

# PIERS 2008 Hangzhou

---

Progress In Electromagnetics Research Symposium

Abstracts

---

March 24–28, 2008

Hangzhou, China

---

[www.emacademy.org](http://www.emacademy.org)  
[www.piers.org](http://www.piers.org)

**PIERS 2008 Hangzhou Abstracts**

Copyright © 2008 The Electromagnetics Academy. All rights reserved.

Published by

The Electromagnetics Academy

777 Concord Avenue, Suite 207

Cambridge, MA 02138

[www.emacademy.org](http://www.emacademy.org)

[www.piers.org](http://www.piers.org)

ISSN: 1559-9450

ISBN: 978-1-934142-03-5

# Progress in Electromagnetics Research Symposium

March 24–28, 2008

Hangzhou, CHINA

## PIERS 2008 HANGZHOU ORGANIZATION

### PIERS Chair

J. A. Kong, MIT, USA

### PIERS 2008 Hangzhou International Advisory Committee

L. C. Botten	C. H. Chan	W. C. Chew	H.-T. Chuah
S. T. Chun	N. Engheta	A. K. Fung	Z.-H. Gu
T. M. Habashy	M. Hallikainen	Y. Hara	H.-C. Huang
A. Ishimaru	Z. Lemnios	L.-W. Li	I. V. Lindell
S. G. Liu	K.-M. Luk	S. Mano	G. D. McNeal
Y. Miyazaki	P. Pampaloni	A. Priou	K. Senne
M. Tateiba	L. Tsang	K. Yasumoto	J. Zehentner
W. X. Zhang			

### PIERS 2008 Hangzhou Technical Program Committee

A. Baghai-Wadji	G. Berginc	W. M. Boerner	H. Braunisch
H.-S. Chen	K.-S. Chen	T. J. Cui	H. C. Fernandes
L. Gurel	K. Kobayashi	S. Lucyszyn	A. Massa
E. L. Miller	M. Moghaddam	R. Muttukrishnan	Z. P. Nie
R. Ramer	C. M. Rappaport	C. Seo	A. H. Sihvola
D. P. Tsai	J. Vrba	B.-I. Wu	

### PIERS 2008 Hangzhou Symposium Committee

H.-S. Chen	K. S. Chen(Co-Chair)	Y. Du	J. T. Huangfu
Q. Jiang	L. X. Ran	L. F. Shen	H. G. Wang
B.-I. Wu	D. X. Yang	X. M. Zhang(Co-Chair)	

### PIERS 2008 Hangzhou Local Arrangement Committee

H.-S. Chen	X. X. Cheng	Y. Du(Co-Chair)	G. W. Fu
J. T. Huangfu	T. Jiang	L. Li	D. W. Liu
Y. Luo	L. Peng	L. X. Ran(Co-Chair)	F. Wang
Z. Y. Wang	S. Xi	W. Z. Yan	D. X. Ye
J. J. Zhang	W. Zhao	F. Zheng	

### PIERS 2008 Hangzhou Administrative Committee

J. J. Bao	H.-S. Chen(Co-Chair)	W. Feng	J. T. Huangfu(Co-Chair)
Q. Jiang	S. Lee	Z. Y. Li	B.-I. Wu
P. L. Xie	L. Ye	L. Y. Yu	

# **PIERS 2008 HANGZHOU SESSION ORGANIZERS**

---

I. Akduman	P. M. Alsing	J. Canning	L. Capineri
C.-C. Chang	D.-C. Chang	H.-W. Chang	H.-S. Chen
Y. Cheng	C-K. Chou	L. Crocco	H.-T. Ewe
J.-M. R. Fournier	L. M. Gaggero-Sager	R. C. Gauthier	T. M. Grzegorzczuk
M. Gu	Z.-H. Gu	K. Iwatsuki	H. Kikuchi
K. Kobayashi	M. Kristensen	A. N. Lagarkov	K. J. Langenberg
J.-F. Lee	C.-F. Li	L. Li	L. W. Li
J. T. Lue	G. H. Ma	Z. Ma	J. Machac
A. Massa	P. M. Meaney	S. Nakamura	N. Nakashima
Y. Okuno	H. C. Ong	M. Oristaglio	K. Ouchi
M. Piana	J. Pu	L. D. Qiu	M. Qiu
R. Ramer	P. Rocca	R. P. Salathé	A. K. Sarychev
C. Seo	Y. V. Shestopalov	S. Siltanen	M. Tateiba
S. Tjuatja	D. P. Tsai	V. R. Velasco	J. T-K. Wan
C.-F. Wang	C. G. Windsor	B.-I. Wu	C.-J. Wu
G. Xie	S. J. Xu	T. Yamasaki	T.-J. Yang
T. S. Yeo	S. Zeng	H. T. Zhang	W. L. Zhang
G. Y. Zhou			

## **PIERS 2008 HANGZHOU EXHIBITOR**

---

- CST China ([www.cst-china.cn](http://www.cst-china.cn))

## **PIERS 2008 HANGZHOU SPONSORSHIP**

---

- Zhejiang University
- National Natural Science Foundation of China
- National Key Laboratory of Space Microwave Technology
- The Electromagnetics Academy at Zhejiang University
- College of Info Science and Engineering, Zhejiang University
- MIT Center for Electromagnetic Theory and Applications/Research Laboratory of Electronics
- The Electromagnetics Academy

## PIERS 2007 SESSIONS

1AP	Poster Session 1	9
1P1	Recent Advances in Metamaterials and Invisibility Cloaking 1	129
1P2	Femtosecond Photonics: Microfabrication and Optical Data Storage 1	141
1P4	Terahertz Optoelectronics	155
1P5	Remote Sensing and Applications	167
1P6	Electromagnetic Wave Applications in Material Processing and Characterization	179
1P7	Space Microwave Technology	189
1P8	Electromagnetic Modeling, Inversion and Application 1	201
2A1	Plasmonic Photonics 1	217
2A2a	Femtosecond Photonics: Microfabrication and Optical Data Storage 2	227
2A2b	Photonic Crystal Waveguides	235
2A3	Metamaterials at Optical Frequencies	241
2A4	Microwave Photonics and Terahertz Technologies and Their Applications	253
2A5	Methods and Instruments for the Determination of Electromagnetic Properties of Soils and Materials	267
2A6	Electromagnetic Theory and Computational Methods for Passive Dielectric Waveguides and Devices	281
2A7	Fields and Waves	291
2A8	Electromagnetic Modeling, Inversion and Application 2	303
2AP	Poster Session 2	315
2P1a	Plasmonic Photonics 2	431
2P1b	Biophoton, Plasmonic Effects and Materials	437
2P2a	Shaping Optical Forces for Trapping and Binding – Theory	445
2P2b	Shaping Optical Forces for Trapping and Binding – Biology	451
2P3	Metamaterials at Microwave Frequencies	457
2P4	Electromagnetic Field in Optical Materials and Dispersion Engineering of Photonic Crystals	473
2P5	Theoretical Models for Microwave Remote Sensing	487
2P6a	Microwave and Millimeter Wave Circuits and Devices 1	499
2P6b	Mobile Antennas for Communication	509
2P7	RF Safety	521
2P8a	Electromagnetic Imaging: State of the Art and Perspectives	535
2P8b	Electromagnetic Inverse Problems	545
3A1a	Dynamics on the Attosecond Time Scale	551
3A1b	Attosecond Pulse Generation Related Technologies	559
3A2a	Shaping Optical Forces for Trapping and Binding – Near-field	565
3A2b	Shaping Optical Forces for Trapping and Binding – Binding	571

3A3a	Metamaterials Design and Applications .....	579
3A3b	Recent Advances in Metamaterials and Invisibility Cloaking 2 .....	587
3A4	Physical Properties of Photoexcited Semiconductors .....	593
3A5	EM Wave in Atmosphere Propagation and Communication 1 .....	605
3A6	Wireless Communication Component .....	617
3A7	Electromagnetic Techniques for Biomedical Applications 1 .....	627
3A8	Computational Techniques .....	641
3P2a	Shaping Optical Forces for Trapping and Binding – Applications .....	653
3P3a	Wave Propagation and Superresolution in Active and Passive Metamaterials 1 .....	663
3P4a	Physical Properties of Photoexcited Semiconductors 2 .....	673
3P5a	EM Wave in Atmosphere Propagation and Communication 2 .....	681
3P6a	Microwave and Optical Devices, Propagation .....	687
3P7a	Electromagnetic Techniques for Biomedical Applications 2 .....	699
3P8a	Novel Mathematical Methods in Electromagnetics .....	707
4A1a	Modelling and Simulations of Nanophotonic Devices .....	717
4A1b	Nano Scale Electromagnetics, MEMS 2 .....	723
4A2a	3D Femtosecond Laser Microprocessing of Transparent Materials .....	729
4A2b	3D Femtosecond Micromachining and 3D Bio-imaging .....	737
4A3	Wave Propagation and Superresolution in Active and Passive Metamaterials 2 .....	743
4A4	Semiconductor Homostructures and Heterostructures 1 .....	753
4A5	Synthetic Aperture Radar Over Land and Sea .....	765
4A6	Waves in Random and Complex Media — Recent Advances in Theoretical and Computational Analyses .....	777
4A7	Extended/Unconventional Electromagnetic Theory, EHD/EMHD, Electrobiolgy 1 .....	791
4A8	Electromagnetic Techniques for Subsurface Detection and Imaging: Theory, Algorithms, and HW Implementations .....	805
4P1a	Photonic Crystals .....	817
4P1b	Plasmonics and Photonic Crystals for Electromagnetic Field Enhancement .....	825
4P2	Vector Properties of Bound Light Beams and Their Physical Effects .....	833
4P3	Wave Propagation and Superresolution in Active and Passive Metamaterials 3 .....	845
4P4a	Semiconductor Homostructures and Heterostructures 2 .....	859
4P4b	Nano-Semiconductors and Devices .....	865
4P5a	Applied Inverse Problems .....	871
4P5b	Remote Sensing of the Earth, Ocean, Atmosphere and Land/Monitoring the earth .....	877
4P6a	Design and Applications of UWB Antennas .....	883
4P6b	EM Theory and Applications .....	891
4P7	Extended/Unconventional Electromagnetic Theory, EHD/EMHD, Electrobiolgy 2 .....	901
4P8a	Advanced CEM Techniques .....	913
4P8b	Computational Electromagnetic Methods .....	919
5A1	Nano Scale Electromagnetics, MEMS .....	929
5A2	Optics and Photonics, Quantum Well Devices and Technology .....	941
5A3	Wave Propagation and Superresolution in Active and Passive Metamaterials 4 .....	953
5A4	Interaction of EM Waves and Media .....	965

---

5A5 Remote Sensing and Scattering Problem.....	973
5A6 Microwave and Millimeter Wave Circuits and Devices 2.....	985
5A8 Novel Antennas and Array Design.....	993
<b>Author Index</b> .....	1006





# Session 1AP

## Poster Session 1

<p><b>Novel Dual-band Microwave Components Based on Composed Right/Left-handed Transmission Lines</b>  <i>Xiao Liu (Institute of Electronics, Chinese Academy of Sciences, China); Chao Li (Institute of Electronics, Chinese Academy of Sciences, China); Fang Li (Institute of Electronics, Chinese Academy of Sciences, China);</i> .....</p> <p><b>Coplanar Waveguide with Elevated Center Strip Conductor Based on HR-Si Substrate</b>  <i>Xiuzhi Wen (East China Normal University, China); Yanling Shi (East China Normal University, China); Jing Liu (East China Normal University, China); Fuquan Cao (East China Normal University, China); Yanfang Ding (East China Normal University, China); Xi Li (East China Normal University, China); Hao Huang (Shanghai IC Research and Development Center, China); Hongbo Ye (Shanghai IC Research and Development Center, China); Linyan Xue (Shanghai IC Research and Development Center, China);</i> .....</p> <p><b>Miniaturization of Harmonics-suppressed Filter with Folded Loop Structure</b>  <i>Han-Nien Lin (Feng-Chia University, Taiwan, R.O.C.); Wen-Lung Huang (Feng-Chia University, Taiwan, R.O.C.); Jer-Long Chen (National Taiwan Ocean University, Taiwan, R.O.C.);</i> .....</p> <p><b>Broadband Amplifier Gain Slope Equalization Filter</b>  <i>Qian Ma (Zhejiang University, China); Mingbo Ma (Jilin University, China);</i> .....</p> <p><b>The PBG Filter Design</b>  <i>Cheng-Hung Lin (National Taiwan Ocean University, Taiwan); Guan-Yu Chen (National Taipei University of Technology, Taiwan); Jwo-Shiun Sun (National Taipei University of Technology, Taiwan); Kwong-Kau Tiong (National Taiwan Ocean University, ); Y. D. Chen (High Tech Computer Corp. (HTC), Taiwan);</i> .....</p> <p><b>Optimization of the SAW Transducer Design by Probabilistic Global Search Lausanne</b>  <i>Guiling Huang (Nankai University, China); Qida Zhao (Nankai University, China); Luming Zhao (Nankai University, China); Shuhong Li (Nankai University, China); Junfeng Lv (Nankai University, China); Fei Wang (Nankai University, China); Jiping Liao (Nankai University, China);</i> .....</p> <p><b>Scaling Law for Unloaded Q of Microwave Resonators</b>  <i>Ikuo Awai (Ryukoku University, Japan); Taichi Nishimura (Ryukoku University, Japan);</i> .....</p> <p><b>Design of Wideband Filter Using Split-ring Resonator DGS</b>  <i>Zheng-Zheng Hou (Zhejiang Gongshang University, China); Xing-Xing Li (Zhejiang Gongshang University, China); Chao-Kun Hao (Zhejiang Gongshang University, China);</i> .....</p> <p><b>Novel Trisection Cross-coupled Filter Based on Mixed Split-ring Resonators</b>  <i>Bian Wu (Xidian University, China); Zheng-Zheng Hou (Zhejiang Gongshang University, China); Chang-Hong Liang (Xidian University, China);</i> .....</p> <p><b>Some Differences among HiFi, Tuned Amplifiers and Oscillators</b>  <i>Sara Liyuba Vesely (I.T.B., C.N.R., Italy); A. A. Vesely (, Italy);</i> .....</p> <p><b>X-band Low Phase Noise Quadrature CMOS VCO with Transformer Feedback</b>  <i>Yu-Shun Liao (National Chiao Tung University, Taiwan); Christina F. Jou (National Chiao Tung University, Taiwan);</i> .....</p> <p><b>A Image Rejection Low Noise Amplifier for WLAN System</b>  <i>Lien-Sheng Wei (National Chiao Tung University, Taiwan); Christina F. Jou (Chiao Tung University, Taiwan);</i> .....</p> <p><b>A 3-8 GHz Broadband Low Power Mixer</b>  <i>Chih-Hao Chen (National Chiao Tung University, Taiwan); Christina F. Jou (National Chiao Tung University, Taiwan);</i> .....</p> <p><b>Frequency Synthesizer Architecture Design for DRM and DAB Receiver</b>  <i>Jianzheng Zhou (Southeast University, China); Zhigong Wang (Southeast University, China);</i> .....</p> <p><b>Design of Reflectionless Phase Shifter by Coordinate Transformation</b>  <i>Mengyu Wang (Zhejiang University, China); Lixin Ran (Zhejiang University, China); Jin Au Kong (Massachusetts Institute of Technology, USA);</i> .....</p> <p><b>Path Planning during the Geomagnetic Navigation</b>  <i>Lingling Jiang (Zhejiang University, China); Lixin Ran (Zhejiang University, China);</i> .....</p>	<p>15</p> <p>16</p> <p>17</p> <p>18</p> <p>19</p> <p>21</p> <p>22</p> <p>24</p> <p>25</p> <p>26</p> <p>27</p> <p>28</p> <p>29</p> <p>30</p> <p>31</p> <p>32</p>
--	---

<b>Simulation for a Distributed Phase-stable Synchronization System</b>	
<i>J. Long (Zhejiang University, China); Shan Qiao (Zhejiang University, China); Jiangtao Huangfu (Zhejiang University, China); Lixin Ran (Zhejiang University, China);</i> .....	33
<b>A 40 GHz Amplifier Designed by Using CPW</b>	
<i>Zhihong Dong (Tsinghua University, China);</i> .....	35
<b>A 2.5 GHz Voltage Controlled FBAR Oscillator</b>	
<i>Jon-Hong Lin (National Chiao-Tung University, Taiwan); Y. H. Kao (Chung Hua University, Taiwan);</i>	36
<b>High Tunable Capacitor Using a Finger Structured Electrode</b>	
<i>Young Chul Lee (Mokpo National Maritime University (MMU), Korea); Kyung Hyun Ko (Ajou University, Korea);</i> .....	37
<b>CPW-to-stripline Vertical via Transitions for 60 GHz LTCC SoP Applications</b>	
<i>Young Chul Lee (Mokpo National Maritime University (MMU), Korea);</i> .....	38
<b>A Novel Ultra Wideband Transformer-feedback LNA</b>	
<i>Hui I Wu (National Chiao Tung University, Taiwan); Tsung-Ting Lin (National Chiao Tung University, Taiwan); Christina F. Jou (National Chiao Tung University, Taiwan); Chih-Peng Lin (National Chiao Tung University, Taiwan); Pei-Yuan Chiang (National Chiao Tung University, Taiwan);</i> .....	39
<b>The Differential Low Noise Amplifier for WiMAX System Application</b>	
<i>Man-Long Her (Feng Chia University, Taiwan); Chi-Feng Lin (Feng Chia University, Taiwan); Yu-Hsiang Chen (Feng Chia University, Taiwan);</i> .....	40
<b>DDS Based Radar Signal Generator for Microwave Remote Sensing</b>	
<i>C. Z. Gu (Zhejiang University, China); Shan Qiao (Zhejiang University, China); Jiangtao Huangfu (Zhejiang University, China); Lixin Ran (Zhejiang University, China);</i> .....	41
<b>Ambiguity Function of Chaotic Radar with Colpitts Oscillator</b>	
<i>Tao Jiang (Zhejiang University, China); Shan Qiao (Zhejiang University, China); Zhiguo Shi (Zhejiang University, China); Lixin Ran (Zhejiang University, China);</i> .....	42
<b>A Broadband Low Noise Amplifier Design</b>	
<i>Ying Wang (Xi'an Institute of Space Radio Technology, China); Yi Fu (Xi'an Institute of Space Radio Technology, China); Wan-Zhao Cui (Xi'an Institute of Space Radio Technology, China); Wei Ma (Xi'an Institute of Space Radio Technology, China);</i> .....	43
<b>A 10~18 GHz Wide-band Transformer Feedback LNA</b>	
<i>Pei-Yuan Chiang (National Chiao Tung University, Taiwan); Christina F. Jou (National Chiao Tung University, Taiwan);</i> .....	44
<b>Region Feature Extraction Based on Improved Regularization Method in SAR Image</b>	
<i>Feng Xu (National Disaster Reduction Center of China, China); Chao Wang (Chinese Academy of Sciences, China);</i> .....	45
<b>Reducing the Time Steps of FDTD Predictions of High-Q Cavities</b>	
<i>Juan Chen (Xi'an Jiaotong University, China); Jianguo Wang (Xi'an Jiaotong University, China);</i>	46
<b>Reduction of EMI and Mutual Coupling in Array Antennas by Using DGS and AMC Structures</b>	
<i>A. Mahmoudian (Tarbiat Modares University, Iran); Jalil A. Rashed-Mohassel (University of Tehran, Iran);</i> .....	47
<b>The Phase Invariance Condition for the Ultra-wideband Voltage Controlled Attenuator</b>	
<i>O. V. Stukach (Tomsk Polytechnic University, Russia);</i> .....	48
<b>Facilitating EMI/EMC Modeling by Predicting Voltage Interference in an EMI/EMC Environment by Two Wires as the Pick-up Model of EM Waves</b>	
<i>Atanu Roy (IIT Kharagpur, India); Saswati Ghosh (IIT Kharagpur, India); Ajay Chakrabarty (IIT Kharagpur, India);</i> .....	49
<b>Interaction between Magnetoresistor and Magnetotransistor in the Two-dimensional Folded Vertical Hall Devices</b>	
<i>Guo-Ming Sung (National Taipei University of Technology, Taiwan, R.O.C.); Chih-Ping Yu (National Taipei University of Technology, Taiwan, R.O.C.);</i> .....	50
<b>Multifunctional Piezomagnetic Ferrite Materials and Their Newly Acoustical and Vibration Control Devices</b>	
<i>Quanlu Li (Shaanxi Normal University, China); Yuan Li (Fourth Military Medical University, China); Zhaohui Huang (Fourth Military Medical University, China);</i> .....	52
<b>Development of Smart Antenna Array Signal Processing Algorithm for Anti-Jam GPS Receiver</b>	
<i>Anindya Kundu (Indian Institute of Technology, India); Soham Ghosh (Netaji Subhash Engineering College, India);</i> .....	53
<b>Time Domain Studies of Ultra Wideband Dielectric Loaded Monopole Trans-receive Antenna System</b>	

<i>Atanu Roy (IIT Kharagpur, India); Saswati Ghosh (IIT Kharagpur, India); Ajay Chakrabarty (IIT Kharagpur, India);</i> .....	54
<b>Study and Improvement in Operational Characteristics of Mid Air Collision Aversion System (TCAS)</b>	
<i>Vikrant Kumar Sharma (Jaypee Institute of Information Technology (JIIT), India);</i> .....	55
<b>Design of Three-layer Circular Mushroom-like EBG Structures</b>	
<i>S. Mahdi Moghadasi (Ferdowsi University of Mashhad, Iran); Amir Reza Attari (Ferdowsi University of Mashhad, Iran); M. M. Mirsalehi (Ferdowsi University of Mashhad, Iran);</i> .....	56
<b>Circular Polarized Rhombic Loop Antenna over a Mushroom-like EBG Surface</b>	
<i>S. Mahdi Moghadasi (Ferdowsi University of Mashhad, Iran);</i> .....	58
<b>Bandwidth Enhancement of Single-feed Circularly Polarized Equilateral Triangular Microstrip Antenna</b>	
<i>Sara Sadat Karimabadi (Ferdowsi University of Mashhad, Iran); Yalda Mohsenzadeh (Ferdowsi University of Mashhad, Iran); Amir Reza Attari (Ferdowsi University of Mashhad, Iran); S. Mahdi Moghadasi (Ferdowsi University of Mashhad, Iran);</i> .....	60
<b>Design of Ultra-wideband Monopole Antenna with Band-notched and GPS Circular Polarization Characteristics</b>	
<i>Han-Nien Lin (Feng-Chia University, Taiwan, R.O.C.); Che-Min Shao (Feng-Chia University, Taiwan, R.O.C.); Jer-Long Chen (National Taiwan Ocean University, Taiwan, R.O.C.);</i> .....	62
<b>Small Antenna Measurement Facilities</b>	
<i>Guan-Yu Chen (National Taipei University of Technology, Taiwan); Jwo-Shiun Sun (National Taipei University of Technology, Taiwan); Cheng-Hung Lin (National Taiwan Ocean University, Taiwan); Kwong-Kau Tiong (National Taiwan Ocean University, Taiwan); Y. D. Chen (High Tech Computer Corp. (HTC), Taiwan);</i> .....	63
<b>Microstrip Antenna Design for Ultra Wideband Application by Using Two Slots</b>	
<i>N. Ghassemi (Sistan and Baluchistan University, Iran); Jalil A. Rashed-Mohassel (University of Tehran, Iran); Mohammad Hassan Neshati (SistanBaluchistan University, Iran);</i> .....	65
<b>The GPS Antenna Design and Measurement</b>	
<i>Kuo-Liang Wu (National Taipei University of Technology, Taiwan); Guan-Yu Chen (National Taipei University of Technology, Taiwan); Jwo-Shiun Sun (National Taipei University of Technology, Taiwan); Cheng-Hung Lin (National Taiwan Ocean University, Taiwan); Kwong-Kau Tiong (National Taiwan Ocean University, Taiwan); Y. D. Chen (High Tech Computer Corp. (HTC), Taiwan);</i> .....	66
<b>The Wideband Character of Self-structuring Antenna</b>	
<i>Hongtao Zhang (Xidian University, China); Yingzeng Yin (Xidian University, China); Wenbo Wei (Xidian University, China);</i> .....	68
<b>Shaping Design of Side-fed Offset Cassegrain Reflector Antennas</b>	
<i>Shao-Dong Liu (Xi'an Institute of Space Radio Technology, China); S. F. Liu (Xidian University, China); Yong-Chang Jiao (Xidian University, China); F. S. Zhang (Xidian University, China);</i> ....	69
<b>On Resonant Frequency of Pin Shorted Gap-coupled Circular Patch Antennas</b>	
<i>Pradeep Kumar (Mody Institute of Technology and Science, India); G. Singh (Mody Institute of Technology and Science, India); S. Bhooshan (Mody Institute of Technology and Science, India); T. Chakravarty (Mody Institute of Technology and Science, India);</i> .....	70
<b>Super-compact UWB Bandpass Filter Using a Partially-grounded Interdigital Gap Structure</b>	
<i>Ryosuke Nakamura (Kansai University, Japan); Toshiaki Kitamura (Kansai University, Japan); Yasushi Horii (Kansai University, Japan); Toshitaka Kojima (Kansai University, Japan);</i> .....	72
<b>Folded Dual-mode Microstrip Filter</b>	
<i>Katsuhisa Tagashira (Kansai University, Japan); Toshiaki Kitamura (Kansai University, Japan); Yasushi Horii (Kansai University, Japan); Toshitaka Kojima (Kansai University, Japan);</i> .....	73
<b>Planar Leaky-wave Antenna with Aperture Coupled Feed</b>	
<i>Alireza Mahmoudian (Tarbiat Modares University, Iran); Hamidreza Dalili Oskouei (Tarbiat Modares University, Iran); Keyvan Forooraghi (Tarbiat Modares University, Iran);</i> .....	74
<b>A Novel Broadband Compact Circular Disk Microstrip Antenna for Wireless Applications</b>	
<i>Husam El-Din Ahmed Osman (Arab Academy for Science and Technology and Maritime Transport, Egypt); Esmat Abdel-Fattah Abdallah (Electronics Research Institute, Egypt); Abdel-Hamid Abdel-Rhim (Arab Academy for Science and Technology and Maritime Transport, Egypt);</i> .....	75
<b>Novel Planar Wideband Omni-directional Antenna for RFID Applications</b>	
<i>Heng-Tung Hsu (Yuan Ze University, Taiwan);</i> .....	76
<b>Clover Polarimetric Detector — A Novel Design of an Ortho-mode Transducer at 150 and 225 GHz</b>	
<i>Philip Mausekopf (Cardiff University, UK); Peter Ade (Cardiff University, UK); Stafford Withington (University of Cambridge, UK); Jin Zhang (Cardiff University, UK); Paul Grime (Oxford University, UK);</i> .....	77
<b>Circular Polarization GPS Patch Antennas with Self-biased Magnetic Films</b>	

<i>Guomin Yang (Northeastern University, USA); Andrew Daigle (Northeastern University, USA); Nian-Xiang Sun (Northeastern University, USA); Krishna Naishadham (Draper Laboratory, USA); .....</i>	78
<b>The Dipole Antenna Array Design with Balun Integration</b>	
<i>Guan-Yu Chen (National Taipei University of Technology, Taiwan); Jwo-Shiun Sun (National Taipei University of Technology, Taiwan); Cheng-Hung Lin (National Taiwan Ocean University, Taiwan); Kwong-Kau Tiong (National Taiwan Ocean University, Taiwan); Y. D. Chen (High Tech Computer Corp. (HTC), Taiwan); .....</i>	79
<b>Printed Digital Audio Broadcast Antennas</b>	
<i>The-Nan Chang (Tatung University, Taiwan); Cheng-Min Jen (Tatung University, Taiwan); .....</i>	81
<b>Two-layer Variable Slot Length Reflectarray</b>	
<i>The-Nan Chang (Tatung University, Taiwan); Chia-Hsin Chung (Tatung University, Taiwan); .....</i>	82
<b>The Planar V-dipole Antenna Fed by Marchand Balun</b>	
<i>Cheng-Hung Lin (National Taiwan Ocean University, Taiwan); Guan-Yu Chen (National Taipei University of Technology, Taiwan); Jwo-Shiun Sun (National Taipei University of Technology, Taiwan); Kwong-Kau Tiong (National Taiwan Ocean University, Taiwan); Y. D. Chen (High Tech Computer Corp. (HTC), Taiwan); .....</i>	83
<b>A Single Feed Circularly Polarized Fractal Shaped Microstrip Antenna with Fractal Slot</b>	
<i>P. Nageswara Rao (National Institute of Technology, India); N. V. S. N. Sarma (National Institute of Technology, India); .....</i>	85
<b>Compact Microstrip-fed Annular-slot Antenna Combined with C-shaped Slot for Broad Dualband Operation</b>	
<i>Xiu Long Bao (Dublin Institute of Technology, Ireland); M. J. Ammann (Dublin Institute of Technology, Ireland); .....</i>	86
<b>Design and Implementation of Aperture Coupled Microstrip IFF Antenna</b>	
<i>Mahmoud Niroo Jazi (Université Québec, Canada); Zaker Hossein Firouzeh (Amirkabir University of Technology (AUT), Iran); Hamid Mirmohammad-Sadeghi (Isfahan University of Technology (IUT), Iran); Gholamreza Askari (Isfahan University of Technology (IUT), Iran); .....</i>	87
<b>Design of the Spiral Monopole Antenna for Multi-band Mobile Communication and SAR Analysis</b>	
<i>Sang-Myeong Park (Chungbuk National University, Korea); Nam Kim (Chungbuk National University, Korea); Seung-Woo Lee (Chungbuk National University, Korea); Ho-Min Lee (Chungbuk National University, Korea); Sung-Wu Park (Chungbuk National University, Korea); .....</i>	88
<b>Design and SAR Measurement of the Trapezoidal Shape Antenna</b>	
<i>Seungwoo Lee (Chungbuk National University, Korea); Sang-Myeong Park (Chungbuk National University, Korea); Nam Kim (Chungbuk National University, Korea); Sung-Wu Park (Chungbuk National University, Korea); Seung-Yeup Lee (Chungbuk National University, Korea); .....</i>	89
<b>Design of Dual-band PIFA for WLAN</b>	
<i>Sung-Keun Jeon (Chungbuk National University, Korea); Nam Kim (Chungbuk National University, Korea); Seung-Woo Lee (Chungbuk National University, Korea); Sang-Myeong Park (Chungbuk National University, Korea); Byoung-Jun Jang (Kookmin University, Korea); .....</i>	90
<b>Dual Frequency Operate Circular Array of Triangular Patches with RF-MEMS Switches</b>	
<i>Naveen Kumar Saxena (Agra College, India); Bhoopendra Singh (Agra College, India); P. K. S. Pournish (Agra College, India); .....</i>	91
<b>12 GHz Planar Array Antenna for Satellite Communication</b>	
<i>Adel Mohamed Abdin (Shorouk Academy, Egypt); .....</i>	92
<b>The Helical Antenna for Handset Design and Phantom Effect</b>	
<i>Kuo-Liang Wu (National Taipei University of Technology, Taiwan); Guan-Yu Chen (National Taipei University of Technology, Taiwan); Jwo-Shiun Sun (National Taipei University of Technology, Taiwan); Cheng-Hung Lin (National Taiwan Ocean University, Taiwan); Kwong-Kau Tiong (National Taiwan Ocean University, ); Y. D. Chen (High Tech Computer Corp. (HTC), Taiwan); .....</i>	93
<b>A Comprehensive Study on Performance of IEEE 802.15.4</b>	
<i>Shuai Fang (Zhejiang University, China); Lu Rong (Shanghai Research Center for Wireless Communications, China); Qiang Xu (Zhejiang University, China); Yang Du (Zhejiang University, China); .</i>	95
<b>Performance Analysis of Unsaturated Slotted IEEE 802.15.4 Medium Access Layer</b>	
<i>Shuai Fang (Zhejiang University, China); Lu Rong (Shanghai Research Center for Wireless Communications, China); Qiang Xu (Zhejiang University, China); Yang Du (Zhejiang University, China); .</i>	96
<b>Energy-efficient Sleeping Schedule and Performance Analysis for IEEE 802.15.4 Device</b>	
<i>Qiang Xu (Zhejiang University, China); Lu Rong (Shanghai Research Center for Wireless Communications, China); Shuai Fang (Zhejiang University, China); Yang Du (Zhejiang University, China); .</i>	97
<b>SIP-based Mobility Management</b>	

<i>Bing Zhao (Zhejiang University, China); Lu Rong (Shanghai Research Center for Wireless Communications, China); Peng Qiao (Zhejiang University, China); Yang Du (Zhejiang University, China);</i>	98
<b>Numerical Study of MAC Scheduling Schemes for IEEE 802.15.3</b>	
<i>Guangdi Yang (Zhejiang University, China); Lu Rong (Shanghai Research Center for Wireless Communications, China); Dingyuan Tu (Zhejiang University, China); Rufeng Lin (Zhejiang University, China); Yang Du (Zhejiang University, China);</i>	99
<b>Throughput Analysis of Delayed Acknowledgement over 802.15.3 WPAN with Hybrid ARQ Retransmission</b>	
<i>Rufeng Lin (Zhejiang University, China); Lu Rong (Shanghai Research Center for Wireless Communications, China); Qiang Xu (Zhejiang University, China); Yang Du (Zhejiang University, China);</i>	100
<b>MIMO Channel Model and Its Impact on the Channel Capacity</b>	
<i>Jun Wang (Xi'an Institute of Space Radio Technology, China); Quan Zhou (Xi'an Institute of Space Radio Technology, China); Wei Ma (Xi'an Institute of Space Radio Technology, China); Lede Qiu (Xi'an Institute of Space Radio Technology, China);</i>	101
<b>The Influence of the Climatic Peculiarities on the Electromagnetic Waves Attenuation in the Baltic Sea Region</b>	
<i>Mindaugas Zilinskas (Vilnius University, Lithuania); Milda Tamosiunaite (Vilnius University, Lithuania); Stasys Tamosiunas (Vilnius University, Lithuania); Milda Tamosiuniene (Semiconductor Physics Institute, Lithuania);</i>	102
<b>Outdoor Exposure to the RF-radiation of WiFi for Wireless City Applications</b>	
<i>Gilbert Decat (VITO, Belgium); Meynen Guy (VITO, Belgium); Daniel Wilczek (VITO, Belgium);</i>	103
<b>OFDM System Location Determination with 4-element Antenna Array Using Frequency Domain Matrix Pencil (FDMP) Method</b>	
<i>Mohamed A. Labib (Alexandria University, Egypt); Hassan M. Elkamchouchi (Alexandria University, Egypt);</i>	104
<b>WCDMA 3D Location Determination with 3D Polarization Using Four 3-element Arrays</b>	
<i>Mohamed A. Labib (Alexandria University, Egypt); Hassan M. Elkamchouchi (Alexandria University, Egypt);</i>	105
<b>Location Determination for 2G/3G/4G Using Time Delay Matrix Pencil (TDMP) Method</b>	
<i>Mohamed A. Labib (Alexandria University, Egypt); Hassan M. Elkamchouchi (Alexandria University, Egypt);</i>	106
<b>To the Glory of J. F. Maxwell: Electromagnetic Theory of the Origin of Saturn's Rings</b>	
<i>Vladimir V. Tchernyi (Scientific Agency "SAIBR", Russia);</i>	107
<b>Analyses on Frequency Dependence of Permeability and Power Loss for NiZn Ferrites</b>	
<i>Hua Su (University of Electronic Science and Technology of China, China); Huaiwu Zhang (University of Electronic Science and Technology of China, China); Xiaoli Tang (University of Electronic Science and Technology of China, China); Zhiyong Zhong (University of Electronic Science and Technology of China, China);</i>	108
<b>Strip Casting of Immiscible Alloys in a Static Magnetic Field</b>	
<i>H. L. Li (Institute of Metal Research, China); Jiuzhou Zhao (Institute of Metal Research, Chinese Academy of Sciences, China);</i>	109
<b>Two Different Sets of Integral Equations for Modeling Electromagnetic Scattering from Arbitrary Concave Perfectly Conducting Objects</b>	
<i>Jia-Jun Niu (Shanghai Jiao Tong University, China); Bin Yuan (Shanghai Jiaotong University, China); Yu Rong (Shanghai Jiao Tong University, China);</i>	110
<b>A Hybrid GAM/SM-AIM Formulation for Quasi-planar Structures above a Planar Aperture Array</b>	
<i>Nicola Truschi (University of Florence, Italy); Alberto Di Maria (University of Florence, Italy); Angelo Freni (University of Florence, Italy);</i>	111
<b>Electrical Transport in Manganite Structures: The Random Fuse Network Study</b>	
<i>Jian-Chun Wu (Suzhou University, China); Hua Sun (Suzhou University, China); Hai-Xia Da (Suzhou University, China); Zhen-Ya Li (Suzhou University, China);</i>	112
<b>A Hybrid Iterative Method for Computing Electromagnetic Scattering of Large Perfectly Conducting Cavities</b>	
<i>Jia-Jun Niu (Shanghai Jiao Tong University, China); Bin Yuan (Shanghai Jiaotong University, China); Yu Rong (Shanghai Jiao Tong University, China);</i>	113
<b>Inward-outward Hybrid Iterative Method for Analyzing Electromagnetic Scattering by Complex Perfectly Conducting Objects including Large Cavities</b>	
<i>Jia-Jun Niu (Shanghai Jiao Tong University, China); Bin Yuan (Shanghai Jiaotong University, China); Yu Rong (Shanghai Jiao Tong University, China);</i>	114
<b>Technique for Detecting Chirp in Femtosecond Pulse by Autocorrelator</b>	

<i>Yan Ling (Fudan University, China); Fang Lu (Fudan University, China);</i> .....	115
<b>3D Microwave Module Interconnect Using Fuzz Button</b>	
<i>Lei Xia (University of Electronic Science and Technology of China, China); Ruimin Xu (University of Electronic Science and Technology of China, China); Bo Yan (University of Electronic Science and Technology of China, China);</i> .....	116
<b>Design and Analysis of Quad-band PCB Embedded Antenna for Mobile Handset Applications</b>	
<i>Soon-Ho Hwang (Samsung Electronics Co., LTD, Republic of Korea); Kyu-Bok Park (Samsung Electronics Co., LTD, Republic of Korea); Joon-Ho Byun (Samsung Electronics Co., LTD, Republic of Korea);</i> .....	117
<b>Reconfigurable Stacked Patch Antenna for Wireless Power Beaming and Data Telemetry</b>	
<i>Guangli Yang (Antenna Technology Center of Excellence, MDa, Motorola Inc., USA);</i> .....	118
<b>An High Gain Omni-directional Planar Array Antenna</b>	
<i>Yuanbo Shang (Xidian University, China); T. Zhang (Xidian University, China); Yong-Chang Jiao (Xidian University, China); F. S. Zhang (Xidian University, China);</i> .....	119
<b>Analysis of Technical Conditions for Sharing Frequency Spectrum</b>	
<i>Taekjin Hwang (Electronics and Telecommunication Research Institute, Korea);</i> .....	120
<b>Dynamic Sector Synthesis of Antenna Array Using Genetic Algorithm</b>	
<i>Abdelaziz Abdelmonem Abdelaziz (Misr International University (MIU), Egypt); Hanan A. Kamal (Cairo University, Egypt);</i> .....	121
<b>Mie Particles and Quasiparticles in Ag Thin Films</b>	
<i>M. Gnanavel (University of Hyderabad, India); D. Bharathi Mohan (University of Coimbra, Portugal); C. S. Sunandana (University of Hyderabad, India);</i> .....	122
<b>Surface Plasmon Polaritons in Dual-sided Corrugated Metal Films</b>	
<i>Xin Wu (Nanjing University, China); Z. J. Zhang (Nanjing University, China); R. W. Peng (Nanjing University, China); J. S. Zhang (Nanjing University, China); J. Li (Nanjing University, China); K. Wei (Nanjing University, China); De Li (Nanjing University, China); R. L. Zhang (Nanjing University, China);</i> .....	123
<b>On The Concept of Vector (Polarization) Electromagnetic Inverse Boundary Conditions for the Perfectly and Imperfectly Conducting Cases and Its Applications: Why Is Renewed Interest in EM-IBC Forthcoming?</b>	
<i>Wolfgang-Martin Boerner (University of Illinois at Chicago, USA);</i> .....	124
<b>Recent Advances in Polarimetric and Interferometric Radar Remort Sensing</b>	
<i>Wolfgang-Martin Boerner (University of Illinois at Chicago, USA);</i> .....	126
<b>Need for Developing Repeat-pass Differential POL-SAR Interferometry</b>	
<i>Wolfgang-Martin Boerner (University of Illinois at Chicago, USA); Kun-Shan Chen (NCU-CSRSR, Taiwan);</i> .....	127
<b>Mechanical and Electric Fields in Quantum-wire and Quantum-dot Nanostructures</b>	
<i>E. Pan (The University of Akron, USA); K. Y. Xu (Shanghai University, China);</i> .....	128

## Novel Dual-band Microwave Components Based on Composed Right/Left-handed Transmission Lines

Xiao Liu, Chao Li, and Fang Li

Institute of Electronics, Chinese Academy of Sciences, Beijing, China

**Abstract**— Employing right/left-handed transmission lines (CRLH-TLs), a dual-band branch-line coupler (BLC), a dual-band band-pass filter (BPF) and a dual-band series 3-port power divider are presented. These components are designed, fabricated and measured. Simulated and measured results demonstrate that the size of the BLC operating at 0.9 GHz and 1.8 GHz is as small as that of the conventional BLC based on quarter-wavelength TL with single operating frequency at 0.9 GHz. For the dual-band BPF, CRLH structure with phase shift of  $0^\circ$  and  $-180^\circ$  at two arbitrary frequencies are synthesized. The two measured central frequencies are  $f_1 = 1.47$  GHz and  $f_2 = 2.3$  GHz, with fractional bandwidths  $W_1 = 10.2\%$  and  $W_2 = 13.0\%$ , respectively. Moreover, it has a comparatively compact size. The dual-band series 3-port power divider using dual-band matching technique provides equal power splitting to all 3 ports, which can be extended to an arbitrary number of output ports, and meanwhile it is compact. These proposed novel dual-band microwave components can mitigate some of the problems between the dual-band work and the need for compact size, which are of great use in practical applications.

## Coplanar Waveguide with Elevated Center Strip Conductor Based on HR-Si Substrate

Xiuzhi Wen<sup>1,2</sup>, Yanling Shi<sup>1,2</sup>, Jing Liu<sup>1</sup>, Fuquan Cao<sup>1</sup>, Yanfang Ding<sup>1</sup>, Xi Li<sup>1</sup>  
Hao Huang<sup>3</sup>, Hongbo Ye<sup>3</sup>, and Linyan Xue<sup>3</sup>

<sup>1</sup>Department of E. E., East China Normal University, China

<sup>2</sup>State Key Laboratories of Transducer Technology, China Academy of Sciences, China

<sup>3</sup>Shanghai IC Research and Development Center, China

**Abstract**— Coplanar waveguide lines (CPW) is an important component in microwave field and it is widely used in monolithic microwave integrated circuits and modern communication systems. Practical application of integrated circuits requires operation over radio frequency. The investigation on the performances of CPW on Si-based substrate as a function of frequency gains interest.

The overall CPW loss can be divided into integration substrate loss and strip metal loss. The loss of CPW lines on low-resistivity silicon is high in the traditional IC technology. The high-resistivity silicon can reduce substrate loss effectively. The magnetic-field which brings loss concentrates near the center strip conductor. In this paper, an elevated CPW based on high-resistivity silicon is presented. The center strip conductor is elevated on a silicon dioxide layer which is easily fabricated by thermal oxidation. This extra silicon dioxide layer under the center strip conductor weakens the magnetic-field, which could be validated by the HFSS simulation. Compared with the conventional CPW with the center strip and ground planes on the same plane, the elevated CPW's insertion loss can be decreased. And the process flow is compatible with the mainstreamed CMOS technology.

According to the simulated results by HFSS, 50  $\Omega$  Aluminum CPW lines are fabricated on HR-Si of 1000  $\Omega$ -cm resistivity. The length of CPW lines is 2000  $\mu\text{m}$ . The width of the center strip conductor is 39  $\mu\text{m}$  and the gap between the center strip conductor and the ground plane is 24  $\mu\text{m}$ . The Aluminum lines are isolated from Si substrate by oxide layer. Three CPW lines with different heights of oxide layer have been fabricated. The height of  $\text{SiO}_2$  under the ground planes is 0.1  $\mu\text{m}$  while those under the center strip conductor are 0.1  $\mu\text{m}$ , 0.2  $\mu\text{m}$ , 0.3  $\mu\text{m}$  separately. The measured and simulated results all show that the elevated CPW can decrease the insert loss. At 10 GHz, the elevated CPW with 0.3  $\mu\text{m}$   $\text{SiO}_2$  under the center strip conductor has an insertion loss of 1.91 dB which is 0.11 dB smaller than that with 0.2  $\mu\text{m}$   $\text{SiO}_2$ , and it is 0.33 dB smaller than that of the conventional CPW. The simulated and measured results are in good agreement. Thus this elevated CPW structure can improve the transmission performance and it is available for low-loss Si-MMIC applications up to radio frequency.



# Miniaturization of Harmonics-suppressed Filter with Folded Loop Structure

Han-Nien Lin<sup>1</sup>, Wen-Lung Huang<sup>2</sup>, and Jer-Long Chen<sup>3</sup>

<sup>1</sup>Department of Communications Engineering, Feng-Chia University, Taiwan, R.O.C.

<sup>2</sup>Department of Electrical Engineering, Feng-Chia University, Taiwan, R.O.C.

<sup>3</sup>Department of Electrical Engineering, National Taiwan Ocean University, Taiwan, R.O.C.

**Abstract**— This article utilized a loop resonator as a base for designing and realizing a band-pass filter. A quarter-wavelength open stub was then incorporated to suppress the second and third harmonics. The signal between the feed and resonator enhanced by coupling feed and therefore can improve the insertion loss. The transmission zero for the electric and magnetic coupling in the lower and upper stopbands in the filter was implemented by a narrow coupling gap and connected via the ground to improve the signal-to-noise ratio (S/N ratio) of the complete circuit. The proposed methodology is different from the cross couple technique but can be implemented to achieve the same performance. It also has the additional advantage of effectively reducing the circuit size. Since the original prototype of the original circuit is a resonator based on one wavelength structure, it is slightly larger compared with the other structures. We therefore utilize folding the loop of the circuit to achieve miniaturization. The reduction of the circuit size is about 30%. The circuit with folded structure not only can reduce the size but also can maintain the performance as original structure with only a little degradation on the third harmonic. The obvious loss observed in the original structure at the high frequencies can introduce the improper electromagnetic interference. The lossy effect could be eliminated by using EMI routing technique to effectively suppress the unwanted loss mechanism and make the circuit more stable in electromagnetic environment. The results of the measurement and simulation are in good agreement within experimental errors and provide a sound experimental verification of the suitable EMI design technique.

## Broadband Amplifier Gain Slope Equalization Filter

Qian Ma<sup>1</sup> and Mingbo Ma<sup>2</sup>

<sup>1</sup>Zhejiang University, China

<sup>2</sup>Jilin University, China

**Abstract**— Since the achievable gain of transistors typically falls off as the frequency increases, an equalization filter with positive gain slope is necessary to compensate for the gain roll-off of broadband amplifiers. This paper proposed a novel structure of equalization filter with characteristics of wide frequency band, low excess loss and low non-linear distortion.

The proposed structure consists of a gain slope equalizer followed by a SIW-PBG (substrate integrated waveguide-photon band gap) filter. The equalizer is designed to provide a linear gain slope from  $-10$  dB to  $0$  dB. Apart from the traditional models [1], the series resonant circuit is substituted by series microstrip gap and high-resistance microstrip lines (Figure 1) to minimize the parasitic effects. The SIW-PBG filter is applied to enhance the selectivity of the system. Based on the models proposed in Zhang-Cheng Hao's work [2], the structure of the filter is modified to adapt to the cut-off frequencies and the passband requirements (Figure 2).

The whole system is simulated by ADS schematic simulator and CST EM simulator. The results show that a  $-10$  dB to  $0$  dB linear positive gain slope is achieved in the spectrum of  $8.5$  GHz to  $18.5$  GHz. Except for the excess loss of  $0.88$  dB at  $18.5$  GHz, the non-linear ripple is no more than  $0.33$  dB, showing characteristics of good impedance matching, low excess loss, and sharp out-of-band.

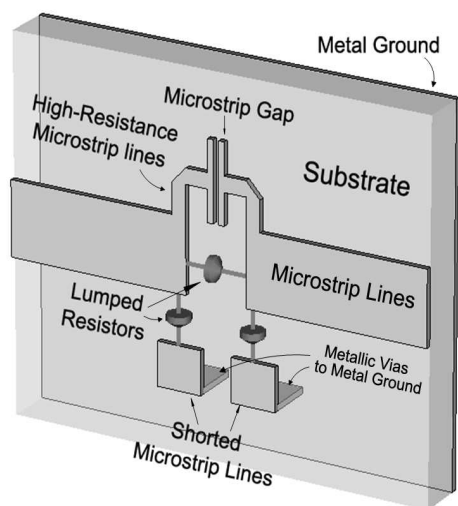


Figure 1: The novel equalizer structure.

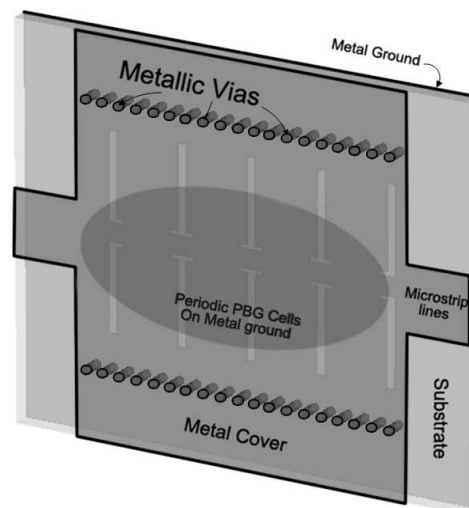


Figure 2: The SIW-PBG filter structure.

### REFERENCES

1. Vendelin, G., A. Pavio, and U. Rohde, *Microwave Circuit Design Using Linear and Nonlinear Techniques*, J. Wiley and Sons, New York, 1990.
2. Hao, Z.-C. W. Hong, J.-X. Chen, X.-P. Chen, and K. Wu, "Compact super-wide bandpass substrate integrated waveguide (SIW) filters," *IEEE*, 0018-9480, 2005.

## The PBG Filter Design

Cheng-Hung Lin<sup>1</sup>, Guan-Yu Chen<sup>2</sup>, Jwo-Shiun Sun<sup>2</sup>, Kwong-Kau Tiong<sup>1</sup>, and Y. D. Chen<sup>3</sup>

<sup>1</sup>Department of Electrical Engineering, National Taiwan Ocean University, Taiwan

<sup>2</sup>Department of Electronic Engineering, National Taipei University of Technology, Taiwan

<sup>3</sup>Antenna and EMC Laboratory, High Tech Computer Corp. (HTC), Taiwan

**Abstract**— The performances of the periodic surface structures of defected shapes on the ground plane for low-pass filter (LPF) co-design are studied. Simulated results with full wave electromagnetic analyses are in good agreement with those experimental data. The optimal structure of double periodic structure bringing about the perturbation electromagnetic waves will be determined. The proposed LPF has defect ground surface with the characteristics of band-gap characteristics.

**Introduction:** The periodic surface structure is like photonic band-gap (PBG) [1–3] structures are effective in RF and microwave application that provides an effective control of electromagnetic waves along specific direction and performance. Controlling the periodic distance of PBG that exist band reject characteristic. Periodic and defected ground structure (DGS) have some excellent performance applied microwave transmission line guide such as the microstrip PBG, coplanar waveguide PBG, coplanar-stripline PBG, uniplanar compact PBG and multiplayer PBG. The perforation patterns of PBG on the ground surface with band-stop and slow wave characteristics are studied.

**Design & Results:** In this paper, a traditional LPF (Fig. 1) placed at center the DGS with various PBG structures (Fig. 2) is studied, then proposed high harmonic reject low pass characteristic on PBG microstrip line. By the way of measurement and simulation (Fig. 3) to detect this structure exist obvious passband, stopband and leaky wave band region then compare with interrelate research papers. Via measurement to calculate EM structures on band-gap region, then find DGS structure can apply high reject band characteristic as a perfect low-pass filter circuit. FR4 substrate (dielectric constant 4.4, loss  $\delta \tan = 0.015$  and height 1.6 mm) was used for this design and implement.

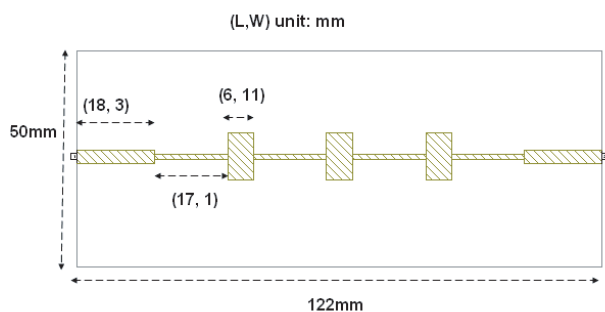


Figure 1: Traditional LPF design with perfect ground plane.

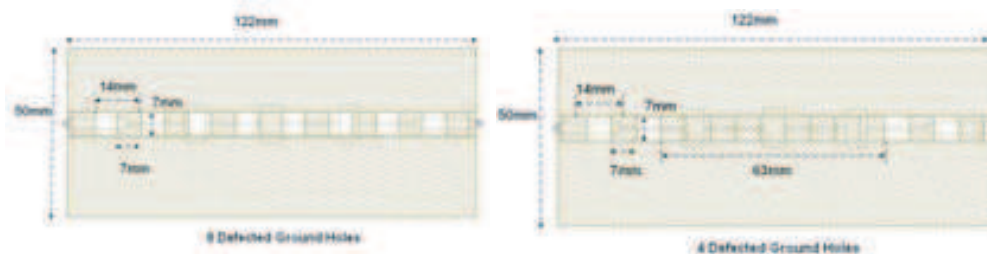


Figure 2: LPF design with periodic and non-periodic ground plane.

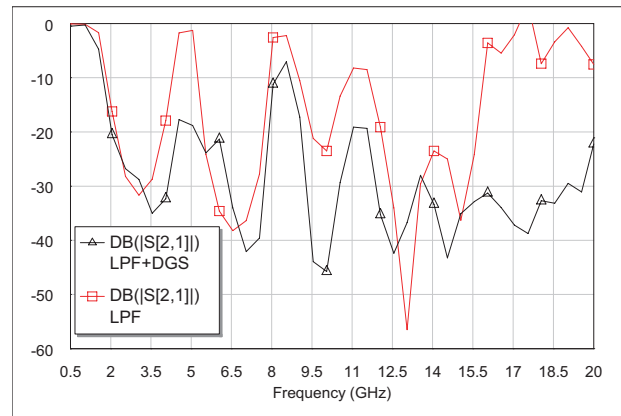


Figure 3: The data of LPF embedded DGS and traditional LPF.

**Conclusion:** This paper describes a harmonic tuning for embedded defected ground plane. EM modeling for a LPF embedded defected ground plane structure co-design is determined. The structure with stop-band characteristic for broadband harmonic rejection tuning has been experimentally verified. Method of moment is applied to simulate the fields and currents distribution of the design. The results of full wave electromagnetic analyses are in good agreement with those experimental data. An optimal structure of the LPF and defected ground plane structure is determined.

#### REFERENCES

1. Munk, B. A., *Frequency Selective Surfaces: Theory and Design*, John Wiley, New York, c2000.
2. Soukoulis, C. M., *Photonic Band Gaps and Localization*, Plenum Press, New York, c1993.
3. Robert E. Collin, *Field Theory of Guided Waves*, 2nd, IEEE Press, New York, c1991.

# Optimization of the SAW Transducer Design by Probabilistic Global Search Lausanne

Guiling Huang<sup>1,2</sup>, Qida Zhao<sup>1</sup>, Luming Zhao<sup>3</sup>, Shuhong Li<sup>1</sup>  
Junfeng Lv<sup>1</sup>, Fei Wang, and Jiping Liao<sup>1</sup>

<sup>1</sup>Institute of Modern Optics, Nankai University, Tianjin 300071, China

<sup>2</sup>Institute of Photo Electronic Thin Film Devices & Technology  
Nankai University, Tianjin 300071, China

<sup>3</sup>Department of Physics, Nankai University, Tianjin 300071, China

**Abstract**— Complexity is a main shortcoming for designing surface acoustic wave transducer. It is effective to use the optimization program to design SAW transducer IDTs to aim at improvement in the filter characteristics and shortening of the lead time of the product design. In general, it is difficult to apply the gradient method because there are a lot of semi-optimal solutions in the allowable range of the design parameters. Some researches have done by using global optimization algorithms, in which Genetic algorithms (GAs) are the most widely used. In this paper, a new and promising method based on Probabilistic Global Search Lausanne (PGSL), a new global optimization algorithm which was proposed by Benny Raphael is proposed. It is a direct search algorithm that utilizes global sampling for finding the minimum of a user defined objective function. The power of PGSL is in handling blackbox objective functions (the objective function does not require to be expressed in an explicit mathematical form) and constraints. Gradients are not needed and no special characteristics of the objective functions (such as convexity) are required. PGSL is founded on the assumption that optimal solutions can be identified through focusing search around sets of good solutions. The algorithm includes four nested cycles: Sampling cycle, Probability updating cycle, Focusing cycle and Subdomain cycle. In the sampling cycle (innermost cycle), a certain number of samples (NS) are generated randomly according to the current probability density function (PDF). Each point is evaluated by the user-defined objective function and the best point is selected. In the next cycle, probabilities of regions containing good solutions are increased and probabilities decreased in regions containing less attractive solutions. In the third cycle, search is focused on the interval containing the best solution after a number of probability updating cycles by further subdivision of the interval. In the subdomain cycle, the search space is progressively narrowed by selecting a subdomain of smaller size centered on the best point after each focusing cycle. Each cycle serves a different purpose in the search for a global optimum. The sampling cycle permits a more uniform and exhaustive search over the entire search space than other cycles. Probability updating and focusing cycles refine search in the neighborhood of good solutions. Many tests carried out on complex nonlinear objective functions indicate that PGSL performs better than Gas. An attractive characteristic of PGSL is that there are not a large number of interrelated parameters in it need to be appropriately fixed. An example of design optimization using PGSL on SAW transducer is reported.

## Scaling Law for Unloaded $Q$ of Microwave Resonators

Ikuo Awai and Taichi Nishimura

Department of Electronics & Informatics, Ryukoku University  
2-1 Yokotani, Seta-oecho, Otsu 520-2194, Japan

### Abstract—

**Introduction:** Scaling laws for unloaded  $Q$  of a resonator versus the resonant frequency are derived based on Maxwells equations. Three types of structure, one, two and three-dimensional resonators are discriminated, together with three origins of power loss, conductor, dielectric and radiation losses. Each case shows different dependencies on the resonant frequency, which is confirmed by E/M field simulation and experiment. Only one-dimensional resonators are explained here.

**Theory:** (1) Conductor  $Q$  Dissipated power at the conductor surface is given by

$$P_c = R_s \iint_s |H_t|^2 dS \quad (1)$$

$$R_s = \sqrt{\omega \mu_0 / \sigma} \quad (2)$$

where  $H_t$  is the tangential magnetic field.

The stored energy, on the other hand, is written as

$$W = \iiint_v \mu_0 |\mathbf{H}|^2 dV = \int_0^\ell \iint_s \mu_0 |\mathbf{H}(S, z)|^2 dS dz \quad (3)$$

Considering that the surface resistance of the conductor is proportionate to  $f_0^{1/2}$  as shown in Eq. (2), we have

$$Q_c = \frac{\omega_0 W}{P_c} \propto \frac{f_0 f_0^{-1}}{f_0^{1/2} f_0^{-1}} \propto f_0^{1/2} \quad (4)$$

This square root dependency is the scaling law for  $Q_c$  of one dimensional resonator.

### (2) Dielectric $Q$

The dielectric loss is given by

$$P_d = \omega \varepsilon'' \iiint_{v_d} |\mathbf{E}|^2 dV \quad (5)$$

where  $V_d$  is the volume of the lossy dielectric. If one assumes is independent of the frequency, which is often the case, one have the following relatyons using the dimension of resonator  $N$  ( $= 1, 2$  or  $3$ ),

$$P_d \propto f_0 \ell^N = f_0 f_0^{-N} = f_0^{1-N} \quad (6)$$

$$W \propto \ell^N = f_0^{-N} \quad (7)$$

$$Q_d = \frac{\omega_0 W}{P_d} \propto \frac{f_0 f_0^{-N}}{f_0^{1-N}} = f_0^0 \quad (8)$$

Therefore, it is noted that the dielectric  $Q$  is independent of the resonant frequency irrespective of the dimension of resonators.

### (3) Radiation $Q$

The radiation power is given by

$$\mathbf{L} = \iint_s \mathbf{i}_m(r) e^{-jk_0 \hat{r} \cdot \mathbf{r}} dS \quad (9)$$

$$P_r = \frac{k_0^2}{6\pi\eta_0} (|L_\theta|^2 + |L_\varphi|^2) \quad (10)$$

For one dimensional open resonator, the radiation surfaces are located on each end. Therefore the integral in Eq. (10) is constant even when the resonator length changes. Thus, the radiation  $Q$  is calculated

$$Q_r = \frac{\omega_0 W}{P_r} \propto \frac{f_0 f_0^{-1}}{f_0^2} \propto f_0^{-2} \tag{11}$$

**Simulation (Microstrip Line Resonator):** The substrate thickness  $\tan \delta$ , dielectric constant and  $\tan \delta$  are assumed to be 0.74 mm, 3.27 and 0.0036, respectively. Solid lines are the theoretical curves given by Eqs. (4), (8) and (11).

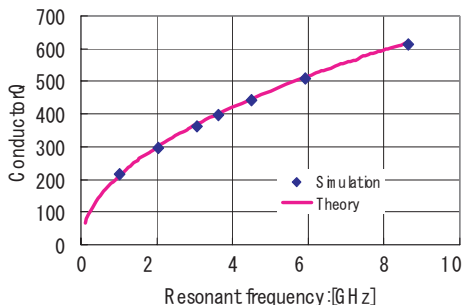


Figure 1: Conductor  $Q$ .

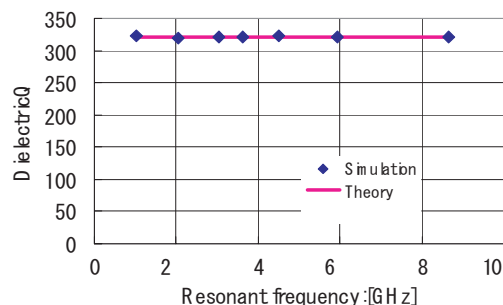


Figure 2: Dielectric  $Q$ .

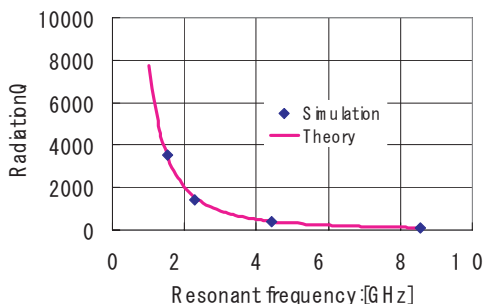


Figure 3: Radiation  $Q$ .

**Experiment:**

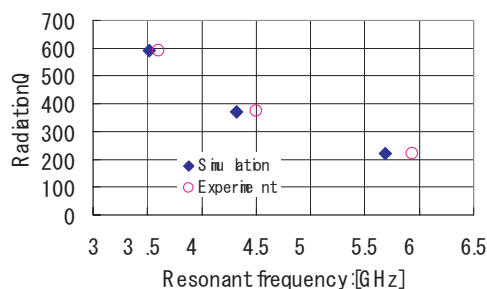


Figure 4: Measured and simulated radiation  $Q$ .

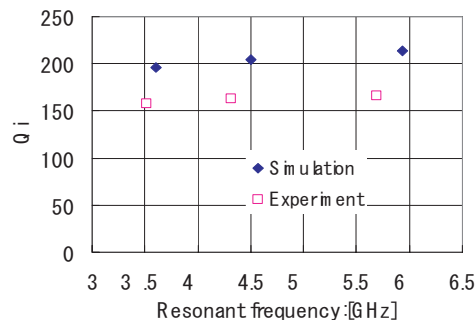


Figure 5: Combined  $Q$  of conductor and dielectric losses.

**Conclusion:** Scaling laws for microwave resonators have been derived successfully. Theory, simulation and experiment agree quite well for microstrip line resonators. Though only one-dimensional resonator is presented, higher-dimensional ones have already been analyzed and partly verified by experiment. They will be published in other chances.

## Design of Wideband Filter Using Split-ring Resonator DGS

Zheng-Zheng Hou, Xing-Xing Li, and Chao-Kun Hao

College of Information and Electronic Engineering, Zhejiang Gongshang University  
Hangzhou 310018, China

**Abstract**— Defected ground structure was firstly proposed by Park et al. based on the idea of photonic band-gap (PBG) structure [1] in 1999, and had found its application in the design of planar circuits and low-pass filters [2, 3]. Defected ground structure is realized by etching a defective pattern in the ground plane of the micro-strip line, which disturbs the shield current distribution in the ground plane, then change the characteristics of a transmission line such as equivalent capacitance and inductance to obtain the slow-wave effect and band-stop property. Compared with the conventional PBG structures, defected ground structure requires only one defected unit to obtain the forbidden-gap property, and the center frequency of the gap is fully determined by the configuration of the defected unit, so it has the advantages of small size, compact structure as well as the facility of equivalent-circuit analysis and filter design [4–6].

Split-ring resonator DGS is becoming one of the most popular DGS types in recent years [7, 8], which introduces a transmission zero at the out-of-band, so it has a much steeper slope for the filter design. In this paper, the split-ring resonator DGS is successfully applied to the design of micro-strip band-pass filter. First, the equivalent-circuit values are extracted by the curve-fitting method; second, a novel wideband filter circuit model is constructed and analyzed; the filter is then realized by using lumped chip capacitances and T-shaped open-circuit stubs and fabricated. Measured pass-band loss is below 1 dB with a wide pass-band from 1 GHz to 2.4 GHz, and from 3 GHz to 8 GHz, the out-band suppression is no less than 25 dB.



# Novel Trisection Cross-coupled Filter Based on Mixed Split-ring Resonators

Bian Wu<sup>1</sup>, Zheng-Zheng Hou<sup>2</sup>, and Chang-Hong Liang<sup>1</sup>

<sup>1</sup>National Laboratory of Antennas and Microwave Technology, Xidian University, Xi'an 710071, China

<sup>2</sup>College of Information and Electronic Engineering, Zhejiang Gongshang University  
Hangzhou 310018, China

**Abstract**— Recent development in wireless communication system has created a need of band-pass filter with low insert loss, high out-of-band suppression and compact size. Cross-coupled filters are widely investigated because they introduce one or more additional coupling between nonadjacent resonators and create finite transmission zeros out of band [1, 2]. Microstrip open-loop or split-ring is one of the most popular resonant units that have been used, it is equivalent to a half-wavelength resonator, the coupling between two split-rings can be electric, magnetic or mixed depending on the orientation of the resonators, and the input/output coupling can be realized by strip-gap or tapped line. This structure can be easily applied to the exact filter design using classical theories of coupled resonator circuits [3–5]. In recent years, there has been an increasing interest in the planar filter design with defected ground structure due to its compact size and band-gap property [6–8].

In this paper, both microstrip split-ring and defected split-ring are applied to the design of a mixed split-ring cross-coupled filter. First, the resonant property of the defected split-ring is studied and compared with that of the microstrip split-ring. Then the defected split-ring is loaded at the bottom of the two-section microstrip split-ring filter, which have a mutual coupling with each other, and a bandpass filter with a pair of transmission zeros is obtained. At last, such a kind of trisection mixed split-ring cross-coupled filter which has a center frequency of 1.4 GHz is fabricated, the experimental results agree well with the simulation that validates the presented method.

## Some Differences among HiFi, Tuned Amplifiers and Oscillators

S. L. Vesely<sup>1</sup> and A. A. Vesely<sup>2</sup>

<sup>1</sup>I.T.B., C.N.R., Italy

<sup>2</sup>via L. Anelli 13, Milano 20122, Italy

**Abstract**— The distinction between amplifiers and oscillators was somewhat ambiguous already with the first MASER. In Gordon, Zeiger, and Townes' [1] paper of 1955, the ammonia MASER is actually considered an amplifier of resonant signals, or alternatively an oscillator, without distinguishing between enhanced signal to noise ratio and frequencies of self-oscillation sustained by the cavity. We think two points in particular deserve paying attention to. In the first place, a wavemeter should deliver information about a sample, which is not compatible with the production of temporally stable carrier waves. Secondly, a MASER working as an oscillator either selectively amplifies thermal noise, so that at thermal equilibrium one cavity mode is amplified, or else exercises a positive feedback on an ammonia emission line, by means of its tuned cavity. Perhaps, experimenters act in different ways if they are seeking to induce a stimulated emission for an inverted ammonia level, buried in thermal noise, than if they try to get better matching conditions between the cavity and the excited gas fed into it.

From a telecommunication theory perspective, a MASER used as a sensitive spectrometer might be considered a signal receiver, but one could retrieve no information from such a MASER. To clarify, HiFi amplification provides for broadband magnification of audio signals without altering their *content*, irrespectively of it being music, voice, noises, etc. For radio receivers narrow-band techniques have also been developed, e.g., superheterodyne. They are useful for discriminating and selectively amplifying transmitted signals, that is the carrier modulation, when they are masked by signals belonging to adjacently allotted channels, that are not wanted. Unwanted signals are also collectively called *noise*, in a broader sense. However, narrow-band processing of radio signals at IF is practicable only when the data flow is parameterized using a single variable, usually time or phase. When the transmitted data flow is not known beforehand, as it is the case with spectra, information cannot be retrieved from narrow-band reception.

Besides the information function, there is also another sense in which an ammonia MASER behaves non-linearly. Its “tuned amplification” is by no means like narrow-band detection because high sensitivity is obtained at the expenses of response linearity: resonance between ammonia and the cavity happens at the self-reversion condition of the 1.25 cm line, that is to say, of the signal. Thus, a MASER can function as a pulsed oscillator provided that its response as an amplifier is essentially of the on/off type. Distortion under CW functioning conditions is even worse. In that case the cavity is exercising a positive feedback on the line. As soon as stationary resonance conditions are met, the frequency undergoes a shift away from the free emission frequency, due to the load modulation that the feedback causes. Therefore, coupling with the cavity determines the vanishing of the relevant line. While the ammonia-line “saturates” because of the resonant couplings with the cavity, it cannot be irradiated with any special strength by the MASER, and power is irradiated at nearby frequencies, which don't belong to the gas-spectrum. In conclusion, we think a good MASER cavity merely serves for passively damping load fluctuations. According to kinetic theory, instead, the noise originates from molecular thermal excitation inside the cavity, while oscillation introduces an ordered cooperative state, that is to say, the cavity actively selects the cooperative state from thermal noise.

### REFERENCES

1. Gordon, J. P., H. J. Zeiger, and C. H. Townes, “The maser-new type of microwave amplifier, frequency standard, and spectrometer,” *Phys. Rev.*, Vol. 99, No. 4, 1264–1274, 1958.

## X-band Low Phase Noise Quadrature CMOS VCO with Transformer Feedback

Yu-Shun Liao and Christina F. Jou

Institute of Communication Engineering, National Chiao Tung University  
Hsinchu 300, Taiwan

**Abstract**— A fully integrated quadrature VCO with transformer feedback is proposed to achieve low-phase-noise and at a x-band using a TSMC 0.18- $\mu\text{m}$  CMOS technology. The VCO is implemented using a transformer-based LC tank and the transformer feedback configuration from the drain to the back-gate of the switching transistors. The proposed VCO, which allows higher oscillation frequency while keeping comparable performances compared to those of the other topologies.

The current source is replaced by resistor providing bias condition and wide-band operation. Besides, two benefits also achieved due to the removal of the current source. First, the current source is the main contributor to the phase noise. Second, when all transistors in the VCO core are put in GHz-switching bias condition, flicker noise will apparently be reduced by about 10 dB.

With parallel coupling transistor to generate the I-Q phase. From the Barkhausen criterion, oscillation only occurs when the loop gain is  $[A(j\omega)]^4 = 1$ , which means  $A(j\omega) = 1 \angle 90^\circ$ . Therefore, this configuration provides quadrature-phase signals from the four outputs of these two proposed VCOs.

The simulation result shows the phase noise is about  $-114 \text{ dBc/Hz}$  at 1 MHz offset and the output frequency tuning range of the QVCO is around 800 MHz ranging from 8.9 to 9.7 GHz. The QVCO core circuit draws only 4.1 mA from a 1.5-V supply. Compared with the recent works, the proposed QVCO topology shows phase noise performance 5 dBc/Hz lower than the original and power consumption of 6.15 mW compared to the original VCO core of 6.84 mW.

## A Image Rejection Low Noise Amplifier for WLAN System

Lien-Sheng Wei and Christina F. Jou

Institute of Communication Engineering, National Chiao Tung University, Hsinchu, Taiwan

**Abstract**— At typical ratio frequency front-ends receiver, proper filtering of image signals is mandatory. The image-rejection (IR) filter usually is an external component, such as surface acoustic wave (SAW) filters. These kinds of filters are often very expensive and large that is not suitable for SOC.

In order to eliminate external SAW filter, the LNA with new on-chip IR techniques have been proposed. This IR LNA uses current-reused structure that works like two common source amplifiers and shares current, so that it can reach low power and high gain. The IR filter is achieved by passive components to save more power than active filter. This passive IR filter that includes a shunt resonator series with a capacitor, then shunts with an inductor. By locating shunt resonator in inter-stage of current-reused circuit, the IR filter can be presented. The output impedance of first transistor at RF frequency and image frequency are highest and lowest, respectively. Because output impedance multiplied by transconductor is gain of common source amplifier, proposed LNA can provide high gain at wanted signal and reject image signal. Therefore, IR LNA can be achieved.

The proposed IR LNA is optimized for 5.8 GHz application for WLAN with IF frequency of 500 MHz based on TSMC 0.18  $\mu\text{m}$  CMOS technology. Consuming a DC power of 5.98 mW from a 1 V supply, the LNA exhibits 15.4 dB gain and  $-18.1$  dB IR. The input and output reflection coefficients are  $-15.9$  and  $-26$ , respectively. The noise figure is 2.85 dB. The IIP3 is  $-11$  dBm and P1dB is  $-19.4$  dBm.

## A 3–8 GHz Broadband Low Power Mixer

Chih-Hau Chen and Christina F. Jou

Institute of Communication Engineering, National Chiao Tung University, Hsinchu, Taiwan

**Abstract**— A 3–8 GHz broadband mixer is presented in this paper. This broadband mixer is low power and high conversion gain. It provides current reuse and ac-coupled folded switching. This mixer is designed in TSMC 0.18- $\mu\text{m}$  CMOS technology. This broadband mixer achieves simulated conversion gain of  $9 \pm 1.5$  dB, a single sideband noise figure lower than 15.2 dB and IIP3 better than  $-7$  dBm. From 3–8 GHz, at supply voltage of 1.5 V power consumption without output buffer is 3.27 mW and power consumption with buffer is about 8mW. The chip area is  $1079 \mu\text{m} \times 761 \mu\text{m}$ .

In transconductor stage, the advantage of using pmos instead of resistor can be amplified RF signal. The pmos can be used as current reuse. It can not only supply high gain but also provide a low power. The capacitor C affords ac-coupled in RF signal and to be isolated of pmos and nmos in DC. In RF signal, the total  $g_m$  is equal to  $g_{mn} + g_{mp}$  ( $g_{mn}$  is the transconductance of nmos, and  $g_{mp}$  is the transconductance of pmos).

Linearity in the mixers is very important. Nonlinearity in the mixer voltage transfer function is caused by operation of the switching transistors in the linear region. The transistors in switching stage will be cutting off by the large voltage swing at the drain of the transconductance. Linearity almost completely decides by the input signal dynamic range. In the folded switching mixer with current reuse, the linearity can be improved by decreasing the DC drain voltages of the transconductance.

# Frequency Synthesizer Architecture Design for DRM and DAB Receiver

Jianzheng Zhou<sup>1,2</sup> and Zhigong Wang<sup>1</sup>

<sup>1</sup>Institute of RF- & OE-ICs, Southeast University, Nanjing, China

<sup>2</sup>School of Computer & Information, Hefei University of Technology, Hefei, China

**Abstract**— A DRM/DAB receiver will need to support several radio standards including AM, DRM, FM, and DAB, and need to provide the necessary flexibility for seamless receiving. A key challenge in the full integration of such a DRM/DAB receiver is the design and implementation of its beating heart, i.e. the reconfigurable frequency synthesizer which acts as the local oscillator (LO) and covers all the frequency bands of the considered standards. This is due to the difficulty in meeting the performance requirements with on-chip components because of the diverse standards it needs to support.

We have proved that a double-conversion low-IF structure is the most suitable architecture for the DRM/DAB receiver, and the first intermediate frequency ( $f_{IF1}$ ) is 36.95 MHz and  $f_{IF2}$  is 2 MHz for DAB, 175 kHz for other bands in this system. The receiver needs two quadrature LO signals, the first one is generated by a synthesizer and the second one is a fixed frequency. So, only the synthesizer which generates the first quadrature LO is discussed in this work.

Some of the main design specifications and considerations are given as follows. Firstly, the output frequency range of synthesizer is 37 ~ 37.3 MHz, 37.4 ~ 38.7 MHz, 39.2 ~ 64 MHz, 112.9 ~ 145 MHz, 210.9 ~ 277 MHz and 1488.9 ~ 1529 MHz for LF, MF, HF, FM, III band and L band, respectively. Its resolution is 3 kHz, 1 kHz, 5 kHz, 25 kHz, 64 kHz and 64 kHz for LF, MF, HF, FM, III band and L band, respectively. Numerical stipulation of phase noise for this design, a typical value of  $-80$  dBc/Hz@1 kHz is chosen. Generally speaking, all sidebands need to be approximately 70 to 80 dB below the main carrier. Initial design switching time of less than 100 ms is aimed. Furthermore, generation of quadrature LO-signals is mandatory for low-IF receiver architecture.

Because of their higher complexity, higher dissipation and larger die area, and thus direct analog frequency synthesizer (DAS) and direct digital frequency synthesizer (DDFS or DDS) are often not suitable for DRM/DAB receivers. Meanwhile, The fractional-N PLL architecture suffers from fractional spurs which degrade the spurious-tone performance. While a single-loop integer-N PLL Synthesizer with an additional frequency divider X placed at the output of the VCO to allow for smaller frequency steps than the loop's reference frequency and improves the lock time, phase noise, and reference spurs. Based on this concept model and the specifications of DRM/DAB receivers, 4 synthesizer structures were designed for the receiver which supports several radio standards including AM, DRM, FM, and DAB. The performance of each synthesizer was analyzed theoretically, including phase noise, spurious, lock time, etc. Comparisons of the characteristics of the four structures are given. Analysis and calculations will prove that the synthesizer structure 1 with a single VCO and a single loop filter is the most suitable one for the DRM/DAB receivers, which need few external components and require no mechanical alignments. Suppose that the  $PN_{floor}$  of the PLL is better than  $-210$  dBc/Hz, we can obtain the performance of the synthesizer structure 1, which is listed in table I.

Table 1: The performance of synthesizer structure 1.

Band	Output Frequency Range (MHz)	Step Size (kHz)	Phase noise dBc/Hz@1 kHz	Ref. spur Reduction	Switch Time (ms)
LF	37-37.3	3	< -112	38 dB	< 0.1
MF	37.4-38.7	1	< -107	38 dB	< 0.3
HF	39.2-64	5	< -107	> 33.6 dB	< 0.1
FM	112.9-145	25	< -103	> 26 dB	< 0.05
III band	210.9-277	64	< -99	> 20 dB	< 0.04
L band	1488.9-1529	64	< -80.4	6 dB	< 0.1

# Design of Reflectionless Phase Shifter by Coordinate Transformation

Mengyu Wang<sup>1,2</sup>, Lixin Ran<sup>1,2</sup>, and Jin Au Kong<sup>1,3</sup>

<sup>1</sup>Electromagnetics Academy at Zhejiang University, Zhejiang University, Hangzhou 310058, China

<sup>2</sup>Department of Information and Electronic Engineering, Zhejiang University, Hangzhou 310027, China

<sup>3</sup>Research Laboratory of Electronics, Massachusetts Institute of Technology, Cambridge, MA 02139, USA

**Abstract**— Recently the use of coordinate transformations to produce material specifications that control electromagnetic fields in interesting and useful ways has been widely studied. Pendry have suggested a method in which the transformation properties of Maxwell's equations and the constitutive relations can yield material descriptions that implement surprising functionality. Using this method, we can control the behavior of any electromagnetic wave by designing the proper devices.

In this article, we suggest a method to design a phase shifter by coordinate transformation. The permittivity and permeability of the media can be obtained by applying form-invariant, spatial coordinate transformations to Maxwell's equations. Any electromagnetic wave that propagates through this media will get its polarization direction changed. Compared with the traditional anisotropic media, this new media has the specialty in that it provides reflectionless properties. Numerical simulations are performed to illustrate these properties.

## Path Planning during the Geomagnetic Navigation

Lingling Jiang<sup>1,2</sup> and Lixin Ran<sup>1,2</sup>

<sup>1</sup>Electromagnetics Academy at Zhejiang University, Zhejiang University, Hangzhou 310027, China

<sup>2</sup>Department of Information and Electronic Engineering, Zhejiang University, Hangzhou 310027, China

**Abstract**— Pigeons can navigate through apparently featureless environments with pinpoint accuracy, over very long distances. Pigeons are also discovered to have the ability to navigate in darkness during night. How they are able to do this remains a mystery and greatly elicits pigeon bionics. Scientists in the University of Auckland report pigeons' apparent orientation to the intensity gradient of the geomagnetic field observed in their homing from sites in and around a magnetic anomaly, in which the behavior occurred is irrespective of the homeward direction, which indicates the geomagnetism may play an impact role in position determination.

But systems of paired coordinates merely consisting of geomagnetic components hypothesized up to now are lack of experimental support. For example, the non-dipole anomalies that cause intensity, inclination and declination to be aligned at high angles to each other cover relatively small areas, and the "inclination with intensity" model proposed by Lohmann have been challenged on the grounds that the two coordinates only vary at high angles to each other over areas that are both relatively small and ephemeral over evolutionary time, whereas the pigeons often navigate over large area.

This paper proposes a novel navigation method similar to pigeons' homing behavior, which depends totally on the geomagnetic environments, without relying on familiar surroundings, cues that emanate from the destination, or information collected along the journey. We choose geomagnetic intensity (or inclination) and declination as paired coordinates, Figure 1 shows the total intensity distribution on earth's surface while Figure 2 demonstrates the declination distribution, these two geomagnetic components are aligned at high angles in relatively larger areas compared with the former hypothesis.

An optimal path planning is introduced in this method, where the position determination is not limited to pigeon's biological behavior but expected to be applicable to human beings' navigations. It only needs acquainting the magnetic data near home and continuous comparing work done during the journey, instead of recording detailed magnetic information of a large scale area in advance (e.g., huge amounts of data required in terrain navigation). Therefore it may be used on the other planets where we do not know detailed magnetic data, as long as these planets have systematic magnetic distributions.

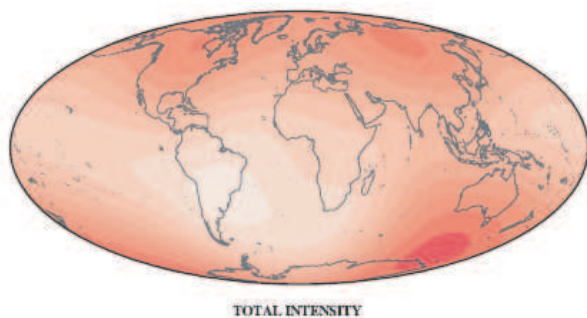


Figure 1: Total intensity distribution.

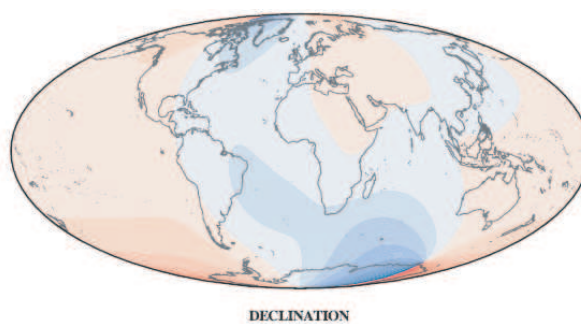


Figure 2: Declination distribution.



# Simulation for a Distributed Phase-stable Synchronization System

J. Long<sup>1</sup>, S. Qiao<sup>3</sup>, J. T. Huangfu<sup>1,2</sup>, and L. X. Ran<sup>1,2</sup>

<sup>1</sup>Department of Information Science and Electronic Engineering  
Zhejiang University, Hangzhou 310027, China

<sup>2</sup>The Electromagnetics Academy at Zhejiang University  
Zhejiang University, Hangzhou 310027, China

<sup>3</sup>City College, Zhejiang University, Hangzhou 310027, China

**Abstract**— In this paper, a distributed phase-stable synchronization system, which is capable

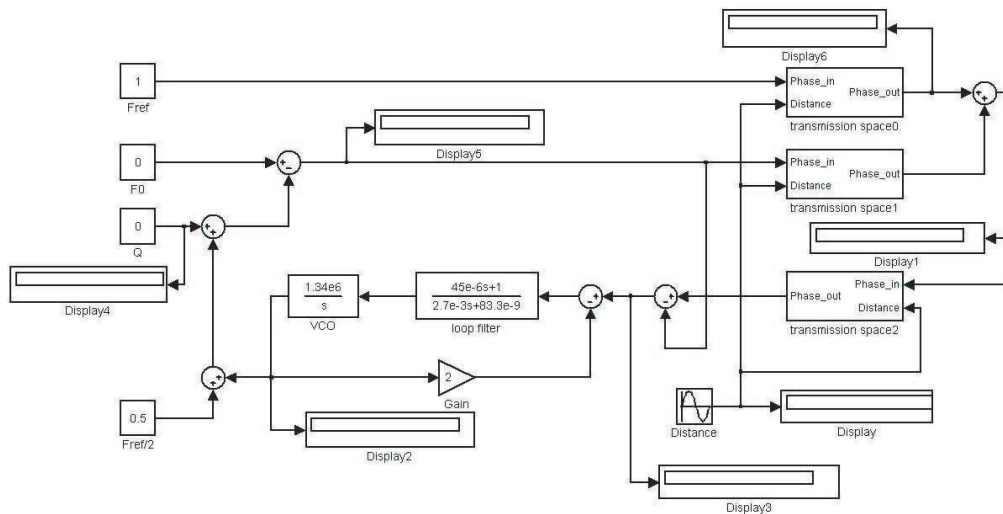


Figure 1: Simulation schematic in matlab.

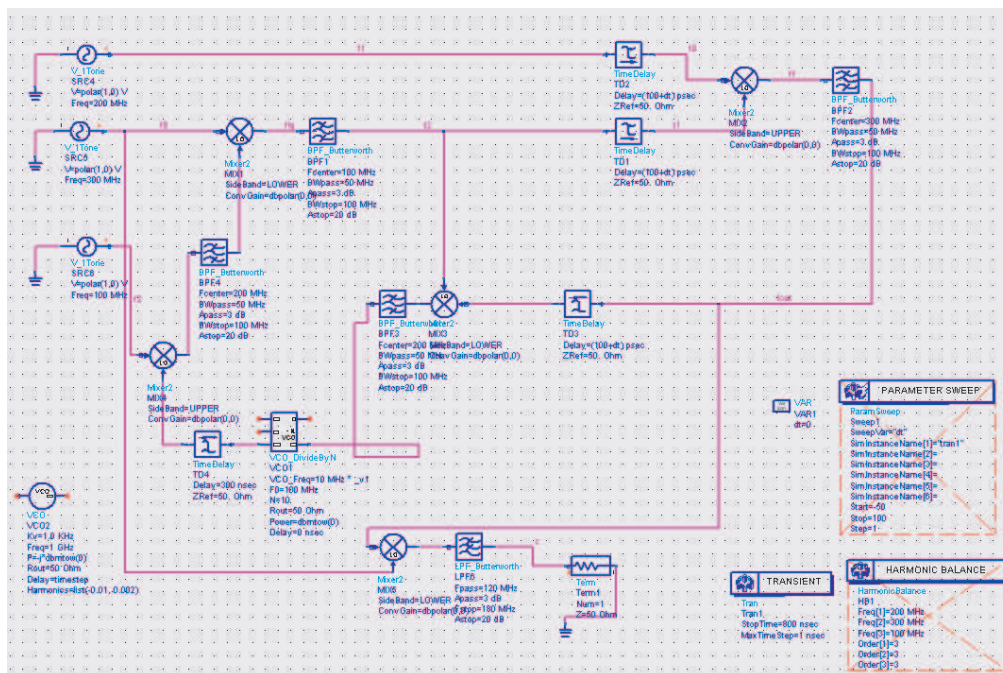


Figure 2: Simulation schematic in ADS.

of sending a phase-synchronous signal from the master base to several slave bases with a distance

by using microwave, is demonstrated. The stability of the phase is the feature of this system. In this paper two methods of simulation are conducted, which are numerical simulation and system simulation. And excellent results are got to show the great performance of the system.

Figure 1 and Figure 2 are the system schematics in simulation. Some methods are used here to test the performance of the system and verify that the system is capable of sending a phase-synchronous signal.

By using different signals as the sources to the system and comparing it with the output, we easily find that the system can lock the majority input signals when some of the conditions, such as distance and noise, are varying. In matlab simulation, we use three different sources, which are constant, ramp and sine, to simulate the system. The result shows that the output signal can be locked in a short time, which is about 0.2ms at most. And we can get the similar result from ADS system simulation.

## A 40 GHz Amplifier Designed by Using CPW

Zhihong Dong

The Institute of Microelectronics, Tsinghua University, China

**Abstract**— In this paper, a 40 GHz amplifier is designed with its matching network and inductors realized by transmission line (CPW).

For mm-wave circuit design, reactive component values are very small, requiring inductance values on the order of 50–250 pH. Direct implementation of these elements (matching networks and resonators) using spiral inductors do not have the required accuracy, so transmission lines are used with the appropriate length and termination. Another benefit of using transmission lines is that the well-defined ground return path confines the magnetic and electric fields and significantly reduces any coupling to adjacent structures.

The amplifier consists of two stages of cascode devices (Figure 2) with input, output, and interstage reactive matching since cascode offers best isolation, low-to-moderate noise, ease of matching, good linearity, higher gain.

For 0.13  $\mu\text{m}$  SMIC 1p8m process, the voltage supply is 1.2 v, the gate voltage of  $Q_1$  and  $Q_3$  is near 0.75 v. For the second stage, there is no source degeneration for the sake of gain, but for the first stage, we have to keep the inductance degeneration for the sake of input matching.

The input and output are designed to be matched to  $50\ \Omega$ . The matching of the input is realized through adjusting  $L_S$  and  $L_G$  as follows, while the output matching is through adjusting  $L_{D2}$  and  $C_{C2}$ , and the interstage matching is through adjusting  $L_{D1}$  and  $C_{C1}$ .

The length of the four transistors is 0.13  $\mu\text{m}$ , while the width of  $Q_1$  and  $Q_2$ , the width is  $3\ \mu\text{m} \times 9 = 27\ \mu\text{m}$  and the width of  $Q_3$  and  $Q_4$  is  $4\ \mu\text{m} \times 10 = 40\ \mu\text{m}$ , after input and output matching, we get  $L_{S1} = 90\ \text{pH}$ ,  $L_G = 275\ \text{pH}$ ,  $C_{C2} = 33\ \text{fF}$ ,  $L_{D2} = 265\ \text{pH}$ . After adjusting interstage matching, we finally set  $L_{d1} = 270\ \text{pH}$  and  $C_{C1} = 50\ \text{fF}$ . After simulation through HSPICE we get the Gain = 12.5, NF = 7.64 dB with power dissipation = 13.8 mw. Note that for this simulation result, we have used the ideal inductance. It is well-known that when using the practical inductance like spiral inductance, there must be great performance degeneration. Besides it is impossible to realize small inductance like 80 pH using spiral inductance, so we choose CPW to realize small inductance.

For simplification, we only replace  $L_{S1}$  by a length of CPW while keeping other inductances ideal. As we all know the  $Q_L$  and characteristic impedance depend on the w/s ratio, if we want the CPW characteristic impedance to be  $50\ \Omega$ , we can set the w/s to be around 10/9 (from ADS simulation), anyway we can verify it through HFSS simulation. First we get the S parameter, then through the following equation we can get the impedance approximates 50 and have the inductance approximates 90 pH. Thus we can use this structure to replace  $L_{S1}$ . After adjusting the length of the CPW to be 120  $\mu\text{m}$ , we get the Gain = 13.3 and NF = 7.61 dB. (Needs further simulation with other inductance and matching network replaced by CPW).

Through HFSS or ADS simulation, we can choose the appropriate w/s, and then we use the first-order electrical model of T-line in HSPICE simulation to get the performance. After comparison the results with the ideal case, we find that transmission line is indispensable for RF application. Through HFSS simulation, we find the Q of the CPW is 15–20, but its performance exceeds the ideal ones, which is the biggest advantage.

## A 2.5 GHz Voltage Controlled FBAR Oscillator

J. H. Lin<sup>1</sup> and Y. H. Kao<sup>2</sup>

<sup>1</sup>Department of Communication Engineering, National Chiao-Tung University, Hsinchu, Taiwan

<sup>2</sup>Department of Communication Engineering, Chung Hua University, Hsinchu, Taiwan

**Abstract**— In high-speed digital communication system, a clock recovery circuit is used for signal integrity. The clock is usually extracted from a phase-look-loop (PLL) circuit with low jitter voltage controlled oscillator (VCO). In optical communications, 2.488 GHz VCO play important role in the jitter filter and frequency translator for 40 Gigabits system, like OC768. Due to the availability of high frequency and high quality resonator, the VCOs were mostly fabricated at 622 MHz either by the fourth harmonic of 155 MHz crystal oscillator (VCXO) or directly 622 MHz saw oscillator (VCSO). Both cases suffer from the increase of floor noise and the degradation factor of  $20 \log(N) = 12$  dB on the phase noise as applications to OC768 at 2488.32 MHz. Thus, high frequency VCO with high-Q resonator using direct oscillation is required to overcome these disadvantages. For this purpose, Film Bulk Acoustic Resonator (FBAR) is the hopeful candidate. In this paper, a high quality film bulk acoustic resonator (FBAR) was designed and fabricated. The FBAR is shown as Fig. 1. The FBAR device is a three-layer structure with the top and bottom electrodes of aluminum and gold sandwiching a middle layer of oriented piezoelectric aluminum nitride. The Modified Butterworth VanDyke (MBVD) equivalent circuit model for the resonator was extracted for oscillator design. Using this resonator, a 2.5 GHz voltage controlled FBAR oscillator is designed and realized with hybrid circuits. The electronic tuning range of the oscillator exceeds  $\pm 6\%$ . The 2nd harmonics of oscillator is suppressed below 40 dB. The oscillator provides 14.5 dBm of output power without output buffer amplifier and consumes 65 mA from +5 V DC power supply.

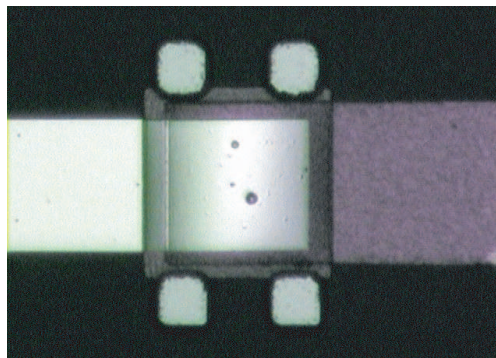


Figure 1: Picture for the film bulk acoustic resonator.

### ACKNOWLEDGMENT

This work is supported by Chung Shan Institute of Science and Technology under contract BV95G1-1P-001P00. The authors would like to thank Dr. P. Y. Chen at Chung Shan Institute of Science and Technology for fabricating the film bulk acoustic resonator.

### REFERENCES

1. Ishii, O., H. Iwata, M. Sugano, and T. Ohshima, "UHF AT-CUT crystal resonators operating in the fundamental mode," *IEEE Int. Frequency Control Symposium*, 975–980, 1998.
2. Nomura, N., M. Itagaki, and Y. Aoyagi, "Small packaged VCSO for 10 Gbit Ethernet Application," *IEEE UFFC*, 68–73, 2004.
3. Rubby, R., J. D. Larson, P. Bradley, and Y. Oshmyansky, "Ultra-miniature, high-Q filter and duplexers using FBAR technology," *ISSC*, Feb. 2001.

# High Tunable Capacitor Using a Finger Structured Electrode

Young Chul Lee<sup>1</sup> and Kyung Hyun Ko<sup>2</sup>

<sup>1</sup>Div. of Marine Electronics and Communication Engineering  
Mokpo National Maritime University (MMU), Korea

<sup>2</sup>Department of Materials Science and Engineering, Ajou University, Korea

**Abstract**— We present a novel tunable metal-insulator-metal (MIM) capacitor with the finger-structure electrode for improving its tunability. The capacitors were fabricated on a low-resistivity Si substrate employing lead zinc niobate (PZN) thin film dielectric. The fabricated capacitor, whose line width and spacing was 2.5  $\mu\text{m}$ , achieved the effective capacitance tunability of 22.8% at 5.5 V. This achieved tunability is higher value of 10% than that of the conventional rectangular MIM at 900 MHz.

## CPW-to-stripline Vertical via Transitions for 60 GHz LTCC SoP Applications

Young Chul Lee

Div. of Marine Electronic and Communication Engineering

Mokpo National Maritime University (MMU), Korea

**Abstract**— In this work, CPW-to-stripline (SL) vertical via transitions using gradually stepped vias and embedded air cavities are presented for V-band LTCC System-on-Package (SoP) applications. In order to reduce radiation loss due to abrupt via discontinuities, gradual via transitions (one and two stepped via structure) are proposed and investigated. In addition, in order to reduce increased parasitic shunt capacitance due to stepped via structures, air cavities are embedded below the transition vias. Using a 3-D EM simulation tool, the proposed transitions are designed and analyzed, compared to the conventional transition. Three-segment transmission lines (CPW-SL-CPW) in 7-layer LTCC dielectrics were fabricated and measured. The two stepped via (STV2) transition with embedded air cavities shows an insertion loss of 1.6 dB and return losses below  $-10$  dB over 60 GHz. The transition loss per one STV2 transition is 0.7 dB at 60 GHz.

## A Novel Ultra Wideband Transformer-feedback LNA

Hui I Wu, Tsung-Ting Lin, Christina F. Jou, Chih-Peng Lin, and Pei-Yuan Chiang

Microwave and Millimeter Wave Laboratory

Institute of Communication Engineering, National Chiao Tung University

Hsinchu, Taiwan

**Abstract**— Ultra wide-band communication techniques have attracted great interests in both academia and industry during the last few years for applications in short-range. A Low-noise amplifier (LNA) is the first stage, after antenna and low-pass filter in the receiver block of a communication system. The UWB LNA face several challenges, such as sufficient power gain through entire bandwidth to suppress the noise of next stage, low noise figure and low power consumption.

In order to connect an antenna port, the first problem facing is 50 Ohm wide-band input matching. There are several existing matching mechanisms for wideband matching network. However, these topologies have some problems such as high noise figure, large chip area or very complicated matching network. The proposed common source based lna using transistor's intrinsic capacitor, intentionally added Miller Capacitors, and a transformer to achieve wide band input impedance matching from 3 GHz to 11 GHz.

However high coupling coefficient transformer and the large transconductance is required for 3–11 GHz bandwidth, and higher magnetic coupling must be achieved by overlaying (i.e., multi-layer) transformer windings; unfortunately, the fifth-layer metal (M5) is a thin metal which would degrade the noise factor of the low noise amplifier. Based on the reasons above, a small Miller capacitor is added between the gate and the drain of first stage transistor, which will help matching the input impedance of the lna to 50 ohm without the need for high coupling coefficient and large transconductance.

The proposed low noise amplifier is designed in TSMC 0.18- $\mu\text{m}$  mixed signal/RF CMOS process. With 1 V bias voltage, the low noise amplifier can achieve a simulated power gain ( $S_{21}$ ) of 12.5 dB from 3–11 GHz while consuming 12 mW. The simulated good noise factor is less than 3.2 dB over the entire UWB frequency band. And the simulated  $S_{11}$  is  $< -12.8$  dB from 3–11 GHz. An output-matching buffer is designed for broadband output impedance matching, The simulated  $S_{22}$  is  $< -14$  dB from 3–11 GHz. Compared with previously reported 018- $\mu\text{m}$  CMOS LNAs in 3–11 GHz range, this circuit has the smallest noise factor with competitive performance.

# The Differential Low Noise Amplifier for WiMAX System Application

Man-Long Her, Chi-Feng Lin, and Yu-Hsiang Chen

Department of Communications Engineering, Feng-Chia University  
100, Wenhwa Rd., Seatwen, Taichung, 40724, Taiwan

**Abstract**— This paper presents the design and post-layout simulated results of an integrated differential low noise amplifier (LNA), which can be applied Worldwide Interoperability Microwave Access (WiMAX) technology of broadband to provide high data rate and transmitting data in long distance. Although the WiMAX standard (IEEE 802.16) has not been completed universally, most of the proposed applications are allowed to transmit in a band between 2 and 11 GHz (2.5 GHz, 2.8 GHz, 3.5 GHz, and 5.8 GHz etc.) [1].

Figure 1 shows the simplified configuration of the differential LNA. In the gain amplifier, this LNA employs cascode transistor  $M_1$  and  $M_2$  to reduce miller effect of gate-drain capacitor  $C_{gd}$  and enhance gain. Inductor  $L_1$  is for simultaneous noise and gain matching for the impedance matching of the LNA. Resistor  $R_1$  is a shunt feedback resistor added to the conventional cascode narrowband LNA. The capacitor  $C_2$  is for ac signal coupling purposed [2]. In the last stage of the design,  $M_5$  and  $M_6$  form the phase splitter, which uses the  $L_3$  and  $C_4$  feedback circuit to achieve a gain balance and  $180^\circ$  phase differences between its two outputs. The simulation results of a 3 GHz to 4 GHz differential LNA are shown in Figure 2. The proposed differential LNA is designed and simulated based on a  $0.18\ \mu\text{m}$  1P6M standard RF CMOS process Design Kit (PDK) from Taiwan Semiconductor Manufacturing Company (TSMC). A post-layout simulation was extracted using the Agilent ADS simulator. We adopted the modified the LC branch filter circuit with RC shunt-feedback circuit for input impedance matching circuit to achieve the optimized input return loss ( $S_{11}$ ) less than  $-10\ \text{dB}$ , and the maximum power gain ( $S_{21}$ ,  $S_{31}$ ) are less than  $17.5\ \text{dB}$  within the noise figure between  $2.4\text{--}2.5\ \text{dB}$  from 3 to 4 GHz can be obtained. The phase difference between its two outputs is only  $180^\circ \pm 0.4^\circ$ . The current dissipation of the differential LNA is  $17\ \text{mA}$  from a  $1.2\ \text{V}$  power supply.

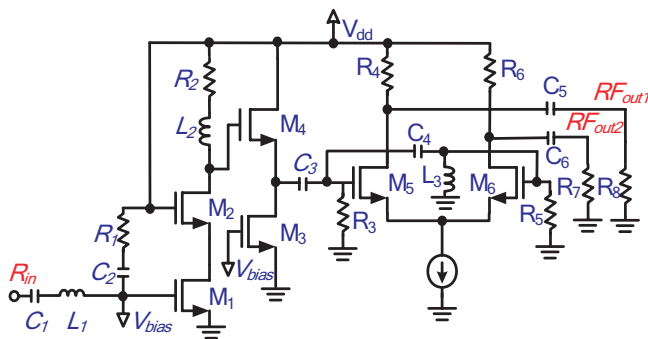


Figure 1: Proposed differential CMOS LNA.

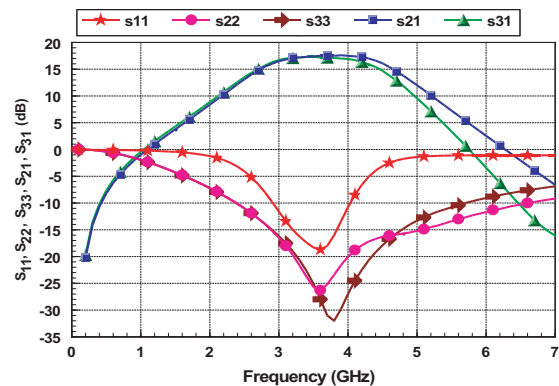


Figure 2: Simulation performance of differential CMOS LNA.

## REFERENCES

1. Bisla, B., R. Eline, and M. F. Luiz, "RF system and circuit challenges for WiMAX," *Intel Technology Journal*, Vol. 08, 189–200, Aug. 2004.
2. Lu, Y., K. S. Yeo, A. Cabuk, J. Ma, M. A. Do, and Z. Lu, "A novel CMOS low-noise amplifier design for 3.1–10.6 GHz ultra-wideband wireless receivers," *IEEE Circuits and Systems Society*, Vol. 53, Issue 8, 1683–1692, Aug. 2006.



# DDS Based Radar Signal Generator for Microwave Remote Sensing

C. Z. Gu<sup>1</sup>, S. Qiao<sup>3</sup>, J. T. Huangfu<sup>1,2</sup>, and L. X. Ran<sup>1,2</sup>

<sup>1</sup>Department of Information Science and Electronic Engineering  
Zhejiang University, Hangzhou 310027, China

<sup>2</sup>The Electromagnetics Academy at Zhejiang University  
Zhejiang University, Hangzhou 310027, China

<sup>3</sup>City College, Zhejiang University, Hangzhou 310015, China

**Abstract**— Microwave Remote Sensing (MRS) has become a targeted area of intensive research for its great application in diverse situations. We utilized the DDS technique to design a signal generator for the use in MRS. To overcome the disadvantages due to the inherent characteristics of DDS, we put forward two methods, a 3-order Butterworth filter and the pre-distortion technique. Real test results show that the in-band spectrum is greatly ameliorated.

Figure 1 shows the architecture of the DDS radar signal generator. To generate radar signals, waveform data are read out of the DataFlash to the high-speed SDRAM and DACs, with the phase-encoding address sequence generated by FPGA as the address for waveform memory. The DACs convert digital data to analog outputs, which are further filtered to remove undesirable frequency waveforms. The mixer modulates baseband signals to radio frequency (RF) output that is amplified to a required power level for the ultimate radar signal output.

The clutter noise comes from three aspects: the nonlinearities of logic circuit and devices, especially DACs, the Finite Word-length Effect of memories and DACs, and aliased harmonics predicted by sampling theory. The role of the filter is to remove unwanted signal frequency, or to decline the frequency component below a certain level. The filter should be a low-pass filter, with the 3 dB cut-off frequency 80 MHz and off band attenuation at 250 MHz no less than 20 dB. Figure 2 shows the RF output with and without the designed filtered inserted.

Figure 3 shows the spectrum before and after employing the pre-distortion method. The pre-distortion method is used to improve the flatness of in-band spectrum. The waveform generation process includes a signal sampling process. So, as long as the amplitude and phase compensation values are made, it is convenient to program and calculate the value after pre-distortion for each sample point. Following are the details of the process of the pre-distortion method: obtain spectrum data from the spectrum analyzer → use filtering algorithm to analyze the spectrum envelop → obtain the pre-distortion compensation coefficient for each sampling point → obtain waveform value for each sampling point according to the pre-distortion compensation coefficient → download waveform data. In order to achieve the desired in-band gain flatness, the above process may be repeated several times.

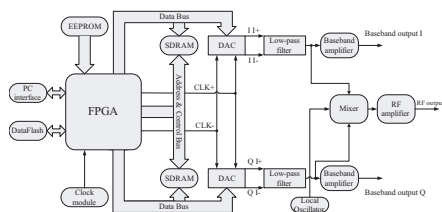


Figure 1

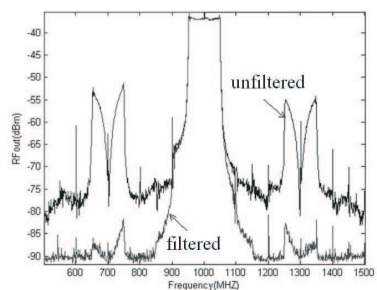


Figure 2

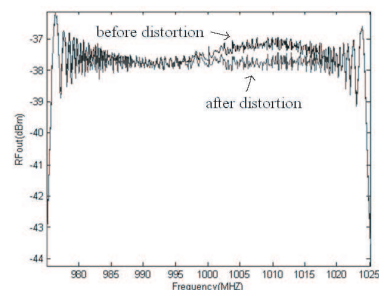


Figure 3

## Ambiguity Function of Chaotic Radar with Colpitts Oscillator

Tao Jiang<sup>1,2</sup>, Shan Qiao<sup>1,3</sup>, Zhi Guo Shi<sup>1</sup>, and Lixin Ran<sup>1,2</sup>

<sup>1</sup>Dept. of Information and Electronic Engineering, Zhejiang University, 310027, China

<sup>2</sup>Electromagnetics Academy at Zhejiang University, Zhejiang University, 310027, China

<sup>3</sup>Zhejiang University City college, Zhejiang University, 310027, China

**Abstract**— The ambiguity function of a kind of chaotic radar uses Colpitts oscillator is investigated and compared from different points of view. The Colpitts oscillator with specific value of capacitance and inductance can generate chaotic signal with frequency band from direct current to several gigahertz. The auto-ambiguity functions show that the chaotic signal of such oscillator is ideal for Radar application with both high range and range rate resolution. The cross-ambiguity functions also indicate the chaotic signal has excellent capabilities in the electronic counter- countermeasures (ECCM).

## A Broadband Low Noise Amplifier Design

Ying Wang, Yi Fu, Wan-Zhao Cui, and Wei Ma

National Key Laboratory of Space Microwave Technology  
Xi'an Institute of Space Radio Technology, Xi'an 710100, China

**Abstract**— Low noise amplifier (LNA), as the first stage of RF and microwave receivers, is a very important elements in communication systems. It is imperative to accelerate the production process of the space LNA by developing the broadband LNA with high reliability. At present, the space LNA is made up of the packaged MESFET or HEMT. Because of the parasitic effects in packaged MESFET or HEMT itself, it is difficult for electronic engineers to design the broadband LNA.

In this paper, a new design method for space LNA is proposed. Firstly, the resonance network is used as the LNA's input matching network. Secondly, by optimizing elements' values of the resonance network, the port impedance is matched to the optimal noise impedance of the low noise element in a broad frequency band based on simulations and the broadband noise matching is obtained. A C-band two stages broadband LNA is designed on the basis of our method. The circuit and EM simulation are shown by lumped elements and microstrip elements in Agilent ADS software, which proves the availability and practicality of our method. Compared with those LNA's designed by traditional ways using the same low noise element, the LNA's performance obtained here can be improved, and 30% bandwidth is achieved in noise factor.

## A 10~18 GHz Wide-band Transformer Feedback LNA

Pei-Yuan Chiang and Christina. F. Jou

Institute of Communication Engineering, National Chiao Tung University, Hsinchu, Taiwan

**Abstract**— A wide-band (10~18 GHz) low noise amplifier (LNA) is presented. With transformer feedback and parasitic capacitance ( $C_{gd}$ ,  $C_{gs}$ ) in the traditional common gate cascode amplifier, good input matching is achieved from 10 GHz to 18 GHz. Wide-band communication system (like UWB for 3.1 to 10 GHz; 57 to 64 GHz millimeter wave system) have received much attention due to high data rate and high speed communication. In such a wideband system, LNA is in the first stage after antenna in the front-end receiver block. To interface with the antenna and the preselect filter, LNA requires input match to  $50\ \Omega$  over the bandwidth. Meanwhile LNA must provide high gain and the most important, low noise.

There is no input-matching elements in the input gate of the input amplifier, so that the LNA can achieve lower NF. Due to the transformer feedback, signal current at drain will couple into source. The noise circle and input matching circle will more close over 10~18 GHz. Therefore the LNA can achieve low noise and good input matching.

The LNA is designed based on CMOS TSMC 0.18  $\mu\text{m}$  mixed signal/RF process. With 1.8 V supply voltage and three stage amplifiers to achieve wider gain bandwidth, the LNA can achieve input-matching of  $-12\ \text{dB}$  from 10 to 18 GHz; minimum NF 2.4 dB; gain ( $S_{21}$ ) of 17 dB and 1 dB gain compression (P1 dB) at  $-22.6\ \text{dB}$ . The noise figure is below 3.5 dB over 10–18 GHz. The power consumption is 37.6m W (exclude buffer).

# Region Feature Extraction Based on Improved Regularization Method in SAR Image

Feng Xu<sup>1</sup> and Chao Wang<sup>2</sup>

<sup>1</sup>National Disaster Reduction Center of China  
Beijing 100053, China

<sup>2</sup>China Remote Sensing Satellite Ground Station  
Chinese Academy of Sciences  
Beijing 100086, China

**Abstract**— The noise existed in Synthetic Aperture Radar (SAR) image weakens the detailed features of region of interest (ROI) such as target and shadow. It also leads to the serious performance reduction of subsequent target detection, classification and recognition. The conventional regularization method could enhance target features in SAR image; however, the high computation complexity limits the real-time application of it. An improved regularization method is introduced in this paper, which increases processing speed of region feature extraction for SAR image significantly. It is theoretically proved that, by optimizing SAR projection operator, computation complexity could be reduced from  $O(M^3N^3)$  to  $O(MN)$  without ability losing of the region-based feature enhancement. MSTAR SAR image data is employed for algorithm experiment. The result shows that our method can increase target-to-clutter ratio significantly while restraining the noise in ROI, and then extract target and shadow from background clutters in SAR image more accurately.

## Reducing the Time Steps of FDTD Predictions of High-Q Cavities

Juan Chen<sup>1</sup> and Jianguo Wang<sup>1,2</sup>

<sup>1</sup>School of Electronic and Information Engineering, Xi'an Jiaotong University, Xi'an 710049, China

<sup>2</sup>Northwest Institute of Nuclear Technology, P. O. Box 69-15, Xi'an 710024, China

**Abstract**— Finite-difference time-domain (FDTD) method is an effective tool for shielding effectiveness analysis. But due to the high Q of the cavity considered, the conventional second-order FDTD method requires a very large number of time steps for a pulse excitation to decay to a value that is sufficiently close to zero for accurate Fourier transformation of the time-domain fields into the frequency domain. This paper demonstrates the long FDTD time steps for generating accurate frequency domain parameters can be reduced by introducing an infinite ground plane at the bottom of the enclosure. The ground plane has no effect on the shielding effectiveness, but can improve the calculation efficiency. Compared with the method of introducing of an artificial loss into the solution space, this method has much higher accuracy, which is validated by numerical examples.

## Reduction of EMI and Mutual Coupling in Array Antennas by Using DGS and AMC Structures

A. Mahmoudian<sup>1</sup> and J. Rashed-Mohassel<sup>2</sup>

<sup>1</sup>Microwave Lab., Department of Electrical Engineering, Tarbiat Modares University, Tehran, Iran

<sup>2</sup>Center of Excellence on Applied Electromagnetic Systems, School of Electrical and Computer Engineering, University of Tehran, Iran

**Abstract**— Considering the difficulty of via construction in EBG structures and the cost of lossy materials and absorbers, in this paper, we look for implementing DGS and AMC to reduce mutual coupling in enclosures and array antennas particularly in CBS antennas. Circular ring defected ground structure and capacitive loaded AMC strips are designed and optimized to have electromagnetic band gaps and incident wave reflection features, respectively, in the resonant frequency band of cavity backed slot (CBS) antenna. The complete structure consists of CBS antenna with circular ring DGS and CLS-AMC. These structures are investigated and enhancement in EMI and the radiation patterns of this antenna is observed.

# The Phase Invariance Condition for the Ultra-wideband Voltage Controlled Attenuator

O. V. Stukach

Tomsk Polytechnic University, Russia

**Abstract**— In the multi-channel wideband systems of the microwave amplifiers, antenna arrays, the signal auto-phasing, power control, radar etc. in many cases the independence of the response phase shift concerning effect at controlling of source signal amplitude is required. A voltage controlled attenuator (VCA) is especially one of the most important devices. The function of the phase invariant attenuator is to change the amplitude in the processing of microwave signal with minimal impact to the phase characteristic.

Novelty of this paper consists of new necessary condition of minimum phase shift at the attenuation adjusting for the linear attenuator. It is possible a new design of phase invariant attenuator based on this condition.

Also the paper discloses details of the new VCA structure based on the cross-coupling circuits and discusses its performance. Its main difference from known consists in ultra wide band feature and large range of attenuation where minimum of the phase shift is provided. As a result, the output parameters and adjusting parameters of diodes are founded.

The possibility of ultra-wideband VCA development is defined by reactive parameters of controlled elements. Their values should be small and constant during adjusting. In this connection the improvement of attenuator is connected with improvement of controlled elements and their effective using. The most spreading elements are p-i-n diodes, which parasitic reactances provide the growing of attenuation with frequency increase, and consequently, to reduction of transfer factor. Therefore the phase shift cannot be reduced more than up to 2–5 degrees.

It is shown that for attenuator designing it is necessary to unit a crossed circuit with  $\pi$  or T-form structure of connection of controlled elements. Hereon it is necessary to calculate parameters of adjusting elements.

The base structure of the experimental VCA with one p-i-n diode in serial arm and two in parallel has been developed. Phase stability is provided by inductances, which combined with the diode's parasitic capacities and compensate for the phase shift variation when the attenuation is adjusted.

The maximum phase shift variation within the attenuation range up to 20 dB does not exceed  $2^\circ$  in a frequency band of 0.1–2 GHz. In another attenuation ranges the phase shift is more less. In the attenuator without correction the phase shift in same band reaches 500. Thereby, phase shift is reduced to the account of correction almost in 25 times. The maximum attenuation is 26 dB.

It is of interest that the adjusting inductance is very small. It once again proves that the circuit topology satisfying to the condition of phase invariance is more important, than parameters of adjusting circuits.

The p-i-n diode attenuator was fabricated on a polycore layout. Parameters of the matching circuits in the frequency band of 0.1, ..., 3 GHz and attenuation  $K(f) = 3, \dots, 35$  dB has been optimized. Minimum of phase shift for attenuation  $K_i(0) = 1, \dots, 26$  dB,  $i = 0, \dots, 5$  has been received. For the last  $K_5(0) = 26$  dB the phase error becomes essential. It is possible to reduce the phase shift only increasing the frequency band, but it is difficultly, or with use of diodes with smaller parasitic parameters. In this circuit, series-connected p-i-n diodes operate as attenuators, while a shunt-connected diode operates as a phase-shift compensation circuit.

The low phase shift attenuator is shown to overcome some disadvantages of the existing phase shift attenuator. In the paper it is shown what conditions must satisfy a transfer function.

Modern techniques demand a theory to developing a new generation of components at lower costs. The use of the correction circuits permits to achieve a more constant phase shift via regulation of the transfer factor by a sufficiently simple method.



# Facilitating EMI/EMC Modeling by Predicting Voltage Interference in an EMI/EMC Environment by Two Wires as the Pick-up Model of EM Waves

Atanu Roy<sup>1</sup>, Saswati Ghosh<sup>2</sup>, and Ajay Chakrabarty<sup>1</sup>

<sup>1</sup>Department of Electronics & Electrical Communication Engineering, IIT Kharagpur, India

<sup>2</sup>Kalpana Chawla Space Technology Cell, IIT Kharagpur, India

**Abstract**— EMI the silent threat or it may be silent killer is present everywhere, inside and outside of all electrical equipments. The successful detection and elimination of EMI require a systematic search for EMI sources as well as knowledge of interference susceptibilities of the equipment. Familiarity with the environment in which the equipment will work as well as possible alternative environments are fundamental to effective EMI reduction to a required minimum level. In this paper we designed a simple two wire model to predict EMI when this model is illuminated by a distant source antenna. The proposed model is being fabricated at Indian Institute of Technology, India. Measured and simulated results are shown. Simulations were being carried out at Kalpana Chawla Space Technology Cell, IIT Kharagpur, India.

The model that we fabricated is a simplified version of the more exact transmission line model, but it will be suitable for prediction purposes. We consider a parallel-wire transmission of length  $\ell$  that has a uniform plane wave incident on it. The wires are separated by a distance  $s$  and have load resistances  $R_S$  and  $R_L$ . In order to quantify our results, we will place the two wires in the  $xy$  plane, with  $R_S$  located at  $x = 0$  and  $R_L$  at  $x = \ell$ . The wires are parallel to the  $x$  axis. Our interest is in predicting the terminal voltages  $\hat{V}_S$  and  $\hat{V}_L$ . The induced voltage is being contributed by the incident EM field.

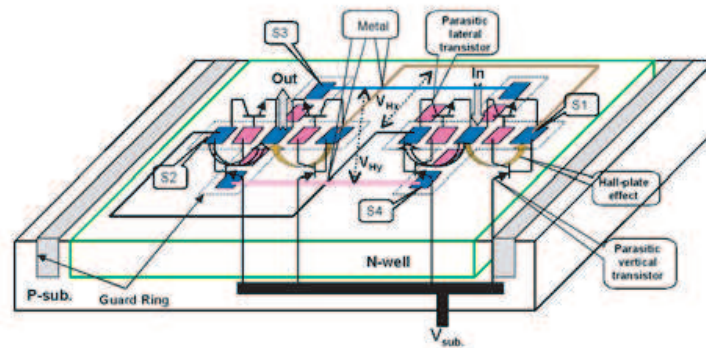
# Interaction between Magnetoresistor and Magnetotransistor in the Two-dimensional Folded Vertical Hall Devices

Guo-Ming Sung and Chih-Ping Yu

Department of Electrical Engineering, National Taipei University of Technology  
1, Sec. 3, Chung-Hsiao E. Rd., Taipei 106, Taiwan, R.O.C.

**Abstract**— This study presents a novel 2-D folded vertical Hall device, fabricated in a standard 0.35- $\mu\text{m}$  CMOS process. The maximum supply-current related sensitivity,  $S_{RI}$ , of 95% V/A·T is measured with a 20-mA bias current. By properly adjusting the supplied bias currents to the doped areas of  $p^+$ - and  $n^+$ - implants, the measured data shows that the dominant mechanism, evoked by the bulk parasitic magneto-transistor, is the hybrid effect of the Hall effect and the filament magneto-sensitivity effect. Furthermore, the maximum supply-voltage-related sensitivity of the bulk parasitic magnetotransistor is about 19 and 15 times better than that of Hall-plate magneto-resistor and vertical parasitic magneto-transistor, respectively. At the same time, the maximum induced Hall voltage is superior to those of the Hall-plate magneto-resistor and vertical parasitic magneto-transistor by 44 and 3 times, respectively. Note that the largest supply-current-related sensitivity is 62.34% (V/AT).

**Two-dimensional Folded Vertical Hall Device:** If the magnetic field is applied in the  $x$ -direction, the induced Hall voltages  $V_{Hx}$  and  $V_{Hy}$  are detected in the  $x$ -direction and  $y$ -direction, respectively. After the measured process is completed, the same procedure will be processed once again as the magnetic field is put on the  $y$ -direction. The additional  $P^+$ -implant contacts are used to establish the vertical parasitic magnetotransistor and the bulk magnetotransistor and to enhance the magnetosensitivity of the Hall-plate by changing the trajectories of majority carriers.



**Experimental Setup:** There are three cases, Hall-plate magnetoresistor, vertical parasitic magnetotransistor and bulk parasitic magnetotransistor, are considered within the proposed 2-D magnetic sensor. Case 1 is that all of the  $p^+$ - implants and the p-substrate are connected with the negative voltage to turn the vertical parasitic magnetotransistors off. In case 2, all of the  $p^+$ -implant contacts are connected to the positive voltage, but the  $n^+$ -implant contacts are supplied with the negative voltage. This means that all of the vertical parasitic magnetotransistors are in saturation, and all of the Hall-plate magnetoresistors are off. The main effect is the magnetic effect of the vertical parasitic magnetotransistor. Next, case 3 is designed to understand the magnetic effect of the bulk parasitic magnetotransistor by connecting all of the  $p^+$ - implant and  $n^+$ - implant contacts with a negative voltage. This leads to turn off the magnetic functions of the Hall-plate magnetoresistor and the vertical parasitic magnetotransistor. Therefore, the bulk parasitic magnetotransistors dominate the effect.

**Conclusions:** The results show that the folding design is effectively improve the linearity of the proposed magnetic sensor. And that, the magnetosensitivity of the bulk parasitic magnetotransistor is better than that of the Hall-plate magnetoresistor and that of the vertical parasitic

magnetotransistor. In other words, the bulk parasitic magnetotransistor dominates the magnetic effect in the proposed 2-D folding magnetic device. The mechanism can be described as follows: when the magnetic field is applied in the  $y$ -direction, the majority carriers of the Hall-plate magnetoresistor and the vertical parasitic magnetotransistor will distract the base currents on the base region of the bulk parasitic magneto-transistors to increase the induced Hall voltages. In the meanwhile, the emitter current filaments, which are deflected by the Lorentz force, have the same effect.

# Multifunctional Piezomagnetic Ferrite Materials and Their Newly Acoustical and Vibration Control Devices

Quanlu Li<sup>1</sup>, Yuan Li<sup>2</sup>, and Zhaohui Huang<sup>2</sup>

<sup>1</sup>Institute of Applied Acoustics, School of Physics and Information Technology  
Shaanxi Normal University, Xi'an 710062, China

<sup>2</sup>Department of Prevention Medicine, Fourth Military Medical University  
#17, Changlexi Street, Xi'an 710033, China

**Abstract**— The design, preparation etc of newly multipurpose ferrites (i.e., a magnetoelectric ceramic materials)  $\text{Ba}_{6-x}\text{R}_{2x}(\text{Nb}_{1-x}\text{Fe}_{2+x})\text{O}_3$ , etc, which it exhibiting the piezoelectricity and the piezomagnetic effect, then, preparation and selection of magnetorheological fluids (MRF) have been studied, respectively. The functional integrated devices which is a newly acoustical and vibration control devices combining multipurpose ferrites  $\text{Ba}_{6-x}\text{R}_{2x}(\text{Nb}_{1-x}\text{Fe}_{2+x})\text{O}_3$ , etc and magnetorheological fluids, and their applications have been investigated, and, emphasis was given to the applications in acoustics and vibration control, etc, as may be noted.

# Development of Smart Antenna Array Signal Processing Algorithm for Anti-Jam GPS Receiver

Anindya Kundu<sup>1</sup> and Soham Ghosh<sup>2</sup>

<sup>1</sup>Kalpana Chawla Space Technology Cell (KCSTC)

Department of Electronics and Electrical Communication Engineering  
Indian Institute of Technology, Kharagpur 721 302, West Bengal, India

<sup>2</sup>Department of Electronics Communication Engineering (ECE)  
Netaji Subhash Engineering College, Kolkata 700152, West Bengal, India

**Abstract**— GPS guidance uses low power signals from satellites which are 11000 NMI away. The satellite transmitter power is modest nearly 10 W orders of magnitude. Neither satellite nor receivers have the luxury of very high antenna gain since both entities have significant field of view requirements. These factors result in a very low power density incident on a GPS receiver antenna. The signal received is generally 165 dB down than the thermal noise level. Such signals are notoriously easy to jam either by intentional noise sources (Jammer) or unintentionally from harmonics of broadcasting stations or other out of band sources.

Here in this paper we will show how a nulling antenna or controlled reception pattern antenna with adaptive spatial filtering technique efficiently mitigate the intentional and non intentional interferences. A beamforming antenna array is a set of antennas whose outputs are weighted by complex values and combined to form the array output. The effect of the complex valued weights is to steer main lobes of the array pattern to desired directions. These directions may be unknown and so the antenna weights must be adjusted adaptively until some measure of array performance is improved, indicating proper lobe or null placement. An adaptive algorithm to adjust the complex weights of an antenna array is presented that nulls high power signals while allowing reception of GPS signals as long as the signals arrive from different directions.

The GPS signals are spread spectrum modulated and have very low average power, on the order of background thermal noise. Simulations of the adaptive algorithm minimize the output power of the array to within 5 dB of the background noise level. The technique which will be adopted to optimize the weight values is steepest descent algorithm and implements an efficient, exact gradient calculation. With M antennas in the array, only M-1 weights are adjustable. It appears that M-1 adjustable antenna weights can null M-1 unwanted signals (jammers). However, in the course of the algorithm development, a few configurations of antennas and jammer arrival directions were found where this is not true. Even when the jammer arrival directions are known, certain configurations are mathematically impossible to cancel out the intentional interferences.

The basic requirements of an adaptive Nulling antenna array are that it should provide enough gain margin to the user (or users) to satisfy the link calculations and at the same time suppressing the interfering signals. To achieve this, the elements of the antenna should have enough gain individually and should be physically configured in such a way as to be able simultaneously to point pattern nulls in the direction of interfering sources. The algorithm is the most crucial in steering the main beam in the direction of the SOI (signal of interest). Incoming signal to the array are of three types 1. GPS Signal 2. Jammer signal 3. Noise The GPS signal and Noise are considered to have low power of the order of background noise level, while Jammers have assumed to have much higher power level. The strategy behind this adaptive nulling aiming on reducing the array output Jammer power to a level comparable to the output GPS signal power, so that the later can be detected with spread spectrum technology. So we can conclude that this onboard Adaptive antenna processing efficiently mitigate the intentional interference from jammers and keep military GPS receiver accurate.

## Time Domain Studies of Ultra Wideband Dielectric Loaded Monopole Trans-receive Antenna System

Atanu Roy<sup>1</sup>, Saswati Ghosh<sup>2</sup>, and Ajay Chakrabarty<sup>1</sup>

<sup>1</sup>Department of Electronics and Electrical Communication Engineering, IIT Kharagpur, India

<sup>2</sup>Kalpna Chawla Space Technology Cell, IIT Kharagpur, India

**Abstract**— This paper presents the time domain studies of a wideband trans-receive antenna system consisting of a quarter-wave monopole loaded with an annular dielectric resonator antenna. This antenna has recently become attractive to antenna designers due to its broadband characteristics. However, while using this antenna in ultra wideband trans-receive system, the time domain characterization of the whole system is required and investigation on this has not yet been performed by other researchers. In this paper, the transmit antenna is excited by a wideband signal. The time domain waveform of the received voltage developed at the load end of the receive antenna is presented both for far field and near field position of the receive antenna. The results are simulated using CST Microwave Studio, version 5.

The monopole loaded with dielectric resonator antenna (DRA) has found important application as broadband antenna. A very interesting work on the guidelines for the design of this antenna was presented in recent literature. The broadband characteristics of the hybrid antenna both in transmit and receive mode as EMI sensor in frequency domain had already been studied. There has been considerable interest on the studies of different loaded and dielectric resonator antennas for their wideband characteristics. However, the authors have not noticed any appreciable work on the time domain analysis of this antenna in a wideband trans-receive antenna system including the mutual coupling between the antenna elements and concentrated on this. In this paper, the time domain studies of the trans-receive antenna system including the medium is presented for far field and also considering the near field coupling between the antennas.

## Study and Improvement in Operational Characteristics of Mid Air Collision Aversion System (TCAS)

Vikrant Kumar Sharma

Department of Electronics and Communications  
Jaypee Institute Of Information Technology (JIIT)  
Noida, Uttar-Pradesh-124001, India

**Abstract**— The drawbacks in the current system of TCAS are studied in this paper along with the changing needs because of rising air traffic. Improving the maneuvering capability by making a new algorithm for calculating the path, and also by establishing an exclusive communication link enhanced threat handling. It was found that the horizontal steering in a threat situation has to be implied by studying the air traffic in the vicinity. Steering vertically can create a problem when a/c are present above and below. All paths are calculated by taking the distance and climb or decent rate of the individual a/c around the main a/c, which would be necessary to avoid collision with them. This procedure is followed at the other confronting a/c too. The best path which is taken ensures aversion of collision between them and nullifies the possibility of a threat situation with another a/c because of it. These findings were found to be helpful in situations where density of air traffic is high and with them a better probability of collision avoidance is achieved as compared to the present system. It doesn't involve changing the full equipments such as the transponder and the antennae, but some modifications in the processor based on the new algorithm.

## Design of Three-layer Circular Mushroom-like EBG Structures

S. Mahdi Moghadasi<sup>1,2</sup>, A. R. Attari<sup>1</sup>, and M. M. Mirsalehi<sup>1</sup>

<sup>1</sup>Electrical Engineering Department, Ferdowsi University of Mashhad, Mashhad, Iran

<sup>2</sup>Communications and Computer Research Center, Ferdowsi University of Mashhad, Mashhad, Iran

**Abstract**— In this paper two types of three-layer mushroom-like electromagnetic band-gap (EBG) surfaces with circular patches are investigated. One of them consists of a square array of circular patches and the other one consists of a triangular array of circular patches in upper and lower layers. Using reflection phase characteristics, guidelines for designing a ground plane for low profile antenna applications are presented. The effect of radius of patches in each layer, gap size, dielectric constant and thickness of each layer on reflection phase characteristic is studied. The frequency band inside of which a wire antenna adjacent to the three-layer EBG surface has good matching is achieved by means of the reflection phase characteristics of the EBG ground plane.

**Summary:** In recent years, unique properties of electromagnetic band-gap (EBG) structures have made them applicable in many antenna and microwave applications. Two main interesting features associated with EBG structures are suppression of surface waves and in-phase reflection coefficient for plane waves [1–3]. Suppression of surface waves results in higher efficiency, smoother radiation pattern, and less back lobe and side lobe levels in antenna applications [1, 2]. On the other hand, these structures can be used in design of low profile antennas because the radiating current can lie directly adjacent to the ground plane without being shorted [1, 3].

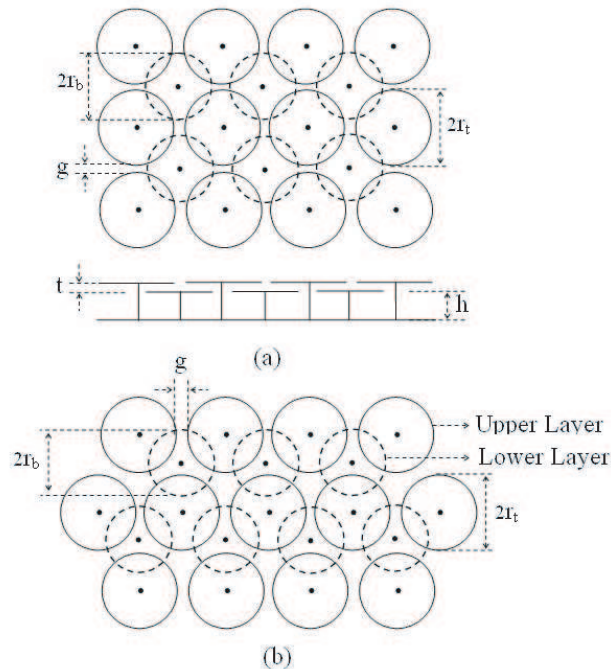


Figure 1: Three-layer mushroom like EBG surface with circular patches (a) Square array, (b) Triangular array.

The main reason for designing three-layer EBG surfaces is that lower zero reflection phase frequency can be achieved comparing to two-layer structures. This property can be shown by the reflection phase of the structure when a normal incident plane wave is illuminated to the surface. The relation between the reflection phase characteristic of an EBG surface and the input-match frequency band of a wire antenna using the surface as a ground plane is investigated in [3]. It is shown that the frequency region where the EBG surface has a reflection phase between  $45^\circ$  and  $135^\circ$  is very close to the input-match frequency band of the low profile wire antenna using the surface as a ground plane. Therefore, one can use the reflection phase curve to identify the input-match frequency band of the antenna.



Reflection phase of a periodic surface can be computed using one unit cell of the structure with periodic boundary condition as described in [4].

In this paper we investigate the effect of both structures parameters on the reflection phase characteristic. By means of these curves, design guidelines for a three-layer circular mushroom-like EBG ground plane are obtained.

#### REFERENCES

1. Engheta, N. R. and W. Ziolkowski, "Metamaterials physics and engineering explorations," Wiley, New York, 2006.
2. Sievenpiper, D., L. Zhang, R. F. J. Broas, N. G. Alexopolus, and E. Yablonovitch, "High-impedance electromagnetic surfaces with a forbidden frequency band," *IEEE Trans. Microwave Theory Tech.*, Vol. 47, 2059–2074, Nov. 1999.
3. Yang, F. and Y. Rahmat-Samii, "Reflection phase characterizations of the EBG ground plane for low profile wire antenna applications," *IEEE Trans. Antennas Propag.*, Vol. 51, 2691–2703, Oct. 2003.
4. Remski, R., "Analysis of PBG surfaces using Ansoft HFSS," *Microwave J.*, Vol. 43, No. 9, 190–198, Sept. 2000.

# Circular Polarized Rhombic Loop Antenna over a Mushroom-like EBG Surface

S. Mahdi Moghadasi<sup>1,2</sup>

<sup>1</sup>Electrical Engineering Department, Ferdowsi University of Mashhad, Mashhad, Iran

<sup>2</sup>Communications and Computer Research Center, Ferdowsi University of Mashhad, Mashhad, Iran

**Abstract**— In this paper, a low profile rhombic loop antenna is investigated over an EBG surface. A low frequency mushroomlike EBG surface is used as the antenna ground plane. To achieve a low frequency design, it is proposed to use a suspended EBG structure. Center frequency of this structure can be easily decreased by increasing the suspended surface height. In comparison with a PEC ground plane, design of antenna above a suspended EBG ground plane results in significantly reduction of the structure thickness. The investigated antenna is circularly polarized. It is shown that the axial ratio bandwidth ( $< 3$  dB) and return loss bandwidth ( $< 10$  dB) of the rhombic loop antenna above the designed EBG surface are 15% and 12%, respectively.

**Summary:** Electromagnetic band gap (EBG) structures have been studied widely in recent years due to their novel electromagnetic features [1, 2]. These structures are implemented by periodic dielectric and various metallization patterns. There are a wide range of applications associated with EBG structures for two main properties. First they can suppress surface waves' propagation along the structure. Eliminating surface waves by means of EBG structures can enhance the radiation efficiency of different kinds of antennas such as microstrip antennas. The second remarkable property of EBG structures is their reflection phase characteristics which vary continuously from  $180^\circ$  to  $-180^\circ$  in a frequency band [3]. This feature can be seen in mushroom-like EBG surfaces which consist of metallic protrusions arranged in two-dimensional lattice. In a frequency band that the reflected phase is around zero the structure behave as a perfect magnetic conductor. Therefore, these surfaces are also called artificial magnetic conductors. Because of the in-phase reflection property of the surface, a radiating current can be laid directly adjacent to the surface and so it is possible to use this surface as a ground plane in the design of low profile antennas [1, 2].

There has been a wide interest in the design of low profile antennas with circular polarization using a mushroom-like EBG surface. A monopole curl antenna [4] and a square spiral antenna above a mushroom-like EBG surface [5] have been studied for circular polarization. A single loop wire antenna with rhombic configuration has been first proposed in [6]. This antenna has circular polarization due to an air gap at an appropriate position on the loop. It is illustrated that this antenna has wide bandwidth for axial ratio (AR) and return loss.

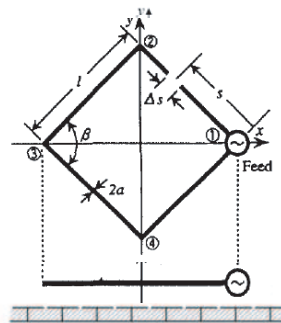


Figure 1: Rhombic loop antenna located above a mushroom-like EBG ground plane.

In this paper, we investigate a rhombic loop antenna over an EBG surface. By using an EBG ground plane it is possible to design a low profile structure. Fig. 1 illustrates a rhombic loop antenna located above a mushroom-like EBG surface. To achieve a low frequency design, it is proposed to use a suspended EBG structure. We first design a wideband low frequency suspended mushroom-like EBG surface. Then performance of a rhombic loop antenna placed at a distance of  $\lambda/20$  above the designed EBG surface is investigated.

**REFERENCES**

1. Engheta, N. and R. W. Ziolkowski, *Metamaterials Physics and Engineering Explorations*, Wiley, New York, 2006.
2. Sievenpiper, D., L. Zhang, R. F. J. Broas, N. G. Alexopolus, and E. Yablonovitch, "High-impedance electromagnetic surfaces with a forbidden frequency band," *IEEE Trans. Microwave Theory Tech.*, Vol. 47, 2059–2074, Nov. 1999.
3. Yang, F. and Y. Rahmat-Samii, "Reflection phase characterizations of the EBG ground plane for low profile wire antenna applications," *IEEE Trans. Antennas Propag.*, Vol. 51, 2691–2703, Oct. 2003.
4. Yang, F. and Y. Rahmat-Samii, "A low profile circularly polarized curl antenna over electromagnetic band-gap (EBG) surface," *Microwave Opt. Technol. Lett.*, Vol. 31, No. 3, 165–168, 2001.
5. Nakano, H., K. Tatsuzawa, D. Togashi, H. Mimaki, and J. Yamauchi, "Effects on the radiation characteristics of using a corrugated reflector with a helical antenna and an electromagnetic band-gap reflector with a spiral antenna," *IEEE Trans. Antennas Propag.*, Vol. 53, 191–199, Jan. 2005.
6. Morishita, H. and K. Hirasawa, "Wideband circularly polarized loop antenna," *Proc. IEEE AP-S Int. Symp.*, 1286–1289, 1994.

# Bandwidth Enhancement of Single-feed Circularly Polarized Equilateral Triangular Microstrip Antenna

Sara Sadat Karimabadi<sup>1</sup>, Yalda Mohsenzadeh<sup>1</sup>  
Amir Reza Attari<sup>1</sup>, and S. Mahdi Moghadasi<sup>1,2</sup>

<sup>1</sup>Electrical Engineering Department, Ferdowsi University of Mashhad, Iran

<sup>2</sup>Communications and Computer Research Center, Ferdowsi University of Mashhad, Iran

**Abstract**— Design of dual-band and multi-band antennas has gained increasing demands in modern wireless communication systems in which the backward compatibility and the roaming capability among multistandards are required. For instance, the antenna is preferably designed in 2.4–2.5 and 5–6 GHz bands to meet the standards of IEEE 802.11a=b=g in WLAN systems.

In recent years, unique properties of electromagnetic band-gap (EBG) structures have made them applicable in many antenna and microwave applications. Two main interesting features associated with EBG structures are suppression of surface waves and in-phase reflection coefficient for plane waves [1–3]. Suppression of surface waves results in higher efficiency, smoother radiation pattern, and less back lobe and side lobe levels in antenna applications [1, 2]. On the other hand, these structures can be used in design of low profile antennas because the radiating current can lie directly adjacent to the ground plane without being shorted [1, 3].

This paper presents a compact dual-band slot antenna which is designed over a dual-band mushroom-like EBG surface. By using the EBG ground plane, unidirectional radiation and gain enhancement are achieved. The antenna is printed on a single-layer PCB and fed by a coplanar waveguide (CPW). The slots on the upper layer of the mushroom-like structure cause the dual band reflection phase characteristics of the structure. By sweeping length of the slots, it is possible to change the two zero-reflection phase of the structure.

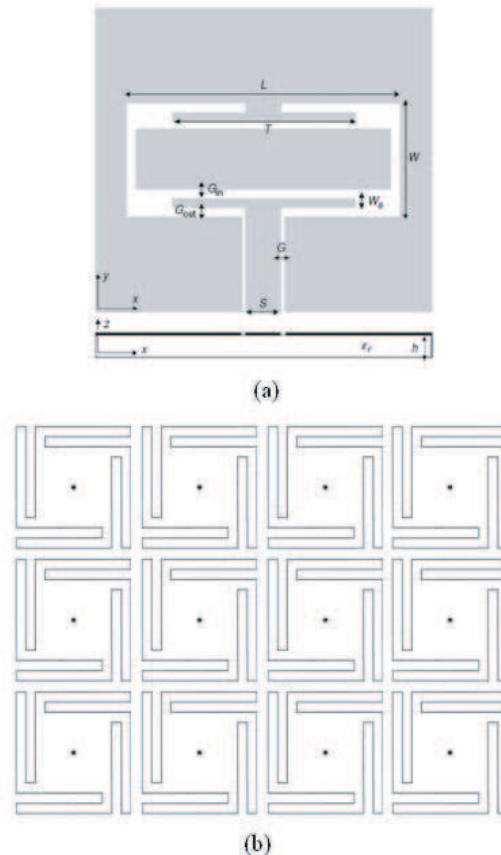


Figure 1: (a) the dual-band CPW-fed slot antenna, (b) slotted patches mushroom-like EBG ground plane.

**REFERENCES**

1. Engheta, N. and R. W. Ziolkowski, *Metamaterials Physics and Engineering Explorations*, Wiley, New York, 2006.
2. Sievenpiper, D., L. Zhang, R. F. J. Broas, N. G. Alexopolus, and E. Yablonovitch, "High-impedance electromagnetic surfaces with a forbidden frequency band," *IEEE Trans. Microwave Theory Tech.*, Vol. 47, 2059–2074, Nov. 1999.
3. Yang, F. and Y. Rahmat-Samii, "Reflection phase characterizations of the EBG ground plane for low profile wire antenna applications," *IEEE Trans. Antennas Propag.*, Vol. 51, 2691–2703, Oct. 2003.
4. Remski, R., "Analysis of PBG surfaces using Ansoft HFSS," *Microwave J.*, Vol. 43, No. 9, 190–198, Sept. 2000.

## Design of Ultra-wideband Monopole Antenna with Band-notched and GPS Circular Polarization Characteristics

Han-Nien Lin<sup>1</sup>, Che-Min Shao<sup>1</sup>, and Jer-Long Chen<sup>2</sup>

<sup>1</sup>Department of Communications Engineering, Feng-Chia University, Taiwan, R. O. C.

<sup>2</sup>Department of Electrical Engineering, National Taiwan Ocean University, Taiwan, R. O. C.

**Abstract**— In this paper, a printed disk monopole antenna with coplanar waveguide (CPW) feeder for ultra-wideband (UWB) and global positioning system (GPS) application is proposed. Because the frequency band between 3.1 to 10.6 GHz assigned for UWB system by FCC will cause interference to the existing wireless communication systems, for example the wireless local area network (WLAN) for IEEE 802.11a operating in 5.15–5.35 GHz and 5.725–5.825 GHz bands, therefore the UWB antenna with a band-notched is required. The antenna is structured with the conventional radiating disk element that would have benefit on manufacturing process and cost effective. In addition, it implements annular stub to reduced current distributions of right-hand side radiating element to achieve circular polarization (CP) for GPS application at 1.575 GHz. The characteristics of axial ratio (AR) can be optimized by tuning the length of stub and the distance between the stub and radiating element. The optimal AR will be achieved at 1.575 GHz, meanwhile  $AR < 3$  can be achieved for the frequency range from 1.558 to 1.595 GHz. By modifying the edges of the ground, the antenna is observed to provide an enhanced impedance bandwidth. The band-stop characteristic is realized by cutting a U shaped slot on the radiating disk. The frequency of stop-band can be adjusted by changing the length and width of the inserted slot. The impedance bandwidth of the proposed antenna can range from 3 GHz to 11 GHz for  $VSWR < 2$  with the band rejection characteristic in the frequency band of 5 GHz to 6 GHz. Since the antenna presents a notched band from 5 to 6 GHz, it can prevent the RF interference from the wireless local area network (WLAN) 802.11a. This proposed antenna shows a monopole-like radiation pattern and good agreement has been obtained between the simulation and experiment results.

## Small Antenna Measurement Facilities

Guan-Yu Chen<sup>1</sup>, Jwo-Shiun Sun<sup>1</sup>, Cheng-Hung Lin<sup>2</sup>, Kwong-Kau Tiong<sup>2</sup>, and Y. D. Chen<sup>3</sup>

<sup>1</sup>Department of Electronic Engineering, National Taipei University of Technology, Taiwan

<sup>2</sup>Department of Electrical Engineering, National Taiwan Ocean University, Taiwan

<sup>3</sup>Antenna and EMC Laboratory, High Tech Computer Corp. (HTC), Taiwan

**Abstract**— The mobile phone under test of far-field range testing has been the plan (Fig. 1) at the Cellular Telecommunications & Internet Association (CTIA) certification program test requirements for performing radiated power and receiver performance measurement. In this papers [1–4], facilities of mobile phone measurement have recently commissioned a spherical far-field measurement system (Fig. 2). The low profile far-field spherical scan system provides significant advantages over the older far-field testing including elimination of problem of simple theta ( $\theta$ ) and phi ( $\phi$ ) rotary axis with indoor far-field range testing, complete measurement characterization of the antenna, and improved accuracy. This paper will discuss the antenna and wireless system integration tested with the TRP/TIS and spherical antenna measurement for far-field system, and the results being achieved.

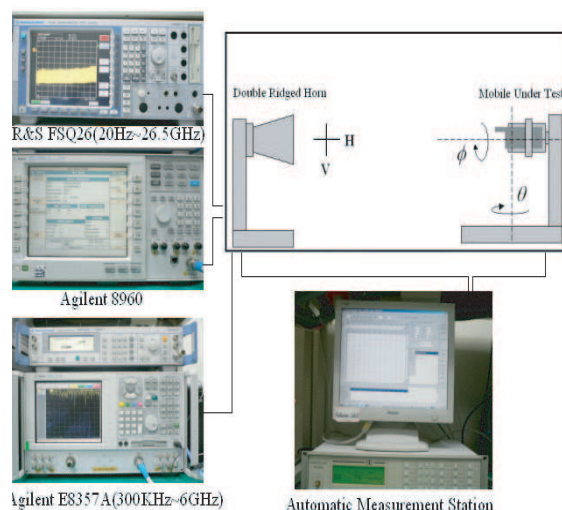


Figure 1: The proposed 3D measurement system and wireless system networking.

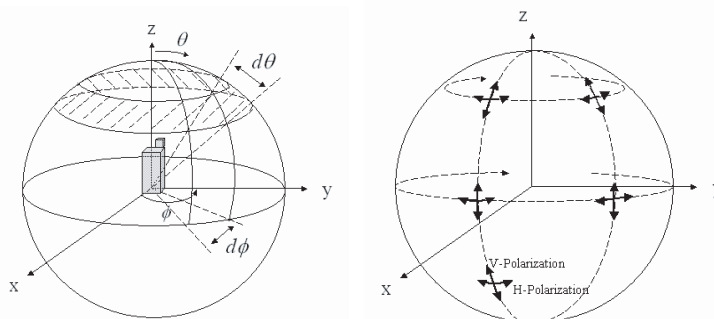


Figure 2: Spherical coordinates and field scanning.

### REFERENCES

1. Chen, G. Y., J. S. Sun, and Y. D. Chen, "The 3D far-field antenna measurement technology for radiation efficiency, mean effective gain and diversity antenna operation," *2006 The 7th International Symposium on Antennas, Propagation, and EM Theory (2006 ISAPE)*, 42–45, Guilin, China, Oct. 2006.

2. Chen, G. Y., J. S. Sun, S. Y. Huang, Y. D. Chen, C. H. Lin, and J. Y. Yang, "Flexible monopole antenna for mobile phone co-design and 3d far-field antenna scanning technique apply to total radiation efficiency and mean effective gain measurement," *2006 China-Japan Joint Microwave Conference (2006 CJMW)*, 89–92, Chengdu, China, Aug. 2006 (ISBN 7-900668-43-8).
3. Chen, G. Y., J. S. Sun, S. Y. Huang, Y. D. Chen, C. H. Lin, and J. Y. Yang, "Manufacture, design, measurement and FPC antennas integration for PDA phone," *2006 China-Japan Joint Microwave Conference (2006 CJMW)*, 416–419, Chengdu, China, Aug. 2006 (ISBN 7-900668-43-8).
4. Chen, G. Y., J. S. Sun, S. Y. Huang, Y. D. Chen, C. H. Lin, and J. Y. Yang, "Mobile handset measurement for wireless system networking," *2006 China-Japan Joint Microwave Conference (2006 CJMW)*, 698–701, Chengdu, China, Aug. 2006 (ISBN 7-900668-43-8).



# Microstrip Antenna Design for Ultra Wideband Application by Using Two Slots

N. Ghassemi<sup>1</sup>, J. Rashed-Mohassel<sup>2</sup>, and M. H. Neshati<sup>1</sup>

<sup>1</sup>Electrical Engineering Department, Sistan and Baluchistan University, Zahedan, Iran

<sup>2</sup>Center of Excellence on Applied Electromagnetic Systems, University of Tehran, Tehran, Iran

**Abstract**— In recent year applications of Broadband Microstrip antennas have been proposed for radar systems in the frequency range of 10–18 GHz [1, 2] due to their simplicity and ease of fabrication. In this paper, a new antenna of this type for broadband application is presented. In this structure as is shown in Fig. 1, a multiresonator microstrip antenna using a rectangular patch located on top of two slots, with different lengths and excited by a non symmetric U-shaped feed line is discussed. The patch and slots are separated by a substrate with low dielectric constant and an air gap. The structure has three resonant frequencies. The distance between the slots ( $S_1$ ), their positions ( $L_5$  and  $L_6$ ) and their lengths ( $L_7$  and  $L_8$ ) have an important effect on the resonant frequencies and the impedance bandwidth of the antenna. By changing these parameters one can set the resonant frequencies with respect to each other to increase the impedance and gain bandwidth of the antenna. The results show that the bandwidth of the antenna increases by using two slots. Fig. 2 shows an antenna in which with  $VSWR < 2$  from 9.8 GHz to 22 GHz and 6.1 GHz (42%) gain bandwidth (above 7 dB) is obtained. The simulated gain of the antenna is over 5 dB from 9.8 GHz to 19 GHz, with a maximum gain of 9.16 dB at the frequency of 14 GHz.

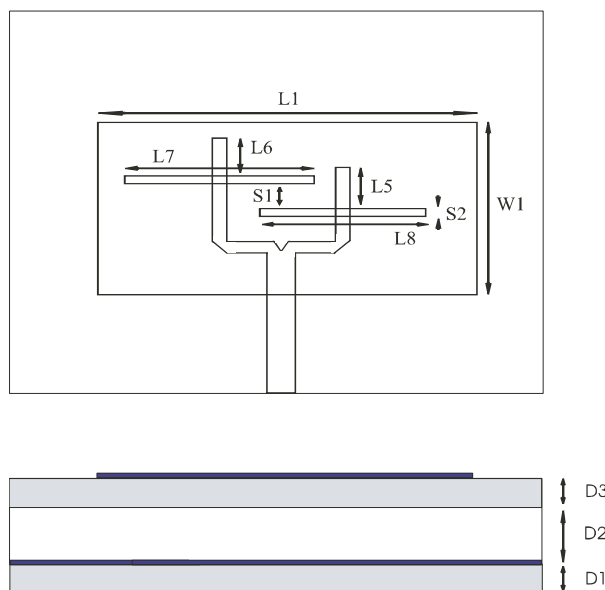


Figure 1: Antenna structure: (a) Top view of the antenna with two slots, (b) Side view of the antenna.

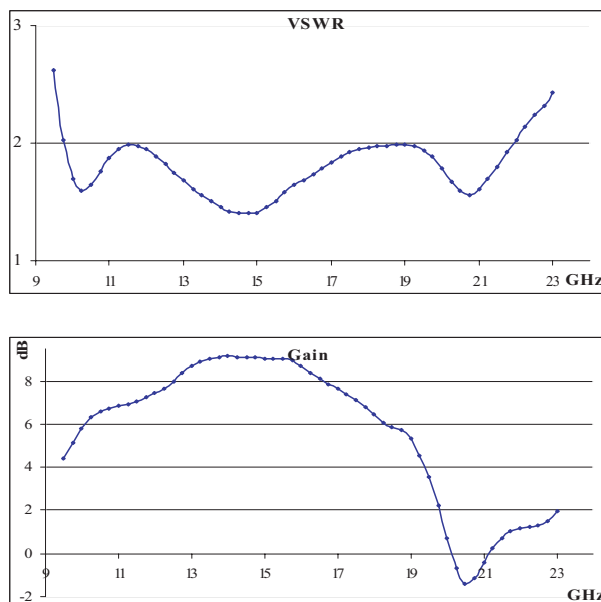


Figure 2: (a) VSWR, (b) Gain of the antenna with two slots.

## REFERENCES

1. Chai, W. W., X. J. Zhang, and J. B. Liu, "A novel wideband antenna design using U-slot," *Progress In Electromagnetics Research Symposium 2007*, 1292–1295, Beijing, China, March 26-30, 2007.
2. Ghassemi, N., M. H. Neshati, and J. Rashed-Mohassel, "Investigation of multilayer probe-fed microstrip antenna for ultra wideband operation," *Asia Pacific Microwave Conference 2007*, Bangkok, Thailand, December 11-14, Accepted for oral presentation.

## The GPS Antenna Design and Measurement

Kuo-Liang Wu<sup>1</sup>, Guan-Yu Chen<sup>1</sup>, Jwo-Shiun Sun<sup>1</sup>, Cheng-Hung Lin<sup>2</sup>  
Kwong-Kau Tiong<sup>2</sup>, and Y. D. Chen<sup>3</sup>

<sup>1</sup>Department of Electronic Engineering, National Taipei University of Technology, Taiwan

<sup>2</sup>Department of Electrical Engineering, National Taiwan Ocean University, Taiwan

<sup>3</sup>Antenna and EMC Laboratory, High Tech Computer Corp. (HTC), Taiwan

**Abstract**— This paper accomplished a GPS band for meander inverted-F monopole antenna structure and easy applied mobile cellular phone application. The measured and simulated data including return loss, antenna gain and radiation patterns are presented.

**Introduction:** The general GPS functions of PDA support the assisted functionality in 2.5/3 G wireless networks. Traditional antennas such as monopoles, dipoles and patches are not suitable to meet the requirements of modern wireless communication and highly demanding mobile GPS systems. As a result, there is the need for alternative approaches to small antenna and high performance design. This paper describes a miniaturized meander shorting monopole for integration in modern GPS wireless systems.

**Design and Results:** The resonance mode of a shorting meander wire antenna (Fig. 1 and Fig. 2) covers the GPS communication bandwidth of 1571.42–1579.42 MHz. The simple wire tuning expansion are introduced to confine the resonance mode region and to facilitate the frequency modes and impedance match expansion easily for antenna and wireless system integration design. The design requirements for GPS antenna is combined into multiple objective goals, such as simplicity of the antenna geometry, radiation pattern, return loss, antenna impedance and polarizations. This design in general to a mobile communication apparatus and global positioning system antenna, and more particularly to a mobile communication system, which utilizes a small-scale metal for the GPS antenna design. In this paper, the experiment setup has done [1, 2]. The phase of the two field components is measured relative to the signal generator, and a double ridge horn serves as a source antenna. Equations (1) and (2) may be expanded to give simple expressions that can be inserted into data logging software to provide a direct conversion from dual linear to RHCP and LHCP at each measurement angle.

$$E_{RHCP} = \frac{1}{\sqrt{2}}(E_H + jE_V) \quad (1)$$

$$E_{LHCP} = \frac{1}{\sqrt{2}}(E_H - jE_V) \quad (2)$$

This antenna also offers a characteristic of high radiation efficiency. Antenna bandwidth of 3.8% (1.53 to 1.59 GHz) was experimentally obtained for a return loss  $-10$  dB. In well known antenna design techniques a matching structure is typically employed to provide matching between the antenna and the GPS circuitry for efficient transfer of energy.

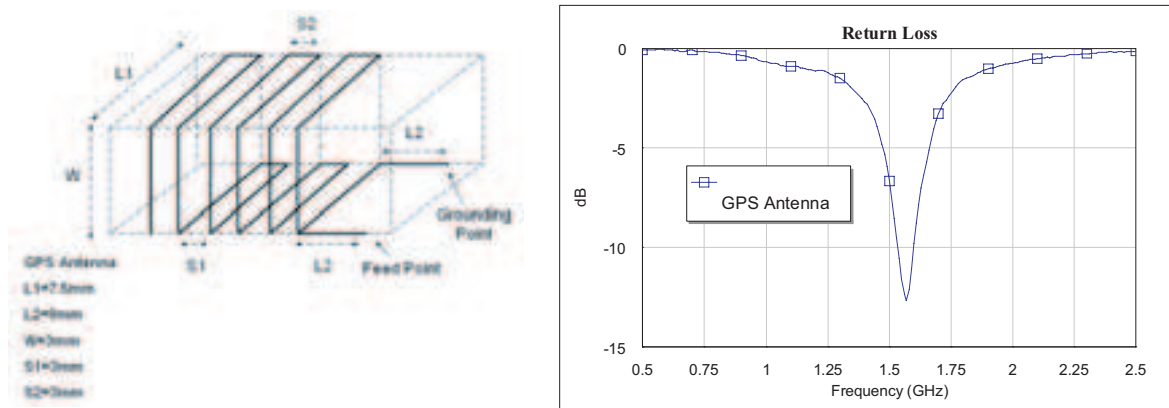


Figure 1: Meander wire antenna design for GPS band and structure layout and measured data.

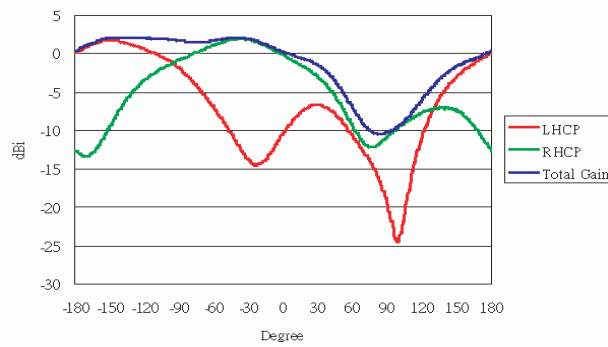


Figure 2: The measured pattern of H-Plane.

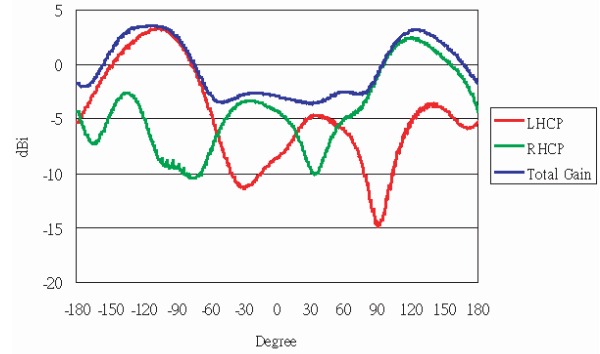


Figure 3: The measured pattern of E-Plane.

## REFERENCES

1. Kraus, J. D. and R. J. Marhefka, *Antennas for All Applications*, McGraw-Hill, 2002.
2. Toh, B. Y., R. Cahill, and V. F. Fusco, "Understanding and measuring circular polarization," *IEEE Transactions on Education*, Vol. 46, No. 3, 313–318, Aug. 2003.

## The Wideband Character of Self-structuring Antenna

Hongtao Zhang, Yingzeng Yin, and Wenbo Wei

National Laboratory of Antennas and Microwave Technology, Xidian University  
Xi'an 710071, Shaanxi, China

**Abstract**— In This paper, a self-structuring antenna (SSA) with 23 controllable switches is analyzed and designed. The controllable switches are chosen PHEMT GaAs IC SPDT Switch AS179-92 of the company SKYWORKS and are controlled by Single Chip. The Hex inverter 74HC04 is used to reduce the number of control lines. The proposed antenna is simulated by the genetic algorithm (GA) combined with method of moment (MOM) and numerical results with measure results are presented and shown that the proposed antenna has a VSWR bandwidth of 40 MHz to 450 MHz with VSWR less than 1.6. From the results of measurement, it can be seen that in some combination of switches states, the proposed antenna has wide frequency band.

## Shaping Design of Side-fed Offset Cassegrain Reflector Antennas

S. D. Liu<sup>1,2</sup>, S. F. Liu<sup>2</sup>, Y. C. Jiao<sup>2</sup>, and F. S. Zhang<sup>2</sup>

<sup>1</sup>Xi'an Institute of Space Radio Technology, Xi'an 710000, China

<sup>2</sup>Xidian University, Xi'an 710071, China

**Abstract**— In satellite communication systems, shaped coverage and frequency reuse require satellite antennas to provide multiple high-quality spot beams over the entire  $18^\circ$  field of view. The Side-fed Offset Cassegrain (SFOC) reflector antenna has good scan properties due to the large foci of its main reflector, but the gain loss becomes serious at larger scanning angles. To improve the scanning capability of the SFOC reflector antenna, a shaping technique is presented. Firstly the ray-tracing technique is employed to obtain the path lengths and directions of the outgoing rays emanating two specified feeds. Then the path length and direction errors of these rays are minimized by adjusting the antenna's main- and sub-reflector surfaces.

A numerical example with the main reflector diameter of 400 wavelengths is given. By shaping its main- and sub-reflector surfaces which are paraboloid and hyperboloid, respectively, the antenna achieves two focal points which results in a scanning range of about 59 percent wider than the original antenna. The radiation fields of the antenna are calculated based the physical optics and the peak gains versus scan angle for the original and shaped antennas are obtained. It shows that the gain loss of the shaped antenna due to phase errors is relatively constant over the field of view and is superior to the original antenna at greater scanning angles.

## On Resonant Frequency of Pin Shorted Gap-coupled Circular Patch Antennas

Pradeep Kumar, G. Singh, S. Bhooshan, and T. Chakravarty  
Mody Institute of Technology and Science, USA

**Abstract**— This article discusses the simulated results of pin-shortened gap-coupled circular patch antennas. The effect of pin shorting and variation of diameter of shorting pin on the resonant frequency have been simulated. The effect of the location of shorting pin on the patches is also studied. This simulation has been carried out using Method-of-Moments based software (IE3D).

The trend for technology in recent times is towards miniaturization and the demand for more compact and robust designs has been growing. The revolution in semiconductor manufacturing and device design methodologies has helped to achieve very high data rates transmission and compact size. In wireless devices, the antenna still remains a matter of concern as regards to its size. Microstrip antennas and arrays are extensively used in several applications; however, they are limited by their size, inspite of their other advantages. However, using high dielectric constant substrates increases the surface wave effect, which yields poor performance in terms of radiation efficiency. One effective way to reduce antenna size is to use a shorted quarter wavelength patch [3–5]. This approach takes advantage of the fact that the electric field component beneath the patch-between the patch and the ground plane-is approximately a cosinusoidal function of the length. It has a maximum value at the edge, goes to zero at the middle plane, and returns to a maximum at the other edge. Because the electric field is null at the middle plane, a short circuit can be placed at this position without affecting the antenna's basic operations. This short circuit at the zero-potential plane reduces the size of the microstrip antenna to half of its original length. It is not necessary to short the whole zero-potential plane; only a few points of this plane need to be shorted. This can be done by simply using shorting pins between the patch and the ground plane [3].

The bandwidth of the microstrip antenna can be increased by several methods such as by reducing the dielectric constant of substrate, by loading a patch and by using thicker substrate [6, 7]. The use of thicker substrate causes spurious radiation. Also, by using gap-coupling the bandwidth of the microstrip antenna can be increased [8]. In gap-coupled microstrip antenna, two patches are placed close to each other. One patch is fed and other is excited by the gap-coupling. For increasing the bandwidth of the microstrip antennas, researchers have designed various types gap-coupled microstrip antennas like rectangular gap-coupled microstrip antennas [9, 10], trian-

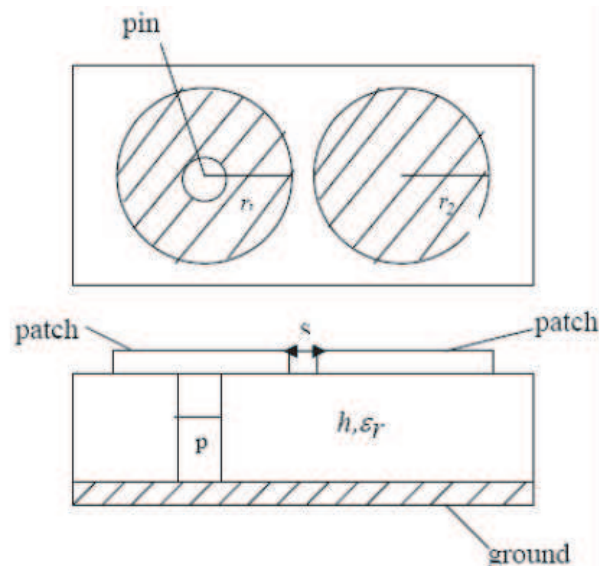


Figure 1: Geometry of pin shorted gap-coupled microstrip antennas.

gular microstrip antennas [11, 12], semicircular microstrip antennas [10] and circular microstrip antennas [13, 14] are few.

In the present paper, we have simulated two conventional gap-coupled circular microstrip patch antenna and pin shorted gap-coupled circular patch microstrip antenna. The simulation work has been performed using the method-of-moment based software (IE3D from M/S Zeland software).

The geometry of two gap-coupled pin shorted circular microstrip antennas is shown in Fig. 1. The patch of radius ' $r_1$ ' is feed patch and the patch of radius ' $r_2$ ' is the parasitic patch.

The parasitic patch is excited by the gap-coupling. The feed patch is shorted by a pin of diameter ' $p$ ' as shown in Fig. 1. The height and permittivity of the substrate is ' $h$ ' and ' $\epsilon_r$ ' respectively. The gap between the adjacent edges is ' $s$ '. In the Fig. 1 the shorting pin is placed at the centre of the fed patch, but the results also taken with the variation of pin location.

# Super-compact UWB Bandpass Filter Using a Partially-grounded Interdigital Gap Structure

Ryosuke Nakamura<sup>1</sup>, Toshiaki Kitamura<sup>1</sup>, Yasushi Horii<sup>2</sup>, and Toshitaka Kojima<sup>1</sup>

<sup>1</sup>Graduate School, Kansai University  
3-3-35, Yamate-cho, Suita-shi, Osaka 564-8086, Japan

<sup>2</sup>Graduate School, Kansai University  
2-1-1, Ryozenji-cho, Takatsuki-shi, Osaka 569-1095, Japan

**Abstract**— Ultra wide-band (UWB) technology has attracted much attention for the purpose of close-range large-capacity wireless communications since the U.S. Federal Communications Commission authorized the unlicensed use of UWB (frequency range of 3.1–10.6 GHz) for commercial use. Recently, various kinds of methods and structures have been developed for the UWB bandpass filters. In addition to the basic filtering characteristics, “compactness” of the size is the most important factor in the practical filter design. In this paper, we propose a super-compact microstrip UWB bandpass filter. This filter is composed of four narrow microstrip lines with 0.4 mm width and 5.0 mm length, two of which are connected to a 50 ohm input microstrip line and the rest of which are to an output microstrip line so as to form an interdigital gap (IDG) structure on a dielectric substrate. The spacing of the narrow microstrip lines is 0.4 mm each, and the dielectric constant and the thickness of the substrate are 2.62 and 0.8 mm, respectively. To create a clear UWB response, metallic posts are introduced to the outer narrow lines in the IDG, and the middle of these lines is connected to the ground plane. Thanks to the posts, a UWB passband from 5.0 GHz to 10.0 GHz and an attenuation pole around 12.5 GHz were realized with filter dimensions of 2 mm × 5 mm in the initial simulation. We also fabricate the filter, and examine the characteristics through experiments.



## Folded Dual-mode Microstrip Filter

Katsuhisa Tagashira<sup>1</sup>, Toshiaki Kitamura<sup>1</sup>, Yasushi Horii<sup>2</sup>, and Toshitaka Kojima<sup>1</sup>

<sup>1</sup>Graduate School, Kansai University

3-3-35, Yamate-cho, Suita-shi, Osaka 564-8086, Japan

<sup>2</sup>Graduate School, Kansai University

2-1-1 Ryozenji-cho, Takatsuki-shi, Osaka 569-1095, Japan

**Abstract**— Compact and high performance microwave filters are highly demanded in wireless communications such as satellite and mobile communication systems. Dual-mode filters are one of the candidates that can achieve such purposes. They have the advantage that a single resonator can be used as a doubly tuned resonator. Therefore, the number of the resonators can be reduced and it can result in size-reduction of the filter. And they also have the benefit that attenuation poles can easily arranged in both sides of the passband. For such reasons, many kinds of dual-mode filters have been proposed so far.

On the other hand, multilayering technology such as LTCC (Low Temperature Co-fired Ceramics) has attracted much attention in order to achieve size-reduction of the devices. From such a background, we propose a new folded dual-mode microstrip filter. The filter utilizes the dual planes of the substrate. On the upper and lower planes, the microstrip and coplanar resonators are arranged, respectively. By connecting the resonators on both planes through conductor wires, the folded loop resonators are formed. We investigate the filtering characteristics through numerical simulations. Especially, we study how the dual-mode resonance occurs by examining the electromagnetic field distribution of the resonators. We also fabricate the filter and examine the characteristics through experiments.

## Planar Leaky-wave Antenna with Aperture Coupled Feed

A. Mahmoudian, H. Dalili Oskouei, and K. Forooraghi

Microwave Lab., Department of Electrical Engineering, Tarbiat Modares University  
Tehran, Iran

**Abstract**— In this paper we study a new design of a two-dimensional (2-D) planar leaky-wave antenna. The antenna consists of a two dimensional periodic array of square patches which are excited by an aperture coupled feed. Dispersion diagram for periodic array of patches on top of a grounded dielectric slab is obtained by using the Floquet theorem for periodic structure and HFSS software. The appropriate frequency band for leaky wave excitation is derived and an aperture coupled design is performed for this frequency band. At last two high gain radiation patterns for two frequencies are observed.

# A Novel Broadband Compact Circular Disk Microstrip Antenna for Wireless Applications

Husam El-Din Ahmed Osman<sup>1</sup>, Esmat Abdel-Fattah Abdallah<sup>2</sup>  
and Abdel-Hamid Abdel-Rhim<sup>1</sup>

<sup>1</sup>Arab Academy for Science & Technology and Maritime Transport, Egypt

<sup>2</sup>Electronics Research Institute, Egypt

**Abstract**— The modern wireless communication networks need compatible antennas for compactness and broad bandwidth. Circular and annular ring microstrip antennas are the best candidate configurations for compactness. But these microstrip antennas suffer from the inherent narrow bandwidth. This paper investigates several approaches for improving the bandwidth of an antenna used in the Wireless Local Area Network (WLAN) operating at 5.2 GHz. The percentage bandwidths of conventional circular disk and annular ring microstrip antenna designed at this frequency are found to be 3.4% and 3.7%, respectively. The dielectric substrate is RT-Duroid 5880 ( $\epsilon_r = 2.2$ ,  $h = 1.575$  mm). A study of circular and annular ring microstrip antenna supported by a layer of air is presented in both the normal and inverted configurations by changing the air thickness. Consequently, the percentage bandwidth for circular disk microstrip antenna in the normal and inverted configuration is found to be 15.5% and 12.36%, respectively and for the annular ring microstrip antenna is 7.23% and 6.22%, respectively at an optimum air thickness of 3 mm. On the other hand, embedding a suitable slot on the surface of the patch leads to increasing the percentage bandwidth as long as the resonance frequencies of the slot and the patch are close to each other [1]. A percentage bandwidth of circular disk with U-slot is found to be more than 24%. A novel shape is proposed having a reduction of the conventional size by 85% (see Fig. 1). Two substrate layers of the same parameter ( $\epsilon_r = 2.2$ ,  $h = 1.575$  mm) are stacked and spaced by an air layer of thickness 3 mm. The feeding layer (coaxial probe) contains a simple conventional circular disk with radius 10.65 mm while the radiating layer contains the proposed novel shape that has slightly reduced radius of 9.65 mm (see Fig. 2). The feed location is about 6 mm from the center with radius of 0.4 mm. The suggested design is optimized by the electromagnetic ready-made software Zeland IE3D. Fortunately, a percentage bandwidth of more than 33% is found (see Fig. 3) covering the frequency range from 4.8 GHz up to 6.1 GHz compared to 11% achieved before at 2.4 GHz [2].

W=3mm  
L=6mm  
Feed Location from the Center=2.2mm  
Feed Radius=0.35mm

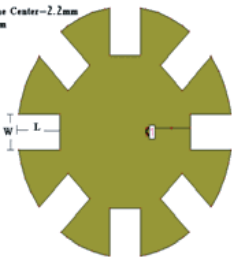


Figure 1: Novel shape.

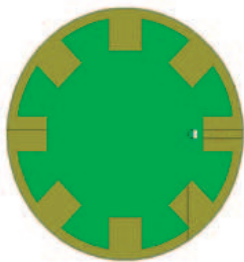


Figure 2: Stacked novel shape.

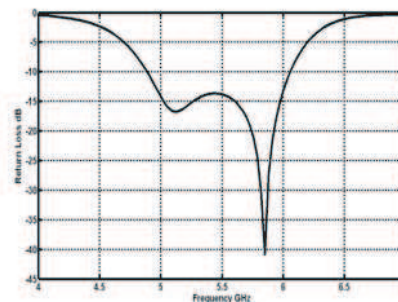


Figure 3:  $S_{11}$  vs. Frequency.

## REFERENCES

1. Bhalla, R. and L. Shafai, "Resonance behavior of single U-slot microstrip patch antenna," *Microwave and Optical Technology Letters*, Vol. 32, No. 5, 333–335, March, 2002.
2. Abdullah, R., D. Yoharaaj, and A. Ismail, "Bandwidth enhancement technique in microstrip antenna for wireless application," *PIERS*, Vol. 2, No. 6, 633–639, 2006.

# Novel Planar Wideband Omni-directional Antenna for RFID Applications

Heng-Tung Hsu

Department of Communications Engineering, Yuan Ze University  
135 Yuan-Tung Road, Chung-Li 32003, Taiwan, R.O.C.

**Abstract**— The technology breakthrough has spurred the large-scale deployment of RFID system with various applications. Lots of RFID applications have imposed very stringent requirements on the tag antennas especially the insensitivity to the environment. In this paper, a novel and simple wideband planar omni-directional antenna is proposed. The proposed antenna has very low-profile and can be easily integrated with standard manufacturing process for cost reduction purposes. The simultaneously wideband and omni-directional characteristics of the proposed structure are achieved by adding two mutually-coupled elements to the conventional dipole antenna. This proposed structure is able to extend the bandwidth ( $VSWR < 2 : 1$ , at UHF band) to 30% compared to simple dipole antennas while maintaining an omni-directional radiation pattern with maximum gain of 2.2 dBi. Additionally, the proposed antenna has larger difference in radar cross section (RCS) values for different states which suggests longer read range than that of the traditional dipole.

## Clover Polarimetric Detector — A Novel Design of an Ortho-mode Transducer at 150 and 225 GHz

Philip Mauskopf<sup>1</sup>, Peter Ade<sup>1</sup>, Stafford Withington<sup>3</sup>, Jin Zhang<sup>1</sup>, and Paul Grime<sup>2</sup>

<sup>1</sup>Astronomy Instrumentation Group, Cardiff University, UK

<sup>2</sup>Experimental Radio Cosmology Group, Oxford University, UK

<sup>3</sup>Cavendish Laboratory, University of Cambridge, UK

**Abstract**— The existence of primordial gravitational waves in the universe is a fundamental prediction of the inflationary cosmological paradigm, and determination of the level of this tensor contribution to primordial fluctuations is a uniquely powerful test of inflationary models. The project CLVOER is to measure this tensor contribution via its effect on the B-mode polarization of the Cosmic Microwave Background (CMB) down to a sensitivity limited by the foreground contamination due to lensing. This project comprises three independent telescopes operating at 97, 150 and 225 GHz.

This paper presents the design of an ortho-mode transducer (OMT) to separate two orthogonal linearly polarized signals traveling in a circular waveguide. The design concept compromises two key issues:

The first is to design a four-probe OMT that can be integrated with a set of TES detectors, the waveguide needs to be split in order to get the OMT signals out to the detectors. This results in a loss of signal propagating out of the gap between the incoming waveguide and the backshort section. The effect of this waveguide gap has been presented in this paper.

The second issue is to design a planar structure that will couple well to the rectangular probes. The design adopted microstrip for two main advantages: the field is confined in a microstrip and therefore the parameters of the waveguide gap has no effect on the microstrip impedance; the microstrip line is the most compact transmission line and therefore the only type that is possible to be used for carrying the signal over the thermally isolating silicon nitride legs of the TES detectors.

Simulations (in HFSS) are presented to determine the optimal probe geometry and feed impedance to achieve good coupling to the optimized probes over a wide bandwidth with corresponding feed impedances for telescopes operating at 150 and 225 GHz. The simulations have been conducted mainly at a frequency range of 180–280 GHz where the tolerancing and the fabrication are most difficult. The results show that at 150 GHz band, the return loss can reach below  $-20$  dB from 126 GHz to 180 GHz with the cross polarization reach below  $-40$  dB. At 225 GHz band, the return loss can reach below  $-20$  dB from 190 GHz to 260 GHz with the polarization isolation more than 32 dB.

## Circular Polarization GPS Patch Antennas with Self-biased Magnetic Films

G. M. Yang<sup>1</sup>, A. Daigle<sup>1</sup>, N. X. Sun<sup>1</sup>, and K. Naishadham<sup>2</sup>

<sup>1</sup>Center for Microwave Magnetic Materials and Integrated Circuits  
Department of Electrical and Computer Engineering  
Northeastern University, Boston, MA 02115, USA

<sup>2</sup>RF Communications Group, Draper Laboratory, Cambridge, MA 02139, USA

**Abstract**— Achieving relative permeability larger than 1 ( $\mu_r > 1$ ) in patch antenna substrates can lead to antenna miniaturization, enhanced bandwidth, tunable radiation frequency, polarization diversity, and beam steering, etc. Bulk ferrite materials, composites of ferrite particles in polymer matrix, metamaterials with embedded metallic circuits, etc., have been used as antenna substrates for achieving  $\mu_r > 1$ . However, these antenna substrate approaches are too lossy to be used at frequencies  $> 500$  MHz, and large biasing magnetic fields are needed for ferrite materials in antenna substrate. In order to be practically feasible in miniature antenna applications, such as handheld wireless communication devices, it is important for antenna substrates to be comprised of self-biased magnetic materials, in which no external bias field is applied. However, it has been challenging to achieve self-biased magnetic materials for antenna substrate applications in the GHz frequency range.

Magnetic thin films provide a unique opportunity for achieving self-biased magnetic patch antenna substrates with  $\mu_r > 1$  at GHz frequency range. The strong demagnetization field for magnetic thin films,  $H_{\text{demag}} = 4\pi M_s$ , allows for high ferromagnetic resonance (FMR) frequencies (up to several GHz), and self-biased magnetization as well, which are essential for microwave magnetic devices. In this work, a new type of patch antennas with metal magnetic films was designed, fabricated, and tested at 2.1 GHz, leading to self-biased electronically tunable magnetic patch antennas with enhanced performance at 2.1 GHz. The magnetic patch antennas showed an enhanced bandwidth of  $> 50\%$  over the non-magnetic patch antennas, a large radiation frequency tunability of 50% of the  $-10$  dB bandwidth, a significantly enhanced directivity, and a large tunability of the radiation field intensity at a low applied magnetic field of  $\sim 20$  Oe. In addition these metallic magnetic films are shown to be temperature stable for antenna applications. These new patch antennas with magnetic films show great promise for achieving *self-biased* miniaturized patch antennas on magnetoelectric substrate with significantly enhanced bandwidth, improved directivity, and high efficiency when multilayers of magnetic films are introduced into antenna substrates. In addition, these magnetic antennas can be made conformably at a low cost with physical vapor deposition method at room temperature, making these patch antennas with metal magnetic films very promising for real applications.

### ACKNOWLEDGMENT

Financial supports from ONR Award N00014-07-1-0761 and from Draper Laboratory are gratefully acknowledged.

## The Dipole Antenna Array Design with Balun Integration

Guan-Yu Chen<sup>1</sup>, Jwo-Shiun Sun<sup>1</sup>, Cheng-Hung Lin<sup>2</sup>, Kwong-Kau Tiong<sup>2</sup>, and Y. D. Chen<sup>3</sup>

<sup>1</sup>Department of Electronic Engineering, National Taipei University of Technology, Taiwan

<sup>2</sup>Department of Electrical Engineering, National Taiwan Ocean University, Taiwan

<sup>3</sup>Antenna and EMC Laboratory, High Tech Computer Corp. (HTC), Taiwan

**Abstract**— In this paper, the array antenna design is suitable for wireless LAN, radio identification, wireless sensor and short range intelligent wireless communication. In this design, the  $1 \times 2$  dipole antenna feed network with magic T and divider two wide bandwidth planar tapered balun is studied.

**Array Antenna Design and Results:** The design and experimental results of low profile embedded dipole antenna array (Fig. 1 and Fig. 2) with tapered balun shows fairly good performances and antenna gain. The feed network of the design with wider bandwidth and lower power loss tapered microstrip line to coplanar stripline (CPS) transition that provided unbalanced to balanced line with balanced equal power output of  $180^\circ$  phase difference. The achieved planar embedded wider band dipole antenna array exhibits antenna bandwidths (Fig. 3) cover WLAN (IEEE 802.11a/b), RFID (ISM band) and DSRC (IEEE 802.11p), respectively. Apply full wave EM analyses and shows good agreement with those experimental data. The 3D antenna measured method [1–4] and data are shown in Fig. 4 and Fig. 5.

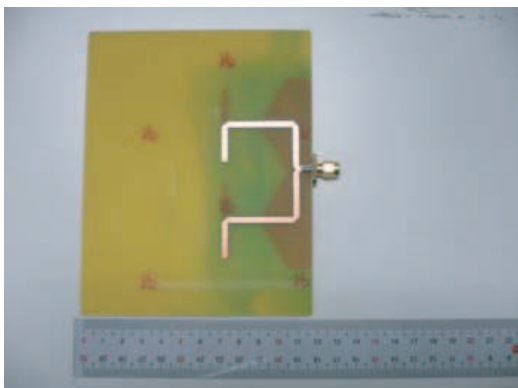


Figure 1: The proposed  $1 \times 2$  dipole array (top).

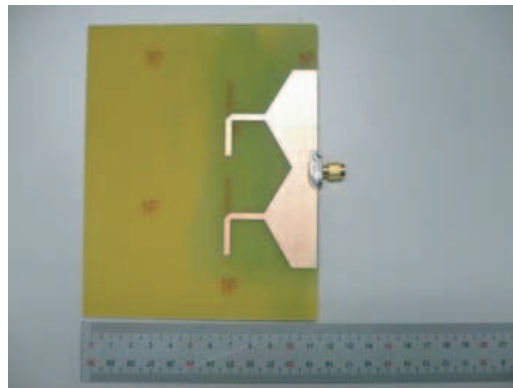


Figure 2: The proposed  $1 \times 2$  dipole array (bottom).

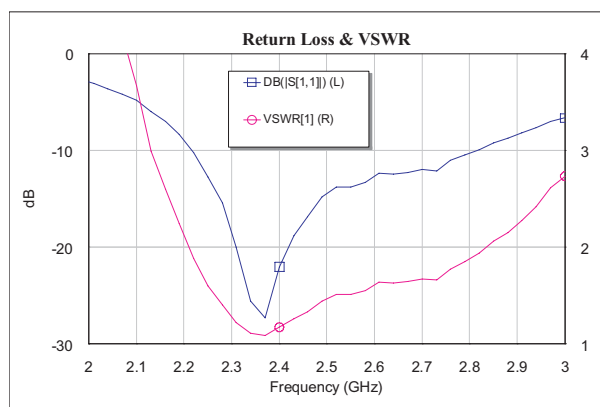


Figure 3: The measured data of return loss and VSWR.

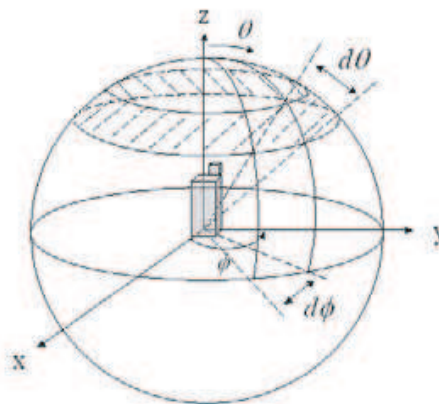


Figure 4: 3D antenna measurement.

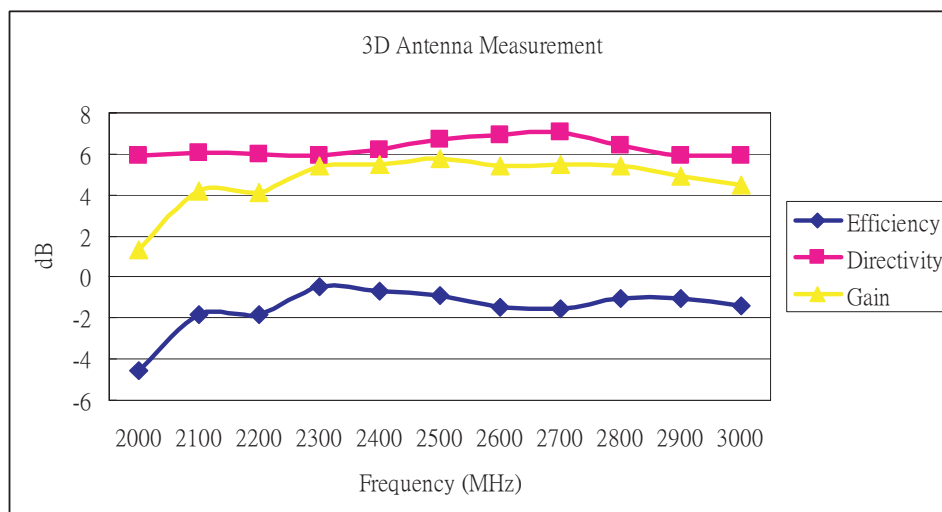


Figure 5: The measured data of 3D antenna performance.

#### REFERENCES

1. CTIA, <http://www.ctia.org/>.
2. "Test plane for mobile station over the air performance," Revision 2.1, Cellular Telecommunications & Internet Association (CTIA), Washington, D.C., Apr. 2005.
3. Stutzman, L. W., *Antenna Theory and Design*, John Wiley, c1998.
4. Balanis, A. C., *Antenna Theory*, John Wiley, c2005.



## Printed Digital Audio Broadcast Antennas

The-Nan Chang and Cheng-Min Jen

Graduate Institute of Communication, Tatung University, Taiwan

**Abstract**— In this paper, printed antennas were studied for digital broadcast reception. The first one is a meandered loop antenna. Being in a meandered form, it can be made very compact. However, the gain and efficiency are quite low. In our study, the measured gain is only  $-30$  dBi. Aside from low gain, the bandwidth is also narrow. Therefore, this configuration may not be practical in use.

We then studied a bow-tie antenna. Bow-tie antenna is typically considered to have more bandwidth than the meandered configuration. Its gain increases up to  $1.85$  dBi. Measured bandwidth is around  $8\%$ . For DAB reception in upper half of Band III, a required bandwidth of  $13\%$  is needed. We found that the bandwidth can be increased by half-sizing the bow-tie antenna without reducing too much of its gain. This half sized bow-tie antenna (HBTA) takes an area of  $475$  mm by  $110$  mm. Measured  $10$  db return loss bandwidth ranges from  $192$  to  $236$  MHz, or  $21\%$  bandwidth centered at  $214$  MHz. The gain is  $1.78$  dBi within the whole band.

## Two-layer Variable Slot Length Reflectarray

The-Nan Chang and Chia-Hsin Chung

Graduate Institute of Communication, Tatung University, Taiwan

**Abstract**— In this paper, a microstrip patch loaded with a co-plane slot and an atop-patch is used to realize a 12 GHz reflectarray on a two-layer substrate. Phase of reflection is adjusted by tuning the length of each slot. The length of the atop-patch is also varied and is used as a mask so that we can select required phase range section by section to have a full  $360^\circ$  range.

## The Planar V-dipole Antenna Fed by Marchand Balun

Cheng-Hung Lin<sup>1</sup>, Guan-Yu Chen<sup>2</sup>, Jwo-Shiun Sun<sup>2</sup>, Kwong-Kau Tiong<sup>1</sup>, and Y. D. Chen<sup>3</sup>

<sup>1</sup>Department of Electrical Engineering, National Taiwan Ocean University, Taiwan

<sup>2</sup>Department of Electronic Engineering, National Taipei University of Technology, Taiwan

<sup>3</sup>Antenna and EMC Laboratory, High Tech Computer Corp. (HTC), Taiwan

**Abstract**— The Marchand balun for microwave band as a feeding network structure that effectively excited tapered V-dipole antenna geometry is proposed. The microstrip line to coplanar strip line transition then to fed tapered V-dipole antenna. The designed quasi-tapered TEM horn (V-dipole) antenna has the merits such as wideband, simple feeding network, low profile compact size with fairly good antenna performances such as return loss, peak gain and radiation patterns.



Figure 1: V-dipole antenna fed by Marchand balun.

**Introduction:** The radiation mechanism of a TEM horn antenna is based on traveling wave propagation along the tapered aperture slot, which results in an end-fire antenna. TEM horn

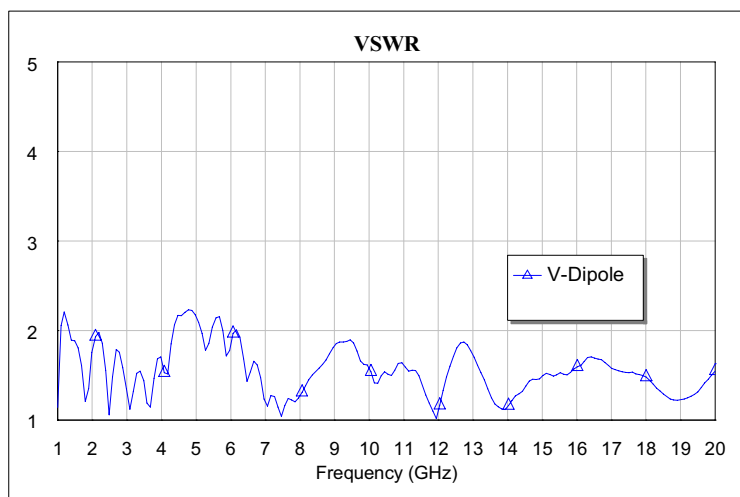


Figure 2: Measured data of VSWR.

or tapered slot antenna (TSA) exhibits some advantages such as wideband, wide scanning, high gain, low cross polarization and symmetrical E and H plane radiation patterns [1] for an array or embedded circuits as antenna radiating elements. In this paper, the Marchand balun with a balanced to unbalanced transition is shown good impedance matching and easy to integration and fabrication and the frame of the planar structure on tapered TEM horn (V-dipole) was experimentally investigated. Measured results indicate that effects have significant impacts on the return loss, input impedance, radiation patterns and antenna gain of the TEM horn (V-dipole) antenna.

**Quasi-TEM Horn (V-dipole) Antenna:** The coplanar stripline to feed planar tapered V-shape as quasi-TEM antenna radiator. The V-dipole antenna is a kind of traveling wave antenna that wave propagating along the tapered slot for heading radiation. The basic geometry of the designed TEM horn antenna is like a double ridge as shown in Fig. 1 and performance result (Fig. 2). The transition provides wider balanced equal outputs, as well as a matching section for the traveling tapered slot of TEM horn antenna. The FEM software based on full wave frequency domain method was adopted to perform the simulation of the designed low profile and planar TEM horn antenna. The planar quasi-TEM horn was fabricated on the FR4 substrate (dielectric constant = 4.4 and dielectric loss = 0.02). The simple quasi-TEM horn antenna structures exhibits broadband and low profile compact structure for UWB and impulse radio applications. The radiation characteristics of the TEM horn antenna based on the spherical coordinate and 3D chamber system are measured. The measured data of H-plane and E-plane are shown in Fig. 3.

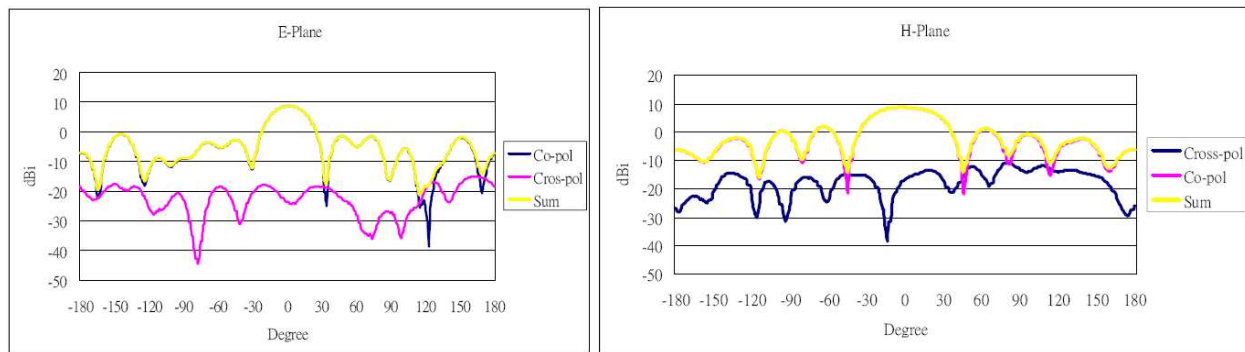


Figure 3: Measured 3 GHz antenna gain pattern of E and H plane.

**Conclusion:** The designed V-dipole antenna fed by coplanar stripline and the transition is presented. It exhibits the merits of geometric simplicity, wide bandwidth, lightweight, low cross polarization, and high peak gain. This V-dipole antenna is suitable for UWB impulse radio operation and application.

## REFERENCES

1. Lee, K. F. and W. Chen, *Advances in Microstrip and Printed Antennas*, John Wiley & Sons, Inc. 1997.

## A Single Feed Circularly Polarized Fractal Shaped Microstrip Antenna with Fractal Slot

P. Nageswara Rao and N. V. S. N. Sarma

Department of Electronics and Communications Engineering  
National Institute of Technology, Warangal, India

**Abstract**— A single feed circularly polarized fractal shaped Microstrip antenna is presented. Applying fractal geometry to the Microstrip antennas to reduce the real estate of the patch and to make the antenna operate at multiple bands is a new trend in printed antennas. When the fractal curves are used as boundary to the Euclidean shaped antennas, the antenna operates at lower frequency which is an indication of reduction in size. The reduction in size is mainly due to the increase of electrical length of patch through which the surface current travels. Applying the concept of fractals to get circular polarization is again a new and innovative idea. By doing so it is possible to obtain a better axial ratio very close to unity and better 3 db Axial ratio bandwidth greater than 1%. With regular shaped antennas like square, triangular or circular patches the 3 db axial ratio more than 1% with single feed may not be possible. In this paper a Koch fractal boundary Microstrip antenna with a fractal shaped slot is used to excite two orthogonal near degenerate modes with same amplitude, which are prerequisite for getting circular polarization. It is always simple to use single feed than two feed to get circular polarization since it is not required to design a  $90^\circ$  phase shifter. With this proposed antenna the 3 db axial ratio bandwidth of about 1.2% is obtained in addition to reducing the size. The purity of circular polarization can be visualized with the help of smith chart in which the curve will have a loop with zero area, then the two orthogonal modes are very near to each other. The geometry of the antenna, axial ratio, radiation pattern and variation of input impedance with frequency are given. The measurement results will be submitted in the full paper. The analysis is done using IE3D electromagnetic simulator.

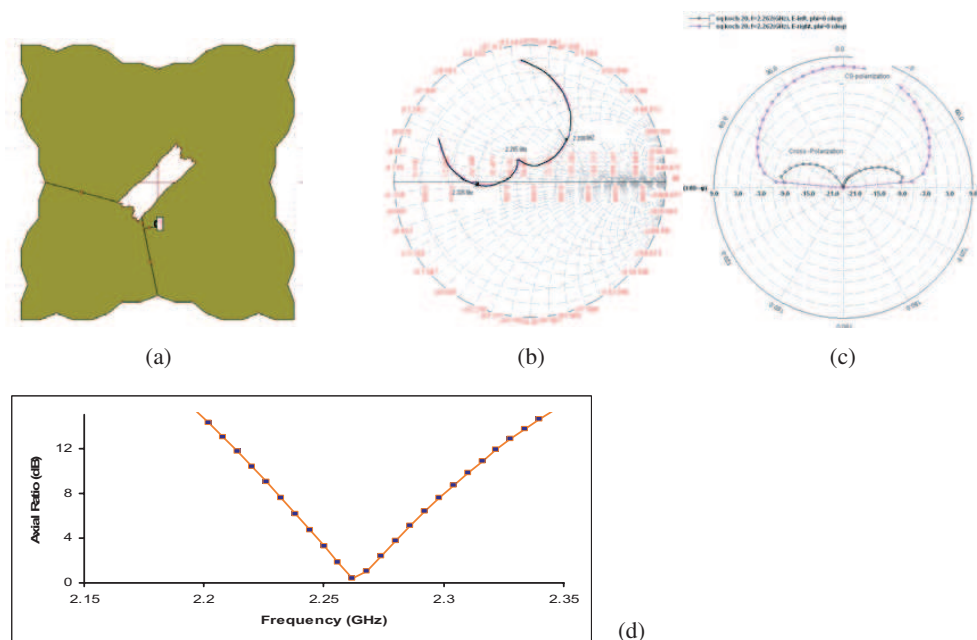


Figure 1: (a) Geometry, (b) S11, (c) radiation pattern, (d) axial ratio.

## Compact Microstrip-fed Annular-slot Antenna Combined with C-shaped Slot for Broad Dualband Operation

X. L. Bao and M. J. Ammann

Centre for Telecommunications Value-chain Research  
School of Electronic & Communications Engineering  
Dublin Institute of Technology, Kevin Street, Dublin 8, Ireland

**Abstract**— Recently, annular-slot antennas have been of great interest to antenna designers because of good performance, such as relatively wide bandwidth, low profile, light weight, and ease of fabrication. Dual-band and multi-band annular-slot antennas had been reported of late and impedance bandwidths in the range 10%–20% have also been realised by adjusting the feedline and slot structure.

In this paper, an antenna comprising a compact annular-slot combined with a small concentric annular split-ring slot is presented. The antenna is fed by a T-shaped microstrip line. By using the T-shaped microstrip feedline to tune the level of electromagnetic coupling between annular-slot and feedline, good matching can be achieved. The proposed antenna can effectively enlarge the length of the annular-slot by introducing the concentric annular split-ring slot, so it can lengthen the surface current path, thus significantly reducing the resonant frequency.

For the proposed antenna, the length and width of microstrip feedline and the width of annular-slot are the key parameters which determine the antenna performance because of the electromagnetic coupling through the strip and slot. By optimizing these parameters, a broadband dual-frequency slot antenna is realised.

The measured results of return loss show good agreement with simulated values. The results show that bandwidth for the lower band is about 27.2% (490 MHz) from 1.556 GHz to 2.046 GHz, and the bandwidth for the high band is about 34.1% (1798 MHz) from 4.366 GHz to 6.164 GHz. The ratio of centre frequencies for the lower and high bands is 2.92. The radiation patterns are omnidirectional. The slot antenna is proposed for wireless communication applications which require broadband dual-frequency operation.

# Design and Implementation of Aperture Coupled Microstrip IFF Antenna

M. N. Jazi<sup>1</sup>, Z. H. Firouzeh<sup>2</sup>, H. Mirmohammad-Sadeghi<sup>3</sup>, and G. Askari<sup>3</sup>

<sup>1</sup>Institut National de la Recherche Scientifique, Université de Québec, Canada

<sup>2</sup>Department of Electrical Engineering, Amirkabir University of Technology, Iran

<sup>3</sup>Information and Communication Technology Institute, Isfahan University of Technology, Iran

**Abstract**— Microstrip antennas are simple planar structures that have advantages such as low profile, conformal availability, simple fabrication using printed circuit technology, low cost and compatibility with integrated circuits. In spite of limitations such as small bandwidth, low gain and low power handling capability, microstrip antennas have been used in variety applications such as military, industry and wireless communication due to their advantages. Different techniques have been used to improve the bandwidth of microstrip antenna. Increasing dielectric thickness is the simple method to improve the antenna bandwidth up to a few percent. Aperture coupled stacked patch microstrip antenna can improve the bandwidth greater than 50 percent at the expense of increasing in back lobe radiation level. To reduce back radiation, metallic rods or resonance planes are used in the back of the antenna or appropriate cavities are put next to the coupling aperture. In this paper, both techniques have been used to increase the bandwidth and decrease the back radiation.

To improve radiation performance of the microstrip antenna four structures are investigated. Simulated and measured results show that antenna with air substrate has the maximum frequency bandwidth and best radiation performance. Experimental results of frequency bandwidth and radiation patterns of the optimum structure agree with the simulation results. The antenna has the gain of 8.5 dB, the bandwidth of greater than 25% at the central frequency of 1060 MHz, and F/B better than 15 dB. This aperture coupled microstrip antenna can be used as an element of microstrip array antennas in Identification Friend or Foe (IFF) systems or Secondary Surveillance Radar (SSR) systems.

## Design of the Spiral Monopole Antenna for Multi-band Mobile Communication and SAR Analysis

S. M. Park<sup>1</sup>, N. Kim<sup>1</sup>, S. W. Lee<sup>1</sup>, H. M. Lee<sup>2</sup>, and S. W. Park<sup>1</sup>

<sup>1</sup>Division of Information and Communication Eng., Chungbuk National University, Korea

<sup>2</sup>Department of Bioelectronics, BIT Graduate school, Chungbuk National University, Korea

**Abstract**— In this paper, spiral-line planar monopole antenna mounted on CDMA/WCDMA handset is designed. Frequency characteristics optimized with various design parameters are analyzed and designed. The two spiral lines are adopted in order to implement CDMA frequency bandwidth and WCDMA frequency bandwidth with small-sized antenna. The bandwidth of a realized antenna is 0.805 ~ 0.892 GHz and 1.867 ~ 2.302 GHz for return loss below -10 dB which contain the required bandwidth of CDMA/WCDMA. And the simulated and measured values of 1 g and 10 g averaged SAR on human head caused by the spiral-line planar monopole antenna mounted on folder-type handsets were analyzed and discussed. As a result, the measured 1 g and 10 g averaged SARs was similar to simulated values and were lower than the 1.6 W/kg, 2 W/kg of 1 g and 10 g averaged peak SAR limits.



## Design and SAR Measurement of the Trapezoidal Shape Antenna

S. W. Lee<sup>1</sup>, S. M. Park<sup>1</sup>, N. Kim<sup>1</sup>, S. W. Park<sup>1</sup>, and S. Y. Rhee<sup>2</sup>

<sup>1</sup>Chungbuk National University, Korea

<sup>2</sup>Chonnam National University, Korea

**Abstract**— In this paper, we designed the trapezoidal shape antenna which can be used in WLAN services. The trapezoidal shape would be working in the 2 GHz band and 5.2 GHz, and the small rectangular pieces in the trapezoidal shape were making the frequency shift from 5.2 GHz to 5.7 GHz. In addition, we found out the best values of the antenna parameters by sweeping some characteristics. The designed antenna has occurred resonances of which the first band is 2 GHz ~ 2.6 GHz and the second band is 5.2 GHz ~ 5.9 GHz below the return loss of -10 dB. Also, we will measure the SAR (Specific Absorption Rate) values for the human body.

## Design of Dual-band PIFA for WLAN

Sung-Keun Jeon<sup>1</sup>, Nam Kim<sup>2</sup>, Seung-Woo Lee<sup>2</sup>  
Sang-Myeong Park<sup>2</sup>, and Byoung-Jun Jang<sup>3</sup>

<sup>1</sup>Department of Bioelectron, BIT Graduate School, Chungbuk National University, Korea

<sup>2</sup>Division of Information and Communication Eng., Chungbuk National University, Korea

<sup>3</sup>Collage of Electrical Engineering, Kookmin University, Korea

**Abstract**— This paper proposed a new dual-band PIFA (Planar Inverted-F Antenna) for WLAN. Two patches were used in order to embody each WLAN band. The shorting strip and meander-type radiation patches were used in order to minimize the size of the antenna. The  $-10$  dB return loss bandwidth of a realized antenna was  $1.95 \sim 2.65$  GHz and  $5.47 \sim 6.03$  GHz which contains WLAN. The measured bandwidth contain two WLAN band ( $2.4 \sim 2.4835$  GHz,  $5.725 \sim 5.825$  GHz).

## Dual Frequency Operate Circular Array of Triangular Patches with RF-MEMS Switches

Naveen Kumar Saxena, Bhoopendra Singh, and P. K. S. Pourush

Microwave Lab, Department of Physics, Agra College, Agra, PIN 282002 (U.P), India

**Abstract**— A microstrip reconfigurable array antenna with integrated RF-MEMS switches is proposed which can operate at dual frequencies with the help of programming language. The switches are incorporated to equilateral triangular patch to control or change the frequency. The computer controlling and array of these equilateral triangular patches gives more directivity and scanning power, which makes it very useful in many communication system.

## 12 GHz Planar Array Antenna for Satellite Communication

Adel M. Abdin

Department of Communications, Faculty of Engineering  
Shorouk Academy, Shorouk City, Cairo, Egypt

**Abstract**— A novel microstrip antenna array of 32 elements is designed and built for broadcasting satellite orbital positions. It is working in the 12.43–12.53 MHz band (space-to-Earth). A corporate feeding network is used to give equal amplitude and phase to each element. The theoretical analysis is based on IE3D (Zeland) software and genetic algorithm to optimize the performance of planar array. A dummy column of elements is assumed around the excited 32 elements. The effect of these dummy elements is tested using IE3D (Zeland) software. This effectiveness is investigated on the return loss, voltage standing wave ratio (VSWR), number of main lobes of the radiation pattern, and the center frequency. The simulation shows the return loss and VSWR decrease as number of columns of parasitic elements increases. On the other hand the center frequency and number of main lobes increase as number of parasitic elements increases. The side-lobe level of the planar array is inspected using genetic algorithm under the variation of the spacing between elements and the excitation technique. The return loss and VSWR are measured and compared with the simulated results. They are very close. Both the theoretical and experimental results are presented and discussed.

## The Helical Antenna for Handset Design and Phantom Effect

Kuo-Liang Wu<sup>1</sup>, Guan-Yu Chen<sup>1</sup>, Jwo-Shiun Sun<sup>1</sup>, Cheng-Hung Lin<sup>2</sup>  
Kwong-Kau Tiong<sup>2,3</sup>, and Y. D. Chen<sup>3</sup>

<sup>1</sup>Department of Electronic Engineering, National Taipei University of Technology, Taiwan

<sup>2</sup>Department of Electrical Engineering, National Taiwan Ocean University, Taiwan

<sup>3</sup>Antenna and EMC Laboratory, High Tech Computer Corp. (HTC), Taiwan

**Abstract**— A high performance wire and patch co-design monopole antenna fabricated using two kinds of folded wire and metal patch as radiator is presented. A prototype of the proposed monopole antenna with a compact area size is implemented, and the antenna shows a wide operating bandwidth of about 300 and 50 MHz for low band and high band bandwidth, making it easy to cover the GSM, EDGE, CDMA, CDMA 2000, W-CDMA and UMTS band for wireless communication and 2.5G/3G dual mode operation of a mobile handset phone.

**PDA Antenna Operation** A low profile and compact helical (Fig. 1) antenna with multi-asymmetric helix turns is designed and measured (Fig. 2). The helical antenna, which is placed along the axis of a RF coaxial line fed through the ground plane, can be operated at multi resonant frequencies. The helix wire radiator [1, 2], which is designed to operate at the normal mode radiation performance, is mounted directly on the PDA ground environment. The finite element method (FEM) is used to obtain the numerical solution of far-field radiation patterns, which are found in good agreement compared to the experimental results. The bandwidth performance in multi-frequencies operation would also be explicitly studied.



Figure 1: The multi-bands helical antenna.

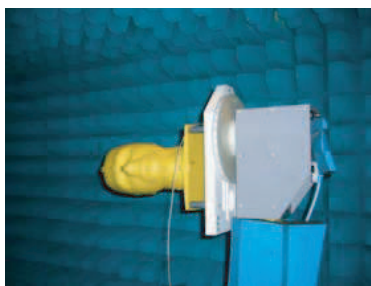


Figure 2: The multi-bands helical antenna for phantom effect.

The design of a miniaturized helical antenna is proposed and presented for 2.5G/3G mobile communication bands. The measured data is shown in Table 1. In this paper, a compact and low profile internal helical antenna for multi-bands has been proposed. This antenna was designed and measured for phantom effect. A good agreement between measurement and analysis has been obtained. The proposed antenna shows a wider operating bandwidth (Fig. 3) and it is easy to cover the GSM, EDGE, CDMA, CDMA 2000, W-CDMA and UMTS band for wireless communication and 2.5G/3G dual mode operation of a mobile handset phone, co-design, co-integration and PDA application.

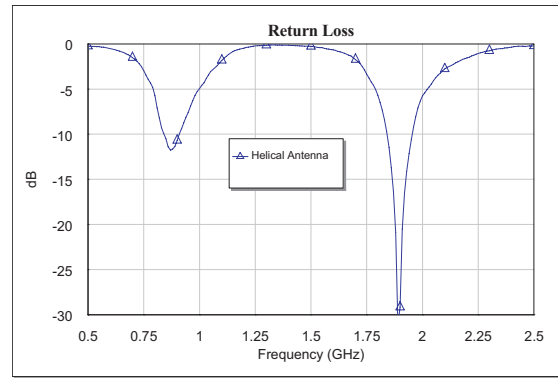


Figure 3: The measured data of helical antenna.

Table 1: The antenna gain.

Frequency (MHz)	800	850	900	950
Peak Gain (dBi)	-0.6	-0.4	0.9	-0.15
Frequency (MHz)	1000	1700	1750	1800
Peak Gain (dBi)	-0.1	-0.2	-0.15	-0.3
Frequency (MHz)	1850	1900	1950	2000
Peak Gain (dBi)	-0.2	-0.3	-0.25	-1.6

## REFERENCES

1. Stutzman, L. W., *Antenna Theory and Design*, John Wiley, c1998.
2. Balanis, A. C., *Antenna theory*, John Wiley, c2005.

## A Comprehensive Study on Performance of IEEE 802.15.4

Shuai Fang<sup>1</sup>, Lu Rong<sup>2</sup>, Qiang Xu<sup>1</sup>, and Yang Du<sup>1</sup>

<sup>1</sup>The Electromagnetics Academy, Zhejiang University, Hangzhou 310058, China

<sup>2</sup>Shanghai Research Center for Wireless Communications, Shanghai 200050, China

**Abstract**— IEEE 802.15<sup>TM</sup> working group has designed the IEEE 802.15.4 standards to target the low-rate wireless personal area network (LR-WPAN) which is characterized by low complexity, low cost and low power. The IEEE 802.15.4 standards specify operations of the physical layer (PHY) and medium access control (MAC) sublayer. These standards are to ensure acceptable system performance in terms of network PHY collisions, MAC collisions, throughput, average transmission delay and energy efficiency. Yet there are a number of factors that may affect the system performance, including beacon order (BO), backoff exponent (BE), contention window (CW), existence of hidden terminal problem, and existence of acknowledgement (ACK) mechanism. Understanding the impacts of these factors is of great importance in system design to improve performance. These impacts are examined numerically via network simulator (NS2) in the current work, which leads to some nontrivial findings.

## Performance Analysis of Unsaturated Slotted IEEE 802.15.4 Medium Access Layer

Shuai Fang<sup>1</sup>, Lu Rong<sup>2</sup>, Qiang Xu<sup>1</sup>, and Yang Du<sup>1</sup>

<sup>1</sup>The Electromagnetics Academy, Zhejiang University, Hangzhou 310058, China

<sup>2</sup>Shanghai Research Center for Wireless Communications, Shanghai 200050, China

**Abstract**— In this paper, we analyze the performance of unsaturated slotted medium access layer (MAC) as specified by the IEEE 802.15.4 standard. The analytical tool that we use to model the behavior of uplink transmission of a standard compliant device is the Markov chain model, a general framework that also used by some other researchers (e.g., Bianchi, Pollin, Misic). Yet we deviate from their approaches essentially in one way or another. We consider different types of traffic, including saturated and unsaturated, with the source process being Poisson. In the unsaturated case, the idle time is allowed to be random to reflect the realistic scenario. We discard the assumption about independent carrier sensing probabilities among devices, except for the first transmission attempt. When retransmission is required due to collision, there are conditions under which independence of carrier sensing may or may not hold. Such conditions are explicitly identified and incorporated in our model. The effect of beacon order (BO) is also included. Validity of our model is verified by good agreement between model predictions and numerical simulations via Network Simulation (NS2) of key model parameters and of system performance descriptors such as throughput.



# Energy-efficient Sleeping Schedule and Performance Analysis for IEEE 802.15.4 Device

Qiang Xu<sup>1</sup>, Lu Rong<sup>2</sup>, Shuai Fang<sup>1</sup>, and Yang Du<sup>1</sup>

<sup>1</sup>The Electromagnetics Academy, Zhejiang University, Hangzhou 310058, China

<sup>2</sup>Shanghai Research Center for Wireless Communications, Shanghai 200050, China

**Abstract**— Low-rate personal area network (LR-WPAN) specified by the IEEE 802.15.4 standards is characterized by low complexity, low cost and low power. It holds great potential in many fields, such as telemetry, patient monitoring, and industrial automated control. Yet one of the most important determining factors is the power consumption, since most standards compliant devices are believed to be battery-powered.

In this paper, we analyze power consumption of the sleep mode, specifically, the indirect mode in downlink transmission and the direct mode in uplink transmission. Analysis by other researchers and by our own indicates that overhearing presents a significant problem in energy waste and should be avoided. Yet unlike the case of IEEE 802.11 wireless local area network (WLAN) where RTS/CTS mechanism is specifically adopted to this end, LR-WPAN is designed to operate without RTS/CTS to reduce system complexity. To attack the overhearing problem, we propose a sleep mechanism in the backoff stage in uplink transmission. The efficiency of such mechanism is evaluated analytically using the system model that we have recently developed and is verified numerically via network simulator (NS2).

## SIP-based Mobility Management

Bing Zhao<sup>1</sup>, Lu Rong<sup>2</sup>, Peng Qiao<sup>1</sup>, and Yang Du<sup>1</sup>

<sup>1</sup>The Electromagnetics Academy, Zhejiang University, Hangzhou 310058, China

<sup>2</sup>Shanghai Research Center for Wireless Communications, Shanghai 200050, China

**Abstract**— The EU IST project My personal Adaptive Global NET (MAGNET) project aims at user-centric service provision, with an emphasis on personalisation, adaptation, interoperability, personal networking and interconnecting heterogeneous networks. It strives to provide users secure and seamless communications. Yet it is a challenging task to maintain a guaranteed QoS for all in-session traffic flows when a moving cluster of a personal network (PN) causes the micro- or macro-mobility handoff. The primary QoS parameters of concern are end-to-end packet delay and packet loss. The high data rate (HDR) services of MAGNET project to large degree belong to the QoS sensitive streaming multimedia traffic, thus require a handoff delay under 100 ms according to the ETSI QoS specification.

In this paper, we propose a handoff scheme that incorporates two mechanisms: 1) make-before-break to realize soft handoff; 2) SIP, since its operation is transparent to the underlying network, thus well suitable for interconnecting heterogeneous networks, and in the meanwhile it is heavily deployed in the 3GPP standards.

However, there are still other issues to be considered. For instance, in the old SIP handoff scheme, it will send a new INVITE to establish connection after obtaining the new IP address, which causes packet loss and considerable re-connection delay. To deal with this issue, we propose to use the INVITE/JOIN mechanism. The associated potential redundancy at both the mobile host (MH) and corresponding host (CH) is also well taken care of. Finally we present some numerical results to demonstrate the effectiveness of our approach.

## Numerical Study of MAC Scheduling Schemes for IEEE 802.15.3

Guangdi Yang<sup>1</sup>, Lu Rong<sup>2</sup>, Dingyuan Tu<sup>1</sup>, Rufeng Lin<sup>1</sup>, and Yang Du<sup>1</sup>

<sup>1</sup>The Electromagnetics Academy, Zhejiang University, Hangzhou 310058, China

<sup>2</sup>Shanghai Research Center for Wireless Communications, Shanghai 200050, China

**Abstract**— In this paper we examine the performance of a variety of HDR MAC scheduling schemes using numerical simulations, with a focus on channel aware schemes. The performance determinant factors, such as traffic characteristics, terminal mobility, and channel conditions, are included in this study in order to ensure the results more relevant to realistic wireless personal area network (WPAN) scenarios.

The scheduling algorithms under consideration are 1) SRPT; 2) the exponential rule (EXP); 3) the modified largest weighted delay first rule (M-LWDF); 4) the proportionally fair rule (PROP-FAIR); and 5) the maximum rate rule (MAX-RATE). We find that under good channel conditions and light network load, the EXP and M-LWDF algorithms tend to have better performance in terms of average throughput and job failure than others; on the other hand, under heavy traffic conditions, these two schedulers suffer from a drastic performance degradation, since none of them gives sufficient consideration for the cases of packet loss or timeout. SRPT rule appears to have the minimal system response time in this case. In addition, because of its non-preemptive characteristic, SRPT is fairly robust among these schedulers against adverse channel conditions and heavy traffic load. However, since SRPT prefers small packets to large ones, it is unsuitable for cases where large packets are important.

Our findings shed light on the features of the prevailing scheduling algorithms and their suitability in WPAN flow scheduling, and are useful in designing new scheduling algorithms.

## Throughput Analysis of Delayed Acknowledgement over 802.15.3 WPAN with Hybrid ARQ Retransmission

Rufeng Lin<sup>1</sup>, Lu Rong<sup>2</sup>, Qiang Xu<sup>1</sup>, and Yang Du<sup>1</sup>

<sup>1</sup>The Electromagnetics Academy, Zhejiang University, Hangzhou 310058, China

<sup>2</sup>Shanghai Research Center for Wireless Communications, Shanghai 200050, China

**Abstract**— Transmission of redundancy information is one of the main factors that limit the performance of High Data Rate (HDR) Wireless Personal Area Network (WPAN). In order to reduce redundancy information during transmission and to improve channel utilization, IEEE 802.15.3 standard defines Delayed-ACK (Dly-ACK) mechanism that acknowledges a burst of data frames by one ACK frame instead of acknowledging each data frame. However, effective deployment of the Dly-ACK mechanism is still an open issue.

In this paper, we propose to combine Dly-ACK with the Hybrid-ARQ (HARQ) retransmission scheme, and provide an analytical model for analyzing the system performance. The expression of throughput is derived as a function of payload length, data rate, BER, number of retransmissions of data frame and ACK frame, interval between frames, and burst size, etc. This model is useful in helping one to determine the optimal payload size for a given transmission setting and channel BER.

Our results show that based on the HARQ scheme, the optimal throughput is significantly higher than that with ARQ, and larger payload size is proposed to further improve the performance. The performance gain is even more evident with increasing BER.

# MIMO Channel Model and Its Impact on the Channel Capacity

Jun Wang, Quan Zhou, Wei Ma, and Lede Qiu

National Key Laboratory of Space Microwave Technology  
Xi'an Institute of Space Radio Technology, Xi'an 710100, China

**Abstract**— In order to study the impacts of array configuration and channel model parameters including antenna spacing and scattering angle on the channel capacity of an S-MIMO (Satellite Multiple Input Multiple Output) system, a novel method is proposed to explore the channel capacity under flat fading. A novel channel model is constructed based on the fading correlation matrix which depends on the array configuration. And then using the properties of Wishart distribution, closed-form expressions for the upper and lower bounds on the ergodic capacity of N by M MIMO system are presented in detail. The novel method also could be generalized to MIMO-OFDM systems with any number of transmit and receive antennas. Computer simulation results show that for small spacing the UCA yields higher channel capacity than ULA. The channel capacity is maximized when the antenna spacing increases to a certain point, and further more, the larger the scattering angle, the quicker the channel capacity converges to its maximum. And at high SNR, the upper and lower bounds on the ergodic capacity are close to its true value.

## The Influence of the Climatic Peculiarities on the Electromagnetic Waves Attenuation in the Baltic Sea Region

M. Zilinskas<sup>1,2</sup>, M. Tamosiunaite<sup>2,3</sup>, S. Tamosiunas<sup>2,3</sup>, and M. Tamosiuniene<sup>4</sup>

<sup>1</sup>Communications Regulatory Authority of the Republic of Lithuania

Department of Radio Communication, Algirdo 27, LT-03219 Vilnius, Lithuania

<sup>2</sup>Faculty of Physics, Vilnius University, Sauletekio 9, LT-10222 Vilnius, Lithuania

<sup>3</sup>Institute of Materials Science and Applied Research, Vilnius University  
Sauletekio 9, LT-10222 Vilnius, Lithuania

<sup>4</sup>Semiconductor Physics Institute, A. Gostauto 11, LT-01108 Vilnius, Lithuania

**Abstract**— It is very important to predict the electromagnetic waves attenuation due to the rain and the clouds when new wireless communication systems are planning. Most of the rain attenuation prediction methods require the knowledge of the values of the rain rates. Though there have been developed many models for determination of the electromagnetic waves attenuation due to the rain and the clouds in varied regions, the electromagnetic waves attenuation due to the rain and the clouds in the Baltic Sea area has been analyzed not enough. Lithuania, being in the transitional geography zone from the Baltic Sea climate to Atlantic and continentals East Europe climate, may be distinguished for its variable climate. This circumstance causes that the rain attenuation prediction methods are not always suitable for use in Baltic Sea area. The peculiarities of the climatic conditions in Lithuania are reviewed. The values of rain rates measured in the Lithuanian weather Stations with the 10-minutes integration time have been presented. According to the presented data, a relation between the rain rate and the annual precipitation has been derived. The model for one-minute rain rate calculations on the months starting from May up to September in Lithuania has been presented. The values of the electromagnetic waves attenuation due to the rain have been determined by using the known relation and the values of rain rates obtained by using the model mentioned above.

The methods for calculation of the specific cloud attenuation have been reviewed. The semi empirical method for determination of the cloud attenuation has been used. The cloud attenuation has been computed by using the meteorological data measured at the ground level. The suitable to the Lithuanian climatic conditions relation between temperature and height above the ground level was chosen when the latitude of the locality and the average daily temperature were considered. The values of the relative humidity and the temperature have been used in calculation of the values of water content in the cloud. The values of the specific attenuation under conditions of cloud cover have been determined.

Concluding it may be pointed, that there is a need to take into account the peculiarities of the Baltic Sea region climate when determining the values of the specific rain attenuation in this region. The model for cloud attenuation is very practical because it requires only the meteorological factors measured at the ground level.

## Outdoor Exposure to the RF-radiation of WiFi for Wireless City Applications

Gilbert Decat, Meynen Guy, and Daniel Wilczek  
VITO, Boeretang 200, BE 2400 Mol, Belgium

**Abstract**— When we think about wifi (wireless fidelity) applications we tend to think about wireless PC- indoor only and less about wireless outdoor city applications where the wifi technology is used for the communication between the assess points (AP) and the personal digital assistant (PDA) for managing a maximum of commercial and other city related applications.

Because a so called wireless city can be seen as a city with a network containing a substantial amount of wifi-AP's, one expects that the general public is exposed to an amount of RF-radiation from which nor the magnitude of the exposure neither the risks of the exposure are known. Therefore, and since Belgium is one the world leaders in this domain via the i-City research lab, we were assessing the up- and downlink exposure of the general public to the RF-radiation when using this application.

The RF-signal and the magnitude of the signal of about 30 AP's were analyzed and measured in 30 different streets by means of two adequate spectrometers (Fieldcop and Narda SRM 3000). The E-field (V/m) which is a measure of the RF-exposure strength was measured in up- and downlink and the spatial distribution of the E-field was defined following a well-designed cubic grid system. In each point the rms and the peak value of the E-field were measured: while the rms was averaged over 6 minutes the hold peak value was equal to the maximum E-field measured over a 6 minutes' period.

From the first results of the analyses there is a tendency to conclude that the magnitude of the E-field the user of the wireless city PDA is exposed to is weak with respect to the national and international exposure limits and that people passing inactivated AP's are exposed to a negligible E-field strength. It has to be noted that this is a conclusive trend based on the analyses of only 1 AP. The results and conclusions of the complete AP sample (30 units) will be presented more extendedly in the full-length paper.

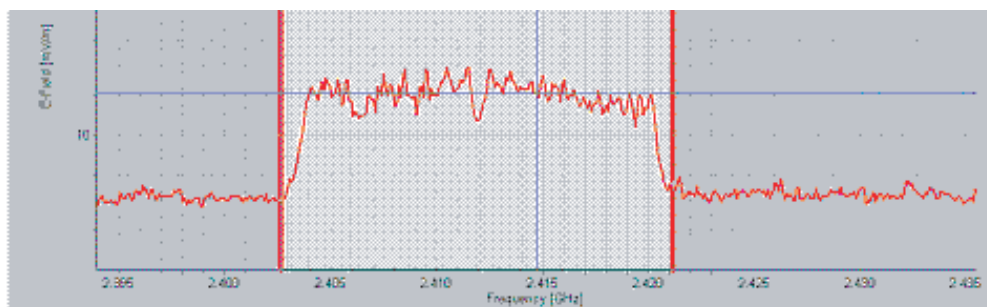


Figure 1: E-field (mV/m) of wifi AP.

## OFDM System Location Determination with 4-element Antenna Array Using Frequency Domain Matrix Pencil (FDMP) Method

Mohamed A. Labib and Hassan M. Elkamchouchi

Department of Electrical Engineering, Alexandria University, Alexandria, Egypt

**Abstract**— A 3D location determination method using only four elements antenna is proposed for Orthogonal Frequency Division Multiplexing (OFDM) systems which are commonly used in the Fourth Generation (4G). A group of frequencies is received from the transmitter (on mobile phone) or returned signals (Radar). The Matrix Pencil method is used to identify the length of each path. Depending on the geometrical distribution of the four elements, the phase shifts are determined for each path. Knowing the phase shift between the elements helps to find the Direction of Arrival (DOA) for each path. Small dipole antennas are used in the numerical examples to clarify this location determination method in the presence of complex noise in the OFDM systems.



## WCDMA 3D Location Determination with 3D Polarization Using Four 3-element Arrays

Mohamed A. Labib and Hassan M. Elkamchouchi

Department of Electrical Engineering, Alexandria University, Alexandria, Egypt

**Abstract**— A 3D location determination method uses only four 3-element arrays, each 3-element array consists of three orthogonal dipoles to achieve the vertical, horizontal and orthogonal one to both of them. The non line-of-sight path would change the polarization at the receiver which can affect the quality and the strength of the received signal. This method is proposed for WCDMA mobile systems which are commonly used in the third generation (3G). The receiver RAKE is used to identify the multipath and the time delay between the elements for each polarization state. Depending on the geometrical distribution of the four arrays, the phase shifts are determined for each path. Knowing the phase shift between the elements helps to find the Direction of Arrival (DOA) for each path. The path distance is determined via the traveling time of the message response between the transmitter and the receiver. The received signals of the antenna elements are combined on the Maximum Ratio Combining (MRC) for signal maximization also.

## Location Determination for 2G/3G/4G Using Time Delay Matrix Pencil (TDMP) Method

Mohamed A. Labib and Hassan M. Elkamchouchi

Department of Electrical Engineering, Alexandria University, Alexandria, Egypt

**Abstract**— A 3D location determination method using only four elements antenna is proposed depending on a Time Delay Matrix Pencil (TDMP) method. A group of signal symbols in time variant domain is received from the transmitter (on mobile phone 2G/3G/4G) or returned signals (Radar), then transferred to the frequency domain using FFT. The Matrix Pencil method is applied to identify the length of each path. Depending on the geometrical distribution of the four elements, the phase shifts are determined for each path. Knowing the phase shift between the elements helps to find the Direction of Arrival (DOA) for each path. Small dipole antennas are used in the numerical examples to clarify this location determination method in the presence of complex noise for GSM, WCDMA and OFDM systems.

## To the Glory of J. F. Maxwell: Electromagnetic Theory of the Origin of Saturn's Rings

Vladimir V. Tchernyi

SAIBR, Vavilova St., 97. Fl. 14, of. 35, Moscow 117335, Russia

**Abstract**— The reason for the coming into being and stable existence of the rings of Saturn has been a mystery and an unsolved scientific problem for 400 years. In 1859 Maxwell deduced that the rings consisted of solid and separate particles. Further experiments proved that the ring particles contain frozen water with inclusions of ammonia, methane, sulphuric and organic compounds, ferrosilicates and other substances. The particles of the rings move as they should according to Kepler laws. Gravitation force compensated by centrifugal force for any particle.

Numerous attempts to explain the origin of the rings with the use of notions about gravitation, particles' interaction with solar wind or emergence from dust plasma have not been successful. Moreover, the existing theories of the rings are characteristically heterogeneous and not united by a single physical nature of their origin. But most importantly they cannot explain a multitude of the phenomena observed. A paradoxical situation has taken shape, where, with the exception of a huge database on the properties of the rings, excellent photographs and radar data obtained by means of expensive devices on board the space probes, no full-value physical picture of the rings of Saturn existed till today.

According to the new understanding, the rings of Saturn took shape from superconductive ice particles of the protoplanetary cloud that initially surrounded Saturn. After the magnetic field of Saturn came into being the superconductive particles of the protoplanetary cloud began drifting to the plane of the magnetic equator, which as a result led exactly to the formation of the highly flattened disk around Saturn. Similar to magnetic particles creating dense and rarefied areas in a nonuniform magnetic field the superconductive ice particles also form their groups, which from outside look like a system of rings. The superconductivity of the ring particles is confirmed by the fact that the ring particles are relics of the early days of the Solar system and were never subject to coalescence and heating. The superconductive particles cannot stick together as the magnetic field emanates from them and pushes the particles apart. Indeed, the Sun heats the rings weakly, the temperature in area of the rings being only around one hundred degrees above the absolute zero. And high-temperature superconductivity discovered in 1986 can already be observed under such temperatures, and in the same 1986 experimentally demonstrated superconductivity of ice.

The discovery of the superconductivity of the matter of the ring particles allows to explain many experimental data on land-based and space research of Saturn: how the rings came into being, how they were grouped into the disk; why the ring particles do not get mixed; why the microwaves of the circular polarization are reflected from the ring as if from a magnetic mirror; why the magnetic field is pushed out from the rings; why the spokes take shape; why non-polarized electromagnetic radiation ranging from kilohertz to megahertz emerges; where from some kind of an atmosphere appears near the rings; how density waves and bended waves take shape; why earth type planet does not have a rings, and a lot more.

### REFERENCES

1. Tchernyi, V. V. and A. Yu. Pospelov, "About hypothesis of the superconducting origin of the Saturn's rings," *Astrophysics and Space Science*, Vol. 307, No. 4, 347–356, Springer, 2007.
2. Tchernyi, V. V. and A. Yu. Pospelov, "Possible electromagnetic nature of the Saturn's rings: superconductivity and magnetic levitation," *Progress In Electromagnetic Research (PIER)*, Vol. 52, 277–299, Cambridge, MIT, MA, 2005.
3. Tchernyi, V. V. and E. V. Chensky, "Movements of the protoplanetary superconducting particles in the magnetic field of Saturn lead to the origin of rings," *IEEE Geoscience and Remote Sensing Letters*, Vol. 2, No. 4, 445–446, 2005, Corrections: Vol. 3, No. 2, 2006.

## Analyses on Frequency Dependence of Permeability and Power Loss for NiZn Ferrites

Hua Su, Huaiwu Zhang, Xiaoli Tang, and Zhiyong Zhong

State Key Laboratory of Electronic Thin Films and Integrated Devices

University of Electronic Science and Technology of China

Chengdu 610054, China

**Abstract**— Microstructures and magnetic properties of NiZn ferrite are very sensitive to the preparation technics. This paper focuses its discussion on microstructures, frequency dependence of permeability and power loss for NiZn samples sintered at different temperatures. It was found with increasing sintering temperature, average grain size increased monotonously. However, initial permeability first increased, then decreased slightly. This result was attributed to simultaneous influences of grain size and closed pores in grains. When average grain size enhancing too much, the frequency stability of permeability became worse, which was attributed to low-frequency- resonance induced by big grain size. The sample with large grain size and closed pores could obtain lower  $P_{cv}$  (power loss) when excited under large flux density. This fact was attributed to that the closed pores were not easy to block domain wall movement and grain boundaries became the predominant domain wall pinning factor. However, for the low induction condition, the closed pores in grain size reduced the distance between pinned edges and easily blocked domain wall movement, so the sample with small grain size had lower  $P_{cv}$ . With increasing testing frequency, sample with small grain size had better performance on  $P_{cv}$ . This result was explained in terms of the influences of  $P_e$  (eddy current loss) and  $P_r$  (residual loss) to  $P_{cv}$ .

## Strip Casting of Immiscible Alloys in a Static Magnetic Field

H. L. Li and J. Z. Zhao

Institute of Metal Research, CAS. 72 Wenhua Road, Shenyang 110016, China

**Abstract**— The solidification behavior of the alloys with a miscibility gap in the liquid state (immiscible alloys) has gained great interest scientifically in recent years. It has been indicated the strip casting, especially the strip casting in a static magnetic field, has great potentials in the manufacturing of this kind of alloys. In order to understand the microstructure formation mechanism, strip casting experiments were carried out with Al-Pb alloys in the constant magnetic field. The solidification microstructure was analyzed. It is indicated the application of the magnetic field is favorable for the obtaining of the immiscible alloys with a well dispersed microstructure. A model has been developed by taking into account the common action of the nucleation, the diffusional growth, the spatial motions of the minority phase droplets and the convections of the matrix liquid to describe the microstructure evolution in an immiscible alloy strip cast in a magnetic field. Calculations have been performed according to the practical experimental conditions to investigate the microstructure formation process. It has been shown that an undercooled region appears in front of the solid/liquid interface and the liquid-liquid decomposition takes place there. If the solidification velocity is high enough, a steady state of solidification can be established and a fine dispersion of Pb-particles in the Aluminium matrix can be obtained. A static magnetic field can lower down the convections of the matrix liquid and is, therefore, favorable for the obtaining of a well dispersed microstructure of immiscible alloys.

## Two Different Sets of Integral Equations for Modeling Electromagnetic Scattering from Arbitrary Concave Perfectly Conducting Objects

Jia-Jun Niu, Bin Yuan, and Yu Rong

Department of Electronic Engineering, Shanghai Jiao Tong University, Shanghai, China

**Abstract**— This paper discusses two different sets of integral equations for Modeling Scattering from Arbitrary Concave Objects such as both the inner and outer walls of cavities. These two sets of integral equations are derived first using the equivalence theorem and then the property is shown that these two sets of integral equations are respectively suitable for solving in direct moment methods and in hybrid iterative method. After implementation of both sets of integral equations for solving scattering problem of arbitrary three-dimensional cavities including inner and outer walls, numerical results are given to show the correctness and numerical behavior of these two sets of integral equations.

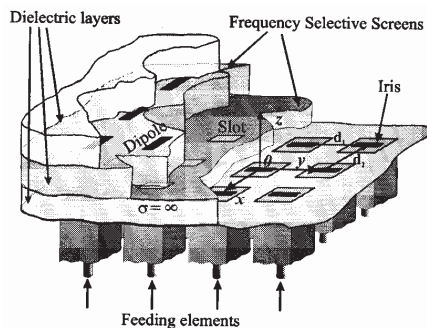
## A Hybrid GAM/SM-AIM Formulation for Quasi-planar Structures above a Planar Aperture Array

N. Truschi, A. Di Maria, and A. Freni

Dept. of Electronics and Telecommunications, University of Florence  
Via di S. Marta 3, Florence, Italy

**Abstract**— To increase the performance of a planar array of slots, apertures and/or stepped horns, we can place a periodic or an aperiodic metallic structure just above them. When the structure is periodic, it usually acts as a frequency and/or polarization filter, which can be located both in the far or the near field of the array. In the former case, we generally speak of frequency selective surface or dichroic filters, and we can analyze the electromagnetic interaction by considering one or just a few homogeneous plane waves impinging on the periodic structure. Since the excitation and the geometry of the scatterer are periodic, a periodic Green's function can be used, and the structure can be analyzed by considering only a basic cell. Conversely, when the structure is located close to the array, the excitation cannot be considered periodic, and a more complex analysis is required. An aperiodic structure can act as a lens that shapes the beam or reduce the side lobes. It can also be used when two or more antennas operating at different frequencies have to share a common aperture in a space-limited environment: superimposed dichroic microstrip antenna arrays [1] are a typical example of this structure. Furthermore, when we consider an array of cavities radiating on a conducting screen, an improved illumination and an increase in directivity can be obtained by using the aperiodic structure as a partially reflecting sheet in front of the antenna array, parallel to the conducting screen.

If we are interested in aperiodic structures located close to the array, a numerical analysis is necessary. However, since the aperiodic structure is usually large in terms of wavelength, the direct application of the classical Method of Moments (MoM) is inadmissible due to the prohibitive requirement of computation resources. In this communication we present a hybrid technique, called quasi-Planar Structure above a Planar Aperture Array (qPS-PA<sup>2</sup>), that allows the full-wave analysis of finite quasi-planar structures of electrically large dimensions located nearby a planar array of apertures. The technique combines the generalized admittance method (GAM) and the sparse matrix/adaptive integral method (SM/AIM). The former formulation results very efficient for the analysis of array of slots/apertures and their feeding network while the latter is an *ad hoc* version of the AIM developed for the analysis of very large quasi-planar 3D microstrip structures. Given its specialized use in the analysis of quasi-planar structures, however, the SM/AIM method appears efficient also in the case of not very extended structures. The quasi-planar structure can have arbitrary shape, and is modeled using sub-domain triangular patch basis functions. The overall method numerical complexity results  $O(N \log N)$  while the memory requirement  $O(N)$ . Furthermore, the formulation allows us to obtain the radiation characteristics of the array with and without the presence of the quasi-planar structure simultaneously, maintaining the description of the field on the radiating aperture in terms of waveguide modes. This makes it consistent with pre-existing tools based on GSM or GAM methods, developed for the analysis of guiding structures.



### REFERENCES

1. James, J. R., et al., *IEE Proc.*, Vol. H-135, 5, 304–312, 1988.

# Electrical Transport in Manganite Structures: The Random Fuse Network Study

Jian-Chun Wu, Hua Sun, Hai-Xia Da, and Zhen-Ya Li

Key Laboratory of thin films in Jiangsu Province

Department of Physics, Suzhou University

Suzhou 215006, China

**Abstract**— Manganites with the perovskite-type structure have attracted many interest in this decade. Very recently, many anomalous electrical transport effects, such as negative differential resistance (NDR) multisteps, current oscillations, et al., have been reported in these inhomogeneous structures and the Joule heating effect has been regarded as the critical factor to induce these impressive effects.

In our work, a random fuse network model is proposed to study the anomalous electrical transport characteristics due to local Joule heating-induced metal-insulator transition in manganite structures. We focus on the size effects observed in spatially confined manganite structures and the interesting time-dependence due to the self-heating effect. We show that fuses are broken gradually rather than collapse at once by analyzing the sequence of external voltages that induce failure in the hottest fuse in a random fuse network with strong conductance fluctuation. With the increasing of the applied voltage, negative differential resistance (NDR) multisteps are reproduced and the corresponding evolution of current morphology with fuses broken gradually is present. Simulations results for the networks with various size show that confined geometry will sharpen the steplike NDR response in current-voltage curves. Considering the small thermal conductance in such inhomogeneous structures, the bonds may be annihilated (fuse broken) and created (fuse revived) alternatively due to the competition between heating and dissipating and a non-vanishing breaking/reviving time may lead to the history-dependence of the resistivity state. The oscillation frequency depends on material parameters such as thermal conductance as well as the environments.



## A Hybrid Iterative Method for Computing Electromagnetic Scattering of Large Perfectly Conducting Cavities

Jia-Jun Niu, Bin Yuan, and Yu Rong

Department of Electronic Engineering, Shanghai Jiao Tong University, China

**Abstract**— A hybrid iterative method (HIM) is developed for analyzing scattering from electrically large perfect conducting cavities. The HIM uses the combination of Kirchhoff's approximation and the first-order scattering as sources to initiate the inner iterative process involving only the magnetic field integral equation (MFIE) for currents on the interior cavity walls. After several inner iterations, the outer iteration involving both the electric field integral equation (EFIE) and the MFIE is performed once in which the sources at the aperture are updated with new scattering fields to initiate next inner iterative process. The iterative process continues until an appropriate convergence criterion has been achieved. Compared with two similar current-based iterative methods, iterative physical optics (IPO) method and field iterative method (FIM), the HIM has remarkable advantages in memory requirement and the number of iterations demanded for convergence. Numerical results are presented which demonstrate the convergence and accuracy of the HIM by comparison with results from methods of moment (MM), IPO and FIM.

# Inward-outward Hybrid Iterative Method for Analyzing Electromagnetic Scattering by Complex Perfectly Conducting Objects including Large Cavities

Jia-Jun Niu, Bin Yuan, and Rong Yu

Department of Electronic Engineering, Shanghai Jiao Tong University, Shanghai, China

**Abstract**— An inward-outward iteration process is combined with the hybrid iterative method (HIM) to analyze the scattering by complex perfectly conducting objects including large cavities. The HIM is originally designed for computing the scattered fields from the interior of large cavities regardless of the contribution from external surface and other exterior complex parts. With the help of inward-outward iteration process in which the whole space is divided into two regions, the interior and exterior of the large cavity, two coupled iterative processes are performed sequentially. In the interior region, the original HIM is used to compute the fields at the aperture which are regarded as the sources in the exterior region. As long as the artificial sources are known, the hybrid EFIE-MFIE (HEM) method is used to compute the fields outside the cavity which may update the fields at the aperture used as the sources for the HIM to initiate a new iterative process. This inward-outward iterative process continues until an appropriate convergence criterion has been achieved. This inward-outward HIM (IOHIM) may be considered as a combination of the HIM and traditional current-based hybrid methods. Numerical results are given and indicate that IOHIM calculations are in reasonable agreement with moment method (MM) calculations, while far less computation time and memory are required.

## Technique for Detecting Chirp in Femtosecond Pulse by Autocorrelator

Yan Ling and Fang Lu

Surface Physics Laboratory, Laboratory of Advanced Materials, Physics Department  
Fudan University, Shanghai 200433, China

**Abstract**— We introduce a new method for detecting chirp in femtosecond pulse by autocorrelator. The chirp in femtosecond pulse is another characteristic other than the profile, the duration and frequency. While it is relatively more often to give attention to others, measuring the chirp is more complicated and given less attention. The setup for the measurement is the same as that used for Measurements of femtosecond pulse temporal profile by means of Michelson interferometer with Schottky junction [1]. The interference of two pulses is employed rather than the Second Harmonic Generation (SHG) with an autocorrelator. Usually the measurements of femtosecond pulse is realized by an interferometer in combination with a nonlinear optical material, while the measurement described in this paper is realized by means of a Michelson interferometer with Schottky junction. Only a metal-semiconductor (MS) junction (Schottky junction) is needed, and neither the nonlinear optical material nor a photo-detector is included. When the pulse has chirp, the signal inner oscillations when the two pulse at superposition and at partly superposition are different. By fitting from the experimental result, the pulse chirp degree can be got easily. This technique can used for pulse at kinds of durations and frequencies, and is a complementarity for the technique described in Ref. 1, to measure the characteristics of femtosecond pulse.

### REFERENCES

1. Ling, Y. and F. Lu, "Measurements of femtosecond pulse temporal profile by means of a Michelson interferometer with a Schottky junction," *Appl. Opt.*, Vol. 45, 9087–9091, 2006.

## 3D Microwave Module Interconnect Using Fuzz Button

Lei Xia, Ruimin Xu, and Bo Yan

School of Electronic Engineering

University of Electronic Science and Technology of China, Chengdu, China

**Abstract**— 3D stacking packaging could provide improved performance of the system that cannot be achieved using conventional 2-D packaging technologies. Fuzz button is fabricated by randomly wound wire approximately 0.5 mm diameter inserted into an organic carrier to form a coaxial-like structure. It is one of the most commonly solder-less connection in microwave modules, and it works excellent at severe vibration environment without being damaged while maintaining a good connection and allowing easy rework.

This paper presents general face to face 3D vertical interconnect structure using fuzz buttons, improving its performance by inductor and capacitor compensation. The stack of two substrates realized with a rectangular metal frame separating them. Three fuzz buttons hold together by a dielectric that enables vertical interconnection between conductor backed coplanar waveguide on two adjacent modules, the dielectric embedded in a frame which supporting the two modules. According to vertical interconnect equivalent circuit, the vertical interconnect can be equivalent as a low pass filter. The value of the filter components can be calculated by parameter extracting, and then obtain equivalent characteristic impedance. The equivalent characteristic impedance less than  $50\ \Omega$ , so the inductor and capacitor compensation is needed to attain better matching, the matching can be improved by changing the CPW line or its ground. The bandwidth of the vertical interconnect extended with the improving of impedance match. To demonstrate abovementioned, a microwave vertical interconnect manufactured by RF60A substrate, test results show better performance at X-band.

# Design and Analysis of Quad-band PCB Embedded Antenna for Mobile Handset Applications

Soon-Ho Hwang, Kyu-Bok Park, and Joon-Ho Byun

Telecommunication R & D Center, Samsung Electronics Co., LTD, Republic of Korea

**Abstract**— In recent years, mobile handsets have been not only becoming smaller and slimmer but also covering multiple service bands to satisfy with user's requirement. Because of reduced mobile handsets, its antenna is also needed to be miniaturized simultaneously having good operations. The Planar Inverted F Antenna(PIFA) is mostly used in small mobile handsets due to its attractive features of compact size and good performance. Furthermore, the PCB embedded antenna is very useful in slim mobile handsets, due to low profile, low manufacturing cost, and easy fabrication.

In this paper, the proposed antenna is a PIFA and PCB embedded type. This covers GSM(890–960 MHz), PCS(1850–1990 MHz), GPS(1575 MHz), and Bluetooth(2400–2480 MHz) bands. This antenna is designed for commercial mobile phone. The size of antenna part and total dimension is  $32 \times 14 \text{ mm}^2$  and  $40 \times 80 \text{ mm}^2$ , respectively. The substrate is a FR4 whose permittivity is 4.4. Figure 1 and 2 are a geometry and VSWR of the proposed antenna. Through the meandered radiating element, this proposed antenna whose slits and lengths are optimized resonates at 4 service bands. Each meandered line has an electrical length of each service band. This proposed antenna is very suitable for small and slim mobile handset. Further study is going to be considered in special cases which are under effects of plastic case, hand, and head related to SAR.

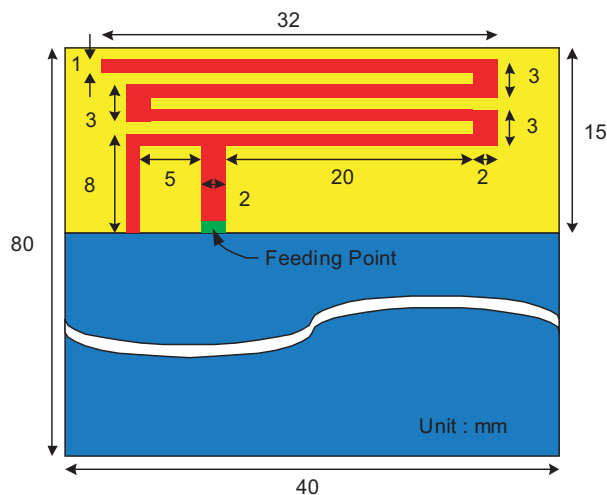


Figure 1: Geometry of the proposed antenna.

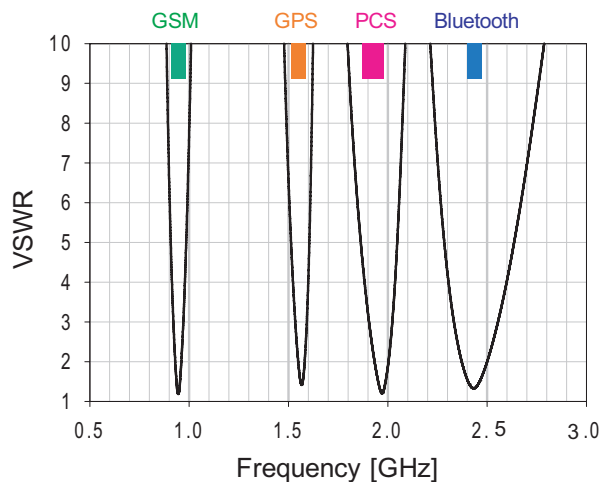


Figure 2: VSWR of each service band.

## REFERENCES

1. Wong, K., "Planar antennas for wireless communications," John Wiley and Sons, New York, 2003.
2. Gao, Y. and X. Chen, "Study of a miniature PIFA," *APMC 2005*, Vol. 4, Dec. 2005.
3. Ansoft HFSS.

# Reconfigurable Stacked Patch Antenna for Wireless Power Beaming and Data Telemetry

Guangli Yang

Antenna Technology Center of Excellence, MDb, Motorola Inc.

Libertyville, IL 60048, USA

**Abstract**— Hundreds of years ago, humanity has dreamed of converting the solar energy to electricity, this is infeasible until rectifying antenna, or rectenna, is developed for wireless power transmission. The history of using rectenna can be trace back to 100 years ago when Tesla successfully lighted two light bulbs from uncollimated radiated energy formed from oscillators operating up to 100 MV at 150 KHz. Wireless power transmission was studied in the 1920s and became a reality with the development of high-power high-efficiency microwave tubes by the Raytheon Company, Waltham, MA, in the 1950s [85]. Since then, researchers have developed many kinds of rectennas in various frequencies from MHz to GHz.

In this paper a reconfigurable stacked patch rectenna is introduced for possible wireless power beaming and data telemetry application. The proposed antenna operates at 5.8 GHz with 9.5 dBi gain and 7.6% bandwidth. At a lower frequency 2.45 GHz the antenna operates as a planar inverted-F antenna (PIFA) with 3.3 dBi gain and 2.2% bandwidth. Switching between the two regimes of operation is achieved using PIN diodes. It is proposed that the antenna can be used for wireless power reception in sensors at 5.8 GHz and for data telemetry in between sensors or a sensor and a control station at 2.45 GHz. The wireless power reception ability of this antenna was tested by applying a high efficiency schottky diode rectifying circuit with the RF-to-dc conversion efficiency of 70% for an input power density level of  $1 \text{ mW/cm}^2$  and a load resistance of  $200 \Omega$ .

## An High Gain Omni-directional Planar Array Antenna

**Y. B. Shang, T. Zhang, Y. C. Jiao, and F. S. Zhang**  
National Laboratory of Antennas and Microwave Technology  
Xidian University, Xi'an 710071, China

**Abstract**— An novel planar array antenna is proposed in this paper. Prototype of the proposed antenna have been constructed and tested. The experimental results show that the antenna can good omni-directional radiations in the desired frequency bands have been achieved. The proposed antenna with relatively low profile is suitable for wireless applications.

## Analysis of Technical Conditions for Sharing Frequency Spectrum

**Taekjin Hwang**

Electronics and Telecommunication Research Institute, Korea

**Abstract**— A frequency sharing technique is necessary for using the limited frequency resources efficiently. In this paper we study the condition for sharing frequency bands in two cases. One is the case that the frequency band is already allocated to the specific communication. The other is the case of allocating the new frequency bands to communication systems having interference avoiding techniques. For each case we investigate the conditions for sharing frequency bands and the suggestions for that are presented in this paper.



## Dynamic Sector Synthesis of Antenna Array Using Genetic Algorithm

Abdelaziz A. Abdelaziz<sup>1</sup> and Hanan A. Kamal<sup>2</sup>

<sup>1</sup>Faculty of Engineering, Misr International University (MIU), Cairo, Egypt

<sup>2</sup>Faculty of Engineering, Cairo University, Giza, Egypt

**Abstract**— This paper introduces a new application of genetic algorithm (GA) in dynamic sector synthesis of antenna array for mobile base transceiver station (BTS). The basic objective is to have narrow beam widths in heavy handoff areas and wider beam widths in areas with low traffic density. By predefining the beam widths and thus the beams of each sector, optimal sectoring can be achieved using GA at different time of the day as traffic changes. The proposed algorithm consists of the simple GA with new adaptive mutation mechanism. When compared with simple GA, the proposed algorithm shows faster convergence. The results obtained are more stable and having higher fitness.

## Mie Particles and Quasiparticles in Ag Thin Films

M. Gnanavel<sup>1</sup>, D. Bharathi Mohan<sup>2</sup>, and C. S. Sunandana<sup>1</sup>

<sup>1</sup>School of Physics, University of Hyderabad, Hyderabad 500 046, India

<sup>2</sup>Department of Mechanical Engineering, University of Coimbra, Coimbra, Portugal

**Abstract**— Thin films (2 nm–100 nm thick) of Ag obtained from vacuum thermal evaporation exhibit thickness-dependent optical transmission characteristic of a variety of nano scale structures. While ultrathin films (< 10 nm) give evidence of Mie particles [1,2] thicker films exhibit red-shifted plasmon resonances that transform from surface-to-volume resonance. Partially iodized Ag films exhibit an interesting plasmon-exciton ‘transition’ [3]. These results could be understood from the perspective of surface thermodynamics of the metallic nanostructures.

### REFERENCES

1. Bharathi Mohan, D. and C. S. Sunandana, *J. Appl. Phys.*, Vol. 100, 064314, 2006.
2. Bharathi Mohan, D. and C. S. Sunandana, *Physics Chemistry and Applications of Nanostructures (Nanomeeting 2007)*, Eds. V. E. Borisenko, S. V. Gopananko and V. S. Gurin, World Scientific, New Jersey.
3. Bharathi Mohan, D., K. Sreejith, and C. S. Sunandana, *Appl. Phys. B*, Vol. 89, 59–63, 2007.

## Surface Plasmon Polaritons in Dual-sided Corrugated Metal Films

Xin Wu, Z. J. Zhang, R. W. Peng, J. S. Zhang, J. Li  
K. Wei, De Li, and R. L. Zhang

National Laboratory of Solid State Microstructures and Department of Physics  
Nanjing University, Nanjing 210093, China

**Abstract**— In recent years, there has been great interests in the study of subwavelength surface plasmon polariton optics. The surface plasmon polariton (SPP) is a surface electromagnetic wave localized at the interface between dielectric and metallic materials. By altering the periodic structure of metallic films, the electromagnetic field can be periodically modulated. In this work, we investigate the SPPs and their effect on optical properties in dual-sided corrugated metal films. Based on Rayleigh hypothesis, infinite hierarchy of coupled amplitude equations are deduced to describe the propagation of electromagnetic waves in this system. It is shown that when the wave vector of incident light matches the SPP at the interface, SPPs will be excited. If the metallic film is thin enough, the SPP on two interfaces will interact each other via evanescent wave. The interaction of SPPs makes the surface modes splitting to be the symmetric mode and the asymmetric mode, respectively. The interaction of SPPs depends on the interfacial geometry of the metallic film. We consider two kinds of interfacial cases, i.e., the symmetric profile film and asymmetric profile film. The dispersion curve and the field distribution of SPPs are calculated in both cases. It is shown that the dispersion relation can be tuned by the geometry of the metallic film, including the thickness of the film, the period and the amplitude of the corrugation in the metallic film. Furthermore, it is demonstrated that when the SPP is excited, electromagnetic field is enhanced dramatically at corresponding frequency of incident light, which may achieve potential applications on near-field optical devices.

### ACKNOWLEDGMENT

This work is supported by the grant from National Natural Science Foundation of China.

# On The Concept of Vector (Polarization) Electromagnetic Inverse Boundary Conditions for the Perfectly and Imperfectly Conducting Cases and Its Applications: Why Is Renewed Interest in EM-IBC Forthcoming?

Wolfgang-Martin Boerner

UIC-ECE Communications, Sensing and Navigation Laboratory  
900 W. Taylor St., SEL (607) W-4210, M/C 154, Chicago, IL 60607-7018, USA

**Abstract**— The inverse problem of electromagnetic scattering pertains to the problem of recovering the size, shape, material surface and interior constituents of an unknown scatterer, given the incident and the scattered fields every where, together with the laws governing the interaction. In the direct problems of scattering and diffraction, the electric size, the shape and the material surface and interior constituents are known *a priori* together with the pre-specified incident field in terms of a computational coordinate system so that their unknown vector electric and vector magnetic fields can be derived from Maxwell's equations by incorporating the known parameters into the boundary conditions which are well established. In contrary, in the inverse problem such local boundary conditions must be sought which *in particular* do not depend on either the size, shape or the surface normal and material properties of the scattering body and its enclosing surface, but must allow to specify these parameters uniquely from the recovered near fields. Here two separate cases are considered, a perfectly and an imperfectly conducting closed-shaped smooth body for which the total complex vector electric fields  $\mathbf{E} = \mathbf{E}^{inc} + \mathbf{E}^{scat}$  and  $\mathbf{H} = \mathbf{H}^{inc} + \mathbf{H}^{scat}$  are assumed to be given everywhere and expressed in terms of a computational coordinate system, where for a

1. Perfectly conducting closed-shaped, convex and smooth body, the following inverse boundary conditions hold

$$\mathbf{E}\mathbf{H} = 0 \quad \text{and} \quad |\mathbf{E}^{inc}| = |\mathbf{E}^{scat}| \quad \text{necessary and sufficient} \quad (1)$$

$$\mathbf{E} \times \mathbf{E}^* = 0 \quad \text{necessary and not locally sufficient} \quad (2)$$

2. Imperfectly conducting closed-shaped, convex and smooth body, for which the following inverse boundary conditions are derived from the Leontovich direct boundary condition

$$\mathbf{E} \times \mathbf{n} = \eta \mathbf{n} \times (\mathbf{H} \times \mathbf{n}) \quad (3)$$

where  $\hat{\mathbf{n}}$  denotes outward local surface normal,  $\eta$  defines the local normal Leontovich surface impedance. By inverting this Equation (3), two characteristic orthogonal vector quantities, A and B, are obtained which are tangential to the local surface and independent of its local normal

$$\mathbf{A} = \mathbf{E} \times \mathbf{E}^* - \eta \eta^* \mathbf{H} \times \mathbf{H}^* \quad \text{and} \quad \mathbf{B} = \eta \mathbf{E}^* \times \mathbf{H} - \eta^* \mathbf{E} \times \mathbf{H}^* \quad (4)$$

Satisfying the following three necessary but not locally yet globally sufficient conditions

$$\mathbf{A}\mathbf{B} = 0 \quad \text{orthogonality condition} \quad (5a)$$

$$A^2 = B^2 \quad \text{normality condition} \quad (5b)$$

$$\hat{\mathbf{n}}\mathbf{A} = 0 \quad \text{and} \quad \hat{\mathbf{n}}\mathbf{B} = 0 \quad \text{tangentiality condition} \quad (5c)$$

These two sets of boundary conditions are tested for the case of cylinders and spheres of different radii and for two slightly different frequencies for verifying that these conditions are indeed satisfied for (i) the perfectly conducting and (ii) the imperfectly conducting cases explaining why these conditions are exact, and why all of these conditions are necessary but some of the conditions are not locally but only globally sufficient.

Although attempts had been made soon after these vector inverse electromagnetic boundary conditions were first discovered forty years ago, verifying them with experimental data was not possible at that time due to the lack of measurement capabilities and accuracy. However, within the past decade this has changed and sufficiently accurate measurement data for near and far field measurements are now becoming available for testing them which is of considerable relevance to non-destructive material testing and also for advancing vector electromagnetic inverse scattering theory and techniques.

**REFERENCES**

1. Boerner, W.-M. (V. H. Weston), "A bistatic electromagnetic inverse scattering technique," *Can. J. Physics*, Vol. 47, No. 11, 1177–1184, 1969.
2. Boerner, W.-M. and H. P. S. Ahluwalia, "On a continuous wave electromagnetic inverse boundary condition," *Canadian Journal of Physics*, Vol. 50, No. 23, 3023–3061, 1972.
3. Boerner, W.-M. (H. P. S. Ahluwalia), "Application of a set of electromagnetic inverse boundary conditions to the profile characteristics inversion of imperfectly conducting cylindrical shapes," *IEEE Trans.*, Vol. AP 21, No. 5, 663–672, 1973.
4. Boerner, W.-M. (H. P. S. Ahluwalia), "Profile characteristics inversion of spherical shapes," *IEEE Trans.*, Vol. AP 22, No. 5, 673–682, 1974.
5. Boerner, W.-M. and O. A. Aboul-Atta, "On the concept of electromagnetic inverse boundary conditions," *1975 Int. IEEE/AP-S Symposium Proc.*, 130–135, Urbana, IL, USA, 2–5 June, 1975.
6. Boerner, W.-M. (O. A. Aboul-Atta), "Vectorial impedance identity for the natural dependence of harmonic fields in closed boundaries," *Can. Journal of Phys.*, Vol. 53, 1404–1407, 1975.

## Recent Advances in Polarimetric and Interferometric Radar Remot Sensing

Wolfgang-Martin Boerner

UIC-ECE Communications, Sensing and Navigation Laboratory  
900 W. Taylor St., SEL (607) W-4210, M/C 154, Chicago, IL 60607-7018, USA

**Abstract**— Radar Polarimetry Radar Interferometry and Polarimetric SAR Interferometry represent the current culmination in ‘*Microwave Remote Sensing*’ technology, but we still need to progress very considerably in order to reach the limits of physical realizability. Whereas with *radar polarimetry* the textural fine-structure, target orientation, symmetries and material constituents can be recovered with considerable improvement above that of standard ‘*amplitude-only*’ *radar*; by implementing ‘*radar interferometry*’ the spatial (in depth) structure can be explored. With Polarimetric Interferometric Synthetic Aperture Radar (POL-IN-SAR) imaging, it is possible to recover such co-registered textural and spatial information from POL-IN-SAR digital image data sets simultaneously, including the extraction of DEMs from either Polarimetric (scattering matrix) or Interferometric (dual antenna) SAR systems. Simultaneous Polarimetric-plus-Interferometric SAR Imaging offers the additional benefit of obtaining co-registered textural-plus-spatial three-dimensional POL-IN-DEM information, which when applied to *Repeat-Pass Image-Overlay Interferometry* provides differential background validation and environmental stress-change information with highly improved accuracy. Then, by either designing multiple dual polarization antenna POL-IN-SAR systems or by applying advanced POL-IN-SAR image compression techniques, will result in ‘POL-arimetric TOMO-graphic’ SAR or POL-TOMO-SAR imaging. By advancing these EWB-D-POL-IN/TOMO-SAR Imaging modes, we are slowly but steadily approaching the ultimate goal of eventually realizing air-borne and space-borne monitoring of the Terrestrial and Planetary Covers.

## Need for Developing Repeat-pass Differential POL-SAR Interferometry

Wolfgang-Martin Boerner<sup>1,2</sup> and Kun-Shan Chen<sup>2</sup>

<sup>1</sup>UIC-ECE Communications, Sensing and Navigation Laboratory  
900 W. Taylor St., SEL (607) W-4210, M/C 154, Chicago, IL 60607-7018, USA

<sup>2</sup>Space Wave Scattering and Remote Sensing Laboratory, NCU-CSRSR  
300 Chong-da Road, R3-413, Chung-Li 32054, Taiwan

**Abstract**— Radar Polarimetry, Radar Interferometry and Polarimetric SAR Interferometry represent the current culmination in ‘*Microwave Remote Sensing*’ technology, but we still need to progress very considerably in order to reach the limits of physical realizability. Whereas with *radar polarimetry* the textural fine-structure, target orientation, symmetries and material constituents can be recovered with considerable improvement above that of standard ‘*amplitude-only*’ *radar*; by implementing ‘*radar interferometry*’ the spatial (in depth) structure can be explored. With Polarimetric Interferometric Synthetic Aperture Radar (POL-IN-SAR) imaging, it is possible to recover such co-registered textural and spatial information from POL-IN-SAR digital image data sets simultaneously, including the extraction of Digital Elevation Maps (DEM) from either Polarimetric (scattering matrix) or Interferometric (dual antenna) SAR systems. Simultaneous Polarimetric-plus-Interferometric SAR Imaging offers the additional benefit of obtaining co-registered textural-plus-spatial three-dimensional POL-IN-DEM information, which when applied to *Repeat-Pass Image-Overlay Interferometry* provides differential background validation and environmental stress-change information with highly improved accuracy.

However, hitherto only single-polarization-channel repeat-pass IN-SAR was developed and considered; and therefore the aim of this paper is to scrutinize and determine why and for what specific problems fully polarimetric differential RP-POL-IN-SAR imaging is required.

# Mechanical and Electric Fields in Quantum-wire and Quantum-dot Nanostructures

E. Pan<sup>1</sup> and K. Y. Xu<sup>2,3</sup>

<sup>1</sup>Department of Civil Engineering, the University of Akron  
Akron, OH 44325, USA

<sup>2</sup>Department of Mechanics, Shanghai University  
99 Shangda Road, Shanghai 200444, China

<sup>3</sup>College of Engineering, Michigan Technological University  
1400 Townsend Drive, Houghton, MI 49931, USA

**Abstract**— Research progresses on novel features associated with lattice-misfit induced elastic/electric fields in nanoscale quantum-wire (QWR) and quantum-dot (QD) structures are presented. Especially, the fully coupled piezoelectric model have received wide attention recently, accurate prediction of the induced fields still remains a challenge: 1). The elastic and piezoelectric coefficients depend strongly on the lattice-misfit value; 2). Edges, corners, and interfaces in QWR/QD structures exhibit field concentration and even singularity; and 3). Multiple QWRs/QDs or QWR/QD arrays (of large number) interact to each other. Review continuum mechanics (CM) method combined with molecule dynamics (MD) simulation for calculation of the induced elastic/electric fields in nanoscale QWR/QD structures. Propose some interesting issues including 1). develop a fully coupled MD model based on the thermodynamic principle to predict the lattice misfit-dependent QWR/QD material behavior, 2). derive a novel multi-domain BEM formulation to analyze the coupled elastic/electric fields in nanoscale QWRs/QDs using the fully coupled piezoelectric model, and 3). develop a fast BEM to simulate the elastic and piezoelectric fields in QWR/QD superlattice nanostructures.

Although BEM has the well-known advantage of treating concentration and singularity easily and accurately, its applications are largely within the conventional engineering field. Even in this area, practical application of BEM is still impeded by its size limitation. However, renewed interests emerge recently due to the adoption of FMM to BEM, which shows certain new and attractive features, bringing BEM back again as an active and competitive computational tool. Combining with the reliable material properties from our new MD simulation, it will initiate the very first application of FMM accelerated BEM to nanoscale quantum structures and therefore could greatly impact various nanotechnology fields, where elastic anisotropy and multiphase coupling are involved. Furthermore, combined with the ab initio technique for, and the experimental measurement of, the optoelectronic properties of QWR/QD nanodevices, the long-standing unsolved yet critical issues on electromechanical coupling and nonlinearity will be possibly eventually solved.



# Session 1P1

## Recent Advances in Metamaterials and Invisibility Cloaking 1

<p><b>Transformation Optics</b>  <i>Ulf Leonhardt (University of St Andrews, UK); Thomas G. Philbin (University of St Andrews, UK);</i></p> <p><b>Electromagnetic Materials with a Polarization Independent Wave Velocity: Wormhole Construction and Inverse Problem</b>  <i>Allan Greenleaf (University of Rochester, USA); Yaroslav Kurylev (University College London, USA); Matti Lassas (University of Technology, Finland); E. Somersalo (University of Technology, Finland); Gunther Uhlmann (University of Washington, USA);</i></p> <p><b>Optimization of the Optical Invisibility Cloak Constructed of Concentric Layered Nanostructure</b>  <i>Yijun Feng (Nanjing University, China); Xiaofei Xu (Nanjing University, China); Ying Huang (Nanjing University, China); Tian Jiang (Nanjing University, China);</i></p> <p><b>A Rigorous Analysis in the Time and Frequency Domains of Full Wave Electromagnetic Invisibility Cloaks</b>  <i>Ricardo Weder (Universidad Nacional Autónoma de México, México);</i></p> <p><b>Manipulating Light Polarizations by Anisotropic Meta-materials: A Generalized <math>4 \times 4</math> Transfer-matrix Method</b>  <i>Jiaming Hao (Fudan University, China); Lei Zhou (Fudan University, China);</i></p> <p><b>Spherical Cloak Makes both Passive and Active Devices Invisible</b>  <i>Hongsheng Chen (Zhejiang University, China); Baile Zhang (Massachusetts Institute of Technology, USA); Bae-Ian Wu (Massachusetts Institute of Technology, USA); Jin Au Kong (Massachusetts Institute of Technology, USA);</i></p> <p><b>Differential Forms, Metrics, and the Electromagnetic Masking of Scattering Objects</b>  <i>Burkay Donderici (The Ohio State University, USA); Kezhong Zhao (Ansoft Corporation, USA); Fernando Lisboa Teixeira (The Ohio State University, USA); Jin-Fa Lee (The Ohio State University, USA);</i></p> <p><b>Transformation Media that Rotate Electromagnetic Fields</b>  <i>Huanyang Chen (Shanghai Jiao Tong University, China); Hongru Ma (Shanghai Jiao Tong University, China); C. T. Chan (Hong Kong University of Science and Technology, China);</i></p> <p><b>A General Method for Cloaking Design</b>  <i>Yu Luo (Zhejiang University, China); Jingjing Zhang (Zhejiang University, China); Hongsheng Chen (Zhejiang University, China); Lixin Ran (Zhejiang University, China); Jin Au Kong (Massachusetts Institute of Technology, USA);</i></p> <p><b>Invisibility Cloaking of Active Devices</b>  <i>Matti Lassas (Helsinki University of Technology, Finland); Allan Greenleaf (University of Rochester, USA); Yaroslav Kurylev (University College London, UK); Gunther Uhlmann (University of Washington, USA);</i></p>	<p>130</p> <p>131</p> <p>132</p> <p>133</p> <p>134</p> <p>135</p> <p>136</p> <p>137</p> <p>138</p> <p>139</p>
---	---

## Transformation Optics

Ulf Leonhardt and Thomas G. Philbin

University of St Andrews, UK

**Abstract**— Modern metamaterials offer remarkable control over electromagnetic fields with applications ranging from invisibility devices to perfect lenses. Imagine there were no practical limits on the electromagnetic properties of materials. Given a desired function, how do we find the design of the device that turns this function into fact? We show that general relativity provides clear recipes for calculating the required material properties. In the early 1920's Gordon noticed that moving isotropic media appear to electromagnetic fields as certain effective space-time geometries. Tamm generalized this geometric approach to anisotropic media and briefly applied this theory to the propagation of light in curved geometries. In 1960 Plebanski formulated the electromagnetic effect of curved space-time or curved coordinates in concise constitutive equations. Dielectric media act on electromagnetic fields as geometries and geometries act as effective media. Only very recently meta-material implementations of coordinate transformations were considered as engineering tools, ideas we take further here: we show that general relativity lends the most natural recipes for such engineering applications. The adaptability of metamaterials is mirrored in the arbitrary choice of coordinates in general relativity. Media that actively perform coordinate transformations are known as transformation media. The most interesting properties of such media seem to stem from non-trivial topologies: spaces with holes in the case of invisibility devices, coordinate folds for negative refraction, multi-valued physical space for the Aharonov-Bohm effect and multiple sheets of electromagnetic space-time mapped on to physical space-time in the case of artificial event horizons.

# Electromagnetic Materials with a Polarization Independent Wave Velocity: Wormhole Construction and Inverse Problem

A. Greenleaf<sup>1</sup>, Y. Kurylev<sup>2</sup>, M. Lassas<sup>3</sup>, E. Somersalo<sup>3</sup>, and G. Uhlmann<sup>4</sup>

<sup>1</sup>Department of Mathematics, University of Rochester, Rochester, NY 14627, USA

<sup>2</sup>Department of Mathematics, University College London, Gower Street, London, WC1E 5BT, UK

<sup>3</sup>Institute of Mathematics, University of Technology, P. O. Box 1100, Helsinki 02015, Finland

<sup>4</sup>Department of Mathematics, University of Washington, Seattle, WA 98195, USA

**Abstract**— There have been recently a significant progress in developing electromagnetic metamaterials with a very high ratio of anisotropy. Such metamaterials may be used, for example, to develop invisibility cloaking, see e.g., [1] for some striking experimental results and [2, 3] for a complete theoretical analysis. An important feature of the metamaterials used is that they represent a special case of electromagnetic materials with the wave velocity which is independent of polarization.

In this talk we, firstly, develop another possible application of such metamaterials, namely, to construct electromagnetic wormholes. Geometrically, a wormhole can be imagined as a 3-dimensional Euclidean space with an attached 3-dimensional handle. Clearly, such construction changes dramatically the picture of the electromagnetic wave propagation. We show how to realize such a construction, using metamaterials, within the framework of the usual 3-dimensional Euclidean space (without any handles attached!) and discuss some possible applications.

In the second part of the talk, we show that it is possible to recover, up to a change of coordinates, the electromagnetic parameters for general materials with a polarization independent wave velocity. This can be done using measurements in the time-domain which are made on a portion of the boundary of the regions occupied by the material under the assumption that the electromagnetic properties do not depend upon the frequency.

The first part of this work is carried out with A. Greenleaf, M. Lassas and G. Uhlmann, the second part — with M. Lassas and E. Somersalo.

## REFERENCES

1. Schurig, D., J. Mock, B. Justice, S. Cummer, J. Pendry, A. Starr, and D. Smith, “Metamaterial electromagnetic cloak at microwave frequencies,” *Science Online*, Oct. 19, 2006.
2. Greenleaf, A., M. Lassas, and G. Uhlmann, “On nonuniqueness for Calderon’s inverse problem,” *Math. Res. Lett.*, Vol. 10, 685–693, 2003.
3. Greenleaf, A., Y. Kurylev, M. Lassas, and G. Uhlmann, “Full invisibility of active devices at all frequencies,” *Comm. Math. Phys.*, published online, Aug. 15, 2007.
4. Greenleaf, A., Y. Kurylev, M. Lassas, and G. Uhlmann, *Electromagnetic Wormholes via Handlebody Construction*, Preprint arXiv:0704.0914, 2007.
5. Greenleaf, A., Y. Kurylev, M. Lassas, and G. Uhlmann, *Electromagnetic Wormholes and Virtual Magnetic Monopoles*, Preprint math-ph/0703059, 2007.
6. Kurylev, Y., M. Lassas, and E. Somersalo, “Maxwell’s equations with a polarization independent wave velocity: Direct and inverse problems,” *J. Math. Pure et Appl.*, Vol. 86, 237–270, 2006.

# Optimization of the Optical Invisibility Cloak Constructed of Concentric Layered Nanostructure

Yijun Feng, Xiaofei Xu, Ying Huang, and Tian Jiang

Department of Electronic Science and Engineering, Nanjing University, Nanjing 210093, China

**Abstract**— The basic idea of cloaking objects from the observation by electromagnetic fields proposed by J. Pendry [1], is to use anisotropic transform medium whose permittivity and permeability are obtained from a homogeneous isotropic medium, by transformations of coordinates. The idea has been successfully confirmed by experimental demonstration at microwave frequencies [2]. However, the design uses artificially structured metamaterial with inclusions of subwavelength metallic split-ring resonators, and cannot be easily implemented for an optical cloak, which is certainly of particular interest. Recently, W. Cai et al. have proposed an optical cloaking device for transverse magnetic polarization [3], but their design still requires metamaterial with anisotropic distribution of the permittivity, which is realized by subwavelength inclusions of metal wires in the radial direction embedded in a dielectric material.

In this presentation, we will propose an optical cloak structure that does not require metamaterials with subwavelength structured inclusions to realize the anisotropy or inhomogeneity of the material parameters. We construct a concentric layered nanostructure of alternating homogeneous isotropic materials that can be treated as an effective medium with the required radius-dependent anisotropy. With optimized design of the permittivity or the thickness of the alternating layers through genetic algorithm, we will demonstrate the improvement of low-reflection and power-flow bending properties of the proposed cloaking structure through rigorous analysis of the scattered electromagnetic fields. The proposed cloaking structure could be possibly realized by nano-structured normal materials, therefore may lead to a practical path to an experimental demonstration of electromagnetic cloaking in the optical range.

## ACKNOWLEDGMENT

Supported by the National Basic Research Program of China (2004CB719800), the National Nature Science Foundation (No. 60671002), and the Specialized Research Fund for the Doctoral Program of Higher Education (No. 20030284024).

## REFERENCES

1. Pendry, J. B., D. Schurig, and D. R. Smith, *Science*, Vol. 312, 1780–1782, 2006.
2. Schurig, D., J. J. Mock, B. J. Justice, S. A. Cummer, J. B. Pendry, A. F. Starr, and D. R. Smith, *Science*, Vol. 314, 977–980, 2006.
3. Cai, W., U. K. Chettiar, A. V. Kildishev, and V. M. Shalaev, *Nature Photonics*, Vol. 1, 224–227, 2007.

# A Rigorous Analysis in the Time and Frequency Domains of Full Wave Electromagnetic Invisibility Cloaks

Ricardo Weder

Instituto de Investigaciones en Matemáticas Aplicadas y en Sistemas  
Universidad Nacional Autónoma de México, Apartado Postal 20-726, DF 01000, México

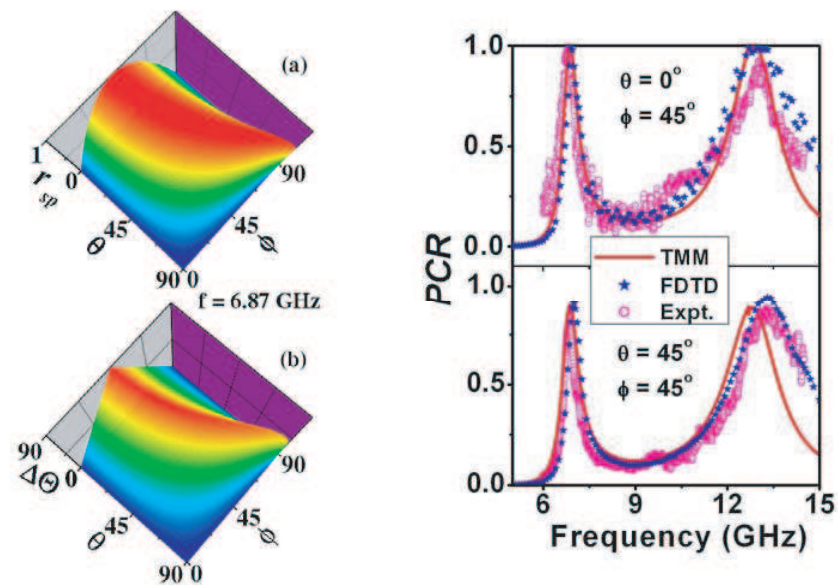
**Abstract**— We present a rigorous analysis of electromagnetic invisibility cloaks in the time and frequency-domains. We study the initial value problem for Maxwell's equations in *transformation media*. We prove that there is only one time evolution outside of the cloaked objects that conserves electromagnetic energy. This statement has many consequences. It implies that the cloaked objects completely decouple from the electromagnetic waves outside of them. Electromagnetic waves inside and outside of the cloaked objects are completely independent of each other. Furthermore, the scattering operator is the identity, i.e., the scattering amplitudes are identically zero. We prove this both in the time-domain, and at each fixed frequency in the frequency domain. We formulate cloaking as a boundary value problem outside of the cloaked objects, at each fixed frequency, and we derive the unique *cloaking boundary condition* that is allowed by energy conservation. We prove our results for media that are obtained by transformations of coordinates of general anisotropic media. This proves that it is possible to cloak objects inside general crystals.

# Manipulating Light Polarizations by Anisotropic Meta-materials: A Generalized $4 \times 4$ Transfer-matrix Method

Jiaming Hao and Lei Zhou

Physics Department, Fudan University, Shanghai 200433, China

**Abstract**— The anisotropic meta-materials have drawn considerable attention recently. In many previous studies on such problems, simplifications were made to assume that either the electric field or the magnetic field is along a principle axis of the anisotropic material. Here we present a generalized  $4 \times 4$  transfer-matrix method to study the scatterings of electromagnetic (EM) waves by anisotropic meta-materials in a more general situation, with incident waves taking arbitrary polarization and propagation directions. Employing this method, we illustrate how to manipulate EM wave polarizations freely through reflections by several types of meta-material reflectors [1]. These results show that the polarization states of electromagnetic waves can be manipulated through reflections by an anisotropic metamaterial reflector, and *all* possible polarizations (circular, elliptic and linear) are realizable via choosing appropriate material parameters [2]. In particular, we show it possible to rotate the polarization direction of a linearly polarized EM wave by an arbitrary angle using a planar double-layer meta-material reflector of thickness much less than wavelength. Microwave experiments were performed to successfully realize these ideas and results are in excellent agreement with finite-different-time-domain simulations (see figures blow).



## REFERENCES

1. Hao, J. M. and L. Zhou, unpublished.
2. Hao, J. M., Y. Yuan, L. X. Ran, T. Jiang, J. A. Kong, C. T. Chan, and L. Zhou, *Phys. Rev. Lett.*, Vol. 99, 063908, 2007.

## Spherical Cloak Makes both Passive and Active Devices Invisible

Hongsheng Chen<sup>1,2</sup>, Baile Zhang<sup>2</sup>, Bae-Ian Wu<sup>2</sup>, and Jin Au Kong<sup>1,2</sup>

<sup>1</sup>The Electromagnetics Academy at Zhejiang University, Zhejiang University, China

<sup>2</sup>Research Laboratory of Electronics, Massachusetts Institute of Technology, Cambridge, MA 02139, USA

**Abstract**— Invisibility cloaking has received much attention recently. The design process for the cloak is mostly based on a coordinate transformation. The functionality of the cloak has been demonstrated analytically in the geometrical optics limit or in the electrostatic or magnetostatic limit. In this paper, we use an analytical scattering method to demonstrate the functionality of the spherical cloak, which can cloak both passive and active devices. We show that for an ideal cloak, the total scattering cross section is absolutely zero. When an active device is inside a cloak, extraordinary electric and magnetic surface voltages are induced at the inner boundary of the cloak. These surface voltages prevent electromagnetic waves from going out. Our analytical derivations also show that the surface voltages due to an electric dipole with an arbitrary position inside the cloak is exactly equal to the auxiliary scalar potentials, which consequently gain physical counterparts in this special case.

# Differential Forms, Metrics, and the Electromagnetic Masking of Scattering Objects

Burkay Donderici<sup>1</sup>, Kezhong Zhao<sup>2</sup>, Fernando L. Teixeira<sup>1</sup>, and Jin-Fa Lee<sup>1</sup>

<sup>1</sup>The Ohio State University, USA

<sup>2</sup>Ansoft Corporation, USA

**Abstract**— We discuss the possibility of *electromagnetic masking* of objects via metamaterial blueprints, whereby the scattering field of a given object is made identical to a scattered field of a different object. Metamaterial blueprints for this purpose can be systematically derived by exploiting the metric invariance of Maxwell equations in a manner akin to used in the derivation of electromagnetic cloaking [1].

Metric invariance is a basic property of Maxwell equations first discovered by Van Dantzig [2] in 1934 and rediscovered many times ever since [3–5]. Metric invariance essentially means that a continuous change on the metric of space (diffeomorphism) can be made equivalent (in a precise sense) to a change on the constitutive parameters. The change on the constitutive parameters is such that the permittivity and the permeability become inhomogeneous and anisotropic [6, 7]. Even though this property is not immediate to see when Maxwell equations are written in the standard vector calculus language, it becomes obviated when Maxwell equations are written in the differential forms language [8].

## REFERENCES

1. Pendry, J. B., D. Schurig, and D. R. Smith, “Controlling electromagnetic fields,” *Science*, Vol. 312, 1780–1782, June 2006.
2. Van Dantzig, D., “The fundamental equations of electromagnetism, independent of metrical geometry,” *Proc. Cambridge Phil. Soc.*, Vol. 37, 421–427, 1934.
3. Deschamps, G., “Electromagnetics and differential forms,” *Proc. IEEE*, Vol. 69, No. 6, 676–696, June 1981.
4. Ward, A. J. and J. B. Pendry, “Refraction and geometry in Maxwell’s equations,” *J. Mod. Opt.*, Vol. 43, 773–793, 1996.
5. Teixeira, F. L. and W. C. Chew, “Lattice electromagnetic theory from a topological viewpoint,” *J. Math. Phys.*, Vol. 40, No. 1, 169–187, 1999.
6. Teixeira, F. L., “Closed-form metamaterial blueprints for electromagnetic masking of arbitrarily shaped, convex PEC objects,” *IEEE Antennas Wireless Propagat. Lett.*, Vol. 6, 163–164, 2007.
7. Zhao, K., Ph.D. Dissertation, The Ohio State University, September 2007.
8. Teixeira, F. L. and W. C. Chew, “Differential forms, metrics, and the reflectionless absorption of electromagnetic waves,” *J. Electromagn. Waves Appl.*, Vol. 13, No. 5, 665–686, 1999.



# Transformation Media that Rotate Electromagnetic Fields

Huanyang Chen<sup>1,2</sup>, Hongru Ma<sup>1</sup>, and C. T. Chan<sup>2</sup>

<sup>1</sup>Institute of Theoretical Physics, Shanghai Jiao Tong University, Shanghai 200240, China

<sup>2</sup>Department of Physics, Hong Kong University of Science and Technology  
Clear Water Bay, Kowlong, Hong Kong, China

**Abstract**— The authors suggest a way to manipulate electromagnetic waves by introducing a rotation mapping of coordinates that can be realized by a specific transformation of the permittivity and permeability of a shell surrounding an enclosed domain. Inside the enclosed domain, the information from the outside will appear as if it is coming from a different angle. Numerical simulations were performed to illustrate these properties.

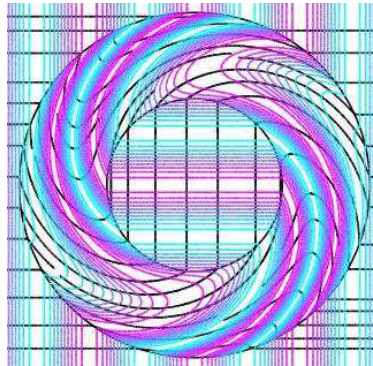


Figure 1: The magnetic-field distribution in the vicinity of the rotation coating with the power-flow lines (in black) to show the smooth deviation of EM power.

## REFERENCES

1. Chen, H. and C. T. Chan, *Appl. Phys. Lett.*, Vol. 90, 241105, 2007.
2. Chen, H., B. Hou, S. Chen, X. Ao, W. Wen, and C. T. Chan, unpublished results, 2007.

## A General Method for Cloaking Design

Yu Luo<sup>1</sup>, Jingjing Zhang<sup>1</sup>, Hongsheng Chen<sup>1,2</sup>, Lixin Ran<sup>1,2</sup>, and J. A. Kong<sup>1,2</sup>

<sup>1</sup>The Electromagnetics Academy at Zhejiang University, Zhejiang University, China

<sup>2</sup>Research Laboratory of Electronics, Massachusetts Institute of Technology  
Cambridge, MA 02139, USA

**Abstract**— The idea of using the coordinate transformation approach to design a cloak of invisibility has received much attention. Up to now, most of the discussions on cloaking are based on the linear transformation. If different transformations are adopted, cloaks with different performances can be achieved. This paper gives an analytical field solutions on a spherical cloak created with a general class of transformation functions. The analytical expressions of the electromagnetic field in the whole space are calculated, and the field distributions of cloaks with different parameters are analyzed. This analytical full wave method is a very computational efficient validation method compared with numerical simulations. It also provides a better physical insight into the effect of the transformation function on the performance of devices.

### REFERENCES

1. Pendry, J. B., D. Schurig, and D. R. Smith, *Science*, Vol. 312, 1780, 2006.

## Invisibility Cloaking of Active Devices

M. Lassas<sup>1</sup>, A. Greenleaf<sup>2</sup>, Y. Kurylev<sup>3</sup>, and G. Uhlmann<sup>4</sup>

<sup>1</sup>Helsinki University of Technology, Finland

<sup>2</sup>University of Rochester, USA

<sup>3</sup>University College of London, UK

<sup>4</sup>University of Washington, USA

**Abstract**— We consider the mathematical theory of invisibility cloaking and its practical implications. We prove existence and non-existence results for solutions of Maxwell's equations in cloaking constructions. In particular, we show how a Soft-and-Hard Surface inside the cloaking metamaterial improves the cloaking effect in the cloaking of a cylinder.

One of the main theme of the talk is to consider how to formulate Maxwell's equations rigorously with a singular permittivity and permeability that appear in several constructions of cloaking devices. The basic idea of such constructions, used in the papers of Leonhardt and Pendry et al. in 2006 [1, 2] for Maxwell's equations and in papers [3, 4] for the electrical impedance tomography in 2003, is to use a singular transformation that pushes isotropic electromagnetic parameters forward into singular, anisotropic ones.

In the talk, based on results of [5, 6], we define the notion of finite energy solutions of the Helmholtz and Maxwell's equations for such singular electromagnetic parameters, and study the behavior of the solutions on the entire domain, including the cloaked region and its boundary. We prove that the obtained construction cloaks passive objects, i.e., those without internal currents, at a given frequency. Due to the singularity of the metric, one needs to work with weak solutions. Analyzing the behavior of such solutions inside the cloaked region, we show that, depending on the chosen construction, there appear new "hidden" boundary conditions at the surface separating the cloaked and uncloaked regions. We also consider the effect on invisibility of active devices inside the cloaked region, interpreted as collections of sources and sinks or internal currents. When these conditions are overdetermined, as happens for Maxwell's equations, generic internal currents prevent the existence of finite energy solutions and invisibility is compromised. This non-existence of finite energy solutions can be viewed as a failure of the invisibility construction when there are active sources inside the cloaked region. However, invisibility can be restored by modifying the coating construction, by either inserting a physical surface at the boundary of the cloaked object.

We consider also cloaking of an infinite cylinder. Then invisibility results for Maxwell's equations are valid if the coating material is lined on with a surface satisfying the soft and hard surface (SHS) boundary condition (see [7, 8]), but in general not without such a lining, even for passive objects.

### REFERENCES

1. Leonhardt, U., "Optical conformal mapping," *Science*, Vol. 312, 1777–1780, 23 June, 2006.
2. Pendry, J. B., D. Schurig, and D. R. Smith, "Controlling electromagnetic fields," *Science*, Vol. 312, 1780–1782, 23 June, 2006.
3. Greenleaf, A., M. Lassas, and G. Uhlmann, "On nonuniqueness for Calderon's inverse problem," *Mathematical Research Letters*, Vol. 10, 685–693, 2003.
4. Greenleaf, A., M. Lassas, and G. Uhlmann, "Anisotropic conductivities that cannot be detected in electrical impedance tomography," *Physiological Measurement*, Vol. 24, 413–420, 2003.
5. Greenleaf, A., Y. Kurylev, M. Lassas, and G. Uhlmann, "Full-wave invisibility of active devices at all frequencies," To appear in *Communications in Mathematical Physics*.
6. Greenleaf, A., Y. Kurylev, M. Lassas, and G. Uhlmann, "Effectiveness and improvement of cylindrical cloaking with the SHS lining," arXiv:0707.1315v1 [physics.optics].
7. Kildal, P.-S., "Definition of artificially soft and hard surfaces for electromagnetic waves," *Electron. Lett.*, Vol. 24, 168–170, 1988.
8. Hanninen, I., I. Lindell, and A. Sihvola, "Realization of generalized soft-and-hard boundary," *Progress in Electromagnetics Research*, PIER 64, 317–333, 2006.



# Session 1P2

## Femtosecond Photonics: Microfabrication and Optical Data Storage 1

Photonic Band Gap Materials: Engineering Light-matter Interactions, Part I	142
<i>Sajeev John (University of Toronto, Canada);</i> .....	
Photonic Band Gap Materials: Engineering Light-matter Interactions, Part II	143
<i>Sajeev John (University of Toronto, Canada);</i> .....	
Towards 3D Microfabrication of Photonic and Plasmonic Components by Two-photon Polymerization	144
<i>Boris N. Chichkov (Laser Zentrum Hannover e.V., Germany);</i> .....	
Quantum Entanglement and Single Photon Emission in Photonic Crystals	145
<i>Xue-Hua Wang (Sun Yat-Sen University, China);</i> .....	
Three Dimensional Femtosecond Laser Structuring in Optical Materials	146
<i>Saulius Juodkazis (Hokkaido University, Japan); V. Mizeikis (Hokkaido University, Japan); H. Misawa (Hokkaido University, Japan); Kenji Kitamura (National Institute for Materials Science, Japan); Shunji Takekawa (The Australian National University, Australia); E. G. Gamaly (National Institute for Materials Science, Japan); A. V. Rode (National Institute for Materials Science, Japan); Wieslaw Krolikowski (National Institute for Materials Science, Japan);</i> .....	
Nanometer Resolution and Designable Assembly in Two-photon 3D Micronanofabrication	147
<i>Xuan-Ming Duan (Chinese Academy of Sciences, China); Xian-Zi Dong (Chinese Academy of Sciences, China); Wei-Qiang Chen (Chinese Academy of Sciences, China); Zhen-Shang Zhao (Chinese Academy of Sciences, China);</i> .....	
Fabrication and Characterisation of Photonic Devices in Laser Media by Femtosecond Laser Writing	148
<i>Daniel Jaque Garcia (Universidad Autonoma de Madrid, Spain); Airan Rodenas (Universidad Autonoma de Madrid, Spain); Jorge Lamela (Universidad Autonoma de Madrid, Spain); Francisco Jaque (Universidad Autonoma de Madrid, Spain); Gustavo Torchia (Universidad de Salamanca, Spain); Cruz Mendez (Universidad de Salamanca, Spain); Luis Roso (Universidad de Salamanca, Spain);</i> ...	
Femtosecond Laser Fabrication of High Precision Three-dimensional Woodpile Photonic Crystals and Their Near-field Characterisation	149
<i>Baohua Jia (Swinburne University of Technology, Australia); Min Gu (Swinburne University of Technology, Australia);</i> .....	
Three-dimensional Chiral Photonic Crystals	150
<i>M. Thiel (Universität Karlsruhe (TH), Germany); G. Von Freymann (Universität Karlsruhe (TH), Germany); M. Wegener (Universität at Karlsruhe (TH), Germany);</i> .....	
3D Structuring of Materials by Femtosecond Pulses	151
<i>Saulius Juodkazis (Hokkaido University, Japan); H. Misawa (Hokkaido University, Japan);</i> .....	
Direct Femtosecond Fabrication in High Refractive Index Materials	152
<i>Guangyong Zhou (Swinburne University of Technology, Australia); Min Gu (Swinburne University of Technology, Australia);</i> .....	
Photonic Quasi-crystals: A Review	153
<i>Robert C. Gauthier (Carleton University, Canada);</i> .....	

# Photonic Band Gap Materials: Engineering Light-matter Interactions, Part I

Sajeev John

Department of Physics, University of Toronto  
60 Saint George Street, Toronto, Ontario, M5S 1A7, Canada

**Abstract**— Photonic Band Gap (PBG) materials [1, 2] are artificial, periodic, dielectrics that enable engineering of the most fundamental properties of electromagnetic waves. These include the laws of refraction, diffraction, and spontaneous emission of light [3, 4]. Unlike traditional semiconductors that rely on the propagation of electrons through an atomic lattice, PBG materials execute their novel functions through selective trapping or “localization of light” [5]. Three dimensional (3D) PBG materials offer a unique opportunity to simultaneously (i) synthesize micron-scale 3D optical circuits that do not suffer from diffractive losses [6] and (ii) engineer the electromagnetic vacuum density of states in this 3D optical micro-chip [7]. This combined capability opens a new frontier in integrated optics as well as the basic science of radiation-matter interactions.

I review recent approaches to micro-fabrication of photonic crystals with a large 3D PBG centered near 1.5 microns. These include direct laser-writing techniques [8], holographic lithography [9], silicon double inversion [10], and a newly invented optical phase mask lithography technique [11].

## REFERENCES

1. John, S., “Strong localization of photons in certain disordered dielectric superlattices,” *Phys. Rev. Lett.*, Vol. 58, 2486, 1987.
2. Yablonovitch, E., *Phys. Rev. Lett.*, Vol. 58, 2059, 1987.
3. John, S. and J. Wang, “Quantum electrodynamics near a photonic band gap: Photon bound states and dressed atoms,” *Physical Rev. Letters*, Vol. 64, 2418, 1990.
4. John, S. and T. Quang, “Spontaneous emission near the edge of a photonic bandgap,” *Physical Review A*, Vol. 50, 1764, 1994.
5. John, S., “Electromagnetic absorption in a disordered medium near a photon mobility edge,” *Phys. Rev. Lett.*, Vol. 53, 2169, 1984.
6. Chutinan, A. and S. John, “3+1 dimensional integrated optics with localized light in a photonic band gap,” *Optics Express*, Vol. 14, No. 3, 1266–1279, Feb. 6, 2006.
7. Wang, R. Z. and S. John, “Engineering the electromagnetic vacuum for controlling light with light in a photonic band gap micro-chip,” *Physical Review A*, Vol. 70, 043805, 2004.
8. Deubel, M., M. Wegener, A. Kaso, and S. John, “Direct two-photon writing and characterization of slanted pore photonic crystals,” *Applied Physics Letters*, Vol. 85, 1895, 2004.
9. Chan, T., O. Toader, and S. John, “Photonic band gap synthesis by optical interference lithography,” *Physical Review E*, Vol. 71, 046605, 2005.
10. Tetreault, N., G. von Freymann, M. Deubel, M. Hermatschweiler, F. Perez-Willard, S. John, M. Wegener, and G. A. Ozin, “New route towards three-dimensional photonic band gap materials: Silicon double inversion of polymeric templates,” *Advanced Materials*, Vol. 18, No. 4, 457+, Feb. 17, 2006.
11. Chan, T., O. Toader, and S. John, “Photonic band gap formation by optical phase mask lithography,” *Physical Review E*, Vol. 73, 046610, 2006.

# Photonic Band Gap Materials: Engineering Light-matter Interactions, Part II

Sajeev John

Department of Physics, University of Toronto  
60 Saint George Street, Toronto, Ontario, M5S 1A7, Canada

**Abstract**— I discuss the theoretical prediction of nonlinear Bloch waves [1] in photonic crystals that have been embedded with resonant nonlinear oscillators and which are incoherently pumped. Nonlinear Bloch waves are periodic, nondecaying, exact solutions of Maxwell's equations in a strongly scattering medium with complex, nonlinear, frequency-dependent dielectric function with regions of loss and gain. They are relevant to lasing in dielectric photonic crystals. Nonlinear Bloch waves may also appear in electrically-driven, metallic, photonic crystal filaments [2] and may have applications to high efficiency incandescent lighting.

Finally, I describe a novel and fundamental quantum mechanical effect predicted [3, 4] to occur in carefully fabricated PBG-Quantum Well Hetero-structures. We suggest that the dynamics of bound electron-hole pairs (excitons) in the quantum well can be significantly modified by the PBG environment. In particular, the exciton acquires a very large electromagnetically-induced mobility as well as long lifetime, when its radiative recombination energy coincides with a photonic band edge. This may enable Bose condensation of excitons at elevated temperatures.

## REFERENCES

1. Kaso, A. and S. John, "Nonlinear bloch waves in resonantly doped photonic crystals," *Physical Review E*, Vol. 74, 046611, 2006.
2. Kaso, A. and S. John, "Nonlinear bloch waves in metallic photonic band gap filaments," (submitted for publication).
3. John, S. and S. J. Yang, "Electromagnetically induced exciton mobility in a photonic band gap," *Physical Review Lett.*, Vol. 99, 046801, 2007.
4. Yang, S. J. and S. John, "Exciton dressing and capture by a photonic band edge," *Physical Review B*, Vol. 75, 235332, 2007.

## Towards 3D Microfabrication of Photonic and Plasmonic Components by Two-photon Polymerization

**Boris N. Chichkov**

Laser Zentrum Hannover e.V., Hollerithallee 8, 30419 Hannover, Germany

**Abstract**— Recent advances in the development of high resolution, direct laser writing technologies for the fabrication of three-dimensional (3D) microstructures will be discussed. By tightly focusing femtosecond laser pulses into the volume of a photosensitive material any 3D micro-structure can be fabricated by two-photon polymerization (2PP). In this presentation, microstructuring of different organic-inorganic hybrid materials (also nonlinear materials) will be reported. Different examples of 3D microstructures, such as microoptic and plasmonic components, and 3D photonic crystals, including investigations of their optical properties will be presented. Biomedical applications of 2PP technique will be highlighted.



# Quantum Entanglement and Single Photon Emission in Photonic Crystals

Xue-Hua Wang

School of Physics & Engineering, Sun Yat-sen University, Guangzhou 510275, China

**Abstract**— Photonic crystals are a new type of optical materials with periodic dielectric structures. They are the optical analogue of semiconductors for the electrons, known as “photon semiconductor”. The band gaps and Bloch property of electromagnetic fields in photonic crystals provide a unique way to control propagation of light and interaction between photons and quantum systems (such as atoms, molecules, and quantum dots, so on). Many novel quantum optics phenomena have been predicted, such as inhibition and coherent control of spontaneous emission, enhanced quantum interference effects, non-Markovian effects, wide lifetime distribution, nonclassic decay, etc. [1–13].

In this presentation, we discuss the possible application of photonic crystals to quantum computation and quantum information. Photonic crystals have the superior capability of controlling and engineering the quantum dynamic behaviors of two-level systems due to photonic band gap and Bloch property of the electromagnetic field. It is shown that the photonic crystals can fundamentally change the property of the coupling interaction between quantum dots or atoms, which results in novel entanglement properties and enhances efficiency of single photon emission. This will open a unique way to control quantum entanglement between atoms or quantum dots and to develop new approaches of quantum information processing.

## REFERENCES

1. John, S. and J. Wang, *Phys. Rev. Lett.*, Vol. 64, 2418, 1990.
2. John, S., et al., *Phys. Rev. Lett.*, Vol. 74, 3419, 1995.
3. Bay, S., et al., *Phys. Rev. Lett.*, Vol. 79, 2654, 1997.
4. Zhu, S. Y., et al., *Phys. Rev. Lett.*, Vol. 84, 2136, 2000.
5. Li, Z. Y., L. L. Lin, and Z. Q. Zhang, *Phys. Rev. Lett.*, Vol. 84, 4341, 2000.
6. Wang, X. H., B. Y. Gu, et al., *Phys. Lett. A*, Vol. 308, 116, 2003.
7. Wang, X. H., B. Y. Gu, et al., *Phys. Rev. B*, Vol. 67, 155114, 2003.
8. Wang, X. H., R. Wang, B. Y. Gu, and G. Z. Yang, *Phys. Rev. Lett.*, Vol. 88, 093902, 2002.
9. Petrov, E. P., et al., *Phys. Rev. Lett.*, Vol. 81, 77, 1998.
10. Megens, M., et al., *Phys. Rev. A*, Vol. 59, 4727, 1999.
11. Wang, X. H., B. Y. Gu, R. Wang, and H. Q. Xu, *Phys. Rev. Lett.*, Vol. 91, 113904, 2003.
12. Wang, X. H., Y. S. Kivshar, and B. Y. Gu, *Phys. Rev. Lett.*, Vol. 93, 073901, 2004.
13. Zhou, Y. S., X. H. Wang, B. Y. Gu, and F. H. Wang, *Phys. Rev. Lett.*, Vol. 96, 103601, 2006.

## Three Dimensional Femtosecond Laser Structuring in Optical Materials

S. Juodkazis<sup>1</sup>, V. Mizeikis<sup>1</sup>, H. Misawa<sup>1</sup>, Kenji Kitamura<sup>2</sup>  
Shunji Takekawa<sup>3</sup>, E. G. Gamaly<sup>2</sup>, A. V. Rode<sup>2</sup>, and W. Krolikowski<sup>2</sup>

<sup>1</sup>CREST-JST and Research Institute for Electronic Science, Hokkaido University  
CRIS Bldg. N-21-W-10, Sapporo 001-0021, Japan

<sup>2</sup>Optronic Materials Center, National Institute for Materials Science, Tsukuba 305-0044, Japan

<sup>3</sup>Laser Physics Centre, Research School of Physical Sciences and Engineering  
The Australian National University, Canberra ACT 0200, Australia

**Abstract**— We present results of experimental and theoretical studies of the formation of optical micro-structures using high power femtosecond laser pulses. We discuss three basic recording mechanisms: dielectric breakdown, photovoltaic effect in photorefractive crystals and photo-darkening via the nonlinear absorption. We demonstrate efficient recording of single bits in variety of optical media including silica, Lithium Niobate and Lithium Tantalate crystals as well as arsenic chalcogenide glass. We discuss application of the femtosecond pulse structuring for read/write/erase optical memories.

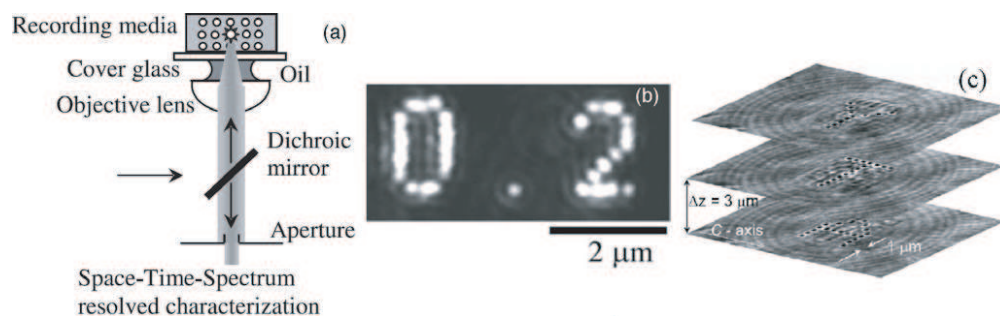


Figure 1: (a) Principle of 3D bit recording and reading using femtosecond pulses; (b) Image of a ‘bit’ pattern recorded via the dielectric breakdown in the volume of silica; (c) Layered recording of bits forming letters Y, T, and A in photorefractive Fe: LiNbO<sub>3</sub>.

### REFERENCES

1. Juodkazis, S., A. V. Rode, E. G. Gamaly, S. Matsuo, and H. Misawa, *Appl. Phys. B*, Vol. 77, 361, 2003.
2. Joudkazis, S., et al., *Appl. Phys. Lett.*, Vol. 89, 062903, 2006.
3. Juodkazis, S., T. Kondo, H. Misawa, A. Rode, M. Samoc, and B. Luther-Davies, *Optics Express*, Vol. 14, 7751–7756, 2006.

# Nanometer Resolution and Designable Assembly in Two-photon 3D Micronanofabrication

Xuan-Ming Duan, Xian-Zi Dong, Wei-Qiang Chen, and Zhen-Shang Zhao

Laboratory of Organic NanoPhotonics (LaONP), Technical Institute of Physics and Chemistry  
Chinese Academy of Sciences, Beijing 100080, China

**Abstract**— Three-dimensional (3D) micronanofabrication based on two-photon polymerization (TPP) has been established as a unique technique for micro/nanostructure fabrication due to its capability of intrinsic 3D processing in the past decade. Various micromachines and microdevices have been reported, such as microspring, microgear, micropump, 3D photonic crystals (PhCs) [1–6]. These achievements exhibited the excellent potential of TPP technique in the application field of micromachines and microdevices (MEMS). On the other hand, the spatial fabrication resolution based TPP has improved to be 100 nm on the surface of substrate [7] and 30 nm as suspended line [8]. In this paper, we report the newly developed method for improving spatial resolution of TPP and the results, in which the fabrication resolutions were further achieved to be 50 nm on substrate [9, 10] and sub-15 nm as suspended lines [11]. We also propose a simple and practicable method of fabricating integrated MEMS via parallel laser microfabrication by designing configurations of multiple beams, and demonstrate customisable fabrication of assembled 2D and 3D microstructures using multiple beam two-photon processing (MBTPP) (Figure 1) [12].

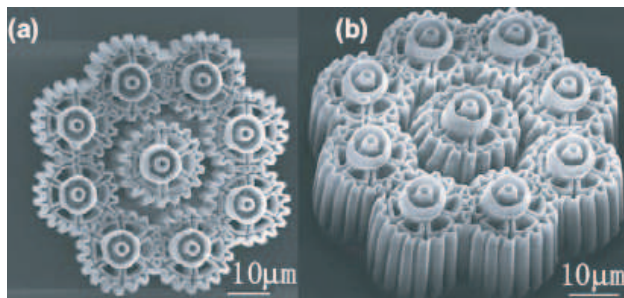


Figure 1: Top (a) and side (b) views of assembled microgears set fabricated by MBTPP.

## REFERENCES

1. Kawata, S., H.-B. Sun, T. Tanaka, and K. Takada, *Nature*, Vol. 412, 697, 2001.
2. Galajda, P. and P. Ormos, *Appl. Phys. Lett.*, Vol. 78, 249, 2001.
3. Maruo, S. and H. Inoue, *Appl. Phys. Lett.*, Vol. 89, 144101, 2006.
4. Kaneko, K., H.-B. Sun, X.-M. Duan, and S. Kawata, *Appl. Phys. Lett.*, Vol. 83, 2091, 2003.
5. Duan, X.-M., H.-B. Sun, K. Kaneko, and S. Kawata, *Thin Solid Films*, Vol. 453–454, 518, 2004.
6. Sun, Z.-B., X.-Z. Dong, S. Nakanishi, W.-Q. Chen, X.-M. Duan, and S. Kawata, *Appl. Phys. A*, Vol. 86, 427, 2007.
7. Takada, K., H.-B. Sun, and S. Kawata, *Appl. Phys. Lett.*, Vol. 86, 071122, 2005.
8. Juodkazis, S., V. Mizeikis, K. K. Seet, M. Miwa, and H. Misawa, *Nanotechnology*, Vol. 16, 846, 2005.
9. Xing, J.-F., X.-Z. Dong, W.-Q. Chen, X.-M. Duan, N. Takeyasu, T. Tanaka, and S. Kawata, *Appl. Phys. Lett.*, Vol. 90, 131106, 2007.
10. Dong, X.-Z. and X.-M. Duan, *Opt. Precision Eng.*, Vol. 15, 441, 2007.
11. Tan, D., Y. Li, F. Qi, H. Yang, Q. Gong, X.-Z. Dong, and X.-M. Duan, *Appl. Phys. Lett.*, Vol. 90, 071106, 2007.
12. Dong, X.-Z., Z.-S. Zhao, and X.-M. Duan, *Appl. Phys. Lett.*, Vol. 91, 2007, in press.

## Fabrication and Characterisation of Photonic Devices in Laser Media by Femtosecond Laser Writing

Daniel Jaque Garcia<sup>1</sup>, Airan Rodenas<sup>1</sup>, Jorge Lamela<sup>2</sup>, Francisco Jaque<sup>2</sup>, Gustavo Torchia<sup>3</sup>  
Cruz Mendez<sup>3</sup>, and Luis Roso<sup>3</sup>

<sup>1</sup>GIEL, Departamento de Fisica de Materiales, Universidad Autonoma de Madrid, Madrid 28049, Spain

<sup>2</sup>Departamento de Fisica de Materiales, Universidad Autonoma de Madrid, Madrid 28049, Spain

<sup>3</sup>Grupo de Optica, Universidad de Salamanca, Spain

**Abstract**— Femtosecond laser writing has been used to modify, at the micrometric scale, the local refractive index of solid state laser media leading to the creation of optically active photonic devices. Due to the possibility of optical amplification, the obtained devices have been demonstrated to be capable of light generation and manipulation. As an example, femtosecond laser writing has been used to fabricate optically active channel waveguides and non-collinear diode pumped lasers.

In order to evaluate the potential application of the obtained photonic structures it is necessary to investigate how the original properties of the irradiated laser media have been modified by the physical phenomena at the origin of the permanent modifications induced after femtosecond irradiation. In this work we present a novel approach to this problem consisting in the combination of Confocal-Micro-Luminescence and Near Field Optical Microscopy. We have found that the spectroscopic properties of the active ions, responsible of optical gain, are quite sensible to the structural modifications induced by femtosecond pulses. Taking advantage of this fact we have been able to locate spatially a rich variety of effects activated by femtosecond pulses including local compression and dilatation, local amorphization and local crystallographic re-orientations. The results obtained from the analysis of Confocal-Micro-Luminescence have been found in excellent agreement with the micro-pictures obtained with the Near Field Scanning Microscope which has also revealed the presence of defect formation, self-focusing induced micro-explosions and shock wave propagation above the elastic limits of the irradiated material.

The information provided from both techniques has been found of great relevance not only from the applied point of view but also from the fundamental one since it gets information about the light matter interaction at the femtosecond time scale.

# Femtosecond Laser Fabrication of High Precision Three-dimensional Woodpile Photonic Crystals and Their Near-field Characterisation

Baohua Jia and Min Gu

Centre for Micro-Photonics and CUDOS, Faculty of Engineering and Industrial Sciences  
Swinburne University of Technology, P. O. Box 218, Hawthorn 3122, Australia

**Abstract**— The femtosecond laser facilitated two-photon polymerisation (2PP) technique is a power fabrication tool for various arbitrary shaped micro-optical devices, among them photonic crystals (PCs) representing a hot topic [1]. Due to their unique optical properties and potential capability to miniaturise optical system, three-dimensional (3D) PCs have attracted much interest in the last two decades. Various fabrication techniques have been proposed and demonstrated. However challenge remains when near-infrared (NIR) or visible PCs compatible with the current telecommunication infrastructure are fabricated because periodicities comparable to the wavelength of illumination light have to be achieved. In this paper, by using the femtosecond laser facilitated 2PP technique, high precision 3D polymer woodpile PCs possessing NIR ( $\sim 1.1 \mu\text{m}$ ) bandgaps with nearly 100% suppression in transmission have been achieved. The NIR photonic bandgaps can be continuously tuned to a shorter wavelength region by employing a thermal annealing process, and eventually leads to woodpile PCs having bandgaps at a wavelength shorter than  $1 \mu\text{m}$ . To characterise the 3D PCs and to optimise the fabrication process, near-field optical microscopy has been employed to obtain both the morphology and optical properties of the PCs simultaneously. The experimental results demonstrate that the near-field measurements provide significant additional information about the optical properties of the devices, which has been previously inaccessible [2].

## REFERENCES

1. Jia, B., J. Li, and M. Gu, "Two-photon polymerisation for three-dimensional photonic devices in polymer and nanocomposites," *Austr. J. Chem.*, Vol. 60, 484–495, 2007.
2. Jia, B., J. Li, and M. Gu, "Near-field characterization of three-dimensional woodpile photonic crystals fabricated with two-photon polymerization," *Frontiers in Optics 2006 The 90th OSA Annual Meeting*, Rochester, New York, USA, October 8–12, 2006.

# Three-dimensional Chiral Photonic Crystals

M. Thiel<sup>1</sup>, G. von Freymann<sup>1,2</sup>, and M. Wegener<sup>1,2</sup>

<sup>1</sup>Institut für Angewandte Physik and DFG-Center for Functional Nanostructures (CFN)  
Universität Karlsruhe (TH), Karlsruhe 76131, Germany

<sup>2</sup>Forschungszentrum Karlsruhe in der Helmholtz-Gemeinschaft, Karlsruhe 76021, Germany

**Abstract**— Direct laser writing (DLW) [1–5] based on tightly focused femtosecond laser pulses has become a routine technique for the rapid fabrication of complex three-dimensional (3D) photoresist structures with lateral feature sizes down to 100 nm. Indeed, DLW has even become commercially available quite recently (see, e.g., [www.nanoscribe.de](http://www.nanoscribe.de)).

In this talk, we present our recent corresponding work on 3D Photonic Crystals. Especially we concentrate on chiral microstructures. Periodic chiral dielectric or metallic nanostructures have recently attracted considerable attention because of the possibility of obtaining giant circular dichroism or giant gyrotropy in the optical regime. To date, chiral dielectric structures outperform chiral metallic structures by a large margin regarding losses.

Interesting dielectric candidates are the recently introduced circular-spiral designs [6–10] — three-dimensional nanostructures of considerable complexity. While it is conceivable that high-quality circular-spiral structures might be fabricated on large areas at low cost via holographic lithography, it would be highly desirable to have blueprints at hand that are accessible by a variety of different approaches suitable for large-area low-cost mass fabrication. Regarding a distinct class of periodic structures, namely photonic-band-gap materials, layer-by-layer approaches such as the famous woodpile structure have proven to be accessible by a large variety of different techniques. Thus, chiral layer-by-layer structures appear to be attractive as well.

We fabricate and characterize polymeric three-dimensional layer-by-layer chiral photonic crystals via direct laser writing in the commercially available photoresist SU-8. The obtained circular dichroism from polarization stop bands is comparable to that of recently demonstrated circular-spiral photonic crystals [8–10]. For the here presented layer-by-layer chiral photonic crystals, the transmittance in the polarization stop band centered around 1.55  $\mu\text{m}$  wavelength is about 91% for right-handed circular incident polarization (RCP) impinging on a left-handed structure and about 2% for left-handed circular incident polarization (LCP) and the same structure. As expected for ideal structures without unintentional linear birefringence, LCP and RCP interchange for a right-handed structure [8–10].

## REFERENCES

1. Kawata, S., et al., *Nature*, Vol. 412, 697, 2001.
2. Deubel, M., et al., *Nature Mater.*, Vol. 3, 444, 2004.
3. Deubel, M., et al., *Appl. Phys. Lett.*, Vol. 85, 1895, 2004.
4. Deubel, M., et al., *Appl. Phys. Lett.*, Vol. 87, 221104, 2005.
5. Deubel, M., et al., *Opt. Lett.*, Vol. 31, 805, 2006.
6. Lee, J. and C. T. Chan, *Opt. Express*, Vol. 13, 8083–8088, 2005.
7. Lee, J. and C. T. Chan, *Appl. Phys. Lett.*, Vol. 90, 051912, 2007.
8. Thiel, M., et al., *Adv. Mater.*, Vol. 19, 207, 2007.
9. Thiel, M., et al., *Opt. Lett.*, in press, 2007.
10. Thiel, M., et al., *Appl. Phys. Lett.*, submitted, 2007.

## 3D Structuring of Materials by Femtosecond Pulses

S. Juodkazis and H. Misawa

Research Institute for Electronic Science, Hokkaido University  
N21W10 CRIS Bldg., Sapporo 001-0021, Japan

**Abstract**— Photonic crystals are periodic dielectric structures which are expected to play important role in optics and optoelectronics due to their unique capabilities of controlling the emission and propagation of light via photonic band gap (PBG) effects. These capabilities can be best exploited in three-dimensional (3D) photonic crystals. Since the direct, large scale 3D microfabrication of photonic crystals from semiconductors has proven to be tedious, cheaper and simpler fabrication strategies are highly demanded. Some of these strategies involve microfabrication of so-called photonic crystal templates using more feasible techniques and materials. The templates can be subsequently infiltrated by other materials having higher refractive index. Also, the photo-polymerized templates can be coated by metals using electroless deposition, which forms an uniform layer of 50–200 nm of metal (Ni, Ag, Au, etc.) over the frame of the structure. Such metal coated photonic structures perform as edge filters with a controllable spectral position of the edge in IR spectral region. Similar structures can be used for plasmonic applications as well.

Femtosecond lasers enable to perform large-scale 3D microstructuring of materials with typical feature sizes of 0.2–1  $\mu\text{m}$ . These characteristics make femtosecond laser microfabrication a highly suitable technique for the fabrication of 3D photonic crystals and their templates. Here, we outline the physical principles underlying the 3D laser microstructuring techniques: holographic [1] and direct laser writing [2]. We describe application of these techniques for the fabrication of 3D photonic crystals, and demonstrate some of the results achieved in this field and discuss the mechanisms of 3D material processing.

### REFERENCES

1. Kondo, T., S. Juodkazis, V. Mizeikis, S. Matsuo, and H. Misawa, *New J. Phys.*, Vol. 8, No. 10, 250–266, 2006.
2. Seet, K. K., V. Mizeikis, S. Matsuo, S. Juodkazis, and H. Misawa, *Adv. Mat.*, Vol. 17, No. 5, 541–545, 2005.

# Direct Femtosecond Fabrication in High Refractive Index Materials

Guangyong Zhou and Min Gu

Centre for Micro-Photonics and Centre for Ultrahigh-bandwidth Devices for Optical Systems (CUDOS)  
Faculty of Engineering and Industrial Sciences, Swinburne University of Technology  
P. O. Box 218, Hawthorn VIC 3122, Australia

**Abstract**— Photonic crystals (PhCs) are believed to be the basic platform for many advanced applications such as ultrasensitive optical sensing devices, ultra-low threshold lasers and ultra-fast data processing and telecommunications. To realize these cutting-edge devices, the PhCs need to have 3D complete bandgap. In other words, the PhCs need to be fabricated in high refractive index materials. Another very important feature is that the materials need to have large nonlinearity to realize functional devices. Lithium niobate ( $\text{LiNbO}_3$ ) and chalcogenide glasses (ChGs) are excellent candidates which can meet both criteria.  $\text{LiNbO}_3$  has a high refractive index of  $\sim 2.2$  and a large transparent range of  $0.45\text{--}5\ \mu\text{m}$  which makes it a suitable candidate for near-infrared photonic crystal fabrication. ChGs are amorphous materials containing one of the chalcogen elements (e.g., S, Se, Te) and a wide array of other elements (e.g., As, Ge, Cd, etc). This class of glasses have high refractive index ( $> 2.4$ ) and excellent transparency in the infrared wavelength region ( $1\ \mu\text{m}\text{--}15\ \mu\text{m}$ ).

The direct laser writing technique has been proved to be an efficient method to fabricate PhCs in low refractive index materials [1–3]. However, in high refractive materials the refractive index mismatch between materials and immersion medium introduces very strong aberration distorts the focus region [4]. Although previous results show that 3D PhCs can be fabricated directly in  $\text{LiNbO}_3$  by using the femtosecond laser induced microexplosion method [5, 6] and in  $\text{As}_2\text{S}_3$  by using the two photonic polymerization method [7], strong aberration still cause serious distortion at the focus region and therefore deteriorate the quality of the PhCs. Here we will review the problems of direct laser writing in high refractive index materials and aberration compensation using the adaptive optics method.

## ACKNOWLEDGMENT

The work is jointly supported by an Australian Research Council (ARC) Discovery project and ARC Centres of Excellence Program. CUDOS is an ARC Centre of Excellence.

## REFERENCES

1. Zhou, G., M. Ventura, M. Straub, and M. Gu, “In-plane and out-of-plane band-gap properties of a two-dimensional triangular polymer-based void channel photonic crystal,” *Appl. Phys. Lett.*, Vol. 84, 4415–4417, 2004.
2. Zhou, G., M. Ventura, M. Vanner, and M. Gu, “Use of ultrafast-laser-driven microexplosion for fabricating three-dimensional void-based diamond-lattice photonic crystals in a solid polymer material,” *Opt. Lett.*, Vol. 29, 2240–2242, 2004.
3. Zhou, G., M. Ventura, M. Vanner, and M. Gu, “Fabrication and characterization of face-centered-cubic void dots photonic crystals in a solid polymer material,” *Appl. Phys. Lett.*, Vol. 86, 011108, 2005.
4. Gu, M., *Advanced Optical Imaging Theory*, Springer, Berlin, 2000.
5. Zhou, G. and M. Gu, “Anisotropic properties of ultrafast laser-driven microexplosions in lithium niobate crystal,” *Appl. Phys. Lett.*, Vol. 87, 241107, 2005.
6. Zhou, G. and M. Gu, “Direct optical fabrication of three-dimensional photonic crystals in high refractive index  $\text{LiNbO}_3$  crystal,” *Opt. Lett.*, Vol. 31, 2783–2785, 2006.
7. Wong, S., M. Deubel, F. Pérez-Willard, S. John, G. A. Ozin, M. Wegener, and G. von Freymann, “Direct laser writing of three-dimensional photonic crystals with a complete photonic bandgap in chalcogenide glasses,” *Adv. Mater.*, Vol. 18, 265–269, 2006.



## Photonic Quasi-crystals: A Review

**Robert C. Gauthier**

Department of Electronics, Carleton University  
Ottawa, Ontario K1S-5B6, Canada

**Abstract**— The generally known photonic crystals are those that contain an intricate mix of two dielectric materials showing a spatial translational symmetry in the pattern. Due to this translational symmetry, computation techniques extracted from solid state physics can be applied in determining the optical properties of the dielectric structure, most importantly, the band structure and location of bandgaps. The introduction of an irregularity in the pattern “defect” enables a host of optical device configurations. The photonic quasi-crystal is an intricate mix of two dielectric materials that shows only a rotational symmetry in the pattern. Computations, using techniques such as FDTD, indicate that photonic quasi-crystal also possesses a photonic bandgap and that defects and waveguides can be introduced to facilitate optical devices. This presentation will review recent developments in photonic quasi-crystal research, focussing on computation techniques, structure patterning and applications. A new class of photonic quasi-crystal will be presented which contains rotational as well as radial periodicity about the central location of the pattern.



# Session 1P4

## Terahertz Optoelectronics

<p><b>Experimental Study on Generation of THz Radiation Using Periodically and Aperiodically Poled Lithium Niobate</b></p> <p><i>Zhen Tian (Tianjin University, China); Changlei Wang (Tianjin University, China); Qirong Xing (Tianjin University, China); Jianqiang Gu (Tianjin University, China); Lu Chai (Tianjin University, China); Yanfeng Li (Tianjin University, China); Qingyue Wang (Tianjin University, China); Yiqiang Qin (Nanjing University, China); Yongyuan Zhu (National Laboratory of Solid State Microstructures, China);</i> .....</p>	156
<p><b>Waveguide Structures for Generation of Terahertz Radiation by Electro-optical Process in GaAs and ZnGeP<sub>2</sub> Using 1.55 μm Fiber Laser Pulses</b></p> <p><i>Tianxin Yang (Tianjin University, China); Shupeng Song (Tianjin University, China); Hongtao Dong (Tianjin University, China); Rongsheng Ba (Tianjin University, China);</i> .....</p>	157
<p><b>The Role of Non-resonant Effect in Terahertz Transmission through Subwavelength Holes</b></p> <p><i>Jianguang Han (Oklahoma State University, USA); Xinchao Lu (Oklahoma State University, USA); Abul K. Azad (Oklahoma State University, USA); Mufei Gong (Oklahoma State University, USA); Weili Zhang (Oklahoma State University, USA);</i> .....</p>	158
<p><b>Very Deep Subwavelength Metallic Gratings with Like-lens Properties at THz Frequency Region</b></p> <p><i>Dong Liang (Tianjin University, China); Changlei Wang (Tianjin University, China); Qirong Xing (Tianjin University, China); Yanfeng Li (Tianjin University, China); Zhen Tian (Tianjin University, China); Jianqiang Gu (Tianjin University, China); Lu Chai (Tianjin University, China); Qingyue Wang (Tianjin University, China);</i> .....</p>	159
<p><b>Electromagnetic Metamaterials for Terahertz Applications</b></p> <p><i>Hou-Tong Chen (MPA-CINT, Los Alamos National Laboratory, USA); Willie J. Padilla (Boston College, USA); Richard D. Averitt (Boston University, USA); Joshua M. O. Zide (University of California, USA); Arthur C. Gossard (University of California, USA); Clark Highstrete (Sandia National Laboratories, USA); Mark Lee (Sandia National Laboratories, USA); Abul K. Azad (MPA-CINT, Los Alamos National Laboratory, USA); John F. O'Hara (MPA-CINT, Los Alamos National Laboratory, USA); Antoinette J. Taylor (MPA-CINT, Los Alamos National Laboratory, USA);</i> .....</p>	160
<p><b>Interference and Spectral Shaping of Terahertz Pulses</b></p> <p><i>Zhen Tian (Tianjin University, China); Qirong Xing (Tianjin University, China); Changlei Wang (Tianjin University, China); Jianqiang Gu (Tianjin University, China); Lu Chai (Tianjin University, China); Yanfeng Li (Tianjin University, China); Qingyue Wang (Tianjin University, China);</i> .....</p>	161
<p><b>Time-frequency Analysis of Ultrafast THz Pulse in Metal Waveguide Based on THz-TDS</b></p> <p><i>Jianqiang Gu (Tianjin University, China); Haiyan Wen (Tianjin University, China); Qirong Xing (Tianjin University, China); Zhen Tian (Tianjin University, China); Feng Liu (Tianjin University, China); Changlei Wang (Tianjin University, China); Yanfeng Li (Tianjin University, China); Mingxia He (Tianjin University, China); Lu Chai (Tianjin University, China); Qingyue Wang (Tianjin University, China);</i> .....</p>	162
<p><b>Terahertz Response of Bulk and Nanostructured ZnO</b></p> <p><i>Jianguang Han (Oklahoma State University, USA); Wei Chen (University of Texas at Arlington, USA); J. Zhang (Inner Mongolia University, China); Mingxia He (Tianjin University, China); A. K. Azad (MPA-CINT, Los Alamos National Laboratory, USA); S. Ray (Oklahoma State University, USA); Y. Zhao (University of Georgia, USA); Weili Zhang (Oklahoma State University, USA);</i> .....</p>	163
<p><b>Terahertz Time-domain Spectroscopy of MgO Nanoparticles</b></p> <p><i>Jianguang Han (Oklahoma State University, USA); Xinchao Lu (Oklahoma State University, USA); Mei Sang (Tianjin University, China); Wei Chen (University of Texas at Arlington, USA); Weili Zhang (Oklahoma State University, USA);</i> .....</p>	164
<p><b>Terahertz Time-domain Spectroscopy Signature of Animal Tissues</b></p> <p><i>Mingxia He (Tianjin University, China); Meng Li (Tianjin University, China); Weili Zhang (Oklahoma State University, USA);</i> .....</p>	165

## Experimental Study on Generation of THz Radiation Using Periodically and Aperiodically Poled Lithium Niobate

Zhen Tian<sup>1,2</sup>, Changlei Wang<sup>1,2</sup>, Qirong Xing<sup>1,2</sup>, Jianqiang Gu<sup>1,2</sup>  
Lu Chai<sup>1,2</sup>, Yanfeng Li<sup>1,2</sup>, Qingyue Wang<sup>1,2</sup>, Yiqiang Qin<sup>3</sup>, and Yongyuan Zhu<sup>3</sup>

<sup>1</sup>Ultrafast Laser Laboratory, College of Precision Instrument & Optoelectronics Engineering  
Tianjin University, Tianjin 300072, China

<sup>2</sup>Key Laboratory of Opto-electronics Information and Technical Science (Ministry of Education)  
Tianjin University, Tianjin 300072, China

<sup>3</sup>National Laboratory of Solid State Microstructures, Nanjing University, Nanjing 210093, China

**Abstract**— Recently there is a considerable research activity in the development of the new sources in the terahertz (THz) region of the electromagnetic spectrum. Over the past decade years, many new techniques were developed for generating broadband or narrowband THz radiation. And optical rectification of femtosecond pulses in nonlinear materials is an efficient method to generate ultra-short terahertz (THz) pulses in a wide frequency range extending from 100 GHz to well above 10 THz. Lithium niobate (LN) is well suited for such a purpose despite the high absorption in the THz range. In this paper, we have discussed experimentally and compared various schemes to generate THz radiation in periodically and aperiodically poled LN using femtosecond pulses. These schemes allow us to produce broadband as well as narrowband but tunable THz radiation. And multi-frequency modes THz radiation has been achieved using aperiodically poled LN. Such THz source with multi-frequency modes can provide THz radiation in a wide range of frequencies whose spectral power can be adjusted by structure parameters. Moreover we have designed a structure to generation broadband and narrowband THz radiation in a single LN crystal. At last, despite the discussion being focused on LN, these results can easily be applied to other nonlinear materials.

# Waveguide Structures for Generation of Terahertz Radiation by Electro-optical Process in GaAs and ZnGeP<sub>2</sub> Using 1.55 $\mu\text{m}$ Fiber Laser Pulses

T. Yang, S. Song, H. Dong, and R. Ba

College of Precision Instruments and Opto-electronics Engineering  
Laboratory of Optoelectronics Information Technical Science, Educational Ministry of China  
Center for Terahertz Waves, Tianjin University, China

**Abstract**— The usage of a 1550-nm ultrafast fiber laser will make the THz time domain spectroscopy system a more compact one with much lower costs. By discussing the basic schemes of the THz generation methods based on the 1550-nm ultrafast lasers briefly, GaAs and ZnGeP<sub>2</sub> are likely to be promising nonlinear optical crystals for THz waves generation by using electro-optical process because of their high second-order nonlinearity, and low absorption in the infrared, and wide THz spectral transmission. However, the mismatches of velocities between the THz wave and optical pulses are so large that the lengths of interaction are quite short, for example, the phase-matching coherent length of 0.7 mm for GaAs and 0.3 mm for ZnGeP<sub>2</sub> at 2 THz around, respectively. That limited extremely the applications of these bulk nonlinear optical crystals in the field of THz wave generation. In this paper, we have exploited the structure of parallel-plate waveguide (PPWG) to increase the phase velocity of THz wave in order to extend the interaction length between THz and optical pulses. Based on the dispersion properties of GaAs and ZnGeP<sub>2</sub> and the theory of waveguide mode propagation, the effective coherent lengths have been calculated for a variety of PPWG configurations in which a thin slice of nonlinear optical crystal is tightly sandwiched between two metallic plates. A figure of merit (FOM) of the nonlinear optical crystal used for optical rectification in PPWG versions is defined in the terms of relevant parameters of nonlinear optical crystals, especially including the absorption coefficients for the THz radiation. Comparison of a large set of the well known nonlinear optical crystals for PPWG configurations has been done theoretically by using published values. Meanwhile, a graded-index (GRIN) cylindrical lens of which axis is parallel to the PPWG width is introduced to reshape and focus the beam of optical pulses to enhance the lateral section of interaction and the optical intensity in the core of PPWG, and a model calculations predict that a new stack configuration of PPWGs could enable efficient generation of high energy THz pulses.

# The Role of Non-resonant Effect in Terahertz Transmission through Subwavelength Holes

Jianguang Han<sup>1,2</sup>, Xinchao Lu<sup>1</sup>, Abul K. Azad<sup>1</sup>, Mufei Gong<sup>1</sup>, and Weili Zhang<sup>1</sup>

<sup>1</sup>School of Electrical and Computer Engineering, Oklahoma State University  
Stillwater, Oklahoma 74078, USA

<sup>2</sup>Department of Physics, National University of Singapore, 2 Science Drive 3, 117542, Singapore

**Abstract**— The extraordinary transmission of light in metallic films perforated with periodic array of subwavelength holes has stimulated enormous interest due in part to their large span of promising applications in plasmonics, bioengineering, and nanofabrication, as well as the rich physics behind the phenomenon [1, 2]. Generally, the enhanced transmission is attributed to resonant excitation of surface plasmons (SPs) set up by the periodicity of the holes, where light is coupled into SPs on the incidence surface of the array, and then reemit from the other surface. The resonant interaction between electron-charged oscillations near the surface of metal and the electromagnetic field creates SPs and results in rather unique properties. The recent advance focusing on this topic has been achieved in the far-infrared terahertz regime by use of terahertz time-domain spectroscopy. At terahertz frequencies, the highly conductive nature of metals has generated unique interest in the investigation of extraordinary transmissions. Experimentally, the role of hole shape, polarization, dielectric properties of metal and substrate, and the thickness of the arrays on SP-enhanced terahertz transmission have been studied [3–8]. The characteristic excitation of terahertz SPs has enabled a further in-depth understanding of their physical mechanisms. Here, we study a series of subwavelength hole arrays with various hole widths that correspond to filling fractions of metal ranging from 81.3% to 34.4%. The measured hole width-dependent transmission spectra present a characteristic evolution, including well-regulated change in transmittance, linewidth broadening, and blueshift of peak frequencies. We show that such a characteristic evolution is resulted from the coupling between the discrete resonant excitation of SPs and the continuum non-resonant transmission through the holes. Numerical analysis based on the Fano model and the measured angle-resolved transmission band structures agree well with our experimental observations.

## REFERENCES

1. Ebbesen, T. W., H. J. Lezec, H. F. Ghaemi, T. Thio, and P. A. Wolff, *Nature*, Vol. 391, 667, 1998.
2. Barnes, W. L., A. Dereux, and T. W. Ebbesen, *Nature*, Vol. 424, 824, 2003.
3. Qu, D., D. Grischkowsky, and W. Zhang, *Opt. Lett.*, Vol. 29, 896, 2004.
4. Han, J. G., A. K. Azad, M. F. Gong, X. C. Lu, and W. Zhang, *Appl. Phys. Lett.*, Vol. 91, 071122, 2007.
5. Azad, A. K., Y. Zhao, and W. Zhang, *Appl. Phys. Lett.*, Vol. 86, 141102, 2005.
6. Azad, A. K. and W. Zhang, *Opt. Lett.*, Vol. 30, 2945, 2005.
7. Azad, A. K., Y. Zhao, W. Zhang, and M. He, *Opt. Lett.*, Vol. 31, 2637, 2006.
8. Zhang, W., A. K. Azad, J. Han, J. Xu, J. Chen, and X.-C. Zhang, *Phys. Rev. Lett.*, Vol. 98, 183901, 2007.

## Very Deep Subwavelength Metallic Gratings with Like-lens Properties at THz Frequency Region

Dong Liang, Changlei Wang, Qirong Xing, Yanfeng Li  
Zhen Tian, Jianqiang Gu, Lu Chai, and Qingyue Wang

Ultrafast Laser Lab, School of Precision Instruments and Optoelectronics Engineering  
Key laboratory of Optoelectronics Information and Technical Science  
Tianjin University, Tianjin 300072, China

**Abstract**— Existing and emerging applications of terahertz (THz) technology in medicine, imaging, biology, compact radar ranges, industrial controls, remote sensing, terahertz tomography, terahertz microscopy, space exploration and homeland security have stimulated intensive research in developing new elements for controlling THz waves. In this article, it is proposed that very deep metallic gratings with chirped slit width can be used to focus the THz beam. On the condition that the wavelength of the input wave is far larger than the grating period, the effective refractive index of the very deep subwavelength metallic gratings for the THz frequency region can be obtained by strict theoretical deduction. Based on the theoretical model, we propose a kind of subwavelength metallic grating with chirped slit width, which has similar characteristics with common optical lenses. Numerical simulations by finite difference time domain method are presented, which shows that the wave front will be bended when p-polarized THz plane wave transmits through the metallic grating. As a result it is proven that the present subwavelength metallic grating has like-lens properties for THz waves. The factors affecting the focus of this kind of lens are also discussed.

## Electromagnetic Metamaterials for Terahertz Applications

Hou-Tong Chen<sup>1</sup>, Willie J. Padilla<sup>2</sup>, Richard D. Averitt<sup>3</sup>  
Joshua M. O. Zide<sup>4</sup>, Arthur C. Gossard<sup>4</sup>, Clark Highstrete<sup>5</sup>  
Mark Lee<sup>5</sup>, Abul K. Azad<sup>1</sup>, John F. O'Hara<sup>1</sup>, and Antoinette J. Taylor<sup>1</sup>

<sup>1</sup>MPA-CINT, Los Alamos National Laboratory  
P.O. Box 1663, MS K771, Los Alamos, NM 87545, USA

<sup>2</sup>Department of Physics, Boston Collage  
140 Commonwealth Avenue, Chestnut Hill, MA 02467, USA

<sup>3</sup>Department of Physics, Boston University  
590 Commonwealth Avenue, Boston, MA 02215, USA

<sup>4</sup>Materials Department, University of California, Santa Barbara, CA 93106, USA

<sup>5</sup>Sandia National Laboratories, P.O. Box 5800, Albuquerque, NM 87185-1415, USA

**Abstract**— Development in terahertz (THz) science and technology is prevented mainly by the deficiency of suitable material responses. The useful electronic and photonic responses at microwave and optical regimes, respectively, both degrade significantly at this frequency regime. Over the last couple of decades many efforts associated with filling this so-called “THz gap” have resulted in moderate progress in THz generation and detection as well as various demonstrations of promising applications. Functional devices to control and manipulate THz waves, which are crucial in many applications, are still largely not available. An optimistic solution to this problem is found in the recently developed class of artificially structured composite materials termed metamaterials. The resonance responses of electromagnetic metamaterials significantly enhance their interaction with THz waves, thereby providing new opportunities to construct devices for THz applications. We have developed a series of planar electrical metamaterials at THz frequencies, which were characterized by THz time domain spectroscopy and all showed a strong electrical resonance response. Alteration of the properties of substrates upon which the metamaterials were fabricated has resulted in actively or dynamically tunable THz metamaterial devices. High efficiency electrical THz switching and modulation operating at room temperature have been accomplished by the use of a hybrid metamaterial and Schottky diode structure. The THz transmission was easily and effectively switched and/or modulated by applying a relatively small voltage bias. Dynamical switching of THz radiation was also achieved by photo-doping of the semiconductor substrates, where ultrafast switching has been demonstrated by the use of ErAs/GaAs nanoisland superlattice substrates. We show that electromagnetic metamaterials are promising in building various high efficiency and frequency agile functional devices for THz applications.



## Interference and Spectral Shaping of Terahertz Pulses

Zhen Tian, Qirong Xing, Changlei Wang, Jianqiang Gu, Lu Chai  
Yanfeng Li, and Qingyue Wang

Ultrafast Laser Laboratory, College of Precision Instrument & Optoelectronics Engineering  
Key Laboratory of Opto-electronics Information and Technical Science (Ministry of Education)  
Tianjin University, Tianjin 300072, China

**Abstract**— Over the past 20 years, the generation and the detection of free-space electromagnetic pulses in the terahertz frequency range have been widely considered one of the greatest developments in the field of ultrafast optics. And terahertz free-space radiation has been used in many applications such as coherent time-domain spectroscopy (TDS) and imaging. On the other hand, some applications, such as optical computing, radar and microwave communications and signal processing may favor interference and pulse shaping or spectral shaping of terahertz pulses, sometimes narrow-band terahertz pulse. For this reason, a terahertz Michelson interferometer was built in this paper, and we report on interference and spectral shaping of terahertz pulses. By using terahertz Michelson interferometer, freely propagating femtosecond laser pulses are superimposed on a ZnTe crystal leading to interference of terahertz pulses. The interference pattern represents the sum of the pulses with high fidelity. And controlling the relative phase of femtosecond laser pulses, mutual annihilation and amplification have been respectively achieved. Then varying time delay of the two femtosecond laser pulses, spectral shaping of terahertz pulse has been achieved. Our experimental setup is simpler and more convenient than other terahertz interference setup. At last the applications of interference and spectrum shaping for optical computing and communications have been discussed.

## Time-frequency Analysis of Ultrafast THz Pulse in Metal Waveguide Based on THz-TDS

Jianqiang Gu, Haiyan Wen, Qirong Xing, Zhen Tian, Feng Liu  
Changlei Wang, Yanfeng Li, Mingxia He, Lu Chai, and Qingyue Wang

Ultrafast Laser Laboratory, College of Precision Instrument & Optoelectronics Engineering  
Key Laboratory of Optoelectronics Information and Technical Science (Ministry of Education)  
Tianjin University, Tianjin, China

**Abstract**— In the recent 20 years, thanks to the breakthrough in THz sources and detectors, a new electromagnetic technology named THz-TDS (Terahertz time-domain spectroscopy) has been developed, accelerating the research based on ultrafast THz waves. The transmission THz pulses in metal waveguides is an important field in broadband THz research. Most research on THz waveguides is based on the THz-TDS system in which the electric field of THz pulse waveforms is detected directly. Fourier analysis generally plays an important role in this technology. Comparison between the THz pulses passing through and not passing through the waveguide reveals the sample's characteristics such as absorption and dispersion. But Fourier transforming THz pulses means losing all time information. So, deeper understanding requires time-frequency analysis. Our work is based on a typical THz-TDS system but uses continuous wavelet transform (CWT) to analyze the THz pulses. The result is a coefficient matrix which represents the magnitude or phase for a certain frequency of the pulses at a certain time. Through our investigation, we find this new approach gives more accurate and more obvious dispersion information. In addition and more importantly, CWT can distinguish between different modes existing in the waveguide, each mode showing its own group velocity, absorption factor and cutoff frequency. All these information is present clearly on a single CWT coefficient map. We think it will be a very powerful method in the THz field and we call it THz wavelet domain spectroscopy.

# Terahertz Response of Bulk and Nanostructured ZnO

Jianguang Han<sup>1,2</sup>, Wei Chen<sup>3</sup>, J. Zhang<sup>4</sup>  
Mingxia He<sup>1,5</sup>, A. K. Azad<sup>1</sup>, S. Ray<sup>1</sup>, Y. Zhao<sup>6</sup>, and Weili Zhang<sup>1</sup>

<sup>1</sup>School of Electrical and Computer Engineering, Oklahoma State University  
Stillwater, Oklahoma 74078, USA

<sup>2</sup>Department of Physics, National University of Singapore, 2 Science Drive 3, 117542, Singapore

<sup>3</sup>Department of Physics, University of Texas at Arlington, Arlington, TX 76019, USA

<sup>4</sup>College of Chemistry and Chemical Engineering, Inner Mongolia University  
Hohhot, Inner Mongolia 010021, China

<sup>5</sup>Center for Terahertz waves and College of Precision Instrument and Optoelectronics Engineering  
Tianjin University, Tianjin 300072, China

<sup>6</sup>Department of Physics and Astronomy, University of Georgia, Athens, GA 30602, USA

**Abstract**— Understanding the far-infrared (IR) optical and dielectric properties of zinc oxide (ZnO) is essential for its terahertz applications. With a direct band gap (3.37 eV) at room temperature and their unique properties, ZnO is one of the most promising semiconductors and has attracted enormous interest with applications in electro-optic, acousto-optic and optoelectronic devices, ultraviolet-light emitters, chemical sensors, and piezoelectric materials [1–4]. ZnO possesses a number of advantages that facilitate its use for terahertz device applications, such as ease in fabrication, wide band gap, rather high mobility and resistivity, and transparency at terahertz frequencies. Pulsed terahertz radiation has been demonstrated from a photoconductive switch fabricated on high-resistivity, single-crystal ZnO [5]. The experimental result showed that its high breakdown electric field enables ZnO to be an intriguing semiconductor in high power terahertz generation. Recently, particular attention has been paid to ZnO nanostructures not only for fundamental research on material properties in the terahertz regime but also for promising device applications. Here, we present terahertz time-domain spectroscopy (THz-TDS) characterization of far-IR optical and dielectric properties of ZnO of different morphologies, including bulk single-crystal, nanowires, tetrapods, tubes, and prisms. The THz-TDS results are analyzed and well fit with dielectric theory combined with effective medium models. Our results indicate that different ZnO nanostructure morphologies exhibit different characteristics due to diverse resonance mechanisms dominated by either free electrons or phonons. The dielectric function of tubular and prismlike structures exhibits the Drude-like behavior, while it is dominated by low-frequency phonon resonances for nanowires and tetrapods. The overall low-frequency phonon resonances of these nanostructures are measured by Raman scattering spectroscopy, showing good consistency with those of bulk wurtzite single-crystal ZnO.

## REFERENCES

1. Wang, Z. L., *J. Phys: Condens. Matter*, Vol. 16, 829, 2004.
2. Fang, Z. and J. G. Lu, *J. Nanosci. Nanotech.*, Vol. 5, 1561, 2005.
3. Özgür, Ü., Y. I. Alivov, C. Liu, A. Teke, M. A. Reshchikov, S. Doğan, V. Avrutin, S. J. Cho, and H. Morkoç, *J. Appl. Phys.*, Vol. 98, 041301, 2005.
4. Han, J. G., W. Zhang, W. Chen, S. Ray, J. Zhang, M. X. He, A. Azad, and Z. Y. Zhu, *J. Phys. Chem. C*, Vol. 111, 13000, 2007.
5. Ono, S., H. Murakami, A. Quema, et al., *Technical Digest of CLEO' 2005*, Baltimore, MD (CD ROM), Paper CThX6, May 22–27, 2005.

# Terahertz Time-domain Spectroscopy of MgO Nanoparticles

Jianguang Han<sup>1</sup>, Xinchao Lu<sup>1</sup>, Mei Sang<sup>2</sup>, Wei Chen<sup>3</sup>, and Weili Zhang<sup>1</sup>

<sup>1</sup>School of Electrical and Computer Engineering, Oklahoma State University  
Stillwater, Oklahoma 74078, USA

<sup>2</sup>Center for Terahertz waves and College of Precision Instrument and optoelectronics Engineering  
Tianjin University, Tianjin 300072, China

<sup>3</sup>Department of Physics, University of Texas at Arlington, Arlington, TX 76019, USA

**Abstract**— Magnesium oxide (MgO) is an important semiconductor due to its fascinating physical and chemical properties and promising applications in a broad range of disciplines, particularly in terahertz optoelectronics. With rock-salt structure of NaCl, MgO does not show any phase transition at least up to 227 GPa, and thus make it a better pressure medium in high pressure solid state devices. It is well known that as an inert material with a high melting point, MgO is widely used as a catalyst in important chemical reactions and as a good substrate for many materials. The characteristic high melting point makes MgO a basic refractory material for lining crucibles and fireproofing applications. Pressed MgO is also used as an optical material and has an essential use for in optical devices [1–3]. Here, the optical and dielectric properties of MgO nanoparticles and bulk single-crystal MgO are studied by use of terahertz time-domain spectroscopy over a broad frequency range from 0.3 to 3.5 THz. The terahertz system used in our measurements is a photoconductive switch-based terahertz spectrometer which is aligned into an 8F confocal geometry in order to achieve a 3.5-mm frequency-independent beam waist, as well as the excellent beam coupling between the transmitter and receiver [4]. Both the reference and sample pulses in the time domain are Fourier transformed to obtain corresponding complex amplitude spectra. The measured refractive index, power absorption, and complex dielectric function are obtained and well analyzed by a dielectric theory. In comparison to its bulk materials, MgO nanostructures often present quite different properties. Hence, the investigation of low-frequency optical characteristics represented here in MgO nanoparticles compared with its bulk single crystal is essential to clearly understand their dielectric properties, optical mode behavior, and size effect. This is also of great interest in future device applications of both crystalline and nanostructured MgO in the terahertz regime.

## REFERENCES

1. Duffy, T. S., R. J. Hemley, and H. K. Mao, *Phys. Rev. Lett.*, Vol. 74, 1371, 1995.
2. Williams, Q. and E. J. Garnero, *Science*, Vol. 273, 1528, 1996.
3. Strachan, A., T. Cagin, and W. A. Goddard, *Phys. Rev. B*, Vol. 60, 15084, 1999.
4. Han, J. G., W. Zhang, W. Chen, L. Thamizhmani, A. K. Azad, and Z. Y. Zhu, *J. Phys. Chem. B*, Vol. 110, 1989, 2006.

# Terahertz Time-domain Spectroscopy Signature of Animal Tissues

Mingxia He<sup>1</sup>, Meng Li<sup>1</sup>, and Weili Zhang<sup>1,2</sup>

<sup>1</sup>Center for Terahertz Waves, College of Precision Instrument and Optoelectronics Engineering  
Tianjin University, Tianjin 300072, China

<sup>2</sup>School of Electrical and Computer Engineering, Oklahoma State University  
Stillwater, Oklahoma 74078, USA

**Abstract**— The terahertz time-domain spectroscopy becomes a promising technology in studies of biological tissues, genetic analysis, and cancer diagnosis. Due to the fact that biological tissues possess high level of hydration, it results in strong absorption at terahertz frequencies. Here, we present terahertz time-domain spectroscopy characterization of animal tissues, including skin, fat, and muscles from porcine and rat samples. The experimental data reveal different frequency-dependent responses to terahertz radiation for difference types of tissues from these two animals.

The results show the power absorption coefficients of the porcine samples. Among different type of the porcine tissues, muscle shows the highest absorption and the frequency-dependent value is compatible with the previous measurements. As being consistent with the estimation from the time-domain transmitted pulses and the corresponding spectra, the absorption coefficient of skin tissue is obviously lower than that of muscle by an average of 10%. Compared to skin and muscle, the fat tissue shows extremely low absorption at terahertz frequencies due to very low water content. At 0.5 THz, the power absorption coefficients of skin and lean pork are all above  $100 \text{ cm}^{-1}$ , while it is only  $15 \text{ cm}^{-1}$  for porcine fat.

We have also carried out THz-TDS characterization of rat tissues. The tissues were measured within 24 hours of the euthanasia of the six-month-old rats. The skin and muscle tissues with thickness of 0.53 and 0.96 mm, respectively, were characterized. The power absorption coefficients of the rat tissues have very similar values compared to the results obtained in porcine tissues.



# Session 1P5

## Remote Sensing and Applications

<b>Interferometric ISAR Imaging on Squint Model</b>	
<i>Changzheng Ma (National University of Singapore, Singapore); Tat Soon Yeo (National University of Singapore, Singapore); Hwee Siang Tan (National University of Singapore, Singapore); Guangyue Lu (Xi'an Institute of Post and Telecommunications, China);</i>	168
<b>Avian Detection and Monitoring Using Frequency-stepped Chirp Signal Radar</b>	
<i>Qun Zhang (AFEU, China); Ying Luo (AFEU, China); Dong Liang Hu (Naval University of Engineering, China); Bin-feng Luo (Naval University of Engineering, China); Y. S. Zeng (AFEU, China);</i>	169
<b>Model of Man-made Target beneath Foliage Using PolInSAR</b>	
<i>Bin Zou (Harbin Institute of Technology, China); Hongjun Cai (Harbin Institute of Technology, China); Lamei Zhang (Harbin Institute of Technology, China); Maoliu Lin (Harbin Institute of Technology, China);</i>	170
<b>A Hybrid Entropy Decomposition and Maximum Likelihood Method for Image Classification</b>	
<i>Chue-Poh Tan (Technology Park Malaysia, Malaysia); Hong-Tat Ewe (Technology Park Malaysia, Malaysia); Hean-Teik Chuah (Multimedia University, Malaysia);</i>	171
<b>Comparison of Methods for Target Detection and Applications Using Polarimetric SAR Image</b>	
<i>Lamei Zhang (Harbin Institute of Technology, China); Junping Zhang (Harbin Institute of Technology, China); Bin Zou (Harbin Institute of Technology, China); Ye Zhang (Harbin Institute of Technology, China);</i>	173
<b>Light Reflection from a Rough Liquid Surface Including Wind-wave Effects in a Scattering Atmosphere: Polarized Light Case</b>	
<i>Santo V. Salinas (National University of Singapore, Singapore); Soo Chin Liew (National University of Singapore, Singapore);</i>	174
<b>Retrieval of Sea Water Attenuation Coefficient and Water Depth from Hyperspectral Imagery</b>	
<i>Soo Chin Liew (National University of Singapore, Singapore); Santo V. Salinas (National University of Singapore, Singapore); Chew Wai Chang (National University of Singapore, Singapore);</i>	175
<b>Localization in Near Field with Wideband Signal: Trade-off between Bandwidth and Number of Sensors</b>	
<i>Hongyang He (University of Nantes, France); Yide Wang (University of Nantes, France); Joseph Sallard (Universite de Nantes, France);</i>	176
<b>Investigation of Novel Surface Acoustic Wave (SAW) Gas Sensor Used in Sensor Network</b>	
<i>Mitsutaka Hikita (Kogakuin University, Japan); Keiya Minami (Kogakuin University, Japan); Koki Takimoto (Kogakuin University, Japan); Yasushi Hiraizumi (Kogakuin University, Japan);</i>	177

## Interferometric ISAR Imaging on Squint Model

Changzheng Ma<sup>1,2</sup>, Tat Soon Yeo<sup>1</sup>, Hwee Siang Tan<sup>1</sup>, and Guangyue Lu<sup>3</sup>

<sup>1</sup>Department of Electrical and Computer Engineering, National University of Singapore, Singapore

<sup>2</sup>School of Electric and Information Engineering, Zhongyuan University of Technology, China

<sup>3</sup>Telecommunication Engineering Department, Xi'an Institute of Post and Telecommunications, China

**Abstract**— Conventional interferometric inverse synthesis aperture radar three dimensional imaging only consider broadside imaging condition. In this paper, squint model imaging configuration is discussed and the coordinate transform equation is given. The ISAR range profile envelope alignment problem among different antennas are also discussed. Simulation results show the effectiveness of our proposed method.



# Avian Detection and Monitoring Using Frequency-stepped Chirp Signal Radar

Q. Zhang<sup>1,2</sup>, Y. Luo<sup>1</sup>, D. L. Hu<sup>3</sup>, B. F. Luo<sup>3</sup>, and Y. S. Zeng<sup>1</sup>

<sup>1</sup>Institute of Telecommunication Engineering, AFEU, Xi'an 710077, China

<sup>2</sup>Key Laboratory of Wave Scattering and Remote Sensing Information (Ministry of Education)  
Fudan University, Shanghai 200433, China

<sup>3</sup>Naval University of Engineering, Wuhan 430033, China

**Abstract**— The bird aircraft strike hazard (BASH) is a worldwide problem to aviation, which brings billions of dollars in damage and loss of life every year. Statistics suggested that about 10,000 bird strike accidents happened all around the world per year, and 90 percents occurred during take-off and landing in the vicinity of airports. Avian radar systems are necessary to be developed for avian surveillance and early warning. Experiments point out that 3-centimeter wavelength surveillance radar (e.g., BIRDRAD) can detect the departure of migrants from different types of habitat within a range of 6 kilometers of the radar, and the Doppler weather surveillance radar (WSR-88D) can measure the density of birds in the radar beam as they begin a migratory movement within 60 kilometers, but trying to identify the type of bird is problematic. The abilities to distinguish types of targets (birds, insects or aircraft with small size, such as Unmanned Aerial Vehicle), identity types of birds, and determine flock sizes are considered to be important goals for future research and development.

The radar imaging with high resolution is a potential technique to solve the problems. To exploit the movement features of birds, the ultra-large-wideband signal is necessary to be utilized for high range resolution. In this paper, the frequency-stepped chirp signal is applied to synthesize a signal with a bandwidth 3 GHz for a range resolution 5 cm. By means of synthetic bandwidth with frequency-stepped chirp signals, high range resolution can be realized as well as alleviation of computing load of digital signal processor.

The range resolution obtained via frequency-stepped chirp signal is high enough to explore the micro-Doppler information of birds. The rotating structures in a radar target or mechanical vibrations of the target body may induce additional frequency modulation on returned signals and generate side-bands about the center frequency of the body Doppler frequency, called the micro-Doppler effect. Different micro-motions can induce different micro-Doppler features, that is to say, micro-Doppler can be regarded as a unique signature of the target, and provides additional information for target detection, recognition and identification. The swings of bird's wings can also cause the micro-Doppler phenomenon, which offers a new approach to identify the birds: transmitting frequency-stepped chirp signals to the birds, and then extracting the micro-Doppler information from the echoes.

This paper is organized as follows: Section 1 describes the principle of frequency-stepped signal; the micro-Doppler effect is introduced in Section 2; some discussion about the extraction of micro-Doppler is presented in Section 3; finally, some computer simulations are given in the last Section.

## Model of Man-made Target beneath Foliage Using PolInSAR

Bin Zou, Hongjun Cai, Lamei Zhang, and Maoliu Lin

Harbin Institute of Technology, No. 92 West Dazhi Street, Harbin 150001, China

**Abstract**— Polarimetric SAR Interferometry can be used for parameter inversion of ground. An appropriate model is of most importance for parameters inversion. This paper derives a series of scattering model that can be used for parameter inversion of forestry area, such as RV, RVoG, OV and OVoG. These models can reveal the characteristics of forestry area as well as establish the relationship between observed data and parameters of test area. Finally, a multi-layer random scattering model that can be used for parameter inversion of forestry area containing a man-made target is derived. An improved model is examined by the simulated data of the single-baseline polarimetric SAR interferometry. The result turns out that the improved RVoG scattering model is correct.

# A Hybrid Entropy Decomposition and Maximum Likelihood Method for Image Classification

Chue-Poh Tan<sup>1</sup>, Hong-Tat Ewe<sup>2</sup>, and Hean-Teik Chuah<sup>2</sup>

<sup>1</sup>Centre for Advanced Informatics, MIMOS Berhad, Technology Park Malaysia  
57000 Kuala Lumpur, Malaysia

<sup>2</sup>Multimedia University, Jalan Multimedia  
63100 Cyberjaya, Selangor, Malaysia

**Abstract**— This paper presents the development of Synthetic Aperture Radar (SAR) image classifier based on the hybrid method of “Entropy Decomposition and Maximum Likelihood” (EDML) for agricultural crop type classification. Entropy Decomposition is an effective technique to obtain valuable decomposed parameters for image interpretation with analysis of the underlying scattering mechanisms. However, the main disadvantage of Entropy Decomposition is that the decision boundaries of the analysis plane are arbitrary. To overcome this problem, Maximum Likelihood technique is taken into consideration to help to determine the decision boundaries based upon Gaussian probability model. Hence, the hybrid EDML is developed to provide alternative way to improve the classification accuracy. In this paper, this novel classifier has been applied on a multi-crop region of Flevoland, Netherlands with multi-polarization data for crop type classification. Validation of the classifiers has been carried out by comparing the classified image obtained from EDML classifier and ML classifier. The final outcome of this research clearly indicates that EDML has the ability in improving the classification accuracy for agricultural crop type classification.

The potential of SAR in discriminating among different agricultural crop type has been demonstrated in several studies [1–10]. Previously, Van Zyl [11] proposed an unsupervised classification to classify terrain types by identifying the scattering process as odd bounce, even bounce or diffuse scattering. The ocean surface and flat ground basically have the characteristics of Bragg scattering (odd bounce) while the city blocks, buildings, and hard targets have the characteristics of double bounce scattering (even bounce) and forest and heavy vegetation have the characteristics of volume scattering (diffuse scattering). It is interesting to find that this classification algorithm provides information for terrain type identification. For a refined classification into more classes, Cloude and Pottier [12] proposed an unsupervised classification algorithm based on their target decomposition theory that utilized two parameters: the entropy,  $H$ , and alpha,  $\bar{\alpha}$ . However, the main disadvantage of this algorithm is the arbitrary location of decision boundaries in the  $H - \bar{\alpha}$  feature space [13]. To surmount this insufficiency, we propose a combined method of Entropy Decomposition and Maximum Likelihood (EDML) to perform the agricultural crop type classification.

## REFERENCES

1. Tan, C. P., J. Y. Koay, H. T. Ewe, H. T. Chuah, and S. Bahari, “Applications of remote sensing in the monitoring of rice crops,” *IEM Journal*, Vol. 67, No. 4, Dec. 2006.
2. Tan, C. P., J. Y. Koay, K. S. Lim, H. T. Ewe, and H. T. Chuah, “Classification of multi-temporal SAR images for rice crops using combined entropy decomposition and support vector machine technique,” *Progress In Electromagnetics Research*, PIER 71, 19–39, 2007.
3. Tan, C. P., H. T. Ewe, and H. T. Chuah, “A hybrid entropy decomposition and support vector machine for agricultural crop type classification,” *Proceedings of the Progress in Electromagnetics Research Symposium (PIERS 2007)*, 42–46, Beijing, China, 26–30 March, 2007.
4. Lim, K. S., C. P. Tan, J. Y. Koay, V. C. Koo, H. T. Ewe, Y. C. Lo, and A. Ali, “Multitemporal C- band radar measurement on rice fields,” *Proceedings of the Progress in Electromagnetics Research Symposium (PIERS 2007)*, 36–39, Beijing, China, 26–30 March, 2007.
5. Lim, K. S., S. Bahari, C. P. Tan, J. Y. Koay, M. Y. Chua, V. C. Koo, H. T. Ewe, A. Halim, and M. Safid, “Rice field measurement using C-band scatterometer,” *4th National Microwave Remote Sensing Seminar*, MACRES, Kuala Lumpur, 28 November, 2006.
6. Tan, C. P., J. Y. Koay, K. S. Lim, H. T. Teng, H. T. Ewe, H. T. Chuah, and S. Bahari, “Image classification of rice growth stages using combination of entropy decomposition and support vector machine (EDSVM),” *Proceedings for PacRim AIRSAR Significant Results Symposium*, MACRES, Kuala Lumpur, 26–28 June, 2006.

7. Koay, J. Y., C. P. Tan, H. T. Ewe, H. T. Chuah, and S. Bahari, "Theoretical modelling and measurement comparison of season-long rice field monitoring," *Proceedings of the Progress in Electromagnetics Research Symposium (PIERS 2005)*, 25–28, Hangzhou, China, 22–26 August, 2005.
8. Ulaby, F. T., R. K. Moore, and A. K. Fung, *Microwave Remote Sensing: Active and Passive*, Artech House, Norwood, MA, 1986.
9. Bouman, B. A. M. and D. H. Hoekman, "Multi-temporal multi-frequency radar measurements of agricultural crops during the Agriscatt-88 campaign in The Netherlands," *Int. J. Remote Sens.*, Vol. 14, 1595–1614, 1993.
10. Tran, T. N., R. Wehrens, D. H. Hoekman, and L. M. C. Buydens, "Initialization of markov random field clustering of large remote sensing images," *IEEE Trans. Geosci. Remote Sensing*, Vol. 43, No. 8, 1912–1919, 2005.
11. Van Zyl, J. J., "Unsupervised classification of scattering behavior using radar polarimetry data," *IEEE Trans. Geosci. Remote Sensing*, Vol. 27, No. 1, 36–45, Jan. 1989.
12. Cloude, S. R. and E. Pottier, "An entropy based classification scheme for land applications of polarimetric SAR," *IEEE Trans. Geosci. Remote Sensing*, Vol. 35, No. 1, 68–78, Jan. 1997.
13. Yahia, M. and Z. Belhadj, "Unsupervised classification of polarimetric SAR images using neural networks," *IEEE International Conference Information and Communication Technologies 2004*, 335–337, 2004.

## Comparison of Methods for Target Detection and Applications Using Polarimetric SAR Image

Lamei Zhang, Junping Zhang, Bin Zou, and Ye Zhang

Harbin Institute of Technology, No. 92 West Dazhi Street, Harbin 150001, China

**Abstract**— Polarimetric SAR (PolSAR) is sensitive to the orientation and characters of object and polarimetry could yield several new descriptive radar target detection parameters and lead to the improvement of radar detection algorithms. Target decomposition theory has been used for information extraction in PolSAR, and it can also explore the phase message in PolSAR data. In this paper, a comparison of polarimetric target decomposition methods is proposed. We generate a validity test for these methods using DLR ESAR L-band full polarized data. Results show that among many target decomposition algorithms, the coherent and incoherent formulations are quite comparable in distinguishing natural targets and man-made buildings. Pauli decomposition, Cameron decomposition and Freeman decomposition are suitable for the detection of natural targets. On the other hand, SDH decomposition, OEC decomposition, and Four-component model, in particular, are very useful for man-made target extraction.

# Light Reflection from a Rough Liquid Surface Including Wind-wave Effects in a Scattering Atmosphere: Polarized Light Case

Santo V. Salinas and Soo Chin Liew

Centre for Remote Imaging, Sensing and Processing, National University of Singapore, Singapore

**Abstract**— Surface phenomena, such as wind-generated waves, gravity and capillary waves, internal waves, ocean slicks, surface currents, density fluctuations etc., modulate the ocean's surface roughness with a direct effect on the Sun's reflection pattern (Sun glint) observed over the ocean. At the same time, the Sun glint is affected by the scattering effects of molecules and aerosols present in the atmosphere. To understand these wind and wave related effects on the Sun glint pattern, Salinas et al. [1] have developed an atmospheric radiative transfer model that incorporates a new wind-wave description for the mean square slope of the sea surface. This model solves the scalar radiative transfer equation and includes wind interaction and wave states, such as wave age, as the main factors contributing to surface roughness. In this paper, we extend the above mentioned work and include light polarization effects originating from aerosol and molecular scattering and from the roughness of the surface. Polarization is considered by using the 4-Stokes vector formalism and the  $4 \times 4$  scattering phase matrix for aerosols and molecules. Simulation results showing polarization effects on the simulated, top of the atmosphere, Sun glint are presented. These computations were performed for a range of wind speeds and wave age parameter relevant to remote sensing. The model can have possible applications to the retrieval of wind and wave states, such as wave age, near a Sun glint region and for the study of of ocean surface roughness characteristics arising from air-sea interaction.

## REFERENCES

1. Quant, J., *Spectrosc. Radiat. Transfer*, Vol. 105, 414–424, 2007.

# Retrieval of Sea Water Attenuation Coefficient and Water Depth from Hyperspectral Imagery

Soo Chin Liew, Santo V. Salinas, and Chew Wai Chang

Centre for Remote Imaging, Sensing and Processing, National University of Singapore, Singapore

**Abstract**— The reflectance of sea water depends on the backscattering and absorption properties of water. The penetration of electromagnetic (EM) waves into sea water depends on the water attenuation coefficient at the particular wavelengths of the EM waves. For pure water, the attenuation coefficient is about  $0.01 \text{ m}^{-1}$  near 420 nm (blue region) and increases to about  $0.6 \text{ m}^{-1}$  at 700 nm (red region). Thus, the characteristic penetration depth, i.e., the inverse of the attenuation coefficient, is about 100 m in the blue end and decreases to about 1.5 m in the red end of the spectrum. Coastal waters typically contain suspended particles and dissolved material that increase the scattering and absorption coefficients, and hence decrease the penetration depth. If the sea is shallower than the penetration depth, reflection from the sea bottom would also contribute to the reflectance measured above the water surface. Models exist that relate the above-water reflectance to the water depth, absorption and backscattering coefficients, and the sea bottom reflectance. In this paper, we use an optimization procedure to retrieve these parameters from the reflectance spectra measured above the water surface. Three sets of reflectance spectra were tested. The first set was a synthetic data set generated from a forward simulation model. The second data set was measured using a hand-held spectrophotometer during field trips in coastal waters around Singapore. The third set was obtained from an air-borne imaging spectrometer. Coincidental in-situ measurements of water depth and water absorption and attenuation coefficients were available for validation of the retrieval results. For the air-borne data set, effects of atmosphere need to be considered. The atmospheric effects were included in the optimization model and the atmospheric parameters were retrieved together with the water parameters.

## Localization in Near Field with Wideband Signal: Trade-off between Bandwidth and Number of Sensors

H. He, Y. Wang, and J. Saillard

Laboratoire IREENA, Polytech'Nantes, University of Nantes, France

**Abstract**— Source localization using sensor arrays is one of the important applications of radar, sonar... etc. During last few decades, the wideband (WB) technique has been well used in source localization for the sake of high resolution when the size of antenna arrays is limited. However, to determine the resolution capacity of a WB localization system remains a problem. In this article, we propose firstly a method for the wideband source localization in the near field, and secondly we present a comparison of the resolution for wideband signal and narrow band (NB) signal with larger size of antenna arrays. Finally, a proximate method to determine the resolution capacity of a WB system is based on the comparison.

In the first part of this article, the WB localization method is stated. To summate the information carried by different frequencies, the coherent summation method is employed. This method is widely used in the far field. we show that it can also be applied in near field with the pre-estimation of the steering vector (knowing as directional vector for far field source localization). After coherent focalization, the covariance matrix of the received signal at sensors is established for a certain frequency. Finally, the precise position of the target is given with the help of MUSIC method.

In the second part, the comparison of the resolution for WB system and NB system is presented. We take the 3 dB-beamwidth of the pseudo-spectrum in two axes as the criterion for the comparison of resolution. With this criterion, we can define an equivalent NB system with larger size of antenna array which gives the same resolution as a WB system. The relation between the bandwidth and the number of antennas can be found proximately through the comparison. Finally, we can simply calculate the needed bandwidth for the WB system with the resolution achieved by a NB system.



# Investigation of Novel Surface Acoustic Wave (SAW) Gas Sensor Used in Sensor Network

Mitsutaka Hikita, Keiya Minami, Koki Takimoto, and Yasushi Hiraizumi  
Kogakuin University, Nishi-Shinjuku, Shinjuku-ku, Tokyo, Japan

**Abstract**— Mobile communications, e.g., cellular phones, have become very widespread. A new concept called “Sensor Network” has been proposed with the development of such communications systems. Sensed signals from many sensor nodes arranged in a wide area are gathered to a center node by technology similar to that used in mobile communications. Home/office circumstance control, environment monitoring and protection, etc can be conducted based on the collected data. We propose a new SAW (Surface Acoustic Wave) subtle-gas sensor, which can be used in these sensor nodes.

One of the most successful SAW gas-sensors is a SAW GC (gas chromatography) invented by E. J. Staple et al. [1, 2]. However, it has a rather complicated structure using not only a SAW sensor but also a trap and a column tubes to separate gases according to their molecule weight. Due to the rather large size and the high power consumption, it can not be adopted in “Sensor Network”. Moreover, only Quartz crystal substrates have been used in these kinds of conventional SAW gas sensors, because SAW sensors require very good temperature characteristics for the piezoelectric substrates. We have invented a new SAW sensor structure, which can remove such a limited selection for piezoelectric crystal substrates. The proposed sensor consists of three SAW delay lines, two delay lines of which are used to generate standard in-phase (I-phase) and quadrature-phase (Q-phase) signals. The third one is used for sensing of gasses. Phase shift for propagating SAW due to mass loading effect of sensing gasses is measured based on the standard I-phase and Q-phase signals from the other two delay lines which are isolated from the sensing gasses. The influence from temperature is same for the three delay lines, which provides temperature-compensated characteristics between phase of the sensing delay line and I-/Q-phases of the standard delay lines.

ZigBee has been regulated by IEEE 802.15.4 [3] and ZigBee Alliance as a wireless-communications medium for the “Sensor Network”. One of the most important features for ZigBee is the extremely low-power consumption, which provides several-year operation by a single battery. In ZigBee, 2.4 GHz is used to connect sensor nodes mutually in “Sensor Network”. They can provide not only conventional star-link but also new mesh-link type network topology. Our sensor is also designed to be combined with 2.4-GHz ZigBee. Sensing signals with several hundred MHz are generated by division and multiplication of 2.4-GHz signal, which can remove the necessity of a VCO (Voltage-Controlled Oscillator) used in the conventional SAW sensors. Moreover, the dynamic range of our sensor is expanded by using not only fundamental but also 3-rd harmonic frequency SAWs to detect gasses. For example, 150 MHz obtained from 2.4 GHz divided by 16 is used in coarse sensing, while 450 MHz, 150 MHz multiplied by 3, is used in fine sensing. It is predicted that new “Sensor Network” in which our sensors are installed will possibly provide hydrogen-gas leakage sensing for future fuel-cell cars and environmental-pollution gas sensing.

## REFERENCES

1. Staples, E. J., “Dioxin/Furan detection and analysis using a SAW based electronic nose,” *IEEE Ultrason. Symp. Proc.*, 521–525, 1998.
2. Electronic Sensor Technology HP, “Chemical sensor for the 21 century,” (<http://www.estcal.com/>).
3. IEEE Standard 802.15.4: *Wireless Medium Access Control (MAC) and Physical Layer (PHY) Specifications for Low Rate Wireless Personal Area Networks (LR-WPANs)*, 2003.



# Session 1P6

## Electromagnetic Wave Applications in Material Processing and Characterization

<p><b>EXAFS and Raman Characterization of <math>x\text{La}(\text{Mg}_{1/2}\text{Sn}_{1/2})\text{O}_3-(1-x)\text{La}(\text{Mg}_{1/2}\text{Ti}_{1/2})\text{O}_3</math> Microwave Ceramics</b></p> <p><i>Chih-Ta Chia (National Taiwan Normal University, Taiwan); Tsan-Yuan Yu (National Taiwan Normal University, Taiwan); Chieh-Han Lu (National Taiwan Normal University, Taiwan); G. Santosh Babu (IIT - Madras, India); Venkatachalam Subramanian (IIT - Madras, India); V. R. K. Murthy (IIT - Madras, India); I-Nan Lin (Tamkang University, Taiwan);</i> .....</p>	180
<p><b>Dynamic Optical and Terahertz Responses of YBCO Films with Various In-plane Orientations</b></p> <p><i>Zen-Chi Lin (National Tsing Hua University, Taiwan, R.O.C.); Pao-An Lin (National Tsing Hua University, Taiwan, R.O.C.); Kuo-Chien Hsu (National Tsing Hua University, Taiwan, R.O.C.); Hsin-Chia Ho (National Tsing Hua University, Taiwan, R.O.C.); Shyh-Shii Pai (National Tsing Hua University, Taiwan, R.O.C.); Cheng-Chung Chi (National Tsing Hua University, Taiwan, R.O.C.);</i> .....</p>	181
<p><b>Anisotropic Ultrafast Dynamics in Doped <math>\text{Y}_{1-x}\text{Ca}_x\text{Ba}_2\text{Cu}_3\text{O}_{7-\delta}</math> Superconducting Thin Films</b></p> <p><i>C. W. Luo (National Chiao Tung University, Taiwan); K. H. Wu (National Chiao Tung University, Taiwan); J.-Y. Lin (National Chiao Tung University, Taiwan); T. M. Uen (National Chiao Tung University, Taiwan); Y. S. Gou (National Taiwan Normal University, Taiwan); Jenh-Yih Juang (National Chiao Tung University, Taiwan);</i> .....</p>	182
<p><b>Growth of Carbon Nanotubes and Its Applications in Quantum Transport Behavior and Hydrogen Storage</b></p> <p><i>H. Y. Miao (Tunghai University, Taiwan); L. W. Chang (National Tsing Hua University, Taiwan); Juh Tzeng Lue (National Tsing Hua University, Taiwan);</i> .....</p>	183
<p><b>Surface Plasma and Growth Mechanism of Gold Nanorods</b></p> <p><i>Ru-Shi Liu (National Taiwan University, Taiwan); H. M. Chen (National Taiwan University, Taiwan); S. F. Hu (National Taiwan Normal University, Taiwan);</i> .....</p>	184
<p><b>Far-infrared, Raman Spectroscopy and Microwave Dielectric Properties of <math>\text{La}(\text{Mg}_{0.5}\text{Ti}_{0.5-x}\text{Sn}_x)\text{O}_3</math> Ceramics</b></p> <p><i>I-Nan Lin (Tamkang University, Taiwan, China); Chih-Ta Chia (Taiwan Normal University, Taiwan, China); Hsiang-Lin Liu (Taiwan Normal University, Taiwan, China); Hsiu-Fung Cheng (National Taiwan Normal University, Taiwan, China); G. Santosh Babu (IIT-Madras, India); V. Subramanian (IIT-Madras, India); V. R. K. Murthy (IIT-Madras, India);</i> .....</p>	185
<p><b>Conductivities for Direct Current and Microwaves with Domain Wall Scattering for Ni-Fe Alloy Thin Films</b></p> <p><i>Yi-Chen Yeh (National Tsing Hua University, Taiwan); Juh Tzeng Lue (National Tsing Hua University, Taiwan);</i> .....</p>	186
<p><b>Photoelectric Effect of Silicon Nanopillar</b></p> <p><i>Shu-Fen Hu (National Taiwan Normal University, Taiwan); Ting-Wei Liao (National Taiwan Normal University, Taiwan); Chao-Yuan Huang (National Taiwan Normal University, Taiwan);</i> .....</p>	187
<p><b>The Studies of Defects in Phosphorous Ion-implanted Si(111) by Reflective Second Harmonic Generation</b></p> <p><i>Kuang-Yao Lo (National Chiayi University, Taiwan); Yi Jen Huang (National Chia Yi University, Taiwan);</i> .....</p>	188

## EXAFS and Raman Characterization of $x\text{La}(\text{Mg}_{1/2}\text{Sn}_{1/2})\text{O}_3-(1-x)\text{La}(\text{Mg}_{1/2}\text{Ti}_{1/2})\text{O}_3$ Microwave Ceramics

Chih-Ta Chia<sup>1</sup>, Tsan-Yuan Yu<sup>1</sup>, Chieh-Han Lu<sup>1</sup>, G. Santosh Babu<sup>2</sup>, V. Subramanian<sup>2</sup>  
V. R. K. Murthy<sup>2</sup>, and I. N. Lin<sup>3</sup>

<sup>1</sup>Department of Physics, National Taiwan Normal University, Taipei 11681, Taiwan

<sup>2</sup>Department of Physics, IIT - Madras, Chennai-600 036, India

<sup>3</sup>Department of Physics, Tamkang University, Tamsui, Taipei 251, Taiwan

**Abstract**— The 1:1 ordered  $x\text{La}(\text{Mg}_{1/2}\text{Sn}_{1/2})\text{O}_3-(1-x)\text{La}(\text{Mg}_{1/2}\text{Ti}_{1/2})\text{O}_3$  microwave ceramics with  $x = 0, 0.25, 0.5, 0.75$  and  $1$  were examined by Raman scattering and Extended X ray Absorption Fine Structure (EXAFS) to reveal the correlation of the micro-structure with the microwave dielectric properties. The microwave  $Qxf$  value has reached minimum value around 46000 with  $x = 0.5$ , while the dielectric constant decreases with Sn concentration. EXAFS found that the Sn atoms are sitting at Ti lattice site, and the Sn-O bond length increases with Sn concentration. This is mainly due to the larger ionic radius and heavy mass of  $\text{Sn}^{4+}$ , as compared with  $\text{Ti}^{4+}$  ions. Therefore, the volume of oxygen-octahedron increasing with Sn concentration is expected. However, the La-O bond length decreases with Sn concentration, that is the volume of  $\text{LaO}_8$  decreases, as revealed by EXAFS. Raman measurement found that the oxygen-octahedral vibrations mostly are redshifted by Sn doping, and the vibrations regarding to the La-site vibration are mostly blueshifted with Sn concentration. Raman measurement is consistent with the EXAFS results. EXAFS indicates the volume of oxygen-octahedron is increased with  $x$ , however, the density of oxygen-octahedron is also increased with  $x$  due to the heavy mass of  $\text{Sn}^{4+}$ . Therefore, it is the main reason that causes the dielectric constant to reduce with  $x$ . The width of oxygen-octahedral phonon is strongly correlated with the microwave  $Qxf$  value, which indicates the propagation of the microwave is similar to the propagation of oxygen-octahedral phonon.

## Dynamic Optical and Terahertz Responses of YBCO Films with Various In-plane Orientations

Zen-Chi Lin<sup>1</sup>, Pao-An Lin<sup>2</sup>, Kuo-Chien Hsu<sup>2</sup>, Hsin-Chia Ho<sup>3</sup>  
Shyh-Shii Pai<sup>2,3</sup>, and Cheng-Chung Chi<sup>1,2</sup>

<sup>1</sup>Institute of Photonics Technologies, National Tsing Hua University, Taiwan, R.O.C.

<sup>2</sup>Department of Physics, National Tsing Hua University, Taiwan, R.O.C.

<sup>3</sup>Instrument Technology Research Center, National Applied Research Laboratories, Taiwan, R.O.C.

**Abstract**— Biepitaxial superconducting structures have been studied by many researchers for their versatility and device application potential. Novel fabrication techniques and detailed physical measurements of these materials both are important for realizing their potentials. In this study, we focus on the terahertz (THz) and optical responses of superconducting  $\text{YBa}_2\text{Cu}_3\text{O}_{7-\delta}$  (YBCO) films with various in-plane orientations. We report results and analyses of THz time domain spectroscopy and time-resolved photoinduced reflectivity experiments on four in-plane orientated superconducting YBCO films grown on yttria-stabilized zirconia substrates. High quality  $0^\circ$  and  $45^\circ$  in-plane orientations films were obtained by using the growth temperatures at  $810^\circ\text{C}$  and  $660^\circ$ , respectively. As the growth temperature decreases from  $810^\circ\text{C}$ , the dominant orientation shifts gradually from  $0^\circ$  to  $45^\circ$  in the mixture of  $0^\circ$  and  $45^\circ$  domains. Our study of the transmissions of THz time domain spectroscopy indicates a higher value of conductivity at room temperature for the  $0^\circ$ -orientation films than the  $45^\circ$ -films. Using the optical pump-THz probe scheme, we observed combinations of positive and negative THz transmission transients relative to a thermal equilibrium level with different relaxation times of about 0.9 and 9.0 ps respectively for all samples containing  $45^\circ$ -domains. On the other hand, pure  $0^\circ$ -orientation films show only positive transients with a relaxation time of about 1.1 ps. Furthermore, by using optical pump-probe photo-reflectivity measurement we observed faster relaxations for the  $45^\circ$ -film than the  $0^\circ$ -films. Possible physical mechanisms for the relaxations related with in-plane orientations of YBCO films will be discussed.

## Anisotropic Ultrafast Dynamics in Doped $Y_{1-x}Ca_xBa_2Cu_3O_{7-\delta}$ Superconducting Thin Films

C. W. Luo<sup>1</sup>, K. H. Wu<sup>1</sup>, J.-Y. Lin<sup>2</sup>, T. M. Uen<sup>1</sup>, Y. S. Gou<sup>3</sup>, and J.-Y. Juang<sup>1</sup>

<sup>1</sup>Department of Electrophysics, National Chiao Tung University, Hsinchu, Taiwan, R.O.C.

<sup>2</sup>Institute of Physics, National Chiao Tung University, Hsinchu, Taiwan, R.O.C.

<sup>3</sup>Department of Physics, National Taiwan Normal University, Taipei, Taiwan, R.O.C.

**Abstract**— The anisotropic dynamics of photoinduced quasiparticle in the  $Y_{1-x}Ca_xBa_2Cu_3O_{7-\delta}$  is revealed by using the orientation-resolved femtosecond reflection spectroscopy. This bulk-sensitive spectroscopy, combined with the well-textured (110)- and (100)- $Y_{1-x}Ca_xBa_2Cu_3O_{7-\delta}$  thin films, serves as an effective probe to quasiparticle relaxation dynamics in different crystalline orientations. The significant anisotropy in both the magnitude of the photoinduced transient reflectivity change ( $\Delta R/R$ ) and the characteristic relaxation time ( $\tau$ ) indicates that the nature of the relaxation channel is intrinsically different in various axes and planes. Two distinctly temperature-dependent characteristics of quasiparticle dynamics in the nodal ( $ab$ -diagonal) and antinodal ( $b$ -axis) directions are clearly identified. One type of temperature dependence has been observed along  $ab$ -diagonal and  $b$ -axis, while the other type of temperature dependence related to the opening of the superconducting gap appears along  $b$  axis.

The transient reflectivity changes along nodal and antinodal directions are totally different in the slow relaxation process which relates to the opening of superconducting gap. The relaxation time ( $\tau$ ) diverges at  $T_c$ , and appears to be governed by a temperature-dependent gap  $\Delta(T)$  at  $T < T_c$ . Furthermore, for  $T > T_c$ , a monotonic increase of  $\tau$  with decreasing  $T$  along nodal and antinodal directions was observed. The results lend support to recombination dominant scenario of quasiparticle dynamics. However, the quasiparticle thermalization may take part along the nodal direction in the highly underdoped samples.

This novel spatial dichotomy between the nodal and antinodal quasiparticle dynamics and the evolution of gap symmetry with hole doping are discussed for enlightenment on the nature of the phase diagram of hole-doped cuprates.

## Growth of Carbon Nanotubes and Its Applications in Quantum Transport Behavior and Hydrogen Storage

H. Y. Miao<sup>1</sup>, L. W. Chang<sup>2</sup>, and J. T. Lue<sup>3</sup>

<sup>1</sup>Department of Electrical Engineering, Tunghai University, Taichung, Taiwan

<sup>2</sup>Department of Electrical Engineering, National Tsing Hua University, Hsin Chu, Taiwan

<sup>3</sup>Departments of Physics, National Tsing Hua University, Hsin Chu, Taiwan

**Abstract**— Carbon nanotubes (CNTs) are successfully grown on alloy substrates made of copper and iron groups by hot-filament chemical vapor deposition method with self-bias induced by a radio-frequency-field. Carbon nanotubes were also directly grown on the ends of micro-electrodes that were fabricated by photolithography. The sample with a single CNT across nickel electrodes was tediously selected by a scanning electron microscope (SEM) to measure the I-V characteristic at a closed cycle He refrigerator. A discontinuous step of the I-V curve was observed at low temperatures as the current is above certain values. We also developed a one-dimensional transport theory for conductors that can qualitatively portray the quantum behavior of the I-V characteristic. The ability of hydrogen uptake of several carbonize material experiments have been carried out and compared. Purified Single-wall and Multi-wall carbon nanotubes (MWCNTs) produced by arc discharge and microwave (MW) CVD, Taiwan bamboo charcoal with MWCNTs on it are compared and discussed. Because of high hydrogen storage capacity, low-produce cost and high mass production speed, Taiwan bamboo charcoal shows excellent results irrespective to be pretreated with or without alkali or acid solvent.

## Surface Plasma and Growth Mechanism of Gold Nanorods

R. S. Liu<sup>1</sup>, H. M. Chen<sup>1</sup>, and S. F. Hu<sup>2</sup>

<sup>1</sup>Department of Chemistry, National Taiwan University, Taipei 106, Taiwan

<sup>2</sup>Department of Physics, National Taiwan Normal University, Taipei 106, Taiwan

**Abstract**— A new approach to fabricate long length of gold nanorods by controlling the volume of growth solution will be reported. The shape evolutions ranging from fusiform nanoparticles to 1-D rods were observed. Increasing the addition of growth solution can control the length of nanorods. The length of rods can be extended to 2  $\mu\text{m}$ , and nanorods with aspect ratios of up to  $\sim 70$  could be obtained. Moreover, X-ray absorption spectroscopy (XAS) is applied herein to elucidate the growth mechanism of gold nanorods. The gold ions were directly reduced to gold atoms by ascorbic acid during the reaction, and then gold atoms were deposited on the surface of gold seeds that were introduced into the reaction. Extended X-ray absorption fine structure (EXAFS) confirmed the growth of gold and the environment around Au atoms over the reaction. The XAS are expected to have wide applications in the growth of gold and other related materials. The corresponding surface plasma phenomenon of gold nanorods will be also presented.



## Far-infrared, Raman Spectroscopy and Microwave Dielectric Properties of $\text{La}(\text{Mg}_{0.5}\text{Ti}_{(0.5-x)}\text{Sn}_x)\text{O}_3$ Ceramics

I-Nan Lin<sup>1</sup>, Chia-Ta Chia<sup>2</sup>, Hsiang-Lin Liu<sup>2</sup>  
Hsiu-Fung Cheng<sup>2</sup>, G. Santosh Babu<sup>3</sup>, V. Subramanian<sup>3</sup>, and V. R. K. Murthy<sup>3</sup>

<sup>1</sup>Department of Physics, Tamkang University, Tamsui, Taipei, Taiwan 251, Republic of China

<sup>2</sup>Department of Physics, National Taiwan Normal University, Taipei, Taiwan 116, Republic of China

<sup>3</sup>Department of Physics, IIT-Madras, Chennai 600 036, India

**Abstract**—  $\text{La}(\text{Mg}_{0.5}\text{Ti}_{(0.5-x)}\text{Sn}_x)\text{O}_3$  perovskite ceramics with composition ( $x = 0.0 - 0.5$ ) are prepared by the solid state reaction method. The ceramics are characterized by X-ray diffraction, Far-Infrared reflectance, Raman spectroscopy and microwave dielectric properties. The symmetry of ceramics is monoclinic with  $P2_1/n$  space group. Intrinsic dielectric constant and loss are estimated by fitting reflectance to the four-parameter semi quantum model. TO (transverse optic) phonon mode strengths and average phonon damping are calculated. The modes corresponding to B-site ordering are identified in Raman spectra and the  $A_{1g}$  mode of  $\text{La}(\text{MgTi})_{0.5}\text{O}_3$  is analyzed by assuming two merging modes. The variation of long range order (LRO) is correlated with full width half maximum (FWHM) of  $A_{1g}$  mode. Microwave measurements are carried out in the frequency range of 8–10 GHz. The dielectric constant ( $\epsilon'$ ) is found to gradually decrease from 28.4 to 19.7 with the increase in tin concentration whereas the temperature coefficient of resonant frequency ( $\tau_f$ ) decreases from  $-68$  ppm/ $^\circ\text{C}$  to  $-84$  ppm/ $^\circ\text{C}$ . Product of the quality factor and resonant frequency ( $Q \times f$ ) obtained for  $\text{La}(\text{MgTi})_{0.5}\text{O}_3$  is 55,000 GHz, that decreases to 46,000 for  $x = 0.25$  composition and then increases to 63,000 GHz for  $\text{La}(\text{MgSn})_{0.5}\text{O}_3$ .

## Conductivities for Direct Current and Microwaves with Domain Wall Scattering for Ni-Fe Alloy Thin Films

Yi-Chen Yeh<sup>1</sup> and Juh Tzeng Lue<sup>2</sup>

<sup>1</sup>Institute of Photonics Technologies, National Tsing Hua University, Hsin Chu, Taiwan

<sup>2</sup>Department of Physics, National Tsing Hua University, Hsin Chu, Taiwan

**Abstract**— Stripe domain characteristic for Permalloy thin film under external magnetic field are observed with the variation of applying magnetic field measured. The DC resistivity for currents conducting parallel to domain walls (CIW) is significantly smaller than that of the perpendicular (CPW) case as inspected by a magnetic force microscopy (MFM). As the applied frequencies approach the microwave frequency no difference in conductivities for CPW and CIW is observed. This can be expressed that when the signal frequency is up to microwaves, the electron spin scattering with the magnetic domain walls is diminished by the turn-around of carriers before they arrived next domain walls as measured by a *T*-junction micro-strip line resonator.

## Photoelectric Effect of Silicon Nanopillar

Shu-Fen Hu<sup>1</sup>, Ting-Wei Liao<sup>2</sup>, and Chao-Yuan Huang<sup>1,2</sup>

<sup>1</sup>Department of Physics, National Taiwan Normal University, Taiwan

<sup>2</sup>Institute of Electro-Optical Science and Technology, National Taiwan Normal University, Taiwan

**Abstract**— A device is composed of triple quantum dots sandwiched between electrodes and is highly sensitive to the surrounding electrostatic environment. We show that the photoelectric effect resulting from the capture of photo-excited carriers by quantum dots produces a detectable change in the source-drain resistance of the transistor. Current-voltage characteristics measured at  $T = 300\text{ K}$  as a function of source-drain bias for sample device 1 under dark and various intensities of  $\sim 580\text{ nm}$  illumination are shown in Fig. 1. The photocurrent increased as the illumination intensity increased. As presented in Fig. 2, the black curve was measured at dark showing quasilinear characteristics. The red curve in Fig. 2 shows the measured current under the  $580\text{ nm}$  illuminations, the incident radiant energy is  $\sim 2.2 \times 10^{-7}\text{ J/second}$ . Dramatically an increase in the measured current is observed across the entire bias range. The green curve in Fig. 2 appears the measured current under manually chopped  $580\text{ nm}$  illumination, where the illumination was switched on or off at 5 second intervals during the bias sweep. The observed I-V characteristics clearly exhibit almost complete recovery of the device after illumination is removed. We found the devices responsivities of approximately  $R = 3.98 \times 10^6\text{ A/W}$  for  $V_d = 0.18\text{ V}$  and  $R = 9.1 \times 10^5\text{ A/W}$  for  $V_d = 0.05\text{ V}$ , and external quantum efficiency of more than 8.6%.

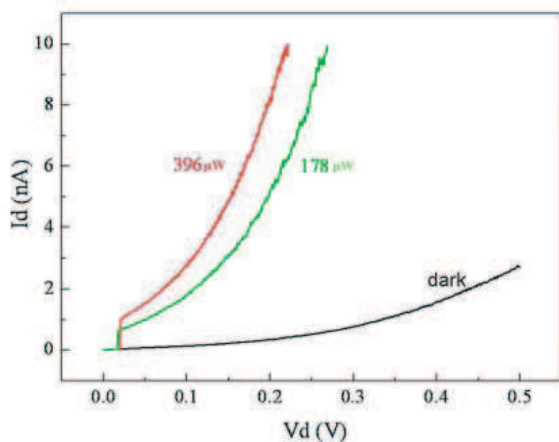


Figure 1: Current-Voltage (I-V) characteristics of the quantum dots acquired in the dark and use the optical gate of controllable illumination intensities of  $396\ \mu\text{W}$ ,  $178\ \mu\text{W}$  and dark, respectively.

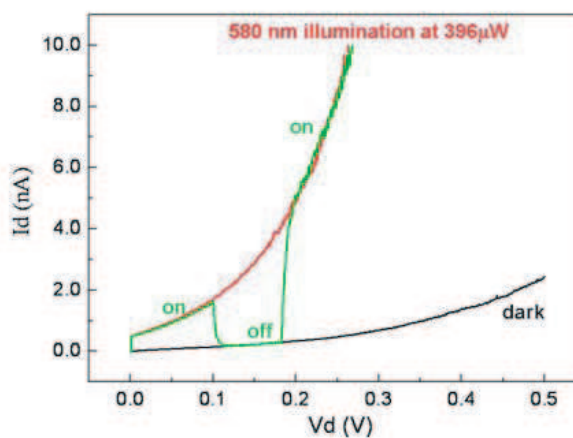


Figure 2: Current-Voltage (I-V) characteristics of the quantum dots acquired in the dark (black line) and use the optical gate at  $396\ \mu\text{W}$  of  $580\text{ nm}$  illumination (red Line). Reversible switching in I-V curve measured every 5 second on/off under manually chopped  $580\text{ nm}$  illumination is also shown (green line).

### ACKNOWLEDGMENT

This work was supported by the National Science Council of Taiwan under contract number NSC 96-2112-M-003 -005.

## The Studies of Defects in Phosphorous Ion-implanted Si(111) by Reflective Second Harmonic Generation

Kuang Yao Lo<sup>1</sup> and Yi Jen Huang<sup>2</sup>

<sup>1</sup>Department of Applied Physics, National Chia Yi University, Chia Yi 600, Taiwan, R.O.C.

<sup>2</sup>Institute of Optoelectronics and Solid State Electronics  
National Chia Yi University, Chia Yi 600, Taiwan, R.O.C.

**Abstract**— Reflective Second Harmonic generation (RSHG) is used to analyze the defects of the implanted Si(111). Under the condition of low-energy and high-dose implantation, RSHG is sensitive on the surface region as the short projected range and high absorption coefficient of SHG light. The isotropic contribution ( $a_0$ ) of p-polarized RSHG with s-polarized fundamental light irradiation (SP-RSHG) corresponds to the defects in the implanted Si(111) during rapid thermal annealing (RTA) process. The value of  $a_0$  is not only arisen from the contribution of the residual electric dipoles but also from the excess point defects after RTA process. Supersaturated phosphorous atoms in the recrystallized silicon will precipitate at lower RTA temperature and its result leads to the raise of  $a_0$ . The measurements of the sheet resistance give the same tendency to illustrate the defect distribution on the surface region.

# Session 1P7

## Space Microwave Technology

<a href="#">Analysis of Equivalence of Standing-wave Dipole Model and Traveling-wave Monopole Model</a>	
<i>Shi-Wei Dong (Xi'an Institute of Space Radio Technology, China); Wei Ma (Xi'an Institute of Space Radio Technology, China); Wanzhao Cui (Xi'an Institute of Space Radio Technology, China); She Shang (Xi'an Institute of Space Radio Technology, China); Hong-Tai Zhang (Xi'an Institute of Space Radio Technology, China); Hong Chen (Xi'an Institute of Space Radio Technology, China);</i>	190
<a href="#">Research on the Electromagnetic Interference of Antennas on the Satellite</a>	
<i>Bin Zhou (Xi'an Institute of Space Radio Technology, China); Qizhong Liu (Xidian University, China); Xinyang He (Xi'an Institute of Space Radio Technology, China);</i>	191
<a href="#">Ka-band Solid-state Amplifier Using Spatial Power-combining Technique</a>	
<i>Lei Wang (Xi'an Institute of Space Radio Technology, China); Shiwei Dong (Xi'an Institute of Space Radio Technology, China); Wei Ma (Xi'an Institute of Space Radio Technology, China);</i>	192
<a href="#">Analysis of BPSK Homodyne Intersatellite Optical Communication Link with Optical Field Misalignment</a>	
<i>Qinggui Tan (Xi'an Institute of Space Radio Technology, China);</i>	193
<a href="#">New Method of Amplitude Modulation for Detection of Multipaction</a>	
<i>Yan Ping Li (Xi'an Institute of Space Radio Technology, China); Yi Ming Ma (Xi'an Institute of Space Radio Technology, China);</i>	194
<a href="#">Peculiar Radar Cross Section Properties of Metamaterials</a>	
<i>Wan-Zhao Cui (Xi'an Institute of Space Radio Technology, China); Wei Ma (Xi'an Institute of Space Radio Technology, China); Ledu Qiu (Xi'an Institute of Space Radio Technology, China);</i>	195
<a href="#">Rectangular Waveguide Band Pass Filter with Capacitive Coupling Iris</a>	
<i>Shengxian Li (Xi'an Jiaotong University, China); Junmei Fu (Xi'an Institute of Space Radio Technology, China); Xuda Wu (Xi'an JiaoTong University, China);</i>	196
<a href="#">Study on W-band PLL Frequency Synthesizer for Space Communications</a>	
<i>Haihong Ma (Xi'an Institute of Space Radio Technology, China); Xiaohong Tang (University of Electronic Science and Technology of China, China);</i>	197
<a href="#">Theoretical Analysis of Composite Right/Left-handed Coupled Transmission Line Resonators</a>	
<i>Tiancun Hu (Xi'an Institute of Space Radio Technology, China); Wei Ma (Xi'an Institute of Space Radio Technology, China);</i>	198
<a href="#">Automatic Digital Modulation Recognition Using Feature Subset Selection</a>	
<i>Jie Li (Xi'an Institute of Space Radio Technology, China); Jun Wang (Xi'an Institute of Space Radio Technology, China); Xiaoyan Fan (Xi'an Institute of Space Radio Technology, China); Yi Zhang (Xi'an Institute of Space Radio Technology, China);</i>	199

## Analysis of Equivalence of Standing-wave Dipole Model and Traveling-wave Monopole Model

Shi-Wei Dong, Wei Ma, Wan-Zhao Cui, She Shang, Hong-Tai Zhang, Hong Chen

National Key Laboratory of Space Microwave Technology

Xi'an Institute of Space Radio Technology, Xi'an, China

**Abstract**— The standing-wave dipole model and the traveling-wave monopole model are often employed in time-domain radiation research of wire antenna. The two models are introduced firstly. Then they are demonstrated to be equivalent theoretically from the view point of radiated fields. It should be noted that the field point can be freely located in the space outside the models, which is different from references [1, 2].

Standing-wave dipole model and traveling-wave monopole model have both found extensive employment in research of transient radiation of wire antenna. M. Rubinstein, M. A. Uman, A. Safaeinili and M. Mina have demonstrated their equivalence; But strict limitation was imposed on, that is the equivalent field point must be located on the perpendicular halving plane of the dipole. This paper releases the limitation and deduces the generalized demonstration.

In Section 2 and 3 standing-wave dipole model and traveling-wave monopole model are investigated respectively. In Section 4 a standing-wave dipole is regarded as four traveling-wave monopole. According to law of superposition it is demonstrated that they are equivalent at any location outside the dipole. In this section movement of charges is also analyzed. This paper concludes with Section 5.

All in all the equivalence is theoretically demonstrated of standing-wave dipole model and traveling-wave monopole model. During the demonstration the field point can be selected freely in the space outside the models.

# Research on the Electromagnetic Interference of Antennas on the Satellite

Bin Zhou<sup>1</sup>, Qizhong Liu<sup>2</sup>, and Xinyang He<sup>1</sup>

<sup>1</sup>Research Office of Microwave Technology  
Xi'an Institute of Space Radio Technology, Xi'an 710100, China

<sup>2</sup>National Laboratory of Antennas and Microwave Technology  
Xidian University, Xi'an 710071, China

**Abstract**— The antennas on the satellite would interfere each other due to the complex framework of the satellite and the considerable quantity, the similar structure, the adjacent location, the superposed working frequency of antennas. The mutual influence between antennas and satellite, and the interference among the antennas would be inevitable. So, it is urgent for the antennas working normally under the complex electromagnetic interference conditions.

It would consume huge computing resource with low efficiency to analyze the radiation field of the satellite by full wave method, for example Method of Moment (MoM). Thus, the approximate algorithm-Uniform Geometrical Theory of Diffraction (UTD) with advantage of distinct conception and convenient calculation is adopted to analyze the electromagnetic interference of antennas on the satellite. In order to solve this problem, the following engineering effort must be carried out in turn.

- The unit patterns of antennas could be acquired by the professional software, which is the pretreatment of the analysis of radiation patterns of antennas on the satellite.
- The satellite could be equivalent to the combination of some simple structures, and the antennas could be equivalent to the point source with the same patterns, which would be convenient for analyzing by UTD.
- The influence of the satellite on the antennas, and the interference among the antennas on the satellite could be analyzed by UTD, including the patterns of the antennas on the satellite, and the interference power and isolation among the antennas on the satellite.
- Finally, the position scheme of the antennas on the satellite would be forecasted according to the calculating results.

In 1970s, the patterns and the isolation of the antennas on the airplane were analyzed by UTD and UAT in State University of Ohio and Illinois University, which had been applied to the military and civil aviation successfully. The error between the measured results and the calculated results of State University of Ohio is 3.76 dB. At present, the position scheme of the antennas is decided by the experience and the repeating tests mostly at home, which would be difficult to realize optimization and consume a lot of manpower and material resources. Especially for the complex carrier, the huge errors make the forecast be failing.

In this paper, the electromagnetic interference of a certain antenna system on the satellite is analyzed by the approximate algorithm-UTD, associated with China Academy of Space Technology pre-research projects. The patterns of the antennas on the satellite and the isolation between transmit antennas and receive antennas are investigated in detail. Then, the analyzable software is offered, which provide the scientific proof of the position scheme and frequency setting of antennas on the satellite. So, the method is more precise than the estimated method, and is widely applied to the engineering calculation.

## Ka-band Solid-state Amplifier Using Spatial Power-combining Technique

Lei Wang, Shiwei Dong, and Wei Ma

National Key Laboratory of Space Microwave Technology  
Xi'an Institute of Space Radio Technology, Xi'an 710100, China

**Abstract**— The successful application and development of millimeter-wave solid-state system are greatly determined by the system output power. The approach of power combing is an effective solution for greater output power, when restricted by the output of single device. Especially, new technology of power combining is the key of millimeter-wave solid-state power transmitting when the old ways meet some difficulties. A new method of waveguide-based spatial power combining is used in millimeter-wave in this paper. The theory and structure has been analyzed and a project of Ka band power combiner based on overmoded waveguide has developed.

The broad-band spatial power-combining technique addresses all these issues by combining the output power of a large quantity of microwave monolithic integrated circuit (MMIC) amplifiers in a overmoded waveguide environment, while maintaining good linearity and improving phase noise of the MMIC amplifiers. A waveguide was used as the host of the combining circuits for broader bandwidth and better uniformity by equally distributing the input power to each element. A new compact overmoded combiner with much smaller size is investigated. Broad-band filine to microstrip-line transition is integrated for better compatibility with commercial MMIC amplifiers. Thermal simulations are performed and an improved thermal management scheme over previous designs is employed to improve the heat sinking in high-power application. In this paper, A Ka-band power amplifier using the spatial power-combining design is built and demonstrated to have a bandwidth from 26 to 27 GHz with 5 W maximum output power.



# Analysis of BPSK Homodyne Intersatellite Optical Communication Link with Optical Field Misalignment

Qinggui Tan

Xi'an Institute of Space Radio Technology, Xi'an 710100, China

**Abstract**— There is a trend towards inter-satellite communication links with increasing data rates. Compared with conventional communication systems, laser communication terminals offer the advantages of higher data rate and larger link distance with lower mass, lower size, and lower power dissipation since the antennae gain is much higher due to the shorter carrier wavelength. Among of all the optical modulation schemes, homodyne BPSK (binary phase shift keying) is the modulation scheme with highest sensitivity for communication and tracking. Furthermore BPSK modulation scheme providing full immunity against sunlight.

In homodyne BPSK intersatellite optical communication link, homodyne detection is based on the interference that results when two mutually coherent electromagnetic waves  $E_{LO}$  and  $E_S$  overlap in space (see Figure 1). In the homodyne receiver, the optical field produced by a laser local oscillator (LO)  $E_{LO}$  is optically mixed with the received-signal optical field  $E_S$  prior to photodetection.

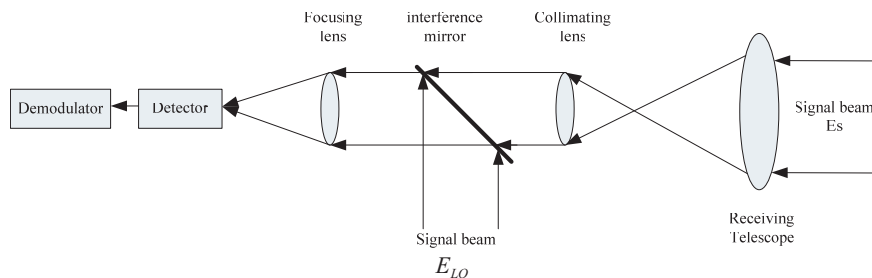


Figure 1: Block diagram of a typical homodyne receiver.

High homodyne efficiency requires that the received signal optical field and LO field be precisely aligned along the same optical axis so that their focused images overlap on the detector surface. Misalignment of two fields can reduce the degree of photomixing, and then degrades the signal to noise ratio (SNR) and bit error rate (BER) of homodyne BPSK intersatellite optical communication link. In real homodyne intersatellite optical communication link with tracking and pointing error, perfect alignment and matching diffraction patterns, affected by tracking and pointing error, are extremely difficult to achieve and the system performance is degraded.

In this paper, the basic principle and characteristics of a homodyne optical receiver is described. The BER expression of homodyne BPSK intersatellite optical communication link in the presence of Rayleigh-distributed random pointing and tracking error is derived. And the performance degradation resulting from optical field misalignment of  $E_{LO}$  and  $E_S$  is analyzed. The results show that the misalignment caused by tracking and pointing error is a critical factor degrading the SNR and BER of homodyne BPSK intersatellite optical communication link. And the optical field misalignment is a critical factor defining the system transmitting optical power required and telescope aperture size. The results can be helpful to the design of homodyne BPSK intersatellite optical communication system.

## New Method of Amplitude Modulation for Detection of Multipaction

Yan Ping Li and Yi Ming Ma

Xi'an Institute of Space Radio Technology, Xi'an 710100, China

**Abstract**— Multipaction is a radio frequency (RF) field-driven resonant discharge in vacuum. A free electron inside a microwave device is accelerated by the electric field with one of the device walls, and consequently secondary electrons are emitted. In the space industry, multipaction is a well-known phenomenon, lots of prevention methods are taken to avoid this problem. As the satellites of today are high-power systems, tests are often needed during the satellites design and manufacture phase. Several different methods of detection are available and can be divided into two fairly distinct groups-global and local methods. Different frequency band detection methods have been build. In china, L. S. C. Ku bands multipaction test method of second harmonic and forward/reverse power nulling have been builded in Xi'an Institute of Space Radio Technology. As the millimeter frequency band technolgy is developed ,the global methods being used which is limited by instruments and system can not well accommodate the needs of multipaction test, new method research for detection of multipaction became important and impendent.

The paper introduces a new global method of amplitude modulation for multipaction detection on the the basis of idea of the article. The crucial point of the method is the fact that if a small amplitude modulation is superimposed on the microwave signal, the amplitude modulation signal harmonic will not be discernible in the noise spectrum unless a multipaction is present. The underlying physical processes are discussed based on power and frequency. The experiments are carried out with the methods of second harmonic and forward/reverse power nulling detection. The results of experiments demonstrat the new detection method. Finally the advantages and disadvantages of the existing global methods as well as of the amplitude modulation method are discussed. Thoery and experiments show this method is sensitive and the system is simply, moreover, constrast with other multipaction detectioan method, the method can be used in Ka frequency band.

### REFERENCES

1. Udiljak, R., D. Anderson, P. Ingvarson, and U. Jordan, "New method for detection of multipaction," *IEEE Transction Science*, Vol. 31, No. 3, Jun. 2003.

# Peculiar Radar Cross Section Properties of Metamaterials

Wan-Zhao Cui, Wei Ma, and Lede Qiu

National Key Laboratory of Space Microwave Technology

Xi'an Institute of Space Radio Technology, Xi'an 710100, Shannxi Province, China

**Abstract**— In 1968, lossless propagation of an electromagnetic wave in the materials with negative permittivity ( $\epsilon$ ) and negative permeability ( $\mu$ ) was first investigated by V. G. Veselago [1], and was experimentally verified in 2001 based on split-ring resonators and rods [2]. These materials were named “Left-Handed Metamaterials” (LHMs) because the vectors  $E$ ,  $H$ , and  $k$  form a left-handed triplet. V. G. Veselago speculated on the possible existence of LHMs and anticipated their unique electromagnetic properties such as the reversal of Snell’s Law, the Doppler effect, and the Vavilov-Cerenkov effect [1]. LHMs support electromagnetic waves with group and phase velocities that are antiparallel, known as backward waves [3] while wavefronts travel backward toward the source in an LHM when energy still travels away from the source. The unique properties of LHMs have allowed novel applications, concepts, and devices to be developed [4]. Science magazine even named LHMs as one of the top ten scientific breakthroughs of 2003 [3].

Planar metamaterials including zero index of refraction metamaterials have been realized experimentally by several research groups [5]. Zero index of refraction metamaterials [6] have properties of a passive, dispersive metamaterial matched to free space, and both the permittivity and permeability are zero at a specified frequency. Some researchers have shown that in both the source and scattering configurations the electromagnetic fields in a matched zero-index medium take on a static character in space, yet remain dynamic in time, in such a manner that the underlying physics remains associated with propagating fields. Moreover, zero phase variation at various points in the zero-index medium if steady-state conditions are satisfied. These researches have found a zero index of refraction metamaterials, such as a zero-index electromagnetic band-gap structured medium, significantly narrows the far-field pattern associated with an antenna located within it, and a matched zero index refraction slab could be used to transform curved wave fronts into planar ones.

We give an overview of some results of our theoretical analysis of anomalous scattering phenomena for metamaterials involving zero index of refraction metamaterials, and the connection of a dynamic electromagnetic variable, the radar cross section, and a static parameter, the polarizability are discussed, respectively. These results provide some physical insights and ideas for potential applications.

## REFERENCES

1. Veselago, V. G., “The electrodynamics of substances with simultaneously negative values of  $\epsilon$  and  $\mu$ ,” *Sov. Phys.-Usp.*, Vol. 10, No. 4, 509–514, 1968.
2. “Breakthrough of the year: The runners-up,” *Science*, Vol. 302, No. 5653, 2039–2045, 2003.
3. Shelby, R. A., D. R. Smith, and S. Schultz, “Experimental verification of a negative index of refraction,” *Science*, Vol. 292, No. 5514, 77–79, 2001.
4. Caloz, C. and T. Itoh, *Electromagnetic Metamaterials: Transmission Line Theory and Microwave Applications*, Wiley, New York, 2005.
5. Engheta, N. and R. W. Ziolkowski, *Metamaterials: Physics and Engineering Explorations*, IEEE Press, 2006.
6. Ziolkowski, R. W., “Propagation in and scattering from a matched metamaterial having a zero index of refraction,” *Phys. Rev. E*, Vol. 70, 046608, 2004.

# Rectangular Waveguide Band Pass Filter with Capacitive Coupling Iris

Shengxian Li<sup>1,2</sup>, Junmei Fu<sup>2</sup>, and Xuda Wu<sup>1</sup>

<sup>1</sup>School of Electronics and Information Technology  
Xi'an Jiaotong University, Xi'an 710049, China

<sup>2</sup>Xi'an Institute of Space Radio Technology, Xi'an 710100, China

**Abstract**— Rectangular waveguide band pass filters (BPFs) are used widely in microwave system, such as satellite communication system, radar system, etc., and inductive irises are often used as coupling elements, so the response at out of band is usually asymmetric for this kind of BPF, the rejection at low frequency stop-band is larger than that at high frequency stop-band.

Capacitive coupling iris is usually used in the waveguide low pass filter, it is not reported that capacitive iris is defined as coupling element in waveguide BPF. In this paper, rectangular waveguide BPF with capacitive coupling iris is presented. Different performance between capacitive and inductive coupling iris is simulated by mode matching method (MMT) and discussed. The total BPFs with capacitive and with inductive coupling iris are analyzed by MMT, and the rigorous  $S$  parameters are achieved, so different stop-band performance between them is obtained.

As example, one Ku band waveguide BPF with capacitive coupling iris is simulated and realized, the measured response show that the rejection performance at high frequency stop-band is better than that at low frequency stop-band.

# Study on W-band PLL Frequency Synthesizer for Space Communications

Haihong Ma<sup>1</sup> and Xiaohong Tang<sup>2</sup>

<sup>1</sup>Laboratory of Microwave Technology  
Xi'an Institute of Space Radio Technology, Xi'an 710100, China

<sup>2</sup>School of Electronic Engineering  
University of Electronic Science and Technology of China, Chengdu 610054, China

**Abstract**— With the rapid development of millimeter wave technology, it is widely used at the fields of radar systems and space communication. Due to atmospheric absorption, frequency around 60 GHz cannot be utilized effectively, so W-band (75–100 GHz) is considered as a “technological frontier” for space communication. Because of the unknown channel behavior and the development level of hardware at these frequencies, actual disquisition on W-band space communication systems are mainly based on feasibility studies. At 2006, NASA launched a new LEO satellite mission (CloudSat) to study clouds and climate, and a weather W-band radar at 94 GHz was on board, which was the first mission carrying a space-qualified W-band radar system.

Millimeter wave frequency synthesizer is one of the key parts of millimeter wave systems. The demand for it with good performances is more and more urgent than ever, especially in W-band. Because of the high frequency, the W-band frequency synthesizer can not be achieved by the sole use of DDS or PLL.

In this paper, a W-band PLL frequency synthesizer with low phase noise has been presented. With the combination of the technique of PLL, DDS and multiplier, an X-band frequency synthesizer with low phase noise is designed. Then, the microwave local frequency and the basic frequency of millimeter wave VCO are mixed through harmonic mixing to obtain millimeter wave interim frequency. After the interim frequency is locked by PLL, the W-band frequency synthesizer is finally achieved. Such W-band frequency synthesizer is characterized by nice performances, which has good foreground for its application in millimeter wave systems.

# Theoretical Analysis of Composite Right/Left-handed Coupled Transmission Line Resonators

Tiancun Hu and Wei Ma

National Key Laboratory of Space Microwave Technology  
Xi'an Institute of Space Radio Technology, Xi'an 710100, China

**Abstract**— The concept of Left-handed materials (LHMs) was first presented by V. G. Veselago in 1968 [1]. The experimental realization of LHMs with resonance structures was demonstrated by Smith in 2000 [2]. However, it seems of little practical interest for engineering applications because of high loss and narrow bandwidth. Another realization of LHMs with microstrip structure was composite right/left-handed transmission line (CRLH-TL) presented by Caloz and Itoh [3]. The CRLH-TL has gained significant interest because of low loss and broad bandwidth. Theoretical Analysis of CRLH-TL was studied rapidly. Also, many microwave devices based on CRLH-TL have been presented. In fact, it is necessary to form coupling between two conductors of two CRLH-TLs in order to design filter, coupler, impedance transformer, resonance loop and so on. As a result, the two transmission lines affect each other. The characteristics are different from the single characteristics. The composite right/left-handed coupled transmission line (CRLH-CTL) can describe the CRLH-TL with two close conductors.

In this paper, a novel resonator based on CRLH-CTL is designed. The CRLH-CTL resonator is analyzed using the even and odd mode approach. It is shown that there are two resonance frequencies which are the odd mode and even mode resonance frequency, and the quality factor of the even mode resonance is higher than the quality factor of odd mode. The simulation of the composite right/left-handed coupled transmission line resonator is accomplished with the planar EM simulation tool of Ansoft designer. The simulation results agree well with the theoretical analysis.

## REFERENCES

1. Veselago, V. G., "The electrodynamics of substances with simultaneously negative values of  $\epsilon$  and  $\mu$ ," *Soviet Physics Uspekhi*, Vol. 10, No. 4, 509–514, Jan., Feb. 1968.
2. Shelby, R. A., D. R. Smith, and S. Schultz, "Experimental verification of a negative index of refraction," *Science*, Vol. 292, 77–79, April 2001.
3. Caloz, C. and T. Itoh, "Novel microwave devices and structures based on the transmission line approach of meta-materials," *IEEE-MTT Int'l Symp.*, Vol. 1, 195–198, Philadelphia, PA, June 2003.

# Automatic Digital Modulation Recognition Using Feature Subset Selection

Jie Li, Jun Wang, Xiaoyan Fan, and Yi Zhang

National Key Laboratory of Space Microwave Technology  
Xi'an Institute of Space Radio Technology, Xi'an 710100, China

**Abstract**— Signal modulation type is one of the important characteristics used in signal monitoring and identification. Modulation recognition systems have to be able to correctly classify the incoming signal's modulation scheme in the presence of noise. For military applications, signal identification is used for purposes such as surveillance, electronic warfare and threat assessment. Some civilian applications are signal confirmation, interference identification and spectrum management.

Automatic recognition of digital modulation signals has seen increasing demand nowadays. The use of artificial neural networks for this purpose has been popular since the late 1990s.

In this paper, a new automatic digital modulation recognition method using ECOC-SVMs and GA is introduced. A new feature set combined statistical and spectral feature subset is used for modulation classification to make the SVMs classifier more robust in Gaussian noise environment. Moreover, GA is used to perform feature selection to reduce the input dimension and increase performance of the ECOC-SVMs classifier. Compared to the conventional ANN method and the decision theoretic algorithm, the proposed method can recognize more digital modulation types. Furthermore, significant improvements can be seen particularly at a low SNR.





# Session 1P8

## Electromagnetic Modeling, Inversion and Application 1

<a href="#">Object-oriented Philosophy in Designing Adaptive FEM Package for 3D Elliptic Differential Equations</a>	
<i>Zheng Yong Ren (Central South University, China); Jing Tian Tang (Central South University, China); Chang Sheng Liu (Central South University, China); Xiao Xiao (Central South University, China); Hua Kun Du (Central South University, China); Ye Wang (Central South University, China); Ji Feng Zhang (Central South University, China);</i>	202
<a href="#">GL EM Mechanical and Acoustic Field Time Domain Modeling for Materials and Exploration with Dispersion</a>	
<i>Ganquan Xie (GL Geophysical Laboratory, USA); Jianhua Li (GL Geophysical Laboratory, USA); Lee Xie (GL Geophysical Laboratory, USA); Feng Xie (GL Geophysical Laboratory, USA);</i>	203
<a href="#">Evaluating Surface Impedance Models for Normal Metals in the Extreme Anomalous Region</a>	
<i>Stepan Lucyszyn (Imperial College London, United Kingdom);</i>	204
<a href="#">State-of-the-Art Microwave Filter Modeling and Design Using Neural Network Technique</a>	
<i>Humayun Kabir (Carleton University, Canada); Ming Yu (COM DEV Ltd., Canada); Qijun Zhang (Carleton University, Canada);</i>	205
<a href="#">A GLEMFHS EMS Imaging Using the GL EM-Flow-Heat-Stress Coupled Modeling</a>	
<i>Jianhua Li (GL Geophysical Laboratory, USA); Lee Xie (GL Geophysical Laboratory, USA); Ganquan Xie (GL Geophysical Laboratory, USA); Jing Li (GL Geophysical Laboratory, USA); Daxin Zuo (GL Geophysical Laboratory, USA);</i>	206
<a href="#">Simulation on EMI Coupling from Driving System of Fuel Cell Vehicle</a>	
<i>Jiawei Sun (Tongji University, China); Min Zhang (Tongji University, China);</i>	207
<a href="#">Properties of Motion of Microscopic Particles in Nonlinear Systems and Nonlinear Quantum Mechanics</a>	
<i>Xiao-Feng Pang (University of Electronic Science and Technology of China, China);</i>	208
<a href="#">3D-2D AGILD EM Inversion for GPR Imaging in Multiple Lines' Data Configuration</a>	
<i>Ganquan Xie (GL Geophysical Laboratory, USA); Michael Oristaglio (Schlumberger-Doll Research, USA); L. Xie (GL Geophysical Laboratory, USA); Jianhua Li (GL Geophysical Laboratory, USA);</i>	210
<a href="#">Three Component Time-domain Electromagnetic Surveying: Modeling and Data Analysis</a>	
<i>Chow-Son Chen (National Central University, Taiwan); Wei-Hsuan Chiu (National Central University, Taiwan); Ching-Ren Lin (Academia Sinica, Taiwan);</i>	211
<a href="#">Experimental Study on Noise Coupling among Multiple Power Areas through Edge Coupling and via Penetrations</a>	
<i>Gang Feng (Missouri University of Science and Technology, USA); Jun Fan (Missouri University of Science and Technology, USA);</i>	212
<a href="#">Analogy between Electromagnetic and Acoustic</a>	
<i>Z. E. A. Fellah (Laboratoire de Mecanique et d'Acoustique, France); N. Sebaa (, Belgium); E. Ogam (Laboratoire de Mecanique et d'Acoustique, France); M. Fellah (Laboratoire de Physique Theorique, Faculte de Physique, Algerie); C. Depollier (Laboratoire d'Acoustique de l'Universite du Maine, France); W. Lauriks (Katholieke Universiteit Leuven, Belgium);</i>	214
<a href="#">High-frequency Ferromagnetic Properties and Monte Carlo Simulation of FeCoHf Thin Films Prepared by Gradient Sputtering</a>	
<i>Meimei Liu (Fujian Normal University, China); Shandong Li (Fujian Normal University, China); Jenq-Gong Duh (National Tsing Hua University, Taiwan);</i>	215
<a href="#">Green's Function of Reduced Wave Equation for a Nonhomogeneous Medium</a>	
<i>Evgeny Grigoryevich Saltykov (Lomonosov Moscow State University, Russia);</i>	216

## Object-oriented Philosophy in Designing Adaptive FEM Package for 3D Elliptic Differential Equations

Zheng Yong Ren, Jing Tian Tang, Chang Sheng Liu, Xiao Xiao  
Hua Kun Du, Ye Wang, and Ji Feng Zhang

School of Info-physics and Geomatics Engineering, Central South University, Changsha, China

**Abstract**— Although adaptive finite-element (AFE) analysis is becoming more and more focused in scientific and engineering fields, its efficient implementations are remain to be a discussed problem as its more complex procedures. In this paper, we propose a clear C++ framework implementation to show the powerful properties of Object-oriented philosophy (OOP) in designing such complex adaptive procedure. In terms of the modal functions of OOP language, the whole adaptive system is divided into several separate parts such as the mesh generation or refinement, a-posterior error estimator, adaptive strategy and the final post processing. After proper designs are locally performed on these separate modals, a connected framework of adaptive procedure is formed finally. Based on the general elliptic differential equation, little efforts should be added in the adaptive framework to do practical simulations. To show the preferable properties of OOP adaptive designing, two numerical examples are tested. The first one is the 3D direct current resistivity problem in which the powerful framework is efficiently shown as only little divisions are added. And then, in the second induced polarization IP exploration case, new adaptive procedure is easily added which adequately shows the strong extendibility and re-usage of OOP language. Finally we believe based on the modal framework adaptive implementation by OOP methodology, more advanced adaptive analysis system will be available in future.

# GL EM Mechanical and Acoustic Field Time Domain Modeling for Materials and Exploration with Dispersion

Ganquan Xie, Jianhua Li, Lee Xie, and Feng Xie  
GL Geophysical Laboratory, USA

**Abstract**— In the last few years, we have proposed EM, Mechanical, Acoustic and Flow GL Modeling and applications in the frequency domain then we covert them to time domain. In this paper, we propose a new EM and mechanical GL modeling in the time domain directly. We derive the new time domain EM and mechanical integral equation. Based on these time domain integral equations, we construct EM and mechanical time domain GL modeling. Similar with our GL method in the frequency domain, the time domain GL method does not need to solve any large matrix, only  $6 \times 6$  and  $9 \times 9$  matrices are needed to solve in the time domain EM and mechanical GL modeling respectively. Moreover, the artificial boundary and absorption condition are unnecessary in our time domain GL method. The time domain EM and mechanical GL method have wide application. Many applications are described in this paper.

## REFERENCES

1. Xie, G., F. Xie, L. Xie, and J. Li, "New GL method and its advantages for resolving historical difficulties," *Progress in Electromagnetics Research*, PIER 63, 141–152, 2006.
2. Xie, G., J. Li, L. Xie, and F. Xie, "GL metro carlo EM inversion," *Journal of Electromagnetic Waves and Applications*, Vol. 20, No. 14, 1991–2000, 2006.

# Evaluating Surface Impedance Models for Normal Metals in the Extreme Anomalous Region

Stepan Lucyszyn

Department of Electrical and Electronic Engineering  
Imperial College London, Exhibition Road  
London, SW7 2AZ, United Kingdom

**Abstract**— Radio frequency circuits and systems need to be modelled to high accuracy to account for losses in transmission lines and poor unloaded quality factors in resonators. This is especially important at millimeter-wave frequencies, where carrier and signal powers generated may be at a premium, subsystems' efficiencies are inherently poor and received signal power levels can be close to, or below, the thermal noise floor. There are a number of well-known techniques for calculating the surface impedance of normal metals at room temperature; from the most basic classical skin-effect model to semiclassical methods [1–3]. Moreover, at relatively low temperatures, additional models exist; from the most basic 'ineffectiveness' concept proposed by Pippard [4] to the extreme anomalous models derived by Reuter and Sondheimer [5]. For the first time, some of the more well-known extreme non-classical models will be compared to the semiclassical solution [5]. It will be shown that a number of researchers suggest inappropriate models to calculate surface impedance for normal metals in the extreme anomalous region [6–8], where the mean distance between collisions for the conducting valence electrons is much greater than the classical skin depth. To this end, derivations for the various models will be shown from first principles. The basic assumptions and approximations will be highlighted, with a view to identifying their weaknesses. The relationship between conductivity, frequency and temperature will be explored with a view to compare and contrast errors in predicted performance for realistic transmission lines, resonators and filters operating at millimeter-wave frequencies and at cryogenic temperatures.

## REFERENCES

1. Lucyszyn, S., "Investigation of anomalous room temperature conduction losses in normal metals at terahertz frequencies," *IEE Proc. - Microwaves, Antennas and Propagation*, Vol. 151, No. 4, 321–329, Aug. 2004.
2. Lucyszyn, S., "Investigation of Wang's model for room temperature conduction losses in normal metals at terahertz frequencies," *IEEE Transactions on Microwave Theory Tech.*, Vol. 53, No. 4, 1398–1403, Apr. 2005
3. Lucyszyn, S., "Evaluating surface impedance models for terahertz frequencies at room temperature," TEA PIERS Online, ISSN 1931–7360, Vol. 3, No. 4, 554–559, June 2007.
4. Pippard, A. B., "The surface impedance of superconductors and normal metals at high frequencies: II The anomalous skin effect in normal metals," *Proc. Royal Society*, Vol. A191, 385–398, 1947.
5. Reuter, G. E. H. and E. H. Sondheimer, "The theory of the anomalous skin effect in metals," *Proc. Royal Society*, Vol. A195, 336–364, 1948.
6. Matick, R. E., *Transmission Lines for Digital and Communication Networks*, McGraw-Hill Book Co., New York, 1969 (re-printed Wiley-IEEE Press, Dec. 2000).
7. Abrikosov, A. A., *Fundamentals of the Theory of Metals*, North-Holland, Amsterdam, 1988
8. Ilyinsky, A. S., G. Ya. Slepian, and A. Ya Slepian, *Propagation, Scattering and Dissipation of Electromagnetic Waves*, Peter Peregrinus Ltd., London, 1993.

# State-of-the-Art Microwave Filter Modeling and Design Using Neural Network Technique

H. Kabir<sup>1</sup>, M. Yu<sup>2</sup>, and Q. J. Zhang<sup>1</sup>

<sup>1</sup>Department of Electronics, Carleton University, Ottawa, Ontario, Canada

<sup>2</sup>COM DEV Ltd., Cambridge, Ontario, Canada

**Abstract**— This paper presents recent advances in microwave filter modeling and design using neural network technique. Microwave filters are an integral part of satellite and ground based communication systems. The design procedure of these filters usually requires several iterations using EM-based models, which takes a considerable amount of time. The entire procedure has to be repeated each time a new filter needs to be designed. Due to increased complexity of microwave filters and multiplexers and shorter design time requirement, we need a faster method to design these filters. Neural network can capture any device behavior accurately and the evaluation time of a neural network model is fast. Once developed neural network model can be used over and over again for different filter dimension. For these reasons neural network modeling technique is an appropriate alternative of EM-based modeling. In the past some results have been published in microwave filter modeling using neural network technique. These filters were simpler in structure and in the form of either waveguide or planar structure. Neural network models for these filters were developed relating physical parameters to electrical parameters (for example, width and length of microstrip as inputs and s-parameter as output). Though these neural network models are faster than EM-based models, they need to be iterated to obtain the design variables for a desired filter response. Recently neural network has been used to obtain the design variables directly not using an iterative approach. In this approach coupling matrix is used to correctly characterize complex filter function. Training data were generated using an EM-based model and then these data were reorganized so that the design variables become output of the neural network model. Neural network and filter equivalent circuits are combined in a special way to obtain design variables quickly. A waveguide dual mode filter with an elliptic filter function was considered for this work. The amount of training data required to cover the entire range of all the variables were large. To reduce the training data generation and neural network training time the entire structure was decomposed into three modules each representing a different filter junction. Neural network models were developed for each module. Due to the coupling between orthogonal modes, GSM of the junctions in the filter is necessary to characterize most of the modules. Instead of trying to model the GSM directly, equivalent circuit variables such as coupling value and insertion phase are extracted from EM data first. Neural network models are then developed for the circuit variables. A four pole filter with 2 transmission zeros were designed using the neural network model. Using the neural network models circuit variables was generated hundreds of times faster than the EM-based model and all the dimensions found were very accurate. In this work advanced methods for modeling and designing microwave filters using neural network technique are presented. Innovative approaches were taken to model and design complex filters. Very good correlation was found between neural network predicted dimensions and that using EM-based model. Design time is also reduced significantly by using the neural network models.

# A GLEMFHS EMS Imaging Using the GL EM-Flow-Heat-Stress Coupled Modeling

Jianhua Li, Lee Xie, Ganquan Xie, Jing Li, and Daxin Zuo

GL Geophysical Laboratory, USA

**Abstract**— We have proposed 3D GL and AGILD Electromagnetic (EM)-Flow-Heat-Stress coupled modeling (GLEMFHS) in PIERS 2007 in Beijing and published the method in PIERS Online. In this paper, we propose a dynamic electromagnetic stirring (EMS) imaging using the GLEMFHS coupled modeling, in short, we call it GLEMFHS EMS imaging. The GLEMFHS EMS imaging can be used to display the EM, flow, heat, and stress field dynamically in the steel cast processes and recover, monitor, and control the parameters, such that the steel continuous cast products high quality steel. Recent 10 years, the EMS is almost installed in all steel continuous cast factories. However, all EMS system is blind operating. The steel expert and technician can not see the steel flow and temperature imaging in the real time. An automatically EMS dynamic to monitor, display, and real time control system for EMS is lacking and necessary. Our GLEMFHS EMS imaging system using the GL EM-flow-heat-stress coupled modeling will perform automatically the EMS dynamic monitor, display, and real time controlling for EMS in steel continuous cast.

## REFERENCES

1. Xie, G., J. Li, L. Xie, F. Xie, and J. Li, "The 3D GL EM-flow-heat-stress coupled modeling," *PIERS Online*, Vol. 3, No. 4, 411–417, 2007.
2. Xie, G., J. H. Li, J. Li, and F. Xie, "3D and 2.5D AGLID EMS stirring modeling in the cylindrical coordinate system," *PIERS Online*, Vol. 2, No. 5, 505–509, 2006.
3. Xie, G., J. Li, J., and J. H. Li, "New AGILD EMS electromagnetic field modeling," *PIERS Online*, Vol. 1, No. 2, 168–172, 2005.
4. Li, J., G. Xie, and Z. Liao, "Electromagnetic stirring using GL electromagnetic field," *Proceeding of PIERS2005 in Hangzhou*, 180, 2005.
5. Xie, G., F. Xie, L. Xie, and J. Li, "New GL method and its advantages for resolving historical difficulties," *Progress In Electromagnetics Research*, Vol. PIER 63, 141–152, 2006.
6. Xie, G., J. Li, L. Xie, and F. Xie, "GL metro carlo EM inversion," *Journal of Electromagnetic Waves and Applications*, Vol. 20, No. 14, 1991–2000, 2006.

## Simulation on EMI Coupling from Driving System of Fuel Cell Vehicle

Jiawei Sun and Min Zhang

Modern Integrated Electromagnetic Simulation R and D Center (MIEMS)  
Tongji University, Shanghai, China

**Abstract**— Compared with traditional internal combustion engine vehicles, fuel cell vehicles have more serious electromagnetic compatibility problem because of the application of inverter and electric motor. It has proved that the DC-DC and DC-AC converters in power control unit (PCU) of fuel cell vehicles are the main electromagnetic noise sources due to high and fast switching current. On the other hand as space for wiring harness is limited in vehicles, the high voltage cables between power control unit and electric motor are arranged close to the other low voltage cables. Hence these cables are the important EMI coupling path in the driving system of fuel cell vehicle. In this paper the operating principles and typical output current waveform of the inverter in vehicle are analyzed. Current waveform is measured on a test PCU. This waveform is applied in a cabling EMC software — CableMod with a realistic set-up of power control unit in a body chassis. Current distribution in cables obtained with CableMod is used in a system-level EMC software — CST MICROWAVE STUDIO® for EMC analysis of the whole car. Emission analysis on both shielded and unshielded cables is carried out. The simulation results obtained is used to determine the noise level compared with related EMC standards.

# Properties of Motion of Microscopic Particles in Nonlinear Systems and Nonlinear Quantum Mechanics

Xiao-Feng Pang

Institute of Life Science and Technology

University of Electronic Science and Technology of China, Chengdu 610054, China

**Abstract**— As known, quantum mechanism is the foundation of modern science. So-called quantum mechanics is just the science describing properties and rules of motion of microscopic particles, which the matters in the world are composed of Nonlinear quantum mechanics (NLQM) then is to study the law of motion of microscopic particles in nonlinear systems. Thus the quantum mechanics established by several great-scientists containing N. Bohr, M. Born, E. Schrodinger and W. Heisenberg, etc. in early 1900s is referred to as linear quantum mechanics (LQM). Pang Xiao-feng built the nonlinear quantum mechanics which were described in the book of “quantum mechanics in nonlinear quantum mechanics” by Pang et al. which was recently published in World Scientific Publishing Co., and is on sale extensively in the around world, at present. This is first book as to this problem. This book is essentially composed of three parts. The first presents a review of the LQM, as well as theoretical and experimental fundamentals that establish the nonlinear quantum mechanical theory. The theory itself and its essential features are covered in the second part. In the final part, extensive applications of this theory in physics, biology and polymer are introduced. The whole volume forms a complete system of the NLQM. Concrete contents are included in 88 sections in 10 chapters about 650 pages, they are as follows. Linear quantum mechanics: its successes and problems; macroscopic quantum effects and properties of motion of quasiparticles; the fundamental principles and theory of nonlinear quantum mechanics; wave-corpucle duality of microscopic particles (MIP) in the NLQM; nonlinear interaction and localization of the MIP; nonlinear versus linear quantum mechanics; the problems solving in the NLQM; properties and states of the MIP in different nonlinear systems; nonlinearly quantum-mechanical properties of the excitons and phonons; properties of nonlinear excitations and motions of protons, polarons and magnons in different systems.

For the development of quantum mechanics from linear range to nonlinear domain Pang work at and investigate this problem about 20 years. He firstly sought the roots of these problems existed in the LQM. When restrictions of the elementary hypotheses for the independence of the Hamiltonian of the systems on the states of the particles and the linearity of the theory in the LQM were broken through we proposed and established elementary principles and theory of the NLQM, based on the close relations among the nonlinear interaction and soliton motions and macroscopic quantum effect and incorporating modern theories of superconductor and superfluid and soliton, according to the features and theory of macroscopic quantum effects and soliton theory. The fundamental principles of nonlinear quantum mechanics (NLQM) are that (1) microscopic particles in a nonlinear quantum system are described by the following wave function,  $\phi(\vec{r}, t) = \varphi(\vec{r}, t) e^{i\theta(\vec{r}, t)}$ , where  $\varphi(\vec{r}, t)$  and  $\theta(\vec{r}, t)$  are functions of space and time.

(2) In the nonrelativistic case,  $\phi(\vec{r}, t)$  satisfies he generalized nonlinear Schrodinger equations

$$i\hbar \frac{\partial \phi}{\partial t} = -\frac{\hbar^2}{2m} \nabla^2 \phi \pm b |\phi|^2 + V(\vec{r}, t) \phi + A(\phi),$$

or

$$\mu \frac{\partial \phi}{\partial t} = -\frac{\hbar^2}{2m} \nabla^2 \phi \pm b |\phi|^2 \phi + V(\vec{r}, t) \phi + A(\phi),$$

In the relativistic case,  $\phi(\vec{r}, t)$  satisfies the nonlinear Klein-Gordon equation (NLKGE):

$$\frac{\partial^2 \phi}{\partial t^2} - \frac{\partial^2 \phi}{\partial x_j^2} = \beta \sin \phi + \gamma \frac{\partial \phi}{\partial t} + A(\phi), \quad \frac{\partial^2 \phi}{\partial t^2} - \frac{\partial^2 \phi}{\partial x_j^2} \mp \alpha \phi \pm \beta |\phi|^2 \phi = A(\phi) \quad (j = 1, 2, 3)$$

According to these principles we built the fundational theory of NLQM, such as superposition theory, Fourier Transformaation theory, quantization theory and eigenvalue theory, and so on. We obtained the invariance and conservation laws of mass,energy and momentum and angular momentum for the microscopic particles, which are also some elementary and universal laws of matters in the NLQM and give further the methods and ways solving the above questions. We



discover also that the laws of motion of the MIPs in such a case are completely different from that in the LQM. They have a lot of new properties, for example, the particles possess the real wave-corpucle duality, obey the classical rule of motion and conservation laws of energy, momentum and mass, satisfy minimum uncertainty relation, can be localized due to the nonlinear interaction, its position and momentum can be also determined, etc.. Therefore the NLQM is a new subject, it could solve these problems disputed long-times about one centenary by the scientists in the LQM. Meanwhile, the self- consistence and validity of this theory have been also checked in detial, we can give a lot of new results and explain a large number of physical phenomena occurred in physics, biology and polymer utilized the NLQM theory. Thus the NLQM is a necessary result of development of quantum mechanics and correct representation form in the nonlinear systems. Establishing the NLQM can promotes development of physics and can raise the knowledge and recognition levels to the essences of the microscopic matters. Therefore, the NLQM built are very necessary and correct. We can predicate thaat the nonlinear quantum mechanics has extensive applicaations in physics, chemistry, biology and polymer, etc.

#### REFERENCES

1. Pang, X.-F. and Y.-P. Feng, *Quantum Mechanics in Nonlinear Systems*, World Scientific Publishing Co., New Jersey, 2005.
2. Pang, X.-F., *Theory for Nonlinear Quantum Mechanics*, Chongqing Press, Chongqing, 1994.
3. Pang, X.-F., *Soliton physics*, Sichuan. Scie. Tech. Press, Chengdu, 2003.

## 3D-2D AGILD EM Inversion for GPR Imaging in Multiple Lines' Data Configuration

Ganquan Xie<sup>1</sup>, Michael Oristaglio<sup>2</sup>, L. Xie<sup>1</sup>, and Jianhua Li<sup>1</sup>

<sup>1</sup>GL Geophysical Laboratory, USA

<sup>2</sup>Schlumberger Doll Research, USA

**Abstract**— In this paper, we propose a 3D-2D AGILD electromagnetic (EM) inversion for ground penetration radar (GPR) imaging in multiple lines' data configuration. The GPR data sources and receivers are arranged in multiple lines. For each source exciting, the EM wave field is propagation in the half space with inhomogeneous anomalous EM parameters in finite domain of the underground of the Earth. We use the 3D AGILD EM modeling method to simulate the EM wave field in the 3D anomalous EM parameters domain which is embedded in the half space background media. The inhomogeneous EM parameters, conductivity, dielectric, and magnetic permeability parameters, are updated by the 2D AGILD inversion in the multiple line vertical sections by the difference between the multiple lines' measured data and 3D AGILD EM modeling data restricting on these configuration data lines. The synthetic data tests show that the 3D-2D AGILD GPR imaging using multiple lines' data has high resolution in the corrected depth-frequencies matching band. Some 3D-2D EM field mine exploration data AGILD GPR imaging shows our AGILD GPR imaging method has reasonable resolution and can be useful for practical GPR geophysical oil and mine exploration and engineering geophysical exploration and environmental clear and detection.

### REFERENCES

1. Li, J., G. Xie, M. Oristaglio, L. Xie, and F. Xie, "3D-2D AGILD EM modeling and inversion," *PIERS Online*, Vol. 3, No. 4, 423–429, 2007.
2. Xie, L., J. Li, M. Oristaglio, C. C. Lin, and G. Xie, "The GPR imaging using the AGILD Metro Carlo EM inversion," *PIERS 2007 in Prague Proceeding*, to appear in *PIERS Online*.
3. Xie, G. and J. Li, "New parallel stochastic global integral and local differential equation modeling and inversion," *Physics D*, Vol. 133, 477–487.
4. Xie, G., J. Li, and F. Xie, "Advanced GILD EM modeling and inversion," *PIERS Online*, Vol. 1, No. 1, 105–109, 2005.
5. Xie, G., J. Li, and F. Xie, "2.5D AGLID EM modeling and inversion," *PIERS Online*, Vol. 2, No. 4, 390–394, 2006.
6. Li, J. and G. Xie, "A cubic-hole finite element for 3D resistivity modeling," *Three-Dimensional Electromagnetics*, No. 7, 591–599, edited by Michael Oristaglio, Geophysical Development.

## Three Component Time-domain Electromagnetic Surveying: Modeling and Data Analysis

Chow-Son Chen<sup>1</sup>, Wei-Hsuan Chiu<sup>1</sup>, and Ching-Ren Lin<sup>2</sup>

<sup>1</sup>Institute of Geophysics, National Central University, Taiwan

<sup>2</sup>Institute of Earth Sciences, Academia Sinica, Taiwan

**Abstract**— In the frequency-domain electromagnetic methods of exploration, the secondary electromagnetic (EM) fields due to induced currents from conductors, together with the primary EM field, are recorded with a suitable receiver at various points in space. In general, the secondary EM field at the receiver, which contains all the information regarding the underground conductors, may be several orders of magnitude smaller than the primary field. Under these conditions the separation of the measured total EM field into its primary and secondary parts is difficult. This fact led to the idea of using time-domain electromagnetic measurements (TEM), often referred to as transient EM techniques. In TEM measurements, the secondary fields are measured in the absence of the primary field.

A comparative survey using single component (measuring the vertical component of the field,  $H_z$ ) TEM receiver and three component (measuring  $H_x$ ,  $H_y$  and  $H_z$ ) TEM receiver was undertaken at a test site, NCU campus. Although this was a metal detection survey, it was particularly useful as a research effort, since the anomalies was almost a certainty. Unlike the single component data, results from the three component data are unambiguous as to the location and orientation of conductors. Measuring adding of the horizontal components of the secondary magnetic field may allow the use of fewer field setups and usually leads to more confidence in the interpretation of azimuth, orientation and size of the conductor. From this and other surveys, it is apparent that the  $H_z$  data, which displays only uni-polar, positive anomalies, are usually the strongest, cleanest data, and provide the best indication of target location, while  $H_x$  and  $H_y$  data are by nature weaker, but can be used to determine direction to off-line 3D targets. Modeling of the data using the programme PLATE (Dyck et al., 1980), which gives first approximation of a theoretical plate-style buried conductor in air, for 3D conductor gives a good fit in the mid-delay time. As a result, the 3-component TEM experiment combined with 3D TEM modelling is a useful tool for the purpose of deep unexploded ordnance detection, or even to the engineering purpose.

# Experimental Study on Noise Coupling among Multiple Power Areas through Edge Coupling and via Penetrations

Gang Feng and Jun Fan

Electromagnetic Compatibility Laboratory  
 Department of Electrical and Computer Engineering  
 Missouri University of Science and Technology  
 (University of Missouri-Rolla)  
 Rolla, MO 65409, USA

**Abstract**— With the progress in semiconductor technology year by year, the frequency of digital circuit becomes higher and higher. Multilayer power/ground plane structure is widely used in high speed PCB and high-performance package designs to achieve very low impedance of the power distribution network (PDN). The power integrity problems are concerned much more than before. We adopt cavity model and segmentation method to perform fast analyzing the noise coupling between different power areas in a multilayer power/ground plane structure. Since the size of the power plane is always much larger than the thickness of the dielectric, a pair of power planes acts essentially as a 2D cavity resonator, where the  $TM_z$  modes are the dominant propagation modes (let  $\hat{z}$  be the direction normal to the plane). Because the skin effect is more significant at high frequencies, the vertical coupling through the conductor plane can be neglected. When the power areas at different voltages overlap together, the noise current can only flow on the surface of a metal plane and detour to the other surface at the edges or via holes of the overlapped power areas. So, the general analyzing steps can be the following: (1) The power/ground structure is decomposed into a series of plane pairs according to the shapes of overlapping areas; (2) Each plane pair can be characterized as a multi-port network by applying the cavity's analytical formulas. A lot of internal ports are defined at the edges and via hole positions for inter-connection and some external ports are defined for observing noise coupling; (3) The impedance matrix among external ports can be obtained by applying voltage and current continuity conditions to the internal ports in each plane pair. Then the noise coupling feature is obtained by the transfer impedance matrix. It should be noticed that the fringing effect (horizontal electric field) is neglected in the process of connecting the equivalent networks, because

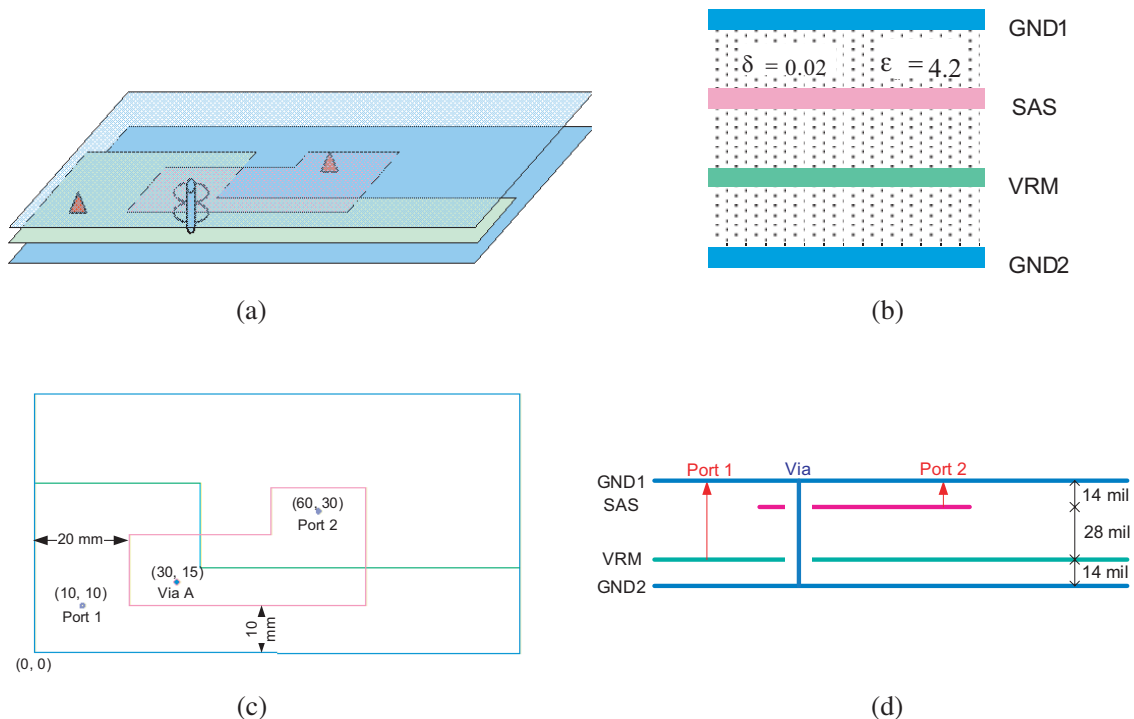


Figure 1: Test board structure, (a) Overview, (b) Stackup, (c) Top view, (d) Side view.

the TMz modes are assumed to be the dominant modes. This assumption is accurate for large power planes with small dielectric thickness. Otherwise, additional circuit elements are needed to take into account the second order effects. The simulation and measurement results verified that the assumption is correct. In this article, a four layer test board is analyzed by the proposed method and full wave method (FEM), as shown in Figure 1. The results agree well with each other up to 2 GHz (Figure 2).

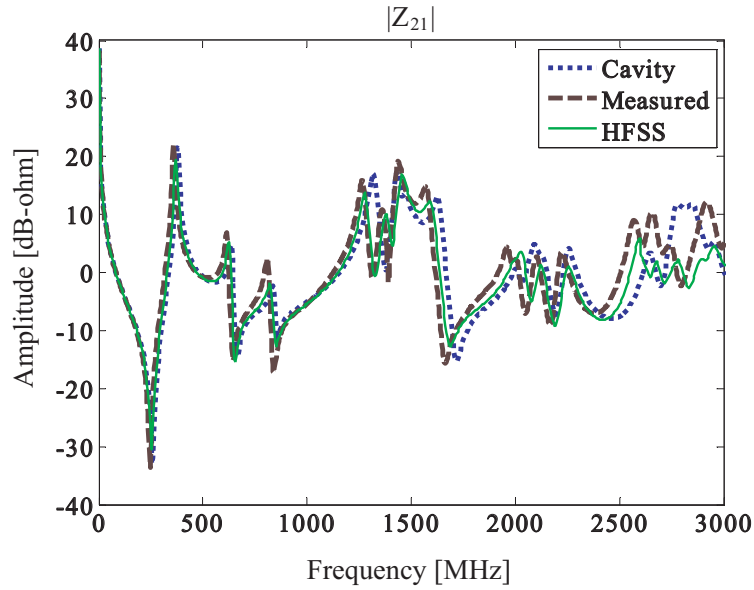


Figure 2: The simulated and measured transfer impedance.

## Analogy between Electromagnetic and Acoustic

Z. E. A. Fellah<sup>1</sup>, N. Sebaa<sup>2</sup>, E. Ogam<sup>1</sup>, M. Fellah<sup>3</sup>, C. Depollier<sup>4</sup>, and W. Lauriks<sup>2</sup>

<sup>1</sup>Laboratoire de Mécanique et d'Acoustique

CNRS-UPR 7051, 31 chemin Joseph Aiguier, Marseille, 13402, France

<sup>2</sup>Laboratorium voor Akoestiek en Thermische Fysica, Katholieke Universiteit Leuven

Celestijnenlaan 200 D, B-3001 Heverlee, Belgium

<sup>3</sup>Laboratoire de Physique Théorique, Faculté de Physique

USTHB, BP 32 El Alia, Bab Ezzouar 16111, Algérie

<sup>4</sup>Laboratoire d'Acoustique de l'Université du Maine, UMR-CNRS 6613, Université du Maine

Avenue Olivier Messiaen 72085 Le Mans Cedex 09, France

**Abstract**— In this communication, the analogy between the propagation of electromagnetic waves in materials media and the propagation of acoustic waves in porous materials is given. It is shown that this analogy is an efficient tool for the understanding of the physics of porous materials and for the development of a propagation models. The study of acoustic waves in a viscothermal media may be transposed to the electromagnetic case and the analysis of transient phenomena in the porous solids may be deduce from the electromagnetic case. This show that it is possible to use the same calculus codes for the simulation the propagation of acoustics waves and electromagnetic waves in complex media when the analogy is established. The direct and inverse problem are solved in porous media and a comparison between experiment and theory is discussed for transmitted and reflected waves.

# High-frequency Ferromagnetic Properties and Monte Carlo Simulation of FeCoHf Thin Films Prepared by Gradient Sputtering

Meimei Liu<sup>1</sup>, Shandong Li<sup>1,2</sup>, and Jenq-Gong Duh<sup>2</sup>

<sup>1</sup>Department of Physics, Fujian Normal University, Fuzhou 210093, China

<sup>2</sup>Department of Materials Science and Engineering, National Tsing Hua University  
Hsinchu 30013, Taiwan

**Abstract**— During the last decade, the application of high-frequency soft magnetic films on the power, reading and writing head, and wireless communication, etc., was widely investigated. In this study, FeCoHf films were prepared by a gradient sputtering method at ambient temperature. The film was subsequently annealed at 400°C for 1 hr in the presence of a magnetic field of 2 kGs along the gradient direction. Field emission electron probe microanalyzer showed a Hf composition gradient from 9.1 to 19.6 at% was present in the film from one side to the other. It was revealed that magnetic properties of the films dramatically depend on the Hf composition. With the increase of Hf composition, the saturation magnetization of the films increased from 20 to 22 kG at first, then decreased to 15.8 kG. A distinct Hf composition depended uniaxial anisotropy up to 400 Oe was obtained. On the other hand, high resonance frequency over 3 GHz and permeability in excess of 100 were achieved in the magnetic annealed films. Considering the intrinsic stress in the gradient films, the Hf composition depended hysteresis loops were simulated using Monte Carlo method. The simulation revealed that uniaxial anisotropy in the gradient films as well as the promising high-frequency ferromagnetic properties can be attributed to the uniaxial stress gradient, which is induced by uniaxial Hf composition gradient.

## Green's Function of Reduced Wave Equation for a Nonhomogeneous Medium

**Evgeny G. Saltykov**

Department of Computational Mathematics and Cybernetics  
Lomonosov Moscow State University, Moscow, Russia

**Abstract**— A method is proposed for constructing the Green's function for the reduced wave equation with a complex-valued coefficient and with an inhomogeneous term of the delta-function type. This equation describes a wave propagation in the Earth which is characterized by the complex-valued coefficient  $k(z, x)$  depending on two independent variables  $z, x$ .

The problem solution has the form of the spectral expansion with respect to fundamental functions of a one-dimensional nonself-adjoint Sturm-Liouville operator for a two-layer medium on entire real line  $z$ . The fundamental functions depend on the parameter  $x$ . The spectral expansion coefficients satisfy the system of two second kind integral equations. In the weak dependence case of the wave number  $k(z, x)$  on a coordinate  $x$ , the systems of two integral equations can be solved by the successive approximation method.



# Session 2A1

## Plasmonic Photonics 1

<p><b>Design, Fabrication, and Integration of Micro/Nano-scale Plasmonic Waveguide Devices for VLSI Photonic Integrated Circuit Application</b></p> <p><i>El-Hang Lee (INHA University, South Korea); S. H. Song (Hanyang University, South Korea); . . . .</i></p> <p><b>Optical Superresolution through Super-oscillations</b></p> <p><i>F. M. Huang (University of Southampton, UK); Vasily Fedotov (University of Southampton, UK); Yifang Chen (Central Microstructure Facility, UK); F. Javier Garcia de Abajo (Instituto de Optica — CSIC, Spain); Nikolay Zheludev (University of Southampton, UK); . . . . .</i></p> <p><b>Multidimensional Optical Data Storage Based on Plasmonic Nanophotonics</b></p> <p><i>Min Gu (Swinburne University of Technology, Australia); . . . . .</i></p> <p><b>Nanoparticle-based Molecular Plasmonics</b></p> <p><i>Andrea Csaki (Institute for Photonic Technology (IPHT), Germany); Andrea Steinbrueck (Institute for Photonic Technology (IPHT), Germany); Norbert Jahr (Institute for Photonic Technology (IPHT), Germany); Kathrin Ritter (Institute for Photonic Technology (IPHT), Germany); Thomas Schueler (Universitat Jena, Germany); Robert Moeller (Universitat Jena, Germany); Wolfgang Fritzsche (Institute for Photonic Technology (IPHT), Germany); . . . . .</i></p> <p><b>Metallic Structures with Nanometer Scale Resolution Fabricated by Direct Laser Photoreduction and Selected Surface Metallization</b></p> <p><i>Xuan-Ming Duan (Technical Institute of Physics and Chemistry, Chinese Academy of Sciences, China); Yao-Yu Cao (Technical Institute of Physics and Chemistry, Chinese Academy of Sciences, China); Wei-Kang Wang (Technical Institute of Physics and Chemistry, Chinese Academy of Sciences, China); Xian-Zi Dong (Technical Institute of Physics and Chemistry, Chinese Academy of Sciences, China); Wei-Qiang Chen (Technical Institute of Physics and Chemistry, Chinese Academy of Sciences, China); Nobuyuki Takeyasu (RIKEN, Japan); Takuo Tanaka (RIKEN, Japan); Satoshi Kawata (RIKEN, Japan); . . . . .</i></p> <p><b>Superlens from Complementary Anisotropic Metamaterials</b></p> <p><i>G. X. Li (Hong Kong Baptist University, China); H. L. Tam (Hong Kong Baptist University, China); F. Y. Wang (Hong Kong Baptist University, China); Kok Wai Cheah (Hong Kong Baptist University, China); . . . . .</i></p> <p><b>Optimized Plasmonic Nanostructures for Nanolithography</b></p> <p><i>Y. Chue (National Taiwan University, Taiwan); Y. Cheng (National Taiwan University, Taiwan); Jia-Han Li (National Taiwan University, Taiwan); . . . . .</i></p> <p><b>Slow Light and Extraordinary Magneto-optical Effects in Magnetic and Plasmonic Nanostructures</b></p> <p><i>Vladimir I. Belotelov (A. M. Prokhorov General Physics Institute, Russia); A. K. Zvezdin (A. M. Prokhorov General Physics Institute, Russia); A. N. Kalish (A. M. Prokhorov General Physics Institute, Russia); E. A. Shevchenko (A. M. Prokhorov General Physics Institute, Russia); . . . . .</i></p>	<p>218</p> <p>219</p> <p>220</p> <p>221</p> <p>222</p> <p>223</p> <p>224</p> <p>225</p>
--	---

# Design, Fabrication, and Integration of Micro/Nano-scale Plasmonic Waveguide Devices for VLSI Photonic Integrated Circuit Application

El-Hang Lee<sup>1,2</sup> and S. H. Song<sup>3</sup>

<sup>1</sup>OPERA National Research Center for VLSI Photonics Technology  
INHA University, Incheon 402-751, South Korea

<sup>2</sup>Graduate School of Information Technology and Telecommunication  
INHA University, Incheon 402-751, South Korea

<sup>3</sup>Department of Physics, College of Natural Sciences  
Hanyang University, Seoul 133-791, South Korea

**Abstract**— We present an overview of our work on the theory, design, fabrication, and integration of micro/nano-scale plasmonic waveguide devices for VLSI photonic integrated circuit applications. We first examine the characteristics and use of the slow light propagation and the fast light propagation on the design of various functions. We design both horizontally parallel directional couplers and vertically parallel directional couplers and compare their performances. For this, we designed and fabricated vertical directional couplers consisting of metal stripe waveguides embedded in polymer. The coupling length of the fabricated vertical directional coupler consisting of 20 nm thin and 5  $\mu\text{m}$  wide gold stripes was 260  $\mu\text{m}$ . The extinction ratio was about 28 dB and the separation distance of the two metallic waveguides was 4.2  $\mu\text{m}$ . The fabricated vertical directional couplers were 9 mm long in total length with the arm separation of 200  $\mu\text{m}$  at the input/output section. The total insertion loss was measured as  $\sim 24$  dB and the additional loss was about  $\sim 3$  dB. We also designed and fabricated a novel metal-waveguide structure for sustaining long-range surface-plasmon-polaritons(LR-SPP), which is basically composed of two asymmetric metal layers: a very thin, finite-width metal strip on top of a metal slab with a dielectric gap in between. Mode cut-off of LR-SPPs excited on the asymmetric double-metal waveguides is characterized by investigating their dispersion relations and mode profiles. We confirm experimentally the existence of low-loss, well-confined LR-SPP modes by measuring far-field outputs emerging from an edge of the asymmetric double-metal waveguides. We then fabricated several types of SPP waveguide devices including straight line, S-bend, Y-branch, and couplers for the gold strip patterns (20 nm-thick, 5  $\mu\text{m}$ -wide). The Overall propagation loss of the asymmetric double-metal waveguides is comparable to that of single metal-strip waveguides. In addition, the mode sizes can be tuned by increasing the dielectric gap between the metal layers to get a higher coupling efficiency to single-mode fibers in telecom wavelength. This novel structure may open up new possibilities of realizing SPP-waveguides for sensors or nonlinear SPP-waveguide by replacing the gap dielectric with a bio-fluid or a nonlinear medium. These plasmonic devices are then integrated with other micro/nano-photonic devices, either on a board or on a chip, for VLSI photonic integrated circuit applications. We will present examples of devices and integrated circuits along with the scientific and engineering issues arising from the various mismatches between devices of diverse functional characteristics and properties.

## Optical Superresolution through Super-oscillations

Fu Min Huang<sup>1</sup>, Vasily Fedotov<sup>1</sup>, Yifang Chen<sup>2</sup>  
F. Javier Garcia de Abajo<sup>3</sup>, and Nikolay Zheludev<sup>1</sup>

<sup>1</sup>EPSRC Nanophotonics Portfolio Centre, Optoelectronics Research Centre  
University of Southampton, SO17 1BJ, UK

<sup>2</sup>Central Microstructure facility, Rutherford Appleton Laboratory  
Didcot, Oxon, OX11 0QX, UK

<sup>3</sup>Instituto de Optica — CSIC, Serrano 121, 28006 Madrid, Spain

**Abstract**— Most ideas for achieving super-resolution in optics are based on the recovery of evanescent fields which are commonly believed to be the necessary components to form sub-wavelength field concentrations. For instance, the famous Veslago-Pendry idea for a far-field super-lens is based on the recovery of evanescent information by “amplifying” the fading evanescent components in a slab of a negative-index material. However, evanescent fields may not be needed to achieve subwavelength concentration of light: according to a phenomenon called superoscillations, band-limited functions are able to oscillate arbitrarily faster than the highest Fourier components they contain.

Here we present experimental demonstration and theoretical analysis of optical super-oscillation generators based on 1D arrays of nano-holes and slits, and on 2D array of nano-holes in metal screen and show that they generate sub-wavelength localizations of light.

We also show that properly designed arrays of nano-holes can be used as a far-field imaging super-lens thus opening a new way of achieving optical resolution beyond Rayleigh limit, which is different from many existing approaches depending on the recovery of evanescent fields.

# Multidimensional Optical Data Storage Based on Plasmonic Nanophotonics

Min Gu

Centre for Micro-Photonics, Faculty of Engineering and Industrial Sciences  
Swinburne University of Technology, Hawthorn 3122, VIC, Australia

**Abstract**— Two-photon-induced three-dimensional (3D) optical data storage systems have attracted significant interest due to a potential storage density of Tbits/cm<sup>3</sup>. Development of integrated optics compels the need for further expanding the current storage density by either breaking the diffraction limit of light or involving other physical dimensions. Here we introduce a new concept of multi-dimensional optical storage based on nanophotonics, in particular, involving nanostructured materials. In this new technology, the information can be stored not only in different positions of a thick volume medium but also in a polarisation and spectral domains. The nanostructured materials comprise of semiconductor metallic nanorods. The tuneability of optical properties of the plasmonic properties of anisotropic gold nanorods provide the polarisation and spectral encoding mechanisms in the same spatial position to break the data density limit imposed by the 3D optical storage technology. This nanophotonic approach will lead to a horizon of the new-generation optical data storage technology. This talk will present our recent advance in the nanoparticle-assisted third generation optical data storage technology.

## Nanoparticle-based Molecular Plasmonics

Andrea Csaki<sup>1</sup>, Andrea Steinbrueck<sup>1</sup>, Norbert Jahr<sup>1</sup>, Kathrin Ritter<sup>1</sup>, Thomas Schueler<sup>2</sup>  
Robert Moeller<sup>2</sup>, and Wolfgang Fritzsche<sup>1</sup>

<sup>1</sup>Nanobiophotonics Department, Institute for Photonic Technology (IPHT), Jena, Germany

<sup>2</sup>Jenaer BioChip Initiative, Friedrich-Schiller-Universität Jena, Germany

**Abstract**— The plasmonic properties of metal (e.g., gold or silver) nanoparticles are in the focus of our work. The control of these properties (also in connection with molecular components) and their use for sensing purposes are main goals. One approach for particles with designed plasmonic features is the use of composite particles with defined layers of one metal covering a core of another metal. We studied such particles with various methods and even on-line during the synthesis in order to understand the influence of the various parameters on the resulting optical properties. Such designer particles were combined with molecular tools (e.g., DNA) in order to realize novel constructs such as pairs or cauliflower arrangements. Other approaches included the use of enzymes to induce particle formation of special, anisotropic geometries. In order to get a thorough understanding of the processes involved, microscopic as well as spectroscopic studies were conducted on a single molecule level.

Applications often require parallel measurements but defined readout of just one measurement event. In order to realize such arrangements, various approaches for integration of plasmonic functional units were studied, usually based on microstructured chips and often supported by specific molecular interactions. Also nanoaperture arrangements were studied in order to characterize their plasmonic properties and to understand how to control their properties.

Another line of research is focused of the use of light in order to induce damages to the area surrounding particles with nanometer resolution using the particles as nanoantennas that convert the incoming light into heat. The study of this effect including modeling and systematic experiments will lead to an understanding of the basic principles in order to exploit this effect for various envisioned applications.

## Metallic Structures with Nanometer Scale Resolution Fabricated by Direct Laser Photoreduction and Selected Surface Metallization

Xuan-Ming Duan<sup>1</sup>, Yao-Yu Cao<sup>1</sup>, Wei-Kang Wang<sup>1</sup>, Xian-Zi Dong<sup>1</sup>, Wei-Qiang Chen<sup>1</sup>  
Nobuyuki Takeyasu<sup>2</sup>, Takuo Tanaka<sup>2</sup>, and Satoshi Kawata<sup>2</sup>

<sup>1</sup>Laboratory of Organic NanoPhotonics (LaONP), Technical Institute of Physics and Chemistry  
Chinese Academy of Sciences, Beijing 100080, China

<sup>2</sup>Nanophotonics Laboratory, RIKEN, Wako, Saitama 351-0189, Japan

**Abstract**— Multiphoton processes have been widely used to fabricate micro/nanometer-scaled patterns in the past decade as one of the recognized powerful lithography tools. A number of two-dimensional (2D) and three-dimensional (3D) microstructures have been successfully created using multiphoton processes toward photonic, electronic and plasmonic applications with polymers, dielectrics and metals. Progress has been made on patterning metal with the demonstration of 2D and 3D microstructures. However, comparing to the spatial resolution of nanometer scale achieved with polymers, obtaining the resolution in nanometer scale with laser photoreduction is still a hard challenge for fabricating continuous metallic structures. On the other hand, selected metallization on polymeric structures has been proposed as a useful route to obtain complex metallic structures. In this paper, we report the laser direct patterning of metal nanoparticles with the association of surfactant, which improve the resolution upon diffraction limit in the fabrication of metallic microstructure. We also successfully fabricated metallic structures by selected metallization on prepared polymeric structures. With the further modification of the surface of metallic micro/nanostructures, the functional devices could be developed and expected to play an important role as plasmonic photonics interdisciplinary research fields, i.e., plasmonic photonics, nanoimaging, nanodetection, nanomanipulation and so on.

## Superlens from Complementary Anisotropic Metamaterials

G. X. Li, H. L. Tam, F. Y. Wang, and K. W. Cheah

Department of Physics, Hong Kong Baptist University  
Kowloon Tong, Hong Kong SAR, China

**Abstract**— Metamaterials with isotropic property have been shown to possess novel optical property such as negative refractive index that can be used to design as superlens. Recently it was shown that metamaterials with anisotropic property can translate the high frequency wave vector,  $k$ , values from evanescence to propagating. Using this property and introducing bilayer metamaterials that have complementary anisotropic property, a superlens device can be designed. The simulation further shows that the design can be achieved using metal/oxide multilayer.

In fact in an earlier work, S. A. Ramakrishna et al. proposed a highly effective anisotropic layered system which has potential to be a perfect lens. This shows that anisotropic metamaterials negative refraction and near-field focusing can exist. These anisotropic metamaterials, especially for which not all of the principal elements of the permeability and permittivity tensors have the same sign, have many optically novel phenomena. In 2005, Podolskiy et al. developed a nonmagnetic left-handed system which can work at the optical and infrared frequencies using the strongly anisotropic waveguide in which the negative refraction occurs. They also demonstrated this kind of anisotropic can be effectively used for imaging. Recently, Wood, Pendry and Tsai described in detail the novel optical property of the layered  $\text{SiO}_2$ -Ag system in which the ordinary evanescent waves can propagate and these modes travel in a preferred direction. Zubin Jacob et al. used similar idea to obtain far-field imaging beyond the diffraction limit using an anisotropic cylindrical geometry.

We proposed a new superlens configuration that can give sub-wavelength resolution image in the optical frequency range. This was done through using a complementary anisotropic slab (C-slab includes slab1 and slab2) which supports both propagating waves and evanescent waves and the negative refraction at the interface of the two slabs to form a sub-diffraction limit image. A pair of slits with width 30 nm and center to center separation of 60 nm can be easily resolved by the proposed C-slab superlens with working wavelength 365 nm.

The transfer matrix method has been used to analyze the transmission coefficients of the practical C-slab superlens, and Magnetic flux distribution of the double slits imaging is mapped by the commercial software COMSOL Multiphysics 3.3a in both C-slab and free space. Calculated results demonstrate that the C-slab superlens can go beyond the near-field diffraction limit although the optical properties of slab1 and slab2 independently does not possess the standard superlens conditions. Based on the C-slab and effective medium theory idea, practical anisotropic C-slab superlens which is less sensitive to the metal loss and has higher imaging resolution can be designed by fine tuning the working wavelength and the host dielectrics.

# Optimized Plasmonic Nanostructures for Nanolithography

Y. Chue, Y. Cheng, and J. Li

Department of Engineering Science and Ocean Engineering, National Taiwan University  
Taipei 10617, Taiwan

**Abstract**— In 1998, Ebbesen et al. found that the optical signals can transmit through sub-wavelength hole arrays in metallic films [1]. Then, a lot of researches related to this field are reported [2–5] and the nanowriting or nanolithography systems based on plasmonics-assisted devices are studied [6–8]. The transmission characteristics through small apertures in metallic films can be described by the waveguide mode analysis and numerical simulations [9]. These findings show that the metal-dielectric nanostructures with specific geometry can reconstruct the light intensity distribution and can have the great potential for nanolithography application.

Based on the finite difference time domain method, we study several metal-dielectric nanostructures with different shapes for the incident plane waves with different wavelengths, especially for visible light. The simulation results show that the light enhancement varies with structures and incident waves. Using the optimization procedures in parameters of geometry and the incident waves, some plasmonic nanostructures with careful design are found to have the superior converging properties for visible light and they can focus the light in a small region which is below the diffraction limit. An analytical model is established based on the simulation results to describe the light behavior in the complex nanostructures. Considering the fabrication limits, several optimized plasmonic nanostructures can be designed for nanolithography experiments.

## REFERENCES

1. Ebbesen, T. W., H. J. Lezec, H. F. Ghaemi, T. Thio, and P. A. Wolff, “Extraordinary optical transmission through sub-wavelength hole arrays,” *Nature*, Vol. 391, 667–669, 1998.
2. Martín-Moreno, L., F. J. García-Vidal, H. J. Lezec, A. Degiron, and T. W. Ebbesen, “Theory of highly directional emission from a single subwavelength aperture surrounded by surface corrugations,” *Phys. Rev. Lett.*, Vol. 90, No. 16, 167401, 2003.
3. Barnes, W. L., W. A. Murray, J. Dintinger, E. Devaux, and T. W. Ebbesen, “Surface plasmon polaritons and their role in the enhanced transmission of light through periodic arrays of subwavelength holes in a metal film,” *Phys. Rev. Lett.*, Vol. 92, No. 10, 107401, 2004.
4. Degiron, A., H. J. Lezec, N. Yamamoto, and T. W. Ebbesen, “Optical transmission properties of a single subwavelength aperture in a real metal,” *Opt. Comm.*, Vol. 239, 61–66, 2004.
5. Fu, Y., W. Zhou, L. E. N. Lim, C. L. Du, and X. G. Luo, “Plasmonic microzone plate: Superfocusing at visible regime,” *Appl. Phys. Lett.*, Vol. 91, 061124, 2007.
6. Lee, C. K., C. L. Lin, D. Z. Lin, T. D. Cheng, C. K. Chang, L. B. Yu, and C. S. Yeh, “Developing a nanowriter system: simulation and experimental set-up of a plasmonic-based lens design,” *Mater. Sci. Forum*, Vol. 505-507, 1–6, 2006.
7. Inao, Y., S. Nakasato, R. Kuroda, and M. Ohtsu, “Near-field lithography as prototype nanofabrication tool,” *Microelectron. Eng.*, Vol. 84, 705–710, 2007.
8. Kik, P. G., S. A. Maier, and H. A. Atwater, “Surface plasmons for nanofabrication,” *Prof. of SPIE*, Vol. 5347, 215–223, 2004.
9. Webb, K. J. and J. Li, “Analysis of transmission through small apertures in conducting films,” *Phys. Rev. B*, Vol. 73, 033401, 2006.



# Slow Light and Extraordinary Magneto-optical Effects in Magnetic and Plasmonic Nanostructures

V. I. Belotelov<sup>1,2</sup>, A. K. Zvezdin<sup>1</sup>, A. N. Kalish<sup>1,2</sup>, and E. A. Shevchenko<sup>1</sup>

<sup>1</sup>A. M. Prokhorov General Physics Institute, Russia

<sup>2</sup>M. V. Lomonosov Moscow State University, Russia

**Abstract**— Optical properties of the plasmonic nanostructured materials, i.e. materials which can sustain the propagation of the surface plasmon-polariton (SPP) waves, are shown to have some peculiarities leading to new optical effects like the effect of the extraordinary optical transmission [1]. At the same time, it was revealed, that magneto-optical properties of plasmonic systems also demonstrate rather interesting behavior at the frequency domains of the SPPs excitation [2, 3]. Thus, the Faraday effects enhancement by an order of magnitude was reported recently [2].

In this we consider a bilayer system of the periodically perforated with the hole arrays metallic layer and a dielectric layer magnetized either in longitudinal or transversal geometry. By varying the thickness of the dielectric layer it is possible to achieve either waveguiding or SPPs conditions. Magneto-optical Faraday and Kerr effects along with intensity effects are found to have pronounced resonance peaks. While for large thicknesses (much larger than wavelength) the enhancement is associated with the excitation of SPPs and Rayleigh anomalies, for layers of micron or submicron thickness the quasi-guided modes play a crucial role.

We also investigate a physical nature of the influence of the periodicity and SPPs on the magneto-optical effects. The correlation between wave group velocity and the Faraday rotation peaks is found. It is demonstrated that the Faraday rotation in the periodic systems is strongly related with the group velocity  $V_g$  and gets its maximum values at the vanishing  $V_g$ . In the case of the considered heterostructure this dependence of the specific Faraday angle can be written by  $\Phi_{F0} = \langle Q \rangle \omega / 2V_g$ , where  $\langle Q \rangle$  is the matrix element of the magneto-optical parameter [2]. Thus, the increase of the magneto-optical effects in magnetic periodic systems is related to the phenomenon of slow light.

## ACKNOWLEDGMENT

Work is supported by RFBR (06-02-17507, 07-02-91588, 07-02-01445), and Russian foundation “Dynasty”.

## REFERENCES

1. Ebbesen, T. W., H. J. Lezec, H. F. Ghaemi, T. Thio, and P. A. Wolff, *Nature*, Vol. 391, 667, 1998.
2. Belotelov, V. I., L. L. Doskolovich, and A. K. Zvezdin, *Phys. Rev. Lett.*, Vol. 98, 77401, 2007.
3. Inoue, M., R. Fujikawa, H. Uchida, K. H. Shin, and et al., *PIERS 2007*, Prague, 153, 2007.



# Session 2A2a

## Femtosecond Photonics: Microfabrication and Optical Data Storage 2

<b>Femtosecond Photonics for Multilayered Optical Memory</b>	
<i>Yoshimasa Kawata (Shizuoka University, Japan); M. Miyamoto (Shizuoka University, Japan); M. Nakabayashi (LINTEC Corp., Japan); .....</i>	228
<b>Rewriteable Three-dimensional Optical Memory by Using Spatial Valence State Manipulation of Rare-earth Ions</b>	
<i>Jianrong Qiu (Zhejiang University, China); K. Miura (Kyoto University, Japan); K. Hirao (Kyoto University, Japan); .....</i>	229
<b>Polarization-dependent Memory of Light via Ultrashort Pulse Laser Irradiation</b>	
<i>Yasuhiko Shimotsuma (Kyoto University, Japan); Masaaki Sakakura (Kyoto University, Japan); Peter G. Kazansky (University of Southampton, UK); Jianrong Qiu (Zhejiang University, China); Kiyotaka Miura (Kyoto University, Japan); Kazuyuki Hirao (Kyoto University, Japan); .....</i>	230
<b>Fs Laser Micro Fabrication Method and Its Application in Multilayer Data Storage</b>	
<i>Wenhao Huang (University of Science and technology of China, China); .....</i>	231
<b>Lasing with the Shortest Wavelength in Substituted ZnO and Laser Spectroscopy Study on High Density Exciton in Nanocrystal</b>	
<i>Jian-Wen Dong (The Hong Kong University of Science and Technology, China); C. R. Ding (Zhongshan (Sun Yat-Sen) University, China); B. C. Chen (Zhongshan (Sun Yat-Sen) University, China); S. W. Li (Zhongshan (Sun Yat-Sen) University, China); He-Zhou Wang (Zhongshan University, China); .....</i>	232
<b>Optical Filter Based on One Dielectric Reflector</b>	
<i>Ken Liu (National University of Defense Technology, China); Wei-Min Ye (National University of Defense Technology, China); Xiao-Dong Yuan (National University of Defense Technology, China); ..</i>	233

# Femtosecond Photonics for Multilayered Optical Memory

Y. Kawata<sup>1</sup>, M. Miyamoto<sup>1</sup>, and M. Nakabayashi<sup>2</sup>

<sup>1</sup>Mechanical Engineering, Shizuoka University, Japan

<sup>2</sup>R&D Division, LINTEC Corp., Japan

## Abstract—

**Introduction:** Three-dimensional (3-D) optical memory has been studied by many researchers in order to overcome the data storage capacity that is limited by the diffraction limit of light [1, 2]. 3-D optical memories based on two-photon excitation are the most promising techniques, because many technologies for current optical memories, such as pick-up optics, servo and tracking systems, will be used with some extensions or modifications.

In this paper, we propose a novel fabrication method of multilayered media by a laminating process using pressure sensitive adhesives (PSA). The proposed technique is very easy to pile up many layers and control the film thickness, so this technique is applicable to mass production of multilayered media.

**Multilayered Medium Using PSA:** We fabricated a multilayered media by wet coating and laminating process using PSA. First, the photosensitive layer and the PSA as a transparent layer were deposited on polyethyleneterephthalate (PET) release liner films, respectively. The photosensitive layer and the PSA layer were laminated together, peeling away the release liner film from the PSA film. Second, it was laminated on a substrate under the constant pressure, and then the two layered sheets were superposed on other layers repeatedly.

We have succeeded the fabrication of twenty recording layers as the multilayered medium. Figure 1 shows the cross section along axial direction observed with a reflection confocal microscope. The film thickness of the photosensitive layer was  $1.6\ \mu\text{m}$  and film thickness of the transparent layer was  $4.6\ \mu\text{m}$ .

Figure 2 shows recording and reading results of twenty recording layers. Bit distance is  $2.0\ \mu\text{m}$ . The recorded bits in all layers were clearly observed with high contrast. It was also recognized that the crosstalks between neighboring layers were small enough.

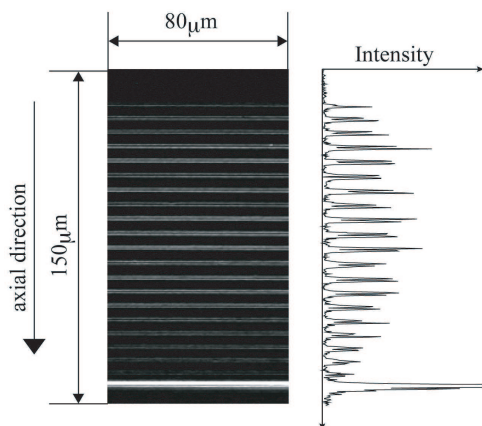


Figure 1: Cross sectional view of multilayered medium.



Figure 2: Recording and readout results of twenty layers.

## REFERENCES

1. Kawata, S. and Y. Kawata, *Chem. Rev.*, Vol. 100, 1777, 2000.
2. Miyamaoto, M., M. Nakakno, M. Nakabayashi, S. Miyata, and Y. Kawata, *Appl. Opt.*, Vol. 45, 8424, 2006.

## Rewriteable Three-dimensional Optical Memory by Using Spatial Valence State Manipulation of Rare-earth Ions

Jianrong Qiu<sup>1</sup>, K. Miura<sup>2</sup>, and K. Hirao<sup>2</sup>

<sup>1</sup>State Key Laboratory of Silicon Materials, Zhejiang University  
Hangzhou 310027, China

<sup>2</sup>Department of Material Chemistry, Graduate School of Engineering  
Kyoto University, Sakyo-ku, Kyoto 606-8501, Japan

**Abstract**— We review recent research development on the recording, readout, and erasure of three-dimensional optical memory using the spatial valence-state manipulation of rare-earth ions. The mechanism of the femtosecond laser-induced localized photoreduction of rare-earth ions from  $\text{Re}^{3+}$  to  $\text{Re}^{2+}$  in glasses is discussed. Three-dimensional optical memory with ultrahigh storage density has been demonstrated. Photoreduction bit of 200 nm diam is recorded in a  $\text{Sm}^{3+}$ -doped glass with a femtosecond laser and readout clearly by detecting the fluorescence as a signal with excitation at 488 nm  $\text{Ar}^+$  laser. The photoreduction bit that is stable at room temperature can be erased by photo-oxidation with a cw laser at 514.5 nm  $\text{Ar}^+$  laser. Since photoreduction bits can be spaced 150 nm apart in a layer within glass, a multilayer structure with several hundred layers could be used to record data. A memory capacity of as high as 1 Tbit could thus be achieved in a glass piece with dimensions of 10 mm×10 mm×1 mm. We also point out the future tendencies of the related research.

# Polarization-dependent Memory of Light via Ultrashort Pulse Laser Irradiation

Y. Shimotsuma<sup>1</sup>, M. Sakakura<sup>1</sup>, P. G. Kazansky<sup>2</sup>  
J. Qiu<sup>3</sup>, K. Miura<sup>4</sup>, and K. Hirao<sup>4</sup>

<sup>1</sup>Innovative Collaboration Center, Kyoto University, Japan

<sup>2</sup>Optoelectronics Research Centre, University of Southampton, United Kingdom

<sup>3</sup>Department of Materials Science and Engineering, Zhejiang University, China

<sup>4</sup>Department of Material Chemistry, Kyoto University, Japan

**Abstract**— The remarkable phenomena in ultrafast light-matter interactions manifested as a localized structural change in transparent material and an evolution of one-dimensional metal nanoparticles in liquid ablation are observed. The periodic nanostructures composed of oxygen depleted regions of 20 nm size with periods as small as 140 nm inside silica glass, are aligned perpendicular to the laser polarization. The polycrystalline copper nanowires with a length of 1.0  $\mu\text{m}$  and a diameter of 85 nm are also successfully formed only under the linear-polarized laser irradiation. The growth mechanism of copper nanowires under the femtosecond laser irradiation was suggested to be a nucleation growth process. The periodic nanostructures inside silica glass and the copper nanowires in ethanol solution can be interpreted in terms of a created pattern via coupling between photon and plasmon waves; consequently a material could memorize the direction of the light polarization.

## Fs Laser Micro Fabrication Method and Its Application in Multilayer Data Storage

Wenhao Huang

Department of Precision Machinery and Instrumentation  
University of Science and technology of China  
Hefei 230026, China

**Abstract**— In this talk our recent progress of femtosecond laser micro-fabrication method is presented. It includes the fabrication apparatus, the laser-materials interaction, the optimizing method for novel micro optical and photonic devices, and the applications in living cell and in optical multi-layer data storage. Some challenges of improving the laser spot quality and optical driving are discussed.

## Lasing with the Shortest Wavelength in Substituted ZnO and Laser Spectroscopy Study on High Density Exciton in Nanocrystal

J. W. Dong, C. R. Ding, B. C. Chen, S. W. Li, and H. Z. Wang

State Key Laboratory of Optoelectronic Materials and Technologies

Zhongshan (Sun Yat-Sen) University, Guangzhou 510275, China

**Abstract**— At femtosecond pulse laser pumping, stimulated emissions are observed in  $\text{Zn}_x\text{Mg}_{1-x}\text{O}$  epilayers. Among them, spectral blue shifts are dependent on the Mg substitution concentration; and the highest lasing photon energy (in ZnO series materials even reported) of 3.51 eV is observed. Furthermore, experimental results also show that by high concentration Mg substitution, a red shift of the electron-hole plasma stimulated emission is reduced and its efficiency doesn't decrease with the Mg substitution concentration. These results imply that the lasing frequency of ZnO series materials can be modified by substitution. Study on the high density excitons in single semiconductor nano-crystal by femtosecond laser spectroscopy, an interesting new collective behavior of high density excitons in single semiconductor nano-crystal is revealed. We anticipate our discovery to be a starting point for new developments of active nano-optoelectronic devices, which not only benefits to the development of nano-technology but also quantum information processing and quantum communication.



## Optical Filter Based on One Dielectric Reflector

Ken Liu, Wei-Min Ye, and Xiao-Dong Yuan

Research Center of Photonic Crystals, College of Optoelectronic Engineering  
National University of Defense Technology, Changsha 410073, Hunan, China

**Abstract**— By theoretically analysis both in frequency domain and time domain, we demonstrate a dielectric compact optical filter based on only one reflector. The structure analyzed is a dielectric omnidirectional mirror suspended in air and perforated with rectangular lattice of air holes. The periodic dielectric index provides resonance features, sharp resonant modes with nearly complete transmission appear. Based on this phenomenon, when resonant modes are in band gap of the mirror and can radiate out of the mirror, the structure can then act as an optical filter. This kind of transmission filter is more compact than the conventional dielectric thin film devices. Resonant states in a filter depend on the lattice constant, radius of the air holes, and thickness of each layer of the reflector, without changing the reflector's thickness, a transmission mode can be determined by lattice constant and radius of the air holes, thus different filters can be easily integrated in one reflector, space-variant optical transmission filter are achieved.

Furthermore, there are several parameters can be changed to change center wavelength, shape of resonant modes, by carefully changing lattice constant, radius of air holes and thickness of layers, two resonant modes can overlap each other, flat-top optical-filters are developed and achieved. To design this kind of flat top filter do not need additional layers as conventional dielectric thin film devices, the more number of defect layers the conventional dielectric filter has, the more square the band shape.

This kind of filter is expected to be used in optical communication devices and vertical cavity surface emitting lasers.



# Session 2A2b

## Photonic Crystal Waveguides

<p><b>Manipulating Polarisation in 2D Photonic Crystal Silicon-On-Insulator (SOI) for Novel Photonic Filters</b>  <i>John Canning (University of Sydney, Australia); Martin Kristensen (University of Aarhus, Denmark); Nina Skivesen (University of Aarhus, Denmark); Lars H. Frandsen (Technical University of Denmark, Denmark); Amelie Tetu (University of Aarhus, Denmark); Jacques Chevallier (University of Aarhus, Denmark); Cicero Martelli (University of Aarhus, Denmark); .....</i></p> <p><b>Fresnel Fibres and Components</b>  <i>John Canning (University of Sydney, Australia); .....</i></p> <p><b>Scattering of UV Light through Photonic Crystal Fibre Triangular Lattices and Impact on Grating Writing</b>  <i>John Canning (University of Sydney, Australia); John Holdsworth (University of Newcastle, Australia); .....</i></p> <p><b>Polymer Photonic Crystal Waveguides in Orthodontics</b>  <i>Maura Milsczewski (Universidade Tecnologica Federal do Parana, Brasil); John Canning (University of Sydney, Australia); Cicero Martelli (University of Sydney, Australia); Hypolito Kanilowski (Universidade Tecnologica Federal do Parana, Brasil); Jose Simoes (Universidade de Aveiro, Portugal); Michael Stevenson (University of Sydney, Australia); Paolo Talaia (Universidade de Aveiro, Portugal); .....</i></p> <p><b>Making Porphyrin Nanowires for Silicon Photonic Crystal Waveguides</b>  <i>Cicero Martelli (University of Aarhus, Denmark); Nina Skivesen (University of Aarhus, Denmark); John Canning (University of Aarhus, Denmark); Martin Kristensen (University of Aarhus, Denmark); Maxwell J. Crossley (The University of Sydney, Australia); .....</i></p>	<p>236</p> <p>237</p> <p>238</p> <p>239</p> <p>240</p>
---	--

## Manipulating Polarisation in 2D Photonic Crystal Silicon-On-Insulator (SOI) for Novel Photonic Filters

John Canning<sup>1,2</sup>, Martin Kristensen<sup>1</sup>, Nina Skivesen<sup>1</sup>, Lars H. Frandsen<sup>3</sup>  
Amelie Tetu<sup>1</sup>, Jacques Chevallier<sup>1</sup>, and Cicero Martelli<sup>1</sup>

<sup>1</sup>iNANO and Department of Physics and Astronomy, University of Aarhus, Århus, Denmark

<sup>2</sup>School of Chemistry, University of Sydney, Sydney, Australia

<sup>3</sup>COM·DTU, Department of Communications, Optics and Materials  
Technical University of Denmark, Denmark

**Abstract**— Photonic crystal 2-D waveguides and components offer substantive compact dispersion for increasing functionality within a photonic chip. For most devices propagation of quasi-TE light is primarily considered. We have recently characterized the polarisation conversion properties found in simple linear 2D silicon-on-insulator photonic crystal waveguide devices. Based on these properties we propose and demonstrate novel narrow pass filters and narrow transmission polarisation converters by exploiting the input and output polarisations of the photonic crystal. The basic configuration for doing this is illustrated in Figure 1. A supercontinuum source is used to probe the linear SOI crystal. The transmission spectra are monitored on an optical spectrum analyser. Polarisation is adjusted at the input end with polarisation controllers and polarisers. The output polarisation is monitored using a second polariser and another controller. In this way we are able to map the polarisation space of the device, including any cross coupling between eigenstates. By adjusting these input and output devices we are able to obtain very narrow pass band and rejection filters, shown in Figure 2. Given the possibility of integrating many of these components directly onto a photonic chip, this offers a unique and practical approach to creating such filters based on phase matching the eigenstates using the large difference in polarisation dispersion of the 2D crystal. These devices raise interesting questions regarding the practical identification of the crystal band edge compared with the theoretical edge. Applications of such filters include polarisation converters to ensure proper polarisation eigenstate matching in chip devices operating on one eigenstate only, and straightforward filters.

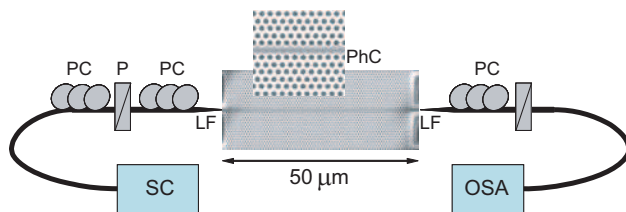


Figure 1: Schematic of setup employed and SEM image of a 50  $\mu\text{m}$  photonic crystal waveguide inserted as the PhC. The inset shows a close-up of the structure. Also not shown because of size restraints in the imaging process is the SOI tapered input waveguides leading into the structure. PhC — photonic crystal; PC — polarisation controller; P — polariser; LF — lensed fibre; SC — supercontinuum source; OSA — optical spectrum analyser.

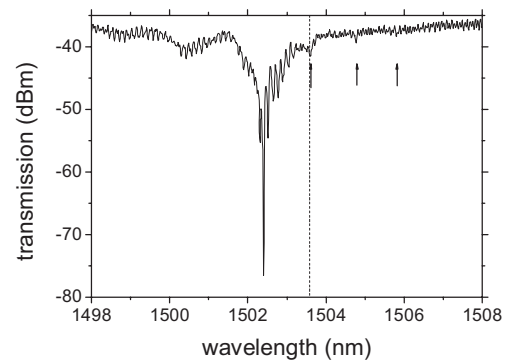


Figure 2: Ultra narrow transmission notch which is created before the band edge of the crystal. The band edge is marked by the dashed line.

## Fresnel Fibres and Components

**John Canning**

School of Chemistry, University of Sydney, Sydney, Australia

**Abstract**— Fresnel fibres were introduced by Canning to describe how to optimize scattering such that field propagation occurs along the waveguide. In a 2-D cylindrical distribution of refractive index, the simplest conditions are analogous to Yariv and Yeh's Bragg and chirped Bragg fibres. These can be replaced with air holes positioned approximately along the circular Fresnel zones to the waveguide. However, other solutions are possible including hyperbolic Fresnel fibres which can have holes placed along the hyperbolic zone plates of the waveguide thereby producing even more exotic profiles for dispersion and other phenomena associated with light traveling down a waveguide. So long as the phase scattering mechanism is constructive in the direction of propagation, the propagating field can be shaped arbitrarily using such extended Fresnel sources. The concept of the Fresnel fibre is the recognition of such Fresnel sources as the basic point at which light and its group velocity and other properties can be shaped and manipulated. From such fibres comes a number of basic components that can be integrated into the fibre structure, the most demonstrated one being the Fresnel lens. This has been done both by etching conventional fibres such that a chirped Bragg structure exists at the end of the fibre or by splicing onto a conventional fibre a short piece of Fresnel fibre with holes distributed within the zone plates of the fibre. From a functional point of view very broadband Fresnel fibres have a bandgap-like property where light over a considerably larger spectral region than conventional band gap fibres travel along the waveguide. In this presentation I review some of these properties.

# Scattering of UV Light through Photonic Crystal Fibre Triangular Lattices and Impact on Grating Writing

John Canning<sup>1</sup> and John Holdsworth<sup>1,2</sup>

<sup>1</sup>OFTC, School of Chemistry, University of Sydney, Australia

<sup>2</sup>School of Mathematical and Physical Sciences, University of Newcastle, Australia

**Abstract**— Using commercially available finite difference time domain (FDTD) software, simulations of UV light (193 nm) scattering through the side of an air-silica photonic crystal fibre were carried out. The figure below shows the results which indicate, despite large scattering by the air holes, when the laser light is aligned orthogonal to one of the lattice axes, the lattice acts to focus some of the light into the back of the fibre core. This suggests grating writing is possible without using index matching fluids within the holes. We have written gratings into such fibres shown in Figure 2. Slight angular deviations suggest that this focusing is dissipated and grating writing is quickly spoilt. We investigate this experimentally.

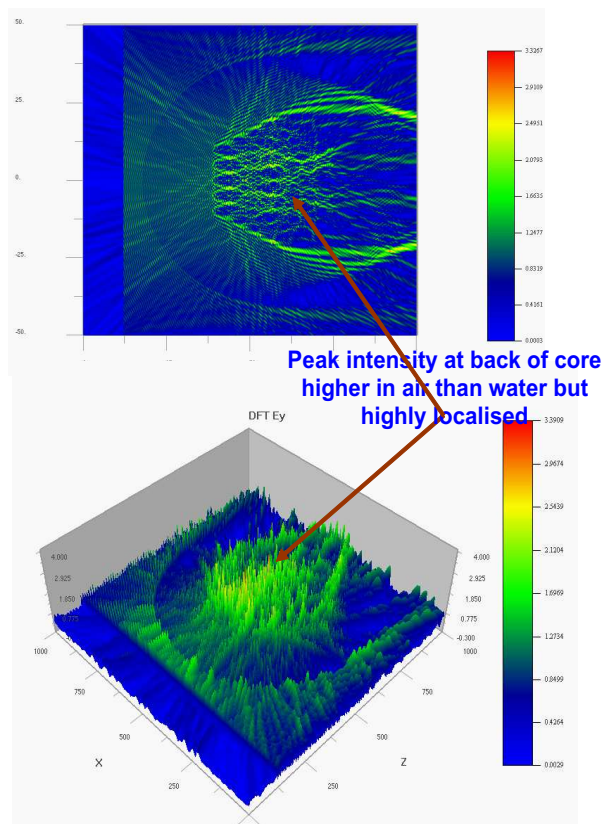


Figure 1: FDTD simulations of 193 nm light striking crystal lattice fibre from the side. Case for both air and water simulated.

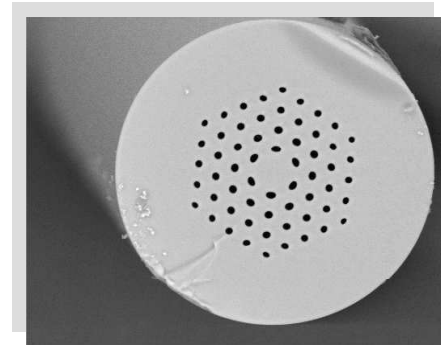


Figure 2: Cross-section of photonic crystal fibre manufactured at Sydney University.

## Polymer Photonic Crystal Waveguides in Orthodontics

Maura Milsczewski<sup>1,2</sup>, John Canning<sup>2</sup>, Cicero Martelli<sup>3</sup>, Hypolito Kanilowski<sup>1</sup>  
Jose Simoes<sup>4</sup>, Michael Stevenson<sup>2</sup>, and Paolo Talaia<sup>4</sup>

<sup>1</sup>Universidade Tecnológica Federal do Paraná, 80230-901 Curitiba, Brasil

<sup>2</sup>School of Chemistry, University of Sydney, Sydney, Australia

<sup>3</sup>School of Electrical and Information Engineering, University of Sydney, Australia

<sup>4</sup>Departamento de Engenharia Mecânica, Universidade de Aveiro, Portugal

**Abstract**— Photonic crystal fibres made from polymer materials have a feature which distinguishes them from silica — They are sensitive to strain and pressure perturbations. For example, applied local pressure can be measured directly as a form of attenuation of transmitted light. Whilst this deformation issue has been problematic in evaluation the potential usefulness of such fibres for communications it in fact makes them ideal sensing systems. We describe recent developments we have made in the area of orthodontics using polymer photonic crystal fibre as the sensing element itself. Localised pressure is fundamental to the correction of teeth and these fibres are ideal for their measurement. To our knowledge this is the first direct measurements of orthodontic forces and heralds a new era of applied photonics health monitoring.

Transversal pressure deforms the fibre structure proportionally to the applied load causing light to leak out. Figure 1, shows a photograph of the apparatus used. The characterization for transversal pressure demonstrates linear behaviour within the studied load range 0.09 to 4.7 N. For the orthodontic measurements the sensor is placed between the orthodontic appliance and only one tooth. Loads ranging over 0.98 to 8.82 N, simulating extra oral appliances, are applied over the orthodontic system at the first molar region. The surface of the tooth experiences forces ranging from 0 to  $\sim 0.63$  N compatible with forces required for dental movement.

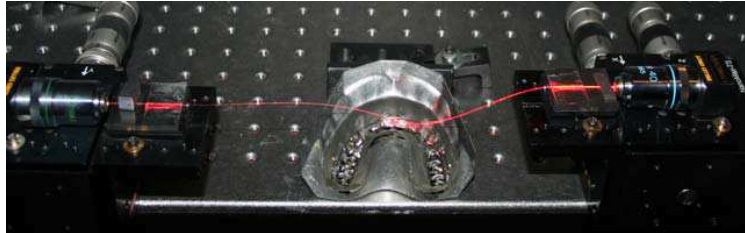


Figure 1: Photograph of a polymer photonic crystal fibre localised pressure sensor on a clinical trial mandible for assessment of applied dental forces typical of corrective adjustment during tooth realignment.

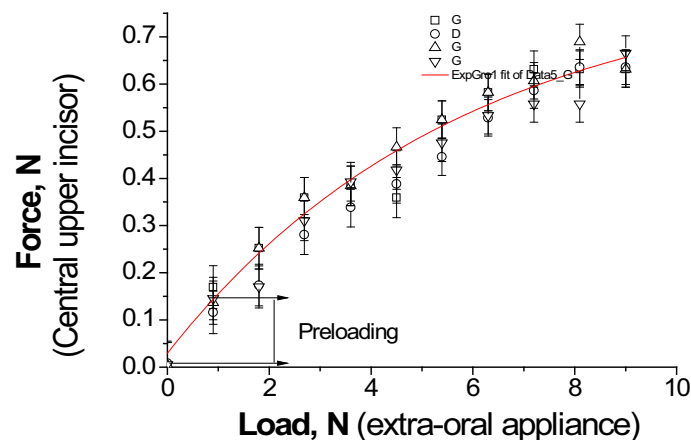


Figure 2: Measured force as applied load is increased.

# Making Porphyrin Nanowires for Silicon Photonic Crystal Waveguides

Cicero Martelli<sup>1,2</sup>, Nina Skivesen<sup>1</sup>, John Canning<sup>1,3</sup>  
 Martin Kristensen<sup>1</sup>, and Maxwell J. Crossley<sup>3</sup>

<sup>1</sup>iNANO and Department of Physics and Astronomy, University of Aarhus, Århus, Denmark

<sup>2</sup>School of Electrical and Information Engineering, The University of Sydney, Australia

<sup>3</sup>School of Chemistry, The University of Sydney, NSW 2006, Australia

**Abstract**— The functionality of photonic crystal waveguides can be increased using a number of materials. A system of particular importance is porphyrins since they have a number of properties useful for optical and electronic applications. However, the development and understanding of formation of structures based on porphyrins has a long way to go. In this work we report on the self assembly of porphyrin nanowires on silicon. Atomic force microscopy is used to characterise these structures for the first time. By understanding how they form on flat silicon, it is expected that this work will provide insights on how best to deposit such active material on SOI crystal waveguides.

Figure 1 shows a dark-field optical micrograph of the wires deposited on the Si substrate. The aspect ratio (length/width) of the wires is  $\sim 30$ . For comparison, the scale grid shows a 2D 50  $\mu\text{m}$  long SOI photonic crystal waveguide. Therefore, the porphyrin worms are in excess of 50  $\mu\text{m}$  in length and can in principle be laid across the entire length of the crystal waveguide to allow strong interaction with an optical field. Figure 2 shows AFM images of one of these wires. The surface is found to be ultra smooth within resolution.

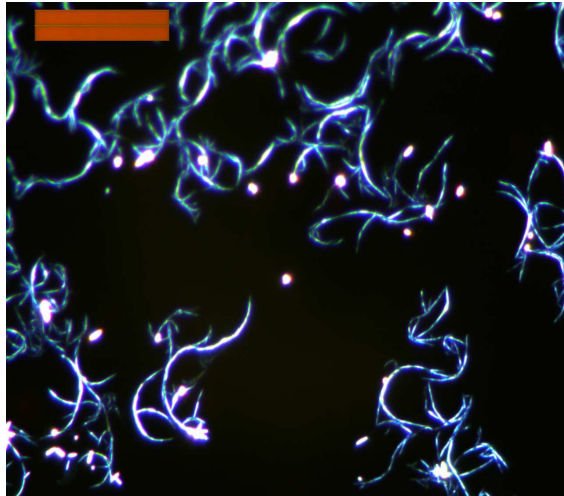


Figure 1: Dark-field optical images of the wires formed on a silicon substrate, the scale lines corresponds to a 2D 50  $\mu\text{m}$  photonic crystal waveguide.

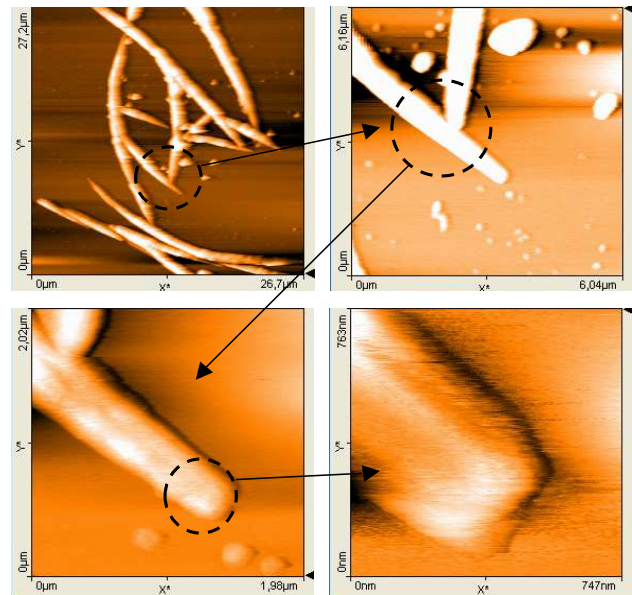


Figure 2: AFM images of the self-assembled porphyrin worms. Resolution  $\geq 7$  nm.



# Session 2A3

## Metamaterials at Optical Frequencies

### Phase-engineered Metamaterial Structures and Devices

*Christophe Caloz (École Polytechnique de Montréal, Canada); Shulabh Gupta (École Polytechnique de Montréal, Canada);* ..... 242

### Optical Activity Introduced by Magnetic Plasmon Resonance in Metamaterial

*Hui Liu (Nanjing University, China); D. A. Genov (University of California, USA); Tao Li (Nanjing University, China); Shu-Ming Wang (Nanjing University, China); Fu-Ming Wang (Nanjing University, China); Shi-Ning Zhu (Nanjing University, China); X. Zhang (University of California, USA);* ..... 243

### Realization of Three-dimensional Photonic Metamaterials at Optical Frequencies

*Na Liu (Universität Stuttgart, Germany); Hongcang Guo (Universität Stuttgart, Germany); Liwei Fu (Universität Stuttgart, Germany); Stefan Kaiser (Universität Stuttgart, Germany); H. Schweizer (University of Stuttgart, Germany); Harald W Giessen (University of Stuttgart, Germany);* ..... 244

### Dielectric Metamaterials with Accessible Tunability

*Xian Qi Lin (Southeast University, China); Jessie Yao Chin (Southeast University, China); Xin Mi Yang (Southeast University, China); Di Bao (Southeast University, China); Qiang Cheng (Southeast University, China); Tie Jun Cui (Southeast University, China);* ..... 246

### Does Planar Left-handed Material Slab Resolve Subwavelength Details in the Image?

*M. Yu. Barabanenkov (Russian Academy of Sciences, Russia); Yurii Nicolaevich Barabanenkov (Russian Academy of Sciences (IRE RUS), Russia); S. A. Nikitov (Russian Academy of Sciences, Russia);* .... 247

### Widening the Negative Effective Parameter Frequency Band of Resonant SNG Metamaterials

*Jan Zehentner (Czech Technical University, Czech Republic); Jan Machac (Czech Technical University, Czech Republic);* ..... 248

### Resonance-induced Transparencies of Opaque Waveguides and Doppler Effects of a Light Source on a Meta-material Slab

*Hao Xu (Fudan University, China); Weihua Wang (Fudan University, China); Jiaming Hao (Fudan University, China); Lei Zhou (Fudan University, China);* ..... 249

### From Photonic Crystals to Metamaterials: A General Mean-field Theory

*Peter Halevi (Instituto Nacional de Astrofisica, Optica y Electronica, Mexico); F. Pérez-Rodríguez (Benemerita Universidad Autonoma de Puebla, Mexico); J. A. Reyes-Avendaño (Instituto Nacional de Astrofisica, Optica y Electronica, Mexico); E. Reyes-Ayona (Instituto Nacional de Astrofisica, Optica y Electronica, Mexico);* ..... 250

### Coupling Light to Delocalized Magnetic Excitations: Magnetic Plasmon Polaritons and Antisymmetric SPP Mode

*Tao Li (Nanjing University, China); Hui Liu (Nanjing University, China); Shu-Ming Wang (Nanjing University, China); Fu-Ming Wang (Nanjing University, China); Jia-Qi Li (Nanjing University, China); Shi-Ning Zhu (Nanjing University, China);* ..... 251

### Influence of Dephasing on Electromagnetically Induced left-handedness in Optically Excited Atomic Media

*Shang-Bin Li (Shanghai Research Center of Amertron-global, China);* ..... 252

## Phase-engineered Metamaterial Structures and Devices

Christophe Caloz and Shulabh Gupta

École Polytechnique de Montréal, Canada

**Abstract**— Electromagnetic metamaterials are inherently dispersive: their constitutive parameters (permittivity  $\varepsilon$  and permeability  $\mu$ ) are functions of frequency or, equivalently, their dispersion relation  $[\beta(\omega)]$  is a nonlinear function of frequency [1]. In the particular case of double negative (DNG) metamaterials ( $\varepsilon < 0$  and  $\mu < 0$ ), also called left-handed (LH) or negative refractive index (NRI) metamaterials, dispersion is a direct consequence of energy positiveness, which is related to causality.

Since the invention of the superheterodyne receiver by Edwin Armstrong in 1918 and, later, the development of efficient harmonic signal generators, most radio communication systems have been narrow-band in nature. However, the explosion of needs for high data-rate wireless links is currently producing a paradigmatic shift of radio toward broadband and ultra-wideband spectrum operation [2]. In this context, the unprecedented and tailorable dispersive properties of metamaterials may provide solutions to several new challenges. While the past decades have focused on *magnitude engineering and filter design* [3], we predict that the forthcoming decades will experience major interest in *phase engineering* (where the term “phase engineering” is intended to represent both “dispersion and nonlinearity” engineerings) and “*chirper design*” (where the term “chirper” is a neologism suggested here to designate a phase-engineered device). In both case, metamaterials are expected to play an important role.

Phase-engineered metamaterials devices may be operating either in the *harmonic-regime* or in the *impulse-regime*.

In harmonic-regime phase-engineered metamaterial devices, the phase relation is engineered so as to provide desired functionalities at different narrow-band frequencies; a typical example is the case of multi-band devices, where for instance a CRLH (composite right/left-handed) metamaterial transmission line is inherently dual-band [1] (Sec. 5.1) while a Lorentz-extended CRLH metamaterial is inherently tri-band [4].

Impulse-regime phase-engineered metamaterial devices are excited by pulses, i.e., ultra wideband signals, for which the designs of most conventional components need to be revisited. The first impulse-regime metamaterial devices have been recently developed and demonstrated by our group [5, 6]. They include tunable pulse delay lines, pulse position modulators (PPMs), Talbot pulse train multipliers, frequency discriminators and real-time Fourier transformers, spectrogram analyzers and soliton-based devices with diverse functionalities.

### REFERENCES

1. Caloz, C. and T. Itoh, *Electromagnetic Metamaterials, Transmission Line Theory and Microwave Applications*, Wiley-Interscience, Wiley and IEEE Press, 2005.
2. Yang, L. and G. B. Giannakis, “Ultra-wideband communications, an idea whose time has come,” *IEEE Trans. Sig. Proc. Mag.*, 26–54, Nov. 2004.
3. Matthaei, G. L., L. Young, and E. M. T. Jones, *Microwave Filters, Impedance-Matching Networks, and Coupling Structures*, Artech House, 1964.
4. Rennings, A., T. Liebig, C. Caloz, and I. Wolff, “Double Lorentz transmission line metamaterials and their applications to triband devices,” *IEEE MTT-S Int. Microwave Symp.*, 1427–1430, Honolulu, June 2007.
5. Abielmona, S., S. Gupta, and C. Caloz, “Experimental demonstration and characterization of a tunable CRLH delay line system for impulse/continuous wave,” *IEEE Microwave Wireless Compon. Lett.*, Dec. 2007 (to be published).
6. Caloz, C. and S. Gupta, “Dispersion and nonlinearity engineered metamaterial devices,” *Metamaterial Conference*, Rome, Oct. 2007 (to be published).

# Optical Activity Introduced by Magnetic Plasmon Resonance in Metamaterial

H. Liu<sup>1,2</sup>, D. A. Genov<sup>2</sup>, T. Li<sup>1</sup>  
S. M. Wang<sup>1</sup>, F. M. Wang<sup>1</sup>, S. N. Zhu<sup>1</sup>, and X. Zhang<sup>2</sup>

<sup>1</sup>Department of Physics, National Laboratory of Solid State Microstructures  
Nanjing University, Nanjing 210093, China

<sup>2</sup>5130 Etcheverry Hall, Nanoscale Science and Engineering Center  
University of California, Berkeley, California 94720-1740, USA

**Abstract**— In 1999, Pendry reported that a nonmagnetic metallic element, referred to as double split ring resonator, with size smaller than the wavelength of radiation, exhibits a strong resonant response to the magnetic component of an incident electromagnetic field. [1] It was also suggested that a combination of magnetic response and chirality could be used as an alternative route to negative refraction.[2] Various electromagnetic chiral structures have been reported in the microwave spectral range, such as helical wire spring, swiss-rolé metal structure, [2] rotating rosette shape [3–4]. Recently, novel metallic elements have been demonstrated, with magnetic response in the near-infrared and visible spectral region [5–13]. This provides new possibilities to engineer magnetically coupled systems and realize artificial chiral effect at optical frequency.

In this letter, we investigate the magnetic plasmon response of a subwavelength nanostructure, referred to as a magnetic dimer (MD). The magnetic dimer constitutes of two single split-ring resonators (SSRR) coupled through magnetic induction. The fundamental MD resonances are viewed as bonding and antibonding combinations of individual SSRRs eigenmodes. A new type of optical activity is observed in the coupled system which is not an inherent property of the individual magnetic resonators. [14] For instance, a linearly polarized light flips into an elliptically polarized state as it passes through an array of magnetic dimers. Overall, all types of wave polarization are accessible with the proposed magnetic plasmon (MP) based metamaterial.

## REFERENCES

1. Pendry, J. B., et al., *IEEE Trans. Microwave Theory Tech.*, Vol. 47, 2075, 1999.
2. Pendry, J. B., *Science*, Vol. 306, 1353, 2004.
3. Papakostas, A., et al., *Phys. Rev. Lett.*, Vol. 90, 107404, 2003.
4. Rogacheva, A. V., et al., *Phys. Rev. Lett.*, Vol. 97, 177401, 2006.
5. Yen, T. J., et al., *Science*, Vol. 303, 1494, 2004.
6. Linden, S., et al., *Science*, Vol. 306, 1351, 2004.
7. Enkrich, C., et al., *Phys. Rev. Lett.*, Vol. 95, 203901, 2005.
8. Zhou, J., et al., *Phys. Rev. Lett.*, Vol. 95, 223902, 2005.
9. Ishikawa, A., et al., *Phys. Rev. Lett.*, Vol. 95, 237401, 2005.
10. Liu, H., D. A. Genov, et al., *Phys. Rev. Lett.*, Vol. 97, 243902, 2006.
11. Wang, F. M., H. Liu, et al., *Phys. Rev. E*, Vol. 95, 016604, 2007.
12. Li, T., H. Liu, et al., *Phys. Rev. E*, Vol. 96, 016606, 2007.
13. Wang, F. M., H. Liu, et al., *Phys. Rev. E*, Vol. 76, 075110, 2007.
14. Liu, H., D. A. Genov, et al., *Phys. Rev. B*, Vol. 76, 073101, 2007.

# Realization of Three-dimensional Photonic Metamaterials at Optical Frequencies

Na Liu, Hongcang Guo, Liwei Fu, Stefan Kaiser, Heinz Schweizer, and Harald Giessen

4. Physikalisches Institut, Universität Stuttgart, D-70569, Stuttgart, Germany

**Abstract**— We present a general recipe to manufacture three-dimensional optical metamaterials through a layer-by-layer technique. Specifically, we introduce a fabrication process by means of planarization, lateral alignment, and stacking. We demonstrate stacked metamaterials, investigate the interaction between adjacent stacked layers, and analyze the optical properties of stacked metamaterials with respect to an increasing number of layers.

In the last two years, a lot of effort has been dedicated towards the investigation of stacked metamaterials. Among them, a bulk optical metamaterial consisting of 2D perforated metal-dielectric stacks with a thickness much larger than the free space wavelength was theoretically studied, exhibiting negative refractive index [1]. Very recently, a three-functional-layer optical metamaterial was fabricated, however requiring a delicate lift-off procedure [2]. This structure encountered problems such as nonrectangular side walls and a very limited number of layers, therefore diminishing the capability for further stacking.

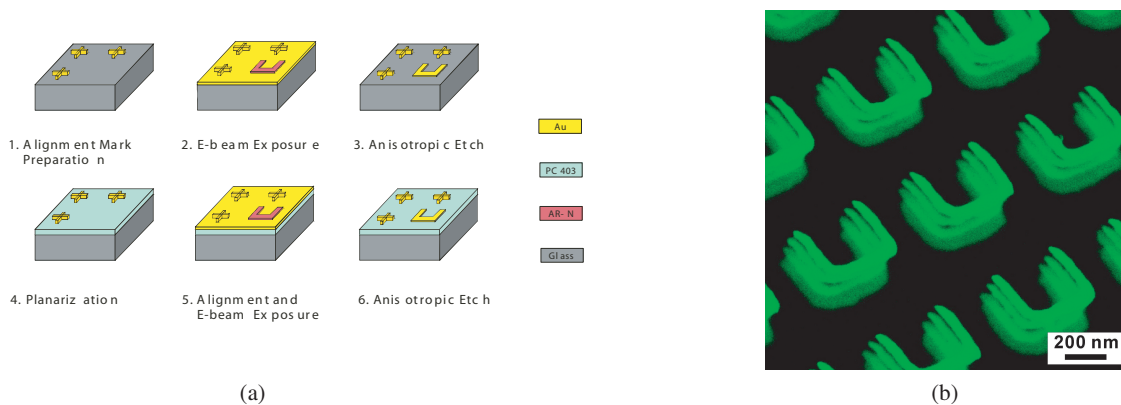


Figure 1: (a) Processing flow scheme of the structure fabrication. (b) Scanning electron microscopy image of the fabricated fourlayer SRR metamaterial.

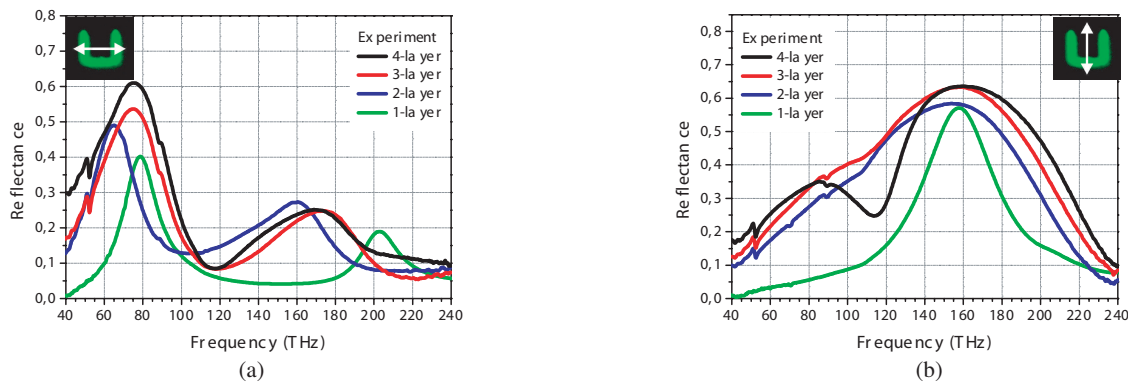


Figure 2: Evolution of optical spectra with increasing number of SRR layers for polarizations (a) parallel and (b) perpendicular to the gap-bearing sides of SRRs, respectively.

In this contribution, we develop and demonstrate an effective alternative for the realization of 3D optical metamaterials through a layer-by-layer technique [3]. The aforementioned difficulties from the lift-off procedure are completely avoided. A split-ring resonator (SRR) structure is selected as the basic unit cell for the stacking demonstration, and a well-aligned fourlayer SRR

metamaterial is nicely implemented. The optical properties of the fabricated structure are investigated experimentally and numerically. The coupling effects between adjacent stacked layers are elegantly interpreted using the method of plasmon hybridization [4]. The evolution of the optical response with increasing stacked layer numbers demonstrates an increased bandwidth. We are going to provide general design principles as well as further insight into the optimization of 3D metamaterials at optical frequencies.

#### REFERENCES

1. Zhang, S., W. J. Fan, N. C. Panoiu, K. J. Malloy, R. M. Osgood, and S. R. J. Brueck, *Opt. Express*, Vol. 14, 6778, 2006.
2. Dolling, G., M. Wegener, and S. Linden, *Opt. Lett.*, Vol. 32, 551, 2007.
3. Qi, M. H., et al., *Nature*, Vol. 429, 538, 2004.
4. Prodan, E., C. Radloff, N. J. Halas, and P. Nordlander, *Science*, Vol. 302, 419, 2003.

## Dielectric Metamaterials with Accessible Tunability

Xian Qi Lin, Jessie Yao Chin, Xin Mi Yang, Di Bao, Qiang Cheng, and Tie Jun Cui  
The State Key Laboratory of Millimeter Waves, School of Information Science and Engineering  
Southeast University, Nanjing 210096, China

**Abstract**— Resonant particles, due to their intrinsic electric or magnetic dipoles, have been the major access to artificial electromagnetic metamaterials, which have largely broadened the range of material parameters at hand. More recently, it has been reported that lattice of high dielectric resonators are possible to present double-negative behavior [1, 2]. The physical explanation lies in the manipulation of displacement currents. Based on this idea, we propose a new metamaterial particle which is composed of a dielectric cylinder and a metal rod screwed inside. The dielectric cylinder has a relative permittivity of 36.7 and is nonmagnetic, and hence is easily available. With the rod screwing up and down, it provides an agreeable tunability and gives a range of available material parameters at each frequency. Arraying the particles into a lens, we are able to shift the refracted beam by changing the height of metal rods gradually while keeping the loss suppressed. It can be applied to design novel components to steer the electromagnetic waves.

In order to prove the novel controllable metamaterials, we simulate the case of  $5 \times 3$  metal-dielectric disks inside a planar waveguide. By changing the heights of metal screws  $h$ , we can conveniently tune the deflected angles of the electromagnetic waves. Figure 1(a) illustrates the real parts of the relative refraction indexes for a single disk with different  $h$ . Figure 1(b) shows the field distributions inside the waveguide under the excitation of plane waves, with two obvious deflection of 30 and  $-30$  degrees by the gradient-metamaterial lens.

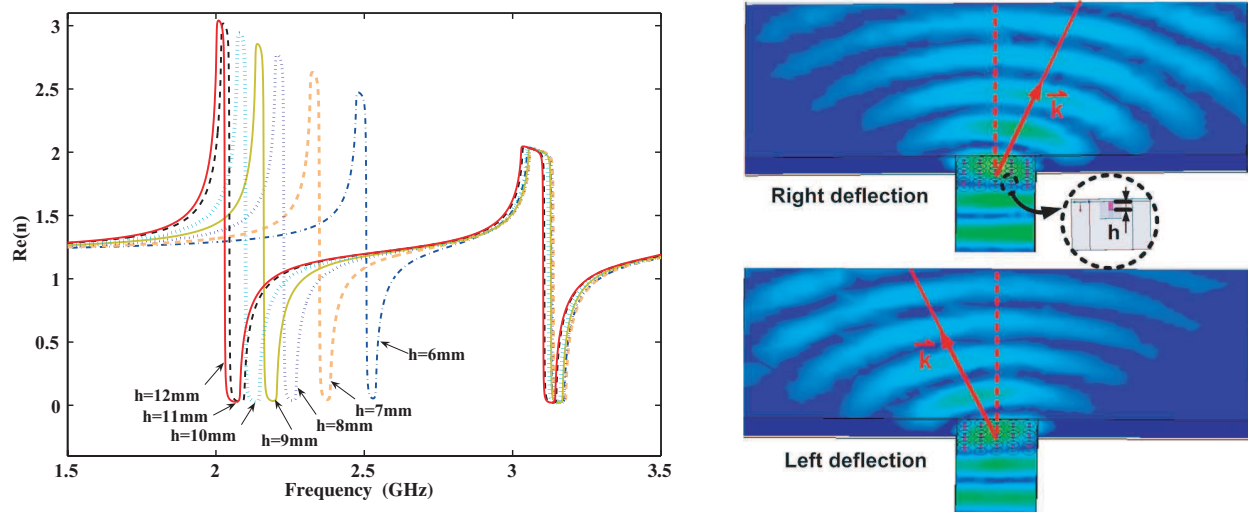


Figure 1: Electromagnetic wave controlled by tunable dielectric metamaterials with gradient indexes. (a) Real parts of the gradient indexes. (b) Deflection of planer waves at the frequency of 2.56 GHz.

### REFERENCES

1. Peng, L., L. X. Ran, H. S. Chen, H. F. Zhang, J. A. Kong, and T. M. Grzegorzczuk, "Experimental observation of left-handed behavior in an array of standard dielectric resonators," *Phys. Rev. Lett.*, Vol. 98, 157403, Apr. 2007.
2. Ueda, T., A. Lai, and T. Itoh, "Demonstration of negative refraction in a cutoff parallel-plate waveguide loaded with 2-D square lattice of dielectric resonators," *IEEE Trans. on Microw. Theory Tech.*, Vol. 55, No. 6, 1280–1287, June 2005.

## Does Planar Left-handed Material Slab Resolve Subwavelength Details in the Image?

M. Yu. Barabanenkov<sup>1</sup>, Yu. N. Barabanenkov<sup>2</sup>, and S. A. Nikitov<sup>2</sup>

<sup>1</sup>Institute of Microelectronics Technology and superpure materials, Russian Academy of Sciences  
142432 Chernogolovka, IMT RAS, Russia

<sup>2</sup>Institute of Radioengineering and Electronics, Russian Academy of Sciences, 125009 Moscow, Russia

**Abstract**— It is common knowledge that conventional lenses collect electromagnetic fields emitted by an object and refocus them to an image. Even perfect conventional lenses cannot resolve in the image subwavelength details of the object at the operating wavelength. However, Pendry [1] extending Veselago's analysis [2], called in question mentioned fundamental limitation and showed a possibility to construct a lens that can approach a perfect electromagnetic reconstruction of the object. In essence, to perfectly reconstruct an image including exponentially decaying away from the object near field components requires an amplifier to restore fields to their original intensity. A slab of materials in which the electrical permittivity and the magnetic permeability are both equal to minus one, i.e., perfect planar left-handed material slab that is the so called perfect Veselago lens, performs the necessary amplification. On the other hand, we studied [3] the energy emission effect from electromagnetic evanescent wave at scattering by a dielectric structure. These two concurrent opposite effects of evanescent wave amplifying and energy emission promise [4] an operation of evanescent wave intensity using a medium with negative and inhomogeneous dielectric permittivity and magnetic permeability. In particular, we show that an object wave field is transferred identically by Veselago lens, with image source point giving Veselago rule for negative refraction. Thus, it appeared that Veselago lens is near field carrier only and subwavelength resolution is quite separated problem. The latter is the main issue of the present report.

Starting with equation for the energy flux in the direction of incident evanescent wave amplitude decay and using 1D grating with linelike rulings as a dielectric structure, we consider the distant-spatial and interference-spatial spectroscopy of evanescent waves. Both these scenarios of evanescent wave spatial spectroscopy are illustrated on examples of evanescent waves created by a planelike source with electrical current density being parallel to rulings of the grating. These examples are related to the problem to access optical details within the unit cell of a photonic crystal beyond the diffraction limit and to the problem of retrieving lower subwavelength spatial harmonics of temperature distribution along a planelike heated object, using the object thermal radiation. Note, the total transmitted field is comprised of (a) the transmitted through a structure energy flux coming from evanescent incident spectral orders and (b) the flux caused by the interference of incident propagating and evanescent wave spectral orders. We demonstrate that these two fluxes are separated by applying the 1D grating with line rulings and with a forbidden gap in the spectrum of radiation transmission for the incident propagating spectral order when the energy flux transmitted through the grating consists of contribution of evanescent spectral orders in the incident electric field only.

### REFERENCES

1. Pendry, J. B., *Phys. Rev. Lett.*, Vol. 85, 3966, 2000.
2. Veselago, V. G., *Sov. Phys. Usp.*, Vol. 10, 509, 1968.
3. Barabanenkov, M. Yu., Yu. N. Barabanenkov, Yu. V. Gulyaev, and S. A. Nikitov, *Phys. Lett. A*, Vol. 364, 421, 2007.
4. Barabanenkov, Yu. N., M. Yu. Barabanenkov, and S. A. Nikitov, "Operation of evanescent wave intensity using metamaterials of negative permittivity and permeability," *PIERS 2007 Prague Program*, 25, Prague, Czech Republic, August 27-30, 2007.

# Widening the Negative Effective Parameter Frequency Band of Resonant SNG Metamaterials

J. Zehentner and J. Machac

Czech Technical University in Prague, Technicka 2, 16627 Prague 6, Czech Republic

**Abstract**— Volumetric single negative (SNG) metamaterials, i.e., metamaterials with negative permittivity and positive permeability, or vice versa, generally consist of resonant particles with anisotropic behavior. The frequency band in which one of the effective parameters of these metamaterials is negative is very narrow, due to the resonant character of the particles. This seriously limits their practical application. The paper summarizes a few ways to widen this frequency band. The demand for an isotropic medium is an additional, very important consideration in metamaterial applications.

Our investigated SNG metamaterial with negative permeability consists of planar broadside coupled split ring resonators (BC-SRR) [1]. The metamaterial with negative permittivity consists of a planar electric dipole loaded by a loop inductor [2, 3].

One way to extend the frequency band of a resonant circuit response is by utilizing a concept of coupled circuits. The overall resonant feature of the coupled circuits depends on the value of the coupling coefficient. The equivalent circuit of the resonant particles that are used is more complex than the equivalent circuit of a simple LC resonant circuit. For this reason, the frequency dependence of the transmission coefficient of a pair of BC-SRRs located in the R32 waveguide behaves slightly differently than does a pair of simple LC resonant circuits. The widening of the particle response depending on the mutual location of two BC-SRRs has been documented.

A more effective way to achieve the same effect is by utilizing a system consisting of a large number of particles distributed properly in a hosting material. We now have two mechanisms for widening the metamaterial frequency response. The particles are coupled to each other, and we observe the same effect as is exhibited by a couple of resonant circuits. The particles in the system differ slightly from each other due to the tolerances of the fabrication process in the geometrical dimensions of the conducting layout, and even due to the non-homogeneity of the substrate thickness and its permittivity. Consequently each particle has a different resonant frequency and the frequency band of the system of particles is wider than that of a single particle. Generally, the more particles are present in the system, the wider the band will be. We have documented these effects using three different composites in the case of both epsilon-negative and mu-negative particles. The first system consisted of a periodic distribution of particles oriented in the same direction. Naturally, the response of this medium remained anisotropic, as it did for a single particle. This system was obtained, with the frequency band of the response considerably wider than that of a single particle. At the same time the isotropic response was obtained using quasi-randomly [2, 3] or fully randomly [1] distributed particles. The effect of the widening the frequency band of the response is similar as in the case of the particles distributed periodically.

## REFERENCES

1. Jelinek, L., J. Machac, and J. Zehentner, "A magnetic material composed of randomly oriented SRRs," *PIERS 2007*, CD-Rom, 474–477, Beijing, China, March 2007.
2. Machac, J., P. Protiva, and J. Zehentner, "Isotropic epsilon-negative particles," *2007 International Microwave Symposium Digest*, CD-Rom, TH4D-03, Honolulu, Hawaii, USA, June 2007.
3. Protiva, P., J. Machac, and J. Zehentner, "Particle for an isotropic metamaterial with negative permittivity," *EMTS 2007 C International Electromagnetic Theory Symposium URSI*, CD-ROM, Ottawa, ON, Canada, July 2007.

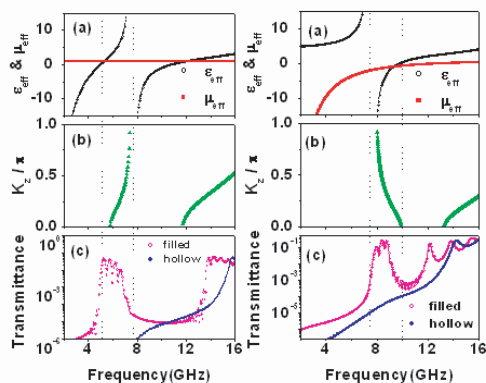


# Resonance-induced Transparencies of Opaque Waveguides and Doppler Effects of a Light Source on a Meta-material Slab

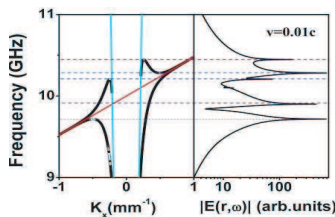
Hao Xu, Weihua Wang, Jiaming Hao, and Lei Zhou

Physics Department, Fudan University, Shanghai 200433, China

**Abstract**— This talk contains two parts. First, we show that a metallic waveguide behaves as an electric (magnetic) plasma for transverse-electric (transverse-magnetic) polarized electromagnetic (EM) waves. Inserting *anisotropic* resonance structures of either electric or magnetic type into a waveguide, we find extraordinary transmissions of EM waves with different polarizations through the waveguide at frequencies well below the waveguides cut-off value, following two different mechanisms. We design realistic electric/magnetic resonance structures, and perform finite difference time domain simulations on realistic systems to successfully demonstrate all theoretical predictions (see figure below).



Second, we apply a rigorous Green's function theory to study the Doppler effects of a light source placed on top of a meta-material slab. When the receiver is in motion with the source and the slab, we find that, in addition to a mode corresponding to the conventional Doppler effect, there are several other frequency components which do not obey the standard frequency-shift rule. We show that such new effects are caused by the coupling between the radiated electromagnetic waves and the surface modes of the meta-material slab, whose dispersion relation varies as the functions of velocity in the moving reference frame (see figure below).



# From Photonic Crystals to Metamaterials: A General Mean-field Theory

P. Halevi<sup>1</sup>, F. Pérez-Rodríguez<sup>2</sup>, J. A. Reyes-Avendaño<sup>1</sup>, and E. Reyes-Ayona<sup>1</sup>

<sup>1</sup>Instituto Nacional de Astrofísica, Óptica y Electrónica, Apdo. Post. 51, Puebla, México

<sup>2</sup>Instituto de Física, Benemérita Universidad Autónoma de Puebla  
Apdo. Post. J-48, Puebla, México

**Abstract**— A very general homogenization theory is presented for a photonic crystal (dielectric or metallo-dielectric) that can have three- or two- or one-dimensional periodicity. The Bravais lattice and the shape of the inclusions within the unit cell are arbitrary. The material properties are described by a generalized conductivity defined at every point in the unit cell. The electromagnetic fields have been averaged over the unit cell, resulting in the replacement of the Bloch fields by plane waves. This enables us to define the derived  $\mathbf{D}$  and  $\mathbf{H}$  fields in terms of the primary fields  $\mathbf{E}$  and  $\mathbf{B}$ . In the most general case, such a response turns out to be *bi-anisotropic*, having terms associated with the permittivity ( $\boldsymbol{\varepsilon}$ ), permeability ( $\boldsymbol{\mu}$ ), and magneto-electric ( $\boldsymbol{\gamma}$  and  $\boldsymbol{\delta}$ ) dyadics:

$$\mathbf{D} = \boldsymbol{\varepsilon} \cdot \mathbf{E} + \boldsymbol{\gamma} \cdot \mathbf{H}, \quad \mathbf{B} = \boldsymbol{\delta} \cdot \mathbf{E} + \boldsymbol{\mu} \cdot \mathbf{H}.$$

We have derived explicit expressions for the four dyadics  $\boldsymbol{\varepsilon}$ ,  $\boldsymbol{\gamma}$ ,  $\boldsymbol{\delta}$ , and  $\boldsymbol{\mu}$  in terms of the geometry, material parameters of the inclusions, circular frequency  $\omega$ , and wave vector  $\mathbf{k}$ . This response, of course, pertains to an effective *uniform* material which can display exotic behaviour — a photonic *metamaterial*. We note that, in general, the principal axes of  $\boldsymbol{\mu}$  depend on the direction of  $\mathbf{k}$  and do not coincide with the principal axes of  $\boldsymbol{\varepsilon}$ . The response dyadics simplify considerably for small  $\mathbf{k}$ 's (local limit). Indeed, in this case, if the unit cell is centro-symmetric, there is no magneto-electric response ( $\boldsymbol{\gamma} = \boldsymbol{\delta} = 0$ ). Further, if the unit cell has cubic symmetry, the response then becomes *bi-isotropic*, characterized by scalar  $\boldsymbol{\varepsilon}$  and  $\boldsymbol{\mu}$ . These results have strong consequences for the Crystal Optics and optical response of anisotropic photonic materials. Since  $\boldsymbol{\varepsilon}$ ,  $\boldsymbol{\gamma}$ ,  $\boldsymbol{\delta}$ , and  $\boldsymbol{\mu}$  can be computed for any specified structure of the unit cell by means of matrix inversions, the design of broadband, low-loss metamaterials should be facilitated.

In the special cases of small spheres and narrow cylinders (wires) we have successfully reduced our general formulae for  $\boldsymbol{\varepsilon}$  to well known expressions. We have also computed the bi-anisotropic response of a 2D photonic crystal of metallic (plasma) cylinders for different filling fractions, propagation directions, and polarizations. It turns out that the metamaterial is paramagnetic (diamagnetic) when the electric (magnetic) field is parallel to the cylinders. We are also in the process of applying our theory to 3D metallo-dielectric photonic crystals with unit cells that, presumably, will give rise to  $\boldsymbol{\varepsilon}(\omega)$  and  $\boldsymbol{\mu}(\omega)$  both negative in the same spectral range, that is, to *left-handed* metamaterials.

## ACKNOWLEDGMENT

This WORK was partially supported by CONACYT project SEP-2004-CO1-46425.

# Coupling Light to Delocalized Magnetic Excitations: Magnetic Plasmon Polaritons and Antisymmetric SPP Mode

Tao Li, Hui Liu, Shu-Ming Wang, Fu-Ming Wang, Jia-Qi Li, and Shi-Ning Zhu

National Laboratory of Solid State Microstructures

Department of Physics, Nanjing University

Nanjing 210093, China

**Abstract**— Since Pendry proposed the genius design of split resonant ring (SRR) as the artificial “magnetic atom” in 1999 [1], this structure is widely used to construct the meta-magnetism and negative index metamaterials (NIM). However, this SRR structure meet great difficulty in fabrication in very small size for realizing the ultimate optical metamaterial. After many efforts in development, two realistic structures emerge with convinced NIM performance at NIR frequency. One the metal strip pairs [2] and the other is a sandwich structure perforated with hole arrays [3]. Afterwards, both designs were further improved and exhibit artificial magnetic response and negative refraction at visible frequency. At present, the second type design interest us greatly, due to its structural similarity to the perforated metal film, which has been proved to exhibit extraordinary optical transmission (EOT) [4]. Although many discussions have been involved in the origin of such EOTs, surface plasmon polariton (SPP) is undoubtedly considered as an important contributor.

As the second type metamaterial (metal/dielectric/metal fishnet) is concerned, we propose two kinds of delocalized magnetic excitations, which can be coupled to incident light to form two kinds of polaritons. One is a plasmonic behavior of the “magnetic atoms” as they are excited by the incident light. Beyond Ref [3] and the related reports revealed, in this structure the magnetic excitations may not be isolated but coupled together via magnetic inductions in the 2D plane, and lead to a plasmonic behavior as is called magnetic plasmon polariton (MPP) [5]. Our experiments expectedly provide two pronounced magnetic modes in combination with the strong SPP transmission band. Detailed analyses and theoretical simulation definitely confirm that they correspond to two MPP modes associated with the reciprocal lattice vectors  $G(0,1)$  and  $G(1,1)$ . As consequences, we expectedly modulated the MPP modes by adjusting the lattice parameter as well. The other delocalized magnetic mode is actually the antisymmetric SPP mode. Our numerical results clearly demonstrated the physical pictures of symmetric and antisymmetric SPP modes in homogenous dielectric background [6]. In antisymmetric mode, the longitudinal electric field remained in the middle layer builds up the virtual current loops to form a strong magnetic response. We definitely find the great change in the retrieved the magnetic permeability, which confirms the magnetic mode.

## REFERENCES

1. Pendry, J. B., et al., *IEEE Trans. Microwave Theory Tech.*, Vol. 47, 2075, 1999.
2. Shalaev, V. M., et al., *Opt. Lett.*, Vol. 30, 3356, 2005.
3. Zhang, S., et al., *Phys. Rev. Lett.*, Vol. 95, 137404, 2005.
4. Ebbesen, T. W., et al., *Nature*, London, Vol. 391, 667, 1998.
5. Li, T., et al., *Appl. Phys. Lett.*, Vol. 90, 251112, 2007.
6. Li, T., et al., *Phys. Rev. E*, Vol. 76, 016616, 2007.

## Influence of Dephasing on Electromagnetically Induced left-handedness in Optically Excited Atomic Media

Shang-Bin Li

Shanghai research center of Amertron-global, Zhangjiang High-Tech Park  
299 Lane, Bisheng Road, No. 3, Suite 202, Shanghai 201204, China

**Abstract**— The influence of dephasing on electromagnetically induced left-handedness in optically excited atomic media is investigated.

# Session 2A4

## Microwave Photonics and Terahertz Technologies and Their Applications

<p>Microwave Photonic Devices and Their Applications to Communications and Measurements  <i>Tadao Nagatsuma (NTT Corporation, Japan); Yuichi Kado (NTT Corporation, Japan);</i> .....</p> <p>Terahertz Emission from Two-dimensional Plasmons in High-electron-mobility Transistors Stimulated by Optical Signals  <i>Yahya Moubarak Meziani (Tohoku University, Japan); Tetsuya Suemitsu (Tohoku University, Japan); Taiichi Otsuji (Tohoku University, ); Eiichi Sano (Hokkaido University, );</i> .....</p> <p>Resonant Band Gaps from a Narrow Slit at Terahertz Frequencies  <i>Yan Zhang (Capital Normal University, China); Kuo Meng (Capital Normal University, China); Yanhua Wang (Capital Normal University, China);</i> .....</p> <p>Beam Pattern Investigation of Terahertz Quantum Cascade Lasers  <i>Saeed Fatholoulumi (University of Waterloo, Canada); Dayan Ban (University of Waterloo, Canada); Hui Luo (Institute for Microstructure Sciences, National Research Council, Canada); Peter Grant (Institute for Microstructure Sciences, National Research Council, Canada); Sylvain R. Laframboise (Institute for Microstructure Sciences, National Research Council, Canada); Zbig R. Wasilewski (National Research Council, Canada); Margaret Buchanan (Institute for Microstructural sciences, National Research Council, Canada); H. C. Liu (Institute for Microstructure Sciences, National Research Council, Canada);</i> .....</p> <p>Fabrication of Terahertz Coupling Structures by Electron Beam Lithography  <i>Grahame Rosolen (Commonwealth Scientific and Industrial Research Organisation, Australia);</i> .....</p> <p>Terahertz Sensing for Ensuring the Safety and Security  <i>Yuichi Ogawa (TOHOKU UNIVERSITY, Japan); Shinichiro Hayashi (Tohoku University, Japan); Chiko Otani (Institute of Physical and Chemical Research (RIKEN), Japan); Kodo Kawase (Nagoya University, Japan);</i> .....</p> <p>Live Electro-optic Imaging (LEI) for Real-time Analyses of Electric Near-fields over Microwave Circuits  <i>Kiyotaka Sasagawa (National Institute of Information and Communications Technology, Japan); Atsushi Kanno (National Institute of Information and Communications Technology, Japan); Masahiro Tsuchiya (National Institute of Information and Communications Technology (NICT), Japan);</i></p> <p>Latest Trends in Millimeter-wave Imaging Technology  <i>Soichi Oka (NTT Microsystem Integration Laboratories, Japan); Hiroyoshi Togo (NTT Microsystem Integration Laboratories, Japan); Naoya Kukutsu (NTT Microsystem Integration Laboratories, Japan); Tadao Nagatsuma (NTT Corporation, Japan);</i> .....</p> <p>Trends in Next Generation Optical Access Networks and a Proposed Hybrid Optical/Wireless Wide-area Access Network  <i>Junichi Kani (NTT Access Network Service Systems Laboratories, Japan);</i> .....</p> <p>Development of Radio on Free Space Optics System for Ubiquitous Wireless  <i>Katsutoshi Tsukamoto (Osaka University, Japan); Takeshi Higashino (Osaka University, Japan); Takuya Nakamura (Osaka University, Japan); Koichi Takahashi (Osaka University, Japan); Yuji Aburakawa (Osaka University, Japan); Shozo Komaki (Osaka University, Japan); Kazuhiko Wakamori (Waseda University, Japan); Toshiji Suzuki (Waseda University, Japan); Kamugisya Kazaura (Waseda University, Japan); Alam Mohammad Shah (Waseda University, Japan); Kazunori Omae (Waseda University, Japan); Mitsuji Matsumoto (Waseda University, Japan);</i> .....</p> <p>Photonic Millimeter-wave Generation and Distribution System Applicable to the ALMA Radio Telescopes  <i>Hitoshi Kiuchi (National Astronomical Observatory of Japan (NAOJ), Japan); Tetsuya Kawanishi (National Institute of Information and Communications Technology (NICT), Japan); Masumi Yamada (National Astronomical Observatory of Japan (NAOJ), Japan); Takahide Sakamoto (National Institute of Information and Communications Technology (NICT), Japan); Masahiro Tsuchiya (National Institute of Information and Communications Technology (NICT), Japan); Jun Amagai (National Institute of Information and Communications Technology (NICT), Japan); Masayuki Izutsu (National Institute of Information and Communications Technology (NICT), Japan);</i> .....</p>	<p>255</p> <p>256</p> <p>257</p> <p>258</p> <p>259</p> <p>260</p> <p>261</p> <p>262</p> <p>263</p> <p>264</p> <p>265</p>
--	--



# Microwave Photonic Devices and Their Applications to Communications and Measurements

Tadao Nagatsuma<sup>1,2</sup> and Yuichi Kado<sup>1</sup>

<sup>1</sup>NTT Microsystem Integration Laboratories, NTT Corporation  
3-1 Morinosato Wakamiya, Atsugi, Kanagawa 243-0198, Japan

<sup>2</sup>Graduate School of Engineering Science, Osaka University  
3-1 Machikaneyama, Toyonaka, Osaka 565-8650, Japan

**Abstract**— The recent explosive growth in communications has been brought about by wired (fiber-optic) and wireless (radio-wave) communications technologies. These two technologies have started to merge to create a new interdisciplinary area called Microwave Photonics (MWP). In addition, viewing the electro-magnetic spectrum with wavelengths progressively decreasing to the millimeter and submillimeter-wave bands on the radio-wave side and wavelengths progressively increasing to the infrared region on the light-wave side, we see that there is a large gap in utilization on the boundary between radio waves and light waves, i.e., the frequency band between 100 GHz and 10 THz. This untapped region represents a major resource for humankind in the 21st century.

MWP technology aims at achieving advancement and improved functions in telecommunications systems that cannot be achieved by extension of individual technologies, mainly through the combination of radio-wave technology and photonic technology. At the same time, MWP technology is also expected to open up unused frequency bands through the fusion of different fields. The opening of new application fields other than communications is also expected.

This paper provides an overview of the status of MWP technology, focusing on a system concept and enabling devices, and describes some of the latest applications, such as high-speed wireless communications, non-invasive electric-field sensors, and spectroscopy.

# Terahertz Emission from Two-dimensional Plasmons in High-electron-mobility Transistors Stimulated by Optical Signals

Y. M. Meziani<sup>1</sup>, T. Suemitsu<sup>1</sup>, T. Otsuji<sup>1</sup>, and E. Sano<sup>2</sup>

<sup>1</sup>RIEC, Tohoku University, Sendai, Japan

<sup>2</sup>RCIQE, Hokkaido University, Japan

**Abstract**— Two-dimensional (2D) plasmons in high-electron mobility transistors (HEMT's) have attracted much attention due to their potentiality promoting emission of terahertz radiation. This paper reviews recent advances in our original, room-temperature operating HEMT-based terahertz emitters.

We have recently proposed a novel device structure of optically-pumped plasmon-resonant terahertz emitter incorporating doubly interdigitated grating gates and a vertical cavity onto HEMT. When the dual grating gates are biased at different levels, the sheet carrier density is periodically modulated, making periodic 2D plasmon cavities along with the grating. When the device is photoexcited by laser irradiation, photoelectrons, injected to the cavities, excite the plasmons. The plasmon itself is non-radiative. Hence, in order to emit the THz wave, an antenna is necessary to transform this longitudinal wave to a radiative transverse electromagnetic wave. The grating gate in the device works as an antenna, leading to emission of terahertz radiation.

The first version was designed and fabricated into an InGaP/InGaAs/GaAs high-electron mobility transistor structure. The 2D-plasmon layer is formed with a quantum well in the InGaAs channel layer. The grating gate is formed with 60-nm thick Ti/Au. The fabricated device was subjected to 1550-nm, 1-mW (a) a single CW-laser, and (b) a 70-fs pulsed-laser illumination at room temperature. In case of (a), terahertz emission was detected by a Si bolometer under certain bias conditions, which is inferred to be due to the self oscillation stimulated by the plasmon instability. In case of (b), an impulsive radiation followed by relaxation oscillation was measured by electrooptic sampling, whose Fourier spectrum exhibits resonant peaks of plasmons' harmonic modes up to 4 THz. Estimated radiation power exceeds 0.1  $\mu$ W, resulting in excellent conversion efficiency of the order of  $10^{-4}$ .

Theoretical study reveals that a low-conductive gate electrode, in which the electron concentration should be comparable to that of 2D-plasmon layer, is preferred to enhance the efficiency of field emission. In this case a highly conductive metal gate has a disadvantage. Thus, the second version introduced a double-decked HEMT structure, where the upper deck channel serves as the grating antenna to convert the non-radiative plasmonic wave in the lower-deck HEMT channel to radiative THz electromagnetic wave. Experimental results confirmed that the conversion efficiency and radiation power are successfully enhanced to the order of  $10^{-3}$  (by one order of magnitude higher than those for a conventional metal grating-gate device), which is higher by two orders of magnitude than that for state-of-the art transit-time-based devices such as uni-traveling-carrier photodiodes.



# Resonant Band Gaps from a Narrow Slit at Terahertz Frequencies

Yan Zhang, Kuo Meng, and Yanhua Wang

Beijing Key Lab for Terahertz Spectroscopy and Imaging, Key Laboratory of Terahertz Optoelectronics  
Ministry of Education, Department of Physics, Capital Normal University  
Beijing 100037, China

**Abstract**— Surface plasmonic sub-wavelength optics opened a new door for fabricating optical devices with wavelength scale. It brings great benefits to the terahertz (THz) frequency regime which has a relatively long wavelength. Due to the wide application foreground of the THz wave, the tools with smaller size such as sources, lenses, and switches with in this range are quite necessary for system integration. The progresses on THz generation and detection such as THz quantum cascade lasers have been reported. However, devices to control and manipulate THz wave are extensively behind. We report a simple sub-wavelength device for resonant band gaps generation at the THz frequencies. Employing the surface plasmon polaritons, only a single sub wavelength slit can cut out the THz spectrum effectively. The transmission spectrum of thus device is measured using the THz time domain spectroscopy system. With the slit becomes narrower, the transmission peaks move to the high frequency direction and the depth of the forbidden gap increase. Theoretical simulations are also carried out by using the FDTD method. It has been demonstrated that the simulation results agree with experimental results well. This kind of devices can provide an approach to control the THz photons.

# Beam Pattern Investigation of Terahertz Quantum Cascade Lasers

S. Fatholouloumi<sup>1,2</sup>, D. Ban<sup>2</sup>, H. Luo<sup>1</sup>, P. Grant<sup>1</sup>, S. R. Laframboise<sup>1</sup>  
Z. Wasilewski<sup>1</sup>, M. Buchanan<sup>1</sup>, and H. C. Liu<sup>1</sup>

<sup>1</sup>Institute for Microstructure Sciences, National Research Council, Ottawa, Canada

<sup>2</sup>Department of Electrical and Computer Engineering, University of Waterloo, Waterloo, Canada

**Abstract**— Terahertz (THz) quantum cascade lasers (QCL) are becoming a major technology for THz compact, coherent and single-frequency radiation sources. Such a source has many potential applications, particularly in spectroscopy, imaging, and local oscillators for heterodyne receivers. THz QCLs are fabricated by growing multiple periods of GaAs/Al<sub>0.15</sub>Ga<sub>0.85</sub>As quantum wells (MQW) using molecular beam epitaxy (MBE) followed by patterning laser ridge using photolithography techniques. Due to the time limitation of MBE growth duration, the active region of a QCL device is typically not thicker than 10  $\mu\text{m}$ . Various ridge width (30–100  $\mu\text{m}$ ) and cavity length ( $\sim 1$  mm) of the device can be defined separately during subsequent device fabrication processing. Considering the wavelength of THz laser beam (30  $\mu\text{m}$  to 300  $\mu\text{m}$ ), the sub-wavelength dimensions of laser ridge facet suggests that output beam pattern is not a Gaussian beam anymore, but rather becomes a diffractive-like pattern. Therefore, it is crucial to carefully characterize and study output beam profile of THz QCLs.

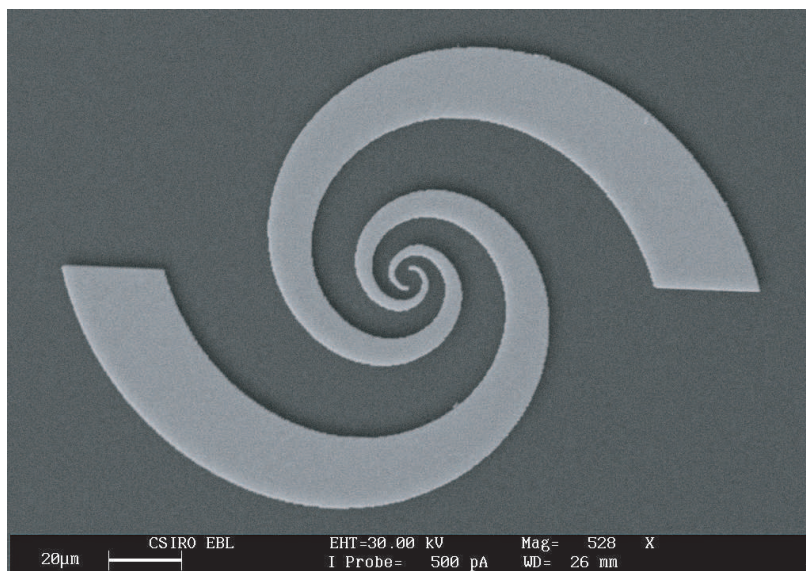
In this paper we present far-field beam pattern measurement results of in house fabricated THz QCLs with ridge widths of 30  $\mu\text{m}$  and 100  $\mu\text{m}$ . The devices have a GaAs/AlGaAs quantum cascade active region with a thickness of 10  $\mu\text{m}$  and are cleaved into Fabry-Perot resonators with a cavity length of 1 mm. The laser beam pattern data of each device were acquired by moving a THz detector along a QCL device-centered circle. Both devices show diffractive-like beam patterns in the vertical direction (perpendicular to semiconductor heterojunction plane). In the lateral direction (parallel to semiconductor heterojunction plane), the device with a wider ridge width (100  $\mu\text{m}$ ) shows a Gaussian-like beam profile. The full width at half maximum (FWHM) of the Gaussian-like beam profile is measured to be 18 degree. A radio-frequency (RF) design simulator (HFSS) was deployed to simulate far-field beam pattern of the QCL devices. The simulation results yield a Gaussian beam profile with a FWHM of 16 degree along the lateral direction, which is in good agreement with the measured value (18 degree). In the vertical direction, simulated far-field pattern shows good consistence with the experimental data for the portion above the laser/package interface plane. Discrepancy between the experimental and simulation results is observed for the portion below the laser/package interface plane, which could be attributed to the presence of the gold package underneath of the QCL devices.

## Fabrication of Terahertz Coupling Structures by Electron Beam Lithography

Grahame Rosolen

Information and Communication Technologies Centre  
Commonwealth Scientific and Industrial Research Organisation  
Vimiera Road, Marsfield, NSW 2121, Australia

**Abstract**— In order to design electromagnetic radiation coupling structures such as antennas and photonic crystals the critical dimensions of the structures must be commensurate with the wavelengths of the radiation of interest. In the case of Terahertz radiation the characteristic wavelength is in the range 1 mm to 30  $\mu\text{m}$ . To achieve high quality structures the fabrication technique must have a resolution capability considerably finer than the wavelength. For Terahertz coupling structures this constraint is at the limit of many conventional machining based fabrication capabilities. One technique to overcome this resolution issue is to pattern structures using electron beam lithography (EBL) and then use semiconductor fabrication techniques to produce the final structures. This technique provides a flexible patterning capability for fabricating devices with a wide range of topologies and sizes. The principle advantages of EBL are the ability to pattern features with dimensions in the micron and sub-micron range as well as the ability to directly pattern structures on a substrate without the need for a prefabricated mask. The technique also affords the flexibility to change the pattern topology by altering the lithography data file and it provides the ability to fabricate structures containing elements ranging in size from microns up to millimetres on the same substrate. This enables structures which operate over a wide band of Terahertz frequencies to be patterned. The structures are defined using conventional CAD drafting packages and then converted into lithography data files for exposure. The structures are patterned using a scanning electron microscope which has been modified for direct write EBL. The planar structures are exposed in a layer of electron sensitive resist, which after developing produces an opening in the resist in the shape of the desired structure. This opening is used for the deposition of metal. The resist is then removed leaving the structure on the substrate. In situations where electrical contact is required part of the structure can be patterned to form the contacts for bonding to other components in a system. An example of a coupling structure patterned using this technique is shown below.



## Terahertz Sensing for Ensuring the Safety and Security

Y. Ogawa<sup>1</sup>, S. Hayashi<sup>1,2</sup>, C. Otani<sup>2</sup>, and K. Kawase<sup>1,2,3</sup>

<sup>1</sup>Tohoku University, Japan

<sup>2</sup>RIKEN, Japan

<sup>3</sup>Nagoya University, Japan

**Abstract**— We are studying a few THz sensing methods for ensuring the safety and security of the lives of people, such as, i) Nondestructive detection of illicit drugs using spectral fingerprints, ii) Label-free detections of protein-protein interactions for allergy test. The absence of non-destructive inspection techniques for illicit drugs hidden in mail envelopes has resulted in such drugs being freely smuggled across international borders. We have developed a basic technology for THz imaging which allows detection and identification of drugs concealed in envelopes by introducing the component spatial pattern analysis. The spatial distribution and the composition of the targets are obtained from THz multispectral transillumination images, using absorption spectra measured with a tunable THz wave source.

A label-free biological sensor, which is based on the resonant transmission phenomenon of a thin metallic mesh, is proposed in the THz wave region. By using this sensor, we demonstrate the highly sensitive detection of small amounts of protein. A distinct shift of the transmission dip frequency is observed for fmol order of protein printed on the metallic mesh, indicating the significantly high sensitivity of our sensor. In this presentation, a feasibility study for producing simplified determination of allergen in food material using label-free biological sensor will be reported.

## Live Electro-optic Imaging (LEI) for Real-time Analyses of Electric Near-fields over Microwave Circuits

Kiyotaka Sasagawa, Atsushi Kanno, and Masahiro Tsuchiya  
National Institute of Information and Communications Technology, Japan

**Abstract**— Live electro-optic imaging (LEI) system is described in this paper, which enables the real-time imaging functionality of electrical signals on up to 10 GHz-class circuits in real-time on a screen at video frame rates as high as 30 frames per second. In the system, photonics provides important features of the system: its  $100 \times 100$ -channel parallel detection and the low invasiveness of electrooptic crystal. With the LEI system, novel diagnostic methods are provided through instantaneous and intuitive analyses of RF signal distribution changes. As an example, LEI observation results for a coplanar waveguide with a moving metal plate are presented.

## Latest Trends in Millimeter-wave Imaging Technology

S. Oka, H. Togo, N. Kukutsu, and T. Nagatsuma

NTT Microsystem Integration Laboratories

3-1, Morinosato Wakamiya Atsugi-shi, Kanagawa 243-1908, Japan

**Abstract**— This paper presents the latest survey of millimeter-wave imaging. Recent advances in millimeter-wave technology have expanded various feasibility of new inspection method. In order to develop diagnostic imaging systems by millimeter-wave, many types of passive or active sensing devices have been proposed in this frequency range.

One of the most traditional applications of millimeter-wave imaging is for security inspection in airport for military purpose. In these practical devices, their sophisticated millimeter-wave parts and computational image processing techniques are integrated to obtain high-resolution fluoroscopic images. In addition to these works, we also propose our application which is aimed for a nondestructive inspection of civil engineering as below.

Alarm in regards to decrepit concrete structures (such as expressways built in the booming post-war years) and recently-built apartment buildings with faked earthquake-proof certification is becoming a serious social problem. To check such concrete structures, crack inspection is common though the crack is often hidden by wall coating such as wall paper, lining paint, and tile.

To solve this problem, we developed a compact millimeter-wave scanner called “Crack Scan”. The millimeter-wave passes through wall coating, but they are scattered on impact with fine cracks. Even though the spatial resolution of general imaging systems is in the range of wavelength, Crack Scan is able to find sub-millimeter widths crack (specified in civil engineering standards) by detecting dispersion in the near field.

# Trends in Next Generation Optical Access Networks and a Proposed Hybrid Optical/Wireless Wide-area Access Network

Junichi Kani

NTT Access Network Service Systems Laboratories, NTT Corporation, Japan

**Abstract**— In the recent few years, the optical access service based on Fiber-to-the-Home (FTTH) have been proven as the most promising fixed Internet access service; the number of its customers in Japan has exceeded that of ADSL since early in 2007. The Gigabit-Ethernet passive optical network typically used provides 1 Gb/s total bandwidth shared among 32 subscribers. A complementary solution to support the broadband access is the wireless LAN using microwave frequency, that is applicable in the last one step of the access network, e.g., inside the stations/floors. In these networks, average bandwidth per user is assumed as around several 10 Mb/s.

This paper first reviews technologies and standardization trends toward the next-generation optical access networks (NG-OAN), whose target can be assumed as providing new services with the average bandwidth of several 100 Mb/s to several Gb/s. One of the key points is how to utilize the optical multiplexing technologies including wavelength-division multiplexing (WDM) in the NG-OAN [1]. It also overviews the fiber-wireless access technology as a candidate to provide wireless connection in the last one step of the future access network.

Secondly, a novel hybrid dense-WDM and fiber-wireless access network is proposed and described. It is based on an optical multi-carrier generator which has been reported as the centralized light source for a wide-area WDM access network [2]. The proposed network utilizes each of the wavelength sets generated by the multi-carrier generator for wavelength-dedicated services via full-fiber access or wavelength-shared services via fiber-wireless access depending on the necessity. The detailed configuration, some features such as upgradability in terms of the wavelength set and basic performance will be discussed in the paper.

## REFERENCES

1. Kani, J., K. Iwatsuki, and T. Imai, "Optical multiplexing technologies for access-area applications," *IEEE Journal of Selected Topics in Quantum Electronics*, Vol. 12, Issue 4, 661-668, July–Aug. 2006.
2. Kani, J., M. Teshima, K. Akimoto, N. Takachio, H. Suzuki, K. Iwatsuki, and M. Ishii, "A WDM-based optical access network for wide-area gigabit access services," *IEEE Communication Magazine*, Vol. 41, Issue 2, S43–S48, February 2003.

## Development of Radio on Free Space Optics System for Ubiquitous Wireless

Katsutoshi Tsukamoto<sup>1</sup>, Takeshi Higashino<sup>1</sup>, Takuya Nakamura<sup>1</sup>, Koichi Takahashi<sup>1</sup>  
Yuji Aburakawa<sup>1</sup>, Shozo Komaki<sup>1</sup>, Kazuhiko Wakamori<sup>2</sup>, Toshiji Suzuki<sup>2</sup>  
Kamugisya Kazaura<sup>2</sup>, Alam Mohammad Shah<sup>2</sup>, Kazunori Omae<sup>2</sup>, and Mitsuji Matsumoto<sup>2</sup>

<sup>1</sup>Graduate School of Engineering, Osaka University, Japan

<sup>2</sup>GITI, Waseda University, Japan

**Abstract**— In ubiquitous network society, users want an environment to access any communication services at any time, any place, and any situations. In order to realize the ubiquitous networks, a combination of IP network and broadband heterogeneous wireless access services will play an important role. A large diversification appears in air interfaces of wireless access. A suitable wireless service should be provided according to users' different demands for applications, quality, latency, and moreover users' situations such as indoor, outdoor, and fast/slow mobility. Therefore, a universal platform for heterogeneous wireless services will become a key issue to realize ubiquitous networks, however, currently leads redundant equipments and investments on infrastructures, and these problems prevent the quick start of a new wireless service and employing microcellular architecture. These are revealed especially in in-building at urban areas, and rural areas with less broadband fiber-infrastructure.

Radio on Fiber (RoF) with layer 1 routing capability can realize a cost effective universal platform for future ubiquitous wireless services. The layer 1 routing concept can be realized by not only RoF but also RoFSO (Radio on Free Space Optics) or RoR (Radio on Radio) networks, which provide a free space for heterogeneous wireless services in Free Space Optics or millimeter wave radio. We have started developing a new advanced RoFSO system. This paper describes its concept and features, and furthermore, discusses about its role in future ubiquitous wireless.



# Photonic Millimeter-wave Generation and Distribution System Applicable to the ALMA Radio Telescopes

H. Kiuchi<sup>1</sup>, T. Kawanishi<sup>2</sup>, M. Yamada<sup>1</sup>, T. Sakamoto<sup>2</sup>  
M. Tsuchiya<sup>2</sup>, J. Amagai<sup>2</sup>, and M. Izutsu<sup>2</sup>

<sup>1</sup>National Astronomical Observatory of Japan, Japan

<sup>2</sup>National Institute of Information and Communications Technology, Japan

**Abstract**— Research into optical modulators has made remarkable progress in recent years. This paper discusses the possibility of applying the high extinction ratio optical modulator to a high stability and high frequency (over 100 GHz) optical reference signal generator. High-frequency reference signals are generated by a highly stable optical two-tone generator. High-frequency signals are used in recent high-rate communication, National frequency standard distribution and astronomical application. ALMA (Atacama Large Millimeter/sub-millimeter Array) is a high-frequency radio interferometer array currently under development, and each of the ALMA antennas has a 10-band receiver, and its highest receiving frequency reaches 950 GHz. To receive such high frequencies, higher reference frequency is required for the 1st local (as much as over 100 GHz), and stability to maintain the signal coherence is also required. To address these issues, we have developed a new method to generate and transmit a reference signal in the form of frequency difference between two coherent light waves. One method to generate two optical signals is producing them from a pair of laser sources using optical phase lock loop for feed back control, however, optical phase lock loop has a stability problem in its operation. A good alternative method to the optical phase lock scheme is the LiNbO<sub>3</sub> Mach-Zehnder optical intensity modulator which is capable of generating two highly stable optical signals (upper sideband and lower sideband components) by applying a sinusoidal microwave signal to an input laser signal. The two optical signals require phase stability better than  $10^{-13}$  in the Allan standard deviation, vibration robustness and polarization maintaining capability. The signal coherence loss estimated from the phase stability of the two optical signals generated by the Mach-Zehnder modulator shows that the modulator has the ability to generate highly stable optical signals.



## Session 2A5

# Methods and Instruments for the Determination of Electromagnetic Properties of Soils and Materials

Microwave Dielectric Spectroscopy of Moist Soils in the Problem of Radar and Radiometric Remote Sensing of the Land <i>V. L. Mironov (Kirensky Institute of Physics, Siberian Branch, Russian Academy of Sciences, Russia);</i>	268
An International Agreement on the Characterisation of the Effects of Soils on Ground Penetrating Radars and Metal Detectors <i>Yann Yvinec (Royal Military Academy, Belgium);</i>	271
Soil Electromagnetic Properties and Landmine (Metal) Detectors: An Overview of Canadian Research <i>Yogadhis Das (Defence R and D Canada, Canada);</i>	272
Mapping of Landmine Detection Interferences in Soil Prior to Operation <i>T. J. Katsube (Geological Survey of Canada, Canada); Yogadhis Das (Defence R and D Canada, Canada);</i>	273
Estimation of Relative Permittivity of Shallow Soils by Using the Ground Penetrating Radar Response from Different Buried Targets <i>Lorenzo Capineri (University of Florence, Italy); David J. Daniels (ERA Technology, UK); Pierluigi Falorni (Universita di Firenze, Italy); Olga Lucia Lopera (Royal Military Academy, Belgium); Colin G. Windsor (United Kingdom Atomic Energy Authority (UKAEA), UK);</i>	274
Electrodynamic Model for Near-field Microwave Microscopy of Layered Samples <i>A. N. Reznik (Institute for Physics of Microstructures, Russia); V. V. Talanov (Solid State Measurements, Inc., USA);</i>	275
An Example of Holographic Radar Using at Restoration Works of Historical Building <i>Vladimir V. Razevig (Bauman Moscow State Technical University, Russia); Sergey I. Ivashov (Bauman Moscow State Technical University, Russia); Anton P. Sheyko (Bauman Moscow State Technical University, Russia); Igor A. Vasilyev (Bauman Moscow State Technical University, Russia); A. V. Zhuravlev (Bauman Moscow State Technical University, Russia);</i>	276
Device Fatigue-fracture Caused by High Current Density <i>Jianhua Xiao (Henan Polytechnic University, China);</i>	277
Magnetic Layer Plasma Thruster Using in Liquid Crystal Alignment <i>Bing-Hung Chen (National Dong-Hwa University, Taiwan, R.O.C.); Pei. Ci. Li (National Dong-Hwa University, Taiwan, R.O.C.);</i>	278
Anomalous Negative Magnetostriction in $Tb_{0.3}Dy_{0.7}Fe_{1.95}$ Alloys under Magnetomechanical Loading <i>Y. Pei (Tsinghua University, China); Dai-Ning Fang (Beijing Institute of Technology, China);</i>	279

# Microwave Dielectric Spectroscopy of Moist Soils in the Problem of Radar and Radiometric Remote Sensing of the Land

V. L. Mironov

Kirensky Institute of Physics SB RAS, Russia

**Abstract**— In aerospace radar and radiometric remote sensing of soils and vegetation cover, a dielectric model of moist soils is considered to be a most important block of data processing algorithms. For the radio sounding of soil moisture, biomass, thawed or frozen state of the land, and classification of soils by mineral and granulometric contents, the relationships between these geophysical characteristics and the moist soil dielectric constant represent a critical basis of physical origin [1,2]. Such dielectric models must include the dependence on temperature, mineral contents parameters, volumetric or gravimetric moisture, and frequency.

For developing the data processing algorithms in radio sounding from space, the semiempirical mixing dielectric model (SMDM) proposed in [3] is most widely employed, so that it has become a kind of classical model. In this model, there are used dielectric spectra and spectral parameters of the Debye origin, which concern the water out of soil. While the dielectric spectrum of soil water, which is bound on the surface of solid soil particles, mineral or organic is ignored. Hence, the parameters of a bound water spectrum can not be involved in predicting the dielectric spectra of moist soils. Instead, in the SMDM, the impact of the mineral and granulometric composition of soil, which completely determines the dielectric spectrum of bound soil moisture, is taken into account only empirically, through modifying the dependence of dielectric constant on the content of moisture. In particular, for this reason, the SMDM can not be applied to frozen moist soils, as their dielectric frequency dispersion is completely induced by the bound (unfrozen) soil moisture.

Spectroscopy of moist soils in the microwave frequency band underwent further development in the works of the author and his coauthors [4–18]. In works [4, 5], there were created the methodical basis for dielectric spectroscopy of moist soils, in which the Debye spectroscopic parameters were employed for both the bound and unbound soil water, and techniques for deriving these physical quantities from dielectric measurements were proposed [4–7]. The model suggested in [4, 5] was named the generalized refractive mixing dielectric mode (GRMDM).

In this presentation, an analytical review is given as to the results obtained in this area. Specifically, there was considered the dependence of dielectric spectroscopic parameters pertaining to moist soils on the granulometric composition of solid fraction and the fraction of organic matter in soil [7–11]. The study was conducted on the basis of data set measured for a conglomerate of soils collected in the chernozem area in the European part of Russia, in some steppe, forest, and forest-tundra territories in Siberia, as well as in Kansas and Mississippi states (USA). As a result of that study, a dielectric model was developed, in which the temperature, clay and humus content, volumetric moisture, and electromagnetic field frequency are the only input parameters allowing to make predictions for dielectric spectra of moist soils in the microwave frequency band [12–14]. This model, named the mineralogy based soil dielectric model (MBSDM), was shown to be as simple in usage as the SMDM is, ensuring dielectric predictions with less error, than classical dielectric model of [3], over the significantly extended range of granulometric and mineralogical parameters.

In the frame of the GRMDM, the temperature dependences of spectroscopic parameters were studied on the basis of the bentonite clay [15] and some types of arctic soils in Alaska [16]. In addition, there was created a physically appropriate model of dielectric frequency dispersion in the moist frozen soils, accounting for the contribution of both bound soil water and transitional bound water in soil. Moreover, for the first time, the processes of converting liquid soil water into bound soil water of transitional type was observed, and the dependences of dielectric spectroscopic parameters with regard to transitional bound water were studied, describing gradual transition of its phase state to that of the ice.

Using the GRMDM for the soils including water solution, there was carried out analysis to study how spectroscopic parameters of bound water containing ions depend on the temperature, with frozen soils being spanned. A technique was also proposed to make estimations of dielectric spectra for salt solution in the unbound soil water, which ensured dielectric predictions in the case of saline moist soils [17, 18].

With the use of the GRMDM, the impact of soil humus on the retrieved values of soil moisture was distinctly taken into account when processing the radiometric remote sensing data [19].

There was also noticeably decreased the error of prediction for the diurnal cycle of bare soil radiobrightness [20]. This spectroscopic model was found to be an effective mean to make prediction of the radiobrightness, radar backscatter and its polarization pattern, as well as to develop a physical basis for subsurface radar sounding, in the condition of freezing or thawing of the active permafrost layer [21–25].

Henceforth, the methodology suggested for microwave dielectric spectroscopy will ensure dielectric databases to be developed for the moist top-soil cover. A principle difference of such databases is that they will be using spectroscopic parameters as a primary element, which ensure taking into account the mineral and organic composition of soils, as well as the seasonal weather variations for a concrete physiographic territory. With the use of such dielectric databases, the reliability of data processing algorithms is expected to be substantially increased in regard with the aerospace radar and radiometric remote sensing of the Earth.

## REFERENCES

1. Ulaby, F. T., R. K. Moor, and A. K. Fung, *Microwave Remote Sensing, Active and Passive*, Vol. III, Artech House, Dedham, MA, 1986.
2. Komarov, S. A. and V. L. Mironov, *Microwave Remote Sensing of Soils*, Nauka, Novosibirsk, Russian, 2000.
3. Dobson, M. C., F. T. Ulaby, M. T. Hallikainen, and M. A. El-Rayes, "Microwave dielectric behavior of wet soil-part II: dielectric mixing models," *IEEE Trans. Geosci. Remote Sensing*, Vol. 23, No. 1, 35–46, 1985.
4. Mironov, V. L., M. C. Dobson, V. H. Kaupp, S. A. Komarov, and V. N. Kleshchenko, "Generalized refractive mixing dielectric model for moist soils," *Proc. IGARSS*, Vol. 6, 35563558, Toronto, Canada, 2002.
5. Mironov, V. L., M. C. Dobson, V. H. Kaupp, S. A. Komarov, and V. N. Kleshchenko, "Generalized refractive mixing dielectric model for moist soils," *IEEE Trans. Geosci. Remote Sensing*, Vol. 42, No. 4, 773–785, 2004.
6. Mironov, V. L., P. P. Bobrov, L. G. Kosolapova, V. N. Mandrygina, and S. V. Fomin, "Data processing technique for deriving soil water spectroscopic parameters in microwave," *Proc. IGARSS, Denver*, Vol. 6, 2957–2961, USA, 2006.
7. Mironov, V. L., L. G. Kosolapova, and S. V. Fomin, "A method for developing a moist-soil dielectric database in the microwave band," *Radiophysics and Quantum Electronics*, Vol. 50, No. 4, 339–349, USA, 2007.
8. Mironov, V. L. and P. P. Bobrov, "Soil dielectric spectroscopic parameters dependence on humus content," *Proc. IGARSS'03*, Vol. II, 1106–1108, Toulouse, France, 2003.
9. Mironov, V. L., P. P. Bobrov, and V. N. Mandrygina, "Bound water spectroscopy for the soils with varying mineralogy," *Proc. IGARSS, Anchorage*, Vol. V, 3478–3480, USA, 2004.
10. Mironov, V. L., "Spectral dielectric properties of moist soils in the microwave band," *Proc. IGARSS'04*, Vol. V, 3474–3477, Anchorage, USA, 2004.
11. Mironov, V. L., P. P. Bobrov, A. P. Bobrov, V. N. Mandrygina, and V. D. Stasuk, "Microwave dielectric spectroscopy of moist soils for a forest-tundra region," *Proc. IGARSS'05*, Vol. VII, 4485–4488, Seoul, Korea, 2005.
12. Mironov, V. L., L. G. Kosolapova, and S. V. Fomin, "Validation of the soil dielectric spectroscopic models with input parameters based on soil composition," *Proc. IGARSS'07*, Barcelona, Spaine, 22–27 July, 2007.
13. Mironov, V. L., L. G. Kosolapova, and S. V. Fomin, "Physically and mineralogically based spectroscopic dielectric model for moist soils," *IEEE Trans. Geosci. Remote Sensing*, (submitted paper), 2007.
14. Bobrov, P. P., V. L. Mironov, O. A. Ivchenko, and V. N. Krasnoukhova, "Microwave spectroscopic dielectric model of moist soils using physical and hydrological characteristics as input parameters," *Proc. IGARSS'07*, Barcelona, Spaine, 22–27 July, 2007.
15. Mironov, V. L., V. H. Kaupp, S. A. Komarov, and V. N. Kleshchenko, "Frozen Soil dielectric model using unfrozen water spectroscopic parameters," *Proc. IGARSS*, Vol. 7, 4172–4174, Toulouse, France, 2003.
16. Mironov, V. L., R. D. Roo, and I. V. Savin, "Dielectric spectroscopic model for tussock and shrub tundra soils," *Proc. IGARSS'07*, Barcelona, Spain, 22–27 July, 2007.
17. Mironov, V. L., S. A. Komarov, and V. N. Kleshchenko, "Microwave dielectric spectroscopy for bound water in saline soil," *Proc. IGARSS*, Vol. 5, 3196–3199, Seoul, Korea, 2005.

18. Mironov, V. L., S. A. Komarov, and V. N. Kleshchenko, "Dielectric model for saline moist soils in the microwave band," *Proc. of the All Russian Conference on Physics of Radio Waves*, Vol. 3, 17–20, Tomsk, Russia, 2002.
19. Mironov, V. L., P. P. Bobrov, O. A. Ivchenko, S. V. Krivaltsevitsh, and A. S. Jaschenko, "Dynamic radiobrightness for drying soils as a function of humus content," *Proc. IGARSS'05*, Vol. II, 1127–1130, Seoul, Korea, 2005.
20. Mironov, V. L., V. V. Scherbinin, A. S. Komarov, and A. A. Bogdanov, "Measurement and simulation of diurnal radiobrightness variations for a bare unfrozen soil," *Proc. IGARSS'07*, Barcelona, Spaine, 22–27 July, 2007.
21. Mironov, V. L., P. P. Bobrov, P. V. Zhirov, S. V. Krivaltsevitsh, A. S. Jaschenko, and R. D. de Roo, "Radiobrightness dynamics of freezing/thawing processes for different soil," *Proc. IGARSS'06*, Vol. 6, 3015–3018, Denver, USA, 2006.
22. Komarov, A., V. L. Mironov, and S. Li, "SAR polarimetry for permafrost active layer freeze/thaw processes," *Proc. IGARSS'02*, Vol. V, 2654–2656, Toronto, Canada, 2002.
23. Mironov, V. L., S. A. Komarov, S. Li, V. E. Romanovsky, T. V. Baikalova, and V. V. Skoroglyadov, "Freeze-thaw processes radar remote sensing: Modeling and image processing," *Proc. IGARSS'05*, Vol. I, 608–611, Seoul, Korea, 2005.
24. Mironov, V. L., S. A. Komarov, T. V. Baikalova, and V. V. Skoroglyadov, "Influence of snow and plant covers on the seasonal radar remote sensing signal variations," *Proc. of IGARSS*, Vol. 6, 2705–2707, Denver, USA, 2006.
25. Komarov, S. A., V. L. Mironov, and K. V. Muzalevsky, "GPR signal simulations in the course of freeze/thaw process for a permafrost area," *Proc. IGARSS'05*, Vol. VII, 4600–4603, Seoul, Korea, 2005.

# An International Agreement on the Characterisation of the Effects of Soils on Ground Penetrating Radars and Metal Detectors

Yann Yvinec

Royal Military Academy, Belgium

## Abstract—

**Objectives:** The paper describes an international agreement on the soil properties to measure in order to characterise the effects that soils have on the performance of ground penetrating radars (GPRs) and metal detectors, how to measure these properties and how to relate them to sensor performance.

**Motivation:** Soils can affect the performance of GPRs and metal detectors. Since metal detectors are widely used in humanitarian demining characterising the effects of soils on its performance has become a major concern to the mine action community. GPRs are now being combined with metal detectors into dual-sensor mine detectors. Therefore the soil effects on GPR performance have received great attention too.

This is why it has been decided to find an agreement on how to characterise the soil effects on these two sensors through tests that could be carried out not only in laboratory but also in the field by users.

**Status of the Agreement:** The document is written by a Workshop working under the guidelines set by the European Standard Committee (CEN). It will be a CEN Workshop Agreement (CWA), that is, a document based on a consensus among the Workshop participants. Before being published by CEN, the CWA will have to be open for public comments.

**Procedure:** A call for participants occurred in 2007 and people from universities, mine action organisations, and sensor providers have joined the Workshop. Three work groups have been set up: soil characterisation for metal detectors, soil characterisation for GPRs and soil classification.

## Soil Electromagnetic Properties and Landmine (Metal) Detectors: An Overview of Canadian Research

Y. Das

Defence R&D Canada, Suffield, Canada

**Abstract**— The metal detector, working on the principle of electromagnetic induction, has been one of the most commonly used tools to detect buried landmines. The signal produced in a detector by a metal object depends on many factors including the object's size, shape, orientation, material and the parameters of the detector electronics. One of the other important factors that can influence this signal is the host soil. The adverse effect of certain types of soil on metal detectors was recognized during World War II and some detector models were fitted with a means to reduce this effect. As well, during the period 1945-47, the effect of different rocks and soils on the performance of the mine detector, in use by the United States, was studied. In the intervening time since these studies were done, the issue of dependence of metal detector performance on soil properties appears to have been largely ignored by the mine detection community. On the other hand, in recent years, as a result of the worldwide use of the metal detector in humanitarian demining, users were once again finding that certain soils, mostly in tropical regions, can (1) reduce the sensitivity of detectors to an extent that they cannot detect targets to desired depths; (2) cause false targets; and (3) in extreme cases, render some detectors totally unusable. This so-called "soil problem" may appear to be much more severe at the present time than during previous conflicts. This is because current metal detectors are made much more sensitive so that they can detect antipersonnel landmines which contain a minimal amount of metal and are presently very common and widely used.

About five years ago, being faced with the above situation, The Canadian Centre for Mine Action Technologies (CCMAT) initiated a research effort to address the need to clarify and advance the knowledge of the effect of soil properties on the functioning of metal detectors and its implication for humanitarian demining. This presentation will give a very brief overview of this research, which has achieved the following to date:

1. A systematic analytical framework, complemented with numerical computations and experiments, was developed to study various aspects of the interaction of soil electromagnetic properties and metal detectors. This study adequately explained which electromagnetic properties are important and to what extent they affect the performance of metal detectors of various designs, employing continuous wave as well as pulse induction principles.
2. Instruments and measurement protocols to characterize and develop models for relevant soil properties were investigated. One of the outcomes was the development of an instrument that can measure the complex magnetic susceptibility of soil over a frequency band of interest in metal detection. Data from this instrument which operates over 96 Hz to 96 kHz were used to estimate soil model parameters needed to study the effect of soil magnetism on metal detectors. Similar efforts to estimate soil electrical conductivity are ongoing.
3. CCMAT proposed and is continuing to promote the idea of developing a database of identified soil electromagnetic properties for soils in landmine affected regions. Such a database will help demining organizations select equipment and predict its performance in their particular environment; help equipment developers and researchers assess the potential of their proposed technologies in various parts of the world; and help researchers develop test facilities that simulate realistic demining environments existing in different parts of the world.



# Mapping of Landmine Detection Interferences in Soil Prior to Operation

T. J. Katsube<sup>1</sup> and Y. Das<sup>2</sup>

<sup>1</sup>Geological Survey of Canada, 601 Booth St., Ottawa, ON K1A 0E8, Canada

<sup>2</sup>Defence R&D Canada Suffield, P. O. 4000, Station Main, Medicine Hat AB, T1A 8K6, Canada

**Abstract**— Many soil physical and chemical properties can interfere with landmine detection. Therefore, it is essential to obtain prior knowledge of the distribution of these interferences in order to improve detection technology selection and demining safety. Since rapid mapping of these properties over wide areas is essential for meeting military and economic requirements, it is proposed to use a combination of remote sensing, airborne and ground surface geophysics, as required.

For example, in areas where electromagnetic signal interference from iron-oxide or other metallic particles are possible, Landsat imagery combined with a few lines of airborne or specially designed ground surface electromagnetic surveys could be effective. In areas where the source of interferences could be due to electrical conductivity resulting from soil moisture or distribution of certain chemicals also due to soil moisture, fusion of various Landsat images and RADARSAT images for dry and wet periods combined with various geophysical surveys could prove effective. The source of interference in soils or surface geological material can be very variable and complex. However, today, there are various rapid mapping technologies by remote sensing and geophysical methods that have the possibility of meeting many requirements, in particular when fused. In this presentation, it is planned to show several examples of these fused tests that have been carried out.

# Estimation of Relative Permittivity of Shallow Soils by Using the Ground Penetrating Radar Response from Different Buried Targets

L. Capineri<sup>1</sup>, D. J. Daniels<sup>2</sup>, P. Falorni<sup>1</sup>, O. L. Lopera<sup>3</sup>, and C. G. Windsor<sup>4</sup>

<sup>1</sup>Dipartimento Elettronica e Telecomunicazioni, Università di Firenze, Italy

<sup>2</sup>ERA Technology, United Kingdom

<sup>3</sup>Royal Military School, Belgium

<sup>4</sup>116 East Hagbourne, OX11 9LD, United Kingdom

**Abstract**— Ground penetrating radar (GPR) for landmine detection has reached the stage where portable equipment for field operations is commercially available. Dual sensor systems in which high performance metal detectors (MD) are combined with GPR have been extensively trialled.

The operating conditions for the GPR are strongly affected by the electromagnetic characteristics (magnetic susceptibility and complex relative permittivity) of the soil. These can change in space (soil inhomogeneities) and also in time (environmental factors like moisture, temperature). These variations are the main reasons why the GPR systems need either manual or auto-calibration before their use as a mine detector.

This paper describes an assessment of methods that can be used by operators in the field for the estimation of the relative permittivity ( $\epsilon_r$ ) of the soil at shallow depth. The estimation of  $\epsilon_r$  is obtained indirectly by the propagation velocity  $v = c/\sqrt{\epsilon_r}$ , where  $c$  is the speed of light in vacuum.

Experiments were carried out using the MINEHOUND dual sensor system jointly developed by Vallon GmbH and ERA Technology at the test site of the latter. Different metal targets were buried at different depths in a soil defined as ballast. The time-of-flight was estimated from data acquired in a 10 second scan above the target.

The MINEHOUND antenna uses two linearly polarised parallel elements separated by 8.3 cm, one transmitting and the other receiving and has a centre frequency of 1 GHz. The equation of the minimum time-of-flight from the target reflection (antenna over the target centre) is:

$$TOF_{\min} = \frac{2}{c} \sqrt{\left(\frac{S}{2} - \frac{S}{2} \frac{Z_0}{Z_0 + h} \frac{1}{\sqrt{\epsilon_R}}\right)^2} + h^2 + \frac{2}{c} \sqrt{\epsilon_R} \sqrt{\left(\frac{S}{2} \frac{Z_0}{Z_0 + h} \frac{1}{\sqrt{\epsilon_R}}\right)^2} + Z_0^2 \quad (1)$$

where  $Z_0$  is the target depth,  $h$  is the antenna height from soil surface.

The received signals also contain another reflection from the air-soil interface that, with the bistatic antenna configuration, corresponds to the following time-of-flight equation:

$$TOF_{Air-soil} = \frac{2}{c} \sqrt{\left(\frac{S}{2}\right)^2} + h^2 \quad (2)$$

By suitable processing of the experimental data the difference of the various times-of-flight (Eq. (1)–Eq. (2)) can be evaluated and the value of  $\epsilon_r$  can be estimated. Note that Eq. (1) is non-linear for the unknown  $\epsilon_r$ . The effect of the variability of  $h$  during the sweep also needs to be considered, because it impacts on the uncertainty of the estimate of  $\epsilon_r$ .

In this paper we assess which of several different metal targets provides the best calibration target for a measurement procedure in the field:

1. metal pipe
2. metal sphere
3. metal planar reflector

The analysis includes the following points:

- Radar response
- Influence of burying procedures on soil properties
- Cost and availability

# Electrodynamic Model for Near-field Microwave Microscopy of Layered Samples

A. N. Reznik<sup>1</sup> and V. V. Talanov<sup>2</sup>

<sup>1</sup> Institute for Physics of Microstructures, Nizhnii Novgorod 603950, Russia

<sup>2</sup> Solid State Measurements, Inc., 110 Technology Dr., Pittsburgh, PA 15275, USA

**Abstract**— Near-Field (NF) microwave microscopy has emerged in the past decade as a powerful technique for investigating materials microwave (MW) properties with high spatial resolution. The main feature of a near-field microscope (NFM) is the probe with size  $D \ll \lambda$ , where  $\lambda$  is the operating wavelength. Spatial resolution of NFM is governed by the probe size rather than the radiation wavelength and for modern NFMs  $D/\lambda \sim 10^{-5} - 10^{-6}$ . In this work we have developed and verified experimentally a new electrodynamic model for NF-microscopy of the plain-layered media. We also have investigated the applicability of our model for characterization of thin dielectric films.

We model the probe as an electrically small antenna, which is placed a distance  $h$  above the sample with vertically stratified complex dielectric permittivity  $\varepsilon = \varepsilon(z) = \varepsilon_1(z) + i\varepsilon_2(z)$ . To calculate the probe input impedance  $Z = R + iX$  we model it as an antenna with external surface current given by two-dimensional distribution with characteristic length scale  $D$ . We have developed an effective algorithm for calculation of electromagnetic (EM) field around the antenna, which is based on the theory of EM-field propagation in one-dimensional media (including quasi-stationary fields). We also used the integral relations of the Poynting theorem, which relates the impedance components  $R$ ,  $X$  with electric and magnetic fields. To calculate the EM response measured by NFM we have modeled such device as MW resonator loaded with antenna. We proposed the equivalent circuit of the resonator, which contains impedance  $Z$  as a load. The value of  $Z$  is sensitive to  $\varepsilon(z)$ , therefore information about  $\varepsilon$  of the sample can be obtained from the measurements and calculations of NFM resonator frequency response. We have designed a computer algorithm and program, which rapidly calculates the NFM response for each given distribution  $\varepsilon(z)$ .

We have verified our model using NFM data for thin dielectric films. The operating frequency of NFM was  $\sim 4$  GHz and its probe an aperture  $D \sim 5 \mu\text{m}$ . The films were  $\text{SiO}_2$  ( $\varepsilon \approx 3,9$ ) thermally grown on conductive Si substrates. The films thickness varied from  $0,1 \mu\text{m}$  to  $1,5 \mu\text{m}$ . In the calculations we used  $D$  as the fitting parameter, which value was determined during the calibration measurements. The NFM resonance frequency shift as a function of the probe height  $h$  for different  $\text{SiO}_2$  film thicknesses has been analyzed and very good agreement between theoretical and experimental results was obtained. We also used our calculations for clarification of some important features of the empirical technique, which was developed earlier for dielectric films metrology. Finally, we proposed an alternative technique for such measurements, which yields accuracy  $\sim 5-7\%$  for thin films dielectric constant.

## An Example of Holographic Radar Using at Restoration Works of Historical Building

V. V. Razevig, S. I. Ivashov, A. P. Sheyko, I. A. Vasilyev, and A. V. Zhuravlev

Remote Sensing Laboratory, Bauman Moscow State Technical University

5, 2nd Baumanskaya str., Moscow 105005, Russia

**Abstract**— The former Senate building, Saint-Petersburg, Russia is being refitted for using it by Constitutional court of Russian Federation. The team of the Remote Sensing Laboratory was invited to participate in this work. The case is that the underfloor water heating system has been installed in the Senate building. The arrangement of pipes hasn't been precisely documented. Besides there are electricity and communications cables as well as metal mesh under concrete floor of the building. Workers were afraid of damage pipes and cables during laying of parquet floor. Main purpose was to investigate building floor and to define exact position of pipes and cables with the help of subsurface holographic radars developed by Remote Sensing Laboratory.

Main work was made with the help of RASCAN-4/2000 radar. The total area of the scanned surface was 16.7 sq. m. Overall time of work (disregarding the time for equipment installation) was about 5 hours. More than half of that time consumed scanning while the rest was spent in plotting the layout of pipes and cables on the floor. The surveyed area was divided into fragments with the size of 1.7 by 2.0 m. After recording a radar image of each fragment, the operator analyzed the image and drew the results by the chalk on the floor.

There was no difference between pipes and metal mesh in the parallel polarization radar images. In the cross polarization radar images, the plastic pipes were clearly visible. An algorithm of numerical filtration was proposed to improve quality of radar images.

Summarizing the results of work one may state that RASCAN-4/2000 radar is useful for doing such tasks. Possible productivity of the device in current configuration is up to 50 sq. m per day.

## Device Fatigue-fracture Caused by High Current Density

Jianhua Xiao

Henan Polytechnic University, Jiaozuo 454000, Henan, China

**Abstract**— The electrons-migration under high current density can cause the distortion of molecules. The molecules deformation has two possible stable configurations when the electrons-migration is not symmetric in space. Geometrically, the non-symmetric electrons-migration behaves as a local rotation. When the electrons-migration is incompressible flow feature, the conductor may suffer fatigue effects, this is the normal case. However, when the electrons-migration is highly non-symmetric, only one stable configuration is possible, the conductor will produce fracture. The condition of fracture is described by an intrinsic parameter of critical local rotation angular, which is related with the yield stress of conductor material. This research gives the current density condition for the fatigue-fracture deformation. It shows that to increase the ability to against the fatigue-fracture deformation, one can increase the critical angular of material (that is to say, increase the yield stress of material while at the same time reduce the elastic modulus). For fractured conductors, the current density will accelerate the fatigue-fracture process in the fractured position of conductor as it forms a high charge density there when the reference charge density is determined by initial or boundary condition.

# Magnetic Layer Plasma Thruster Using in Liquid Crystal Alignment

Bing-Hung Chen and Pei. Ci. Li

Institute and Department of Electrical Engineering, National Dong-Hwa University  
No. 1, Sec. 2, Da-Xue Rd., Shoufeng, Hualien, Taiwan, R.O.C.

**Abstract**— Thruster plasma is one of the most potential candidates to be the next generation non-contact liquid crystal alignment technology in the flat panel display manufacturing. Magnetic layer plasma thruster is one kind of Hall thruster, which has a longer acceleration channel and lower electron temperature compared with anode layer plasma thruster, and more sensitive to the magnetic field distribution in the channel where magnetic field should have Gaussian form and maximum at the exit. Hence the channel length must satisfy the condition  $(2eV_d/m_e)^{1/2} < L < (m_i/eB)(2eV_d/m_i)^{1/2}$  where  $V_d$  is the applied voltage. According to above, we made a magnetic layer thruster with dimension of 62 mm inner diameter, 70 mm outer diameter, 8 mm channel width and 12 mm channel length, and cathode is carried out by hollow-cathode type located near the exit for 4 cm separation. Magnetic field is created by 4 outer coils with 400 turns and one inner coil with 550 turns, then it can reach 650 gauss at exit when  $V_d$  is chosen 450 V and currents are 2 and 3.2 A respectively. The plasma is ignited and measured by Langmuir probe and getting parameters  $T_e \sim 4.32 - 8.12$  eV and  $n_e \sim 2.11 - 7.87 \times 10^{11}$  cm<sup>-3</sup> at 10<sup>-4</sup> torr. Applying it in polyimide alignment which is the key process related to liquid crystal monomer reacting with polyimide surface. Pre-tilt angle and anchoring energy are the index of this interaction. We can get pre-tilt angle  $\sim 8^\circ$  and anchoring energy  $\sim 8.43 \times 10^{-5}$  J/m<sup>2</sup> at the conditions of 30° incident angle and 3 min process time. The data show better pre-tilt angle for wide-view technology but relatively weaker anchoring energy compared with conventional rubbing method.

## Anomalous Negative Magnetostriction in $\text{Tb}_{0.3}\text{Dy}_{0.7}\text{Fe}_{1.95}$ Alloys under Magnetomechanical Loading

Y. Pei<sup>1,2</sup> and D. Fang<sup>1</sup>

<sup>1</sup>Department of Engineering Mechanics, Tsinghua University, Beijing 100084, China

<sup>2</sup>School of Science, Beijing Institute of Technology, 100081, China

**Abstract**— The anomalous negative magnetostriction has been studied in detail for the positive magnetostrictive material of Terfenol-D under two types of magnetomechanical loading. Under the application of the axial compressive stress  $\sigma$  and the axial magnetic field  $H$ , the axial negative magnetostriction  $\bar{\lambda}$  is observed when  $H_{\parallel}$  increases to coercive field around, which is similar with the butterfly hysteresis in PZT. The amplitude of  $\bar{\lambda}$  increases firstly, and then decrease with the increasing of  $\sigma$ . The initial negative magnetostriction is attributed to the rotation of magnetic domains parallel or antiparallel to the field direction. Firstly, the domains parallel to the field direction will rotate away from the field and stress axis to keep the total free energy lower at appropriate fields. Secondly, the domains antiparallel to the field direction will rotate across the direction perpendicular to the rod axis, which is similar with the mechanism that the  $180^{\circ}$  domain switch consists of two steps of  $90^{\circ}$  domain switch used in ferroelectric materials.





# Session 2A6

## Electromagnetic Theory and Computational Methods for Passive Dielectric Waveguides and Devices

<b>Field Analysis of Dielectric Waveguide Devices Based on Coupled Transverse-mode Integral Equation</b>	282
<i>Hung-Wen Chang (National Sun Yat-Sen University, Taiwan, R.O.C.); Shih-Ming Lu (National Sun Yat-sen University, Taiwan, R.O.C.);</i> .....	
<b>Numerical Analysis of Polarization Splitter Based on Vertically Coupled Microring Resonator</b>	283
<i>Xinlun Cai (University of Bristol, UK); Siyuan Yu (University of Bristol, UK); Dexiu Huang (Wuhan National Laboratory for Optoelectronics, China);</i> .....	
<b>Numerical Approaches for Solving Coupled Mode Theory-Part I: Uniform Fiber Bragg Gratings</b>	284
<i>Jiun-Jie Liao (I-Shou University, Taiwan); Nai-Hsiang Sun (I-Shou University, Taiwan); Ru-Yen Ro (I-Shou University, Taiwan); Po-Jui Chiang (I-Shou University, Taiwan); Shih-Chiang Lin (I-Shou University, Taiwan);</i> .....	
<b>Numerical Approaches for Solving Coupled Mode Theory-Part II: Apodized Fiber Bragg Gratings</b>	285
<i>Jiun-Jie Liao (I-Shou University, Taiwan); Nai-Hsiang Sun (I-Shou University, Taiwan); Ru-Yen Ro (I-Shou University, Taiwan); Jung-Sheng Chiang (I-Shou University, Taiwan); Shih-Chiang Lin (I-Shou University, Taiwan);</i> .....	
<b>Hybrid FD-FD Method for Medium Scaled Dielectric Waveguide Devices</b>	286
<i>Hung-Wen Chang (National Sun Yat-Sen University, Taiwan); Wei-Chi Cheng (Sun Yat-sen University, Taiwan);</i> .....	
<b>A New Simple Technique for Suppress the Spurious Response at Twice the Passband Frequency</b>	287
<i>Homayoon Oraizi (Iran University of Science and Technology, Iran); Hoggat-Allah Nemati (Iran University of Science and Technology, Iran);</i> .....	
<b>Numerical Calculations of PCs Structures by Pseudospectral Method</b>	289
<i>Po-Jui Chiang (I-Shou University, Taiwan); Nai-Hsiang Sun (I-Shou University, Taiwan);</i> .....	
<b>Full Eigen Mode Expansoin Technique for Large Scale Dielectric Waveguide Devices with One-way Traffic</b>	290
<i>Hung-Wen Chang (National Sun Yat-Sen University, Taiwan); Sen-Eon Liu (National Sun Yat-sen University, Taiwan);</i> .....	

# Field Analysis of Dielectric Waveguide Devices Based on Coupled Transverse-mode Integral Equation

Hung-Wen Chang and Shih-Ming Lu

Institute of Electro-optical Engineering National Sun Yat-Sen University, Kaohsiung 80424, Taiwan

**Abstract**— Planer lightwave circuit (PLC) devices are building blocks of next generation optical communication systems. PLC examples include the power dividers, directional couplers, micro-ring cavities, waveguide crossing and arrayed waveguide gratings. Rigorous analysis of these waveguide devices is very difficult due to the shear size of the problem and numerical difficulties of handling bi-directional multi-mode traffic in these devices. Approximation methods such as the beam propagation method (BPM), time-domain finite-difference (FD-TD) and frequency-domain finite-difference (FD-FD) methods are used to analyze and optimize the design. However each of these methods has its limitation. In this paper, we propose an integral-equation formulation for analyzing EM field of 2-D dielectric waveguide devices. We first apply stair-case approximation of and turn the device into many vertical slices of 1-D parallel layered structures. The entire electromagnetic mode field is completely determined transverse field components on the interfaces between slices. These interfacial functions are governed by a system of transverse-mode integral equations made of layered modes from each slice. These unknown tangential field functions are solved by coupled matrix equation. The reflection/transmitted coefficients or the scattering functions of complex dielectric devices are then obtained. Examples of waveguide devices such as multi-mode interferometer, waveguide crossing and quasi-adiabatic tapered waveguides are studied using present formulation.

## Numerical Analysis of Polarization Splitter Based on Vertically Coupled Microring Resonator

Xinlun Cai<sup>1,2</sup>, Siyuan Yu<sup>1</sup>, and Dexiu Huang<sup>2</sup>

<sup>1</sup>Department of Electrical & Electronic Engineering, University of Bristol, UK

<sup>2</sup>Wuhan National Laboratory for Optoelectronics, China

**Abstract**— A novel polarization splitter which exploits the strong polarization dependence of vertical coupled microring resonator is presented. Based on a combination of a three dimensional, full vectorial film mode matching method (FMM) with a three dimensional full vectorial coupled mode theory (CMT), the device performance of vertically coupled microring resonator is rigorously investigated. Three steps are taken to model the structure: First, the propagation constants and the eigenmodes of straight and bent waveguides are computed using FMM; second, the scattering matrix describing the behavior of coupling region is obtained by means of CMT; and finally the spectral responses of microring resonator for TE and TM mode are calculated. By this method, one obtains a complete three dimensional vectorial microring resonator description without any free parameters, which permits a convenient investigation of the influence of geometrical parameters on the spectral response. The calculated result shows that the response of microring resonator is indeed strongly polarization dependent and the resonance wavelengths are different for the two polarizations. The resonance wavelengths of the two orthogonal polarization states are different because of the difference in modal index and scattering matrix for different polarizations, hence the different polarized light can be transferred to different output port at specific wavelength. Such property allows for the design of integrated polarization splitter. The investigation of the influence of geometrical parameters on splitting ratio demonstrated that a splitting ratio greater than 20 dB at 1.55  $\mu\text{m}$  can be achieved in this device.

## Numerical Approaches for Solving Coupled Mode Theory-Part I: Uniform Fiber Bragg Gratings

Jiun-Jie Liao<sup>1</sup>, Nai-Hsiang Sun<sup>1</sup>, Ru-Yen Ro<sup>2</sup>, Po-Jui Chiang<sup>1</sup>, and Shih-Chiang Lin<sup>2</sup>

<sup>1</sup>Department of Electrical Engineering, I-Shou University, Kaohsiung, Taiwan, R.O.C.

<sup>2</sup> Department of Communication Engineering, I-Shou University, Kaohsiung, Taiwan, R.O.C

**Abstract**— In this paper, we use the eigenvalue technique (EVT) and the forth-order Runge-Kutta method (RKM) to solve the coupled mode theory (CMT) for uniform fiber Bragg gratings (FBGs). The eigenvalue technique is the rigorous method to solve the linear differential equations. Therefore, the analytical solution of a uniform FBG can be obtained. On the other hand, the RKM is the most common used numerical method to solve the initial value problem of the ordinary differential equation. Therefore, the forth order Runge-Kutta method is applied to calculate the couple mode theory in uniform FBGs as well. The transmission and reflection coefficients of uniform FBGs are analyzed in this paper. Compare the calculated results obtained by EVT with that by RKM. The RKM reaches to 8-digit accurate when the steps of the RKM is 1000.

## Numerical Approaches for Solving Coupled Mode Theory-Part II: Apodized Fiber Bragg Gratings

Jiun-Jie Liao<sup>1</sup>, Nai-Hsiang Sun<sup>1</sup>, Ru-Yen Ro<sup>2</sup>, Jung-Sheng Chiang<sup>1</sup>, and Shih-Chiang Lin<sup>2</sup>

<sup>1</sup>Department of Electrical Engineering, I-Shou University, Kaohsiung, Taiwan, R.O.C.

<sup>2</sup>Department of Communication Engineering, I-Shou University, Kaohsiung, Taiwan, R.O.C

**Abstract**— The eigenvalue technique (EVT) and the fourth-order Runge-Kutta method (RKM) are used to solve the coupled mode theory (CMT) for apodized fiber Bragg gratings (FBGs). The Gaussian-apodized structure of fiber gratings are simulated in this paper. Since the eigenvalue technique is the rigorous method to solve the linear differential equations, the analytical solution of a uniform FBG can be obtained by EVT. However, the index distribution of gratings varies with the propagation distance for apodized FBGs. Therefore, the piecewise-uniform technique with EVT is applied to calculate the couple mode theory in apodized FBGs. The characteristics of transmission and reflection of apodized FBGs are analyzed in this paper. Compare the calculated results obtained by EVT with that by RKM. The results show that RKM is faster and more accurate than EVT.

# Hybrid FD-FD Method for Medium Scaled Dielectric Waveguide Devices

Hung-Wen Chang and Wei-Chi Cheng

Institute of Electro-optical Engineering, National Sun Yat-sen University

Kaohsiung 80424, Taiwan

**Abstract**— We combine hybrid analytic mode expansion method with finite-difference, frequency-domain (FD-FD) method to study planer lightwave circuit (PLC) waveguide devices. To reduce FD-FD computational domain, an analytic layer-mode based absorbing boundary condition (ABC) and an index averaging scheme are developed for this hybrid method. The FD region handles only the complex propagating and scattering sections. The input and output sections are modeled analytically with reflection/transmission vectors. The resulting matrix equation is still too large for the standard matrix direct solver. On the other hand a fast and robust iterative solver does not exist for Helmholtz FD equation. We proposed a direct method using a modified Thomas method. As a result, we have greatly reduced excessive page faults and cut down the prolonged elapsed time compared with a sparse matrix solver. The combination of all the previously mentioned techniques makes it possible to run medium scale 2-D waveguide devices (up to one hundred wavelengths in each dimension) on a PC. A typical run may generate two-hundred thousand unknowns and take less than 5 minutes to complete. Numerical examples include a micro-ring cavity and a quasi-adiabatic tapered waveguide will be shown to demonstrate the effectiveness of this method.

# A New Simple Technique for Suppress the Spurious Response at Twice the Passband Frequency

Homayoon Oraizi and Hoggat-Allah Nemati

Iran University of Science and Technology, Narmak, Tehran 16846-13114, Iran

**Abstract**— A double radial stub technique is applied to parallel-coupled or hairpin line band-pass filters for spurious response suppression. The shunt branches of series-resonant circuits are used for realizing the finite-frequency transmission zeros. The double radial stub structure has a flat low-pass characteristic and a moderate band stop due to the introducing of transmission zero of elliptic function.

**Introduction:** Some methods are used to equalize the even and odd mode phase velocities for coupled-line microstrip filters. Due to the unequal even and odd mode phase velocities, this filter suffers from the spurious responses at  $2f_0$ , twice that of the passband frequency. hairpin bandpass filter (H-BPF) structure, resembles the parallel coupled line filter [1, 2], and it is widely used and preferable because of its compact size. Like parallel-coupled structures, this hairpin BPF also suffers from the spurious response. Several techniques have been proposed to tackle this problem. The solution is mainly obtained by providing different strip-lengths to equalize phase velocities.

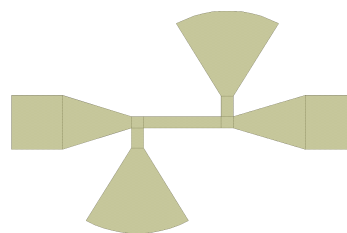
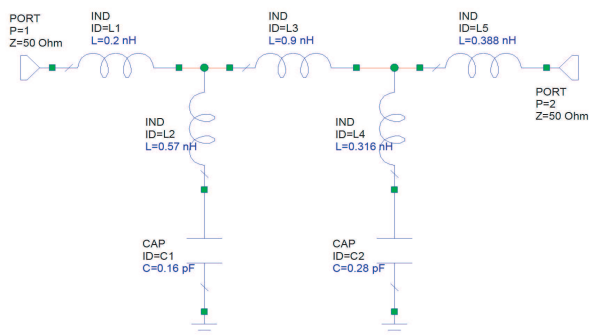


Figure 1: Lumped model of double radial stub.

Figure 2: Microstrip structure of double radial stub (7 mm × 5 mm).

Some DGS's have a flat low-pass and a narrow band gap characteristics due to the introducing a transmission zero of elliptic function. They can be utilized for harmonic suppression. DGS and PBG structures with some patterns etched in the ground plane have been proposed to reject a harmonic. The proposed methods have no simple analytical solution and for their implementation

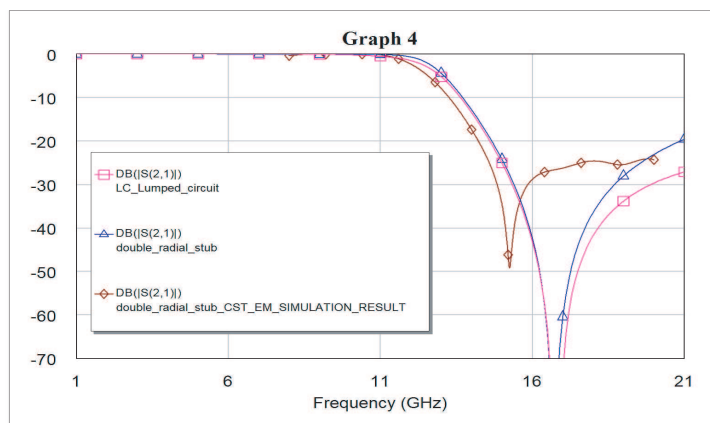


Figure 3: Simulation results of double radial stubs.

an EM simulation is needed. Wiggly-line filter based on the strip-line modulation is proposed to suppress the spurious passband at the second harmonic of the operating frequency.

The new proposed method of double radial stub can be designed by analytical methods with easy implementation.

**Design Procedure:** A prototype of the double radial stub may have an elliptic function response. Fig. 1 shows an elliptic function low pass filter that has two series-resonant branches connected in shunt that short out transmission at their resonant frequencies, and thus give two finite-frequency attenuation poles. Note that at  $f = \infty$  these two branches have no effect, and the inductances  $L_1$ ,  $L_3$  and  $L_5$  block transmission by having infinite series reactances, whereas the capacitance  $C_6$  shorts out transmission by having infinite shunt susceptance [2].

**Implementation:** A sample double radial stub is designed by the proposed method. and its performance is compared with that of Microwave Office simulation software, CST, and the lumped model in Fig. 3. The designed double radial stub is suitable for elimination of the second harmonic component of the hairpin filter with center frequency 10 GHz with bandwidth 1 GHz. As it can be seen there is good agreement between the simulations and the proposed method.

#### REFERENCES

1. Matthaei, G., L. Young, and E. M. T. Jones, *Microwave Filters, Impedance-Matching Networks, and Coupling Structures*, Boston, Artech House, Nov. 1985.
2. Hong, J. S. and M. J. Lancaster, *Microwave Filters for RF/Microwave Applications*, 38–64, John Wiley & Sons, New York, 2001.



# Numerical Calculations of PCs Structures by Pseudospectral Method

Po-Jui Chiang and Nai-Hsiang Sun  
I-Shou University, Taiwan

**Abstract**— To analyze leaky waveguides we employ the perfectly matched layer (PML) into full-vectorial multidomain pseudospectral mode solver as the computational window border for calculating leaky modes. The PML can absorb the outgoing wave based on multidomain pseudospectral methods, which can help us estimate the attenuation in the waveguides. The formulations are applied to Honeycomb fibers and remarkable accuracy is demonstrated.

## Full Eigen Mode Expansion Technique for Large Scale Dielectric Waveguide Devices with One-way Traffic

Hung-Wen Chang and Sen-Eon Liu

Institute of Electro-optical Engineering, National Sun Yat-sen University  
Kaohsiung 80424, Taiwan

**Abstract**— Many PLC (planar lightwave circuit) devices based on optical interfering principle have only one-way (forward propagating) traffic going in the devices. These devices include MMI (multi-mode interferometers), AWG (arrayed waveguide grating), MZI (Mach-Zehnder interferometers) and many other adiabatic waveguide devices. In opto-electronic industry, BPM (beam propagation method) is most widely used numerical method for studying par-axial light-wave propagation in these devices. Although BPM can calculate very fast, it can not accurately model wide-angle EM wave traffic due to its intrinsic limitation of the par-axial approximation.

Recently, FD-TD (finite difference-time domain) method is becoming very popular for its capability of performing full-wave analysis of PLC devices. However, when the size of waveguide device is many times larger than the optical wavelength, FD-TD can not run on computers with limited RAM memory. Large-scale parallel computation will be called for to perform the computational task. When there is very little reflection in the waveguide devices, we propose to use one-way full eigen-mode expansion technique (FEMET), which is a simplification of our full-wave rigorous CTMIE (coupled transverse-mode integral equation) formulation, to simplify the computational task. Like CTMIE, in FEMET, the device is first divided into many sections made of slices of layered dielectric waveguides. The orthonormal eigen modes are first constructed. The transmission coefficients of each layer are then obtained by direct integration of the junction field with the particular eigen mode. Each eigen mode propagation is then performed with each layer and the process repeats itself to the next slice until the fields in the entire device are all calculated. Examples of FEMET calculations vs. FD-FD and CTMIE results will be discussed in this paper.

# Session 2A7

## Fields and Waves

<a href="#">Wave Field Imaging</a>	
<i>Karl Joerg Langenberg (University of Kassel, Germany); Klaus Mayer (University of Kassel, Germany); René Marklein (University of Kassel, Germany);</i>	292
<a href="#">The Theory of Low-Frequency Wave Physics Revisited</a>	
<i>George Venkov (Technical University of Sofia, Bulgaria); Martin W. McCall (Imperial College London, United Kingdom); Dan Censor (Ben-Gurion University of the Negev, Israel);</i>	293
<a href="#">Radiation Emission in a Medium with Time-dependent Permittivity</a>	
<i>Peter Halevi (Instituto Nacional de Astrofísica, Óptica y Electrónica, México);</i>	294
<a href="#">Analysis of Layered Crossed Gratings Using Method of Integral Functionals Based on a Model of Double Periodic Magneto-dielectric Layer</a>	
<i>Vladimir Yachin (Institute of Radio Astronomy of the National Academy of Sciences of Ukraine, Ukraine); Kiyotoshi Yasumoto (Kyushu University, Japan);</i>	295
<a href="#">Performance of Multigrid in the Context of Beam Dynamics Simulations</a>	
<i>Gisela Poplau (Rostock University, Germany); Ursula van Rienen (Rostock University, Germany);</i>	296
<a href="#">Trends in Computational Electromagnetics</a>	
<i>Thomas Weiland (Technische Universität Darmstadt, Germany);</i>	297
<a href="#">Incorporation of the Continuous Spectrum in Closed Form Expressions for Layered Media Green's Functions</a>	
<i>Rafael R. Boix (University of Seville, Spain); Francisco L. Mesa (University of Seville, Spain); Francisco Medina (University of Seville, Spain);</i>	298
<a href="#">Fiber-optical Analog of the Event Horizon</a>	
<i>Ulf Leonhardt (University of St Andrews, UK); Thomas G. Philbin (University of St Andrews, UK); Friedrich König (University of St Andrews, UK);</i>	299
<a href="#">Trapped Surface Wave and Lateral Wave in the Presence of a Four-layered Region</a>	
<i>Yi Hui Xu (Zhejiang University, China); Kai Li (Zhejiang University, China); Liang Liu (Zhejiang University, China);</i>	300
<a href="#">A New Type of Mechanically Tunable Frequency Selective Surface</a>	
<i>Da Ma (Southeast University, China); Wen Xun Zhang (Southeast University, China);</i>	301
<a href="#">An Efficient Highways Coverage Technique for the High Altitude Platforms Mobile Communications</a>	
<i>Yasser Albagory (Faculty of Electronic Engineering, Egypt); Moawad Dessouky (Faculty of Electronic Engineering, Egypt); Hamdy Shashar (Faculty of Electronic Engineering, Egypt);</i>	302

## Wave Field Imaging

Karl J. Langenberg, Klaus Mayer, and René Marklein

Department of Electrical Engineering, University of Kassel, 34121 Kassel, Germany

**Abstract**— Three topics have been selected to demonstrate the practical feasibility of wave field imaging in terms of linearized diffraction tomography:

1. Imaging of concealed objects on persons with electromagnetic waves,
2. assessing the integrity of concrete with electromagnetic and elastic waves,
3. assessing the integrity of dissimilar welds with elastic waves.

Electromagnetic and elastic waves in solids share some common features: They satisfy linear first order partial differential equations involving a time derivative of appropriate fields and relating it to spatial derivatives in terms of particular del-operations (gradient, gradient dyadic, divergence, curl). Therefore, the same modelling as well as imaging algorithms apply with pertinent modifications.

We utilize an FMCW radar sensor with a centre frequency of 90 GHz to scan objects (handgun, ceramic knife) concealed under clothing on a Styrofoam torso within a two-dimensional synthetic aperture. The resulting data are processed with a frequency diversity version of the Fourier Diffraction Slice Theorem yielding three-dimensional images.

Non-destructive testing of concrete (e.g., bridges) involves the integrity assessment of tendon ducts, i.e., eventually finding grouting defects. This is a two-step procedure: Finding the tendon ducts below the steel bar reinforcement and then finding potential grouting defects. The first problem can be attacked with electromagnetic waves, whereas the second one requires the utilization of ultrasound (elastic waves). Again, diffraction tomography is a suitable tool for data processing of either kind.

Dissimilar welds in the primary circuits of nuclear power plants have an inhomogeneous anisotropic material composition. Elastic wave field imaging can account for that, if rays are properly back-propagated according to their energy velocity diagrams; the resulting algorithm is the time domain version of frequency diversity diffraction tomography. It turns that the proper consideration of the weld material characteristics yields more precise information about the location of defects as compared to disregarding it.

# The Theory of Low-Frequency Wave Physics Revisited

George Venkov<sup>1</sup>, Martin W. McCall<sup>2</sup>, and Dan Censor<sup>3</sup>

<sup>1</sup>Department of Applied Mathematics and Informatics  
Technical University of Sofia, 1756 Sofia, Bulgaria

<sup>2</sup>Department of Physics, The Blackett Laboratory  
Imperial College of Science, Technology and Medicine  
Prince Consort Road, London SW7 2AZ, UK

<sup>3</sup>Department of Electrical and Computer Engineering  
Ben-Gurion University of the Negev  
84105 Beer-Sheva, Israel

**Abstract**— The Stevenson approach to low-frequency time-harmonic wave scattering, that expanded the electric and magnetic fields in power series of  $k$ , essentially the inverse wavelength, is scrutinized. Stevenson's power series approach performance implies a variable frequency  $\omega$ , i.e., a variable wave-number  $k$ , an assumption challenged here.

Presently the three major linear wave physics models: acoustics, electromagnetics, and elastodynamics, are put on an equal footing by introducing the self-consistent system concept. Accordingly any low-frequency series expansion starts with the pertinent Helmholtz equation. Far-field surface-integrals are derived for each case.

To verify our approach, an example of low-frequency electromagnetic scattering by a long cylinder is elaborated, the results are compared to, and agree with the exact Hankel-Fourier series solution.

# Radiation Emission in a Medium with Time-dependent Permittivity

P. Halevi

Instituto Nacional de Astrofísica, Óptica y Electrónica  
Apdo. Post. 51, Puebla, Pue., México

**Abstract**— There are many studies of radiation emission in inhomogeneous media, with *position*-dependent characteristic parameters. However, to my knowledge, radiation in a medium whose properties vary with *time* has not been considered previously. As will become evident below, the behavior of power emission in a material characterized by a time-dependent permittivity  $\varepsilon(t)$  is qualitatively different from that in a stationary medium and has the potential to lead to unusual applications. And, many methods for producing such a dynamic medium — in real time — can be suggested: nonlinear modulation of the permittivity of an insulator, employing the thermo-electric effect, infilling a material by a liquid crystal and tuning the latter by means of external agents, manipulation of the free-carrier density in semiconductors, etc.

The medium considered is assumed to be a boundless (bulk), non-magnetic dielectric with a *real*, arbitrarily varying, permittivity  $\varepsilon(t)$ . The source of radiation is an embedded current density  $\mathbf{J}(\mathbf{r},t)$ , that can be replaced by a harmonically oscillating point dipole  $\mathbf{p}(t)\delta(\mathbf{r})$ . While this is a classical theory, as is well known, replacement of  $\mathbf{p}$  by twice the atomic transition-dipole moment yields a valid quantum-mechanical result — provided that the emitted light is weakly coupled to the dipole. With this proviso, the conclusions below are expected to hold valid for *spontaneous emission*. This is a modal theory, the normal modes being those of the sourceless, dynamic dielectric. Then, a carefully designed and calculated Green's function  $G(\mathbf{r},t;\mathbf{r}',t')$  leads to the vector potential  $\mathbf{A}(\mathbf{r},t)$ , the radiated field  $\mathbf{E}(\mathbf{r},t)$ , and *instantaneous* power  $P(t)$ . This is expressed in terms of the dipole moment  $\mathbf{p}$  and frequency  $\omega_o$  and integrals that involve  $\varepsilon(t)$  and the vector potential  $a_{\mathbf{k}}(t)$  of the normal modes (which satisfies the Sturm-Liouville differential equation),  $\mathbf{k}$  being the wave vector of these modes.

I have applied this general theory to the case of a periodically varying medium, the frequency of modulation being  $\Omega$ . Then the spectrum  $k(\omega)$  is periodic, with  $k(\omega + \Omega) = k(\omega)$ , and exhibits *k*-gaps. As a consequence, whenever the modal frequency  $\omega$  is equal to a multiple integer of  $\Omega/2$ , the group velocity is infinite and the modal density vanishes. The important result follows that *the radiated power vanishes for  $\omega_o = \Omega/2, \Omega, 3\Omega/2$ , etc.* I have also derived perturbational formulae for harmonic variation, namely  $\varepsilon(t) = \varepsilon_o[1 + \kappa \sin(\omega t)]$ , where  $\kappa \ll 1$ . I find that, if  $\Omega \ll \omega_o$ , *radiation occurs not only at the dipole frequency  $\omega_o$ , but also at satellite frequencies  $\omega_o \pm \Omega$ !* At the central frequency  $\omega_o$  the well known classical result is modified by a weak contribution that oscillates in time as  $\sin(\Omega t)$ . The satellite lines oscillate in the same way, they have, however, an amplitude that is proportional to  $\kappa \omega_o / \Omega$  — not necessarily small. If the spectrometer were designed to have a temporal resolution  $\Delta t < 2\pi/\Omega$ , then these interesting features should be readily observable. And, if the variation is *not* perturbational ( $\kappa \geq 1$ ), then radiation should occur at all the frequencies  $\omega_o, \omega_o \pm \Omega, \omega_o \pm 2\Omega$ , etc.

These ideas, in addition to their intrinsic physical interest, could lead to the development of novel, dynamic light sources.

# Analysis of Layered Crossed Gratings Using Method of Integral Functionals Based on a Model of Double Periodic Magneto-dielectric Layer

Vladimir Yachin<sup>1</sup> and Kiyotoshi Yasumoto<sup>2</sup>

<sup>1</sup>Institute of Radio Astronomy of the National Academy of Sciences of Ukraine  
4, Chervonopraporna str., 61002, Kharkov, Ukraine

<sup>2</sup>Department of Computer Science and Communication Engineering, Kyushu University  
Fukuoka 819-0395, Japan

**Abstract**— Periodic dielectric or metallic structures have been a subject of continuing interest because of their wide applications to frequency selective or polarization selective components in microwaves to optical wave regions. Among them, crossed gratings, sometimes referred to as three-dimensional gratings, have many applications such as antireflection layers, beam splitters, phase plates, narrow-band filters, substrates for radiating elements, and so on. The cross grating is formed by arranging the diffractive elements periodically in two non-collinear directions on a planar structure. There are two generic geometries of the cross gratings that are typically discussed in the literatures. The first geometry, usually referred to as a surface relief grating, consists of a dielectric layer with periodically implanted dielectric blocks. The difference of the relative permittivity between the layer and the blocks is relatively small. The second geometry is a metallic grating comprised of a metal layer periodically perforated with apertures or an array of periodic metallic elements implanted in a dielectric layer. In this case, the contrast in the relative permittivity between the layer material and the diffractive elements is very large. In the microwave region the metal is treated as a perfect electric conductor (PEC).

In this work, we shall discuss a novel numerical method in the frequency domain that can be applied to dielectric, metallic, and PEC gratings under the same algorithm. The method uses a concept of the double periodic magneto-dielectric layer to a cross grating and formulates a set of vectorial volume integral equations for the equivalent electric and magnetic polarization currents of the assumed periodic layer. The integral equations are solved using the integral functionals [1] related to the polarization currents distributions and the technique of double Floquet-Fourier series expansions. Once the integral functionals are determined, the scattered fields outside the layer can be calculated accordingly without performing the modal analysis of the electric and magnetic fields inside the grating layer. The unit cell of the layer is comprised of several parallelepiped segments of materials characterized by the complex-valued relative permittivity and permeability of step functions profiles. For the magneto-dielectric object with relative permittivity  $\varepsilon$  and permeability  $\mu$ , it is known [2] that the scattered fields outside the object tends to those for a PEC object of the same geometry when the material parameters are chosen so as to satisfy the extremes  $|\varepsilon| \gg 1$  and  $\varepsilon\mu \simeq 1$ . This situation is referred to as a PEC-like material. Using this fact, the arbitrary profiles of cross gratings comprised of dielectric, metallic, or PEC layers can be flexibly modeled by properly choosing the material parameters and sizes or locations of the parallelepiped segments in the unit cell.

## REFERENCES

1. Gal, L. K. and N. A. Khizhnyak, "The scattering of oblique incident wave on thin metallic cylinder of elliptic cross-section," *Izvestiya Vyzov Radiofizika (in Russian)*, English translation in *Radiophysics and Quantum Electronics*, Vol. 14, 1596–1610, 1971.
2. Yachin, V., K. Yasumoto, and N. Sidorchuk, "Method of integral functionals in problems of electromagnetic wave scattering by doubly-periodic magneto-dielectric structures," *Proc. of 2004 Korea-Japan Joint Conference on AP/EMC/EMT*, 223–226, Seoul, 2004.

# Performance of Multigrid in the Context of Beam Dynamics Simulations

G. Pöplau and U. van Rienen  
Rostock University, Germany

**Abstract**— The design of future light sources and colliders requires increasingly precise 3D beam dynamics simulations. In so-called tracking simulations the particle trajectory is determined which is described by the relativistic equation of motion. The equation of motion is solved by means of an appropriate time integration scheme. In regimes of rather low energy, this implies that the space charge fields have to be taken into account in each time step of the numerical integration. Recently, the efficient calculation of 3D space charge fields gained particular importance in the context of electron cloud studies for the ILC (International Linear Collider) damping rings.

Based on the geometric multigrid technique fast Poisson solvers have been developed and successfully applied for 3D space charge simulations. In theory, these multigrid Poisson solvers have optimal performance, i.e., the numerical effort depends linearly on the number of mesh points.

Unfortunately, this optimal convergence rate can sometimes not be achieved in simulations of real life problems. Possible reasons are that some of the components of multigrid, i.e., relaxation, coarsening, grid transfer operators, are not sufficiently adapted to the problem. In this paper the performance of the geometric multigrid technique is investigated in the context of space charge calculation. Some suggestions for an appropriate application and implementation of geometric multigrid will be deduced.

Another problem is the behavior of the multigrid Poisson solver within the particle tracking procedure. Since space charge fields have to be computed in each time step of the numerical integration, the calculated fields of the previous time step can be used as initial guess for the iterative Poisson solver. With this approach the effort for the new space charge calculation can be reduced. Recently, certain simulations have shown that other iterative algorithms like the method of preconditioned conjugate gradients can gain so much from this approach that they are faster than multigrid. The question under investigation is how multigrid can compete with other iterative algorithms for real life tracking simulations.

The iterative Poisson solvers are available as software package MOEVE 2.0 (MOEVE: **M**ultigrid for **n**on-**e**quidistant grids to solve Poisson's **e**quation). Furthermore, these Poisson solvers are implemented in the tracking code Astra of K. Flöttmann (DESY, Hamburg, Germany) and the tracking code GPT (General Particle Tracer) of Pulsar Physics (Eindhoven, the Netherlands).

## ACKNOWLEDGMENT

This work was supported by DESY, Hamburg, Germany.



## Trends in Computational Electromagnetics

**Thomas Weiland**

Fachbereich Elektrotechnik und Informationstechnik

Institut fuer Theorie Elektromagnetischer Felder (TEMF), Technische Universitaet Darmstadt  
Schlossgartenstrasse 8, D-64289 Darmstadt, Germany

**Abstract**— Research in Computational Electromagnetics over the last decades has resulted in a large variety of different algorithms in time- or frequency-domain and on surface- or volume-meshes, to name only the most imphant groups. The wide choice makes the decision, which method to choose for a given problem, a quite difficult task. We will present an approach to select the most appropriate algorithm in order to obtain the required accuracy in the shortest computational time.

# Incorporation of the Continuous Spectrum in Closed Form Expressions for Layered Media Green's Functions

R. R. Boix<sup>1</sup>, F. Mesa<sup>2</sup>, and F. Medina<sup>1</sup>

<sup>1</sup>Department of Electronics and Electromagnetism, College of Physics, University of Seville  
Av. Reina Mercedes, s/n, Seville 41012, Spain

<sup>2</sup>Department of Applied Physics 1, School of Computer Engineering, University of Seville  
Av. Reina Mercedes, s/n, Seville 41012, Spain

**Abstract**— The application of the method of moments (MoM) to the solution of mixed potential integral equations (MPIE) has proven to be an efficient numerical tool for the analysis of planar circuits and antennas [1]. In order to solve the MPIE arising from the analysis of planar structures, it is necessary to calculate the spatial domain Green's functions (GF) for the scalar and vector potentials in multilayered media. These GF can be determined via numerical computation of infinite integrals that are commonly known as Sommerfeld integrals (SI). However, the highly-oscillatory nature of the integrands involved makes the numerical computation of SI cumbersome and time consuming. Among the many different methods that have been proposed for speeding up the evaluation of Sommerfeld integrals, the most efficient ones are the discrete complex image method (DCIM) [2] and the rational function fitting method (RFFM) [3]. These two methods lead to closed-form expressions of the GF that consist of either spherical waves (DCIM) or cylindrical waves (RFFM).

Whereas the DCIM usually fails to reproduce the far field behavior of the GF of a multilayered substrate [4], the RFFM is especially suitable for that purpose because the far field behavior of the GF is frequently dominated by cylindrical surface waves whose amplitudes and propagation constants are well predicted by the RFFM [5]. Unfortunately, the far field behavior of the spatial domain GF is not only contributed by the surface waves but is also contributed by the so-called continuous spectrum (the surface waves are related to poles of the spectral domain GF located on the proper Riemann sheet, and the continuous spectrum is related to the branch point singularities of the spectral domain GF). In lossless multilayered media, the surface waves contribution usually dominates over the continuous spectrum contribution in the far field (there are exceptions to this rule, as it happens in the case of GF without TM spectral proper poles at frequencies where TE surface waves are not excited), and then the RFFM tends to provide accurate results in the far field. However, in lossy multilayered media the continuous spectrum dominates the far field [6], and in this case the RFFM fails to provide accurate results in the far field.

In this paper we present a novel implementation of the RFFM approach described in [5], which leads to accurate values of the GF in the far field when the far field is dominated by surface waves as well as by the continuous spectrum. In the novel approach, the far field contribution of the continuous spectrum to the GF is first derived in closed form both in the spatial domain and in the spectral domain. In fact, although the far field behavior of the continuous spectrum when all the poles are far from the branch points is known to be different from that observed when some of the poles are very close to the branch points [6, 7], these two different situations are conveniently handled by the expression of the far field contribution of the continuous spectrum that has been derived in the paper. Once this contribution is available, its spectral version is explicitly extracted from the spectral domain GF functions and the method of total least squares is subsequently applied to the resulting expressions [5]. This procedure leads to closed-form expressions of the spatial domain GF that explicitly contain information about the far field contributions of both the surface waves and the continuous spectrum. Thus, these closed-form expressions accurately reproduce the far field behavior of the spatial domain Green's functions in all scenarios.

## REFERENCES

1. Michalski, K. A., et al., *IEEE-AP*, Vol. 45, 508–519.
2. Aksun, M. I., *IEEE-MTT*, Vol. 44, 651–658.
3. Kourkoulos, V. N., et al., *IEEE-AP*, Vol. 54, 1568–1576.
4. Shuley, N., et al., *IEEE-MTT*, Vol. 50, 2185–2192.
5. Boix, R. R., et al., *IEEE-MTT*, Vol. 55, 268–280.
6. Mosig, J. R., et al., *IEEE-AP*, Vol. 51, 3200–3208.
7. Demuyne, F. F., et al., *IEEE-AP*, Vol. 46, 397–406.

## Fiber-optical Analog of the Event Horizon

Ulf Leonhardt, Thomas G. Philbin, and Friedrich König  
University of St Andrews, UK

**Abstract**— We have embarked on an experimental programme to create optical analogues of the event horizon, artificial black holes made of light, using ultrashort light pulses in photonic-crystal fibres. The optical properties of these fibres are dominated by their microstructure, arrangements of longitudinal holes with diameters smaller than the wavelength. (In this respect the fibres are metamaterials.) Our experiment is based on the simple idea that black holes resemble moving media. The horizon is the place where the velocity of the medium matches the speed of light in the material. Thanks to the optical Kerr effect, an ultrashort pulse changes the refractive index, acting like a moving medium. Since the medium is made by light, it naturally travels at the speed of light. The additional contribution of the pulse to the refractive index turns out to be sufficient to establish horizons. Recently we obtained the first data: we measured the classical frequency shifts at optical analogues of the event horizon. Such artificial black holes may be capable of demonstrating the spontaneous creation of quantum particles at horizons predicted by Stephen Hawking in 1974. This is one of the intellectually most influential predictions of theoretical physics, having inspired literally thousands of research papers. It has been used as one of the benchmarks of the theories that attempt to unify the physics of the small, quantum mechanics, with the physics of the very large, gravity and cosmology, an unsolved theoretical mystery. But even the benchmark for the most advanced theories of physics, Hawking effect, has been purely theoretical so far. Our scheme offers a realistic chance of succeeding in the first observation of this effect. Such experimental demonstrations are vital, because physics is an empirical science after all. Theory without experiment frequently poses the wrong questions and does not always follow the correct pathways. For example, while working on the theory behind our experiment we noticed that several methods developed in the quantum field theory of curved space fail when they are confronted with a real laboratory system.

# Trapped Surface Wave and Lateral Wave in the Presence of a Four-layered Region

Yi Hui Xu, Kai Li, and Liang Liu

The Electromagnetics Academy, Zhejiang University, Hangzhou 310058, China

**Abstract**— The problem of the electromagnetic field generated by a dipole source in a layered region has been studied by many investigator in the past decades because of its wide useful applications like subsurface and closed-to-the surface communication, radar, and geophysical prospecting and diagnostics. In the Wait's pioneering works, the electromagnetic field of a dipole source in the layered region was examined by using surface-impedance technique [1]. Lately, further developments on the electromagnetic field of a dipole source in a three-layered have been carried out by *King et al.* [2], especially, the lateral wave is addressed carefully.

In 1998, Wait [4] wrote a comment on the 1994 paper by King and Sandle [3] and regarded that the terms of the trapped surface wave, which varies as  $\rho^{-1/2}$  in the far region, should be considered for the three-layered case. The debates rekindled several investigators to re-visit the problem again. In 2002, *Zhang and Pan* [5] had addressed the electromagnetic field of a vertical dipole in the presence of three-layered region. It has been demonstrated that the trapped surface wave, which is contributed by the sums of residues of the poles, should be considered in the three-layered case. It is concluded, naturally, that the trapped surface wave can also be excited efficiently by a dipole source in the four-layered region.

In this paper, the propagation model considers the region as a perfect conductor, coated with the two layer dielectrics, and air above. Propagation of the electromagnetic field in the presence of a four-layered region is examined in detail when a vertical electric dipole and observation point are located in the air. Similar to the three-layered case, analytical results are found for the electromagnetic field, which includes four wave modes: a direct wave, an ideal reflected wave, trapped surface waves, and lateral waves. The wave number of the trapped surface wave, which is contributed by the sums of residues of the poles, is between the wave numbers  $k_0$  in the air and  $k_2$  in the lower dielectric layer. The lateral wave is evaluated by the integrations along the branch cut. Analysis and computations shows that the trapped surface wave play a major role in communication at large distance when both the source point and observation point are on or close to the boundary between the air and the upper dielectric layer.

## REFERENCES

1. Wait, J. R., *Electromagnetic Waves in Stratified Media*, 2nd Ed., Pergamon Press, New York, 1970.
2. King, R. W. P., M. Owens, and T. T. Wu, *Lateral Electromagnetic Waves: Theory and Applications to Communications, Geophysical Exploration, and Remoting Sensing*, Springer-Verlag, 1992.
3. King, R. W. P. and S. S. Sandler, "The electromagnetic field of a vertical electric dipole in the presence of a three-layered region," *Radio Sci.*, Vol. 29, No. 1, 97–113, 1994.
4. Wait, J. R., "Comment on 'The electromagnetic field of a vertical electric dipole in the presence of a three-layered region' by Ronold, W. P. King and Sheldon S. Sandler," *Radio Sci.*, Vol. 33, No. 2, 251–253, 1998.
5. Zhang, H. Q. and W. Y. Pan, "Electromagnetic field of a vertical electric dipole on a perfect conductor coated with a dielectric layer," *Radio Science*, Vol. 37, No. 4, 2002.

# A New Type of Mechanically Tunable Frequency Selective Surface

Da Ma and Wen Xun Zhang

State Key Lab. of Millimeter Waves, Southeast University, Nanjing 210096, China

**Abstract**— The purpose of this paper is to study the characteristics of a mechanically tunable frequency selective surface (MTFSS), which has many advantages such as simple structure, easy fabrication, low-cost, and large tunable range with extensive potential engineering applications.

Compared to the previous study on MTFSS, two improvements have been done: one is an improved “quasi-sandwich” structure with air-gap to reduce insertion loss; another is employing square-loop slot as elements of MTFSS for good frequency response characteristic and polarization adaptability. With comparison to different structures of elements, which exhibits relative good performance, under normal and oblique incidence of plane wave. Simulated results indicate that such MTFSS has good stability for different incident angles. The tunable range covers 1.90~3.20 GHz which corresponds to 54.17% almost linear shift of resonant frequency shift referring to 2.40 GHz as design. Besides, the characteristic of MTFSS with Y slot elements is also studied.

As validation of this approach, a prototype of MTFSS with square-loop slot elements is designed, fabricated and measured. The tested data in agreement with simulated results, it shows the availability of this approach.

## An Efficient Highways Coverage Technique for the High Altitude Platforms Mobile Communications

Yasser Albagory, Moawad Dessouky, and Hamdy Shashar

Department of Electronics and Electrical Communications Engineering

Faculty of Electronic Engineering, Egypt

**Abstract**— This paper proposes a novel beamforming technique for the high altitude platforms (HAPs) mobile communications to generate adaptive radio coverage worm-shaped cells covering the main highways which carry a heavy traffic of mobile users. This technique is based on pattern summation of individual low-sidelobe narrow beams -which constitute the desired cell pattern- weighted by an adaptive amplitude correcting function. The new shaped cell differs from the conventional hexagonal or elliptical cells as it follows the curvatures of the highway for long distances, therefore it has an important role in reducing the frequent handoff and signaling traffic of location updating from moving users over long highways.

## Session 2A8

# Electromagnetic Modeling, Inversion and Application 2

<a href="#">The Electromagnetic and Seismic Field Coupled Modeling for Pores Media</a>	
<i>Jing Ba (Tsinghua University, China); Huizhu Yang (Tsinghua University, China); Michael Oristaglio (Schlumberger-Doll Research, USA); Ganquan Xie (GL Geophysical Laboratory, USA);</i>	304
<a href="#">Energy-efficient Data Aggregation Protocol Based on Static Clustering for Wireless Sensor Networks</a>	
<i>S.-G. Deng (Southeast University, China); L.-F. Shen (Southeast University, China); X.-R. Zhu (Southeast University, China);</i>	305
<a href="#">An Inverse-scattering Iterative Algorithm for EM and Seismic Imaging</a>	
<i>Jing Ba (Tsinghua University, China); Huizhu Yang (Tsinghua University, China); Jianhua Li (GL Geophysical Laboratory, USA);</i>	306
<a href="#">A Weight Regression Analysis of the Spectroscopy and Chromatography Measurement Data</a>	
<i>Juan Fan (Hunan Environmental Monitoring Center, China); Jianhua Li (GL Geophysical Laboratory, USA); Chien-Chang Lin (Dayeh University, Taiwan);</i>	307
<a href="#">AGILD Low Frequency EM Field Simulation for Earth Ionosphere Large Scale Waveguide</a>	
<i>Qingyun Di (Institute of Geology and Geophysics, Chinese Academy of Sciences, China); Ganquan Xie (GL Geophysical Laboratory, USA); Jianhua Li (GL Geophysical Laboratory, USA); Tong Kang (Communication University of China, China);</i>	308
<a href="#">AGILD DC Mechanical and Electric Modeling for Industrial and Environmental Engineering</a>	
<i>Chien-Chang Lin (Dayeh University, Taiwan); Jianhua Li (GL Geophysical Laboratory, USA); Jing Li (Hunan KMD Electric Technology Company, China); Ganquan Xie (GL Geophysical Laboratory, USA);</i>	309
<a href="#">A Method of Improving Image Quality of an Uncooled Infrared Focal Plane Array</a>	
<i>Xia Zhang (Institute of Microelectronics of Chinese Academy of Sciences, China); Dapeng Chen (Institute of Microelectronics of Chinese Academy of Sciences, China); Chaobo Li (Institute of Microelectronics of Chinese Academy of Sciences, China); Shali Shi (Institute of Microelectronics of Chinese Academy of Sciences, China); Binbin Jiao (Institute of Microelectronics of Chinese Academy of Sciences, China); Yi Ou (Institute of Microelectronics of Chinese Academy of Sciences, China);</i>	310
<a href="#">Management of the Operation and Environment in the EM Stirring</a>	
<i>Jing Li (GL Geophysical Laboratory, USA); Jianhua Li (GL Geophysical Laboratory, USA); Daxin Zuo (GL Geophysical Laboratory, USA); Ganquan Xie (GL Geophysical Laboratory, USA); Henghua Li (Hunan KMD Electric Technology Company, China);</i>	311
<a href="#">AGILD WMT Ray-tracing Tomography and Its Application</a>	
<i>Jianhua Li (GL Geophysical Laboratory, USA); Chien-Chang Lin (Dayeh University, Taiwan); Ganquan Xie (GL Geophysical Laboratory, USA); Michael Oristaglio (Schlumberger-Doll Research, USA);</i>	312
<a href="#">Improved Isoparameter FEM for Plastic and EM Modeling</a>	
<i>Chien-Chang Lin (Dayeh University, Taiwan); Jianhua Li (GL Geophysical Laboratory, USA); Ganquan Xie (GL Geophysical Laboratory, USA); Michael Oristaglio (Schlumberger-Doll Research, USA);</i>	313
<a href="#">AGILD Seismic Modeling For Double-porosity Media</a>	
<i>Jing Ba (Tsinghua University, China); Huizhu Yang (Tsinghua University, China); Ganquan Xie (GL Geophysical Laboratory, USA);</i>	314

# The Electromagnetic and Seismic Field Coupled Modeling for Pores Media

Jing Ba<sup>1</sup>, Huizhu Yang<sup>1</sup>, Michael Oristaglio<sup>2</sup>, and Ganquan Xie<sup>3</sup>

<sup>1</sup>Tsinghua University, China

<sup>2</sup>Schlumberger Doll Research, USA

<sup>3</sup>GL Geophysical Laboratory, USA

**Abstract**— In this paper, we present the electromagnetic (EM) and seismic field coupled modeling for pores media using AGILD method. The EM and seismic differential integral equation are discretized in the boundary strip zone by collocation FEM method. The EM and seismic Galerkin equation are discretized by FEM method in internal domain. Both integral discretization on the strip zone and Galerkin FEM in the internal domain are used to construct AGILD EM and seismic wave field coupled modeling. Using the seismic and EM AGILD coupled modeling simulation, we investigated the mechanical and EM properties of the pores media that is very useful for geophysical and Earthquake exploration and environmental engineering and sciences applications.

## REFERENCES

1. Li, J., G. Xie, M. Oristaglio, L. Xie, and F. Xie, "3D-2D AGILD EM modeling and inversion," *PIERS Online*, Vol. 3, No. 4, 423–429, 2007.
2. Li, J. and G. Xie, "A cubic-hole finite element for 3D resistivity modeling," *Three-dimensional Electromagnetics*, No. 7, 591–599, edited by Michael Oristaglio, Geophysical Developments.
3. Li, J., G. Xie, and F. Xie, "New stochastic AGLID EM modeling and inversion," *PIERS Online*, Vol. 2, No. 5, 490–494, 2006.
4. Li, J., G. Xie, and J. Li, "3D and 2.5D AGLID EMS stirring modeling in the cylindrical coordinate system," *PIERS Online*, Vol. 2, No. 5, 505–509, 2006.
5. Xie, G., J. Li, M. Majer, D. Zuo, and M. Oristaglio, "3D electromagnetic modeling and nonlinear inversion," *Geophysics*, Vol. 65, No. 3, 804–822, 2000.
6. Xie, G. and J. Li, "New parallel stochastic global integral and local differential equation modeling and inversion," *Physics D*, Vol. 133, 477–487.
7. Xie, G., J. Li, and F. Xie, "Advanced GILD EM modeling and inversion," *PIERS Online*, Vol. 1, No. 1, 105–109, 2005.
8. Xie, G., J. Li, and F. Xie, "2.5D AGLID EM modeling and inversion," *PIERS Online*, Vol. 2, No. 4, 390–394, 2006.
9. Xie, G., F. Xie, L. Xie, and J. Li, "GL method and its advantages for resolving historical difficulties," *Progress in Electromagnetics Research*, PIER 63, 141–152.
10. Xie, G., J. Li, and J. Li, "New AGILD EMS electromagnetic field modeling," *PIERS Online*, Vol. 1, No. 2, 168–172, 2005.
11. Xie, G., F. Xie, and J. Li, "New GL and GILD superconductor electromagnetic modeling," *PIERS Online*, Vol. 1, No. 2, 173–177, 2005.



# Energy-efficient Data Aggregation Protocol Based on Static Clustering for Wireless Sensor Networks

S.-G. Deng<sup>1,2</sup>, L.-F. Shen<sup>1</sup>, and X.-R. Zhu<sup>1</sup>

<sup>1</sup>National Mobile Communications Research Laboratory, Southeast University, China

<sup>2</sup>Hunan City University, China

**Abstract**— Using clustering and aggregation enables better resource allocation and helps improve power control in wireless sensor networks (WSNs). Nevertheless, repeated clustering would increase the overhead and reduce network lifetime. An energy-efficient data aggregation protocol based on static clustering (EDASC) is proposed to acquire good network performance. Simulation results show that this approach makes network lifetimes much longer and remarkably reduces control overhead.

# An Inverse-scattering Iterative Algorithm for EM and Seismic Imaging

Jing Ba<sup>1</sup>, Huizhu Yang<sup>1</sup>, Jianhua Li<sup>2</sup>, and Mengqiu Guo<sup>3</sup>

<sup>1</sup>Tsinghua University, China

<sup>2</sup>GL Geophysical Laboratory, USA

<sup>3</sup>Geological and Geophysical Institute, China

**Abstract**— Based on the inverse-scattering series (ISS) theory, we presented an iterative algorithm which can numerically solve a higher order ISS term with all the lower order ISS terms determined. This work differs from the leading order inverse scattering (LOIS) algorithm [3, 7] and the higher order scattering (HOIS) algorithm that non ISS terms are ignored in the multi-dimensional imaging. Born and WKBJ approximations are used to solve the first order term in ISS series, while the higher order terms are calculated through a band-limited discrete Fourier transform. The algorithm hold high precision for singularity imaging, but face the problem of huge computing and long calculation time. In the iterative method, we used seismic and electromagnetic differential integral equations to reduce the costs. Our method can be used to solve seismic and electromagnetic inverse problem in geophysics and environmental engineering etc. applications.

## REFERENCES

1. Clayton, R. W. and R. H. Stolt, "A Born-WKBJ inversion method for acoustic reflection data," *Geophysics*, Vol. 46, 1559–1567, 1981.
2. Liu, F., A. B. Weglein, etc., "Multi-dimensional seismic imaging using the inverse scattering series," *SEG Annual Meeting*, New Orleans, 2006.
3. Shaw, S. A., "An inverse scattering series algorithm for depth imaging of reaction data from a layered acoustic medium," PhD thesis, University of Houston, 2005.
4. Shaw, S. A., A. B. Weglein, etc., "Isolation of a leading order depth imaging series and analysis of its convergence properties for a 1D acoustic medium," *Journal of Seismic Exploration*, Vol. 13, 99–120, 2004.
5. Stolt, R. H., "Migration by Fourier transform," *Geophysics*, Vol. 43, 23–48, 1978.
6. Weglein, A. B., F. A. Gasparotto, etc., "An inverse-scattering series method for attenuating multiples in seismic reflection data," *Geophysics*, Vol. 62, 1975–1989, 1997.
7. Weglein, A. B., D. J. Foster, etc., "Predicting the correct spatial location of reflectors without knowing or determining the precise medium and wave velocity: Initial concept, algorithm and analytic and numerical example," *Journal of Seismic Exploration*, Vol. 10, 367–382, 2002.
8. Xie, G., J. Li, M. Majer, D. Zuo, and M. Oristaglio, "3D electromagnetic modeling and nonlinear inversion," *Geophysics*, Vol. 65, No. 3, 804–822, 2000.
9. Xie, G. and J. Li, "New parallel stochastic global integral and local differential equation modeling and inversion," *Physics D*, Vol. 133, 477–487.
10. Xie, G., F. Xie, L. Xie, and J. Li, "GL method and its advantages for resolving historical difficulties," *Progress in Electromagnetics Research*, PIER 63, 141–152.

# A Weight Regression Analysis of the Spectroscopy and Chromatography Measurement Data

Juan Fan<sup>1</sup>, Jianhua Li<sup>2</sup>, and Chien-Chang Lin<sup>3</sup>

<sup>1</sup>Hunan Environmental Monitoring Center, China

<sup>2</sup>GL Geophysical Laboratory, USA

<sup>3</sup>Department of Mechanical and Automation Engineering, Da-Yeh University, Taiwan

**Abstract**— Hunan Environmental Monitoring Center laboratories have the gas chromatography, high-performance liquid chromatography, plasma emission spectroscopy, ion chromatography, atomic absorption spectrophotometer, and a group of instruments. We used the spectroscopy and iron Chromatography to measure the quantity or quality of the metal contamination in the water, in particular, in the drink water. From the electromagnetic field theory and AGILD EM and flow modeling simulation in the spectroscopy and iron chromatography, we proposed a new weight regression analysis for the spectroscopy and chromatography measurement data computational analysis. Our weight regression method can be used to determinate metal contamination distributions in the time and space domain. The method is accurate and fast and can be useful to predict the metal contamination history, currently status, and in the future, also the contamination area and degree. The method can be used to find the contamination sources and find remediation approaches, such that will obtain a well posed equilibrium between the production and environmental protection and safe.

## REFERENCES

1. Li, J., G. Xie, M. Oristaglio, L. Xie, and F. Xie, "3D-2D AGILD EM modeling and inversion," *PIERS Online*, Vol. 3, No. 4, 423–429, 2007.
2. Li, J., G. Xie, and F. Xie, "New stochastic AGLID EM modeling and inversion," *PIERS Online*, Vol. 2, No. 5, 490–494, 2006.
3. Xie, G., J. Li, M. Majer, D. Zuo, and M. Oristaglio, "3D electromagnetic modeling and nonlinear inversion," *Geophysics*, Vol. 65, No. 3, 804–822, 2000.
4. Xie, G. and J. Li, "New parallel stochastic global integral and local differential equation modeling and inversion," *Physics D*, Vol. 133, 477–487, 1999.
5. Xie, G., J. Li, and F. Xie, "Advanced GILD EM modeling and inversion," *PIERS Online*, Vol. 1, No. 1, 105–109, 2005.
6. Xie, G., F. Xie, and J. Li, "New GL and GILD superconductor electromagnetic modeling," *PIERS Online*, Vol. 1, No. 2, 173–177, 2005.
7. Xie, G., J. Li, F. Xie, and L. Xie, "3D GL EM and quantum mechanical coupled modeling for the nanometer materials," *PIERS Online*, Vol. 3, No. 4, 418–423, 2007.
8. Xie, G., T. Kang, and J. Li, "AGILD EM dispersion modeling for photonic crystals," to be appear in PIERS 2008 in Hangzhou.

# AGILD Low Frequency EM Field Simulation for Earth Ionosphere Large Scale Waveguide

Qingyun Di<sup>1</sup>, Ganquan Xie<sup>2</sup>, Jianhua Li<sup>2</sup>, and Tong Kang<sup>3</sup>

<sup>1</sup>Geological and Geophysical Institute of Chinese Academy, China

<sup>2</sup>GL Geophysical Laboratory, USA

<sup>3</sup>Communication University of China, China

**Abstract**— In this paper, we present the AGILD low frequency electromagnetic (EM) field simulation in the Earth-Ionosphere large scale waveguide. The EM wave field propagation in the Earth-Ionosphere waveguide is very large scale computational research project. The Earth-Ionosphere (EI) waveguide can be the global EI waveguide and the district EI waveguide. The Finite Element method (FEM) and Finite Difference method (FD) can not simulate the EM wave field propagation in the large scale EI waveguide because the matrix is extremely large and artificial boundary condition error reflection will degrade the accuracy of the computational EM field. The AGILD EM modeling overcomes the difficulty for solving extremely large matrix and clears the error reflection from the artificial boundary. We use the AGILD EM modeling method to simulate the low frequency EM field propagation in the district large scale EI waveguide. We presented a brief and primary EI waveguide electric wave propagation in the PIERS 2007 in the Prague and obtained France, Italy and other countries colleagues' strongly interesting. It is emphasized that the "EM filed simulation in the Earth-Ionosphere large scale waveguide" is very important large scale computational EM project in the world. Our AGILD low frequency EM field simulation method in the Earth-Ionosphere large scale waveguide is very useful for global climate changing, global space geophysical science, geophysical and Earthquake exploration, and geophysical and environmental engineering etc. It is great challenge for the extremely large scale EM computation.

## REFERENCES

1. Li, J., G. Xie, M. Oristaglio, L. Xie, and F. Xie, "3D-2D AGILD EM modeling and inversion," *PIERS Online*, Vol. 3, No. 4, 423–429, 2007.
2. Li, J., G. Xie, and F. Xie, "New stochastic AGLID EM modeling and inversion," *PIERS Online*, Vol. 2, No. 5, 490–494, 2006.
3. Xie, G., J. Li, M. Majer, D. Zuo, and M. Oristaglio, "3D electromagnetic modeling and nonlinear inversion," *Geophysics*, Vol. 65, No. 3, 804–822, 2000.
4. Xie, G. and J. Li, "New parallel stochastic global integral and local differential equation modeling and inversion," *Physics D*, Vol. 133, 477–487.
5. Xie, G., J. Li, and F. Xie, "Advanced GILD EM modeling and inversion," *PIERS Online*, Vol. 1, No. 1, 105–109, 2005.
6. Xie, G., J. Li, and F. Xie, "2.5D AGLID EM modeling and inversion," *PIERS Online*, Vol. 2, No. 4, 390–394, 2006.
7. Xie, G., F. Xie, L. Xie, and J. Li, "GL method and its advantages for resolving historical difficulties," *Progress in Electromagnetics Research*, PIER 63, 141–152.
8. Xie, G., F. Xie, and J. Li "New GL and GILD superconductor electromagnetic modeling," *PIERS Online*, Vol. 1, No. 2, 173–177, 2005.

# AGILD DC Mechanical and Electric Modeling for Industrial and Environmental Engineering

Chien-Chang Lin<sup>1</sup>, Jianhua Li<sup>1,2</sup>, Jing Li<sup>3</sup>, and Ganquan Xie<sup>2</sup>

<sup>1</sup>Da-Yeh University, Taiwan

<sup>2</sup>GL Geophysical Laboratory, USA

<sup>3</sup>Hunan KMD Electric Technology Company, China

**Abstract**— In this paper, we present an AGILD DC mechanical and electric modeling method for industrial and environmental engineering. First, we propose the AGILD DC mechanical modeling. Second, we propose the AGILD DC electric modeling. A differential integral plastic transverse deformation equation and direct electric current differential integral equation are holding on the boundary strip domain. The plastic elastic Galerkin equation and direct current Galerkin equation are holding in the internal domain. Both differential integral equation on the boundary strip and Galerkin equation in internal domain are coupled together to construct AGILD DC mechanical and electric modeling method. The AGILD DC mechanical plastic modeling is useful for the multiple layered thin plastic hectograph plate deformation analysis in the new LTD industrial design in the TV and Laptop developing. The AGILD DC electric modeling is used for DC electric imaging to find water source and detect and monitor the heavier metal contamination in the surface water and ground water. That is very important research project of the environment sciences, monitoring, and remediation engineering. Our AGILD DC electric modeling imaging and spectroscopy imaging can be joint working together for monitoring water's environmental quality and plastic plate large deformation. The AGILD DC mechanical and electric modeling method can be used for industrial production and environmental engineering.

## REFERENCES

1. Lin, C. C., G. Xie, and J. Li, "Nondestructive testing in mechanical engineering by wave inversion," *PIERS Online*, Vol. 3, No. 6, 795–800, 2007.
2. Li, J., G. Xie, M. Oristaglio, L. Xie, and F. Xie, "3D-2D AGILD EM modeling and inversion," *PIERS Online*, Vol. 3, No. 4, 423–429, 2007.
3. Li, J., G. Xie, and F. Xie, "New stochastic AGLID EM modeling and inversion," *PIERS Online*, Vol. 2, No. 5, 490–494, 2006.
4. Xie, G., J. Li, M. Majer, D. Zuo, and M. Oristaglio, "3D electromagnetic modeling and nonlinear inversion," *Geophysics*, Vol. 65, No. 3, 804–822, 2000.
5. Xie, G. and J. Li, "New parallel stochastic global integral and local differential equation modeling and inversion," *Physics D*, Vol. 133, 477–487.
6. Xie, G., J. Li, and F. Xie, "Advanced GILD EM modeling and inversion," *PIERS Online*, Vol. 1, No. 1, 105–109, 2005.
7. Xie, G., J. Li, F. Xie, and L. Xie, "3D GL EM and quantum mechanical coupled modeling for the nanometer materials," *PIERS Online*, Vol. 3, No. 4, 418–423, 2007.

# A Method of Improving Image Quality of an Uncooled Infrared Focal Plane Array

Xia Zhang<sup>1,2</sup>, Dapeng Chen<sup>1</sup>, Chaobo Li<sup>1</sup>, Shali Shi<sup>1</sup>, Binbin Jiao<sup>1</sup>, and Yi Ou<sup>1</sup>

<sup>1</sup>Institute of Microelectronics of Chinese Academy of Sciences, Beijing, China

<sup>2</sup>Department of Photo-electronics, Communication University of China, Beijing, China

**Abstract**— A MEMS micro-cantilever array and optical read out uncooled infrared imaging system is consist of infrared lenses, micro cantilever beam focal plane array (FPA), read out part of visible light, and image acquisition processing components. The heat radiation issued by the infrared radiation sources irradiate to the lens FPA, the thermal effects cause the micro cantilever on FPA to occur displacement and deformation; The read out path of visible light is starting from the foreseeable visible light source, passing a small hole diaphragm and focalizes as a point light source, it passes through the semi permeable semi reflective mirror, and passes the collimator lens to translate into parallel light which strikes into the FPA. Visible light is reflected by deformed cantilever beam on FPA, after the filter, is accepted by CCD device. Because the deformation of the cantilever beam is caused by the infrared absorption thermal effects, so visible lights reflection data recorded in CCD can be used to determinate the infrared absorption thermal effects. In this paper, we present a method of improving image quality of an uncooled infrared focal plane array by experiments. Under experimental conditions without the infrared radiation sources, we used white light and green light source (LED) to irradiate to the black background and make thermal imaging. We compare the system noise impact and disturbance due to two light sources with same illumination light source on the system. From the experimental results, the amount noise distribution of the white light source is higher than the green light source; also, the noise distribution band of white light source is more wide than noise band of the green light source. At the same time, we will use the AGILD etc. optical and electromagnetic modeling to simulate our experiments with white light and the green light sources, respectively. We will calculate intensity distribution and spectral distribution of white light and the green light to interact with materials. By joint investigation and comparison between optical experiments and optical numerical simulations, we will clarify that the thermal imaging quality may be improved by green light source.

## REFERENCES

1. Li, J., G. Xie, and F. Xie, "New stochastic AGLID EM modeling and inversion," *PIERS Online*, Vol. 2, No. 5, 490–494, 2006.
2. Xie, G., F. Xie, L. Xie, and J. Li, "GL method and its advantages for resolving historical difficulties," *Progress In Electromagnetics Research, PIER*, Vol. 63, 141–152, 2006.
3. Xie, G., F. Xie, and J. Li, "New GL and GILD superconductor electromagnetic modeling," *PIERS Online*, Vol. 1, No. 2, 173–177, 2005.
4. Xie, G., J. Li, F. Xie, and L. Xie, "3D GL EM and quantum mechanical coupled modeling for the nanometer materials," *PIERS Online*, Vol. 3, No. 4, 418–423, 2007.
5. Xie, G., T. Kang, and J. Li, "AGILD EM dispersion modeling for photonic crystals," to be appear in PIERS 2008 proceeding, PIERS 2008 in Hangzhou.

# Management of the Operation and Environment in the EM Stirring

Jing Li<sup>1,2</sup>, Jianhua Li<sup>1</sup>, Daxin Zuo<sup>1</sup>, Ganquan Xie<sup>1</sup>, and Henghua Li<sup>2</sup>

<sup>1</sup>GL Geophysical Laboratory, USA

<sup>2</sup>Hunan KMD Electric Technology Company, China

**Abstract**— The electromagnetic stirrer (EMS) is important tool in the metal and steel continuous casting. The EMS has been installed in almost all steel factors. By AGILD electromagnetic stirring modeling simulation, the current exist EMS's magnetic field leaking is still large and its wastage is still high. Moreover, the leaking magnetic field products the induced electric field in the air near and around the continuous cast machine That cause risk hazard workplace for the steel worker in steel factor. Therefore, EMS's optimal design is very necessary. Therefore KMD and GLGEO perform cooperative research to set a scheme management platform to manage the operation and environment in the EM stirring. By the data analysis, when the risk peak is over the threshold, the design operation will make processes and obtain the optimal design under environmental safe and lower contamination constraints. The environmental safe constraint and product developing operation are connection by AGILD Lagrangian method. In the near future, we will use new GLGEO's EMS modeling to improve the control system and increase the efficiency of the KMD EMS and protect environment. The GLGEO's GL and AGILD EMS modeling are new novel Global and Local electromagnetic stirring software. The GL and AGILD method and software and method of management of the EMS operation and environment are patented by GL GEOPHYSICAL Laboratory. The GLGEO EMS modeling software challenge to FEM, FD, and Born like EM modeling. The GLGEO GL and AGILD EMS has many advantages over FEM, FD, and Born like modeling.

## REFERENCES

1. Li, J., G. Xie, and F. Xie, "New stochastic AGLID EM modeling and inversion," *PIERS Online*, Vol. 2, No. 5, 490–494, 2006.
2. Li, J., G. Xie, and J. Li, "3D and 2.5D AGLID EMS stirring modeling in the cylindrical coordinate system," *PIERS Online*, Vol. 2, No. 5, 505–509, 2006.
3. Xie, G., J. Li, M. Majer, D. Zuo, and M. Oristaglio, "3D electromagnetic modeling and nonlinear inversion," *Geophysics*, Vol. 65, No. 3, 804–822, 2000.
4. Xie, G. and J. Li, "New parallel stochastic global integral and local differential equation modeling and inversion," *Physics D*, Vol. 133, 477–487, 1999.
5. Xie, G., J. Li, and F. Xie, "Advanced GILD EM modeling and inversion," *PIERS Online*, Vol. 1, No. 1, 105–109, 2005.
6. Xie, G., J. Li, and F. Xie, "2.5D AGLID EM modeling and inversion," *PIERS Online*, Vol. 2, No. 4, 390–394, 2006.
7. Xie, G., F. Xie, L. Xie, and J. Li, "GL method and its advantages for resolving historical difficulties," *Progress In Electromagnetics Research, PIER*, Vol. 63, 141–152, 2006.
8. Xie, G., J. Li, and J. Li, "New AGILD EMS electromagnetic field modeling," *PIERS Online*, Vol. 1, No. 2, 168–172, 2005.

## AGILD WMT Ray-tracing Tomography and Its Application

Jianhua Li<sup>1,2</sup>, Chien-Chang Lin<sup>1</sup>, Ganquan Xie<sup>2</sup>, and Michael Oristaglio<sup>3</sup>

<sup>1</sup>Department of Mechanical and Automation Engineering, Da-Yeh University, Taiwan

<sup>2</sup>GL Geophysical Laboratory, USA

<sup>3</sup>Schlumberger Doll Research, USA

**Abstract**— To implement and develop a new ray-tracing method that provides a useful tool to analyze optical measurement sites and geophysical surface-to-surface, surface-to-borehole, and crosshole data. To develop next-generation wave propagation algorithm and codes for computational geophysics, computational mechanics, biomedical sciences, and interactive 3D wavelength matching topography. In this paper, A new wavelength matching topology method is developed to generate AGILD finite element mesh. The rays are accurately traced using the known velocity expression in the current element instead of in-layered or stratified medium. The wavelength matching topology and the curve ray tracing are combined to construct the AGILD FEM Ray Tracing tomography forward modeling and inversion algorithm.



## Improved Isoparameter FEM for Plastic and EM Modeling

Chien-Chang Lin<sup>1</sup>, Jianhua Li<sup>1,2</sup>, Ganquan Xie<sup>2</sup>, and Michael Oristaglio<sup>3</sup>

<sup>1</sup>Department of Mechanical and Automation Engineering, Da-Yeh University, Taiwan

<sup>2</sup>GL Geophysical Laboratory, USA

<sup>3</sup>Schlumberger Doll Research, USA

**Abstract**— In this paper, we present an isoparameter finite element method to calculate the electromagnetic (EM) field and the stress and deformation of the very thin multiple layered plastic hectograph or heliotype plate. The isoparameter element has high accurate to simulate the multiple tin plastic plate deformation and EM modeling. The thin multiple layered plastic plate has more advantages than the glass plate in the new LCD screen etc displayer and other industrial engineering applications. In this paper, we present an improved isoparameter finite element method to calculate the stress and deformation of the very thin multiple layered plastic hectograph or heliotype plate and EM field distribution.

## AGILD Seismic Modeling For Double-porosity Media

Jing Ba<sup>1</sup>, Huizhu Yang<sup>1</sup>, and Ganquan Xie<sup>2</sup>

<sup>1</sup>Tsinghua University, China

<sup>2</sup>GL Geophysical Laboratory, USA

**Abstract**— In this paper, we present the seismic field modeling for double-porosity media using AGILD method. The seismic differential integral equations are discretized in the boundary strip zone by collocation FEM method. The seismic Galerkin equations are discretized by FEM method in internal domain. Both integral discretization on the strip zone and Galerkin FEM in the internal domain are used to construct AGILD seismic wave field modeling. The three phases' wavefields are simulated through AGILD method in double-porosity media.

# Session 2AP

## Poster Session 2

<b>Electrical Field and Plasticity for Polar Materials</b>	
<i>Jianhua Xiao (Henan Polytechnic University, China);</i> .....	322
<b>Photoacoustic Effect: A Case in Which Electromagnetic Wave Is Converted into Sound</b>	
<i>Mayo Villagrán-Muniz (Universidad Nacional Autónoma de México, México); J. Andrade-Herrera (Universidad Nacional Autónoma de México, México);</i> .....	323
<b>Study on Initial Stage of Gas Discharge by Numerical Method</b>	
<i>Yun Zhang (Tsinghua University, China); Rong Zeng (Tsinghua University, China); Xiaochuan Wang (Tsinghua University, China); Bo Zhang (Tsinghua University, China); Jinliang He (Tsinghua University, China);</i> .....	324
<b>Genetic Algorithms for Automated Design of the Multilayer Absorbers in the X-Band and Incident Angle Range</b>	
<i>Nadia Lassouaoui (Universite Paris X, Nanterre, France); Habiba Hafdallah Ouslimani (Universite Paris X, Nanterre, France); Alain C. Priou (Universite Paris X, Nanterre, France);</i> .....	326
<b>A Novel Analysis for Circular-groove Guide</b>	
<i>Yinqin Cheng (Northwest University for Nationalities, China);</i> .....	328
<b>PIC Simulation of Surface Charging in the Wake Zone</b>	
<i>Ji Wang (Lanzhou Institute of Physics, China); Jiawen Qiu (Lanzhou Institute of Physics, China); Xiaogang Qin (Lanzhou Institute of Physics, China);</i> .....	329
<b>The Optical Spatial Comb</b>	
<i>Tao Duan (Xi'an Institute of Optics and Precision Mechanics, China); Chun-Fang Li (Xi'an Institute of Optics and Precision Mechanics, China);</i> .....	330
<b>Analysis of High Frequency Interference in Antennas by Implementation of a Novel Efficient Hybrid TLM Method</b>	
<i>M. Bahadorzadeh (Islamic Azad University, Iran); M. Naser Moghaddasi (Islamic Azad University, Iran);</i> .....	331
<b>Asymptotic Expansion of the Scattering Problem by a Rough Periodic or Doubly Periodic Surface</b>	
<i>J.-R. Poirier (LAME- ENSEIHT-INPT, France); A. Bendali (IMT, INSA, France); Pierre Borderies (Office National d'Etudes et de Recherches Aérospatiales, France);</i> .....	332
<b>Physics Based Time Domain Simulation of Magnetic Recording Signal and Noise</b>	
<i>Xiaobin Wang (Seagate Technology, USA); Zhen Jin (Hitachi Global Storage Technology, USA); Xuebing Feng (Seagate Technology, USA); Dimitar Dimitrov (Seagate Technology, USA);</i> .....	333
<b>Ferroelectric Properties of Pulsed Laser Deposited Thin Films for Detecting Electromagnetic Waves</b>	
<i>Hsiu-Fung Cheng (National Taiwan Normal University, Taiwan); P. T. Joseph (National Tsing Hua University, Taiwan); C. C. Hung (National Taiwan Normal University, Taiwan); Y. W. Chen (National Taiwan Normal University, Taiwan); Nyan-Hwa Tai (National Tsing Hua University, Taiwan); I-Nan Lin (Tamkang University, Taiwan);</i> .....	334
<b>Ferroelectric Properties of Nanostructured SBLFT Thin Films Prepared by Pulsed Laser Ablation</b>	
<i>P. T. Joseph (National Tsing Hua University, Taiwan); Nyan-Hwa Tai (National Tsing Hua University, Taiwan); Hsiu-Fung Cheng (National Taiwan Normal University, Taiwan); I-Nan Lin (Tamkang University, Taiwan);</i> .....	335
<b>Modeling of Electron Beam — Bragg Gratings Interaction</b>	
<i>Artem A. Balyakin (Saratov State University, Russia); Elena V. Blokhina (Saratov State University, Russia);</i> .....	336
<b>PIC Simulation of Surface Charging in the Wake Zone</b>	
<i>Ji Wang (Lanzhou Institute of Physics, China); Jiawen Qiu (Lanzhou Institute of Physics, China); Xiaogang Qin (Lanzhou Institute of Physics, China);</i> .....	337
<b>Study on a Novel Permanent Magnet Retarder for Vehicles</b>	
<i>Lezhi Ye (Beijing University of Technology, China); Desheng Li (Beijing University of Technology, China); Z. Y. Lu (Beijing University of Technology, China); Qiaohong Guo (Beijing University of Technology, China);</i> .....	338
<b>Research on a Maglev Ball Control System Based on DSP2812</b>	

<i>Qiaohong Guo (Beijing University of Technology, China); Desheng Li (Beijing University of Technology, China); Zhiyuan Lu (Beijing University of Technology, China); Wei Wang (Beijing University of Technology, China); Lezhi Ye (Beijing University of Technology, China); .....</i>	339
<b>Key Technologies for Lidar Detecting Stealth Targets</b>	
<i>Bin Zhu (Chengdu University, China); Jing Zhang (University of Electronic Science and Technology of China, China); Yan Chen (University of Electronic Science and Technology of China, China); Ke Deng (University of Electronic Science and Technology of China, China); Dagang Jiang (University of Electronic Science and Technology of China, China); Peng Zhang (University of Electronic Science and Technology of China, China); Zoushi Yao (University of Electronic Science and Technology of China, China); Wei Hu (University of Electronic Science and Technology of China, China); .....</i>	340
<b>Enhancement of Microwave-assisted Organic Reactions Using Active Carbon</b>	
<i>Zhibin Li (East China University of Science and Technology, China); Jianhua Chen (East China University of Science and Technology, China); Haisheng Xu (East China University of Science and Technology, China); Shan Hu (East China University of Science and Technology, China); Dong Shen (East China University of Science and Technology, China); .....</i>	341
<b>A Comparison of SRTM and CALIPSO Super-resolution Lidar Altimetry</b>	
<i>Yongxiang Hu (NASA Langley Research Center, USA); .....</i>	343
<b>Universal Radio Frequency Identification Sensing System</b>	
<i>J. H. Lin (BeeDar Technology Inc., Taiwan); J. L. Sun (BeeDar Technology Inc., Taiwan); T. H. Su (BeeDar Technology Inc., Taiwan); P. F. Hsieh (BeeDar Technology Inc., Taiwan); .....</i>	344
<b>Passive Radar Imaging Based on Correlation Motion Compensation</b>	
<i>Xiaoyan Fan (Xi'an Institute of Space Radio Technology, China); She Shang (Xi'an Institute of Space Radio Technology, China); Wei Ma (Xi'an Institute of Space Radio Technology, China); Jie Li (Xi'an Institute of Space Radio Technology, China); Xuan Li (Xi'an Institute of Space Radio Technology, China); .....</i>	345
<b>Enhancement Gradient Pulse Waveforms in MR Tomography</b>	
<i>Eva Gescheidtova (Brno University of Technology, Czech Republic); Radek Kubasek (Brno University of Technology, Czech Republic); .....</i>	346
<b>A Study on Electronic Nose System Based on Integrated Gas Sensors Array and Support Vector Machine</b>	
<i>Guiling Huang (Nankai University, China); Qida Zhao (Nankai University, China); Luming Zhao (Nankai University, China); Shuhong Li (Nankai University, China); Yinping Miao (Nankai University, China); Jiping Liao (Nankai University, China); Fei Wang (Nankai University, China); .....</i>	347
<b>High Vertically Resolved Atmospheric State and Surface/Cloud Parameters Retrieved with IASI Single Field-of-view</b>	
<i>Daniel K. Zhou (NASA Langley Research Center, USA); .....</i>	348
<b>Remote Sensing of Atmosphere and Surface Properties from Ultra-spectral Sensors</b>	
<i>Xu Liu (NASA Langley Research Center, USA); Daniel K. Zhou (NASA Langley Research Center, USA); Allen Larar (NASA Langley Research Center, USA); Willian L. Smith (Hampton University, USA); Peter Schluessel (EUMETSAT, Germany); .....</i>	349
<b>Three-scale Radar Backscattering Model of the Ocean Surface Based on Second-order Scattering</b>	
<i>Ying Yu (Institute of Electronics, China); Xiao-Qing Wang (Institute of Electronics, China); Min-Hui Zhu (Institute of Electronics, China); Jiang Xiao (Institute of Electronics, China); .....</i>	350
<b>Potentiality of Doppler Spectrum of Backscattered Microwave Signal for Detection of Sea Surface Slicks</b>	
<i>Vladimir Yurjevich Karavov (Institute of Applied Physics, Russian Academy of Sciences, Russia); Mikhail Kanevsky (Institute of Applied Physics, RAS, Russia); Eugeny Meshkov (Institute of Applied Physics, RAS, Russia); .....</i>	351
<b>Remote Sensing Image Compression Based on Classification and Detection</b>	
<i>Minqi Li (Xi'an Institute of Space Radio Technology, China); Quan Zhou (Xi'an Institute of Space Radio Technology, China); Jun Wang (Xi'an Institute of Space Radio Technology, China); .....</i>	352
<b>Using AMSR-E Satellite Data to Retrieve Soil Moisture on the Mongolia Plateau</b>	
<i>Yuei-An Liou (National Central University, Taiwan); Tzu-Yin Chang (National Central University, Taiwan); .....</i>	353
<b>Far-field Diffraction Characteristics of a Short Pulse from a Slit with Gaussian form of Transmittance</b>	
<i>Pin Han (National Chung Hsing University, Taiwan); .....</i>	354
<b>Two-step Contrast Source Inverse Method with Phaseless Data for EM Inverse Scattering</b>	
<i>Lianlin Li (Institute of Electronics, Chinese Academy of Sciences, China); Yin Xiang (Institute of Electronics, Chinese Academy of Sciences, China); Fang Li (Institute of Electronics, Chinese Academy of Sciences, China); .....</i>	355
<b>Differential Theory with Genetic Algorithms in Design Periodic Absorbers</b>	

<i>Nadia Lassouaoui (University Paris X, France); Habiba Hafdallah Ouslimani (University Paris X, France); Alain C. Priou (University Paris X, France); .....</i>	356
<b>A Stable and Efficient Numerical Method for Grating Structures</b>	
<i>N.-Y. Shih (National Taiwan University, Taiwan); W.-L. Yeh (National Taiwan University, Taiwan, China); Yih-Peng Chiou (National Taiwan University, Taiwan); .....</i>	358
<b>Optical Response of a Tunable Liquid Crystal Cell with Nano-structured Metal Layer</b>	
<i>Lizhen Ruan (University of Exeter, United Kingdom); J. Parsons (University of Exeter, United Kingdom); W. A. Murray (University of Exeter, United Kingdom); J. Roy Sambles (University of Exeter, United Kingdom); .....</i>	359
<b>Theoretical and Experimental Study of Goos-Hänchen Shifts on Symmetrical Metal-cladding Waveguides</b>	
<i>Zhuangqi Cao (Shanghai Jiao Tong University, China); Honggen Li (Shanghai Jiao Tong University, China); Lin Chen (Shanghai Jiao Tong University, China); Qishun Shen (Shanghai Jiao Tong University, China); Xiaoxu Deng (Shanghai Jiao Tong University, China); .....</i>	360
<b>Optical Mode Parameters of the 2.3-<math>\mu\text{m}</math> Al(In)/GaAsSb/GaSb Ridge-waveguide Laser Diodes and Laser Diode Arrays</b>	
<i>Yimin Chen (Stony Brook University, USA); Dmitry Donetsky (Stony Brook University, USA); ....</i>	361
<b>Wavefront Phase Modulation of Cylindrical Vector Beam in Optical Focusing System</b>	
<i>Xiumin Gao (Hangzhou Dianzi University, China); Jian Wang (Hangzhou Dianzi University, China);</i>	362
<b>Detection of Narrow-band and Multi-frequency Terahertz Generation and Propagation in Periodically Poled MgO: LiNbO<sub>3</sub> (PP-MgO: LN)</b>	
<i>W. M. Liu (National University of Singapore, Singapore); G. Kh. Kitaeva (Moscow State University, Russia); H. C. Guo (National University of Singapore, Singapore); Sing Hai Tang (National University of Singapore, Singapore); .....</i>	363
<b>The Photonics Collapse-revival's of Intensity-dependent Coupling of Lambda Atoms and Fields</b>	
<i>J. Hajivandi (University of Shiraz, Iran); M. M. Golshan (University of Shiraz, Iran); .....</i>	364
<b>High Quality, High Intensity and Narrow Bessel Beams</b>	
<i>O. Brzobohatý (Institute of Scientific Instruments of the ASCR, v.v.i., Czech Republic); T. Čížmár (Institute of Scientific Instruments of the ASCR, v.v.i., Czech Republic); Pavel Zemánek (Institute of Scientific Instruments of the ASCR, v.v.i., Czech Republic); .....</i>	366
<b>Speed Enhancement of Many-body Cluster of Microparticles in Optical Conveyor Belt</b>	
<i>M. Šiler (Institute of Scientific Instruments of the ASCR, v.v.i., Czech Republic); T. Čížmár (Institute of Scientific Instruments of the ASCR, v.v.i., Czech Republic); Pavel Zemánek (Institute of Scientific Instruments of the ASCR, v.v.i., Czech Republic); .....</i>	367
<b>All-optical Switching Structure Using Nonlinear Photonic Crystal Directional Coupler</b>	
<i>Armaghan Eshaghi (Ferdowsi University of Mashhad, Iran); M. M. Mirsalehi (Ferdowsi University of Mashhad, Iran); Amir Reza Attari (Ferdowsi University of Mashhad, Iran); S. A. Malekabadi (Ferdowsi University of Mashhad, Iran); .....</i>	369
<b>Two-color Two-photon Microscopy for Enhancing the Imaging Depth into Highly Scattering Media</b>	
<i>Lingling Qiao (Shanghai Institute of Optics and Fine Mechanics, China); Chen Wang (Shanghai Institute of Optics and Fine Mechanics, China); Ya Cheng (Shanghai Institute of Optics and Fine Mechanics, China); Zhizhan Xu (Shanghai Institute of Optics and Fine Mechanics, Chinese Academy of Sciences, China); .....</i>	370
<b>Multifunctional Microdevices Integration on Glass Chips with Femtosecond Laser Microfabrication</b>	
<i>Fei He (Shanghai Institute of Optics and Fine Mechanics, China); Haiyi Sun (Shanghai Institute of Optics and Fine Mechanics, China); Jian Xu (, China); Yang Liao (Shanghai Institute of Optics and Fine Mechanics, China); Ya Cheng (Shanghai Institute of Optics and Fine Mechanics, China); Zhizhan Xu (Shanghai Institute of Optics and Fine Mechanics, Chinese Academy of Sciences, China);</i>	371
<b>Studying of the Dipole Characteristic of THz from Photoconductors</b>	
<i>Hong Liu (Xi'an University of Technology, China); Weili Ji (Xi'an University of Technology, China); Wei Shi (Xi'an University of Technology, China); .....</i>	372
<b>Influence of External-cavity Length on the Route-to-chaos of Semiconductor Lasers under Optical Feedback</b>	
<i>Moustafa Ahmed (Minia University, Egypt); Minoru Yamada (Kanazawa University, Japan); .....</i>	373
<b>Broadband Terahertz Biological Sensing with a Membrane Device</b>	
<i>H. Yoneyama (RIKEN, Japan); M. Yamashita (RIKEN, Japan); A. Tanabashi (RIKEN, Japan); S. Kasai (RIKEN, Japan); H. Ito (RIKEN, Japan); T. Ouchi (RIKEN, Japan); .....</i>	374
<b>Quadratic Data Storage System in Polymeric Material</b>	
<i>Kokou D. Dorkenoo (Institut de Physique et Chimie des Matériaux de Strasbourg, France); .....</i>	375
<b>Beam Spot Size Evolution of Gaussian Femtosecond Pulses after Angular Dispersion</b>	

<i>Derong Li (Huazhong University of Science and Technology, China); Xiaohua Lv (Huazhong University of Science and Technology, China); Shaoqun Zeng (Huazhong University of Science and Technology, China); Qingming Luo (Huazhong University of Science and Technology, China);</i> .....	376
<b>Propagation of Anomalous Hollow Beams in a Turbulent Atmosphere</b>	
<i>Yangjian Cai (University of Erlangen, Germany); Halil Tanyer Eyyuboglu (Cankaya University, Turkey); Yahya Baykal (Cankaya University, Turkey);</i> .....	377
<b>New Optical Fiber Sensor Based on Hydrogels for Detection of Liquid Leaks</b>	
<i>Guiling Huang (Nankai University, China); Qida Zhao (Nankai University, China); Junfeng Lv (Nankai University, China); Luming Zhao (Nankai University, China);</i> .....	378
<b>Longitudinal Relaxation Time Measurement in MR with Transient-state Magnetization</b>	
<i>Eva Gescheidtova (Brno University of Technology, Czech Republic); Karel Bartusek (Academy of Sciences of the Czech Republic, Institute of Scientific Instruments, Czech Republic);</i> .....	379
<b>The Electromagnetic Interaction with Tissue of a Circular Patch Antenna, Comprising a Concentric Ring and Radially Slotted Groundplane</b>	
<i>S. Curto (Dublin Institute of Technology, Ireland); Xiu Long Bao (Dublin Institute of Technology, Ireland); M. J. Ammann (Dublin Institute of Technology, Ireland);</i> .....	380
<b>Anti-interference Design of Quasi-resonant Tank for Magnetic Induction Heating System</b>	
<i>Cheng-Chi Tai (National Cheng Kung University, Taiwan); Ming-Kum Cheng (National Cheng Kung University, Taiwan);</i> .....	381
<b>The Design of a Half-bridge Series-resonant Type Heating System for Magnetic Nanoparticle Thermotherapy</b>	
<i>Cheng-Chi Tai (National Cheng Kung University, Taiwan); Chien-Chang Chen (National Cheng Kung University, Taiwan);</i> .....	382
<b>Morphological Changes Induced by 53.37 GHz Radiation on Giant Vesicles</b>	
<i>Alfonsina Ramundo-Orlando (National Research Council Establishment, Italy); M. Cappelli (National Research Council Establishment, Italy); G. Longo (National Research Council Establishment, Italy); M. Girasole (National Research Council Establishment, Italy); L. Tarricone (University of Salento, Italy); A. Beneduci (University of Calabria, Italy);</i> .....	383
<b>A Novel Method for Passive Shim Design: II</b>	
<i>Hector Sanchez Lopez (The University of Queensland, Australia); Feng Liu (The University of Queensland, Australia); Ewald Weber (The University of Queensland, Australia); Stuart Crozier (The University of Queensland, Australia);</i> .....	385
<b>Design of Tunable Filter with Fiber Bragg Gratings with Cladding Made of Electro-optic Materials</b>	
<i>Shang-Lin Hou (Lanzhou University of Technology, China); Suo-Ping Li (Lanzhou University of Technology, China); Dao-bin Wang (Lanzhou University, China); Jing-Li Lei (Lanzhou University of Technology, China);</i> .....	387
<b>Fiber Grating Designing Method Based on Multi-subpopulation Competition Evolutionary Algorithm</b>	
<i>Zhaoni Huang (Guangxi Shipping School, China); Songfen Liu (Nankai University, China); Guil-ing Huang (Nankai University, China);</i> .....	389
<b>A Study of Detection Technology for Liquid Leakage Base on Fused-biconical Fiber Couplers</b>	
<i>Zhaoni Huang (Guangxi Shipping School, China); Guiling Huang (Nankai University, China);</i> .....	390
<b>Influence of the Cladding Diameter of Tilted Fiber Bragg Grating on the Refractive Index Sensitivity Characteristic</b>	
<i>Yinping Miao (Nankai University, China); Qida Zhao (Nankai University, China); Bo Liu (Nankai University, China); Bo Dong (Nankai University, China); Guiling Huang (Nankai University, China);</i> .....	391
<b>A Compact Filter with Good Performance Based on Super-compact Multilayered Left-handed Transmission Line</b>	
<i>Hao Hu (Xi'an Jiaotong University, China); Anxue Zhang (Xi'an Jiaotong University, China); Yan-sheng Jiang (Xi'an Jiaotong University, China); Zhuo Xu (Xi'an Jiaotong University, China);</i> .....	392
<b>Scattering Characteristics of a New Dielectric Periodic Array Composed of Left-handed Gratings</b>	
<i>Weihai Fang (University of Science and Technology of China, China); Shanxia Xu (University of Science and Technology of China, China);</i> .....	393
<b>Propagation Characteristics of a Novel NRD Guide with Double-LHM Slab Layer</b>	
<i>Yongmei Pan (University of Science and Technology of China, China); Shanxia Xu (University of Science and Technology of China, China);</i> .....	394
<b>Realization of Even Amplitude and Phase Distributions in Series Feed Configuration with Composite Right/Left-handed Transmission Line</b>	

<i>Yuanchun Li (University of Science and Technology of China, China); Qi Zhu (University of Science and Technology of China, China); Jun Zhang (University of Science and Technology of China, China); Jiali Lai (University of Science and Technology of China, China); Shanjia Xu (University of Science and Technology of China, China);</i> .....	395
<b>Design of Microstrip Array with Series Fed Configuration</b>	
<i>Wenhui Mao (University of Science and Technology of China, China); Qi Zhu (University of Science and Technology of China, China); Yuanchun Li (University of Science and Technology of China, China); Shanjia Xu (University of Science and Technology of China, China);</i> .....	396
<b>The Research on Application of Composite Meta-material in Rectangular Waveguide</b>	
<i>Man-na Han (Communication University of China, China); Qiang Sui (Communication University of China, China); Chao Li (Institute of Electronics, Chinese Academy of Sciences, China);</i> .....	397
<b>Magneto-tunable Left-handed Material Based on Yttrium Iron Garnet</b>	
<i>Hongjie Zhao (Tsinghua University, China); Ji Zhou (Tsinghua University, China); Qian Zhao (Tsinghua University, China); Bo Li (Tsinghua University, China); Lei Kang (Tsinghua University, China); Yang Bai (University of Science and Technology, China); Xing Zhang (University of Texas at Arlington, USA);</i> .....	398
<b>Experimentally Demonstration of Isotropic Negative Permeability in a Three-dimensional Dielectric Composite</b>	
<i>Qian Zhao (Tsinghua University, China); Lei Kang (Tsinghua University, China); Bo Du (Tsinghua University, China); Hongjie Zhao (Tsinghua University, China); Qin Xie (Tsinghua University, China); Xueguang Huang (Tsinghua University, China); Bo Li (Tsinghua University, China); Ji Zhou (Tsinghua University, China); Longtu Li (Tsinghua University, China);</i> .....	399
<b>The Negative Parameters of Left-handed Materials Consisting of Granular Composite</b>	
<i>Xiumin Gao (Hangzhou Dianzi University, China);</i> .....	400
<b>Hydrogenated Amorphous Silicon-based Thin Film Solar Cells</b>	
<i>S. Khalefa (Plasma Research Laboratory, Libya); M. Sbeta (Center for Solar Energy Studies αLibya, Libya); A. Abugalia (Center for Solar Energy Studies αLibya, Libya);</i> .....	401
<b>Electromagnetic Field Quantization in an Anisotropic Magnetodielectric Medium with External Charges</b>	
<i>Majid Amooshahi (University of Isfahan, Iran); Fardin Kheirandish (University of Isfahan, Iran);</i> ..	402
<b>Study on Elliptical Cylinder and Elliptical Sphere Electromagnetic Cloakings</b>	
<i>Kan Yao (Institute of Electronics, Chinese Academy of Science, China); Chao Li (Institute of Electronics, Chinese Academy of Sciences, China); Fang Li (Institute of Electronics, Chinese Academy of Sciences, China);</i> .....	403
<b>Microscopic Origins of Nonlinearity in Superconducting Microwave Devices</b>	
<i>Alexander Zhuravel (National Academy of Science of Ukraine, Ukraine); Alexey V. Ustinov (University of Erlangen, Germany); Steven M. Anlage (University of Maryland, USA);</i> .....	404
<b>Omni-directional Vibration Sensor Based on Dynamic Image Understanding</b>	
<i>Yi-Ping Tang (Zhejiang University of Technology, China); Wu-Jie He (Zhejiang University of Technology, China); Yi-Hua Zhu (Zhejiang University of Technology, China);</i> .....	405
<b>Rotation of the Leaky Dielectric Particle in a Spinning Electric Field</b>	
<i>Yu. Dolinsky (Ben-Gurion University of the Negev, Israel); T. Elperin (Ben-Gurion University of the Negev, Israel);</i> .....	406
<b>Real Time Fire Detection Based on Omni-directional Vision</b>	
<i>Yi-Ping Tang (Zhejiang University of Technology, China); Shun-jing Jin (Zhejiang University of Technology, China);</i> .....	407
<b>Research on Audio Information Hiding Arithmetic Based on BP Neural Network</b>	
<i>Hong Wang (Wuhan University of Technology, China); Qiong Sun (Wuhan University of Technology, China); Yi Sun (Wuhan University of Technology, China);</i> .....	408
<b>Model Error Estimate in Quantitative Remote Sensing Inversion</b>	
<i>Zheng Lu (Beijing Normal University, China); Hua Yang (Beijing Normal University, China); Xi-ang Ma (Beijing Normal University, China); ZhiXing Ren (Beijing Normal University, China);</i> .....	409
<b>Fabrication of Focusing Optic for Soft X-Ray Microscope</b>	
<i>Kwon Su Chon (Wonkwang University, Republic of Korea); Kwon-Ha Yoon (Wonkwang University, Republic of Korea);</i> .....	410
<b>Schlieren Imaging with Coherent and Incoherent Light Sources and with Proper Fourier Filters</b>	
<i>Boris Zakharin (University of Arizona, USA); Josef Stricker (Technion -I. I. T., Israel);</i> .....	411
<b>Polarization-independent Microwave Directional Anisotropy in Magnetophotonic Crystal</b>	
<i>H. X. Da (Suzhou University, China); J. C. Wu (Suzhou University, China); Zhen-Ya Li (Suzhou University, China);</i> .....	412

<b>Scaling Invariance Band Gaps in 1D Periodic Structures Containing Metamaterials</b>	
<i>Zhiguo Wang (Tongji University, China);</i> .....	413
<b>Influence of Subjective Material on the Energy Transferring Process between Phosphorescent Material and Fluorescent Material</b>	
<i>Yuan Li (Beijing Jiaotong University, China); Suling Zhao (Beijing Jiaotong University, China); Zheng Xu (Beijing Jiaotong University, China); Fujun Zhang (Beijing Jiaotong University, China); Yanrui Li (Beijing Jiaotong University, China); Yaru Yang (Beijing Jiaotong University, China); Jinglu Song (Beijing Jiaotong University, China);</i> .....	414
<b>Implementation of Range-gated Underwater Laser Imaging System</b>	
<i>Mingsong Chen (Guilin University of Electronic Technology, China); Faliang Ao (Guilin University of Electronic Technology, China); Ning He (Guilin University of Electronic Technology, China);</i> .....	415
<b>Band Engineering and Waveguide Design for THz Si/SiGe Quantum Cascade Laser</b>	
<i>Guijiang Lin (Xiamen University, China); Hongkai Lai (Xiamen University, China); Cheng Li (Xiamen University, China); Songyan Chen (Xiamen University, China); Jinzhong Yu (Xiamen University, China);</i> .....	416
<b>Far-field Distortion Characteristics of Annular Lasers from Confocal Unstable Resonators through the Natural Atmosphere</b>	
<i>Yufeng Peng (Henan Normal University, China); Li Liu (Henan Normal University, China); V. S. Egorov (St. Petersburg State University, Russia); Zuhai Cheng (Wuhan National Laboratory for Optoelectronics, China); Minggao Zhang (Henan Normal University, China);</i> .....	417
<b>Subwavelength Terahertz Imaging and Plasmonically Transferred Image through an Array of Periodically Corrugated Metal Rods</b>	
<i>Yongyao Chen (Tianjin University, China); Ching-Yue Wang (Tianjin University, China);</i> .....	418
<b>Surface Optical Breathers in Semiconductor Quantum Dots</b>	
<i>G. T. Adamashvili (Technische Universität Berlin, Germany); A. Knorr (Technische Universität Berlin, Germany);</i> .....	419
<b>Spatial Light Modulators for Cold Atom Manipulation</b>	
<i>Michael Mestre (Univ Paris Sud, France); Fabienne Diry (Univ Paris Sud, France); Bruno Viaris de Lesegno (Univ Paris Sud, France); Laurence Pruvost (Univ Paris Sud, France);</i> ....	420
<b>Active III-V Photonic Crystal Devices Integrated onto Silicon Wafers</b>	
<i>F. Raineri (Laboratoire de Photonique et de Nanostructures (CNRS UPR20), France); G. Vecchi (Laboratoire de Photonique et de Nanostructures (CNRS UPR20), France); A. M. Yacomotti (Laboratoire de Photonique et de Nanostructures (CNRS UPR20), France); T. Karle (Laboratoire de Photonique et de Nanostructures (CNRS UPR20), France); A. Levenson (Laboratoire de Photonique et de Nanostructures (CNRS UPR20), France); R. Raj (Laboratoire de Photonique et de Nanostructures (CNRS UPR20), France);</i> .....	421
<b>From Fast Optical Bistability to Thermo-optical Excitability in a Two Dimensional Photonic Crystal</b>	
<i>A. M. Yacomotti (Laboratoire de Photonique et de Nanostructures (CNRS UPR20), France); P. Monnier (Laboratoire de Photonique et de Nanostructures (CNRS UPR20), France); F. Raineri (Laboratoire de Photonique et de Nanostructures (CNRS UPR20), France); R. Raj (Laboratoire de Photonique et de Nanostructures (CNRS UPR20), France); A. Levenson (Laboratoire de Photonique et de Nanostructures (CNRS UPR20), France);</i> .....	422
<b>The Localized Modes for Random Laser</b>	
<i>Sheng Li (Physics Department of Zhejiang Normal University, China); Xin Sun (Fudan University, China); Thomas F. George (University of Missouri-St.Louis, USA);</i> .....	423
<b>Nitride-based LEDs with MQW Active Regions Grown by Different Temperature Profiles</b>	
<i>S. C. Wei (National Cheng Kung University, Taiwan); A. T. Cheng (National Cheng Kung University, Taiwan); Yan-Kuin Su (Cheng Kung University, Taiwan, China);</i> .....	424
<b>Optical Tunneling through a Disordered Stack of Metamaterials</b>	
<i>Wei-Hua Sun (Nanjing University, China); Ye Lu (Nanjing University, China); R. W. Peng (Nanjing University, China); De Li (Nanjing University, China); X. Wu (Nanjing University, China); L. S. Cao (Nanjing University, China); Mu Wang (Nanjing University, China);</i> .....	425
<b>Optical Propagation in One-dimensional Random <math>n</math>-mer Dielectric Systems</b>	
<i>Zeng Zhao (Nanjing University, China); F. Gao (Nanjing University, China); Ru-Wen Peng (Nanjing University, China); K. Wei (Nanjing University, China); L. S. Cao (Nanjing University, China); De Li (Nanjing University, China); Z. Wang (Nanjing University, China); Mu Wang (Nanjing University, China);</i> .....	426
<b>Voltage-controlled Light Storage in Vertically Coupled InGaAs/GaAs Quantum Dots</b>	
<i>Ka-Di Zhu (Shanghai Jiao Tong University, China);</i> .....	427



**Effect of 50 Hz Power Frequency Magnetic Field on Microfilament Cytoskeleton Assembly of Human Amnion FL Cell**

*Keping Chu (East China Normal University, China); Yukun Zhang (East China Normal University, China); Danying Zhang (Zhejiang University, China); Qunli Zeng (Zhejiang University, China); Zhiyin Cai (East China Normal University, China); Shude Chen (East China Normal University, China); Ruohong Xia (East China Normal University, China); ..... 428*

**Goos-Hänchen Shift and Pulse Widening for Step-index Fiber**

*Yaoju Zhang (Wenzhou University, China); Jianping Bai (Nanyang Normal University, China); .... 429*

**An Inverse Model for Localization of Low-diffusivity Regions in the Heart Using Ecg/Mcg Sensor Arrays**

*Ashraf Atalla (McMaster Univerisity, Canada); Aleksandar Jeremic (McMaster University, Canada); 430*

## Electrical Field and Plasticity for Polar Materials

Jianhua Xiao

Henan Polytechnic University, Jiaozuo, Henan 454000, China

**Abstract**— For polar materials, the polar molecular will rotate locally when electrical field is applied. When the electrical field is big enough, the fractures will appear in material. In this paper, the material composed by rigid polar molecular is studied. The elastoplastic deformation under electrical field is theoretically formulated to explain the relation between micro geometry and macro geometry. The macro geometry is defined by the traditional strain. The micro geometry is described the base vector transformation of material coordinators. The research shows that there are the two basic plastic configurations of macro geometry. They are named as type-I and type-II elastoplasticity. The type-I elastoplasticity is characterized with plastic contraction on the normal plane of electrical field. The type-II elastoplasticity is characterized with plastic expansion on the electrical field direction. The critical field strength is expressed by the material yield-stress. When the electrical field is bigger than the critical value, the volume ratio of voids or cracks is expressed by the field strength.

## Photoacoustic Effect: A Case in Which Electromagnetic Wave Is Converted into Sound

Mayo Villagrán-Muniz<sup>1</sup> and J. Andrade-Herrera<sup>2</sup>

<sup>1</sup>CCADET, Universidad Nacional Autónoma de México  
Apartado Postal 70-186, Código Postal 04510, México D.F., México

<sup>2</sup>Facultad de Ciencias, Universidad Nacional Autónoma de México  
Apartado Postal 70-186, Código Postal 04510, México D.F., México

**Abstract**— The photoacoustic effect is not well known and here we present a simple way to show it. When a continuous chopped or pulsed electromagnetic wave irradiates a sample of matter, they can be absorbed and the resulting energy will then be radiated as heat. This heat causes detectable sound waves due to pressure variation in the surrounding medium. Depending on the excitation conditions (for example short or long lights pulses), different acoustic transducers (sonic or ultrasonic) are needed. In this work, a microsecond light pulse produced by a flash photographic camera was sent to one extreme of a cylindrical metallic rod. Light pulses generate sounds waves that are detected by a microphone attached to the other extreme of the rod. Sound velocity and attenuation in the rod can be easily measured.

## Study on Initial Stage of Gas Discharge by Numerical Method

Yun Zhang, Rong Zeng, Xiaochuan Wang, Bo Zhang, and Jinliang He  
Department of Electrical Engineering, Tsinghua University, Beijing 100084, China

**Abstract**— The progress and characteristics of initial stage of gas discharge is studied in this paper by numerical simulation. A program based on the FE-FCT method in its full two-dimension form is developed and employed for the solution of transport equations of charged species under the effect of space-charge electric field. The initial stage of gas discharge between parallel plate electrodes, including the development of avalanche and progression of Townsend or streamer discharge are presented. The influences of length of gap and applied electric field on the mechanism and process of breakdown are analyzed and the breakdown voltage and formative time of discharge are predicted by the numerical method, and is well agree with the experimental result. The actions of cathode secondary emission on discharge are investigated, and photoemission is found to be more efficient than ion-electron emission.

**Introduction:** The initial stage is a very important part in gas discharge, especially in short air gap. It determines whether the discharge mechanism is Townsend or streamer, the break down electric field and the formative time delay of the discharge. Therefore, it is very essential to study the initial stage of gas discharge by numerical method carefully for understanding the characteristics and pushing forward the study of gas discharge.

In this paper the numeric method is utilized to study the initial stage of the discharge. The program based on hydrodynamic model and a fully two-dimensional FE and FCT algorithm was developed for numerical simulation of gas discharge. Then the method is utilized to simulate the development of avalanche and the formation of Townsend or streamer discharge. The distribution of electrons, ions and electric field, current evolution, criterion of breakdown and streamer velocity are acquired.

**Numerical Method:** The hydrodynamic fluid model is adopted in this paper. It consists of the continuity equations for electrons, positive ions and negative ions (to account for the development of the space-charge) and Poisson's equation (to account for the modification of the electric field due to space-charge). The continuity equations in their multidimensional form are:

$$\begin{aligned}\frac{\partial N_e}{\partial t} &= S + N_e\alpha |\mathbf{W}_e| - N_e\eta |\mathbf{W}_e| - N_eN_p\beta_{ep} - \nabla \cdot (N_e\mathbf{W}_e - D\nabla N_e) \\ \frac{\partial N_p}{\partial t} &= S + N_e\alpha |\mathbf{W}_e| - N_eN_p\beta_{ep} - N_nN_p\beta_{np} - \nabla \cdot N_p\mathbf{W}_p \\ \frac{\partial N_n}{\partial t} &= N_e\eta |\mathbf{W}_e| - N_nN_p\beta_{np} - \nabla \cdot (N_n\mathbf{W}_n)\end{aligned}\quad (1)$$

where  $t$  is the time,  $N_e$ ,  $N_p$  and  $N_n$  are the charge densities for electrons, positive ions and negative ions.  $\mathbf{W}_e$ ,  $\mathbf{W}_p$  and  $\mathbf{W}_n$  are the drift velocities for electrons, positive ions and negative ions, respectively and  $D$  is the electron diffusion coefficient which are all functions of reduced electric field  $\mathbf{E}/n$ ,  $n$  is the neutral gas number density. The symbols  $\alpha$ ,  $\eta$ ,  $\beta_{ep}$  and  $\beta_{np}$  denote the ionization, attachment, electron-positive ion recombination and negative-positive ion recombination coefficients, respectively. The term  $S$  is the source term due to photoionization and cathode secondary emission.

Poisson's equation is given by

$$\nabla \cdot (\varepsilon_r \nabla \phi) + \frac{e}{\varepsilon_0} (N_p - N_n - N_e) = 0 \quad (2)$$

where  $\varepsilon_0$  is the dielectric constant of free space,  $\varepsilon_r$  the relative permittivity,  $e$  the electron charge and  $\phi$  the electric potential.

The finite element-flux corrected transport (FE-FCT) algorithm is adopted for the continuity equations. Poisson's equation is solved using standard Taylor-Galerkin method. In the calculation, the adaptive meshing and parallel computing methods were also adopted to improve the computing efficiency.

**Result:** Using the method above, the initial stage of gas discharge of 1 cm paralleled plane gap is simulated first to study the details of development of avalanche and the formation of Townsend or streamer discharge. When the applied voltage is higher than 32 kV, the avalanche is formed

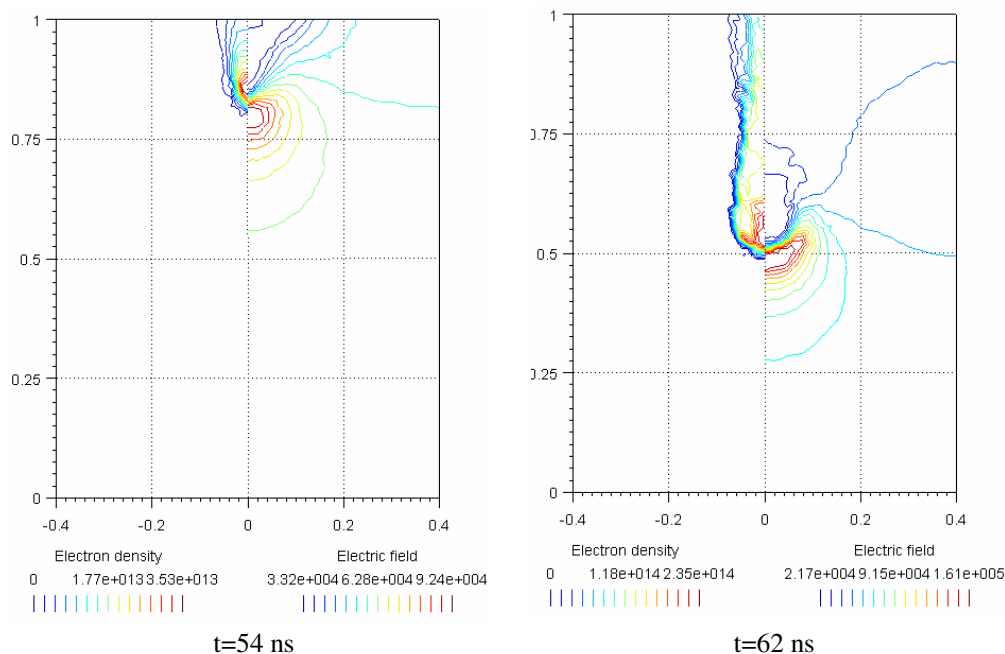


Figure 1: Streamer propagation, the left half is the contours of electron density ( $\text{cm}^{-3}$ ), the right half electric field (V/cm).

and Townsend breakdown is observed. If the voltage is higher than 38 kV, the discharge appears as streamer discharge, as is shown in Figure 1. The  $x$ -coordinate is the radial distance from the center of the plane while the  $y$ -coordinate is axial distance from cathode.

From the figure we can see the electron density of first avalanche increases to be  $10^{13} \text{ cm}^{-3}$  when it reaches the anode, the space charges sharply intensify the electric field below the avalanche head to about 80 kV/cm, then streamer forms.

The influence of gap length on discharge mechanism is also investigated. When the gap length increases, each avalanche travels longer distance in electric field, so its density can increase to the criterion of formation of streamer under lower voltage. When the gap length increases to 3 cm, streamer is observed under 30 kV/cm electric field in our simulation.

## Genetic Algorithms for Automated Design of the Multilayer Absorbers in the X-Band and Incident Angle Range

N. Lassouaoui, H. Hafdallah Ouslimani, and A. Priou

University Paris X, Nanterre, Pole Scientifique and Technique, Ville d'Avray  
Applied Electromagnetism Group (GEA) 50  
rue de Sèvre 92410, Ville d'Avray, France

**Abstract**— In this paper, we developed genetic algorithms (Gas) to find the thicknesses, the electric and magnetic constants of the multilayer absorbers blades. We optimize the geometrical and physical properties of the multilayer absorbing structure that can minimize the reflection coefficient on a wide frequency band as well as for a wide incidence angle. In this multidimensional research, we construct an electromagnetic analysis and a synthesis method.

The electromagnetic analysis deals with the electromagnetic problem and necessitates the exact or the approximate calculation of the reflection parameter ( $S_{11}$ ). In the case of the studied flat layers absorbing structure, the literature proposes several methods allowing an exact computation of  $S_{11}$ :

- using Parratt's recursion and Fresnel equations,
- using the input impedance [1],
- using the transfer matrix and layer matrix of each slab layer [2].

For the synthesis method accomplished by the GAs [3, 4], the parameters are calculated according to the diversity of the populations in order to ensure a best exploration of research space and an automatic genetic processing. At the first beginning, we generate randomly a fixed number of solution candidates. We follow two steps:

- Optimization according to the frequencies for a fixed incidence angle  $\theta_i$ : for each candidate and each frequency, we point out the worst case corresponding to the poor reflectivity (maximum reflectivity in dB) witch can measure the minimal expected performance in this frequency band.
- Optimization according the incidence angles: for a fixed frequency, the final solutions of the last step (1) are used. The same optimization process is engaged for each candidate for variable incidence angle (from 0 to  $\pm 90$  deg).

Figure 1 shows the obtained results (worst cases) for the transverse electric (TE) mode with a three layers absorbing structure over the X-band frequency and total angular band. The GAs optimize 15 variables since each layer is characterized by the thickness, the real and imaginary parts of the permittivity ( $\epsilon$ ) and the permeability ( $\mu$ ). For energy constraints, we select positive Imaginary parts of  $\epsilon$  and  $\mu$ . We achieve  $-80$  dB for a normal incidence at 10 GHz. For the angular evolution, the performance decreases when we approach the grazing incidence angle.

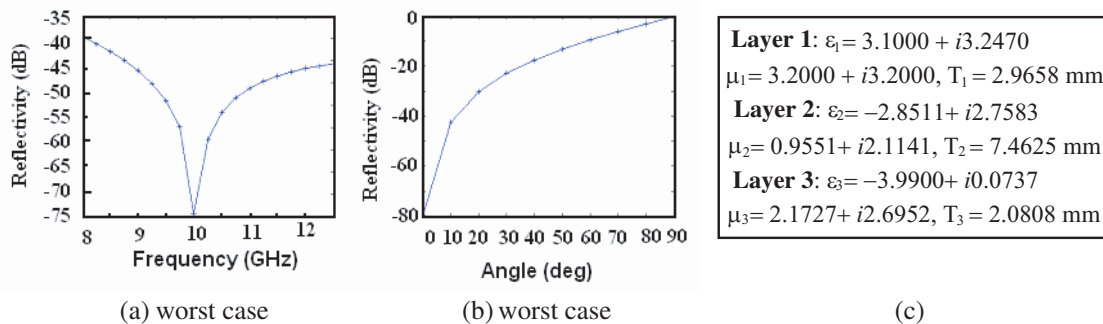


Figure 1: TE Mode; (a) frequency response, (b) angular response of obtained configuration (c).

**REFERENCES**

1. Vinoy, K. J. and R. M. Jha, *Radar Absorbing Materials*, Kluwer Academic Publishers, 1996.
2. Petit, R., *Electromagnetic Waves in Radio Electricity and Optics*, Masson Edition, 1992.
3. Hall, J. M. "A novel, real-valued genetic algorithm for optimizing radar absorbing materials," NASA/CR-2004-212669, March 2004.
4. Goldberg, D. E., *Genetic Algorithms in Search, Optimization and Machine Learning*, Addison-Wesley, 1989.

## A Novel Analysis for Circular-groove Guide

**Yinqin Cheng**

Northwest University for Nationalities, China

**Abstract**— Using method of moment, the circular-groove guide has been studied. The characteristic equation of circular-groove guide has been gotten with this method. The transmission characteristics of the dominant mode have been obtained and discussed.



## PIC Simulation of Surface Charging in the Wake Zone

J. Wang, J. W. Qiu, and X. G. Qin

National Key Lab. of Vacuum & Cryogenics Technology and Physics  
Lanzhou Institute of Physics, Lanzhou 730000, China

**Abstract**— Space charging process in the wake zone is reviewed and calculated with particle-in-cell (PIC) simulation under the interactions of two-plate and plasma in auroral region. Because of low ion ratio in the wake of large space structures, encountering high energy auroral electron and less secondary electron emission, small body in the wake may be charged to high negative voltages, which seriously influences spacecraft docking or extravehicular activity of astronauts.

A model of two-body immersing in the macro ion and electron flows is built in the paper to numerically simulate the interaction of two-body with auroral plasma. These macro particles move in manner of 2-D electrostatic PIC algorithm, which solves Poisson equation with leap-frog format. In the two-plate model, a large conductor denotes spacecraft and a small insulator denotes free flyer all keeping relative stationary in LEO/PEO while macro particles spreads with resultant velocity. The secondary electron emission from the surface of small body is treated as an inner boundary condition. Another inner condition is that the conductor only emits backscatter electron while ambient electron injecting. The surface charging voltages of the two bodies are calculated with current balance equations to simplify the calculation and shorten computing time.

The simulation provides a quantitative estimation of electric field of the existence of the wake zone as well as charging voltage of the free body in the wake zone. It also validates that the same severe charging conditions as literatures described are indispensable to achieve several kilovolts voltage of the small body in the wake zone.

## The Optical Spatial Comb

Tao Duan<sup>1,3</sup> and Chun-Fang Li<sup>1,2</sup>

<sup>1</sup>State Key Laboratory of Transient Optics Technology, Xi'an Institute of Optics and Precision Mechanics  
Academia Sinica, Xi'an 710119, China

<sup>2</sup>Department of Physics, Shanghai University, 99 Shangda Road, Shanghai 200444, China

<sup>3</sup>Graduate School of the Chinese Academy of Sciences, Beijing 100049, China

**Abstract**— When a beam of light is incident on a plane-parallel dielectric slab surrounded by transparent medium a series of reflection (or transmission) beams will be emerging on each side of the slab. However, the amplitudes are continuously divided by the surface of the dielectric slab, so the amplitude of the reflection beams diminish and become about zero quickly. If the dielectric slab has active (gain) or absorptive (attenuation), the interesting phenomena will occur. The reflection of a beam on a lower-index absorptive medium at greater than the critical angle is known as the attenuated total internal reflection(ATIR)where the reflectivity is less than unity. On the contrary, the reflected beam is more intense compared to the beam that is incident on a lower-index active medium, which is the enhanced total internal reflection effect (ETIR). As a result, the amplitude of a series of reflection light beam will be amplified when the incident light beam is through the isotropic optically active dielectric slab of lower refractive index surrounded by transparent medium at lower than the critical angle. It will be shown that the optical spatial comb emerges on the each side surface of the isotropic optically active dielectric slab. That is to say, a series of amplified reflection (or transmission) light beam of the same amplitudes and the same spatial distance between adjacent beam on condition that the active index of the active dielectric slab, the incident angle and slab thickness are choice properly.

## Analysis of High Frequency Interference in Antennas by Implementation of a Novel Efficient Hybrid TLM Method

M. Bahadorzadeh and M. Naser Moghaddasi

Department of Electrical Engineering, Islamic Azad University  
Science & Research Campus, Hesarak, Tehran, Iran

**Abstract**— A new method for analysis of interference in high frequency has been used for evaluation of the interference of two loop antennas. The method is based on the Transmission Line Matrix (TLM) method augmented with a time-domain integral equation Formulation to account for the radiation of equivalent source and to evaluate the interfering electromagnetic fields. A comparison between this method which is referred as the IRIS method (Interference and Radiation of Internal Surfaces) and different approaches for the Analysis of Interference has been performed. The result of classical TLM analysis and the IRIS method analysis for interfering of loop antennas has been represented.

# Asymptotic Expansion of the Scattering Problem by a Rough Periodic or Doubly Periodic Surface

J.-R. Poirier<sup>1</sup>, A. Bendali<sup>2</sup>, and P. Borderies<sup>3</sup>

<sup>1</sup>LAME-ENSEEIH-INPT, 2 rue Charles Camichel, 31071 Toulouse cedex, France

<sup>2</sup>IMT, INSA, Complexe Scientifique de Rangueil, 31007 Toulouse Cedex 4, France

<sup>3</sup>ONERA, 2 avenue Edouard Belin, 31055 Toulouse Cedex 5, France

**Abstract**— Scattering of electromagnetic waves by rough surfaces is for long a research topic of great interest with recently an increasing trend due for instance to the strong demand from the remote sensing community. To avoid heavy computations which may rapidly become intractable when the surface under consideration is rapidly oscillating or presents some multi-scale features, it is desirable to incorporate the effects of the small details through an homogenization process. A method to build an asymptotic expansion of the field incorporating the effect of rapid variations of a perfectly conducting surface on the scattering of a scalar, E-polarized, time-harmonic electromagnetic wave has been previously developed [1, 2]. The derivation of the asymptotic expansion is based on a decomposition of the field in two parts. The first part describes the overall behavior of the wave and the second one deals with its small scale variations. The asymptotic expansion is rigorously constructed for periodic surfaces presenting a large-scale global periodicity to suppress the boundary effects and a small local period to describe the rapid variations.

The present work presents a convergence study for the impedance boundary condition obtained from an asymptotic expansion of the field. The study is done in terms of several numerical experiments. We consider a model surface with rapid oscillations which can be represented by a function with two-scale variations. The amplitude and the extent of the variations are assumed to be comparable to each other and small as compared to the wavelength. In the case of periodic surface, the field can be obtained through a Floquet expansion and the convergence of the field, outside a zone near to the surface, can be naturally coincides with that of propagative modes.

We will show that the homogenization process yields accurate results and converges at the expected rate of convergence. We also present the computation time which has been used to obtain the solution of the homogenized problem, hence illustrating the efficiency of the method, in particular for a surface with a small height and very oscillating variations.

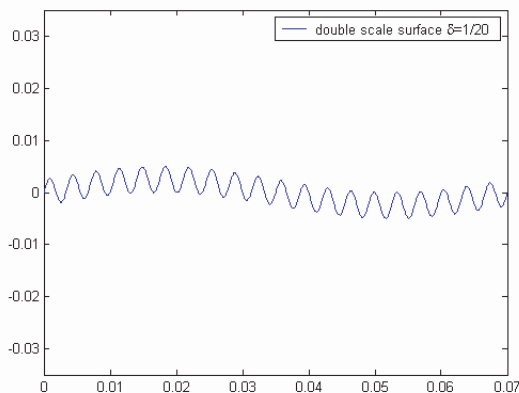


Figure 1: Double scale surface.

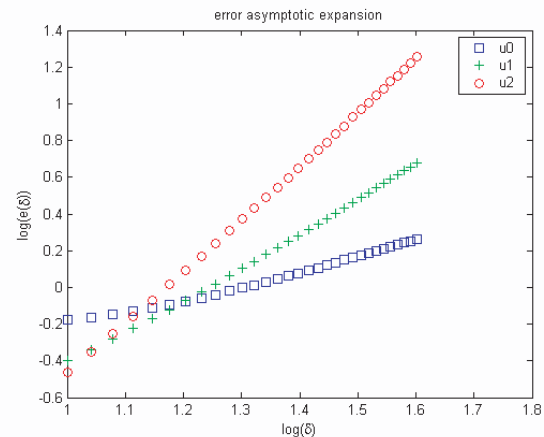


Figure 2: Log scale convergence curves.

## REFERENCES

1. Poirier, J.-R., A. Bendali, and P. Borderies, "Impedance boundary conditions for the scattering of time harmonic waves by rapidly varying surfaces," *IEEE Transactions on Antennas and Propagation*, Vol. AP-54, No. 3, Aug. 2006.
2. Poirier, J.-R., "Modélisation électromagnétique de effets de rugosité surfacique," thèse de doctorat, soutenue le 14 décembre, 2000.

# Physics Based Time Domain Simulation of Magnetic Recording Signal and Noise

Xiaobin Wang<sup>1</sup>, Zhen Jin<sup>2</sup>, Xuebing Feng<sup>1</sup>, and Dimitar Dimitrov<sup>1</sup>

<sup>1</sup>Seagate Technology, Bloomington, USA

<sup>2</sup>Hitachi Global Storage Technology, San Jose, USA

**Abstract**— Simulating accurate signal and noise waveform from basic recording head and media parameter is a challenge task. This paper reports the progress of a fast time domain simulator for magnetic recording signal and noise. The simulator is a combination of recording physics calculation [1, 2], micro-magnetic simulations [3] and experimental data information extracting [4]. The simulator takes physics parameters as inputs and can be calibrated to measurements at current density and scaled to recording system at higher density. It can generate millions of bits in short times, suitable for equalized SNR and channel BER simulation. In order to illustrate our techniques of generating signal and noise waveforms from basic recording physics parameters, the paper is focused on following topics: 1) newly developed formula to calculate transition noise considering physics limitations at high recording density and its calibration to micro-magnetic simulation. 2) Synthesizing time domain position-dependent transition jittering noise and colored electronic noise from measurement data. 3) Non-saturation DC noise treatment and its effects on equalized SNR. 4) Simulation of head jittering noise.

## REFERENCES

1. Wang, X. and N. H. Bertram, “A simple transition parameter expression including grain size and intergranular exchange,” *Journal of Applied Physics*, Vol. 93, No. 10, 7005–7007, May 2003.
2. Jin, Z., X. Wang, and N. H. Bertram, “An analytical model for the cross-track correlation length including inter-granular interactions,” *IEEE Transactions on Magnetics*, Vol. 39, No. 5, 2603–2605, Sept. 2003.
3. Internal code from Seagate
4. Wang, X., X. Feng, Z. Jin, and J. Fernandez-de-Castro, “Effects of reader response on medium noise modes,” *Journal of Applied Physics*, Vol. 99, No. 8, p08k502, 2006.

## Ferroelectric Properties of Pulsed Laser Deposited Thin Films for Detecting Electromagnetic Waves

H. F. Cheng<sup>1</sup>, P. T. Joseph<sup>2</sup>, C. C. Hung<sup>1</sup>, Y. W. Chen<sup>1</sup>  
N. H. Tai<sup>2</sup>, and I. N. Lin<sup>3</sup>,

<sup>1</sup>Department of Physics, National Taiwan Normal University, 116, Taiwan

<sup>2</sup>Department of Materials Science and Engineering, National Tsing Hua University, 300, Taiwan

<sup>3</sup>Department of Physics, Tamkang University, 251, Taiwan

**Abstract**— Ferroelectric properties of pulsed laser deposited (PLD)  $x(0.94\text{Pb}(\text{Zn}_{1/3}\text{Nb}_{2/3})\text{O}_3 + 0.06\text{BaTiO}_3) + (1-x)(1-y)\text{PbZrO}_3 + y\text{PbTiO}_3$  (PBZNZT) ( $x = 0.6$ ,  $y = 0.52$ ) thin films were investigated in this work. Buffer layers of  $\text{Ba}(\text{Mg}_{1/3}\text{Ta}_{2/3})\text{O}_3$  (BMT) thin films were deposited on to substrates prior to the fabrication of PBZNZT thin films. We have found that, the variation of the oxygen pressures in the PLD process for fabricating BMT buffer layers greatly influenced the coercive field ( $E_c$ ) of the prepared PBZNZT thin films. The value of  $E_c$  was decreased from around 522 kV/cm to 422 kV/cm with the increased oxygen pressure from 0.5 mbar to 0.9 mbar. The detailed calculation of electrical properties from the ferroelectric properties of PBZNZT thin films were also carried out and reported. Furthermore, this study suggests that PBZNZT thin film materials are potential candidate for electromagnetic waves detecting applications.

## Ferroelectric Properties of Nanostructured SBLFT Thin Films Prepared by Pulsed Laser Ablation

P. T. Joseph<sup>1</sup>, N. H. Tai<sup>1</sup>, H. F. Cheng<sup>2</sup>, and I. N. Lin<sup>3</sup>

<sup>1</sup>Department of Materials Science and Engineering, National Tsing Hua University, Hsinchu, Taiwan

<sup>2</sup>Department of Physics, National Taiwan Normal University, Taipei, Taiwan

<sup>3</sup>Department of Physics, Tamkang university, Tamsui, Taiwan

**Abstract**— Nanostructured ferroelectric  $\text{SrBi}_{4.25}\text{La}_{0.75}\text{FeTi}_4\text{O}_{18}$  (SBLFT) thin films have been synthesized using pulsed laser ablation technique. The thin films of SBLFT materials were grown on Pt(111)/TiO<sub>2</sub>/SiO<sub>2</sub>/Si substrates for electrical measurement and analysis. The crystalline structure and microstructure of SBLFT thin films were examined and determined, respectively, using x-ray diffraction (XRD) and field emission scanning electron microscopy (FESEM). The XRD results show that the films are in (1111) preferred orientation. The grain size of prepared SBLFT thin films is lesser than 100 nanometers, which was confirmed from the FESEM images. The SBLFT thin films have exhibited room temperature ferroelectric properties with saturated electric polarization ( $P_s$ ) of  $8.0 \mu\text{C}/\text{cm}^2$ , and coercive electric voltage ( $V_c$ ) of 2.5 V. The results imply that SBLFT ferroelectric thin films have potential applications in nano devices such as electro-optic detectors and ferroelectric random access memories.

## Modeling of Electron Beam — Bragg Gratings Interaction

Artem A. Balyakin and Elena V. Blokhina

Saratov State University, 83 Astrakhanskaya st., Saratov 410012, Russia

**Abstract**— We present the results of numerical simulation of interaction between electron beam and periodic structure (Smith-Parcell effect) for 2-D case. Two models are considered: the infinitely narrow electron beam and the beam of a finite width. We discuss both linear and nonlinear case. The obtained results show the possibility to excite the electromagnetic wave in a periodic structure.

In recent years the opportunity to construct vacuum microwave amplifiers and oscillators, operating in terahertz band and using traditional for microwave electronics mechanisms of electron beam interaction with electromagnetic wave has attracted a great interest. One strives to create the analogues of conventional vacuum electron devices (BWO, TWT, klystrons), as well as devices of a new type, with typical waveguide structure of micron size. The importance of terahertz radiation is connected with perspectives to use it in spectroscopy, medicine, information processing and transmission.

Here we discuss one of perspective schematics of such devices, where a sheet electron beam interacts with a field of periodic dielectric structure (in particular, nonlinear one). Actually, such a device is a kind of orotron (amplifier and oscillator using Smith-Parcell radiation that, in fact, is one of a type of Cherenkov's radiation). We emphasize that although it utilizes the traditional interaction mechanism of O-type, the direct application of existing TWT theories is difficult, since the beam and waveguide structure cannot be described in terms of 1-D model. Thus we developed a 2-D code using FDTD method to directly solve Maxwell's equations in such a system.

We modeled open system where boundary conditions are put in a form of so called perfectly matched layers. The parameters of the system were chosen to describe real devices (period of Bragg gratings  $0.5 \mu\text{m}$ , width of the system  $6.275 \mu\text{m}$ , frequency corresponding to Bragg resonance  $2 \cdot 10^{14} \text{ Hz}$ ). We present the results of numerical simulation for the following models. First, we considered rather simple model when periodic structure is linear and electron beam has an infinitely narrow width (in computer modeling equal to one step of space discretization). Second, we discuss the electron beam having a width comparable with the period of the structure. Our results prove that such a system can operate in a terahertz diapason. Then we introduce nonlinearity in the system. In that case with the increase of the electron beam intensity the amplitude of the excited radiation in the structure also grows that can lead to the shift of a dispersion curve and thus the regimes of gating and non-gating can be observed.

### ACKNOWLEDGMENT

The authors thank A.G. Rozhnev, and N.M. Ryskin for useful discussions. This work was supported by the RFBR grants 06-02-16773. A.A. Balyakin's work was also supported by CRDF grant Y3-P-06-02.



## PIC Simulation of Surface Charging in the Wake Zone

J. Wang, J. W. Qiu, and X. G. Qin

Lanzhou Institute of Physics, China

**Abstract**— In order to realize the levitation of the globe the authors utilize the hybrid-excited magnets to take advantages of permanent magnet and electrical magnet. The former has the characteristics of economic energy, working dependably, the simple construction and high efficiency, and the later has the advantage that the magnetic field can be controlled well. The authors study the working principle and the mathematical model of the system by the methods of the mechanics analysis and theoretical calculation and obtain parameters based on experiments. According to the data the authors deduce the transfer functions of the controlled globe and system. The authors utilize a PDF (Pseudo-Derivative-Feedback) control arithmetic to design the PDF controller which has no high qualification to the mathematical model. The authors also analyses the systemic stability, robustness and the control precision. The study shows the PDF control method is predominant in the engineering application to the nonlinear and instable system. The method has the characteristics of robustness and high control precision.

## Study on a Novel Permanent Magnet Retarder for Vehicles

L. Z. Ye, D. S. Li, Z. Y. Lu, and Q. H. Guo

School of Mechanical Engineering and Applied Electronics Technology  
Beijing University of Technology, China

**Abstract**— This paper proposes a novel permanent magnet retarder (PMR) whose the stator subassembly is a magnetic equipment having independent work system. We focus on designing and analyzing its structural parameters. It is simple and feasible that optimize the structural parameters of the magnetic equipment by using magnetic circuit design method, but the precision of the result is not enough. We can get the relative curve between the structural parameters and its magnetic force by using the finite element method (FEM). According to the optimal parameters we design four kinds of magnetic equipment of PMR. Compared with the analytical and experimental results, it is confirmed that FEM is suitable for optimizing the structural parameters of magnetic equipment.

## Research on a Maglev Ball Control System Based on DSP2812

Q. H. Guo, D. S. Li, Z. Y. Lu, W. Wang, and L. Z. Ye

College of Mechanical Engineering and Applied Electronics Technology  
Beijing University of Technology, Beijing 100022, China

**Abstract**— As the basis of maglev technology, a single freedom ball suspension control system with hybrid electromagnets is introduced in this paper. According to the physical model of the system we designed, the linear model and control strategies were established and analysed. A fixed-point digital signal processor TMS320F2812 is chosen as the controller of the system for its high speed and high efficiency of calculation and control. A/D module and the eventmanager(EV) module are used in the system. PID algorithm which is applied frequently in industry is adopted and DSP's output signal — PWM signal is used to control the driver. Both the simulation by matlab and actual control results show the magnet suspension system works well.

## Key Technologies for Lidar Detecting Stealth Targets

Bin Zhu<sup>1</sup>, Jing Zhang<sup>2</sup>, Yan Chen<sup>2</sup>, Ke Deng<sup>2</sup>  
Dagang Jiang<sup>2</sup>, Peng Zhang<sup>2</sup>, Zoushi Yao<sup>2</sup>, and Wei Hu<sup>2</sup>

<sup>1</sup>Chengdu University, Chengdu 610106, China

<sup>2</sup>University of Electronic Science and Technology of China, Chengdu 610054, China

**Abstract**— Detecting and tracking stealth targets have drawn more and more attention. With the advantages of high resolution and anti-jamming to mature radar technologies, the lidar has become a new and unique radar mechanism. Key technologies of lidar detecting stealth target have been proposed based on two methods called multi-band and multi-static anti-stealth. The combination of the visible, infrared and laser technologies can improve the detection probability of stealth targets.

# Enhancement of Microwave-assisted Organic Reactions Using Active Carbon

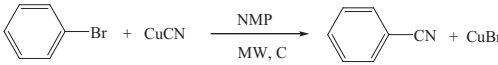
Zhibin Li, Jianhua Chen, Haisheng Xu, Shan Hu, and Dong Shen

Laboratory of Chemical Physics, East China University of Science and Technology  
Shanghai 200237, China

**Abstract**— Microwave has been widely used in synthetic chemistry to reduce reaction time and increase product yield. However, when the reaction substrate and solvent are unpolar, it does not work because of the poor absorption of microwave. To solve this problem, ionic liquids and cylinders of sintered silicon carbide were used in unpolar microwave reactions.

Here we reported the use of active carbon to enhance the microwave-assisted organic reactions. Active carbon has strong absorption of microwave and can be heated up very rapidly under microwave irradiation so can be used as energy-transfer medium to heat the reaction mixtures. Cyanation of bromobenzene and Diels-Alder reaction of anthracene with diethyl maleate were chosen to study the effect in an open vessel. The results showed that active carbon significantly enhanced the microwave reactions with medium polarity from middle to low, especially for low polar or nonpolar reactions which were not working under microwave irradiation, active carbon helped finish the reaction within a short time. Active carbon is stable, easily available, convenient to use and their waste disposal is easy and environment friendly, so it is reasonable to expect this method to have great application in organic chemistry.

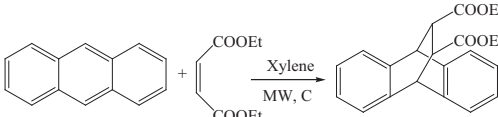
Table 1: The yields of adding different quantities of active carbon in different irradiation time.



C (g)	Y (%) <sup>a</sup> (40 min.)	Y (%) (60 min.)	Y (%) (80 min.)
0.0	11.49	51.04	95.19
0.2	45.74	93.25	96.62
0.3	47.58	96.77	97.67
0.4	48.15	96.86	97.64

<sup>a</sup> Conversion.

Table 2: The yields of adding different quantities of active carbon in different irradiation time.



C (g)	Y (%) <sup>a</sup> (40 min.)	Y (%) (80 min.)
0.0	0.0	0.0
0.3	37.5	82.1
0.4	39.4	84.1
0.4 <sup>b</sup>		89.8

<sup>b</sup>500 W power, 76 min. irradiation time were employed.

Tables 1, 2 were the results of the reactions, for the cyanation of bromobenzene the yields with shorter reaction time were significantly improved by adding active carbon, and for the Diels-Alder

reaction of anthracene with *cis*-diethyl maleate, in the absence of active carbon due to the weak microwave absorption of xylene, the reaction did not work after 80 min (300 W) irradiation and no anthracene consumption was detected by NMR. When 0.3 g active carbon was added, the mixture refluxed after 20 min. irradiation and 82.1% of anthracene consumed (determined by NMR) after 80 min.. With stronger power (500 W) and more active carbon (0.4 g), the consumption of anthracene was increased to 89.8% after 76 min. irradiation (Employing high power could damage the reactor in the case of low microwave absorption!). A test for investigating the effect of active carbon on nonpolar reaction was performed by the Diels-Alder reaction of anthracene with *trans*-dibutyl fumarate in p-xylene. 0.4 g active carbon and 400 W of power were employed, after irradiation for 80 min., 85.6% consumption of anthracene was reached.

## A Comparison of SRTM and CALIPSO Super-resolution Lidar Altimetry

Yongxiang Hu

NASA Langley Research Center, USA

**Abstract**— Land surface elevation derived from Shuttle Radar Topography Mission (SRTM) is compared with the surface elevation derived from space-based lidar measurements over every continent of the globe where SRTM data are available. The lidar altimetry data are derived from the Cloud-Aerosol Lidar and Infrared Pathfinder Satellite Observation (CALIPSO) spacecraft using a technique we refer to as Elevation Information in Tail (EIT) [1], developed to provide improved lidar altimetry from space-based lidar data. The EIT technique is demonstrated using CALIPSO data and is applicable to other similar lidar systems with low-pass filters. The technique relies on an observed relation between the shape of the surface return signals (peak shape) and the detector photo-multiplier tube transient response (transient response tail). Application of the EIT to CALIPSO data resulted in at least an order of magnitude or better improvement in the CALIPSO land surface 30-meter elevation measurements. The results of EIT compared very well with the elevation measurements from the Shuttle Radar Topography Mission (SRTM) over all continents of the globe.

### REFERENCES

1. Hu, et al., “Elevation in Tail (EIT) technique for lidar altimetry,” *Optics Express*, 2007, submitted.

## Universal Radio Frequency Identification Sensing System

J. H. Lin, J. L. Sun, T. H. Su, and P. F. Hsieh  
BeeDar Technology Inc., Tainan County 741, Taiwan

**Abstract**— In recent years, contactless radio frequency identification (RFID) systems have received much attention in security, logistics and medical fields. The RFID system is constructed by readers and tags. The passive tags are powered by rectification of the radio signal sent by the reader. A RFID tag which can be integrated with a sensor for temperature, pressure or bio-signal is developed in this work. When tag with sensor is implanted inside animal or human body, HF or UHF radio signal is suitable to be chosen as the power source of the tags. Because some kinds of sensors consume higher driving current, the tags need to receive more power to let the sensors work normally. So the readers should transmit higher power to fulfill the power requirement of the tags. The high power of HF or UHF radio signal may cause uncertain harm for animal or human body. The 125 kHz low frequency radio frequency identification (RFID) tag structure based on ISO 18000-2 is chosen for the basis of this system. The block diagram of the Universal Radio Frequency Identification Sensing System is shown as Fig. 1. An internal digital to analog (D/A) converter designed to perform the analog to digital (A/D) function with a comparator and successive-approximation algorithm executed by the digital control unit. The n bits resolution of the built-in internal D/A determines the maximum resolution of the A/D function. The number of bits of A/D resolution can be configured via the reader with a protocol and be stored within the universal radio frequency identification sensing system's memory, such that the successive-approximation algorithm does not need to go all the way though to n bits of resolution. The universal radio frequency identification sensing system is configured and embodied to transmit an indicative signal of an analog measuring device by using RFID communication method.



Figure 1: Universal radio frequency identification sensing system.

### REFERENCES

1. US Patent US 11/162,410, BeeDar Technology Inc.



## Passive Radar Imaging Based on Correlation Motion Compensation

Xiaoyan Fan, She Shang, Wei Ma, Jie Li, and Xuan Li

National Key Laboratory of Space Microwave Technology  
Xi'an Institute of Space Radio Technology, Xi'an 710100, China

**Abstract**— A novel method of passive radar imaging for moving target, which uses external illuminators as its transmitters, has become an interesting research. There exist several external illuminator based algorithms for passive radar imaging, such as polar coordinate algorithm, convolution reverse projection algorithm and direct FFT algorithm. All the algorithms are accomplished by using single/multiple illuminator and single/multiple receiver to analyze the relation of received signal and target scattering function in passive radar imaging system. These algorithms are based on turntable model but motion compensation is not considered. In fact, motion component can make image defocus in range and azimuth direction. Until now, there is a cross-correlation algorithm, minimum entropy and keystone transformation algorithm for motion compensation algorithm of target imaging by using wideband pulse signal. No attentions have been made on the narrow-band continues broadcast or television signal.

This paper presents a new motion compensation algorithm based on passive radar imaging. The algorithm uses the maximal value of the correlation function between the two adjacent echoes to estimate the compensation factor, and then reconstructs target image using the direct FFT algorithm. Simulation results show that the algorithm can achieve a better performance for an actual target moving model than traditional method.

When motion factor is considered, a few factors such as direction and velocity of target motion, television station position and receiving station position affect the bistatic angle which is the main factor of imaging. A better image can be obtained by reasonable placed stations, which limit the action scope of system. That is, the target which flies in a certain scope of direction can just be imaged. Theoretically, the problem can be resolved by adding the amounts of receiving station. There are several other factors on passive radar imaging, such as analyses of signal waveform, effect of direct wave, and low signal noise ratio, which demand further research.

## Enhancement Gradient Pulse Waveforms in MR Tomography

E. Gescheidtova and R. Kubasek

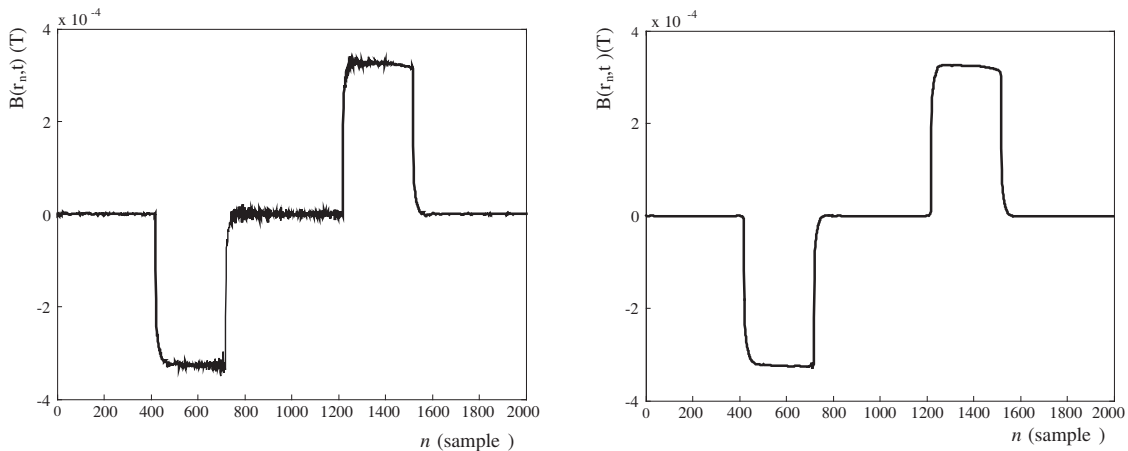
Department of Theoretical and Experimental Engineering  
Faculty of Electrical Engineering and Communication, Brno University of Technology  
Kolejni 2906/4, 612 00 Brno, Czech Republic

**Abstract**— The magnetic resonance (MR) imaging techniques of tomography and spectroscopy are exploited in many applications. For the MR instruments to function properly it is necessary to maintain a high quality of homogeneity of the fundamental magnetic field. The pre-emphasis compensation of the generated gradient field increases the homogeneity of the generated magnetic field and reduces the minimum switching times of the gradients. This enables measuring the MR images of incisions in the human body, the relaxation properties of nuclei, self-diffusion processes, flows of liquids and movements of solids faster and more accurately.

When defining the area being measured in localized spectroscopy and tomography, the gradient field is excited by very short pulses of sufficient magnitude. This gives rise to a fast changing magnetic field, which induces eddy currents in the conducting material near the gradient coils. These currents then cause retrospectively unfavourable deformation of the total magnetic field. The effect of eddy currents acts against the fast temporal changes in the magnetic field. The basic idea of a method that compensates this effect consists in replacing the missing leading edge of the field waveform by an overshoot of excitation current.

To have the best possible compensation it is necessary to find an optimum shape of excitation pulse. Basically, this consists in obtaining the spectrometer response pulse, inverting it and using this inversion to filter the excitation (usually square) pulse. The term pre-emphasis compensation method is based on the fact that the compensation filter is in the nature of a differentiating element (high-pass filter).

At the present time, pre-emphasis filters are implemented by digital means, most frequently digital signal processors. At the Institute of Scientific Instruments, Academy of Sciences of the Czech Republic in Brno, pre-emphasis filters are implemented on a Motorola 96002 DSP as a fifth-order IIR filter in the first canonical form.



Measured waveform of magnetic inductance and waveform of magnetic inductance after denoising filtering.

The application of pre-emphasis compensation of gradient magnetic field has led to a qualitative improvement in the parameters of the magnetic field generated in an MR tomograph. It can therefore be expected that better results will be obtained in all regions of MR tomography and spectroscopy where the generation of gradient fields of a defined waveform with minimum switching times is required. Today the minimum applicable switching time of gradients in MR tomography is a limiting factor in the application of fast imaging sequences in MRI. Shortening the gradient edges and improving the magnetic field homogeneity after a gradient impulse result in shortening the minimum applicable switching time of magnetic field gradients and the waiting time between gradient impulses, when the magnetic field is required to drop to the level of the homogeneity of the basic magnetic field  $B_0$ . In that case the images of incisions in the human body can be measured faster and more accurately.

## A Study on Electronic Nose System Based on Integrated Gas Sensors Array and Support Vector Machine

Guiling Huang<sup>1,2</sup>, Qida Zhao<sup>1</sup>, Luming Zhao<sup>1</sup>, Shuhong Li<sup>1</sup>, Yinping Miao<sup>1</sup>  
Jiping Liao<sup>1</sup>, and Fei Wang<sup>1</sup>

<sup>1</sup>Institute of Modern Optics, Nankai University, Tianjin 300071, China

<sup>2</sup>Institute of Photo electronic Thin Film Devices & Technology, Nankai University  
Tianjin, China

**Abstract**— By using the technology of sensor array and appropriate pattern recognition techniques, the quantitative analysis of gases have become a hot area in the field of sensor research. In this paper, we tried support vector machine(SVM) ,a new algorithm which has not been paid enough attention in a mixed gases (NO<sub>x</sub>, and CO) measurement system based on surface acoustic wave (SAW) sensor array. Traditional classification methods, such as neural network approaches, have suffered difficulties with generalization, producing models that can overfit the data. The SVM approach is considered a good candidate because of its high generalization performance. Acoustic Wave Sensors are useful for a broad range of sensing devices. The SAW consists of two sets of interdigitated fingers at each end of a membrane, one set for generating the SAW and one for detecting it. The surfaces of the SAW devices are useful platforms to convert property changes such as mass into detectable electrical signals. SAW gas sensors are made by applying a thin chemically sensitive film onto the surface of the SAW delay line. In general the detection principle of the SAW gas sensor relies on the change of the SAW velocity upon adsorption of the reactant by the sensor film. This velocity change are related to the following effects: the change in the mass density of the film, the change in its electrical conductivity or the change in its elastic constants. From both theory and experiment, it is indicated that the proposed method can increase effectively the credibility of the sensing data.

## High Vertically Resolved Atmospheric State and Surface/Cloud Parameters Retrieved with IASI Single Field-of-view

Daniel K. Zhou

NASA Langley Research Center, Hampton, VA 23681, USA

**Abstract**— The Infrared Atmospheric Sounding Interferometer (IASI) on the MetOp satellite was launched on October 19, 2006. IASI possesses an ultra-spectral resolution of  $0.25 \text{ cm}^{-1}$  and a spectral coverage from 645 to  $2760 \text{ cm}^{-1}$ . Ultra-spectral resolution infrared spectral radiance obtained from near nadir observations provide atmospheric, surface, and cloud property information. An advanced retrieval algorithm with a fast radiative transfer model, including cloud effects, is used for atmospheric profile and cloud parameter retrieval. This physical inversion scheme has been developed, dealing with cloudy as well as cloud-free radiance observed with ultraspectral infrared sounders, to simultaneously retrieve surface, atmospheric thermodynamic, and cloud microphysical parameters. A fast radiative transfer model, which applies to the clouded atmosphere, is used for atmospheric profile and cloud parameter retrieval. A one-dimensional (1-d) variational multi-variable inversion solution is used to improve an iterative background state defined by an eigenvector-regression-retrieval. The solution is iterated in order to account for non-linearity in the 1-d variational solution. It is shown that relatively accurate temperature and moisture retrievals can be achieved below optically thin clouds. For optically thick clouds, accurate temperature and moisture profiles down to cloud top level are obtained. For both optically thin and thick cloud situations, the cloud top height can be retrieved with relatively high accuracy (i.e., error  $< 1 \text{ km}$ ). Preliminary retrievals of atmospheric soundings, surface properties, and cloud optical/microphysical properties with the IASI observations are obtained and presented. These retrievals are further inter-compared with those obtained from airborne FTS system, such as the NPOESS Airborne Sounder Testbed-Interferometer (NAST-I), dedicated dropsondes, radiosondes, and ground based Raman Lidar. The capabilities of satellite ultra-spectral sounder such as the IASI are investigated.

## Remote Sensing of Atmosphere and Surface Properties from Ultra-spectral Sensors

Xu Liu<sup>1</sup>, Daniel K. Zhou<sup>1</sup>, Allen Larar<sup>1</sup>, William L. Smith<sup>2</sup>, Peter Schluessel<sup>3</sup>

<sup>1</sup>NASA Langley Research Center, MS401A, Hampton, VA 23681, USA

<sup>2</sup>Hampton University, VA 23668 and University of Wisconsin-Madison, Madison, WI 53706, USA

<sup>3</sup>EUMETSAT, Am Kavalleriesand 31, 64 295 Darmstadt, Germany

**Abstract**— The Infrared Atmospheric Sounding Interferometer (IASI) was launched successfully on board the MetOp-A satellite on 19 October 2006. It is an ultraspectral instrument with 8461 channels covering the spectral range from 645 to 2760  $\text{cm}^{-1}$ . We will describe a retrieval algorithm using a Principal Component-based Radiative Transfer Model (PCRTM) for generating atmospheric temperature/moisture/ozone profiles and surface properties (such as surface skin temperature and surface emissivities). The retrieval algorithm performs both the radiative transfer calculations and inversions in the Principal Component (PC) domain. Due to the high computational efficiency of this retrieval algorithm, all 8461 IASI channels are used in the inversion process. The PCRTM calculates the PC coefficients and the associated Jacobian in the compressed PC space directly. Channel radiances can be obtained simply by a linear combination of significant PC vectors using the PC coefficients as weights. The inversion algorithm is based on a non-linear Levenberg-Marquardt method with climatology covariance matrices and *a priori* information as constraints. One advantage of this approach is that it uses all information content from the ultraspectral data so that the retrieval is less sensitive to instrument noise and eliminates the need for selecting a sub-set of the channels. We will also use data collected during the Joint Airborne IASI Validation Experiment (JAIVEx) field campaign to validate the algorithm and IASI retrievals.

## Three-scale Radar Backscattering Model of the Ocean Surface Based on Second-order Scattering

Ying Yu<sup>1,2</sup>, Xiao-Qing Wang<sup>1</sup>, Min-Hui Zhu<sup>1</sup>, and Jiang Xiao<sup>1</sup>,

<sup>1</sup>National Key Laboratory of Microwave Imaging Technology  
Institute of Electronics, Beijing 100080, China

<sup>2</sup>Graduate University of Chinese Academy of Sciences, Beijing 100049, China

**Abstract**— In recent years, airborne and spaceborne imaging radars have received considerable attentions in the area of ocean observation. But it is expensive and difficult to obtain accurate data in the measurement due to complicated conditions on the ocean surface. Therefore, a number of radar backscattering models are given, which have been important approaches in the remote sensing of the ocean.

Based on the second-order composite surface and stochastic multi-scale models, an ocean surface backscattering model is presented in this paper, including both the large-/intermediate-small-scale scattering and the second-order Bragg scattering. Firstly, we get the radar backscatter cross section expression for large-scale surface by means of traditional Kirchhoff method and for intermediate-small-scale surface by simplifying Kirchhoff integral formulation of backscatter. Secondly, we derive the second-order Bragg scattering expressions within this frame, and develop an analytic solution of hydrodynamic modulation function according to weak hydrodynamic interaction theory. In addition, tilt modulation is implemented through the observation angle transform between nominal and local coordinate systems. Finally, we divide ocean surface into intermediate-small-scale and large-scale spectra. The hydrodynamic/tilt modulations of intermediate-small-scale/ Bragg waves by the large ones are calculated accordingly. The hydrodynamic modulation of Bragg waves by intermediate-scale waves in a resolution cell can also be simulated, which is included in the second-order Bragg scattering. The total radar backscatter cross section is the sum of the large-scale, intermediate-small-scale and the second-order Bragg scatter cross section.

The result shows that reasonable agreement between measured and simulated data is obtained, and this model is better than the two models mentioned above. Consequently, this model can provide a reliable means of simulation in remote sensing of the ocean.

## Potentiality of Doppler Spectrum of Backscattered Microwave Signal for Detection of Sea Surface Slicks

Vladimir Karaev, Mikhail Kanevsky, and Eugeny Meshkov

Institute of Applied Physics, RAS  
46 Uljanova str., 603950, Nizhny Novgorod, Russia

**Abstract**— The problem of the detection of films is very important, therefore, intensive investigations in this area are executing in many countries. However, the most of the algorithms are based on the using of normalized radar cross section.

In our paper the analysis of possibilities of Doppler spectrum of microwave radar for detection of slicks at nadir probing is fulfilled. The analytical investigation of the influence of a surfactant film on the Doppler spectrum width at nadir probing for the microwave radar with a narrow and knife-like antenna beam is carried out for the first time.

The advanced model of the Doppler spectrum for radar with wide antenna beam was developed for our analysis. The width of the Doppler spectrum depends on the variance of the orbital velocities for fixed radar and on the slope variance for a moving radar. The dependence of width of the Doppler spectrum on wind speed, parameters of film, radar wavelength and the speed of radar platform was investigated.

It is shown that the requirements to the radar antenna depend on radar platform speed. In case of the fixed radar for detection of slicks it is necessary to use a narrow antenna beam, however, for diagnostic of the slicks from the moving radar we must apply the radar with a knife antenna beam.

The study has shown, that the detection of slicks using the algorithm based on the width of a Doppler spectrum is being improve with the decrease of wave length of the radar, and for the decision of a problem of diagnostic it is desirable to use radar wavelengths which do not exceed 2–3 cm.

In the whole, the contrast of slicks on the width of a Doppler spectrum is less than contrast on the radar cross section, however spatial and temporal fluctuations of a Doppler spectrum width are less than fluctuations of power of a backscattered signal. It allows us to consider a Doppler spectrum as the perspective detecting instrument of presence of slicks on water surface.

# Remote Sensing Image Compression Based on Classification and Detection

Minqi Li, Quan Zhou, and Jun Wang

National Key Laboratory of Space Microwave Technology, Xi'an Institute of Space Radio Technology  
Xi'an, China

**Abstract**— The major bottleneck of remote sensing satellites is the transmission of the obtained images to the ground station. Traditional compression algorithms can not process the huge data volume captured by the high resolution sensors. In this paper, a novel compression scheme based on classification and detection algorithms is proposed. In the proposed scheme, based on the regions of interest, the image of high compression ratio is obtained which is compressed in different strategy. And also its computational complexity is low and tends to be realized. The novel scheme is appropriate for on-board processing.



## Using AMSR-E Satellite Data to Retrieve Soil Moisture on the Mongolia Plateau

Yuei-An Liou<sup>1,2</sup> and Tzu-Yin Chang<sup>2</sup>

<sup>1</sup>Center for Space and Remote Sensing Research, National Central University, Chungli 320, Taiwan

<sup>2</sup>Institute of Space Sciences, National Central University, Chungli 320, Taiwan

**Abstract**— Soil moisture plays a crucial role in the land-atmosphere energy balance. It is one of few directly observable hydrological and atmospheric variables. In this study, we use AMSR-E satellite data to retrieve soil moisture on the Mongolia Plateau. The Mongolia Plateau is chosen because it is a very high plateau and considered as a cold source of the atmosphere in winter, and has an important impact on the Asian monsoon system. Two retrieval schemes are implemented for this study of radiometric sensing of soil moisture. They include the  $\tau$ - $\omega$  model and the R model. The latter one is developed based on a land surface process and radiobrightness (R) model for bare soil and vegetated terrain (Liou, 1999). Compared with the in situ ground measurements, the soil moisture retrieved from the R model and the  $\tau$ - $\omega$  model is underestimated in dry season. The scattering effect is then incorporated into the R model. Better retrievals of soil moisture are hence obtained. In future, we will attempt to apply the modified R model with the AMSR-E 6.925 GHz brightness temperature measurements to monitor long-term soil moisture variation over the Mongolia Plateau.

## Far-field Diffraction Characteristics of a Short Pulse from a Slit with Gaussian form of Transmittance

**Pin Han**

Institute of Precision Engineering, National Chung Hsing University  
250, Kuo Kuang Road, Taichung 402, Taiwan, R.O.C.

**Abstract**— The spectrum changes of a Gaussian pulse in the far-field is studied with Fresnel diffraction integral when it is incident on a slit with Gaussian form transmittance. It is found that the side-lobes of the spectral intensity which exist in normal slit with unit transmittance will be eliminated under such a condition. This effect could be useful for optical engineering or optical communications.

## Two-step Contrast Source Inverse Method with Phaseless Data for EM Inverse Scattering

Lianlin Li, Yin Xiang, and Fang Li

Institute of Electronics, Chinese Academy of Sciences, Beijing 100080, China

**Abstract**— In recent years, electromagnetic inverse scattering techniques grow more attractive because of their sensitivity to the dielectric properties, which is useful for detecting and reconstructing quantitatively unknown objects in a noninvasive fashion. At present, the main research focuses on the stable approaches to the forward/inverse problem and the cheaper radar instrument. As for the method of finding the solution of inverse problem, there are two kinds of strategies as stochastic approach (such as genetic algorithm, particle swarm optimization, simulated annealing etc.) and determined approach (such as Born approximation, extend Born approximation, contrast source inversion method, and so on). However, all of them require the measurement of not only the intensity of the scattered wave but also its phase. Phase measurements generally present considerable practical difficulties and non-negligible hard cost. Recently some approaches for the inverse problem from phaseless data have been proposed and tested to circumvent the problem of phase measurement.

In this presentation, the two-step approach for the EM inverse scattering problem has been developed, where the first step is to find the initial trial for the second step based on the Rytov (or Born) approximation with intensity-only data proposed by Li, the second step is to find the required solution iteratively based on the CSI strategy. However, different from the standard CSI, the data equationthe domain integral equation for the measured datais modified which are suitable for electromagnetic inverse scattering with phaseless data. Some numerical experiments are tested to validate the proposed approach.

## Differential Theory with Genetic Algorithms in Design Periodic Absorbers

N. Lassouaoui, H. Hafdallah Ouslimani, and A. Priou

University Paris X, Nanterre, Pole Scientifique and Technique, Ville d'Avray  
Applied Electromagnetism Group (GEA) 50, rue de Sèvre 92410, Ville d'Avray, France

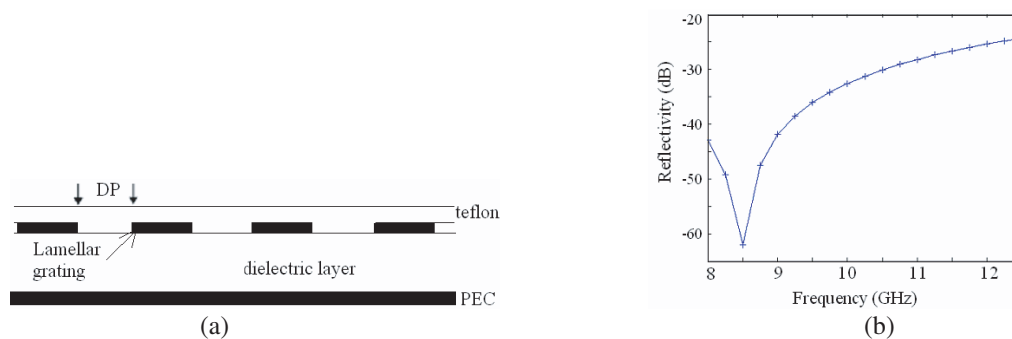
**Abstract**— Based on encouraging results in using evolutionary search in electromagnetic field, here in, a realvalued genetic algorithm (GA) was implemented to specify the characteristics (thickness  $T$ , period  $P$ , permittivity  $\varepsilon$  and permeability  $\mu$ ) which ensure the minimization of the reflectivity by periodic gratings on a wide frequency band. In our GA, we have used several kinds of operators; the parameters are computed in automatic way; we check the best exploring of research space; and the reflectivity of the grating is used as fitness to direct the research towards the minimum.

Thus, we need to study the diffraction problem. This latter is the necessity to find the scattered field which satisfies [1]: Helmholtz equation in each media; Quasi-periodicity; The continuity of the total field on the boundary surface between two media; Radiation condition; Energy finiteness.

A huge number of approaches exist in area of diffraction by periodic surfaces [1, 2], such as: the moment method, the finite-difference time-domain method, the finite element method. Here in, we choose the differential theory DT of gratings; since it is well established and provided both simplicity and versatility [1]. With DT, the Maxwell equations are applied to periodic media, they are projected onto a Fourier basis; which provide a set of differential equations. However, to solve them, the initial values of the total fields and the derivatives are not known, we have only the link between the functions and their derivatives. So, the shooting method [1] is used for solving this boundary-value differential problem. It is based by constructing  $N$  linearly independent initial values, then; a process of  $N$  integrations is performing from  $\theta$  to depth of layer. Since the linearity of the fields, we can obtain the true values of the fields and the reflectivity parameter [1].

Here in, we present results obtaining for TE mode of a stack (Figure 1) constituted respectively by a homogeneous layer ( $\mu_1, \varepsilon_1, T_1$ ) (in the bottom), lamellar periodic structure along  $x$  ( $\mu_2, \varepsilon_2, T_2, P$ ) and layer of Teflon with  $T = 0.5$  mm. All are backed by a PEC. Firstly, we study the stability of the computes according  $N$  (number of Fourier components), we need at least 35 components.

Figure 1(b) shows the reflectivity in X-band for incidence normal of the solution obtained after 100 generations, we reach a reflectivity of  $-62$  dB.



<b>Homogeneous Layer:</b>	$\varepsilon_1=1.4000+i0.5433$	$\mu_1=0.4000+i0.2000$	$T_1=5.8345$ mm
<b>Periodic Layer:</b>	$\varepsilon_2=0.2089+i0.8000$	$\mu_2=1.0000+i0.0000$	$P=8.6573$ mm, $DP=1.4$ mm, $T_2=9.5954$ mm

Figure 1: (a) Schema of grating, (b) frequency response of obtained solution at 100 iterations.

### REFERENCES

1. Neviere, M. and E. Popov, *Light Propagation in Periodic Media, Differential Theory and Design*, published by Marcel Dekker, 2003.
2. Vinoy, K. J. and R. M. Jha, *Radar Absorbing Materials*, Kluwer Academic Publishers, 1996.

3. Hall, J. M., "A novel, real-valued genetic algorithm for optimizing radar absorbing materials," NASA/CR-2004-212669, March 2004.
4. Goldberg, D. E., *Genetic Algorithms in Search, Optimization and Machine Learning*, Addison-Wesley, 1989.

## A Stable and Efficient Numerical Method for Grating Structures

N.-Y. Shih<sup>1</sup>, W.-L. Yeh<sup>1</sup>, and Y.-P. Chiou<sup>2</sup>

<sup>1</sup>Institute of Photonics and Optoelectronics, National Taiwan University  
No. 1, Sec. 4, Roosevelt Road, Taipei 10617, Taiwan

<sup>2</sup>Department of Electrical Engineering, National Taiwan University  
No. 1, Sec. 4, Roosevelt Road, Taipei 10617, Taiwan

**Abstract**— A pseudo-spectral method is applied to solve the grating structures. Compared with frequently used rigorous coupled wave analysis (RCWA), it is more stable and shows high efficiency in calculating metallic gratings. In this presentation, we will demonstrate the fast convergence and outstanding stability of the method. Its success lies in dividing the computational domain into subdomains conforming to the problem geometry and combining the polynomial approximations with patching conditions derived from the problem physics. The method holds great promise for modeling more elaborate photonic structures.

## Optical Response of a Tunable Liquid Crystal Cell with Nano-structured Metal Layer

L. Z. Ruan, J. Parsons, W. A. Murray, and J. R. Sambles

Electromagnetic Materials Group, School of Physics, University of Exeter, UK

**Abstract**— There is presently much interest in exploiting the dielectric response of structured metals to construct photonic materials. Almost a decade ago Ebbesen and colleagues [1] reported that a metal film perforated with an array of holes of diameter much less than the wavelength, gave rise to optical transmission orders with magnitude greater than predicted by standard aperture theory. This study stimulated an enormous surge of research interest [2] into the exploration of enhanced transmission through a variety of different metal structures. Apart from its fundamental interest, this extraordinary effect also has potential application in optical chip technology, optical sensing, flat-panel displays, organic light emitting devices and wavelength-tunable filters etc. The majority of the work thus far has focused on combinations of perforated metal films with passive dielectric layers.

In this study we use liquid crystals with director profiles which can be easily changed by the application of a low electric field. This provides a tunable dielectric, and allows the exploration of the voltage dependent optical response in very thin liquid crystal cells having a perforated silver slit layer on one surface of the cell. Reflectivity spectra from such cells are explored with various slit sizes and applied fields.

### REFERENCES

1. Ebbesen, T. W., J. J. Lezec, H. F. Ghaemi, T. Thio, and P. A. Wolff, *Nature*, Vol. 391, 667, 1998.
2. Barnes, W. L., A. Dereux, and T. W. Ebbesen, *Nature*, Vol. 424, 824, 2003.

## Theoretical and Experimental Study of Goos-Hänchen Shifts on Symmetrical Metal-cladding Waveguides

Zhuangqi Cao, Honggen Li, Lin Chen, Qishun Shen, and Xiaoxu Deng

Guided-wave Photonics Group, National Laboratory on Local Fiber-Optic Communication Networks and Advanced Optical Communication System, Shanghai Jiao Tong University  
Shanghai 200240, China

**Abstract**— In this paper, large positive and negative Goos-Hänchen(GH) shifts on a symmetrical metal-cladding waveguide (SMCW) were investigated both theoretically and experimentally. The SMCW is simply a glass slab with several hundred micrometers sandwiched between two gold films. A recently developed free-space coupling technique was used to transfer the light energy into the ultrahigh order modes of the SMCW. It is shown that during the resonant excitation, and the intrinsic damping coincides with the radiative damping of the modes, the lateral shifts of reflected beam are enhanced to as large as hundreds of micrometers. It is also known that sign of the GH shift is totally dependent on the difference between the radiative damping and the intrinsic damping. GH shifts with sub-millimeter scale were experimentally observed. The experimental results show good agreement with theoretical prediction.



## Optical Mode Parameters of the 2.3- $\mu\text{m}$ Al(In)GaAsSb/GaSb Ridge-waveguide Laser Diodes and Laser Diode Arrays

Yimin Chen and Dmitry Donetsky

Department of Electrical and Computer Engineering, MS-2350  
Stony Brook University, NY 11794, USA

**Abstract**— Patterned optical waveguides can be applied to photonic devices such as semiconductor laser diodes to improve the parameters of output emission. One of the major advantages is that it enables decrease of the light beam divergence with modification of the optical losses for different modes with diffraction-limited output beam as an ultimate goal. In this study, we simulated waveguides with arrays of coupled ridges, and optimized the parameters for 2.3- $\mu\text{m}$  GaSb-based laser diodes [1].

Simulation of multilayer slab waveguide was performed. Refractive indices of core layer and cladding layers were determined to be 3.9 and 3.3 respectively. A single ridge structure was simulated in order to determine the ridge geometry optimal for the laser diodes. The waveguide structure and relationships between the optical absorption loss and waveguide dimensions were determined with accounting for the absorption in the covering metal layer. The goal was to obtain less optical loss for the basic mode compared to the higher order modes utilizing different field distributions in the lateral direction. The waveguide with array of 10 ridges on the p-side cladding layer was simulated. In the simulation, ridge depth ranged from 1  $\mu\text{m}$  to 1.5  $\mu\text{m}$ , with three different ridge widths of 5  $\mu\text{m}$ , 10  $\mu\text{m}$  and 20  $\mu\text{m}$ . The relationships between the ridge parameters such as depth and width, and optical loss for different modes were found. The waveguide simulation was done by the commercial software BeamProp from Rsoft. The waveguides were created in BeamProp CAD and simulated based on the Beam Propagation Method (BPM). The batch data processing was done in MathCad. During simulations, interconnection between two programs was automated, favoring the reduction time for the repetitive data manipulations in the future studies.

It was shown that the thickness of the waveguide cladding layer can be decreased from the current design, resulting in lower electrical and thermal resistances of the laser diode structure, with the optical losses within the tolerable range. The optimal ridge width and depth were determined. Finally, for ridge waveguide with 5  $\mu\text{m}$  width and 1.15  $\mu\text{m}$  depths, the waveguide geometry providing the three-fold difference in optical losses between the basic mode and higher order modes was identified. This geometry ensures adequate conditions for generation of only basic mode with near diffraction-limited divergence of the laser output beam divergence.

### REFERENCES

1. Donetsky, D., G. Kipshidze, L. Shterengas, T. Hosoda, and G. Belenky, "2.3  $\mu\text{m}$  type-i quantum well GaInAsSb/AlGaAsSb/GaSb laser diodes with quasi-CW output power of 1.4 W," *Electron. Lett.*, Vol. 43, No. 15, 810–812, 2007.

# Wavefront Phase Modulation of Cylindrical Vector Beam in Optical Focusing System

X. Gao and J. Wang

Electronics and Information College, Hangzhou Dianzi University  
Hangzhou 310018, China

**Abstract**— Cylindrical vector beams have become very attractive recently for their unique properties and promising applications. In this paper, the wavefront phase modulation is employed in focusing system of cylindrical vector beams to form concentric piecewise section, and focusing properties of the concentric piecewise cylindrical vector beams is investigated theoretically. Section of the beam consists of three concentric portions, center circle portion, inner annular portion and outer annular portion. The center circle portion and outer annular portion are radial polarized, and the inner annular portion is generalized polarized. The phase of the inner annular portion is tunable. Numerical simulations show that the evolution of the focal shape is very considerable by changing the radius and polarization rotation angle of each portion of the vector beam. And some interesting focal spots may occur, such as two-peak or three-peak focus, dark hollow focus, ring focus, and two-ring-peak focus. For certain geometric parameters of the beam, the focal shift occurs and can be adjusted by phase shift and polarized direction of inner annular portion. For some case, three-peak focal pattern may occur, and peaks shift in same direction with one local minimum also shift. For other some case, two-peak focal pattern may occur with shifting peaks. The tunable quantitative focal shift is illustrated in detail. In addition, some gradient force patterns is also computed, including cup shell shape trap, rectangle shell shape trap, dumbbell optical trap, spherical shell optical trap, which shows that the concentric piecewise cylindrical vector beam can be used to construct controllable optical tweezers.

# Detection of Narrow-band and Multi-frequency Terahertz Generation and Propagation in Periodically Poled MgO: LiNbO<sub>3</sub> (PP-MgO: LN)

W. M. Liu<sup>1</sup>, G. Kh. Kitaeva<sup>2</sup>, H. C. Guo<sup>1</sup>, and S. H. Tang<sup>1</sup>

<sup>1</sup>Department of Physics, National University of Singapore, 119260, Singapore

<sup>2</sup>Faculty of Physics, Moscow State University, Moscow 119992, Russia

**Abstract**— The generation and control of terahertz (THz) radiation remains an area of intensive research during the last decade. This range of electromagnetic spectrum is very attractive due to a variety of promising applications in spectroscopy, outer-space communication, biomedical imaging and tomography. There are essentially two methods for THz wave generation. The first method employs ultra-short laser pulse to illuminate a photoconductive semiconductor to induce a transient electrical current which results in THz emission. The other method is via optical rectification in nonlinear dielectric crystals pumped by ultra-short laser pulses. The later method can be used to generate broad-band, single-cycle THz waves under phase matching condition as well as to generate narrow-band, multi-cycle THz waves under quasi-phase matching condition.

We studied the narrow-band and multi-frequency terahertz generation and propagation in an after-grown periodically poled MgO: LiNbO<sub>3</sub> (PP-MgO: LN) crystal using a femtosecond pump-probe technique. Using a pump beam at the central wavelength of 800 nm as excitation, a well-pronounced optical probe signal which reflects the evolution of the THz wave was observed in the crystal with a domain periodicity of 30  $\mu\text{m}$ . The power spectrum of the Fourier transform of THz wave exhibits a backward THz wave with frequency 1.36 THz and a forward wave 3.15 THz generated in the crystal. A general theoretical model was developed to explain the nature of signal formation, taking into considerations the following three factors: (1) pump-beam-induced THz generation by quasi-phase matching; (2) the sum- and difference-frequency mixing between the THz wave and an optical probe wave in the PP-MgO: LN crystal; (3) THz wave detection by a detector using the lock-in technique. The experimental results are in good agreement with the theoretical predictions.

# The Photonics Collapse-revival's of Intensity-dependent Coupling of Lambda Atoms and Fields

J. Hajivandi and M. M. Golshan

Department of Physics, University of Shiraz, Shiraz, Iran

**Abstract**— In the present report, we have extended the Jaynes-Cummings model, in a Kerr-like media and with an intensity dependent coupling [1], to the three-level  $\Lambda$  atoms. In our model, the  $\Lambda$  atom placed in a Kerr medium, interacts with two fields, one of them is initially coherent while the other one is not. The noncoherent field is coupled to the atoms through the Kerr effect and intensity dependent coupling constants. These two effects, which may be obtained from the q-deformation of field operators commutation relations, are shown to drastically influence the collapse-revivals of the noncoherent field. We do this, by introducing the appropriate Hamiltonian, determining the time evolution of the initial density matrix and thereby calculating the two photonic mean numbers, as functions of time.

In Figures 1–3 the noncoherent photonic mean numbers as functions of time, and for different values of Kerr constant,  $\chi$ , and nonlinear coupling constant,  $k$ , are presented. From these figures the following conclusions are made.

1. The noncoherent field, in spite of its noncoherency, follows the pattern of collapse-revivals.
2. The period of collapses (revivals) decreases as the nonlinear factors increase. For extreme values of the nonlinear coupling constant, the pattern is destroyed.
3. The effect of the Kerr medium on the period of collapses (revivals) is much more than that of the intensity-dependent coupling.

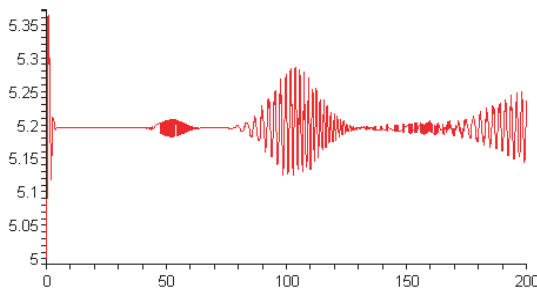


Figure 1: Noncoherent photonic mean number, for  $k = \chi = 0$ .

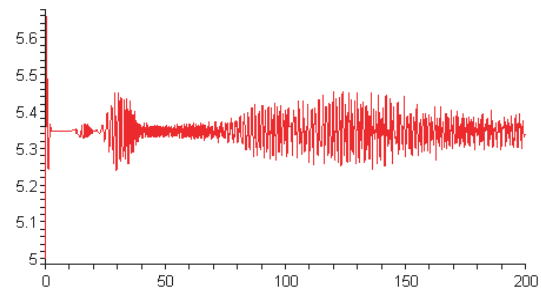


Figure 2: Noncoherent photonic mean number for  $k = 1, \chi = 0$ .

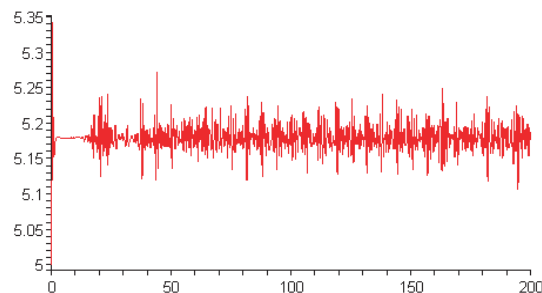


Figure 3: Noncoherent photonic mean number for  $k = 0, \chi = 1$ .

**REFERENCES**

1. Sivakumar, S., "Nonlinear Jaynes-Cummings model of atom-field interaction," *arXiv: quant-ph/0302046*, Vol. 1, 2003.
2. Faisal, A. A., E. Orany1, "Revival-collapse phenomenon in the quadrature squeezing of the multiphoton Jaynes-Cummings model with the binomial states," *arXiv: quant-ph/0704.2347*, Vol. 1, 2007.

## High Quality, High Intensity and Narrow Bessel Beams

O. Brzobohatý, T. Čižmár, and P. Zemánek

Institute of Scientific Instruments of the ASCR, v.v.i. Academy of Sciences of the Czech Republic  
Kralovopolska 147, Brno 612 64, Czech Republic

**Abstract**— A special group of so called non-diffracting beams — Bessel beams found in the last five years many applications in the field of optical micro-manipulation [1, 2], communications [3], photopolymerization [4]. Majority of these experiments are based on the unique properties of Bessel beams [5], i.e., invariable optical intensity along the beam propagation. However, the practical realization of Bessel beams is mainly based on conical lenses illuminated by a Gaussian beams. The beam formed behind the axicon is in this case called pseudo-non-diffracting beam because its intensity is not constant and varies [4, 6]. However, this description supposed an ideal axicon with sharp tip which is not satisfied for real commercially available axicons. They have oblate tip close to a spherical surface. Therefore the beam generated behind the axicon is not a Bessel beam but an interference field obtained by a Bessel beam and a spherical wave coming from the axicon tip. This unwanted interference creates an axial modulation of the field behind the axicon tip with a period  $\lambda/(1 - \cos \alpha)$ , where  $\alpha$  is the polar angle between the plane waves forming the Bessel beams and  $\lambda$  is the laser wavelength in the medium. The left-hand part of Fig. 1 shows the Bessel beam profile which suffers with the unwanted interference described above. Sever modulations of the intensity are clearly visible. To get rid of this modulation we carefully determined size of an obstacle which we placed to the Fourier plane to block majority of the spherical wave intensity. The right-hand part of Fig. 1 demonstrates improvement of the beam profile. Side-effect of this method is desirable shift of the axial intensity maximum of the Bessel beam far from the axicon tip. This beam was used in pioneering experiments of optical binding in counter-propagating Bessel beams.

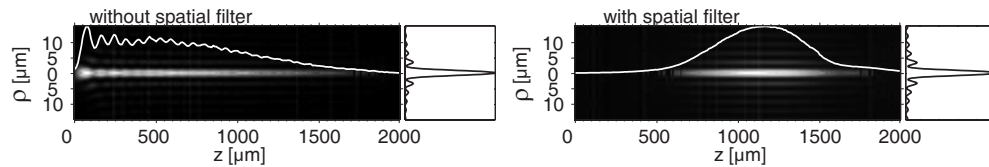


Figure 1: Comparison of spatial profile of filtered and unfiltered Bessel beam generated behind non-perfect axicon with an apex angle  $\tau = 170^\circ$  illuminated by a Gaussian beam (wavelength 1064 nm, maximal power 10 W, beam-waist diameter 5 mm). The beam formed behind the axicon was transformed by a telescope formed from lenses  $f_1 = 50$  mm and  $f_2 = 11$  mm to a Bessel beam of core diameter equal to  $2.4 \mu\text{m}$ .

### ACKNOWLEDGMENT

This work was partially supported by Ministry of Education, Youth, and Sports of the Czech Republic (project No. LC06007) and Institutional Research Plan of the Institute of Scientific Instruments (AV0Z20650511).

### REFERENCES

1. Garcés-Chávez, V., et al., “Simultaneous micromanipulation in multiple planes using a self-reconstructing light beam,” *Nature*, Vol. 419, 145–147, 2002.
2. Čižmár, T., et al., “Optical conveyor belt for delivery of submicron objects,” *Appl. Phys. Lett.*, Vol. 86, 174101–1–174101–3, 2005.
3. Bouchal, Z. and R. Čelechovský, “Mixed vortex states of light as information carriers,” *New J. Phys.*, Vol. 6, 131, 2004.
4. Ježek, J., et al., “Formation of long and thin polymer fiber using nondiffracting beam,” *Opt. Express*, Vol. 14, 8506–8515, 2006.
5. Durnin, J., et al., “Diffraction-free beams,” *Phys. Rev. Lett.*, Vol. 58, 1499–1501, 1987.
6. Jarutis, V., et al., “Focusing of laguerre-gaussian beams by axicon,” *Opt. Commun.*, Vol. 184, No. 1–4, 105–112, 2000.

# Speed Enhancement of Many-body Cluster of Microparticles in Optical Conveyor Belt

M. Šiler, T. Čižmár, and P. Zemánek

Institute of Scientific Instruments of the ASCR, v.v.i., Academy of Sciences of the Czech Republic  
Kralovopolska 147, 612 64 Brno, Czech Republic

**Abstract**— Interactions between many colloidal particles placed into the laser beams causes principal deviations in their behavior comparing to the single particle placed in laser beams. The most wellknown phenomenon (also called optical binding) is self-organization of colloidal particles into various one or two-dimensional structures without the necessity to create optical trap for each particle [1–4]. Most frequently only static behavior of created structures is studied. In our paper we focused on behavior of more particles delivered in travelling standing wave (conveyor belt) [5] and we show that with the same velocity of the travelling wave more particles are delivered faster.

We used an interference of two counterpropagating evanescent waves to create an array of optical traps near the surface. The controllable movement of the whole structure is achieved by changing the phase in one wave. We obtained so-called travelling standing wave (TSW) [5]. Colloidal particle follows the movement of the TSW however its mean velocity is lower comparing to TSW. The reason are hops over the potential barrier between neighboring optical traps. We moved the TSW bi-directionally with constant speed  $\pm 100 \mu\text{ms}^{-1}$ . Single bead moved with average velocity  $16 \mu\text{ms}^{-1}$ , however more particles formed a one-dimensional cluster (chain) and moved with higher average velocities. Speed increase by 15% has been already reported for two beads guided by a waveguide and propelled by radiation pressure [6]. However we observed speed increase from 23% for 2 beads up to 280% for 8 beads comparing to single particle. The stability of the cluster was done by a combination of optical gradient forces, forces coming from the interaction between particles and hydrodynamic binding. However the speeds of the edge particles in the cluster was the lowest. Figure 1 compares motion of particle chains formed from one to eight beads and taken at four times.

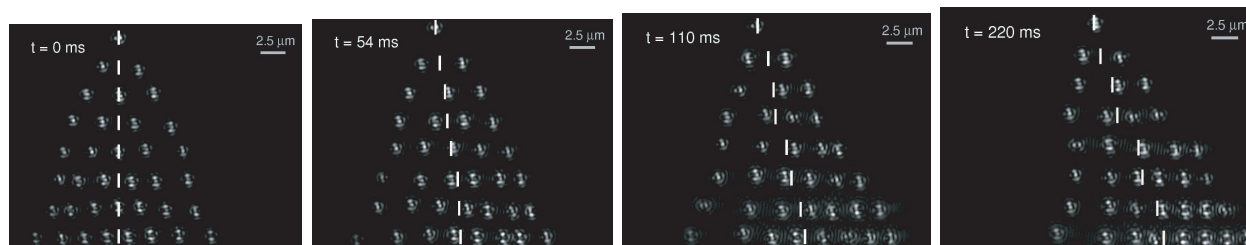


Figure 1: Light scattered by chains of 1–8 polystyrene beads of diameter 520 nm placed in water. The images compare chain positions and particles locations inside each cluster at four different moments. For clarity the positions of the center of the mass at the  $t = 0$  were vertically aligned. The positions of the centers of the mass is shown by the vertical bars and the horizontal bar in top-right corner shows distance of  $2.5 \mu\text{m}$ .

## ACKNOWLEDGMENT

This work was partially supported by MEYS CR (project No. LC06007) and IRP of the ISI (AV0Z20650511).

## REFERENCES

1. Burns, M. M., et al., “Optical binding,” *Phys. Rev. Lett.*, Vol. 63, 1233–236, 1989.
2. Tatarkova, S. A., et al., “One-dimensional optically bound arrays of microscopic particles,” *Phys. Rev. Lett.*, Vol. 89, 283901, 2002.
3. Mellor, C. D., et al., “Array formation in evanescent waves,” *Chem. Phys. Chem.*, Vol. 7, 329–332, 2006.
4. Reece, P. J., et al., “Experimental observation of modulation instability and optical spatial soliton arrays in soft condensed matter,” *Phys. Rev. Lett.*, Vol. 98, 203902, 2007.

5. Čižmár, T., et al., “Optical sorting and detection of sub-micron objects in a motional standing wave,” *Phys. Rev. B*, Vol. 74, 035105, 2006.
6. Grujic, K. and O. G. Hellesø, “Dielectric microsphere manipulation and chain assembly by counter-propagating waves in a channel waveguide,” *Opt. Express*, Vol. 15, 6470–6477, 2007.



# All-optical Switching Structure Using Nonlinear Photonic Crystal Directional Coupler

A. Eshaghi, M. M. Mirsalehi, A. R. Attari, and S. A. Malekabadi  
Department of Electrical Engineering, Ferdowsi University of Mashhad, Iran

**Abstract**— A new all-optical switching structure with efficient transmission of waves through the switch is presented. Switching is accomplished by means of embedded Kerr nonlinear rods in the coupling region. Modifying the supermodes dispersion relation cause the switching length to be as small as  $18a$ , where  $a$  is the lattice constant.

**Introduction:** In a directional coupler consisting of two parallel waveguides, the wave confined to one of the waveguides consists of even and odd supermodes with a phase difference. If the phase difference is equal to  $(2n + 1)\pi$ , the wave will transfer to the other waveguide, this means

$$(k_{\text{even}} - k_{\text{odd}})L_c = (2n + 1)\pi \quad (1)$$

where  $k_{\text{even}}$  and  $k_{\text{odd}}$  are the wavenumbers of even and odd supermodes, respectively, and  $L_c$  is the coupling length. For performing switching, the phase difference should change to  $2m\pi$ . When photonic crystal fabrication is finalized,  $L_c$  is fixed. Through the use of nonlinearity, one can change the effective index of refraction and as a result, the wavenumbers of the supermodes will change and switching operation can be obtained.

It can be shown that switch length, is proportional to  $1/(\Delta k_{\text{even}} - \Delta k_{\text{odd}})$ , where  $\Delta k_{\text{even}}$  and  $\Delta k_{\text{odd}}$  are the difference between the wavenumbers of even and odd supermodes in two states of switch operation, respectively.

**Switch Structure:** Figure 1 shows the schematic view of the structure. The PC is formed by a 2D triangular lattice of rods in air. The radius of the rods is  $r = 0.2a$ , where  $a$  is the lattice constant. The structure has a bandgap for TM modes in the range  $0.334 < a/\lambda < 0.508$ . Two parallel waveguides are obtained by removing two rows of the rods. By introducing a new coupling region structure, the difference between the wavenumbers of linear and nonlinear regimes is enlarged so the coupling region length is reduced to  $18a$ . The radius of the rods in coupling region and beside the waveguides and the position of this rods are the design parameters. These parameters are adjusted to the following values,  $r_c = 0.18a$ ,  $r_{d1} = 0.19a$ ,  $r_{d2} = 0.2a$ ,  $l_1 = 0.18a$  and  $l_2 = 0$ .

Using modified  $60^\circ$  bend structure, transmission spectra from input to outputs have improved in comparison with the conventional  $60^\circ$  bend.

In the linear regime the switch is in cross state, and in the nonlinear regime, the switch works in bar state. Power ratio between the output ports is more than 25 dB.

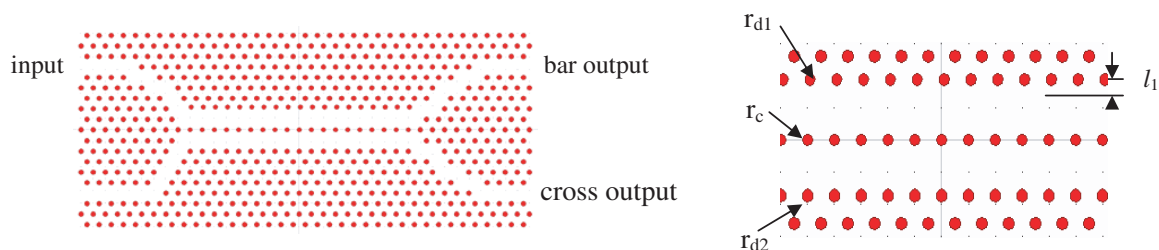


Figure 1: Schematic view of the structure.

## Two-color Two-photon Microscopy for Enhancing the Imaging Depth into Highly Scattering Media

Lingling Qiao, Chen Wang, Ya Cheng, and Zhizhan Xu

State Key Laboratory of High Field Laser Physics, Shanghai Institute of Optics and Fine Mechanics  
P. O. Box 800-211, Shanghai 201800, China

**Abstract**— With the development of the biomedicine, biological imaging has become more and more important. Two-photon excitation fluorescence (2PE) microscopy has been a valuable technique in the world of biological imaging in tissue explants and living animals. However, 2PE has difficulties in improving the imaging depth in highly scattering media. In a highly scattering medium, the 2PE imaging has low signal-to-noise ratio (SNR) because of two reasons [1]: (1) the number of fluorescence photons generated from the focal volume decreases in evidence and (2) the number of (background) fluorescence photons from the out-focus plane increases inevitably. In two-color two-photon (2C2P) excitation fluorescence microscopy, 2CE fluorescence is generated only in the region where the two different beams overlap with each other in both space and time [1, 2]. Although scattering decreases the in-focus fluorescence, it only minimally increases the unexpected fluorescence background unlike in the 2PE case [3]. Compared to 2PE, 2CE has higher SNR, 2CE has distinct advantage over 2PE when observing fluorescence objects through highly scattering media. In this paper, we discuss the scattering problem in the medium and propose a meaningful approach to overcome the out of focus fluorescence problem. In our approach, we use two excitation wavelengths of 800 nm and 1200 nm, and detect fluorescence signal at 480 nm emission wavelength, the 800 nm pulse is from a 40 fs Ti-sapphire laser and the 1200 nm pulse is provided by a OPA setup. We shape the two beams to make them only overlap with each other at the focus, so we substantially reduce the fluorescence background and increase the SNR. We expect that the method can be applied to a variety of imaging task in thick tissue and in live animals, especially, it is possible to use this approach to examine the cancer living cell in real-time.

### REFERENCES

1. Cambaliza, M. O. and C. Saloma, *Opt. Commun.*, Vol. 184, 25, 2000.
2. Gryczynski, I., H. Malak, and J. R. Lakowicz, *Biospect.*, Vol. 3, 97, 1996.
3. Caballero, M. T., P. Andres, A. Pons, J. Lancis, and M. Martinez-Corral, *Opt. Commun.*, Vol. 246, 313, 2005.

# Multifunctional Microdevices Integration on Glass Chips with Femtosecond Laser Microfabrication

Fei He, Haiyi Sun, Jian Xu, Yang Liao, Ya Cheng, and Zhizhan Xu

State Key Laboratory of High Field Laser Physics, Shanghai Institute of Optics and Fine Mechanics  
P. O. Box 800-211, Shanghai 201800, China

**Abstract**— Conception of lab-on-a-chip revolutionized various fields, such as chemical and biological fields for human gene and protein analysis, new drug development, medical inspection, synthesis of new materials, environmental monitoring, and so on [1]. However, difficulties in their functional integration on small spatial scales have been a major challenging issue. Recent advances in femtosecond laser microfabrication provide a potential technique to it [2]. This development enables us to form various functional microdevices including optical, fluidic, electronic, and thermal elements, which can be integrated on the same glass chips. In this paper, the formation of microfluidic optical waveguide and selective metallization microstructures irradiated by femtosecond laser on glass substrates are presented, respectively [3–4].

Firstly, we describe the fabrication of microfluidic channel structures on the surface of borosilicate glass by femtosecond laser direct writing for optical waveguiding application. Liquid with a variable refractive index was fed in the microchannels, serving as the cores of the waveguides. We observed the evolution of the transverse modes in the microfluidic waveguides following the change of refractive index of the liquid core using a CCD imaging system. By controlling the refractive index of the liquid, either a multimode or a single-mode waveguiding can be achieved [3]. Then, we present an easy and efficient approach for selective metallization of glass based on ultrafast laser modification combined with electroless plating. The process is mainly composed of three steps: (1) formation of silver nitrate thin films on glass substrates; (2) generation of silver particles in the irradiated area by ultrafast laser direct writing; (3) selective electroless copper plating in the modified area. Possible mechanisms as well as electrical properties are also investigated. Using this approach, the electrical control and thermal control in multifunctional microdevices will be easily realized [4]. These results demonstrate the potential to integrate multi-functional devices for the lab-on-a-chip applications using femtosecond laser pulses.

## REFERENCES

1. Figeys, D. and D. Pinto, *Anal. Chem.*, Vol. 72, 330, 2000.
2. Sugioka, K., Y. Cheng, and K. Midorikawa, *Appl. Phys. A*, Vol. 81, 1, 2005.
3. Sun, H., F. He, Z. Zhou, Y. Cheng, Z. Xu, K. Sugioka, and K. Midorikawa, *Opt. Lett.*, Vol. 32, 1536, 2007.
4. Xu, J., Y. Liao, H. Zeng, Z. Zhou, H. Sun, J. Song, X. Wang, Y. Cheng, and Z. Xu, *Opt. Express*, submitted.

## Studying of the Dipole Characteristic of THz from Photoconductors

Hong Liu, Weili Ji, and Wei Shi

School of Automation and Information Engineering, Xi'an University of Technology, China

**Abstract**— Under the different experimental conditions, THz waveform which was generated by the different GaAs photoconductive switch provided with diverse carrier lifetimes triggered by femo-second laser pulse are calculated. The results indicate the main course of the dipole characteristic of THz waveforms emitting from low-temperature grown GaAs is the lifetime of optical-generated carriers less than the generation time; To SI-GaAs photoconductive semiconductor switches with the lifetime of optical-generated carriers more than 100 ps, the dipole characteristic of THz waveforms is mainly because of intra-valley scatter and the space charge field screening on different experimental conditions (different biased electric field and different optical pulse energy).

# Influence of External-cavity Length on the Route-to-chaos of Semiconductor Lasers under Optical Feedback

Moustafa Ahmed<sup>1</sup> and Minoru Yamada<sup>2</sup>

<sup>1</sup>Department of Physics, Faculty of Science, Minia University, 61519 El-Minia, Egypt

<sup>2</sup>Division of Electrical Engineering and Computer Science  
Graduate School on Natural Science and Technology, Kanazawa University  
Kakuma-machi, Kanazawa 920-1192, Japan

**Abstract**— This paper investigates influence of the external-cavity length on the route-to-chaos when semiconductor lasers operate under external optical feedback (OFB). The study is based on numerical solution of an improved time-delay model of laser rate equations. The length of the cavity varies from 1 to 20 cm. The frequency ratio (FR) of the external-cavity mode-separation frequency to the relaxation frequency is used to classify influence of the external-cavity length. The time variation of the laser intensity and its Fourier transform are examined in the first and second routes-to-chaos that corresponds to the weak and intermediate ranges of OFB, respectively. The laser is assumed to operate above threshold. The results show that, under weak OFB the laser operates in continuous wave (CW). The steady-state solution then bifurcates first into a stable limiting cycle and further into a torus followed by a chaotic state. The torus may be period doubling, sub-harmonic or quasi-periodic depending on the FR. The limiting cycle corresponds to periodic oscillation (PO). The oscillation frequency changes with the variation of the FR around the relaxation frequency and decreases with the increase of OFB. When the FR is higher than unity, the sequence of laser dynamics is CW  $\rightarrow$  PO  $\rightarrow$  period doubling (PD) $\rightarrow$  period multiplication (PM)  $\rightarrow$  chaos. The PD is characterized by the oscillation frequency of the bifurcation point and its half-harmonic, whereas the PM is characterized by a higher frequency and its sub-harmonics. When the FR is less than but near to unity, the sequence of laser dynamics is CW  $\rightarrow$  PO  $\rightarrow$  quasi-periodicity at the frequency of the bifurcation point and its rational sub-harmonics  $\rightarrow$  chaos. However, when the FR is much less than unity the sequence is CW  $\rightarrow$  PO  $\rightarrow$  quasi-periodicity at a frequency lower than but near to the external-cavity mode-separation frequency associated with components at the difference of these frequencies  $\rightarrow$  chaos.

## Broadband Terahertz Biological Sensing with a Membrane Device

H. Yoneyama<sup>1</sup>, M. Yamashita<sup>1</sup>, A. Tanabashi<sup>1</sup>, S. Kasai<sup>1,2</sup>  
H. Ito<sup>1</sup>, and T. Ouchi<sup>1,2</sup>

<sup>1</sup>Terahertz Biological Sensing Research Lab., RIKEN, 2-1, Hirosawa, Wako-shi, Saitama 351-0198, Japan

<sup>2</sup>Canon Research Center, Canon Inc., 3-30-2, Shimomaruko, Ohta-ku, Tokyo 146-8501, Japan

**Abstract**— Terahertz (THz) technology is expected to be a useful for the biosensing applications. Unfortunately, due to the strong terahertz attenuation from water, most of experiments have been limited to measurement pellet samples. In this study, we propose a membrane device that consists of micro-filter membranes and wells for holding samples in solution. The membranes used in the device can pass through THz waves and the attenuations of the materials origin are almost not found. This membrane device allows small amounts of sample to be prepared easier than current methods and enables us to analyze samples in solution after dried. Over hundred molecules were measured with this membrane device, including sugars, nucleosides, DNAs, proteins, harmful food additives, physiologically active substances and environmental hormones. We found that almost of them have their vibrational features like signature peaks in THz ranges. We will show some of experimental results in this presentation. Although several techniques have been employed for analyzing these molecules, most of methods used oxidation reagent or fluorescent reagent or radioactive label, the direct measurement methods have not been advanced yet. This membrane device is effective for direct measurements in broadband THz ranges with terahertz time domain spectroscopy (TDS) measurement system and Fourier-transform infrared spectrometry (TF-IR) measurement system. Results suggest that this membrane device is an excellent one for analyzing biomolecules. This approach promotes the understanding of the relationships between biomolecules with THz radiations. THz spectrum technology has the potential to be a useful tool in clinical diagnosis applications.

## Quadratic Data Storage System in Polymeric Material

**Kokou D. Dorkenoo**

Institut de Physique et Chimie des Matériaux de Strasbourg, UMR 7504 CNRS-ULP  
23 rue du Loess, BP 43, F-67034 Strasbourg cedex 2, France

**Abstract**— We describe an accurate method to encode a continuous gray scale image in thin films made of polymer doped with an azo dye using multi-photon processes. In this technique, the push-pull azo-chromophores have first to be oriented and then frozen in a given orientation through conventional poling techniques. This provides us with a starting condition where all the film generates a second harmonic signal (SHG) (all pixels set to “white”). In the writing process, the two-photon absorption (TPA) is used to locally disorient the chromophores in desired microscopic volumes via cis-trans isomerization cycles. The resulting decrease in second harmonic intensity is directly related to the amount of induced disorientation. The image is read back by measuring the SHG intensity point-by-point with a photomultiplier. The 3D spatial selectivity of TPA allows us to obtain 2D and 3D data storage. We also demonstrate that below a certain power there is no irreversible damage done to the sample so that the written spots can be erased by re-poling above the glass transition temperature. Near IR depoling of azo dye co-polymers provides the basis for an erasable, high density (terabits/cm<sup>3</sup>), data storage device.

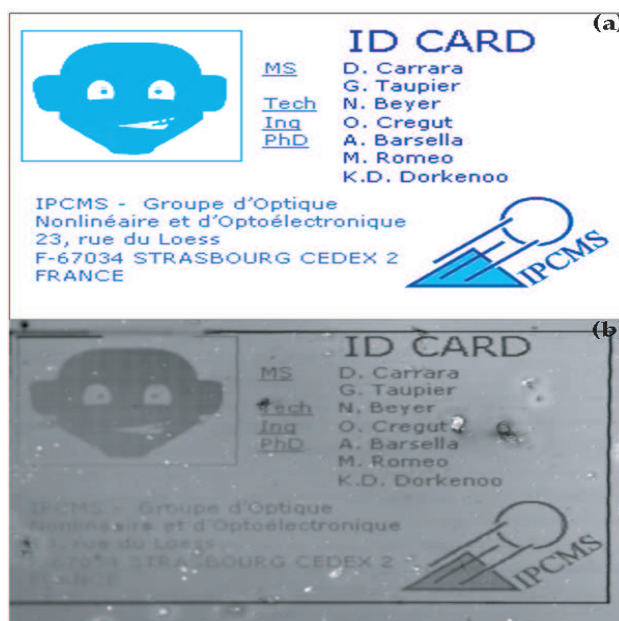


Figure 1: Gray-scale image: (a) Starting image, (b) SHG scanning microscopy image.

## Beam Spot Size Evolution of Gaussian Femtosecond Pulses after Angular Dispersion

Derong Li, Xiaohua Lv, Shaoqun Zeng, and Qingming Luo

Britton Chance Center for Biomedical Photonics, Wuhan National Laboratory for Optoelectronics  
Huazhong University of Science and Technology, Wuhan 430074, China

**Abstract**— Beam spot size evolution of Gaussian femtosecond pulses after angular dispersion is analyzed based on Gaussian beam model and verified with experiments using an acousto-optic deflector. Analytical expressions of beam spot size at arbitrary propagation distance are acquired, which indicates that beam spot size evolution after angular dispersion is determined by the direct interaction of spectra lateral walkoff by angular dispersion and the original divergence of the Gaussian beam. This work reveals insights for the propagation of Gaussian femtosecond laser beam after angular dispersion, and may be important for the generation and application of the Gaussian femtosecond laser.



## Propagation of Anomalous Hollow Beams in a Turbulent Atmosphere

Yangjian Cai<sup>1</sup>, Halil T. Eyyuboğlu<sup>2</sup>, and Yahya Baykal<sup>2</sup>

<sup>1</sup>Department of Electronic and Communication Engineering, Çankaya University  
Öğretmenler Cad. 14, Yüzüncüyıl 06530 Balgat Ankara, Turkey

<sup>2</sup>Max-Planck-Research-Group, Institute of Optics, Information and Photonics  
University of Erlangen, Staudtstr. 7/B2D-91058 Erlangen, Germany

**Abstract**— Propagation of a circular or elliptical anomalous hollow beam with a circular or elliptical solid core in a turbulent atmosphere is investigated in detail. The electric field of a circular or elliptical anomalous hollow beam is expressed as superposition of a finite sum of stigmatic or astigmatic Gaussian beam and stigmatic or astigmatic doughnut hollow beam. Based on the extended Huygens-Fresnel integral, analytical formulae for the average irradiance of a circular or elliptical anomalous hollow beam propagating in a turbulent atmosphere are derived. The irradiance and spreading properties of circular and elliptical anomalous hollow beams in a turbulent atmosphere and in free space are studied numerically. It is found that a circular or elliptical anomalous hollow beam at short propagation distance in turbulent atmosphere has similar propagation properties to that of free space, while at long propagation distance, a circular or elliptical anomalous hollow beam eventually becomes a circular Gaussian beam in a turbulent atmosphere, which is much different from its propagation properties in free space. The conversion from an anomalous hollow beam to a circular Gaussian beam becomes quicker and the beam spot in the far field spreads more rapidly for a larger structure constant, a shorter wavelength and a smaller waist size of the initial beam.

# New Optical Fiber Sensor Based on Hydrogels for Detection of Liquid Leaks

Guiling Huang<sup>1,2</sup>, Qida Zhao<sup>1</sup>, Junfeng Lv<sup>1</sup>, and Luming Zhao<sup>1</sup>

<sup>1</sup>Institute of Modern Optics, Nankai University, Tianjin 300071, China

<sup>2</sup>Institute of Photo electronic Thin Film Devices and Technology  
Nankai University, Tianjin 300071, China

**Abstract**— Various industrial fields require leak detection sensors because water, oil, and other hazardous liquid leaks provoke serious accidents. In this paper, a new kind of optical fiber sensor for the determination of leaking liquid is designed. The sensor uses a swellable polymer material, hydrogels, as the active sensing component. The sensing mechanism in this device is based on the effect of bending losses of the fiber connected to the hydrogel. The sensor can be used to respond to different trigger stimulus. This research provides a novel technique to detect leaks in underground storage tanks and oil pipeline. The system has the priority of simple, cheap and safe. It is well known that the losses of the fundamental mode in single-mode optical fibers is influenced by fiber curvature microbend loss has always been an undesirable effect that causes problems in fiber-optic communication links. However, this phenomenon has been exploited profitably in the fabrication of a variety of fiber-optic sensors to measure, e.g., pressure, temperature, and displacement. In this paper, we develop the optical fiber sensors based on hydrogels to detect liquid leaks. Hydrogels are cross-linked polymers which swell to an appreciable extent in water. The water content depends on the polymer structure, and can be made responsive to environmental factors. The outline of this paper is as follows. Section 2 introduce the basic principle of the optical fiber sensor based on hydrogels; The numerical simulation and experiment results are given in section 3, and finally the main conclusions are given in section 4.

# Longitudinal Relaxation Time Measurement in MR with Transient-state Magnetization

E. Gescheidtova<sup>1</sup> and K. Bartusek<sup>2</sup>

<sup>1</sup>Department of Theoretical and Experimental Engineering  
Faculty of Electrical Engineering and Communication, Brno University of Technology  
Kolejni 2906/4, 612 00 Brno, Czech Republic

<sup>2</sup>Academy of Sciences of the Czech Republic, Institute of Scientific Instruments  
Kralovopolska 147, 612 64 Brno, Czech Republic

**Abstract**— To measure the relaxation times  $T_1$  of polarized gases an unusual method has been proposed that makes use of the transient state of the magnetization of the nuclei being measured. The transient state is the result of multiple excitations by RF pulses with a small flip angle and an appropriate repetition time  $T_R$ .

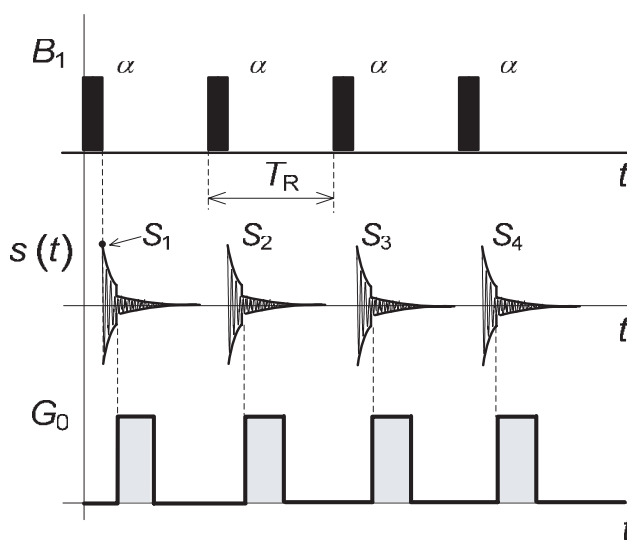
The method was designed and experimentally tested for measuring the relaxation times  $T_1$  of polarized gases with transient-state magnetization, based on measuring the MR signal levels after the termination of RF pulses.

For a higher precision of determining  $T_1$  two measurements with different repetition times were performed. The relaxation time was calculated from one or two measurements, using an optimization method. In the method described no precise calibration of the flip angle of RF pulses is necessary. The measuring precision achieved was better than 1%, and it depends on a precise determination of the magnitude of MR signal. The technique described will be used when measuring the properties of polarized gases or even liquids in porous materials.

For proposed method to be measured with sufficient accuracy it is necessary to fulfill two prerequisites:

- 1) The nuclei of the sample being measured must be excited by a series of regularly repeated RF pulses with identical flip angles  $\alpha$  and with identical repetition time  $T_R$ .
- 2) The other important prerequisite of the method is a short spin-spin relaxation time of the medium being measured; the condition  $T_2 \ll T_R$  must be fulfilled.

The pulse sequence of the proposed method for a simple series of RF pulses is illustrated in figure.



# The Electromagnetic Interaction with Tissue of a Circular Patch Antenna, Comprising a Concentric Ring and Radially Slotted Groundplane

S. Curto, X. L. Bao, and M. J. Ammann  
Dublin Institute of Technology, Ireland

**Abstract**— The study of a novel compact circular patch with a concentric ring and radial slots in the ground plane for a hyperthermia applicator at the 434 MHz ISM band shows that it exhibits an enhanced E-field coupling into simulated human tissue models. In RF-hyperthermia applicators, reducing the size of the applicator for the treatment of tumours located at curved sites of the body and the efficient delivery of electromagnetic energy are priority considerations. Designed for a small size and a low cost alternative to large resonant loops, square patches, dielectric loaded horns or dipole arrays, the lightweight antenna can be deployed in close proximity to a patient undergoing a clinical course of superficial hyperthermia treatment. Arbitrary near-field loading of an antenna by various tissue types requires that its input impedance be sufficiently insensitive to in-band resonant detuning, that it have matched bandwidth to a high powered source and that the fields in the tissue can be targeted to selected areas in the patient.

The antenna has been modelled using CST's MWS and reported here are E-fields, input impedances, surface currents and specific absorption rates. The antenna's design and properties are discussed for performance in very close proximity to human tissue models. For contrast, the free-space behaviour illustrates the tissue loading effect on the antenna. The resonant modes on the compact patch are analyzed to evaluate the coupling of fields into the tissue. As tissue layer thicknesses vary around the body and between patients, a range of skin, fat and muscle thicknesses are used to estimate appropriate distances between the antenna applicator and the patient.

## Anti-interference Design of Quasi-resonant Tank for Magnetic Induction Heating System

Cheng-Chi Tai and Ming-Kun Cheng

Department of Electrical Engineering, National Cheng Kung University, Tainan 70101, Taiwan

**Abstract**— The electromagnetic inducing of heat has been extensively studied for the treatment of local hyperthermia, wherein case deposited magnetic particles are used to locally heat human tissues. Application of magnetic materials for local hyperthermia of biological tissue has been known, in principle, for more than four decades. The main idea of hyperthermia is to raise the tissue temperature up to  $41.5 \sim 46^\circ\text{C}$  to kill malignant cells while preserving normal cells. At least two full-sized human prototypes have been built by magnetic fluid hyperthermia (MFH) and had been used shortly for the first clinical trials of hyperthermia. However, these systems usually are too bulky and with poor heating efficiency. Therefore, we intend to develop a more compact and efficient heating applicator.

Applying magnetic nanoparticle (MNP) in curing cancers has been a significant subject to the medical research. The majority of MNP heating system was performed in an induction coil or in the air-gap of a magnetic inductor, cooled by water or air. Although the structure of the electromagnetic applicator looks simple, its higher frequency and higher current mechanism are very complicated.

In the paper, we presents the design of a quasi-resonant tank for magnetic induction heating system, discusses some anti-interference applications using a half-bridge inverter with optimal construction of the circuits and decoupling design. The paper also presents a method for the design of the applicator and the place of the decoupling capacitor. By using this method, the problems of high-frequency voltage interference can be significantly reduced.

Experiments indicated that this magnetic induction heating system can satisfy well the heating requirement of a magnetic nanoparticle with a resonant frequency of approximately 220 kHz.

# The Design of a Half-bridge Series-resonant Type Heating System for Magnetic Nanoparticle Thermotherapy

Cheng-Chi Tai and Chien-Chang Chen

Department of Electrical Engineering, National Cheng Kung University, Tainan, Taiwan

**Abstract**— Application of magnetic materials for hyperthermia of biological tissue has been known, in principle, for more than four decades. Many empirical works were done in order to confirm a therapeutic effect on several types of tumors by performing experiments with animals or using cancerous cell cultures. The main idea of magnetic nanoparticle thermotherapy is to utilize 7- to 50-nm diameter of ferric oxide ( $\text{Fe}_3\text{O}_4$ ) particles which are heated up to  $42^\circ\text{C}$  under AC magnetic field for cancer therapy applications. In order to achieve the goal of killing cancer cells using the AC magnetic field, we designed a heating system to generate magnetic field which can be focused and frequency adjustable.

This study adopts the half-bridge series-resonant type circuit as the core scheme of the heating system, and utilizes the frequency-adjustable design to conduct the heating experiment. In this work, we also study the characteristics of coil from impedance aspect to improve the heating efficiency of magnetic field. Since the impedance value must be kept unchanged in the operation so as to make the current in coil and the magnetic field in a stable state, the impedance analyzer is used in the light of raising the system stability and coil impedance measurement. As for the design of coil structure, we utilize finite-element simulation software to find the place with even and more concentrated magnetic field. The experiment results show that the designed coil and the heating system can warm up the magnetic nanoparticle  $6^\circ\text{C}$  in 30 minutes, which has attained the expected heating result for the study.

## Morphological Changes Induced by 53.37 GHz Radiation on Giant Vesicles

A. Ramundo-Orlando<sup>1</sup>, M. Cappelli<sup>1,2</sup>, G. Longo<sup>3</sup>  
M. Girasole<sup>3</sup>, L. Tarricone<sup>2</sup>, and A. Beneduci<sup>4</sup>

<sup>1</sup>INMM, National Research Council Establishment, Via Del Fosso del Cavaliere, 100, Roma 00133, Italy

<sup>2</sup>Department of Innovation, University of Salento, Lecce, Italy

<sup>3</sup>ISM, National Research Council Establishment, Via Del Fosso del Cavaliere, 100, Roma 00133, Italy

<sup>4</sup>Department of Chemistry, University of Calabria, Arcavacata di Rende (CS), Italy

**Abstract— Objectives:** As reported in literature [1,2] the biological response to millimeter waves (MMWs) appears deeply related to the frequency range and the level of power radiation. A part from the thermal effects that occur at high powers ( $> 10 \text{ mW/cm}^2$ ), it was conjectured that the interaction between MMWs and biological systems could involve resonant/non-thermal mechanisms at very low powers [3]. Since the biophysical mechanisms underlying these effects are still unknown, studies to fill important gaps in knowledge focused on possible health hazards of electromagnetic fields are recommended by European and WHO reports [4]. To significantly reduce the uncertainty in the current scientific information researchers are encouraged to use a modeling approach for testing how EMF interact with biological systems. Previous studies [5,6] in our laboratory have indicated that vesicles are an eligible model to study changes on lipid membranes induced by 2.45 GHz and 130 GHz, so that physical and biochemical processes may be isolated and analyzed in molecular terms.

Here, we report an approach to a real time evaluation (i.e., during the irradiation to 53.37 GHz) of morphological changes induced on giant vesicles.

**Methodology:** We used giant unilamellar vesicles (GUVs) consisting of egg yolk phosphatidylcholine (Sigma) prepared by electroformation method [7]. We worked with alternating current (ac) electric fields and specially constructed investigation chamber containing two parallel platinum wires where lipids are deposited and formed. In order to visualize the effects on shape, size and budding process of the bilayer induced by irradiation, we directly observed GUVs with phase contrast microscopy (OLYMPUS IX70). Fluorescence images were also obtained after incubation of GUVs with di-8-ANEPPS (2 mM). The irradiation was carried out by means of a MMWs Band low intensity device (IMG-53.37 manufactured by Micro Med Tech, Russia) during overall microscopy observation. The temperature was measured by using thermocouples (positioned at different points in the medium) and an infrared camera.

**Results and Conclusion:** Preliminary results have shown that, when irradiated at 53.37 GHz, spherical vesicles assume prolate shapes (Fig. 1). Similar shape deformation of giant vesicles

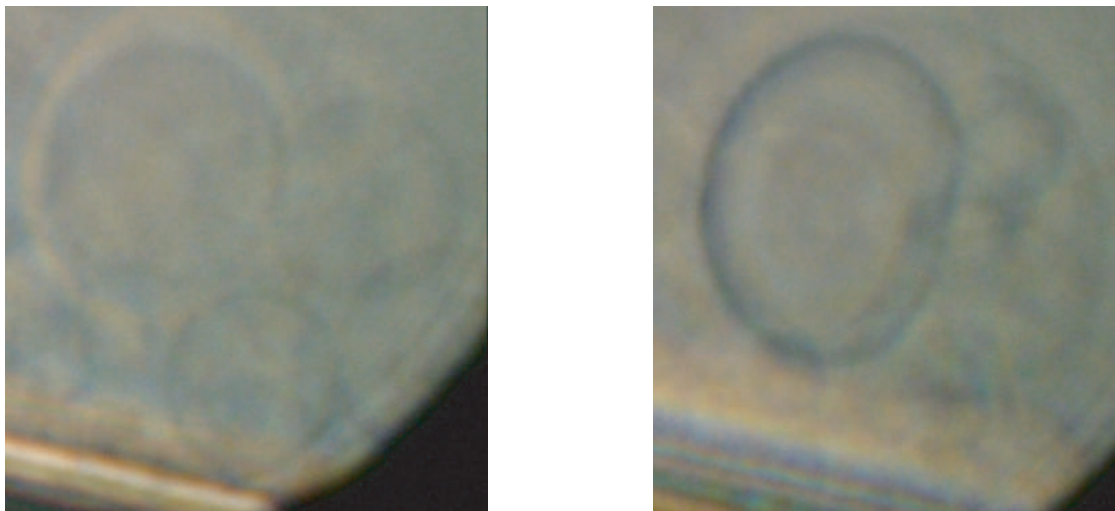


Figure 1: Phase contrast microscopy observation of giant vesicles. Sham samples (left) showing spherical giant vesicles. Under 53.37 GHz radiation for 5' (right) sphere-to prolate transformation is observed.

has already been reported for exposure to AC fields depending on several parameters, including field strength, frequency, and conductivities of the media [8]. However, no relaxation back to the initial vesicles shapes were observed after the 53.37 GHz radiation has been turned off, indicating that other factors were involved in the observed phenomenon. The fluorescence analysis revealed an enhancement of the vesicles motion respect to the wires position. Di-8-ANEPPS has been used to enhance the contrast of the vesicles' edges. During the irradiation a sharp increase in the diffusion of the dye has been observed resulting in a blurring of the vesicle edges. The membrane model used in these studies appears to be a sensitive system to MMWs radiation at low power density (about  $10 \text{ mW/cm}^2$ ). Future studies will provide a better evaluation of all exposure conditions so as to optimize the application of the MMWs radiation and to assure a complete monitoring of external conditions.

#### REFERENCES

1. Pakhomov, A. G., et al., *Bioelectromagnetics*, Vol. 19, 393–413, 1998.
2. Fedorov, V. I., et al., *Int. J. Infrared and Millimeter Waves*, Vol. 24, 1235–1254, 2003.
3. Fröhlich, H., *Biological Coherence and Response to External Stimuli*, 1–24, (H. Fröhlich Ed.), 1988.
4. 2006 WHO Research Agenda for Radio Frequency Fields ([www.who.int](http://www.who.int)).
5. Ramundo-Orlando, A., et al., *Bioelectromagnetics*, Vol. 15, 303–313, 1994.
6. Ramundo-Orlando, A., et al., *Bioelectromagnetics* on line, 2007.
7. Angelova, M. I. and D. S. Dimitrov, *Faraday Discuss. Chem. Soc.*, Vol. 81, 303–11, 1986.
8. Dimova, R., et al., *Soft Matter*, Vol. 3, 817–827, 2007.



## A Novel Method for Passive Shim Design: II

Hector Sanchez Lopez, Feng Liu, Ewald Weber, and Stuart Crozier

School of Information Technology & Electrical Engineering

The University of Queensland

St. Lucia, Brisbane Qld 4072, Australia

**Abstract**— This paper presents a new passive shim design method and a novel shimming procedure to correct the magnetic field inhomogeneities generated by biplanar partially open Magnetic Resonance Imaging magnets. The method produces biplanar passive shim solutions capable of generating harmonics with high purity and using a minimal number of ferrosims. The magnetic coupling among shim pieces is considered and its effect over high harmonic order is analysed for linear and nonlinear ferrosim.

**Introduction:** Magnetic resonance imaging (MRI) requires a main magnet to produce a strong and very homogeneous magnetic field (a few parts per million) within the imaging region. Reproducing the magnet theoretical dimensions as accurately as possible in the manufacturing process is very difficult. Due to machining tolerances unavoidable errors are introduced in the permanent magnet and poles positions and therefore in the expected magnetic field homogeneity and as a consequence a passive and/or active correction process is required [1]. In this paper we present a novel passive shimming approach for biplanar shim where the thickness is expressed as a sum of orthogonal functions multiplied by unknown amplitudes. The thickness is expressed as a function of the azimuthal angle and shim domain radius and hence, an optimal shimming procedure can be achieved for a set of particular harmonics impurities, DSV size, and pole face dimension.

**Materials and Methods:** We assume an isotropic and homogenous ferromagnetic disk of radius  $\rho_{\max}$ , uniformly magnetized ( $M_z e_z$ ) along the axial axis. The disk thickness  $t$  is much smaller than the axial distance ( $Z_0^\pm$ ) between the two pole faces and thick enough to produce an induced magnetization  $M_z$  along the axial axis. The volume of the magnetized element in the continuous shim domain is written as:  $dV' = \rho' \cdot t(z, \phi')^\pm d\rho' d\phi'$ , where the scalar magnitude  $t(\rho', \phi')^\pm$  represents the element thickness at the point  $(\rho', \phi')$  and can be expressed as a sum of orthogonal functions multiplied by unknowns amplitudes. The sign (+ and -) are used to identify the pole faces. The coefficients corresponding to the magnetic field oscillating harmonics are written as:

$$A_{nm} = \int_{\rho_{\min}}^{\rho_{\max}} \int_0^{2\pi} C_{nm}(\rho', \phi') \cos m\phi' d\rho' d\phi' \quad \text{and} \quad B_{nm} = \int_{\rho_{\min}}^{\rho_{\max}} \int_0^{2\pi} C_{nm}(\rho', \phi') \sin m\phi' d\rho' d\phi',$$

where  $C_{nm}$  contains the function  $t(\rho', \phi')^\pm$ . A least squares optimization algorithm is used to obtain the optimal amplitudes of the  $t(\rho', \phi')^\pm$  thickness function that minimizes the disk weight  $W(\rho', \phi')$  and at the same time, cancel the target harmonics and control the high orders field components excluded in the target set. From the continuous thickness map, a valid domain (regions with positive thickness) is set and discrete pieces of shim are chosen. A linear programming optimization algorithm is then employed to obtain the discrete thickness distribution. An iterative process for thickness calculation taken into account the magnetic coupling is performed until no significant variation of the shim thickness is produced.

**Results and Conclusions:** This approach was applied for a case where a combination of harmonics forms the harmonic target set. The target harmonic produces a peak-to-peak magnetic field inhomogeneity equivalent to 447.46 ppm. Fig. 1 (+a, -b) shows the thickness map and the valid domain (+c, -d) (the starting point for placing discrete shim pieces). The addition of the un-shimmed magnetic field and the magnetic field generated by the discrete shim array shown in Fig. 1 (+e, -f) reduces the peak-to-peak magnetic field inhomogeneity to 2.87 ppm. The figure of merit value corresponding to the discrete array was  $\eta = 7.96 \cdot 10^{-5} \text{ T}/(\text{kg}\cdot\text{ppm})$  and the weight of the iron shim set was 1.29 kg. The shim profile obtained by considering the field contribution of all the shims uniformly distributed on the pole face surface (traditional technique) generates a figure of merit  $\eta = 3.30 \cdot 10^{-5} \text{ T}/(\text{kg}\cdot\text{ppm})$ . This value is 2.41 times smaller than the same parameter produced with our approach. The corrected peak-to-peak field inhomogeneity was 8.79 ppm using 1.4 kg of iron. The total shim set weight was nearly less of that needed when using classical approach (i.e., to search directly for the shimming solution without using a continuous map as a starting point) and the homogeneity was improved 3 times using the profile shown in Fig. 1(g). The ferrosims thickness expressed as a sum of orthogonal series

in functions of the azimuthal angle and shim domain radius, provides a useful map where the shim shape and thickness is well defined. The placement of the ferroshim pieces in the effective domain significantly reduces the shim weight and improves the field homogeneity. The new shim profiles presented in this research generates highly pure harmonics and high orders in an efficient manner. The magnetic coupling effect produces a small impact over the low order harmonics and very high impact over high order and degrees when linear iron is used for shimming. When using nonlinear iron and the magnetic coupling is no taken into account the large impact over the orders and degrees can lead toward wrong path in the shimming procedure and the target field homogeneity could never be reached.

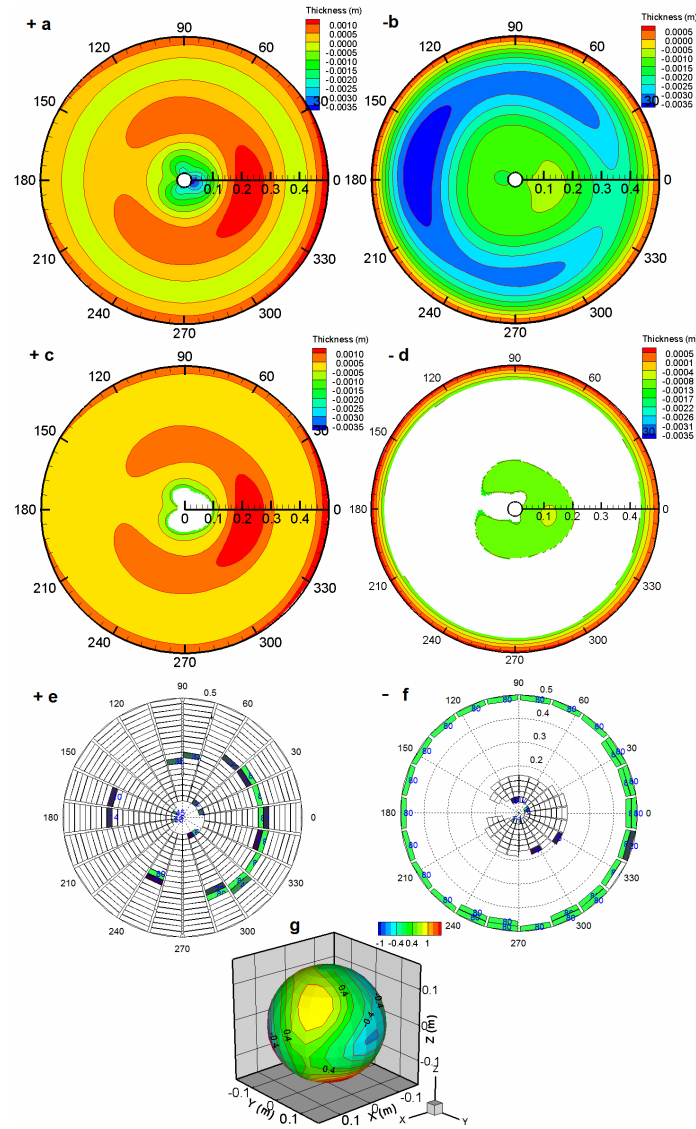


Figure 1.

## ACKNOWLEDGMENT

Financial support for this project from the Australian Research Council is gratefully acknowledged.

## REFERENCES

1. Sanchez Lopez, H., F. Liu, E. Weber, and S. Crozier, "A novel method for passive shim design: I," submitted to *PIERS08*.

# Design of Tunable Filter with Fiber Bragg Gratings with Cladding Made of Electro-optic Materials

Shang-Lin Hou<sup>1,2</sup>, Suo-Ping Li<sup>1</sup>, Dao-Bin Wang<sup>1</sup>, and Jing-Li Lei<sup>1</sup>

<sup>1</sup>School of Science, Lanzhou University of Technology, Lanzhou 730050, China

<sup>2</sup>Key Laboratory of Optical Communication & Lightwave Technologies of Ministry of Education Beijing University of Posts and Telecommunications, Beijing 100876, China

**Abstract**— Fiber gratings have developed rapidly since the optical sensitivity was described in 1978. Numerous applications have been demonstrated that utilize fiber grating as dispersion compensator, density wavelength division multiplexer (DWDM), fiber laser, fiber sensors and so on. Fiber Bragg gratings can be used as spectrum filter due to its superior reflectivity. The index contribution has a great impact on the reflectivity of the fiber Bragg gratings. Uniaxial anisotropic electro-optic crystal material, i.e.,  $\text{LiNbO}_3$ , is complex due to its indices difference along its various axes. Electro-optic effect and elasto-optic effect in a chirped fiber grating with cladding made of uniaxial crystal material are theoretically analyzed in 2004 and the results indicate that the reflected spectra of the chirped grating can be changed by the electric field and the strain applied to the fiber grating cladding along  $z$ -axis. The characteristics of a new type of fiber Bragg grating with cladding made of uniaxial crystal material were predicted in 2007 and the calculated results indicate that parameter  $K_{cl}$ , i.e., the ratio of the extraordinary ray refractive index to the ordinary ray index, has a strong impact on the reflectivity and the Bragg wavelength. Thus, the index contribution can be adjusted to design the characteristics of the fiber if its cladding is made of the uniaxial material.

In this work, first, we presented the electro-optic effect of uniaxial anisotropic electro-optic crystal material, i.e.,  $\text{LiNbO}_3$ , then the wave equations were established in both the cladding and the core, at last the reflectivity of this kind of fiber Bragg grating was investigated using coupling theory and numeric solution.

Following the analysis mentioned above, we designed a new tunable spectrum filter based on the fiber Bragg grating with cladding made of uniaxial anisotropic electro-optic crystal material, i.e.,  $\text{LiNbO}_3$ , whose optical axis is parallel to the axis of fiber Bragg grating. The filter is made up of a Fiber Circulator, a fiber Bragg grating and an electric field generator as shown in the following figure. Tuning is achieved by changing the voltage applied to the electrodes of the electric field generator to induce the electric field running along the axis of the fiber Bragg grating to vary the refractive-index difference expressed by parameter  $K_{cl}$ , i.e., the ratio of the extraordinary ray refractive index to the ordinary ray index, which eventually changes the reflectivity and the Bragg wavelength of the fiber Bragg grating.

By changing the index distribution of the cladding, you will tune the filter at difference wavelength ( $\lambda_B$ ). Since tuning is done by an electric field, tuning speed is very high. Low loss, easy coupling, a narrow bandwidth, and high resolution are the advantages of this kind of fiber Bragg grating tuning filter, while its dynamic range can reach the order of 10 nm and it can be spreading by cascading several this kind of filter with different center Bragg wavelengths.

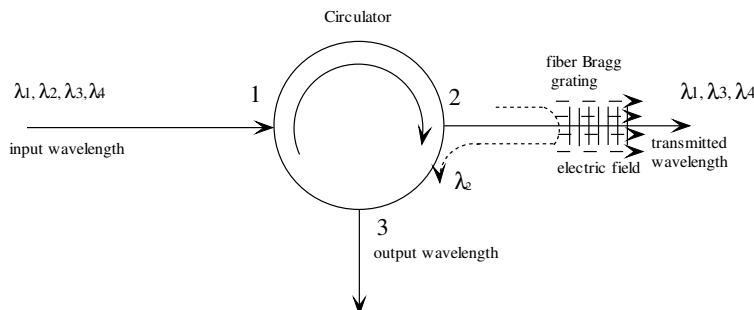


Figure 1: Sketch of the tunable filter based on fiber Bragg grating with uniaxial anisotropic electro-optic crystal material.

**ACKNOWLEDGMENT**

Project supported by the Natural Science Foundation of Gansu Province, China (Grant No. 3ZS062-B25-036) and the Training Plan Fund for Outstanding Young Teachers of Lanzhou University of Technology.

# Fiber Grating Designing Method Based on Multi-subpopulation Competition Evolutionary Algorithm

Zhaoniu Huang<sup>1,2</sup>, Songfen Liu<sup>3</sup>, and Guiling Huang<sup>4</sup>

<sup>1</sup>Guangxi Shipping School, Guangxi 530007, China

<sup>2</sup>Guilin University of Electronic Technology, Master's Degree of Engineering

<sup>3</sup>Department of Physics, Nankai University, Tianjin 300071, China

<sup>4</sup>Institute of Modern Optics, Nankai University, Tianjin 300071, China

**Abstract**— This paper presented a promising method to synthesize the physical parameters of fiber Bragg grating numerically from FBG reflection spectrum. The method is based on a Multi-subgroup competition evolutionary algorithm. The novel method was applied to design the structure parameters of uniform FBG for filtering, and chirped FBG for dispersion compensation. The inverse problem is a classical problem in applied physics and engineering fields. An example of such a problem is to synthesize or reconstruct the physical parameters (such as length of grating  $L$ , grating period  $\Lambda$ , and difference in refractive indices  $\Delta n$ ) of a fiber Bragg grating (FBG) structure from its reflectivity. Such research is most important for both device design and characterization purposes. Many synthesis methods have been proposed and achieved various degrees of success in recent years, such as the Fourier transform technique, the GLM method, time-frequency signal representations and layer peeling techniques, which have been shown to be effective in the design of some special FBG devices. But all these methods require information on both the amplitude and the phase of the FBG reflection coefficient. Other powerful synthesis methods are the optimization methods based on some global optimization techniques. Evolutionary algorithms are the most widely used optimization methods. The analysis curve of the gratings designed here shows a good agreement with the expected curve and the algorithm is better than classical evolutionary programming algorithm in the aspects of global optimization and convergence.

## A Study of Detection Technology for Liquid Leakage Base on Fused-biconical Fiber Couplers

Zhaoniu Huang<sup>1</sup> and Guiling Huang<sup>2</sup>

<sup>1</sup>Guangxi Shipping School, Guangxi 530007, China

<sup>2</sup>Institute of Modern Optics, Nankai University, Tianjin 300071, China

**Abstract**— This paper presents a novel detection technology for liquid leakage, whose sensing elements are fused-biconical single-mode optic fiber couplers. The sensing principle of this new class fiber optic sensor is based on the fact that when the waist of a fused-biconical single-mode optic fiber coupler is dip in the liquid, the absorption of the evanescent wave changes and the coupling ratio also changes. Using fiber sensors and fiber cable, we can measure, monitor and analysis the leakage situation of the liquid tanks far away from the liquid tanks on line. The proposed system consists of a light source, transmitting fiber, fused-biconical single-mode optic fiber coupler, a photodetector (PD), and a digital multimeter for output voltage monitoring. Recently, Liquid tanks leak detection has been domestic and international concerns. Specially the oil leak will not only bring about great economic losses, a negative impact to the surrounding ecological environment, but also are susceptible to fire and explosion incidents, the oil leakage detection of a very practical meaning. With the development of fiber optic sensing technology, optical fiber sensors are gradually being applied to industrial process control and measurement detection. The optical fiber sensor detection modules and optical fiber signal transmission lines do not contain current, which itself is a safe system. The technology and system presented in the paper has the advantages of simple, easy fabricated, low cost. In particular, by using the coupling ratio of the output power, the fluctuations in transmission loss can overcome. The system can be developed to a quasi-distributed sensor network for remote monitoring.

## Influence of the Cladding Diameter of Tilted Fiber Bragg Grating on the Refractive Index Sensitivity Characteristic

Yinping Miao, Qida Zhao, Bo Liu, Bo Dong, and Guiling Huang  
Institute of Modern Optics, Nankai University, Tianjin 300071, China

**Abstract**— Short-period fiber Bragg grating with weakly tilted grating planes generates a large number of narrowband cladding mode resonances in transmission. In this letter, we present a simple high-sensitivity optical chem-sensor device based on tilted fiber Bragg grating (TFBG) and post-sensitized by a hydro-fluoric (HF) etching treatment. This technique is based on the global monitoring of cladding modes in the transmitted spectrum. Owing to the presence of the Bragg grating resonance in the transmitted spectrum, the sensor is intrinsically sensitive to temperature change with in the range of 20°C–100°C. This feature is particularly useful since the refractive index varies with temperature. The cladding-mode resonances can be enhanced greatly by etching the cladding of the TFBG. When the cladding diameter is reduced, due to surrounding medium refractive index modifications, it will lead to the cladding-mode resonance wavelengths shifts. In order to analyze the evolution of the cladding modes couplings in the surrounding medium, We use a set of index oils and measure the fiber diameter with respect to different etching time by a microscope. Our experimental results show that the measurement of the refractive index of the medium surrounding the fiber for values between 1.003 ~ 1.45 with an accuracy approaching  $1 \times 10^{-4}$  and analyzed the refractive sensitivity characteristic of TFBG theoretically by using the three-layer media optical wave-guide. In this way a refractometer with high accuracy and high sensitivity can be achieved. This way can provide fast results and be used in real-time operating systems. So it is potential use in accurate refractometry.

## A Compact Filter with Good Performance Based on Super-compact Multilayered Left-handed Transmission Line

Hao Hu, Anxue Zhang, Yansheng Jiang, and Zhuo Xu

School of Information and Electronics Engineering, Xi'an Jiaotong University, China

**Abstract**— In this paper, an improved structure for the design of bandpass filters with obviously size reduction and good performance at high frequency is presented. This structure is based on super-compact multilayer-ed (ML) composite-right/left-handed (CRLH) transmission line (TL), firstly proposed by the authors Yasushi Horii, Christophe Caloz and Tatsuo Itoh in the article “Super-Compact Multilayered Left-Handed Transmission Line and Diplexer Application” on April 2005. The ML architecture, designed by the authors, consists of the periodic repetition of pairs of U-shaped parallel plates provided the left-handed (LH) series capacitance, connected to a ground enclosure by meander lines which provided the LH shunt inductance. The right-handed parasitic series inductance and shunt capacitance are generated by the metallic connections in the direction of the propagation and by the voltage gradient from the TL to the ground enclosure, respectively. However the frequency of this structure is low (about 0.4 GHz) and the performance in the passband is not desired. To improve this, some research has been done on the architecture properties with the commercial 3D electromagnetic stimulation tool-CST, and then we draw some conclusions such as using the rectangle line in the LH unit cell instead of the meander lines can greatly increase the frequency, and the larger the width of the rectangle line is, the higher the frequency will be. And also some influence on frequency and performance made by the space between the U-shaped parallel plates, the distance between the ground enclosure and the unit cell, the length of metallic connection and the height of the ground enclosure. Moreover, some improvements have been made by using much narrower rectangle line in the middle layer of the architecture to eliminate the undesired resonances when frequency increases and more layers to improve the performance in the band pass. Based on these research, an improved filter has been proposed, not only exhibiting particularly small dimensions, less than 5 by 4 mm on a very high frequency (e.g., 9.5 GHz), but also have the distinct advantage of less than 0.7 dB in-band loss, greater than 18 dB return loss in the passband and 1GHz bandwidth. In addition, this proposed filter can be implemented using modern low-temperature co-fired ceramic (LTCC) processes.



# Scattering Characteristics of a New Dielectric Periodic Array Composed of Left-handed Gratings

Wei-hai Fang and Shan-jia Xu

Department of Electronics Engineering and Information Science  
University of Science and Technology of China, Hefei, Anhui 230027, China

**Abstract**— The scattering characteristics of a new dielectric periodic array composed of left-handed gratings are carefully investigated by a method which combines the multimode network theory with the rigorous mode matching method. The variations of the frequency selective characteristics with the number of periodic layers are presented and comparisons of scattering properties between the left-handed and right-handed periodic arrays are also shown with some explanations. Guidelines for accurate design of the millimeter wave frequency selective surface are given.

## ACKNOWLEDGMENT

This work is supported by the National Natural Science Foundation of China (No. 60471037, 60531020).

## Propagation Characteristics of a Novel NRD Guide with Double-LHM Slab Layer

Yongmei Pan and Shanjia Xu

Department of Electronics Engineering and Information Science  
University of Science & Technology of China, Hefei 230027, China

**Abstract**— A new waveguiding structure based on Nonradiative Dielectric (NRD) guide with a double Left Hand Material (LHM) slab layer is carefully investigated. Rigorous multi-mode network treatment combining with mode matching method is carried out to analyze the propagation characteristics of the structure. Theoretical analysis results reveal that depending on the choice of the permittivity and permeability of the two dielectric slabs, the guiding structure is of series distinct and interesting properties, such as anomalous dispersion, opposite polarization modes coupling, and the existence of the complex mode. Besides, the new configuration can also be used as a leaky wave antenna working in the dominant or the first higher mode. All these particular features create various applications in electromagnetic engineering. Physical insights and intuitive justifications for the mathematical findings are also presented.

### ACKNOWLEDGMENT

The work described in this paper is supported by the National Natural Science Foundation of China (No. 60471037) and (No. 60531020).

## Realization of Even Amplitude and Phase Distributions in Series Feed Configuration with Composite Right/Left-handed Transmission Line

Yuanchun Li, Qi Zhu, Jun Zhang, Jiali Lai, and Shanjia Xu

Dept. of EEIS, University of Science & Technology of China, Hefei 230027, China

**Abstract**— Based on Composite Right/Left-Handed Transmission line (CRLH-TL), a novel series feed configuration is proposed, which realize even amplitude and phase distributions among different output ports in a large array within a relatively wide bandwidth. In the structure, single stubs and double stubs are employed to realize even amplitude distributions among different ports, while CRLH-TLs are used to compensate the phase delay caused by the different length of Right-Handed transmission line because Left-handed Transmission lines' group velocities and phase velocities are reversed. Finally, a series feeding network has been designed as an example.

### ACKNOWLEDGMENT

This work is supported by the National Natural Science Foundation of China (No. 60471037, 60531020).

## Design of Microstrip Array with Series Fed Configuration

Wenhui Mao, Qi Zhu, Yuanchun Li, and Shanxia Xu

Dept. of EEIS, University of Sci. & Tech. of China, Hefei 230027, China

**Abstract**— Based on composite Right/Left-handed transmission line (CRLH-TL) and microstrip antenna with broad beamwidth, a novel microstrip array with series feeding configuration working at large angles is presented here. In the structure of the microstrip array element, a conducting cylinder and the coupling aperture are used to obtain a 3-dB beamwidth of  $170^\circ$ , which is much wider than that of traditional microstrip antenna. Meanwhile, because Left-handed Transmission lines' group velocities and phase velocities are reversed, even phase distribution among elements in a series feeding array can be achieved by means of CRLH. As an example, a microstrip array with present broad beamwidth microstrip antenna and CRLH-TL series fed configuration has been designed. Numerical results reveals that present array working at large angle, has higher gain and lower side lobe level than those of traditional parallel and series fed microstrip arrays. Moreover, the novel microstrip antenna array shows other advantages, such as simple in structure, small in area, low insertion loss and high efficiency.

### ACKNOWLEDGMENT

This work is supported by the National Natural Science Foundation of China (No. 60471037, 60531020).

# The Research on Application of Composite Meta-material in Rectangular Waveguide

Man-na Han<sup>1</sup>, Qiang Sui<sup>1</sup>, and Chao Li<sup>2</sup>

<sup>1</sup>Communication University of China, Beijing, China

<sup>2</sup>Institute of Electronics, Chinese Academy of Sciences, Beijing, China

**Abstract**— In this paper, the application of meta-material on the design of rectangular waveguide filters is presented and discussed. Split-ring resonators (SRRs) and complementary split-ring resonators (CSRRs) are applied in rectangular waveguide, the influence of SRR and CSRR on the propagation property in rectangular waveguide has been investigated.

A fearfully narrow-band band pass filter which based on the combination of rectangular waveguide irises and split-ring resonators (SRRs) was designed and fabricated. In the filter, the rectangular waveguide irises as an inductive window offered a negative permittivity, and the SRRs which accreted on the medium offered a negative permeability. Then the combination of irises and SRRs is applied as an resonator, we obtained its equivalent circuit, and designed the filter based on it. Experimental verification of the rectangular waveguide band pass filter has been carried out, the results of the simulation and measured are given in the paper. However, the final response has been shifted a little as compared to the simulation. This is probably due to the fact that dimensions are very close to the limits, and the effective distances between irises do not exactly correspond to the nominal values.

A band reject filter is also discussed in this paper, an array of CSRRs has been etched on the underside of the rectangular waveguide to produce a negative permeability, and then it can be a band reject filter. We etched CSRRs in the longitudinal of the rectangular waveguide, namely the direction of propagation. We had simulated several arrays of CSRRs, and the response of this form is the best, because the electric along the direction of propagation is the strongest. The device produces a deep rejection frequency band with sharp cutoff, and exhibits a flat and lossless passband, the simulated result has been given in the paper. The structure based on CSRRs has been used on designing filters after the concept was proposed in 2004. To the authors' knowledge, the application of CSRRs is always on planar circuit, such as microstrip lines, not in rectangular waveguide filters. However, the rejection frequency band is not as deep as CSRRs etched on microstrip lines, it provides a new thread about the application of the CSRRs in rectangular waveguide.

# Magneto-tunable Left-handed Material Based on Yttrium Iron Garnet

Hongjie Zhao<sup>1</sup>, Ji Zhou<sup>1</sup>, Qian Zhao<sup>1</sup>, Bo Li<sup>1</sup>, Lei Kang<sup>1</sup>  
Yang Bai<sup>2</sup>, and Xing Zhang<sup>1</sup>

<sup>1</sup>State Key Laboratory of New Ceramics and Fine Processing  
Department of Materials Science and Engineering  
Tsinghua University, Beijing 100084, China

<sup>2</sup>Corrosion and Protection Center, Key Laboratory of Environmental Fracture (Ministry of Education)  
University of Science and Technology, Beijing 100083, China

<sup>3</sup>Department of Physics, University of Texas at Arlington, Arlington, TX 76019, USA

**Abstract**— A magneto-tunable left-handed material (LHM) consisting of yttrium iron garnet (YIG) slab and metallic wires has been demonstrated by experiments and simulations. The left-handed passband through the LHM can be dynamically and continuously tuned in a wide frequency region by an applied magnetic field. The tunability of the passband is attributed to that of the negative permeability induced by ferromagnetic resonance in the YIG slab. We proposed a convenient means to design tunable LHM based on the ferromagnetic materials as an alternative to tunable split ring resonators.

## Experimentally Demonstration of Isotropic Negative Permeability in a Three-dimensional Dielectric Composite

Qian Zhao, Lei Kang, Bo Du, Hongjie Zhao, Qin Xie, Xueguang Huang, Bo Li  
Ji Zhou, and Longtu Li

State Key Lab of New Ceramics and Fine Processing, Department of Materials Science and Engineering  
Tsinghua University, Beijing 100084, China

**Abstract**— Isotropic negative effective permeability resulting from Mie resonance was demonstrated experimentally and numerically in a three-dimensional (3D) dielectric composite consisting of dielectric ceramic cube arrays. It shows that a strong sub-wavelength magnetic resonance can be excited in dielectric cubes corresponding to the first Mie resonance mode, where the negative effective permeability is verified by analyzing the dispersion properties. Such sub-wavelength magnetic resonance results from the enhancement of the displacement current inside each dielectric particles, distinct from that of metallic SRRs, and can be easily controlled by the size, volume ratio, and permittivity properties of the dielectric cubes. Microwave scattering experiments are performed on the combined BST cubes/metal wires medium, and the results shows that a pass-band appears within the forbidden band of the BST cubes, which confirms that the effective permeability of the BST cubes composite is negative in the region. The performance of such composite shows a promise of isotropic 3D left-handed materials with more simple structure and in higher frequency.

# The Negative Parameters of Left-handed Materials Consisting of Granular Composite

**X. Gao**

Electronics and Information College, Hangzhou Dianzi University  
Hangzhou 310018, China

**Abstract**— Recently, left-handed material (LHM) has received much attention for potential applications and their interesting properties. And aiming at constituting LHM, some approaches have been proposed including granular composite method. There are some investigations in the possibility of preparing LHM with metallic magnetic granular composites. The effective refractive index of a kind of granular composite, which consists of granular metallic and magnetic granular inclusions with different radius embedded in a host medium, is theoretically investigated in this paper. Simulation results show that for certain volume fractions of these two inclusions, the negative permittivity peak shifts to low frequency and the peak value increases with increasing radius ratio of the magnetic granulae to that of metallic granulae. Simultaneously, peak value of permeability decreases with the radius ratio, and value peak shifts to high frequency with increasing volume fraction of magnetic inclusion. In addition, the possibility of constructing tunable granular composite LHM by using electrorheological and Magnetorheological effect also investigated. By altering the external electric and magnetic fields, the granulae can be arrayed and clustered, which maybe lead to certain concentration of the two kinds of particles, in turn forms tunable granular composite LHM.



## Hydrogenated Amorphous Silicon-based Thin Film Solar Cells

S. Khalefa<sup>1</sup>, M. Sbeta<sup>2</sup>, and A. Abugalia<sup>2</sup>

<sup>1</sup>Plasma Research Laboratory, Libya

<sup>2</sup>Center for Solar Energy Studies œ Libya, Libya

**Abstract**— The electric and the photo characteristics of solar cells were studied at TU-Delft (Holland). The deposition technique that was used is an rf PECVD AMOR deposition system “radio frequency Plasma Enhanced Chemical Vapor Deposition” on an amorphous thin films that has been deposited on a supporting substrate made from glass. The system is monitored and controlled by a computer system. The control system manipulates the robotic arm transport mechanism, gas flow rates, pressure, temperature and rf power level. A high quality thin films were deposited at temperature of 180Co and an rf power of 4 watts, while CVD “Chemical Vapor Deposition” techniques require higher temperature range to produce similar quality films. Another system is used (Leybold deposition system cvd) for depositing metallic contacts from either silver (Ag) or aluminum (Al). Amor and Leybold systems were used to deposit devices and layers with different specifications. Two substrates were used for layer; glass-based and c-Si wafer-based while tco-coated glass substrate was used for devices. Three types of glass-based layers; p, n and i were deposited with 300 nm thickness each. Three 300 nm intrinsic layers of c-Si based-wafer were deposited at three different rf powers; 3 W, 4 W and 5 W. On the other hand three devices with three different thicknesses; 150 nm, 300 nm and 450 nm were deposited on tco-coated substrate.

## Electromagnetic Field Quantization in an Anisotropic Magnetodielectric Medium with External Charges

Majid Amooshahi and Fardin Kheirandish

Department of Physics, University of Isfahan, Isfahan, Iran

**Abstract**— In order to quantize electromagnetic field in the presence of an anisotropic magnetodielectric medium we enter the medium directly in the process of quantization modelling it by two independent set of harmonic oscillators which we call them  $E$  and  $M$  quantum fields. The  $E$  and  $M$  fields describe polarizability and magnetizability of the medium, respectively. This means that in our approach the electric and magnetic polarization densities of the medium are defined, respectively as linear combinations of the ladder operators of the  $E$  and  $M$  quantum fields. Some coupling tensors are introduced which couple the medium with electromagnetic field. The coupling tensors have a key role in this quantization scheme so that the electric and magnetic susceptibility tensors of the magnetodielectric medium are obtained in terms of these coupling tensors. Also, the explicit forms of the noise polarization densities are obtained in terms of the coupling tensors and the ladder operators of the  $E$  and  $M$  fields at  $t = 0$ . It can be shown that when the medium tends to a non-absorbing one, the noise densities also tend to zero and this quantization scheme reduced to the usual quantization in these media. Using a Hamiltonian in which the electric and magnetic polarizations interact minimally respectively with the displacement and magnetic fields, the Maxwell equations, the constitutive equations of the medium and the equations of motion of the external charged particles are obtained as the Heisenberg equations of the total system. As a simple application, the spontaneous decay rate of a two-level atom is calculated in the presence of an anisotropic magnetodielectric medium.

## Study on Elliptical Cylinder and Elliptical Sphere Electromagnetic Cloakings

Kan Yao, Chao Li, and Fang Li

Institute of Electronics, Chinese Academy of Sciences, China

**Abstract**— Recently, the design of medium which exhibit complex and interesting electromagnetic behavior has been widely studied. The concept of using coordinate transformations to produce material of special properties opened an exciting gateway for electromagnetic cloaking and invisibility. In this concept, the properties of an electromagnetic medium in a space with non-flat topology may be studied under series of proper coordinate transformations.

Prof. Schurig and Pendry have presented cloaking structures based on an anisotropic medium whose permittivity and permeability are obtained from a homogeneous medium, by transformations of coordinates. The results of radial transformations are studied, such as situations of cylindrical and spherical cloaking. In this paper, we study elliptical cylinder and elliptical sphere cloaking by a series of transformations. The analytical and the simulated results are both given and they agree well with each other. These new cloakings may lead to more practical applications since their shapes are more flexible as compared to cylindrical and spherical ones.

# Microscopic Origins of Nonlinearity in Superconducting Microwave Devices

Alexander Zhuravel<sup>1</sup>, Alexey Ustinov<sup>2</sup>, and Steven M. Anlage<sup>3</sup>

<sup>1</sup>B. Verkin Institute for Low Temperature Physics and Engineering  
National Academy of Science of Ukraine, Kharkov, Ukraine

<sup>2</sup>Physics Institute III, University of Erlangen, Nuremberg, Germany

<sup>3</sup>Physics Department, Center for Nanophysics and Advanced Materials  
University of Maryland, College Park, MD 20742-4111, USA

**Abstract**— High power applications of superconducting microwave devices are limited by extrinsic defects that produce nonlinearity, as seen through intermodulation distortion, for example. The technique of low-temperature Laser Scanning Microscopy (LSM) [1] has been applied to the investigation of local microwave properties in superconducting  $\text{YBa}_2\text{Cu}_3\text{O}_7/\text{LaAlO}_3$  thin-film resonators patterned into a meandering strip transmission line. By using a modified newly developed procedure of spatially-resolved complex impedance partition, the influence of inhomogeneous current flow on the formation of nonlinear microwave response in such planar devices is analyzed in terms of the independent impact from resistive and inductive components [2]. The modified procedure developed here is dramatically faster than our previous method. The LSM capability to probe the spatial variations of two-tone, third-order intermodulation photoresponse on micron length scales is used to find the 2D distribution of the local sources of microwave nonlinearity [3]. The results show that the dominant sources of microwave nonlinearity are strongly localized in the resistive domains formed by the highest microwave current densities at the edges of the strips, structural defects like twin-domain blocks, and topological inhomogeneities including the edge shape and the inner corners of the resonator structure.

## REFERENCES

1. Zhuravel, A. P., A. G. Sivakov, O. G. Turutanov, A. N. Omelyanchouk, S. M. Anlage, and A. V. Ustinov, "Laser scanning microscope for HTS films and devices," *Low Temperature Physics*, Vol. 32, 592–607, 2006.
2. Zhuravel, A. P., S. M. Anlage, and A. V. Ustinov, "Measurement of local reactive and resistive photoresponse of a superconducting microwave device," *Appl. Phys. Lett.*, Vol. 88, 212503, 2006.
3. Zhuravel, A. P., S. M. Anlage, and A. V. Ustinov, "Imaging of microscopic sources of resistive and reactive nonlinearities in superconducting microwave devices," *IEEE Trans. Appl. Supercond.*, Vol. 17, 902–905, 2007.

# Omni-directional Vibration Sensor Based on Dynamic Image Understanding

Yi-Ping Tang, Wu-Jie He, and Yi-Hua Zhu

Institute of Information Engineering, Zhejiang University of Technology  
Hangzhou 310014, China

**Abstract**— Intelligent vibration sensor is on the cutting edge of vibration measurement technique, and some popular researches have focused on the push of computer vision technique and image processing technique in vibration measurement up to now. And in order to deal with the drawbacks existed in current researches, using vibration mathematical model, brand new theory and mechanisms related to design a kind of intelligent, omni-directional, and visualized vibration sensors embedded with vibration analysis, image processing, and network communication, are proposed to realize omni-directional vibration sensing, vibration visualization, omni-directional area surveillance, and sharing of information captured by sensors based on dynamic image understanding.

In the paper, we consider to solve three complementary questions, which are 1) how to design the sensor to detect and sense the vibration efficiently and sensitively enough; 2) given initial conditions, how to describe the vibration dynamics without solving the vibration mathematical equations; and 3) given the parameters which determine the vibration, how to specify initial conditions which yield the vibration.

And we provide a complete answer to Question 1. Spring pendulum system is imported to implement to detect and sense vibration or swing of the pendulum bob caused by the force which is applied from all directions with the help of omni-directional vision sensor (ODVS) and embedded system. As to question 2, Analytical descriptions are derived from the vibration amplitude, precession angle and period in term of the invariants of the motion, which are computed by image processing algorithm, especially entropic threshold algorithm based on color difference. Thus, the vibration dynamics can be deduced from the initial conditions. Question 3 is more recondite, but we can give a positive answer for physically interesting case of vibration. We derive approximate conditions from the angular momentum and the change of displacement in terms of the vibration amplitude in both vertical and horizontal direction based on the vibration mathematical model. Initial conditions can then be determined which yield the desired vibration to a good level of approximation based on dynamic image understanding with vibration environment monitoring via ODVS, which implement of intrusion detection.

Eventually, experimental investigation is carried out based on the prototype. Considering the different application of omni-directional vibration sensor, we chose to take the box with universal wheel as the simulated target to test the sensitivity and performance of the omni-directional vibration sensor in different conditions. Additionally, experimental data are reported which are recorded from different vibration mode, including vibration and swing caused by the force applied from all directions, and good agreement is found with the theory proposed.

## Rotation of the Leaky Dielectric Particle in a Spinning Electric Field

Yu. Dolinsky and T. Elperin

The Pearlstone Center for Aeronautical Engineering Studies  
Department of Mechanical Engineering, Ben-Gurion University of the Negev  
P. O. B. 653, Beer-Sheva 84105, Israel

**Abstract**— We study rotation of a weakly conducting particle around its axis of symmetry under the action of the external electric field which spins in the plane normal to the axis of symmetry of the particle. The particle is imbedded in a homogeneous stationary medium with finite electric conductivity and permittivity that are different from the corresponding parameters of the particle. We determined the dependence of the particle angular velocity upon the amplitude and angular velocity of the electric field. It is showed that depending upon the ratios of the particle electric conductivity and permittivity to the corresponding parameters of the host medium, the direction of rotation of the particle can be identical or opposite to the direction of rotation of the external electric field. We determined the amplitude dependent critical angular velocity of the external electric field that separates the domains with two possible regimes of rotation of the particle. In the first domain the particle rotates only in one direction while in the second domain the particle may rotate in two directions. We investigated also the stability of different regimes of rotation of the particle. The results obtained in this study complement the results of previous investigations which considered renormalization of the viscosity of particle suspension in the presence of DC electric field. The obtained results allow us to determine in the explicit form the critical shear that separates the domain of bi-stability from the domain where only the main regime occurs. The obtained results also allow us to determine the critical amplitude of the external electric field as a function of vorticity of the shear flow and the explicit dependence of the effective viscosity upon the amplitude of the electric field.

# Real Time Fire Detection Based on Omni-directional Vision

Yi-Ping Tang and Shun-jing Jin

Institute of Information Engineering, Zhejiang University of Technology, Hangzhou 310014, China

**Abstract**— Some of the defects of existing image based fire detection technology including: 1) using ordinary CCD camera cannot get the panoramic image of the scene; 2) only concerning about flame recognition, lack the analysis of how burning combustion goes into fire disaster; 3) difficult to locate the fire position in real world. This paper proposes a fire detection method based on omni-directional vision to solve these problems, which is related to dynamic image understanding and integrated fire characteristics analysis. This method has the advantage to 1) detect fire in real-time, 2) reduce the false alarm rate significantly, and 3) locate the fire position exactly.

Omni-directional Vision Sensor (ODVS) is introduced into this paper to achieve the real-time panoramic video surveillance of a large scale scene. ODVS can go beyond the vision limits of human to reach the  $360^\circ$  view, it is capable to compact all information of a hemisphere into a two-dimension omni-directional image. Therefore, a single ODVS can replace various types of vision sensors (such as cradle head camera, multiple cameras, etc.), which makes the collection of vision information, detection and tracking of target objects in video much easier. Further more, the accuracy target position can be located easily by employing the imaging principle of ODVS.

The main purpose of this paper is to make computer observe and detect fire as human. In order to achieve this goal, flame in video should be identified firstly, since it could be dangerous to detect flame where it should not be. Then the behavior of flame is further analyzed to distinguish between controllable and uncontrollable combustion, this is because uncontrollable combustion has high possibility to cause a fire disaster, but controllable combustion not.

The recognition of flame in video is as following: 1) extract the foreground pixels through background subtraction; 2) discard the interference pixels by analysis the fire color and flicker characteristics; then 3) recognize the flame region through connection component labeling, filling and concatenating. The process of classify flame into uncontrollable combustion is as following: 1) analyze the change of flame area to calculate the growing rate; 2) analyze the movement of flame to calculate the spreading rate. A flame is only classified into uncontrollable combustion when both the growing rate and spreading rate are high.

Among the factors related to fire, flame and human are concerned in this paper to make a final fire disaster decision: 1) if flame is detected but no person in the scene, then the flame is very likely to cause a fire, alarm should be triggered; 2) if both flame and human are detected, and flame is further classified into uncontrollable combustion, then the probability of fire is high, alarm should be triggered.

# Research on Audio Information Hiding Arithmetic Based on BP Neural Network

Hong Wang, Qiong Sun, and Yi Sun

School of Information Engineering, Wuhan University of Technology, Hubei, China

**Abstract**— This paper proposes an audio information hiding algorithm based on BP neural network. The algorithm adopts 256 grey scales image as embedded information and audio as the carrier. Utilize learning samples to train the neural network, and then extract image information by the trained network.

The embedded information used in the algorithm is 256 grey scales images. Divide audio signal into segments, and embed the constructed pixel points and grey image in the piecewise audio signals in turn. The aim of constructing pixel points to simulate hiding grey image, thus to train BP neural network approach to the best. The method trains pixel points which are gradually ergodic in 256 grey scales, and each grey scale could be trained uniformly.

The experimental results show that the amount of embedded data is large and the times of extracting data is short by the algorithm of this paper. The speed of extracting grey image by this algorithm is about 20 times higher than the traditional method. Anti-attack robustness of this algorithm is strong, because not only embedded data but also samples will suffer from the same attack. Through BP network training, the network can adapt to the attack in some degree and overcome the harm of attack, thus restored image has preferable effect. However, this algorithm trains NN using constructed pixel points which is different from hiding image. Therefore, extracted information probably has little distortion even without any attack. On the whole, if the training effect of NN is adequate, the distortion could be controlled in extraordinarily tiny intervals and the quality of output information is perfect.



# Model Error Estimate in Quantitative Remote Sensing Inversion

Lu Zheng<sup>1</sup>, Yang Hua<sup>1</sup>, Ma Xiang<sup>2</sup>, and Ren Zhixing<sup>1</sup>

<sup>1</sup>State Key Laboratory of Remote Sensing Science, Beijing Normal University, China

<sup>2</sup>School of Mathematics, Beijing Normal University, Beijing 100875, China

**Abstract**— The essence of quantitative remote sensing is inversion. Model is one component of it. However, model is approximation of true scene, the difference between them called model error. It may due to the hypothesis when modeling. Thus the error will affect the precision of inverse result. In this paper, taking SAIL (Scattering by Arbitrarily Inclined Leaves) model as an example, its error is simulated and its distribution function is estimated.

SAIL model, a classic radiative transfer model for homogenous canopy, is a four-flux and nine-parameter non-linear model. LAI (Leaf Area Index), one of its parameter, is one of the most important parameters for precise agriculture, crop remote sensing monitoring, etc. As high demand of LAI accurate, different inversion algorithms and models are investigated. But seldom consider the model error. In this paper, radiosity model, a compute simulation model, is taking as the reality. Differences of model results between them under different groups of observational angles and spectrum conditions take as model error. Prior knowledge using in quantitative remote sensing inversion is proved valid to solve the ill-posed problems in some extent. Taking model error as one kind of prior knowledge using in inversion should know its distribution. Multiple regression method is used to estimate model error's distribution function. Results show the function is a 2-dimension Gaussian.

To verify the necessary of considering model error and right of our estimated distribution function, inversion results compared of this distribution with normal distribution. Result is satisfactory. Theory of model errors distribution estimating and its application in remote sensing inversion need study further.

## Fabrication of Focusing Optic for Soft X-Ray Microscope

**Kwon Su Chon and Kwon-Ha Yoon**

Institute for Radiological Imaging Science, Wonkwang University  
344-2 Sinyong, Iksan, Jeonbuk 570-749, Republic of Korea

**Abstract**— There have been many attempts to investigate nanometer-scale fine structures. A soft X-ray microscope can be used to investigate hydrated specimens, particularly living cells, with a high resolution about several times better than that of a visible light microscope. It can also extend to material science, plasma fusion research, magnetic research, environment science, and so on. The reflecting optics used in a soft X-ray microscope require supersmooth surfaces and a highly accurate figure. We consider a Wolter type I mirror as a condenser optic for a biological application. This consists of two axially symmetric confocal surfaces of revolution, i.e., an ellipsoid and a hyperboloid. A Wolter type I mirror used in a soft X-ray microscope has small diameter and long mirror length because of very small grazing incidence angle of X-rays. This geometrical shape may result in fabrication difficulty in direct machining of reflecting surfaces. In this case, a replication method is much better. A replicated mirror can be fabricated from a master mandrel, which has a counter shape of the desired mirror, through several replication steps. A Wolter type I microscope mirror with an axial symmetry was successfully fabricated by a epoxy replication method. The quality of the replicated mirror critically depended on the surface roughness and shape accuracy of the master mandrel. The replicated gold mirror was 1.3 nm rms in average surface roughness and 160 nm P-V in figure error, respectively. The epoxy replication method showed very good copy ability in terms of surface roughness and figure. In addition, several mirrors could be fabricated using only one master mandrel without destroying their surface roughness and figure.

# Schlieren Imaging with Coherent and Incoherent Light Sources and with Proper Fourier Filters

Boris Zakharin<sup>1</sup> and Josef Stricker<sup>2</sup>

<sup>1</sup>Aerospace and Mechanical Engineering Department  
University of Arizona, Tucson, AZ 85721, USA

<sup>2</sup>Faculty of Aerospace Engineering  
Technion-I. I. T., Technion City, Haifa 32000, Israel

**Abstract**— Coherence of light illumination has an important influence on image quality. This is especially true for schlieren imaging. For incoherent schlieren system with ordinary knife-edge filter, experiments revealed, that the geometrical optics interpretation holds, namely the image intensity is proportional to the object phase derivative. For the systems with coherent point source and with the knife-edge as a Fourier filter the image intensity is proportional to the Hilbert transform of the object phase (J. W. Goodman “Introduction to Fourier Optics”). While the dynamic range of the incoherent systems is easily adjustable, permitting the measurement of the phase object with large phase variance, the measurements with the coherent system are limited typically to the values of the phase less than one. However the range of the coherent schlieren can be significantly increased, by using proper graded filters. Currently there is much controversy in the literature about the theoretical interpretation of the schlieren images. The purpose of this study is to clarify existing disagreements by providing consistent wave optics theory for the schlieren systems with different sources and filters. Such a theory will permit correct and precise interpretation of the measurement results.

The main tool for the current analysis is the Fourier optics technique. To characterize the imaging properties, the schlieren amplitude and intensity point-spread functions were introduced for the coherent and incoherent systems accordingly. The calculations reveal that for the coherent system with graded filter the modified geometrical optics interpretation is valid as well, according to which the EM field of the image is proportional to the object refraction. Finally, the imaging properties of the schlieren systems with different sources and filters are considered.

# Polarization-independent Microwave Directional Anisotropy in Magnetophotonic Crystal

H. X. Da, J. C. Wu, and Z.-Y. Li

Key Laboratory of Thin Films in Jiangsu Province  
Department of Physics, Suzhou University  
Suzhou 215006, China

**Abstract**— Symmetry breaking in a solid can occasionally give rise to some intriguing phenomena. For example, Faraday effect and natural optical activity are associated with the broken time reversal symmetry and space inversion symmetry, respectively. Symmetry arguments have shown that broken time reversal and space inversion symmetries simultaneously can produce magneto-chiral effect (MCHA) or optical magnetoelectric effect (OME). The special feature of them is the independence of the polarization state of the light. The former can be realized in the chiral media subject to a static magnetic field, while the latter occurs in any media lack of both time reversal and space inversion symmetries. For example, a single crystal  $\text{Cr}_2\text{O}_3$ , cubic paramagnetic and multiferroic materials. At present, the frequency region of such effects is mainly concentrated on visible light, infrared frequency and the x-ray region. However, there is no report on nonreciprocal directional anisotropy at the microwave regime.

Magnetophotonic crystals (MPCs) are spatially periodic structure with at least one of the constitutive components being a magnetically polarized material. In MPCs, the Kerr or Faraday rotation of the polarization plane of incident linearly polarized light can be enhanced due to the localization effect of light. Especially interesting, asymmetric spectrum can be realized when the geometry of the periodic array of MPCs meets certain symmetry criterion. Frozen mode and unidirectional properties in such system have been investigated from theoretical, simulation and experimental aspects. In MPCs, to combine two anisotropic dielectric layers with misaligned in plain anisotropy with ferromagnetic material will break both space inversion and time reversal symmetries. Then, the question naturally comes to mind if polarization-independent directional anisotropic property can exist in MPCs without the presence of chiral material or multiferroics?

Polarization-independent microwave directional anisotropy, a feature that has not been appreciated in the literature so far, in the above mentioned configuration is investigated. We have known that such a configuration exhibits asymmetric spectrum at the certain microwave regime. The existence of microwave directional anisotropic (MDA) effect is examined according to  $4 \times 4$  Muller matrix method based on the asymmetric properties of the system. Our results show that this effect can be realized in such magnetophotonic crystals without the existence of magnetization and polarization simultaneously. Furthermore, the order of this unique electromagnetic effect can be up to  $10^{-3}$ .

## Scaling Invariance Band Gaps in 1D Periodic Structures Containing Metamaterials

Zhiguo Wang

Department of Physics, Tongji University, Shanghai 200092, China

**Abstract**— The band structures of 1D periodic structures are studied in the sub-wavelength limit. In 1D photonic crystal (PC), a “spatial-averaged single-negative” (SASN) gap whose edges corresponding to zero (volume) averaged permittivity and zero (volume) averaged permeability will appear when metamaterial is included. Unlike the Bragg gap, the frequency range of the SASN gap is invariant to the geometrical scaling and insensitive to the incident angle and disorder. In the sub-wavelength limit, both the zero- $\bar{n}$  gap in negative-index 1D PC and the zero-effective-phase gap in the single-negative 1D PC can be understood as SASN gaps. When the sub-wavelength condition is not fulfilled, the zero- $\bar{n}$  gap and zero-effective-phase gap begin to act differently. Next, we discuss the band structures of comb-like PCs with backbones constructed of negative index materials (NIMs). The result shows the existence of a special sub-wavelength band gap which is insensitive to the geometrical scaling and disorder. The behavior of its gap-edges is asymmetric. One gap-edge is decided by the average permittivity whereas the other is only subject to the changing of the permeability of the backbone. This makes the broadening of the gap easily. Then, the transmission properties of loop structures with finite segments made of NIMs are studied. We demonstrate that there exists a special band gap which is a sub-wavelength band gap and is invariant upon a change of scale length. Analytic expressions of its edges are obtained under sub-wavelength condition. The width of this gap can be enlarged easily with tuning structure parameters. In addition, this method is applied to multi-channel systems.

## Influence of Subjective Material on the Energy Transferring Process between Phosphorescent Material and Fluorescent Material

Yuan Li, Suling Zhao, Zheng Xu, Fujun Zhang, Yanrui Li, Yaru Yang, and Jinglu Song

Institute of Optoelectronics Technology, Beijing Jiaotong University, China

**Abstract**— As the role of sensitization in fluorescence, phosphorescent material (PM) improves the efficiency of energy transferring process in adulterating system. It could be divided into three process among three kind of materials, like PVK:Ir(ppy)<sub>3</sub>:Rubrene. At the same time, the subjective materials, for instance PVK, CBP and TPD, are the foremost subjective material influencing the whole energy transferring process. We fabricated three devices, which using Ir(ppy)<sub>3</sub> as phosphorescent sensitizing material, Rubrene as the fluorescent material, and PVK, CBP and TPD as the fluorescent subjective materials. Finally, CBP is the best subjective material due to the maximal overlap between emitting spectrum and absorb spectrum and the energy level relationship.

# Implementation of Range-gated Underwater Laser Imaging System

Mingsong Chen, Faliang Ao, and Ning He

School of Information & Communication, Guilin University of Electronic Technology, Guilin 541004, China

**Abstract**— The novel system uses a Q-switched Nd:YAG solid state laser operating at a wavelength of 532 nm (green). The operating principle for the Underwater Laser Imaging System (ULIS) is distance-triggered model. The implementation for synchronization controlling set of the imaging system is one of the key techniques. The programmable pulse width synchronous controlling set is carefully introduced in this paper. We try to use the synchronization set to fulfill the Underwater Laser Imaging System (ULIS) operating at distance-triggered model. We have been trying our best to put forward the corresponding solving method of the whole Underwater Laser Imaging System (ULIS). As the development of the digital signal processing technology, the chip of digital signal processing developing from 1980s has powerful ability to deal with digital signal. Therefore in the Underwater Laser Imaging System (ULIS), the DSP chip TMS320VC5416 is used to deal with the images which get from the Underwater Laser Imaging System (ULIS). In order to reduce the noise in the image, and keep the original details in the images, the median filtering was introduced and used in the digital image processing system. We apply the CCD as the imaging detector, use the pulsed laser as the flash source and adopt the controlled system as the controlling part to realize the laser distance-triggered model imaging system. The design of the synchronization control set for Underwater Laser Imaging System (ULIS) by distance trigger is one of the key techniques in the whole system. This paper has introduced the performance request to the synchronization control set, which Underwater Laser Imaging System (ULIS) needs, and has introduced the design principle and realization process for the synchronization control set using with CPLD which fits the related requirement. The paper has also explained the implementation process to conveniently adjust the pulse delay and the pulse width. At the same time this paper has presented the practical principle and the testing condition. At the end the design principle and the practical realization process have also been implemented.

# Band Engineering and Waveguide Design for THz Si/SiGe Quantum Cascade Laser

Guijiang Lin<sup>1</sup>, Hongkai Lai<sup>1</sup>, Cheng Li<sup>1</sup>, Songyan Chen<sup>1</sup>, and Jinzhong Yu<sup>1,2</sup>

<sup>1</sup>Semiconductor Photonics Research Center, Department of Physics  
Xiamen University, Xiamen 361005, China

<sup>2</sup>State Key Laboratory on Integrated Optoelectronics, Institute of Semiconductors  
The Chinese Academy of Sciences, Beijing 100083, China

**Abstract**— Efficient terahertz (THz) sources are the keys to high resolution molecular spectroscopy, imaging, and high-speed communications. Quantum cascade structures based on Si/SiGe material are likely to operate over a broader THz range and have better thermal conductivity to the substrate and device packages than III-V semiconductor heterostructures. Operation of a Si/SiGe quantum cascade laser (QCL) at terahertz range requires good modeling and analysis of carrier transport in the quantum cascade structures and light propagation in the waveguide.

Optimized band parameters are used to calculate the hole subband structure of Si/SiGe quantum well using a six-band *kp* method. By considering the selection rules of hole intersubband transitions in valence band, appropriate Si/SiGe quantum well structures for THz devices are obtained. The intersubband transitions between HH2 and HH1 reach at THz frequencies for lower Ge content when the SiGe active well width becomes larger than 6 nm. Transition from the subbands of the light hole LH2 to the ground state of the heavy hole HH1 lies in long wavelength but out of THz frequencies. And it is the most convenient to modulate the energy separations between HH2 and LH1 in THz frequencies. Lower Ge content should be used in Si/SiGe QCL based on interwell transitions between HH1 and LH1.

Based on a simple Si/SiGe superlattice, with just two confined subbands (one heavy hole HH1 and one light hole LH1). A waveguide for Si/SiGe QCL operating at THz waves based on a double-metal clad waveguide and a metal-metal silicide clad waveguide with heavily doped SiGe layer was designed. Material parameters considerations have been described and different THz waveguides were theoretically evaluated and optimized to minimize loss and maximize modal confinement. Calculations showed that higher confinement factor and lower loss coefficients with low thickness of waveguide is practicable by using double metal waveguide. The Al-WSi<sub>2</sub> confinement waveguide provides relative higher  $\alpha/\Gamma$  ratio than the other Al-metal silicide waveguides. The quality factor  $\alpha/\Gamma$  increase as increasing the contact layer thickness and decrease as increasing the active layer thickness, and the appropriate layers thicknesses optimization of the THz Si/SiGe QCL waveguide are also obtained.



# Far-field Distortion Characteristics of Annular Lasers from Confocal Unstable Resonators through the Natural Atmosphere

Yufeng Peng<sup>1,2</sup>, Li Liu<sup>1</sup>, V. S. Egorov<sup>2</sup>, Zuhai Cheng<sup>3</sup>, and Minggao Zhang<sup>1</sup>

<sup>1</sup>College of Physics and Information Engineering, Henan Normal University, Xinxiang 453007, China

<sup>2</sup>Department of Optics, St. Petersburg State University, Petrodvorets 198504, Russia

<sup>3</sup>Wuhan National Laboratory for Optoelectronics, Wuhan 430074, China

**Abstract**— With the rapid development in the use of lasers in the fields of communications links, radar, etc, propagation characteristics of laser beams through atmosphere, such as intensity and phase fluctuations in the presence of atmospheric turbulence, were widely paid attention to during the past years. In particular, the advent of a high-power laser has greatly enhanced the research on such fluctuations due to their significance in laser communications through the atmosphere. In recent years, annular or dark-hollow beams have attracted more and more attentions because of their wide applications in modern optics and atomic optics. Y. Baykal and H. T. Eyyuboğlu et al. presented the propagation of higher-order annular beams in free space as well as their log-amplitude and phase fluctuations in the presence of atmospheric turbulence, in order to examine the suitability of various beams for broadband access free space optics (FSO) communication links.

In this paper, Based on the laser field from a positive confocal unstable resonator (ab initio), the propagation characteristics of the beam through atmosphere are investigated by means of fast Fourier transform (FFT), and it is assumed that the refractive index and absorption of atmosphere are only decided by the air molecules. Considering the thermal effects of the laser beam and wind velocity of air, we evaluate the beam offsets, beam spreading, and beam qualities of the laser field transmitting from the resonator through the natural atmosphere. Meanwhile, the far-field intensity distributions of the laser beam with various intensities in the atmosphere are obtained. It is shown that the far-field diffraction patterns are deformed due to absorption of air and wind velocity.  $\beta$ -parameter and Strehl ratio, which are usually used for high-power lasers, are introduced to estimate the beam quality characteristics. With increasing the intensity of the beam, the far-field diagram patterns are outspreaded, the peak intensities decreased, the peak centers shifted, and the beam quality characteristics greatly degraded.

# Subwavelength Terahertz Imaging and Plasmonically Transferred Image through an Array of Periodically Corrugated Metal Rods

Yongyao Chen and Ching-Yue Wang

Ultrafast Laser Lab, School of Precision Instruments and Optoelectronics Engineering  
Key Laboratory of Optoelectronic Information Technical Science  
Tianjin University, Tianjin 300072, China

**Abstract**— Metal rods with periodically circular grooves can sustain Surface-Plasmon-like modes, and the effective surface plasmon frequency of the metal wire can be tailored to reach the Terahertz (THz) region. In this way, tightly confined THz surface plasmon polaritons (SPPs) can be sustained on the surface of metal rod. Moreover, by using an array of such structured metal rods (typical configuration is a hexagonal arrangement), we can make a THz imaging system with subwavelength resolution. The picture on the object plane was plasmonically transferred through the rod array to reproduce the pattern on the image plane in the other side. These devices enable an efficient transfer of image with subwavelength resolution in the THz or microwave region, and open the way to important applications such as integrated optics, near field microscopy, and high resolution image transfer systems in the THz band.

# Surface Optical Breathers in Semiconductor Quantum Dots

G. T. Adamashvili<sup>1,2</sup> and A. Knorr<sup>1</sup>

<sup>1</sup>Institut für Theoretische Physik, Nichtlineare Optik und Quantenelektronik  
Technische Universität Berlin, Hardenbergstr. 36, D-10623 Berlin, Germany

<sup>2</sup>Georgian Technical University, Kostava str. 77, Tbilisi, 0179, Georgia

**Abstract**— During the last years optical coherent nonlinear properties of semiconductor quantum dots have been a major research topic [1]. In particular, experimental investigations on the possibility of optical solitons and self-induced transparency in semiconductor quantum dot waveguides have been reported [2]. Recently, also theoretical investigations of breathers of self-induced transparency have been considered for plane waves in semiconductor quantum dots (SQD), and explicit analytical expressions for the parameters of the resonance breathers have been presented [3].

Up to now at the considerations of nonlinear waves in SQD of existence the borders of crystals have been ignored. Taking into account of borders of a crystal results in occurrence of surface conditions for electrons, excitons, phonons and other quasi-particles. For the description of surface branches of energetic of spectrum of the crystals it is necessary to take into account boundary conditions. On the boundary of the division such media the surface electromagnetic waves can be propagating. The properties of the surface modes when one of the connected medium is semiconductor are investigated in detail [4]. On the other hand, in the boundary of semiconductors with another medium, can be growing the SQD, which can form a thin transitive layer. In the work [5] surface optical solitons in SQD have been investigated.

In this contribution, a theory of optical breathers (pulsing-solitons) for the nonlinear coherent interaction of surface TM-modes with a layer of an ensemble of inhomogeneously broadened SQD is developed. Explicit analytical expressions for the surface soliton ( $0 < \pi >$  pulse) in the presence of single and biexciton transitions are obtained in the regime of self-induced transparency. The analysis shows that realistic parameters for breather formation can be reached in current experiments.

## REFERENCES

1. Bimberg, D., M. Grundmann, and L. Lednetsov, *Quantum Dot Heterostructures*, Wiley, 1999.
2. Schneider, S., P. Borri, W. Langbein, U. Woggon, J. Forstner, A. Knorr, R. Sellin, D. Ouyang, and D. Bimberg, *Appl. Phys. Lett.*, Vol. 83, 3668–3671, 2003.
3. Adamashvili, G. T. and A. Knorr, *Opt. Lett.*, Vol. 31, 74–78, 2006.
4. Sovremennye problemi nauki o kondensirovannich sred, Poverchnostnie polaritoni, *Elektromagnitnie volni na poverchnostiach i granicah pazdela sred*, Edited by V. M. Agranovich and A. A. Maradudin, Moscow, Nauka, 1985.
5. Adamashvili, G. T. and A. Knorr, *Phys. Lett. A.*, Vol. 367, #3, 220–223, 2007.

## Spatial Light Modulators for Cold Atom Manipulation

Michael Mestre, Fabienne Diry, Bruno Viaris de Lesegno, and Laurence Pruvost

Laboratoire Aimé Cotton, Univ Paris Sud, CNRS UPR3321, F-91405 Orsay, France

**Abstract**— Spatial Light Modulators (SLM's) are programmable optical elements that can act as dynamical holograms, providing flexible control over the light intensity of a laser in a given plane. Thus, the operator can manipulate small objects using the forces that arise from the dipole force. They are being used for a wide range of applications, including biology, condensed matter physics, quantum optics and atomic physics.

Our group is performing experiments using SLM for cold atom manipulation. First we have focused on response time and diffraction pattern quality issues. We have demonstrated an AOM/SLM device with a refresh time of some micro-seconds and without bleed effect during the hologram changes [1]. This device would be well-suited for cold atom manipulation with time-dependent dipole potentials.

Now, we are experimenting with cold Rubidium atom guiding using hollow Laguerre-Gaussian beams obtained by applying helical-phase holograms to laser beam. Being far-detuned from resonance and dark where the atoms spend most of their time, the light field causes little scattering-induced losses and guiding is efficient.

Future applications of this technique will be presented and discussed in the context of cold atoms or Bose-Einstein Condensates experiments.

### REFERENCES

1. Mestre, M., B. Viaris de Lesegno, R. Farcy, L. Pruvost, J. Bourderionnet, A. Delboulbé, B. Loiseaux, and D. Dolfi, "Fast reconfigurable and transient-less holographic beam-shaping realized by a AOM-SLM device," *EPJApp*, accepted.

# Active III-V Photonic Crystal Devices Integrated onto Silicon Wafers

F. Raineri, G. Vecchi, A. M. Yacomotti, T. Karle, A. Levenson, and R. Raj

Laboratoire de Photonique et de Nanostructures (CNRS UPR20)

Route de Nozay, 91460 Marcoussis, France

**Abstract**— Hybrid integrated structures allow us more freedom to tailor the optical properties of our devices. By bonding active and passive wafers together, we can combine many different functionalities on one chip. Optical sources and detectors have already been demonstrated in III-V materials coupled to the Silicon-On-Insulator waveguide system, in which compact filters and interconnects have been fabricated. The main advantage is that we are no longer restricted by the linear absorption of active-waveguiding structures. Additionally, the optimum materials for particular non-linear functions can be selected. The admixture of different physical material properties can benefit the optical properties of the devices, for example, permitting CW, room temperature operation of novel lasers, as we will discuss.

As a first step with a hybrid material system we report on the continuous wave operation of a band edge laser at room temperature near  $1.55\ \mu\text{m}$  in an InGaAs/InP photonic crystal. The photonic crystal slab is integrated onto a Silicon chip by means of Au/In bonding technology, which combines two advantages, efficient heat sinking and broad band reflectivity. A flat dispersion band-edge photonic mode is used for surface normal operation. The laser characteristic is plotted in Fig. 1. The emission linewidth is measured to be 80 pm and the threshold around 5 mW. The next step is to couple light between the III-V and the SOI waveguides, allowing for efficient modulation and switching.

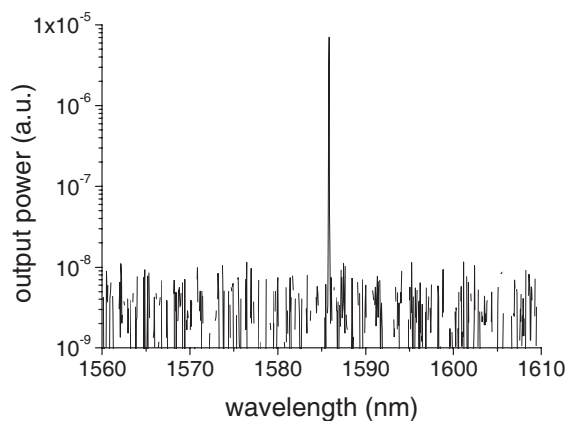


Figure 1: Laser characteristic.

# From Fast Optical Bistability to Thermo-optical Excitability in a Two Dimensional Photonic Crystal

A. M. Yacomotti, P. Monnier, F. Raineri, R. Raj, and A. Levenson

Laboratoire de Photonique et de Nanostructures (CNRS UPR 20)  
Route de Nozay, Marcoussis 91460, France

**Abstract**— Optical bistability is the building block for optical memories and logic gates in photonic integrated circuits. In such context, fast switching between the two stable states is needed. Among the few recent demonstrations of bistability in photonic crystals (PCs), two fast bistable systems have been reported so far: two photon absorption-induced bistability in a four point defect of a Si triangular PC lattice [1], and a refraction index-induced bistable operation in a perfectly periodic InP graphite PC lattice [2]. Here we focus on the latter which results from the combination of the refractive index change due to carrier injection in the quantum wells and a low group velocity mode at the  $\Gamma$  point of the Brillouin zone. As a result, the 2D PC acts as a nonlinear distributed resonator.

In order to observe fast bistable operation, thermal effects must be minimised. Our vertical structure (a  $\text{SiO}_2$  cladding underneath the InP membrane) ensures good heat sinking to the Si substrate. Additionally, the modulation of the injection beam is also necessary in order to reduce thermal loading. In these conditions, hysteresis cycles as the one showed in the figure have been observed in our system. Switching times are less than 1 ns, and may be as short as 200 ps which is the carrier recombination time.

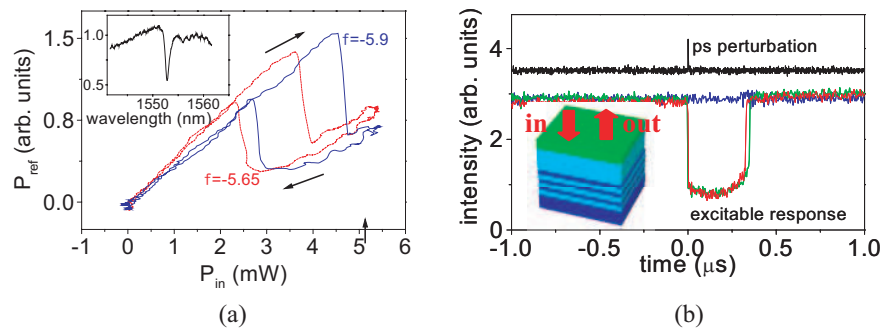


Figure 1: (a) Hysteresis cycles under 200 ns-duration, 100 kHz repetition rate injection pulses, showing bistable operation of a 2DPC, for two different detuning of the injection wavelength with respect to the photonic resonances. (b) Excitable response (red and green line) for an external light perturbation (black line) above a 1 pJ threshold. Inset: sketch of the PC and the geometry of the injection.

Turning off the modulation, thermal effects arise affecting the dynamics in time scales of the order of the thermal dissipation time ( $1 \mu\text{s}$ ). Experimentally, the low reflection bistable state observed in the hysteresis cycle (the “hot state” where the light enters into the resonator) is no longer a stable one, but a transient signal which switches back to the the high reflection state in a fixed time ( $\sim 300 \text{ ns}$ ). As a result, a light pulse — rather than a bistable operation — can be induced with an external perturbation, which can be interpreted in terms of a nonlinear dynamical phenomenon called excitability [3], at the origin of neuronal spiking. We will discuss possible applications of excitability, from low threshold coupled optical neurons to the realisation of all-optical delay lines.

## REFERENCES

1. Tanabe, T., et al., *Opt. Lett.*, Vol. 19, 2575, 2005.
2. Yacomotti, A. M., et al., *Appl. Phys. Lett.*, Vol. 88, 231107, 2006.
3. Yacomotti, A. M., et al., *Phys. Rev. Lett.*, Vol. 97, 143904, 2006.

## The Localized Modes for Random Laser

Sheng Li<sup>1,2,3</sup>, Xin Sun<sup>2</sup>, and Thomas F. George<sup>3</sup>

<sup>1</sup>Physics Department of Zhejiang Normal University, Jinhua, Zhejiang 321004, China

<sup>2</sup>Research Center for Quantum Manipulation, Fudan University, Shanghai 200433, China

<sup>3</sup>Office of the Chancellor and Center for Nanoscience

Departments of Physics and Biochemistry and Physics and Astronomy  
University of Missouri-St.Louis, St.Louis, Missouri 63121, USA

**Abstract**— When a wide-gap semiconductor polycrystalline film, such as III-V semiconductor, is pumped by a pulsed laser, a special light pulse can be generated. During the propagation of this light pulse, strong multiple scattering not only traps coherent and localized modes inside the sample, but also leaks non-coherent extensive modes outside. As the gain of the external laser pulse approaches a critical threshold value, the leaked energy, which is caused by non-coherent extensive modes, can be counteracted to drive the photons into the localized modes. Once the external gain surpasses the critical value, the localized mode serves as a laser mode to emit coherent radiation, and forming so-called random laser. Meanwhile, based on the phase vector diagram describing the collective behavior of the random laser, it becomes possible to distinguish these laser modes and show the “invisible” microcavities of random laser.

# Nitride-based LEDs with MQW Active Regions Grown by Different Temperature Profiles

S. C. Wei, A. T. Cheng, and Y. K. Su

Advanced Optoelectronic Technology Center  
Institute of Microelectronics & Department of Electrical Engineering  
National Cheng Kung University, Taiwan

**Abstract**— We report on the use of temperature cycling method to further improve the quality of the MQW structure and the performance of nitride-based LEDs grown by metalorganic vapor phase epitaxy. During the growth of MQW active region, three different temperature profiles (process A, B, and C) were used. The MQW active regions consist of 5 periods of 3-nm-thick InGaN well layers and 15-nm-thick GaN barrier layers for all LEDs. It can be seen that forward voltages of three LEDs were almost identical. However, the reverse leakage can be significantly reduced using both temperature ramping and temperature cycling methods. From double crystal *X*-ray diffraction (DCXRD) spectra of three LEDs, the satellite peaks are not clearly visible for sample B, which suggests poor interfaces in the MQW region of the conventional LED. On the contrary, clear satellite peaks with small full-width-half-maxima (FWHM) were observed for samples A and C. For the electrostatic discharge (ESD) characteristics of these devices, it was found that the conventional LED (i.e., sample B) could only endure ESD pulse of  $-1100$  V. However, samples A and C could well endure ESD pulse of  $-3500$  and  $-2800$  V, respectively. With a 20 mA current injection, the output powers were 5.5, 6.0 and 7.9 mW, which correspond to external quantum efficiencies of 10.3%, 11.2% and 14.8% for samples A, B and C, respectively. The larger EL intensity observed from sample C is attributed to the improved crystal quality of barrier layers and the prevention of possible impurity incorporation using temperature cycling method.

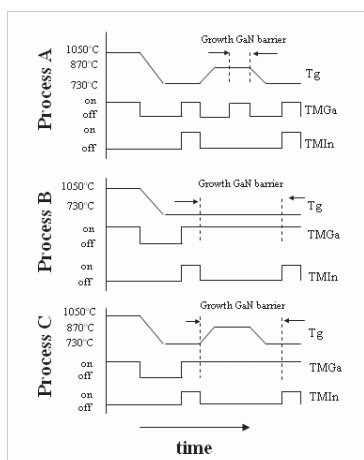


Figure 1: The three different temperature profiles used to grow the MQW active regions in this study.

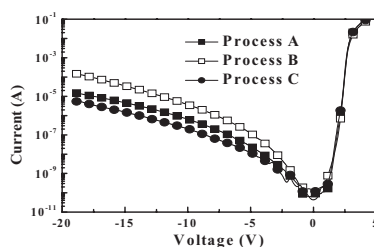


Figure 2: I-V characteristics of three LEDs.

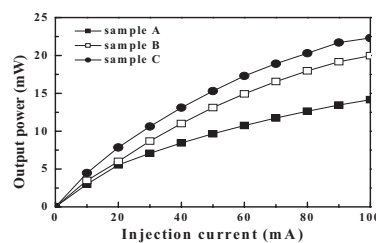


Figure 3: L-I characteristics of three LEDs.



## Optical Tunneling through a Disordered Stack of Metamaterials

Wei-Hua Sun, Ye Lu, R. W. Peng, De Li, X. Wu, L. S. Cao, and Mu Wang

National Laboratory of Solid State Microstructures and Department of Physics  
Nanjing University, Nanjing 210093, China

**Abstract**— It is well known that in conventional photonic crystals, Bragg scattering gives rise to the photonic band gap. The defect mode will appear within the Bragg gap when the periodicity is broken such as by introducing a defect in the structure. Both the Bragg gap and the defect mode will shift dramatically when the incident angle of light varies. It becomes interesting to overcome the angular effects and obtain omnidirectional transmission properties by using the metamaterials. In this work, we present the propagation of electromagnetic wave through a type of metamaterial, where positive and negative index materials are randomly stacked. It is found that electromagnetic waves can transmit perfectly and omnidirectionally through this system. This kind of transparency in the photonic band gap is robust against incident angles, optical polarization and system disorder. The numerical calculations are in good agreement with the analytical predictions. The findings are expected to achieve the potential applications in the optoelectronic devices.

# Optical Propagation in One-dimensional Random $n$ -mer Dielectric Systems

Zeng Zhao, F. Gao, R. W. Peng, K. Wei, L. S. Cao  
De Li, Z. Wang, and Mu Wang

National Laboratory of Solid State Microstructures and Department of Physics  
Nanjing University, Nanjing 210093, China

**Abstract**— Photonic localization in a dielectric microstructure can be considered as an analogy to the electronic localization in crystals. Up to now, the photonic localization has been demonstrated in periodic, quasiperiodic and other deterministic aperiodic systems, which achieves a photonic bandgap and presents potential applications in optoelectronics. In this work, we have both theoretically and experimentally investigated the optical propagation in an one-dimensional random  $n$ -mer(RN) dielectric system. The localization-delocalization transitions of photons have been demonstrated in this correlated disorder system. Multiple resonant transmissions are observed, which agrees with the analytical expectation. At each resonant mode, zero-Lyapunov exponent and undecayed field distribution have been found through the whole system. Meanwhile channels are opened for photonic transport. As a result, the density of states enhances significantly at each resonant mode. The localization-delocalization transition of photon has been demonstrated experimentally by the observations on the  $\text{SiO}_2/\text{TiO}_2$  multilayer films in visible and near infrared regions of light. The photon behavior presented here provides a possible way to manipulate the photons in photonic bandgap, and may have the applications in designing filters and waveguide of electromagnetic waves.

## ACKNOWLEDGMENT

This work is supported by the grant from National Natural Science Foundation of China.

## Voltage-controlled Light Storage in Vertically Coupled InGaAs/GaAs Quantum Dots

Ka-Di Zhu

Department of Physics, Shanghai Jiao Tong University  
800 Dongchuan Road, Shanghai 200240, China

**Abstract**— Electromagnetically induced transparency (EIT) has proven to be an important issue in modern quantum optics and quantum information processing. EIT is a very powerful technique that can eliminate the absorption and refraction at the resonant frequency of a transition and greatly enhance nonlinear susceptibility in the spectral region of the induced transparency of the medium. This phenomenon can be used to slow down optical pulses, or even bring them to a complete stop. In the present paper, we demonstrate theoretically that it is possible to stop quantum light in vertically coupled InGaAs/GaAs quantum dots systems simply by applying an external voltage. This stopping is based on the form-stable polaritons consisting of quantum light and indirect exciton associated with EIT using tunneling instead of pump laser. The indirect exciton dark-state polaritons in the two coupled quantum dots can then be reaccelerated and converted back into a photon pulse via a tunable voltage. The device system has possible applications in quantum information processing by using modern electro-optical technology.

## Effect of 50 Hz Power Frequency Magnetic Field on Microfilament Cytoskeleton Assembly of Human Amnion FL Cell

Keping Chu<sup>1</sup>, Yukun Zhang<sup>1</sup>, Danying Zhang<sup>2</sup>  
Qunli Zeng<sup>2</sup>, Zhiyin Cai<sup>1</sup>, Shude Chen<sup>1</sup>, and Ruohong Xia<sup>1</sup>

<sup>1</sup>Key Laboratory of Optical and Magnetic Resonance Spectroscopy, Physics Department  
East China Normal University, China

<sup>2</sup>Bioelectromagnetics Laboratory of Zhejiang Province  
Zhejiang University School of Medicine, China

**Abstract**— The relationship between extremely low frequency magnetic fields and tumors occurrences is one of the most concerned issues to the present environmental and health investigations. Tumor cells usually behave abnormal proliferation and cell migration. These properties are directly linked to the signal transduction pathways of growth factors and that of cell cytoskeleton. In this research, methods such as immunohistochemical method, Western blotting, a confocal microscope, a scanning electron microscope and an atomic force microscope were used to detect the effect of 50 Hz power frequency magnetic field on microfilament assembly of human amnion FL cell. Further investigations were carried out to understand the mechanism.

The results can be concluded as follows: 0.2 mT, 50 Hz magnetic fields (MF) induced a decrease in cell skeleton stress fibers in FL cell. New filopodia appeared at the cell periphery after exposure. The mean height of microfilament cytoskeleton decreased after exposure observed with a confocal microscope. The cell shapes became more flat and lamellipodia appeared after exposure with a scanning electron microscope. The epidermal growth factor receptor (EGFR) mass associated with the detergent-insoluble cytoskeleton increased after exposure. The assembly of actin in vitro was not affected by magnetic field, but the efficiency of assembly decreased. The changes of microfilament induced by MF could not be inhibited after clearing the free radical using -Tocopherol, or blocking the EGFR tyrosine kinase by PD153035, or chelating the calcium ions in the medium by Ethylen glycol-bis ( $\beta$ -aminoethylether) -N, N, N', N'-tetraacetic acid (EGTA). But, the changes of microfilament induced by MF could be obviously inhibited by PD153035 associated with EGTA.

The effect on microfilament induced by MF may fundamentally relate to the decrease on assembly efficiency of F-actin, the clustering of EGFR and the inflow of calcium ions.

# Goos-Hänchen Shift and Pulse Widening for Step-index Fiber

Yaoju Zhang<sup>1</sup> and Jianping Bai<sup>2</sup>

<sup>1</sup>College of Physics and Electronic Information, Wenzhou University, Wenzhou 325027, China

<sup>2</sup>School of Physics and Electronic Engineering, Nanyang Normal University, Nanyang 473061, China

**Abstract**— The pulse widening in fiber communications causes a significant restriction of bit rate. The intermodal dispersion occurs not only in grade-index multimode fibers but also in the two-core singlemode fiber. The Goos-Hänchen shift is not considered in the conventional analysis based on the geometric optics. The Goos-Hänchen shift is calculated in the step-index fiber in this paper. The analytic expression is derived for calculating the pulse widening from intermodal dispersion in the multimode fiber. The analytic and numerical results show that Goos-Hänchen shift has an important effect on the intermodal dispersion. The positive Goos-Hänchen shift can decrease the pulse widening.

## An Inverse Model for Localization of Low-diffusivity Regions in the Heart Using Ecg/Mcg Sensor Arrays

Ashraf Atalla and Aleksandar Jeremic

Department of Electrical and Computer Engineering, McMaster University, Hamilton, Ontario, Canada

**Abstract**— The phases of myocardial action potentials and processes of myocardial depolarization and repolarization are well studied and described in most handbooks of electrophysiology and electrocardiography. The underlying processes controlling the (re)polarization in the cardiac activation can be described, on a molecular level, as diffusion of ions through various channels (Na, K, etc.) giving a rise to ionic current which in turn creates electromagnetic field on the torso surface which can be externally measured.

Modeling the cardiac activation on a cellular level has been a subject of considerable research interest resulting in numerous models related to membrane potential (e.g., Hodgkin-Huxley model). However, these models are mainly suitable for forward modeling in which the cardiac activation is simulated using *a priori* knowledge of various parameters. Complimentary to this approach is inverse modeling in which information on cardiac activation (and some physiological parameters) is deduced from ECG/MCG measurements.

One of the most important parameters controlling the activation wavefront propagation is myocardium conductivity. Namely, significant conductivity changes can cause occurrence of irregular activation patterns and lead to various pathological conditions such as arrhythmia, early after-depolarization, etc. From a physiological point of view, conductivity changes usually occur due to ion depletion from a particular region of the heart. As a result, the diffusivity in this region becomes very small preventing the propagation of the activation wavefront and causing the aforementioned irregular patterns. Therefore, any algorithm capable of detecting these anomalies can potentially be useful to predict the onset of these cardiac physiopathologies.

In this paper we propose a new activation model based on the diffusion equation. Although the FitzHugh-Nagumo model is based on the diffusion equation its applicability to inverse approach and real data is limited because of its isotropic and homogeneous nature. First we develop cardiac activation model based on the reaction-diffusion equation with non-homogeneous and anisotropic diffusion tensor. Such a model can be used for detecting different physiological conditions such as conductivity anomalies, which can predate onset of various pathological conditions such as cardiac arrhythmia, early after-depolarization, etc. Then we derive the statistical and measurements model using Geselowitz equations corresponding to our diffusion based source. Using these models we derive the generalized least squares (GLS) estimator for localizing conductivity anomalies/disorders.

# Session 2P1a

## Plasmonic Photonics 2

Electric and Magnetic Dipole Moments and Lifetimes of Eigenstates of Finite-length Cylinders and Cylinder-clusters	
<i>David J. Bergman (Tel Aviv University, Israel);</i> .....	432
Localization Characteristics of Two-dimensional Metal Nanoparticle Structures	
<i>Jian-Wen Dong (The Hong Kong University of Science and Technology, China); Kin Hung Fung (The Hong Kong University of Science and Technology, China); Che Ting Chan (Hong Kong University of Science and Technology, China); He-Zhou Wang (Zhongshan (Sun Yat-Sen) University, China);</i> .....	433
Ponderomotive Force-induced Nonlinearity for Surface Plasma Wave in Plasma-insulator-plasma Structure	
<i>Yung-Chiang Lan (Cheng Kung University, Taiwan, China);</i> .....	434
Focusing of Light beyond the Diffraction Limit	
<i>Kuan-Ren Chen (National Cheng Kung University, Taiwan, China);</i> .....	435
A Study of the Motion of Surface Plasmons on Silver Nanotrack	
<i>Sheng Chung Chen (Far East University, Taiwan, R.O.C.); Zheng Yu Lin (National Taiwan University, Taiwan, R.O.C.); Kuo Pin Chiu (National Taiwan University, Taiwan, R.O.C.); Din Ping Tsai (National Taiwan University, Taiwan, R.O.C.);</i> .....	436

# Electric and Magnetic Dipole Moments and Lifetimes of Eigenstates of Finite-length Cylinders and Cylinder-clusters

David J. Bergman

Raymond and Beverly Sackler School of Physics and Astronomy  
Sackler Faculty of Exact Sciences, Tel Aviv University, IL-69978 Tel Aviv, Israel

**Abstract**— Approximate closed form expressions for the electromagnetic eigenstates of an isolated, finite-length circular cylinder and for the interactions between such states of different cylinders are used to obtain the eigenstates and eigenvalues for a pair of such cylinders. This is done by numerical diagonalization of an infinite matrix representation of the integro-differential operator whose eigenstates are solutions of Maxwell's equations with an equally strong incoming and outgoing part. This representation is obtained by using as a basis for the Hilbert space of divergence-free vector fields the collection of isolated-cylinder eigenstates of all the different isolated cylinders. In that basis, the above-mentioned integro-differential operator has diagonal elements which are just the isolated-cylinder eigenvalues, while the off-diagonal elements are calculated as overlap integrals between pairs of eigenstates of two different isolated cylinders.

Once the eigenstates are known, their electric and magnetic dipole moments can be calculated. The local physical electric field which exists inside such a system when an external or volume averaged uniform field  $E_0$  is applied can be written as a linear combination of the isolated-cylinder eigenstates. The resulting electric and magnetic polarizations can then be found from the corresponding dipole moments of the isolated-cylinder moments. In this way useful expressions for the macroscopic electric and magnetic response, i.e., for the macroscopic electric permittivity  $\kappa_e$  and for the macroscopic magnetic permeability  $\mu_e$ , are found.

The eigenvalues found by following the procedure outlined above are all real, since the integro-differential operator and the resulting infinite matrix are self-adjoint. Those eigenstates are the ones to use when one is trying to calculate the macroscopic response of an “unlimited” composite medium, where a monochromatic electromagnetic field can propagate but where no radiation losses may occur. A particular case of this is when that medium is a periodic collection of identical inclusions. In that case the numerical computation of the eigenstates is further facilitated by the existence of a Bloch theorem.

In cases where the composite medium is limited to one inclusion or a small cluster of such inclusions, an incident plane wave will not only result in a local field which propagates through the cluster, but there will also be some scattering of the incident radiation. In that case a better set of eigenstates for expanding the physical field is obtained by using a different integro-differential operator, namely one whose eigenstates automatically satisfy outgoing-wave boundary conditions at large distances. In that case, the integro-differential operator is non-self-adjoint. Consequently, its eigenvalues are non-real. Moreover, the imaginary part of each eigenstate has the “wrong sign”: It expresses the creation of energy, at a rate which compensates for the rate at which energy is radiated out to infinity in that scattering eigenstate. Because of that, the imaginary part of the eigenvalue actually provides the radiative lifetime of that scattering eigenstate. That lifetime increases to infinity as the ratio of cylinder radius  $a$  to wavelength  $\lambda$  decreases. In order to calculate the lifetime when  $a/\lambda \ll 1$ , we use the eigenvector of the real eigenvalue problem to calculate the expectation value of the non-self-adjoint scattering operator.



# Localization Characteristics of Two-dimensional Metal Nanoparticle Structures

Jian-Wen Dong<sup>1,2</sup>, Kin Hung Fung<sup>1</sup>, C. T. Chan<sup>1</sup>, and He-Zhou Wang<sup>2</sup>

<sup>1</sup>Department of Physics, The Hong Kong University of Science and Technology  
Clear Water Bay, Hong Kong, China

<sup>2</sup>State Key Laboratory of Optoelectronic Materials and Technologies  
Zhongshan (Sun Yat-Sen) University, Guangzhou 510275, China

**Abstract**— Recently, there has been great interest in the plasmon excitation of metal nanoparticles and their aggregates because of their novel properties and some plausible applications. We present the results on plasmonic modes of metal nanoparticles arranged in the two-dimensional quasi-crystalline patterns. In previous studies on the wave transport characteristics in quasi-periodic electronic and phononic systems, the localization of eigenmodes in real space has been the main focus. Two dimensional quasi-periodic arrays of particles are in fact more complex, as the eigenmodes can couple with free photons. We systemically investigated the spatio-temporal localization characteristics in a variety of quasi-crystals consisting of silver nanoparticles. We found rich and complex phenomena. Some ring-like mode modes are found to be highly localized in real space, and have high fidelity.

# Ponderomotive Force-induced Nonlinearity for Surface Plasma Wave in Plasma-insulator-plasma Structure

Yung-Chiang Lan

Institute of Electro-Optical Science and Engineering, National Cheng Kung University  
No. 1 University Road, Tainan 701, Taiwan, China

**Abstract**— Surface plasma wave (SPW) is the coherent fluctuations of the electron charges at the plasma-insulator interface and with the fields highest at the interface and decaying exponentially into both media. Associated with SPW, the plasma-insulator-plasma (PIP) structure is an effective subwavelength waveguide [1]. The ponderomotive force is a nonlinear force that a charged particle experiences in an inhomogeneous electromagnetic field [2]. When SPW propagating along the plasma-insulator interface, the electromagnetic field inhomogeneity in the direction perpendicular to the interface will generate the ponderomotive force and cause the electrons becoming redistributed and moving to field-free regions. Consequently, the local refractive index of the plasma becomes nonlinear and depends on the amplitude of the incident field.

From the perturbation scheme, the time-averaged charge density can be expressed as  $n = n_0 + n_2$ , where the ponderomotive force-induced density perturbation  $n_2 = \frac{1}{2} \frac{\nabla^2 |E^2|}{m \omega^2}$  [3, 4]. Then the relative dielectric constant of the plasma can be expressed as  $\varepsilon_m = 1 - \left(\frac{\omega_p}{\omega}\right)^2 - \frac{\omega_p^2}{2mn_0} \frac{\nabla^2 |E^2|}{\omega^4}$ .

In this study, the characteristics of SPW in the PIP structure considering the nonlinear ponderomotive force are investigated. Regarding the continuity of the normal component of  $\vec{D}$  and the tangential components of  $\vec{E}$  at the plasma-insulator interface, the wave equations and the dispersion relations are solved numerically. Then the incident field-dependent dispersion relations of the SPW will be drawn and compared with those in the ponderomotive force-free case. The field profiles of the SPW along the direction perpendicular to the plasma-insulator interface are also examined. Finally, the distinctions between the SPW and the waveguide modes in the PIP structure will be discussed.

## REFERENCES

1. Maier, S. A., *Plasmonics: Fundamentals and Applications*, Springer, 2007.
2. Chen, F. F., *Introduction to Plasma Physics and Controlled Fusion*, Plenum Press, 1974.
3. Mendonça, J. T., et al., *Phys. Lett. A*, Vol. 239, 373, 1998.
4. Ginzburg, P. and M. Orenstein, *Book of Abstract for the 3rd International Conference on Surface Plasmon Photonics*, 53, 2007.

## Focusing of Light beyond the Diffraction Limit

K. R. Chen

Physics Department, Institute of Electro-optics, National Cheng Kung University, Taiwan, China

**Abstract**— Diffraction, a general characteristic of wave phenomena, occurs whenever a portion of wave front encounters and propagates past an obstruction, was first referenced in the work of Leonardo da Vinci in 1400 s, and has being studied in detail since Francesco Grimaldi in the 1600 s. Explanation based on a wave theory was not noticed until 1800 s. Diffraction sets a lower limit on the spot size of light and thus the ultimate resolution of numerous diagnostic and fabrication instruments. In fact, the diffraction limit inspired Heisenberg for his uncertainty principle of quantum mechanics; they can be deduced from each other. It is shown that, in passing through a grooved metallic subwavelength aperture including a patterned exit structure, an incident light can be focused to a single-spot size beyond the diffraction limit and then propagates to far zone. The wave function across the slits of a sub-limit scale is not considered in the conventional optical and quantum theories, and thus not within their scope. A combination of factors, surface plasma, light bending, subwavelength antenna and constructive interference, are found to be responsible for this unusual effect. The light focusing process, besides its academic interest, is expected to open up a wide range of application possibilities such as lithography, imaging, sensing, optical storage, photonic circuit and many others.

## A Study of the Motion of Surface Plasmons on Silver Nanotrack

Sheng Chung Chen<sup>1</sup>, Zheng Yu Lin<sup>2</sup>, Kuo Pin Chiu<sup>2</sup>, and Din Ping Tsai<sup>2</sup>

<sup>1</sup>Department of Electrical Engineering, Far East University, Tainan, Taiwan, R.O.C.

<sup>2</sup>Department of Physics, Center of Nanostorage Research  
National Taiwan University, Taipei, Taiwan, R.O.C.

**Abstract**— The propagation of the surface plasmons is allowed on the interface of the metal and dielectric. Thus, it is possible to make the motion of surface plasmons on a nanostructure if it meets the propagating conditions. We numerically construct a silver nanotrack of which length is equal to wavelength, and the results of the simulation show that surface plasmons, on both ends of the nanotrack, move toward to each other during the illumination.

Surface Plasmon is generated by the collective motion of free electrons on the metal surface. Thus, it is possible to see the motion of surface plasmon if the nanostructure just meets the corresponding conditions. We numerically construct a nanotrack by two silver nanowires and illuminating the nanotrack by an optical plane wave, as shown in Figure 1. The polarization of the wave is parallel to the nanotrack. The wavelength of the light and the length of the nanotrack both are 600 nm, the diameter of the nanotrack is 60 nm, the spacing between two nanowires is 40 nm. The simulations are made by three-dimensional Finite-Difference Time-Domain (3D FDTD) method, the results show that, there are some hot spots (surface plasmons) generated between the silver nanowires. Initially, two hot spots appear near the ends of the nanotrack, and then, both the hot spots move toward to each other, and the intensity of the hot spots are stronger and stronger, as the six snapshots shown in Figure 1.

We will further to study the factors influence speed of the surface plasmons and the mechanism of the motion.

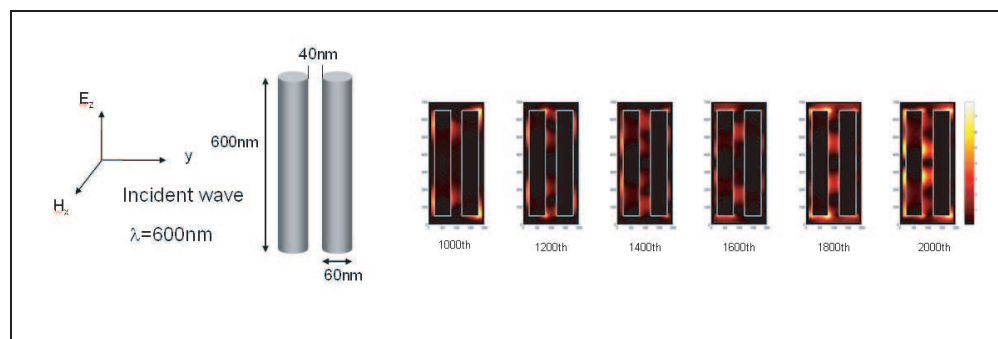


Figure 1: The configuration of the two silver nanotracks and the polarized incident optical wave. The six sequential pictures are snapshotted from 1000th to 2000th time steps. It can be seen that the surface plasmons between nanotracks are moving from the ends toward to the middle during the illumination.

### ACKNOWLEDGMENT

This research is supported by the National Science Council of Taiwan, R.O.C. through the grant number NSC 96-2221-E-269 -005 -.

# Session 2P1b

## Biophoton, Plasmonic Effects and Materials

<p><a href="#">Cloaking of Metallic Cube by Plasmonic Shell in Quasistatic Limit</a>  <i>Adnan Noor (The University of Manchester, UK); Zhirun Hu (The University of Manchester, UK);</i></p> <p><a href="#">Theoretical and Experimental Investigations on Surface Plasmon Cross Coupling Mediated Emission from ZnO</a>  <i>Dangyuan Lei (The Chinese University of Hong Kong, China); H. C. Ong (The Chinese University of Hong Kong, China);</i></p> <p><a href="#">Theoretical and Experimental Studies of the Optical Properties of One-dimensional Metallic Gratings</a>  <i>Wai Chun Luk (The Chinese University of Hong Kong, China); Heping Ying (The Chinese University of Hong Kong, China); Jia Li (The Chinese University of Hong Kong, China); Pak Ming Hui (The Chinese University of Hong Kong, China); Hock Chun Ong (The Chinese University of Hong Kong, China);</i></p> <p><a href="#">The Optical Properties of Large Area Two-dimensional Plasmonic Nanobottle Arrays</a>  <i>Hei Iu (The Chinese University of Hong Kong, China); Jia Li (The Chinese University of Hong Kong, China); Hock Chun Ong (The Chinese University of Hong Kong, China); Jones Tsz-Kai Wan (The Chinese University of Hong Kong, China);</i></p> <p><a href="#">Resonance as a Tool to Transfer Informations to Living Systems</a>  <i>Antonella Lisi (Istituto di Neurobiologia e Medicina Molecolare, C.N.R., Italy); Deleana Pozzi (Università “La Sapienza”, Italy); Mario Ledda (Istituto di Neurobiologia e Medicina Molecolare, C.N.R., Italy); Flavia De Carlo (Istituto di Neurobiologia e Medicina Molecolare, C.N.R., Italy); Roberto Gaetani (Università “La Sapienza”, Italy); Enrico D’Emilia (ISPESL, DIPIA, Italy); Livio Giuliani (ISPESL, DIPIA, Italy); Francesca Bertani (Università “La Sapienza”, Italy); Isotta Chimenti (Università “La Sapienza”, Italy); Lucio Barile (Università “La Sapienza”, Italy); Alberto Foletti (Medico Chirurgo, Specialista in Chirurgia Generale, Italy); Settimio Grimaldi (Istituto di Neurobiologia e Medicina Molecolare, C.N.R., Italy);</i></p> <p><a href="#">High-sensitivity Exploration of Very Thin Liquid Crystal Layers — Coupled Surface Plasmon and Guided Modes</a>  <i>Fuzi Yang (Tsinghua University, China); Lizhen Ruan (University of Exeter, United Kingdom); J. Roy Sambles (University of Exeter, United Kingdom);</i></p>	<p>438</p> <p>439</p> <p>440</p> <p>441</p> <p>442</p> <p>443</p>
--	---

## Cloaking of Metallic Cube by Plasmonic Shell in Quasistatic Limit

Adnan Noor and Zhirun Hu

The University of Manchester, Manchester, UK

**Abstract**— In this paper cloaking of a cubic metallic object by plasmonic cover is investigated and numerically analysed. Cloaking of PEC objects by plasmonic covers, especially plasmonic shells, has been recently investigated [1], and promising results have been produced. Most of these work concern with cloaking of sub-wavelength PEC spheres. Cloaking of electrically large objects has also been reported [2], requiring complex spatial variation of permittivity and permeability.

The object investigated here is an aluminium cube, while the cloak is spherical plasmonic shell. Monostatic and bistatic RCS are calculated using Ansoft HFSS, and compared to that of un-cloaked cube. The reduction of RCS is also compared to the case of metallic sphere, the structure investigated in [1]. The operating frequency is selected to be 1.2 GHz.

Simulation results as good as that for cloaked metallic sphere are obtained for the metallic cube, implying that for monostatic case the object geometry is not very critical. The cloaked structure is also investigated in presence of losses in the plasmonic shell. In case of losses the performance degrades slightly, however the reduction in RCS is still sufficient for potential practical applications.

In our study, an aluminium cube is enclosed in a plasmonic shell (relative permittivity 0.1, relative permeability 5.1) with outer radius of 57.5 mm and inner radius of 50 mm. Dimensions of the cube are chosen such that it would fit in the shell. The structure is simulated using Ansoft HFSS.

For shell with no losses the monostatic RCS decreases by more than 99%. Simulation is repeated with losses (bulk conductivity 0.001 Siemens, dielectric loss tangent 0.001, and magnetic loss tangent of 0.001), and the resulting reduction in RCS is 98%, 1% lower than that of lossless case. For practical applications this is still sufficient.

The bistatic RCS depends on angle of a receiver with respect to source, therefore only maximum bistatic RCS is considered. For lossless case the bistatic RCS decreases by more than 93%, whereas for lossy case the reduction in maximum bistatic RCS is about 92%.

### REFERENCES

1. Engheta, N. and A. Alù, "Plasmonic materials in transparency and cloaking problems: Mechanism, robustness, and physical insights," *Optics Express*, Vol. 15, No. 6, 19 March, 2007.
2. Schurig, D., J. J. Mock, B. J. Justice, S. A. Cummer, J. B. Pendry, A. F. Starr, and D. R. Smith, "Metamaterial electromagnetic cloak at microwave frequencies," *Science*, Vol. 314, 10 November, 2006.

# Theoretical and Experimental Investigations on Surface Plasmon Cross Coupling Mediated Emission from ZnO

D. Y. Lei and H. C. Ong

The Chinese University of Hong Kong, China

**Abstract**— Surface Plasmons (SPs) are the collective oscillations of the electron charges at metal/dielectric interface. Due to the high field strength of SPs, the transition rates of nearby light emitting dipoles can be strongly affected. As metal electrode is invariably used as a medium for injecting carriers into semiconductor, SPs arising from metal/semiconductor interface therefore can evolve as an effective means to increase the emission efficiency of light emitting diodes (LEDs). Although works have been demonstrated on how to use SPs to enhance the emission of organic [1] and inorganic [2, 3] semiconductors, they all are in the backward geometry in which light is emitted via the substrate. However, for an opaque substrate, only the forward emission is useful. Therefore, it is beneficial to realize the SP mediated forward emission from semiconductor.

Here, we have realized SP mediated emission from ZnO in the forward geometry by making use of SP cross coupling (SPCC). In general, there are two processes involved. First, the emission efficiency of ZnO can be increased by SP resonant coupling. We have developed a method of using metal alloy to tune the SP resonance energy to match with the emission energy of semiconductor so that resonant coupling can be achieved. Plasmonic density of states (DOS) and Purcell factor ( $F_P$ ) for  $\text{Al}_x\text{Ag}_{1-x}$ -capped ZnO,  $\text{Al}_x\text{Au}_{1-x}$ -capped ZnTe and  $\text{Ag}_x\text{Au}_{1-x}$ -capped CdSe have been theoretically determined. Large DOS and  $F_P$  can be obtained at certain alloy composition. Experimentally,  $\text{Al}_x\text{Ag}_{1-x}$  thin films have been deposited on ZnO and their optical properties have been studied. It is found that the largest emission enhancement can be observed from  $\text{Al}_{0.8}\text{Ag}_{0.2}/\text{ZnO}$ , which agrees well with theory. Secondly, we have employed metal-insulator-metal (MIM) structure as a medium to increase the transmission of the metal system and thereby to increase the forward emission. Simulations and experiments have shown that, due to the cross coupling of the radiative SP mode in the structure, MIM has a sharp transmission peak that is highly depending on the thickness of the insulator. By tailoring the insulator thickness so that the transmission matches with the emission peak of ZnO, the forward emission from MIM/ZnO can be enhanced by 7 times compared with its bare counterpart.

## REFERENCES

1. Neal, K., K. Okamoto, and A. Scherer, "Surface plasmon enhanced emission from dye doped polymer layers," *Opt. Express*, Vol. 13, 5522, 2005.
2. Okamoto, K., I. Niki, A. Shvartser, Y. Narukawa, T. Mukai, and A. Scherer, "Surface-plasmon-enhanced light emitters based on InGaN quantum wells," *Nature Mater*, Vol. 3, 601, 2004.
3. Lai, C. W., J. An, and H. C. Ong, "Surface-plasmon-mediated emission from metal-capped ZnO thin films," *Appl. Phys. Lett.*, Vol. 86, 251105, 2005.

# Theoretical and Experimental Studies of the Optical Properties of One-dimensional Metallic Gratings

Wai Chun Luk, Haiping Yin, Jia Li, Pak Ming Hui, and Hock Chun Ong

Department of Physics, The Chinese University of Hong Kong, Shatin, N.T., Hong Kong, China

**Abstract**— In the recent years, there have been many experimental and theoretical interests about the extraordinary transmission of light through two-dimensional (2-D) periodic sub-wavelength hole arrays fabricated on a thin layer of metal film. However, the underlying mechanism of this transmission effect remains unclear. In particular, whether the transmission is assisted by surface plasmon polaritons (SPPs) or waveguide modes is still under debate. On the other hand, metallic grating, which is the one-dimensional (1-D) counterpart, also possesses interesting optical properties. As 1-D structure can easily support propagating waveguide modes normal to the film surface while 2-D can not, study on 1-D metallic gratings may provide not only more physical insight on the transmission mechanism of 2-D hole arrays but also some new phenomena. In this presentation, we have fabricated 1-D metallic gratings with subwavelength grooves by interference lithography and measured their dispersion relations by using angle-dependent reflectivity and transmittance. Strong angle dependent reflection and transmission features are frequently observed from the reflection and transmission spectra indicating the excitation of SPPs. By varying the groove depth, we have observed new localized plasmon modes that are independent of angle gradually evolve. In particular, strong interaction between SPPs and localized modes can be seen at groove depth of 200 nm, 380 nm and 570 nm. By using the Rigorous Coupled-Wave Analysis (RCWA) method, we have simulated the optical spectra and field patterns as a function of angle for different groove depths and our calculations agree well with the experiment. Our results unambiguously prove the presence of two channels in assisting the extraordinary transmission in 1-D metallic gratings.



# The Optical Properties of Large Area Two-dimensional Plasmonic Nanobottle Arrays

Hei Iu, Jia Li, Hock Chun Ong, and Jones Tsz-Kai Wan

Department of Physics, The Chinese University of Hong Kong, Shatin, N.T., Hong Kong, China

**Abstract**— In recent years, discussion on the applications of surface plasmon polaritons (SPPs) has been intensive in photonics and biotechnology communities. However, how to gain control on SPPs with great precision and flexibility is still under developed. With better control of SPPs, the local fields can be engineered to serve for various applications such as second harmonic generation, surface-enhanced Raman, etc. Mimicking the photonic crystal analogy, plasmonic structure can also be used for manipulating this surface waves by localizing the fields within certain regions. In this presentation, we will talk about our recent progress on the optical properties of large area two-dimensional (2-D) plasmonic crystal. By using interference lithography and thin film deposition technique, we have fabricated 2-D metallic nanobottle arrays with period varied from 400 to 800 nm in cubic form. In particular, the aperture, or the neck, of bottle can be controlled from 50 to 300 nm by changing the thickness of metal coating. Angle-dependent reflectivity measurements are then carried out on the arrays to map out the dispersion relations. With the aid of finite-difference time domain (FDTD) simulations, we are able to identify the Bragg scattered SP and localized SP modes from the dispersion relation. In addition, the field patterns of these resonance modes have been mapped out accordingly. By comparing the experiments and simulations, we have found by changing the aperture of the bottle, one could easily modify the confinement of the localized modes and thus the field strength. As a result, the nanobottle arrays are expected to find potential applications in areas such as bio-sensing and surface-enhanced Raman scattering.

## Resonance as a Tool to Transfer Informations to Living Systems

Antonella Lisi<sup>1</sup>, Deleana Pozzi<sup>2</sup>, Mario Ledda<sup>1</sup>, Flavia de Carlo<sup>1</sup>  
Roberto Gaetani<sup>2</sup>, Enrico D'Emilia<sup>3</sup>, Livio Giuliani<sup>3</sup>, Francesca Bertani<sup>2</sup>  
Isotta Chimenti<sup>2</sup>, Lucio Barile<sup>2</sup>, Alberto Foletti<sup>4</sup>, and Settimio Grimaldi<sup>1</sup>

<sup>1</sup>Istituto di Neurobiologia e Medicina Molecolare, C.N.R., Rome, Italy

<sup>2</sup>Dipartimento di Medicina Sperimentale, Università "La Sapienza", Rome, Italy

<sup>3</sup>ISPESL DIPIA, Italy

<sup>4</sup>Bititalia, Milano, Italy

**Abstract**— In the middle of the eighties there were attempts to understand the physical mechanisms of resonance action of combined static and alternate magnetic fields (MFs). A. Liboff (Liboff, 1985;), considering the motion of free ions in the vacuum (cyclotron) under action of these MFs, supposed a mechanism similar could be applied to understand one of the operating way to transfer information in the living systems. But at room temperature this idea could be realized only in very large systems capable to include the long radius of ion rotation measured by meters. The idea (Lednev, 1991); on participation of parametric resonance in such sort of effects was not very fruitful for lack of a necessary low frequency harmonic oscillator in living systems. The Larmor precession could not help in this situation, not being such an oscillator because of lack of restoring force with proper parameters. The problem solving had come from Quantum Electrodynamics of Condensed Matter. According to the quantum electro-dynamical theory by Preparata (1995), the liquid water consists of two components: coherent and incoherent ones. The coherent component is contained within spherical so called "coherence domains" (CDs) where all molecules synchronously oscillate with the same phase. CDs are surrounded by the incoherent component where molecules oscillate with casual phases regarding each other. Diameters of CDs are measured by tenths of a micron, and at room temperature the total volume of domains is about 40% of the whole water media. At resonance action of the calcium ion cyclotron frequency the ion is accelerated by the MFs, increasing its kinetic energy till its escape from CD jumping into the incoherent component of the water molecule where the ion became biologically available. We have recently demonstrated the possibility to obtain Cardiac Stem Cells (CSCs), from human endomyocardial biopsy specimens. CSCs self-assemble into multi-cellular clusters known as cardiospheres (CSps) that engraft and partially regenerate infarcted myocardium.

CSps and Cardiospheres-derived-Cells CDCs were exposed for five days in an incubator inside a solenoid system with temperature and humidity and CO<sub>2</sub> regulated. This exposure system were placed in an amagnetic shielded room in the simultaneous presence of a static MF and a low-alternating-frequency-MF, close to the cyclotron frequency corresponding to the charge/mass ratio of Ca<sup>++</sup> ion. In this exposure conditions CSps and CDCs modulate their differentiation turning on cardiogenesis and turning off vasculogenesis. Cardiac markers such as Troponin I (TnI) or Myosin Heavy Chain (MHC) were up-regulated (Fig. 1), conversely angiogenic markers such as Vascular Endothelial Growth Factor (VEGF) or Kinase Domain Receptor (KDR) (Fig. 2) were down-rugulated as evidenced by immunocytochemistry. The improvement in the cardiogenic differentiation was confirmed by Real-Time PCR and Western Blotting. Interestingly, an increase in the proliferation (particularly of the CDCs) was observed and evidenced by Brd-U incorporation (ELISA) and cell counting kit-8 (WST-8) analysis.

**Conclusion:** Exposure to Calcium ion ICR can modulates the cardiogenic *versus* angiogenic differentiation process of *ex vivo* expanded CSCs.

This may pave the way for novel approaches in tissue engineering and cell therapy.

# High-sensitivity Exploration of Very Thin Liquid Crystal Layers — Coupled Surface Plasmon and Guided Modes

Fuzi Yang<sup>1,2</sup>, Lizhen Ruan<sup>2</sup>, and J. R. Sambles<sup>2</sup>

<sup>1</sup>Chemistry Department, Tsinghua University, Beijing 100084, China

<sup>2</sup>Electro-Magnetic Materials, School of Physics, University of Exeter  
Exeter, EX4 4QL, United Kingdom

**Abstract**— Knowledge of the molecular director profile very near to the boundaries of a liquid crystal (LC) cell and its dynamic behaviour under external influence, e.g., an applied voltage, is key information to both fundamental research and practical device design. A very sensitive optical method for exploring the surface situation of LC molecules is thus important for the study of liquid crystal cells.

For a LC cell with thin silver claddings it is possible to excite both a surface plasmon and ordinary optical guided modes. In a situation where the tilt of the director varies from homogeneous to homeotropic through the cell, then for p-polarized incident radiation the p-polarized surface plasmon mode and the ordinary guided waves may couple to each other. When the plane containing the director is normal to the incident plane, there is also polarisation conversion leading to strong coupling between the p-polarised surface plasmon and s-like guided modes [1].

In this study a half leaky guided mode (HLGM) geometry [2] with a single metal-cladding layer, composed of a hybrid aligning nematic (HAN) LC cell, has been used to explore the distribution of the LC director very near the surface. From theoretical analyses together with numerical modelling it is shown how this coupled spectrum gives a high sensitivity to the surface director tilt profile near the walls which is higher than that of the surface plasmon mode alone. The HLGM geometry studied here uses a low-index bottom glass plate to replace a thick metal-coating in a double-metal cladding HAN cell technique developed recently by us [1]. Because the low-index plate is a better total reflector than a metal-coating for a certain incident-angle range, then not only can the coupling spectrum be excited, but also it allows for simple sample fabrication while the theoretical fitting is easier because of the lack of the bottom metal coating. The experimental results fully confirm the model predictions showing that this modified geometry also provides a powerful tool for near-surface director studies like as in work [1].

## REFERENCES

1. Yang, F., L. Ruan, S. A. Jewell, and J. R. Sambles, *New Journal of Physics*, Vol. 9, 49, 2007.
2. Yang, F. and J. R. Sambles, *J. Opt. Soc. Am.*, Vol. B10, 858, 1993.



# Session 2P2a

## Shaping Optical Forces for Trapping and Binding – Theory

<a href="#">Bored Helical Phases: Dynamics of Intensity Profiles and Poynting Vector Calculation upon Propagation</a>	446
<i>Nathaniel P. Hermosa II (Ateneo de Manila University, Philippines); Stein C. Baluyot (Ateneo de Manila University, Philippines);</i> .....	
<a href="#">Optical Trapping in Interfering Laser Beams: Principles and Applications</a>	447
<i>Pavel Zemánek (Institute of Scientific Instruments of the ASCR, v.v.i., Czech Republic); T. Čížmár (Institute of Scientific Instruments of the ASCR, v.v.i., Czech Republic); M. Šiler (Institute of Scientific Instruments of the ASCR, v.v.i., Czech Republic); P. Jákł (Institute of Scientific Instruments of the ASCR, v.v.i., Czech Republic); M. Sery (Institute of Scientific Instruments of the ASCR, v.v.i., Czech Republic);</i> .....	
<a href="#">Theory for Trapping Efficiency of Arbitrary Beams in Optical Tweezers</a>	448
<i>Antonio A. R. Neves (Universita di Lecce, Italy); A. Fontes (Federal University of Pernambuco, Brazil); C. L. Cesar (Universidade Estadual de Campinas, Brazil); A. Camposeo (Universita di Lecce, Italy); R. Cingolani (Universita di Lecce, Italy); D. Pisignano (Universita di Lecce, Italy);</i> .....	
<a href="#">Dual-beam Interferometric Laser Trapping of Rayleigh and Mesoscopic Particles</a>	449
<i>Vincent L. Y. Loke (The University of Queensland, Australia); Timo A. Nieminen (The University of Queensland, Australia); N. R. Heckenberg (The University of Queensland, Australia); Halina Rubinsztein-Dunlop (The University of Queensland, Australia);</i> .....	
<a href="#">Giant Optical Forces and Size-selective Manipulation for Microspheres Using Evanescent Wave Excitation of Whispering Gallery Modes</a>	450
<i>Jack Ng (The Hong Kong University of Science and Technology, China); Che Ting Chan (The Hong Kong University of Science and Technology, China);</i> .....	

## Bored Helical Phases: Dynamics of Intensity Profiles and Poynting Vector Calculation upon Propagation

Nathaniel P. Hermosa II and Stein C. Baluyot

School of Science and Engineering, Ateneo de Manila University

Loyola Heights, Quezon City, 1108 Philippines

**Abstract**— A modified helical phase is presented. The phases of these beams are made by boring a hole at the center of a helical phase as,

$$\Phi_{\ell}(r, \theta) = \begin{cases} 0 & 0 \leq r \leq r_i, \\ \ell\theta & r > r_i \end{cases} \quad (1)$$

where  $r_i$  is the cavity radius and  $\ell$  is the number of  $2\pi$  windings around the azimuth. The beams are propagated numerically via the “Split-Step” algorithm introduced by Feit and Fleck. We observe that the intensity profiles of these beams vary with the cavity radius. When the ratio between the cavity radius and the beam radius ( $r_i/r_o$ ) is less than 0.15, the beams’ intensity profiles are similar to the profiles of the Laguerre-Gaussian beams. However at  $r_i/r_o$  greater than 0.50, the beams produce  $\ell$  intense distinct arms. We surmise that the number of arms is due to an integral  $2\pi$  phase difference between the bore and the helical phase. In between ratios 0.15 and 0.50, the intense arms of the beams are not yet distinct and the intensity profiles still resemble distorted circles. We have experimentally verified the intensity profiles with the use of computer generated holograms.

Upon propagation in free space, these beams rotate around the propagation axis while keeping their intensity profiles. The intensity profiles are the same upon scaling, up to a certain propagation distance. The rotation is a function of  $\ell$  and is dependent on  $r_i$ . The rate of rotation with propagation distance is faster for small  $\ell$  and the rate decreases with increasing  $\ell$ . Beams with similar  $\ell$  but with different  $r_i$  seem to have the same rotation rate.

We also present calculations of the Poynting vector of these beams as they propagate. Specifically, we compute for the linear momentum of these beams in anticipation of possible applications in optical micromanipulation.

# Optical Trapping in Interfering Laser Beams: Principles and Applications

P. Zemanek, T. Cizmar, M. Siler, P. Jakl, and M. Sery

Institute of Scientific Instruments of the ASCR, v.v.i.

Academy of Sciences of the Czech Republic, Kralovopolska 147, 612 64 Brno, Czech Republic

**Abstract**— The classical tool for optical micromanipulations — single-beam optical tweezers — has been known for more than 20 years and, apart from life sciences, it influenced also colloidal and aerosol chemistry, atomic physics, hydrodynamics, and basic physics. However, many new and exciting applications were introduced in the last five years. Some of the most remarkable examples are based on engineering of laser beam wavefront via dynamically reconfigurable phase or amplitude masks (so called holographic tweezers) or exploiting the interference of several laser beams.

This last mentioned light-shaping technique is the prerequisite for various methods of sorting of colloidal particles or living cells according to their size or refractive index in optical lattices, Bessel beams, traveling standing waves; simultaneous optical confinement of thousands of objects in spatially periodic interference structures and their delivery over millimeter distances. The above list illustrates clearly the application potential of the interferometric optical micromanipulation techniques. They can be combined with microfluidic systems to sort microobjects and increase further the sensitivity and versatility of lab-on-a-chip systems dealing with very small volumes of analyte; they can be used in laboratories where non-contact manipulation with large amount of objects is needed or interactions between these objects have to be analyzed. However, more confined objects scatter more light that interferes with the trapping light pattern and can lead to loss of stability of the trapped structure.

We are going to present how the trapping in spatially periodic fields, with emphasis on the standing waves trapping, depends on the object size and material, how to employ it for optical sorting with and without the fluid flow, how to use traveling periodic potential profiles for object delivery and how the number of objects influences confinement properties of the whole structure comparing to the single particle.

## ACKNOWLEDGMENT

This work was partially supported by MEYS CR (project No. LC06007) and IRP of the ISI (AV0Z20650511).

# Theory for Trapping Efficiency of Arbitrary Beams in Optical Tweezers

A. A. R. Neves<sup>1</sup>, A. Fontes<sup>2</sup>, C. L. Cesar<sup>3</sup>, A. Camposeo<sup>1</sup>, R. Cingolani<sup>1</sup>, and D. Pisignano<sup>1</sup>

<sup>1</sup>National Nanotechnology Laboratory of CNR-INFM, Distretto Tecnologico, Scuola Superiore ISUFI  
Università di Lecce, via Arnesano I-73100, Lecce, Italy

<sup>2</sup>Federal University of Pernambuco, Recife, Pernambuco, Brazil

<sup>3</sup>CePOF, Instituto de Física, Universidade Estadual de Campinas, Brazil

**Abstract**— Today optical tweezers setup has become a highly sensitive force measurement, and in the last few years different theories were developed to determine the theoretical optical forces on a dielectric microsphere acting as a probe. Initial works separated the trapping domain in two distinct size regime, (Rayleigh and Geometrical Optics) for the particle size compared to the wavelength of the trapping beam, but for most trapping experiments the probe size is of the order of the wavelength, consequently a full range Mie regime has to be adopted. Also for a certain size ratio, of the microsphere diameter with respect to wavelength, may be such to give rise to morphology dependent resonances, which must certainly be taken into account since the scatterer cross section will change abruptly. Even though the scatterer is spherically symmetric, the trapping force is dependent on polarization and does not share the spherical symmetry of the microsphere. To account for polarizations in the high numerical aperture (NA) focal region, different approximations of the non-paraxial beam has been adopted, but only with an angular spectrum representation could the vectorial EM fields in the focal region satisfy Maxwell's equation exactly. The correct beam description represents one of the main problems for proper determination of optical forces. Recently it has been shown that with an integral relation the partial wave expansion coefficients of this focused vectorial EM fields could be determined analytically, thus gaining significant physical insight into the dependence of the optical forces through the use of the generalized Lorenz-Mie theory. Diffraction effects and aberrations due to the refractive index mismatch of the immersion oil objective are observed on the optical trapping force profiles for an arbitrary beam profile and polarization. Here we present this optical force theory, solved without approximations, providing further insight into the physics of optical trapping, in term of easily obtainable experimental parameters.



## Dual-beam Interferometric Laser Trapping of Rayleigh and Mesoscopic Particles

V. L. Y. Loke, T. A. Nieminen, N. R. Heckenberg, and H. Rubinsztein-Dunlop  
The University of Queensland, Australia

**Abstract**— There has been a significant amount of experimental work with counter-propagating, crossed-beam, and other interferometric laser trapping of neutral dielectric particles. Apart from the benefits of these configurations, such as the compensation or neutralization of scattering forces, there are a number of interesting applications. For example, the optical lattice resulting from interference can be used to sort particles of different refractive indices or sizes. The system can also be used to study thermal hopping between potential wells or to investigate Brownian motion subject to a quasi-periodic external potential.

Most theoretical work on dual-beam systems has been focused on Rayleigh particles. For mesoscopic particles, where Rayleigh scattering is not applicable, we employ the generalized Lorenz–Mie theory (GLMT) which is synonymous with the T-Matrix method when considering spherical particles. GLMT is an exact method which is applicable in both the Rayleigh and mesoscopic regimes.

We calculate the fields and optical forces on the particles in the vicinity of the trapping region for several dual beam configurations such as counter-propagating, axially offset, and crossed beams, and with different particle sizes. We present the intensity profiles which demonstrate the interference fringes and the force vectors to predict the positions where a given particle can be localized. Surprisingly, our results show that sub-wavelength localization by interference fringes of particles that are much larger than the wavelength (or fringes) of the trapping beams is possible. The competition between such localization by interference fringes and attraction to the focus can be controlled by the beam convergence angle, or, equivalently, the numerical aperture of the focussing system.

# Giant Optical Forces and Size-selective Manipulation for Microspheres Using Evanescent Wave Excitation of Whispering Gallery Modes

Jack Ng and C. T. Chan

The Hong Kong University of Science and Technology, Hong Kong, China

**Abstract**— One of the state-of-the-art techniques to determine the size of a microsphere is to utilize the extremely sharp fluorescence peaks of its WGM, where an accuracy of  $\sim 0.05\%$  has been experimentally achieved for a 5-micron-diameter sphere [2]. However, there is a desire to search for methods that are automatic and/or parallel, and therefore they have higher throughputs. Here we propose an approach base on WGM induced optical forces that will potentially allow one to select microspheres of a particular size or resonant frequency, and possibly in large quantities.

Evanescent waves have the unique ability to couple to the WGMs while preserving its high- $Q$ . By exciting the WGM of a microsphere with an evanescent wave, it is shown that one can exert a giant size-selective optical force on individual microsphere (see Fig. 1), with strength proportional to  $Q$  and the size-sensitivity  $\sim Q^{-1}$  (where  $Q$  is the quality factor of the WGM). For a 5  $\mu\text{m}$ -diam microsphere, one can easily achieve a force exceeding  $\sim 100$  pN (76 nN for a perfect sphere with no absorption) at a moderate light intensity ( $10^4$  W/cm $^2$ ), and with a size-sensitivity of better than 0.1%. Such resonant force is potentially useful for accurate size-selective manipulation, and for selecting microcavities that have the same size and resonant frequency (potentially with a state-of-the-art accuracy), in a fully automatic, parallel, and high throughput manner.

**Methodology:** We calculate the optical forces that act on a high- $Q$  microsphere by an evanescent wave (or inhomogeneous plane wave). We found that evanescent waves can couple efficiently to whispering gallery modes (WGM) and the optical force is greatly enhanced at resonance. The formalism we employ is based on a multiple-scattering and Maxwell Stress Tensor formalism [1].

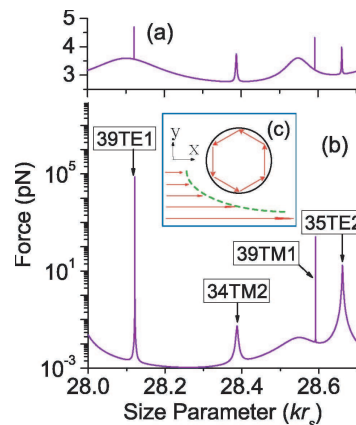


Figure 1: The optical force acting on a microsphere along the propagating direction of the incident wave. The parameters are incident wavelength  $\lambda = 520$  nm, the dielectric constant of the sphere  $\epsilon_{\text{sphere}} = 2.5281$ , and the sphere radius  $r_s = 2.317 - 2.375$   $\mu\text{m}$ . (a) The incident wave is a linear polarized homogeneous plane wave with a uniform intensity of  $I_0 = 10^4$  W/cm $^2$ . (b) The incident wave is an s-polarized evanescent wave with  $k_0/k = 1.427$  and  $I_0 = 10^4$  W/cm $^2$  at the bottom of the sphere. (c) A schematic illustration of how an evanescent wave excites a WGM. Efficient excitation.

## REFERENCES

1. Ng, J., Z. F. Lin, C. T. Chan, and P. Sheng, *Phys. Rev. B*, Vol. 72, 085130, 2005.
2. Mukaiyama, T., et al., *Phys. Rev. Lett.*, Vol. 82, 4623, 1999.

# Session 2P2b

## Shaping Optical Forces for Trapping and Binding – Biology

Optical Micro-assembly in Parallel	
<i>Jesper Glückstad (Technical University of Denmark, Denmark);</i> .....	452
Spectroscopy Nanofabrication and Biophotonics	
<i>Enzo Di Fabrizio (CNR-INFN, Italy);</i> .....	453
Feeling for Cells with Light	
<i>Josef A. Käs (University of Leipzig, Germany);</i> .....	454
Investigating Cellular Signaling Reactions at the Nanometer and Attoliter Scale	
<i>Horst Vogel (Swiss Federal Institute of Technology (EPFL), Switzerland);</i> .....	455
PicoNewton Force Spectroscopy for Motile Structures of the Axon's Growth Cone	
<i>Dan Cojoc (CNR-INFN, Italy); E. Ferrari (CNR-INFN, Italy); F. Di Fato (International School for Advanced Studies (SISSA-ISAS), Italy); R. Shahapure (International School for Advanced Studies (SISSA-ISAS), Italy); J. Laishram (International School for Advanced Studies (SISSA-ISAS), Italy); M. Righi (International School for Advanced Studies (SISSA-ISAS), Italy); Enzo Di Fabrizio (CNR-INFN, Italy); V. Torre (International School for Advanced Studies (SISSA-ISAS), Italy);</i> .....	456

## Optical Micro-assembly in Parallel

Jesper Glückstad

Optics and Plasma Research Department, Risø National Laboratory  
Technical University of Denmark, DK-4000 Roskilde, Denmark

**Abstract**— The parallel assembly of minute components with sizes in the range of 1–100 micro-meters remains to be an exciting scientific challenge within micro-mechanics. The research into real-time, massively parallel and three-dimensional micro-assembly schemes may lead to revolutionary developments of new and reconfigurable micro-opto-electromechanical-systems. In particular, micro-assembly done within a liquid environment seems attractive to pursue due to the fact that undesirable effects of van der Waals and surface interactions can be kept at a minimum.

Real-time reconfigurable arrays of a plurality of interactive optical traps are potentially a very attractive approach to enable precise assembly of freely suspended microstructures. Multiple optical traps are capable of holding, positioning and rotating a plurality of mesoscopic objects in three dimensions [1]. In the past year, we have demonstrated the first all-optical, directed micro-assembly scheme [2] by tiling a plurality of microscopic structural elements on a planar substrate using real-time reconfigurable optical traps from a variant of the parallel optical manipulation schemes we have previously reported on [3, 4]. The number of optical traps, their intensity profiles and spatial locations were all controlled either interactively or in an automated way using an advanced computer interface. Under computer-automated control, the system demonstrated the capability for fully autonomous search-and-collect routines without the need for any user intervention [5]. Our experimental demonstrations showed that optical traps of a few milli-Watts are able to achieve good positional and rotational control of the assembled micro-structures. Efficient tiling also benefited from applying shape-complementarity among the micro-puzzle pieces having identical geometrical shapes and in-plane rotational symmetry. Finally, the puzzle pieces had elongated aspect ratio so that orientations were conveniently determined by an image analysis subroutine — making it easy to orient the projected elongated optical traps. The micro-fabrication of the puzzle pieces was achieved by a standard femto-second laser two-photon polymerization technique.

### REFERENCES

1. Glückstad, J., P. J. Rodrigo, and I. Perch-Nielsen, “Optical 3D manipulation and observation in realtime (invited paper),” *J. Robotics Mechatronics*, Vol. 18, No. 6, 692–697, 2006.
2. Rodrigo, P. J., L. Kelemen, C. A. Alonzo, I. Perch-Nielsen, J. S. Dam, P. Ormos, and J. Glückstad, “2D optical manipulation and assembly of shape-complementary planar microstructures,” *Opt. Express*, Vol. 15, 9009–9014, 2007.
3. Rodrigo, P. J., I. Perch-Nielsen, C. A. Alonzo, and J. Glückstad, “GPC-based optical micro-manipulation in 3D real-time using a single spatial light modulator,” *Opt. Express*, Vol. 14, 13107–13112, 2006.
4. Rodrigo, P. J., I. Perch-Nielsen, and J. Glückstad, “Three-dimensional forces in GPC-based counterpropagating-beam traps,” *Opt. Express*, Vol. 14, 5812–5822, 2006.
5. Perch-Nielsen, I., P. J. Rodrigo, C. A. Alonzo, and J. Glückstad, “Autonomous and 3D real-time multi-beam manipulation in a microfluidic environment,” *Opt. Express*, Vol. 14, 12199–12205, 2006.

## Spectroscopy Nanofabrication and Biophotonics

Enzo Di Fabrizio

CNR-INFM, Italy

**Abstract**— In recent years, there was an increasing interest on design and fabrication of nanostructures devoted to photonic applications such as photonic crystals fabrication [1], spectroscopy analysis, detection of single molecules and fundamental studies on well confined electromagnetic field. Different materials, fabrication techniques and applications were especially devoted to the use of plasmonic enhancement to the study of molecules of biological interest. The main task was the control the enhancement of the local electrical field, in order to overcome the low scattering cross section of the Raman effect, when single molecule has to be detected.

In this work we present the fabrication of a novel plasmonic nanostructure for Surface Enhanced Raman Scattering for single molecule detection. High sensitivity measurements of a few tens of molecules will be presented. The choice of nanolithography as fabrication techniques is due to the fact that it is now necessary to investigate, in a controllable and reproducible way the effect of 3D geometry on the generation of plasmonpolaritons on such material and devices. The structures were tested optically with different set up, and we found significant improvement in the spectra quality and in the detection sensitivity, down to a few tens of molecules.

### REFERENCES

1. Gerace, D., et al., *Appl. Phys. Lett.*, Vol. 87, 211116, 2005.
2. Stockman, M. I., *Phys. Rev. Lett.*, Vol. 93, 137404-1-4, 2004.

## Feeling for Cells with Light

Josef A. Käs

University of Leipzig, Germany

**Abstract**— The cytoskeleton a compound of highly dynamic polymers and active nano-elements inside biological cells is responsible for a cell's stability and organization. It mechanically senses a cell's environment and generates cellular forces sufficiently strong to push rigid AFM-cantilevers out of the way. These forces are generated in the lamellipodium — which can be considered a thin polymeric film — by molecular motor-based nano-muscles, and by polymerization through mechanisms similar to Feynman's hypothetical thermal ratchet. The active polymer networks as basic element of the lamellipodium are described by a new type of polymer physics since nano-sized molecular motors and active polymerization overcome the inherently slow, often glass-like brownian polymer dynamics. Light has been used to observe cells since Leeuwenhoek's times; however, we use the forces caused by light described by Maxwell's surface tensor to feel the cytoskeleton. The optical stretcher exploits the nonlinear, thus amplified response of a cell's mechanical strength to small changes between different cytoskeletal proteomic compositions as a high precision cell marker that uniquely characterizes different cell types. Consequentially, the optical stretcher detects tumors and their stages with accuracy unparalleled by molecular biology approaches. This precision allows us to isolate adult stem cells for regenerative medicine without contamination through molecular markers.

# Investigating Cellular Signaling Reactions at the Nanometer and Attoliter Scale

Horst Vogel

Swiss Federal Institute of Technology (EPFL), CH 1015 Lausanne, Switzerland

**Abstract**— Classically, cellular signaling is investigated measuring different optical or electrical properties of either single cells or microliter volumes of suspensions of live cells. Here we show how ligand binding to cell surface receptors and subsequent signaling reactions can be monitored both in single cells and in single, submicrometer sized vesicles, which are either produced by reconstitution from individual components or derived from living biological cells. Such vesicles are the smallest autonomous containers capable of performing cellular signaling reactions, thus opening the door to downscale analysis of cellular functions to the nanometer and attoliter range. We describe a method that allows the massively parallel isolation of such attoliter-sized experimental volumes and their organization in ordered arrays by optical trapping. Our approach of miniaturization using advanced microfluidics combined with multiple optical tweezers opens novel routes in functional proteomics such as multiplexing single cell bioanalytics or investigating receptor mediated signaling in multiarray format. In this context ensemble and single molecule spectroscopies of suitably labeled proteins are used to investigate transmembrane signaling within individual live cells and native vesicles. We will report on our recent findings of cellular signaling reactions mediated by ligand-gated ion channels and G-protein coupled receptors.

## REFERENCES

1. Pick, H., et al., “Investigating cellular signaling in single attoliter vesicles,” *J Am Chem Soc*, Vol. 127, 2908, 2005.
2. Meyer, B. H., et al., “FRET imaging reveals that functional neurokinin-1 receptors are monomeric and reside in membrane microdomains of live cells,” *Proc Natl Acad Sci*, Vol. 103, 2138, USA, 2006.
3. Jacquier, V., et al., “Visualizing odorant receptor trafficking in living cells down to the single-molecule level,” *Proc Natl Acad Sci*, Vol. 103, 14325, USA, 2006.
4. Danelon, C, M. G Jenke, C. Schreiter, G. M. Kim, J. B. Perez, C. Santschi, J. Brugger, and H. Vogel, “Micro- and nanostructured devices for the investigation of biomolecular interactions,” *Chimia*, Vol. 60, A754–A760, 2006.
5. Grandl, J., E. Sakr, F. Kotzyba-Hibert, S. Bertrand, D. Bertrand, H. Vogel, M. Goeldner, and R. Hovius, “Fluorescent epibatidine agonists for neuronal and muscle-type nicotinic acetylcholine receptors,” *Angew. Chem. Int. Ed.*, Vol. 46, 3505–3508, 2007.

# PicoNewton Force Spectroscopy for Motile Structures of the Axon's Growth Cone

D. Cojoc<sup>1,3</sup>, E. Ferrari<sup>1</sup>, F. Di Fato<sup>2</sup>, R. Shahapure<sup>2</sup>  
 J. Laishram<sup>2</sup>, M. Righi<sup>2</sup>, E. Di Fabrizio<sup>1,4</sup>, and V. Torre<sup>2</sup>

<sup>1</sup>Laboratorio Nazionale TASC, CNR-INFM, Area Science Park, Basovizza, Trieste, Italy

<sup>2</sup>International School for Advanced Studies (SISSA-ISAS), Trieste, Italy

<sup>3</sup>Centro Biomedicina Molecolare(CBM), Trieste, Italy

<sup>4</sup>Università Magna Graecia di Catanzaro, Italy

**Abstract**— The migration of the axons of neuronal cells is driven by guidance cues sensed by receptors located on the growth cone [1]. Filopodia and lamellipodia, the highly motile structures extruding from the tip of the growth cone, explore the environment. Their motion has been analyzed, but little is known about the force these neuronal structures exert on the structures they might find during their navigation. In fact, the analysis of this force has been limited to theoretical considerations and experimental analysis have been restricted to samples of isolated filaments [2] or to migrating cells [3]. In this study, we used optical tweezers [4] to measure the forces exerted by filopodia and lamellipodia with a millisecond temporal resolution.

Silica beads of 1  $\mu\text{m}$  in diameter, functionalised with amino groups to reduce sticking, were trapped with an 1064 nm infrared (IR, mW power at the sample) optical tweezers close to the growth cone of a migrating axon (Fig. 1(a)) [5]. The growth cone displaced the bead both laterally and axially from its equilibrium position by even 2 or 3 microns (Fig. 1(b)). At the end the bead did not remain attached to the growth cone and could return to its original position in the trap (Fig. 1(c)). We measured the lateral force exerted by the growth cone  $F_{neu} = (F_x, F_y)$  by following the bead position both by using back focal interferometry with quadrant photo diode (QPD) [4] and by video tracking.

We have analysed collisions between growth cones and trapped beads in more than 200 experiments. Each experiment lasted for 3 minutes and in many experiments several collisions significant for statistical analysis were observed. These collisions produced maximal forces ranging from less than 1 pN to at least 20 pN with a maximal rate of increase of 10 pN/second. These collisions lasted from less than 1 sec to about 40–60 seconds. Larger forces were usually observed during long lasting collisions. As these forces extend over a wide range of intensities and durations, we measured separately the forces developed by filopodia and lamellipodia for hundreds experiments in order to have a good statistics.



Figure 1: Snapshots, at three different moments of time, of a growth cone displacing a bead out of the optical trap. The red cross indicates the equilibrium position inside the optical trap. Scale bar 2  $\mu\text{m}$ .

## REFERENCES

1. Song, H. and M. Poo, *Nat. Cell Biol.*, Vol. 3, E81, 2001.
2. Marcy, Y., J. Prost, M. F. Carlier, and C. Sykes, *Proc. Natl. Acad. Sci.*, Vol. 101, 5992, USA, 2004.
3. Prass, M., K. Jacobson, A. Mogilner, and M. Radmacher, *J. Cell Biol.*, Vol. 174, 767, 2006.
4. Neuman, K. C. and S. M. Block, *Rev. Sci. Instrum.*, Vol. 75, 2787, 2004.
5. Cojoc, D., E. Ferrari, F. Difato, R. Shahapure, J. Laishram, M. Righi, E. Di Fabrizio, and V. Torre, *PlosOne*, accepted September 2007.



# Session 2P3

## Metamaterials at Microwave Frequencies

<p>Negative-index Materials Are Different from Left-handed Materials: Bi-isotropic Constitutive Relations Revisited</p> <p><i>Ari Henrik Sihvola (Helsinki University of Technology, Finland);</i> .....</p> <p>Extraordinary Transmission through Periodically Perforated Screens from a Circuit Theory Perspective</p> <p><i>Francisco Medina (University of Seville, Spain); Francisco L. Mesa (University of Seville, Spain); Mario Sorolla (Universidad Publica de Navarra, Spain);</i> .....</p> <p>An Inhomogeneous Model of Periodic Structures for Negative Index Material</p> <p><i>Ling Li Hou (Lanzhou University, China); Jessie Yao Chin (Southeast University, China); Qiang Cheng (Southeast University, China); Ruopeng Liu (Southeast University, China); Fu Yong Xu (Lanzhou University, China); Tie Jun Cui (Southeast University, China);</i> .....</p> <p>Development of Thin Soft Magnetic Amorphous Microwires for High Frequency Magnetic Sensors Applications</p> <p><i>Arcady P. Zhukov (Universidad del Pais Vasco, Spain); M. Ipatov (Universidad del Pais Vasco, Spain); C. García (Universidad del Pais Vasco, Spain); J. Gonzalez (Universidad del Pais Vasco, Spain); Larissa V. Panina (University of Plymouth, UK); J. M. Blanco (Universidad del Pais Vasco, Spain); V. Zhukova (Universidad del Pais Vasco, Spain);</i> .....</p> <p>Design of Metamaterial Based-on Ferromagnetic Substrate</p> <p><i>Boren Zheng (University of Electronic Science and Technology of China, China); Guangjun Wen (University of Electronic Science and Technology of China, China); Zhenghai Shao (University of Electronic Science and Technology of China, China); Yunjian Cao (University of Electronic Science and Technology of China, China); Kang Xie (University of Electronic Science and Technology of China, China);</i> .....</p> <p>Analysis of Varactor-tunable High-impedance Surfaces and Waveguides</p> <p><i>O. Luukkonen (TKK Helsinki University of Technology, Finland); C. R. Simovski (St. Petersburg Institute of Fine Mechanics and Optics, Russia); A. V. Räisänen (TKK Helsinki University of Technology, Finland); Sergei Tretyakov (Helsinki University of Technology, Finland);</i> .....</p> <p>A Novel Wideband Microstrip Patch Antenna with Left-handed Element and Enhanced Horizontal Radiation</p> <p><i>Ya-Nan Li (National University of Singapore, Singapore); Cheng-Wei Qiu (National University of Singapore, Singapore); Le-Wei Li (National University of Singapore, Singapore); Juan R. Mosig (Ecole Polytechnique Federale de Lausanne, Switzerland);</i> .....</p> <p>Left-handed Behavior of Ferrite Loaded Waveguide</p> <p><i>Kensuke Okubo (Okayama Prefectural University, Japan); Makoto Tsutsumi (Fukui University of Technology, Japan);</i> .....</p> <p>Transmission Properties of Omega Shaped Bianisotropic Metamaterial</p> <p><i>Koray Aydin (Bilkent University, Turkey); Zhaofeng Li (Bilkent University, Turkey); Serafettin Bilge (Bilkent University, Turkey); Ekmel Ozbay (Bilkent University, Turkey);</i> .....</p> <p>Lossless DNG-DPS Bilayer Structures for Tunneling and Zero Reflection</p> <p><i>Homayoon Oraizi (Iran University of Science and Technology, Iran); Majid Afsahi (Iran University of Science and Technology, Iran);</i> .....</p> <p>Periodic Ferrite-semiconductor Layered Composite with a Tunable Negative Index of Refraction</p> <p><i>Ai-Min Jiang (Nanjing University, China); Rui-Xin Wu (Nanjing University, China);</i> .....</p> <p>Studies of Pulse Propagation in Strongly Dispersive Media</p> <p><i>J. Qi (Helsinki University of Technology, Finland); Ari Henrik Sihvola (Helsinki University of Technology, Finland);</i> .....</p> <p>On the Study of Left-handed Coplanar Waveguide Coupler on Ferrite Substrate</p> <p><i>Mahmoud A. Abdalla (University of Manchester, UK); Zhirun Hu (University of Manchester, UK);</i> .....</p>	<p>458</p> <p>459</p> <p>460</p> <p>462</p> <p>463</p> <p>464</p> <p>465</p> <p>466</p> <p>467</p> <p>468</p> <p>470</p> <p>471</p> <p>472</p>
---	--

# Negative-index Materials Are Different from Left-handed Materials: Bi-isotropic Constitutive Relations Revisited

A. Sihvola

Electromagnetics Laboratory, Helsinki University of Technology  
P. O. Box 3000, FI-02015 TKK, Espoo, Finland

**Abstract**— This presentation focuses on two aspects of complex materials effects: the handedness character in chiral materials on one hand, and the negative-index effects on the other. Also more general bi-isotropic materials are connected to the discussion. The four complex material parameters in the bi-isotropic relations are restricted by physical principles. The presentation will look at these restrictions from the point of view of the metamaterials paradigm. Also complex materials terminology will be discussed.

**Introduction:** Within the metamaterials paradigm [1], the material parameters appearing in the constitutive relations are allowed to have a wider variation domain than in the earlier “strict electromagnetics”. At least research seems to be focused much more into such materials, like, for example, materials with negative permittivity and permeability, that are capable of producing new and counterintuitive phenomena and effects.

Bi-isotropic materials (media without any special direction in their structure but with magneto-electric effect) have their constitutive relations coupled [2]:

$$\mathbf{D} = \epsilon \cdot \mathbf{E} + \sqrt{\mu_0 \epsilon_0} \xi \cdot \mathbf{H} \quad (1)$$

$$\mathbf{B} = \sqrt{\mu_0 \epsilon_0} \zeta \cdot \mathbf{E} + \mu \cdot \mathbf{H} \quad (2)$$

between the electric  $\mathbf{E}$  and magnetic  $\mathbf{H}$  fields and electric  $\mathbf{D}$  and magnetic  $\mathbf{B}$  flux densities. The four material parameters  $\epsilon$ ,  $\mu$ ,  $\xi$ , and  $\zeta$  are dictated by the microstructure of the medium. The connection of the magnetoelectric parameters  $\xi$  and  $\zeta$  to the possibilities of negative refraction in at least one of the eigenwaves has been the object of certain research interest lately. This discussion is continued in the presentation with a revision of the characteristics of basic problems involving bi-isotropic media.

## REFERENCES

1. Sihvola, A., “Metamaterials in electromagnetics,” *Metamaterials*, Vol. 1, No. 1, 2–11, 2007.
2. Lindell, I. V., A. H. Sihvola, S. A. Tretyakov, and A. J. Viitanen, *Electromagnetic Waves in Chiral and Bi-isotropic Media*, 332, Artech House, Boston and London, 1994.

# Extraordinary Transmission through Periodically Perforated Screens from a Circuit Theory Perspective

Francisco Medina<sup>1</sup>, Francisco Mesa<sup>1</sup>, and Mario Sorolla<sup>2</sup>

<sup>1</sup>Microwaves Group, University of Seville, Seville, Spain

<sup>2</sup>Department of Electrical and Electronics Engineering, University of Navarra, Pamplona, Spain

**Abstract**— Extraordinary transmission of light through periodically perforated metal screens using subwavelength holes has attracted the attention of many researchers since the discovery of such phenomenon in 1998 [1]. Excitation of surface plasmons in the metal/air interface was first proposed as the explanation of this phenomenon [2]. However, it was soon recognized that if the holes are practiced in perfect conductors (metals at microwave frequencies are almost perfect conductors) extraordinary transmission is also present [3]. Indeed, enhanced transmission can be observed even if the perforated slab is a perfect dielectric [4]. Since perfect conductors and dielectric materials do support surface plasmons a different mechanism must be acting. Correlation of extraordinary transmission wavelengths with the period of the structure, rather than with the specific size or shape of the holes, clearly suggests that diffraction by a periodic grid is the key point. Dynamical diffraction theory has been then successfully applied to explain the extraordinary transmission peaks observed in the experiments [5, 6]. It can still be argued that surface plasmons are also supported by the periodically perforated screens itself even if metal is perfect (it has been well known for decades that periodically structured perfect conductor surfaces can support surface waves). However, this interpretation makes both points of view very close.

The purpose of this contribution is to review the problem from the point of view of classical theory of frequency selective surfaces (FSS). Practitioners of FSS know that total transmission through a perforated thin perfect metal layer is possible at the resonance frequency of the practiced holes. In this case the holes are not electrically small and this phenomenon can not be considered extraordinary transmission (as it has been done in some published works). Nevertheless a sharp transmission peak can also be observed when the holes are much smaller than the wavelength of the incident radiation. But this phenomenon also admits a relatively simple explanation in terms of circuit models usually employed in the frame of the analysis of FSS. For normal incidence, the problem posed by the FSS reduces to the analysis of scattering of a TEM mode supported by a rectangular cross section transmission line loaded with an iris practiced on a metal screen perpendicular to the wave propagation direction. This transmission line corresponds to each of the unit cells that can be identified in the infinite periodic problem. It will be shown that the reactive energy associated to the excitation of the first higher order mode near its cutoff frequency provides full explanation of the extraordinary transmission. Incidentally, the transmission zero known as Wood's anomaly, which is very close to the extraordinary transmission frequency, is also easily explained using this approach. Some details of the spectrum near the Wood's anomaly in the case of thick metal screens will also be explained using this simple transmission line model.

## REFERENCES

1. Ebbesen, T. W., H. J. Lezec, H. F. Ghaemi, T. Thio, and P. A. Wolff, "Extraordinary optical transmission through sub-wavelength hole arrays," *Nature*, Vol. 391, 667–669, 1998.
2. Martin-Moreno, L., F. J. Garcia-Vidal, H. J. Lezec, K. M. Pellerin, T. Thio, D. E. Grupp, J. B. Pendry, and T. W. Ebbesen, "Theory of extraordinary optical transmission through subwavelength hole arrays," *Phys. Rev. Lett.*, Vol. 86, 1114, 2001.
3. Beruete, M., M. Sorolla, I. Campillo, J. S. Dolado, L. Martin-Moreno, J. Bravo-Abad, and F. J. Garcia-Vidal, "Enhanced millimeter-wave transmission through subwavelength hole arrays," *Optics Lett.*, Vol. 29, 2500–2502, 2004.
4. Catrysse, P. B. and S. Fan, "Near-complete transmission through subwavelength hole arrays in phononpolaritonic thin films," *Phys. Rev. B*, Vol. 75, 075422, 2007.
5. Lezec, H. J. and T. Thio, "Diffracted evanescent wave model for enhanced and suppressed optical transmission through subwavelength hole arrays," *Optics Express*, Vol. 12, 3629–3651, 2004.
6. García-de-Abajo, F. J., R. Gómez-Medina, and J. J. Sáenz, "Full transmission through perfect-conductor subwavelength hole arrays," *Phys. Rev. E*, Vol. 72, 016608, 2005.

# An Inhomogeneous Model of Periodic Structures for Negative Index Material

Ling Li Hou<sup>1,2</sup>, Jessie Y. Chin<sup>2</sup>, Qiang Cheng<sup>2</sup>  
 Ruopeng Liu<sup>2</sup>, Fu Yong Xu<sup>1</sup>, and Tie Jun Cui<sup>2</sup>

<sup>1</sup>School of Information Science and Engineering, Lanzhou University, Lanzhou 730000, China

<sup>2</sup>State Key Laboratory of Millimeter Wave, School of Information Science and Engineering  
 Southeast University, Nanjing 210096, China

**Abstract**— S-parameter retrieval has proved to be an efficient approach to obtain electromagnetic parameters of negative index material(NIM) from reflection and transmission coefficients, where a slab of NIM with finite thickness is regarded as a homogeneous medium slab with the same thickness. Nevertheless, NIM structures composed of sub-wavelength unit cells are different from homogeneous materials and the published retrieval method is, under certain circumstances, not accurate enough. In this paper, we propose advanced parameter retrievals for NIM slabs using an inhomogeneous model. Due to the coupling effects of unit cells in a slab, the roles of edge and inner cells are different. Hence the equivalent medium parameters for edge and inner cells are different either, which results in the inhomogeneous property of the NIM slab. We propose the retrievals of medium parameters for edge and inner cells from S parameters by considering two-cell and three-cell NIM slabs, respectively. Then we set up an inhomogeneous three-layer model for arbitrary NIM slabs, which is much more accurate than the traditional homogeneous model. Numerical simulations verify the above conclusions.

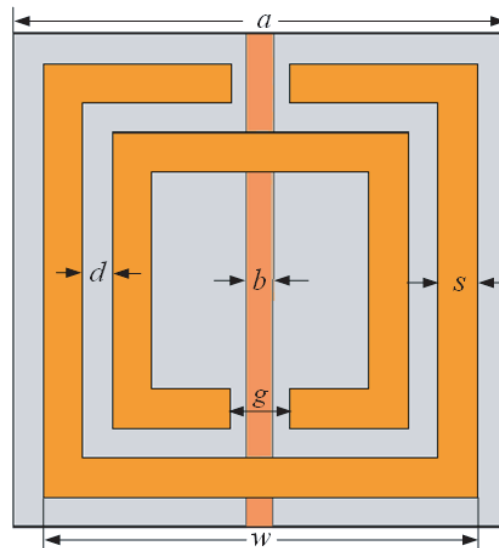


Figure 1: One unit cell NIM.

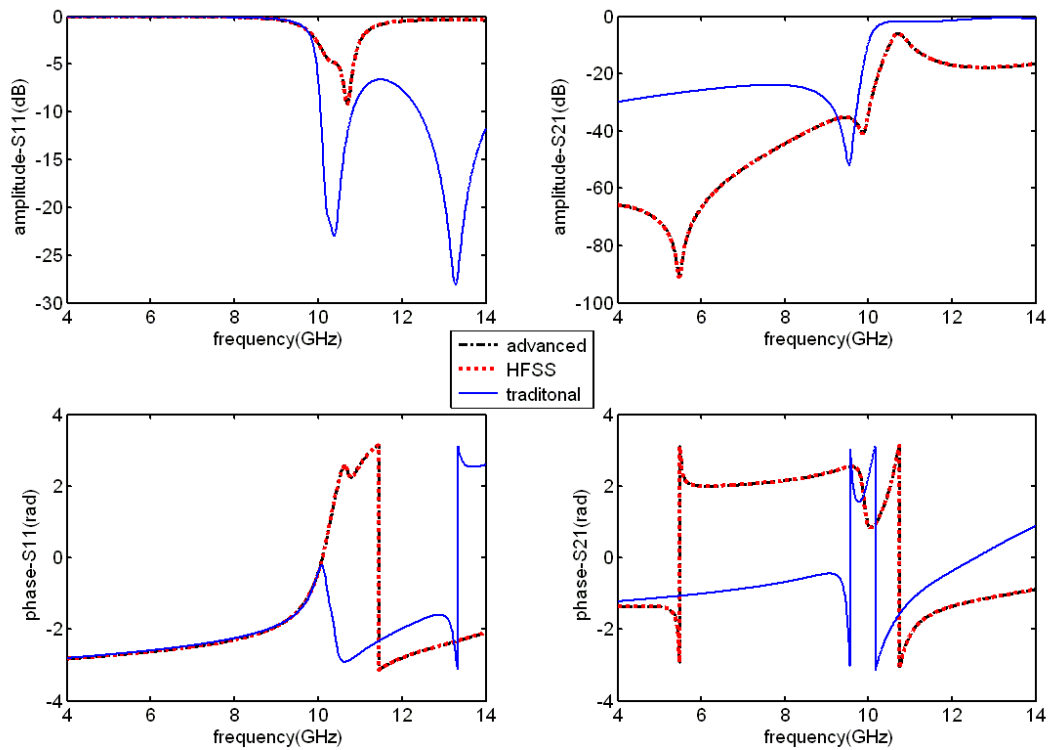


Figure 2: S-parameter of two units cell NIM.

#### REFERENCES

1. Pendry, J. B., A. J. Holden, D. J. Robbins, and W. J. Stewart, *IEEE Trans. Microwave Theory and Tech.*, Vol. 47, 2075, 1999.
2. Schurig, D., J. J. Mock, and D. R. Smith, *Appl. Phys. Lett.*, Vol. 88, 041109, 2006.
3. Liu, R., A. Degiron, J. J. Mock, and D. R. Smith, *Appl. Phys. Lett.*, Vol. 90, 263504, 2007.

## Development of Thin Soft Magnetic Amorphous Microwires for High Frequency Magnetic Sensors Applications

A. Zhukov<sup>1</sup>, M. Ipatov<sup>1</sup>, C. García<sup>1</sup>, J. Gonzalez<sup>1</sup>  
L. Panina<sup>1,2</sup>, J. M. Blanco<sup>3</sup>, and V. Zhukova<sup>3</sup>

<sup>1</sup>Dpto. de Física de Materiales, Fac. Químicas  
Universidad del País Vasco, San Sebastián 20009, Spain

<sup>2</sup>School of Computing, Communications and Electronics  
University of Plymouth, PL4 8AA, UK

<sup>3</sup>Dpto. de Física Aplicada, EUPDS  
Universidad del País Vasco, San Sebastián 20009, Spain

**Abstract**— Studies of thin magnetically soft amorphous microwires attract recently great attention owing to their excellent magnetic properties and extremely thin dimensions [1] allowing it use in miniaturized magnetic sensors and tuneable composite materials. Understanding of the mechanisms determining the magnetization process of these materials allows to tailor their magnetic softness and obtain improved high frequency stress sensitive giant magneto-impedance, GMI, effect [1]. GMI effect becomes a hot topic of applied magnetism owing to the large sensitivity (up to 600%) to the DC magnetic field, when the high-frequency current flows along the magnetic conductor [2]. Recently new types of stress-tuneable composite materials based on thin ferromagnetic wires with the effective microwave permittivity depending on an external dc magnetic field or tensile stress recently have been introduced [3].

In this paper we report novel results on hysteretic properties and GMI effect (diagonal and off-diagonal components) at high frequency region (between 10 MHz and 500 MHz) in thin amorphous microwires (Fe-rich, Co-rich and Co-Fe-rich with nearly-zero magnetostriction constant) with metallic diameter between 5 and 15  $\mu\text{m}$ . Control of the samples composition and geometry allows to tailor their magnetoelastic anisotropy and respectively magnetic softness and GMI.

On the other hand special thermal treatment allowing inducing the magnetic anisotropy by stress and/or magnetic field annealing allows to improve their magnetic softness and stress sensitivity.

Excellent magnetic softness, high GMI effect and linear and non-hysteretic off-diagonal MI curves has been obtained in Co-rich microwires with diameters between 6 and 12  $\mu\text{m}$ .

### REFERENCES

1. Zhukova, V., A. Chizhik, A. Zhukov, A. Torcunov, V. Larin, and J. Gonzalez, *IEEE Trans. Magn.* Vol. 38, No. 5, 3090, part I, 2002.
2. Panina, L. V. and K. Mohri, *Appl. Phys. Lett.*, Vol. 65, 1189, 1994.
3. Panina, L. V., S. I. Sandacci, and D. P. Makhnovskiy, *J. Appl. Phys.*, Vol. 97, 13701, 2005.

## Design of Metamaterial Based-on Ferromagnetic Substrate

Boren Zheng<sup>1,2</sup>, Guangjun Wen<sup>1</sup>, Zhenghai Shao<sup>1</sup>, Yunjian Cao<sup>1</sup>, and Kang Xie<sup>1</sup>

<sup>1</sup>Key Laboratory of Broadband Optical Fiber Transmission & Communication Networks  
University of Electronic Science and Technology of China, Chengdu 610054, China

<sup>2</sup>School of Computer and Information, Chongqing Jiaotong University, Chongqing 400074, China

**Abstract**— In this paper, a metamaterial operating in the x-band has been designed by use of a ferromagnetic substrate embedded with a array of metal wire or strip. The transmission and reflection characteristics of EM wave in the designed metamaterial and at the interface between metamaterial and positive refraction index material was simulated by HFSS EDA tools, the effective permittivity, effective permeability and refraction index of the composite substance were extracted out by the transfer matrix method. The simulation result shown that the effective refraction index of the composite substance are negative in the frequency range from 8.5 GHz to 10.7 GHz. The refraction feature of EM wave passing through a prism made of the designed metamaterial has been simulated too, and negative refraction phenomena at the interface between metamaterial and positive refraction index material were observed in the above frequency range. The results demonstrated the method to synthese metamaterial based on ferromagnetic substrate embedded with a array of metal wire or strip is viable.

### ACKNOWLEDGMENT

Projects 60571024, 60771046 and 60588502 supported by National Natural Science Foundation of China.

# Analysis of Varactor-tunable High-impedance Surfaces and Waveguides

O. Luukkonen<sup>1</sup>, C. Simovski<sup>2</sup>, A. V. Räsänen<sup>1</sup>, and S. A. Tretyakov<sup>1</sup>

<sup>1</sup>Radio Laboratory/SMARAD, TKK Helsinki University of Technology  
P. O. 3000, FI-02015 TKK, Finland

<sup>2</sup>Department of Physics, St. Petersburg Institute of Fine Mechanics and Optics  
197101, Sablinskaya 14, St. Petersburg, Russia

**Abstract**— Artificial impedance surfaces offer exotic properties that can be utilized in antenna designs, absorbers, and waveguides. These surfaces have been commonly composed of a capacitive grid over a metal-backed dielectric slab. The grid can be comprised of capacitive strips, array of patches, or even inductive strips with lumped capacitive loads. The capacitive response of the grid together with the inductive response of the metal-backed dielectric slab form a resonant structure, and near the resonance frequency of the surface the (input) surface impedance of this type of a structure reaches very high values. This type of surfaces are therefore commonly referred to as *high-impedance surfaces*. The frequency band of the applications of these high-impedance surfaces range typically from the microwave region to the lower millimeter wave region.

In waveguides the artificial impedance surfaces have been used to create quasi-TEM waveguides [1], analog phase shifters [2], and tunable lenses capable of beam scanning [3]. In [2] and [3] the tunability in the applications is realized by using electrically tunable high-impedance surfaces. Commonly the tuning of the impedance surfaces has been realized by varying the capacitive response of the grid. When designing analytically an application that utilizes high-impedance surfaces it is necessary to model the response of the surfaces accurately even for oblique angles of incidence. In addition to this, the capacitive tuning of the surface needs to be taken into account correctly. In this presentation a simple and accurate model for a high-impedance surface structure is presented. Furthermore, we include the effect of electrically controllable lumped capacitors to the analysis.

We will further use the present model to study modes in a waveguide that has high-impedance surfaces as sidewalls. The results of modes in the parallel-plate waveguide with tunable impedance surface sidewalls will be presented. The results will be compared to those in [4], and, in addition, “mode-switching” between the metallic waveguide modes in the vicinity of the resonance frequency of high-impedance surfaces will be shown. The analytical results are verified with full-wave simulations.

## REFERENCES

1. Yang, F.-R., K.-P. Ma, Y. Qian, and T. Itoh, “A novel TEM waveguide using uniplanar compact photonic-bandgap (UC-PBG) structure,” *IEEE Transactions on Microwave Theory and Techniques*, Vol. 47, No. 11, 2092–2098, 1999.
2. Higgins, J. A., M. Kim, J. B. Hacker, and D. Sievenpiper, “The application of photonic crystals to quasi-optic amplifier,” *IEEE Transactions on Microwave Theory and Techniques*, Vol. 47, No. 11, 2139–2143, 1999.
3. Xin, H., J. B. West, J. C. Mather, J. P. Doane, J. A. Higgins, H. Kazemi, and M. J. Rosker, “A two-dimensional millimeter wave phase scanned lens utilizing analog electromagnetic crystal (EMXT) waveguide phase shifters,” *IEEE Transactions on Antennas and Propagation*, Vol. 53, No. 1, 151–159, 2005.
4. Kehn, M. N. M., M. Nannetti, A. Cucini, S. Maci, and P.-S. Kildal, “Analysis of dispersion in dipole-FSS loaded hard rectangular waveguide,” *IEEE Transactions on Antennas and Propagation*, Vol. 54, No. 8, 2275–2282, 2006.



# A Novel Wideband Microstrip Patch Antenna with Left-handed Element and Enhanced Horizontal Radiation

Ya-Nan Li<sup>1</sup>, Cheng-Wei Qiu<sup>1</sup>, Le-Wei Li<sup>1,2</sup>, and Juan R. Mosig<sup>2</sup>

<sup>1</sup>ECE Department, National University of Singapore, Singapore

<sup>2</sup>Swiss Federal Institute of Technology, Lausanne, Switzerland

**Abstract**— Microstrip patch antennas usually have the strongest radiation in the vertical direction (while the patch is placed horizontally). At the mean time, the radiation along the plane of patch usually causes unwanted radiated power and thus causes coupling among array elements so as to reduce the efficiency. Dielectric polarization currents are confirmed as physical sources of this unwanted radiation. Several techniques were proposed to compensate these currents and suppress radiation in horizontal directions. In practical applications, it is, however, desirable to have the radiation along the horizontal plane to be enhanced by taking advantages of the horizontal radiation and suppressing the vertical radiation. Of course, difficulty exists because the horizontal radiation is much lower than the vertical radiation if antennas are printed on substrates with low-permittivity (like foam) or placed in the air.

In this paper, we present a novel microstrip antenna with planar left-handed material structure patterns. It is developed, based on a conventional patch antenna, where isolated triangle gaps and crossed strip-line gaps are etched on the metal patch and ground plane, respectively. This pattern was proven in literature to have left-handed characteristics. In this way, the wave propagating along the patch is strongly enhanced, and the working band is significantly broadened from a few hundred MHz to a few GHz. FDTD-based simulation results show that most energy is radiated in horizontal direction during the whole working band, while the vertical radiation being suppressed. Also, this new patch antenna has very high efficiency, very low loss and low VSWR. Finally, practical experiments demonstrate a good agreement between the simulation and measured results.

## ACKNOWLEDGMENT

This work has been supported in part by the US Air Force Office for Scientific Research via a grant FA4869-07-1-4024 (AOARD/AFOSR Project: AOARD-07-4024), an ARC grant from Ministry of Education, Singapore, and Swiss Federal Institute of Technology, Lausanne, Switzerland. Helpful discussion with Dr. Hai-Ying Yao in Temasek Labs at the National University of Singapore is grateful.

# Left-handed Behavior of Ferrite Loaded Waveguide

Kensuke Okubo<sup>1</sup> and Makoto Tsutsumi<sup>2</sup>

<sup>1</sup>Okayama Prefectural University, Japan

<sup>2</sup>Fukui University of Technology, Japan

**Abstract**— Studies on left-handed transmission lines are very active subject in recent years. One of them is a periodic structure of ferrite and dielectric slab in the rectangular metal waveguide under cutoff which shows new propagation effect through LH behavior [1]. This paper proposes non periodical ferrite waveguide magnetized transversely and longitudinally to the wave propagation together with experiments.

A ferrite slab of thickness  $d$  magnetized transversely to wave propagation is located into the center of a rectangular waveguide of width of  $w$  below cutoff in which a surface mode can propagate. If ratio of  $w$  to  $d$  is three, typical negative group velocity characteristics appears due to LH operation. This was explained with magnetostatic surface wave mode influenced by metal plate [2, 3]. A ferrite slab magnetized longitudinally to wave propagation is completely filled into rectangular waveguide of small cross section, in which a volume mode can propagate. A new ferrite waveguide mode with negative group velocity characteristics was numerically confirmed with a help of HFSS technique. And electromagnetic field theory in approximate form.

Experiments were carried out using  $1 \times 5 \times 10 \text{ mm}^3$  single crystal of YIG slab. Surface mode was excited at  $S$  band, and compared with scattering parameters of surface mode calculated numerically by HFSS. Typical tunable filter characteristics of surface mode was observed. Experiment on volume mode longitudinally magnetized ferrite slab was also undertaken using  $2 \times 5 \times 10 \text{ mm}^3$  single crystal of YIG slab and a result is shown in figure. LH volume ferrite mode can be seen in the figure along with magnetostatic backward volume wave (MSBVW) mode, and it was good agreement with numerical result of HFSS.

As a conclusion if their LH ferrite waveguide structure are arranged in two dimension, ferrite lens may be realized with small size at  $X$  band which focusing phenomenon of microwave can be controlled by the magnetic field.

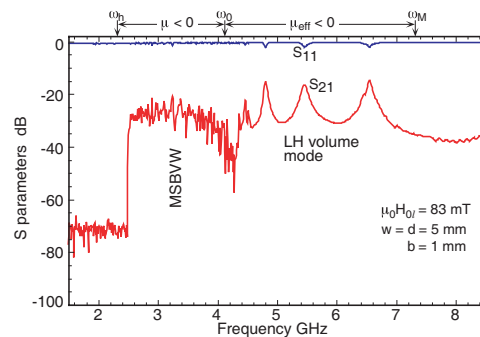


Figure 1: Experiment on frequency response of LH ferrite mode along with magnetostatic backward volume mode.

## REFERENCES

1. Ueda, T. and M. Tsutsumi, *IEEE Trans. Magn.*, Vol. 41, No. 10, 3532–3527, Oct. 2005.
2. Van, de Vart, *Electronics Letters*, Vol. 6, No. 19, 601–602, Sept. 1970.
3. Okubo, K. and M. Tsutsumi, *Intermag Dig.*, EU-01, 2006.

# Transmission Properties of Omega Shaped Bianisotropic Metamaterial

Koray Aydin, Zhaofeng Li, Serafettin Bilge, and Ekmel Ozbay

Nanotechnology Research Center

Department of Physics and Department of Electrical and Electronics Engineering

Bilkent University, Bilkent, 06800 Ankara, Turkey

**Abstract**— Omega structures are composite electromagnetic materials with a proper combination of  $\Omega$ -shaped metallic inclusions in a host dielectric medium. These metamaterials could be regarded as bianisotropic or pseudo-chiral media. Electric and magnetic polarizations are induced by both electric and magnetic fields in bianisotropic media. In this study, we report the transmission properties of omega shaped metallic inclusions on a dielectric medium that exhibits bianisotropic properties. The resonance frequencies of single omega resonators are investigated experimentally and numerically. The resonance frequency of a  $\Omega$  structure depends on its orientation with respect to the incident electric field. Increasing the tail length of the  $\Omega$  resonator causes a decrease in resonance frequency. Band gaps due to the magnetoelectric resonances are observed for various types of periodic omega arrays. A transmission band is observed when a periodic  $\Omega$  media is combined with a negative permittivity media of periodic thin wires. The transmission band appears below the band gap of periodic omega media, in turn indicating a right-handed behavior. Dual transmission band is obtained by composing two different types of metamaterials that are arranged periodically [1].

## REFERENCES

1. Aydin, K., Z. Li, and E. Ozbay, *New J. Phys.*, to be published.

# Lossless DNG-DPS Bilayer Structures for Tunneling and Zero Reflection

Homayoon Oraizi and Majid Afsahi

Iran University of Science and Technology, Narmak, Tehran 16846-13114, Iran

**Abstract**— Distribution of the electromagnetic field and power flux inside and outside of a lossless DNG-DPS bilayer structure are investigated by the Transmission Line Transfer Matrix Method (TLTMM) and appropriate conditions are determined that under which complete wave tunneling occurs with no reflection at any angle of incidence and at all frequencies.

**Introduction:** By an iterative method [1] and by a full wave analysis method [2], it just mentioned without details that under appropriate conditions the reflection from a lossless DNG-DPS bilayer structure becomes zero. Also, field and power flux distribution is determined inside and outside of a lossless MNG-ENG bilayer by a full wave method [2].

In this paper, which is complementary to [1, 2], field and power flux distribution is determined inside and outside of a DNG-DPS bilayer under TM plane wave incidence by the TLTMM method [3, 4].

**Problem Formulation:** Consider a lossless DNG-DPS bilayer, with thicknesses  $d_1$  and  $d_2$ . A TM plane wave is incident on it at an arbitrary angle of incidence in the y-z plane as shown in Fig. 1. It is necessary to select the correct sign for the characteristic impedances and propagation constants in metamaterials [5]. The necessary and sufficient conditions for tunneling may be obtained from the equivalent transmission lines as

$$\begin{aligned} Z_1 &= Z_2, \\ \beta_1 d_1 &= -\beta_2 d_2 \end{aligned} \quad (1)$$

$$\theta_{r=0} = \arcsin \sqrt{\frac{\varepsilon_1 \varepsilon_2 (\varepsilon_2 \mu_1 - \varepsilon_1 \mu_2)}{\mu_0 \varepsilon_0 (\varepsilon_2^2 - \varepsilon_1^2)}} \quad (2)$$

The DNG-DPS bilayer may be designed by the TM Brewster angle of no reflection.

**Example:** As an example, the reflection coefficient of a DNG-DPS layer is drawn in Fig. 2 for the Brewster angle of  $\theta_{r=0} = 45^\circ$  and the set of parameters shown in the figure. It is seen that the reflection coefficient becomes zero at any angle of incidence for the case  $\varepsilon_2 = -\varepsilon_1$ ,  $\mu_2 = -\mu_1$ ,  $d_2 = d_1$ . It is observed that the reflection coefficient becomes zero at any frequency, under such conditions. The field and power flux of this structure are drawn versus distance in Fig. 3 for the TM incident wave at the angle of incidence  $\theta_{r=0} = 45^\circ$ .

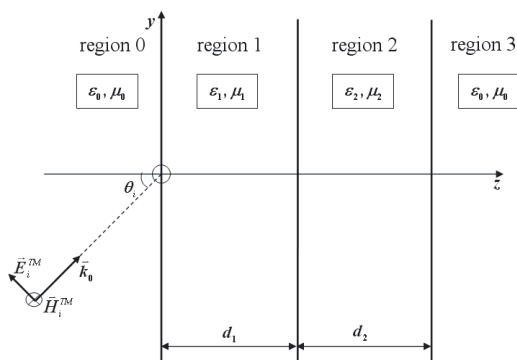


Figure 1: A DNG-DPS bilayer under oblique incidence of a TM plane wave.

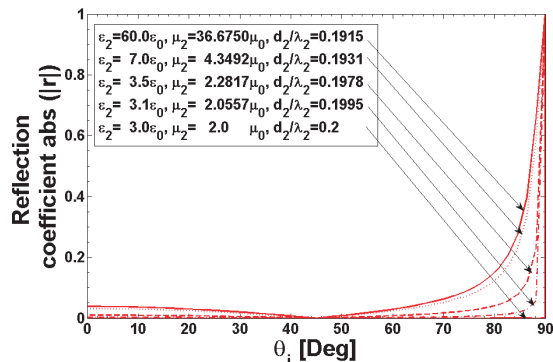


Figure 2: Variation of reflection coefficient versus incidence angle of a TM plane wave. The design is for Brewster angle of  $45^\circ$  at frequency  $f_0$ . The DNG parameters are  $\varepsilon_1 = -3\varepsilon_0$ ,  $\mu_1 = -2\mu_0$ ,  $d_1/\lambda_1 = 0.2$  and those of DPS are shown in the caption.

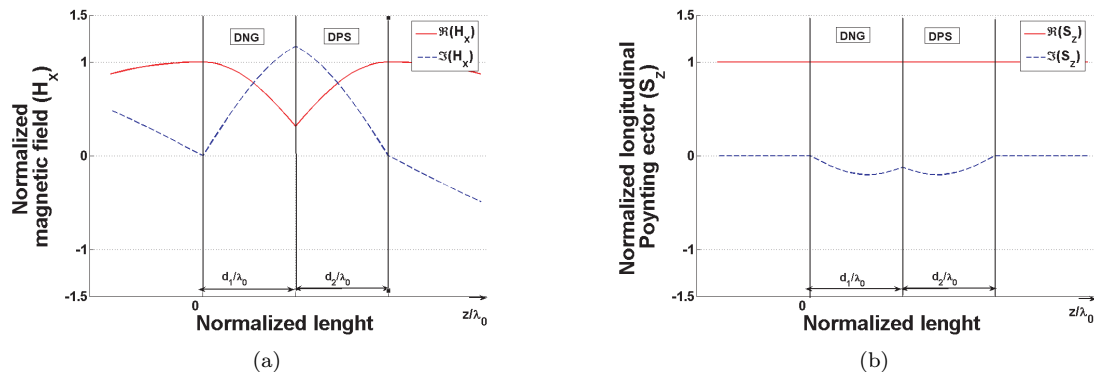


Figure 3: Field and power flux variation versus distance in the layers. The angle of incidence of TM plane wave is  $45^\circ$  and the parameters are  $\varepsilon_2 = -\varepsilon_1 = 3\varepsilon_0$ ,  $\mu_2 = -\mu_1 = 2\mu_0$ ,  $d_2/\lambda_2 = d_1/\lambda_1 = 0.2$ ,  $r = 0$ ,  $t = 1$ . (a) Normalized magnetic field; (b) Normalized Poynting's vector.

#### ACKNOWLEDGMENT

This research was in part supported by Iran Telecommunication Research Center under contract number 500/1911 dated 2007/5/8.

#### REFERENCES

1. Cory, H. and C. Zach, "Wave propagation in metamaterial multi-layered structures," *Microwave and Optical Technology Letters*, Vol. 40, No. 6, 460–465, Mar. 2004.
2. Alù, A. and N. Engheta, "Pairing an epsilon-negative slab with a mu-negative slab: resonance, tunneling and transparency," *IEEE Trans. on Antennas and Propagation*, Vol. 51, No. 10, 2558–2571, Oct. 2003.
3. Oraizi, H. and M. Afsahi, "Analysis of planar dielectric multilayers as FSS by transmission line transfer matrix method (TLTMM)," *Progress In Electromagnetics Research*, PIER 74, 217–240, 2007.
4. Oraizi, H. and M. Afsahi, "Application of transmission line transfer matrix method (TLTMM) for the analysis of wave propagation in metamaterial multilayer mtructures as FSS," under submission.
5. Oraizi, H. and M. Afsahi, "Determination of correct values for propagation constant, intrinsic impedance and refraction index of metamaterials," under submission.

# Periodic Ferrite-semiconductor Layered Composite with a Tunable Negative Index of Refraction

**Ai-min Jiang and Rui-xin Wu**

Department of Electronic Sciences and Engineering  
Nanjing University, Nanjing 210093, China

**Abstract**— We have studied the index of refraction of layered ferrite-semiconductor composite. We found that the composite could have negative index of refraction with applied magnetic fields. We studied the relationship between the index of refraction and the parameters of the materials, and found not only the permeability and the permittivity but also the thickness ratio of the ferrite and the semiconductor influences the existence of the negative index. At long wave limitation, we derived the effective index of refraction of the composite, which indicate the size unit cell could be much smaller than the working wavelength.

The studied shows the negative index of the composite is basically based on the negative permeability of the ferrite, which is tunable with applied magnetic field. Therefore, the negative index of the composite can be tuned. The effect of magnetic parameters of the ferrite, such as magnetic damping, on the index have been studied Full-wave simulations of the YIG-semiconductor layered composite has been done and the results confirm the theoretical studies. It is demonstrated that the index of the composite can be easily changed by external magnetic field when the structure is fixed, which has some applications such as beam scanning for example.

## Studies of Pulse Propagation in Strongly Dispersive Media

J. Qi and A. Sihvola

Electromagnetics Laboratory, Helsinki University of Technology  
P. O. Box 3000, FI-02015 TKK, Espoo, Finland

**Abstract**— Along with the present interest in metamaterials [1], the question about physical limitations of the values of permittivity are relevant. The allowed ranges for negative permittivities are always band-limited and causality principles set restrictions to the global behavior of the permittivity function. Losses and refractive spectra are connected. In this presentation, strongly dispersive Lorentz media are considered. Pulses with different temporal variations are propagated through such medium and characteristic changes in the parameters of the pulse are studied and classified.

### REFERENCES

1. Sihvola, A., “Metamaterials in electromagnetics,” *Metamaterials*, Vol. 1, No. 1, 2–11, 2007.

## On the Study of Left-handed Coplanar Waveguide Coupler on Ferrite Substrate

M. A. Abdalla and Z. Hu

MACS Group, School of EEE, University of Manchester  
P. O. Box 88, Manchester M60 1QD, UK

**Abstract**— Recently, there has been a great interest in using left handed materials (LHMs) i.e., both permittivity and permeability are negative, for RF/microwave circuit applications. The LHMs have been realized in different planar configurations. Recently, left-handed (LH) coplanar waveguides (CPW) for RF/microwave applications have been proposed and demonstrated experimentally, where different types of loading series capacitors and parallel inductors have been analyzed.

Ferrite medium substrate has tunable dispersive properties depending on the direction and value of the applied magnetic bias to the ferrite substrate. Therefore, a tunable LH transmission line (TL) is expected on ferrite substrates which has been recently, demonstrated in different planar configurations.

Microwave coupler is one of the desirable devices in microwave applications. The different types of conventional microwave couplers have a trade off between bandwidth, coupling level, and structure implementation constraints. The conventional quarter wave coupled line coupler has broad bandwidth which is typically more than 25%. But, it has two disadvantages. First, it has the difficulties of not 3-dB backward wave coupling level as that requires very small spacing between the two lines (typically less than 10 dB). Second, the forward coupling level increases with increasing either physical or electrical length of the TL.

The novel properties of the LH TL can lead to novel performance of LH coupled line coupler. The LH coupler can provide arbitrary high coupling level, even 0 dB, over a broad bandwidth (more than 35%) with relatively wide lines separation. Also, it has high forward coupling at lower frequency without the need to increase the physical length. Recently, dielectric LH coupled line couplers were introduced mainly in microstrip configuration.

In this paper we will present a uniplanar LH CPW coupled line coupler on ferrite substrate. An external DC magnetic field is applied horizontally to the ferrite substrate which causes it to have the saturation magnetization in the same direction. The proposed coupler consists of two parallel LH TLs, instead of the conventional (right-handed) RH TLs, in a symmetric configuration. The individual LH CPW TLs were designed using planar segment wires as shunt inductors and interdigital capacitors as series capacitors.

The proposed structure is analyzed using full wave numerical simulation and the equivalent analytical circuit of the structure is presented.

The proposed coupler has the advantages of its compact size and high coupling level. Also, it has the capability of being tunable and nonreciprocal due to the effect of the ferrite substrate. Moreover, in comparison with ferrite microstrip configuration, the ferrite CPW one requires lower dc magnetic bias since it has much smaller demagnetization factor.



# Session 2P4

## Electromagnetic Field in Optical Materials and Dispersion Engineering of Photonic Crystals

<a href="#">One-dimensional Arrays of Ultra-small Josephson Junctions under Microwave Irradiation</a>	
<i>Watson Kuo (National Chung Hsing University, Taiwan); Saxon Liou (National Chung Hsing University, Taiwan); Y. W. Suen (National Chung Hsing University, Taiwan); C. D. Chen (Institute of Physics, Academia Sinica, Taiwan);</i>	474
<a href="#">The Effect of Cooling Systems on HTS Microstrip Antennas</a>	
<i>Shu-Fang Liu (Xidian University, China); Shao-Dong Liu (Xi'an Institute of Space Radio Technology, China);</i>	475
<a href="#">GL Time Domain Modeling for EM Acoustic and Elastic Wave Field with Dispersion in Crystal and Porous Material</a>	
<i>Jianhua Li (GL Geophysical Laboratory, USA); Ganquan Xie (GL Geophysical Laboratory, USA); Lee Xie (GL Geophysical Laboratory, USA); Feng Xie (GL Geophysical Laboratory, USA);</i>	476
<a href="#">A Novel Decoupled Scheme of the Potential-based Finite Element Method for 3-D Transient Eddy-current Problems</a>	
<i>Tong Kang (Communication University of China, China); Kwang Ik Kim (Pohang University of Science and Technology, Republic of Korea);</i>	477
<a href="#">Influence of Electric-field on Conductivity Properties of Proton Transfer in Hydrogen-bonded Systems</a>	
<i>Xiao-Feng Pang (University of Electronic Science and Technology of China, China);</i>	478
<a href="#">Optical Properties of a Superconducting Distributed Bragg Reflector</a>	
<i>Chien-Jang Wu (National University of Kaohsiung, Taiwan);</i>	479
<a href="#">Fabrication of Polymer Bragg Grating Waveguide Devices Using MEMS Technology</a>	
<i>Kun-Yi Lee (China Institute of Technology, Taiwan); Wei-Ching Chuang (National Formosa University, Taiwan); Yen-Juei Lin (China Institute of Technology, Taiwan); Wei-Yu Lee (China Institute of Technology, Taiwan);</i>	480
<a href="#">Optical Dispersion of Indefinite Media Based on a Special Physical Model</a>	
<i>Linfang Shen (Zhejiang University, China); Tzong-Jer Yang (Chung-Hua University, Taiwan); Yuan-Fong Chau (Chin Yuan University, Taiwan);</i>	481
<a href="#">High-sensitivity Nuclear Magnetic Resonance Spectrometer for Hyperpolarized <sup>3</sup>He and Water by Using High-T<sub>c</sub> Superconducting Quantum Interference Devices</a>	
<i>Hong-Chang Yang (National Taiwan University, Taiwan); Shu-Hsien Liao (National Taiwan Normal University, Taiwan); Heng-Er Horng (National Taiwan Normal University, Taiwan); S. Y. Yang (National Taiwan Normal University, Taiwan);</i>	482
<a href="#">Frequency-dependent Negative Refraction of Photonic Crystals: Experimental Observations on Super-prisming and Super-chromatic-aberration Effects</a>	
<i>Shieh-Yueh Yang (National Taiwan Normal University, Taiwan); J. Y. Wu (National Taiwan Normal University, Taiwan); H. E. Horng (National Taiwan Normal University, Taiwan); Chin-Yih Hong (Nan-Kai Institute of Technology, Taiwan); H. C. Yang (National Taiwan University, Taiwan);</i>	483
<a href="#">AGILD EM Dispersion Modeling For Photonic Crystals</a>	
<i>Ganquan Xie (GL Geophysical Laboratory, USA); Tong Kang (Communication University of China, China); Jianhua Li (GL Geophysical Laboratory, USA);</i>	484
<a href="#">Fast and Accurate Full-model Simulation Algorithm for the Analysis of Frequency Selective Surfaces and Periodic Structures</a>	
<i>Heng-Tung Hsu (Yuan Ze University, Taiwan);</i>	485
<a href="#">Design and Implementation of Novel Switching-mode Output Driver with Off-chip Transmission Speed up to 640 Mb/s</a>	
<i>Heng-Shou Hsu (Feng-Chia University, Taiwan);</i>	486

# One-dimensional Arrays of Ultra-small Josephson Junctions under Microwave Irradiation

Watson Kuo<sup>1</sup>, Saxon Liou<sup>1</sup>, Y. W. Suen<sup>1</sup>, and C. D. Chen<sup>2</sup>

<sup>1</sup>Department of Physics, National Chung Hsing University, Taichung 402, Taiwan

<sup>2</sup>Institute of Physics, Academia Sinica, Nankang, Taipei 105, Taiwan

**Abstract**— The zero-bias resistance of one-dimensional arrays of Josephson junctions irradiated with microwaves is studied [1]. The measured arrays are composed of aluminum islands, having two sub-microm sized junctions connected in parallel to their neighbors to form superconducting quantum interference devices (SQUIDs) [2]. The junction can be tuned from over-damped to under-damped because the Josephson coupling energy can be tuned using a small magnetic field perpendicular to the SQUID loops. In the over-damped regime, the zero-bias resistance oscillates as the irradiating microwave amplitude increases. In the under-damped regime, the zero-bias resistance monotonically decreases as the microwave amplitude increases. The experimental data is analyzed with an ac-current bias single Josephson junction model.

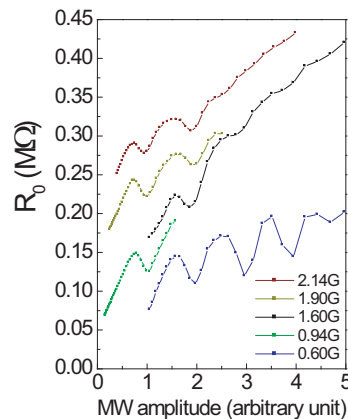


Figure 1: The zero-bias resistance,  $R_0$  as a function of rescaled microwave amplitude when the Josephson coupling energy is tuned maximal shows an oscillatory behavior at various microwave frequencies. Due to different coupling strength, the scaling parameters for each frequency are different. Notice that  $R_0$  are shifted for clarity.

## REFERENCES

1. Liou, S., W. Kuo, Y. W. Suen, W. H. Hsieh, C. S. Wu, and C. D. Chen, "Shapiro steps observed in a superconducting single electron transistor," *Chin. J. Phys.*, Vol. 45, No. 2-II, 230–236, 2007.
2. Kuo, W. and C. D. Chen, "Scaling analysis of magnetic-field-tuned phase transitions in one-dimensional Josephson junction arrays," *Phys. Rev. Lett.*, Vol. 87, No. 18, 186804, 2001.

# The Effect of Cooling Systems on HTS Microstrip Antennas

S. F. Liu<sup>1</sup> and S. D. Liu<sup>2</sup>

<sup>1</sup>Xidian University, Xi'an 710071, China

<sup>2</sup>Xi'an Institute of Space Radio Technology, Xi'an 710000, China

**Abstract**— HTS antennas must work at a temperature below the critical temperature of the HTS material, so a cooling system is needed and the antenna should be placed in it. Would the cooling system influence the properties of the HTS antenna? And if any, how does it? To answer these questions, some studies are made.

A cryocooler, which consists of a compressor, a cold head, a vacuum chamber and other related parts, is often used to cool HTS antennas because of its easy handling and convenience compared with liquid  $N_2$ . Among all these parts, the vacuum chamber influences the properties of HTS antenna most, so a 3-D model is constructed to simulate it. In the 3-D model, a cylindrical cavity of perfect conductor is used to model the cylindrical stainless jacket of the vacuum chamber as well as the stainless flange at the bottom. The dielectric window of vacuum chamber is assumed as a circle dielectric plate with a certain thickness, which has the same radius as that of the cylinder and serves as a cover of the cylindrical cavity. The height and radius of the cylinder is denoted as  $H$  and  $R$  respectively, and the distance between the antenna and the underside of the dielectric plate is denoted as  $d$ . With variations of the configuration parameters, simulations are done for a rectangular HTS patch antenna placed inside the cavity. The results show that when the vacuum chamber has an appropriate dimension the antenna can obtain a remarkably enhanced gain.

# GL Time Domain Modeling for EM Acoustic and Elastic Wave Field with Dispersion in Crystal and Porous Material

Jianhua Li, Ganquan Xie, Lee Xie, and Feng Xie  
GL Geophysical Laboratory, USA

**Abstract**— The magnetic field and electric field differential integral equation were proposed by authors in 1995 in which the Green's kernel is integrative. In this paper, we propose a new EM time domain GL modeling directly based on the magnetic field, and electric field differential integral equation in the time domain. We derive the new magnetic field and electric field differential integral equation in the time domain. Based on these time domain magnetic and electric differential integral equations, we construct magnetic and electric field time domain GL modeling. Similarly, we derive a mechanical time domain differential integral equation and propose a new mechanical time domain GL modeling. The EM field and mechanical field is different field in physical theory and application. However, the EM and mechanical field have some relationship in the mathematical physical research topics. In the macro scope and macro to micro mixed scope the coupled EM and mechanical field play important role. The EM founder Maxwell was an elastic mechanical researcher and then he moved to EM research field. Our GL method can be used for EM, mechanic, acoustic, flow, quantum mechanics and their mixed coupled field modeling. The time domain GL method does not need to solve any large matrix, only  $3 \times 3$  and  $6 \times 6$  matrices are needed to solve in the time domain Magnetic, electric and mechanical GL modeling respectively. Moreover, the artificial boundary and absorption condition are unnecessary in the time domain GL method. Some applications in material science and exploration are described in this paper.

## REFERENCES

1. Xie, G., F. Xie, L. Xie, and J. Li, "New GL method and its advantages for resolving historical difficulties," *Progress In Electromagnetics Research*, Vol. PIER 63, 141–152, 2006.
2. Xie, G., J. Li, L. Xie, and F. Xie, "GL metro carlo EM inversion," *Journal of Electromagnetic Waves and Applications*, Vol. 20, No. 14, 1991–2000, 2006.
3. Li, J., G. Xie, L. Xie, and F. Xie, "A 3D GL EM modeling and inversion for forest exploration and felling," *PIERS Online*, Vol. 3, No. 4, 402–410, 2007.
4. Xie, G., J. Li, F. Xie, and L. Xie, "3D GL EM and quantum mechanical coupled modeling for the nanometer materials," *PIERS Online*, Vol. 3, No. 4, 418–422, 2007.
5. Xie, G., J. Li, L. Xie, F. Xie, and J. Li, "The 3D GL EM-flow-heat-stress coupled modeling," *PIERS Online*, Vol. 3, No. 4, 411–417, 2007.
6. Xie, G., "A new iterative method for solving the coefficient inverse problem of wave equation," *Comm. on Pure and Applied Math.*, Vol. 39, 307–322, 1986.
7. Xie, G. and J. Li, "Nonlinear integral equation of coefficient inversion of acoustic wave equation and TCCR iteration," *Science in China*, Vol. 32, No. 5, 513–523, 1989.
8. Xie, G. and J. Li, "New iterative method for solving scattering problem of 3-D wave equation," *Science in China*, Vol. 31, No. 10, 1195–1202, 1988.

# A Novel Decoupled Scheme of the Potential-based Finite Element Method for 3-D Transient Eddy-current Problems

Tong Kang<sup>1</sup> and Kwang Ik Kim<sup>2</sup>

<sup>1</sup>Department of Applied Mathematics, School of Sciences  
Communication University of China, Beijing 100024, China

<sup>2</sup>Department of Mathematics, Pohang University of Science and Technology  
Pohang 790-784, Republic of Korea

**Abstract**— In this paper, we investigate the potential-based finite element method (the  $A-\phi$  method) for 3-D eddy-current problems. In our models, the source coil carries a pulse excitation current instead of a time harmonic current, which produces transient physical fields. As distinguished from the traditional coupled scheme which needs to solve an equation system including both vector and scalar unknowns at every time-step after time discretization, a novel decoupled scheme is presented here. Because the vector and scalar unknowns are calculated in two different equation systems respectively, it decreases the total CPU time and the storage amount of non-zero entries of coefficient matrix. Hence, it spends less costs of computation. Some computer simulation results of the magnetic flux and eddy-current densities for two 3-D eddy-current models (IEEJ model and TEAM Workshop Problem 7) are demonstrated to verify the feasibility and efficiency of our algorithm.

## Influence of Electric-field on Conductivity Properties of Proton Transfer in Hydrogen-bonded Systems

Xiao-Feng Pang

Institute of Life Science and Technology, University of Electronic Science and Technology of China  
Chengdu 610065, China

**Abstract**— We study and calculate the mobility and conductivity of proton transfer and influence of temperature on it by pang's dynamic model in hydrogen bonded systems, which coincide with experiments.

Hydrogen bonded systems consisting of series of hydrogen bonds,  $\dots X-H \dots X-H \dots X-H \dots$ , where X is a heavy ion or oxygen atom in ice, occur extensively in condensed matter, polymers and biological systems. Experiments discovered that there are a considerable electrical conductivity, even though electron transport through these systems is hardly supported. This is a quite intriguing feature. We recently proposed a new model in which we suggest that motion of the proton between a pair of heavy ions crossed over the barrier in the intrabond, which results in occurrence of the ionic defect, is mainly determined by the double-well potential. When the proton approaches the neighboring heavy ions the coupled interaction will be greatly enhanced and can be so much larger than the double-well potential which results in appearance of the bond. Thus, the both kinds of defects are produced by competition of the double-well potential and non-linear coupled interaction. Hamiltonian of the systems is denoted by [1-5]

$$\begin{aligned}
 H = H_p + H_{ion} + H_{int} = & \sum_n \left[ \frac{1}{2} p_n^2 + \frac{1}{2} m \omega_0^2 R_n^2 - \frac{1}{2} m \omega_1^2 R_n R_{n+1} + U_0 \left[ 1 - \left( \frac{R_n}{R_0} \right)^2 \right]^2 \right] \\
 & + \sum_n \left[ \frac{1}{2M} P_n^2 + \frac{1}{2} \beta (u_n - u_{n-1})^2 \right] \\
 & + \sum_n \left[ \frac{1}{2} \chi_1 m (u_{n+1} - u_{n-1}) r_n^2 + m \chi_2 (u_{n+1} - u_n) R_n R_{n+1} \right] \quad (1)
 \end{aligned}$$

where the proton displacements and momentum are  $R_n$  and  $p_n = mR_n$ ,  $R_0$  is the distance between the central maximum and one of the minima of the double-well,  $U_0$  is the height of the barrier of the double-well potential.  $u_n$  and  $P_n = Mu_n$  are the displacement of the heavy ion and its conjugate momentum,  $\chi_1$  and  $\chi_2$  are coupling constants between the proton and heavy ion sublattices. From Eq. (1) we obtained new method for influence of electric-field on conductivity properties of proton transfer in hydrogen-bonded systems.

### REFERENCES

1. Pang, X.-F. and H. J. W. Miiller-Kirsten, *J. Phys. Condens Matter*, Vol. 12, 885, 2000.
2. Pang, X.-F. and H. J. W. Miiller-Kirsten, *Phys. Stat. Sol. (B)*, Vol. 236, 34, 2003.
3. Pang, X.-F. and H. J. W. Miiller-Kirsten, *Soliton Physics*, Sichuan Sci. and Tech. Press, Sin. Chengdu, 687-752, 2003.
4. Pang, X. F. and Y. P. Yuan, *Chem. Phys. Lett.*, Vol. 373, 392, 2003.
5. Pang, X.-F. and Y. P. Yuan, *Quantum Mechanics in Nonlinear Systems*, World Scientific Publishing Co., New Jersey, 2005.

# Optical Properties of a Superconducting Distributed Bragg Reflector

**Chien-Jang Wu**

Department of Applied Physics, National University of Kaohsiung, Kaohsiung 811, Taiwan

**Abstract**— In this work we theoretically study the optical properties of a superconducting distributed Bragg reflector (SuDBR) made of superconducting/dielectric periodic bilayers. Optical wave properties are numerically investigated from the reflectance response calculated based on the transfer matrix method together with the two-fluid model of superconductors. The frequency-dependent reflection responses of TE and TM modes are illustrated at different angles of incidence, and at different dielectric constants of dielectric layer under the condition of equal length layers. The reflection band structures in such a SuDBR shows some fundamental differences from those of a dielectric DBR. The effects band shrinking of a TM wave and band widening of a TE one are both demonstrated. The existence of omnidirectional band is also displayed. In the case of unequal length layers, it is found the omnidirectional band width will be reduced compared to the equal length layers.

## Fabrication of Polymer Bragg Grating Waveguide Devices Using MEMS Technology

Kun-Yi Lee<sup>2</sup>, Wei-Ching Chuang<sup>1</sup>, Yen-Juei Lin<sup>2</sup>, and Wei-Yu Lee<sup>2</sup>

<sup>1</sup>Department of Electro-Optics Engineering, National Formosa University, Yunlin, Taiwan

<sup>2</sup>Department of Electrical Engineering, China Institute of Technology, Taipei, Taiwan

**Abstract**— In this paper, we proposed a novel process to replicate the polymer submicron range Bragg grating wavelength filter by using holographic interference techniques, soft lithography, and micro molding. The grating structure on a polymer is fabricated first using holographic interferometry and micro-molding processes. In this experiment, the master of the periodic structure was created on an i-line submicrometer positive photoresist film by a holographic interference using a He-Cd (325 nm) laser. A subsequent mold using polydimethylsiloxane (PDMS) polymer was cast against this master and used as a stamp to transfer the grating pattern onto a UV cure epoxy. Based on our AFM and SEM results, we found that the grating period and the corresponding depth of the grating pattern can be accurately controlled down to less than 1% error. We also found that a high aspect ratio of almost 0.7 : 1 between the depth and the period of the grating structure could be obtained using this process.

The polymeric wavelength filters are produced by a two-step molding process where the master mold is first formed on a negative tone photoresist and subsequently transferred to a PDMS mold; following this step, the PDMS silicon rubber mold was used as a stamp to transfer the pattern of the polymeric wavelength filters onto a UV cure epoxy. Initial results show good pattern transfer in physical shape. The waveguide properties including the mode pattern and the effective index were simulated using the beam propagation method. The effective index of the waveguide is 1.5447 from the simulation. The Bragg wavelength is 1553.9 nm as calculated from the Bragg reflection condition. The transmission of the optical filter was also calculated by using coupled mode theory. The calculated transmission minimum of the optical filter is  $-19.5$  dB. The spectral characteristics of the optical filter were measured using an optical spectrum analyzer. The measured result shown, at the Bragg wavelength, a transmission dip of  $-18.5$  dB was obtained, and the 3-dB-transmission bandwidth was about 8 nm. The result is consistent with the calculation of the coupled mode theory. The measured Bragg wavelength is 1554.02 nm, which is off by 0.12 nm from the theoretical prediction.



## Optical Dispersion of Indefinite Media Based on a Special Physical Model

Linfang Shen<sup>1</sup>, Tzong-Jer Yang<sup>2</sup>, and Yuan-Fong Chau<sup>3</sup>

<sup>1</sup>Department of Information Science and Electronic Engineering, Electromagnetic Academy  
Zhejiang University, Hangzhou, Zhejiang Province, China

<sup>2</sup>Department of Electrical Engineering, Chung-Hua University, Hsinchu 300, Taiwan

<sup>3</sup>Department of Electronic Engineering, Chin Yuan University, Jung Li 320, Taiwan

**Abstract**— The dispersion behavior of indefinite media is studied by a special physical material model. Interesting phenomena associated with the finite period, such as the upper cutoff for propagating waves, additional propagating mode in the anti-cutoff region predicted by the homogenized medium, and refraction of wave on a special indefinite material boundary, are illustrated. By comparing the dispersion features of a particular material and its dipole model, the effect of dimension included on dispersion is also investigated. The dispersion behavior of near zero transverse dielectric constant will be discussed.

# High-sensitivity Nuclear Magnetic Resonance Spectrometer for Hyperpolarized $^3\text{He}$ and Water by Using High- $T_c$ Superconducting Quantum Interference Devices

Hong-Chang Yang<sup>1</sup>, Shu-Hsien Liao<sup>2</sup>, Heng-Er Horng<sup>2,3</sup>, and S. Y. Yang<sup>3</sup>

<sup>1</sup>Department of Physics, National Taiwan University, Taipei 116, Taiwan

<sup>2</sup>Department of Physics, National Taiwan Normal University, Taipei 106, Taiwan

<sup>3</sup>Institute of Electro-optical Science and Technology

National Taiwan Normal University, Taipei 116, Taiwan

**Abstract**— We designed a low field nuclear magnetic resonance (NMR) spectrometer by using a high- $T_c$  superconducting quantum interference device (SQUID) and flux coupling for water and optically pumped hyperpolarized  $^3\text{He}$  gas. For optically pumped hyperpolarized  $^3\text{He}$  gas the NMR signal of the  $^3\text{He}$  procession spin is coupled to SQUID with a flux coupling, in which the pickup coil and input coil forms a tank circuit. By using a flux coupling we significantly improved the NMR signal. This spectrometer shows an S/N gain of 773 compared to that directly measured by a SQUID for an OP cell. For water the parameters to optimize the measurement of longitudinal relaxation time detection using a high- $T_c$  superconductive quantum interference device magnetometer are investigated [1]. These parameters include the pre-polarization field,  $B_p$ , the pre-polarization time,  $T_{Bp}$ , and the delay time,  $T_d$ , to turn on pulses after turning off the pre-polarization field. Furthermore, the decreasing of magnetization with the increasing  $T_d$  of the applied pulse was analyzed to determine the longitudinal relaxation time. We estimated the longitudinal relaxation time to be  $2.11 \pm 0.04$  s and  $2.29 \pm 0.04$  s respectively for water determined from nuclear magnetic resonance (NMR) signals as a function of  $T_{Bp}$  and  $T_d$  at  $24^\circ\text{C}$  in a measuring field of  $95 \mu\text{T}$ . The data are consistent with the derived longitudinal relaxation time of water measured from the increase of magnetization with the duration of the polarizing field [2].

## REFERENCES

1. Yang, H.-C., S.-H. Liao, H.-E. Horng, S.-L. Kuo, H.-H. Chen, and S. Y. Yang, "Enhancement of high- $T_c$  SQUID-detected NMR signals with pre-polarization of magnetization in microtesla magnetic field," *Appl. Phys. Lett.*, Vol. 88, 252505, 2006.
2. Liao, S.-H., H.-E. Horng, H.-C. Yang, and S.-Y. Yang, "Longitudinal relaxation time detection using a high- $T_c$  superconductive quantum interference device magnetometer," *J. Appl. Phys.*, Vol. 102, 033914, 2007.

# Frequency-dependent Negative Refraction of Photonic Crystals: Experimental Observations on Super-prisming and Super-chromatic-aberration Effects

S.-Y. Yang<sup>1</sup>, J. Y. Wu<sup>1</sup>, H. E. Horng<sup>1</sup>, Chin-Yih Hong<sup>2</sup>, and H. C. Yang<sup>3</sup>

<sup>1</sup>Institute of Electro-optical Science and Technology  
National Taiwan Normal University, Taipei 116, Taiwan

<sup>2</sup>Department of Mechanical Engineering  
Nan-Kai Institute of Technology, Nantou County 542, Taiwan

<sup>3</sup>Department of Physics, National Taiwan University, Taipei 106, Taiwan

**Abstract**— By detecting the spatially distributed intensity of a transmitted microwave whose incident angle is well controlled, the propagating path, the refractive angle, and the refractive index  $n_{PC}$  of the transmitted microwave can be determined. We then experimentally investigated the frequency-dependent negative refractive index of photonic crystals while microwaves of various frequencies were being transmitting out of the photonic crystals. It was found that  $n_{PC}$  is negative for microwaves having frequencies a little bit higher than the forbidden band, and approaches to zero when the frequency is far from the forbidden band. The negative refraction of photonic crystals was found not only for an incident continuous-wave microwave, but also for microwave with amplitude-modulation. The highly dispersive relationship between the negative refractive index and the frequency of microwave that was observed shows promise in being used in a microwave wavelength multiplexer by utilizing the negative-refraction super-prisming effect of photonic crystals.

On the other hand, the super-lensing effects of photonic-crystal concave lens for microwaves having various frequencies are studies experimentally. In addition to observing the focusing effect of photonic-crystal concave lens involving negative refraction, the effective focal length (FL) as a function of microwave frequency is explored. It was observed that FL becomes larger as the frequency of the negative-refraction microwave increases. Super-chromatic-aberration effect utilizing negative refraction was found for photonic crystals. According to the experimental results on the dependencies of  $n_{PC}$  and FL on microwave frequency, we find that the relationship between FL and  $n_{PC}$  follows  $FL = R/(1 - n_{PC})$ , where R is the curvature radius of the photonic-crystal concave lens.

## AGILD EM Dispersion Modeling For Photonic Crystals

Ganquan Xie<sup>1</sup>, Tong Kang<sup>2</sup>, and Jianhua Li<sup>1</sup>

<sup>1</sup>GL Geophysical Laboratory, USA

<sup>2</sup>School of Sciences, Communication University of China, China

**Abstract**— In this paper, we propose an Advanced Global Integral and Local Differential (AGILD) Electromagnetic (EM) dispersion modeling for photonic crystals. We present a periodic Green's function differential integral equation in the strip of lattice unit cell, Also, a Galerkin equation in the internal of the lattice cell. Both differential integral equation and Galerkin integral Bloch equations are used to construct the AGILD EM dispersion modeling for phonic crystals. Our method is fast and parallel. It can clear the error boundary reflection and numerical dispersion error. The AGILD EM dispersion modeling can be useful for simulation in the dispersion engineering of photonics crystals and other advanced optical device and fiber design and nanometer materials investigation.

### REFERENCES

1. Li, J., G. Xie, M. Oristaglio, L. Xie, and F. Xie, "3D-2D AGILD EM modeling and inversion," *PIERS Online*, Vol. 3, No. 4, 423–429, 2007.
2. Li, J., G. Xie, and F. Xie, "New stochastic AGLID EM modeling and inversion," *PIERS Online*, Vol. 2, No. 5, 490–494, 2006.
3. Xie, G., J. Li, M. Majer, D. Zuo, and M. Oristaglio, "3D electromagnetic modeling and nonlinear inversion," *Geophysics*, Vol. 65, No. 3, 804–822, 2000.
4. Xie, G. and J. Li, "New parallel stochastic global integral and local differential equation modeling and inversion," *Physics D*, Vol. 133, 477–487, 1999.
5. Xie, G., J. Li, and F. Xie, "Advanced GILD EM modeling and inversion," *PIERS Online*, Vol. 1, No. 1, 105–109, 2005.
6. Xie, G., J. Li, and F. Xie, "2.5D AGLID EM modeling and inversion," *PIERS Online*, Vol. 2, No. 4, 390–394, 2006.
7. Xie, G., F. Xie, L. Xie, and J. Li, "GL method and its advantages for resolving historical difficulties," *Progress In Electromagnetics Research, PIER*, Vol. 63, 141–152, 2006.
8. Xie, G., J. Li, and J. Li, "New AGILD EMS electromagnetic field modeling," *PIERS Online*, Vol. 1, No. 2, 168–172, 2005.
9. Xie, G., F. Xie, and J. Li, "New GL and GILD superconductor electromagnetic modeling," *PIERS Online*, Vol. 1, No. 2, 173–177, 2005.
10. Xie, G., J. Li, F. Xie, and L. Xie, "3D GL EM and quantum mechanical coupled modeling for the nanometer materials," *PIERS Online*, Vol. 3, No. 4, 418–423, 2007.

# Fast and Accurate Full-model Simulation Algorithm for the Analysis of Frequency Selective Surfaces and Periodic Structures

Heng-Tung Hsu

Department of Communications Engineering, Yuan Ze University  
135 Yuan-Tung Road, Chung-Li 32003, Taiwan, R.O.C.

**Abstract**— This paper proposed a fast and accurate electromagnetic simulation algorithm for the analysis of frequency selective surfaces (FSS) with full models. FSS basically composed of periodic assemblies of identical elements arranged in a one- or two-dimensional array. These periodic structures are either an array of apertures in a thin metallic sheet or metallic patches on a dielectric substrate and have found wide spreading applications in the areas of signal filtering or antenna beam shaping. Conventionally, only the unit cell was analyzed electromagnetically and the performance of the overall structure was obtained through proper summation with array factors. Such method had certain limits and could not predict the diffraction caused by the edges of the apertures especially when the observation position was relatively close to the structure. In this paper, a fast and accurate method based on the finite integration algorithm in time domain is proposed. Such method can take the full model into consideration during analysis and has been proven accurate with calculation time comparable to that of analyzing a unit cell. Same algorithm can also be applied in the cases for analyzing period structures for various electromagnetic applications.

## Design and Implementation of Novel Switching-mode Output Driver with Off-chip Transmission Speed up to 640 Mb/s

Heng-Shou Hsu

Department of Electronic Engineering, Feng-Chia University  
100 Wenhwa Road, Seatwen, Taichung 40724, Taiwan, R.O.C

**Abstract**— This paper proposed the design and implementation of novel switching-mode output driver according to optimal off-chip transmission speed through the suppression of possible electromagnetic interference. While the on-chip transmission rate can be easily optimized to the desired performance by careful circuit-level simulation, the inevitable off-chip performance degradation is addressed through full wave electromagnetic simulation. Electromagnetic analysis results revealed that the interference could be minimized only when the complex impedance level was maintained at the desired output impedance of the output stage with the imaginary part minimized over the highest frequency range of operation. The proposed novel output driver possesses the advantages of less power consumption under lower transmission rate and better signal integrity when transmission rate up to 640 Mb/s. The circuits were implemented in a 3.3 v 0.35  $\mu\text{m}$  CMOS process. Simulation results demonstrate the novel output driver is suitable for off chip data transmission and has wide application on interface circuitry.

## Session 2P5

# Theoretical Models for Microwave Remote Sensing

<a href="#">Digital Bathymetry and Correction Model for Multibeam Bathymetric Sonar System</a>	
<i>Lei Yan (Peking University, China); Jia Cheng Yu (Beijing Institute of Technology, China); Yue Feng Liu (Peking University, China); Jia Bin Chen (Beijing Institute of Technology, China); ...</i>	488
<a href="#">A Broadband Proximity Antenna for Subsurface Sensing</a>	
<i>Suman K. Gunnala (The University of Texas at Arlington, USA); Mingyu Lu (The University of Texas Arlington, USA); Jonathan W. Bredow (The University of Texas at Arlington, USA); Saibun Tjuatja (The University of Texas at Arlington, USA); .....</i>	489
<a href="#">Surface Bistatic Scattering Based on IEM Model</a>	
<i>T. D. Wu (National Taiwan Ocean University, Taiwan); Kun-Shan Chen (National Central University, Taiwan); Jiancheng Shi (University of California at Santa Barbara, USA); .....</i>	490
<a href="#">FDTD Modeling of Emission from Finite-size Object</a>	
<i>Luis M. Camacho (The University of Texas at Arlington, USA); Mingyu Lu (The University of Texas Arlington, USA); Saibun Tjuatja (The University of Texas at Arlington, USA); .....</i>	491
<a href="#">Multi-temporal Backscattering Behavior of Rice Crop Canopies Based on Dense Medium Model Simulations</a>	
<i>Jun-Yi Koay (Multimedia University, Malaysia); Hong Tat Ewe (Multimedia University, Malaysia); Hean-Teik Chuah (Multimedia University, Malaysia); .....</i>	492
<a href="#">A Study of Optimized Observation Configuration in Determining Sea Ice Thickness Using Multilayer Backscattering Model in Antarctica</a>	
<i>Mohan Dass Albert (Multimedia University, Malaysia); Hong-Tat Ewe (Multimedia University, Malaysia); Hean-Teik Chuah (Multimedia University, Malaysia); .....</i>	493
<a href="#">Localization of Passive Targets Based on a Radar Sensor Network</a>	
<i>Tsungyin Wu (The University of Texas at Arlington, USA); Mingyu Lu (The University of Texas Arlington, USA); Kartik Trasi (The University of Texas at Arlington, USA); Saibun Tjuatja (The University of Texas at Arlington, USA); .....</i>	494
<a href="#">Use of Numerical Methods for Assessing Validity Domains of the Approximations Involved in Electromagnetic Interaction Modeling with Vegetation</a>	
<i>Pierre Borderies (Office National d'Etudes et de Recherches Aerospatiales (ONERA), France); J.-R. Poirier (LAME-ENSEEIH- INPT, France); S. Tournier (ONERA, France); C. Lauprette (ONERA, France); Ludovic Villard (Office National d'Etudes et de Recherches Aerospatiales (ONERA), France); Pascale Dubois-Fernandez (ONERA, France); N. Floury (ESA-ESTEC/TEC-EEP, The Netherlands); .....</i>	495
<a href="#">Analysis of the Impact of Forest Structure on Radar Backscattering Based on Three-dimensional Radar Coherent Model</a>	
<i>Dawei Liu (Zhejiang University, China); Guoqing Sun (University of Maryland, USA); Yang Du (Zhejiang University, China); Wenzhe Yan (Zhejiang University, China); Jin Au Kong (Massachusetts Institute of Technology, USA); .....</i>	496
<a href="#">On the Convergency Properties of Translational Addition Theorems</a>	
<i>Wenzhe Yan (Zhejiang University, China); H. Wu (Zhejiang University, China); Yang Du (Zhejiang University, China); Q. W. Xiao (Zhejiang University, China); Dawei Liu (Zhejiang University, China); Jin Au Kong (Massachusetts Institute of Technology, USA); .....</i>	497

## Digital Bathymetry and Correction Model for Multibeam Bathymetric Sonar System

L. Yan<sup>1</sup>, J. C. Yu<sup>1,2</sup>, J. B. Chen<sup>2</sup>, and Y. F. Liu<sup>1</sup>

<sup>1</sup>Beijing Key Laboratory of Spatial Information Integration and Applications  
Peking University, Beijing 100871, China

<sup>2</sup>Department of Automatic Control, School of Information Science and Technology  
Beijing Institute of Technology, Beijing 100081, China

**Abstract**— Multibeam Bathymetric Sonar System (MBSS) is a complex system that is used to survey seafloor terrain. As it has the characteristic of wide covering, high scanning density, high precision and efficiency, it is playing a important role in practical work and attracting more and more attention.

This paper presents a digital bathymetry model in terms of principle of Multibeam Bathymetric Sonar System, and a correction method of water depth survey due to effect of angular beamwidth is given. Accordingly, terrain maps are constructed to imitate the realtime terrain.

On doing seafloor simulation experiment, in general, the reference depth map (RDM) has been obtained beforehand, but the local depth map (LDM) is unknown. When the position of autonomous underwater vehicles (AUV) is needed precisely, the terrain matching should be performed between RDM and LDM. Meanwhile, for the sake of cost of equipment, the model of MBSS is needed to give the LDM to substitute for it. In addition, as the seafloor terrain is complex, when depth survey is operating, there are some errors due to the coupling effect between angle beam-width and diverse terrain. So water depth data measured by MBSS should be corrected according to practical situation.

This paper takes the practical system for an example to construct its model. The practical system is shown as Fig. 1. It has 16 beams with  $2^\circ \times 2^\circ$  angular beamwidth. When it works, a swath will be formed. With geometrical analysis, It's model can be obtained.

In surveying process, the acquired distance between transducer and seabed is shorter than the real for the coupling of beamwidth and fluctuant terrain. By analyzing their correlation, the depth compensation can be reckoned, thus the surveying precision will be increased.

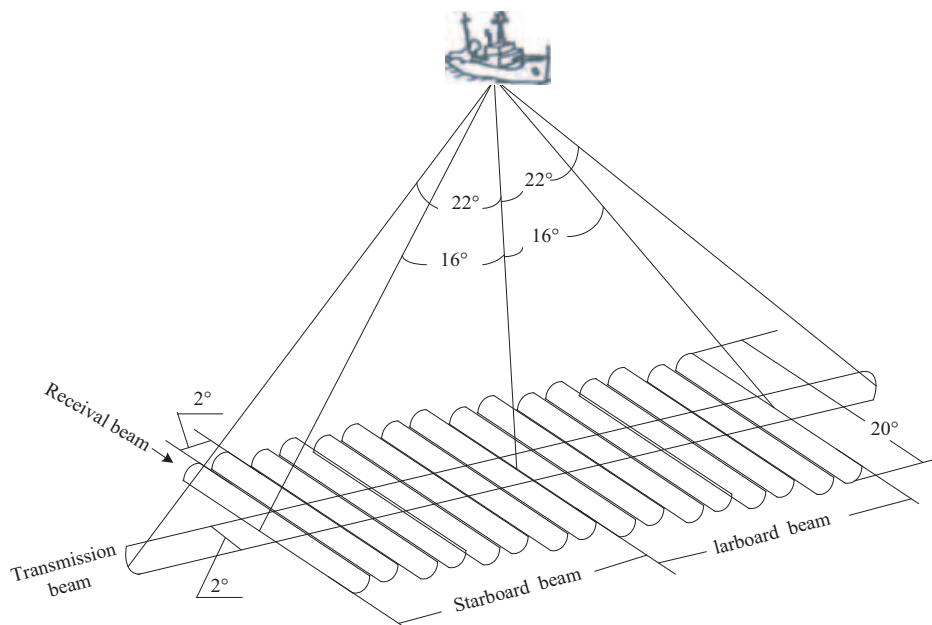


Figure 1: Working principle of MBSS.



## A Broadband Proximity Antenna for Subsurface Sensing

Suman K. Gunnala, Mingyu Lu, Jonathan W. Bredow, and Saibun Tjuatja

Wave Scattering Research Center, Department of Electrical Engineering  
The University of Texas at Arlington  
UTA Box 19016, Arlington, TX 76019-0016, U.S.A.

**Abstract**— In ground penetrating radars (GPR), direct reflection from ground constitutes the major source of clutters [1]. Many researchers have developed various signal processing techniques to suppress signals from the ground reflection [2]. This study aims at minimizing the ground clutter through designing conformal antennas that reside in the proximity of ground (very close to or touching the ground) and directly couple electromagnetic power into the ground. The proposed antenna array is composed of cavity-backed slot elements. Compared to patch antennas, cavity-backed slots have a few advantages. First, it is relatively easier to achieve large bandwidth. Our initial simulation and measurement results show a 35% input impedance bandwidth. Second, mutual coupling among cavity-backed slots is minimal, and radiation characteristics are insensitive to the substrate truncation [3]. Third, slots are more efficient than patches in that there is no dielectric loss. And fourth, slots have higher power tolerance. In the novel proximity antenna, each cavity-backed slot element is designed to operate in the two-halfspace configuration: one halfspace is air; and the other is soil. Over a pretty broad band (2.5 GHz to 4 GHz in our initial design), microwave power fed to the antenna is delivered into the soil to the maximal extent; and at the same time, there is little crosstalk among antenna elements. The proposed antenna is tested in realistic scenarios where metallic objects are buried underneath ground. Because the proximity antenna avoid direct reflection from ground through hardware design, GPR equipped with these novel antennas are expected to outperform conventional GPR that rely on signal processing to suppress ground clutters, especially when the distance between buried objects and ground surface is small. Measurement results and theoretical modeling of the subsurface wave-target interactions using the proposed broadband proximity antenna demonstrated significant improvement on the scattered signal. Detail measurement results and model analysis will be presented in the paper.

### REFERENCES

1. Rappaport, C., M. El-Shenawee, and H. Zhan, "Suppressing GPR clutter from randomly rough ground surfaces to enhance nonmetallic mine detection," *Subsurface Sensing Technologies and Applications*, Vol. 4, No. 4, 311–326, October 2003.
2. Zhao, A.-X., Y.-S. Jiang, and W.-B. Wang, "Exploring independent component analysis for GPR signal processing," *Presented at Progress in Electromagnetics Research Symposium*, Hangzhou, China, August 2005.
3. Zheng, B. and Z. Shen, "Effect of a finite ground plane on microstrip-fed cavity-backed slot antennas," *IEEE Transactions on Antennas and Propagation*, Vol. 53, 862–865, 2005.

## Surface Bistatic Scattering Based on IEM Model

T. D. Wu<sup>1</sup>, Kun-Shan Chen<sup>2</sup>, and Jiancheng Shi<sup>3</sup>

<sup>1</sup>Department of Electrical Engineering, National Taiwan Ocean University, Taiwan

<sup>2</sup>Center for Space and Remote Sensing Research, National Central University, Chung-Li 32054, Taiwan

<sup>3</sup>Institute of Computational Earth System Science, University of California at Santa Barbara  
Santa Barbara, CA 93117, USA

**Abstract**— The IEM model was derived starting from the estimation of the surface tangential fields [1–2]. Once the surface fields are known, then the far zone scattered fields is calculated through the Stratton-Chu formula. Ensemble averages are then carried out over the randomly rough surface, assuming a Gaussian height distribution, to obtain the scattering coefficients. To estimate the surface tangential fields, the magnetic field integral equations and the electric field integral equations, for the upper medium and lower medium, that governing the surface currents, are rewritten in a form of the Fredholm integral equation of the second kind so that the iterative scheme can be applied to obtain the estimates. Up to second order solutions are approximated the exact solution. The first order solution corresponds to the so-called Kirchhoff field, while the second order solution corresponds to the complementary field [1]. Because of the coherent process, the resulting scattering power consists of three terms: the Kirchhoff term, the cross term, and the complementary term, so as the scattering coefficients. It has been demonstrated that the classical Kirchhoff model (KM) and small perturbation model (SPM) are special IEM cases in both the high and low frequency regions for backscattering, respectively. The Advanced IEM (AIEM) [3–5] based on original IEM version has been reported to improve the prediction accuracy. The main focus was on the backscattering direction and the surface emissivity. For the bistatic cases, the IEM was shown to unsatisfactorily match the classical Kirchhoff Model. This is due to that the sum of two terms including the Fresnel reflection coefficients in Kirchhoff tangential field are dropped out to simplify the derivation of the Kirchhoff field coefficient. In this paper we rederive a complete expression of the Kirchhoff field coefficients in IEM model. After quite intricate mathematical manipulations, new but still compact expressions of the Kirchhoff field coefficients are obtained. We investigate the impact of these terms on the bistatic scattering. It is found that with the new expression, the model prediction for bistatic scattering is much accurate as compared to the original one.

### REFERENCES

1. Fung, A. K., Z. Li, and K. S. Chen, “Backscattering from a randomly rough dielectric surface,” *IEEE Trans. Geosci. Remote Sensing*, Vol. 30, 356–369, Mar. 1992.
2. Fung, A. K., *Microwave Scattering and Emission Models and Their Applications*, Artech House, 1994.
3. Chen, K. S., T. D. Wu, and A. K. Fung, “A note on multiple scattering in an IEM model,” *IEEE Trans. Geoscience and Remote Sensing*, Vol. 38, No. 1, 249–256, 2000.
4. Wu, T. D., K. S. Chen, A. K. Fung, and M. K. Tsay, “A transition model for the reflection coefficient in surface scattering,” *IEEE Trans. Geoscience and Remote Sensing*, Vol. 39, No. 9, 2040–2050, 2001.
5. Chen, K. S., T. D. Wu, L. Tsang, Q. Li, J. C. Shi, and A. K. Fung, “The emission of rough surfaces calculated by the integral equation method with a comparison to a three-dimensional moment method simulations,” *IEEE Trans. Geoscience and Remote Sensing*, Vol. 41, No. 1, 90–101, 2003.

## FDTD Modeling of Emission from Finite-size Object

Luis M. Camacho, Mingyu Lu, and Saibun Tjuatja

Wave Scattering Research Center, Department of Electrical Engineering  
The University of Texas at Arlington, UTA Box 19016, Arlington, TX 76019-0016, USA

**Abstract**— Microwave emission from an object in a given direction is generally partially polarized. Kirchhoff radiation law relates the partially polarized intensities, represented using the Stokes parameters, to the absorption properties of the object. The far-field flux of energy emitted into a particular direction of space and with a particular polarization is proportional to the absorption cross section for a monochromatic plane wave incident upon the body from the opposite direction and with the same polarization. The complexity of analytical relation between object's Stokes parameters and its absorption properties is determined by geometry and dielectric properties of the object. Simplifying assumptions are usually made in the derivation of the analytical model for emission from finite size object. In this study, a Finite-Difference Time-Domain (FDTD) numerical model is utilized to determine the emission from a finite size object with arbitrary shape and dielectric value. The total scattering cross-section of an object is calculated using a 3D FDTD algorithm. Microwave emission from the object for a given direction and polarization is determined from its total scattering with the same polarized incident but with opposite incident direction. Calculated results from objects with arbitrary shape and discussion of the modeling issues will be included in the presentation.

## Multi-temporal Backscattering Behavior of Rice Crop Canopies Based on Dense Medium Model Simulations

J. Y. Koay, H. T. Ewe, and H. T. Chuah  
Multimedia University, Malaysia

**Abstract**— In recent years, efforts to study the backscattering behavior of rice crop canopies have resulted in the measurement of the multi-temporal backscattering coefficient of rice crops over various incident angles, frequencies and polarizations through the use of space-borne radars and ground-based scatterometers. With the availability of all these data, different scattering models have been developed for rice crop canopies in an attempt to further analyze the results obtained [1, 2]. One such model is based on the radiative transfer equations, and incorporates the Dense Medium Phase and Amplitude Correction Theory (DM-PACT) [3] as well as the amplitude and Fresnel phase corrections [4] to take into account coherent effects and Fresnel field effects of closely spaced scatterers, respectively. Hence, the canopy is modeled as a dense medium. An early variation of the dense medium model for rice crops employs needle-shaped scatterers to simulate the leaves of the rice plants [5]. In this study, the phase matrix of the rice crop canopy is obtained using the scattered field of elliptic disk-shaped scatterers (with the inclusion of the Fresnel field effects) to model the leaves. This model is then used in the simulation of the backscattering coefficient of rice crop canopies at different stages of growth, through which the contribution of the different scatterers in the canopy and the backscattering mechanisms involved are then analyzed. This enables a better understanding of the multi-temporal backscattering behavior of rice crop canopies, particularly that of the sensitivity of the rice crop backscattering coefficient to the different scatterers in the medium and the input parameters of the model.

### REFERENCES

1. Le Toan, T., F. Ribbes, L. F. Wang, N. Floury, K. H. Ding, J. A. Kong, M. Fujita, and T. Kurosu, "Rice crop mapping and monitoring using ERS-1 data based on experiment and modeling results," *IEEE Transactions on Geoscience and Remote Sensing*, Vol. 35, 41–56, 1997.
2. Wang, L., J. A. Kong, K. H. Ding, T. Le Toan, F. Ribbes-Baillarin, and N. Floury, "Electromagnetic scattering model for rice canopy based on Monte Carlo simulation," *Progress in Electromagnetics Research*, Vol. 52, 153–171, 2005.
3. Chuah, H. T., S. Tjuatja, A. K. Fung, and J. W. Bredow, "A phase matrix for a dense discrete random medium: Evaluation of volume scattering coefficient," *IEEE Transactions on Geoscience and Remote Sensing*, Vol. 34, No. 5, 1137–1143, 1996.
4. Ewe, H. T. and H. T. Chuah, "A study of fresnel scattered field for non-spherical discrete scatterers," *Progress In Electromagnetics Research*, Vol. PIER 25, 189–222, 2000.
5. Koay, J. Y., C. P. Tan, K. S. Lim, S. Bahari, H. T. Ewe, H. T. Chuah, and J. A. Kong, "Paddy fields as electrically dense media: theoretical modeling and measurement comparisons (Periodical style-Accepted for publication)," *IEEE Transactions on Geoscience and Remote Sensing*, to be published.

# A Study of Optimized Observation Configuration in Determining Sea Ice Thickness Using Multilayer Backscattering Model in Antarctica

M. D. Albert<sup>1</sup>, H. T. Ewe<sup>2</sup>, and H. T. Chuah<sup>1</sup>

<sup>1</sup>Faculty of Engineering, Multimedia University, Malaysia

<sup>2</sup>Faculty of Information Technology, Multimedia University, Malaysia

**Abstract**— Global warming has been a topic highly interested by the research community. Researchers have been relating global warming to Antarctica and the increase in global temperature may speed up the melting of ice in the southern continent. This vast volume of ice has significant effects on climate, ocean salinity, current as well as its biological ecosystem. It is our interest to monitor physical changes in Antarctica, especially the sea ice condition, for global warming study using remote sensing technique.

Since Antarctica is a huge continent, monitoring the physical changes could be challenging. Therefore, remotely sensing the continent using satellite would be a perfect choice but the retrieval of physical parameters of sea ice from the satellite images needs a thorough understanding of interaction between microwave and sea ice.

In this paper, a multilayer model based on radiative transfer theory is developed to represent sea ice terrain in Antarctica. Unlike some single layer models in the literature, the multilayer model can represent the snow and sea ice layers more accurately. In this model, the snow and sea ice layers are considered electrically dense and therefore the Dense Medium Phase and Amplitude Correction Theory (DMPACT) is incorporated to consider the close spacing effect among the scatterers. The air-snow interface, snow-sea ice interface and sea ice-ocean interface are modeled using the Integral Equation Method (IEM). In order to better understand the interaction between microwave and snow and sea ice media, it is important to choose good observation configurations, such as frequency, incident angle and polarization of the wave. In this study, the optimization of observation configuration will be carried out and how various scattering mechanisms and also the physical parameters of sea ice and snow media can affect the backscattering coefficient with different observation configuration will be presented. This serves as practical guideline for future ground truth measurement in Antarctica and satellite monitoring in Antarctica.

# Localization of Passive Targets Based on a Radar Sensor Network

Tsungyin Wu, Mingyu Lu, Kartik Trasi, and Saibun Tjuatja

Wave Scattering Research Center, Department of Electrical Engineering  
The University of Texas at Arlington  
UTA Box 19016, Arlington, TX 76019-0016, USA

**Abstract**— In this study, a radar sensor network is deployed for passive target detection. Each sensor behaves as short-range impulse radar. It transmits impulse signals to all directions. When there is a target present, the distance between target and radar sensor is found by measuring the time difference between the transmitted impulse and the echo signal through correlation. The exact location of the target is determined by synthesizing information from multiple sensors. Each individual sensor consists of an omni-directional wideband antenna, an impulse transceiver, and signal processing unit. The quasi-planar conical antennas developed in [1] are good candidates for the sensor antennas. They are wideband (matched to 50-ohm from 1.5 GHz to 20 GHz), omni-directional, mechanically stable, light-weighted, and of low cost. In our data acquisition process, the transceiver is realized using vector network analyzer; and signal processing is performed on personal computers. The sensor network is tested in anechoic chamber and in realistic noisy environments, for metallic and dielectric targets with various physical sizes. Multiple algorithms are applied for the target localization, including Iteratively Refined-Minimum Mean Square Estimate (IR-MMSE) [2], Hough Transform [3], and Grid Based Location Estimation [4]. A modified grid based algorithm is demonstrated to offer the best performance in presence of large range estimation errors. Presently, existing localization algorithms for radar sensor network assumed that the target behaves as point scatterer. In this study, we extend the network sensing model to include finite size target. The non-point target scattering model for radar network sensing is expected to further improve the localization accuracy.

## REFERENCES

1. Lu, M., J. W. Bredow, S. Jung, and S. Tjuatja, "Theoretical and experimental study of a quasi-planar conical antenna," Presented at *The 2007 IEEE Antennas and Propagation Society Symposium*, Honolulu, HI, June 2007.
2. Liu, D., P. Ning, and W. K. Du, "Attack-resistant location estimation in sensor networks," Presented at *The Fourth International Symposium on Information Processing in Sensor Networks*, Los Angeles, CA, April 2005.
3. Chang, C. and A. Sahai, "Object tracking in a 2D UWB sensor network," Presented at *The Thirty-Eighth Asilomar Conference on Signals, Systems and Computers*, Pacific Grove, CA, November 2004.
4. Fretzagias, C. and M. Papadopouli, "Cooperative location-sensing for wireless networks," Presented at *The Second IEEE Annual Conference on Pervasive Computing and Communications*, Orlando, FL, March 2004.

# Use of Numerical Methods for Assessing Validity Domains of the Approximations Involved in Electromagnetic Interaction Modeling with Vegetation

P. Borderies<sup>1</sup>, J.-R. Poirier<sup>2</sup>, S. Tournier<sup>1</sup>, C. Lauprette<sup>1</sup>  
L. Villard<sup>1</sup>, P. Dubois-Fernandez<sup>1</sup>, and N. Floury<sup>3</sup>

<sup>1</sup>ONERA, 2 avenue Edouard Belin, 31 055 Toulouse Cedex 5, France

<sup>2</sup>LAME-ENSEEIH-INT, 2 rue Charles Camichel, 31071 Toulouse cedex, France

<sup>3</sup>ESA-ESTEC/TEC-EEP, Noordwijck, The Netherlands

**Abstract**— Electromagnetic models of interaction with natural land media are extensively used to analyze and foresee the Synthetic Aperture Radar observables, and may be used to study the robustness of retrieval algorithms. However, usually, these models rely on approximations of various origin which may jeopardize the relevancy of some simulations, all the more so as retrieval algorithms rely more and more on complex sets of observables including polarimetry and interferometry, which makes the requirements toward these models still more demanding than for the mere radiometric outputs.

In particular, the most basic bricks used in most interaction models (either radiative transfer ones or born type coherent ones) are the scattering matrices of the discrete scatters describing the vegetation. They are based on analytical approaches involving electromagnetic approximations which implications on the accuracy of scattering matrix terms and further the retrieval possibilities need to be investigated. Numerical techniques when applicable are then very helpful to perform such study. However they have to face some specific challenges among which the high dielectric constant encountered in natural media and the thinness of some components like leaves, together with the requirements in computational power. The purpose of the present paper is first to evaluate the relevancy of several numerical techniques for this purpose of modeling electromagnetic interaction with piece of vegetation using some reference solutions and then to show the results obtained on the most used basic scattering elements which are the finite length cylinder and the flat ellipsoid.

## Analysis of the Impact of Forest Structure on Radar Backscattering Based on Three-dimensional Radar Coherent Model

Dawei Liu<sup>1</sup>, Guoqing Sun<sup>2</sup>, Yang Du<sup>1</sup>, Wenzhe Yan<sup>1</sup>, and Jin Au Kong<sup>1,3</sup>

<sup>1</sup>The Electromagnetics Academy, Zhejiang University, Hangzhou 310058, China

<sup>2</sup>Department of Geography, University of Maryland, College Park, MD 20742, USA

<sup>3</sup>Department of Electrical Engineering and Computer Science  
Massachusetts Institute of Technology, Cambridge, MA 02139, USA

**Abstract**—Vegetation spatial structure including plant height, biomass, vertical and horizontal heterogeneity, is an important factor influencing the exchanges of matter and energy between the landscape and atmosphere, and the biodiversity of ecosystems. Radar backscattering, especially the phase information, is dependent on the spatial structure of vegetation canopies. In this study the three-dimensional radar coherent model is used to simulate the backscattering coefficient of forest and analyze the effect of forest structure on radar backscattering scattering. The 3-D structure of forest stands could be obtained from field data, or from combined use of forest growth model and fractal tree model. Simulated forest stands from a forest growth model parameterized using local environmental parameters can serve as a database of forest stands for radar modeling. A fractal tree model (L-system) was used to simulate 3-D tree structure of different age or height. The data sets from the simulation can be used to help explore the effects of canopies of different species and age structure on radar backscatter. The coherent radar backscatter model takes the 3-D forest scene as input and simulates the coherent radar backscattering signature.

In this study, different data sets (forest with equal biomass) will be generated using forest growth model and fractal model: two different structural distributions of deciduous tree in the forest, two different structural distributions of coniferous tree in the forest and three different structural distributions of deciduous and coniferous mixing in the forest. The data sets from the simulation are putted into the radar coherent model, and then the coherent radar backscattering signatures are simulated. The results indicate that the change of forest structure (tree distribution and the species of tree) has a considerable effect on the radar backscattering. The analysis of the effect of forest structure on radar backscattering should improve our ability to monitor forest ecosystems.



## On the Convergency Properties of Translational Addition Theorems

W. Z. Yan<sup>1</sup>, H. Wu<sup>1</sup>, Y. Du<sup>1</sup>, Q. W. Xiao<sup>1</sup>, D. W. Liu<sup>1</sup>, and J. A. Kong<sup>1,2</sup>

<sup>1</sup>The Electromagnetics Academy, Zhejiang University, Hangzhou 310058, China

<sup>2</sup>Department of Electrical Engineering and Computer Science  
Massachusetts Institute of Technology, Cambridge, MA 02139, USA

**Abstract**— Translational addition theorems are powerful analytic tools to translate a multipole expansion of an electromagnetic field from one to another coordinate system and are of considerable importance for a wide range of electromagnetic scattering problems. For instance, to study the multiple volumes scattering behavior, a coupled linear system may be used, where the electromagnetic fields are expanded in terms of vector spherical harmonics, which may need to be translated from the center of a scatterer to that of another. The convergence property of translational addition theorem thus bears its influence on the convergence of the linear system.

In this paper we review several efficient methods for calculating both scalar and vector translation additional coefficients and check the convergence properties of translational addition theorem from a numerical point of view. As expected the convergence behavior depends on the configuration and the harmonic function. For the extreme cases there may only need a few addition terms to guarantee convergence on one hand and a few hundred terms on the other hand. The latter case indicates that caution may need to be taken against common engineering practice where several tens of terms are commonly used. We illustrate such effect through multiple-sphere scattering problems.



# Session 2P6a

## Microwave and Millimeter Wave Circuits and Devices

### 1

<b>40 GHz Band Down/Up Converter with E-Plane Circuit</b>	
<i>Yozo Utsumi (National Defense Academy, Japan); Nguyen Thanh (National Defense Academy, Japan); Toshihisa Kamei (National Defense Academy, Japan); Hirosuke Suzuki (KEYCOM Corporation, Japan);</i> .....	500
<b>An Experimental Study of Improved Low Pass Filter Using Post-wall Grounding Configuration</b>	
<i>Ka Sing Lim (Multimedia University, Malaysia); Manimaran Nagalingam (Multimedia University, Malaysia);</i> .....	502
<b>Use of Ground Plane Windows and Floating Conductors in Microstrip SIR Filters</b>	
<i>Maria del Castillo Velázquez-Ahumada (University of Seville, Spain); Jesús Martel (University of Seville, Spain); Francisco Medina (University of Seville, Spain);</i> .....	503
<b>A Millimeter-wave Sampled-Line Six-port Reflectometer at 300 GHz</b>	
<i>Guoquan Wu (University of Virginia, USA); Zhiyang Liu (M/A-COM, USA); Stephen H. Jones (Virginia Diodes, Inc., USA); Robert M. Weikle (University of Virginia, USA);</i> .....	504
<b>Parallel-coupled Microstrip Filter with Super Wide Stopband</b>	
<i>Shry-Sann Liao (Feng-Chia University, Taiwan); Shih-Yi Yuan (Feng-Chia University, Taiwan); Pou-Tou Sun (Feng-Chia University, Taiwan); Yi-Hao Chang (Feng-Chia University, Taiwan); Hung-Liang Lin (Feng-Chia University, Taiwan);</i> .....	505
<b>Design and Optimization of Microstrip Interdigital Bandpass Filters with Impedance Matching</b>	
<i>Homayoon Oraizi (Iran University of Science and Technology, Iran); Nima Azadi-Tinat (Iran University of Science and Technology, Iran); Shahrokh Saeedi (Iran University of Science and Technology, Iran);</i>	506

## 40 GHz Band Down/Up Converter with E-Plane Circuit

Y. Utsumi<sup>1</sup>, N. Thanh<sup>1</sup>, T. Kamei<sup>1</sup>, and H. Suzuki<sup>2</sup>

<sup>1</sup>National Defense Academy, Japan

<sup>2</sup>KEYCOM Corporation, Japan

**Abstract**— In Japan, 2003 marked the introduction of digital terrestrial broadcasting in major urban areas, and analog broadcasting throughout the country is scheduled to go digital by 2011. Terrestrial broadcasting is therefore expected to take on a multi-channel format in time, and the transmission capacity of cable television is likewise predicted to increase significantly. At present, urban cable television features a bandwidth of 450 MHz, but this will have to be increased to 700 MHz due to the conversion to digital. In situations where laying cable for commercial circuits from the cable company's head end to housing complexes and other buildings is difficult, the current scheme is to use wireless transmission in the 23-GHz band (bandwidth: 400 MHz; one-way transmission in the downlink). Studies are now being conducted on the use of wireless transmission in the 40-GHz band (bandwidth: 1 GHz) to enable broadband and bidirectional transmission in future systems.

To this end, we report on a prototype frequency down-converter and frequency up-converter using an E-plane planar circuit that can be mounted in a waveguide. These converters will enable the high-frequency section of a transmit/receive circuit to be integrated with filters and other devices in a waveguide. They are slated to be used in high-quality and inexpensive bidirectional wireless transmission systems for urban cable television of the future.

Figure 1 shows the structure of the down/up converter using an E-plane planar circuit. It features inductive strips (copper-plate thickness  $t = 100 \mu\text{m}$ ) inserted into a divided waveguide achieved by splitting a waveguide (WRJ-400) at the center of the H plane, and is designed under image-short conditions. Specifically, the converter consists of local rejection filter L (dielectric resonator: 35.6 GHz), capacitive strip C for RF signal matching, Schottky-barrier mixer diode D,  $\lambda/4$  transformer ridge guide T, image-short ridge guide S, RF rejection filter R made with a strip line, and local band pass filter P (35.6 GHz), all achieved on a single E-plane planar circuit.

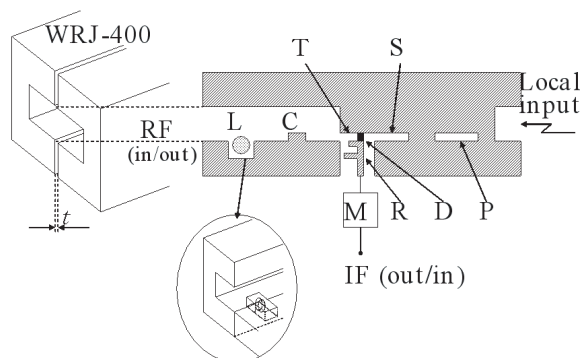


Figure 1: The structure of the E-plane circuit Down/Up converter with inductive strips.

Table 1 summarizes the frequency relation of the down/up converters designed for the downlink and uplink of a cable-television bidirectional wireless transmission system.

Table 1: The frequency relation of the Down/Up converter.

	Down converter	Up converter
Local freq.	35.6 GHz	35.6 GHz
IF freq.	5.17~5.87 GHz (700 MHz)	6.49~6.535 GHz (45 MHz)
RF freq.	40.77~41.47 GHz (700 MHz)	42.09~42.135 GHz (45 MHz)

Figure 2 shows experimental results. Fig. 2(a) shows the characteristics of the down converter and Fig. 2(b) the characteristics of the up converter (including IF-matching-circuit M). Measurements were performed with the input local level at +18 dBm and input RF/IF signal level at -15 dBm.

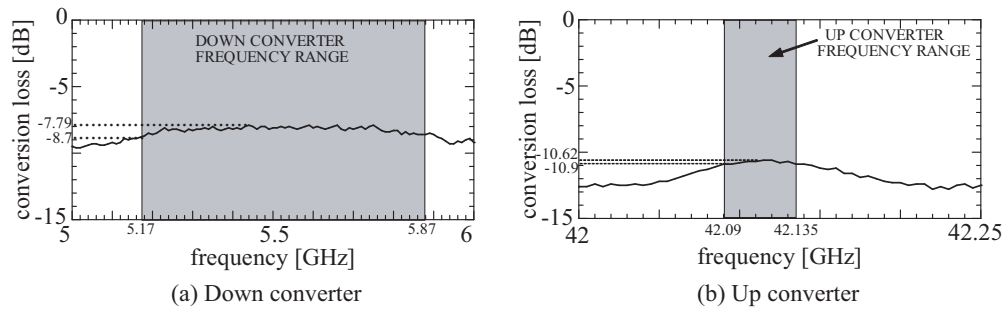


Figure 2: Conversion loss of the Down/Up converter.

The conversion loss of the down converter was found to be 7.79–8.70 dB and that of the up converter 10.6–10.9 dB. The greater loss of the latter can be explained as follows. Back impedance of the IF terminal is low at  $17\ \Omega$ , and though IF-matching-circuit M was designed to convert it to  $50\ \Omega$ , matching could not be achieved across the entire band.

# An Experimental Study of Improved Low Pass Filter Using Post-wall Grounding Configuration

Ka Sing Lim and Manimaran Nagalingam

Faculty of Engineering, Multimedia University, Jalan Multimedia, 63100 Cyberjaya, Selangor, Malaysia

**Abstract**— In this paper, an improved Post-Wall Stepped-Impedance Low Pass Filter (PWSILPF) is presented with a maximally flat response and a cut-off frequency of 2.5 GHz. The proposed PWSILPF has flat pass band from 0 Hz to 2.5 GHz with better overall performance. An additional post-wall grounding is configured as an improvement technique to minimize the parasitic capacitance effect and to ensure the feasibility of using FR4 in microwave circuit design. The hardware is constructed based on simulated result and the performance of the filter is analyzed using Vector Network Analyzer (VNA).

The proposed filter of PWSILPF utilizes the distributed element from the microstrip line and post-wall grounding surrounding the circuit board. It is more flexible to be designed, as it can change the geometry of each section according to desired characteristics [1]. Fig. 1 shows the constructed low pass filter using conventional grounding method and its measured result is used as a reference for comparison with the proposed PWSILPF design as shown in Fig. 2. It is possible to use this technique to improve the microwave filters design up to acceptable results. Simulated results in Fig. 3 show a flat pass band from DC up to 2.5 GHz. Comparison of the measured results of both constructed filters is shown in Fig. 4. The frequency response of constructed PWSILPF has a close agreement with the simulated result under perfect ground plane configuration. It is also shown that the frequency response of the proposed PWSILPF is able to minimize the parasitic capacitance effect on microstrip board and maintain its flat band response.

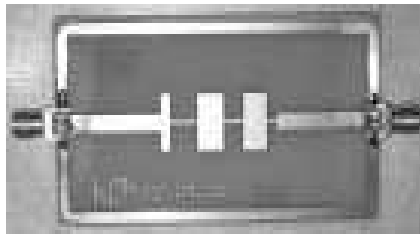


Figure 1: Filter design using conventional technique.

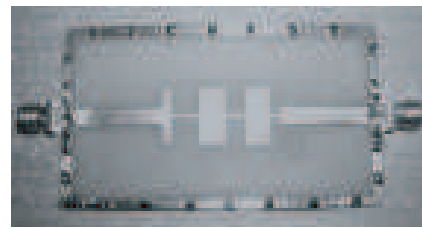


Figure 2: Filter design of proposed PWSILPF design.

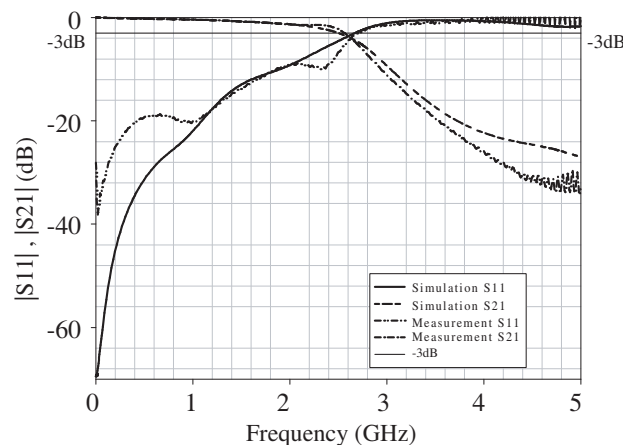


Figure 3: Simulated frequency response of designed LPF.

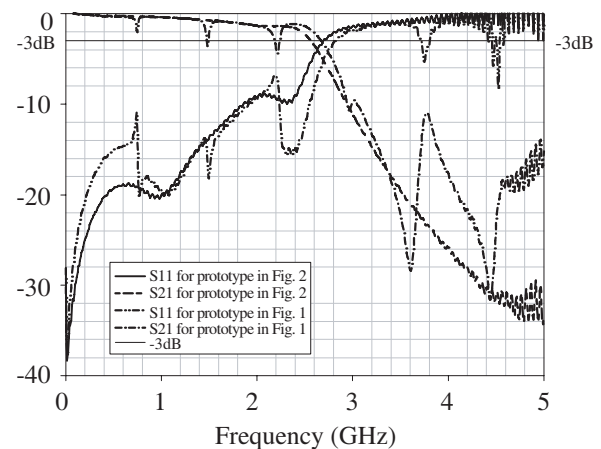


Figure 4: Comparison of measured frequency response.

## REFERENCES

1. Li, W. and J. Vandewege, "Practical design considerations on lumped element filters for microwave applications," *IEEE Electronics, Circuits and Systems. International Conference*, Vol. 1, 394–397, Dec. 2000.

## Use of Ground Plane Windows and Floating Conductors in Microstrip SIR Filters

M. C. Velázquez-Ahumada, Jesús Martel, and Francisco Medina  
Microwaves Group, University of Seville, Seville, Spain

**Abstract**— Microstrip filters for RF and microwave circuits operating in the low end of the microwave spectrum have been a popular topic of research during the last years due to increasing demands of wireless systems. Miniaturization has been a principal issue since relatively large wavelength yields large circuits if conventional distributed designs are used [1]. Stepped impedance resonators (SIR) have been exploited during the last years due to their unique properties that make them very useful to improve spurious response of microstrip filters and to reduce the size of otherwise relatively large coupled open loop resonators [2]. In this contribution we propose a new class of miniaturized SIR for bandpass microwave and RF filter design. These resonators combine the concept of SIR resonator with defected ground structures (DGS). Both size and filter response have been improved by using ground plane windows and floating conductors in the backside of the substrate where folded SIR have been printed. The use of ground plane windows increases the characteristic impedance of the inductive regions of the resonators. Therefore, the resonator and the whole filter size is reduced with respect to the conventional implementation. But more significantly, the ground plane windows open a new way of coupling between the resonators and, consequently, the bandwidth of the designed filters can be increased. Another advantage of the proposed structures is that the out-of-band rejection level and bandwidth (between the first and second transmission bands of the filter) is improved when the ground plane portion below the capacitive region of the resonators is substituted by a floating conducting patch. Due to size reduction, the individual resonators are electrically small around the transmission band of the filter. This simplifies design because the resonator can be considered a quasi-lumped element and simple quasi-static concepts can be directly applied in the design process. A detailed study of the individual resonator response and comparison with other available alternative structures is presented. Experimental characterization of single resonators as well as measurements of some filters will be provided in the presentation to illustrate the behavior of the new components.

### REFERENCES

1. Hong, J. S. and M. J. Lancaster, *Microstrip Filters for RF/Microwave Applications*, Wiley, New York, 2001.
2. Gu, J., F. Zhang, C. Wang, Z. Zhang, M. Qi, and X. Sun, "Miniaturization and harmonic suppression open-loop resonator bandpass filter with capacitive terminations," *IEEE International Microwave Symposium*, 373–376, San Francisco, CA, USA, 2006.

## A Millimeter-wave Sampled-Line Six-port Reflectometer at 300 GHz

Guoguang Wu<sup>1</sup>, Zhiyang Liu<sup>2</sup>, Stephen H. Jones<sup>3</sup>, and Robert M. Weikle, II<sup>1</sup>

<sup>1</sup>University of Virginia, Charlottesville, VA 22904, USA

<sup>2</sup>M/A-COM, Lowell, MA 01853, USA

<sup>3</sup>Virginia Diodes, Inc., Charlottesville, VA 22902, USA

**Abstract**— The six-port reflectometer has long been recognized as an attractive approach to scattering parameter measurement systems due to the relative simplicity of its architecture as well as its potentially low cost [1]. In particular, the six-port holds much promise for realizing network analyzers operating well into the submillimeter part of the spectrum. In this work, the design of a submillimeter-wave sampled-line six-port reflectometer is described and a prototype version of the instrument is applied to characterize a number of different devices under test (DUT). Measurement results from the six-port reflectometer are compared to those performed with a commercial network analyzer (Agilent 8510C with millimeter-wave extension modules from Oleson Microwave Laboratories) as well as with theoretical results based on electromagnetic simulation. The basic measurement system consists of a frequency multiplier chain manufactured by Virginia Diodes, Inc. that provides power over the 280 GHz to 325 GHz band. The reflectometer consists of a section of WR-2.8 waveguide and set of three probes feeding zero-bias Schottky diodes. The voltage response of the diodes are read with a Keithley multimeter and processed by a laptop computer via a USB-GPIB interface.

The devices under test (DUT) include a sliding load, sliding short-circuit, a set of fixed offset shorts, and a 90-degree-rotated waveguide terminated with an offset short. The reflection coefficient (magnitude and phase) are found through calibration of the instrument by using a flush short-circuit and seven offset shorts to implement the 6-port-to-4-port reduction originally described by Engen. Following this, a short-circuit, 2 offset shorts and an open-ended waveguide are used to complete the calibration. Using the calibration procedure outlined above, a number of standard devices are measured, including a sliding load, a variety of offset shorts, and a 90-degree-rotated offset short. Results obtained from these measurements are assessed by comparison with theoretical calculations based on electromagnetic theory. It was found that the six-port reflectometer measurements are in good agreement with these theoretical calculations and provide results that are approximately as accurate as those obtained with the Agilent 8510C with Oleson Microwave extension modules.

### REFERENCES

1. Engen, G. F., "The six-port reflectometer: An alternative network analyzer," *IEEE Trans. Microwave Theory Tech.*, Vol. 25, 1075–1080, 1977.



## Parallel-coupled Microstrip Filter with Super Wide Stopband

Shry-Sann Liao, Shih-Yi Yuan, Pou-Tou Sun, Yi-Hao Chang, and Hung-Liang Lin

RF/MW Circuits Design Laboratory, Department of Communication Engineering  
Feng-Chia University, 100, Wen-Hua Rd., Taichung, Taiwan 407, R.O.C.

**Abstract**— Bandpass filters play an important rule in satellite and mobile communication system to pick out wanted signal. Wide stopband and high selectively are usually required to enhance the overall system performance. The parallel-coupled microstrip filter has been used due to its planar structure, ease of synthesis method, and the low cost. But as we know it suffers from the spurious responses. Many methods have been proposed to overcome these problem [1–3]. [1] used over-coupled end stages to approach  $2f_0$  suppression. Half length open ended resonator and discontinuities and reposition of the coupling section are proposed to suppress 3-order passband in [2]. Stepped impedance resonator (SIR) and tapped line technology are another ways to have wide stopband [3]. In this work, we proposed one filter which is center frequency at 900 MHz, and it has super wide stopband with  $6f_0$  harmonic suppression and high selectivity.

This filter was designed by traditional parallel coupled microstrip bandpass filter, over coupled effect and for the wide harmonic suppression below 20 dB at least the four times passband frequency. And then we change the position of tapped-line at input/output and coupling length. Based on that, the filters can suppression more than six times of spurious responses shown in Fig. 1. All the simulated S-parameters of this filter are obtained from the full-wave Sonnet em simulator. The implemented circuit in this paper are fabricated on the FR4 substrate ( $\epsilon_r = 4.7$ ,  $\tan \delta = 0.022$ , thickness = 0.8 mm, and the metal thickness = 0.02 mm) and is measured by Agilent 8510C.

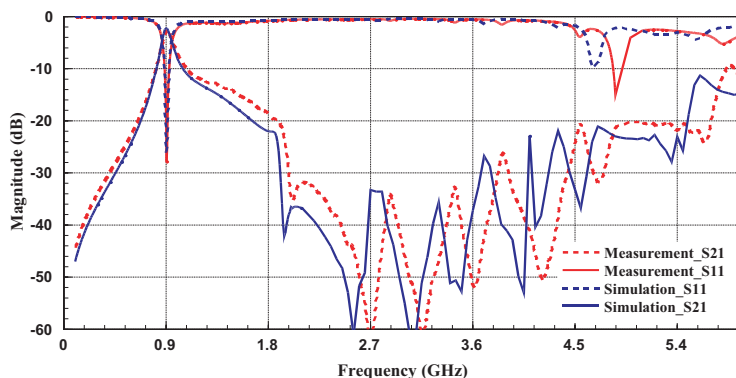


Figure 1: Measurement and Simulation of S-parameterer.

### REFERENCES

1. Kuo, J.-T., S.-P. Chen, and M. Jiang, "Parallel-coupled microstrip filters with over-coupled end stages for suppression of spurious responses," *Microwave and Wireless Components Letters, IEEE* [see also *IEEE Microwave and Guided Wave Letters*], Vol. 13, 440–442, 2003.
2. Hong, S. and K. Chang, "A parallel-coupled microstrip bandpass filter with suppression of both the 2nd and the 3rd harmonic responses," *Microwave Symposium Digest*, 365–368, June 2006.
3. Kuo, J.-T. and E. Shih, "Stepped impedance resonator bandpass filters with tunable transmission zeros and its application to wide stopband design," *Microwave Symposium Digest IEEE MTT-S International*, 1613–1616, June 2002.

# Design and Optimization of Microstrip Interdigital Bandpass Filters with Impedance Matching

Homayoon Oraizi, Nima Azadi-Tinat, and Shahrokh Saeedi

Iran University of Science and Technology, Narmak, Tehran 16846-13114, Iran

**Abstract**— A least square based method is developed for the design and optimization of microstrip interdigital bandpass filters. The  $N$  coupled transmission line theory is employed to take into account the couplings among adjacent and nonadjacent conducting strips. The algorithm also incorporates the load and source impedance matching. The minimization of error function determines the length, width and spacing of strips.

**Introduction:** Interdigital filters were fabricated by inserting metallic round rods in rectangular cavities [1], and were fabricated to obtain better than 10 percent bandwidth. Since that time, different types of interdigital filters have been devised and used in microwave circuits. Microstrip interdigital filters have also been developed, but their design procedures have usually ignored the significant nonadjacent resonant strip couplings. As reference [2] indicated that the coupling among consecutive strips on nonhomogeneous microstrip structures decreases gradually rather than abruptly, the nonadjacent strip couplings [3] need to be considered in the design. Furthermore, the  $N$  different phase velocities on the  $N$  coupled strips need to be included in the design procedure. Accordingly, in this paper a numerical procedure based on the method of least squares is proposed for the design of the interdigital bandpass filters, which utilizes the theory of  $N$  coupled transmission lines [4]. The adjacent and nonadjacent couplings among strip lines, their distinct phase velocities, and dispersion relations are readily incorporated in the design method. Furthermore, impedance matching of load and source impedances over a frequency bandwidth is also incorporated into the design algorithm.

**Numerical Procedure:** An error function is constructed for the specified insertion loss in the lower and upper stopbands, transition bands and the passband, as shown in Fig. 2.

$$e = \sum_{k=1}^{K_{SL}} w_k (IL_k - ILSB_k)^2 + \sum_{k=K_{PL}}^{K_{PU}} w_k (IL_k - ILPB_k)^2 + \sum_{k=K_{SU}}^K w_k (IL_k - ILSB_k)^2$$

where  $IL_k = -20 \log |s_{21}|_k$  is the insertion loss calculated at the  $k$ th frequency and  $ILSB$  and  $ILPB$  are their specified values in the stopband and passband, respectively. The frequency band is divided into  $K$  discrete frequencies and  $w_k$  is the weighting function.

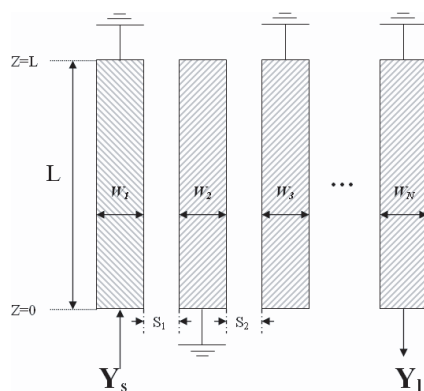


Figure 1: Circuit model of the narrow band microstrip interdigital filter.

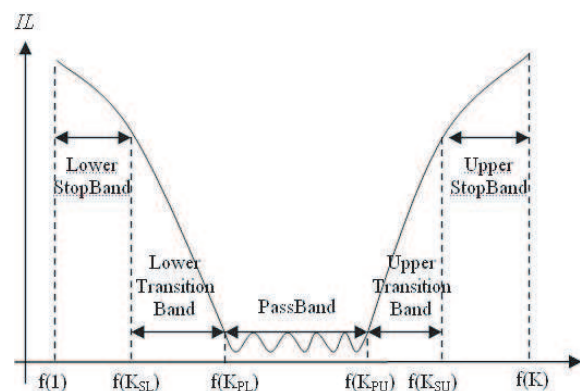


Figure 2: Frequency response of a bandpass interdigital filter.

**Implementation:** A sample filter is designed and optimized by the proposed method. The filter is fabricated and its performance is measured and compared with that of Microwave Office simulation software and that computed by the proposed method in Fig. 3.

The characteristics of the interdigital bandpass filter are: Filter degree is three or five microstrip lines, center frequency 2 GHz in the range 1 to 3 GHz,  $K = 300$  for 300 discrete frequencies for the error function, frequency bandwidth in the passband is 120 MHz (or 6%),  $w_k = 1$ , input and output impedances equal to  $50 \Omega$ .

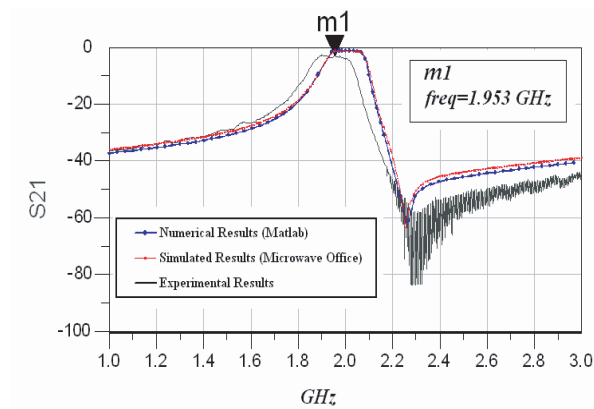


Figure 3: Circuit model of the narrow band microstrip interdigital filter.

#### REFERENCES

1. Matthaei, G., L. Young, and E. M. T. Jones, *Microwave Filters, Impedance-Matching Networks, and Coupling Structures*, 614–647, Artech House, Boston, Nov. 1985.
2. Milligan, T. A., “Dimensions of microstrip coupled lines and interdigital structure,” *IEEE Trans. Microwave Theory Tech.*, Vol. 25, No. 5, 405–410, May 1977.
3. Gentili, G. and M. Salazar-Palma, “The definition and computation of modal characteristic impedance in quasi-TEM coupled transmission lines,” *IEEE Trans. Microwave Theory Tech.*, Vol. 43, No. 2, 338–343, Feb. 1995.
4. Tripathi, V. K., “Asymmetric coupled transmission lines in an inhomogeneous medium,” *IEEE Trans. Microwave Theory Tech.*, Vol. 23, No. 9, Sept. 1975.



# Session 2P6b

## Mobile Antennas for Communication

<p><b>Simple Multiband Antenna for Mobile Phone Application Based on a Dual-arm Monopole Structure</b>  <i>David Delaune (Fujikura Ltd., Japan); Ning Guan (Fujikura Ltd., Japan); Koichi Ito (Chiba University, Japan);</i> .....</p> <p><b>Antennas Made of Transparent Conductive Films</b>  <i>Ning Guan (Fujikura Ltd., Japan); Hiroataka Furuya (Fujikura Ltd., Japan); David Delaune (Fujikura Ltd., Japan); Koichi Ito (Chiba University, Japan);</i> .....</p> <p><b>A 35-GHz Quasi-Yagi Antenna on Silicon Substrate</b>  <i>Jun Liao (Rensselaer Polytechnic Institute, USA); Zhaoran (Rena) Huang (Rensselaer Polytechnic Institute, USA); Kenneth Connor (Rensselaer Polytechnic Institute, USA);</i> .....</p> <p><b>Application of Artificial Dielectric Material for a PIFA Antenna</b>  <i>Jwo-Shiun Sun (National Taipei University of Technology, Taiwan); Guan-Yu Chen (National Taipei University of Technology, Taiwan); Cheng-Hung Lin (National Taiwan Ocean University, Taiwan); Kwong-Kau Tiong (National Taiwan Ocean University, Taiwan); Y. D. Chen (High Tech Computer Corp. (HTC), Taiwan);</i> .....</p> <p><b>Bandwidth Enhancement of Balanced Folded Loop Antenna Design for Mobile Handsets Using Genetic Algorithms</b>  <i>Dawei Zhou (Bradford University, UK); Raed A. Abd-Alhameed (Bradford University, UK); Peter S. Excell (Bradford University, UK);</i> .....</p> <p><b>Design Considerations of MIMO Antennas for Mobile Phones</b>  <i>Muhammad Usman (University of Bradford, UK); Raed A. Abd-Alhameed (University of Bradford, UK); Peter S. Excell (University of Bradford, UK);</i> .....</p> <p><b>A Simple Antenna Design of Implantable RFID based on EFAB Technology</b>  <i>Donghui Guo (Xiamen University, China); Huajun Chen (Xiamen University, China); L. L. Cheng (City University of Hong Kong, China);</i> .....</p>	<p>510</p> <p>512</p> <p>513</p> <p>514</p> <p>516</p> <p>518</p> <p>520</p>
--	--

# Simple Multiband Antenna for Mobile Phone Application Based on a Dual-arm Monopole Structure

David Delaune<sup>1</sup>, Ning Guan<sup>1</sup>, and Koichi Ito<sup>2</sup>

<sup>1</sup>Optics and Electronics Laboratory, Fujikura Ltd., Japan

<sup>2</sup>Department of Medical System Engineering, Chiba University, Japan

## Abstract—

**Introduction:** Recently, multi-band operation in mobile phones tends to become popular especially for quad-band or penta-band operation [1]. For the quad-band antenna design, the targeted bands are the GSM band (880–960 MHz) and the DCS/PCS/UMTS band (1710–2170 MHz) [2]. To meet the above-mentioned requirement, a low-profile monopole antenna is a promising antenna design. In this paper, a printed monopole antenna with a very low profile as compared to others (4 mm only in height), protruded from the top edge of the ground plane is proposed aimed at multiband application in the mobile phone including the GPS band. The proposed antenna has been fabricated and results match well with the simulated ones.

**Composition:** The configuration of the proposed antenna is shown in Fig. 1. The antenna is located above the top edge of the system ground plane ( $40 \times 70 \text{ mm}^2$ ) with a small distance of 3 mm between the lower part of the antenna and the ground plane. The antenna is composed of two branches formed by a longer resonant strip (strip 1) and a shorter resonant strip (strip 2) located near a matching board used to increase the bandwidth. Strip 1 generates a fundamental mode at 925 MHz and a second mode at about 1900 MHz. This lower band is used for the GSM operation. Strip 2 generates a fundamental mode at about 2100 MHz, which overlaps with the second mode of strip 1 to form a wide band hence enabling the coverage of GPS/DCS/PCS/Bluetooth bands.

The matching board results in good impedance matching for strip 2 thus leading to an improved bandwidth of the upper band.

**Performances:** Figure 2 shows the voltage standing wave ratio (VSWR) for the antenna. The obtained impedance bandwidths of the lower and upper bands are about 100 MHz for a VSWR of 3.5 (or  $S_{11} < -5.1 \text{ dB}$ ) and 1130 MHz for a VSWR of 2.8 (or  $S_{11} < -6.5 \text{ dB}$ ), respectively.

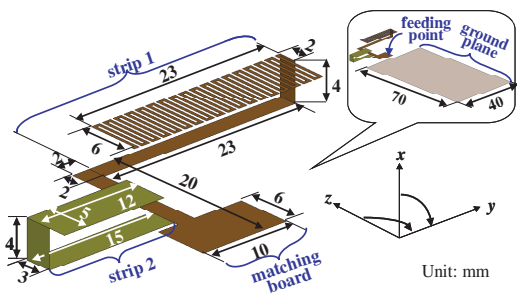


Figure 1: Composition of the antenna.

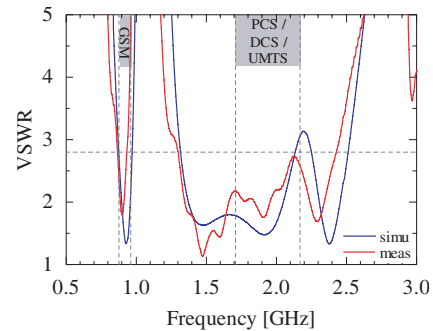


Figure 2: VSWR of the proposed model.

Radiation characteristics of the antenna (not shown here for brevity) are also studied. Almost omni-directional radiation patterns are observed in the  $xy$  plane and figure-of-eight shaped radiation patterns are observed in the other planes. The antenna peak gains are experimentally 0.1 dBi in the lower band and 0.9 dBi in the upper band.

**Conclusions:** A printed monopole antenna for quad-band operation in the mobile phone including GPS has been proposed and studied. The antenna occupies a volume of  $40 \times 20 \times 4 \text{ mm}^3$  with a very low height as compared to others, yet it can cover two wide bands centered at about 925 MHz and 2100 MHz to realize GSM/GPS/DCS/PCS operation. Good radiation characteristics of the antenna over the operating bands have also been observed. The proposed antenna is very promising for application in the mobile phone as an internal antenna for quad-band operation, which furthermore includes a GPS function.

**REFERENCES**

1. Wong, K. L., *Planar Antennas for Wireless Communications*, John Wiley & Sons, New York, USA, 2003.
2. Lee, H.-J., et al., "The compact quad-band planar internal antenna for mobile handsets," *Proceedings of the 2007 IEEE Antennas and Propagation International Symposium*, 2045–2048, Hawaii, USA, June 2007.

## Antennas Made of Transparent Conductive Films

N. Guan<sup>1</sup>, H. Furuya<sup>1</sup>, D. Delaune<sup>1</sup>, and K. Ito<sup>2</sup>

<sup>1</sup>Optics and Electronics Laboratory, Fujikura Ltd., Japan

<sup>2</sup>Department of Medical System Engineering, Chiba University, Japan

**Abstract**— As mobile wireless communications have progressed drastically in recent years, mobile terminals are becoming smaller and smaller, and miniaturization of the antennas installed in mobile devices is required accordingly. The designing of antennas for small mobile devices is becoming much more difficult not only because the space is getting limited but also because other electrical parts influence the performance of the antennas. Transparent conductive films, such as indium tin oxide (ITO) and fluorine-doped tin oxide films, allow the transmission of electric currents while retaining the optically transparency [1]. Applying the transparent conductive films to construct antennas is a good alternative to meet the space requirement because the transparent antennas can be installed on the surface or the display window of the mobile devices without much visible design problem. The interference from the other electric parts can also be suppressed thanks to the location of the antenna.

In this paper, two antennas widely used for small mobile devices are investigated: one is a monopole antenna that consists of one-half of a bow-tie dipole antenna [2] and another a planar inverted-F antenna (PIFA) that consists of a rectangular patch. Considering from the designing point of view, we made the whole monopole antenna by the transparent conductive film but only the patch of the PIFA by the film. The antennas are designed to work at 2.4 GHz and their performances are compared with each other. The antennas are studied experimentally and theoretically. A wire-grid model based on the moment method is applied for the numerical analysis. The resistance of the transparent film is taken into account by directly loading a resistance on every discretized element. The theory agrees with the experiment very well.

A fabricated ITO film with a sheet resistivity of  $1 \Omega/\text{sq}$  has a transmittance at a wavelength of 550 nm as high as 72%. By using this film, the monopole antenna shows a gain of  $-0.47 \text{ dB}$  and a radiation efficiency of 89% at 2.4 GHz and the PIFA does a gain of  $-1.2 \text{ dB}$  and a radiation efficiency of 76% at the same frequency, respect to a copper antenna with the same dimension, respectively. As the film becomes thinner, the transparency increases but the sheet resistivity increases too and this makes the performance of the antennas deteriorate. It is shown that while a gain lowering rate is  $0.20 \text{ dB}/\Omega/\text{sq}$  and an efficiency lowering rate is  $2.7\%/ \Omega/\text{sq}$  for the monopole antenna, the gain lowering rate is  $0.47 \text{ dB}/\Omega/\text{sq}$  and the efficiency lowering rate is  $4.5\%/ \Omega/\text{sq}$  for the PIFA. The resistance of the film has more serious influence on the PIFA than on the monopole antenna because the PIFA behaves like a resonator and hence excites large current distribution on the patch. Nevertheless, if we use an ITO film with sufficient small resistivity, we can obtain a radiation performance good enough for the practical applications.

It is expected that the transparent films can be also applied for other types of antennas, such as slot antenna, loop antenna, patch antenna and so on. It is hoped that the transparent antennas can provide a useful means for the antennas integration when employed in mobile terminals in the near future.

### REFERENCES

1. Kawashima, T., H. Matsui, and T. Tanabe, "New transparent conductive films: FTO coated ITO," *Thin Solid Films*, Vol. 445, No. 2, 241–244, 2003.
2. Guan, N., H. Furuya, D. Delaune, and K. Ito, "Radiation efficiency of monopole antenna made of a transparent conductive film," *Proc. 2007 IEEE AP-S Int. Symp.*, 221–224, Hawaii, USA, June 2007.



## A 35-GHz Quasi-Yagi Antenna on Silicon Substrate

Jun Liao, Z. Rena Huang, and Kenneth Connor

Department of Electrical, Computer, and System Engineering, Rensselaer Polytechnic Institute  
110 8th St. Troy, NY 12180, USA

**Abstract**— The atmosphere attenuation reaches a local minimum at the electromagnetic wave transmission window of  $\sim 35$  GHz. This band is very attractive because of its potential bandwidths of up to several GHz, which offers the possibility of wireless communication at several gigabits per second according to the Nyquist sampling theorem. Thus, it is of great interest to develop antennas that operate at 35 GHz for various applications.

The CMOS technology for a voltage-controlled oscillator and amplifier at tens of gigahertz has already been developed. In this paper, we will present our design of a quasi-Yagi antenna with a dual split director on silicon substrate operating at 35 GHz. The planar quasi-Yagi antenna has demonstrated high directivity, which makes it suitable for integration with other elements to form on-chip RF CMOS transceivers. In addition, radiation at millimeter wavelength permits the integration of multiple antennas in an array on one chip to achieve improved efficiency of a wireless system.

The radiation characteristics of a quasi-Yagi antenna on a high dielectric substrate are affected by the surface wave excited in the substrate. The induced current in the director and reflector dramatically affect the gain and radiation pattern of antenna. In our design, we place a number of split directors in the forward radiation direction of the antenna to improve the gain and the front-to-back ratio. The optimization of antenna parameters is modeled finite element method using CST microwave studio. Different from the antenna on Duroid substrate at K band, the antenna on silicon substrate suffers extremely high loss at high operation frequency. In order to reduce the loss in the Si substrate, a silicon oxide layer is used on the substrate. Full wave analysis is employed to calculate the loss of the microstrip and the coplanar strip line. Both frequency independent dielectric loss and frequency dependent conductor loss are evaluated.

With our design and optimization, a high directivity, broadband planar antenna on silicon substrate for 35 GHz application can be achieved. This antenna is compatible with CMOS technology and will be a key building block of monolithic microwave integrated circuits (MMIC) for future wireless applications.

## Application of Artificial Dielectric Material for a PIFA Antenna

Jwo-Shiun Sun<sup>1</sup>, Guan-Yu Chen<sup>1</sup>, Cheng-Hung Lin<sup>2</sup>, Kwong-Kau Tiong<sup>2</sup>, and Y. D. Chen<sup>3</sup>

<sup>1</sup>Department of Electronic Engineering, National Taipei University of Technology, Taiwan

<sup>2</sup>Department of Electrical Engineering, National Taiwan Ocean University, Taiwan

<sup>3</sup>Antenna and EMC Laboratory, High Tech Computer Corp. (HTC), Taiwan

**Abstract**— Artificial materials of periodic dielectrics which exhibit electromagnetic band-gap (EBG) performance have been proposed and applied on a planar inverted-F antenna (PIFA) design in this paper. The artificial defected dielectric material has some useful characteristics such as harmonic rejection, band suppression and surface wave suppression. A three-dimensionally periodic dielectric structure with a compact and low profile electromagnetic band gap material is presented. The artificial dielectric material (ADM) enhances radiation performance, bandwidth, radiation gain and efficiency of the designed antenna.

In one embodiment of the implementation, the ADM substrate for a PIFA antenna comprises the frequency selective material. The general approach to reduce an antenna's size is to load the antenna with dielectric material. The ADM is better than the traditional uniform dielectric material with its good electromagnetic effects and easy integration with low profile antenna. Fig. 1 is the proposed ADM structure. Fig. 2 is a designed PIFA with an ADM structure. Fig. 3 shows the comparison data in between PIFA with ADM and a traditional PIFA.

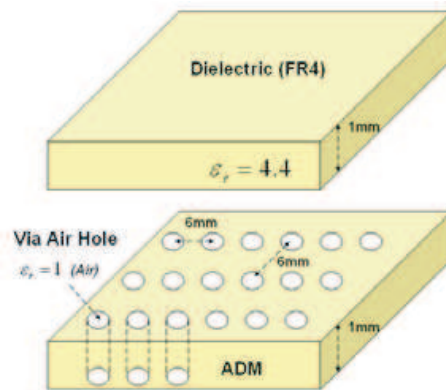


Figure 1: The proposed ADM structure.

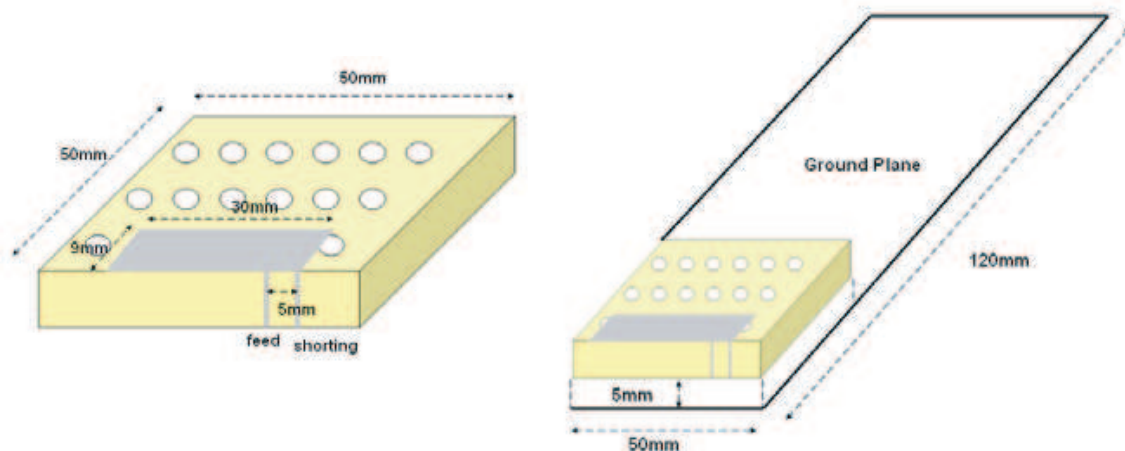


Figure 2: A designed PIFA with an ADM structure.

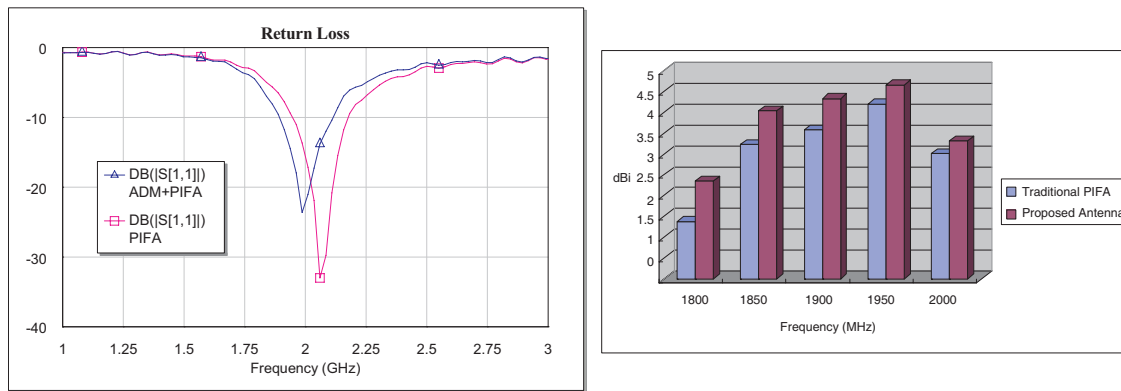


Figure 3: Comparisons of an ADM PIFA and a traditional PIFA.

The ADM applied for a PIFA antenna radiator has been developed. This designed antenna covers WCDMA and UMTS band from 1900 MHz to 2200 MHz. Evidently, it should be useful for many wireless applications.

# Bandwidth Enhancement of Balanced Folded Loop Antenna Design for Mobile Handsets Using Genetic Algorithms

D. Zhou, R. A. Abd-Alhameed, and P. S. Excell

Mobile and Satellite Communications Research Centre, University of Bradford  
Richmond Road, Bradford, West Yorkshire, BD7 1DP, UK

**Abstract**— In this paper, a simple folded loop antenna (FLA) for handsets with relatively wideband impedance, designed and optimized using genetic algorithms (GA). The geometry of proposed FLA was adopted from a previous work [1] (see Fig. 1) and applied here for this study due to its simple structure for the mobile antenna applications. The FLA antenna configuration dimensions used were optimized and evaluated using GA in collaboration with NEC-2. The FLA was optimized with GA using real-valued chromosomes. The intended antenna was designed for GSM1800 applications (1710–1860 MHz). Performance of the randomly generated antenna samples was computed using NEC-2 and its result was compared with desired fitness using a cost function. The objective was to find the optimal solution that satisfies certain constraints including a specific antenna volume.

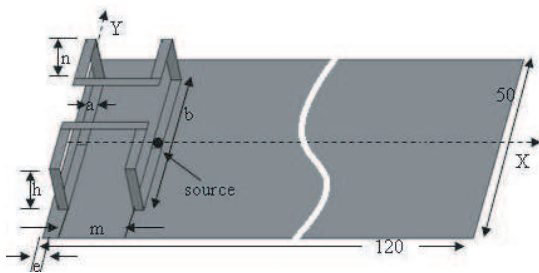


Figure 1: Geometry of the folded loop antenna with decreased-scaled ground plane.

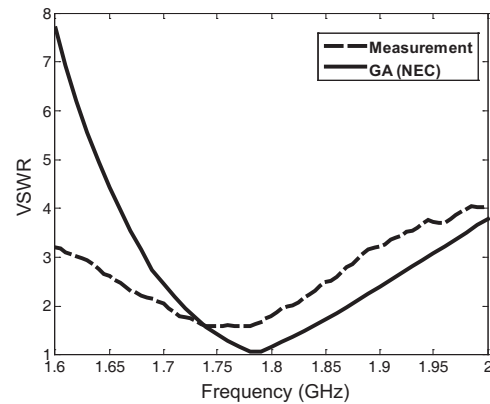


Figure 2: Comparison of the simulated return loss of the proposed antenna.

Configuration of optimal FLA antennas with excellent VSWR covering entirely required GSM1800 frequency bands was found within the maximum generation; antenna parameters of the best fit designs are shown in Table 1. A prototype antenna was tested to verify and validate the GA-optimized antenna structure and the comparative resultant VSWR are presented in Fig. 2. The measured data have shown good agreement with predicted ones. In addition, the performance of the proposed antenna with human effect is also investigated, in order to demonstrate the advantage of mobile antenna design using balanced technique.

Table 1: Summary of GA input parameters, antenna variables and best solutions.

GA parameters	FLA for GSM1800	
	Parameters (m)	Optimal (m)
Number of population size = 6	Wire radius (a) (0.0004–0.0008)	0.00074
Number of parameters = 7	FLA length (b) (0.03–0.04)	0.03978
Probability of mutation = 0.02	FLA height (h) (0.003–0.012)	0.01173
Maximum generation = 500	FLA arm length (n) (0.002–0.015)	0.008785
Number of possibilities = 32768	Parallel wires distance (m) (0.005–0.015)	0.01489
Ground plane size (120 × 50 mm)	FLA distance to GP edge (e) (0.0–0.002)	0.0008643
	Distance between FLA and GP ( $h_0$ ) (not shown in Fig. 1) (0.001–0.003)	0.001112

**REFERENCES**

1. Morishita, H., Y. Kim, Y. Koyanagi, and K. Fujimoto, "A folded loop antenna system for handsets," *IEEE AP-S Proc.*, Vol. 3, 440–443, July 2001.

## Design Considerations of MIMO Antennas for Mobile Phones

M. Usman, R. A. Abd-Alhameed, and P. S. Excell

Mobile and Satellite Communications Research Centre  
Richmond Road, University of Bradford, Bradford, West Yorkshire, BD7 1DP, UK

**Abstract**— MIMO for short, which stands for Multiple Input, Multiple Output systems are theoretically able to provide increased throughput, and better error performance than traditional systems [1, 2]. The particular aspect that is used by MIMO systems is called *Multi-Path* propagation [2]. This effect occurs when the radio signals sent from the transmitter bounce off intermediate objects before reaching the receiver. Some of these reflected signals may travel along entirely separate paths, and even reach the receiver at different times. Currently, there are a number of MIMO applications, development platforms, and tools that are showing great promise in the quest for wireless systems with higher bandwidth and greater capabilities. The major advantage of MIMO technology is the digital beam forming, which is now making its way out of research laboratories and into real-world applications with great speed.

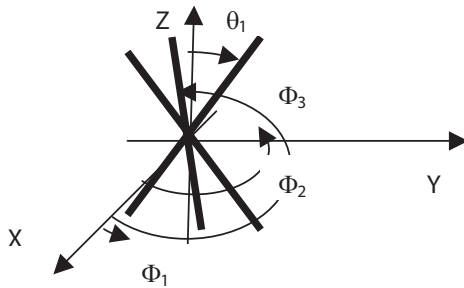


Figure 1: Basic antenna geometry.

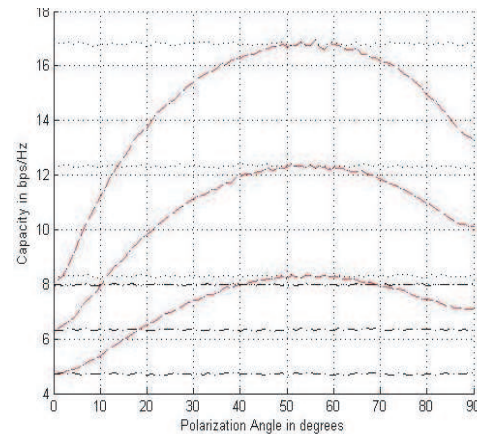


Figure 2: The channel capacity of  $3 \times 3$  MIMO system as oriented in Fig. 1 as a function of the polarization angle for different SNR starting from 10 dB, 15 dB and 20 dBs.

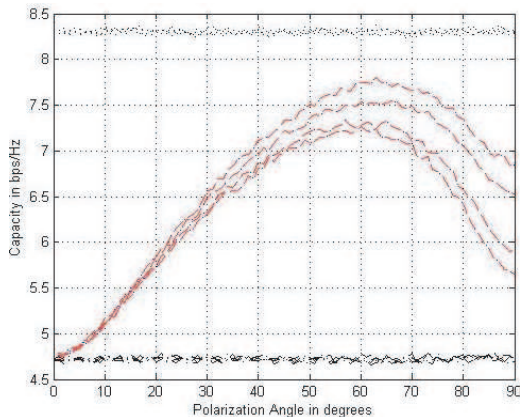


Figure 3: The channel capacity of  $3 \times 3$  MIMO system as oriented in Fig. 1 as a function of the polarization angle and azimuth Laplacian spectrum of  $\sigma_\phi$  (5, 10, 20, 30 degrees).

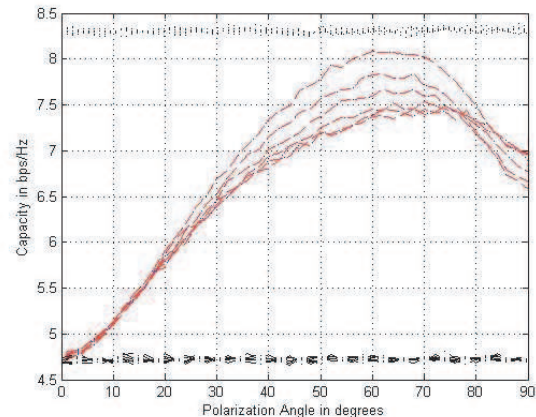


Figure 4: Similar to Fig. 3 except the Gaussian azimuth power spectrum was considered for different values of variance angles as  $\sigma_\phi$  (5, 10, 20, 30 degrees).

Spatial correlation using polarization issues for MIMO applications has great interest [4] since the size of the actual radiating elements can be reduced. This study has great advantages if a MIMO system needs to be implemented on a mobile handset.

This paper considers the spatial polarization technique and how this technique can improve the capacity of the system. A MIMO system of  $2 \times 2$  and  $3 \times 3$  elements are presented for implementations on mobile handsets. The system was discussed under Raleigh fading channel and the results were compared to linear or planer array antenna MIMO system. More over different types of power azimuth spectrums were taken under considerations for system evaluation. The antenna geometry samples shown in Fig. 1, where as several results are presented in Figs. 2 to 4. Gaussian and laplacian azimuth power spectrums shown in Figs. 3 and 4 were considered for their accuracy to much as possible the real practical problem implementation.

#### REFERENCES

1. Wallace, J. W. and M. A. Jensen, "Modeling the indoor MIMO wireless channel," *IEEE Trans. Antennas Propag.*, Vol. 50, No. 5, 591–599, May 2002.
2. Wallace, J. W., M. A. Jensen, A. L. Swindlehurst, and B. D. Jeffs, "Experimental characterization of the MIMO wireless channel: Data acquisition and analysis," *IEEE Trans. Wireless Commun.*, Vol. 2, No. 2, 335–343, Mar. 2003.
3. Gesbert, D., H. Bölcskei, D. A. Gore, and A. Paulraj, "Outdoor MIMO wireless channels: Model and performance prediction," *IEEE Trans. Commun.*, Vol. 50, No. 12, 1926–1934, Dec. 2002.
4. Dong, L., H. Choo, R. W. Heath, and H. Ling, "Simulation of MIMO channel capacity with antenna polarization diversity," *IEEE Transactions on Wireless Communications*, Vol. 4, No. 4, 1869–1873, July 2005.

## A Simple Antenna Design of Implantable RFID based on EFAB Technology

Donghui Guo<sup>1,2</sup>, Huajun Chen<sup>1</sup>, and L. L. Cheng<sup>3</sup>

<sup>1</sup>EDA Lab, Physics Department, Xiamen University, Fujian 361005, China

<sup>2</sup>Department of Electronic Engineering, Xiamen University, Fujian 361005, China

<sup>3</sup>Electronic Engineering Department, City University of Hong Kong, China

**Abstract**— This paper is to present a new technology for implantable RFID antenna design. As implantable RFID are popularly used as active devices for animal identification, bio-medical sensor etc. Size miniature and high working efficiency are the basic requirements for these implantable devices which cause no discomforts for a body. A new MEMS process called EFAB is introduced. The implantable RFID antenna design is based on the use of micro-coil. With EFAB design rules and parameters, the simulation results have shown that we can satisfy the requirements of implantable RFID antenna.



# Session 2P7

## RF Safety

<b>Informing the Public about EMF and Health: Scientists' Responsibility</b>	522
<i>Michael H. Repacholi (University of Rome "La Sapienza", Italy);</i> .....	
<b>Advances in RF Bioeffect Mechanisms</b>	523
<i>Asher R. Sheppard (Asher Sheppard Consulting, USA); Mays L. Swicord (Motorola Inc., USA);</i>	
<i>Quirino Balzano (University of Maryland, USA);</i> .....	
<b>Design and Achievement of a Stirring Mode Chamber for Animal Exposure</b>	525
<i>Tongning Wu (France Telecom RD, RESA/FACE, France); F. Lacroux (France Telecom RD,</i>	
<i>RESA/FACE, France); Y. Toutain (Antennessa-Satimo, France); O. Picon (Universite Paris-Est</i>	
<i>Marne-La-Vallee, France); Man-Fai Wong (France Telecom R and D, France); Joe Wiart (France</i>	
<i>Telecom R and D, France);</i> .....	
<b>Dependence of the Induced Current of the Liquid-type Human-body Equivalent Antenna on Its Height</b>	526
<i>Ally Y. Simba (National Institute of Information and Communications Technology, Japan);</i>	
<i>Yoshilide Takahashi (National Institute of Information and Communications Technology, Japan);</i>	
<i>Soichi Watanabe (National Institute of Information and Communications Technology, Japan);</i>	
<i>Takuji Arima (Tokyo University Agriculture and Technology, Japan); Toru Uno (Tokyo University</i>	
<i>of Agriculture and Technology, Japan);</i> .....	
<b>SAR of Wireless Communication Terminals Operated near the Human Body Using the Example of PCM-CIA Data Cards</b>	528
<i>Yi Zhou (University of Wuppertal, Germany); Joachim Streckert (University of Wuppertal, Germany);</i>	
<i>H. Ndoumbè Mbonjo Mbonjo (University of Wuppertal, Germany); Volkert Hansen (University of</i>	
<i>Wuppertal, Germany);</i> .....	
<b>Active Implantable Medical Devices (AIMD) and Radio Frequency (RF) Fields</b>	529
<i>Veronica Ivans (Medtronic CRDM, USA);</i> .....	
<b>An Estimate for Human Health that Influenced by Electromagnetic Wave from Mobile Phone and the Relay Stations</b>	530
<i>Hung-Yao Pai (Chienkuo Technology University, Taiwan);</i> .....	
<b>Cardiophysiological Studies on Patients with Dual-chamber Pacemaker During Exposure to RF-fields Emitted by Cellular Phones</b>	531
<i>Maila Hietanen (Finnish Institute of Occupational Health, Finland); Kari Tahvanainen (Finnish Insti-</i>	
<i>tute of Occupational Health, Finland); Juanita Nino (Finnish Institute of Occupational Health, Finland);</i>	
<i>Juha Hartikainen (Kuopio University Hospital, Finland); Antti Hedman (Kuopio University Hospital,</i>	
<i>Finland); Tom Kuusela (Turku University, ); Harri Lindholm (Finnish Institute of Occupational</i>	
<i>Health, Finland);</i> .....	
<b>Behavioral and Cognitive Effects of MW Electromagnetic Field Exposures Updated</b>	532
<i>Sheila A. Johnston (Independent Neuroscience Consultant, Ireland);</i> .....	
<b>RF Bioeffect Research to Address Human Safety Concerns</b>	534
<i>Chung-Kwang Chou (Motorola Labs, USA); Joe A. Elder (Motorola Florida Research Laboratories,</i>	
<i>USA);</i> .....	

## Informing the Public about EMF and Health: Scientists' Responsibility

Michael H. Repacholi

Department of Electronic Engineering, University of Rome "La Sapienza"

Via Eudossiana 18, Roma 00184, Italy

**Abstract**— Studies on possible health effects of exposure to electromagnetic fields have been ongoing since the early 1950's when RADARs were first used in the Second World War and the Korean War. Since this period over 6000 scientific studies have been published that relate to this topic. Within this large database of information there are studies claiming both positive and negative effects for the same end-points. For the general public, and many scientists, this presents a confusing situation that must be resolved using logical and well-established methodology.

To assess health risks from any physical, chemical or biological agent, the World Health Organization (WHO) and most national scientific review committees conduct a formal process of health risk assessment that relies on a weight-of-evidence approach. Following the rules for health risk assessment, recently described by WHO (see: [http://www.who.int/peh-emf/standards/EMF\\_standards\\_framework%5b1%5d.pdf](http://www.who.int/peh-emf/standards/EMF_standards_framework%5b1%5d.pdf), and in the Preamble of [http://www.who.int/peh-emf/publications/EHC\\_232.Preamble.pdf](http://www.who.int/peh-emf/publications/EHC_232.Preamble.pdf)), papers are assessed for quality and methodology, and the final health risks determined by weighing the evidence for and against there being a real effect. Criteria for this assessment have been used by WHO for over 50 years and have been shown to give reliable conclusions.

Once high quality reviews have been conducted, the general public needs to be informed, in easily understood language, so they can know whether an agent is a health hazard or not. While new research results may challenge the conclusions in such as review, it must be remembered that single studies cannot overturn the review conclusions; single studies must be judged along with similar studies to determine whether the weight-of-evidence changes.

It is the responsibility of scientists to be balanced when they inform the public. Topics like the health effects of EMF exposure, are sensitive issues and stir emotions among members of the general public, especially when effects on children are discussed.

This presentation will briefly discuss the health risk assessment process and how it affects scientists' responsibility to be balanced when informing the general public about EMF-induced health effects. Elements of a good risk communications strategy will also be discussed.

## Advances in RF Bioeffect Mechanisms

Asher R. Sheppard<sup>1</sup>, Mays L. Swicord<sup>2</sup>, and Quirino Balzano<sup>3</sup>

<sup>1</sup>Asher Sheppard Consulting, Redlands, CA 92373, USA

<sup>2</sup>Motorola Inc, Ft. Lauderdale, FL 33304, USA

<sup>3</sup>Department of Electrical and Computer Engineering, University of Maryland  
College Park, MD 20742, USA

**Abstract**— The complexity of interactions of electromagnetic fields up to  $10^{12}$  Hz with the ions, atoms and molecules of biological systems has given rise to a large number of established and speculative biophysical mechanisms applicable over a wide range of time and distance scales, field amplitudes, frequencies, and waveforms. This paper focuses on the physical principles that guide quantitative assessment of mechanisms applicable for exposures at or below the level of endogenous electric fields (generally, 1 to  $10^2$  V·m<sup>-1</sup>), with emphasis on conditions where temperature increases are insignificant ( $\ll 1$  K).

Experiment and theory demonstrate possible demodulation at membrane barriers for frequencies  $\lesssim 10$  MHz, but not at higher frequencies. Although signal levels somewhat below system noise can be detected, signal-to-noise ratios substantially less than 0.1 cannot be overcome by cooperativity, signal averaging, coherent detection, or by nonlinear dynamical systems. Sensory systems and possible effects on biological magnetite suggest paradigms for extreme sensitivity at lower frequencies, but there are no known radiofrequency analogues. At the molecular level, vibrational modes are so overdamped by water molecules that excitation of molecular modes below the far infrared cannot occur. However, below approximately 150 MHz, effects on the rate of certain chemical reactions can occur through radical-pair spin-coupled reactions [4].

The hypothesis of nonlinear effects triggered by demodulation of RF carriers amplitude modulated at extremely low frequencies suffers from the strong attenuation of any demodulated components. For an ideal hypothetical lossless detection process where the reverse biased nonlinear device acts as a lossless capacitor  $C$ , the attenuation of  $I$ , the current across the energy gap at a material discontinuity, is inversely proportional to the angular frequency  $\omega (= 2\pi f)$  of the signal, that is, the gap voltage  $V(\omega) = I/j\omega C$ . Consequently, in the example of a 900 MHz carrier amplitude-modulated at 16 Hz, a perfect square law detector would attenuate the signal power at base band in the proportion 16/900,000,000, or by about 77 dB. An attenuation of 90–100 dB is more likely because of leakage losses across the hypothesized potential barrier in living tissue. For attenuation of this order, a  $10^{-3}$  W (1 mW) RF carrier 100% amplitude modulated at 16 Hz can be expected to yield a demodulated signal power of no more than  $10^{-12}$  W at the 16-Hz baseband frequency.

Measurements showed that the ELF E-field detected by a nonlinear material from an incident ELF amplitude-modulated RF electric field of  $100$  V·m<sup>-1</sup> would be no more than approximately  $3 \times 10^{-3}$  V·m<sup>-1</sup> in the ELF band [1]. Consequently, the voltage across a  $10^{-8}$  m thick membrane could be no more than  $3 \times 10^{-11}$  V. This astonishingly small signal is approximately  $10^7$  times (140 dB) smaller than the low-frequency membrane voltage noise that limits physiologically significant events in excitable cells [2] and would be equally far below the cell membrane voltage noise of  $10^{-6}$  V·Hz<sup>-1/2</sup> observed by [3] in the band from 1 Hz to 104 Hz. These fundamental considerations show that for any practical exposure the demodulated ELF signal that may exist across the membrane would be irretrievably lost in membrane noise.

In conclusion, two RF mechanisms plausibly may affect biological matter under common exposure conditions. For frequencies below approximately 150 MHz, shifts in the rate of chemical reactions can be mediated by radical pairs and at all frequencies, dielectric and resistive heating can raise temperature and increase the entropy of the affected biological system.

### REFERENCES

1. Balzano, Q., V. Hodzic, R. W. Gammon, and C. C. Davis, "A doubly resonant cavity for detection of rf demodulation by living cells," *Bioelectromagnetics*, (in press), 2007.
2. Jacobson, G. A., K. Diba, A. Yaron-Jakoubovitch, Y. Oz, C. Koch, I. Segev, and Y. Yarom, "Subthreshold voltage noise of rat neocortical pyramidal neurones," *The Journal of Physiology Online*, Vol. 564, 145–160, 2005.
3. Roa, R. L. and W. F. Pickard, "The use of membrane electrical noise in the study of Characean electrophysiology," *J. Exp. Bot.*, Vol. 27, 460–472, 1976.

4. Woodward, J. R., C. R. Timmel, P. J. Hore, and K. A. McLauchlan, "Oscillating magnetic field effects on chemical reaction yields," *RIKEN Review*, Vol. 44, 79–81, 2002.

# Design and Achievement of a Stirring Mode Chamber for Animal Exposure

T. Wu<sup>1</sup>, F. Lacroux<sup>1</sup>, Y. Toutain<sup>2</sup>, O. Picon<sup>3</sup>, M. F. Wong<sup>1</sup>, and J. Wiart<sup>1</sup>

<sup>1</sup>France Télécom R & D, RESA/FACE, 38 rue du Général Leclerc  
92794 Issy-les-Moulineaux cedex 9, France

<sup>2</sup>Antennessa-Satimo, Bât. Ponant, Avenue la Pérouse 29280 Plouzané, France

<sup>3</sup>Université Paris-Est Marne-La-Vallée Cité Descartes 5  
bd Descartes Champs sur Marne 77454 MARNE LA VALLEE CEDEX 2, France

**Abstract**— There is a public concern about the effects of electromagnetic waves on health and in particular about children. WHO has recommended studies to analyse the possible effects on young biological system. Dealing with adult animal, previous studies have been conducted with constrained animal in exposure system (e.g., rat in a rocket). Another approach is to use a stirring mode chamber (SMC) that allows free movement of the animals.

The present communication presents simulation and measurement of an exposure system based on an SMC and having 6 antennas emitting randomly at 2450 MHz. In order to steer the mode several metallic slabs have been attached perpendicularly to the side wall and 3 corners have been modified to split the wave. In the simulation six  $\lambda/2$  dipole antennas have been located at about (to avoid symmetries) the centre of each face of the cavity. The six antennas are controlled by a programme which enables only one of them emit while others keep idle. The emitting cycle is random. The choice is made at random from the temporal view. All the methods mentioned above act actually as the function of stirrer in the reverberation chamber. It changes the boundary condition of the field distribution and generates different modes as much as possible.

The movement of the animal must not influence the power emitted by the antennas and must not change the exposure. By using non-uniform FDTD (Finite Difference In time domain), such influence has been studied. The impedance of the antenna versus the position of the animals has been analysed. The uniformity of the incident field as well as the uniformity of the exposure have been studied. Taking into account of these simulations, an SMC of about 1.5 m\*1.5 m\*1.5 m has been built. The simulation and the measurement results are compared.

# Dependence of the Induced Current of the Liquid-type Human-body Equivalent Antenna on Its Height

Ally Y. Simba<sup>1</sup>, Yoshihide Takahashi<sup>1,2</sup>, Soichi Watanabe<sup>1</sup>, Takuji Arima<sup>2</sup>, and Toru Uno<sup>2</sup>

<sup>1</sup>National Institute of Information and Communications Technology  
Koganei, Tokyo, Japan

<sup>2</sup>Graduate School of Engineering, Tokyo University Agriculture and Technology  
Koganei, Tokyo, Japan

## Abstract—

**Introduction:** At Very High Frequency (VHF) bands (30–300 MHz) the power absorption by the human body due to RF exposure reaches maximum values. This is because the whole-body resonant absorption frequencies lie within this region [1]. It is known that large current flows at the ankle if the human body stands on the ground at the whole-body resonant condition. The local SAR around the ankle (SAR<sub>ankle</sub>) can be estimated from the induced ankle current (I<sub>ankle</sub>) and the equivalent section area of the ankle (A<sub>ankle</sub>), i.e.,  $SAR_{ankle} = (I_{ankle}/A_{ankle})^2/\sigma$ . As a result, the induced ankle current is used as an additional exposure limit in the VHF bands in the ICNIRP and IEEE guidelines. The liquid-type human-body equivalent antenna that can be used for measuring these currents was proposed recently [2]. In order to optimize this antenna, we are currently carrying out numerical investigations of the antenna for the plane wave and near field exposure conditions and compares the results with those obtained from the anatomically Japanese models [3].

**Antenna Structure:** Figure 1 shows the structure of the human equivalent antenna, where  $h_a$  and  $h_l$  are the height of the acrylic board and tissue equivalent liquid. The  $h_l$  chosen in this

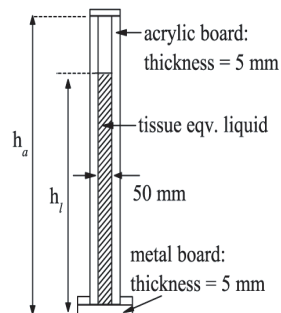


Figure 1: Liquid-type human body equivalent antenna.

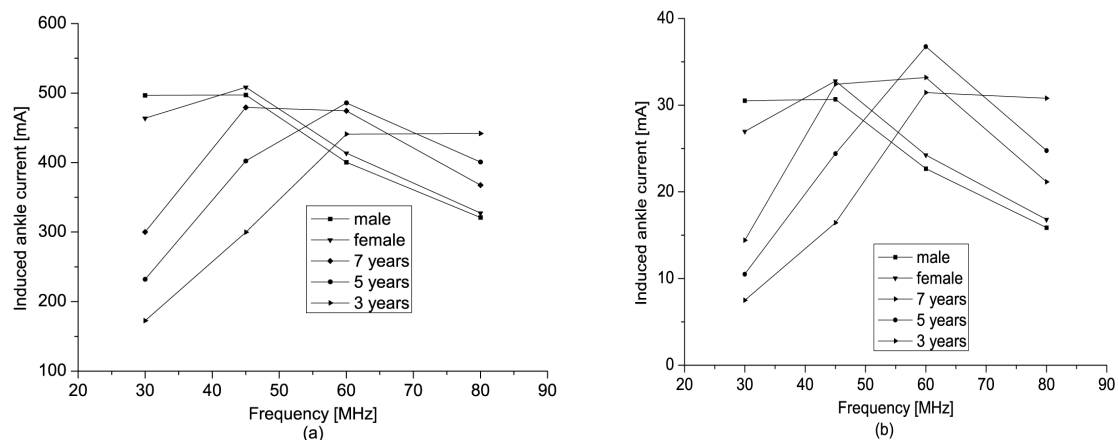


Figure 2: Induced ankle current of the human body equivalent antenna exposed to (a) plane wave with  $1 \text{ mW/cm}^2$ , (b) near field of monopole antenna with 1 W incident power.

work are 1730, 1610, 1205, 1040, and 880 mm corresponding to the heights of the Japanese adults male and female, 7, 5 and 3 years children models, respectively. The cross-sectional area of the antenna ( $2500 \text{ mm}^2$ ) is the same for all cases. For the near field exposure, the equivalent antenna is placed at a distance of 3 m from a monopole antenna having 1 W input power. In the case of plane wave exposure, the incident power density of  $1 \text{ mW/cm}^2$  is assumed. The calculations in this work are carried out using the FDTD technique.

**Results and Discussions:** The induced currents of the human body equivalent antenna for both plane wave and the near field exposure are shown in Fig. 2. Similar frequency characteristics appear between far and near field exposure. The results of the anatomically human model will be presented at the conference.

#### REFERENCES

1. Dimbylow, P. J., *Phys. Med. Biol.*, 2835–2846, 2002.
2. Takahashi, Y., et al., *Abstract of BEMS*, 292–295, 2007.
3. Nagaoka, T., et al., *Phys. Med. Biol.*, 2319–2329, 2003.

## SAR of Wireless Communication Terminals Operated near the Human Body Using the Example of PCMCIA Data Cards

Y. Zhou, J. Streckert, H. Ndoumbè Mbonjo Mbonjo, and V. Hansen  
University of Wuppertal, Germany

**Abstract**— Many wireless communication terminals are operated neither in direct contact to the human body nor far away, but often at distances of some centimetres to some decimetres. Typical examples are base stations of cordless phones, wireless LAN routers and network cards for PCs or notebooks.

The exposure of a user to the radiated electromagnetic fields of such devices is expressed by means of the SAR within the human body. The SAR distribution can only be determined from numerical calculations with help of electromagnetic field solvers using computer models for the human body as well as for the communication terminals. From these calculations, the two important characteristic parameters, whole body SAR and maximum localized SAR (10g avg.), can be derived and related to the recommended basic restrictions.

Four highly resolved anatomical body models derived from the data set of the 'visible human project' are used (adult and adolescent, both standing and sitting). The computer models for the terminals are developed with special attention to the antenna design. The models for the human body and for the terminal under test are embedded in a user-typical environment. Since the test volume is not too large, the related field problem is solved with the FDTD method implemented as a parallelized in-house code running on a multiprocessor system.

For the investigations the following 4 types of wireless communication terminals are selected: PCMCIA network card for operation of GPRS, UMTS and W-LAN, Bluetooth USB adapter, W-LAN router and DECT base station.

Detailed computer models of the terminals are developed and the radiation characteristics are calculated and measured in order to perform a mutual quality check between theory and practice.

The field and SAR distributions for several scenarios are computed at all relevant frequencies. Both, whole body and maximum localized SAR are derived.

The resulting SAR values are taken as a reference for the next step: The topology of the terminal and/or the antenna design is modified and the effect on the SAR is investigated. During this the quality of communication is checked by calculating the channel capacity for a SISO system.



# Active Implantable Medical Devices (AIMD) and Radio Frequency (RF) Fields

Veronica Ivans

Medtronic CRDM, 1015 Gramsie Road, MS Z110, St. Paul, MN 55126, USA

**Abstract**— This presentation intends to give an overview of implantable pacemakers and ICDs (implantable cardioverter defibrillators) operation, potential responses, technologies and international standards addressing safety in the presence of ElectroMagnetic Fields (EMF).

During the recent years there has been a rapid proliferation of emitters across the entire frequency spectrum, most notably in the RF range. New therapies using RF fields have been developed as well. On the other hand, there has been a demand for smaller size implantable pacemakers and ICDs, and more sophisticated systems (such more lead wires) with more sophisticated features that would allow physicians to provide and their patients to receive better health care and quality of life.

All the above factors combined have raised the visibility to potential interference from RF fields and its effects on patient safety.

Topics addressed:

1. Definitions of implantable cardiovascular systems
2. Operation of the following implantable systems: pacemakers, implantable cardioverter defibrillators (ICDs)
3. RF sources and impact on patient safety
  - Non-controlled environment:
    - Power lines
    - Electric trains
    - Mobile telephones/personal communications devices
    - Electronic Article Surveillance Systems
    - Metal detectors
    - RFID (Radio Frequency Identification for item management) equipment
    - Recreation devices, such as iPods, game consoles, etc.
    - Remote keyless entry systems
    - Hybrid vehicles
  - Controlled and therapeutic environment:
    - MRI Systems
    - Electrocauterys
    - External Defibrillation
    - Diathermy
4. Safety of RF Telemetry
5. Design solutions for EMI protection
6. International standards addressing RF fields and pacemakers and ICDs safety
  - European Standards: EN 45502-1, EN 45502-2-1 and -2-2
  - International: ISO 14708-1, ISO 14708-2
  - USA: ANSI/AAMI PC69

## An Estimate for Human Health that Influenced by Electromagnetic Wave from Mobile Phone and the Relay Stations

Hung-Yao Pai

E. E. Department, Chienkuo Technology University, Taiwan

**Abstract**— This study first used two measurement devices (including three-axis and single-axis type) to measure the magnitude of electromagnetic field/wave of the mobile phone (including 22 types) and the relay stations in the west Taiwan, and used the MEAD (Meridian Energy Analysis Device) tool and Health Banco energy display instrument to measure 28 users of mobile phone including before and after a call, and observe the changes of 12 Meridians and energy in body for estimating the influence degree of the users' health. The duration of this study is seven months. The frequency of the test is 84. The research found that the users' meridians and energy of heart (blood), bladder, pericardium and liver were more influenced by their mobile phone. Second, the researcher and 10 students went to the relay stations of mobile phone in Changhua and Taichung city to measure the magnitude of their electromagnetic field/wave. The researcher also designed a set of questionnaire to survey the opinions of citizens that live at the area of the relay stations in the two above-mentioned cities. We sent out 400 questionnaires and the response rate is 51.75 percent. The majority of respondents had not uncomfortable in body but worried in mind, and were afraid to lead to cancer. There were also few against events of setting up the relay stations in the two cities. Finally, the findings from the two methodologies (including experimentation and survey method) are valuable for the study and teaching of electromagnetic field/wave.

# Cardiophysiological Studies on Patients with Dual-chamber Pacemaker During Exposure to RF-fields Emitted by Cellular Phones

Maila Hietanen<sup>1</sup>, Kari Tahvanainen<sup>1</sup>, Juanita Nino<sup>1</sup>, Juha Hartikainen<sup>2</sup>, Antti Hedman<sup>3</sup>  
Tom Kuusela<sup>3</sup>, and Harri Lindholm<sup>1</sup>

<sup>1</sup>Finnish Institute of Occupational Health, Finland

<sup>2</sup>Kuopio University Hospital, Finland

<sup>3</sup>Turku University, Finland

**Abstract**— This study is a continuum to a recent study by our group which evaluated effects of exposure to 900 and 1800 MHz GSM phones on blood pressure and cardiac autonomic reflexes at rest and during physiological challenges (Tahvanainen et al.). In the double-blind trial, cardiovascular responses of 32 healthy subjects were evaluated during controlled breathing test, spontaneous breathing test, head-up tilt table test, Valsalva manoeuvre and deep breathing test. The results indicated that there were no statistically significant differences in blood pressure and heart rate between RF exposure and sham exposure on the cardiovascular autonomic nervous system in healthy humans. There has been, however, suspicions on possible adverse cardiophysiological effects of RF fields from cellular phones on persons wearing cardiac pacemakers.

The effects of GSM (1800 MHz) and TETRA (380 MHz) phones on cardiac pacing were studied in 57 patients with implanted dual-chamber pacemakers from three manufacturers. The patients were studied in supine position during their routine polyclinic visits for function adjustment of earlier implanted dual-chamber pacemaker. In order to evaluate possible pacemaker malfunction in the presence of external RF disturbance produced by the two mobile phone types, the pacemakers were programmed to different pacing modes by a clinical cardiologist. The phones were adjusted to operate at the allowed maximum antenna powers (OFF for 20s and ON for 20s). Four consecutive mobile phone locations were applied during clinical testing: 1) on the contralateral ear, 2) on the ipsilateral ear, 3) at a distance of 15 cm from skin above the pacemaker, and 4) on skin just above the pacemaker.

Various physiological signals (ECG, telemetrically measured intra-cardiac signals and continuous finger blood pressure, if available) were recorded with simultaneous recording of the relative intensity signal of RF field. Sophisticated data analysis of the recorded signals was conducted in this trial by a special feature extraction of ECG, blood pressure and pacemaker function signals to obtain accurately the time-synchronized time series of cardiovascular variabilities during different pacemaker function modes.

Contrary to some earlier reports, our results indicate that RF field emissions by GSM 1800 MHz and TETRA 380 MHz phones do not cause interference to pacemaker functions. The only observed harmful effects were found in signal telemetry with GSM phones, when the phone was located in close proximity to pacemaker above the chest. However, RF exposures did not change the programmed function of the pacemaker. As a conclusion, normal use of GSM or TETRA phones by pacemaker patients does not induce any significant clinical problems on intra-cardiac sensing and pacing.

## REFERENCES

1. Tahvanainen, K., J. Niño, P. Halonen, T. Kuusela, T. Laitinen, E. Länsimies, J. Hartikainen, M. Hietanen, and H. Lindholm, "Cellular phone use does not acutely affect blood pressure or heart rate of humans," *Bioelectromagnetics*, Vol. 25, 73–83, 2004.

## Behavioral and Cognitive Effects of MW Electromagnetic Field Exposures Updated

Sheila A. Johnston

Independent Neuroscience Consultant, Ballyellery Cottage, Lahinch, County Clare, Ireland

**Abstract**— This paper presents an updated [2007] overview of the interaction of microwave [MW] electromagnetic fields as external stimuli to the nervous systems and to behavior and cognition of humans and laboratory animals. Replicated scientific studies of MW exposure thresholds for adverse perception and cognitive effects are part of the scientific basis for IEEE and ICNIRP exposure limits. These established adverse MW effects form the basis for an occupational whole body exposure restriction of  $0.4 \text{ W kg}^{-1}$  that provides a 10X margin of safety [9, 10]. The public standard has an additional 5x margin of safety (0.08 W/kg) for both the IEEE [9] and ICNIRP standards [10]. In human cognitive studies with low level MW exposures, replication studies appear to have eliminated the “false positives” with standardized protocols, larger samples [7], multicentered replications [6], better experimental controls, double blind conditions, and Bonferroni or other statistical corrections for multiple comparisons [14] and factoring in the measurement of scientific uncertainty of the results [11, 16]. In animal spatial memory studies the weight of evidence from seven research groups using two species of mammals is that there is no effect on spatial learning as tested by many spatial learning paradigms at whole body or local (head) MW exposures within guideline limits and also well above the whole body and partial body limits, when whole body temperature did not measurably rise. These replications are of particular note because of the extensive basic research ([8, 12], Nobel, 2000) that has established scientific evidence of the neurophysiological and neuroanatomical correlates of spatial memory in animals and man. If the strong evidence for homology of memory is accepted at this time, there does not seem to be any further requirement for studies in this area. However, it is generally preferred to have confirmatory MW exposure, spatial memory experiments in humans for health risk assessment. Controversy has followed reports that low level MW exposure caused toxic leakage through the blood brain barrier [BBB] that could lead to brain cell death and cognitive impairment. In many follow-up studies, most researchers could not replicate the low level BBB permeability changes or could show the effect only at high intensity levels, when the heating of the brain tissue was obvious D’Andrea et al. [4, 5]. Recently McQuade et al. [2005], Kuribayashi et al. [13] and Cosquer et al. [2] have reported no leakage in the BBB after MW exposure at low SARs [2, 0.2, 0.02, 0.002 W/kg]. Further BBB updates and large long-term exposure cognitive studies over 3 generations of rats [Bornhausen et al., in prep.] and human sleep studies [3, 15] will be presented. Since changes in temperature are the biologically relevant information for setting the standards, progress in experimental dosimetry underway to predict thermal responses to SAR exposure levels will be indicated. Precise thermophysiological dosimetry may help resolve any remaining uncertainty of whether or not MWs could have any effects thermal or otherwise on human or animal nervous functions [1] below IEEE and ICNIRP limits.

### REFERENCES

1. Adair, E. R., Workshop “Subtle temperature effects of RF-EMF,” London, November 12–13, 2002, <http://www.cost281.org/>.
2. Cosquer, B., et al., “Blood-brain barrier and electromagnetic fields: Effects of scopolamine methylbromide on working memory after whole-body exposure to 2.45 GHz microwaves in rats,” *Behav. Brain Res.*, Vol. 161, 229–237, 2005.
3. Danker-Hopfe, H., et al., “Do high frequency electromagnetic fields of the GSM and/or the UMTS standard for mobile communication affect sleep?” 6-2:100, *Bems*, Kanazawa, June 2007, <http://www.bioelectromagnetics.org/doc/bems2007-abstracts.pdf>.
4. D’Andrea, J., et al., “Behavioral and cognitive effects of microwave exposure,” *BEMS Suppl.*, Vol. 6, S39–S62, 2003.
5. D’Andrea, J., et al., “Microwave effects on the nervous system,” *BEMS*, Vol. I6, S107–S147, 2003.
6. Haarala, C., et al., “Effect of a 902 MHz EMF emitted by mobile phones on human cognitive function: A replication study,” *BEMS*, Vol. 24, 283–288, 2003.
7. Hamblin, D., et al., “The sensitivity of human event-related potentials and reaction time to mobile phone emitted EMFs,” *BEMS*, Vol. 27, No. 4, 265–273, 2006.

8. Hawkins, R., E. Kandel, and C. Bailey, "Molecular mechanisms of memory storage in *Aplysia*," *Review. Biol. Bull.*, Vol. 210, No. 3, 174–191, 2006.
9. IEEE Std C95.1-2005, *IEEE Standard for Safety Levels with Respect to Human Exposure to Radio Frequency Electromagnetic Fields, 3 kHz to 300 GHz*, The Institute of Electrical and Electronic Engineers, New York, 2006.
10. "ICNIRP Guidelines for limiting exposure to time-varying electric, magnetic and electromagnetic fields up to 300 GHz," *Health Phys.*, Vol. 74, 494–522, 1998.
11. Johnston, S. A. and J. A. D'Andrea, "Behavioral and cognitive effects of electromagnetic field exposures," B. Greenebaume and F. Barnes [eds], *Handbook of Biological Effects of EMF*, CRC Press, Fla, 2006.
12. Kandel, E., et al. (eds) *Principles of Neural Science*, 4th Edn., McGraw Hill, London, 2000.
13. Kuribayashi, M., et al., "Lack of effects of 1439 MHz near field exposure on blood-brain barrier in immature and young rats," *BEMS*, Vol. 26, No. 7, 578–88, 2005.
14. Regel, S. J., et al., "UMTS base station-like exposure, well-being, and cognitive performance," *EHP*, Vol. 114, No. 8, 1270–1275, 2006.
15. Regel, S., et al., "Pulsed RF fields: Dose-dependent effects on sleep, sleep EEG and cognitive performance," *J Sleep Res.*, Vol. 16, No. 3, 253–8, 2007.
16. Wager, T. D. and E. E. Smith, "Neuroimaging studies of working memory: A meta-analysis," *Cogn. Affect Behav. Neurosci.*, Vol. 3, No. 4, 255–274, 2003.

## RF Bioeffect Research to Address Human Safety Concerns

C-K. Chou and Joe Elder

Corporate EME Research Laboratory, Motorola Labs, Fort Lauderdale, Florida, USA

**Abstract**— RF safety concerns started in the 1950s with exposure to radar, then radio and TV broadcasting in the 1960s, microwave ovens in 1970s, police radar in 1980s and then most recently wireless communications. These devices emit a form of non-ionizing energy called radiofrequency (RF) signals. The electromagnetic spectrum helps to explain a major difference in non-ionizing and ionizing energy. The well known cumulative damaging effects of ionizing radiation, such as X-rays and atomic bombs, do not occur at frequencies below those in the UV spectrum, including sunlight and infrared frequencies that are forms of non-ionizing energy. Over the past more than 50 years, a large data base on the bioeffects of RF exposure has been accumulated to support health risk assessments of RF exposure. Currently there are about 1600 peer-reviewed articles in the WHO database relating to RF bioeffects. For mobile telephony alone, there are about 600 peer-reviewed papers and another 200 to-be-published papers are listed in the database. The research subjects consist of epidemiological, human, animal and in vitro cell studies. WHO has stated that scientific knowledge in this area is now more extensive than for most chemicals, and concluded that current evidence does not confirm the existence of any health consequences from exposure to low level electromagnetic fields, that is, at exposure levels within the limits set by international standards.

The strongest bioeffects evidence is from animal cancer studies. The weight of scientific evidence in 41 studies shows that RF exposure up to lifetime exposure does not adversely affect carcinogenic processes at whole-body dose rates up to 4 W/kg, 50 times above the general population exposure limit. Long-term animal studies provide no supportive evidence of low-level non-thermal effects. Short-term exposure studies of animals and in vitro studies showing changes in biological responses, even if proven repeatable, are not consistent with results in the long-term (lifetime) exposure studies, and carry less weight for health risk assessment. In the past 10 years, more than 20 independent expert groups and health authorities have reviewed the RF bioeffects literature. These reviews are consistent in their conclusion that there is no credible evidence that RF exposures within internationally accepted limits cause any adverse health effects, but more research is needed. However, it is noteworthy that one can never prove the null hypothesis, i.e., one can never prove that something is absolutely safe. Basically, there is no known mechanism for adverse health effects of RF exposure other than thermal. Due to the current extensive database, it is unlikely that results of ongoing studies will shift the weight of evidence on health effects. WHO estimated that \$250 M has already been spent on mobile telephony bioeffect research, and more than \$130 M is budgeted on national research programs currently in progress.

International standards for measuring mobile phone emissions are available. With proper regulation, all phones should comply with international exposure limits. RF exposures in residential and office building from base stations are in general lower than 1% of international limits and these levels are similar to levels from radio and TV broadcasts. WHO Fact Sheet #304 (May 2006) states “*Considering the very low exposure levels and research results collected to date, there is no convincing scientific evidence that the weak RF signals from base stations and wireless networks cause adverse health effects.*” In conclusion: 1) RF electromagnetic energy does not produce nuclear (ionizing) radiation, 2) the only proven RF interaction mechanism for adverse health effects is thermal, 3) exposure levels near base stations are very low, and 4) RF emissions from mobile phones comply with international safety limits.

# Session 2P8a

## Electromagnetic Imaging: State of the Art and Perspectives

<b>Negative Refraction and Focusing in Magnetically Coupled L-C Loaded Transmission Lines</b>	
<i>Peter Halevi (Instituto Nacional de Astrofísica, Óptica y Electrónica, México); U. Algreto-Badillo (Instituto Nacional de Astrofísica, Óptica y Electrónica, México);</i>	536
<b>The Closed-form Solution to the Reconstruction of the Radiating Current for EM Inverse Scattering</b>	
<i>Lianlin Li (Institute of Electronics, Chinese Academy of Sciences, China); W. J. Zhang (Institute of Electronics, Chinese Academy of Sciences, China); Fang Li (Institute of Electronics, Chinese Academy of Sciences, China);</i>	537
<b>Contrast Field and Contrast Source Formulations for Microwave Imaging — A Comparative Analysis</b>	
<i>Leonardo Lizzi (University of Trento, Italy); Paolo Rocca (University of Trento, Italy); Massimo Donelli (University of Trento, Italy); Andrea Massa (University of Trento, Italy);</i>	538
<b>Diagnosis of Reinforcing Bars in the Concrete Structure by Using Real-coded GA Using Real Data</b>	
<i>Toshiyuki Tanaka (Nagasaki University, Japan); Yuta Mitake (Nagasaki University, Japan); Kenzo Nagatomi (Nagasaki University, Japan); Takashi Takenaka (Nagasaki University, Japan);</i>	539
<b>A Qualitative Approach to Breast Cancer Detection Using Microwaves</b>	
<i>Michele Piana (Università di Verona, Italy); R. Aramini (Università di Trento, Italy); Giovanni Bozza (Università di Verona, Italy); Massimo Brignone (Università di Genova, Italy); J. Coyle (Università di Verona, Italy); F. Delbary (Università di Verona, Italy);</i>	540
<b>Circular Microwave Imaging Setup for Retrieving Soil Moisture Content</b>	
<i>Raphael Lencrerot (Institut Fresnel, Equipe SEMO, France); Amelie Litman (Institut Fresnel, CNRS, France); Herve Tortel (Institut Fresnel, CNRS, France); Jean Michel Geffrin (University of Paris SUPELEC, France);</i>	541
<b>Complete Recovery of Partially Coherent Wave Fields and Applications in Imaging</b>	
<i>Chanh Q. Tran (La Trobe University, Australia); K. A. Nugent (The University of Melbourne, Australia);</i>	542
<b>An Improved Doppler Parameter Estimator for Synthetic Aperture Radar</b>	
<i>Y. Li (National University of Singapore, Singapore); H. Fu (National University of Singapore, Singapore); Pooi Yuen Kam (National University of Singapore, Singapore);</i>	543

## Negative Refraction and Focusing in Magnetically Coupled L-C Loaded Transmission Lines

P. Halevi and U. Algreto-Badillo

Instituto Nacional de Astrofísica, Óptica y Electrónica, Apdo. Post. 51, Puebla, México

**Abstract**— We studied electromagnetic wave propagation in circuits with one- and two-dimensional periodicity. The unit cell is composed of L-C elements, and neighboring cells are magnetically coupled — by means of mutual inductances  $M$ . Using Kirchhoff's voltage law, we derived simple dispersion relations that relate the circular frequency  $\omega$  and the wave vector  $\mathbf{k}$ . For the infinite one-dimensional transmission line, it is given by  $\omega^2 = 1/[2LC + 2MC \cos(ka)]$ ,  $a$  being the period. For a two-dimensional, unbounded, square lattice, we obtain that  $\omega^2 = 1/\{4LC + 2MC[\cos(k_x a) + \cos(k_y a)]\}$ , where  $k_x$  and  $k_y$  are the components of  $\mathbf{k}$  along the lattice axes. This corresponds to pass-band response, with strong anisotropy for the two-dimensional transmission line: this band is roughly twice as wide in the [11] direction as it is in the [10] direction. And, important to note, the group velocity  $\partial\omega/\partial\mathbf{k}$  is positive (negative) for  $M > 0$  ( $M < 0$ ). We also performed sweep AC analysis, using H-spice software, for the corresponding finite-size circuits (1,000 unit cells), resulting in excellent agreement with the above dispersion relations for frequencies on the order of GHz.

We also consider two different two-dimensional transmission lines coupled magnetically along a straight line and we simulate refraction of an electric signal at this interface. The medium on one side of the interface is characterized by positive coupling ( $M > 0$ ), while on the other side we consider the cases of both positive and negative ( $M < 0$ ) coupling. Now, it turns out that the product of the group and phase velocities is proportional to  $M$ . *It follows that the sign of the effective refractive index is the same as the sign of  $M$ , namely, the medium is right (left)-handed for  $M > 0$  ( $M < 0$ ), in the sense of the ideas initiated by Veselago [1].* Indeed, our simulations with a point source successfully demonstrate both positive (for  $M > 0$ ) and negative (for  $M < 0$ ) refraction. Moreover, Snell's law is well satisfied for angles of incidence greater than about  $15^\circ$ , respectively with a positive and negative index, as deduced from contours of constant phase. The negative refraction gives rise to the first (internal) focus, as predicted by Veselago [1]. We are now proceeding with simulations in order to reproduce the second (external) focus as well.

### ACKNOWLEDGMENT

This work was supported by CONACYT under project: SEP-2004-C01-46425.

### REFERENCES

1. Veselago, V. G., *Sov. Phys.-Usp.*, Vol. 10, 509, 1968.



# The Closed-form Solution to the Reconstruction of the Radiating Current for EM Inverse Scattering

Lianlin Li, W. J. Zhang, and Fang Li

Institute of Electronics, Chinese Academy of Sciences, Beijing 100080, China

**Abstract**— In the past few years, the EM inverse scattering problem, whose goal is to find the location, shape and the dielectric properties distribution of the obstacle in noninvasive fashion, has been addressed by many authors. Three main difficulties in solving an inverse electromagnetic scattering problem are huge computation, nonlinearity and instability. To overcome nonlinearity, a common technique is to transform the original problem (nonlinear) into an inverse source one (linear), by the introduction of an equivalent current density inside scatter. Although the equivalent current density linearizes the inverse scattering equation, the resulting operator is still ill-posed and its solution is usually nonstable and nonunique because the scattering operator is compact. In particular, the nonuniqueness is due to the so-called nonradiating currents that do not radiate outside the support of obstacle and hence belongs to measure zero space of the scattering operator. In this case, some regularization techniques have been developed to solve the linear inverse source problem, such as Tikhonov regularization, truncated singular value decomposition (TSVD), and so on. When use these approaches, one must face two disgusting things: (1) the selection of regularization factor, which is very difficult to be determined; (2) huge computation, in particular for the reconstruction of obstacle embedded in layered medium, where solving the Green function is complicated and time-consuming because of the sommerfeld integral with slow convergence and high oscillation. In addition, because above approaches belong to numerical ones, the analysis of image resolution, the optimal work frequency and the optimal number of transmitter/receiver is very difficult when above techniques are implemented. Therefore, the closed-form solution is very appealing.

In the present work, a new analytical solution to the radiating current density for the inverse source problem is derived based on the idea of SVD of the scattering integral operator. A two-dimensional geometry is considered, which can be straightforward generalized into three dimensional and layered medium cases without increasing complexity. Numerical simulations and the analysis of image resolution show the capabilities of the method to reconstruct the radiating current. By virtue of the closed-form solution, there are five main advantages: (1) very short computational time; (2) avoiding finding the regularization factor and (3) the green function for layered medium case; (4) analyzing easily the image resolution and (5) selecting the optimal radar system.

# Contrast Field and Contrast Source Formulations for Microwave Imaging — A Comparative Analysis

L. Lizzi, P. Rocca, M. Donelli, and A. Massa

ELEDIA Research Group at DIT, University of Trento, Via Sommarive 14, I-38050 Trento, Italy

**Abstract**— Inverse scattering techniques are aimed at recovering the profiles, positions and constitutive parameters of unknown objects belonging to an inaccessible region illuminated by known and successive probing fields from the measurements of the scattered field (i.e., the problem data) collected by a set of sensors in an external observation domain. Within such a framework, different methods have been proposed, based either on system matrix inversion or optimization approaches. Since multiple scattering effects cannot be neglected, full non-linear formulations have to be used. The *contrast field inversion* (CFI) and the *contrast source inversion* (CSI) have been widely employed in a lot of practical applications (e.g., biomedical diagnosis or UXO and landmines detection, NDT/NDE, archeology, etc.).

CFI-based techniques recast the inversion problem to the minimization of a cost function of two integral terms both non-linear related to the so-called Data and State/Object Equations [1, 2]. The goal is to determine the unknown contrast function and total field within the investigation domain.

On the other hand, in the CSI algorithm the contrast sources (i.e., the equivalent currents defined in the support of the scatterers) and the contrast itself are iteratively reconstructed [3–5]. In such a case, the cost function is still composed by two-terms, but only one is non-linear.

This contribution proposes a comparison between the CFI and CSI methods in terms of solution accuracy, robustness to local minima and noise, and computational efficiency. The analysis is aimed at pointing out potentialities and limitations of both the inversion formulations when dealing with synthetic as well as experimental datasets. Towards this end, a set of representative results obtained with different minimization techniques both deterministic [6] and stochastic [7] are reported and compared.

## REFERENCES

1. Caorsi, S., A. Massa, and M. Pastorino, “A computational technique based on a real-coded genetic algorithm for microwave imaging purposes,” *IEEE Trans. Geosci. Remote Sensing*, Vol. 38, No. 4, 1697–1708, July 2000.
2. Donelli, M., G. Franceschini, A. Martini, and A. Massa, “An integrated multiscale strategy based on a particle swarm algorithm for inverse scattering problems,” *IEEE Trans. Geosci. Remote Sensing*, Vol. 44, No. 2, 298–312, Feb. 2006.
3. van den Berg, P. M. and A. Abubakar, “Contrast source inversion method: State of art,” *Progress in Electromagnetic Research, PIER*, Vol. 34, 189–218, 2001.
4. Abubakar, A., P. M. van den Berg, and J. J. Mallorqui, “Imaging of biomedical data using a multiplicative regularized contrast source inversion method,” *IEEE Trans. Microwave Theory and Techniques*, Vol. 50, No. 5, 1761–1771, July 2002.
5. Abubakar, A., T. M. Habashy, and P. M. van den Berg, “Nonlinear inversion of multi-frequency microwave fresnel data using the multiplicative regularized contrast source inversion,” *PIERS 2006*, Vol. 2, No. 5, 485–489, Cambridge, USA, 2006.
6. Kleinman, R. E. and P. M. van den Berg, “A modified gradient method for two-dimensional problems in tomography,” *J. Computat. Appl. Math.*, Vol. 42, 17–35, 1992.
7. Donelli, M. and A. Massa, “Computational approach based on a particle swarm optimizer for microwave imaging of two-dimensional dielectric scatterers,” *IEEE Trans. Microwave Theory and Techniques*, Vol. 53, No. 5, 1761–1776, May 2005.

## Diagnosis of Reinforcing Bars in the Concrete Structure by Using Real-coded GA Using Real Data

Toshiyuki Tanaka, Yuta Mitake, Kenzo Nagatomi, and Takashi Takenaka  
Nagasaki University, Japan

**Abstract**— It is necessary to make a close investigation of the condition of concrete structures with respect to cracks, cavities, and corrosion of reinforcing bars in order to prevent dangerous accidents such as drop of a flake or mass of concrete. Additionally the strength investigation of the concrete structure is very important in order to prevent the destruction by the earthquake. Important factors of the strength investigation of the concrete structure are position and size of the reinforcing bars. The strength of the concrete structure will be camouflaged if the size of the reinforcing bars is smaller than a design. The existence of the reinforcing bars in the concrete can be confirmed at the good accuracy with conventional concrete radars. However, it is very hard to estimate the accurate position of the reinforcing bar, if the electric constant of the concrete has not been known. And the size of reinforcing bars can't be estimated by conventional method using concrete radar. We proposed the method for estimating position of reinforcing bar and dielectric constant of the concrete at the same time by using Gauss-Newton method. This method is equivalent to having supposed the value of the radius of the reinforcing bar to be zero.

In this paper, we propose a method to evaluate the position and radius of reinforcing bars with a high degree of accuracy. The estimate process is as follows.

- 1) Estimate the dielectric constant of the concrete using Gauss-Newton method by the assumption of the radius of reinforcing bars with zero.
- 2) Decide the search area of the reinforcing bars by using the Synthesis Aperture Processing.
- 3) Estimate the position and the radius of reinforcing bars by using Real-coded GA.

In case of the estimation of one reinforcing bar, the chromosome is composed of three genes. These genes are radius, location and depth of the reinforcing bar. The exploration of the cavity is also possible, if the dielectric constant is added to the chromosome. Furthermore, when two reinforcing bars are probed, the chromosome may be composed of six genes. The effectiveness of the presented method has been confirmed using real measured data.

## A Qualitative Approach to Breast Cancer Detection Using Microwaves

M. Piana, R. Aramini, G. Bozza, M. Brignone, J. Coyle, and F. Delbary  
Universita di Verona, Italy

**Abstract**— Qualitative methods for inverse scattering allow the reconstruction of inhomogeneities from far- or near-field data in a fast fashion and typically without requiring to a priori know detailed information on the tissue to be imaged. In particular, in a new approach to linear sampling, reciprocity gap functional and factorization methods a reliable estimate of the spatial resolution can be determined in advance, by means of a straightforward analysis of the scattered field. We test this theoretical estimate and the effectiveness of these qualitative approaches in a simulated experiment of microwave tomography for breast cancer detection.

## Circular Microwave Imaging Setup for Retrieving Soil Moisture Content

R. Lencrerot, A. Litman, H. Tortel, and J.-M. Geffrin

Institut Fresnel, Equipe SEMO

Avenue Escadrille Norman die Niemen, Marseille cedex 13397, France

**Abstract**— Soil moisture content is a key information in soil science and agronomy, in particular to understand water resource acquisition by plants roots. Therefore, monitoring the spatial variability of soil moisture content with sub-meter resolution over time is important for effective agricultural irrigation, especially in water-deprived regions. Intensive effort have been under taken to provide non-invasive geophysical methods, in particular using microwave sensors as the real and imaginary part of the soil dielectric constant is linked to its volumetric water content as well as its salinity.

The goal of our project is to demonstrate the potentiality of a non-invasive microwave imaging system for water content monitoring, which would provide a complementary non-invasive measurement setup for intermediate scales between remote sensing scales and ground truth measurement scales. To this end, a microwave circular setup is being designed and optimised in order to provide reconstructed dielectric maps of soil columns which will be placed inside the setup. In that process, our first step is to validate the algorithmic tools which are currently being implemented and to verify the effectiveness of the proposed experimental setup. Comparisons of computed and measured scattered fields for various obstacles placed within the circular setup will be presented. The computed fields are obtained thanks to a 2D finite-element code which implements in a very simple manner the boundary condition on the electromagnetic field.

The imaging process is performed thanks to an iterative gradient-based scheme which minimizes a classical discrepancy criterion. This minimization under constraints is reformulated using a Lagrangian formulation which is well adapted for the given configuration. The gradient is then simply expressed through the introduction of a so-called adjoint field. To check the effectiveness of the imaging process and its robustness in the present configuration, several numerical and experimental examples will be discussed. In particular, we will show the influence of the calibration process as well as the influence of the permittivity of the surrounding medium on the inversion results.

# Complete Recovery of Partially Coherent Wave Fields and Applications in Imaging

C. Q. Tran<sup>1</sup> and K. A. Nugent<sup>2</sup>

<sup>1</sup>Physics Department, La Trobe University, Victoria 3086, Australia

<sup>2</sup>School of Physics, The University of Melbourne, Victoria 3010, Australia

**Abstract**— Accessing the information capacity carried by a partially coherent wave field represents a considerable challenge and a number of methods have been developed. We report the first complete experimental reconstruction of the four-dimensional coherence function from an undulator synchrotron beam line [1]. The analysis is based on the observation that the data are consistent with a coherence function that is mathematically separable. Promising implications of the technique in imaging using spatially incoherent sources will also be discussed.

## REFERENCES

1. Tran, C. Q., *PRL*, Vol. 98, 224801, 2007.

# An Improved Doppler Parameter Estimator for Synthetic Aperture Radar

Y. Li, H. Fu, and P. Y. Kam

Department of Electrical and Computer Engineering, National University of Singapore  
S117576, Singapore

**Abstract**— With the reputation of high resolution and impressive quality of image, synthetic aperture radar (SAR) has played an important role in cartography, oceanography, and numerous military applications [1]. Since the signal energy from a point target is spread in range and azimuth, the purpose of SAR focussing is to collect this dispersed energy into a single pixel in the output image. The optimum focusing of the SAR data is a space-variant and two-dimensional operation, which makes SAR processing a challenge. The most popular SAR processing algorithm is the Range-Doppler technique [2] and its variations; see [3] and [4]. The method is efficient, and in principle, solves the problems of azimuth focussing and range cell migration correction. These imaging algorithms require the accurate estimation of the Doppler parameters, namely, the centroid Doppler frequency and the frequency rate, to perform coherent processing. Our main goal here is to estimate accurately the Doppler parameters to compensate for the motion caused by the radar or the moving targets. This compensation is challenging and important for moving targets, where the motion is non-cooperative as in inverse SAR (ISAR) [5]. Without correct motion compensation, the imaging quality may be degraded in several ways, such as shifting, distortion, defocusing and so on.

In this paper, we derive an improved maximum likelihood (ML) estimator in the time domain for SAR Doppler signals which are obtained after range compression. It shows that for the values of interest of the Doppler parameters [6], our ML estimator leads to a better performance than that of the only existing estimator in the time domain, i.e., the Djuric-Kay (DK) estimator [7]. In most SAR scenarios, the Doppler signal of a discrete backscattering point is appropriately modeled by a chirp signal [6]

$$r(k) = \alpha \exp [j(\phi + \omega_d k + \omega_r k^2/2)] + n(k) \quad k = 0, \dots, N-1 \quad (1)$$

Here,  $r(k)$  is the received Doppler signal sample,  $\alpha$  is the signal amplitude, and  $\{n(k)\}$  is a sequence of independent, identically  $CN(0, \sigma^2)$  distributed, Gaussian noise samples (Throughout this paper,  $CN(u, \Sigma)$  denotes a complex, Gaussian random variable with mean  $u$  and variance  $\Sigma$ .  $|\cdot|$  denotes an absolute value.). We consider  $\phi$ ,  $\omega_d$  and  $\omega_r$  as unknown but deterministic parameters, where  $\phi$  is the phase,  $\omega_d$  the centroid frequency, and  $\omega_r$  the frequency rate [7]. Denote  $\mathbf{p} = [\phi \ \omega_d \ \omega_r]^T$  as the parameter vector to be estimated. Following our technique in [8], the ML estimate of  $\mathbf{p}$  can be shown to be concisely expressed as [9]

$$\hat{\mathbf{p}}^{(N-1)} = \sum_{k=0}^{N-1} \mathbf{w}(k) \angle r(k) \quad (2)$$

where  $\mathbf{w}(k) = [o_\phi(k) \ w_{\omega_d}(k) \ w_{\omega_r}(k)]^T = |r(k)|\beta(k)/\Omega$ , and  $\beta(k) = [\beta_\phi(k) \ \beta_{\omega_d}(k) \ \beta_{\omega_r}(k)]^T$  whose elements are given by  $\beta_\phi(k) = \sum_{j=0}^{N-2} |r(j)|j \sum_{\tau=1}^{N-1-j} |r(j+\tau)|(j+\tau)\rho$ ,  $\beta_{\omega_d}(k) = -\sum_{j=0}^{N-2} |r(j)| \sum_{\tau=1}^{N-1-j} |r(j+\tau)|(2j+\tau)\rho$ , and  $\beta_{\omega_r}(k) = 2 \sum_{j=0}^{N-2} |r(j)| \sum_{\tau=1}^{N-1-j} |r(j+\tau)|\rho$ , with  $\rho = \tau^2[j(j+\tau) - k(2j+\tau+k^2)]$  and  $\Omega = \sum_{k=0}^{N-1} w_\phi(k)$ . From (2), we note that the estimator is a weighted linear combination of the phases of the received signal samples. It makes use of both the magnitudes and the phases of the received signals, where no assumption on the phase model of the received signals is used. Thus, its performance is expected to be better than that of the DK estimator, where only the phase information was exploited based on the approximate phase model proposed in [10].

The estimation error in  $\omega_d$  can cause linear phase errors leading to a displacement in the image domain. The estimation error in  $\omega_r$  introduces a quadratic phase error (QPE) leading to a defocusing in the imaging domain. Assume the knowledge of  $\phi$  is available. The actual values for  $\omega_d$  and  $\omega_r$  are denoted as  $\omega_{d0}$  and  $\omega_{r0}$ , respectively, and the estimation errors are denoted as  $\bar{\omega}_d$  and  $\bar{\omega}_r$ , respectively. We take  $\text{QPE} < \pi/4$  as the criterion [11], and the range migration caused

by the uncompensated linear phase error should be limited by the range resolution  $\rho_r$ . Then, the criteria for the estimation error limits can be obtained, respectively, as

$$|\bar{\omega}_r| \leq \frac{\rho_a^2 \omega_r^2}{2\pi v_a} \quad (3)$$

and

$$|\bar{\omega}_d| \leq \frac{4\rho_r \rho_a \omega_r}{\lambda v_a}. \quad (4)$$

Here,  $\rho_a$  is the azimuth resolution of SAR, and  $v_a$  is the radar velocity.

Figure 1 compares the performance of our ML estimator (2) and that of the DK estimator [7]. The performance is measured by the inverse error variance in dB. The inverse Cramer-Rao lower bound (ICRLB) in dB is given as the benchmark for comparison. Fig. 1 shows the better performance of our estimator than that of DK for the values of interest of the Doppler parameters. The improved estimation of the Doppler parameters, in turn, results in a better system performance, such as a finer range and/or azimuth resolution. Our improved estimator can also be applied to space-time adaptive processing (STAP) to improve the target detection probability, and other applications.

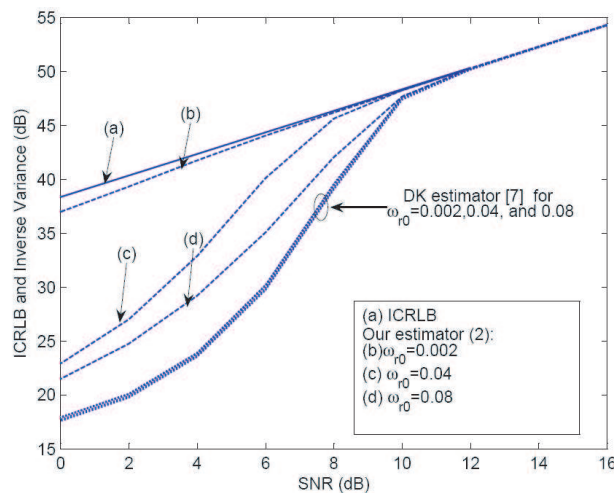


Figure 1: Performance comparison of ML-based estimators for  $\omega_r$ , with  $\omega_{d0} = 0.05$ ,  $\phi_0 = 0.25\pi$ , and  $N = 11$ .

## REFERENCES

- Richards, M. A., *Fundamentals of Radar Signal Processing*, McGraw-Hill, New York, 2005.
- Wu, C., "A digital system to produce imagery from sar data," *In Proc. of the AIAA Systems Design Driven by Sensors Conference*, Oct. 1976.
- Cumming, I. G. and J. R. Bennett, "Digital processing of seasat sar data," *In Proc. of ICASSP*, Apr. 1976.
- Wu, C., K. Y. Liu, and M. Jin, "Modeling and a correlation algorithm for spaceborne sar signals," *IEEE Trans. Aerosp. and Electron. Syst.*, Vol. 18, No. 5, 563–574, 1982.
- Li, J., R. Wu, and V. C. Chen, "Robust autofocus algorithm for isar imaging of moving targets," *IEEE Trans. Acoustics, Speech and Signal Process.*, Vol. 37, 1056–1069, July 2001.
- Curlander, J. C. and R. N. McDonough, *Synthetic Aperture Radar Systems and Signal Processing*, John Wiley and Sons, Inc., 1992.
- Djuric, P. M. and S. M. Kay, "Parameter estimation of chirp signals," *IEEE Trans. Acoustics, Speech and Signal Process.*, Vol. 38, 2118–2126, Dec. 1990.
- Fu, H. and P. Y. Kam, "Map/ml estimation of the frequency of a single sinusoid in noise," *IEEE Trans. Signal Process.*, Vol. 55, 834–845, Mar. 2007.
- Li, Y., H. Fu, and P. Y. Kam, "Improved ml estimators of chirp signal parameters in time domain and its performance analysis," to be submitted to *IEEE Trans. Signal Process.*, 2007.
- Tretter, S., "Estimating the frequency of a noisy sinusoid by linear regression," *IEEE Trans. Info. Theory*, Vol. 31, 832–835, Nov. 1985.
- Carrara, W. G., R. S. Goodman, and R. M. Majewski, *Spotlight Synthetic Aperture Radar: Signal Processing Algorithms*, 209, Artech House, Boston, 1995.



# Session 2P8b

## Electromagnetic Inverse Problems

<b>A Modified Time Reversal Iteration and Inverse Problems</b>	
<i>Matti Lassas (Helsinki Institute of Technology, Finland); Kenrick Bingham (Helsinki Institute of Technology, Finland); Yaroslav Kurylev (University College London, USA); Samuli Siltanen (Tampere University of Technology, Finland);</i> .....	546
<b>Detection of the Inclusions from Localized Boundary Measurements in the Electrical Boundary Measurements</b>	
<i>Takanori Ide (AISIN AW Co., Ltd., Japan);</i> .....	547
<b>Inverse Scattering in a Waveguide</b>	
<i>Hiroshi Isozaki (University of Tsukuba, Japan); Yaroslav Kurylev (University College London, UK); Matti Lassas (Helsinki University of Technology, Finland);</i> .....	548
<b>The D-bar Method for Electrical Impedance Tomography</b>	
<i>Samuli Siltanen (Tampere University of Technology, Finland);</i> .....	549
<b>Experiments in Time-reversed Electromagnetics</b>	
<i>Steven M. Anlage (University of Maryland, USA); Thomas Antonsen (University of Maryland, USA); James Hart (University of Maryland, USA); Biniyam Taddese (University of Maryland, USA); Edward Ott (University of Maryland, USA);</i> .....	550

## A Modified Time Reversal Iteration and Inverse Problems

M. Lassas<sup>1</sup>, K. Bingham<sup>1</sup>, Y. Kurylev<sup>2</sup>, and S. Siltanen<sup>3</sup>

<sup>1</sup>Helsinki University of Technology, Finland

<sup>2</sup>University Collage of London, UK

<sup>3</sup>Tampere University of Technology, Finland

**Abstract**— A novel method to solve inverse problems for the wave equation is introduced. The method is a combination of the boundary control method and an iterative time reversal scheme, leading to adaptive imaging of coefficient functions of the wave equation using focusing waves in unknown medium. The approach is computationally effective since the iteration lets the medium do most of the processing of the data. The iterative time reversal scheme also gives an algorithm for approximating a given wave in a subset of the domain without knowing the coefficients of the wave equation.

## Detection of the Inclusions from Localized Boundary Measurements in the Electrical Boundary Measurements

**Takanori Ide**

AISIN AW Co., Ltd., Japan

**Abstract**— Suppose given physical body in dimension two, and that the electrical conductivity distribution inside the body consists of conductive inclusions in a known background. We propose reconstruction formula for the location of inclusions from localized boundary measurements based on hyperbolic geometry. And we demonstrated the numerical experiments for our proposal algorithm.

## Inverse Scattering in a Waveguide

H. Isozaki<sup>1</sup>, Y. Kurylev<sup>2</sup>, and M. Lassas<sup>3</sup>

<sup>1</sup>Institute of Mathematics, University of Tsukuba, Tsukuba, Ibaraki 305-8571, Japan

<sup>2</sup>Department of Mathematics, University College London, Gower Street, London WC1E 5BT, UK

<sup>3</sup>Institute of Mathematics, Helsinki University of Technology, P. O. Box 1100, Helsinki 02015, Finland

**Abstract**— Let  $(M, g)$  be a waveguide with a single end  $(\Omega \times (0, \infty))$ , i.e.,  $M = M_c \cup (\Omega \times (0, \infty))$ , where  $M_c$  is the compact part of the waveguide. Assume, in addition, that the metric  $g$  in  $\Omega \times (0, \infty)$  is a direct one

$$dl^2 = g_{\alpha\beta}(x)dx^\alpha dx^\beta + dy^2$$

Here  $x = (x^1, \dots, x^{n-1})$  are coordinates in  $\Omega$  and  $0 < y < \infty$  is the coordinate along the end. If  $\lambda_j, \phi_j$  are an eigenvalue and the corresponding eigenfunction of the Laplace operator in  $\Omega$ , then, for  $k^2 > \lambda_j$ , one can send an incoming wave from the right,  $\exp(-i\sqrt{k^2 - \lambda_j}y)\phi_j(x)$  into the waveguide. Being reflected inside  $M$ , it goes back to the right and, measured as  $y \rightarrow \infty$ , looks like a sum

$$\sum_{\lambda_m < k^2} S_{jm}(k^2) \exp\left(i\sqrt{k^2 - \lambda_m}y\right) \phi_m(x)$$

Coefficients  $S_{jm}(k^2)$ ,  $\lambda_j, \lambda_m < k^2$  form a matrix called the (physical) scattering matrix. The main result is that this matrix, known for all  $k^2$ , makes it possible to identify  $M_c$  and the metric  $g|_{M_c}$  in it.

# The D-bar Method for Electrical Impedance Tomography

**Samuli Siltanen**

Tampere University of Technology, Finland

**Abstract**— In electrical impedance tomography (EIT) one recovers the electrical conductivity distribution inside a body from current-to-voltage measurements at the boundary of the body. Applications of EIT include medical imaging, subsurface prospecting, and nondestructive testing.

The imaging problem of EIT is mathematically challenging because it is a nonlinear and ill-posed inverse problem. New direct imaging algorithms for EIT are presented. The methods are based on the mathematical analysis of Nachman [1] and Astala and Paivarinta [2]. The new methods are non-iterative, robust against measurement noise, and produce clinically useful EIT images from both phantom and in vivo human data. Regularization and computational aspects of the methods are discussed.

## REFERENCES

1. *Ann. Math.*, Vol. 143, 1996.
2. *Ann. Math.*, Vol. 163, 2006.

## Experiments in Time-reversed Electromagnetics

Steven M. Anlage, Thomas Antonsen, James Hart, Biniyam Taddese, and Edward Ott

Physics Department, University of Maryland  
College Park, MD 20742-4111, USA

**Abstract**— Recent work in the field of ‘wave chaos’ shows that when waves of short wavelength compared to the system size scatter within a complex enclosure (e.g., a room, stairwell, etc.), the results are extremely sensitive to small changes in the environment [1–3]. In addition, the statistics of these changes can be quantitatively extracted from the theory of random matrices [4, 5]. This extreme sensitivity suggests that this effect can be exploited to make very sensitive detectors. At the same time, there has been much interest in the acoustics community in exploiting the time-reversal symmetry of the wave equation. This property can make a detector (known as a “time-reversal mirror” (TRM)) extremely sensitive to small changes in the acoustic environment. It was also found that a chaotic scattering environment allows one to have a very simple TRM consisting of just one detector! Here we combine these two unique ideas to experimentally investigate time-reversed electromagnetics. We experimentally demonstrate a new electromagnetic one-recording-channel time-reversal mirror that can operate at high frequencies and high bandwidths. The experiments are carried out in a  $1\text{ m}^3$  ray-chaotic enclosure using two simple antennas. The input is a 7.0 GHz signal that is amplitude modulated with a 60 ns-long pulse. The time-reversal focused signal has a peak-signal-to-noise ratio of about 9 dB, and is very sensitive to small perturbations to the ray-chaotic enclosure. The results are consistent with expectations for single-recording-channel time-reversal mirrors, and establish a new platform for study of fundamental issues in time-domain wave chaos, as well as novel applications. Ongoing research is addressing questions of ultimate sensitivity, the ability to determine the precise location of a change, and the roles of attenuation and noise, frequency bandwidth and spectral correlations.

### ACKNOWLEDGMENT

This work is supported by ONR MURI N000140710734 and ONR DURIP N000140710708.

### REFERENCES

1. Hemmady, S., et al., *Phys. Rev. E*, Vol. 74, 036213, 2006.
2. Hemmady, S., X. Zheng, T. M. Antonsen, E. Ott, and S. M. Anlage, “Universal statistics of the scattering coefficient of chaotic microwave cavities,” *Phys. Rev. E*, Vol. 71, 056215, 2005.
3. Hemmady, S., et al., *Phys. Rev. Lett.*, Vol. 94, 014102, 2005.
4. Zheng, X., T. M. Antonsen Jr., and E. Ott, “Statistics of impedance and scattering matrices in chaotic microwave cavities: single channel case,” *Electromagnetics*, Vol. 26, 3, 2006.
5. Zheng, X, T. M. Antonsen Jr., and E. Ott, “Statistics of impedance and scattering matrices of chaotic microwave cavities with multiple ports,” *Electromagnetics*, Vol. 26, 37, 2006.

# Session 3A1a

## Dynamics on the Attosecond Time Scale

<a href="#">Imaging on the Attosecond Time Scale — Promises and Pitfalls</a>	
<i>G. Jordan (Vienna University of Technology, Austria); Ch. Ede (Vienna University of Technology, Austria); Xinhua Xie (Vienna University of Technology, Austria); Armin Scrinzi (Vienna University of Technology, Austria);</i> .....	552
<a href="#">Temporal Characterization of an Attosecond Pulse Train Using the FROG Technique</a>	
<i>Chang Hee Nam (KAIST, Korea); Kyung Taec Kim (KAIST, Korea); Dong Hyuk Ko (KAIST, Korea); Kyung Sik Kang (KAIST, Korea); Ju Yun Park (KAIST, Korea);</i> .....	553
<a href="#">Complete Characterization of Attosecond Pulses by Spectral Shearing Interferometry of Photoelectron Wave Packets</a>	
<i>Taro Sekikawa (Hokkaido University, Japan);</i> .....	554
<a href="#">Classical Trajectory Perspective on Double Ionization Dynamics of Diatomic Molecules Irradiated by Ultrashort Intense Laser Pulses</a>	
<i>Jie Liu (Institute of Applied Physics and Computational Mathematics, China);</i> .....	555
<a href="#">Quantum Control of High Harmonics and Attosecond Pulse Generation</a>	
<i>Peixiang Lu (Huazhong University of Science and Technology, China); Pengfei Lan (Huazhong University of Science and Technology, China); Wei Cao (Huazhong University of Science and Technology, China); Yuhua Li (Huazhong University of Science and Technology, China); Xinlin Wang (Huazhong University of Science and Technology, China);</i> .....	556
<a href="#">Laser Tweezers with a Femtosecond Laser Beam</a>	
<i>Min Gu (Swinburne University of Technology, Australia);</i> .....	557

## Imaging on the Attosecond Time Scale — Promises and Pitfalls

G. Jordan, Ch. Ede, Xinhua Xie, and A. Scrinzi  
Photonics Institute, Vienna University of Technology, Austria

**Abstract**— Fully controlled intense few-cycle laser pulses and precisely synchronized sub-femtosecond XUV pulses are new experimental tools to observe electronic dynamics on the sub-femtosecond time scale [1]. Employing these tools in a variety of experimental setups time-resolved observations of atomic ionization [2], electronic shake-up processes [3] in atoms, and ultra-fast rearrangement of molecules [4] have been and are being investigated. All these experiments involve the exposure of the systems to rather strong laser fields and require a reliable understanding of the impact of the laser on the systems.

We will discuss the new measurement techniques on the examples of “molecular tomography” [5] and of the direct observation of ionization dynamics in atoms and molecules [3]. While a basic understanding of the measurement relies on rather simple models, a quantitatively and often also qualitatively correct interpretation of the results exposes a much more complex picture. The attosecond time structure of ionization can be significantly vary with the systems internal dynamic state, XUV excitation patterns in realistic systems are strongly modulated in presence even of a relatively weak laser field [6], and high harmonic radiation can be the result of the joint action of several electrons. Recent experiments will be discussed by comparison with advanced quantum-mechanical simulations of the few-electron dynamics in atoms and molecules [7].

### REFERENCES

1. Scrinzi, A., M. Y. Ivanov, R. Kienberger, and D. M. Villeneuve, “Attosecond physics,” *J. Phys. B — Topical Review*, Vol. 39, R1–R37, 2006.
2. Drescher, M., M. Hentschel, R. Kienberger, M. Uiberacker, V. Yakovlev, A. Scrinzi, T. Westerwalbesloh, U. Kleineberg, U. Heinzmann, and F. Krausz, “Time-resolved atomic inner-shell spectroscopy,” *Nature*, Vol. 419, 803, 2002.
3. Uiberacker, M., T. Uphues, M. Schultze, A. J. Verhoef, V. Yakovlev, M. F. Kling, J. Rauschenberger, H. Schrder, N. M. Kabachnik, M. Lezius, K. L. Kompa, H.-G. Muller, M. J. J. Vrakking, S. Hendel, U. Kleineberg, U. Heinzmann, M. Drescher, and F. Krausz, “Attosecond real-time observation of electron tunnelling in atoms,” *Nature*, Vol. 446, 627–632, 2007.
4. Baker, S., J. S. Robinson, C. A. Haworth, H. Teng, R. A. Smith, C. C. Chirilă, M. Lein, J. W. G. Tisch, and J. P. Marangos, “Probing proton dynamics in molecules on an attosecond time scale,” *Science*, Vol. 312, 424, 2006.
5. Itatani, J., J. Levesque, D. Zeidler, H. Niikura, H. Pépin, J. C. Kieffer, P. B. Corkum, and D. M. Villeneuve, “Tomographic imaging of molecular orbitals,” *Nature (London)*, Vol. 432, 867, 2004.
6. Xie, X., M. Wickenhauser, W. Boutou, H. Merdji, P. Salieres, and A. Scrinzi, “Sub-cycle dynamics in the laser-ionization of molecules,” *Phys. Rev. A*, 2007.
7. Caillat, J., J. Zanghellini, M. Kitzler, O. Koch, W. Kreuzer, and A. Scrinzi, “Correlated multielectron systems in strong laser fields — an mctdhf approach,” *Phys. Rev. A*, Vol. 71, 012712, 2005.



## Temporal Characterization of an Attosecond Pulse Train Using the FROG Technique

Chang Hee Nam, Kyung Taec Kim, Dong Hyuk Ko, Kyung Sik Kang, and Ju Yun Park  
Department of Physics and Coherent X-ray Research Center, KAIST, Korea

**Abstract**— We have experimentally demonstrated the full temporal reconstruction of an attosecond pulse train by applying the FROG technique to the photoionization process. For the temporal characterization of an attosecond pulse train formed by harmonics from Ar, the photoelectron spectra of He atoms ionized by high harmonic and IR laser pulses were measured while changing the time delay between the two pulses. Then the temporal profile of the attosecond pulse train was retrieved using a FROG inversion algorithm, which revealed the temporal structure of individual attosecond pulses in the attosecond pulse train. From the time-frequency analysis of the attosecond pulses obtained from the full reconstruction, the chirp structure of the attosecond pulses was also analyzed.

# Complete Characterization of Attosecond Pulses by Spectral Shearing Interferometry of Photoelectron Wave Packets

Taro Sekikawa

Department of Applied Physics, Hokkaido University  
Kita13 Nishi 8, Kita-ku, Sapporo 060-8628, Japan

**Abstract**— We propose and demonstrate a simple and robust method to characterize extreme ultraviolet (XUV) attosecond pulses completely by photoelectron (PE) spectral shearing interferometry. Since quantum mechanics postulates that electrons are matter wave, the spectral shape and phase of attosecond pulses are transferred to PE wave packets produced by the photoelectric effect from noble gases. Hence, the characterization of PE wave packets is equivalent to the evaluation of XUV attosecond pulses. The spectral phase of a PE wave packet can be retrieved from an interference pattern in the frequency domain between spectral sheared PE wave packets, ejected from two energy levels splitting from the  $n^2P$  orbital owing to the spin-orbit interaction. This phase retrieval process from the interference pattern in the frequency domain is basically same as spectral phase interferometry for direct electric-field reconstruction (SPIDER), widely used to characterize visible ultrashort laser pulses. Experimentally, we have confirmed the interference of spectral sheared PE wave packets by generating chirped PE wave packets in the above-threshold ionization (ATI) of argon atoms using chirped Ti:sapphire laser pulses. The chirp of laser pulses was controlled by changing the condition of a compressor in the laser system. Spectral change in an ATI PE spectrum with laser chirp was clearly observed. Based on these results, complete characterization of the 19th harmonic of Ti:sapphire laser with a photon energy of 29 eV was demonstrated by measuring PE spectra of neon or argon atoms in comparison with a PE spectrum of helium atoms, corresponding to the case of Fourier-transform limited pulses.

# Classical Trajectory Perspective on Double Ionization Dynamics of Diatomic Molecules Irradiated by Ultrashort Intense Laser Pulses

Jie Liu

Institute of Applied Physics and Computational Mathematics, Beijing, China

**Abstract**— In the present paper, we develop a semiclassical quasi-static model accounting for molecular double ionization in an intense laser pulse. With this model, we achieve insight into the dynamics of two highly-correlated valence electrons under the combined influence of a two-center Coulomb potential and an intense laser field, and reveal the significant influence of molecular alignment on the ratio of double over single ion yield. Analysis on the classical trajectories unveils sub-cycle dynamics of the molecular double ionization. Many interesting features, such as the accumulation of emitted electrons in the first and third quadrants of parallel momentum plane, the regular pattern of correlated momentum with respect to the time delay between closest collision and ionization moment, are revealed and successfully explained by back analyzing the classical trajectories. Quantitative agreement with experimental data over a wide range of laser intensities from tunneling to over-the-barrier regime is presented.

## Quantum Control of High Harmonics and Attosecond Pulse Generation

Peixiang Lu, Pengfei Lan, Wei Cao, Yuhua Li, and Xinlin Wang

Wuhan National Laboratory for Optoelectronics, School of Optoelectronics Science and Engineering  
Huazhong University of Science and Technology, Wuhan 430074, China

**Abstract**— Driven by intense laser pulses, atomic and molecular systems can emit lights at frequencies multiple of that of the laser field. This nonlinear process, known as high harmonic generation (HHG), is a subject of great interest owing to its potential applications for the coherent extreme ultraviolet source and the generation of attosecond pulses. Attosecond extreme ultraviolet pulses, especially the isolated attosecond pulse, allow one to investigate ultrafast electronic processes, opening the door to attophysics. In our work, we propose several schemes for coherent control the HHG. It is shown that single attosecond pulse can be produced using multi-cycle laser pulse via asymmetric molecules, which is more easily carried out in experiments. On the other hand, we show that a broadband supercontinuous high harmonics (with a bandwidth of 180 eV) can be generated with an ultrashort laser pulse in combination with a controlling pulse. And then an isolated sub-100 attosecond pulse can be obtained, which allows one to measure a wide range of ultrafast dynamics not normally accessible before. Moreover, it is shown that this scheme also can be used to steer the launch of attosecond pulses with a high precision. Furthermore, it is demonstrated that UV pulse is a robust tool to control the electron ionization, and so it can be used to control the quantum path of electron in the laser field. With this scheme, an isolated single-cycle attosecond pulse can be produced, and the attosecond pulse yield is enhanced by about two orders.

## Laser Tweezers with a Femtosecond Laser Beam

Min Gu

Centre for Micro-Photonics, Faculty of Engineering and Industrial Sciences  
Swinburne University of Technology, POB 218, Hawthorn 3122, Australia

**Abstract**— Lasers have opened up numerous opportunities for biomedical sciences. Optical tweezers are one of the key biophotonic techniques. They employ the forces of radiation pressure of light to trap and manipulate microscopic particles, and have enormous applications in various disciplines ranging from physics to biology. The trapping volume of the far field optical tweezers is diffraction limited with an elongated axial size. While one deals with very small biological specimens like single cells or molecules, a reduced trapping volume is desirable, which would ideally be provided by a near field trap. In this talk, I will introduce far-field and near-field laser trapping techniques under femtosecond laser illumination. As a result, multiphoton excitation can be combined with laser tweezers. Therefore, the efficiency of whispering gallery modes (WGM) excitation is highly enhanced while a microsphere is trapped. This new mechanism can be used for near-field sensing.



# Session 3A1b

## Attosecond Pulse Generation Related Technologies

### High-order Harmonic Generation in Mixed Gases

*E. J. Takahashi (RIKEN, Japan); T. Kanai (RIKEN, Japan); Y. Nabekawa (RIKEN, Japan); Katsumi Midorikawa (RIKEN, Japan);* ..... 560

### Ultrafast Optics for High-order Harmonics and Attosecond Pulses

*Paolo Villoresi (DEI-University of Padova, Italy);* ..... 561

### Carrier-envelope Phase Controlled 5-fs Optical Pulses for Driving Single Attosecond Pulses Generation

*Zhiyi Wei (Chinese Academy of Sciences, China); Jiangfeng Zhu (Chinese Academy of Sciences, China); Hao Teng (Chinese Academy of Sciences, China); Hainian Han (Chinese Academy of Sciences, China); Qiang Du (Chinese Academy of Sciences, China);* ..... 562

### Attosecond Pulse Generation in Waveform-shaped Two-color Laser Fields

*Zhizhan Xu (Shanghai Institute of Optics and Fine Mechanics, Chinese Academy of Sciences, China); Ya Cheng (Shanghai Institute of Optics and Fine Mechanics, China); Ruxin Li (Shanghai Institute of Optics and Fine Mechanics, China);* ..... 563

### Spatial and Temporal Evolution of Gaussian Femtosecond Pulses after Angular Dispersion

*Shaoqun Zeng (Huazhong University of Science and Technology, China); Xiaohua Lv (Huazhong University of Science and Technology, China);* ..... 564

## High-order Harmonic Generation in Mixed Gases

E. J. Takahashi, T. Kanai, Y. Nabekawa, and K. Midorikawa

Laser Technology Laboratory, RIKEN, Japan

**Abstract**— High-order harmonic generation (HHG) has been recently recognized as one of the best methods of producing an ultrashort coherent light covering a wavelength range from the vacuum ultraviolet to the soft X-ray (XUV) region. High-order harmonics (HH) are applied to a variety of applications. Moreover, HH sources have successfully opened new research areas, such as attosecond science and nonlinear optics in the XUV region. Thus, HHG in pure gases pumped with intense ultrashort lasers is widely accepted as a robust method to obtain ultrashort intense coherent radiation in the XUV region.

Physics of HHG in pure gases is now well understood by the so-called three-step model. HHG in mixed gases, however, has not been noticed both theoretically and experimentally, although it contains profound aspects of HHG. Recently, we have introduced mixed gases as nonlinear media for HHG for the first time and observed destructive and constructive interference of harmonics in a mixed gas of He and Ne and dramatic enhancement of harmonics in a mixed one of He and Xe.

In this paper, novel phenomena caused by interaction of high harmonics generated in mixed gases are reported. Firstly, we determine the excursion times of the electron responsible for HHG in the attosecond region by measuring interference modulation due to the difference between the phase of the harmonics generated in He and Ne gases. Secondly, we demonstrate conclusive experimental evidence of the dramatic enhancement effect of HHG by simultaneous irradiation of seed harmonics to assist optical field ionization.



# Ultrafast Optics for High-order Harmonics and Attosecond Pulses

Paolo Villorosi

Laboratory of Ultraviolet and X-ray Optical Research, CNR-INFM  
DEI-University of Padova, V. Gradenigo 6, 35131 Padova, Italy

**Abstract**— The recent advancement in the nonlinear effects using few-optics-cycle laser pulses have made possible the generation of radiation with extended spectrum in the XUV and duration of the order of one hundred attoseconds. These results are paving the way to a novel class of investigations, in which the probe duration is comparable to the internal time-scale of the atoms and ions. Two methods have proven experimentally the production of isolated attosecond pulses: the high-order harmonics (HHs) cutoff selection [1, 2] and the polarization gating [3, 4]. Other techniques have been used to generate trains of as pulses [5, 6]. These advancements posed the original problem of the pulses compression in order to reach the transform limit of the very large spectrum in the extreme ultraviolet spectral region [3].

This paper will describe first the concept and the performances of a compressor for attosecond pulses in the extreme-ultraviolet spectral region. The exploitation of conical diffraction is expected to confer to this scheme a very high efficiency. The ultimate limit to compression calculated in a case study for the range 10–20 nm resulted lower than 10 as [7].

Moreover, the experimental demonstration of the selection of a portion of the HHs spectrum with a time-compensated scheme will be presented. This leads to the generation of ultrafast and intense XUV pulses of tunable wavelength among the HHs spectrum, using a time-delay compensated monochromator [8–10].

## REFERENCES

1. Hentschel, M., et al., “Attosecond metrology,” *Nature*, Vol. 414, 509–518, 2001.
2. Kienberger, R., et al., “Atomic transient recorder,” *Nature*, Vol. 427, 817–820, 2004.
3. Sola, J., et al., “Controlling attosecond electron dynamics by phase-stabilized polarization gating,” *Nature Physics*, Vol. 2, 319–322, 2006.
4. Sansone, G., et al., “Isolated single-cycle attosecond pulses,” *Science*, Vol. 314, 443–447, 2006.
5. Paul, P., et al., “Observation of a train of attosecond pulses from high harmonic generation,” *Science*, Vol. 292, 1689–1693, 2001.
6. Lopez-Martens, R., et al., “Amplitude and phase control of attosecond light pulses,” *Phys. Rev. Lett.*, Vol. 94, 033001, 2005.
7. Poletto, L., F. Frassetto, and P. Villorosi, “Attosecond pulse compression in the extreme ultraviolet region by conical diffraction,” *CLEO 2007*, Baltimore, 2007.
8. Villorosi, P., “Compensation of optical path lengths in extreme-ultraviolet and soft-x-ray monochromators for ultrafast pulses,” *Appl. Opt.*, Vol. 38, 6040–6050, 1999.
9. Poletto, L., “Time-compensated grazing-incidence monochromator for extreme-ultraviolet and soft X-ray high-order harmonics,” *Appl. Phys. B*, Vol. 78, 1013–1015, 2004.
10. Poletto, L. and P. Villorosi, “Time-compensated monochromator in the off-plane mount for extreme-ultraviolet ultrashort pulses,” *Appl. Opt.*, Vol. 45, 8577–8585, 2006.

# Carrier-envelope Phase Controlled 5-fs Optical Pulses for Driving Single Attosecond Pulses Generation

Zhiyi Wei, Jiangfeng Zhu, Hao Teng, Hainian Han, and Qiang Du

Beijing National Laboratory for Condensed Matter Physics, Institute of Physics  
Chinese Academy of Sciences, Beijing 100080, China

**Abstract**— The generation of single attosecond laser pulses has opened up the new era for research the electron dynamics in attosecond time scale, in general, intense few-cycle optical pulses was used to drive the gas jet to generate high-order harmonic wave for attosecond laser, it has been well known that field reproducibility in each laser shot is predominant for isolated attosecond pulses generation. In this presentation, we report the carrier-envelope phase controlled 5 fs laser at repetition rate of 1 kHz through hollow-core capillary for spectral broadening, white-light continuum was first generated by injecting the 25 fs amplified pulses with pulse energy of 800  $\mu\text{J}$  into a hollow fiber filled with rare gas at high pressure. By dispersion compensation with a set of chirped mirrors, the shortest pulses are measured to be 5.1 fs which is less than two optical cycles, and the pulse energy is up to 400  $\mu\text{J}$ . Following, we carry out carrier-envelope phase stabilization of the few-cycle optical pulses. The carrier-envelope offset frequency of the seed oscillator is fixed at a quarter of the repetition frequency of the oscillator, so every fourth pulse has the same carrier-envelope phase. The phase drift during the amplification stage is monitored by spectral interferometry between an octave spanning white-light continuum generated in a sapphire plate and its second harmonic. Carrier-envelope phase slip is extracted from the interference through Fourier transform and is stabilized by a phase lock loop. The jitter is found to be less than 53 mrad (root-mean-square, RMS). This laser system with carrier-envelope phase stabilized few-cycle pulses enables us to produce coherent soft X-ray emission and open the way to generate single attosecond pulses.

# Attosecond Pulse Generation in Waveform-shaped Two-color Laser Fields

Zhizhan Xu, Ya Cheng, and Ruxin Li

State Key Laboratory of High Field Laser Physics, Shanghai Institute of Optics and Fine Mechanics  
P. O. Box 800-211, Shanghai 201800, China

**Abstract**— In the classical picture of high-order harmonic generation (HHG), an electron is first tunnel-ionized at peak of an electric field, and then is accelerated outward from its parent ion until the laser field reverses its direction. After that, the electron is driven back to the ion and recombines with the ion through the release of an XUV photon [1]. The system composed of the atom and the driving laser field can be regarded as a microscopic X-ray tube where electrons are first accelerated to high energy by an electric field and then collide with a solid target [2]. Therefore, in order to optimize the HHG process, it is crucial to precisely control the electron dynamics in the light field, such as the ionization, acceleration, and recombination, which are completely determined by the light waveform.

From theoretical point of view, generation of arbitrary light waveform can be realized by Fourier synthesis of optical pulses whose frequencies span a broad spectrum. However, this approach is still technically too difficult at present. We will show that, in a general sense, one can effectively control the light waveform using two-color laser fields. In particular, our interest is focused on the optimization of the waveform of few-cycle light field. We demonstrate that isolated single sub-100as extreme ultraviolet (XUV) pulse can be efficiently generated via HHG process by adding a phase-delayed, weak second-harmonic wave upon a few-cycle driving pulse [3]; and high energy photons and electrons as well as tunable XUV coherent radiation can be obtained by adding a weak sub-harmonic wave on the few-cycle pulse [4]. Moreover, quantum path control in few-cycle regime is achievable using these synthesized two-color driving pulses [4]. Some of the theoretical predictions have been proved by recent experiments [5].

## REFERENCES

1. Corkum, P. B., *Phys. Rev. Lett.*, Vol. 71, 1994, 1993.
2. Kapteyn, H., O. Cohen, I. Christov, and M. Murnane, *Science*, Vol. 317, 775, 2007.
3. Zeng, Z., Y. Cheng, X. Song, R. Li, and Z. Xu, *Phys. Rev. Lett.*, Vol. 98, 203901, 2007.
4. Song, X., Z. Zeng, Y. Fu, B. Cai, R. Li, Y. Cheng, and Z. Xu, *Phys. Rev. A*, submitted.
5. Zheng, Y., Z. Zeng, X. Li, X. Chen, H. Lu, S. Zhao, P. Liu, H. Xiong, P. Wei, L. Zhang, Z. Wang, J. Liu, H. Zeng, Y. Cheng, R. Li, and Z. Xu, *Phys. Rev. Lett.*, submitted.

## Spatial and Temporal Evolution of Gaussian Femtosecond Pulses after Angular Dispersion

Shaoqun Zen and Xiaohua Lv

Britton Chance Center for Biomedical Photonics, Wuhan National Laboratory for Optoelectronics  
Huazhong University of Science and Technology, Wuhan 430074, China

**Abstract**— Evolution of femtosecond pulses is an important problem that may be very important for such application as two-photon imaging and femtosecond laser micromachining. Beam spot size and pulse width evolution of Gaussian femtosecond pulses after angular dispersion is analyzed based on Gaussian beam model without the assumption of well collimation. General analytical expression has been found and verified with experiments. The results indicate that beam spot size evolution after angular dispersion is determined by the direct interaction of spectra lateral walkoff by angular dispersion and the original divergence of the Gaussian beam. It is also found that the effects of spectral lateral walk-off, group delay dispersion and the distance traveled on the pulse-width are substantially different when the beam has not been well collimated and when the beam has been collimated. It is showed the difference results from the decaying nature of the angular dispersion of the Gaussian beam sent across a distance. The work here reveals insights for the propagation of Gaussian femtosecond laser beam after angular dispersion, and may be important for the generation and application of the Gaussian femtosecond laser.

# Session 3A2a

## Shaping Optical Forces for Trapping and Binding – Near-field

### Spectral Response of Plasmonic Optical Traps

*Lina Huang (Swiss Federal Institute of Technology Lausanne (EPFL), Switzerland); Olivier J. F. Martin (Swiss Federal Institute of Technology Lausanne (EPFL), Switzerland);* ..... 566

### Trapping Force in Near-field Laser Tweezers

*Baohua Jia (Swinburne University of Technology, Australia); Min Gu (Swinburne University of Technology, Australia);* ..... 567

### Waveguide Based Optical Handling for Biology and Nanofabrication

*Stephane Gétin (CEA-LETI, MINATEC, France); S. Gaugiran (CEA-LETI, MINATEC, France); D. Néel (CEA-LETI, MINATEC, France); P. Ferret (CEA-LETI, MINATEC, France); J.-M. Fedeli (CEA LETI, France); J. Derouard (Universite Joseph Fourier, France);* ..... 568

### Algorithms for Specialized Holographic Optical Tweezers (HOTs): Superresolution, Self-reconstruction, and Evanescent-wave Shaping

*Johannes Courtial (University of Glasgow, UK); L. C. Thomson (University of Glasgow, UK); J. Nelson (University of Glasgow, UK); Michael Mazilu (University of St. Andrews, UK);* ..... 569

### Selfconsistent Collective Dynamics and Stability of an Optically Bound Chain

*Janos Asboth (Universität Innsbruck, Austria); Peter Domokos (Universität Innsbruck, Austria); Helmut Ritsch (Universität Innsbruck, Austria);* ..... 570

## Spectral Response of Plasmonic Optical Traps

Lina Huang and Olivier J. F. Martin

Nanophotonics and Metrology Laboratory

Swiss Federal Institute of Technology Lausanne (EPFL), Switzerland

**Abstract**— The optical forces generated by plasmonic nanostructures deposited on a dielectric substrate are investigated as a function of the excitation wavelength. The various force components show a different behavior as a function of the illumination wavelength. The vertical optical force is particularly relevant to trap particles towards the metallic structure. Fig. 1 (left) shows the dependence of this vertical force as a function of the distance  $z$  above the structure and the illumination wavelength for a  $100\text{ nm} \times 100\text{ nm} \times 40\text{ nm}$  gold structure on a glass substrate illuminated under total internal reflection. When the plasmon resonance is excited in the structure (around a wavelength of  $630\text{ nm}$ ), the magnitude of the vertical force rises quite dramatically, leading to a sharp dip in Fig. 1 (left) since the force is attractive (i.e., negative). Note also that the force decreases rapidly when one moves away from the structure. At a given wavelength, the optical force is not homogeneous over the structure, as illustrated in Fig. 1 (right). This figure shows a map of the vertical component of the optical force over the same  $100\text{ nm} \times 100\text{ nm} \times 40\text{ nm}$  gold structure, at the excitation wavelength of  $630\text{ nm}$ . Note that the strongest force is observed at the edges of the structure. Finally, the utilization of such a plasmonic trapping scheme for lab-on-the-chip applications will be discussed.

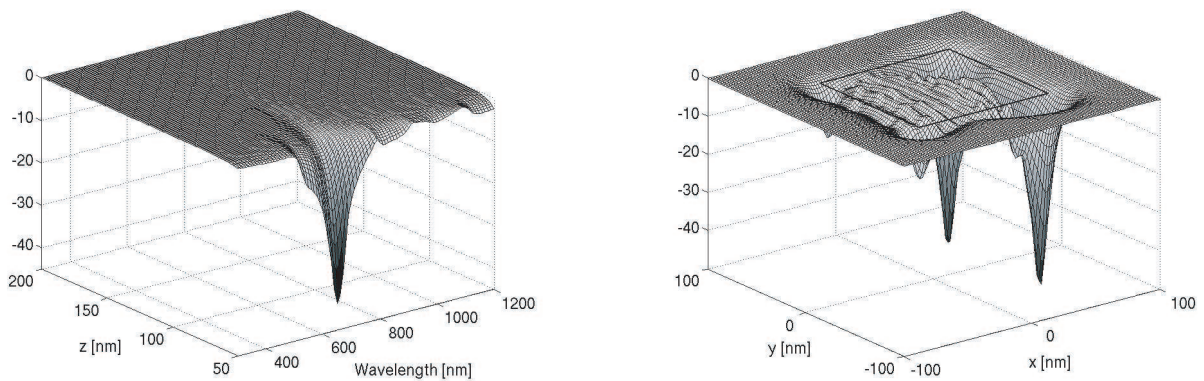


Figure 1: (left) Spectral response of the vertical component of the optical force above a  $100\text{ nm} \times 100\text{ nm} \times 40\text{ nm}$  gold particle as a function of the illumination wavelength and the distance  $z$  above the structure. (right) Distribution of the vertical component of the force over the structure at a  $630\text{ nm}$  wavelength (the projection of the structure is shown in black).

# Trapping Force in Near-field Laser Tweezers

Baohua Jia and Min Gu

Centre for Micro-Photonics, Faculty of Engineering and Industrial Sciences  
Swinburne University of Technology  
P. O. Box 218, Hawthorn 3122, Australia

**Abstract**— Recently near-field trapping using a focused evanescent field generated by a high numerical aperture (NA) total internal reflection (TIR) objective with an annular beam has been proposed and demonstrated to be advantageous over the far-field trapping due to the significantly reduced focal volume, which can substantially suppress the background and heating effect [1,2]. In the mean time, rotation mechanisms, which are of great importance in terms of achieving a complete manipulation of the trapped micro-objects, can be potentially introduced by dynamically controlling the phase, amplitude or even polarization states of the incident beam, whereas in other near-field trapping scheme, such as using a metallic tip, it is rather challenging [3]. To this end Laguerre-Gaussian (LG) beams, which have been commonly used in far-field laser trapping for rotation due to carrying orbital angular momentum, was combined with the focused evanescent illumination. It was revealed by near-field optical microscopy that an anomalous deformation occurs to the focal intensity distribution of a focused evanescent LG beam owing to the phase dislocation originated from the interplay of the phase shift induced by the TIR and the spiral phase front of the LG beam [4]. Under such a circumstance, a complete transverse force mapping is essential to reveal the interaction between the laser focus and the micro-objects since the symmetry of the field is broken. In this paper, theoretical investigations on the two-dimensional transverse trapping efficiency of a dielectric micro-particle under the illumination of a focused evanescent LG beam are presented. The complete 2D trapping force mapping is implemented by using the Maxwell stress tensor approach combined with the vectorial diffraction theory [5]. It is revealed that the severe focal field deformation associated with a focused evanescent LG beam causes significant impact on the transverse trapping performance of the micro-particle. A strong tangential force component is observed in the transverse efficiency mapping, which potentially induces the rotational motion to the particle within a small trapping volume in the optical near-field.

## REFERENCES

1. Gu, M., J.-B. Haumonte, Y. Micheau, J. W. M. Chon, and X. Gan, "Laser trapping and manipulation under focused evanescent wave illumination," *Appl. Phys. Lett.*, Vol. 84, 4236, 2004.
2. Jia, B., X. Gan, and M. Gu, "Direct observation of a pure focused evanescent field of a high numerical aperture objective lens by scanning near-field optical microscopy," *Appl. Phys. Lett.*, Vol. 86, 131110, 2005.
3. Novotny, L., R. X. Bian, and X. S. Xie, "Theory of nanometric optical tweezers," *Phys. Rev. Lett.*, Vol. 79, 645, 1997.
4. Jia, B., X. Gan, and M. Gu, "Anomalous phenomenon of a focused evanescent Laguerre-Gaussian beam," *Optics Express*, Vol. 13, 10360–10366, 2005.
5. Ganic, D., X. Gan, and M. Gu, "Exact radiation trapping force calculation based on vectorial diffraction theory," *Opt. Express*, Vol. 12, 2670, 2004.

# Waveguide Based Optical Handling for Biology and Nanofabrication

S. Gétin<sup>1</sup>, S. Gaugiran<sup>1</sup>, D. Néel<sup>1</sup>, P. Ferret<sup>1</sup>, J.-M. Fedeli<sup>1</sup>, and J. Derouard<sup>2</sup>

<sup>1</sup>CEA-LETI, MINATEC, 17 rue des Martyrs 38054 Grenoble cedex 9, France

<sup>2</sup>Laboratoire de Spectrométrie Physique, UMR 5588 CNRS, Université Joseph Fourier  
BP 87 38402 Saint Martin d'Hères, France

**Abstract**— The evanescent field created on the surface of an ion exchanged waveguide is able to trap and move microparticles [1]. This setup could enable non-invasive devices to concentrate, move, sort and mix micro-nanoparticles and biological objects. Moreover, the manufacturing of these components is compatible with mass production of low cost disposable devices. In this paper, we present the design of high efficiency trapping waveguides and their application to the manipulation of biological cells and nanowires.

A numerical approach of the problem based on the finite element method has been developed. This method enables the calculation of the 3D distribution of the electromagnetic fields around the object. The resulting optical forces are calculated thanks to the Maxwell stress tensor formalism. We have compared the computed forces on different kinds of waveguides. For a given power injected in the waveguide we see that the use of silicon nitride thin films increases the optical forces by a factor of 100 compared to potassium exchanged waveguides. This has been then experimentally confirmed with studies on metal [2] and dielectric particles (latex and glass).

The enhanced propulsion efficiency of particles on silicon nitride waveguides opens the way to cell manipulation. Cells have different optical and physical properties than glass or latex particles: they are bigger (5  $\mu\text{m}$  diameter) and have lower refractive index ( $n \approx 1.4$ ). We worked with two kinds of cells: red blood cells and yeast cells (*Saccharomyces cerevisiae*). On a 10  $\mu\text{m}$  width waveguide, we observed the propulsion of the red blood cells with velocities about 1  $\mu\text{m/s}$  for 60 mW inside the waveguide. For yeast cells, the propulsion velocities are approximately 1  $\mu\text{m/s}$  for a guided power of 40 mW. Like dielectric particles, cells tend to form small chains [3].

With this same technology, we have investigated for the first time to our knowledge the motion of silicon nanowires above silicon nitride waveguides. The nanowires in aqueous solution are attracted towards the waveguide by optical gradient forces. The nanowires align themselves according to the axis of the waveguide and get propelled along the waveguide due to radiation pressure. Movement velocities are up to 40  $\mu\text{m/s}$ . These velocities are studied in relation to the polarization of the injected light (TE or TM).

## REFERENCES

1. Kawata, S. and T. Tani, "Optically driven Mie particles in an evanescent field along a channeled waveguide," *Opt. Lett.*, Vol. 21, 1768, 1996.
2. Gaugiran, S., S. Gétin, J. M. Fedeli, and J. Derouard, "Polarization and particle size dependence of radiative forces on small metallic particles in evanescent optical fields. Evidences for either repulsive or attractive gradient forces," *Opt. Express*, Vol. 15, 8146–8156, 2007.
3. Gaugiran, S., S. Gétin, J. M. Fedeli, G. Colas, A. Fuchs, F. Chatelain, and J. Derouard, "Optical manipulation of microparticles and cells on silicon nitride waveguides," *Opt. Express*, Vol. 13, 6956–6963, 2005.



# Algorithms for Specialized Holographic Optical Tweezers (HOTs): Superresolution, Self-reconstruction, and Evanescent-wave Shaping

J. Courtial<sup>1</sup>, L. C. Thomson<sup>1</sup>, J. Nelson<sup>1</sup>, and M. Mazilu<sup>2</sup>

<sup>1</sup>Department of Physics and Astronomy, University of Glasgow, United Kingdom

<sup>2</sup>School of Physics and Astronomy, University of St Andrews, United Kingdom

**Abstract**— We have devised and implemented algorithms for the calculation of phase-hologram patterns for specialized applications in holographic optical tweezers (HOTs). Our algorithms allow superresolution, that is shaping of the intensity beyond the diffraction limit; self-reconstruction of light beams in arbitrarily many directions simultaneously; and three-dimensional shaping of the intensity of superpositions of evanescent waves.

As optical manipulation ventures into smaller and smaller length scales, it is becoming increasingly important to be able to bring individual optical traps close together without them losing their identities. Superresolution holography can help here. It is a compromise: Our algorithm shapes only the part of the beam that lies within a pre-defined area of interest, while not constraining the beam outside the area of interest. In return, the part of the beam that is being shaped can be shaped beyond the diffraction limit. We will present tweezers-specific simulations of superresolution holography, and discuss its usefulness in practical applications.

One application of optical tweezers is the construction of complex micro structures, for example photonic crystals. In this regime, the effect of the trapped objects on the beam — most notably optical binding — becomes important. On the other hand, some light beams, for example Bessel Beams, are self-reconstructing: if part of the beam is perturbed, the beam's intensity returns to its original shape on further propagation. We have devised an algorithm for the creation of generalized self-reconstructing light beams. Such light beams are self-reconstructing in more than one direction simultaneously, and their 3D intensity distribution can be shaped arbitrarily. We will present computer simulations of light beams shaped using our algorithm.

An area of increasing activity, both because it allows optical manipulation of particles across a large area and because the trapping light can possess sub-wavelength intensity features, is evanescent-wave trapping. We have adapted standard optical-tweezers algorithms to shape three-dimensional evanescent-wave intensity distributions. Our computer simulations demonstrate that it is possible to shape the intensity in the longitudinal direction (for example, the intensity can go through two maxima in the direction in which the evanescent waves decay), but they also demonstrate the limitations of this shaping.

We believe such algorithms will become increasingly useful as optical manipulation advances towards more complex structures and smaller scales.

## Selfconsistent Collective Dynamics and Stability of an Optically Bound Chain

Janos Asboth, Peter Domokos, and Helmut Ritsch

Institut für Theoretische Physik, Universität Innsbruck, Technikerstr. 25, Innsbruck, Austria

**Abstract**— We develop and solve the self-consistent, coupled particle and field equations of motion for a large ensemble of polarizable particles trapped within a far detuned laser field in a 1D standing wave geometry. Cooperative backscattering of the particles strongly modifies the light field distribution and generates long range interactions mediating collective particle oscillation modes. This opto-mechanical coupling is strongly enhanced for asymmetric pumping and leads to a significantly reduced lattice constant at steady state. The collective excitations of the lattice take the form of traveling density waves, which get more pronounced in the asymmetric pump case even in the presence of large viscous cooling. Above a threshold asymmetry this waves are amplified and the lattice becomes unstable.

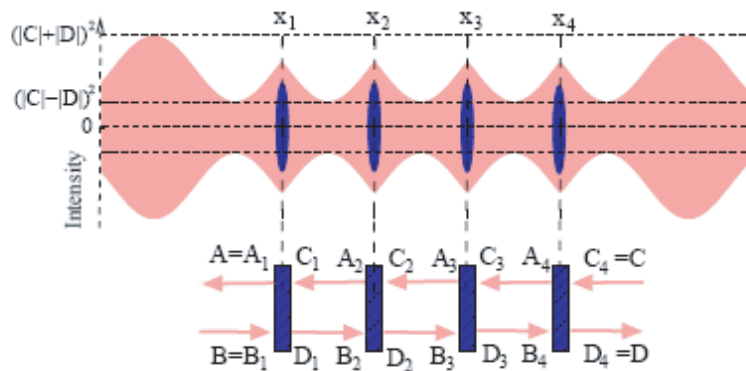


Figure 1: Two laser beams of equal frequency but unequal power create an intensity grating with no nodes. Trapped particles forming disk-shaped clouds are modeled as beam splitters.

### REFERENCES

1. Asbóth, K., H. Ritsch, and P. Domokos, *Phys. Rev. Lett.*, Vol. 98, 203008, 2007.

# Session 3A2b

## Shaping Optical Forces for Trapping and Binding – Binding

<p><a href="#">Longitudinal Optical Binding in Bessel Beams: Theory vs. Experiment</a>  <i>V. Karásek (Institute of Scientific Instruments of the ASCR, v.v.i., Czech Republic); T. Čižmár (Institute of Scientific Instruments of the ASCR, v.v.i., Czech Republic); O. Brzobohatý (Institute of Scientific Instruments of the ASCR, v.v.i., Czech Republic); Pavel Zemánek (Institute of Scientific Instruments of the ASCR, v.v.i., Czech Republic); .....</i></p>	572
<p><a href="#">Advanced Studies of Optical Binding</a>  <i>Tomas Cizmar (University of St Andrews, UK); Peter Reece (University of St Andrews, UK); Klaus Metzger (University of St Andrews, UK); Antonia Carruthers (University of St Andrews, UK); Ewan Wright (University of Arizona, USA); Kishan Dholakia (University of St Andrews, UK); .....</i></p>	574
<p><a href="#">Optical Binding and “Unbinding” in Large-scale Microscopic Particle System</a>  <i>Jack Ng (The Hong Kong University of Science and Technology, China); Zhihong Hang (The Hong Kong University of Science and Technology, China); Che Ting Chan (Hong Kong University of Science and Technology, China); .....</i></p>	575
<p><a href="#">Optical Binding in Evanescent Waves</a>  <i>Luen Yan Wong (Durham University, UK); Matthew R. Cargill (Durham University, UK); Colin D. Bain (Durham University, UK); .....</i></p>	576
<p><a href="#">Full Mie Scattering Model of Optically Bound Particles in Evanescent Waves</a>  <i>Jonathan M. Taylor (Durham University, UK); C. D. Bain (Durham University, UK); G. D. Love (Durham University, UK); .....</i></p>	577

# Longitudinal Optical Binding in Bessel Beams: Theory vs. Experiment

V. Kárásek, T. Čižmár, O. Brzobohatý, and P. Zemánek

Institute of Scientific Instruments of the ASCR, v.v.i. Academy of Sciences of the Czech Republic  
Kralovopolska 147, Brno 612 64, Czech Republic

**Abstract**— We are going to present the latest results concerning sub-micrometer and micrometer size particles self-arrangement in two counter-propagating non-diffracting (Bessel) beams. Experimental set-ups used Bessel beams of typical radii of their cores in the range 1–4  $\mu\text{m}$ . These beams existed over an axial distance of hundreds of micrometres and their axial intensity profiles were smoothed out by a spatial filter. Therefore, the beams intensity variations over a distance of tens of micrometers were negligible in the incident beam and consequently the gradient optical force coming from the incident beam were suppressed enough. These configuration provided an excellent testbed to study 1D optical binding over long range because the interactions between confined objects come mainly from so called optical binding force [1–4].

We carefully measured the parameters of the Bessel beams and used them for numerical simulations based on coupled dipole method [5]. The final goal was to compare the experimental observations and quantitative results with the theoretical simulations for the same input parameters. We compared static behaviour done by the distance between the equilibrium positions of two and more polystyrene beads of diameters 800 and 1070 nm (see Fig. 1). The beads equilibrium configurations were obtained from probability densities to find particles at 1  $\mu\text{m}$  surrounding of certain configuration. The experimental and theoretical results agreed very well withing the experimental error — including the multistability shown in Fig. 1 as wavy force curves.

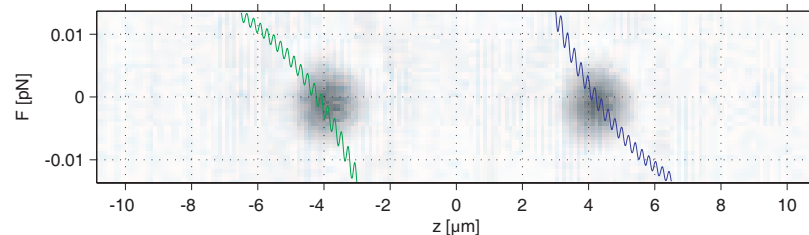


Figure 1: Picture of two polystyrene spheres of diameter 800 nm optically bound in incoherent counter-propagating Bessel beams of core radii 1.8  $\mu\text{m}$  and wavelength 800 nm in water. The wavy curves correspond to the calculated optical forces acting on the right and left sphere for the same parameters as used in the experiment and show multistability of this configuration. Even though the two counter-propagating beams are mutually incoherent, the multistability is caused by the interference of the incident beam with the back-scattered light of the same beam by the rear bead [6].

## ACKNOWLEDGMENT

This project was supported by ISI IRP (AV0Z20650511) and MEYS CR (LC06007).

## REFERENCES

1. Burns, M. M., J.-M. Fournier, and J. A. Golovchenko, "Optical binding," *Phys. Rev. Lett.*, Vol. 63, 1233–1236, 1989.
2. Tatarkova, S. A., A. E. Carruthers, and K. Dholakia, "One-dimensional optically bound arrays of microscopic particles," *Phys. Rev. Lett.*, Vol. 89, 283901, 2002.
3. Singer, W., M. Frick, S. Bernet, and M. Ritsch-Marte, "Self-organized array of regularly spaced microbeads in a fiber-optical trap," *J. Opt. Soc. Am. B*, Vol. 20, 1568–1574, 2003.
4. Metzger, N. K., K. Dholakia, and E. M. Wright, "Observation of bistability and hysteresis in optical binding of two dielectric spheres," *Phys. Rev. Lett.*, Vol. 96, 068102, 2006.
5. Kárásek, V., K. Dholakia, and P. Zemánek, "Analysis of optical binding in one dimension," *Appl. Phys. B*, Vol. 84, 149–156, 2006.

6. Karásek, V. and P. Zemánek, “Analytical description of longitudinal optical binding of two spherical nanoparticles,” *J. Opt. A*, Vol. 9, S215–S220, 2007.

## Advanced Studies of Optical Binding

Tomas Cizmar<sup>1</sup>, Peter Reece<sup>1</sup>, Klaus Metzger<sup>1</sup>  
Antonia Carruthers<sup>1</sup>, Ewan Wright<sup>2</sup>, and Kishan Dholakia<sup>1</sup>

<sup>1</sup>School of Physics and Astronomy, University of St Andrews  
Fife KY16 9SS, Scotland, UK

<sup>2</sup>College of Optical Sciences and Department of Physics, University of Arizona  
Tucson, Arizona 85721, USA

**Abstract**— Optical forces and trapping may dictate the organization and manipulation of colloidal and biological matter at the nanoscopic through to macroscopic level. However full controlled large scale organisation using either of these methods is still an unattained goal. To date have allowed physicists to test several fundamental phenomena including the physics of non-equilibrium systems and optical angular momentum. An ensemble of trapped colloids has a well defined thermodynamic temperature as discovered by Einstein and may be considered as an excellent analogy to extended array of atoms. Insights may be gained on strongly interacting systems such as liquids and phenomena important to condensed-matter physics such as melting, freezing, and the glass transition. The open and to date unaddressed issue is how to use optical fields to initiate large scale assembly of micro and nanoparticles and to fully understand interactions therein. Advanced holographic, beam time-sharing or interferometric techniques may organise several tens of particles. Sculpting the optical field and creating a “tailored optical landscape” can enable experiments elucidating mechanisms at the atomic level. All of these methods have predefined local trap sites in which the matter is situated. Deformation of the light pattern by the very interaction of the particle with the imposed light field is a relevant issue for self assembly of particles at the nano and micro scale but has largely not been addressed. This is where the topic of “optical binding” may play a pivotal and insightful role.

It is noteworthy to state that such “optical binding” is radically different from conventional predefined trapping described in the paragraph above: Here the very interaction between an object and its nearest neighbours creates a self consistent and homogeneous solution that allows a light-particle geometry to, in principle, create a large scale colloidal array. This topic has come again to the fore: work over a decade ago shows this in a geometry by Burns, Golovchenko and Fournier [1]. New and powerful form of longitudinal optical binding in both counter-propagating and vertical beam geometries have come to the fore. The key is that the interparticle spacing here is of the order of microns and indeed the interaction between the particles is creating the bound matter.

Optical bound matter shows rich and interesting particle dynamics including bistable behaviour in particle separations [2] and interesting correlated behaviour in its motion [3]. Recently we have explored the behaviour of larger ensembles of particles in two dimensions on surfaces and seen links between such optical binding and the onset of modulational instability and the formation of optical solitons [4]. In this paper we will review recent experiments at St Andrews in the domain of optical binding and describe new studies looking at the trajectories and forces of particles bound on surfaces. These studies explore various relations between the optical “bonds” and properties of the interacting light-particle system and also verify the existence of transversal binding that might be responsible for unique particle formations observed by Mellor and Bain [5]. Studies varying the coherence of the trapping light will shed new information on the binding process. We believe that the acquirement of controlling these interactions might bring a new level of optical trapping applications together with the possibility to eliminate them in cases where they are not desired.

### REFERENCES

1. Burns, M. M., J. M. Fournier, and J. A. Golovchenko, *Science*, New Series, Vol. 249, No. 4970, 749-754, 1990.
2. Metzger, N. K., K. Dholakia, and E. M. Wright, *Phys. Rev. Lett.*, Vol. 96, No. 068102, 2006.
3. Metzger, N. K., R. F. Marchington, M. Mazilu, R. L. Smith, K. Dholakia, and E. M. Wright, *Phys. Rev. Lett.*, Vol 98, No. 068102, 2007.
4. Reece, P. J., E. M. Wright, and K. Dholakia, *Phys. Rev. Lett.*, Vol. 98, No. 203902, 2007.
5. Mellor, C. D. and C. D. Bain, *ChemPhysChem*, Vol. 7, No. 2, 329–332, 2006.

# Optical Binding and “Unbinding” in Large-scale Microscopic Particle System

Jack Ng, Zhihong Hang, and C. T. Chan

The Hong Kong University of Science and Technology, Hong Kong, China

**Abstract**— A focused laser beam can trap a microscopic particle near its focus. While this optical trapping (OT) technique is developing rapidly and evolving toward simultaneous manipulation of multi-particles, it is not so easy to organize a large number of particles into extended structures. The particles at the boundary of the extended structures will diffract light, consequently the light that reaches the inside of the structure is significantly distorted and will no longer be able to trap particles. Another mechanism of organizing microscopic particles is called “optical binding” (OB) [1, 2], where particles are bound together via multiple scattering of light between the particles. Since in OB, the redistribution of photons by the particles is fully accounted, there is a possibility that OB can lead to large scale light induced organization.

We shall consider OB in large-scale microscopic particle system. We found that OB can organize particles into interesting stable periodic 1D lattices. Interestingly the lattices exhibit a type of stable-unstable transition as the particle’s size, number, and refractive index are increased. Our simulation suggests that for fixed parameters (incident wave, particle size etc.), there is a limit on the maximum number of particles ( $n_{pt}$ ) that can be bounded optically. Furthermore, as the refractive index or the particle size increases,  $n_{pt}$  decreases exponentially. By analyzing the “order of scattering”, we found that the stronger the multiple scattering, the smaller the  $n_{pt}$ .

Aimed at simultaneous organization of a large number of particles, we investigate the cooperation and competition between OT and OB (in an optically-bound 1D lattice). It is found that when OT and OB are working together, one may organize a large number of particles. In general, both OT and OB have a preferred inter-particle separation, and these length scales are in general different and may be tuned by tuning the incident waves. When these two length scales are commensurate, OT and OB are cooperative, and one may optically bind a large number of particles into 1D periodic structure. On the other hand, when these two length scales are incommensurate, only a small number of particles can be bounded. Interestingly, in addition to the reduced stability, the competition between OT and OB induces a long-range structural modulation in the originally periodic chain. The competition of these two length scales is interesting realization of the Frenkel-Kontorova type model.

**Methodology:** We theoretically study light induced optical forces acting on a collection of microscopic particles. In particular, we are interested to see under what condition light can organize particles into a large-scale extended structure. The formalism that we used to compute the optical forces is based on a multiple-scattering and Maxwell Stress Tensor formalism [1].

## REFERENCES

1. Ng, J., Z. F. Lin, C. T. Chan, and P. Sheng, *Phys. Rev. B*, Vol. 72, 085130, 2005.
2. Burns, M. M., J.-M. Fournier, and J. A. Golovchenko, *Science*, Vol. 249, 749, 1990.

## Optical Binding in Evanescent Waves

L. Y. Wong, M. R. Cargill, and C. D. Bain

Department of Chemistry, Durham University, UK

**Abstract**— At PIERS2006 in Cambridge, USA, we reported the formation of two-dimensional arrays of polystyrene particles in the evanescent field of two counter-propagating laser beams at the silica-water interface by optical binding [1–3]. The shapes of the arrays depended on the polarisation of the laser beams and the size of the particles relative to the wavelength of the incident light. In this paper we consider how the nature of the particle affects optical binding. A range of different systems are presently under study and a selection of the more interesting results will be presented

- For a simple hard-sphere system, the only length scale affecting optical binding is the ratio of the particle size to the wavelength of the light. Charge-stabilised polystyrene latices have an additional length scale (the Debye length) associated with the electrostatic repulsion between spheres. Sterically stabilised polymer beads approximate more closely to hard spheres and may simplify theoretical treatments.
- The scattered fields depend strongly on the refractive index contrast between the particles and the solvent. Silica spheres have a lower refractive index contrast than polystyrene in water while titania spheres have a higher refractive index contrast. Experiments with these systems are complicated by the weaker binding in silica and the greater polydispersity of titania, but offer a good testing ground for theories of optical binding.
- Metallic spheres chain in dc and ac-fields, but we are unaware of optical binding studies on such strongly scattering particles. 250-nm diameter gold spheres can be trapped in an evanescent wave and form metastable structures in counterpropagating beams. To date, ordered 2-D arrays have not been observed.
- Optical binding has not been studied with asymmetric particles. While such particles add to the theoretical complexity, they also offer the possibility of creating more complex, anisotropic assemblies. One way of introducing anisotropy that we are exploring is to use Janus particles, which have different dielectric properties on the two sides of a spherical particle.

### REFERENCES

1. Mellor, C. D., C. D. Bain, and J. Lekner, “Pattern formation in evanescent wave optical traps,” *Optical Trapping and Optical Micromanipulation II*, K. Dholakia and G. C. Spalding Eds., *Proc. SPIE 2005*, Vol. 5930, 352–361, 2005.
2. Mellor, C. D. and C. D. Bain, “Array formation in evanescent waves,” *Chem. Phys. Chem.*, Vol. 7, 329–332, 2006.
3. Mellor, C. D., T. A. Fennerty, and C. D. Bain, “Polarization effects in optically bound particle arrays,” *Optics Express*, Vol. 14, 10079–10088, 2006.



## Full Mie Scattering Model of Optically Bound Particles in Evanescent Waves

J. M. Taylor, C. D. Bain, and G. D. Love  
Durham University, UK

**Abstract**— Several groups have recently reported complex self-organizational and dynamic behaviour of microparticles trapped in optical tweezer-like laser beam traps [1–3]. It is important to understand the mechanisms of self-organization if these effects are to be exploited in, for example, the self-assembly of nanostructures.

We present many-particle Mie scattering simulation results for arrays of self-organizing particles in an evanescent wave trap. We compare the calculations with experimental results [2] (also presented in this session) and offer insights into the physical mechanisms which lead to self-organization of the particles.

### REFERENCES

1. Tatarkova, S. A., A. E. Carruthers, and K. Dholakia, “One-dimensional optically bound arrays of microscopic particles,” *Phys. Rev. Lett.*, Vol. 89, No. 28, 283901, 2002.
2. Mellor, C. D., T. A. Fennerty, and C. D. Bain, “Polarization effects in optically bound particle arrays,” *Optics Express*, Vol. 14, No. 21, 10079–10088, 2006.
3. Milne, G., K. Dholakia, D. McGloin, K. Volke-Sepulveda, and P. Zemánek, “Transverse particle dynamics in a Bessel beam,” *Optics Express*, Vol. 15, No. 21, 13972–13987, 2007.



# Session 3A3a

## Metamaterials Design and Applications

<p><a href="#">Design of a 4-bit High Power Phase Shifter Module with Left-handed Transmission Line</a>  <i>Jun Zhang (University of Science and Technology of China, China); Qi Zhu (University of Science and Technology of China, China); Shanjia Xu (University of Science and Technology of China, China);</i></p> <p><a href="#">A Novel Left-handed NRD Guide Directional Coupler without LSE<sub>11</sub> Mode Conversion Loss</a>  <i>Meng Huang (University of Science and Technology of China, China); Shanjia Xu (University of Science and Technology of China, China);</i></p> <p><a href="#">Design of Microstrip Antennas with Composite Right/Left-handed Transmission Lines</a>  <i>Lu Han (University of Sci. and Tech. of China, China); Qi Zhu (University of Science and Technology of China, China); Shanjia Xu (University of Science and Technology of China, China);</i></p> <p><a href="#">Performance Investigation of the Flat Antenna Based on Metamaterials</a>  <i>Dexin Ye (Zhejiang University, China); Lixin Ran (Zhejiang University, China); Jin Au Kong (Massachusetts Institute of Technology, USA);</i></p> <p><a href="#">The Prevention of Multipactor Discharge in Rectangular Waveguide Loaded with Uniaxial Metamaterial</a>  <i>Wan-Zhao Cui (Xi'an Institute of Space Radio Technology, China); Zhiyu Wang (Zhejiang University, China); Tao Jiang (Zhejiang University, China); Dongxing Wang (Zhejiang University, China); Wei Ma (Xi'an Institute of Space Radio Technology, China); Lixin Ran (Zhejiang University, China);</i></p> <p><a href="#">Experimental Study of the Transmission Property of Anisotropic Left-handed Materials</a>  <i>Tao Jiang (Zhejiang University, China); Lixin Ran (Zhejiang University, China); Zhiguo Shi (Zhejiang University, China);</i></p>	<p>580</p> <p>581</p> <p>582</p> <p>583</p> <p>584</p> <p>585</p>
---	---

## Design of a 4-bit High Power Phase Shifter Module with Left-handed Transmission Line

Jun Zhang, Qi Zhu, and Shanjia Xu

Dept. of EEIS, University of Science & Technology of China, Hefei 230027, China

**Abstract**— Based on the structure of left-handed transmission line (LH-TL), a novel integrated 4-bit phase shifter with high power capacity is described. Compared to the traditional Right-hand transmission line based phase shifter, switches are mounted on the fingers of LH-TLs. So the electric current through the switches is only a fraction of that through the whole phase shifter, the power capacity is greatly improved. By alternating the state of switches, multiple phase shifts can be achieved in a single LH-TL element. Also, the phase shifter possesses other advantages such as low cost, small size and easy fabrication.

### ACKNOWLEDGMENT

This work is supported by the National Natural Science Foundation of China (No. 60471037, 60531020).

# A Novel Left-handed NRD Guide Directional Coupler without $LSE_{11}$ Mode Conversion Loss

Meng Huang and Shanjia Xu

Department of Electronics Engineering and Information Science  
University of Science and Technology of China, Hefei, Anhui 230027, China

**Abstract**— In an NRD guidance system with  $LSM_{11}$  mode as its operating mode, the parasitic  $LSE_{11}$  mode will always be excited for asymmetrical discontinuity structures with respect to the longitudinal section. This mode conversion loss can become quite substantial and bring up practical difficulties in an integrated circuit environment. In this paper, we report that this mode conversion effect can be avoided in Left-Handed NRD (LH-NRD) guide structures. Based on this feature, a novel LH-NRD guide directional coupler without mode conversion loss is proposed, its scattering characteristics are analyzed by a method which combines the building block approach and multimode network theory with a rigorous mode-matching procedure. Numerical results verify the feature of mode conversion loss free as expected, and indicate that the proposed coupler is very efficient.

## ACKNOWLEDGMENT

This work is supported by the National Natural Science Foundation of China (No. 60471037 and No. 63531020).

# Design of Microstrip Antennas with Composite Right/Left-handed Transmission Lines

Lu Han, Qi Zhu, and Shanjia Xu

Dept. of EEIS, University of Sci. & Tech. of China, Hefei 230027, China

**Abstract**— Based on the structure of composite right/left-handed transmission lines (CRLH-TLs), a novel high gain printed antenna with CRLH-TLs array is presented here. To improve the gain and the radiation efficiency furthermore, a dual-layered microstrip CRLH-TLs has been developed. As examples, two microstrip antennas with dual-layered CRLH-TLs structure, working at X and L bands respectively, are designed. Compared to the traditional microstrip antenna, the proposed antennas have shown their advantages such as high gain, high radiation efficiency, broad bandwidth, low RCS and small size.

## ACKNOWLEDGMENT

This work is supported by the National Natural Science Foundation of China (No. 60471037, 60531020).

## REFERENCES

1. Caloz, C. and T. Itoh, "Application of the transmission line theory of left-handed (LH) materials to the realization of a microstrip 'LH line'," *Antennas and Propagation Society International Symposium, 2002, IEEE*, Vol. 2, 16–21, June 2002.
2. Yu, F., Q. Zhu, W. Lu, and S. Xu, "Improved structure of left-handed transmission line," submitted to *IEEE AP-S*, 2007.

## Performance Investigation of the Flat Antenna Based on Metamaterials

Dexin Ye<sup>1,2</sup>, Lixin Ran<sup>1,2</sup>, and Jin Au Kong<sup>1,3</sup>

<sup>1</sup>The Electromagnetics Academy at Zhejiang University, Zhejiang University, Hangzhou 310058, China

<sup>2</sup>Department of Information and Electronic Engineering, Zhejiang University, Hangzhou 310027, China

<sup>3</sup>Research Laboratory of Electronics, Massachusetts Institute of Technology, Cambridge, MA 02139, USA

**Abstract**— As the theoretical study of metamaterials developed, Many investigations have examined the theoretical analysis and numerical simulation for this amazing characteristic of metamaterials, more and more artificial structures are designed which have negative permittivity or have negative permeability as well as both negative permittivity and negative permeability. Also epsilon-near-zero (ENZ) and mu-near-zero (MNZ) materials may be properly synthesized as metamaterials at the desired frequency, by embedding suitable inclusions in a host medium. Typical applications of these materials are perfect lenses that are not limited to the usual wavelength limits by employing double negative indexes materials, and most recently, cloaks of invisibility constructed by artificially structured gradient metamaterials. Antennas are also a field in which metamaterials find their amazing applications. In the abstract, isotropic materials with epsilon-near-zero and mu-near-zero and anisotropic materials with special parameters are able to achieve highly directive emission, but whether or not they are able to improve the gain of antenna is still a question. In this paper, we investigate the performance of the flat antenna based on metamaterials. We investigate the flat antennas made of several different materials by simulating and calculating their radiation property and gain. According to the relationship between gain and caliber of parabola antenna, we change the caliber of flat antenna to analyze the changes of gain of the flat antenna. Eventually, we will give a detailed instruction about how to make a flat antenna of metamaterials and how to design relevant artificial structure with desired permittivity and permeability.

## The Prevention of Multipactor Discharge in Rectangular Waveguide Loaded with Uniaxial Metamaterial

Wanzhao Cui<sup>1</sup>, Zhiyu Wang<sup>2</sup>, Tao Jiang<sup>2</sup>  
Dongxing Wang<sup>2</sup>, Wei Ma<sup>1</sup>, and Lixin Ran<sup>2</sup>

<sup>1</sup>National Key Laboratory of Space Microwave Technology  
Xi'an Institute of Space Radio Technology, Xi'an 710000, China

<sup>2</sup>The Electromagnetics Academy at Zhejiang University  
Zhejiang University, Hangzhou 310027, China

**Abstract**— Single-negative uniaxial metamaterial is used to reduce the possibility of multipactor in rectangular waveguide. A waveguide behaves as an E-plasma for TE mode. Single-negative permittivity metamaterial loaded in the waveguide can produce a double-positive passband below the cutoff frequency of the hollow waveguide. Single-negative permeability metamaterial can create both double positive or negative passband depending on the orientation of its optic axis. The metamaterial is inserted in the middle of the waveguide, repeated along the direction of the axis. The TE wave is guided in the region of the uniaxial media. In the other region around, the wave becomes evanescent and attenuates exponentially. As a result, the tangential electric field reduces sharply near the metal boundary, which in agreement with the simulation results. So the probability of electron emission at the metal surface would decrease. Furthermore, this model could be used to control the 1/2-cycle electron transit time between the parallel metal boundary in order to avoid the secondary electron resonance.



# Experimental Study of the Transmission Property of Anisotropic Left-handed Materials

Tao Jiang<sup>1,2</sup>, Lixin Ran<sup>1,2</sup>, and Zhi Guo Shi<sup>1</sup>

<sup>1</sup>Electromagnetics Academy at Zhejiang University, Zhejiang University, Hangzhou 310058, China

<sup>2</sup>Department of Information and Electronic Engineering, Zhejiang University, Hangzhou 310027, China

**Abstract**— The ambiguity function of a kind of chaotic radar using Colpitts oscillator is investigated and compared from different points of view. The Colpitts oscillator with specific value of capacitance and inductance can generate chaotic signal with frequency band from direct current to several gigahertz. The auto-ambiguity functions show that the chaotic signal of such oscillator is ideal for Radar application with both high range and range rate resolution. The cross-ambiguity functions also indicate the chaotic signal has excellent capabilities in the electronic counter-countermeasures (ECCM) and electromagnetic compatibility (EMC).

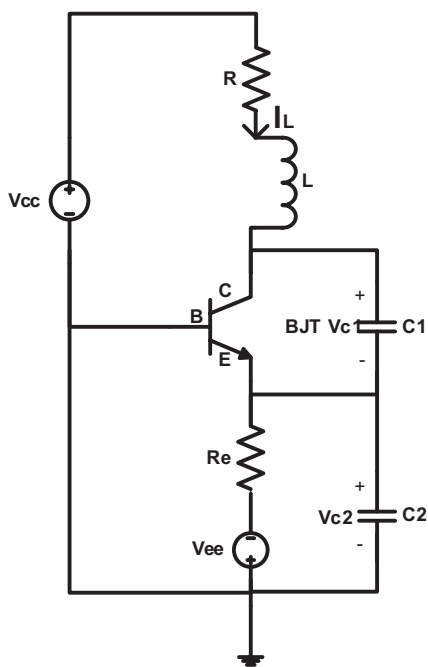


Figure 1: Colpitts oscillator.

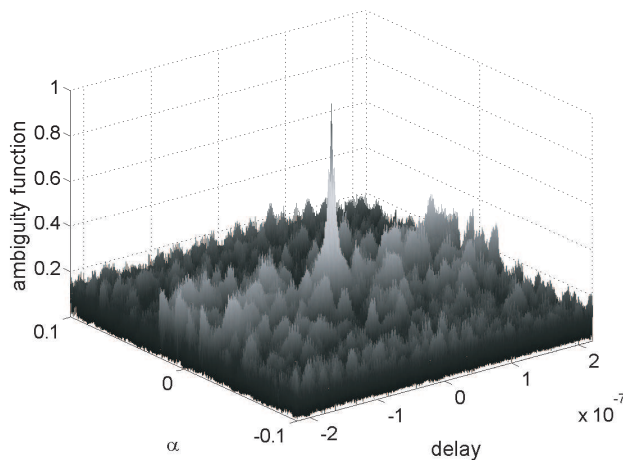


Figure 2: Ambiguity function.

## ACKNOWLEDGMENT

This work is supported by the Key Project of National Science Foundation of China (NSFC) under Contract No. 60531020, and in part by NSFC60671003 and ZJNSF R105253.



# Session 3A3b

## Recent Advances in Metamaterials and Invisibility Cloaking 2

### Cloak Changing with Background

*Jingjing Zhang (Zhejiang University, China); Jiangtao Huangfu (Zhejiang University, China); Yu Luo (Zhejiang University, China); Hongsheng Chen (Zhejiang University, China); Jin Au Kong (Massachusetts Institute of Technology, USA); Bae-Ian Wu (Massachusetts Institute of Technology, USA);* 588

### Cylindrical Cloak Created with Nonlinear Transformations

*Sheng Xi (Zhejiang University, China); Hongsheng Chen (Zhejiang University, China); Bae-Ian Wu (Massachusetts Institute of Technology, USA); Baile Zhang (Massachusetts Institute of Technology, USA); Jiangtao Huangfu (Zhejiang University, China); Dongxing Wang (Zhejiang University, China); Jin Au Kong (Massachusetts Institute of Technology, USA);* ..... 589

### On Extending the Band-width of Electromagnetic Cloaks

*Huanyang Chen (Shanghai Jiao Tong University, China); Xunya Jiang (Institute of Microsystem and Information Technology, CAS, China); Hongru Ma (Shanghai Jiao Tong University, China); C. T. Chan (Hong Kong University of Science and Technology, China);* ..... 590

### Transformation Media for Bend Waveguide

*Jiangtao Huangfu (Zhejiang University, China); Jingjing Zhang (Zhejiang University, China); Sheng Xi (Zhejiang University, China); Hongsheng Chen (Zhejiang University, China); Bae-Ian Wu (Massachusetts Institute of Technology, USA); Dongxing Wang (Zhejiang University, China); Jin Au Kong (Massachusetts Institute of Technology, USA);* ..... 591

### Electromagnetic Absorption by Metamaterial Grating System

*Xiaobing Cai (Beijing Institute of Technology, China); Gengkai Hu (Beijing Institute of Technology, China);* ..... 592

## Cloak Changing with Background

Jingjing Zhang<sup>1,2</sup>, Jiangtao Huangfu<sup>1,2</sup>, Yu Luo<sup>1</sup>  
Hongsheng Chen<sup>1,2</sup>, Jin Au Kong<sup>1,2</sup>, and Bae-Ian Wu<sup>2</sup>

<sup>1</sup>The Electromagnetics Academy at Zhejiang University  
Zhejiang University, Hangzhou 310058, China

<sup>2</sup>Research Laboratory of Electronics, Massachusetts Institute of Technology  
Cambridge, Massachusetts 02139, USA

**Abstract**— Coordinate transformation approach has previously been used for designing cloak which can shield an interior region in a homogeneous medium. In this letter, we consider the case where the background is no longer a homogeneous medium and determine the relative constitutive parameters of the cloak according to the multilayered and gradually changing background. We propose the parameters of cylindrical cloak structures working in multilayered and gradually changing media and the scheme of specifying these parameters could also be applied to the design of cloak in arbitrary isotropic background. The theoretical analysis based on coordinate transformation is given and numerical simulations are performed to illustrate these properties. The simulation results show that the cloaking with the proposed parameters performs well in these inhomogeneous background medium. Potential applications are also discussed.

## Cylindrical Cloak Created with Nonlinear Transformations

Sheng Xi<sup>1,2</sup>, Hongsheng Chen<sup>1,2</sup>, Bae-Ian Wu<sup>2</sup>, Baile Zhang<sup>2</sup>, Jiangtao Huangfu<sup>1,2</sup>  
Dongxing Wang<sup>1</sup>, and Jin Au Kong<sup>1,2</sup>

<sup>1</sup>The Electromagnetics Academy at Zhejiang University, Zhejiang University, Hangzhou 310058, China

<sup>2</sup>Research Laboratory of Electronics, Massachusetts Institute of Technology  
Cambridge, Massachusetts 02139, USA

**Abstract**— We introduce a cylindrical cloak created with a nonlinear transformation. By using the electromagnetic wave scattering theory, we show that the cloak based on the nonlinear transformation is perfect. Since in practical applications, the cloak is usually made of stratified media, and the singularity exists on the inner boundary of the cylindrical cloak is hard to realize, thus the fabricated cloak is usually imperfect. We show the cloak with nonlinear transformation has better performances in practice. The drawbacks affected by the stratification and singularity can be minimized. Numerical simulations are carried out to verify the performances of the non-ideal cloak, showing good agreement with the prediction of the theory.

## On Extending the Band-width of Electromagnetic Cloaks

Huanyang Chen<sup>1,2</sup>, Xunya Jiang<sup>3</sup>, Hongru Ma<sup>1</sup>, and C. T. Chan<sup>2</sup>

<sup>1</sup>Institute of Theoretical Physics, Shanghai Jiao Tong University, Shanghai 200240, China

<sup>2</sup>Department of Physics, Hong Kong University of Science and Technology  
Clear Water Bay, Kowlong, Hong Kong, China

<sup>3</sup>Institute of Microsystem and Information Technology, CAS, Shanghai 200050, China

**Abstract**— Using the idea of a transformation medium, a cloak can be designed to make a domain invisible to all but one target frequency. We examine the possibility of extending the bandwidth of such a cloak. We find that causality requirements impose severe constraints on the system parameters of the transformation medium, and we show that a specific form of “reduction” can help us to create a cloak that offers a reduced cross section in a finite frequency range. We also give a simple inequality that limits the bandwidth of operation.

$$\mu_r = \left( \frac{r - a'}{r} \right)^2, \quad \mu_\theta = 1, \quad \varepsilon_z = \left( \frac{b - \bar{r}}{b - a} \right)^2 \quad (1)$$

$$\omega \frac{dr_0}{d\omega} \geq a \Rightarrow \frac{\Delta\omega}{\omega} \leq \frac{\Delta r_0}{a} \quad (2)$$

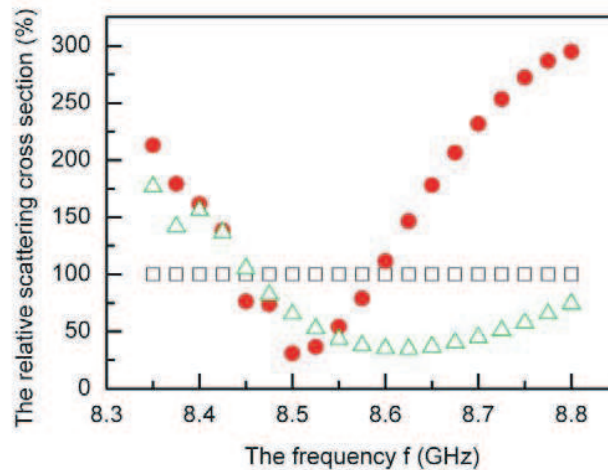


Figure 1: The relative scattering cross sections as a function of frequencies for the dispersive cloak (triangles), the single-frequency cloak (circles) and the PEC cylinder (squares).

### REFERENCES

1. Chen, H., X. Jiang, and C. T. Chan, [http://www.arXiv:0707.1126v2\[physics.optics\]](http://www.arXiv:0707.1126v2[physics.optics]), 2007.
2. Chen, H., Z. Liang, P. Yao, X. Jiang, H. Ma, and C. T. Chan, unpublished results, 2007.

## Transformation Media for Bend Waveguide

Jiangtao Huangfu<sup>1,2</sup>, Jingjing Zhang<sup>1,2</sup>, Sheng Xi<sup>1,2</sup>  
Hongsheng Chen<sup>1,2</sup>, Bae-Ian Wu<sup>2</sup>, Dongxing Wang<sup>1,2</sup>, and Jin Au Kong<sup>1,2</sup>

<sup>1</sup>The Electromagnetics Academy at Zhejiang University, Zhejiang University, Hangzhou 310058, China

<sup>2</sup>Research Laboratory of Electronics, Massachusetts Institute of Technology  
Cambridge, Massachusetts 02139, USA

**Abstract**— The microwave and optical cloaking can be built with the anisotropic inhomogeneous material cloak using coordinate transformation approach. The coordinate transformation approach can also be used to design some complex waveguide device with special properties. In the article, the properties of straight waveguide with transformation media were discussed and confirmed with the simulation results. Another kind of transformation media in bend waveguide based on the coordinate transformation method was presented. Simulation results show that when the material was putted in the bend waveguide, the attenuation of the electromagnetic wave is greatly reduced when propagation through the waveguide junction. Our results provide a good approach for the design of complex waveguide devices with good performance.

# Electromagnetic Absorption by Metamaterial Grating System

Xiaobing Cai and Gengkai Hu

School of Science, Beijing Institute of Technology, Beijing 100081, China

**Abstract**— Total absorption of electromagnetic waves is demonstrated in a system composed of a zero-order diffraction gratings and a rearward metamaterial wall. The grating and the metamaterial wall are separated by an air gap. P-polarized illumination is incident at a random angle to the grating with negative permittivity. Two mechanisms are demonstrated to account for the total absorption. The first one is due to the existence of standing waves in both the grooves of the grating and the air gap. These standing waves trap the electromagnetic waves and induce oscillating surface charge density on the grating surface. The rearward metamaterial with negative permittivity or permeability or double negative parameters are all shown to satisfy the corresponding absorption conditions. The second mechanism is due to excited surface waves at the interface between the air gap and the rearward metamaterial wall. The incident energy are restricted and dissipated at the interface. In this case, only the rearward materials with negative permittivity or left-handed material could excite the surface wave, leading to total absorption.

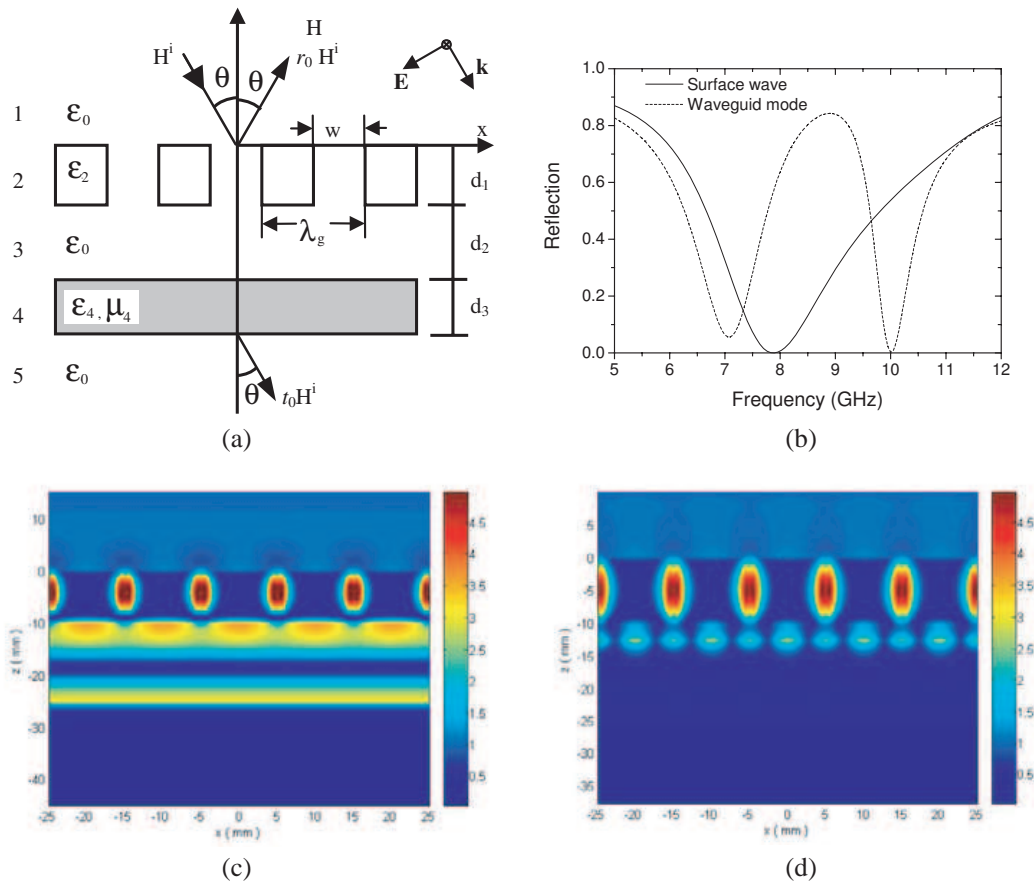


Figure 1: (a) Configuration of the proposed microwave absorbing structure, 1. vacuum, 2. diffraction grating, 3. air gap, 4. metamaterial, 5. vacuum. (b) Reflectance minimums due to waveguide mode and surface wave, respectively. (c) Distribution of magnetic field  $|\mathbf{H}(x, z)|$  as a function of  $x$  and  $z$  over five pitches of the grating with  $\lambda_g = 10.0$  mm,  $d_2 = 30.0$  mm,  $f = 10.0$  GHz. Standing waves appear both in the grooves and the air gap. (d) Distribution of magnetic field  $|\mathbf{H}(x, z)|$  with  $d_2 = 2.7$  mm,  $f = 7.9$  GHz. Strong surface waves are excited at the interface of  $z = -12.7$  mm.



# Session 3A4

## Physical Properties of Photoexcited Semiconductors

<p><a href="#">Optical Emission from Si/<math>\beta</math>-FeSi<sub>2</sub> and C<sub>60</sub>-coupled <math>\beta</math>-FeSi<sub>2</sub> Nanocomposites</a>  <i>Xinglong Wu (Nanjing University, China);</i> .....</p> <p><a href="#">The Manipulation of Tunneling Property by Quantum Dot under Photoexcitation</a>  <i>W. P. Wang (Shanghai Institute of Technical Physics, Chinese Academy of Sciences, China); N. Li (Institute of Technical Physics, Chinese Academy of Sciences, China); Xiaoshuang Chen (Shanghai Institute of Technical Physics, Chinese Academy of Sciences, China); T. X. Li (Shanghai Institute of Technical Physics, Chinese Academy of Sciences, China); Wei Lu (Shanghai Institute of Technical Physics, Chinese Academy of Sciences, China);</i> .....</p> <p><a href="#">Magneto-optical Properties and Spin Dynamics in Novel II-VI and III-V Semiconductor Materials and Nanostructures</a>  <i>I. A. Buyanova (Linköping University, Sweden); W. M. Chen (Linköping University, Sweden); A. A. Murayama (Tohoku University, Japan); Y. Oka (Tohoku University, Japan); C. R. Abernathy (University of Florida, USA); S. J. Pearton (University of Florida, USA);</i> .....</p> <p><a href="#">Exciton-biexciton Dynamics in InGaAs Quantum Wells Studied by Time-resolved Kerr Rotation Spectroscopy</a>  <i>J. Q. Ning (The University of Hong Kong, China); S. J. Xu (The University of Hong Kong, China); X. Z. Ruan (The University of Hong Kong, China); Ji Yang (The University of Hong Kong, China); H. Z. Zheng (The University of Hong Kong, China); H. C. Liu (The University of Hong Kong, China);</i> .....</p> <p><a href="#">Spin Dynamics of Photoexcited Carriers in InGaAs/GaAs Layered Quantum Structures</a>  <i>J. Q. Ning (The University of Hong Kong, China); S. J. Xu (The University of Hong Kong, China); X. Z. Ruan (The University of Hong Kong, China); Ji Yang (The University of Hong Kong, China); H. Z. Zheng (Institute of Semiconductors, Chinese Academy of Sciences, China); H. C. Liu (The University of Hong Kong, China);</i> .....</p> <p><a href="#">Spin Lifetime of Electrons in a High Mobility, Low Density Two-dimensional Electron System</a>  <i>Xue Zhong Ruan (SKLSM, Institute of Semiconductors, Chinese Academy of Science, China); Hai Hui Luo (SKLSM, Institute of Semiconductors, Chinese Academy of Science, China); Yang Ji (SKLSM, Institute of Semiconductors, Chinese Academy of Science, China); Bao Quan Sun (SKLSM, Institute of Semiconductors, Chinese Academy of Science, China); Zhong Ying Xu (SKLSM, Institute of Semiconductors, Chinese Academy of Science, China); V. Umansky (SKLSM, Institute of Semiconductors, Chinese Academy of Science, China);</i> .....</p> <p><a href="#">Designed Fano Resonance in Semiconductor Devices</a>  <i>H. C. Liu (National Research Council, Canada); C. Y. Song (National Research Council, Canada); Z. R. Wasilewski (National Research Council, Canada); J. A. Gupta (National Research Council, Canada); M. Buchanan (National Research Council, Canada);</i> .....</p> <p><a href="#">Dember Effect Induced Photovoltage in Perovskite <math>p</math>-<math>n</math> Heterojunctions</a>  <i>Kui-Juan Jin (Institute of Physics, Chinese Academy of Sciences, China); Kun Zhao (China University of Petroleum, China); Hui-Bin Lu (Institute of Physics, Chinese Academy of Sciences, China); Leng Liao (, China); Guo-Zhen Yang (Institute of Physics, Chinese Academy of Sciences, China);</i> ..</p> <p><a href="#">Photo-excited Carrier Dynamics in Large Bandgap Semiconductor Films and Nanostructures</a>  <i>Kam Sing Wong (Hong Kong University of Science and Technology, China);</i> .....</p> <p><a href="#">Coherent Relaxation of Excitons via Exciton-phonon Interaction and Time Evolution of Excitonic Polaron States</a>  <i>Shi-Jie Xiong (Nanjing University, China); S. J. Xu (The University of Hong Kong, China);</i> .....</p> <p><a href="#">Defects in ZnO Nanorods: Effect of Fabrication Method</a>  <i>Yuk Fan Hsu (The University of Hong Kong, China); Yan Yan Xi (The University of Hong Kong, China); Man Ching Alan Ng (The University of Hong Kong, China); Aleksandra B. Djurišić (The University of Hong Kong, China); Wai Kin Chan (The University of Hong Kong, China);</i> .....</p>	<p>594</p> <p>595</p> <p>596</p> <p>597</p> <p>598</p> <p>599</p> <p>600</p> <p>601</p> <p>602</p> <p>603</p> <p>604</p>
--	--

## Optical Emission from Si/ $\beta$ -FeSi<sub>2</sub> and C<sub>60</sub>-coupled $\beta$ -FeSi<sub>2</sub> Nanocomposites

Xinglong Wu

National Laboratory of Solid State Microstructures, Department of Physics

Nanjing University, Nanjing 210093, China

**Abstract**—  $\beta$ -FeSi<sub>2</sub> is an environment-kind semiconductor material. It has an indirect gap of 0.78 eV and a direct gap of 0.83 eV. The small difference between indirect- and direct-gap energies makes it interesting in optical emission when it is incorporated into a nanocomposite generally consisting of a core and a shell layer. The electronic states of such a nanocomposite are not only determined by the quantum confinement of the core and but also controlled by the surface layer. Its luminescence feature observed experimentally should be a result of interaction between the two nanoparticles (core and shell). In the report, we firstly introduce the fabrication of the Si/FeSi<sub>2</sub> and C<sub>60</sub>-coupled  $\beta$ -FeSi<sub>2</sub> nanocomposites. We adopt Fe ions implantation into Si wafer and then electrochemically etching to form the Si/ $\beta$ -FeSi<sub>2</sub> nanocomposite. Using the bandmixing model of direct and indirect gaps, we then calculate the energy levels of electrons and holes confined in the Si/ $\beta$ -FeSi<sub>2</sub> nanocomposite consisting of nanocrystalline Si core, interfacial  $\beta$ -FeSi<sub>2</sub> layer, and outer Fe<sub>2</sub>O<sub>3</sub> crust. The obtained results explain very well the intensity enhancement and pinning behavior of the observed photoluminescence (PL) peaks after the nanocomposite is stored in air. Afterwards, through reflux treatment of the Si/ $\beta$ -FeSi<sub>2</sub> nanocomposite and further C<sub>60</sub> coupling, we present fabrication of the C<sub>60</sub>-coupled  $\beta$ -FeSi<sub>2</sub> nanocomposite which exhibits a pinned PL peak at 570 nm and a band edge at 370 nm. Spectral analyses suggest that the pinned PL behavior is closely related to both the  $\beta$ -FeSi<sub>2</sub> nanocrystals and the coupled C<sub>60</sub>. We explain the observed PL result using the band-mixing model.

## The Manipulation of Tunneling Property by Quantum Dot under Photoexcitation

W. P. Wang, N. Li, X. S. Chen, T. X. Li, and W. Lu

National Lab for Infrared Physics, Shanghai Institute of Technical Physics  
Chinese Academy of Sciences, 500 Yu Tian Road, Shanghai 200083, China

**Abstract**— The quantum tunneling process is fundamental for both electronic and photoelectronic device. Recently, the quantum dots are combined with the resonant tunneling diode to manipulate the electrical or optical properties, even showing single photon detection behavior at temperature of 4.2 K. Although the excellent opto-electronic behavior has been observed in this new resonant tunneling structure, the working temperature is limited at very low temperature to avoid the temperature smearing effect on the singularity of tunneling current.

In this paper, we present some new approach path to increase the work temperature to use the singularity of tunneling current. We have observed that our proposed new approach path is very sensitive to the photo-excitation on the quantum dot. The quantum step of tunneling current in the surface quantum dot structure has been clearly observed at room temperature, in contrary to the other report where the quantum singularity of tunneling current can only be observed at very low temperature. This big increase of working temperature is well explained by the photo-excitation behavior in quantum dot.

We have also studied the quantum dot combined resonant tunneling diode structure. The pronounce photo-excitation sensitive properties have be observed at 77 K, in contrary to the other report for the observation at 4.2 K. The prototype device gives a very high sensitivity to the photo-excitation. About 10 nA photocurrent is observed for the photon flux of 120 photon/second on the device. The significant increase of the working temperature is well explained by the charging effect of the quantum dot by the electrical bias process.

From our experimental investigation as described above, we found that the change of the electron occupation in quantum dot by the photo-excitation process will strongly manipulate the resonant tunneling current in the quantum dot involved nano-structure. This behavior will open a new approach path to increase the working temperature of opto-electronic device based on the resonant tunneling effect.

## Magneto-optical Properties and Spin Dynamics in Novel II-VI and III-V Semiconductor Materials and Nanostructures

I. A. Buyanova<sup>1</sup>, W. M. Chen<sup>1</sup>, A. A. Murayama<sup>2</sup>, Y. Oka<sup>2</sup>  
C. R. Abernathy<sup>3</sup>, and S. J. Pearton<sup>3</sup>

<sup>1</sup>Department of Physics, Chemistry and Biology, Linköping University  
58183 Linköping, S-58183, Sweden

<sup>2</sup>Institute of Multidisciplinary Research for Advanced Materials  
Tohoku University, Sendai 980-8577, Japan

<sup>3</sup>Department of Materials Science and Engineering, University of Florida  
Gainesville, FL 32611, USA

**Abstract**— Spin-dependent processes in semiconductor materials and related nanostructures are currently attracting increasing interest in view of their importance for novel semiconductor technologies such as spin-dependent electronics (or spintronics), which aims to combine new spin enabling functionality with well-established electronic and optical properties. The success of spintronics relies on the ability to create, control, maintain and manipulate spin orientation over practical time and length scale, which in turn requires full understanding of the corresponding physical processes.

In this talk we shall review our recent results from in-depth investigations of magneto-optical properties, spin transport and spin relaxation processes, by employing cw and time-resolved magneto-optical spectroscopy in combination with tunable laser excitation. Several material systems relevant to spintronic applications will be discussed including ZnMnSe/Zn(Cd)Se quantum wells (QWs) and quantum dots (QDs), GaMnN/Ga(In)N QWs, ZnCdO/ZnO QWs and GaInNP/GaAs heterostructures. We shall show that in ZnMnSe/Zn(Cd)Se two physical mechanisms are responsible for optical spin injection, i.e., (i) commonly believed tunneling of individual carriers or excitons and (ii) energy transfer via localized excitons and spatially separated localized electron-hole pairs (LEHP) located within diluted magnetic semiconductor (DMS). Unexpectedly, the latter mechanism is in fact found to dominate spin injection. We shall also show that spin depolarization in all studied systems is largely determined by efficient spin relaxation within non-magnetic spin detectors, which is an important factor limiting efficiency of spin detection. Detailed physical mechanisms leading to spin depolarization in the investigated structures will be discussed.

## Exciton-biexciton Dynamics in InGaAs Quantum Wells Studied by Time-resolved Kerr Rotation Spectroscopy

J. Q. Ning, S. J. Xu, X. Z. Ruan, Y. Ji, H. Z. Zheng, and H. C. Liu  
Department of Physics, The University of Hong Kong, Pokfulam Road, China

**Abstract**— Time-resolved Kerr rotation (TRKR) technique based on the pump-probe configuration was employed to study the excitonic dynamics in InGaAs quantum wells at 5 K. Decaying oscillation structures are observed in the TRKR measurements, which are due to the exciton-biexciton quantum beating. The oscillations exhibit an oscillation period of  $1.52 \pm 0.01$  ps and a decaying lifetime of  $3.6 \pm 0.4$  ps, both of which are insensitive to the excitation wavelength. The biexciton binding energy of  $2.72 \pm 0.02$  meV is deduced from the oscillation period, and the decaying time is associated with the dephase process of excitons. The oscillation amplitude is found to be strongly dependent on the excitation wavelength, which is proportional to the density of heavy-hole excitons created by the pump pulses. The oscillations only occur at resonant excitation of heavy-hole excitons rather than of light-hole excitons, which suggests that the biexciton formation takes a two-step process and the heavy-hole excitons act as an intermediate state.

## Spin Dynamics of Photoexcited Carriers in InGaAs/GaAs Layered Quantum Structures

J. Q. Ning, S. J. Xu, X. Z. Ruan, J. Yang, H. Z. Zheng, and H. C. Liu  
The University of Hong Kong, Pokfulam Road, China

**Abstract**— Femtosecond time-resolved Kerr rotation (TRKR) method based on degenerate pump-probe configuration was employed to investigate ultrafast spin dynamics of photoexcited carriers in InGaAs/GaAs layered quantum structure. By scanning the photon energy of excitation laser pulses over the heavy- (hh) and light-hole (lh) subbands of the quantum structure successively, the initial time evolution and transient flip of spins of photoexcited carriers can be clearly identified. It is found that both resonant and off-resonant excitations contribute to Faraday rotation while only off-resonant excitations bring about optical activity. Under the action of an additional magnetic field, the photoexcited carriers exhibit composite Larmor precessions with multi-decay time constants and different oscillatory periods, depending sensitively on the initial states of photoexcited carriers. Careful analysis of the experimental data leads to a fine physical picture of the spin dynamics of the photoexcited carriers in the quantum structures. Detailed data and analysis will be reported in this talk.

## Spin Lifetime of Electrons in a High Mobility, Low Density Two-dimensional Electron System

Xue Zhong Ruan, Hai Hui Luo, Yang Ji, Bao Quan Sun  
Zhong Ying Xu, and V. Umansky

SKLSM, Institute of Semiconductors, Chinese Academy of Science  
P. O. Box 912, Beijing 100083, China

**Abstract**— A pump-probe technique (Time-resolved Kerr rotation, TRKR) was employed to study the transverse spin lifetime ( $T_2^*$ ) of electrons in a high mobility, low density two-dimensional electron system (2DES) at low temperature. Embedded in a semiconductor GaAs/Al-GaAs heterostructure, the 2DES has an electron density of  $9.6 \times 10^{10} \text{ cm}^{-2}$  and a mobility of  $3.2 \times 10^6 \text{ cm}^2 \text{ V}^{-1} \text{ s}^{-1}$ . A circularly-polarized pump beam was shined on the sample to generate spin polarized carriers in the 2DES, whose evolution as a function of time, in the presence of a transverse magnetic field, was monitored via measuring the rotation angle of the polarization of a linearly-polarized probe beam. Several resonances, with different spin lifetime and g factors, were observed as the wavelength of the pump beam was tuned to match the energy levels in the 2DES. The electron spin lifetime was also found to depend strongly on the transverse magnetic field and excitation density of the pump beam. As temperature was tuned from 1.5 K to about 40 K, a peak of the spin lifetime of electrons in the ground state of the 2DES appeared around 15 K, on top of an increasing background. The peak is ascribed to that the scattering of electrons in a 2DES becomes strongest as the temperature reaches the same energy scale of the Fermi Energy  $E_f$ . This may be experimental evidence to the theoretical speculation that electron-electron interaction can affect the spin coherent process of electrons.

## Designed Fano Resonance in Semiconductor Devices

H. C. Liu, C. Y. Song, Z. R. Wasilewski, J. A. Gupta, and M. Buchanan  
Institute for Microstructural Sciences, National Research Council, Ottawa K1A 0R6, Canada

**Abstract**— Fano resonance [1] is seen in many areas of physics including atomic and molecular spectroscopy, quantum optics [2], quantum transport [3], and more. It is not only a general physics phenomenon but also useful in applications, for example, lasing without inversion [2]. In order to make use of this quantum interference effect, it is highly desirable if one can design a Fano resonance quantum structure with the coupling strength and other parameters controlled by structural parameters. Semiconductor quantum well is a model system [4, 5] and offers this possibility. We present direct experimental evidence of Fano resonance mediated by intersubband and phonon coupling in a specially designed GaAs/AlGaAs quantum well infrared photodetector. This work presents a new approach for realizing quantum interference [5] in an artificially designed structure and opens new possibilities for making use of Fano resonance in infrared devices.

### REFERENCES

1. Fano, U., *Phys. Rev.*, Vol. 124, 1866–1878, 1961.
2. Nikonov, D. E., A. Imamoglu, and M. O. Scully, *Phys. Rev. B*, Vol. 59, 12212–12215, 1999.
3. Martins, G. B., C. A. Busser, K. A. Al-Hassanieh, E. V. Anda, A. Moreo, and E. Dagotto, *Phys. Rev. Lett.*, Vol. 96, 066802, 1–4, 2006.
4. Capasso, F., *Science*, Vol. 235, 172–176, 1987.
5. Faist, J., F. Capasso, C. Sirtori, L. N. Pfeiffer, and K. W. West, *Nature*, Vol. 390, 589–591, 1997.



## Dember Effect Induced Photovoltage in Perovskite $p$ - $n$ Heterojunctions

Kui-Juan Jin<sup>1</sup>, Kun Zhao<sup>2</sup>, Hui-Bin Lu<sup>1</sup>, Leng Liao<sup>1</sup>, and Guo-Zhen Yang<sup>1</sup>

<sup>1</sup>Beijing National Laboratory for Condensed Matter Physics

Institute of Physics, Chinese Academy of Sciences, Beijing 100080, China

<sup>2</sup>Department of Mathematics and Physics, China University of Petroleum, Beijing 102249, China

**Abstract**— An unusual and rather large transient lateral photovoltage (LPV) has been observed in  $\text{La}_{0.9}\text{Sr}_{0.1}\text{MnO}_3/\text{SrNb}_{0.01}\text{Ti}_{0.99}\text{O}_3$  and  $\text{La}_{0.7}\text{Sr}_{0.3}\text{MnO}_3/\text{Si}$  heterojunctions under the nonuniform irradiation of pulsed laser. The irreversible LPVs on both sides of a  $p$ - $n$  junction challenge the well established model for LPV in conventional semiconductor  $p$ - $n$  junctions, which can be well explained by Dember effect. Much larger LPV is observed in  $\text{La}_{0.7}\text{Sr}_{0.3}\text{MnO}_3/\text{Si}$  than that in  $\text{La}_{0.9}\text{Sr}_{0.1}\text{MnO}_3/\text{SrNb}_{0.01}\text{Ti}_{0.99}\text{O}_3$ . Similar results measured from both substrates of  $\text{SrNb}_{0.01}\text{Ti}_{0.99}\text{O}_3$  and Si also support such a Dember effect. Much larger LPVs in heterojunctions than those in simple samples ( $\text{SrNb}_{0.01}\text{Ti}_{0.99}\text{O}_3$  or Si) suggest a potential application of Dember effect in heterostructures.

# Photo-excited Carrier Dynamics in Large Bandgap Semiconductor Films and Nanostructures

Kam Sing Wong

Department of Physics

Hong Kong University of Science and Technology

Clear Water Bay, Kowloon, Hong Kong, China

**Abstract**— Time-resolved photoluminescence and pump-probe measurements are very powerful techniques to investigate the radiative and nonradiative processes in semiconductor materials. We have used these techniques to study the photo-excited carrier recombination and relaxation dynamics in ZnO and GaN with a range of material morphologies from thin films to nanostructures such as nanorods, nanodots and tetrapods. There has long been controversy on the origin of green emission in ZnO. Our observation of spectral blue shift and logarithmic increase in the green emission peak with increasing excitation intensity and hyperbolic  $t^{-1}$  decay show strong agreement with the tunnel assisted donor-deep-acceptor pair (DAP) model. Most of the ZnO films and nanostructures studied show an ultrafast bandedge exciton emission lifetime in the range of few tens to few hundreds of picoseconds, indicating strong nonradiative recombination process. Our recent work on ZnO tetrapods observed pure radiative exciton recombination at room temperature with emission lifetime of 27.7 ns, which is the longest room temperature exciton recombination lifetime measured so far. For ZnO film, one can easily observed stimulated emission at high excitation intensity, however, for ZnO nanowhisker with parallel end facets, lasing action can be observed with an excitation threshold as low as  $70 \mu\text{J}/\text{cm}^2$ . For some ZnO nanostructures and powders, one often also observed laser-like supernarrow emission; this sharp emission is due to random lasing. However, random lasing has highly chaotic, irregular supernarrow mode emissions, and higher lasing threshold, unlike what we observe in ZnO nanowhiskers where regular longitudinal modes and highly polarized laser emission are seen.

GaN is another large bandgap semiconductor very important for blue LED and laser. Under high excitation, we observed density dependent initial recovery of the photo-induced reflectivity from pump-probe measurement. The onset of this density dependent recovery is consistent with the Mott density, and a model based Auger nonradiative recombination can be used to explain this phenomenon. Our theoretical fitting yield an Auger coefficient of  $\sim 5 \times 10^{-30} \text{ cm}^6\text{s}^{-1}$  for bulk GaN, which is an important parameter for high power device applications. We also investigated the effect of different reactive ion etching process on the carrier recombination dynamics in InGaN/GaN quantum wells based micropillars. It is shown that dry etching under high  $\text{Cl}_2$  concentration strongly affect the exciton recombination lifetime near the etched surface. These results provide important insight into fabricating III-nitride based optoelectronic devices with low dry-etch damage. This work on dry etching damage shows again the important role the surface played in the photo-excited carrier recombination dynamic. In our work on GaN film, we also observed strong nonradiative recombination at the surface using one- and two-photon excitation. More details of our time-resolved work on GaN and ZnO will be presented in the conference.

# Coherent Relaxation of Excitons via Exciton-phonon Interaction and Time Evolution of Excitonic Polaron States

Shi-Jie Xiong<sup>1,2</sup> and S. J. Xu<sup>2</sup>

<sup>1</sup>National Laboratory of Solid State Microstructures and Department of Physics  
Nanjing University, Nanjing 210093, China

<sup>2</sup>Department of Physics and HKU-CAS Joint Laboratory on New Materials  
The University of Hong Kong, Pokfulam Road, Hong Kong, China

**Abstract**— We investigate the time evolution of excitonic polaron states after the creation of an exciton in the presence of exciton-phonon interaction. By solving the time-dependent Schrödinger equation and taking into account the influence of the thermal bath, we obtain a coherent relaxation process from a pure exciton state to an entangled exciton-LO-phonon-bath-phonon complex, via intermediate polaron states consisting of exciton and LO phonons. We formulate the spectrum of spontaneous emission from this relaxation process and the obtained phonon sideband exhibits two characteristics different from those of previous theories: (i) There are two sets of Stokes lines, one corresponds to the exciton-LO-phonon polarons and the other is from the relaxation of the LO-phonon components to the bath phonons. (ii) In certain conditions these two sets are coherent, and this coherence may be reflected by destructive dips in the spectrum. Besides, owing to the complicated component structure of the time evolving state, the intensities of Stokes lines in a set may deviate from the prediction of the Huang-Rhys factors, and the anti-Stokes lines can have asymmetric frequency distribution with respect to the Stokes lines. We also discuss the basic physical features of the relaxation processes.

## Defects in ZnO Nanorods: Effect of Fabrication Method

Yuk Fan Hsu<sup>1</sup>, Yan Yan Xi<sup>1</sup>, Man Ching Alan Ng<sup>1</sup>  
Aleksandra B. Djurišić<sup>1</sup>, and Wai Kin Chan<sup>2</sup>

<sup>1</sup>Department of Physics, The University of Hong Kong, Hong Kong, China

<sup>2</sup>Department of Chemistry, The University of Hong Kong, Hong Kong, China

**Abstract**— In recent years, there has been intensive study of the optical properties of ZnO nanostructures due to a variety of possible morphologies and their great potential for applications in optoelectronic devices. However, the origin of defects causing the visible emission in ZnO nanostructures is still controversial. Among various morphologies of ZnO nanostructures, nanorods/nanowires are among the most useful, since vertical nanorod arrays can be easily integrated into optoelectronic devices using existing semiconductor technologies. While nanorod arrays can be fabricated by many different methods, the fabrication methods and conditions used have a significant effect on the properties of the fabricated nanorods. We performed a detailed study of the properties of nanorod arrays fabricated by hydrothermal synthesis and by vapor deposition of zinc in oxygen/argon gas flow. The structural and optical properties of the fabricated samples were studied by scanning electron microscopy (SEM) and photoluminescence (PL) spectroscopy. The hydrothermally grown nanorods exhibited strong orange defect emission, while the nanorods prepared by vapor deposition exhibited green defect emission. In the case of vapor deposition, change of the growth conditions resulted in the change of both optical properties and morphology, while in the case of hydrothermal growth in all cases nanorods were obtained. However, the rod diameter and orientation, as well as ratio of UV to visible emission, were dependent on the growth conditions. We have limited our study only to the samples exhibiting rod morphology, and annealed the samples at different temperatures and in different environments. The defect emission was strongly affected by the annealing conditions, and the possible origins of different defects have been discussed. Finally, usefulness of the nanorods for practical applications has been demonstrated, and UV emitting light emitting diodes have been fabricated.

# Session 3A5

## EM Wave in Atmosphere Propagation and Communication 1

<a href="#">Stochastic Electromagnetic Beams for Optical Communication Systems Operating in Turbulent Atmosphere</a>	
<i>Olga Korotkova (University of Miami, USA);</i> .....	606
<a href="#">Formulation of Scintillations for Optical Incidence of Arbitrary Field Profile</a>	
<i>Yahya Baykal (Cankaya University, Turkey); Halil Tanyer Eyyubođlu (Cankaya University, Turkey); Yangjian Cai (University of Erlangen, Germany);</i> .....	607
<a href="#">Goos-Haenchen Effect Applied for the Design of Collett-Wolf Beams</a>	
<i>Zu-Han Gu (Surface Optics Corporation, USA); Anting Wang (Surface Optics Corporation, USA);</i> .	608
<a href="#">The Challenges for Optical Communication Using Orbital Angular Momentum of a Laser Beam in Turbulent Atmosphere</a>	
<i>Jixiong Pu (Huaqiao University, China); Ziyang Chen (Huaqiao University, China); Tao Wang (Huaqiao University, China); Yongxin Liu (Huaqiao University, China);</i> .....	609
<a href="#">Propagation of Partially Coherent Beams after a Source Plane Ring Aperture</a>	
<i>Halil Tanyer Eyyubođlu (Cankaya University, Turkey); Yahya Kemal Baykal (Cankaya University, Turkey); Yangjian Cai (University of Erlangen, Germany);</i> .....	610
<a href="#">Second-harmonic Generation by an Astigmatic Partially Coherent Beam</a>	
<i>Yangjian Cai (University of Erlangen, Germany); Ulf Peschel (University of Erlangen, Germany);</i> .	611
<a href="#">The Influence of Atmospheric Turbulence on the Propagation Properties of Partially Coherent Flat-topped Beams</a>	
<i>Xiaoling Ji (Sichuan Normal University, China);</i> .....	612
<a href="#">Design of a Retro-reflected Tag for Free-space Optical Communication</a>	
<i>Zu-Han Gu (Surface Optics Corporation University of California, USA); Tamara A. Leskova (University of California, USA); Alexei Alexei Maradudin (University of California, USA);</i> .....	613
<a href="#">Measurements and Physical Electromagnetic Statistical Modeling of mm Wavelength Propagation</a>	
<i>Zaid Muhi-Eldeen (University of Glamorgan, UK); Miqdad Al-Nuaimi (University of Glamorgan, UK); Leonidas P. Ivrissimtzi (University of Ioannina, Greece);</i> .....	614
<a href="#">Time Domain Analysis of Electromagnetic Monocycle Signals for Communication in Seawater</a>	
<i>Raouf N. Boules (Towson University, USA);</i> .....	615
<a href="#">General Improvement of the Two-flux Kubelka-Munk Approach in the Theoretical Optics of Turbid Media</a>	
<i>Dmitrii A. Rogatkin (Moscow Regional Research and Clinical Institute "MONIKI", Russia); Vladimir V. Tchernyi (Scientific Agency "SAIBR", Russia); V. A. Dybov (Scientific Agency "SAIBR", Russia);</i> .....	616

## Stochastic Electromagnetic Beams for Optical Communication Systems Operating in Turbulent Atmosphere

Olga Korotkova

Department of Physics, University of Miami  
1320 Campo Sano Drive, Coral Gables, FL 33146, USA

**Abstract**— It has been known that *scalar* stochastic (partially coherent) beams can significantly improve performance of optical communication links operating in the turbulent atmosphere. Recent theoretical developments regarding stochastic *electromagnetic* (partially coherent and partially polarized) beams suggest that their use in optical communication systems operating in the turbulent atmosphere can improve performance of the links even better. It is shown how important characteristics of such beams, namely various polarization properties affect scintillation of the beam, and also the signal to noise ratio of a communication channel. In particular, it is found that for unpolarized beams the scintillation index can be reduced up to the factor of two, compared with that of conventionally used linearly polarized beams. Also, unlike partial coherence, being effective only in weak regime of atmospheric fluctuations, partial polarization is effective for both weak and strong fluctuation regimes. Some other advantages of stochastic electromagnetic beams relating to their potential use in communications are also discussed.

# Formulation of Scintillations for Optical Incidence of Arbitrary Field Profile

Y. Baykal<sup>1</sup>, H. T. Eyyuboğlu<sup>1</sup>, and Y. Cai<sup>2</sup>

<sup>1</sup>Department of Electronic and Communication Engineering, Çankaya University  
Öğretmenler Cad. 14, Yüzüncüyıl 06530 Balgat Ankara, Turkey

<sup>2</sup>Max-Planck-Research-Group, Institute of Optics, Information and Photonics, University of Erlangen  
Staudtstr. 7/B2D-91058 Erlangen, Germany

**Abstract**— Scintillation index on the receiver axis is formulated in random medium when an optical source with an arbitrary field profile is employed. To represent the arbitrary source field profile, source is decomposed into pixels and the incident field to form the scintillations is expressed as the superposition of the fields from each pixel area. Thus obtained arbitrary field distribution is then introduced into the weak atmospheric turbulence formulation by using Rytov method. Our result, which is in summation and integral forms, reduces correctly to the known scintillation index of a Gaussian beam wave in atmospheric turbulence.

# Goos-Haenchen Effect Applied for the Design of Collett-Wolf Beams

Zu-Han Gu<sup>1,2</sup> and Anting Wang<sup>1,2,3</sup>

<sup>1</sup>Surface Optics Corporation, 11555 Rancho Bernardo Road, San Diego, CA 92127, USA

<sup>2</sup>Department of Electrical and computer Engineering, University of California, San Diego, CA 92093, USA

<sup>3</sup>Department of Physics, University of Science & Technology of China, Hefei, Anhui 230026, China

**Abstract**— Recent studies show that the control of coherence of laser beams is needed for applications in optical communication in the turbulent atmosphere.

Collett-Wolf beam, which is a partial coherent source, can produce a field as directional as a laser beam, although from a global viewpoint the source is nearly spatially-incoherent. Such a beam with unique features of no speckle noise has been widely used for imaging, illumination, and pointing. However, rotation of the diffuse plate is needed for the design of Collett-Wolf beam.

Goos-Haenchen effect is a lateral displacement of a specularly reflected beam, from the position predicted by geometrical optics considerations, when a Gaussian light beam is incident from an optically denser medium on to its interface with a rarer medium. In most cases, this phenomenon refers to the situation of total reflection.

An optical feedback technique with Goos-Haenchen effect is applied to reduce the spatial coherence of the laser beam by transmitting the beam through the optical feedback loops. The Collett-Wolf beam with optical feedbacks reduces speckle contrast by means of a feedback mechanism.



# The Challenges for Optical Communication Using Orbital Angular Momentum of a Laser Beam in Turbulent Atmosphere

Jixiong Pu, Ziyang Chen, Tao Wang, and Yongxin Liu

Department of Electronic Science & Technology, Huaqiao University  
Quanzhou, Fujian 362021, China

**Abstract**— In recent years there have been increasing interests in studying the optical communication by use of the orbital angular momentum ( $L$ ) of a laser beam. It has been proposed that the  $L$  value of the beam is used as an alphabet for optical messages. In this paper, we present several challenges of using the orbital angular momentum ( $L$ ) of a laser beam in optical communication through turbulent atmosphere. These challenges include the beam spreading of different value of  $L$ , how to keep the value  $L$  unchanged as the beam delivering or received by optical systems with aberration, and the beam propagating through turbulent atmosphere etc. All these processes may cause  $L$  value of the beam change, so that the optical messages may lose. The improvement for avoid the lose of the optical messages is also presented.

# Propagation of Partially Coherent Beams after a Source Plane Ring Aperture

H. T. Eyyuboğlu<sup>1</sup>, Y. K. Baykal<sup>1</sup>, and Y. Cai<sup>2</sup>

<sup>1</sup>Department of Electronic and Communication Engineering, Çankaya University  
Öğretmenler Cad. 14, Yüzüncüyıl, 06530 Balgat, Ankara, Turkey

<sup>2</sup>Max-Planck-Research-Group, Institute of Optics, Information and Photonics, University of Erlangen  
Staudtstr. 7/B2D-91058 Erlangen, Germany

**Abstract**— The propagation properties of partially coherent beams passing through a source placed ring aperture are examined. The derivation is based on the lowest order general beam formulation, such that our results are applicable to a wide range of beams. In this study, our focus is on fundamental Gaussian, cosh-Gaussian, cos-Gaussian, sinh-Gaussian, sin-Gaussian and annular beams. The aperture consists of inner and outer parts, thus the middle hollow part appears in the form of a ring. The propagation environment is turbulent.

From the graphical outputs of the beams investigated, it is seen that despite the existence of the circular ring, during propagation, the beams tend to retain the basic profiles similar to the case of no aperture, but depending on the inner and outer radius dimensions, the propagated beams are reduced in intensity levels and become more spread. It is further observed that, when the inner part of the aperture has nonzero radius, ring formations are developed at the outer edges of the receiver plane intensities.

## Second-harmonic Generation by an Astigmatic Partially Coherent Beam

Yangjian Cai and Ulf Peschel

Institute of Optics, Information and Photonics, Max-Planck-Research-Group  
University of Erlangen-Nuremberg  
Günther Scharowsky-Strasse 1/Bau 24, 91058 Erlangen, Germany

**Abstract**— We investigate second-harmonic generation by a partially coherent twisted anisotropic Gaussian Schell-model beam. An explicit expression for the second-order correlation function of the second-harmonic field is obtained by using a tensor method. The properties of the generated field and the conversion efficiency are studied numerically. We analyze the influence of the crystal's length and of the parameters of the initial pump beam, as e.g., the effective beam width, the transverse coherence length and the twist phase, on the generation of the second-harmonic field. We find that under certain conditions the conversion efficiency of the second-harmonic generation can be increased by using an astigmatic instead of a stigmatic pump beam or by reducing the degree of coherence of the excitation.

## The Influence of Atmospheric Turbulence on the Propagation Properties of Partially Coherent Flat-topped Beams

Xiaoling Ji

Department of Physics, Sichuan Normal University, Chengdu 610068, China

**Abstract**— In 1978 Collett and Wolf predicted that Gaussian Schell-model (GSM) beams may have the same directionality as a fully coherent laser beam, which was confirmed by the experiments. It means that full spatial coherence in free space is not a necessary condition for highly directional light beams. Recently, Shirai, Dogariu and Wolf have extended the result from free space to atmospheric turbulence and have shown that there exist also the equivalent GSM beams in turbulence which under a certain condition may have the same angular spread as a fully coherent Gaussian beam. However, the theoretical and experimental studies about this subject were made for GSM beams. Apart from GSM beams, there are variety of partially coherent beams which can be produced by various sources and have different propagation properties. Thus, an interesting question arises: Does the result hold true for other types of partially coherent beams? This paper is aimed at studying the spreading and directionality of partially coherent flat-topped beams propagating through atmospheric turbulence. The closed-form expression for the mean squared beam width of partially coherent flat-topped beams in turbulence is derived by using the integral transform technique. It is shown that the relative spreading of partially coherent flat-topped beams is less affected by the turbulence than that of fully coherent ones. From the expression for the mean squared beam width, the expression for the angular spread of partially coherent flat-topped beams in turbulence is derived. It is found that two partially coherent flat-topped beams may generate the same angular spread, and there exist equivalent partially coherent flat-topped beams which may have the same directionality as a fully coherent Gaussian beam in free space and also in turbulence.

## Design of a Retro-reflected Tag for Free-space Optical Communication

Zu-Han Gu<sup>1,2</sup>, T. A. Leskova<sup>3</sup>, and A. Maradudin<sup>3</sup>

<sup>1</sup>Surface Optics Corporation, San Diego, CA 92127, USA

<sup>2</sup>Department of Electrical and computer Engineering, University of California  
San Diego, CA 92093, USA

<sup>3</sup>Department of Physics and Astronomy and ISIS, University of California  
Irvine, CA 92679, USA

**Abstract**— Due to its promise of wide bandwidth and fast speed, free space optical communication has emerged in recent years as an attractive alternative to the conventional Radio Frequency RFID. Optical remote identification and target tracking demonstrate a capability to quickly and easily tag an asset and identify and track it from a great standoff range. Optical remote identification and target tracking are a unique combination of emergent technologies that enables performance not possible by other means.

We have studied the bi-directional reflection (BRDF) and mono-static bi-directional reflection (MBR) for a retro-reflected tag at 1.55  $\mu\text{m}$ . The tag is specially designed for strong reflection in the retro-reflection direction for optical communication in free space. Due to multiple scattering, the larger the incident angle, the stronger the MBR.

# Measurements and Physical Electromagnetic Statistical Modeling of mm Wavelength Propagation

Zaid Muhi-Eldeen<sup>1</sup>, Miqdad Al-Nuaimi<sup>1</sup>, and Leonidas P. Ivrissimtzis<sup>2</sup>

<sup>1</sup>University of Glamorgan, UK

<sup>2</sup>University of Ioannina, Greece

**Abstract**— The statistical modeling and field measurements of fixed wireless links at mm-wavelengths operating within an urban or sub-urban propagation channel are presented, with potential applications in the characterization, design and deployment of pertinent networks. A specific goal on the study is the parameterization of the physical attributes of the channel and the associated electromagnetic mechanisms and, ultimately, the representation of the channel in terms of universal probabilistic distribution functions for the line-of-sight (LOS) received field power. Extensive experimental campaign conducted at 40 GHz verified the main postulates of the stochastic representation and assessed the accuracy of channel parameters obtained from the simulations of the statistical model proposed.

Broadband fixed and wireless access (BFWA) systems link design and deployment requires the understanding of the underlying propagation channel and the quantitative description of the fundamental mechanisms that could affect the integrity of the wireless direct link due to attenuation, noise, and interference. Development of analytical and numerical modeling tools enables the rationalization and optimization of the system design and its main constraints, such as cost of deployment (cell size, frequency and polarization planning), antenna parameters (positioning and radiation characteristics), and link performance (coverage and outage probability at the receiver), by accounting for the impairments introduced by the wireless channel.

Although the wireless link is fixed, the propagation channel is time-varying, because of the motion of the objects and the variability of their electromagnetic properties within it, due mainly to varying weather conditions. The study focuses on the analysis and measurements of the effects of scattering on the direct and interfering electromagnetic fields in a BFWA link at mm-waves, taking place in urban or sub-urban residential or industrial environments. The propagation environment, including the reflectivity and refractivity properties of building materials, is statistically modeled from coarse digital GIS data and reflectivity measurements. The EM field and signal at the receiving station is considered random and is calculated employing irregular surface scattering methods, augmented by geometrical optics techniques. The calculations assume realistic transmitting and receiving antenna systems and directive gain patterns. The random nature of the EM fields suggests its representation in terms of Probabilistic Density Functions (PDF's) and their associated moments. Of particular interest, is the parameterization of the random simulations and their association with universal wireless statistical models, such as the Rician distribution, i.e., the description of the field strengths and the characterization of the channel in terms of simple parameters. This parameterization and channel characterization is useful in the classification of the environment and can be utilized in network design and deployment.

# Time Domain Analysis of Electromagnetic Monocycle Signals for Communication in Seawater

Raouf N. Boules

Mathematics Department, Towson University, Towson, MD 21252, USA

**Abstract**— Transient solutions for Maxwell's equations for step function excitation in a general lossy medium were published in 1986 [1]. The case of a rectangular pulse propagating in seawater was more recently investigated [2, 3]. The use of a rectangular pulse is not preferred due to potential problems associated with the antenna design. In this paper a transient time-domain solution for a monocycle sinusoidal pulse propagating in seawater is given. The derivation is through series expansion using step functions as basis. As the signal propagates through seawater, it will be distorted due to medium absorption losses. The distortion is a function of the propagation distance. The signal is further corrupted by additive white noise. A correlator receiver is assumed for detecting the presence or absence of the distorted signal. The performance of the receiver is investigated in terms of false-alarm probability, detection probability, signal-to-noise ratio, and propagation distance.

A conventional radar signal is usually an amplitude-modulated sinusoidal wave. In the simplest case it is a pulse with many cycles of the sinusoidal carrier. The resulting waveform has a small relative bandwidth. Ultrawideband radar is based on signals with large relative bandwidths. Ultrawideband signals are defined [4] as signals with a relative bandwidth of at least 25%. According to this definition, ultrawideband signals are grouped into three recognizable classes: baseband or pulses with no carrier, monocycle, and polycycle waveforms.

The propagation of such signals in loss-free media is treated in the classical electromagnetic literature. Since seawater is far from loss-free this treatment does not apply. Solutions for Maxwell's equations for a step function in a general lossy medium were more recently found [1]. The electric field strength and absorption losses for a baseband rectangular pulse propagating in seawater have been published [2].

In this paper, the solution of Maxwell's equations for a step function is used to derive a solution for a monocycle waveform in seawater. The model we use for seawater is a medium which is charge-free, linear, time-invariant, homogeneous, with constant permittivity  $\epsilon$ , permeability  $\mu$ , and a nonzero conductivity  $\sigma$ . Plots showing the signal distortion for various propagation distances of practical interest are presented.

The solution is then used for investigating the typical radar problem of determining the presence or absence of the returned signal  $s(t)$  which is superimposed on noise  $n(t)$ . The transmitted signal is the monocycle waveform. The returned signal  $s(t)$  is a distorted version of the monocycle. The distortion is due to the high absorption losses of seawater and is function of the propagation distance. The noise process is assumed gaussian white with zero mean. A correlator receiver with a threshold detector is used for detection. The receiver is shown to maximize the detection probability for a given false-alarm probability. The paper gives an analysis of the receiver performance in terms of various relevant parameters such as false-alarm probability, detection probability, and propagation distance.

## REFERENCES

1. Harmuth, H. F., *Propagation of Nonsinusoidal Electromagnetic Waves*, Academic Press, New York, 1986.
2. Boules, R. N., "Absorption losses in seawater for a rectangular electromagnetic pulse," *Proc. IEEE International Symposium on Electromagnetic Compatibility*, 220–221, Cherry Hill, N. J., Aug. 1991.
3. Harmuth, H. F., R. N. Boules, and M. Husain, *Electromagnetic Signals*, Kluwer Publishing, 2000.
4. "Assessment of ultrawideband technology," OSD/DARPA Ultrawideband Radar Review Panel, Report No. R-6280, July 1990.
5. Engler, H. F., Jr., "Advanced technologies for ultrawideband system design," *Proc. IEEE International Symposium on Electromagnetic Compatibility*, 250–253, Dallas, TX, Aug. 1993.

# General Improvement of the Two-flux Kubelka-Munk Approach in the Theoretical Optics of Turbid Media

D. A. Rogatkin<sup>1</sup>, V. V. Tchernyi<sup>2</sup>, and V. A. Dybov<sup>2</sup>

<sup>1</sup>Moscow Regional Research & Clinical Institute "MONIKI"  
Shepkina str., 61/2, Moscow 129110, RF, Russia

<sup>2</sup>Scientific Agency "SAIBR", Vavilova str., 97, fl. 14, off. 35, Moscow, 117335, RF, Russia

**Abstract**— The Kubelka-Munk (KM) two-flux light transport one-dimensional (1D) model is, evidently, the most widely used Radiative Transport theory (RTT) approach in a modern optics of scattering and turbid media because of its simplicity and the existence of its clear analytical solution. Moreover, the KM approach is the best approximation of the general radiative transport equation (TE) in the case of 1D theoretical tasks. But it is well known from the literature that the KM model doesn't allow anyone to obtain an exact solution, especially in the case of highly-absorbing and weakly-scattering media. In the most of publications it is assumed that the light must be diffuse on a surface as well as within the medium for a correct application of the KM equations. However, in our opinion, there are no any reasons to separate light radiation on diffuse and collimated components for a simple 1D theoretical model. In a 1D theoretical task there are no any differences between diffuse and collimated beams because both of them penetrates a medium along 1D "x"-axis only. So, a root of the problem may be located in a far another field. To find out any reasons of the 1D KM approach low accuracy we have examined the general KM equations on the theoretical model of 1D scattering and absorbing medium, for which an exact photometric analytical solution of the light scattering problem can be obtained. It was estimated, that the classical two-flux KM model could give absolutely exact values for the boundary fluxes (transmitted and backscattered radiation) for any cases of scattering and absorbing media by means of small reformulation of initial differential KM equations and by means of more correct initial definition of the transport optical properties of media. It was shown that the main problem of the KM approach as well as of the general RTT consisted in a wrong phenomenological assumption of the existence of two independent optical transport properties of media - absorption and scattering. In the general case of a turbid medium, where an absorption of light is presented, a first coefficient in the right side of the TE and/or KM equations cannot be separated into the two independent transport coefficients - absorption and scattering ("K" and "S" in the KM notations; " $\mu_a$ " and " $\mu_s$ " in the TE notations) - and must be considered as one, united attenuation coefficient "AC". The absorption transport property "K" ( $\mu_a$ ) is included into "AC" as well as into "S" ( $\mu_s$ ), but not additively. Without absorption  $K = 0$  and  $AC = S$ , without scattering  $S = 0$  and  $AC = K$ , like it must be in the classical RTT, but if both an absorption and scattering are presented, then the classical phenomenological assumption  $AC = K + S$  is wrong. It is the main source of errors of the KM approach, for example, if the boundary fluxes are calculated. Only if the absorption into a medium is small, more less than scattering, then the classical assumption can take place. Moreover, such modification of the KM equations showed us an equivalence between absorption coefficients in both theories, i.e., allowed us to estimate exactly that  $K = \mu_a$ , what is contrary to the well-known literature data as well, but, in our opinion, is more reasonable than  $K = 2^* \mu_a$ , what is widely used today in a lot of publications.



# Session 3A6

## Wireless Communication Component

Broadband VCO Using Tunable Metamaterial Transmission Line with Varactor-loaded Split-ring Resonator	618
<i>Jaewon Choi (Soongsil University, Korea); Hyoungjun Kim (Soongsil University, Korea); Chong-min Lee (Soongsil University, Korea); Chulhun Seo (Soongsil University, Korea);</i> .....	
A Frequency and Pattern Reconfigurable Antenna with a Simple Structure	619
<i>Woo Suk Kang (Yonsei University, Korea); Sung Jung Rho (Yonsei University, Korea); Hyung Kuk Yoon (Yonsei University, Korea); Kihun Chang (Yonsei University, Korea); Young Joong Yoon (Yonsei University, Korea);</i> .....	
Design for PCS Antenna Based on WiBro-MIMO	620
<i>Kyeong-Sik Min (Korea Maritime University, Korea); Min-Seong Kim (Korea Maritime University, Korea); Chul-Keun Park (Korea Maritime University, Korea); Manh Dat Vu (Korea Maritime University, Korea);</i> .....	
Dual Band Internal Antenna with Independently Adjusted Resonant Frequencies	622
<i>Jeongpyo Kim (Hanyang University, Korea); Jaehoon Choi (Hanyang University, Korea);</i> .....	
Design of Dual-polarization Stacked Arrays for Wireless Communications	623
<i>Adel Mohamed Abdin (Shorouk Academy, Egypt);</i> .....	
A High Linearity and Efficiency Doherty Power Amplifier for Retrodirective Communication	624
<i>Xiaoqun Chen (Xidian University, China); Yuchun Guo (Xidian University, China); Xiaowei Shi (Xidian University, China);</i> .....	
Effect of the Gap Feeding on the Multi-band Small Antenna Using a Branch Structure	625
<i>Hyengcheul Choi (Hanyang University, Korea); Hojeong Kim (Hanyang University, Korea); Sinhyung Jeon (Hanyang University, Korea); Hyeong Dong Kim (Hanyang University, Republic of Korea);</i>	
Design and Analysis of a 1.2 V, 1.8 GHz, 240.147 $\mu$ W Low Power ASK Transmitter for Wireless Micro Sensor Nodes	626
<i>Thankappan Sasilatha (Anna University, India); J. Raja (SSN College of Engineering, India);</i> .....	

## Broadband VCO Using Tunable Metamaterial Transmission Line with Varactor-loaded Split-ring Resonator

Jaewon Choi, Hyoungjun Kim, Chongmin Lee, and Chulhun Seo  
University of Soongsil, Korea

**Abstract**— In the last few years, the need for more frequency bands has been increasing in the telecommunications with the emergence of new standards. The implementation of multi-band voltage controlled oscillator (VCO) attracts much attention because a tuning range of VCO is one of the most critical elements for multi-standard frequency synthesizers using frequency fractional-N PLL, for example, in which the resolution frequency is infinite. In this paper, the broadband VCO using tunable metamaterial transmission line with varactor-loaded split-ring resonator (VLSRR) is presented. It is demonstrated that VLSRR coupled to microstrip line can lead to metamaterial transmission line with tuning capability. The negative effective permeability is provided by the VLSRR in a narrow band above the resonant frequency. The bias of VLSRR is controlled by the varactor diodes. This is due to the variable capacitance, which allows for certain control of the resonator's frequency. The broadband VCO using this resonance frequency tuning property of VLSRR has presented the phase noise of  $-108.84 \sim -106.84$  dBc/Hz @ 100 kHz in the tuning range, 5.407 ~ 5.84 GHz. The figure of merit (*FOM*) called power-frequency-tuning-normalized (*PFTN*) is 20.144 dB. Compared with VCO using the conventional SRR, the widened tuning range has been 322 MHz (four times), and *PFTN* has been improved in 25.607 dB.

# A Frequency and Pattern Reconfigurable Antenna with a Simple Structure

Woo Suk Kang, Sung Jung Rho, Hyung Kuk Yoon, Kihun Chang, and Young Joong Yoon

Department of Electrical and Electronic Engineering, Yonsei University  
134 Shinchon-dong, Seodaemum-gu, Seoul 120-749, Korea

**Abstract**— Reconfigurable antennas have received much attention since it can provide diversity functions in operating frequency, polarization, and radiation pattern to mobile communication applications. [1,2] Most researches on the reconfigurable antennas are about changing one antenna characteristic while maintaining the other antenna characteristics same. However, it is not enough for those reconfigurable antennas with one characteristic to be used in various applications. For example, the frequency band of the Wireless Broadband Internet (WIBRO) service is 2.3–2.39 GHz, and that of the Satellite Digital Multimedia Broadcasting (SDMB) is 2.63–2.655 GHz. And it is required for the receiver antenna to have an omni-directional radiation pattern for WIBRO service and a directional radiation pattern for SDMB service when it receives the direct signal from the satellite. In this case, the frequency and pattern reconfigurable antenna is required.

In this paper, a simple structure reconfigurable antenna with frequency and radiation pattern is proposed. It is designed to have broadside radiation pattern in WIBRO frequency band and end-fire radiation pattern in SDMB frequency band, by controlling the states of the pin diodes.

## ACKNOWLEDGMENT

This research was supported by the MIC (Ministry of Information and Communication), Korea, under the ITRC (Information Technology Research Center) support program supervised by the IITA (Institute of Information Technology Assessment) (IITA-2005-C1090-0502-0012).

## REFERENCES

1. Cidronali, A., L. Lucci, G. Pelosi, P. Samori, and S. Selleri, "A reconfigurable printed dipole for quad-band wireless applications," *IEEE Antenna and Propagation Society International Symposium*, 217–220, July 2006.
2. Wu, Y.-F., C.-H. Wu, D.-Y. Lai, and F.-C. Chen, "A reconfigurable quadri-polarization diversity aperture coupled patch antenna," *IEEE Transaction on Antenna and Propagation*, Vol. 55, 1009–1012, March 2007.

## Design for PCS Antenna Based on WiBro-MIMO

Kyeong-Sik Min, Min-Seong Kim, Chul-Keun Park, and Manh Dat Vu  
Radio Sciences and Engineering, Korea Maritime University, Korea

**Abstract**— This paper presents a design of wireless broadband (WiBro)-MIMO and personal communication service (PCS) antenna for practical mobile phone. To decrease the mutual coupling of WiBro-MIMO antenna, it is considered on the projected ground structure. In addition, two kind of a PCS band antenna for the multi-function of the mobile phone is designed. The proposed antenna is well tuned in each operating frequency band and the mutual coupling between antenna elements is isolated below  $-15$  dB with 2D and  $-20$  dB with 3D PCS band antenna, respectively.

**Introduction:** A multi-input multi-output (MIMO) antenna system is a well-known technique to enhance the performance of wireless communication systems. The channel capacity that a MIMO antenna system provides is much larger than that provided by the conventional wireless system. Thus, the MIMO antenna system can significantly enhance the performance of the wireless communication system. In this research, a 2-ch wireless broadband (WiBro)-MIMO antenna and 1-ch personal communication service (PCS) band antenna are designed for internal type of mobile phone. The antenna elements are employed the printed meander line antenna and the printed inverted F antenna (IFA), due to its compact size and simple fabrication. All antennas are designed using the modified ground structure for high isolation characteristics.

**WiBro-MIMO and PCS Band Antenna:** Figure 1 shows the photograph of proposed antenna for the 2-ch WiBro-MIMO antenna [1] with the PCS band antenna. The PCS band antennas are designed using the 2D printed IFA and 3D modified IFA between two WiBro antenna elements.

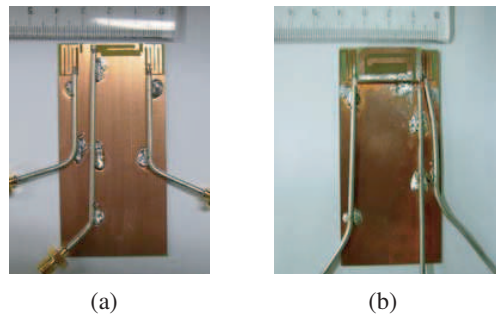


Figure 1: A photograph of proposed antenna. (a) With 2D PCS antenna, (b) with 3D PCS antenna.

Figure 2 shows the S-parameters of proposed WiBro-MIMO antenna with each PCS band antenna. The antenna in Fig. 1(a) has 140 MHz ( $1.74$  GHz  $\sim$   $1.88$  GHz) bandwidth. The isolation

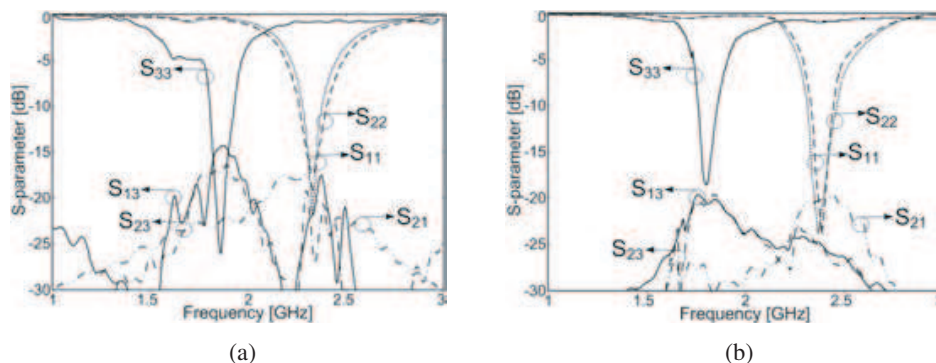


Figure 2: A measured S-parameters of proposed antennas. (a) With 2D PCS antenna, (b) with 3D PCS antenna.

between PCS and WiBro band is observed  $-15$  dB. The bandwidth of 3D PCS is 110 MHz (1.77 GHz  $\sim$  1.88 GHz) and isolation is below  $-20$  dB.

Figure 3 shows the measured radiation patterns of the fabricated PCS band antennas on the WiBro-MIMO antenna. They show the reasonable agreement comparing with calculated ones. The solid and dotted line show the YZ-plane (H-pattern) and XY-plane (E-pattern) of antenna, respectively.

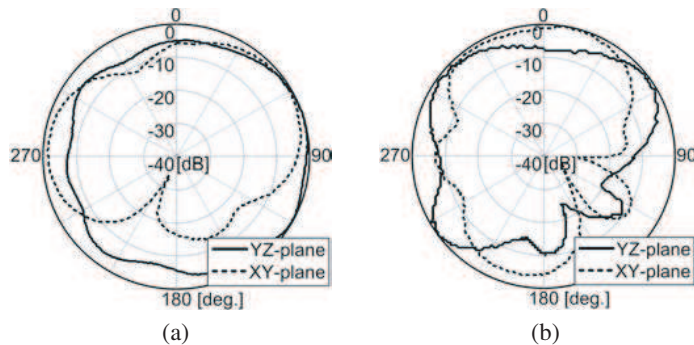


Figure 3: A measured radiation patterns of proposed antennas. (a) 2D PCS antenna, (b) 3D PCS antenna.

**Conclusion:** A compact WiBro-MIMO and two kind of PCS antenna are proposed. The isolation between each WiBro-MIMO antenna elements is considered using projected ground structure. The characteristics of proposed PCS band antennas are satisfied the Korean PCS system. The isolations between WiBro-MIMO and two kind of PCS antenna are below  $-15$  dB with 2D type and  $-20$  dB with 3D type antenna, respectively.

#### REFERENCES

1. Kim, D.-J. and K.-S. Min, "Compact 2-channel MIMO antenna for WiBro handy terminal application," *APMC 2006*, Vol. 3, 214–217, December 2006.

# Dual Band Internal Antenna with Independently Adjusted Resonant Frequencies

Jeongpyo Kim and Jaehoon Choi

Division of Electrical and Computer Engineering, Hanyang University, Seoul, Korea

**Abstract**— We propose a dual band internal antenna. The antenna consists of three planar metal radiators and two resonant circuits including inductors and transmission line between inductors as shown in Fig. 1. The resonant frequencies of the antenna are controlled by mainly inductors not radiators and transmission lines. Fig. 2 and Fig. 3 show that two resonant frequencies are independently adjusted by inductors. Thus, the lower resonant frequency is selected by using L1 and L2, and L3 and L4 are used to fix the higher resonant frequency. The energy in each band is radiated through three radiators not transmission lines. Because the radiators are operated as monopole antennas, the designed antenna has omni-directional radiation patterns at two resonant frequencies. The left and center radiators are operated in the lower band and the higher band signal is radiated at the center and right radiators. The antenna has very compact size of  $40\text{ mm} \times 5\text{ mm} \times 0.8\text{ mm}$  and is operated at GSM 900 and DCS1800 bands as shown in Fig. 4. Since it has very compact size and provides two resonant frequencies that can be independently adjusted by using inductors, the proposed antenna can be easily applied to the multi band mobile terminals. In addition, the characteristics of the antenna are hardly affected by human body because the resonant frequencies are strongly bound by inductors.

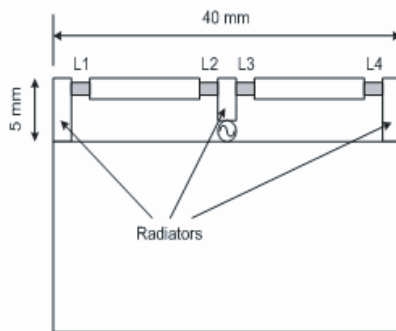


Figure 1: Proposed antenna structure.

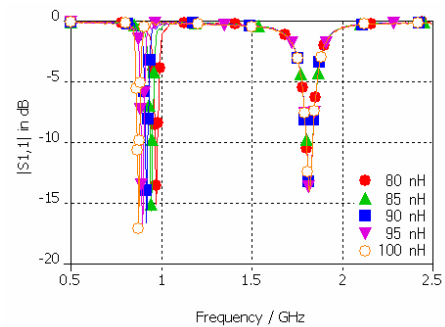


Figure 2: L1 and L2 vs Return loss.

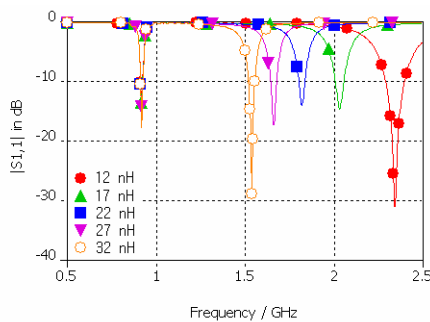


Figure 3: L3 and L4 vs Return loss.

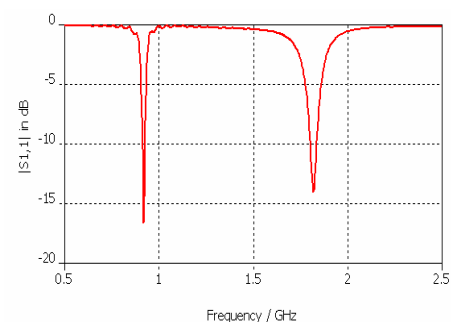


Figure 4: Return loss characteristic.

## Design of Dual-polarization Stacked Arrays for Wireless Communications

Adel Mohamed Abdin

Department of Communications and Electronics, Shorouk Academy, Cairo, Egypt

**Abstract**— A novel dual-polarized stacked antenna array is designed and built for broadcasting satellite orbital positions. It is working in the 12.43–12.53 MHz band (space-to-Earth). It has two layers. The patches in the bottom layer are fed diagonally by a microstrip line to have dual polarization. The lower layer consists of 8-elements with corporate feeding network. This feeding was designed to give equal amplitude and phase to each element. The upper layer is dummy and stacked above the bottom one.

A simulation is carried out to investigate the effects of varying several physical parameters such as dummy patch size, spacing between the lower and upper patches, and spacing between the patches on the performance of the antenna. The return loss ( $S_{11}$ ), voltage standing wave ratio (VSWR), radiation pattern, and impedance characteristics for the designed array are simulated and analyzed using IE3D (Zeland) software.  $S_{11}$  and VSWR are measured and compared with the simulated one.

The designed and fabricated antenna gives  $S_{11} = -35.174$  dB and VSWR = 1.03661 at the center frequency 12.484 GHz. It has a gain of 9.9 dBi, with a minimum half-power beamwidth (HPBW) ( $13.2356^\circ$ ,  $75.3584^\circ$ ) and antenna efficiency is nearly 74%. The measured and simulated results are very close.

The results show that the antenna seems very promising and useful for wireless applications.

## A High Linearity and Efficiency Doherty Power Amplifier for Retrodirective Communication

Xiaoqun Chen, Yuchun Guo, and Xiaowei Shi

National Key Laboratory of Antennas and Microwave Technology, Xidian University  
Xi'an 710071, China

**Abstract**— This paper presents a Doherty power amplifier with advanced design methods for high efficiency and linearity applied to retrodirective communication system for high peak to average power ratio (PAR). It has a high linearity and efficiency across the wideband signal has been studied extensively for the application due to its high efficiency. But the conventional Doherty power amplifier has its limitation. Due to its lower bias point, the current level of the peaking cell is always lower than that of the carrier cell. The load impedances of both cells cannot be fully modulated to the value of the optimum impedance for a high power match. Thus, neither cell can generate full output power. In order to obtain better performance of the Doherty power amplifier, first a special inverted Doherty topology is proposed. This “inverted Doherty” will guarantee the high efficiency at the low drive level. Second, we develop Doherty power amplifier with uneven power drive which is provided more input power to the peak amplifier than carrier amplifier for full power operation and appropriate load modulation. The amplifier with uneven power drive, the linearity of the amplifier is improved due to proper power operation without severe saturation. These methods are applied to implement Doherty power amplifier using GaAs FET. The amplifier is optimized at large power back-off. The power added efficiency (PAE) and adjacent channel leakage ratio (ACLR) are 33.1% and  $-47$  dBc, which improves about 3.2% and 5 dB respectively, its third-order intermodulation distortion (IMD3) has 2.5 dB improvement compared with conventional Doherty power amplifier.



## Effect of the Gap Feeding on the Multi-band Small Antenna Using a Branch Structure

Hyengcheul Choi, Hojeong Kim, Sinhyung Jeon, and Hyeongdong Kim

Department of Electrical and Computer Engineering, Hanyang University  
Haengdang-dong, Seongdong-gu, Seoul, Korea

**Abstract**— Recently, the antenna for mobile handsets is required to be small and to have a multi-band operation. Although a branch structure is often utilized to get a multi-band operation, small antenna using this structure cannot have a sufficient bandwidth because of an inter-coupling capacitor between two radiating elements. This paper examined an effect of inter-coupling capacitance between two radiating elements by using a transmission line model. Fig. 1(a) shows the geometry of small antenna using branch structure and Fig. 1(b) depicts an equivalent circuit of it at a lower frequency.

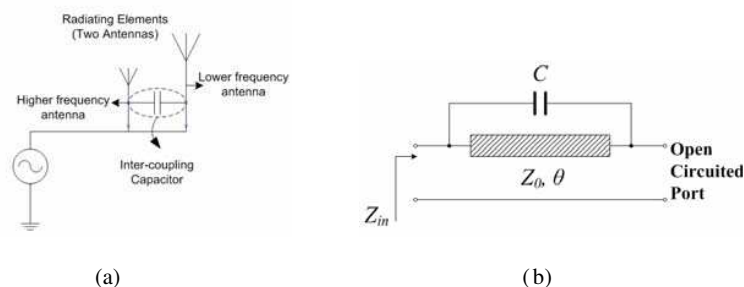


Figure 1: Illustration of small antenna using branch structure, (a) geometry of small antenna using branch structure (b) transmission line model.

To examine the effect of inter-coupling capacitor between two antennas, the input reactance of Fig. 1(b) is shown at Fig. 2. From this graph, it is proved that the inter-coupling capacitor makes the bandwidth of fundamental resonant frequency narrow. Therefore, this paper will propose a gap feeding method to alleviate the influence of the inter-coupling capacitor at branch structure. By comparing two different antennas at which one is adopted a gap feeding and the other is not adopted it, the proposed technique will be detailedly verified in this paper.

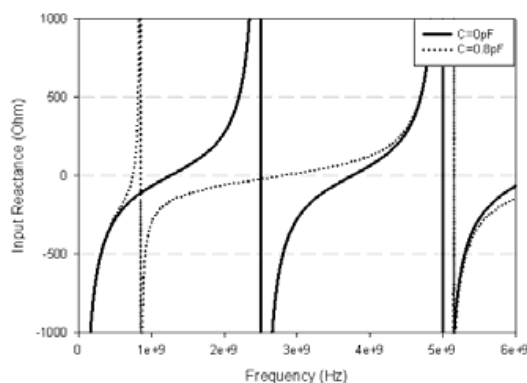


Figure 2: Variation of input reactance with different inter-coupling capacitors.

## Design and Analysis of a 1.2 V, 1.8 GHz, 240.147 $\mu$ w Low Power ASK Transmitter for Wireless Micro Sensor Nodes

T. Sasilatha<sup>1</sup> and J. Raja<sup>2</sup>

<sup>1</sup>Anna University, Chennai, India

<sup>2</sup>SSN College of Engineering, Tamil nadu, India

**Abstract**— A 1.2 V, 1.8 GHz ASK transmitter for low-rate WPAN is designed and implemented. The performance of the transmitter is analyzed to meet the unique requirements of wireless micro sensor nodes. Emphasis was placed on observing device reliability constraints such as leakage current, short circuit current, switching current, supply voltage and the operating frequency at low power to maximize the life time of the wireless sensor nodes. The power consumption in the design is considerably reduced in this approach. The performance of the ASK transmitter is compared with previously reported low power transmitters operating in similar frequency ranges.

# Session 3A7

## Electromagnetic Techniques for Biomedical Applications 1

<b>Biomedical Qualitative Imaging by Means of a Two-step Inverse Scattering Approach</b>	
<i>Manuel Benedetti (University of Trento, Italy); Massimo Donelli (University of Trento, Italy); Dominique Lesselier (CNRS-SUPELEC-UPS 11, France); Andrea Massa (University of Trento, Italy);</i>	628
<b>Wavefront Reconstruction of Breast Microwave Imagery Acquired along Circular Scan Trajectories: A Study on Experimental Feasibility</b>	
<i>Daniel Flores-Tapia (University of Manitoba, Canada); Gabriel Thomas (University of Manitoba, Canada); Stephen Pistorius (University of Manitoba, Canada);</i>	629
<b>A Contrast Source Inversion Algorithm Using a Finite-difference Solver</b>	
<i>Wenyi Hu (Schlumberger-Doll Research, USA); Aria Abubakar (Schlumberger-Doll Research, USA); Peter M. van den Berg (Delft University of Technology, Netherlands); Tarek M. Habashy (Schlumberger-Doll Research, USA);</i>	630
<b>Detection of Breast Tumor by Using a Time-domain Three-dimensional Reconstruction Method</b>	
<i>Hui Zhou (Ocean University of China, China); Takashi Takenaka (Nagasaki University, Japan); Toshiyuki Tanaka (Nagasaki University, Japan);</i>	631
<b>Advancements towards Microwave Tomography for Breast Cancer Screening</b>	
<i>Ilaria Catapano (National Research Council - Institute for Electromagnetic Sensing of Environment, Italy); Lorenzo Crocco (National Research Council - Institute for Electromagnetic Sensing of Environment, Italy); Michele D'Urso (DIET Università di Napoli Federico II, Italy); Tommaso Isernia (DIMET Università Mediterranea di Reggio Calabria, Italy);</i>	632
<b>An Analysis of Algorithms for the Solution of the Magnetoencephalography Inverse Problem</b>	
<i>Michele Piana (Università di Verona, Italy); C. Campi (Università di Verona, Italy); A. Pascarella (Università di Verona, Italy); A. Sorrentino (Università di Genova, Italy);</i>	633
<b>TEM Horn Antenna for Microwave Imaging</b>	
<i>Mark A. Campbell (University of Calgary, Canada); Michal M. Okoniewski (University of Calgary, Canada); Elise C. Fear (University of Calgary, Canada);</i>	634
<b>FDTD Analysis in Hyperthermia and Dosimetry for Biomedical Applications</b>	
<i>Seddik Bri (Equipe Hyperfréquences et Matériaux, ESTM, Maroc); A. Saadi (Equipe Matériaux et Hyperfréquences-ESTM, Maroc); A. Nakheli (Equipe Hyperfréquences et Matériaux, ESTM, Maroc); M. Habibi (Université Ibn Tofail, Maroc); L. Zenkour (Laboratoire d'Electronique et Telecommunications, EMI, Maroc); L. Bellarbi (Equipe Matériaux et Hyperfréquences-ESTM, Maroc); Ahmed Mamouni (Institut d'Electronique, de la Micro'lectronique et de Nanotechnologie, UMR CNRS 8520, IEMN, France);</i>	635
<b>The Design of Planar Transverse Gradient Coils Using a Deformation Algorithm</b>	
<i>Minhua Zhu (Zhejiang University, China); Feng Liu (The University of Queensland, Australia); Ling Xia (Zhejiang University, China); Andrew Mehnert (The University of Queensland, Australia); Hector Sanchez (The University of Queensland, Australia); Qing Wei (The University of Queensland, Australia); Stuart Crozier (The University of Queensland, Australia); Jianfeng Zhu (Zhejiang University, China); Zhaoyang Jin (Zhejiang University, China); Chenghui Zhang (Shandong University, China); Naxin Cui (Shandong University, China); Wenlong Xu (China Jiliang University, China);</i>	636
<b>A Novel Algorithm for Inverse Scattering from Phaseless Measurements of Total Field Based on Rytov Approximation</b>	
<i>Yanli Liu (Institute of Electronics, Chinese Academy of Sciences, China); Lianlin Li (Institute of Electronics, Chinese Academy of Sciences, China); Fang Li (Institute of Electronics, Chinese Academy of Sciences, China);</i>	638
<b>Technical Equipment for Research of Biological Effects of EM Field</b>	
<i>Jan Vrba (Czech Technical University in Prague, Czech Republic); Paolo Togni (Czech Technical University in Prague, Czech Republic); Lukas Visek (Czech Technical University in Prague, Czech Republic); Luca Vannucci (University of Pisa, Czech Republic); Peter Peschke (German Cancer Research Institute, Germany);</i>	639

# Biomedical Qualitative Imaging by Means of a Two-step Inverse Scattering Approach

M. Benedetti<sup>1,2</sup>, M. Donelli<sup>1</sup>, D. Lesselier<sup>2</sup>, and A. Massa<sup>1</sup>

<sup>1</sup>ELEDIA Research Group at DIT, University of Trento, Via Sommarive 14, I-38050 Trento, Italy

<sup>2</sup>Département de Recherche en Électromagnétisme - Laboratoire des Signaux et Systèmes  
CNRS-SUPELEC-UPS 11, 3 rue Joliot-Curie, 91192 Gif-sur-Yvette CEDEX, France

**Abstract**— X-rays imaging and magnetic resonance imaging (MRI) are currently reference methodologies for the non-invasive inspection procedures of biological bodies. In such a framework, microwave methodologies have recently emerged as suitable tools for biomedical diagnosis because of [1]: (a) the non-ionizing nature of microwave, thus the possibility to minimize the collateral effects; (b) the sensibility of microwave to the water content as well as to the contrast variations that exist between malignant and other tissues. In addition, microwave methodologies seem to be less expensive than MRI, as well. Therefore, such approaches can play an important role. As far as microwave inverse scattering techniques are concerned, some qualitative imaging approaches have been recently developed in order to profitably exploit the amount of *a-priori* information on the problem at hand usually available [2]. As an example, some approaches that approximate “contrast” regions (i.e., spatial regions characterized by dielectric differences with respect to “safe” reference distributions) with rectangular shapes have already been proposed [3]. Despite the satisfactory results, such techniques cannot be reliably employed when an accurate knowledge on the shapes of these regions is needed. Notwithstanding, such approximate methods could be profitably used for providing a “first-step” concerned with a rough localization of the “contrast region” to be further improved by means of a successive refinement reconstruction carried out with suitable contour detection methods. Towards this end, this paper presents a two-step procedure aimed at improving the reconstruction of a pathology inside a biological body. More in detail, starting from the knowledge of the scattered field with and without the pathology, the approximate problem where the contrast region is assumed of simple shape (e.g., a rectangle) is reformulated in terms of an inverse scattering one and successively solved by means of the minimization of a suitably-defined cost function. After such a step, the region-of-interest (RoI) is estimated starting from the parameters describing the rough rectangular shape. Then, the second retrieval phase takes place with the application of shape-based optimization technique based on the numerical evolution of a level set function [4]. The outline of the paper is as follows. The mathematical formulation of the proposed approach is presented and the effectiveness of the approach is discussed with reference to a set of representative numerical results in dealing with pathologies within biomedical bodies with noiseless as well as blurred data.

## REFERENCES

1. Fear, E. C., P. M. Meaney, and M. A. Stuchly, “Microwave for breast cancer detection,” *IEEE Potentials*, Vol. 22, No. 1, 12–18, Feb.–Mar. 2003.
2. Benedetti, M., M. Donelli, and A. Massa, “Multicrack detection in two dimensional structures by means of GA-based strategies,” *IEEE Trans. Antennas and Propagat.*, Vol. 55, No. 1, 205–215, Jan. 2007.
3. Caorsi, S., A. Massa, M. Pastorino, and A. Rosani, “Microwave medical imaging: potentialities and limitations of a stochastic optimization technique,” *IEEE Trans. Microwave Theory and Tech.*, Vol. 52, No. 8, 1909–1916, August 2004.
4. Dorn, O. and D. Lesselier, “Level set methods for inverse scattering,” *Inverse Problems*, Vol. 22, R67–R131, 2006.

# Wavefront Reconstruction of Breast Microwave Imagery Acquired along Circular Scan Trajectories: A Study on Experimental Feasibility

Daniel Flores-Tapia<sup>1</sup>, Gabriel Thomas<sup>1</sup>, and Stephen Pistorius<sup>2,3,4</sup>

<sup>1</sup>Department of Electrical and Computer Engineering, University of Manitoba, Winnipeg, Canada

<sup>2</sup>Department of Physics and Astronomy, University of Manitoba, Winnipeg, Canada

<sup>3</sup>Department of Radiology, University of Manitoba, Winnipeg, Canada

<sup>4</sup>Department of Medical Physics, CancerCare Manitoba, Winnipeg, Canada

**Abstract**— During the last decades, Subsurface Radar (SR) has been extensively used on as a non invasive imaging tool in a wide variety of applications such as archeology, soil humidity estimation and landmine detection. Similarly to conventional radar applications, SR systems irradiate electromagnetic waves into the scan area, which is usually formed by two or more layers with different dielectric properties. The received echoes from different buried objects are recorded [1] and displayed in order to be visualized and interpreted. In recent years, SR technology has been used in imaging scenarios where radar techniques theoretically yield high contrast imagery, like breast cancer detection and wood inspection [2, 3]. The data acquisition process in these novel applications is performed along circular or quasi circular scan trajectories in order to adapt better the geometry of the scan area. Also, due to the short distances between the scan locations and the scattering objects, traditional far field focusing techniques are not suitable to properly reconstruct the recorded data.

Currently, there are two main approaches to reconstruct cylindrical SR data: time domain techniques and wavefront reconstruction methods. Time domain focusing techniques perform a shift-sum process over a set of regions of interest in the scan area. The target responses are delayed according to the location where they were collected and their distance from the regions of interest. Next, the shifted responses are added and the square of the sum is the energy at the region of interest. The same process is repeated for all the regions of interest in the scan area. Some examples of this methodology are the confocal mapping algorithm [2] and the polarimetric parameter based reconstruction performed by Kaestner [3].

Wavefront reconstruction techniques focus the recorded SR data by performing a series of operations in the frequency domain. In general, wavefront reconstruction methods work as follows. First, the spectrum of the collected reflections, both in the signal travel time and the scan trajectory directions, is calculated. Afterwards, the spectrum of the recorded signals is compensated using the frequency response of the imaging trajectory. The compensated spectrum is then mapped from the spatial-temporal frequency space in which was originally collected to the imaging area spatial frequency space. Finally, the inverse Fourier transform is applied to the processed data in order to properly visualize the target signatures. Although wavefront reconstruction methods are traditionally used in SR scenarios where the scan trajectory is linear, their potential application on data acquired along circular scan trajectories was shown by the authors in [4] using simulated data sets.

In this work, the experimental feasibility of the wavefront reconstruction approach for circular trajectories proposed by the authors in [4] is illustrated. An experimental data set was collected from phantoms that mimic the dielectric contrast present on breast cancer detection. The focal quality, signal to noise ratio, and spatial accuracy of the focused images were measured in order to quantitatively and qualitatively assess the performance of the reconstruction method. The evaluated technique yielded promising results at an affordable computational cost, encouraging further studies using more complex phantoms.

## REFERENCES

1. Daniels, D., *Ground Penetrating Radar*, IEE Press, London, UK, 2004.
2. Fear, E. C. and M. A. Stuchly, "Microwave detection of breast cancer," *IEEE Transactions on Microwave Theory and Techniques*, Vol. 48, 1854–1863, Nov. 2000.
3. Kaestner, A. P. and L. B. Baath, "Microwave polarimetry tomography of wood," *IEEE Sensors Journal*, Vol. 5, 209–215, April 2005.
4. Flores-Tapia, D. and G. Thomas, "Breast microwave imaging and focusing based on range migration techniques," *16th Int. Zurich Symposium on Electromagnetic Compatibility, Topical Meeting on Biomedical EMC*, Vol. 1, 75–80, Zurich Switzerland, February 2005.

# A Contrast Source Inversion Algorithm Using a Finite-difference Solver

W. Hu<sup>1</sup>, A. Abubakar<sup>1</sup>, P. M. van den Berg<sup>2</sup>, and T. M. Habashy<sup>1</sup>

<sup>1</sup>Schlumberger-Doll Research, USA

<sup>2</sup>Delft University of Technology, The Netherlands

**Abstract**— We present a contrast source inversion (CSI) algorithm for reconstructing unknown electromagnetic or acoustic profile of an inhomogeneous object immersed in a known inhomogeneous background medium from the scattered field data.

Similar to the CSI algorithm using the integral equation (IE) approach, in this new algorithm, the unknown contrast source and the unknown contrast are updated alternately to minimize a pre-defined cost function and there is no full forward problem solution required in each iterative step of the inversion process. However, this new algorithm is based on a finite-difference frequency domain (FDFD) method incorporated with a PML absorbing boundary condition, which enables this algorithm to implement profile reconstruction of an object embedded in an unbounded inhomogeneous background medium. This feature makes this new algorithm more versatile than the CSI using an IE approach which is only capable of handling homogeneous or layered background medium. Numerical experiments show that this new algorithm has excellent performance in both homogeneous and inhomogeneous background medium.

In addition, introducing the finite-difference operator into the algorithm does not deteriorate the efficiency of this algorithm because the stiffness matrix of the finite-difference operator is only dependent on the background medium, which keeps invariant throughout the inversion processes. Therefore, in two-dimensional (2D) configurations, this finite-difference operator only needs to be inverted once and the results can be reused in each iterative step of the inversion process. Furthermore, since a direct matrix inversion technique is employed in our FDFD code, the computational cost to generate the response of an inhomogeneous background medium is limited.

Similar as in the CSI using the IE approach, to enhance the quality of the profile reconstruction, an extra weighted  $L_2$  norm regularization term is added, which is very effective for structures with sharp boundaries, as illustrated in the numerical results. The weighting parameter of this extra regularization term in the cost functional is determined automatically by employing the multiplicative regularization technique. This technique is shown to be very robust in terms of noise-suppressing property and inversion performance with limited measurement data.

## Detection of Breast Tumor by Using a Time-domain Three-dimensional Reconstruction Method

Hui Zhou<sup>1</sup>, Takashi Takenaka<sup>2</sup>, Toshiyuki Tanaka<sup>2</sup>

<sup>1</sup>The College of Marine Geoscience, Ocean University of China, Qingdao, China

<sup>2</sup>Department of Electrical and Electronic Engineering, Nagasaki University  
1-14 Bunkyo-machi, Nagasaki 852-8521, Japan

**Abstract**— Early breast cancer detection is one of the most important and challenging medical subjects because the breast cancer is a leading cause of cancer death among women in Japan. X-ray mammography is currently the most effective detection modality for a front-line mass screening. It has, however, trouble imaging dense breast tissue. Shortcoming in conventional X-ray mammography for breast cancer screening, such as lack of sensitivity (missing up to 15% of tumors) and an unreasonably large amount of false positive readings have led to the search for viable complementary and/or alternative approaches for breast imaging. With an accurate compliment to mammograms, more tumors could be caught at an earlier stage, resulting in a greater treatment success rate.

Microwave has the possibility to identify breast tumors clearly, because tumors show much higher contrast with respect to normal breast tissues at microwave frequencies than at the x-ray frequencies. There are two microwave approaches successful to date: the approach based on radar signal processing originally developed for ground penetrating radars can detect the presence and location of suspicious mass whose tissue properties are different from normal breast tissues, while the approach based on inverse scattering techniques, which is completely different principle, can estimate not only the location and size but also the shape and dielectric properties of a scattering object existing in normal breast tissues, leading to the identification of malignant tumors. We are developing a microwave imaging technology for early breast cancer detection which relies on an inverse scattering technique in the time domain. A microwave mammography based on this technology has the potential to be a low-cost, painless, and safety device for mass screening.

This paper reports numerical simulations of 3-D reconstruction of the relative permittivity profile of a simple breast model consisting of fibroglandular, skin, and normal tissue regions with a tumor by utilizing the forward-backward time-stepping (FBTS) method which we have developed as an inversion technique in the time domain. Measurements are taken in three cross sectional “slices” through the breast numerical phantom. For each cross sectional measurement, each of the 8 antennas is utilized sequentially as a transmitter, with the received signal being measured at each of the 7 available receiving positions. The numerical results show that the quantitative detection of breast cancer is possible by using the FBTS method.

# Advancements towards Microwave Tomography for Breast Cancer Screening

I. Catapano<sup>1</sup>, L. Crocco<sup>1</sup>, M. D'Urso<sup>2</sup>, and T. Isernia<sup>3</sup>

<sup>1</sup>National Research Council - Institute for Electromagnetic Sensing of Environment, Naples, Italy

<sup>2</sup>“Federico II” University of Naples, Naples, Italy

<sup>3</sup>“Mediterranea” University of Reggio Calabria, Reggio Calabria, Italy

**Abstract**— Breast cancer is nowadays one of the main causes of death in women and its early detection is commonly understood as the most effective way to cure this disease. The state-of-the-art screening technique is X-ray mammography which, while sensitive to tumors, has indeed limitations in discriminating amongst malignant tumors and benign ones.

Recently, it has been demonstrated that the electromagnetic properties of the malignant tissues at microwave frequencies are very different from those of the normal ones. Accordingly, microwave tomography has emerged as a complementary diagnostic tool, which can be potentially exploited to perform *morphological* and *functional* screening. On the other hand, the ambitious aim of achieving quantitative information on the imaged tumors involves the solution of a non-linear and ill-posed inverse scattering problem that, besides not-trivial computational issues, claims for reliable approaches capable of avoiding false alarms or lack of detection.

In this communication, in order to address the above problems and proceed towards an effective microwave screening of breast cancer, we will show how, by properly acting on the degrees of freedom of the problem (i.e., type of immersion liquid, working frequency and so on), it is possible to achieve accurate tomographic reconstructions and to actually discriminate between different types of tumors when they are contemporary present.

In particular, by reasoning on the electromagnetic characteristics of the coupling medium, the desired spatial resolution and the factors affecting non-linearity of the underlying inverse scattering problem, we first derive some guidelines for an “optimal” choice of the working frequency and the electromagnetic characteristics of immersion liquid. Then, considering the so determined working conditions, we test the reconstruction capabilities of a Contrast Source inversion approach wherein a regularization by projection is properly exploited in order to increase robustness against false solutions. Numerical examples related to 2D and 3D imaging experiments will be shown at the conference.



## An Analysis of Algorithms for the Solution of the Magnetoencephalography Inverse Problem

M. Piana<sup>1</sup>, C. Campi<sup>1</sup>, A. Pascarella<sup>1</sup>, and A. Sorrentino<sup>2</sup>

<sup>1</sup>Dipartimento di Informatica, Università di Verona, Genova 16146, Italy

<sup>2</sup>Università di Genova, Italy

**Abstract**— Magnetoencephalography (MEG) is a functional imaging modality which allows the measurements of the magnetic fields associated with spontaneous or stimulus-induced neural currents by means of a gradiometer arrangement based on SQUID technology. Due to its formidable temporal resolution (the magnetic signal can be followed with a detail of some milliseconds) MEG is considered as the optimal tool for investigating the dynamical interplay of brain regions during information processing. We provide some insights toward the identification of the optimal method for the solution of the neuromagnetic problem by performing a comparative analysis of three approaches (beamforming, multiple signal classification and particle filtering) to the processing of synthetic data realized according to certain critical but neuroscientifically plausible conditions. Finally an application to real MEG time series is considered.

## TEM Horn Antenna for Microwave Imaging

Mark A. Campbell, M. Okoniewski, and Elise C. Fear

Department of Electrical and Computer Engineering, Schulich School of Engineering  
University of Calgary, Alberta, Canada

**Abstract**— Tissue sensing adaptive radar (TSAR) is a microwave imaging method for the early detection of breast cancer that is under development at the University of Calgary. Short pulses with ultra-wideband (UWB) frequency content are transmitted to and received from the breast, requiring an UWB antenna. This paper reports the design of a TEM horn antenna that works in an immersion medium of canola oil ( $\epsilon_r = 2.5$ ) for this application.

In the open literature there are generally two ways to approach the design of a TEM horn antenna. The first and more conventional method is to design the two metal arms as triangular plates defined by a width angle,  $\alpha$ , and a separation angle,  $\beta$  [1]. The second approach treats each metal arm as the continuation of a parallel plate (PP) transmission line with varying characteristic impedance  $Z_0$  [2]. With the PP design method, the idea of matching the feeding transmission line to free space is often used. These two design methods have been explored for the design of the TSAR antenna, with an emphasis on the PP approach.

When the PP method is used to design a TEM horn antenna, there are a large number of variables available for adjustment. Given a particular envelope of space with a fixed starting and ending location, there are a large number of ways in which the antenna may be designed. Both the metal arm separation and impedance profiles over the antenna length may be varied. To do this, it is necessary to accurately calculate the characteristic impedance of a PP transmission line. A formulation by Wheeler [3] for parallel strips separated by a dielectric sheet in air has been manipulated to allow for calculations in an arbitrary homogeneous medium. Simulations of PP transmission lines performed for confirmation show good agreement. Using the calculation method as a guideline, antenna designs are created using various combinations of linear, exponential, elliptical, circular, near-optimum and other curves for the separation and impedance profiles. Antenna designs were simulated with the MOM software Feko (EM Software and Systems, Stellenbosch, South Africa) because of its ability to model thin curved surfaces efficiently. Performance of the designs is evaluated using VSWR over the frequency range of 2 to 15 GHz.

The simulation results permitted several observations. First, the idea of matching to the intrinsic impedance of the immersion medium has been investigated. Results show this idea to be erroneous (lower VSWR results are obtained with non-matching profiles), though it is still being used as demonstrated in several recent papers [2, 4]. Second, several designs using the PP approach produced better VSWR results than the conventional triangular plate approach. Further investigation of the selected design, including near-field radiation properties, implementation and measurement, is ongoing.

### REFERENCES

1. Lee, R. T., et al., *IEEE Trans. on Ant. and Prop.*, Vol. 52, No. 1, 315–318, Jan. 2004.
2. Chung, K., et al., *IEEE Trans. on Ant. and Prop.*, Vol. 53, Issue 10, 3410–3413, Oct. 2005.
3. Wheeler, H. A., *IEEE Trans. on Mic. Theo. and Tech.*, Vol. 13, Issue 2, 172–185, Mar. 1965.
4. Park, J., *IEEE MTT-S International Microwave Symposium Digest*, 1433–1446, June 2003.

## FDTD Analysis in Hyperthermia and Dosimetry for Biomedical Applications

S. Bri<sup>1,2</sup>, A. Saadi<sup>1,2</sup>, A. Nakheli<sup>1</sup>, M. Habibi<sup>2</sup>, L. Zenkour<sup>1</sup>  
L. Bellarbi<sup>1</sup>, and A. Mamouni<sup>3</sup>

<sup>1</sup>Equipe Matériaux et Hyperfréquences, ESTM, B. P. 3103, Route d'agouray, Meknès, Maroc

<sup>2</sup>Laboratoire des Systèmes des Télécommunications et d'Ingénierie de la Décision (LASTID)  
Faculté des Sciences, Département de physique, Université Ibn Tofaïl, Kénitra, Maroc

<sup>3</sup>Groupe CSAM, Institut d'Electronique, de Microélectronique et de Nanotechnologie  
UMR CNRS 8520 IEMN-DHS, Avenue Poincaré, Cité scientifique  
B. P. 60069 59652, Villeneuve d'Ascq Cedex, France

**Abstract**— In this paper, we present the biological effects of the radio-frequency field, and the interaction mode between RF and the tissue. The simulation of this interaction permitted to analysis the absorption of RF energy in the biological tissue. After we describe a the technique to heat different sizes of tumors and instantaneous follow up of the thermal diffusion, by microwave applicators realized from coaxial monopole surrounded by an absorbing and thermal conductor dielectric material (ATCDM). The Finite Difference Time Domain method “FDTD” with Perfectly Matched Layers for absorbing boundary conditions is used to model the head, the cell phone, microwave applicator and the “ATCDM” material.

# The Design of Planar Transverse Gradient Coils Using a Deformation Algorithm

Minhua Zhu<sup>1</sup>, Feng Liu<sup>2</sup>, Ling Xia<sup>1</sup>, Andrew Mehnert<sup>2</sup>, Héctor Sánchez<sup>2</sup>, Qing Wei<sup>2</sup>  
 Stuart Crozier<sup>2</sup>, Jianfeng Zhu<sup>1</sup>, Zhaoyang Jin<sup>1</sup>, Chenghui Zhang<sup>3</sup>  
 Naxin Cui<sup>3</sup>, and Wenlong Xu<sup>4</sup>

<sup>1</sup>Department of Biomedical Engineering, Zhejiang University, Yu Quan, Hangzhou 310027, China

<sup>2</sup>School of Information Technology & Electrical Engineering, The University of Queensland  
 St. Lucia, Brisbane Qld 4072, Australia

<sup>3</sup>Department of Control Science and Engineering, Shandong University, Jinan 250100, China

<sup>4</sup>Department of Computer Science and Technology, China Jiliang University, Hangzhou 310018, China

## Abstract—

**Introduction:** There are two basic approaches to gradient coil design for MRI. The first is the Fourier (continuous)-space based approach; e.g., the target field method [1]. The second is the real (wire)-space based approach; e.g., the simulated annealing method [2]. Both of these approaches have pros and cons. The first approach uses analytical expressions or series expansions to describe the current densities over a specified surface. It is very efficient for regular-shaped domains but is difficult to implement for domains with arbitrary geometry. The second approach is relatively slower but has the advantage that it can handle more arbitrary geometries and additionally it is easy to incorporate real constraints. In this work we propose a modified, efficient real-space method [2] and apply it to the design of bi-planar gradient coils for open MRI systems. The proposed method permits the placement of current arcs on any desired coil surface. For the case of a planar gradient coil, the design of the z-coils is relatively straightforward; the z- and r-positions of the current ‘loop’ can be adjusted in the optimization process. For the transverse coils, the solution is not as straightforward because it is not feasible to move each segment of the current arcs separately. The solution that we propose in this work is to represent each arc by a closed contour described by parametric equations such that the ensemble of closed contours can be deformed/reshaped in a simple manner controllable by just a few parameters. These parameters are then used to define system rearrangements in the design procedure. An iterative optimization procedure is used to adjust the control parameters to minimize target/cost functions including gradient homogeneity, inductance and other parameters.

**Method:** In the defined coil plane, a series of limaçons (polar equation  $r = a + b \cos \theta$ ) are used to represent the initial current arcs. We use the following parameterization of a limaçon to describe each contour:

$$x(t) = (a + b \cos t) \cos t + k, \quad y(t) = (c + d \cos t) \sin t.$$

The coefficients  $a$ ,  $b$ ,  $c$ ,  $d$ , and  $k$  control the translation and deformation (scaling/shape). We treat these as unknown variables that alter/control the current-arc positions (i.e., x- and y-coordinates). Their values are determined using a quadratic optimization routine. During the

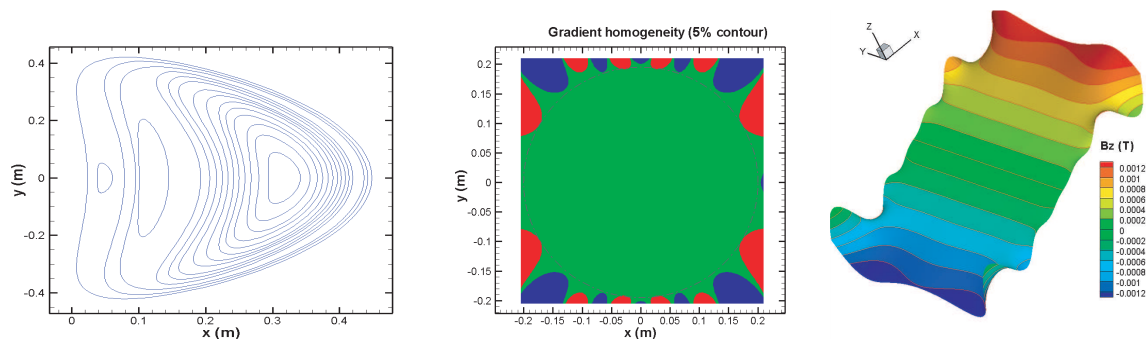


Figure 1: The coil pattern for the symmetrical gradient x-coil (a) and corresponding gradient homogeneity (b) and field profile (c).

optimization, the gradient field over the region of interest is calculated using the Biot-Savart Law. Given that the coil contour is a closed curve, the field evaluation can be efficiently implemented using a 1D Gaussian integration method.

**Result:** Figure 1 shows an example transverse coil pattern and corresponding gradient field homogeneity inside the DSV. It can be seen that the new algorithm can produce a well-connected coil structure and a good gradient linearity.

**Conclusion:** In this work we have demonstrated that a real-space algorithm can be used for complicated gradient coil design through an appropriate parameterization of the current arcs. Both a previous study for a cylindrical system [2] and the current work for a planar system demonstrate the capability of the deformation-space methodology. In the future we will refine this optimization technique; extend it to a variety of geometry domains (including 3D); and consider additional engineering constraints such as energy and inductance.

#### REFERENCES

1. Turner, R., "Gradient coil design: A review of methods," *Magn. Reson. Imag.*, Vol. 11, 903–920, 1993.
2. Crozier, S., L. K. Forbes, and D. M. Doddrell, "The design of transverse gradient coils of restricted length by simulated annealing," *J. Magn. Reson.*, Vol. 107(A), 126–128, 1994.

## A Novel Algorithm for Inverse Scattering from Phaseless Measurements of Total Field Based on Rytov Approximation

Yanli Liu, Lianlin Li, and Fang Li

Institute of Electronics, Chinese Academy of Sciences, Beijing 100080, China

**Abstract**— The problem of determining the properties of a scatter embedded in a non-attenuating or lossy background medium from scattered field data has received considerable attention in recent 30 years or so. Various forms of this problem arise in a number of practical applications in the fields of nondestructive evaluation, surface seismic surveying, ultrasound and optical imaging and geophysical and ultrasound tomography. The ‘properties’ of the scatter that are sought in any given application vary widely and can range from shape and size information to electromagnetic properties. Numerous methods with nondestructive tests and evaluations have been proposed for the reconstruction of the ‘properties’ of the objects.

However, most of these methods require the measurement of not only the intensity of scattered field but also its phase. Phase measurements generally present considerable practical difficulties. Recently some approaches have been proposed to circumvent the problem of direct phase measurements. Some authors have suggested the use of cylindrical lens system or an interferometric technique, but such systems are difficult to construct under certain conditions, and they add both experimental and theoretical complications to the inverse problem. Some variants of diffraction tomography that require only intensity measurements have been proposed that involve iterative algorithms or are restricted to reconstructions of objects whose refractive index is real valued.

In this paper, the linear relationship between the log-amplitude and phase of total field is derived based on Rytov approximation, by which the phase can be easily obtained from the amplitude. From this proposed method, the inverse scattering with amplitude-only data can be easily realized by two-step scheme based on the result of phase information, where the second step is the implement of the standard inverse scattering. It can be found that this method presented in this paper is superior in following ways: (1) The paraxial approximation of field is unnecessary in the process of reconstruction, that is, there is no need to restrict the object to have a well-localized Fourier spectrum. (2) Our formulation can be used for any kind of excited sources except for plane and spherical wave. (3) The tomographic configuration with rotation of the obstacle and a pair of detector planes is not required; moreover, due to the elimination of paraxial approximation, the detector plane can be placed arbitrarily according to the practical requirement. Finally we implement numerically the reconstruction algorithm and present reconstructed images to demonstrate their use and corroborate our theoretical assertions.

# Technical Equipment for Research of Biological Effects of EM Field

Jan Vrba<sup>1</sup>, Paolo Togni<sup>1</sup>, Lukas Visek<sup>1</sup>, Luca Vannucci<sup>2</sup>, and Peter Peschke<sup>3</sup>

<sup>1</sup>Department of EM Field, Czech Technical University in Prague, Prague, Czech Republic

<sup>2</sup>Institute of Microbiology, Czech Academy of Sciences, University of Pisa, Prague, Czech Republic

<sup>3</sup>German Cancer Research Institute, Heidelberg, Germany

**Abstract**— Research of interactions between EM Field and biological systems is of growing interests elsewhere. Also here in Czech Republic there are several groups working in this field, often in international co-operations. We will describe here mainly basic technical equipment developed for 5 different research projects in the discussed area of interactions of EM field and biological systems.

In present time four research institutions here in the Czech Republic run research projects focused on studies of interactions between EM field and biological systems. These institutions are technically supported by Dept. of EM Field of the Czech Technical University in Prague. In this contribution we would like to give more details about that projects and obtained technical results (i.e., description of developed exposition systems).

Three of discussed projects ([1] in Germany and [2] here in Czech Republic) are basic research for simulation of the microwave hyperthermia treatment. Other two projects (both in Czech Republic are focused on simulation of the case of exposition by mobile phone.

In the modern view, cancer is intended as a complex illness, involving the cells that undergo to transformation, their environment, and the general responses at biochemical and biological levels induced in the host. Consequently, the anti-cancer treatment protocols need to be multimodal to reach curative effects. Especially after the technical improvements achieved in the last 15 years by bio-medical engineering, microscopy devices, and molecular biology methods, the combinations of therapeutic procedures are growing in interest in basic and clinical research.

The combination of applied biological research together to the physical sciences can offer important perspectives in anticancer therapy (e.g., different methodologies and technical devices for application of energies to pathological tissues).

The modern bioengineering knowledge applied to traditional tools, as the microscopy, has largely renewed and expanded the fields of their applications (e.g., *in vivo* imaging), pushing the interest for direct morpho-functional investigations of the biomedical problems.

## ACKNOWLEDGMENT

This work was supported by the Czech Academy of Sciences, Institutional Research Concepts No. AV0Z50200510: “Hyperthermia and anticancer immunomodulation, morpho-functional study of micro-environmental interactions in melanoma model”.

## REFERENCES

1. Vrba, J., *Medical Applications of Microwaves*, CTU Press, Prague, In Czech, 2003.
2. Hand, J. and J. R. James(editors), *Physical Techniques in Clinical Hyperthermia*, Wiley, New York, 1986.
3. Franconi, C., J. Vrba, et al., “27 MHz hybrid evanescent-mode applicators,” *Int. Journal of Hyperthermia*, Vol. 9, No. 5, 655–674, 1993.
4. Vrba, J., C. Franconi, et al., “Evanescent-mode applicators for hyperthermia,” *IEEE Trans.on Biomedical Engineering*, Vol. 40, No. 5, 397–407, May 1993.





# Session 3A8

## Computational Techniques

<a href="#">Parallel Computing Methods for Finite-difference Schemes in MRI Research</a>	
<i>Hua Wang (The University of Queensland, Australia); Feng Liu (The University of Queensland, Australia); Adnan Trakic (The University of Queensland, Australia); Stuart Crozier (The University of Queensland, Australia);</i> .....	642
<a href="#">The Effective Current Density Scheme for Drude Model in the Finite-difference Time-domain</a>	
<i>Minfeng Chen (National Taiwan University, Taiwan); Hung-Chun Chang (National Taiwan University, Taiwan, R.O.C.);</i> .....	644
<a href="#">A Numerical Estimation of Human Effects on Electric Field Distribution in Wireless Office LANS Using the FDTD Method</a>	
<i>Louis-Ray Harris (Hokkaido University, Japan); Takashi Hikage (Hokkaido University, Japan); Toshio Nojima (Hokkaido University, Japan); Masahiko Hirono (Hokkaido University, Japan);</i> .....	645
<a href="#">Revisited Implementation of the Spectral Kummer-Poisson's Method for the Efficient Computation of 2-D Periodic Green's Functions in Homogeneous Media</a>	
<i>Rafael R. Boix (University of Seville, Spain); A. L. Fructos (University of Seville, Spain); Francisco L. Mesa (University of Seville, Spain); Francisco Medina (University of Seville, Spain);</i> .....	646
<a href="#">An Improved Matrix Bandwidth and Profile Reduction Algorithm in FEM Problems</a>	
<i>Qing Wang (Xidian University, China); Yuchun Guo (Xidian University, China); Xiaowei Shi (Xidian University, China);</i> .....	648
<a href="#">Scattering of Electromagnetic Waves by Inhomogeneous Dielectric Gratings Loaded with Two Adjacent Perfectly Conducting Strip</a>	
<i>Tsuneki Yamasaki (Nihon University, Japan); Ryosuke Ozaki (Nihon University, Japan); Takashi Hinata (Nihon University, Japan);</i> .....	649
<a href="#">Diffraction on a Magnetic Nanoparticle Array Computed Using Autonomous Blocks with Floquet Channels</a>	
<i>Galina S. Makeeva (Penza State University, Russia); Oleg. A. Golovanov (Penza Military Institute of Artillery, Russia); Martha Pardavi-Horvath (The George Washington University, USA);</i> .....	650
<a href="#">Simulation of Multiple Scattering Scenes for Time Domain Maxwell's Equations by an Hybrid and Parallel Method</a>	
<i>V. Mouysset (ONERA, France); Pierre Borderies (Office National d'Etudes et de Recherches Aeronautiques, France); X. Ferrières (Office National d'Etudes et de Recherches Aeronautiques, France);</i> .....	651

# Parallel Computing Methods for Finite-difference Schemes in MRI Research

Hua Wang, Feng Liu, Adnan Trakic, and Stuart Crozier

School of Information Technology and Electric Engineering

The University of Queensland, Brisbane, Qld 4072, Australia

**Abstract**— With the recent evolution of MRI towards high field strengths in search of better signal to noise ratios (SNR) and improved temporal resolution, the complicated interactions of electromagnetic fields with the patient and resistive MRI system components has increased and requires detailed analyses. Accurate and efficient evaluation of *in situ* electromagnetic field (EMF) distributions is therefore particularly relevant.

The finite-difference time-domain (FDTD) method is well suited to electromagnetic analyses in MRI applications, due to its simplicity and efficiency in wave modelling and its ability to handle field-sample interactions and nonlinear phenomena [1, 2]. In recent years we have developed a series of single-processor based FDTD schemes [3–10], which can be employed to analyze modern MRI problems over a wide range of operating frequencies. For low frequency scenarios, while the dimensions of the material medium are small compared to the wavelength, the induced fields can be treated quasi-statically. In modern MRI, exposures to switched gradient coils and body movements of both patients and health workers through strong, non-uniform static magnetic fields inside and outside of the imager may be able to induce electric currents in tissues. Our previous work [11–13] used single processing quasi-static finite-difference (QSFD) schemes to accurately model the induction of electric fields and associated current densities in human body models exposed to the MRI system in operation.

Electromagnetic modeling of human exposure in MRI settings, however, often requires high spatial resolution and a large problem scale, which imposes a large computational burden. In the realm of large-scale-high-resolution (LSHR) computing, the single processor based methods are limited and are often incapable of managing large memory and computational time requirements. Therefore, to improve the performance of these finite difference schemes, it is necessary to further explore computational strategies such as parallelization. Parallel environments such as the MPI, OPENMP, LAM/MPI, have been used recently in large-scale scientific computations [14–16]. The finite difference methods and related hybrid algorithms, based on their geometrical topology, are highly adaptable to the parallel computing framework, in which the computing task is divided and assigned to many processors with distributed or shared memory allocations. In addition, parallelized conjugate gradient techniques can be applied to solve the sparse matrices obtained by transformation of the original finite difference equations. This is based on the observation that zero elements associated with the free air region surrounding the body model were largely involved in previous  $O(N^3)$  arithmetic operations.

Distinct LSHR problems have been investigated with the aforementioned parallel computing schemes. The FDTD method has been parallelized for the comparative study of the interactions of RF-fields with whole-body human models. A practical case of a human body model, exposed to gradient coil switching indicates computational advantages of the high performance QSFD solver. Compared to previous single processing iterative algorithm, the proposed parallel conjugate gradient method offers significant advantages in terms of improved convergence, smaller memory usage and the ability to handle solution errors. All the problems have been solved at high spatial resolutions, which are already beyond the capability of the conventional non-parallelized finite difference algorithms.

Our long term aim is to generate a complete finite difference model of an MRI system including all the field generating units and an electrical model of a patient. A better understanding of the complex temporal interaction of the fields within the patient and the MRI system components during an MRI scan can provide useful insight into the coil design.

## REFERENCES

1. Collins, C. M., S. Li, and M. B. Smith, “SAR and B1 field distributions in a heterogeneous human head model within a birdcage coil,” *Magn. Reson. Med.*, Vol. 40, 847–856, 1998.
2. Ibrahim, T. S., R. Lee, B. A. Baertlein, Y. Yu, and P. M. L. Robitaille, “Computational analysis of the high pass birdcage resonator: Finite difference time domain solutions for high-field MRI,” *Magn. Reson. Imag.*, Vol. 18, No. 7, 835–856, 2000.

3. Liu, F., S. Crozier, and H. Zhao, "Finite-difference time-domain based studies of MRI pulsed field gradient-induced eddy currents inside the human body," *Concepts Magn. Reson.*, Vol. 15, No. B1, 26–36, 2002.
4. Zhao, H., S. Crozier, and F. Liu, "A FDTD method for modeling the effect of switched gradients on the human body in MRI," *Magn. Reson. Med.*, Vol. 48, 1037–1042, 2002.
5. Zhao, H., S. Crozier, and F. Liu, "An analysis of the high-definition finite-difference time-domain methods," *Appl. Math. Model.*, Vol. 27, 409–419, 2003.
6. Liu, F. and S. Crozier, "A distributed equivalent magnetic current based FDTD method for the calculation of E-fields induced by gradient coils," *J. Magn. Reson.*, Vol. 169, 323–327, 2004.
7. Wei, Q., F. Liu, L. Xia, and S. Crozier, "An object-oriented designed finite-difference time-domain simulator for electromagnetic analysis and design in MRI — Applications to high field analyses," *J. Magn. Reson.*, Vol. 172, 222–230, 2005.
8. Liu, F. and S. Crozier, "An FDTD model for calculation of gradient induced eddy currents in MRI system," *IEEE Trans. Appl. Superconduct.*, Vol. 14, 1983–1989, 2004.
9. Trakic, A., H. Wang, F. Liu, H. S. Lopez, and S. Crozier, "Analysis of transient eddy currents in MRI using a cylindrical FDTD method," *IEEE Trans. Appl. Superconduct.*, [in press 2006].
10. Liu, F., B. L. Beck, B. Xu, J. R. Fitzsimmons, S. J. Blackband, and S. Crozier, "Numerical modelling of 11.1T MRI of a human head using a MoM/FDTD method," *Concepts Magn. Reson.*, Vol. 24, No. B1, 28–38, 2005.
11. Liu, F., H. W. Zhao, and S. Crozier, "On the induced electric field gradients in the human body for magnetic stimulation by gradient coils in MRI," *IEEE Transactions on Biomedical Engineering*, Vol. 50, No. 7, 804–815, 2003.
12. Crozier, S. and F. Liu, "Numerical evaluation of the fields caused by body motion in or near high-field MRI scanners," *Progress in Biophysics and Molecular Biology*, Vol. 87, 267–278, 2005.
13. Liu, F., H. W. Zhao, and S. Crozier, "Calculation of electric fields induced by body and head motion in high-field MRI," *Journal of Magnetic Resonance*, Vol. 161, 99–107, 2003.
14. Guiffaut, A. and K. Mahdjoubi, "A parallel FDTD algorithm using the MPI library," *IEEE Antennas and Propagation Magazine*, Vol. 43, No. 2, 2001.
15. Gedney, S. D., "Finite-difference time-domain analysis of microwave circuit devices in high performance vector/parallel computers," *IEEE Transactions on Microwave Theory and Techniques*, Vol. MTT-43, No. 10, 2510–2514, 1995.
16. Taguchi, K., M. Uchiya, T. Kashiwa, K. Hirayama, H. Kuribayashi, and S. Komatsu, "FDTD large-scale parallel supercomputing and its application to the analysis of radiation characteristics of an antenna mounted on a vehicle," *International Journal of RF and Microwave Computer-Aided Engineering*, Vol. 14, 253–261, 2004.

# The Effective Current Density Scheme for Drude Model in the Finite-difference Time-domain

Minfeng Chen<sup>1,2</sup> and Hung-Chun Chang<sup>1,3</sup>

<sup>1</sup>Graduate Institute of Photonics and Optoelectronics  
National Taiwan University, Taipei, Taiwan, R.O.C.

<sup>2</sup>Department of Physics, Applied Physics, and Astronomy  
Rensselaer Polytechnic Institute, Troy, New York 12180-3590, USA

<sup>3</sup>Department of Electrical Engineering  
National Taiwan University, Taipei, Taiwan 106-17, R.O.C.

**Abstract**— A Finite-Difference Time-Domain (FDTD) mesh is usually made up of cubic lattice for three-dimensional (3-D) problems and square lattice for 2-D problems. Significant difference may arise by comparing the computational mesh and the structure of interest, which leads to reduced accuracy. Extensive methods have been proposed to eliminate such staircase error for conventional dielectric. However, few effort addressed the same issue for dispersive materials, i.e., metals.

Rather than using complicated methods to achieve numerical accuracy, we propose a new and relatively simple scheme to reduce staircase error for Drude material, which characterizes metal. The Drude material is determined by a set of physical quantities:  $\varepsilon_d$  is representative of bounded electrons;  $n$  and  $\tau_p$  correspond to the electron density and relaxation time of free electrons, respectively. Given a FDTD unit cell consisting of various materials, we develop such scheme by taking average for each quantities. The current density is modified at the interface between adjacent materials accordingly. We thus name this scheme the “Effective Current Density” (ECD) scheme. Note that the ECD scheme will return to the conventional index average (IA) scheme by setting  $n = 0$  and  $\tau_p = 0$  (no free electron). Therefore, in a combined material, such as metallodielectric, the ECD scheme still works. In other words, the ECD scheme is an extended version of the IA scheme, which involves the free electron behavior, while the IA scheme only considers dielectric (bounded electrons). The physical interpretation of the ECD scheme will be explained in detail. Finally, we numerically demonstrate the promising accuracy improvement by employing such scheme.

# A Numerical Estimation of Human Effects on Electric Field Distribution in Wireless Office LANS Using the FDTD Method

Louis-Ray Harris, Takashi Hikage, Toshio Nojima, and Masahiko Hirono

Hokkaido University, Sapporo 060-0814, Japan

**Abstract**— In this study, the Finite Difference Time Domain (FDTD) Method is used to examine the variation of the Electric Field Strength distribution in an office environment as the number and position of human models change. The office that has been modeled is based on a room in this department. The results are compared with actual experimental data from measurements taken in the room. (58)

**Method:** Using the FDTD Analysis Method, the electric field strength at every point within a specified area is calculated taking into account physical and electrical properties of all objects defined within that area. The plane in which the data is calculated is 1.0 m from the floor. Results are displayed graphically and an overhead view of the distribution map is also generated. The calculations are performed using the Hokkaido University Information Initiative Centre's supercomputer. The supercomputer is required because the room dimensions of 11.34 m  $\times$  3.64 m  $\times$  15.09 m and a cell size of 1 cm requires a large amount of memory. Exact measurements are used for all objects in the FDTD model. The frequency bands for which the calculations and measurements are performed are the 2 GHz and 5 GHz bands.

If the experimental and simulated datasets agree, it will be possible to proceed with plans to examine ways to improve the E-field strength in various sections of semi-echoic Wireless LAN environments using the FDTD method. This method is more accurate than other methods such as the ray-tracing method because FDTD takes into account the properties of every material in the environment. The cell-size and available memory are the only limiting factors to the accuracy of the results.

# Revisited Implementation of the Spectral Kummer-Poisson's Method for the Efficient Computation of 2-D Periodic Green's Functions in Homogeneous Media

R. R. Boix<sup>1</sup>, A. L. Fructos<sup>1</sup>, F. Mesa<sup>2</sup>, and F. Medina<sup>1</sup>

<sup>1</sup>Department of Electronics and Electromagnetism, College of Physics, University of Seville  
Av. Reina Mercedes, s/n, 41012, Seville, Spain

<sup>2</sup>Department of Applied Physics 1, School of Computer Engineering, University of Seville  
Av. Reina Mercedes, s/n, 41012, Seville, Spain

**Abstract**— The application of the Method of Moments (MoM) to the solution of periodic electromagnetic problems requires the computation of periodic Green's functions. Thus, the free-space 2-D periodic Green's function with 1-D periodicity (2DPGF-1D) has been used in the determination of the scattering matrix of inductive obstacles in rectangular waveguide [1], and the same 2DPGF-1D has also been used in the analysis of the scattering of plane waves from one-dimensional periodic arrays of lossy strips in free space [2]. In the case of multilayered media, the 3-D periodic Green's functions of multilayered media with 2-D periodicity can be obtained in terms of both 3-D periodic Green's functions with 2-D periodicity (3DPGF-2D) in homogeneous media and 2-D periodic Green's functions with 2-D periodicity (2DPGF-2D) in homogeneous media, which has been used in [3] to compute the reflection and transmission properties of frequency selective surfaces embedded in multilayered media. The previous examples show that the development of efficient and accurate algorithms for the computation of the 2DPGF-1D and the 2DPGF-2D in homogeneous media is very useful as an intermediate step for studying the scattering by periodic structures both in homogeneous and multilayered media.

2-D periodic Green's functions in homogeneous media can be written either as spatial infinite series, or as spectral infinite series when Poisson's formula is used. When losses are negligible, both the spatial and the spectral series are slowly converging, and a large number of analytical and numerical methods have been applied in the literature to accelerate the convergence of these series. The most famous analytical methods are the spectral Kummer-Poisson's method, Veisoglu's tranformation method, Ewald's method and the lattice sums method [4, 5], and the most famous numerical methods are Euler's transformation, Shank's transformation, the  $\theta$ -algorithm and the Chebyshev-Toeplitz algorithm [6]. Linton has carried out a comparison among the different acceleration methods that have been used for the computation of 2-D periodic Green's functions in homogeneous media [7], and he has concluded that Ewald's method is the best method in most scenarios because of its versatility and good compromise between accuracy and efficiency.

In this paper the authors presents an algorithm for the acceleration of the series involved in the computation of the 2DPGF-1D and the 2DPGF-2D in homogeneous media. The algorithm is based on an original implementation of the spectral Kummer-Poisson's method. In the algorithm any of the series that has to be accelerated is split into two new series containing unknown coefficients. A judicious choice of these coefficients makes it possible that these two new series converge very fast, one of them with exponential convergence and the other one with algebraic convergence of arbitrarily large order. Whereas other sophisticated algorithms based on Kummer-Poisson's method [8] are heavily dependent on the mathematical expression of the terms of the series that have to be accelerated, the new algorithm presented in this paper is very general and works equally well for 2-D periodic problems with 1-D periodicity and for 2-D periodic problems with 2-D periodicity involving lattices with arbitrarily skewed axes. The CPU times required by the algorithm for the computation of 2-D periodic Green's functions within a predetermined accuracy have been compared with the CPU times required by Ewald's method. The algorithm has been found to be between two and five times faster than Ewald's method in all the cases studied.

## REFERENCES

1. Leviatan, Y., et al., *IEEE-MTT*, Vol. 31, 806–812.
2. Jorgenson, R. E., et al., *IEEE-AP*, Vol. 38, 212–219.
3. Yu, Y., et al., *IEEE-MTT*, Vol. 48, 1623–1627.
4. Valerio, G., et al., *IEEE-AP*, Vol. 55, 1630-1642.
5. Nicorovici, N. A., et al., *Phys. Rev. E*, Vol. 50, 3143–3160.

6. Kinayman, N., et al., *Radio Science*, Vol. 30, 1713–1722.
7. Linton, C. M., *J. Eng. Math.*, Vol. 33, 377–402.
8. Baekelandt, B., et al., *AE Int. J. Electron. Commun.*, Vol. 51, 224–230.

## An Improved Matrix Bandwidth and Profile Reduction Algorithm in FEM Problems

Q. Wang, Y. C. Guo, and X. W. Shi

National Key Laboratory of Antenna and Microwave Technology, Xidian University, Xi'an 710071, China

**Abstract**— It is a key issue to process the stiffness matrices which are sparse, structured and symmetric in FEM (Finite Element Method) problems, such as structural engineering, fluid dynamics, electromagnetic field analysis. Mainly to decrease the volume of the computation data stored, it is necessary to optimize the FEM mesh nodes coding for reducing the bandwidths and profiles of stiffness matrices. The GPS algorithm is a very effective optimization algorithm in bandwidth and profile reduction.

In this paper, a Generalized GPS (GGPS) algorithm is proposed. The algorithm has three key-points. First, all the endpoints are found, which can be used as the origins for generating the tree structures which all have the same depth, rather than two endpoints in the GPS (Gibbs Paul & Stockmeyer) algorithm. Then there are more than two tree structures of the graph. Second, a new tree structure is constructed with all the levels structures, which is smaller in width than any tree structure. Third, a new combination rule is used to obtain more sub graphs in order to further reduce the level width. Hence, we can conclude that the increasing of the amount of pseudo diameter-endpoints and sub graphs can be seen as the increasing of the freedom of level structures space, and the bandwidth and profile can be further reduced when the graph is more fractionized.

Simulation results show that the more the amount of nodes, the smaller the bandwidth and profile can be optimized by the GGPS algorithm, which is smaller than the results got by the GPS algorithm by about 5% in bandwidth and 2% in profile respectively in relation to the test data in the paper. It is clear that the GGPS is superior to the GPS in reducing bandwidth and profile.



# Scattering of Electromagnetic Waves by Inhomogeneous Dielectric Gratings Loaded with Two Adjacent Perfectly Conducting Strip

Tsuneki Yamasaki, Ryosuke Ozaki, and Takashi Hinata

Department of Electrical Engineering, College of Science and Technology  
Nihon University, Tokyo, 101-8308, Japan

**Abstract**— The scattering and guiding problems of inhomogeneous dielectric gratings have been of considerable interest such as optical fiber gratings, photonic bandgap crystals, frequency selective devices, and other applications by the development of manufacturing technology of optical devices. Recently, many analytical and numerical methods which are applicable to the arbitrarily dielectric gratings have been proposed. However, most theoretical and numerical studies have considered the periodic structures in which the material forming grating was either metallic or dielectric.

In this paper, we proposed a new method for the scattering of electromagnetic waves by inhomogeneous dielectric gratings loaded with two adjacent perfectly conducting strips using the combination of improved Fourier series expansion method and point matching method.

In the inhomogeneous dielectric region  $S_2(0 < x < D)$ , the permittivity profile  $\varepsilon_2(x, z)$  is generally not separable with respect to the  $x$  and  $z$  variables. Main process of our methods are as follows: (1) The inhomogeneous layer is approximated by a stratified layers of modulated index profile with  $D$ . (2) Taking each layer as a modulated dielectric grating, the electromagnetic fields are expanded appropriately by a finite Fourier series. (3) In the perfectly conducting strip and gap regions at  $C_1$ (or  $\bar{C}_1$ ) for the boundary, the electromagnetic fields are matched using an orthogonality relation. (4) In the perfectly conducting strip and gap regions at  $C_2$ (or  $\bar{C}_2$ ) for the boundary, it makes the matrix relation on both sides using point matching method. (5) Finally, all stratified layers include the metallic regions are matched using appropriate boundary conditions to get the inhomogeneous dielectric gratings loaded with three perfectly conducting strips.

Numerical results are given for the transmitted scattered characteristics for the case of incident angle and frequency with  $\delta$  for TE waves.

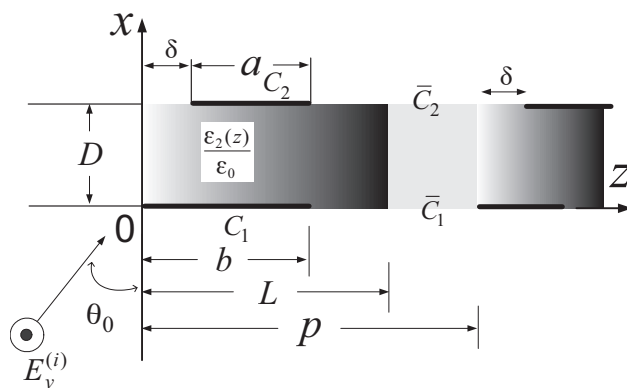


Figure 1: Structure of inhomogeneous dielectric gratings loaded with two adjacent perfectly conducting strips.

# Diffraction on a Magnetic Nanoparticle Array Computed Using Autonomous Blocks with Floquet Channels

Galina S. Makeeva<sup>1</sup>, Oleg A. Golovanov<sup>2</sup>, and Martha Pardavi-Horvath<sup>3</sup>

<sup>1</sup>Penza State University Krasnaya, 40, Penza 440026, Russia

<sup>2</sup>Penza Military Institute of Artillery, Penza-5, 440005, Russia

<sup>3</sup>Department of Electrical and Computer Engineering, The George Washington University  
Washington, D.C. 20052, USA

**Abstract**— A new approach for the rigorous analysis of the diffraction and interactions of electromagnetic waves (EMW) with magnetic nanostructures was developed using the decomposition approach by autonomous blocks (AB) with virtual Floquet channels (FABs) [1]. The drawbacks of minimal ABs [2] and multimode ABs [3] are eliminated in FAB, because in FAB virtual channels for TEM- and higher order modes (including evanescent modes) are taken into account. Exactly solvable models for EMW propagation and its interactions with magnetostatic oscillations in magnetic nanoparticles were developed to solve the 3D diffraction boundary problem based on the Maxwell's equations, complemented by the Landau-Lifshitz equation

A monochromatic plane EMW is incident on an array of ferrite spheres. A bias magnetic field is normal to the direction of propagating EMW. The modulus of scattering parameters of the multimode S matrix were calculated by the FAB method [1]. The results of computing of transmission coefficients  $|S_{12}|$ , depending on the normalized frequency are obtained for the separations of spheres. The minima in  $|S_{12}|$  correspond to eigenfrequencies of homogeneous and inhomogeneous low- or higher order modes of precession of magnetization in ferrite sphere [4]. The excitation of collective modes in magnetic nanoparticle system critically depends on the separation of spheres.

## ACKNOWLEDGMENT

The work of G. S. Makeeva and O. A. Golovanov was supported by The Russian Foundation For Basic Research, Grant 05-08-33503a.

## REFERENCES

1. Golovanov, O. A., *Radiotekh. Elektron*, Vol. 51, 1423, 2006.
2. Nikol'skii, V. V. and O. A. Golovanov, *Radiotekh. Elektron*, Vol. 24, 1070, 1979.
3. Nikol'skii, V. V. and T. I. Lavrova, *Radiotekh. Elektron*, Vol. 23, 241, 1978.
4. Gurevich, A. G. and G. A. Melko, *Magnetic Oscillations and Waves*, CRC Press, Boca Raton, 1996.

# Simulation of Multiple Scattering Scenes for Time Domain Maxwell's Equations by an Hybrid and Parallel Method

V. Mouysset<sup>1</sup>, P. Borderies<sup>2</sup>, X. Ferrières<sup>2</sup>, and P. A. Mazet<sup>1</sup>

<sup>1</sup> Information Modelling and Processing Department, ONERA, Toulouse, France

<sup>2</sup> Electromagnetism and Radar Department, ONERA, Toulouse, France

**Abstract**— A significant challenge in the numerical simulation of electromagnetic compatibility (EMC) is to accurately render for coupling between multiple scatterers and source. In [1] we proposed a new decomposition method in sub-domains to treat this problem in time domain.

Principle of the method, see Figure 1, is to create separated domains  $D^i$  and solve into each  $D^i$

$$\begin{cases} \varepsilon(x)\partial_t E^i + \sigma(x)E^i - \text{rot}H^i = E^{src} + \mathbf{n}^{\mathcal{H}} \times \left( \sum_{j \neq i} H^j \right), \\ \mu(x)\partial_t H^i + \text{rot}E^i = H^{src} - \mathbf{n}^{\mathcal{H}} \times \left( \sum_{j \neq i} E^j \right), \end{cases} \quad (1)$$

where  $(E^j, H^j)$ -fields provided by other  $D^j$ ,  $j \neq i$  are evaluated according to a specific integral formula [1]. Main interest of this method in regard of other existing ones is inherent of its construction: the error of approximation introduced when replacing the complete Green formula by the proposed integral formula, and error of sampling reconstruction above the Huygens face of each domain  $\mathcal{H}^i$  are explicitly given in  $O(\delta/d)$  where  $\delta$  is an adaptive local parameter and  $d$  is geometrically linked to the studied scene. Moreover, it gives a straightforward strategy of parallelization.

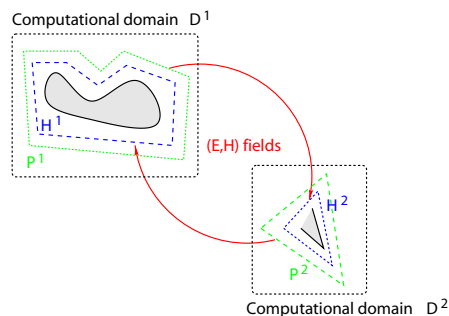


Figure 1: Principle of the multi-domain decomposition.

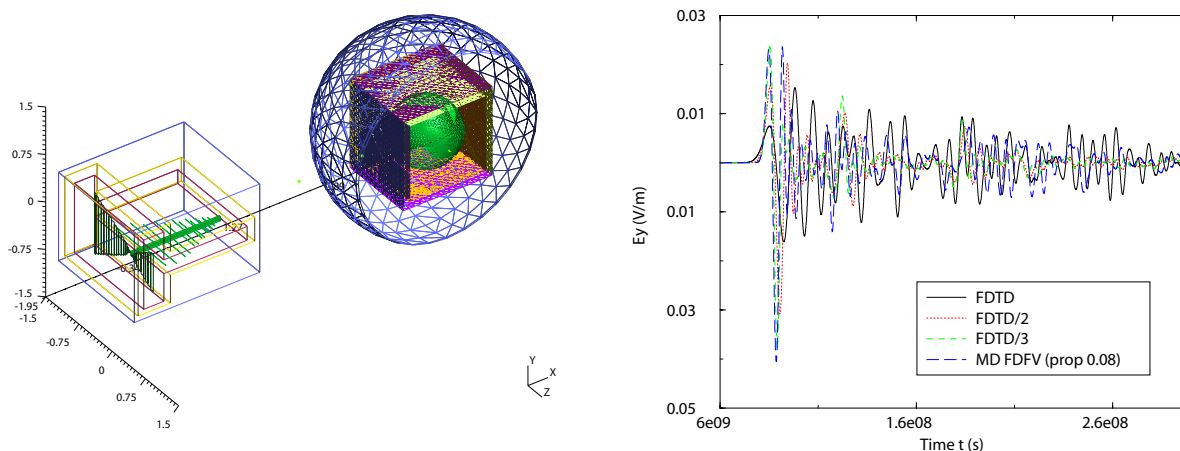


Figure 2: Example of multi-domain decomposition and comparisons between hybrid FDTD-FVTD and mono-domain FDTD results.

In this paper we want to show and augment the domain of interest of this method by applying it to EMC problems. Hence, we are going to study its behaviour according to the scene disposition and the accuracy on  $\delta/d$  we choose, in order to point out when it becomes interesting, in terms of costs (CPU time and memory storage) and accuracy, comparatively to one domain computations.

Then, we will use this method as a way to hybridize schemes, here finite difference (FDTD) and finite volumes (FVTD), see Figure 2, and discuss about its advantages/disadvantages.

At last, by a very intuitive *inter-domain* time step, we propose to free the numerical simulation from a global CFL condition and thus fasten the calculus.

#### REFERENCES

1. Mouysset, V., P. A. Mazet, and P. Borderies, "Efficient treatment of 3D time-domain electromagnetic scattering scenes by disjointing sub-domains and with consistent approximations," *Progress In Electromagnetics Research*, PIER 71, 41–57, 2007.

# Session 3P2a

## Shaping Optical Forces for Trapping and Binding – Applications

<b>Tailoring Particles for Optical Trapping and Micromanipulation: An Overview</b>	
<i>Timo A. Nieminen (The University of Queensland, Australia); T. Asavei (The University of Queensland, Australia); Y. Hu (The University of Queensland, Australia); M. Persson (The University of Queensland, Australia); R. Vogel (The University of Queensland, Australia); Vincent L. Y. Loke (The University of Queensland, Australia); S. J. Parkin (The University of Queensland, Australia); N. R. Heckenberg (The University of Queensland, Australia); Halina Rubinsztein-Dunlop (The University of Queensland, Australia); .....</i>	654
<b>Optical Trapping and Binding in Fresnel Diffraction</b>	
<i>Jean-Marc R. Fournier (Imaging and Applied Optics Institute, Switzerland); Pierre Jacquot (Nanophotonics and Metrology Laboratory, Switzerland); Fabrice Merenda (Imaging and Applied Optics Institute, Switzerland); Johann Rohner (Imaging and Applied Optics Institute, Switzerland); Rene Paul Salathe (Imaging and Applied Optics Institute, Switzerland); .....</i>	655
<b>Laser Tweezers Arrays, Micro-fluidics, and Bio-analytics: From Concept to Reality</b>	
<i>Rene Paul Salathe (Imaging and Applied Optics Institute, Switzerland); Fabrice Merenda (Ecole Polytechnique Federale de Lausanne, Switzerland); Johann Rohner (Ecole Polytechnique Federale de Lausanne, Switzerland); Jean-Marc R. Fournier (Ecole Polytechnique Federale de Lausanne, Switzerland); .....</i>	656
<b>Optical Angular Momentum Transfer on Open and Closed Line Patterns of Light</b>	
<i>A. Jesacher (Innsbruck Medical University, Austria); C. Maurer (Innsbruck Medical University, Austria); A. Schwaighofer (Innsbruck Medical University, Austria); S. Fürhapter (Innsbruck Medical University, Austria); S. Bernet (Innsbruck Medical University, Austria); Monika Ritsch-Marte (Innsbruck Medical University, Austria); .....</i>	657
<b>Confined Brownian Motion Studied by Optical Trapping Interferometry</b>	
<i>Sylvia Jeney (Ecole Polytechnique Fédérale de Lausanne (EPFL), Switzerland); Branimir Lukić (Ecole Polytechnique Fédérale de Lausanne (EPFL), Switzerland); Jonas Kraus (Ludwig-Maximilians-Universität München, Germany); Thomas Franosh (Ecole Polytechnique Fédérale de Lausanne (EPFL), Switzerland); László Forró (Ecole Polytechnique Fédérale de Lausanne (EPFL), Switzerland); .....</i>	658
<b>Circular Movement Control of Micro Spheres Using Weak Focused Laser Beams</b>	
<i>Naoki Kagawa (Fukuyama University, Japan); Shinsuke Hashimoto (Fukuyama University, Japan); Satoru Takahashi (Fukuyama University, Japan); .....</i>	659
<b>Optical Sculpting of Emulsion Droplets</b>	
<i>David Woods (Durham University, UK); Christopher D. Mellor (National Institute for Medical Research, UK); Colin D. Bain (Durham University, UK); Amanda Lewis (Rutherford Appleton Laboratory, UK); Andrew D. Ward (Rutherford Appleton Laboratory, UK); .....</i>	660
<b>Vortices and Persistent Currents: Rotating a Bose-Einstein Condensate Using Photons with Orbital Angular Momentum</b>	
<i>Kristian Helmerson (National Institute of Standards and Technology, USA); .....</i>	661

# Tailoring Particles for Optical Trapping and Micromanipulation: An Overview

T. A. Nieminen<sup>1</sup>, T. Asavei<sup>1</sup>, Y. Hu<sup>1,2</sup>, M. Persson<sup>1</sup>, R. Vogel<sup>1</sup>  
V. L. Y. Loke<sup>1</sup>, S. J. Parkin<sup>1</sup>, N. R. Heckenberg<sup>1</sup>, and H. Rubinsztein-Dunlop<sup>1</sup>

<sup>1</sup>The University of Queensland, Australia

<sup>2</sup>Rice University, USA

**Abstract**— Optical trapping and micromanipulation has developed from an interesting novelty to a powerful and widely used tool, with the capability to move or trap microscopic live biological specimens and measure forces on the order of piconewtons, typical of forces in microbiological systems. Despite this, the range of particles typically trapped or manipulated is quite small, and it is unusual to see applications involving objects other than biological specimens or homogeneous isotropic microspheres, typically polymer or silica.

However, particles can be modified or specially fabricated to expand the possible applications of optical tweezers. For example, while non-absorbing homogeneous isotropic spheres cannot be rotated, optically anisotropic spheres can, and can function as microscopic torque sensors, extending the usual translational micromanipulation and force measurement to rotational manipulation and torque sensing. The development of such particles has led to applications in microscale metrology and biophysics, along with potential deployment of optically-driven micromachines in lab-on-a-chip devices.

We present an overview of our work on the tailoring of microparticles for versatile optical trapping and micromanipulation. This includes approaches based on controlled chemistry—nano-assembly—and optical microfabrication. Beginning with the production of anisotropic vaterite microspheres, we review some of the applications, and difficulties encountered along the way. Some of these difficulties can be overcome by coating of the vaterite microspheres, which, in turn, suggests the use of anti-reflection coating to allow strong trapping of high refractive index particles. We also discuss the alternative strategy of producing arbitrarily shaped polymer microstructures through two-photon photopolymerization, which can be used to produce optically-driven microrotors or structurally anisotropic microspheres to replace vaterites for particular applications.

# Optical Trapping and Binding in Fresnel Diffraction

Jean-Marc Fournier<sup>1</sup>, Pierre Jacquot<sup>2</sup>, Fabrice Merenda<sup>1</sup>  
Johann Rohner<sup>1</sup>, and René-P. Salathé<sup>1</sup>

<sup>1</sup>Imaging and Applied Optics Institute, École Polytechnique Fédérale de Lausanne  
station 17, CH-1015 Lausanne, Switzerland

<sup>2</sup>Nanophotonics and Metrology Laboratory, École Polytechnique Fédérale de Lausanne  
station 17, CH-1015 Lausanne, Switzerland

**Abstract**— Optical traps are often generated in the far field [1], also trapping is efficiently performed in the evanescent field [2]. Meanwhile, the Fresnel diffraction regime offers remarkable possibilities for constructing traps, which have been explored by a few authors [3]. We revisit this regime to produce very high intensity gradients and to trap efficiently, in 3D, micron size dielectric objects. Atypical intensities landscapes are derived from various schemes taking advantage of optical interference. We explore different schemes leading to ensemble of massively parallel optical traps. Strong trapping has been established with many settings realizing multiple beam superposition, and is verified and tested in microfluidic environment.

Optical binding is known to produce self-assembly, then generating optical crystals for which the lattice characteristic depends on the optical interaction between the particles forming the assemblage [4–6]. This is studied experimentally in a two-dimensional crystal constructed with polystyrene spheres by combining gradient trapping and optical binding [5]. Observations and measurements performed in the reciprocal space give information on the crystal properties, in particular on the inter-particle spacing [7]. Gaps between spheres depending on their size has been measured for particles up to two microns in diameter. The manufacturing of large crystals of particles is limited in size and leads to formation of dislocations in the optical arrangement. This is currently under investigation.

## REFERENCES

1. Ashkin, A., “Acceleration and trapping of particles by radiation pressure,” *Physical Review Letters*, Vol. 24, No. 4, 156–159, 1970.
2. Kawata, S. and T. Sugiura, *Opt. Lett.*, Vol. 17, 772, 1992.
3. Jesacher, A., S. Furrer, S. Bernet, and M. Ritsch-Marte, “Diffractive optical tweezers in the Fresnel regime,” *Optics Express*, Vol. 12, 2243–2250, 2004.
4. Maystre, D. and P. Vincent, “Phenomenological study of binding in optically trapped photonic crystals,” *JOSA A*, Vol. 24, 2383–2393, 2007.
5. Burns, M. M., J. M. Fournier, and J. A. Golovchenko, “Optical matter — Crystallization and binding in intense optical-fields,” *Science*, Vol. 249, No. 4970, 749–754, 1990.
6. Mellor, C. D., M. A. Sharp, C. D. Bain, and A. D. Ward, “Probing interactions between colloidal particles with oscillating optical tweezers,” *Journal of Applied Physics*, Vol. 97, No. 10, 2005.
7. Rohner, J., “Light structuring for massively parallel optical trapping,” PhD dissertation, EPFL, Lausanne, 2007.

## Laser Tweezers Arrays, Micro-fluidics, and Bio-analytics: From Concept to Reality

Rene Paul Salathe, Fabrice Merenda, Johann Rohner, and Jean-Marc Fournier  
Ecole Polytechnique Federale de Lausanne, Station 17, CH-1015 Lausanne, Switzerland

**Abstract**— Combining laser tweezers, micro-fluidics and fluorescence spectroscopy offers unique possibilities for developing novel concepts for complex functional screening and compound production techniques. Progress in miniaturization of lasers, optics, and photo-detectors allows increasing the number of tweezers and decreasing at the same time the volume of the whole unit. Optic-, laser-, fluidic-, and detection-parameters have to be optimized for achieving best performance. We discuss some constraints and trade-offs for miniaturization in terms of optical layout, laser power, fluid speed, detection bandwidth, and S/N-ratio. We demonstrate two different approaches for realizing compact platforms with arrays of high N.A. laser tweezers allowing 3D trapping of free-floating cells and vesicles in micro-fluidics. The first one, based on refractive micro-lens arrays, can be used with standard fluorescence microscopes [1]. Here, up to 100 objects can be trapped simultaneously. The traps can hold objects at fluid flows exceeding 100 micrometers per seconds. Parallel fluorescence excitation and detection on the ensemble of trapped particles is shown. We also demonstrate the possibility of selectively releasing particles from the tweezers array after fluorescence detection.

The field of view of high-NA microscope objectives is limited. This restricts the number of trapped particles that can be monitored simultaneously. A second platform has been developed in order to overcome this limitation and to reduce the overall equipment costs. It is based on an array of high N.A. micro-mirrors that are integrated into the micro-fluidic chip [2]. This concept allows multiple trapping in a highly scalable approach. Micro-mirrors are potentially inexpensive and mass producible, e.g., using mold casting techniques. Every trap disposes of its own miniaturized focusing element, thus the total number of traps is not restricted as in schemes relying on microscope objectives. Trapping efficiencies comparable to those obtained with microscope objectives are achieved. The achromatic focusing property of the mirrors combined with broadband reflective coatings allows highly efficient trapping, fluorescence excitation, and — detection with the same element. Simultaneous fluorescence detection on the ensemble of trapped particles is also demonstrated. Such scalable miniaturized stand-alone devices, based on disposable micro-fluidic circuits have a huge application potential ranging from parallel single cell analytics/genomics/proteomics to parallel single molecule chemistries and analytics.

### REFERENCES

1. Merenda, F., et al., “Refractive multiple optical tweezers for parallel biochemical analysis in micro-fluidics,” *Complex Light and Optical Forces, Proc. SPIE*, Vol. 6483-08, 2007.
2. Merenda, F., et al., “Miniaturized high-NA focusing-mirror multiple optical tweezers,” *Opt. Express*, Vol. 15, No. 10, 6075–6086, 2007.



## Optical Angular Momentum Transfer on Open and Closed Line Patterns of Light

A. Jesacher, C. Maurer, A. Schwaighofer, S. Fürhapter, S. Bernet, and M. Ritsch-Marte  
Division for Biomedical Physics, Innsbruck Medical University, Austria

**Abstract**— Diffractive phase holograms at spatial light modulators (SLMs) can generate arbitrary lines of light, such as ellipses or triangles, in the focal plane of a microscope. We have previously shown that imaging an object with a spiral phase filter results in strong edge-enhancement. If the imaging is carried out with a 4f-telescope setup, where the first lens generates the Fourier transformation of the image and a spiral phase filter is introduced into this plane, the desired edge enhancement results in the object plane of the microscope.

Here we show that the convolution with a spiral phase filter of helicity  $\ell = 1$  also offers new ways of optical micromanipulation along these bright “flow lines”, since the helical charge of the spiral phase filter “imprints” a tangential phase gradient depending on the curvature of the object’s outline. Although the *total* amount of orbital angular momentum for a closed light pattern is given by the helical charge of the spiral phase filter, regions of different curvature along the light contours differ in orbital angular momentum. Thus particles trapped on the line, which are pushed along the light contour by transfer of angular momentum, experience a *variable* velocity that *depends on the local curvature* of the shape. In the case of a triangle, for instance, the particles speed up around the corners. For convex/concave shapes one may observe that particles locally move against the dominant sense of direction, until they are pushed out of this region by fast in-coming particles.

## Confined Brownian Motion Studied by Optical Trapping Interferometry

Sylvia Jeney<sup>1</sup>, Branimir Lukić<sup>1</sup>, Jonas Kraus<sup>2</sup>, Thomas Franosh<sup>1</sup>, and László Forró<sup>1</sup>

<sup>1</sup>Institut de Physique de la Matière Complexe, Ecole Polytechnique Fédérale de Lausanne (EPFL)  
CH-1015 Lausanne, Switzerland

<sup>2</sup>Arnold Sommerfeld Center for Theoretical Physics (ASC) and Center for NanoScience (CeNS)  
Department of Physics, Ludwig-Maximilians-Universität München  
Theresienstrasse 37, D-80333 München, Germany

**Abstract**— The dynamic behavior of a single colloidal particle in water confined by an optical trap and a plain surface is investigated at time scales where the inertia of the surrounding fluid plays a significant role. A weak optical trap with interferometric position detection allows monitoring a single micron-sized sphere with a spatial resolution better than 1 nm and a temporal resolution on the order of microseconds.

First, we quantify the influence of the confinement created by the harmonic potential of the optical trap on the particle's velocity autocorrelation, mean-square displacement and power spectral density. We find that they are in excellent agreement with the theory for a Brownian particle in a harmonic potential that accounts for hydrodynamic memory effects, which states that the transition from ballistic to diffusive motion is delayed to significantly longer times than predicted by the standard Langevin equation. This delay is a consequence of the inertia of the fluid, introducing a backflow on the particle's fluctuations. At longer times the motion of the particle is dominated by the trapping potential.

By identifying the time below which the particle doesn't "feel" the potential, we can exclude the existence of free diffusive motion as usually assumed in common optical trapping experiments.

Second, the particle is brought close to a hard surface and we observe how the subtle interplay of surface confinement and hydrodynamic backflow changes the decay of the particle's velocity autocorrelations from a slow  $t^{-3/2}$  to a much faster power-law  $t^{-5/2}$ .

These findings show that the temporal resolution of Optical Trapping Interferometry can be extended down to time scales where the nature of the fluid influences diffusion, bringing the long discussed idea of using a Brownian particle as a local reporter of the dynamics of complex biological fluids one step further.

# Circular Movement Control of Micro Spheres Using Weak Focused Laser Beams

Naoki Kagawa, Shinsuke Hashimoto, and Satoru Takahashi

Faculty of Engineering, Department of Electronic and Electrical Engineering  
Fukuyama University, 1 Gakuen-cho, Fukuyama, Hiroshima 729-0292, Japan

**Abstract**— The radiation pressure acts on the direction of the spread axis and the direction of the center of the cross section of a laser beam for a micro-sphere when a gradually focused laser beam is irradiated to a micro-sphere. These are called the radiation force and the gradient force, respectively. Therefore, when the laser beam is opposed, a micro-sphere can be levitated [1]. If one of the lasers is stopped, the micro-sphere will be moved supplemented in the cross section of the beam. Therefore, we tried to compose a polygonal route with two or more out of focused laser beams, and to move a micro-sphere along with the route.

Three lasers were led to the taper fiber respectively, and a triangular route consisted of the radiation beams from the fibers (Fig. 1). Each laser was blinked with the same cycle of 50% duty ratio but shifted 1/3 cycle phase each other. As a result, we had two alternate situations; one laser was blinking or two lasers were doing simultaneously. A micro-sphere was moved to the intersection along with the first beam at the period that one beam irradiated to the micro-sphere. Then, the micro-sphere moved toward the next intersection according to the second laser beam if the irradiation of the first laser beam was stopped. The micro-sphere can be moved circularly by repeating this operation in the route (Fig. 2).

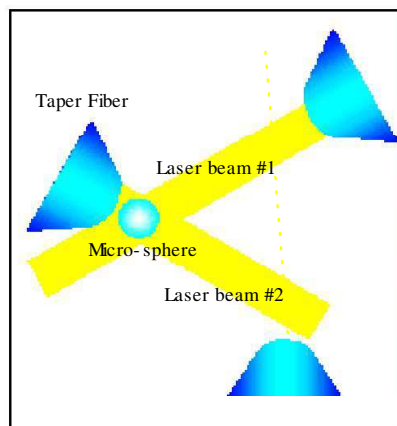


Figure 1: Schematic diagram of triangle route.

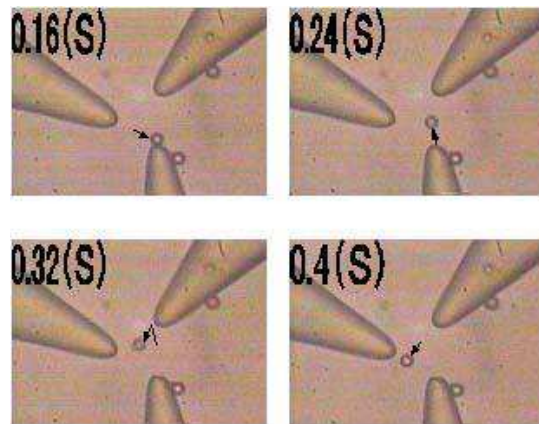


Figure 2: Circular moving micro-sphere on a triangle route.

## REFERENCES

1. Ashkin, A., "Acceleration and trapping of particles by radiation pressure," *Physical Review Letters*, Vol. 24, No. 4, 156–159, 1970.

## Optical Sculpting of Emulsion Droplets

David Woods<sup>3</sup>, Christopher D. Mellor<sup>2</sup>  
Colin D. Bain<sup>3</sup>, Amanda Lewis<sup>1</sup>, and Andrew D. Ward<sup>1</sup>

<sup>1</sup>Central Laser Facility, Rutherford Appleton Laboratory, UK

<sup>2</sup>National Institute for Medical Research, Mill Hill, London, UK

<sup>3</sup>Department of Chemistry, Durham University, UK

**Abstract**— Optical trapping and optical binding are both means of creating ordered arrangements from pre-existing particles. Optical forces can also be used to construct complex shapes by deforming objects. In most cases the optical forces are far too weak to deform a solid object appreciably while the surface tension of liquid droplets normally imposes a spherical shape. Close to microemulsion phase boundaries, however, the interfacial tension of oil drops in water falls to values comparable to the force constant of an optical trap. Optical fields can then be used to deform micron-sized oil drops. In a proof of principle experiment, we have shown (Figure 1) how two, three or four coplanar traps can create dumbbell, triangular or square oil drops. [1] Non-coplanar traps could easily be used to control the shape of a droplet in 3-dimensions.

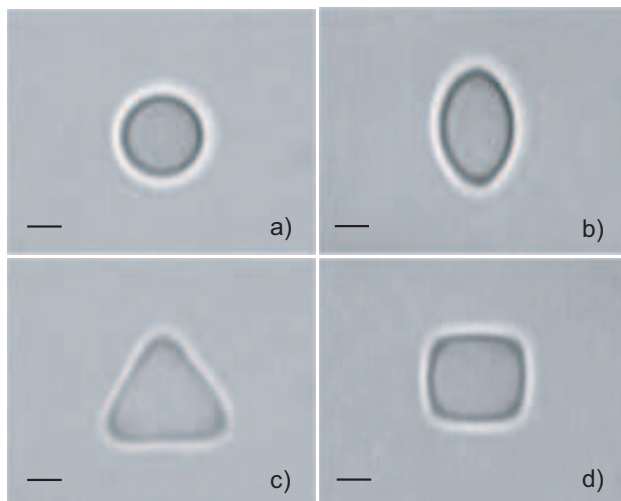


Figure 1: Deformation of an emulsion droplet in a heptane/AOT/brine mixture by 1, 2, 3 or 4 optical traps. The scale bar is 2  $\mu\text{m}$ . [1].

When an oil drop is divided in two by optical tweezers, the ligament or thread connecting the two drops thins to a diameter that is invisible in an optical microscope but remarkably the thread does not break. Scaling arguments suggest that the diameter of this thread is of the order of 100 nm or less. If one daughter droplet is released it recoils towards the remaining droplet with a piconewton force. Optical pressure can be used to drive flow between the drops through the invisible pipe. Networks can be constructed with 3-way junctions and closed loops of droplet can be connected by threads. The physics behind these nanofluidic systems will be discussed.

### REFERENCES

1. Ward, A. D., M. G. Berry, C. M. Mellor, and C. D. Bain, "Optical sculpture: Controlled deformation of emulsion droplets with ultralow interfacial tensions using optical tweezers," *Chem. Comm.*, 4515–4517, 2006.

# Vortices and Persistent Currents: Rotating a Bose-Einstein Condensate Using Photons with Orbital Angular Momentum

Kristian Helmerson<sup>1,2</sup>

<sup>1</sup>Physics Laboratory, National Institute of Standards and Technology  
Gaithersburg, Maryland 20899-8424, USA

<sup>2</sup>Joint Quantum Institute, University of Maryland/NIST  
College Park, Maryland, USA

**Abstract**— The interaction of photons with atoms inevitably involves the exchange of momentum. The transfer of spin angular momentum from a photon to an atom has been well understood for some time and can be used, very effectively, to change the internal state of an atom. Similarly, the past couple of decades have witnessed a tremendous growth in the use of light to control the center-of-mass motion of atoms. For example, the linear momentum of light can be utilized to laser cool and trap atoms. Light, in addition to carrying spin and linear momentum, can also carry orbital angular momentum. The orbital angular momentum of light, which is associated with its spatial mode, has been used to rotate macroscopic objects; however, the rotation of atoms due to the orbital angular momentum of photons has not been directly observed.

I will describe experiments in which we demonstrate [1] the coherent transfer of the orbital angular momentum of a photon to an atom in quantized units of  $\hbar$ . Using a 2-photon stimulated Raman process with Laguerre-Gaussian beams, which carry orbital angular momentum, we generate an atomic vortex state in a Bose-Einstein condensate (BEC) of sodium atoms. We show that the process is coherent by creating superpositions of different vortex states, where the relative phase between the states is determined by the relative phases of the optical fields. Furthermore, we create vortices of charge 2 by transferring to each atom the orbital angular momentum of two photons, each with orbital angular momentum  $\hbar$ .

We subsequently use this technique to generate rotational flow of a BEC confined in a toroidal shaped trap. The toroidal trap is formed by using a blue detuned laser beam to exclude atoms from the central region of an elliptically shaped magnetic trap. We measure that the flow of atoms persists for up to 10 seconds, which we interpret as the first direct evidence of a persistent current in a superfluid Bose gas. Stable flow was only possible in the multiply-connected geometry of the toroidal trap, and was observed for a BEC fraction as small as 15%. We also observed flow with higher angular momentum (winding number), and its splitting into singly-charged vortices when the trap topology was changed from multiply- to simply-connected.

## REFERENCES

1. Andersen, M. F., et al., *Phys. Rev. Lett.*, Vol. 97, 170406, 2006.



# Session 3P3a

## Wave Propagation and Superresolution in Active and Passive Metamaterials 1

<p>Electromagnetic Eigenstates of Finite Cylinders and Cylinder-clusters: Application to Macroscopic Response of Meta-materials</p> <p><i>David J. Bergman (Tel-Aviv University, Israel);</i> .....</p> <p>Negative Refraction as a Source of Some Pedagogical Problems</p> <p><i>V. G. Veselago (A.M. Prokhorov Institute of General Physics, Russian Academy of Sciences, Russian Federation);</i> .....</p> <p>Wide-angle Absorption by the Use of a Metamaterial Plate</p> <p><i>Andrey N. Lagarkov (Institute of Theoretical and Applied Electrodynamics, Russia); Vladimir N. Kisel (Institute for Theoretical and Applied Electromagnetics, Russia); V. N. Semenenko (Institute for Theoretical and Applied Electromagnetics, Russia);</i> .....</p> <p>Metamaterial-based Microwave Absorber</p> <p><i>Andrey N. Lagarkov (Institute of Theoretical and Applied Electrodynamics, Russia); Vladimir N. Kisel (Institute for Theoretical and Applied Electromagnetics, Russia); V. N. Semenenko (Institute for Theoretical and Applied Electromagnetics, Russia);</i> .....</p> <p>Covariant Perspectives on Negative Refraction</p> <p><i>Martin W. McCall (Imperial College of Science, Technology and Medicine, UK);</i> .....</p> <p>Magnetic Metamaterials and Left-handed Materials towards Optical Frequencies</p> <p><i>Maria Kafesaki (Institute of Electronic Structure and Laser (IESL), Greece); Th. Koschny (Institute of Electronic Structure and Laser (IESL), Greece); E. N. Economou (Institute of Electronic Structure and Laser (IESL), Greece); C. M. Soukoulis (Institute of Electronic Structure and Laser (IESL), Greece);</i> .....</p> <p>Superconducting Metamaterials</p> <p><i>Steven M. Anlage (University of Maryland, USA); Michael Ricci (University of Maryland, USA); Nathan Orloff (University of Maryland, USA); Hua Xu (University of Maryland, USA); Laura Adams (University of Maryland, USA);</i> .....</p>	<p>664</p> <p>665</p> <p>668</p> <p>669</p> <p>670</p> <p>671</p> <p>672</p>
---	--

# Electromagnetic Eigenstates of Finite Cylinders and Cylinder-clusters: Application to Macroscopic Response of Meta-materials

David J. Bergman

Raymond and Beverly Sackler School of Physics and Astronomy  
Sackler Faculty of Exact Sciences, Tel Aviv University, IL-69978 Tel Aviv, Israel

**Abstract**— Closed form, approximate expressions are found for the electromagnetic eigenstates of an isolated, finite-length, circular cylinder, of radius  $a$  and length  $L$ , for the case where  $ka \ll 1$  but  $kL$  can be greater than 1 ( $k$  is the wavenumber in the surrounding medium). These eigenstates are standing waves of surface plasmons which propagate along the cylinder axis and are reflected, back and forth, between the cylinder ends. When considering a cluster of such cylinders, the combined set of these non-quasistatic eigenstates, arising from each of the cylinders *in isolation*, form a complete set of vector fields which can be used as a starting point for evaluating the electromagnetic eigenstates of the entire cluster or even of a periodic array of such cylinders. In addition to the isolated-cylinder eigenstates, the interactions between pairs of states on different, parallel cylinders can also be expressed using closed form approximate expressions. Consequently, the integral equation for the eigenstates of a finite cluster or periodic array of such inclusions can be recast as a standard eigenvalue problem of a selfadjoint infinite matrix, which can be solved numerically after suitable truncation. A similar approach was used in the past, successfully, to find the quasistatic eigenstates of an array of spheres [1], and also the non-quasistatic eigenstates of a finite cluster of spheres [2].

Our attention to finite-length circular-cylinders as the basic inclusions in such a meta-material was motivated by the earlier works of Shvets and Urzhumov [3] and of Sarychev, Shvets, and Shalaev [4], who found that resonances of finite-cylinder inclusions had interesting properties vis-a-vis macroscopic electric and magnetic response of a composite medium. Our subsequent work, reported here, is an attempt to develop the properties of such a medium in a systematic fashion.

The isolated-cylinder eigenstates turn out to be very interesting when  $ka \ll 1$  but  $kL \gg 1$ : In that case, the system is not in the strict quasistatic limit, but still exhibits some of the quasistatic forms of behavior. Thus, each eigenstate has an electric multipole moment as well as a magnetic multipole moment. Because of this, it is easy to find eigenstates of a cylinder cluster that have both an electric dipole moment and a magnetic dipole moment, and can thus contribute to the macroscopic quasistatic response to an electric field as well as to a magnetic field. When the system is near such a resonance, the macroscopic response can be tuned significantly by making small changes in the system parameters. This should make such a composite medium interesting in the context of meta-materials, including left-handed materials where the macroscopic electric permittivity  $\varepsilon_e$  and the macroscopic magnetic permeability  $\mu_e$  need to be essentially real and negative: If the composite medium is near an eigenstate which belongs to a discrete portion of the eigenvalue spectrum, then those macroscopic moduli can change their values significantly, in magnitude as well as in sign, as a result of very small changes in the system parameters. Such an approach was used in the past to discuss the macroscopic electric response of a periodic composite medium in the quasistatic limit [5].

## REFERENCES

1. Bergman, D. J., "The dielectric constant of a simple-cubic array of identical spheres," *J. Phys. C*, Vol. 12, 4947–4960, 1979.
2. Bergman, D. J. and D. Stroud, "Theory of resonances in the electromagnetic scattering by macroscopic bodies," *Phys. Rev. B*, Vol. 22, 3527–3539, 1980.
3. Shvets, G. and Y. A. Urzhumov, "Engineering the electromagnetic properties of periodic nanostructures using electrical resonances," *Phys. Rev. Lett.*, Vol. 93, 243902, 2004.
4. Sarychev, A. K., G. Shvets, and V. M. Shalaev, "Magnetic plasmon resonance," *Phys. Rev. E*, Vol. 73, 036609, 2006.
5. Bergman, D. J. and K. J. Dunn, "Bulk effective dielectric constant of a composite with a periodic microgeometry," *Phys. Rev. B*, Vol. 45, 13262–13271, 1992.



## Negative Refraction as a Source of Some Pedagogical Problems

V. G. Veselago

Moscow Institute of Physics and Technology

A. M. Prokhorov Institute of General Physics RAS, Russian Federation

**Abstract**— Introduction to broad scientific circulation the words “metamaterials”, “negative refraction”, “negative index of refraction”, “lefthanded materials” and other terms derived by afore-cited, has brought some unexpected consequences for strategy of teaching of optics, electrodynamics and related disciplines. This fact is bound first of all with fact, that before recent time a index of refraction for isotropic materials always was taken as positive value, equal

$$n = \sqrt{\varepsilon\mu} \quad (1)$$

In this relation electric permeability  $\varepsilon$  and magnetic permeability  $\mu$  also considered as positive values. The recognition of fact, that  $n$ , and  $\varepsilon$  with  $\mu$ , can be, in principle, simultaneously negative values, generates very simple question — in what measure remain equitable many formulas, determinations and correlations, in which enter these values if they will be negative. So, obviously that well-known formula for Snell law

$$\frac{\sin \varphi}{\sin \phi} = n \quad (2)$$

will be valid for negative values of  $n$ , but, of course, it is necessary to define correctly negative angles, as it is shown on Fig. 1.

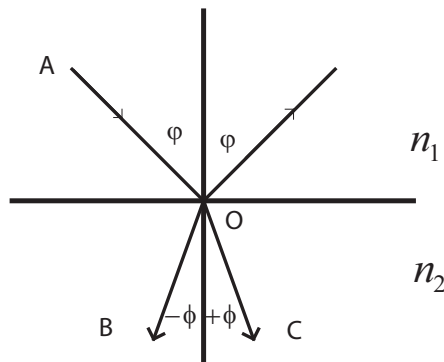


Figure 1: Refraction of beam of light on interface between two isotropic media. In every case  $\sin \varphi / \sin \phi = n_1/n_2 = n$ , but if  $n$  is positive, the beam path is **AOC**, but for negative  $n$  the path is **AOB**.

In the same way, as for Snell law, the equitable well-known formulas for Doppler and Cherenkov effects will remain when we change  $+n \rightarrow -n$ .

However situation sharply changes if consider, for example, the commonly used Fresnel's formulas for material with negative refraction. So, following most of textbooks, reflection coefficient for wave with perpendicular polarization is

$$R_{\perp} = \frac{n_1 \cos \varphi - n_2 \cos \phi}{n_1 \cos \varphi + n_2 \cos \phi} \quad (3)$$

It is clear, that substituting negative  $n_1$  and  $n_2$  in this formula can give undoubtedly wrong value for  $R_{\perp}$ . Really correct formula for  $R_{\perp}$  has the form

$$R_{\perp} = \frac{z_2 \cos \varphi - z_1 \cos \phi}{z_2 \cos \varphi + z_1 \cos \phi} \quad (4)$$

Here values  $z_1$  and  $z_2$  and are so-called wave impedances of two media, and are, accordingly,

$$z_{1,2} = \sqrt{\mu_{1,2}/\varepsilon_{1,2}} \quad (5)$$

Not difficult to see that formula (4) is equivalent with formula (3) in the case when

$$\mu_1 = \mu_2 = 1 \quad (6)$$

and, hereunder,

$$z = \sqrt{1/\varepsilon} = 1/n \quad (7)$$

The Equation (6) is a condition of so-called “nonmagnetic approach”, which implies that we work with nonmagnetic materials, which magnetic permeability is identically unit, and for which correlation (7) is due to (5). Such approach undoubtedly is ineffective for metamaterials in general, and, in particular, to metamaterials with negative refraction, which magnetic permeability can be not only different from unity, but even negative.

Acceptance the identity  $\mu = 1$  is equivalent to acceptance of equality of vectors of magnetic field  $H$  and magnetic induction  $B$

$$B = H \quad (8)$$

and so except term “nonmagnetic approach” such approach can be named as “three-vector approach”. Exactly such approach presents in most textbooks and scientific literature, like, for example, in the book under Landau and Livshitz. As a rule, in such literature presents a phrase like “since magnetic permeability of all known material on enough high frequency is unit, that we shall suppose that vectors  $H$  and  $B$  of these materials are equal”. Naturally that such approach does not leave any place for introduction of wave resistance  $z$ . Hereunder this approach brings rough physical mistakes, for example, very famous statement that condition of absence reflections of wave on the interface between two media is

$$n_1 = n_2 \quad (9)$$

Really this condition must be recorded as equality of two impedances

$$z_1 = z_2 \quad (10)$$

List of some most widely-used formulas written in nonmagnetic approach and in correct form is placed in following table.

Table 1: Some formulas of electrodynamics, written in nonmagnetic and correct forms.

Physical law	Equation for nonmagnetic approach	Correct equation
Snellius, Doppler, Cherenkov $n = \sqrt{\varepsilon} \rightarrow n = \sqrt{\varepsilon\mu}$ if $\varepsilon, \mu < 0$ , than $n < 0$	$\sin \varphi / \sin \psi = n_{21} = \sqrt{\varepsilon_2/\varepsilon_1}$	$\sin \varphi / \sin \psi = n_{21} = \sqrt{\varepsilon_2\mu_2/\varepsilon_1\mu_1}$
Fresnel $n = \sqrt{\varepsilon} \rightarrow 1/z = \sqrt{\varepsilon/\mu}$	$r_{\perp} = \frac{n_1 \cos \varphi - n_2 \cos \psi}{n_1 \cos \varphi + n_2 \cos \psi}$	$r_{\perp} = \frac{z_2 \cos \varphi - z_1 \cos \psi}{z_2 \cos \varphi + z_1 \cos \psi}$
Reflection coefficient for normal fall of light on the border between two media	$r = (n_1 - n_2)/(n_1 + n_2)$	$r = (z_2 - z_1)(z_2 + z_1)$
Condition for full matching	$n_1 = n_2$	$z_1 = z_2$
Brewster angle	$tg \varphi = n$	$tg \varphi = \sqrt{\frac{\varepsilon_2 \varepsilon_2 \mu_1 - \varepsilon_1 \mu_2}{\varepsilon_1 \varepsilon_2 \mu_2 - \varepsilon_1 \mu_1}}$

The motivation of nonmagnetic approach usually come from the fact, that in optical domain magnetic permeability is an unit. This really so for materials, which magnetic characteristics are defined by small particles with atomic sizes. These materials often have a name of so-called “natural” materials, for example like crystals and liquids. However situation greatly differs for the case of “artificial” materials, to which usually refer metamaterials. The magnetic characteristics of these materials are defined by the currents on conducting, metallic elements of these materials. Often this fact is a reason for considering of metamaterials as the media without definite two permeabilities  $\varepsilon$  and  $\mu$ . Indeed difference between so-called natural material and metamaterials is quantitative, rather than principle. Really that one or another material could be described by means of electric or magnetic permeability, necessary that wavelength of radiation will be much more than typical size of elements, forming material and distances between these elements. So if

consider that lattice constant  $\delta$  of majority of natural materials is close to value  $5 \cdot 10^{-5}$  micron, but in optical domain a wavelength  $\lambda$  is close to 0.5 micron, that quotient  $\lambda/\delta$  for these values turns out to be close to  $10^4$ . In first experiments on observation of passing of waves of microwave range through metamaterials this quotient there was about 10. Approximately such value has coefficient  $\lambda/\delta$  in experiments with metamaterials in optical range. Naturally that this value  $\lambda/\delta$  noticeably less than quotient for “natural” material in optical range, but however quotient  $\lambda/\delta \approx 10$  wholly enough for use approach, based on electric and magnetic permeability. Exactly so contraposition “natural” and “artificial” material is deprived the physical sense.

Thereby we see that appearance of metamaterials requires contributing the essential changes to strategy of teaching of electrodynamics and physics. The corresponding courses must begin with consequent introduction of four vectors  $E, D, H, B$ , and obligatory introduction the values of wave impedance  $z = \sqrt{\mu/\varepsilon}$  of media, and only afterwards possible come to three-vector approach if for one or another media magnetic permeability turns out to be identically equal unit, and, accordingly, turns out to be the equitable correlation (8). Herewith in any case it is impossible abandon to notions of wave impedance. It is necessary take into account that even  $\mu \equiv 1$  and, consequently, equation

$$z = \sqrt{1/\varepsilon} = 1/n \quad (11)$$

is valid, so values  $z$  and  $n$  becomes interdependent, their physical sense remains absolutely different. It is necessary to remember that wave impedance for vacuum, equal  $z_0 = 377 \text{ om}$ , is a world constant, exactly in the same way as speed of light in vacuum  $c = 3 \cdot 10^{10} \text{ cm/sec}$ . So electromagnetic characteristics of material wholly possible to describe not on language “ $\varepsilon$  and  $\mu$ ” but also on language “ $n$  and  $z$ ”, using correlations

$$\varepsilon = n/z \quad (12)$$

and

$$\mu = nz \quad (13)$$

However under such approach easy to make a mistake, considering that under negative  $\varepsilon$  and  $\mu$  value  $n$  is positive, but  $z$  — negative. Really value  $z$  always must be taken positive, outside of dependencies from sign  $\varepsilon$  and  $\mu$ . This follows from that fact that value  $z$  defines the attitude of amplitudes of vectors  $H$  and  $E$  in wave, which does not depend on signs of  $\varepsilon$  and  $\mu$ . In this easy make sure, having considered boundary conditions for perpendicular incidence of wave on interface between two media, if one of them is righthanded, but another — lefthanded. Under such turning the fields  $H$  and  $E$  are not changed, and, consequently is not changed value  $z$ , equal

$$z = H/E \quad (14)$$

It is possible also another approach to this problem.

Let us write value  $n$  for the case of negative  $\varepsilon$  and  $\mu$

$$n = \sqrt{\varepsilon\mu} = \sqrt{\varepsilon}\sqrt{\mu} = i\sqrt{|\varepsilon|}i\sqrt{|\mu|} = -\sqrt{|\varepsilon|}\sqrt{|\mu|} < 0 \quad (15)$$

In this case we get undoubtedly negative value of  $n$

Similar calculation gives for  $z$  under negative values of  $\varepsilon$  and  $\mu$  an opposite, undoubtedly positive result

$$z = \frac{\sqrt{\mu}}{\sqrt{\varepsilon}} = \frac{\sqrt{-|\mu|}}{\sqrt{-|\varepsilon|}} = \frac{i\sqrt{|\mu|}}{i\sqrt{|\varepsilon|}} = \frac{\sqrt{|\mu|}}{\sqrt{|\varepsilon|}} > 0 \quad (16)$$

So, it is clear, that wave impedance  $z$  is positive, independently on signs of  $n$ ,  $\varepsilon$  and  $\mu$ .

It is very important, that some formulas for media with arbitrary values of  $\varepsilon$  and  $\mu$  are changed very strong, like, for example formula for Brewster angle (see last row in the table).

All these considerations necessary take into account during process of studying optics and electrodynamics.

This work is supported by the Russian Foundation of Basic Research, grant # 07-02-00233.

## Wide-angle Absorption by the Use of a Metamaterial Plate

A. N. Lagarkov, V. N. Kisel, and V. N. Semenenko

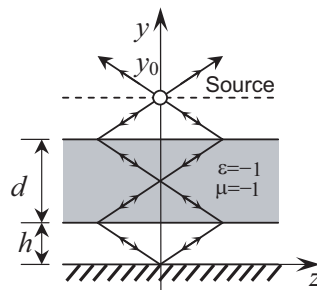
Institute for Theoretical and Applied Electromagnetics, Izhorskaya 13, Moscow 125412, Russia

**Abstract**— Interest to the field propagation along the imperfect surface has about a century-old history, the beginning of which traces back to the Sommerfeld's solution of the classical problem for the dipole radiating above the plane with finite conductivity. Later, as the radio broadcasting evolved, a lot of publications appeared which dealt with electromagnetic field propagation in the presence of an absorbing half-space with the aim to *minimize* the signal losses. Now certain practical needs set questions about how to choose the surface properties of the half-space to ensure absorbing the *maximum* portion of energy radiated by a point source (say, filamentary current), how much the amount of the absorbed energy is and how to create such a surface.

We shall demonstrate that under some circumstances a monochromatic filamentary source located above the plane surface coated by metamaterial does not illuminate the upper half-space at all. It means that one can create such a passive system which secures *total* cancellation of the source field in the upper half-space and, correspondingly, transfers the whole of the emitted energy into the lower half-space.

An example of such a system is given below. Let a filamentary source with a single  $x$ -directed component of the electrical current be placed in the point  $y_0$  over the conducting halfplane  $y = 0$ . Let a focusing flat plane (Veselago's lens) with a thickness of  $d = y_0/2$  made of the metamaterial with  $\varepsilon = -1$ ,  $\mu = -1$  be inserted between the source and the metal plane at the altitude  $h = y_0/4$  (see figure). Then the focusing occurs right at the surface of the conducting plane. Once the total phase advance along ray paths is calculated accounting for the negative phase velocity of the wave traveling through the plane and the phase reversal of the field due to the reflection from the conducting plane, one can discover that the reflected and emitted rays are anti-phased in the half-space of  $y > y_0$ . It means the incidence and secondary fields mutually cancel each other. So in an ideal case, when electromagnetic losses in the plate are infinitesimally small, the total field in the upper half-space tends to zero.

Our experimental investigations and rigorous solution of the corresponding boundary problem confirm this conclusion. Moreover, calculations show that in the case of non-perfect but easy to manufacture metamaterial plate with a rather high losses, say,  $\varepsilon = \mu = -1 - i0.1$  the major portion of energy, as much as 99.4% is transferred into the lower half-space and dissipates there. Besides of the discussed phenomena new designs of the electromagnetic field absorbers and resonators are suggested which may be engineered with the use of metamaterials. Experimental results are discussed with regards to the presented phenomena and suggested applications.



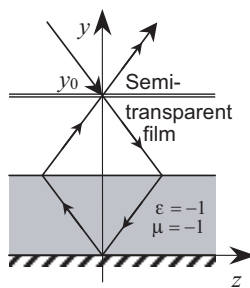
## Metamaterial-based Microwave Absorber

A. N. Lagarkov, V. N. Kisel, and V. N. Semenenko

Institute for Theoretical and Applied Electromagnetics

Izhorskaya 13, Moscow 125412, Russia

**Abstract**— Recently it was shown [1] that under some circumstances a monochromatic filamentary source (say, electrical current) located above and parallel to the plane surface does not illuminate the upper half-space at all. To secure that a flat slab made of the metamaterial with  $\varepsilon = -1$ ,  $\mu = -1$  (Veselago's lens) should be inserted between the source and the metal plane so as to provide for a ray focusing right on the conducting surface. Once the total phase advance along ray paths is calculated accounting for the negative phase velocity of the wave traveling through the plane and the phase reversal of the field due to the reflection from the conducting plane, one can discover that the reflected and emitted rays are anti-phased in the half-space above the current. It means that such a passive system secures total cancellation of the source field in the upper half-space and, correspondingly, transfers the whole of the emitted energy into the lower half-space.



Originating from the discussed principle, we demonstrate here that metamaterials may be efficiently used to create novel absorbers of the electromagnetic energy of a plane wave as well. Their special properties may be achieved, particularly, due to arranging a wave path so as to cross the metamaterial structure with the result of the phase advance compensation. An example of a radar absorber design usable under the incidence of perpendicularly polarized (TM) plane wave is shown in figure. Provided the electromagnetic response of the semi-transparent film, particularly, its transmission and reflection coefficients were properly chosen, the wave reflected from the film cancels the wave penetrated into and returned back from the region  $y < y_0$ . The phenomenon occurs because this latter wave got a negative phase correction when propagated in the metamaterial plate and additional phase reversal because of the reflection from the conducting plane. It is interesting that total phase advance of that wave is equal to  $\pi$  independently on the incidence angle. Therefore, it is possible to achieve a very broad angular range in which such an absorber should operate efficiently, in contrast to classical designs, like Salisbury screen. In fact, only deviations of semi-transparent film properties impose certain limits to the angular performance. Finally, as there are no fundamental physical restrictions on the thickness of the described absorber, it can be made electrically thin (at least, in principle), as well as earlier suggested system of complementary metamaterials [2]. Both calculated and experimental results are discussed with regards to the phenomena and suggested applications.

### REFERENCES

1. Lagarkov, A. N. and V. N. Kisel, "Electromagnetic energy absorption within extensive impedance structures, Electromagnetic materials," *Proc. of the Symposium P, International Conference on Materials for Advanced Technologies, SUNTEC, Singapore, 2007 (ICMAT 2007)*, 3–10, Edited by Lim Hock, Serguei Matitsine, Gan Yeow Beng and Kong Ling Bing, World Scientific, Singapore, 2007.
2. Alu, A., F. Bilotti, N. Engheta, and L. Vegni, "A thin absorbing screen using metamaterial complementary pairs," *Proc. of Joint 9th International Conference on Electromagnetics in Advanced Applications (ICEAA 2005) + 11th European Electromagnetic Structures Conference (EESC 2005)*, ed. Roberto D. Graglia, 229–232, Politecnico di Torino, Torino, Italy, Sept. 12–16, 2005.

## Covariant Perspectives on Negative Refraction

Martin W. McCall

Department of Physics, The Blackett Laboratory  
Imperial College of Science, Technology and Medicine  
Prince Consort Road, London SW7 2AZ, UK

**Abstract**— What is negative refraction? Its key characteristic, that a component of the electromagnetic power flow  $\mathbf{P}$ , opposes the wave vector  $\mathbf{k}$ , is captured through the definition

$$\mathbf{P} \cdot \mathbf{k} < 0, \quad (1)$$

which has inspired the name “Negative Phase Velocity” (NPV) propagation to be used [1]. However, in certain contexts, the condition (1) is ambiguous. In seeking a covariant description of negative refraction, for example, an NPV condition must be devised that is applicable in arbitrary coordinate systems (possibly for frames in relative motion). The condition (1) is not robust to such coordinate changes. In a covariant description, the power flow is expressed as a component of the stress-energy tensor,  $T_{\mu\nu}$ . These issues first surfaced when it was claimed in several publications (e.g., [2]) that gravity can induce negative refraction in the cosmos. Although this theory has now been refuted [3], it does raise some interesting questions concerning the appropriate covariant description of negative refraction *in media*. The definition that extends that given for vacuum [3], and arises naturally from (1), is that the real constant  $C$  is negative in the expression

$$-U^\mu T_{\mu j} = CK_j, \quad (2)$$

where  $U^\mu$  is the 4-velocity of a given observer and  $K_\mu$  is the 4-wavevector. However, in most presentations (e.g., [4]), the form for  $T_{\mu\nu}$  in media is not symmetric, which leads to further ambiguity. In this presentation we will attempt to resolve this. A consistent covariant framework is also required to address the question of whether NPV propagation can be induced by Lorentz transformation, as has been claimed previously [5]. Finally, coordinate frame changes are fundamental to the theory of electromagnetic cloaking [7]. The tools we will present are the best tool kit for discussing how cloaking performance will inevitably deteriorate as the cloak moves relative to the source illumination, thus destroying the delicate resonance conditions fundamental to static negative refraction.

Our principal findings will be presented.

### REFERENCES

1. McCall, M. W., A. Lakhtakia, and W. S. Weiglhofer, “The negative index of refraction demystified,” *Europ. J. Phys.*, Vol. 23, 353, 2002.
2. Mackay, T. G., A. Lakhtakia, and S. Setiawan, “Electromagnetic negative-phase-velocity propagation in the ergosphere of a rotating black hole,” *New Journal of Phys.*, Vol. 7, 171, 2005.
3. McCall, M. W., “Classical gravity does not refract negatively,” *Phys. Rev. Lett.*, Vol. 98, 091102, 2007.
4. Post, E. J., *Formal Structure of Electromagnetics*, Dover, 1997.
5. Mackay, T. G. and A. Lakhtakia, “Negative phase velocity in a uniformly moving, homogeneous, isotropic, dielectric-magnetic medium,” *J. Phys. A: Math. Gen.*, Vol. 37, 5697–5711, 2004.
6. Leonhardt, U. and T. G. Philbin, “General relativity in electrical engineering,” *New J. Phys.*, Vol. 8, 247, 2006.
7. Schurig, D., J. J. Mock, B. J. Justice, S. A. Cummer, J. B. Pendry, A. F. Starr, and D. R. Smith, “Metamaterial electromagnetic cloak at microwave frequencies,” *Science*, Vol. 314, 977–980, 2006.

# Magnetic Metamaterials and Left-handed Materials towards Optical Frequencies

M. Kafesaki<sup>1,2</sup>, Th. Koschny<sup>1,2,3</sup>, E. N. Economou<sup>1,2</sup>, and C. M. Soukoulis<sup>1,2,3</sup>

<sup>1</sup>Foundation for Research and Technology Hellas (FORTH)  
Institute of Electronic Structure and Laser (IESL), Heraklion, Crete, Greece

<sup>2</sup>University of Crete, Greece

<sup>3</sup>Ames Laboratory, and Department of Physics and Astronomy  
Iowa State University, Ames, Iowa, USA

**Abstract**— The novel and unique properties and capabilities of artificial magnetic metamaterials and of left-handed materials made them a subject of intense attention in the last seven years. A large part of the existing efforts in the study of those materials have been devoted to the extension of their operation frequency from the microwaves regime (where left-handed behavior was initially demonstrated) to the optical regime, where telecommunications and imaging applications can undergo revolutionary changes. Here we describe the efforts of our team to design and realize optical magnetic metamaterials and left-handed materials by scaling down well established microwave designs, like split-ring resonators (SRRs) and wires, or wire-pair-based designs. Particular attention is given on the understanding of the behavior of the effective permeability, the resonance frequency and the losses in those designs as they are scaled down from mm to nm scale.

## Superconducting Metamaterials

Steven M. Anlage, Michael Ricci, Nathan Orloff, Hua Xu, and Laura Adams

Physics Department, Center for Nanophysics and Advanced Materials  
University of Maryland, College Park, MD 20742-4111, USA

**Abstract**— The ability to create an artificial material with unique electromagnetic properties has led to much research on metamaterials, especially the class of metamaterials with a simultaneously negative permittivity and permeability, resulting in a negative index of refraction (NIR). These materials offer the promise of super-resolution imaging due to exponential amplification of evanescent waves. Metamaterials hold great promise for disruptive technological applications in the electromagnetic spectrum between RF and the visible. However before these applications emerge, some key enabling properties must be demonstrated. These properties include the ability to make low loss metamaterials, tunability and ‘texturing’ of metamaterials, and scaling metamaterial ‘atoms’ down to dimensions much smaller than the wavelength of interest. Our approach to achieving all of these enabling properties is to employ superconducting metamaterials [1]. To address the loss issue we have created the first left-handed materials made from superconducting (SC) Nb and low-loss dielectrics, and measured their properties in an all-Nb waveguide at low temperatures. We find that the high-Q nature of superconductors requires a different approach to engineering metamaterial devices. For instance, multiple split-ring resonator (SRR) arrays common in normal metal free space experiments are impractical in SC metamaterials, due to the high-Q and strong interactions between the resonators. However, unlike normal-metal SRRs, the properties of a single SC SRR are clearly observable, producing a negative permeability feature in transmission with a  $Q \sim 45000$ . Placing this SRR into an array of SC Nb wires produces an NIR transmission feature with a  $Q \sim 45000$  [2]. The features are tunable with temperature, due to the variable kinetic inductance of the SRRs, and with applied dc and rf magnetic fields. The magnetic tuning mechanisms have been investigated through laser scanning microscopy (imaging the superconducting rf current flow) and magneto-optic microscopy (imaging the penetration of magnetic flux into the SRR) [3]. The high-Q, tunability, and miniaturization of these Nb metamaterials outperform normal-metal counterparts in tight-bandwidth applications, such as narrow-band waveguide notch and passband filters. We also discuss efforts to miniaturize the superconducting metamaterial ‘atoms’.

### ACKNOWLEDGMENT

We thank Alexander Zhuravel, Alexey Ustinov and Ruslan Prozorov for assistance with this work. This work was supported by the NSF through Grant No. NSF/ECS-0322844.

### REFERENCES

1. Ricci, M., N. Orloff, and S. M. Anlage, “Superconducting metamaterials,” *Appl. Phys. Lett.*, Vol. 87, 034102, 2005.
2. Ricci, M. and S. M. Anlage, “Single superconducting split-ring resonator electrodynamics,” *Appl. Phys. Lett.*, Vol. 88, 264102, 2006.
3. Ricci, M., H. Xu, S. M. Anlage, R. Prozorov, A. P. Zhuravel, and A. Ustinov, “Tunability of superconducting metamaterials,” *IEEE Trans. Appl. Supercond.*, Vol. 17, 918, 2007.



# Session 3P4a

## Physical Properties of Photoexcited Semiconductors 2

<b>Multi-photon Up-conversion Blue Lasing of Donor-acceptor Oligofluorenes</b>	
<i>P. L. Wu (Hong Kong Baptist University, China); X. J. Feng (Hong Kong Baptist University, China); H. L. Lam (Hong Kong Baptist University, China); M. S. Wong (Hong Kong Baptist University, China); Kok Wai Cheah (Hong Kong Baptist University, China);</i>	674
<b>Exciton Polariton Lasing in ZnO with Two-photon Excitation</b>	
<i>Xin-Hai Zhang (Institute of Materials Research and Engineering, 3 Research Link, Singapore); S. J. Xu (The University of Hong Kong, China); S. L. Shi (The University of Hong Kong, China); S. J. Chua (Institute of Materials Research and Engineering, 3 Research Link, Singapore); Chi-Ming Che (The University of Hong Kong, China);</i>	675
<b>Size-dependent Two-photon Absorption in Colloidal Semiconductor Quantum Dots</b>	
<i>Wei Ji (National University of Singapore, Singapore);</i>	676
<b>Dynamics of Carriers in Localized States and its Effects on Luminescence of Quantum Dots</b>	
<i>Qing Li (The Australian National University, Australia); S. J. Xu (The University of Hong Kong, China); Lan Fu (The Australian National University, Australia); H. Hoe Tan (The Australian National University, Australia); Chennupati Jagadish (The Australian National University, Australia);</i>	677
<b>Persistent Photo-conductivities from Extended Defects in MBE Grown GaN Films</b>	
<i>Xinhua Li (Institute of Solid State Physics, Chinese Academy of Sciences, China); Fei Zhong (Institute of Solid State Physics, Chinese Academy of Sciences, China); Kai Qiu (Institute of Solid State Physics, Chinese Academy of Sciences, China); Jiannong Wang (The Hong Kong University of Science and Technology, China); Yuqi Wang (Institute of Solid State Physics, Chinese Academy of Sciences, China);</i>	678
<b>Characterization of Fluorine-Plasma-Induced Deep Centers in AlGaIn/GaN Heterostructure by Persistent Photoconductivity</b>	
<i>B. K. Li (The Hong Kong University of Science and Technology, China); K. J. Chen (The Hong Kong University of Science and Technology, China); W. K. Ge (The Hong Kong University of Science and Technology, China); Jian-Nong Wang (The Hong Kong University of Science and Technology, China);</i>	679

## Multi-photon Up-conversion Blue Lasing of Donor-acceptor Oligofluorenes

P. L. Wu<sup>1,3</sup>, X. J. Feng<sup>2,3</sup>, H. L. Lam<sup>1,3</sup>, M. S. Wong<sup>2,3</sup>, and K. W. Cheah<sup>1,3</sup>

<sup>1</sup>Department of Physics, Hong Kong Baptist University, Kowloon Tong, Hong Kong, China

<sup>2</sup>Department of Chemistry, Hong Kong Baptist University, Kowloon Tong, Hong Kong, China

<sup>3</sup>Centre for Advanced Luminescence Materials, Hong Kong Baptist University  
Kowloon Tong, Hong Kong, China

**Abstract**— Multi-photon absorption, in particular two-photon and three-photon absorption, has drawn considerable interest over the years due to its potential applications in various optoelectronics and photonics. Owing to the use of the long-wavelength /low-energy excitation source and the characteristics of the intensity-dependence of the multi-photon absorption process, the multi-photon absorption offer many advantages for the technological applications of high capacity data storage, three-dimensional microfabrication, biological imaging, photodynamic therapy, and frequency up-converted lasing. In spite of significant progress in developing organic molecules with large two-photon absorption (TPA) properties over the past decade, the study/guidelines for structure-three-photon absorption property correlation of organic molecules is/are rather limited. In principle, donor-acceptor chromophores possessing a highly polarizable  $\pi$ -conjugated system are highly two-photon absorption active. To exhibit multi-photon absorption up-converted lasing, molecules are required to possess high fluorescent quantum efficiency, significant multi-photon absorption cross-section, and low fluorescent re-absorption, which could affect the lasing threshold and the attainment of optical gain. As a result, there are only few multi-photon particularly three-photon excited fluorescent dyes can exhibit frequency up-converted lasing and to the best of our knowledge, multi-photon induced up-converted blue-lasing in organic materials has not been demonstrated yet.

As part of our ongoing efforts to probe the structural factors of functional materials that can enhance nonlinear optical responses, we report herein the multi-photon absorption and frequency up-converted blue-lasing properties of novel series of 1, 3, 4-triazole and diphenylamino end-capped  $\pi$ -conjugated oligomers, TAZ-OT(*m*)OF(*n*)-NPh, in which the blue emitting  $\pi$ -conjugated core is derived from either bifluorenyl or terfluorenyl or thienylfluorenyl unit.

In this work, we have demonstrated for the first time that 1, 3, 4-triazole and diphenylamino end-capped  $\pi$ -conjugated oligomers can exhibit efficient multi-photon absorption induced up-converted blue-lasing and the emission/lasing wavelength can be easily tuned by various fluorene-based  $\pi$ -conjugated core.

Three different conjugated length oligomers were investigated for their up-conversion optical properties. Efficient two- and three-photon upconversion photoluminescence were obtained. Pumped by near-infrared femto-second laser at 800 nm, two-photon luminescence colour from green to deep blue was obtained and two-photon upconversion lasing with the same color range was also obtained. The best full width half maximum of the two-photon lasing is about 14 nm. For the three-photon upconversion, femto-second laser at 1344 nm and 1300 nm were the pump wavelengths, and both three-photon photoluminescence and lasing were obtained and the emission color range from sky blue to deep blue. The best full width half maximum of the three-photon lasing is about 6 nm which is one of narrowest reported. This is the first report on a series of organic complexes that exhibit both two-photon and three-photon upconversion photoluminescence and lasing.

## Exciton Polariton Lasing in ZnO with Two-photon Excitation

X. H. Zhang<sup>1</sup>, S. J. Xu<sup>2</sup>, S. L. Shi<sup>2</sup>, S. J. Chua<sup>1</sup>, and C. M. Che<sup>3</sup>

<sup>1</sup>Institute of Materials Research and Engineering, 3 Research Link, 117602, Singapore

<sup>2</sup>Department of Physics and HKU-CAS Joint Laboratory on New Materials  
The University of Hong Kong, Pokfulam Road, Hong Kong, China

<sup>3</sup>Department of Chemistry and HKU-CAS Joint Laboratory on New Materials  
The University of Hong Kong, Pokfulam Road, Hong Kong, China

**Abstract**— ZnO has attracted much attention recently because of its potential applications in optoelectronic devices operating in the ultraviolet (UV) to blue spectral region, owing to its direct wide bandgap of 3.37 eV at room temperature. Compared to other wide bandgap semiconductors, ZnO has an extremely large exciton binding energy (60 meV) and very strong exciton-photon coupling. Polariton condensation and polariton laser with recorded critical temperature of 560 K have been predicted for ZnO based model microcavities. In this work, we observed exciton polariton lasing with two-photon excitation.

The sample used in the present study is a single crystalline ZnO wafer with thickness of  $\sim 1$  mm and (0001) orientation. The optical property of the sample was first studied using continuous wave (cw) photoluminescence (PL). The low temperature cw near-band-edge PL spectrum is dominated by emission lines of bound excitons (BX), two-electron satellites (TES), and their phonon replicas. Very interesting phenomena are observed when the sample is excited with fs pulses centered at 738 nm (1.678 eV), where the photon energy of excitation is smaller than the half of bandgap energy. When the excitation intensity is low, the time-integrated PL spectrum is dominated by the emissions of BX, TES, and their phonon sidebands, similarly as the cw PL spectrum. With increasing the excitation intensity, laserlike oscillating emissions remarkably appear instead of the original BX emission band, and increase rapidly with the excitation intensity. It is interesting to note that the occurrence of the laserlike emissions strongly depends on the excitation wavelength. More specifically, they are observable only when the central excitation wavelength is varied from 730 nm to 750 nm. When the excitation wavelength is beyond this range, they do not appear even with much higher excitation intensity. The laserlike emissions also show strong temperature dependence. They decrease with increasing temperature and totally disappear at 12 K and above. Analysis of the experimental data suggests that laserlike oscillating emissions are due to exciton polariton lasing.

# Size-dependent Two-photon Absorption in Colloidal Semiconductor Quantum Dots

Wei Ji

Department of Physics, National University of Singapore, 117542, Singapore

**Abstract**— Colloidal semiconductor quantum dots (QDs) have received attention because they play a crucial role in two-photon microscopy. [1, 2] CdS QDs, CdSe QDs, CdTe QDs, or ZnSe QDs are considered to be promising candidates because they are capable of being operated at laser wavelengths by commercially available femtosecond lasers with QD sizes from a few to 15 nm. [1] Hence, a comprehensive understanding of size-dependent, two-photon absorption (TPA) is of direct relevance to the applications of semiconductor QDs to two-photon microscopy. Size-dependent TPA of semiconductor QDs have been measured. [3, 4] However, such measurements were carried out with QDs embedded glass, different from the environment for two-photon microscopy. The TPA of colloidal QDs has been investigated with two-photon induced fluorescence (TPIF) technique [5] or nonlinear transmission measurement [6]. The empirical correlation between size and TPA cross-section was obtained with uncertainty since TPIF technique required accurate knowledge of two-photon-excited photoluminescence efficiency. [5] Recently, the TPA of colloidal CdSe and CdTe QDs was unambiguously measured but the systematical study of size-dependent TPA still remained unavailable. [4, 6] Here we report a systematical investigation into the size dependence of TPA in aqueous solutions of organic-capped semiconductor QDs. With femtosecond Z-scan technique at laser wavelengths ranging from 720 to 950 nm, the size-dependent TPA cross-section is unambiguously measured. Based on the effective mass approximation [7], theoretical modeling is also carried out to gain a better understanding of the measurements.

## REFERENCES

1. Michalet, X., F. F. Pinaud, L. A. Bentolila, J. M. Tsay, S. Doose, J. J. Li, G. Sundaresan, A. M. Wu, S. S. Gambhir, and S. Weiss, *Science*, Vol. 307, 538, 2005 and references therein.
2. Larson, D. R., W. R. Zipfel, R. M. Williams, S. W. Clark, M. P. Bruchez, F. W. Wise, and W. W. Webb, *Science*, Vol. 300, 1434, 2003 and references therein.
3. Padilha, L. A., J. Fu, D. J. Hagan, E. W. V. Stryland, C. L. Cesar, L. C. Barbosa, and C. H. B. Cruz, *Opt. Express*, Vol. 13, 6460, 2005.
4. Padilha, L. A., J. Fu, D. J. Hagan, E. W. van Stryland, C. L. Cesar, L. C. Barbosa, C. H. B. Cruz, D. Buso, and A. Martucci, *Phys. Rev. B*, Vol. 75, 075325, 2007.
5. Pu, S. C., M. J. Yang, C. C. Hsu, C. W. Lai, C. C. Hsieh, S. H. Lin, Y. M. Cheng, and P. T. Chou, *Small*, Vol. 2, 1308, 2006.
6. He, G. H., Q. D. Zheng, K. T. Yong, A. I. Ryasnyanskiy, P. N. Prasad, and A. Urbas, *Appl. Phys. Lett.*, Vol. 90, 181108, 2007.
7. Fedorov, A. V., A. V. Baranov, and K. Inoue, *Phys. Rev. B*, Vol. 54, 8627, 1996.

# Dynamics of Carriers in Localized States and its Effects on Luminescence of Quantum Dots

Q. Li<sup>1</sup>, S. J. Xu<sup>2</sup>, L. Fu<sup>1</sup>, H. Hoe Tan<sup>1</sup>, and C. Jagadish<sup>1</sup>

<sup>1</sup>Department of Electronic Materials Engineering, Research School of Physical Sciences and Engineering  
The Australian National University, Canberra ACT 0200, Australia

<sup>2</sup>Department of Physics, The University of Hong Kong, Pokfulam Road, Hong Kong SAR, China

**Abstract**— Spontaneous formation of three-dimensional islands in semiconductors due to the Stranski-Krastanow growth mode has been widely used to produce high-quality quantum dots (QDs). The QDs act as carrier trapping centres in which localised states form due to the quantum confinement effect. The energy of the localised states is affected by many factors such as the size, the shape, the composition and the surrounding strain of the QDs and varies from one dot to another. It is well known that the localised states have a profound effect on the luminescence properties and behaviours of QDs which make them distinguished from the bulk materials and the quantum well materials. For example, the “S”-shaped temperature dependent peak positions and the non-monotonous temperature dependence of emission broadening were frequently observed in QDs samples.

Recently we have developed a model for the luminescence of localised states ensemble. The core of the model is a temperature dependent distribution function which describes the distribution of carriers within the localized states, derived from a rate equation in which the dynamics of carriers, that is, the generation, the thermal escape, the capture and the recombination processes of carriers are taken into account. Based on the distribution function equations describing the temperature dependence of luminescence peak were derived. The model suggests that thermal redistribution of carriers in localised states results in the anomalies in the temperature dependence of the luminescence peak. It is further demonstrated that the model reduces to the well know band-tail model [1] at the high temperature region and the luminescence quenching model of a two-level system [2] when the distribution of localised states approaches a  $\delta$ -function. The model is applied to explain the experimental data of many material systems such as InAs/InP QDs and InGaN quantum wells. Good agreements between the theoretical calculation and the experimental data are achieved.

## REFERENCES

1. Eliseev, P. G., P. Perlin, J. Lee, and M. Osiński, *Appl. Phys. Lett.*, Vol. 71, 569, 1997.
2. Curie, D., *Luminescence in Crystals*, 206, Metheun, London, 1963.

## Persistent Photo-conductivities from Extended Defects in MBE Grown GaN Films

Xinhua Li<sup>1</sup>, Fei Zhong<sup>1</sup>, Kai Qiu<sup>1</sup>, Jiannong Wang<sup>2</sup>, and Yuqi Wang<sup>1</sup>

<sup>1</sup>Key Laboratory of Materials Physics, Institute of Solid State Physics  
Chinese Academy of Sciences, P. O. Box 1129, Hefei 230031, China

<sup>2</sup>Department of Physics, the Hong Kong University of Science and Technology  
Clear Water Bay, Kowloon, Hong Kong SAR, China

**Abstract**— Excitation intensity and spectral dependence of persistent photoconductivity (PPC) in undoped GaN has been measured. The measured current decay behavior cannot simply fitted by stretched exponential functions or other multi-exponential functions. From the experimental results, we can make a conclusion that the photocurrent decay is dependent on excess carriers still existing in the conduct band and independent of incident intensities and wavelength. In order to clarify decay behavior of photocurrent, we proposed the model, in which some extend defects which served as negatively charged centers could be responsible for the excess carrier dependent phenomena. At the ground state, the extended defects are occupied and therefore negatively charged. When light shining on the sample, trapped electrons are excited to the conductance band. After the light is turned off, the recovery of non-equilibrium electrons from conductance band are prevented by the recapture barrier caused by the Coulomb force between the recovering electrons and the electrons still existing in the deep traps. The coulomb force between recovering electrons and trapped electrons would increase with the recovery of excess current. This model results in a fast decrease of photocurrent at the beginning of the decay due to the small capture barriers and a long persistent tail due to the increase of barriers when the excess free electrons is recaptured by the extend defects. Based on this model, time-dependent time-constants at different temperatures are extracted from experimental data. The Arrhnius plots for time constants at different decay stage reveal that the decay processes at the beginning stage dominate by tunnelling process. With the development of the decay process, the processes gradually governed by thermal activation process, and the final barrier is approximately 73 meV.

# Characterization of Fluorine-Plasma-Induced Deep Centers in AlGaIn/GaN Heterostructure by Persistent Photoconductivity

B. K. Li<sup>1</sup>, K. J. Chen<sup>2</sup>, W. K. Ge<sup>1</sup>, and J. N. Wang<sup>1</sup>

<sup>1</sup>Department of Physics, The Hong Kong University of Science and Technology  
Clear Water Bay, Kowloon, Hong Kong, China

<sup>2</sup>Department of Electronic and Computer Engineering  
The Hong Kong University of Science and Technology  
Clear Water Bay, Kowloon, Hong Kong, China

**Abstract**— It has been shown that the F ions induced in the AlGaIn barrier layer can deplete the two-dimensional electron gases (2DEG) in the channel of AlGaIn/GaN high electron mobility transistors (HEMTs) and convert it from depletion mode to enhancement mode [1, 2]. In this work, the properties of F-related deep centers in an AlGaIn/GaN HEMT are studied by the temperature dependent persistent photoconductivity (PPC) and Hall measurements. The growth, structure, and device fabrication of AlGaIn/GaN HEMT are given in Ref. [1]. The gate region of the HEMT is treated by CF<sub>4</sub> plasma in an RIE system at 150 W for 120 seconds and post-gate rapid thermal annealing is conducted at 400°C for 10 minutes. The dark electron density and mobility of both the treated and un-treated HEMTs are measured with temperature varying from 80 K to 305 K. Electron mobility of the treated sample is almost temperature independent in contrast to that of un-treated sample. This suggests a change of scattering mechanism due to induced F-related centers. In comparison with the un-treated sample, a much more pronounced PPC effect is observed for the F-treated sample indicating that the F-related centers are electron traps. Room temperature PPC spectroscopy shows that the optical excitation threshold is about 1.8 eV. Above 200 K, the decay time constant of PPC, modeled by a stretched exponential function, shows thermally activated behavior. An energy barrier for recapture of electrons from the 2DEG channel by the F-related centers is determined as 0.62 eV. Illuminated with 488 nm light the photo-ionization cross section of F-related centers is estimated around  $\sim 10^{-17}$  cm<sup>2</sup> at 305 K. Combining the results from deep-level transient spectroscopy the configuration coordinate diagram of F-related deep center is obtained.

## REFERENCES

1. Cai, Y., Y. G. Zhou, K. J. Chen, and K. M. Lau, *IEEE Electron Device Lett.*, Vol. 26, 435, 2005.
2. Cai, Y., Y. G. Zhou, K. M. Lau, and K. J. Chen, *IEEE Trans. Electron Devices*, Vol. 53, 2207, 2006.





# Session 3P5a

## EM Wave in Atmosphere Propagation and Communication 2

<a href="#">New Approaches to Generation of Helical Laser Beams</a>	
<i>J. Lin (Nanyang Technological University, Singapore); J. Bu (Nanyang Technological University, Singapore); Xiao-Cong Yuan (Nanyang Technological University, Singapore); .....</i>	682
<a href="#">Experimental Reconstruction for Inverse Scattering of One-dimensional Surfaces</a>	
<i>Anting Wang (Surface Optics Corporation, USA); Zu-Han Gu (Surface Optics Corporation, USA); ..</i>	683
<a href="#">Design of Double-frequency Coaxial CTS Antenna</a>	
<i>Bo Sun (Harbin Institute of Technology, China); Jinghui Qiu (Harbin Institute of Technology, China); Lingling Zhong (Harbin Institute of Technology, China); Xiaohang Xing (Harbin Institute of Technology, China); .....</i>	684
<a href="#">Frequency Scanning Using Micro-strip Array Antenna</a>	
<i>Alireza Bayat (Imam Khomeini International University, Iran); Mitra Torabipour Banadkok (Ministry of TCI, Iran); .....</i>	685
<a href="#">New Evidence for an Unexplained Electromagnetic Effect Generating False Acoustic Emission</a>	
<i>Paolo Diodati (Universita' degli Studi di Perugia, Italy); .....</i>	686

## New Approaches to Generation of Helical Laser Beams

J. Lin, J. Bu, and X.-C. Yuan

Photonics Research Centre, School of Electrical and Electronic Engineering  
Nanyang Technological University, Nanyang Avenue, 639798, Singapore

**Abstract**— Laser beams with spiral wavefront are receiving great interest in the field of free-space optical communications where orbital angular momentum is proved to be able to serve as an independent information carrier other than intensity and polarization of light. In this paper, novel ideas on phase plate design for helical beams are proposed and the corresponding Fraunhofer diffraction is studied. Apart from the conventional spiral phase plate whose transmittance is the function of the azimuthal variable, the transmittance of our phase plate depends on both radial and azimuthal coordinates, which provides more flexibility and possible control on the propagation of helical beams in future applications.

## Experimental Reconstruction for Inverse Scattering of One-dimensional Surfaces

Anting Wang<sup>1,2,3</sup> and Zu-Han Gu<sup>1,2</sup>

<sup>1</sup>Surface Optics Corporation, San Diego, CA 92127, USA

<sup>2</sup>Department of Electrical and Computer Engineering  
University of California, San Diego, CA 92093, USA

<sup>3</sup>Department of Physics, University of Science and Technology of China  
Hefei 230026, Anhui, China

**Abstract**— We have studied the inverse scattering problem as an optimization problem for a 1-D surface. As the input data for our self-adaptation genetic algorithm for surface inversion, the scattered intensity has been measured with the laser BRDF instruments. In addition, the reflection and transmission data are collected. The typical reconstruction of inverse scattering for a 1-D random surface is compared with the profile measured by an atomic force microscope (AFM), which can be applied to remote sensing and optical communication.

## Design of Double-frequency Coaxial CTS Antenna

Bo Sun, Jinghui Qiu, Lingling Zhong, and Xiaohang Xing

School of Electronics and Information Technology  
Harbin Institute of Technology, Harbin 150001, China

**Abstract**— Continuous Transverse Stub (CTS) technology is suitable to use with coaxial lines to produce effective microwave antenna structures that radiate omnidirectionally, with high efficiency, low reflection, and useful radiation patterns. In this paper, a new coaxial CTS antenna structure working at double frequency is presented, which reduces the size of antenna without performances changing much. Coaxial CTS antenna consists of several stub elements, and each stub element includes cascade sections of standard coaxial transmission line and open-ended radiating stubs. The proposed antenna consists of five open-ended radiating stubs. Two of the stubs are designed as the low frequency array to operate at 2.45 GHz, while the other three stubs are designed as the high frequency array to operate at 12 GHz. The basic theory and design method are analyzed, and simulation using CST Microwave Studio<sup>®</sup> commercial software is employed to optimize the antenna's properties. Simulation results shows that the radiant efficiency at 2.45 GHz got to be 78.9%, while the  $-10$  dB bandwidth ( $S_{11} < -10$  dB) was 60 MHz. And at 12 GHz, the bandwidth was about 10% which was 1.2 GHz, and within the bandwidth the radiant efficiency was about 98%. At the upper and lower frequency, the radiating patterns in horizon plane were omnidirectional, the gains were 2.8 dB and 4.6 dB, respectively. The proposed coaxial CTS antenna reduces 40% in size, while the radiation efficiency does not become worse obviously. These simple and low cost coaxial CTS structures could be adapted for base station applications in wireless communication, for satellite communication systems, and for personal communication systems.

## Frequency Scanning Using Micro-strip Array Antenna

Alireza Bayat<sup>1</sup> and Mitra Torabipour Banadkok<sup>2</sup>

<sup>1</sup>Department of Communication Engg., Imam Khomeini International University, Iran

<sup>2</sup>Ministry of TCI, Iran

**Abstract**— Micro-strip antennas are ideally suited for arrays which can be used to electronically scan the radiation beam essentially needed for longer detection range and faster data rate (short reaction time). In the present study the micro strip array antenna consists of two series of array which are parallel to each other and each series consists of nineteen elements which is rectangular in shape. Each element functions as a radiator and phase shifter. Unlike a conventional planar array, however, the elements on the array surface are spatially fed using a quarter wave transformers, which is cascade, coupled to each other. With electronic scanning it is possible to obtain practically instantaneous slewing of an antenna radiation beam to any position in the designated sector. Other features, such as scanning exhibited by the proposed antenna tenna is  $120^\circ$  in azimuth as in Fig. 3 which is just, double the scanning reported by Danielson (1). The scanning rate of 0.117 deg/MHz is observed which is better than the earlier reported rate of 0.1 deg/MHz Fig. 4.

# New Evidence for an Unexplained Electromagnetic Effect Generating False Acoustic Emission

Paolo Diodati

Dipartimento di Fisica dell'Università di Perugia, Via A. Pascoli, 1 06100 Perugia, Italy

**Abstract**— Acoustic Emission (AE) measurements are normally performed by sensors made of piezoelectric crystals or ceramics which can generate False Acoustic Emission (FAE), due to the reversible effect. So an ambiguity exists since sensor's vibrations can be driven by elastic oscillations of the medium in contact with the piezoelectric disk, which constitute the Acoustic Emission, as well as by changes of the electric polarity of at least one face of the disk.

In previous papers [1, 2] we communicated that using commercial sensors, FAE was totally due to manmade noise of electromagnetic origin for detected signals in the tunnel of the underground National Laboratory of the Gran Sasso mountain, Italy, while on the same mountain, in the open at 2500 m above sea level, a systematic increase in number and intensity of FAE events was observed, starting from sunset up to about midnight.

On the contrary, AE measurements performed in volcanic areas, in particular in a “rock pile”, such as Stromboli, Italy, show ultrasonic bursts due to micro-movements of the rocks, for whose intensity and number it is not required our method [2] to discriminate FAE from AE.

To answer the question if the noise variation observed on the Gran Sasso mountain [1], which is not due to the electric network or to thermal variation of the rocks, exists also on Stromboli, we made a statistical study, of the signals detected in periods of very low volcanic activity. At Stromboli these periods are characterized by mostly isolated AE bursts of high energy, corresponding to impulsive signals of about 0,1 V up to about 1–2 V [3–5]. The remaining signals, of some mV or less, are due to noise. In this regime ultrasonic precursor signals of seismic events with the highest reliability, were discovered [3], while the study of time and energy distribution of AE in the high-activity regime show scaling laws, interpreted on the paradigm of self-organized criticality [4, 5].

We report here the results of several years of data acquisition. These data, relative to periods of quiescent volcanic activity, were filtered by the discrimination technique described in [2]. The obtained noise shows a modulation similar to that reported in [1]: a systematic increase of number and intensity of FAE events, starting from sunset up to about midnight. In addition a spectacular increase of AE was observed sometime, always starting from sunset. A thermal origin for this FAE, must be rejected for several reasons, as discussed in [1]. Here we underline that rock's dilatation and contraction, due to sun's radiation, generate AE by friction between rock's surfaces, which is considered as true AE by our method [2].

In conclusion, the underground or atmospheric origin of this em effect correlated to the sun's position, must be investigated, being totally unexplained the mechanism generating FAE, the most credible hypothesis, in our opinion, remaining that expressed in [1].

## REFERENCES

1. Diodati, P., et al., “Daily and annual electromagnetic noise variation and acoustic emission revealed on the Gran Sasso mountain,” *Earth and Planetary Science Letters*, Vol. 184, 719–724, 2001.
2. Diodati, P. and S. Piazza, “Simple discrimination method between false acoustic emission revealed by piezoelectric sensors, in Gran sasso mountain measurements,” *J. Acoust. Soc. Am.*, Vol. 116, No. 1, July 2004.
3. Diodati, P., “Ultrasonic precursor signals of seismic events revealed on volcano Stromboli,” *Il Nuovo Cimento*, Vol. 18, No. 2, 239–242, March–April 1995.
4. Diodati, P., F. Marchesoni, and S. Piazza, “Acoustic emission from volcanic rocks: an example of self-organized criticality,” *Phy. Rew. Lett.*, Vol. 67, 2239–2243, 1991.
5. Diodati, P., P. Bak, and F. Marchesoni, “Acoustic emission at the Stromboli volcano: scaling laws and seismic activity,” *Earth and Planetary Science Letters*, Vol. 182, 253–258, 2000.

# Session 3P6a

## Microwave and Optical Devices, Propagation

### Birefringent Azopolymer Long Period Fibre Gratings

*Yanhua Luo (University of Science and Technology of China, China); Zengchang Li (University of Science and Technology of China, China); Qijin Zhang (University of Science and Technology of China, China); Gangding Peng (University of New South Wales, Australia); Rongsheng Zheng (University of Science and Technology of China, China); Ming Hai (University of Science and Technology of China, China); Ru Chen (University of Science and Technology of China, China); Bing Zhu (University of Science and Technology of China, China); .....* 688

### Erasable Azo-polymer Optical Fibre Bragg Gratings

*Yanhua Luo (University of Science and Technology of China, China); Jingli Zhou (University of Science and Technology of China, China); Qing Yan (University of Science and Technology of China, China); Wei Su (University of Science and Technology of China, China); Zengchang Li (University of Science and Technology of China, China); Qijin Zhang (University of Science and Technology of China, China); Gangding Peng (University of New South Wales, Australia); Jintang Huang (University of Science and Technology of China, China); Keyi Wang (University of Science and Technology of China, China); .....* 689

### Cluster Head Selection Using Evolutionary Computing in Wireless Sensor Networks

*Ghufran Ahmed (Ghulam Ishaq Khan Institute of Engineering Sciences and Technology, Pakistan); Noor M. Khan (Mohammad Ali Jinnah University, Pakistan); Rodica Ramer (The University of New South Wales, Australia); .....* 690

### Resonating Modes for Characterization of Low-loss, High Dielectric Constant Materials

*G. M. Banciu (National Institute of Materials Physics, Romania); A. Ioachim (National Institute of Materials Physics, Romania); Rodica Ramer (University of New South Wales (UNSW), Australia); ..* 693

### A Robust Transmission Technique for Arbitrary 3D Images in Wireless Multimedia Sensor Networks

*Ghufran Ahmed (Muhammad Ali Jinnah University, Pakistan); Noor M. Khan (Mohammad Ali Jinnah University, Pakistan); Rodica Ramer (University of New South Wales (UNSW), Australia); .....* 694

### Impact of Cluster Head Energy on the Life Time of Quasi-Centralized Wireless Sensor Networks

*Zubair Khalid (Ghulam Ishaq Khan Institute of Engineering Sciences and Technology, Pakistan); Noor M. Khan (Mohammad Ali Jinnah University, Pakistan); Rodica Ramer (University of New South Wales (UNSW), Australia); .....* 696

## Birefringent Azopolymer Long Period Fibre Gratings

Yanhua Luo<sup>1,2</sup>, Zengchang Li<sup>1</sup>, Qijin Zhang<sup>1</sup>, Gangding Peng<sup>2</sup>  
Rongsheng Zheng<sup>3</sup>, Ming Hai<sup>3</sup>, Ru Chen<sup>4</sup>, and Bing Zhu<sup>4</sup>

<sup>1</sup>Department of Polymer Science and Engineering

University of Science and Technology of China, Hefei 230026, China

<sup>2</sup>School of Electrical Engineering, University of New South Wales, Sydney 2052, NSW, Australia

<sup>3</sup>Department of Physics, University of Science and Technology of China, Hefei 230026, China

<sup>4</sup>Department of Electronic Engineering and Information Science

University of Science and Technology of China, Hefei 230026, China

**Abstract**— We demonstrated that that birefringent long period fiber gratings can be fabricated in azopolymer fiber using polarized 532 nm laser. A 120  $\mu\text{m}$  long-period birefringence grating with a 50% duty cycle has been successfully written within the core of the fibre with 532 nm laser by a mask method. Under polarized microphotography, the grating was observed when the optical axis was set at  $45^\circ$  with the direction of the first polarizing lens of the polarization microscope. And the mechanism forming birefringent fiber gratings was illuminated and simulated further.



## Erasable Azo-polymer Optical Fibre Bragg Gratings

Yanhua Luo<sup>1,2</sup>, Jingli Zhou<sup>1</sup>, Qing Yan<sup>1</sup>, Wei Su<sup>1</sup>, Zengchang Li<sup>1</sup>, Qijin Zhang<sup>1</sup>  
Gangding Peng<sup>2</sup>, Jintang Huang<sup>3</sup>, and Keyi Wang<sup>3</sup>

<sup>1</sup>Department of Polymer Science and Engineering  
University of Science and Technology of China  
Hefei 230026, China

<sup>2</sup>School of Electrical Engineering, University of New South Wales  
Sydney 2052, NSW, Australia

<sup>3</sup>Department of Precision Machinery and Precision Instrumentation  
University of Science and Technology of China  
Hefei 230026, China

**Abstract**— Polymer optical fibre (POF) with a core of azo-polymer has successfully been made with diameter of 114  $\mu\text{m}$  and core of 6  $\mu\text{m}$ , and azobenzene content at 3.2%-wt. Based on the erasable birefringence of azo-polymer materials, a new mechanism of POF gratings has been demonstrated, in which 441.6 nm He-Cd laser is used with the polarization state being periodically modulated. After writing in azo-polymer optical fibre (APOF) by two beams of mutually orthogonal polarizations, a birefringence grating was formed, and then the gratings could be erased almost totally for a short time by the circularly polarized beam at the same wavelength. By manipulating the APOF gratings, the transmittance through APOF at 632.8 nm can be adjustable as revealed by the transmittance change during write-erase-write procedure.

# Cluster Head Selection Using Evolutionary Computing in Wireless Sensor Networks

G. Ahmed<sup>1</sup>, N. M. Khan<sup>1</sup>, and R. Ramer<sup>2</sup>

<sup>1</sup>Mohammad Ali Jinnah University, Pakistan

<sup>2</sup>University of New South Wales, Australia

**Abstract**— Wireless Sensor Network (WSN) comprises of micro sensor nodes with limited energy and processing ability. It is used in military as well as civil applications. In order to enhance the network life time by the period of a particular mission, many routing protocols have been devised. One of these is network clustering, in which network is partitioned into small clusters and each cluster is monitored and controlled by a node, called Cluster Head (CH). The CH should be powerful, closer to the cluster-centroid, less vulnerable [5] and has to have low mobility, so that it can aggregate the data from its own cluster nodes and then send it directly to the Base Station (BS).

Several analyses of energy efficiency of sensor networks have been realized [2, 3, 7, 8] and several algorithms that lead to optimal connectivity topologies for power conservation have been proposed [1, 6, 9–12]. But we still need more energy-efficient solution. In this paper, we are using Evolutionary Computing (EC), also called Genetic Algorithm (GA) for CH selection in a cluster-based WSN. Many aspects of such an evolutionary process are stochastic [4].

Our goal is to search best sensor nodes among hundreds of nodes, so that they can act as CHs. Conventional search methods are not robust, while the GA is a search procedure that uses random choice as a tool to guide a highly exploitative search through a coding of a parameter space. According to Goldberg in [4], the GA has 4 major characteristics:

1. GAs with a coding of the parameter set, not the parameters themselves
2. GAs search from a population of points, not a single point
3. GAs use payoff (objective function) information, not derivatives or other auxiliary knowledge
4. GAs use probabilistic transition rules, not deterministic rules

In many optimization methods, we move carefully from a single point in the decision space to the next using some transition rule to determine the next point. This point-to-point method is dangerous because it is a perfect prescription for locating false peaks in multi modal (many peaked) search spaces. By contrast, GA works from a rich database of points simultaneously (a population of strings), climbing many peaks in parallel; thus, the probability of finding a false peak is reduced over methods that go point-to-point [4].

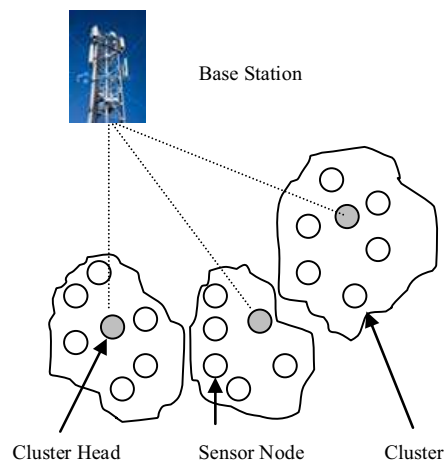


Figure 1: Wireless sensor network.

A GA starts with a population of strings (nodes) and thereafter generates successive populations of strings. A simple GA consists of three operators: 1) Reproduction 2) Crossover and 3) Mutation.

Table 1: Possible values for the attributes.

$X_1$	High	Low
$X_2$	Near	Far
$X_3$	Low	High
$X_4$	Low	High
<b>Digital Value</b>	<b>1</b>	<b>0</b>

The chromosome of the GA contains all the building blocks to a solution of the problem at hand in a form that is suitable for the genetic operators and the fitness function. Each individual sensor node is represented by a 4-bit binary number called ‘gene’. These four-bit genes which define the feature of the node are called “allele” and are represented as follows:

$X_1 X_2 X_3 X_4$

$X_1$  : its remaining battery power,

$X_2$  : distance of a node from the cluster centroid,

$X_3$  : its degree of mobility, and

$X_4$  : its vulnerability index [5].

The possible values of these 4 attributes are shown in Table 1.

Let’s take an example. To start off, select an initial population at random. Here, we select a population of size 4. Each string (node) has some fitness value. This value can be evaluated from a fitness function,  $f(x) = f(x_1, x_2, x_3, x_4)$ . In the case of WSN, the fitness function depends upon the four factors: Nodes with higher energy, low mobility, closer to the cluster centroid and low in vulnerability [5] have high fitness values and can be declared as CHs. For our example, let  $f(x) = x^2$ .

A generation of the GA begins with reproduction. We select the mating pool of the next generation by spinning the weighted roulette wheel four times. From this, the best string get more copies, the average stay even, and the worst die off.

Table 2: CH selection through GA.

No.	Node*	x	$f(x) = x^2$	Pselect <sub>i</sub> ( $f_i/\Sigma f$ )	Expected Count ( $f_i/\text{Avg}(f)$ )	Actual Count**	Mating Pool***	Mate****	Cross-Over Site*****	New Nodes	x	$f(x)=x^2$
1	0110	6	36	0.13	0.52	1	011 0	2	3	0110	6	36
2	1100	12	144	0.52	2.08	2	110 0	1	3	1100	12	144
3	0100	4	16	0.06	0.23	0	11 00	4	2	1101	13	169
4	1001	9	81	0.29	1.17	1	10 01	2	2	1000	8	64
<b>Sum</b>			277	1.00	4.00	4.0						413
<b>Avg.</b>			69.25	0.25	1.00	1.0						103.25

\*Initial population (Randomly Generated Nodes Selected as CHs)

\*\*From Roulette Wheel

\*\*\*After Reproduction (Cross site shown)

\*\*\*\*Randomly selected

The improvement that is provided by GA is not a fluke (a lucky or unusual thing that happens by accident). In our example Table 2, the best string of the first generation (1100) receives two copies because of its high, above average performance. When this combines at random with the next highest string (1001) and is crossed at location 2 (again at random), one of the resulting strings (1101) proves to be a very good choice for CH indeed.

## REFERENCES

1. Chmielewski, D. J., T. Palmer, and V. Manousiouthakis, “On the theory of optimal sensor placement,” *AlChE J.*, Vol. 48, No. 5, 1001–1012, 2002.
2. Slijepcevic, S. and M. Potkonjak, “Power efficient organization of wireless sensor networks,” *Proc. IEEE Int. Conf. on Communications*, 472–476, Helsinki, Finland, 2001.

3. Krishnamachari, B. and F. Ordo'nez, "Analysis of energy-efficient, fair routing in wireless sensor networks through non-linear optimization," *Proc. IEEE Vehicular Technology Conference - Fall*, 2844–2848, Orlando, FL, 2003.
4. Goldberg, D., *Genetic Algorithm in Search, Optimization and Machine Learning*, Addison-Wesley Publishing Company, Inc., 1989.
5. Khalid, Z., G. Ahmed, N. M. Khan, and P. Vigneras, "A real-time energy-aware routing strategy for wireless sensor networks," accepted for presentation in *The 2007 Asia-Pacific Conference on Communications*, Bangkok, Thailand, 2007.
6. Zhou, C. and B. Krishnamachari, "Localized topology generation mechanisms for wireless sensor networks," *IEEE GLOBECOM'03*, San Francisco, CA, December 2003.
7. Trigoni, A., Y. Yao, A. Demers, J. Gehrke, and R. Rajaraman, "WaveScheduling: Energy-efficient data dissemination for sensor networks," *Proc. Int. Workshop on Data Management for Sensor Networks (DMSN)*, in conjunction with *VLDB*, 2004.
8. Mhatre, V., C. Rosenberg, D. Kofman, R. Mazumdar, and N. Shroff, "A minimum cost heterogeneous sensor network with a lifetime constraint," *IEEE Trans. Mobile Comput.*, Vol. 4, No. 1, 4–15, 2005.
9. Ghiasi, S., A. Srivastava, X. Yang, and M. Sarrafzadeh, "Optimal energy aware clustering in sensor networks," *Sensors*, Vol. 2, 258–269, 2002.
10. Rodoplu, V. and T. H. Meng, "Minimum energy mobile wireless networks," *IEEE J. Select. Areas Commun.*, Vol. 17, No. 8, 1333–1344, 1999.
11. Heinzelman, W. R., A. Chandrakasan, and H. Balakrishnan, "Energy-efficient communication protocol for wireless microsensor networks," *Proc. 33rd Hawaii Int. Conf. on System Sciences*, Maui, Hawaii, 2000.
12. Chang, J.-H. and L. Tassiulas, "Energy conserving routing in wireless ad-hoc networks," *Proc. IEEE INFOCOM'00*, 22–31, Tel Aviv, Israel, 2000.

## Resonating Modes for Characterization of Low-loss, High Dielectric Constant Materials

G. M. Banciu<sup>1</sup>, A. Ioachim<sup>1</sup>, and R. Ramer<sup>2</sup>

<sup>1</sup>National Institute of Materials Physics, Magurele, Romania

<sup>2</sup>University of New South Wales, NSW 2052, Australia

**Abstract**— Low loss, high dielectric materials allow miniaturization of microwave devices and circuits. Materials such as  $(\text{Zr}_{0.8}\text{Sn}_{0.2})\text{TiO}_4$  exhibit outstanding temperature stability of their dielectric parameters. This makes them very attractive for microwave and millimeter applications including dielectric resonators, filters, antennas, and substrates for hybrid integrated circuits. In this paper, the resonating modes of samples of high dielectric constant are investigated. A mode chart containing all the transversal electric, transversal magnetic and hybrid modes was drawn, for each set of samples geometrical and dielectric parameters. The mode investigation allows the sample characterization in more frequency points on a wide frequency range. The values of the dielectric constant and of the intrinsic quality factor are evaluated for each sample.

# A Robust Transmission Technique for Arbitrary 3D Images in Wireless Multimedia Sensor Networks

G. Ahmed<sup>1</sup>, N. M. Khan<sup>1</sup>, and R. Ramer<sup>2</sup>

<sup>1</sup>Mohammad Ali Jinnah University, Pakistan

<sup>2</sup>University of New South Wales, Australia

**Abstract**— Wireless Multimedia Sensor Networks (WMSNs) are networks of wirelessly interconnected devices that are able to ubiquitously retrieve multimedia content such as video and audio streams, still images, and scalar sensor data from the environment. With rapid improvements and miniaturization in hardware, a single sensor device can be equipped with audio and visual information collection modules. In addition to the ability to retrieve multimedia data, WMSNs will also be able to store, process in real-time, correlate and fuse multimedia data originated from heterogeneous sources. Potential applications of WMSNs include remote video-based surveillance, traffic monitoring, virtual reality, tracking, home automation, and environmental monitoring.

The wireless medium used in WMSNs is characterized by highly unreliable, mostly caused by multi-path channel fading, and shadowing at the physical layer, collisions or co-channel interference at the MAC layer, high path loss, noise disturbances, and bit error rate (BER), these result in the wireless channel having much lesser capacity than wired channels [3]. Thus, streaming of real-time multimedia data over a wireless sensor network is particularly challenging due to the QoS requirements of a video/audio stream and the unreliability of the wireless medium.

In this paper, we describe a perceptually motivated strategy for transmission of 3D objects represented by texture and mesh over unreliable WMSNs. When transmitting 3D object especially irregular mesh data, not only vertex information but also connectivity information plays a crucial role in 3D reconstruction at the client site. In order to preserve the original geometry of the object, many transmission algorithms suggest retransmission [4] of the base layers to safeguard the successful transmission of important features of the object [1, 2]. Retransmission adds an overhead on bandwidth limited connections, in particular on wireless and mobile networks. Without the need to retransmit the base layer, our goal is to find a robust approach for 3D transmission of arbitrary meshes. Our approach to arbitrary meshes considers stripification of the mesh and distributing nearby vertices into different packets, combined with a strategy that does not need texture or mesh packets to be re-transmitted. Only the valence (connectivity) packets need to be re-transmitted; however, storage of valence information requires only 10% space compared to vertices and even less compared to photo-realistic texture. Thus, less than 5% of the packets may need to be re-transmitted in the worst case to allow our algorithm to successfully reconstruct an acceptable object under severe packet loss. We can transmit real-time data through this approach. In this case, to avoid the delays in requesting re-transmission of packets, it may be wiser to send duplicate packets containing the connectivity information so that real-time visualization of photo-realistic texture mapped 3D objects at high packet loss can be facilitated. The proposed approach can also be used for scalable transmission as well, allowing graceful degradation of a 3D image under limited bandwidth [5].

Our approach focuses on following two factors:

1. Efficient compression based on stripification [5]
2. Robustness to packet loss based on distribution of neighboring vertices into different packets [6]

The sensor nodes encode and group the data (vertices) into different packets and transmit them to sink or base station (BS). After all the packets are received by the BS, first, the mesh is partially reconstructed based on the partial geometry packets and connectivity; following the same order as in the encoding process. Then, the vertices are traversed in the reconstruction order of the valence-driven decoding algorithm [7]. When a vertex with lost geometry,  $L$ , is encountered, the adjacent reconstructed vertices with an edge connected to  $L$ , whose geometry is either not lost or is interpolated previously, are used to interpolate the geometry of  $L$ . A linear interpolation algorithm can be used for the interpolation of the missing vertices.

In Figure 1 (taken from [6]), 30%, 50%, 60%, and 80% randomly selected vertices were lost for a cow meshes. However, the lost geometry was interpolated based on neighboring vertices and valence information, which is transmitted without error. It can be seen that smoothness on the object surface begins to deteriorate at about 60% loss. Visual degradation becomes more obvious at 80% loss; still the object is recognizable as cow.



Figure 1: A cow mesh in left column highlighting the packet loss region before interpolation, while the same cow mesh after the interpolation is shown in the left column. From top to bottom: 30%, 50%, 60% and 80% packet loss [6].

#### REFERENCES

1. Misra, S., M. Reisslein, and G. Xue, "A survey of multimedia streaming in wireless sensor networks," submitted work. [www.fulton.asu.edu/~mre/WSNstreaming.pdf](http://www.fulton.asu.edu/~mre/WSNstreaming.pdf).
2. Limb, J. O., "Distortion criteria of the human viewer," *IEEE Transactions on SMC*, 778–793, 1979.
3. Jakes, W., *Microwave Mobile Communications*, John Wiley and Sons, New York, 1974.
4. Wittenburg, G. and J. Schiller, "A quantitative evaluation of the simulation accuracy of wireless sensor networks," *Proc. of Fachgesprach "Drahtlose Sensornetze" der GI/ITG-Fachgruppe "Kommunikation und Verteilte Systeme"*, Aachen, Germany, July 2007.
5. <http://www.cosy.sbg.ac.at/~held/projects/strips/strips.html>.
6. Cheng, I., L. Ying, and A. Basu, "A perceptually driven model for transmission of arbitrary 3D models over unreliable networks," *Proc. of the Third international Symposium on 3D Data Processing, Visualization, and Transmission (3D PVT'06)*, 421–428, Washington, USA, June 14–16, 2006.
7. Touma, C. and C. Gotsman, "Triangle mesh compression," *Graphics Interface*, 26–34, 1998.

## Impact of Cluster Head Energy on the Life Time of Quasi-Centralized Wireless Sensor Networks

Z. Khalid<sup>1</sup>, N. M. Khan<sup>2</sup>, and R. Ramer<sup>3</sup>

<sup>1</sup>GIK Institute of Engineering Sciences & Technology, Topi, Pakistan

<sup>2</sup>Muhammad Ali Jinnah University, Islamabad, Pakistan

<sup>3</sup>University of New South Wales, Sydney, NSW 2052, Australia

**Abstract**— Wireless Sensor Networks (WSNs) are constrained by deeply embedded routers, resource constrained nodes, highly dynamic networks, frequent topology change and unreliable and asymmetric links. The routing approach must consider and be aware of all these factors. In [1], authors proposed a heterogeneous cluster-based WSN, which lengthens the whole network lifetime by partitioning the whole network into different clusters. Each cluster has a powerful sensor node (SN), which acts as cluster head (CH). CH plays an important role in aggregating and forwarding data sensed by other common nodes [2]. It also manages and controls the entire cluster. In this paper, we investigate the impact of energy ratio of CH and SN on the life time of Quasi-Centralized WSN. It is unproductive to place the CHs with infinite energy because they will be useless after the failure of other nodes of the cluster. Although there are many algorithms for WSN based on clustering in the literature, we take the same approach as discussed in [1].

For simulation setup, we use 100 SNs out of which some have more power than the others. These are the CHs. Network lifetime is considered as the time span from the time of deployment of the network till the time when no node can deliver data to the sink. The average data delivery of all SNs is 1 Kbps. A node is considered as a failed node if it is left with 10% of its original battery power. Fig. 1 shows a plot of network lifetime against the ratio between the energy of CH and that of its individual member nodes. Five different simulations of CH proportion with respect to the total nodes have been simulated. Fig. 1 shows that the lifetime parameters in each plot tend to become constant at some saturation stage. It can be easily observe that the saturation stage is highly dependent on the proportion of CH to the total number of nodes. In other words, we can say that the lower the proportion of CH to total number of nodes, the earlier the saturation stage and vice versa. The plot clearly defines two scenarios of the proportion of CH with respect to the total number of nodes i.e., 0% and 100%. At 0%, the curve would become parallel to the abscissa and at 100% it becomes a straight line toward upper right corner. As far as, the behavior of the lifetime of the WSN with the increase in energy ratio is concerned, it is evident from the plot for any given CH proportion with respect to total number of nodes, that it can be increased up to certain level. Beyond that level, an increase in the energy ratio exerts negligible effect on the network lifetime. It is due to the fact that the SNs die after a certain period of time and CH cannot work without them. Hence, the addition of CH energy (CHE) does not enhance network lifetime after a certain level is reached.

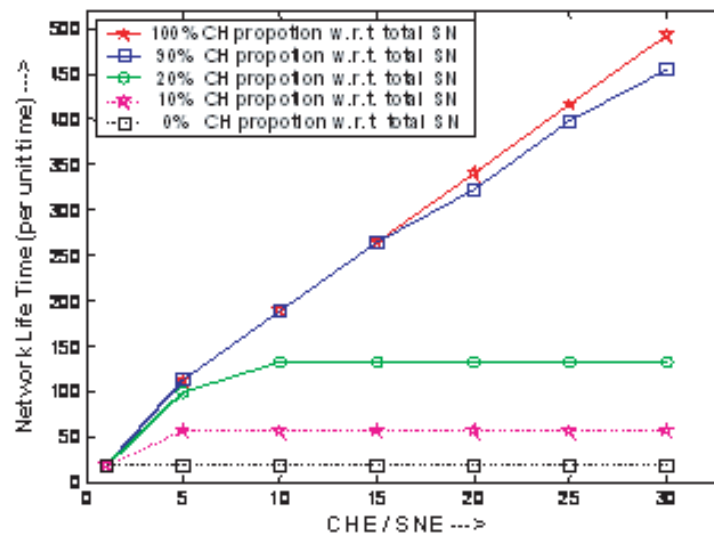


Figure 1: Impact of CH energy on network lifetime.



**REFERENCES**

1. Akkaya, K. and M. Younis, "An energy-aware QoS routing protocol for wireless sensor networks," *Proc. of Int. Conf. Distributed Computing Sys. Workshop (ICDCSW'03)*, 710–715, May 19–22, 2003.
2. Yin, Y., J. Shi, Y. Li, and P. Zhang, "Cluster head selection using analytical hierarchy process for wireless sensor networks," *Proc. of IEEE Int. Symp. Pers. Indoor Mob. Radio Commun. (PIMRC)*, 1–5, September 2006.



# Session 3P7a

## Electromagnetic Techniques for Biomedical Applications 2

### Medical Imaging and Diagnostics Based on Microwaves

*Jan Vrba (Czech Technical University in Prague, Czech Republic); Ladislav Oppl (Czech Technical University in Prague, Czech Republic); Radim Zajicek (Czech Technical University in Prague, Czech Republic); Katerina Novotna (Czech Technical University in Prague, Czech Republic); David Vrba (Czech Technical University in Prague, Czech Republic); ..... 700*

### Some Improvements in Iterative Multi-scaling Strategies

*Xiang Yin (Institute of Electronics, Chinese Academy of Sciences, China); Lianlin Li (Institute of Electronics, Chinese Academy of Sciences, China); Fang Li (Institute of Electronics, Chinese Academy of Sciences, China); ..... 701*

### A Two-step Strategy for Inverse Scattering from Phaseless Data in Free Space

*Wenji Zhang (Institute of Electronics, Chinese Academy of Sciences, China); Lianlin Li (Institute of Electronics, Chinese Academy of Sciences, China); Fang Li (Institute of Electronics, Chinese Academy of Sciences, China); ..... 702*

### Electromagnetic Radiation from Ingested Sources in the Human Intestine at the Frequency of 2.4 GHz

*Lisheng Xu (The Chinese University of Hong Kong, China); Max Q.-H. Meng (The Chinese University of Hong Kong, China); Hongliang Ren (The Chinese University of Hong Kong, China); ..... 703*

### Microwave Thermotherapy — Technical and Clinical Aspects

*Jan Vrba (Czech Technical University in Prague, Czech Republic); ..... 704*

### A Physical Model for Study of Electromagnetic Field Interaction with Cancer Cell

*Dariush Sardari (Amirkabir University, Iran); N. Verga (Carol Davila University, Romania); ..... 705*

## Medical Imaging and Diagnostics Based on Microwaves

Jan Vrba, Ladislav Oppl, Radim Zajicek, Katerina Novotna, and David Vrba  
Department of EM Field, Czech Technical University in Prague, Prague, Czech Republic

**Abstract**— Future trends in medical applications of microwave technique and technology can be seen in development of new diagnostic and imaging methods based on high frequency EM field. A significant importance for the future can be identified for the following methods: Microwave tomography, Microwave radiometry, Measurement of complex permittivity, Imaging in the Terahertz waves band and Microwave diagnostic radars.

Interactions of EM field with biological systems are utilised in the area of therapy (oncology, physiotherapy, urology atp.) from late seventieth of last century. Wideutilization of microwave thermotherapy can be observed in the countries of EU, USA and Japan. Our activities in microwave thermotherapy in former Czechoslovakia started in the year 1981. Since 1990 we are member of ESHO (European Society for Hyprthermia Oncology), which co-operates with NAHS (North American Hyperthermia Society) and ASHO (Asian Society of Hyperthermia Oncology).

Recent trends in microwave medical applications are to study the possibilities to develop new diagnostics based on EM field resp. on microwace technique. A significant importance for the future can be identified for the next methods:

- Magnetic resonance,
- Microwave tomography,
- Microwave radiometry,
- Measurement of complex permittivity,
- Imaging with terahertz waves,
- Microwave diagnostic radar.

We will not talk here about magnetic resonance, as it is just well known and broadly used application of EM field in medical diagnostics. We will focus here on other above mentioned methods (excluding microwave diagnostics radars).

### ACKNOWLEDGMENT

This research is supported by Grant Agency of the Czech Republic, project: “Microwave Imaging for Biomedical Applications” (102/05/0959) and by the research program MSM6840770012 “Transdisciplinary Research in the Area of Biomedical Engineering II” of the CTU in Prague, sponsored by the Ministry of Education, Youth and Sports of the Czech Republic.

### REFERENCES

1. Vrba, J., *Medical Applications of Microwaves*, 1. ed., 168, ISBN 80-01-02705-8, Issued by CTU, Prague, 2003.
2. Semenov, S. Y., et al., “Three-dimensional microwave tomography, initial experimental imaging of animals,” *IEEE Transactions on BME*, Vol. 49, No. 1, 55–63, Jan. 2002.
3. Gabriel, S., R. W. Lau, and C. Gabriel, “The dielectric properties of biological tissue — II. measurements in the frequency range 10 Hz to 20 GHz,” *Phys. Med. Biol.*, Vol. 41, 2251–2269, 1996.

## Some Improvements in Iterative Multi-scaling Strategies

Xiang Yin, Lianlin Li, and F. Li

Institute of Electronics, Chinese Academy of Sciences, Beijing 100080, China

**Abstract**— Inverse scattering problem is in general ill-posed due to the limited measure data corrupted by certain noise, so some additional or *prior* information is needed in the imaging process to cure this pain. The so-called iterative multi-scaling approach (IMSA) has been developed, which exploits the knowledge of the scenario under test obtained at the previous steps, to estimate the location and extension of the obstacle(s) [1, 2]. To ensure a correct solution the zoom in investigation domain must cover the obstacle(s) under test, which is not satisfied by using the original estimation strategy proposed in IMSA if the shape and contrast distribution of obstacle(s) are irregular.

Another property of IMSA is the synthesis of resolutions. That is the contrast and field distribution on each resolution satisfy their own state equations, and the contribution of all resolutions synthesize the scattering field. In the original iterative process of IMSA, it is doubtful that lots of unknowns are to be reconstructed when the resolution level ups. Therefore, the combination of grids (or unknowns) is proposed in this paper.

In summary the novel approach to the estimation of the RoI is proposed, where the formulation for estimating the location and extension of the obstacle is improved and a strategy of discretizing grids in adaptive way are developed. Some numerical experiments are provided to validate them.

### REFERENCES

1. Caorsi, S., M. Donelli, D. Franceschini, and A. Massa, "A new methodology based on an iterative multiscaling for microwave imaging," *IEEE Trans. Microw. Theory Tech.*, Vol. 51, No. 4, 1162–1173, Apr. 2003.
2. Caorsi, S., M. Donelli, and A. Massa, "Detection, location, and imaging of multiple scatterers by means of the iterative multiscaling method," *IEEE Trans. Microw. Theory Tech.*, Vol. 52, No. 4, 1217–1228, Apr. 2004.

# A Two-step Strategy for Inverse Scattering from Phaseless Data in Free Space

Wenji Zhang<sup>1,2</sup>, Lianlin Li<sup>1</sup>, and Fang Li<sup>1</sup>

<sup>1</sup>Institute of Electronics, Chinese Academy of Sciences, Beijing 100080, China

<sup>2</sup>Graduate School of Chinese Academy of Sciences, Beijing 100080, China

**Abstract**— In this paper a two-step strategy for inverse scattering from phaseless data in free space is studied. In the first step both the amplitude and phase of the scattered field is reconstructed from the intensity measurement of the total field. This step can be achieved in a very short time and will not add any burden to the whole inverse scattering problem. Then the contrast function is reconstructed in the second step though the inverse source method using the reconstructed scattered field in the first step. With respect to the single-step method the two-step strategy allows better control of the nonlinearity of the whole inverse problem. The above two-step method is validated against experimental data provided by the CCRM center of Fresnel Institute in France. Excellent reconstruction of the scattered field and the dielectric profile has been obtained for inhomogeneous targets. The experiment results also show that the method is very tolerant to noises.

## Electromagnetic Radiation from Ingested Sources in the Human Intestine at the Frequency of 2.4 GHz

L. S. Xu, Max Q.-H. Meng, and H. L. Ren

Department of Electronic Engineering, The Chinese University of Hong Kong, Shatin, Hong Kong, China

**Abstract**— For the assessment of the compliance of high frequency ingested wireless device with the safety guidelines, the radiation effects and the near fields of the 2.4 GHz ingested wireless devices in the realistic human body model are studied by using the finite-difference time-domain (FDTD) method. Simulations are carried out for three orientations at seven source positions. Specification Absorption Rate (SAR), temperature rise, and near fields are analyzed under these scenarios. Results show that 2.4 GHz can be applied as a transmission frequency of human body implanted antenna although radiation effects and link performances vary greatly with the orientations and positions. All the temperature-rises, peaks of SAR and averaged SAR inside the realistic human body exposed to a realistic 2.4 GHz capsule model are under the safety limits at the input power no more than 26.16 mW. The peaks of SAR, maximums of 1g-averaged SAR, 10g-averaged SAR, and temperature-rises are 1.2871, 0.1529, 0.0564 W/kg and 0.0029°C respectively at the normalized input power of 2.5 mW. The orientation of the ingested wireless device has less influence on the wireless link performance than its position in the gastrointestinal tract. To investigate the link performance of wireless devices under the safety guidelines of radiation exposure, we compared two cases: using antenna array and one antenna to receive the signals transmitted from capsule endoscopes respectively. The antenna array can receive near fields 4 dB higher than one receiving antenna can do at least.

# Microwave Thermotherapy — Technical and Clinical Aspects

Jan Vrba

Department of EM Field, Czech Technical University, Technická 2, Prague 16627, Czech Republic

**Abstract**— We would like to describe our new technical results dealing with microwave thermotherapy in the cancer treatment. Our research interest is to develop applicators for deep local heating and for intracavitary cancer treatment as well. Basic evaluation of clinical results is presented. Deep local and regional applicators

**Deep Local and Regional Applicators:** Microwave thermotherapy (hyperthermia) is being used for cancer treatment since early 80's in many countries around the world. Since 1981 we were interested in the local external applicators working at 434 MHz and 2450 MHz. These applicators were used here in Prague for the treatment of more than 500 patients with superficial or subcutaneous tumours (up to the depth of approximately 4 cm). Now, following new trends in this field, we continue our research in two important directions:

- deep local and regional applicators,
- intracavitary applicators.

For the deep local thermotherapy treatment we develop above all waveguide type applicators based on the principle of evanescent mode waveguide, which is our specific solution and original contribution to the theory of microwave hyperthermia applicators. This technology enable us:

- to design applicators with as small aperture as necessary also for the optimum frequency range for deep local and/or for regional thermotherapy treatment (the frequency band between 27 and 70 MHz).
- using our technology we need not to fill the applicator by dielectric (necessary for deep penetration into the biological tissue — i.e., up to 10 centimetres under the body surface).
- two to four of such applicators can be also used for regional treatment.

Waveguide type applicators are often used in the local external hyperthermia treatment of cancer and other modifications of microwave thermotherapy as they offer very advantageous properties, above all:

- depth of penetration of the EM energy approaching the ideal case of plane wave,
- low irradiation of the energy in the vicinity of the hyperthermia apparatus,
- very good impedance matching, i.e., perfect energy transfer to the biological tissue.

We have studied waveguide applicators heating pattern for the aperture excitation at above and at under the cut-off frequency. It has helped us to get analytical approximations of the electromagnetic field distribution in the treated area of the biological tissue. The most important results for the effective heating depth  $d$  can be characterised as follows:

- at high frequencies (above approx. 1000 MHz) the depth of effective heating  $d$  is above all a function of frequency  $f$  (skin effect),
- below approx. 100 MHz  $d$  is the dominantly function of the diameter  $D$  of applicator aperture ( $d = 0.386D$ ).

**Clinical Results:** In the case of cancer treatment the long term statistics of clinical results can be described as follows:

Complete Response of Tumor	.....	53%
Partial Response of the Tumor	.....	31%
No Significant Response	.....	16%

which corresponds to results obtained also by other groups in Europe.

## ACKNOWLEDGMENT

This research is supported by Grant Agency of the Czech Republic, project: “Microwave Imaging for Biomedical Applications” (102/05/0959) and by the research program MSM6840770012 “Transdisciplinary Research in the Area of Biomedical Engineering II” of the CTU in Prague, sponsored by the Ministry of Education, Youth and Sports of the Czech Republic.



# A Physical Model for Study of Electromagnetic Field Interaction with Cancer Cell

D. Sardari<sup>1</sup> and N. Verga<sup>2</sup>

<sup>1</sup>Faculty of Engineering, Science and Research Campus, Azad University, Tehran, Iran

<sup>2</sup>Carol Davila University, Bucharest, Romania

**Abstract**— It has been known that electromagnetic fields are helpful in treatment of disease. It is already shown that electrostatic, magnetostatic, extremely low frequency electromagnetic fields, and pulsed electromagnetic radiation could be utilized in cancer treatment. These radiations alone or in combination with gamma or X-ray improves the healing of cancer tumors. The healing effect depends on frequency and amplitude of electromagnetic radiation. In the present work a physical model is developed to facilitate study the interaction of electromagnetic fields with the living cell. This model consists of an insulating layer as the cell membrane and a conducting colloid inside as the cytoplasm. In this model, electrical properties of a colloidal liquid is specified. This includes charge mobility and electric conductance. The electric field distribution inside and around the cell is studied. Computer code FLUKA is used to study the interaction between the living cell and electromagnetic field.



# Session 3P8a

## Novel Mathematical Methods in Electromagnetics

<p>Plane Wave Diffraction by Two Parallel, Corrugated Half-planes: Evaluation of the Scattered Field  <i>Jianping Zheng (Chuo University, Japan); Kazuya Kobayashi (Chuo University, Japan); .....</i></p> <p>Plane Wave Diffraction by a Terminated, Semi-infinite Parallel-plate Waveguide with Four-layer Material Loading: The Case of <i>H</i> Polarization  <i>Erhao Shang (Chuo University, Japan); Kazuya Kobayashi (Chuo University, Japan); .....</i></p> <p>Propagation Characteristics of Dielectric Waveguides for the Air-hole Type  <i>Tsuneki Yamasaki (Nihon University, Japan); Ryosuke Ozaki (Nihon University, Japan); Takashi Hinata (Nihon University, Japan); .....</i></p> <p>Analysis of the Diffraction by a Dielectric Body in a Waveguide Using the Method of Volume Integral Equations  <i>Yury G. Smirnov (Penza State University, Russia); Kazuya Kobayashi (Chuo University, Japan); Yury V. Shestopalov (Karlstad University, Sweden); .....</i></p> <p>Method of Integral Equations for Solving 3D Electromagnetic Diffraction Problems in a Perturbed Layer Using Parallel Computations  <i>Yury V. Shestopalov (Karlstad University, Sweden); Yury G. Smirnov (Penza State University, Russia); .....</i></p> <p>Using Preconditioners for Numerical Solution of Integral Equations of Electromagnetics  <i>Alexander B. Samokhin (Moscow Institute of Radio Engineering, Electronics and Automatics, Russia); Ilya Fedotov (Moscow Institute of Radio Engineering, Electronics and Automatics, Russia); .....</i></p> <p>Decompositional Algorithm for Determining Descriptors of Nonlinear Autonomous Blocks with Floquet Channels Using the Iterative Method  <i>Galina S. Makeeva (Penza State University, Russia); Oleg A. Golovanov (Penza Military Institute of Artillery, Russia); Martha Pardavi-Horvath (The George Washington University, USA); .....</i></p> <p>The Iteration Algorithm of Recomposition of Nonlinear Autonomous Blocks with Floquet Channels Using S-Matrices of Linearized Blocks  <i>Galina S. Makeeva (Penza State University, Russia); Oleg A. Golovanov (Penza Military Institute of Artillery, Russia); Martha Pardavi-Horvath (The George Washington University, USA); .....</i></p>	<p>708</p> <p>709</p> <p>710</p> <p>711</p> <p>712</p> <p>713</p> <p>714</p> <p>715</p>
--	---

## Plane Wave Diffraction by Two Parallel, Corrugated Half-planes: Evaluation of the Scattered Field

J. P. Zheng and K. Kobayashi

Chuo University, Japan

**Abstract**— The analysis of wave scattering by gratings and waveguides with periodic structures is important in electromagnetic theory and optics. Various analytical and numerical methods have been developed so far and the diffraction phenomena have been investigated for many kinds of periodic structures. However, there are only a few treatments of the diffraction by periodic structures using rigorous function-theoretic methods. Das Gupta [1] analyzed the plane wave diffraction by a half-plane with sinusoidal corrugation by means of the Wiener-Hopf technique together with the perturbation method. The results presented in [1] have been generalized thereafter by Chakrabarti and Dowerah [2] for the analysis of the  $H$ -polarized plane wave diffraction by two parallel sinusoidal half-planes using the Wiener-Hopf technique. We have considered a finite sinusoidal grating as another important generalization and analyzed the plane wave diffraction by means of the Wiener-Hopf technique [3].

In our previous papers [4–6], we have reconsidered the problem treated by Chakrabarti and Dowerah [2], and analyze the  $E$ -polarized plane wave diffraction by two parallel corrugated half-planes using the Wiener-Hopf technique together with the use of the perturbation method. This paper is in continuation with our previous papers [4–6]. In particular, we shall evaluate the scattered field explicitly based on the results obtained in [4–6]. The field inside the waveguide is expressed in terms of a waveguide mode series, whereas the field outside the waveguide is evaluated asymptotically using the saddle point method leading to a uniform far field expression.

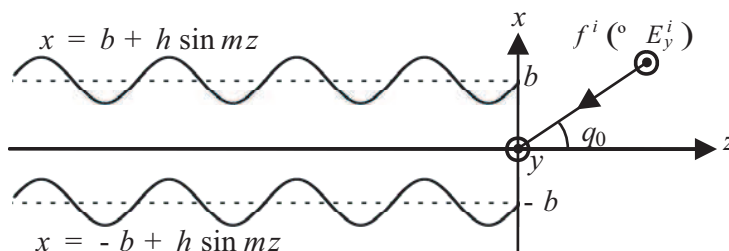


Figure 1: Geometry of the problem.

### REFERENCES

1. Das Gupta, S. P., "Diffraction by a corrugated half-plane," *Proc. Vib. Prob.*, Vol. 3, 413–424, 1970.
2. Chakrabarti, A. and S. Dowerah, "Traveling waves in a parallel plate waveguide with periodic wall perturbations," *Can. J. Phys.*, Vol. 62, 271–284, 1984.
3. Kobayashi, K. and T. Eizawa, "Plane wave diffraction by a finite sinusoidal grating," *IEICE Trans.*, Vol. E74, 2815–2826, 1991.
4. Zheng, J. P. and K. Kobayashi, "Plane wave diffraction by two parallel, corrugated half-planes," *IEEJ Technical Report*, No. EMT-07-39, May 2007.
5. Zheng, J. P. and K. Kobayashi, "Wiener-Hopf analysis of the plane wave diffraction by two parallel, corrugated half-planes," *Proc. 2007 URSI International Symposium on Electromagnetic Theory (EMTS 2007)*, O11-32-6, July 2007.
6. Zheng, J. P. and K. Kobayashi, "Combined perturbation and Wiener-Hopf analysis of the diffraction by two parallel, corrugated half-planes," *Proc. Progress In Electromagnetics Research Symposium (PIERS 2007)*, 59, Prague, August 2007.

# Plane Wave Diffraction by a Terminated, Semi-infinite Parallel-plate Waveguide with Four-layer Material Loading: The Case of $H$ Polarization

E. H. Shang and K. Kobayashi

Chuo University, Japan

**Abstract**— The analysis of the scattering by open-ended waveguide cavities is an important subject in the prediction and reduction of the radar cross section (RCS) of a target. In the previous papers [1, 2], we have considered a terminated, semi-infinite parallel-plate waveguide with three-layer material loading as a canonical two-dimensional cavity geometry, and analyzed the plane wave diffraction for both  $E$  and  $H$  polarizations rigorously using the Wiener-Hopf technique. It has been shown via numerical computation that our Wiener-Hopf solutions are uniformly valid for arbitrary cavity dimensions. As a generalization of the problems analyzed in [1, 2], we have considered in [3–5] a terminated, semi-infinite parallel-plate waveguide with four-layer material loading, and solved the  $E$ -polarized plane wave diffraction by means of the Wiener-Hopf technique.

In this paper, we shall consider the same waveguide geometry as in [3–5], and analyze the diffraction problem for the  $H$ -polarized plane wave incidence using the Wiener-Hopf technique. The analysis procedure is similar to that for the case of  $E$  polarization [3–5]. Taking the Fourier transform of the unknown scattered field and applying boundary conditions in the transform domain, the problem is formulated in terms of the simultaneous Wiener-Hopf equations. The Wiener-Hopf equations are solved via the factorization and decomposition procedure leading to the exact solution. Taking the inverse Fourier transform of the solution in the transform domain, the scattered field inside and outside the waveguide is evaluated explicitly. Representative numerical examples of the RCS are presented and the backscattering characteristics of the waveguide are discussed in detail.

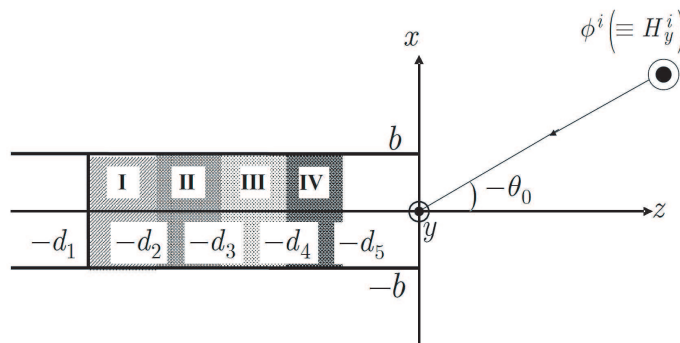


Figure 1: Geometry of the problem.

## REFERENCES

1. Koshikawa, S. and K. Kobayashi, "Diffraction by a terminated, semi-infinite parallel-plate waveguide with three-layer material loading," *IEEE Trans. Antennas Propagat.*, Vol. 45, 949–959, 1997.
2. Koshikawa, S. and K. Kobayashi, "Diffraction by a terminated, semi-infinite parallel-plate waveguide with three-layer material loading: the case of  $H$  polarization," *Electromagnetic Waves & Electronic Systems*, Vol. 5, 13–23, 2000.
3. Shang, E. H. and K. Kobayashi, "Diffraction by a terminated, semi-infinite parallel-plate waveguide with four-layer material loading," *IEEJ Technical Report*, No. EMT-07-38, May 2007.
4. Shang, E. H. and K. Kobayashi, "Diffraction by a terminated, semi-infinite parallel-plate waveguide with four-layer material loading," *Proc. 2007 URSI International Symposium on Electromagnetic Theory (EMTS 2007)*, O11-32-2, July 2007.
5. Shang, E. H. and K. Kobayashi, "Wiener-Hopf analysis of the diffraction by a terminated, semi-infinite parallel-plate waveguide with four-layer material loading," *Proc. Progress In Electromagnetics Research Symposium (PIERS 2007)*, 58, Prague, August 2007.

## Propagation Characteristics of Dielectric Waveguides for the Air-hole Type

Tsuneki Yamasaki, Ryosuke Ozaki, and Takashi Hinata

Department of Electrical Engineering, College of Science and Technology, Nihon University  
1-8-14, Surugadai Kanda Chiyoda-ku, Tokyo, 101-8308, Japan

**Abstract**— Recently, in the optical gratings, the inhomogeneous dielectric gratings are widely used in photonic crystal. Because, the refractive index can easily be controlled to make periodic structures by the development of manufacturing technology of optical devices. Accordingly, the numerical methods which are applicable to inhomogeneous dielectric gratings have been proposed. However, it is not in detail treated the propagation characteristic in the photonic band gap regions.

In this paper, the guiding problems of electromagnetic waves by inhomogeneous dielectric waveguides with both circular air-hole type and rectangular air-hole type are analyzed using the combination of Fourier series expansion method and multilayer method. Our approach for the multilayer method differs from that of other method, so that the order of characteristic matrix equation depends on the modal truncation number, but it does not depend on the number of layers. Therefore our method is effective to the guiding problems of multilayer dielectric waveguides.

Numerical results are given for the propagation characteristics for dielectric waveguides with both circular air-hole type and rectangular air-hole type for TE and TM modes. It is also discussed for the propagation constants by the varying of the radius ( $r = d_1/2$ ), where rectangular air-hole is kept fixed and with the laterally shifting periodically layers.

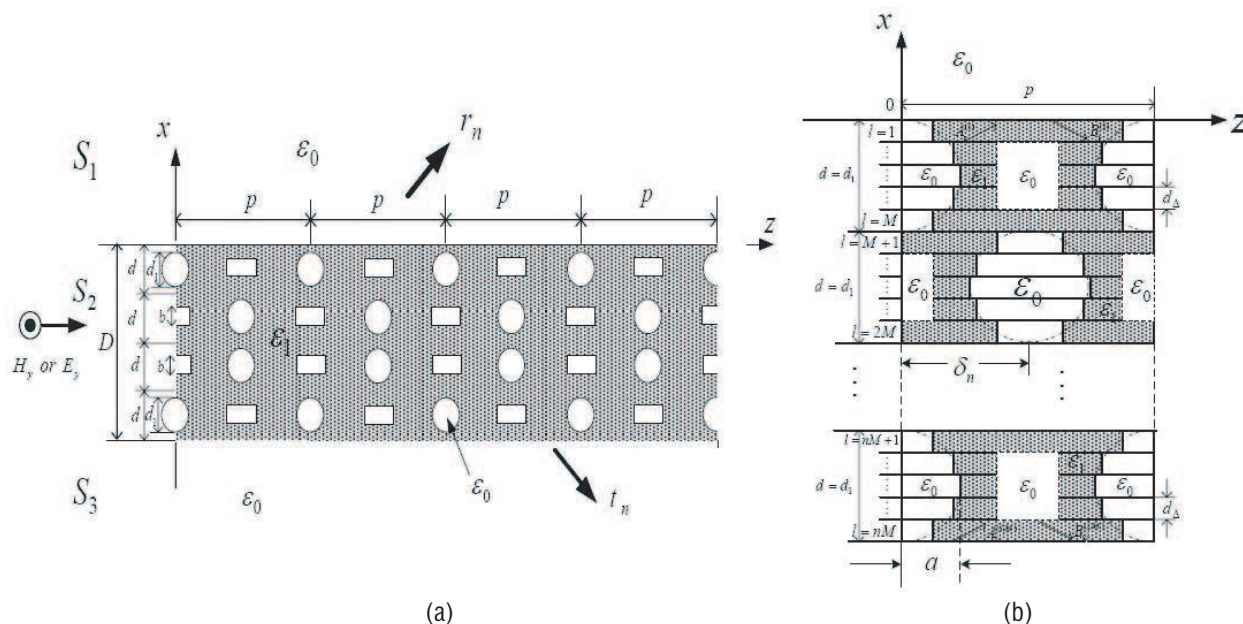


Figure 1: Structure of inhomogeneous dielectric waveguides with both circular air-hole type and rectangular air-hole type, (a) Coordinate system, (b) Approximated air-hole layer.

# Analysis of the Diffraction by a Dielectric Body in a Waveguide Using the Method of Volume Integral Equations

Yu. G. Smirnov<sup>1</sup>, K. Kobayashi<sup>2</sup>, and Yu. V. Shestopalov<sup>3</sup>

<sup>1</sup>Penza State University, Penza, Russia

<sup>2</sup>Chuo University, Tokyo, Japan

<sup>3</sup>Karlstad University, Karlstad, Sweden

**Abstract**— We consider the diffraction of an external electromagnetic field by a locally inhomogeneous dielectric body in a perfectly conducting waveguide of rectangular cross section. The analysis of diffraction by dielectric bodies in resonators and waveguides is important for modeling the processes that take place in microwave ovens and when the scattering of electromagnetic fields by biological objects is considered. Such problems can be solved numerically by the finite element method. However, the direct use of this method is connected with certain difficulties. First, the corresponding boundary value problem (BVP) for Maxwell's equations investigated in [1] is not an elliptic one; therefore, the standard schemes [2] for the proof of the convergence of projection methods cannot be applied. Second, in order to ensure an acceptable accuracy of the calculation of the field in a body with the dielectric constant varying within the range of values from 10 to 20 (when the obstacle mainly consists of water), a fine grid within the inhomogeneity region must be used, which requires that the grid outside the obstacle must be also fine (note that the use of different grid size inside and outside the body gives incorrect results). Since the problem is three-dimensional, the matrices that appear in the finite element method after discretization of the problem are sparse and have a very high order.

We develop the method of volume singular integral equations (VSIE) [3] which is to a big extent free of those drawbacks. In this method, the resulting VSIE operator is elliptic and the integral equation is solved only inside the body (in the inhomogeneity region). We analyze the VSIE on the basis of the corresponding BVP using the equivalence of this BVP and the integral equation. This enables us to prove the existence and uniqueness theorem for the solution of VSIE in the space of square-integrable functions and obtain some results concerning the solutions of BVP. A numerical Galerkin method for the VSIE solution is proposed and its convergence is proved, and some results of numerical experiments are presented.

## REFERENCES

1. Ilinski, A. S. and Yu. G. Smirnov, *Electromagnetic Wave Diffraction by Conducting Screens*, Y. Shestopalov, Ed., VSP Int. Science Publishers, Utrecht, Boston, Köln, Tokyo, 1998.
2. Kress, R., *Linear Integral Equations, Applied Mathematical Sciences*, Vol. 82, Springer-Verlag, New York, 1989.
3. Samokhin, A. B., *Integral Equations and Iteration Methods in Electromagnetic Scattering*, Y. Shestopalov, Ed., VSP Int. Science Publishers, Utrecht, Boston, Köln, Tokyo, 2001.

# Method of Integral Equations for Solving 3D Electromagnetic Diffraction Problems in a Perturbed Layer Using Parallel Computations

Y. V. Shestopalov<sup>1</sup> and Y. G. Smirnov<sup>2</sup>

<sup>1</sup>Karlstad University, Karlstad, Sweden

<sup>2</sup>Penza State University, Penza, Russia

**Abstract**— Boundary value problems (BVPs) for the Maxwell equations in dielectric or magnetic layers with perturbed boundaries arise in mathematical models of electromagnetic wave propagation in irregular waveguides; some typical statements are surveyed in [1]. We develop the solution techniques on the basis of the approach set forth in [2, 3]; the problems in question are reduced to BVPs for the Helmholtz equation, and the BVPs in a layer with perturbed boundaries are considered in Sobolev spaces.

Reduction of BVPs to surface integral equations (IEs) on manifolds with edges is applied in [1] for solving electromagnetic diffraction problems. The IE method enables one to decrease the dimension of the problem and offers a solution technique applicable in domains where the methods based on discretization fail or meet substantial difficulties.

In this study we apply a method of solution to the Dirichlet BVP for the Helmholtz equation in a three-dimensional layer with a local perturbation  $S$  of the boundary based on equivalent reduction to a boundary IE over  $S$ . We prove the unique solvability of the IE and its Fredholm property.

Galerkin method [4] is applied for numerical solution of the problems. The convergence is proved for the numerical method; parallel algorithms and computational techniques are developed, specifically when the boundary perturbation  $S$  consists of a set of many disjoint irregularities. Various numerical results are presented and discussed.

## ACKNOWLEDGMENT

This work is supported by Russian Foundation of Basic Research, grant 06-07-89063.

## REFERENCES

1. Ilyinskii, A. S. and Y. G. Smirnov, *Electromagnetic Wave Diffraction by Conducting Screens*, VSP Int. Sci. Publ., Utrecht, 1998.
2. Morgenröther, K. and P. Werner, “On the principles of limiting absorption and limit amplitude for a class of locally perturbed waveguides. Part 1: time-independent theory,” *Math. Meth. in the Appl. Sci.*, Vol. 10, 125–144, 1988.
3. Werner, P., “Resonance phenomena in local perturbations of parallel-plane waveguides,” *Math. Meth. in the Appl. Sci.*, Vol. 19, 773–823, 1996.
4. Stephan, E. P., “Boundary integral equations for screen problems in  $\mathbb{R}^3$ ,” *Journal of Integral Equations and Operator Theory*, Vol. 10, 236–257, 1987.



# Using Preconditioners for Numerical Solution of Integral Equations of Electromagnetics

**Alexander Samokhin and Ilya Fedotov**

Moscow Institute of Radio Engineering, Electronics and Automatics  
78, Vernadsky av., Moscow 117454, Russia

**Abstract**— Many of tasks in mathematical modeling demand integral equations numerical solution. Matter of computational resources rises up in case of multidimensional equations; situation often becomes more complicated due to non-efficient conditionality and slow convergence iteration methods. The number of iterations required in such cases may be estimated by thousands. Therefore we face the issue of reducing required number of iterations, i.e., increase of convergence rate. One way to increase convergence rate is to use preconditioners.

In this report we propose algorithm of preconditioner construction for numerical solution of integral equations of electromagnetics; the preconditioner based on functional nature of arising linear algebraic equations system. Approximation of integral equations on coarse grid allows to construct the preconditioner and requires few computational resources. In particular, the preconditioner constructed reduces the number of iterations for numerical solution of singular volume integral equations that describe electromagnetic scattering problem on three-dimensional dielectric bodies.

# Decompositional Algorithm for Determining Descriptors of Nonlinear Autonomous Blocks with Floquet Channels Using the Iterative Method

Galina S. Makeeva<sup>1</sup>, Oleg A. Golovanov<sup>2</sup>, and Martha Pardavi-Horvath<sup>3</sup>

<sup>1</sup>Penza State University, Krasnaya, 40, Penza 440026, Russia

<sup>2</sup>Penza Military Institute of Artillery, Penza-5 440005, Russia

<sup>3</sup>Department of Electrical and Computer Engineering  
The George Washington University, Washington, D.C. 20052, USA

**Abstract**— The decompositional approach using the descriptors of autonomous blocks (ABs) as multimode multichannel scattering matrices [1] is available for solving nonlinear boundary problems only in case of ABs filled with “weakly” nonlinear medium. We consider nonlinear AB with Floquet channels (NFAB) in the form of rectangular parallelepiped filled with the homogeneous “strong” nonlinear media and having on its bounds virtual rectangular waveguides with periodic boundary conditions (Floquet channels) as a “waveguide transformer” [1]. The dependence of magnitudes of incident modes on magnitudes of reflected modes on input cross-sections of NFAB is described by nonlinear equations (the descriptor of NFAB).

The computational algorithm for determining of descriptors of NFAB was created using the method of simple iteration. At an each step of iteration the 3D nonlinear diffraction problem based on nonlinear Maxwell’s equations with non-asymptotic radiation boundary conditions [1] on bounds of NFAB was solved.

We find the solution of linearized Maxwell’s equations in the matrix form using multimode scattering matrices of linearized FABs [1] and the radiation vector [2]. We determine the radiation vector by solving the problems of excitation of NFAB by equivalent currents using Vainstein’s method [2]. For the transition to the next step of iteration we redefine the equivalent currents. For this purpose we find electromagnetic fields in the form of reduced series on the eigen fields of rectangular resonators with magnetic or electric walls. Using the projecting model [3] we obtain the system of linear algebraic equations and determine unknown magnitude coefficients in these series .

## ACKNOWLEDGMENT

The work of G. S. Makeeva and O. A. Golovanov was supported by THE RUSSIAN FOUNDATION FOR BASIC RESEARCH, Grant No. 05-08-33503-a.

## REFERENCES

1. Makeeva, G. S. and O. A. Golovanov, *Physics of Wave Processes and Radiotechnics Systems*, Vol. 8, No. 4, 10, 2005.
2. Vainstein, L. A., *Electromagnetic Waves*, M. Radio i Sviaz, 1988.
3. Nikolskiy, V. V., *Izvestiya Vuzov Radiofizika*, Vol. 20, No. 1, 5, 1977.

# The Iteration Algorithm of Recomposition of Nonlinear Autonomous Blocks with Floquet Channels Using S-Matrices of Linearized Blocks

Galina S. Makeeva<sup>1</sup>, Oleg A. Golovanov<sup>2</sup>, and Martha Pardavi-Horvath<sup>3</sup>

<sup>1</sup>Penza State University, Krasnaya, 40, Penza 440026, Russia

<sup>2</sup>Penza Military Institute of Artillery, Penza-5 440005, Russia

<sup>3</sup>Department of Electrical and Computer Engineering  
The George Washington University, Washington, D.C. 20052, USA

**Abstract**— The iterative electrodynamic method of the recomposition of nonlinear autonomous blocks with Floquet channels (NFABs) based on the linearization of descriptors is developed to solve nonlinear 3D diffraction boundary problems for 3D nonlinear microwave devices by using the decompositional algorithm.

Using simple iterations at an each step the descriptor of NFAB are replaced by descriptors of linearized NFABs as multimode multichannel scattering matrices. After then the recomposition of NFABs in accordance with the decomposition scheme [1] of 3D microwave devices is realized.

We represent the nonlinear functions (the dependences of magnitudes of incident modes on the magnitudes of reflected modes on input cross-sections of NFAB) with Taylor's series. Taking into account the partial derivatives up to the first order inclusive in the Taylor's series we reduce the system of nonlinear equations to the system of linear equations at the first approximation. It results the linearized dependences in the matrix form using the S-matrices of NFABs, arranged on combination frequencies, Floquet channels and eigenwaves, and taking into account a radiation vector [2]. We calculate the scattering parameters of these S-matrices using the first order partial derivatives of nonlinear functions. The decomposition scheme of the substitution of NFAB by linearized NFAB with the descriptor as the S-matrix is developed using the auxiliary fictive ABs in the goal to realize a recognizing access for controlling the iterative computational process. At the each iteration we obtain the approximate S-matrix of 3D nonlinear microwave device by combining the S-matrices of linearized NFABs into the decomposition scheme.

## ACKNOWLEDGMENT

The work of G. S. Makeeva and O. A. Golovanov was supported by THE RUSSIAN FOUNDATION FOR BASIC RESEARCH, Grant No. 05-08-33503-a.

## REFERENCES

1. Makeeva, G. S. and O. A. Golovanov, *Physics of Wave Processes and Radiotechnics Systems*, Vol. 8, No. 4, 10, 2005.
2. Vainstein, L. A., *Electromagnetic Waves*, M. Radio i Sviaz, 1988.



# Session 4A1a

## Modelling and Simulations of Nanophotonic Devices

Counter-directional Coupling between Silica Wire and Photonic Crystal Waveguide for Slow Light Generation	
<i>Ziyang Zhang (Royal Institute of Technology (KTH), Sweden); Min Qiu (Royal Institute of Technology (KTH), Sweden); Ulf Andersson (Royal Institute of Technology (KTH), Sweden); .....</i>	718
A Specific Architectures of CMOS Readout for Resonant-cavity-enhanced Devices	
<i>G. Z. Zhan (East China Normal University, China); Fangmin Guo (East China Normal University, China); Wei Lei (East China Normal University, China); J. Huang (East China Normal University, China); Z. Q. Zhu (East China Normal University, China); Junhao Chu (Shanghai Institute of Technical Physics, Chinese Academy of Sciences, China); .....</i>	719
Analyzing the Photovoltaic Characteristic of Carbon Nanotube Device Using Electromagnetic Scattering Model	
<i>Liu Yang (Shanghai Jiaotong University, China); Gaobiao Xiao (Shanghai Jiao Tong University, China); .....</i>	720
Design of Reusable and Flexible Test Access Mechanism Architecture for System-on-Chip	
<i>G. Rohini (St. Joseph's College of Engineering, India); S. Salivahanan (SSN College of Engineering, India); .....</i>	721
Semiconductor Buried-layer Nanopore Photonic Devices	
<i>Michael P. Bradley (University of Saskatchewan, Canada); .....</i>	722

# Counter-directional Coupling between Silica Wire and Photonic Crystal Waveguide for Slow Light Generation

Ziyang Zhang<sup>1</sup>, Min Qiu<sup>1</sup>, and Ulf Andersson<sup>2</sup>

<sup>1</sup>Department of Microelectronics and Applied Physics, Royal Institute of Technology (KTH)  
Electrum 229, 164 40 Kista, Sweden

<sup>2</sup>Center for Parallel Computers, Royal Institute of Technology (KTH)  
100 44 Stockholm, Sweden

**Abstract**— Studies of slow light in two-dimensional photonic crystal slab waveguide have been intensified recently. The applications include compact delay lines for photonic signal processing, dispersion management, enhanced light/matter interaction for lasing and etc. To couple slow light efficiently from a connected dielectric waveguide, a special interface or a mode converter has to be designed. Alternatively, we investigate the evanescent counter-directional coupling between subwavelength-diameter silica wire and photonic crystal waveguide for slow light generation.

The simulations are done using three-dimensional finite-difference time-domain method (3D FDTD). The code, MBfrida, is part of the GEMS suite from Efield AB and is fully parallelized using Message Passing Interface. The computation domain for FDTD updating can be freely divided in three dimensions and the power computation through certain planes can also be divided two-dimensionally.

From the simulations, we have seen an interesting phenomenon that the coupling efficiency improves greatly when the coupling central wavelength moves to the slow light region. To control the coupling point of the two waveguides, one can modify the silica wire properties, i.e., the material refractive index, or more realistically, engineer the dispersion band of the photonic crystal waveguide. We find that by shrinking the line defect width, the dispersion band of the photonic crystal waveguide is effectively flattened at the coupling point, allowing slow light operation. One design gives 82% peak power transmission from silica wire to photonic crystal waveguide over an interacting distance of 50 lattice constants. The group velocity is estimated as 1/35 of light speed in vacuum.

From coupled mode analysis, we find there is a balance between the group velocity and coupling bandwidth in order to achieve optimal coupling efficiency. Though, the dispersion band can be further flattened and group index 40.2 is reached, the coupling bandwidth drops down quickly and the coupling efficiency is reduced to 58%.

## A Specific Architectures of CMOS Readout for Resonant-cavity-enhanced Devices

G. Z. Zhan, F. M. Guo, W. Lei, J. Huang, Z. Q. Zhu, and J. H. Chu

College of Information Science and Technology, East China Normal University, Shanghai 200062, China

**Abstract**— The resonant-cavity enhanced (RCE) photo-detectors have the properties such as wavelength-selectivity, high quantum efficiency, and high-speed response.

Performances of a 1064 nm resonant-cavity-enhanced photodetector (RCE2PD) are investigated. A detailed theoretical analysis on the quantum efficiency of a resonant cavity enhanced (RCE) photo-detector at wavelength of 1.06  $\mu\text{m}$ . High reflectivity AlAs/GaAs DBR used in the device. Under the simulation could find out the optimum periods DBR for RCE photodiodes. And the MQW detector parameters are optimized.

## Analyzing the Photovoltaic Characteristic of Carbon Nanotube Device Using Electromagnetic Scattering Model

Liu Yang and Gaobiao Xiao

Department of Electronic Engineering, Shanghai Jiaotong University  
Dongchuan Road 800, Shanghai 200240, China

**Abstract**— The photovoltaic characteristic of the carbon nanotube such as photoinduced current, absorbed energy, and so on, is critical to the research of the carbon nanotube device-photovoltaic cell. However, it is not a easy task to get the parameter of these characteristics through experiment, so theoretical analysis and computer simulation is necessary and efficient in the research of photovoltaic characteristic of the device. In this paper, we study the absorbed energy of the carbon nanotube photovoltaic cell which was exposed in laser or sunlight. The exciting light to the device was treated as common electromagnetic wave whose frequency is in the frequency band of visible light, about several hundred THz; and the carbon nanotube was treated as a lossy dielectric body with frequency-dependent complex permittivity which could be derived from the quantum theory of carbon nanotube. With some appropriate simplifications of the structure of the device, the corresponding electromagnetic scattering model would be set up. According to the scattering theory, using the dyadic Green's function, the EFIE(electric filed integral equation) of the simplified model of the device could then be conveniently established. In the practical application, periodic carbon nanotube array may be used more often. In this case, based on the single carbon nanotube model above and Floquet theory, we can establish the EFIE for the periodic array device in a similar way. Numerical results of EFIE is presented, and the relationship between the absorbed energy and the frequency can be observed. Through the commercial computational electromagnetic software HFSS, the results and the rationality of the scattering model of this device was validated.



## Design of Reusable and Flexible Test Access Mechanism Architecture for System-on-Chip

G. Rohini<sup>1</sup> and S. Salivahanan<sup>2</sup>

<sup>1</sup>St. Joseph's College of Engineering, Chennai 600 119, India

<sup>2</sup>SSN College of Engineering, Kalavakkam 603 110, India

**Abstract**— Recent advances in IC design methods and manufacturing technologies have led to the integration of a complete system onto a single IC, called system on chip (SoC). These system chips offer advantages such as higher performances, lower power consumption, and decreased size and weight, when compared to their traditional multichip equivalents. However, testing such core-based SoCs poses a major challenge for system integrators. Modular testing of embedded cores in a system-on-chip (SoC) is now recognized as an effective method to tackle the SoC testing problem. In this paper we present an approach to design a TAM architecture and its associated test schedule using a fast and efficient heuristic. The test access mechanism architecture is responsible for the transportation of the test data from the system inputs to the core inputs and from the core outputs to the system outputs and also it could be very useful testing multi-frequency cores in SoC.

## Semiconductor Buried-layer Nanopore Photonic Devices

**Michael P. Bradley**

Department of Physics & Engineering Physics, University of Saskatchewan  
Saskatoon, SK S7N 5E2, Canada

**Abstract**— High dose plasma-based ion implantation provides a new tool for the efficient production of buried-layer semiconductor devices. These buried-layer devices exhibit properties radically different from those of the bulk semiconductors from which they are derived. The properties differ from those of the bulk devices because of the structural modifications which take place on the nanometer scale due to the high-dose ion implantation and the subsequent processing steps. In my laboratory at the University of Saskatchewan we have been able to fabricate a variety of new electroluminescent devices based on nanostructured buried layers in semiconductor matrices. In this talk I will report on the performance of these devices and the fabrication methods used, and also discuss some preliminary ideas for modelling the performance of these devices.

# Session 4A1b

## Nano Scale Electromagnetics, MEMS 2

Design and Simulation of Modified 1-D Electrostatic Torsional Micromirrors with $z$ -axis Displacement	
<i>Lijie Li (University of Strathclyde, UK); Deepak Uttamchandani (University of Strathclyde, UK); Mark Begbie (The Institute for System Level Integration, UK); .....</i>	724
Design and Characterization of a Radio Frequency MEMS Inductor Using Silicon MEMS Foundry Process	
<i>Deepak Uttamchandani (University of Strathclyde, UK); Lijie Li (University of Strathclyde, UK); ..</i>	725
A Concept of Moving Dielectrophoresis Electrodes Based on Microelectromechanical Systems (MEMS) Actuators	
<i>Lijie Li (University of Strathclyde, UK); Deepak Uttamchandani (University of Strathclyde, UK); ..</i>	726
Micro-machined Magnetometers Applied for Nano- and Pico- Satellites	
<i>Zheng You (Tsinghua University, China); Jianzhong Yang (Tsinghua University, China); .....</i>	727

## Design and Simulation of Modified 1-D Electrostatic Torsional Micromirrors with $z$ -axis Displacement

Lijie Li, Deepak Uttamchandani, and Mark Begbie

The Institute for System Level Integration, Alba Campus

Livingston, Scotland EH54 7EG, UK

**Abstract**— Micromirrors based on Micromechanical systems (MEMS) have been essential components in many applications, such as micro confocal microscopy, optical data storage and biomedical imaging [1–3]. A variety of microfabrication and actuation technologies have been used to realize micromirrors, including electrothermal [3], electrostatic [1], etc., of which electrostatic torsional drive has been thought to be the most popular driving mechanism. K. E. Peterson [4] has developed the world first 1-D electrostatic driven torsional micromirror. The Lucent [5] Lambdrouter is one of famous and successful examples of 2-D electrostatic torsional micromirrors. For design improvement of this type of 2-D micromirror, Toshiyoshi et al. [6] have proposed a linearization method based on applying a small control voltage over a large bias voltage. Chiou et al. [7] have presented improved design to demonstrate linear stepping angles of 1-D micromirrors based on multiple electrodes. These developments are focus on realizing linear steps in angle. As mentioned by above articles, there are also displacements in  $z$ -axis as the micromirror is actuated, which have been ignored. The  $z$ -axis displacements have become a significant problem when the micromirrors are used on high resolution spatial scanning. Krishnamoorthy et al. [8] presents a dual-mode 1-D micromirror utilizing stacked multilayer vertical comb drive actuators, which can provide both piston and tilt motion. We have developed a  $z$ -axis displacement compensation concept for 2-D electrostatic torsional micromirrors previously [9].

## Design and Characterization of a Radio Frequency MEMS Inductor Using Silicon MEMS Foundry Process

Deepak Uttamchandani and Lijie Li

Department of Electronic and Electrical Engineering  
University of Strathclyde, Glasgow G1 1XW, UK

**Abstract**— A successful design of RF inductor based on a silicon MEMS foundry process is presented. The suspended inductor has been realized in electroplated thick nickel with front side bulk micromachining of the substrate. The overall size of the inductor is about  $1\text{ mm} \times 1\text{ mm}$ . The inductors have been experimentally characterized and inductances around  $2\text{ nH}$  in the frequency range of  $200\text{ MHz}$ – $7\text{ GHz}$  have been measured with self resonant frequency of  $9.8\text{ GHz}$ . The peak measured value of the Q factor is 12 at a frequency of  $4\text{ GHz}$ . After de-embedding, the Q factor reaches 13 at a frequency of  $4.8\text{ GHz}$ . Simulation based on a parameter extraction method has been carried out for the inductor. There is a good agreement between simulated and experimental results.

## A Concept of Moving Dielectrophoresis Electrodes Based on Microelectromechanical Systems (MEMS) Actuators

Lijie Li and Deepak Uttamchandani

Department of Electronic and Electrical Engineering  
University of Strathclyde, Royal College Building, G1 1XW, UK

**Abstract**— A concept of moving dielectrophoresis electrodes (MDEP) based on Microelectromechanical Systems (MEMS) actuators is introduced in this letter. An example design of tuneable dielectrophoresis filter is presented. Finite Element Analysis of the electrostatic field of the tuneable filter has been conducted. Results show that the trapping force can be adjusted by actuating the MEMS actuators.

## Micro-machined Magnetometers Applied for Nano- and Pico-Satellites

Zheng You and Jianzhong Yang

Department of Precision Instruments and Mechanology  
Tsinghua University, Beijing 100084, China

**Abstract**— Fluxgate magnetic sensors are widely applied since it appeared in early 1930s. They are vector devices which are used to measure the components of magnetic fluxes density vector at one certain point of the dc or low-frequency ac magnetic fields up to 1mT. The theory exploited is based on the saturation of ferromagnetic materials. They have the resolution of 0.1–10 nT, even up to 10 pT, and the absolute precision of 1 nT to 100 nT. Compared with recent anisotropy magnetoresistance (AMR) and giant magnetoresistance (GMR) solid-state magnetic sensors, they have higher temperature stability and better long-term stability as the most primary reasons for their extensive application in satellites and other space vehicles.

Micro fluxgate magnetometers (MFGM), which are based on CMOS or MEMS technology, appeared in 1990s. By compared with traditional fluxgate magnetic sensor, MFGM has some advanced features, such as less mass, smaller size, less power consumption, better performance and batch production. The original goal is to apply of them to hand-held and portable equipments. In addition, there are broad applications in many fields, such as to geomagnetic detection, scientific research, automation, process control of industry, mineral prospecting, and medical appliance, particularly Nano- and/or Pico-Satellites. It is our primary objective to design and microfabricated MFGM as a necessary part of Attitude Determination and Control Subsystem (ADCS) of micro-satellites, used to obtain information about the attitude of the satellite individually or in combination with other parts such as Micro Inertial Measurement Unit (MIMU).

Based on MEMS technology, MEMSMag, a novel type of MFGM( Micro Fluxgate Magnetometer), which exploits magnetic fluxgate principle, has been designed. It has symmetrical geometry, and is flexible for electrical connection, easy to form as a two-axis or a one-axes vector sensor. MEMSMag is easily assembled into a 3-axis subminiature magnetometer and can be applied to measure vector of the weak geomagnetic field. The microfabrication process has been developed. The UV lithography technology in combination with thick positive photoresist was exploited in the microfabrication. The original samples have been produced with the dimension of 1 cm × 1 cm × 100 μm. MEMSMag can be widely applied in the conventional and potential fields, for examples, scientific research, automation, process control of industry, mineral prospecting, medical appliance, especially in micro-satellite (including nano-satellite and pico-satellite) missions.





# Session 4A2a

## 3D Femtosecond Laser Microprocessing of Transparent Materials

<b>Attosecond Physics</b>	
<i>Ferenc Krausz (Ludwig-Maximilians-Universität München, Germany);</i> .....	730
<b>3D Femtosecond Laser Micromachining by Two Photon Polymerization Technique</b>	
<i>Andreas Ostendorf (Laser Zentrum Hannover e. V., Germany);</i> .....	731
<b>Holographic Femtosecond Laser Processing and Three-dimensional Recording in Biological Tissues</b>	
<i>Y. Hayasaki (The University of Tokushima, Japan);</i> .....	732
<b>Single Femtosecond Laser-induced Periodic Microstructures</b>	
<i>Jianrong Qiu (Zhejiang University, China); J. Song (Shanghai Institute of Optics and Fine Mechanics, Chinese Academy of Sciences, China); Zhizhan Xu (Shanghai Institute of Optics and Fine Mechanics, Chinese Academy of Sciences, China); K. Miura (Kyoto University, Japan); K. Hirao (Kyoto University, Japan);</i> .....	733
<b>Nonlinear Pulse Propagation, Filamentation and Refractive Index Change in Glass</b>	
<i>R. Vallée (UniversitéLaval, Canada); Q. Sun (UniversitéLaval, Canada); A. Salimonia (UniversitéLaval, Canada); See Leang Chin (UniversitéLaval, Canada);</i> .....	734
<b>Photonic Waveguide Devices Directly Written into Dielectric Materials Using Femtosecond Laser Pulses</b>	
<i>Martin Ams (Macquarie University, Australia); Graham D. Marshall (Macquarie University, Australia); Peter Dekker (Macquarie University, Australia); Michael Withford (Macquarie University, Australia);</i>	735

# Attosecond Physics

Ferenc Krausz

Max-Planck-Institut für Quantenoptik, Garching  
Ludwig-Maximilians-Universität München, Germany

**Abstract**— Fundamental processes in atoms, molecules, as well as condensed matter are triggered or mediated by the motion of electrons inside or between atoms. Electronic dynamics on atomic length scales tends to unfold within tens to thousands of attoseconds (1 attosecond [as] =  $10^{-18}$  s). Recent breakthroughs in laser science are now opening the door to watching and controlling these hitherto inaccessible microscopic dynamics.

The key to accessing the attosecond time domain is the control of the electric field of (visible) light, which varies its strength and direction within less than a femtosecond (1 femtosecond = 1000 attoseconds). Atoms exposed to a few oscillations cycles of intense laser light are able to emit a single extreme ultraviolet (xuv) burst lasting less than one femtosecond [1, 2]. Full control of the evolution of the electromagnetic field in laser pulses comprising a few wave cycles [3] have recently allowed the reproducible generation and measurement of isolated sub-femtosecond xuv pulses [4, 5], demonstrating the control of microscopic processes (electron motion and photon emission) on an attosecond time scale. These tools have enabled us to visualize the oscillating electric field of visible light with an attosecond “oscilloscope” [6], to control and probe single- and multi-electron dynamics in atoms [7, 8], molecules [9] and solids [10]. Recent experiments indicate the feasibility of extending to frontiers of attosecond metrology towards kiloelectronvolt photon energies [11], Megaelectronvolt electron energies [12], and a temporal resolution approaching the atomic unit of time ( $\sim 24$  as) [13].

## REFERENCES

1. Hentschel, M., et al., *Nature*, Vol. 414, 509, 2001.
2. Kienberger, R., et al., *Science*, Vol. 291, 1923, 2002.
3. Baltuska, A., et al., *Nature*, Vol. 421, 611, 2003.
4. Kienberger, R., et al., *Nature*, Vol. 427, 817, 2004.
5. Goulielmakis, E., et al., *Science*, Vol. 317, 769, 2007.
6. Goulielmakis, E., et al., *Science*, Vol. 305, 1267, 2004.
7. Drescher, M., et al., *Nature*, Vol. 419, 803, 2002.
8. Uiberacker, M., et al., *Nature*, Vol. 446, 627, 2007.
9. Kling, M., et al., *Science*, Vol. 312, 246, 2006.
10. Cavalieri, A., et al., *Nature*, Vol. 449, 1029, 2007.
11. Seres, J., et al., *Nature*, Vol. 433, 596, 2005.
12. Veisz, L., et al., Submitted for Publication, 2008.
13. Goulielmakis, E., et al., Submitted for Publication, 2008.

## 3D Femtosecond Laser Micromachining by Two Photon Polymerization Technique

Andreas Ostendorf

Laser Zentrum Hannover e. V., Hollerithallee 8, D-30419 Hannover, Germany

**Abstract**— One of the rapidly advancing femtosecond laser technologies is three-dimensional micro- and nanostructuring by two-photon polymerization (2PP) technique. In our work, we apply near-infrared Ti: sapphire femtosecond laser pulses (at 800/780 nm) for 3D material processing. When tightly focused into the volume of a photosensitive material (or photoresist), they initiate 2PP process by, for example, transferring liquid into the solid state. This allows the fabrication of any computer-generated 3-D structure by direct laser “recording” into the volume of a photosensitive material. Because of the threshold behavior and nonlinear nature of the 2PP process, a resolution beyond the diffraction limit down to 100 nm can be realized by controlling the laser pulse energy and number of applied laser pulses. In this contribution, recent advances of this technology and future short- and long-term prospects will be described. Main focus will be on the interaction of intense laser pulses with new polymer materials to achieve biodegradable, optical, or specific mechanical properties. Thermal effects are investigated especially for epoxy based resins. Application examples will be discussed with regard to processing speed and reproducibility.

# Holographic Femtosecond Laser Processing and Three-dimensional Recording in Biological Tissues

Yoshio Hayasaki

Department of Optical Science and Technology, Faculty of Engineering  
The University of Tokushima, Japan

**Abstract**— We proposed data recording on biological tissues and prostheses for personal identification. The data recording was performed by femtosecond laser processing because it performs the recording with small thermal damage, a clear edge of recording point, and high data capacity. Because the biological tissues and the prostheses have unexpected movements and individual three-dimensional shapes, the femtosecond laser processing system is required to perform the recording with an adaptability and a high-throughput. The adaptability was performed with a target surface detection composed of an image sensor with a high-frame rate, a guide laser, and a piezoelectric transducer stage. We proposed that the high-throughput was realized by parallel laser processing based on a computer-generated hologram (CGH) displayed on a spatial light modulator (SLM). The use of an SLM enables to perform an arbitrary and variable patterning. The CGH is designed with the multiplexed phase Fresnel lenses (MPFL) we developed, the Fourier iterative method, and the optimal-rotation angle (ORA) method. The MPFL optimized by changing the center phase and size of each phase Fresnel lens has the features of an independent tunability and three-dimensional parallelism of the diffraction peaks. We introduced a compensation of a spatial frequency response of a liquid-crystal SLM in the CGH design using the ORA method to improve the uniformity of the diffraction peaks. We demonstrate the data recording in fingernail (fingernail memory) and dental prostheses (dental memory). We also demonstrate two-dimensional and three-dimensional parallel processing of glass using the holographic femtosecond laser processing.

## Single Femtosecond Laser-induced Periodic Microstructures

Jianrong Qiu<sup>1</sup>, Juan Song<sup>2</sup>, Zhizhan Xu<sup>2</sup>, Kiyotaka Miura<sup>3</sup>, and Kazuyuki Hirao<sup>3</sup>

<sup>1</sup>State Key Laboratory of Silicon Materials, Zhejiang University  
Hangzhou 310027, China

<sup>2</sup>Shanghai Institute of Optics and Fine Mechanics, Chinese Academy of Sciences  
Shanghai 201800, China

<sup>3</sup>Department of Material Chemistry, Graduate School of Engineering, Kyoto University  
Sakyo-ku, Kyoto 606-8501, Japan

**Abstract**— There have been extensive investigations on the formation of periodic microstructures fabricated by laser interference technique in the past decades. In this paper, we introduce unusual single femtosecond laser beam induced periodic microstructures inside solid materials. Polarization-dependent nanograting structure is observed at the focal point inside silica glass. We also have observed self-aligned periodic structure along the propagation direction of the laser beam. The mechanisms of the observed phenomena are reviewed and discussed. The promising applications of the phenomena are proposed.

# Nonlinear Pulse Propagation, Filamentation and Refractive Index Change in Glass

R. Vallée, Q. Sun, A. Saliminia, and S. L. Chin

Center for Optics Photonics and Lasers (COPL), Université Laval, Québec, G1K7P4, Canada

**Abstract**— The nonlinear propagation of ultrashort optical pulses in transparent media was shown [1] to lead to permanent changes of the physical properties of this media, namely of its refractive index. The filamentation process [2], resulting from an interplay between self-focusing and plasma defocusing, was found to play a major role in this material alteration, together with the competing optical breakdown process [3]. Accordingly, there exists for given focusing conditions an energy window for the ultrashort pulses such that smooth changes are induced without structural damages to the glass. In our presentation we show how the conditions for smooth changes and for structural damages are depending on the wavelength and on the focal length. This is leading us to analyse the various conditions for potential applications of this phenomena.

In the first part of our presentation, we will show how one can take advantage of the use of ultrashort pulses at  $1.5\ \mu\text{m}$  to write optical waveguides possessing smoother refractive index changes and showing better performances than those written at  $800\ \text{nm}$ . Conversely, it will be shown in the second part of our talk that the use of short wavelength ultrashort pulses is preferable for the fabrication of photoinduced microchannel in silica glass. To that purpose, a newly developed tunable visible femtosecond laser source was used to fabricate microtracks of defects in silica glass. The results obtained at  $580\ \text{nm}$  will be compared with those obtained at  $800\ \text{nm}$  and  $1300\ \text{nm}$  under similar irradiation conditions. In the last part of our talk, we will present results on the use of diffractive elements (phase masks) in conjunction with ultrashort pulses in order to write Bragg gratings in various types of optical fiber, namely in silica and fluoride glass fibers. It will be shown that the periodic modulation of the refractive index along the fiber core is resulting from a 1-D filamentation process which can be simply modelled by a 1D nonlinear schroedinger equation.

## REFERENCES

1. Davis, K. M., N. Sugimoto, and K. Miura, *Opt. Lett.*, Vol. 21, 1729–1731, 1996.
2. Brodeur, A. and S. L. Chin, *JOSA*, Vol. 16, 637–650, 1999.
3. Saliminia, A., N. T. Nguyen, R. Vallée, and S. L. Chin, *Opt. Commun.*, Vol. 241, 529–538, 2004.

## Photonic Waveguide Devices Directly Written into Dielectric Materials Using Femtosecond Laser Pulses

M. Ams, G. D. Marshall, P. Dekker, and M. J. Withford

Centre for Ultra-high bandwidth Devices for Optical Systems (CUDOS)

Centre for Lasers and Applications (CLA)

Department of Physics, Macquarie University, NSW 2109, Australia

**Abstract**— Significant attention has been directed to the use of laser pulses for fabricating optical components on or inside various materials since the introduction of ultrashort pulsed lasers in the 1980s. In particular, it was demonstrated in 1996 that tightly focussed femtosecond ( $10^{-15}$  s) Ti: Sapphire laser pulses can induce a local internal increase in the refractive index of bulk transparent glasses [1]. This discovery offers unique opportunities for the fabrication of arbitrary 3D photonic waveguide devices inside a wide range of materials simply by translating a sample through the focal point of a focussed femtosecond laser beam. Not only can this direct-write technique be carried out rapidly, it is readily compatible with existing fibre systems, it does not require a lithographic mask and it can be conducted in a regular laboratory environment with the minimum of sample preparation.

In this presentation we will briefly review the present state-of-the-art in the field of femtosecond laser direct written waveguides from research groups around the world and then present our most recent contributions to this field. In particular, at the CUDOS at Macquarie we employed novel femtosecond laser beam delivery techniques [2, 3] in order to fabricate low loss photonic waveguide devices for application in technologies such as telecommunications. After trialling various passive devices including waveguides, 1-N splitters and waveguide-Bragg gratings [4] in non-doped glasses, we transferred our technologies into Erbium/Ytterbium co-doped media resulting in active Photonic devices.

### REFERENCES

1. Davis, K. M., K. Miura, N. Sugimoto, and K. Hirao, *Optics Letters*, Vol. 21, 1729–1731, 1996.
2. Ams, M., G. D. Marshall, D. J. Spence, and M. J. Withford, *Optics Express*, Vol. 13, 5676–5681, 2005.
3. Ams, M., G. D. Marshall, and M. J. Withford, *Optics Express*, Vol. 14, 13158–13163, 2006.
4. Marshall, G. D., M. Ams, and M. J. Withford, *Optics Letters*, Vol. 31, 2690–2691, 2006.





## Session 4A2b

# 3D Femtosecond Micromachining and 3D Bio-imaging

### Femtosecond Laser Writing of Waveguides Inside Glass

*Yan Li (Peking University, China); Dayong Liu (Peking University, China); Hong Yang (Peking University, China); Qihuang Gong (Peking University, China); .....* 738

### 3D Microstructuring of Glass by Femtosecond Laser Direct Writing and Application to Biophotonic Microchips

*Koji Sugioka (RIKEN, Japan); Yasutaka Hanada (RIKEN, Japan); Katsumi Midorikawa (RIKEN, Japan); .....* 739

### Fabrication of Internal Diffraction Gratings in Planar Silica Plates Using Low-density Plasma Formation Induced by a Femtosecond Laser

*Sung-Hak Cho (KIMM (Korea Institute of Machinery and Materials), Korea); Won-Seok Chang (KIMM (Korea Institute of Machinery and Materials), Korea); Jae-Goo Kim (KIMM (Korea Institute of Machinery and Materials), Korea); .....* 740

### Nano-sized 3D Structures Generated by Thin Film Processing by Interfering Femtosecond Laser

*Yoshiki Nakata (Osaka University, Japan); Kunio Tsuchida (Osaka University, Japan); Noriaki Miyanaga (Osaka University, Japan); .....* 741

### Induction of Neuronal Activities with the Femtosecond Laser

*Wei Zhou (Huazhong University of Science and Technology, China); Xiuli Liu (Huazhong University of Science and Technology, China); Shaoqun Zeng (Huazhong University of Science and Technology, China); Qingming Luo (Huazhong University of Science and Technology, China); .....* 742

## Femtosecond Laser Writing of Waveguides Inside Glass

Yan Li, Dayong Liu, Hong Yang, and Qihuang Gong

State Key Laboratory for Mesoscopic Physics and Department of Physics  
Peking University, Beijing 100871, China

**Abstract**— By translation of a sample with respect to the focal point of a femtosecond laser beam, the increase of refractive index can be used to fabricate buried waveguides, optical amplifiers, beam splitters, directional couplers, long-period fiber gratings and birefringent transmission gratings. Using transverse writing, we have fabricated waveguide based photonic devices inside silica glass.

We characterize a  $2 \times 2$  waveguide array, including cross-sectional image of the waveguide area by optical microscope and the correlative analysis. We study the variation of the coupled power between four waveguides as a function of the propagation distance by the coupled-mode theory. These results can provide the basis for future applications for two-dimensional integrated optical devices.

We experimentally study the influence of the focusing depth on both the index change threshold and damage threshold, and on the cross section of the fabricated waveguides. It is mainly attributed to the spherical aberration caused by the refractive index mismatch of the air-glass interface. A  $3 \times 3$  waveguide array was written to demonstrate the influence of focusing depths on the fabrication of three-dimensional waveguide devices. Obvious coupling between waveguides are observed. Because the cross sections are almost the same at one layer but extended at deeper layers, the output intensity distribution is nearly symmetrical at the same layers, but unsymmetrical for different layers. This is useful when an unsymmetrical output is required.

With a low numerical-aperture (NA) focusing lens, multi-mode interference (MMI) waveguides are fabricated with transverse writing method. Not only the MMI waveguides with different widths, but also the long and bent MMI waveguides can be realized. We fabricated MMI waveguides with different widths by changing the effective NA of the focusing objective. The number of output modes increase with the width, which matches the simulation by the beam propagation method. Different output modes are obtained by changing the incident reading beam positions and its wavelength. A  $1 \times 2$  multi-mode splitter is formed of a straight MMI waveguide and a bent MMI waveguide and  $2 \times 3$  output modes are captured at the output facet. We also investigate the influence of the polarization of the writing laser pulses.

## 3D Microstructuring of Glass by Femtosecond Laser Direct Writing and Application to Biophotonic Microchips

Koji Sugioka, Yasutaka Hanada, and Katsumi Midorikawa

The Institute of Physical and Chemical Research, RIKEN

Wako, Saitama 351-0198, Japan

**Abstract**— The use of a femtosecond (fs) laser facilitated the internal modification of transparent materials due to a multiphoton absorption process. One of the most attractive applications of the internal modification process is optical waveguide writing inside glass. In the meanwhile, successive wet chemical etching after the modification can fabricate hollow microstructures three-dimensionally embedded in glass. Three-dimensional (3D) integration of the waveguides and the hollow microstructures realizes highly functional microchips for photonic biosensing.

In this study, we use a commercially available photostructurable glass (Foturan glass) from Schott Glass Corp. The 3D hollow microstructures were fabricated in a glass chip by fs laser direct writing (775 nm, 150 fs, 1 kHz) followed by thermal treatment, chemical wet etching in a 10% hydrofluoric acid solution and additional annealing. By this way, a variety of microfluidic components, micromechanical components like a microvalve, and microoptical components like a micromirror, a microlens, and a microlaser are successfully integrated in a glass chip.

One of the interesting applications of the microchips fabricated by this technique is dynamic observation of living cells and microorganisms. The use of microchip enabled biologists to perform 3D observation and to control the motion of microorganisms as well as to greatly reduce the observation time.

After the hollow microstructure formation, the optical waveguide was further integrated in the identical chip by the internal refractive index modification using the fs laser direct writing. After the waveguide writing, neither thermal treatment nor wet etching were employed. The integrated microchip demonstrated high-sensitivity optical analysis in absorption and fluorescence measurements of liquid samples.

Thus, 3D microstructuring of glass by the fs laser is of great use for manufacture of microchips for dynamic observation of microorganisms and photonic biosensing.

# Fabrication of Internal Diffraction Gratings in Planar Silica Plates Using Low-density Plasma Formation Induced by a Femtosecond Laser

Sung-Hak Cho, Won-Seok Chang, and Jae-Goo Kim

Laser Technology Laboratory Nano Machining Lab, KIMM (Korea Institute of Machinery and Materials)  
171 Jang-dong, Yuseong-gu, Daejeon 305-343, Korea

**Abstract**— Fabrication of internal diffraction grating with photoinduced refractive index modification in planar silica plates was demonstrated using low-density plasma formation excited by a high-intensity femtosecond (100 fs) Ti:sapphire laser ( $\lambda_p = 790$  nm). Temporal behaviors of plasma formation and bulk refractive index modification were observed *in situ*. The refractive index modifications with the diameters ranging from 400 nm to 3  $\mu$ m were photoinduced after plasma formation occurred at the irradiations of peak-intensities more than  $2 \times 10^{13}$  W/cm<sup>2</sup>. The graded refractive index profile was fabricated to be a symmetric form from the center of low-density plasma occurred point. From the diffraction efficiency of *Kogelnik's* coupled mode theory, the maximum value of refractive index change was estimated to be  $1.6 \times 10^{-2}$ . According to the electron spin resonance (ESR) spectroscopic measurement, it was found that the defect concentration of SiE' center increased significantly in the modified region in relation to that of the region without modification. The low-density plasma formation ( $n_e < 1.79 \times 10^{27}$  [1/m<sup>3</sup>]) would induce the refractive index modification with the defects. The diffraction images of the output beam transmitted through the periodically arrayed bulk modification showed that the refractive index modification produced an internal diffraction grating structure. The fabrication method of the internal diffraction grating structure in planar silica plates can be a useful tool for a variety of applications such as arrayed-waveguide grating (AWG) and single-wavelength beam connectors in the fields of wavelength division multiplexing (WDM) system in optical communication and optical sensor.

## Nano-sized 3D Structures Generated by Thin Film Processing by Interfering Femtosecond Laser

Yoshiki Nakata, Kunio Tsuchida, and Noriaki Miyanaga  
Institute of Laser Engineering, Osaka University, Japan

**Abstract**— Femtosecond laser processing has been applied to top-down technique in nanotechnology. We applied interfering femtosecond laser processing of thin film for the generation of new 3D nanostructures such as nano-waterdrop, nanocrown, nanomesh, nanobelt, and dual periodic structure. For example, a nano-waterdrop array was generated by ps laser, and the diameter of the narrowest structure was just about 50 nm. In the case of nanocrown, whiskers were standing at the edge of a nanohole, and the width was just about 80 nm. These structures are much smaller than the wavelength of the laser and the period of the interference. Nanomesh and nanobelt structures were generated by exfoliating the processed periodic structures. Dual periodic structures were generated by multiple shots.

The structures are quite unique and controllable, and aligned structure can be generated automatically because of interference. The adaptability to different material is very good. In practical point of view, no special ambient such as high vacuum, temperature control, special gas or liquid is required, and the cost for ambient condition is low. This method will improve the existing applications and new opportunities of nano-sized structures.

## Induction of Neuronal Activities with the Femtosecond Laser

Wei Zhou, Xiuli Liu, Shaoqun Zeng, and Qingming Luo

Britton Chance Center for Biomedical Photonics, Wuhan National Laboratory for Optoelectronics  
Huazhong University of Science and Technology, Wuhan 430074, China

**Abstract**— Combined with the fluorescence labeling technique, femtosecond laser two-photon microscopy has become an important technique in neuroscience research. To study the effect of input stimulations on the neuronal activity, we exploited the femtosecond laser to irradiate the distal dendrite. The femtosecond laser of 50 mW lasting 30 ms induced the pyramidal neuron a local and a global calcium signals. The technique of femtosecond laser interrogation of neural activities was non-contact, nondestructive, repeatable and requisite of no additional substrates, which would be contribute to the development of neuroscience.

# Session 4A3

## Wave Propagation and Superresolution in Active and Passive Metamaterials 2

Light Polarization and Transmission through Elliptical Nanohole Arrays in the Presence of a Magnetic Field	744
<i>Yakov Strelniker (Bar-Ilan University, Israel); David J. Bergman (Tel-Aviv University, Israel); . . . . .</i>	
Magnetophotonics: Magnetic Nanostructures and Diluted Magnetic Semiconductors	745
<i>Alexander B. Granovsky (Moscow State University, Russia); . . . . .</i>	
Super-resolution in a Two-dimensional Negative-index Metamaterial Superlens	746
<i>Koray Aydin (Bilkent University, Turkey); Ekmel Ozbay (Bilkent University, Turkey); . . . . .</i>	
A Novel Design of Photonic Crystal Lens Based on Negative Refractive Index	747
<i>S. Hazha (University of Kent, UK); F. AbdelMalek (National Institute of Applied Sciences and Technology, Tunisia); . . . . .</i>	
Review of Nonlinear Optics in Metamaterials	748
<i>Yuanjiang Xiang (Hunan University, China); Xiaoyu Dai (Hunan University, China); Shuangchun Wen (Hunan University, China); Dianyuan Fan (Hunan University, China); . . . . .</i>	
Transparency Effect Induced by Elastic Metamaterials	749
<i>Xiaoming Zhou (Beijing Institute of Technology, China); Jin Hu (Beijing Institute of Technology, China); Gengkai Hu (Beijing Institute of Technology, China); . . . . .</i>	
Electromagnetic Smart Screen for Tunable Transmission and Reflection Applications	750
<i>Lie Liu (National University of Singapore, Singapore); Serguei Matitsine (National University of Singapore, Singapore); Peng Khiang Tan (National University of Singapore, Singapore); . . . . .</i>	
Focusing of Light by Disordered Metamaterials	751
<i>A. P. Mosk (University of Twente, The Netherlands); . . . . .</i>	
Nonlinear Effects in Metamaterials	752
<i>Ilya V. Shadrivov (Australian National University, Australia); . . . . .</i>	

# Light Polarization and Transmission through Elliptical Nanohole Arrays in the Presence of a Magnetic Field

Y. M. Strelniker<sup>1</sup> and D. J. Bergman<sup>2</sup>

<sup>1</sup>Department of Physics, Bar-Ilan University, IL-52900 Ramat-Gan, Israel

<sup>2</sup>Raymond and Beverly Sackler School of Physics and Astronomy, Sackler Faculty of Exact Sciences  
Tel Aviv University, IL-69978 Tel Aviv, Israel

**Abstract**— We have studied, analytically and numerically, the extraordinary transmission through perforated metal films with nanosize elliptical holes [1–3]. The films are found to exhibit an extraordinary light transmission at frequencies related to the surface plasmon resonances. Several ways to control the light transmission and light polarization are discussed. We have explained analytically the observed dependence of the polarizations ratio on the aspect ratio of the holes, as well as other features of the extraordinary light transmission found experimentally by R. Gordon, et al. [4]. Our numerical results [3] are in good agreement with experimental data [4]. We also propose to use the magnetic field for getting a strong polarization effect, which depends on the ratio of the cyclotron to plasmon frequencies, and which can be made arbitrarily large [3]. An interesting film material to consider for this purpose is metallic Bismuth, since the low density of charge carriers ( $\sim 3 \times 10^{17} \text{ cm}^{-3}$ ) can help to make the cyclotron frequency of those carriers equal to or greater than their plasma frequency. Another class of interesting materials are semiconductors like GaAs and InAs.

## REFERENCES

1. Strelniker, Y. M. and D. J. Bergman, “Optical transmission through metal films with a sub-wavelength hole array in the presence of a magnetic field,” *Phys. Rev. B*, Vol. 59, R12763–R12766, 1999.
2. Strelniker, Y. M., D. Stroud, and A. O. Voznesenskaya, “Control of extraordinary light transmission through perforated metal films using liquid crystals,” *Eur. Phys. J. B*, Vol. 52, 1–7, 2006.
3. Strelniker, Y. M., “Theory of optical transmission through elliptical nanohole arrays,” *Phys. Rev. B*, Vol. 76, 085409-1–085409-6, 2007.
4. Gordon, R., A. G. Brolo, A. McKinnon, A. Rajora, B. Leathem, and K. L. Kavanagh, “Strong polarization in the optical transmission through elliptical nanohole arrays,” *Phys. Rev. Lett.*, Vol. 92, 037401-1–037401-4, 2004.



# Magnetophotonics: Magnetic Nanostructures and Diluted Magnetic Semiconductors

A. Granovsky

Faculty of Physics, Moscow State University, Moscow 119992, Russia

**Abstract**— The main goal of magnetophotonics is to understand the interaction of electromagnetic waves of a wide spectral range with various magnetic materials and to make useful devices using the acquired knowledge. In some sense magnetophotonics can be considered as spintronics at high frequencies because magnetophotonics involves the interaction between photons, charges and spins. Typical questions that are posed are (a) how to increase the interaction between photons and magnetic materials to develop tunable by a weak magnetic field optical and high frequency devices, (b) how can magnetization be switched and manipulated by electromagnetic waves, (c) what are effective ways and artificial magnetic structures to manipulate photons by an applied magnetic field, (d) what information about electronic, ionic, magnetic structure can be obtained from magnetophotonics experiments.

In the presentation I briefly discuss some of these questions focusing on magneto-optics and magnetorefractive effect in magnetic nanocomposites, discontinuous multilayers, diluted magnetic semiconductors and oxides, magnetophotonic crystals. It is predicted that magnetoreflexion can be enhanced up to 60% in magnetophotonic crystals with built-in magnetic defect possessing magnetorefractive effect.

It is shown that novel room-temperature magnetic semiconductors and oxides semiconductors are very promising materials for magnetophotonics.

# Super-resolution in a Two-dimensional Negative-index Metamaterial Superlens

Koray Aydin and Ekmel Ozbay

Nanotechnology Research Center

Department of Physics and Department of Electrical and Electronics Engineering  
Bilkent University, Bilkent, 06800 Ankara, Turkey

**Abstract**— Left-handed metamaterials (LHM) with negative effective permittivity and permeability are promising candidates for imaging beyond the diffraction limit. The resolution of a positive-index lens is limited to the half-wavelength. The finer details of the image are carried by evanescent waves and quickly decay before reaching the image plane. The perfect reconstruction of the image is possible with a lens having  $\varepsilon_{eff} = \mu_{eff} = -1$ . [1] However, acceptable results could be obtained for deviations from the ideal parameters. In this study, we present a low-loss, impedance matched two-dimensional negative-index metamaterial (NIM) superlens that is capable of resolving subwavelength features with a  $\lambda/8$  resolution [2]. The effective parameters of the LHM are retrieved as  $\varepsilon_{eff} = \mu_{eff} = -1.8$  and they are consistent with the measurements. The flat lens behavior and the effect of lens thickness on the resolving power are discussed. The experimental results on the super-resolving NIM will be provided in this study.

## REFERENCES

1. Pendry, J. B., “Negative refraction makes a perfect lens,” *Phys. Rev. Lett.*, Vol. 85, 3966–3969, 2000.
2. Aydin, K., I. Bulu, and E. Ozbay, *Appl. Phys. Lett.*, Vol. 90, 254102, 2007.

# A Novel Design of Photonic Crystal Lens Based on Negative Refractive Index

S. Haxha<sup>1</sup> and F. AbdelMalek<sup>2</sup>

<sup>1</sup>Photonics Group, Department of Electronics, University of Kent, Canterbury CT2 7NT, UK

<sup>2</sup>National Institute of Applied Sciences and Technology, BP 676 Cedex 1080, Tunis, Tunisia

**Abstract**— Left-handed materials are materials with both negative dielectric permittivity and negative magnetic permeability [1–3]. In 1968, Veselago [1] proposed a material whose permittivity and permeability are simultaneously negative. His theoretical study demonstrated that the electric and magnetic field vectors form a left-handed set of vectors with the wave vector. Later, it became obvious that these materials may be artificially created. Many researchers around the world are now studying different characteristics of the materials with negative refractive index based on photonic crystal structures that operate at optical and microwave frequencies. Several vital ideas and proposals for future application of these materials have been demonstrated, for example, Pendry et al. [4] demonstrated a perfect lens, Ao et al. [5] and Moussa et al. [6] demonstrated subwavelength imaging based on photonic crystals. Photonic crystal slabs based on such materials with negative refraction [7, 8], became candidates to overcome limitations in light focusing. Thus, it is essential to further explore and investigate novel ideas and devices based on photonic crystal with negative refractive index, and application of these devices in various areas such as telecommunication and sensing systems. In this regard, we have proposed a novel model of a lens which serves as a spot-size converter and is based on a two-dimensional photonic crystal structure with a negative refractive index. A numerical method based on two-dimensional Finite-Difference Time-Domain is developed/employed to design the photonic crystal (PC) lens. The configuration geometry of the PC lens is designed, optimized, and integrated into a Photonic Integrated Circuitry (PIC). In other words, this PC lens is deployed to effectively couple the light from a single mode fiber (SMF) with large core size into a photonic crystal waveguide (PCW) with very small structure dimensions. A significant reduction in the device compactness, coupling efficiency and transmission efficiency is demonstrated by optimizing the proposed PC lens and the PCW.

## REFERENCES

1. Veselago, V. G., *Soviet Physics USPEKI*, Vol. 10, 509–514, 1968.
2. Pendry, J. B., A. J. Holden, D. J. Robbins, and W. J. Steward, *Microw. Tech. Trans. MTT*, Vol. 47, 2075–2084, 1999.
3. Smith, D. R., W. J. Padilla, D. C. Vier, S. C. Nemat-Nasser, and S. Schultz, *Phys. Rev. Lett.*, Vol. 84, 4184–4187, 2000.
4. Pendry, J. B., *Phys. Rev. Lett.*, Vol. 85, 3966–3969, 2000.
5. Ao, X. and S. He, “Three-dimensional photonic crystal of negative refraction achieved by interference lithography,” *Opt. Lett.*, Vol. 29, 2542–2544, 2004.
6. Moussa, R., S. Foteinopoulou, L. Zhang, G. Tuttle, K. Guven, E. Ozbay, and C. M. Soukoulis, “Negative refraction and superlens behavior in a two-dimensional photonic crystal,” *Phys. Rev. B*, Vol. 71, 085106-1–5, 2005.
7. Notomi, M., *Phys. Rev. B*, Vol. 62, 10696–10705, 2000.
8. Foteinopoulou S., E. N. Economou, and C. M. Soukoulis, *Phys. Rev. Lett.*, Vol. 90, 107402-1–107402-4, 2003.

## Review of Nonlinear Optics in Metamaterials

Yuanjiang Xiang, Xiaoyu Dai, Shuangchun Wen, and Dianyuan Fan

Research Center of Laser Science and Engineering and School of Computer and Communication  
Hunan University, Changsha 410082, China

**Abstract**— Metamaterials (MMs) are artificial structures that can be pre-designed to show specific electromagnetic properties not commonly found in nature. One of the most exciting opportunities for metamaterials is the development of negative-index metamaterials (NIMs). Thanks to rapidly developing nanofabrication and sub-wavelength imaging techniques, the optical NIMs can now be fabricated. NIMs have opened new doors in optics and have truly excited the imagination of researchers worldwide. The possibility of nonlinear electromagnetic responses, including cubic or quadratic nonlinear responses, in MMs is also demonstrated by the inclusion of nonlinear elements within the MMs, for instance by embedding the split-ring resonators (SRRs) in a Kerr-type dielectric, or by inserting certain nonlinear elements (e.g., diodes) in the split-ring resonators' paths. This will further extend the conventional area of optics, particularly nonlinear optics, and leads to completely new electronic and optical devices.

Although nonlinear optics in MMs remains so far a less developed branch of optics, recent researches demonstrated that a nonlinear MM exhibits a rich spatiotemporal dynamics where both linear and nonlinear effective properties can be tailored simply. This contribution reviews the recent advances on nonlinear interaction between electromagnetic wave with MMs, from the fundamental physical models to unique phenomena and conceived novel devices. The physical origins for the typical nonlinear phenomena, such as second-order harmonic generation (SHG), optical parametric amplification (OPA), four-wave mixing (FWM), optical soliton, self-phase modulation (SPM), cross-phase modulation (XPM), and self-focusing in MMs are explained. Several proposals for applications of nonlinear MMs in manipulating light are demonstrated.

# Transparency Effect Induced by Elastic Metamaterials

Xiaoming Zhou, Jin Hu, and Gengkai Hu

Department of Applied Mechanics, School of Science, Beijing Institute of Technology  
Beijing 100081, China

**Abstract**— Since the pioneer work by Alù and Engheta [1], who found that plasmonic metamaterials can make a dielectric sphere with extremely low total scattering cross section, much works are devoted to analyze the transparency induced by metamaterials. In quasi-static limit, it is shown that the invisibility phenomenon can be well interpreted with the neutral inclusion concept [2], and this neutral inclusion concept is then applied for other more complex configurations, such as a coated ellipsoid and particulate composites. By analogy, the acoustic transparency effect for a coated sphere with acoustic metamaterial can also be achieved [3]. In this talk, we will show how to cloak a solid object with elastic wave metamaterial, where the shear waves in the system are nontrivial. By Mie scattering theory, we show that the effective bulk modulus, mass density, and shear modulus of the assemblage made of the coated spheres dominate the zero, the first and the second order scattering coefficients, respectively. So the transparency condition of a coated sphere with an elastic metamaterial can be obtained by letting the first three scattering coefficients to vanish, this again corresponds to the neutral inclusion concept. Numerical simulations have also shown that the total scattering cross section of an object can be reduced significantly by symmetrically placing some metamaterial spheres around the object, the mechanism concerned is based on the cancellation effect of oppositely-signed dipolar fields. In the end, we show that the Pendry's spherical or cylindrical cloaks [4] can be interpreted based on the Lie symmetry group of the wave equation, this idea is then generated for the design of elliptical cloaks.

## REFERENCES

1. Alù, A. and N. Engheta, "Achieving transparency with plasmonic and metamaterial coatings," *Physical Review E*, Vol. 72, No. 1, 016623, 2005.
2. Zhou, X. M. and G. K. Hu, "Design for electromagnetic wave transparency with metamaterials," *Physical Review E*, Vol. 74, No. 2, 026607, 2006.
3. Zhou, X. M. and G. K. Hu, "Acoustic wave transparency for a multilayered sphere with acoustic metamaterials," *Physical Review E*, Vol. 75, No. 4, 046606, 2007.
4. Pendry, J. B., D. Schurig, and D. R. Smith, "Controlling electromagnetic fields," *Science*, Vol. 312, 1780–1782, 2006.

## Electromagnetic Smart Screen for Tunable Transmission and Reflection Applications

Lie Liu, Serguei Matitsine, and Peng Khiang Tan

Temasek Laboratories, National University of Singapore, Singapore

**Abstract**— In the past few years, electromagnetic left-handed materials and metamaterials have attracted great attention. The main reason lies in that metamaterials can provide certain electromagnetic properties which are not available in nature, such as negative refraction index and sub-wavelength diffraction, etc. The main limitation of metamaterials is that the response is normally within narrow band. Depending on the design of the patterns, the applicable bandwidth is normally not more than few percents of the resonance frequency. One practical solution is to develop tunable screen to extend the working bandwidth.

Electromagnetic smart screen (ESS) containing conductive strip or patch array loaded with pin diodes or varactors was investigated with numerical and experimental approaches. Transmission and reflection coefficient were simulated using finite element method (FEM) with validation by free space measurement. Tunable transmission coefficient of ESS is observed between 3 to 8 GHz, which can be useful for antenna applications. Tunable reflection coefficient ( $-8$  to  $-10$  dB) of a 0.5 mm ESS on top of metallic substrate is observed between 3 to 4 GHz. Good agreement was obtained between simulation and measurement results.

## Focusing of Light by Disordered Metamaterials

A. P. Mosk

MESA+ Institute for Nanotechnology and Department of Science and Technology  
University of Twente, P. O. Box 217, AE Enschede 7500, The Netherlands

**Abstract**— Nanostructured metamaterials offer the prospect of manipulating electromagnetic fields in hitherto impossible ways, in particular, to make images that are much sharper than the Rayleigh resolution limit. Even weak disorder will give rise to strong scattering in these materials which are extremely strongly coupled to the light field. Extremely precise nanofabrication seems to be necessary to avoid disorder-induced scattering. We show experiments where the opposite approach is taken: a fully disordered metamaterial is used to focus light [1]. The essential ingredient is spatial phase control of the incident light field, which we achieve using a liquid-crystal display, which can independently control the phases of many thousands of pixels. The correct phases are found by using feedback from an intensity detector in the target focus, the optimal phases are found using simplified learning algorithms. We have observed that, if suitably phase-shaped light is incident, fully disordered metamaterials, such as strongly photonic titanium dioxide nanoparticles, can focus light to a higher resolution than our aperture-limited programming optics.

Currently we are investigating the possibility to focus light inside disordered materials, using nanoscale fluorescent probes [2], and the feasibility of focusing beyond the diffraction limit using fully disordered metal-dielectric composites, in combination with phase controlled fields. Our results on fully disordered materials lead us to presume that scattering due to small imperfections in nanostructured metamaterials will not be an insurmountable obstacle to their exciting applications.

### REFERENCES

1. Vellekoop, I. M. and A. P. Mosk, "Focusing coherent light through opaque strongly scattering media," *Opt. Lett.*, Vol. 32, 2309, 2007.
2. Vellekoop, I. M., E. G. van Putten, A. Lagendijk, and A. P. Mosk, in preparation, 2007.

## Nonlinear Effects in Metamaterials

Ilya. V. Shadrivov

Nonlinear Physics Centre, Research School of Physical Sciences and Engineering  
Australian National University, Canberra ACT 0200, Australia

**Abstract**— This talk will overview recent theoretical and experimental results obtained in the Nonlinear Physics Centre of the Australian National University in collaboration with the Department of Electrical and Computer Engineering at the University of Wisconsin-Madison.

Novel types of microstructured materials which demonstrate many unusual properties for electromagnetic waves such as negative refraction have been discussed recently in many theoretical studies [1, 2], and currently such materials are being studied experimentally [3]. The simplest composite materials of this type are created by a mesh of metallic wires and split-ring resonators (SRRs), and their unique properties are associated with negative real parts of magnetic permeability and dielectric permittivity for microwaves.

We study both theoretically and experimentally *tunable and nonlinear metamaterial structures* where, e.g., the field intensity can be used for dynamic control of the transmission properties of the composite structure. The dynamic control over metamaterials properties is nontrivial since they possess left-handed properties only in some finite frequency range, which is basically determined by the geometry of the structure. The possibility to control the effective parameters of the metamaterial using nonlinearity has recently been suggested in Refs. [4–6]. The main reason for nontrivial behaviour of nonlinear metamaterials is that the microscopic electric field in the vicinity of the metallic particles forming left-handed structure can be much higher than the macroscopic electric field carried by the propagating wave. This provides a simple physical mechanism for enhancing nonlinear effects in left-handed materials. We overview a range of nonlinear phenomena predicted for metamaterials, including nonlinear resonant response, harmonic generation, and nonlinearity-induced transparency.

We report on the first experimental realization of two-dimensional nonlinear metamaterials, and we study their properties. We demonstrate dynamic control of the left-handed frequency band by incident electromagnetic wave, and show the possibility of the nonlinearity-induced transmission. We study harmonic generation in nonlinear metamaterial, and show that due to the strong frequency dispersion of metamaterial, the intensity of the transmitted second harmonic can be greater than that of the fundamental frequency by two orders of magnitude.

### REFERENCES

1. Pendry, J. B., A. J. Holden, W. J. Stewart, and I. Youngs, *Phys. Rev. Lett.*, Vol. 76, 4773, 1996.
2. Pendry, J. B., A. J. Holden, D. J. Robbins, and W. J. Stewart, *IEEE Trans. Microw. Theory Tech.*, Vol. 47, 2075, 1999.
3. Smith, D. R., W. J. Padilla, D. C. Vier, S. C. N. Nasser, and S. Schultz, *Phys. Rev. Lett.*, Vol. 84, 4184, 2000.
4. Zharov, A. A., I. V. Shadrivov, and Y. S. Kivshar, *Phys. Rev. Lett.*, Vol. 91, 037401, 2003.
5. Lapine, M., M. Gorkunov, and K. H. Ringhofer, *Phys. Rev. E*, Vol. 67, 065601, 2003.
6. Shadrivov, I. V., S. K. Morrison, and Y. S. Kivshar, *Opt. Express*, Vol. 14, 9344, 2006.



## Session 4A4

# Semiconductor Homostructures and Heterostructures 1

Enhancement of the Electronic Confinement Improves the Mobility in $p$ - $n$ - $p$ Delta-doped Quantum Wells in Si	
A. David Ariza-Flores (Universidad Autonoma del Estado de Morelos, Mexico); Isaac Rodriguez-Vargas (Universidad Autonoma de Zacatecas, Mexico); .....	754
Electron Subband Structure and Mobility Trends in $p$ - $n$ Delta-doped Quantum Wells in Si	
A. David Ariza-Flores (Universidad Autonoma del Estado de Morelos, Mexico); Isaac Rodriguez-Vargas (Universidad Autonoma de Zacatecas, Mexico); .....	755
Stark Effect in $p$ -type Delta-doped Quantum Wells	
A. M. Miteva (Space Research Institute, Bulgarian Academy of Sciences, Bulgaria); Stoyan Jelev Vlaev (Universidad Autonoma de Zacatecas, Mexico); V. T. Donchev (University of Sofia, Bulgaria); .....	756
Miniband Structure Formation of $p$ -type Delta-doped Superlattices in GaAs	
Isaac Rodriguez-Vargas (Universidad Autónoma de Zacatecas, México); A. del Rio de Santiago (Universidad Autónoma de Zacatecas, México); J. Madrigal-Melchor (Universidad Autónoma de Zacatecas, México); Stoyan Jelev Vlaev (Universidad Autónoma de Zacatecas, México); .....	757
Quasi-bound Electronic States in Multiple Delta-doped Quantum Wells	
Isaac Rodriguez-Vargas (Universidad Autónoma de Zacatecas, Mexico); A. del Rio De Santiago (Universidad Autónoma de Zacatecas, Mexico); Stoyan Jelev Vlaev (Universidad Autónoma de Zacatecas, Mexico); .....	758
Dimensions of the Spectrum of Elementary Excitations in Heterostructures Mimicking a DNA Sequence	
R. P. Pérez-Álvarez (Universidad Autónoma del Estado de Morelos, México); Miguel Eduardo Mora-Ramos (Universidad Autónoma del Estado de Morelos, México); Luis M. Gaggero-Sager (Universidad Autónoma del Estado de Morelos, México); .....	759
Transmittance and Fractality in a Cantor-like Multibarrier System	
D. S. Díaz-Guerrero (Universidad Autonoma del Estado de Morelos, Mexico); J. J. F. Montoya (Universidad Autonoma del Estado de Morelos, Mexico); Luis M. Gaggero-Sager (Universidad Autonoma del Estado de Morelos, Mexico); R. Pérez-Álvarez (Universidad Autonoma del Estado de Morelos, Mexico); .....	760
The Electrostatic Potential Associated to Interface Phonon Modes in Nitride Single Heterostructures	
Miguel Eduardo Mora-Ramos (Universidad Autónoma del Estado de Morelos, Mexico); R. Pérez-Alvarez (Universidad Autónoma del Estado de Morelos, Mexico); Victor R. Velasco (Instituto de Ciencia de Materiales de Madrid, Spain); .....	761
Electronic Spectrum Study of Parabolic $GaAs/Al_xGa_{1-x}As$ Superlattices	
Isaac Rodriguez-Vargas (Universidad Autónoma de Zacatecas, México); O. Y. Sanchez-Barbosa (Universidad Autónoma de Zacatecas, México); D. A. Contreras-Solorio (Universidad Autónoma de Zacatecas, México); Stoyan Jelev Vlaev (Universidad Autónoma de Zacatecas, México); .....	762
Transport Properties of Delta Doped Field Effect Transistor	
Outmane Oubram (Universidad Autonoma del Estado de Morelos, Mexico); Luis M. Gaggero-Sager (Universidad Autonoma del Estado de Morelos, Mexico); .....	763
Mobility of Doped Graphene	
Gerardo G. Naumis (Universidad Nacional Autonoma de Mexico (UNAM), Mexico); F. J. López-Rodríguez (Universidad Nacional Autonoma de Mexico (UNAM), Mexico); Luis M. Gaggero-Sager (Universidad Autonoma del Estado de Morelos, Mexico); .....	764

## Enhancement of the Electronic Confinement Improves the Mobility in $p$ - $n$ - $p$ Delta-doped Quantum Wells in $Si$

A. David Ariza-Flores<sup>1</sup> and I. Rodriguez-Vargas<sup>2</sup>

<sup>1</sup>Facultad de Ciencias, Universidad Autónoma del Estado de Morelos  
Av. Universidad 1001, Col. Chamilpa, 62209 Cuernavaca, MOR., México

<sup>2</sup>Unidad Académica de Física, Universidad Autónoma de Zacatecas, Calzada Solidaridad Esquina con  
Paseo la Bufa S/N, 98060 Zacatecas, ZAC., México

**Abstract**— The electronic structure and mobility trends in a  $n$ -type delta-doped quantum well in  $Si$ , matched between  $p$ -type delta-doped barriers of the same material, is presented. The distance between the  $n$ -type well and  $p$ -type barriers is varied from 50 Å to 500 Å; and also the impurity density from  $5 \times 10^{12} \text{ cm}^{-2}$  to  $5 \times 10^{13} \text{ cm}^{-2}$ , for both, donors and acceptors. An increase in the mobility by a factor of 1.6 at interwell distance of 50 Å with donor and acceptor concentrations of  $5 \times 10^{12} \text{ cm}^{-2}$  and  $5 \times 10^{13} \text{ cm}^{-2}$  compared with a single delta-doped well without  $p$ -type barriers is found. This improvement in mobility could be attributed to a better confinement of carriers, which favors excited levels with nodes in the donor plane. This trade-off between carrier concentration and mobility could be exploited in high-speed, high-power and high-frequency applications.

# Electron Subband Structure and Mobility Trends in $p$ - $n$ Delta-doped Quantum Wells in $Si$

A. David Ariza-Flores<sup>1</sup> and I. Rodriguez-Vargas<sup>2</sup>

<sup>1</sup>Facultad de Ciencias, Universidad Autónoma del Estado de Morelos  
Av. Universidad 1001, Col. Chamilpa, 62209 Cuernavaca, MOR., México

<sup>2</sup>Unidad Académica de Física, Universidad Autónoma de Zacatecas, Calzada Solidaridad Esquina con  
Paseo la Bufa S/N, 98060 Zacatecas, ZAC., México

**Abstract**— We present the electronic spectrum of a  $n$ -type delta-doped quantum well in  $Si$  coupled to a  $p$ -type delta-doped barrier within the envelope function effective mass approximation. We applied the Thomas-Fermi approximation to derive an analytical expression for the confining potential, and thus, we obtain the electronic structure in a simple manner. We analyzed the electron subband structure varying the distance between the doping planes ( $l$ ) as well as the impurity density in them ( $n_{2D}$ ,  $p_{2D}$ ). We also study the mobility trends through an empirical formula that is based on the electron levels, the electron wave functions and the Fermi level. We find a monotonic decrease in the mobility as the  $p$ -type barrier move away from the  $n$ -type well, and also we find the optimum parameters,  $l = 50 \text{ \AA}$  and  $n_{2D} = 5 \times 10^{12} \text{ cm}^{-2}$  and  $p_{2D} = 1 \times 10^{13} \text{ cm}^{-2}$ , for maximum mobility.

## Stark Effect in p-type Delta-doped Quantum Wells

A. M. Miteva<sup>1</sup>, S. J. Vlaev<sup>2,4</sup>, and V. Donchev<sup>3</sup>

<sup>1</sup>Space Research Institute, Bulgarian Academy of Sciences, Moskovska Str. 6, Sofia 1000, Bulgaria

<sup>2</sup>Unidad Academica de Fisica, Universidad Autonoma de Zacatecas  
Calzada Solidaridad Esquina con Paseo la Bufa, Zacatecas 98060, Zac., Mexico

<sup>3</sup>Department of Condensed Matter Physics, Faculty of Physics, Sofia University  
blvd. James Bourchier 5, 1164-Sofia, Bulgaria

<sup>4</sup>Facultad de Ciencias, Universidad Autonoma del Estado de Morelos  
Av. Universidad 1001, Col. Chamilpa, Cuernavaca 62210, MOR., Mexico

**Abstract**— Many opto-electronic semiconductor devices are based on the quantum confined Stark effect in quantum well structures. The basic problem in the design of such devices is to find the system parameters of the optimal device work. We need a high sensitivity of the Stark shifts with respect to the field, a wide field range and an intensive signal. Realistic numerical calculations can help to resolve this task. There are few theoretical considerations of the Stark effect in delta-doped quantum wells. We present a theoretical study of this effect in p-type delta-doped quantum wells (Be-doped GaAs in (001) growth direction) within the framework of the  $sp^3s^*$  spin dependent tight-binding model. The doping potential is considered as an external one [1] and the electric field is taken into account as in [2]. The Surface Green Function Matching (SGFM) method was applied to consider the interfaces and the linear potential region. The calculations of the Stark shifts and transition probabilities were made in wide interval of impurity concentrations and wide electric field ranges for the ground and the excited states. We found that the p-type delta-doped wells have specific Stark characteristics which can be applied in the practice. There is a parabolic dependence of the Stark shifts magnitude on the electric field strength for some doping concentrations. The critical field values of these wells are higher than in rectangular, parabolic and graded-gap quantum wells. We compare our results with the experimental and theoretical data available in the literature and discuss future studies of the Stark effect in double and multiple delta-doped quantum wells and delta-doped superlattices.

### REFERENCES

1. Vlaev, S. and L. M. Gaggero-Sager, *Phys. Rev. B*, Vol. 58, 1142, 1998.
2. Vlaev, S., V. R. Velasco, and F. G. Moliner, *Phys. Rev. B*, Vol. 49, 11222, 1994.

## Miniband Structure Formation of $p$ -type Delta-doped Superlattices in GaAs

I. Rodriguez-Vargas, A. del Rio de Santiago, J. Madrigal-Melchor, and S. J. Vlaev

Unidad Académica de Física, Universidad Autónoma de Zacatecas  
Calzada Solidaridad Esquina con Paseo la Bufa S/N, Zacatecas 98060, ZAC., México

**Abstract**— We present the electronic structure of finite  $p$ -type delta-doped superlattices in GaAs. We use the first neighbors  $sp^3s^*$  tight-binding approximation including spin for the miniband structure analysis. The calculation is based on an analytical expression for the Hartree-Fock potential of the inhomogeneous part, previously obtained within the Thomas-Fermi (TF) approximation [1]. This potential is considered as external in the computations, so, it is added to the diagonal terms of the tight-binding Hamiltonian [3]. We give a detail description of the delta-doped superlattices, this is, we study the miniband formation as a function of the impurity density ( $n_{2D}$ ) and the superlattice period ( $d$ ) obtaining the ranges of superlattice, multiple well and isolate well behavior. We also compare our results with the theoretical and experimental data available, obtaining a reasonable agreement.

### REFERENCES

1. Gaggero-Sager, L. M., “Exchange and correlation via functional of Thomas-Fermi in delta-doped quantum wells,” *Modelling Simul. Mater. Sci. Eng.*, Vol. 9, No. 1, 1–5, 2001.
2. Valev, S. and L. M. Gaggero-Sager, “Thomas-Fermi approximation in a tight-binding calculation of  $\delta$ -doped quantum wells in GaAs,” *Phys. Rev. B*, Vol. 58, No. 5, 1142–1145, 1998.

# Quasi-bound Electronic States in Multiple Delta-doped Quantum Wells

I. Rodríguez-Vargas, A. del Rio de Santiago, and S. J. Vlaev

Unidad Académica de Física, Universidad Autónoma de Zacatecas  
Calzada Solidaridad Esquina con Paseo La Bufa S/N, Zacatecas 98060, ZAC., México

**Abstract**— Multiple delta-doped quantum wells of  $n$ -type ( $GaAs$  doped with  $Si$ ) and  $p$ -type ( $GaAs$  doped with  $Be$ ) are considered within the semi-empirical  $sp^3s^*$  tight-binding model including spin. The confinement potentials are obtained in the Thomas-Fermi and Thomas-Fermi-Dirac approximations [1] and are added to the Hamiltonian diagonal elements as external potentials [2]. The inhomogeneous doped regions of the multiple quantum wells grown in (001) direction are matched with the semi-infinite homogeneous barriers applying the Surface Green Function Matching Method (SGFM) [3]. The electronic spectra in wide energy intervals above the conduction band and valence band barriers are studied looking for quasi-bound states. The impurity concentrations, the inter-well distances and the number of the wells are varied to obtain very strong energy and spatial localizations. The full-width at half maximum (FWHM) and the mean-life time of the observed quasi-bound states are calculated using a recently published numerical scheme [4]. The conditions and the mechanism of the Capasso states [5] formation are revealed. We have found many quasi-bound states for all doping concentrations in both types of delta-doped wells. Their number depends on the impurity concentration value. A full quantum-mechanical description of these states is given. We have calculated the energies, the spatial distributions and the line shapes of all quasi-bound electronic states for electron and holes. The mean-life times of these states vary between  $10^{-5}$  and  $10^{-7}$  s. The possible experimental observation in time-resolved spectroscopy measurements and some device applications of the quasi-bound states are discussed. We have compared our theoretical results with the results obtained previously in single delta-doped quantum wells of both types.

## REFERENCES

1. Rodríguez-Vargas, I. and L. M. Gaggero-Sager, *J. Appl. Phys.*, Vol. 99, 033702, 2006.
2. Vlaev, S. and L. M. Gaggero-Sager, *Phys. Rev. B*, Vol. 58, 1142, 1998.
3. Vlaev, S., V. R. Velasco, and F. G. Moliner, *Phys. Rev. B*, Vol. 49, 11222, 1994.
4. Vlaev, S. J. and V. M. González-Róbles, *Phys. Stat. Sol. (C)*, Vol. 2, 3653, 2005.
5. Capasso, F., et al., *Nature*, Vol. 358, 565, 1992.

## Dimensions of the Spectrum of Elementary Excitations in Heterostructures Mimicking a DNA Sequence

R. P. Pérez-Álvarez, M. E. Mora-Ramos, and L. M. Gaggero-Sager

Universidad Autónoma del Estado de Morelos, Ave. Universidad 1001, 62209 Cuernavaca, México

**Abstract**— In the few recent years some authors have claimed that there exist certain relationships, or similarities, between the DNA sequences of base pairs and the man-made quasiregular heterostructures [1, 2]. These similarities can be investigated by studying the spectra of elementary excitations in such kind heterostructures. In order to contribute to clarifying this assumed connection, we have calculated the electromagnetic modes that propagate in non-regular dielectric heterostructures mimicking DNA sequences. That is, the structures consist of onedimensional arrays of layers stacked according to a given DNA sequence. In our particular case, the systems under study are dielectric multilayers with delta-like profiles of the refractive indexes. Porous silicon has been the host material chosen.

An important property of the man-made quasiregular layered structures is the fractal character of their spectra. This can be readily verified in the case of Fibonacci and Thue-Morse heterostructures. However, our results indicate that, at least in the analyzed DNA sequences, no similarities can be sustained since the calculated dimension of the spectrum is equal to unity. Nonetheless, there are some yet unexplained peculiarities in the box-counting curves of the mode spectra of these DNA-like systems. This fact indicates that the research on the subject must continue.

### REFERENCES

1. Albuquerque, E. L., M. S. Vasconcelos, M. L. Lyra, and F. A. B. F. de Moura, "Nucleotide correlations and electronic transport of DNA sequences," *Phys. Rev. E*, Vol. 71, 021910, 2005.
2. Roche, S., D. Bicout, E. Maciá, and E. Kats, "Long range correlations in DNA: scaling properties and charge transfer efficiency," *Phys. Rev. Lett.*, Vol. 91, 228101, 2003.

## Transmittance and Fractality in a Cantor-like Multibarrier System

D. S. Díaz-Guerrero, F. Montoya, L. M. Gaggero-Sager, and R. Pérez-Álvarez

Universidad Autónoma del Estado de Morelos, Ave. Universidad 1001, Cuernavaca 62209, México

**Abstract**— The transmittance is studied for a Cantor-like multibarrier system. The calculation are made in the framework of effective mass theory. Some typical values of effective masses and potentials are used in order to have an experimental reference. The techniques of Transfer Matrix are used to calculate the transmittance of the entire structure having some dozens of layers. The results display a complex structure of peaks and valleys. The set of maxima is studied with the tool of the  $q$ -dependent dimension  $D(q)$ . The set of transmittance maxima exhibits a fractal structure, or more exactly, a *multifractal* structure, i.e., a  $q$ -dependent dimension, characterized as usually with limit one when  $q$  parameter tends to  $-\infty$  but with a limit between 0 and 1 when tends to  $+\infty$ . This numerical experiment demonstrate that spatially bounded potential may exhibit fractal character.

### REFERENCES

1. Gaggero-Sager, L. M., E. R. Pujals, and O. Sotolongo-Costa, "Self-similarity in a Cantor-like semiconductor quantum well," *Phys. Stat. Sol. (b)*, Vol. 220, 167–169, 2000.
2. Pérez-Alvarez, R. and F. García-Moliner, "The spectrum of quasiregular heterostructures," invited chapter in *Contemporary Problems of the Condensed Matter Physics*, ed. by S. Vlaev and L. M. Gaggero-Sager, Editorial Nova Science Publishers, Huntington, New York, 2001.
3. Bovier, A. and J. M. Ghez, "Spectral properties of one-dimensional Schrödinger operators with potentials generated by substitutions," *Commun. Math. Phys.*, Vol. 158, No. 1, 45–66, 1993.
4. Pérez-Alvarez, R. and F. García-Moliner, *Transfer Matrix, Green Function and Related Techniques: Tools for the Study of Multilayer Heterostructures*, Universitat Jaume I, Castellón, Spain, 2004.
5. Rasband, S. N., *Chaos Dynamics of Nonlinear Systems*, Wiley Professional Paperback Series, 1997.
6. Pérez-Álvarez, R., F. García-Moliner, and V. R. Velasco, "Some elementary questions in the theory of quasiperiodic heterostructures," *J. of Phys.: Condens. Matter*, Vol. 13, 3689–3698, 2001.



## The Electrostatic Potential Associated to Interface Phonon Modes in Nitride Single Heterostructures

M. E. Mora-Ramos<sup>1</sup>, R. Pérez-Alvarez<sup>1</sup>, and V. R. Velasco<sup>2</sup>

<sup>1</sup>Facultad de Ciencias, Universidad Autónoma del Estado de Morelos, Mexico

<sup>2</sup>Instituto de Ciencia de Materiales de Madrid, CSIC, Spain

**Abstract**— Interface polar optical phonon modes bear the strongest electrostatic character among the long wavelength oscillation modes in polar semiconductor heterostructures. Therefore, they play a leading role in electron-phonon interaction. These modes are typically studied within the so-called dielectric continuum model (DCM). However, recent calculations of interface-phonon-limited electron mobility in nitride-based single heterostructure, using the DCM, have shown that the results thus obtained fall below the experimental reports on this quantity at room temperature for AlGa<sub>N</sub>/Ga<sub>N</sub> systems [1]. In the present work we calculate the electrostatic potential associated to the interface oscillation modes in nitride-based heterostructure by means of the complete phenomenological electroelastic continuum approach for the long wave optical oscillations [2], and the Surface Green Function Matching technique. The crystalline symmetries of zincblende and -isotropically averaged-wurtzite are considered in the sets of input bulk frequencies and dielectric constants.

### REFERENCES

1. Mora-Ramos, M. E., J. Tutor, and V. R. Velasco, *J. Appl. Phys.*, Vol. 100, 123708, 2006.
2. Trallero-Giner, C., R. Pérez-Alvarez, and F. García-Moliner, *Long Wave Polar Modes in Semiconductor Heterostructures*, Pergamon, London, 1998.

## Electronic Spectrum Study of Parabolic $GaAs/Al_xGa_{1-x}As$ Superlattices

I. Rodriguez-Vargas, O. Y. Sanchez-Barbosa, D. A. Contreras-Solorio, and S. J. Vlaev

Unidad Académica de Física, Universidad Autónoma de Zacatecas  
Calzada Solidaridad Esquina con Paseo la Bufa S/N, Zacatecas 98060, ZAC., México

**Abstract**— In the present work the electronic structure of finite parabolic GaAs/AlGaAs superlattices is studied. A detailed analysis of the miniband formation is given and the importance of all system parameters is discussed. The dependence of the equidistant mini-band separation on the superlattice size is revealed. A comparison with different theoretical methods and experimental data is presented. The calculations are conducted in the framework of the semi-empirical  $sp^3s^*$  tight-binding model including spin applying the Green function formalism and the Surface Green Function Matching Method (SGFM) method [1].

### REFERENCES

1. Vlaev, S., V. R. Velasco, and F. García-Moliner, “Electronic states in graded-composition heterostructures,” *Phys. Rev. B*, Vol. 49, No. 16, 11222–11229, 1994.

# Transport Properties of Delta Doped Field Effect Transistor

O. Oubram and L. M. Gaggero Sager

Facultad de Ciencias, Universidad Autónoma del Estado de Morelos  
Av. Universidad 1001, Col. Chamilpa, CP 62209, Cuernavaca, Morelos, Mexico

**Abstract**— The first calculation of mobility and conductivity between source and drain as function of gate voltage in a  $\delta$ -doped Field Effect Transistor is presented. The calculation was performed with a model for the  $\delta$ -FET that was shown in [1]. The mobility was calculated using a phenomenological expression that was presented in [2]. That expression does not have empirical form, neither empirical parameter. For the first time a phenomenological expression of the conductivity is presented, which is derived from the mobility expression. The conductivity shows three different regions: a parabolic region and two linear regions. The parabolic region represents the region at which the conduction channel begins to close. On the other hand, the mobility shows a more different behavior. In the mobility there are four regions. These regions correspond to the disappearance of the different conduction channels that form the subbands of the delta-doped quantum well. The different behavior between mobility and conductivity relies on the depletion of the delta-doped quantum well as the gate potential grows.

## REFERENCES

1. Gaggero-Sager, L. M. and R. Pérez-Alvarez, "A simple model for delta-doped field-effect transistor electronic states," *J. App. Phys.*, Vol. 78, No. 7, 4566–4569, 1995.
2. Rodriguez-Vargas, I., L. M. Gaggero-Sager, and V. R. Velasco, "Thomas-Fermi-Dirac theory of the hole gas of a double p-type delta-doped GaAs quantum wells," *Surf. Sci.*, Vol. 537, No. 1, 75–83, 2003.

## Mobility of Doped Graphene

Gerardo G. Naumis<sup>1</sup>, F. J. López-Rodríguez<sup>1</sup>, and L. M. Gaggero-Sager<sup>2</sup>

<sup>1</sup>Departamento de Física-Química, Instituto de Física  
Universidad Nacional Autónoma de México (UNAM)  
Apartado Postal 20-364, 01000, México D.F., Mexico

<sup>2</sup>Departamento de Física, Fac. de Ciencias  
Universidad Autónoma del Estado Morelos (UAEM)  
Cuernavaca, Morelos, Mexico

**Abstract**— We show that an internal localization mobility edge can appear around the Fermi energy in graphene by introducing impurities in the split-band regimen, or by producing vacancies in the lattice. The edge appears at the center of the spectrum and not at the band edges, in contrast with the usual picture of localization. Such result is explained by showing that the bipartite nature of lattice allows to renormalize the Hamiltonian, and the internal edge appears because of frustration effects in the renormalized lattice. The size in energy of the spectral region with localized states is similar in value to that observed in narrow gap semiconductors.

# Session 4A5

## Synthetic Aperture Radar Over Land and Sea

<p>The Cassini Mission to Saturn: Innovative Design of the Ku Band Titan Radar Mapper  <i>William T. K. Johnson (Jet Propulsion Laboratory, USA);</i> .....</p> <p>Dependency Analysis of Normalized Radar Cross Section of Ocean Surface on Ocean Winds Using an Airborne Dual-frequency Polarimetric Synthetic Aperture Radar  <i>Akitsugu Nadai (National Institute of Information and Communications Technology (NICT), Japan); Toshihiko Umehara (National Institute of Information and Communications Technology, Japan); Makoto Satake (National Institute of Information and Communications Technology (NICT), Japan); Takeshi Matsuoka (National Institute of Information and Communications Technology (NICT), Japan); Seiho Uratsuka (National Institute of Information and Communications Technology, Japan);</i> .....</p> <p>Double Structure of the Wind Jet through the Tsushima Strait  <i>Teruhisa Shimada (Tohoku University, Japan); Hiroshi Kawamura (Tohoku University, Japan);</i> ....</p> <p>Determination of Ocean Wave Imaging Mechanisms by Airborne Synthetic Aperture Radars  <i>C. S. Yang (Korea Ocean Research and Development Institute, Korea); K. Ouchi (National Defense Academy, Japan);</i> .....</p> <p>Surface Wave Parameters Retrieval in Coastal Seas from Spaceborne SAR Image Mode Data  <i>Jian Sun (Tohoku University, Japan); Hiroshi Kawamura (Tohoku University, Japan);</i> .....</p> <p>Some Potential Information in Airborne Single-pass Pol-InSAR Data over Land and Sea  <i>Haipeng Wang (Fudan University, China); Munetoshi Iwakiri (National Defense Academy, Japan); Kazuo Ouchi (National Defense Academy, Japan);</i> .....</p> <p>Extraction of Small Fishing Vessels from ALOS PALSAR Data  <i>Seong In Hwang (National Defense Academy, Japan); Kazuo Ouchi (National Defense Academy, Japan);</i> .....</p> <p>Estimation of Moving Target Parameters in High-resolution SAR Images  <i>Haipeng Wang (Fudan University, China); Kazuo Ouchi (National Defense Academy, Japan); Ya-Qiu Jin (Fudan University, China);</i> .....</p> <p>Experimental Studies on Monitoring Ground Motions with Corner Reflector InSAR  <i>Xiao-Li Ding (The Hong Kong Polytechnic University, China); R. Xiang (The Hong Kong Polytechnic University, China); J. P. Long (The Hong Kong Polytechnic University, China); Z. W. Li (The Hong Kong Polytechnic University, China); Q. Chen (The Hong Kong Polytechnic University, China); Peter Damoah-Afari (The Hong Kong Polytechnic University, China); K. S. Fung (Geotechnical Engineering Office, Civil Engineering and Development Department, China); V. Chan (Geotechnical Engineering Office, Civil Engineering and Development Department, China); Z. Lu (U.S. Geological Survey, EROS Center and Cascades Volcano Observatory, USA);</i> .....</p> <p>Decomposition-based Analysis of Highly Textured Forest Images Acquired by Airborne Polarimetric SAR    <i>Seisuke Fukuda (Institute of Space and Astronautical Science, Japan Aerospace Exploration Agency (ISAS/JAXA), Japan);</i> .....</p>	<p>766</p> <p>767</p> <p>768</p> <p>769</p> <p>770</p> <p>771</p> <p>772</p> <p>773</p> <p>774</p> <p>775</p>
--	---

# The Cassini Mission to Saturn: Innovative Design of the Ku Band Titan Radar Mapper

William T. K. Johnson

Jet Propulsion Laboratory, California Institute of Technology, Pasadena, CA 91109, USA

**Abstract**— The Cassini/Huygens Mission to Saturn was launched in 1997 and arrived in 2004. In addition to the NASA Cassini orbiter, the mission included the Huygens probe, built by the European Space Agency (ESA) to explore the atmosphere and surface of Saturn's moon Titan. Titan has been a mystery for many years, especially since the Voyager spacecraft determined that the dense atmosphere precludes the normal optical observation common to all other moons in the Solar System. This atmosphere, however, is transparent to radar frequencies, and thus a Ku band (13.77 GHz) radar was added to Cassini's complement of instruments. This instrument has many innovative design properties that make it unique among radars. Some of the challenges to the design include: a wide swath; a 4-m diameter, three frequency antenna shared with the telecommunications and radio science subsystems; a very limited time on target; a very limited data volume per Titan pass; and a spacecraft not in orbit around the principal target. The Magellan (Venus) radar had some of the same design difficulties, but it was the lone instrument on a spacecraft in orbit around the target while Cassini includes twelve instruments and passes Titan in a swift, hyperbolic trajectory.

This presentation will explore how many of the design features were selected and how a radar was jointly built by NASA and the Italian Space Agency (ASI) that met or exceeded all the requirements, operating as a radiometer, scatterometer, altimeter, and imaging SAR and, sometimes, an atmospheric probe. Although designed principally as a Synthetic Aperture Radar (SAR), the flexibility of the design has made possible data collection in the scatterometer mode well beyond 500,000 km and SAR mode at twice the initially required altitude. Some data examples will be shown for each radar mode but the focus will be on the instrument design itself.

# Dependency Analysis of Normalized Radar Cross Section of Ocean Surface on Ocean Winds Using an Airborne Dual-frequency Polarimetric Synthetic Aperture Radar

Akitsuugu Nadai, Toshihiko Umehara, Makoto Satake, Takeshi Matsuoka, and Seiho Uratsuka

Applied Electromagnetic Research Center  
National Institute of Information and Communications Technology  
4-2-1 Nukui-Kitamachi, Koganei, Tokyo 184-8705, Japan

**Abstract**— To analyze the coastal environment, the ocean surface wind field with high spatial resolution is important. Because the winds have two components (speed and direction), the external data is needed to determine the ocean surface wind using the SAR with single polarization. The coarse spatial resolution of the external data leads a measurement error of ocean winds using SAR. In this paper, the dependency of normalized radar cross-section (NRCS) of ocean surface on ocean surface winds is analyzed and compared between radar polarizations and frequencies by using the airborne dual-frequency polarimetric SAR with L- and X-band, called Pi-SAR, developed by NICT and JAXA.

The dependency of NRCS of ocean surface on wind direction is analyzed using multiple SAR observations of same area in short time by using a geophysical model function as  $\sigma = a_0 + a_1 \cos(\theta) + a_2 \cos(2\theta)$ , where  $\sigma$  and  $\theta$  is the NRCS and the relative wind direction, respectively. For X-band HH polarization, the magnitude of  $a_1$  is much larger than that of X-band VV polarization. This peculiarity of X-band HH polarization suggests the possibility of measurement of ocean surface wind only using X-band polarimetric SAR data. The polarimetric rate of X-band also changes with the relative wind direction. On the other hand, the NRCSs of L-band parallel components change almost same with the wind direction.

This study suggests the possibility of measurement of the ocean surface wind with high spatial resolution by the X-band polarimetric SAR without any external data.

## Double Structure of the Wind Jet through the Tsushima Strait

Teruhisa Shimada and Hiroshi Kawamura

Center for Atmospheric and Oceanic Studies  
Graduate School of Science, Tohoku University, Sendai, Japan

**Abstract**— We investigate the wind jet blowing through the Tsushima Strait using SAR (ALOS/PALSAR, ENVISAT/ASAR, and RADARSAT) and scatterometer.

First we describe the features of the wind jet through the Tsushima Strait. This strait often promotes the formation of the wind jet when the northeasterly or southwesterly wind blows into the strait. On the other hand, a slender island Tsushima divides the Tsushima Strait into two (west and east) channels. High-resolution wind fields derived from SAR reveal the double structure of the wind jet through the Tsushima Strait. To put it into perspective, the Tsushima Strait can act as a terrestrial gap, accelerating the wind. However, to be exact, both west and east channels can be terrestrial gaps, forming two smaller-scale wind jets. Winds also blow through the terrestrial gap at the midpoint of the Tsushima. Moreover, terrestrial blocking of wind due to the island increase the wind speed differences in the strait.

Then, using 8-year QuikSCAT wind measurements, we obtain wind statistics in the strait. The majority of wind jets blowing from northeast to southwest occur in August–October. On the other hand, the frequency of the wind jets blowing southwest to northeast is large in May–July. The wind speeds are generally larger in northeast-southwest cases (8–13 m/s) than southwest-northeast cases (7–10 m/s).

Monitoring research of this strait is of primary importance from meteorological, oceanographic and disaster-prevention point of view. The results of this study provide us with new insights into the dynamics of the wind jet through the Tsushima Strait and into the impacts on the meteorology and ocean.



# Determination of Ocean Wave Imaging Mechanisms by Airborne Synthetic Aperture Radars

C. S. Yang<sup>1</sup> and K. Ouchi<sup>2</sup>

<sup>1</sup>Ocean Satellite Research Group, Korea Ocean Research and Development Institute  
Sa2-dong 1270, Sangnuk-gu, Ansan, Gyeonggi-do, 426-744, Korea

<sup>2</sup>Department of Computer Science, National Defense Academy  
1-10-20 Hashirimizu, Yokosuka, Kanagawa 239-8686, Japan

**Abstract**— Analysis of ocean waves using synthetic aperture radar (SAR) images is an important issue in oceanography, not only for an academic interest but also for validation and improvement of wave forecasting models and for the utilization in shipping industry and in the field of maritime disaster prevention. Since the launch of the SEASAT satellite with a L-band SAR in 1978, considerable effort has been made to understand the SAR imaging mechanisms of ocean waves, and a large number of publications are available. Consequently, the principal mechanisms of imaging ocean waves by SAR are considered to be well understood. According to the present knowledge, there appear 4 major image modulations to contribute to SAR image formation of ocean waves [1]. The first is the RCS (Radar Cross Section) modulation which is largest for range travelling waves and vanishes for azimuth travelling waves. The second is the velocity bunching modulation arising from the wave motion. This modulation is inherent to SAR, and it is largest for azimuth waves and vanishes for range waves. The third and fourth are the tilt and hydrodynamic modulations associated with the small-scale waves. Among these modulations, velocity bunching still requires some attention, because its theory is not yet, in a strict sense, confirmed by experiment.

In the present article, we analyse airborne Pi-SAR (Polarimetric-Interferometric SAR) X-band images of ocean waves around the Miyake Island at approximately 180 km south from Tokyo, Japan. Two images of a same scene were produced at approximately 40 min. interval from two directions at right angles. One image shows dominant range travelling waves, but the other image shows a different wave pattern. This difference can be caused by the different image modulations of RCS and velocity bunching. We have estimated the dominant wavelength from the image of range waves, and from the wave phase velocity computed from the dispersion relation (though no wave height data were available), the image intensity is computed by using the velocity bunching model [2]. The comparison of the result with the second image at right angle strongly suggests the evidence of velocity bunching.

## REFERENCES

1. Hasselmann, K., R. K. Raney, W. J. Plant, W. Alpers, R. A. Shuchman, D. R. Lyzenga, C. L. Rufenach, and M. J. Tucker, "Theory of synthetic aperture radar ocean imaging: a MARSEN view," *J. Geophys. Res.*, Vol. 90, No. C3, 4659–4686, 1985.
2. Ouchi, K. and D. A. Burrige, "Resolution of a controversy surrounding the focusing mechanisms of synthetic aperture radar images of ocean waves," *IEEE Trans. Geosci. Remote Sens.*, Vol. 32, 1004–1016, 1994.

## Surface Wave Parameters Retrieval in Coastal Seas from Spaceborne SAR Image Mode Data

Jian Sun<sup>1,2</sup> and Hiroshi Kawamura<sup>1</sup>

<sup>1</sup> Graduate School of Science, Tohoku University, Sendai, Japan

<sup>2</sup> Physical Oceanography Laboratory, Ocean University of China, Qingdao, China

**Abstract**— We have developed a retrieval scheme of surface wave parameters (wave height and wave propagation direction) from ERS Synthetic Aperture Radar (SAR) image mode data in coastal seas around Japan. In this study, we investigated the energy of simulated SAR spectrum at different wind speed using nonlinear wave-SAR imaging mechanism, derived the criteria to differentiate swell from wind waves, and accordingly processed SAR images containing swell and wind waves in different way respectively. SAR spectra are converted to surface wave spectra of swell-dominated or wind-wave dominated cases. The SAR spectrum and SAR-derived wind speed are used for the derivation of surface wave spectrum. The wind-wave dominated case and swell-dominated case are differentiated by the wind speed of 6 m/s, and processed in different ways because of their different nonlinear degree. It is indicated that the cutoff wavelength for retrieval of the wind-wave dominated spectrum is proportional to the root of significant wave height, which is consistent with the results of previous studies. We generated 66 match-ups coupling the SAR sub-images and the in-situ surface wave parameters, which were measured by the wave gauges installed in near-shore seas. Among them, the number of swell-dominated case is 57, and the number of wind-wave dominated case is 9. The SAR-derived and in-situ significant wave heights agree well with the bias of 0.24 m, the RMS error 0.92 m and the correlation coefficient of 0.66. The averaged absolute deviation of wave propagation directions is  $18.4^\circ$ , and the agreement tendency does not depend on the wave height. It is proven through the comprehensive validation that the developed SAR surface wave spectrum has high accuracy in the Japanese coastal seas.

# Some Potential Information in Airborne Single-pass Pol-InSAR Data over Land and Sea

Haipeng Wang<sup>1</sup>, Munetoshi Iwakiri<sup>2</sup>, and Kazuo Ouchi<sup>2</sup>

<sup>1</sup>Key Laboratory of Wave Scattering and Remote Sensing  
Department of Communication Science and Engineering, School of Information Science and Engineering  
Fudan University, Shanghai 200433, China

<sup>2</sup>Department of Computer Science, School of Electrical and Computer Science  
National Defense Academy, 1-10-20 Hashirimizu, Yokosuka, Kanagawa 239-8686, Japan

**Abstract**— With rapid advance of SAR (Synthetic Aperture Radar) technology, the most of today's airborne and spaceborne SARs are equipped with fully- or dual-polarimetric and interferometric systems. Accordingly, polarimetric SAR and polarimetric-InSAR (Pol-InSAR) have attracted considerable attention [1, 2]. One of the interesting subjects is the utilization of the coherence property in multi-pass Pol-InSAR data to extract forest and other volume-scattering parameters and to improve the accuracy of image classification [3].

In the present paper, we summarise some potential information in the single-pass fullypolarimetric X-band airborne Pi-SAR (Polarimetric-interferometric SAR) data over the Naruto Strait between the Shikoku Island and mainland of Japan. It is shown that, on the contrary to the coherence of multi-temporal Pol-InSAR interferogram [3], there is high interferometric coherence between HH and VV polarisation images of sea surface due to the Bragg-type single-bounce scattering mechanism; while very low coherence is observed over terrain where multiple or volume scattering dominates. This coherence property can be used to extract man-made objects over the sea. There are several other features observed in the data, including those based on the 4-component decomposition analysis over the sea, which may contain potential information with possible applications to classification of man-made objects such as boats and rafts of marine cultivation. These features are presented and discussed.

## ACKNOWLEDGMENT

This work is supported in part by the Hitachi Ltd., Tokyo, Japan.

## REFERENCES

1. Cloude, S. R. and E. Pottier, "A review of target decomposition theorems in radar polarimetry," *IEEE Trans. Geosci. Remote Sens.*, Vol. 34, 498–518, 1996.
2. Freeman, A. and S. L. Durden, "A three-component scattering model for polarimetric SAR data." *IEEE Trans. Geosci. Remote Sens.*, Vol. 36, 963–973, 1998.
3. Cloude, S. R. and K. P. Papathanassiou, "Polarimetric SAR interferometry," *IEEE Trans. Geosci. Remote Sens.*, Vol. 36, 1551–1565, 1998.

# Extraction of Small Fishing Vessels from ALOS PALSAR Data

SeongIn Hwang and Kazuo Ouchi

Department of Computer Science, School of Electrical and Computer Engineering  
National Defense Academy, 1-10-20 Hashirimizu, Yokosuka, Kanagawa 239-8686, Japan

**Abstract**— Ship detection using spaceborne SAR (Synthetic Aperture Radar) imagery has progressed significantly over the past decade. It has led to the development of algorithms and tools that support the operational use of SAR for monitoring shipping and fishing activities in coastal and offshore areas.

In this paper, attempts were made to extract small fishing vessels using ALOS (Advanced Land Observing Satellite) PALSAR (Phased Array L-band SAR) image data. We deployed 3 types of small fishing vessels of length approximately 9, 12, 14 m at four occasions. The PALSAR data include those in the FBD (Fine Beam Dual-polarization) mode at the nominal incidence angles of  $34.3^\circ$  and  $41.5^\circ$ , FBS (Fine Beam Single-polarization) mode at the incidence angle of  $21.5^\circ$ , and PLR (PoLaRimetric) mode at  $21.5^\circ$  of incidence.

To extract targets we considered two approaches. The first is to utilize coherence images derived from cross-correlation of multilook images [1], and the second is based on CALOG/CFAR (Cell Averaging Logarithmic/Constant False Alarm Rate) [2]. We have succeeded to extract all ships in FBD and FBS modes, but not in PLR mode. From the comparison of SNR (Signal to Noise Ratio) of the resultant images processed by the two techniques, the cross-correlation method is found to be better than the CALOG/CFAR method. Currently, attempts are being made to extract the images of ships that are not visible in the PLR mode by using the polarimetric analysis.

## REFERENCES

1. Ouchi, K., S. Tamaki, H. Yaguchi, and M. Iehara, "Ship detection based on coherence images derived from cross correlation of multilook SAR images," *IEEE Geosci. Remote Sens. Let.*, Vol. 1, No. 3, 184–187, 2004.
2. Schleher, D. C., *Automatic Detection and Radar Data Processing*, Artech House, Boston/London, 1980.

# Estimation of Moving Target Parameters in High-resolution SAR Images

Haipeng Wang<sup>1</sup>, Kazuo Ouchi<sup>2</sup>, and Ya-Qiu Jin<sup>1</sup>

<sup>1</sup>Key Laboratory of Wave Scattering and Remote Sensing  
Department of Communication Science and Engineering  
School of Information Science and Engineering, Fudan University  
Shanghai 200433, China

<sup>2</sup>Department of Computer Science, School of Electrical and Computer Engineering  
National Defense Academy, 1-10-20 Hashirimizu, Yokosuka, Kanagawa 239-8686, Japan

**Abstract**— In this paper, two approaches are proposed to estimate the moving target parameters in high-resolution SAR (Synthetic Aperture Radar) images. PALSAR (Phased Array L-band SAR) on board of ALOS (Advanced Land Observing Satellite) images are exploited in this project. The first approach is the method of split-look (or multilook) image subtraction, where a full-aperture length image is split into two subaperture images. When split-look processing is applied to raw data, there is an inter-look time difference (approximately 1 s), so that the positions of moving targets will be different between the subimages [1]. Therefore, the moving target can be detected by subtracting one look from another. However, since the radar cross section (RCS) is different between looks even for a small angular difference (approximately 1°), the experimental results show that the accuracy of detection is affected by this inter-look RCS difference from stationary targets, and moving targets cannot easily be recognised. One way of utilizing split-look images is to compute the cross-correlation between looks using moving window. In this way, the direction of moving targets can be extracted. The second method is the frequency domain approach, in which the range velocity component of a moving target can be estimated by the center frequency shift in the power spectrum of a single full-look complex image.

Split-look processing is also applied to extract ocean wave parameters including propagation direction, phase velocity and wavelength [2, 3]. Two subimages are produced by non-overlapped subapertures, and analysed in frequency domain. The results show that the estimated wave parameters are in good agreement with the measured truth data.

## ACKNOWLEDGMENT

This project is supported in part by the Hitachi Ltd., Tokyo, Japan, and the National Science Foundation of China under Grants 40637033 and 60571050.

## REFERENCES

1. Ouchi, K., "On the multilook images of moving targets by synthetic aperture radars," *IEEE Trans. Antennas Propagat.*, Vol. 33, 823–827, 1985.
2. Vachon, P. W. and J. C. West, "Spectral estimation technique for multilook SAR images of ocean waves," *IEEE Trans. Geosci. Remote Sens.*, Vol. 30, 568–577, 1992.
3. Ouchi, K., S. Maedoi, and H. Mitsuyasu, "Determination of ocean wave propagation direction by split-look processing using JERS-1 SAR data," *IEEE Trans. Geosci. Remote Sens.*, Vol. 37, 849–855, 1999.

## Experimental Studies on Monitoring Ground Motions with Corner Reflector InSAR

X. L. Ding<sup>1</sup>, R. Xiang<sup>1</sup>, J. P. Long<sup>1</sup>, Z. W. Li<sup>1</sup>, Q. Chen<sup>1</sup>  
P. Damoah-Afari<sup>1</sup>, K. S. Fung<sup>2</sup>, V. Chan<sup>2</sup>, and Z. Lu<sup>3</sup>

<sup>1</sup>Department of Land Surveying and Geo-Informatics, The Hong Kong Polytechnic University  
Hung Hom, Kowloon, Hong Kong, China

<sup>2</sup>Geotechnical Engineering Office, Civil Engineering and Development Department  
Hong Kong Special Administrative Region, Hong Kong, China

<sup>3</sup>U.S. Geological Survey, EROS Center & Cascades Volcano Observatory  
Vancouver, WA, USA

**Abstract**— Six corner reflectors (CR) installed on a hillside slope and on reclaimed land in Hong Kong are used as point targets in our interferometric synthetic aperture radar (InSAR) experiments to study ground motions related to the landslide and ground settlement. Eight ESA ENVISAT SAR images spanning from February 2006 to May 2007 are used in the study. The Least-square AMBiguity Decorrelation Adjustment method (LAMBDA) that was originally developed for phase ambiguity resolution in GPS positioning is used for phase unwrapping in processing the InSAR data. The zenith tropospheric delays determined with 12 continuous GPS stations in Hong Kong are used in the study to determine and correct for the tropospheric delays to the InSAR measurements. Both linear and periodic deformation models are tested in the study. The study demonstrates that the CRInSAR method can be used to monitor ground motions with good accuracy and reliability.

# Decomposition-based Analysis of Highly Textured Forest Images Acquired by Airborne Polarimetric SAR

S. Fukuda

Institute of Space and Astronautical Science  
Japan Aerospace Exploration Agency (ISAS/JAXA), Japan

**Abstract**— Modern high-resolution airborne SAR systems have become able to capture forest texture. Texture in SAR images is fluctuation of radar cross section (RCS) originating from intrinsic spatial variability of distributed targets, and is related to what is called non-Gaussian characteristics of the data. In the previous PIERS, we reported the results of texture analyses over coniferous forests in  $L$ -band images acquired by the Pi-SAR, the Japanese polarimetric airborne sensor [1]. There observed low order parameters of the K-distribution model were related to existence of patch-like sparse forest areas. It was supposed that the spotted sparse areas, where the mean RCS was relatively small due to the poor canopy, certainly enhanced the non-Gaussian property of the forest image including them.

In order to validate the above results, decomposition-based analyses are performed in this study. The decomposition algorithm that A. Freeman recently proposed [2], successfully revealed spotted high contribution of ground (double-bounce or direct) scattering in the forest stand with the low order parameters. On the other hand, volume scattering is dominant in the surrounding forest stands where the data statistics are almost Gaussian. Furthermore the spotted high contribution of ground scattering is only observed in HH polarization; volume scattering is dominant in other polarization. This difference between polarization channels could encourage our understanding of polarimetric variation of forest texture. In this Pi-SAR data, the flight direction also has a certain influence on presence of the spotted ground scattering and the corresponding non-Gaussian characteristics. This direction dependence is physically investigated by analyzing symmetric properties of the forest damaged by the typhoon.

## REFERENCES

1. Fukuda, S. and S. Nakamura, "Statistical analysis of airborne SAR images over a forest region," *IERS 2006*, 398, Tokyo, Japan, Aug. 2006.
2. Freeman, A., "Fitting a two-component scattering model to polarimetric SAR data from forest," *IEEE Trans. Geosci. Remote Sensing*, Vol. 45, No. 8, 2583–2592, Aug. 2007.





# Session 4A6

## Waves in Random and Complex Media — Recent Advances in Theoretical and Computational Analyses

Statistical Characteristics of Transmitted Nano-meter Electromagnetic Waves in Random Bio-medical Tissues for X-Ray Diagnostic Images	778
<i>Yasumitsu Miyazaki (Aichi University of Technology, Japan);</i> .....	
Propagation in Time-dependent Scattering Media	780
<i>Shimshon Frankenthal (Tel Aviv University, Israel); Mark J. Beran (Tel Aviv University, Israel);</i> ...	
Asymptotic Behaviour of Light in a Random Waveguide System	781
<i>Akira Komiyama (Osaka Electro-Communication University, Japan);</i> .....	
The Radar Cross-section of a Cylinder Surrounded by a Phase Changing Screen	782
<i>C. Fujisaki (Mitsubishi Electric Corporation, Japan); K. Haruta (Kyushu University, Japan); Z.-Q. Meng (Fukuoka University, Japan); Mitsuo Tateiba (Kyushu University, Japan);</i> .....	
FDTD Parallel Computing of Microwave Scattering and Attenuation Characteristics Due to Randomly Distributed Rainfalls	783
<i>Yasumitsu Miyazaki (Aichi University of Technology, Japan); Koichi Takahashi (Aichi University of Technology, Japan); Nobuo Goto (The University of Tokushima, Japan);</i> .....	
Local Modes in Random Lasers	785
<i>Allard P. Mosk (University of Twente, The Netherlands);</i> .....	
An Iterative Progressive Numerical Method to the Computation of Scattering from Many Cylinders and Its Parallelization	786
<i>Norimasa Nakashima (Kyushu University, Japan); Mitsuo Tateiba (Kyushu University, Japan);</i> ....	
Field Approximation for Reconstruction of 2D Perfectly Conducting Rough Surfaces	787
<i>Mark Spivack (University of Cambridge, UK); S. Bottone (DataPath Inc, USA); O. Rath (University of Cambridge, UK);</i> .....	
Radar Cross-section of Targets Using Beam Wave Incidence with Linear Polarization	788
<i>Hosam El-Ocla (Lakehead University, Canada);</i> .....	
Polarization of Waves in Reciprocal and Nonreciprocal Uniaxially Bianisotropic Media	789
<i>Xiangxiang Cheng (Zhejiang University, China); Jin Au Kong (Massachusetts Institute of Technology, USA); Lixin Ran (Zhejiang University, China);</i> .....	
Selective Cancellation of Optical Scattering in Random Media	790
<i>Claude Amra (UniversitéPaul Cézanne, France); C. Deumié (UniversitéPaul Cézanne, France); G. Georges (UniversitéPaul Cézanne, France); L. Arnaud (UniversitéPaul Cézanne, France); M. Zerrad (UniversitéPaul Cézanne, France);</i> .....	

# Statistical Characteristics of Transmitted Nano-meter Electromagnetic Waves in Random Bio-medical Tissues for X-Ray Diagnostic Images

Yasumitsu Miyazaki

Department of Media Informatics, Aichi University of Technology  
50-2 Manori, Nishihazama-cho, Gamagori 443-0047, Japan

**Abstract**— Medical image diagnosis and computer aided diagnosis using nano-meter electromagnetic waves and X-ray are very important medical techniques. Particularly, computer tomography techniques are indispensable medical diagnosis based on transmitted X-ray image processing. However, in X-ray image processing with computed radiography for medical diagnosis, physical and physiological phenomena of X-rays are not so much investigated, based on interaction phenomena between bio-medical material and X-ray. Interaction phenomena between bio-medical material and X-ray are concerned with electromagnetic phenomena of a few KeV energy level interactions between deep electrons and nano-meter electromagnetic waves. Photo-electric absorption, Thomson scatterings and Compton scattering are fundamental phenomena in bio-medical tissues, when X-ray is incident into bio-medical materials. Complex refractive index of bio-medical materials consisting of high molecules and polymers for nano-meter electromagnetic waves are real values of less than one and relatively large imaginary values, depending on tissue constructions such as bones, muscles and fats.

Transmitted X-ray responses through biomedical materials are derived by photo-electric absorption and X-ray scatterings. Received X-ray images for medical diagnosis concerned with X-ray absorption are disturbed by X-ray scatterings due to heavy atoms in polymers. If statistical characteristics of X-ray scatterings in random bio-medical tissues are studied and spatial X-ray filter devices for filtering of X-ray scattering for protection of net absorption characteristics are developed, excellent X-ray image diagnosis system may be accomplished.

In this paper, statistical theory of nano-meter electromagnetic waves in bio-medical random media is discussed. Vector wave analysis of X-ray scattering using Green's function is shown for X-ray incident Gaussian beams in short propagation lengths. Based on scattering characteristics for short propagation phenomena, propagation equations for the axial direction are derived using transverse and axial scattering factors correlation function for random bio-medical media. For long distance propagation, large scattering distribution and axial absorption characteristics are studied by axial propagation equation with transverse and axial scattering factors. Scattering factor have properties of homogeneous scatterings for small correlation length of random bio-medical media and forward scatterings for long correlation length. Back scattering and reflection characteristics are concerned with random bio-medical tissues of small correlation lengths. X-ray image responses depend on mainly forward scattering and X-ray absorptions, with scattering losses due to random bio-medical characteristics of small correlation lengths.

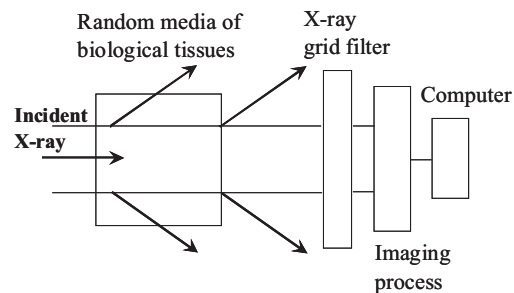


Figure 1: Computer aided diagnosis and scattering X-ray filtering system.

## REFERENCES

1. Miyazaki, Y., "Light scattering of laser beams by random micro-inhomogeneities in glasses and polymers," *Jpn. Jour. Appl. Phys.*, Vol. 13, No. 8, 1238-1248, 1974.

2. Miyazaki, Y., "Electromagnetic characteristics of grid structures for scattering fields of nanometer electromagnetic waves and X-rays," *Proc. of PIERS 2006*, 643–647, Tokyo, Aug. 2006.
3. Miyazaki, Y., "Beam propagation and radiation fields in a uniformly curved X ray dielectric gradient waveguides," *Trans. IEE of Japan*, Vol. 120-C, No. 1, 68–73, Jan. 2000.
4. Miyazaki, Y., "Electromagnetic characteristics of waveguide-type grid filters for scattered nanometer waves in transmitted X-ray diagnostic images," *Proc. of EMTS 2007*, EMTS128, Ottawa, ON, Canada, July 2007.

## Propagation in Time-dependent Scattering Media

Shimshon Frankenthal and Mark J. Beran

Faculty of Engineering, Tel Aviv University, Ramat Aviv, Tel Aviv, Israel

**Abstract**— We have derived equations that govern the range-evolution of the 2nd and 4th order statistics of the forward- and back-propagating components of radiation in media wherein the scattering process (refractivity fluctuations) depends both on space and on time. These are generally integro-difference equations that account for the broadening of the signal spectra due to the time-dependence of the random fluctuations for the scattering media. The solution of these equations is greatly simplified in the so-called quasi-monochromatic regime, where the aforementioned spectral broadening of, say, erstwhile-monochromatic radiation, is limited to a narrow spectral range about the incident frequency. We present relevant results for transversely infinite media, and for propagation in a duct.

Our stochastic treatment is applicable when the correlation-length  $L$  and time  $\tau$  that are associated with the scattering process satisfy the condition  $L/c \ll \tau \ll \ell$ , where  $c$  the average wave-speed in the medium and  $\ell$  a mean scattering length. Consequently, the results of our analysis cannot be expected to apply in the limit  $\tau \rightarrow \infty$  that corresponds to a time-independent medium. However, we can determine the probability density distributions of the power reflection coefficient, and of the various fluxes of the components of an erstwhile plane wave that propagates in a one-dimensionally stratified slab of a time-independent scattering medium. We can thus determine the 2nd and 4th order statistics of the power-fluxes, compare them the corresponding characteristics of the radiation propagating in time-dependent media, and rationalize the differences. We discuss the relevance of this problem to the localization phenomenon, and also examine the distribution of the emerging power-flux and the limitations on the assumption that it possesses a lognormal distribution.

# Asymptotic Behaviour of Light in a Random Waveguide System

Akira Komiyama

Osaka Electro-Communication University  
Hatsu-cho Neyagawa-shi 572-8530, Japan

**Abstract**— The differential equations of the recurrence type describing the light propagation in a random waveguide system can be theoretically derived from the perturbation solution to the coupled mode equations [1, 2], which are given in the matrix form as follows:

$$\frac{dP}{dz} = \kappa a^\downarrow Q^{(1)} + \alpha P^c$$

$$\frac{dQ^{(l)}}{dz} = -\alpha Q^{(l)} + (-1)^l \kappa \left( a^\uparrow Q^{(l-1)} + a^\downarrow Q^{(l+1)} \right), \quad l = 1, 2, 3 \dots$$

where  $P$  and  $P^c$  are the incoherent part and the coherent part of the average power of light, respectively. The forced term  $P^c$  can be obtained from the solution to the coupled mode equations for a system composed of identical cores.  $\alpha$  is the damping factor reflecting randomness of the system and  $\kappa$  is the mode coupling coefficient.  $a^\uparrow$  and  $a^\downarrow$  are the constant matrices.  $Q^{(l)}$ s are the cross powers between cores. By eliminating  $Q^{(l)}$ s, the recurrent differential equations can be reduced to the integro-differential equation [3],

$$\frac{dP}{dz} = -2\kappa^2 \int_0^z K(z-\xi) a^\uparrow P(\xi) d\xi + \alpha P^c$$

where  $K(z)$  is the memory kernel, which is expressed as  $K(z) = a^\downarrow M(z) e^{-\alpha z}$ .  $M(z)$  is a function independent of  $\alpha$  and is easily expanded into powers of  $\kappa z$ . Using partial integrations the integro-differential equation can be rewritten to the convolutionless differential equation,

$$\frac{dP}{dz} = L(z) a^\uparrow P(z) + \alpha P_{cor}^c(z)$$

where  $P_{cor}^c$  is the correction to  $P^c$ . The operator  $L(z)$  is expanded into powers of  $\alpha^{-1}$ . For  $\alpha z \gg 1$ ,  $L(z)$  is reduced to the constant operator  $L(\infty)$ . By replacing the exact operator  $L(z)$  with the constant operator  $L(\infty)$ , the approximate solution can be obtained, which is given by

$$P(z) = \int_0^z R(z-\xi) P_{cor}^c(\xi) d\xi$$

$R(z)$  can be expressed as the integral over all eigenstates of the operator  $L(\infty)$ . Evaluating asymptotically the integral we have  $R(z) \sim z^{-1/2}$  as  $z \rightarrow \infty$ .

## REFERENCES

1. Komiyama, A., *Proceedings of 2004 URSI EMT-S*, 260–262, 2004.
2. Komiyama, A., *Abstracts of PIERS 2006*, 274, Cambridge, 2006.
3. Komiyama, A., *Abstracts of PIERS 2007*, 329, Prague, 2007.

## The Radar Cross-section of a Cylinder Surrounded by a Phase Changing Screen

C. Fujisaki<sup>1</sup>, K. Haruta<sup>2</sup>, Z.-Q. Meng<sup>3</sup>, and M. Tateiba<sup>2</sup>

<sup>1</sup>Communication Systems Center, Mitsubishi Electric Corporation  
8-1-1, Tsukaguchi-Honmachi, Amagasaki, Hyogo 661-8661, Japan

<sup>2</sup>Department of Computer Science and Communication Engineering  
Kyushu University, Fukuoka 812-8581, Japan

<sup>3</sup>Department of Electrical Engineering, Fukuoka University, Fukuoka 814-0180, Japan

**Abstract**— Wave scattering from a body in a random medium is one of important subjects in the fields of radar engineering, remote sensing, astronomy and bioengineering. Because an exact solution for the scattering analysis as a boundary value problem is not easy, a simple but generic model that can explain the scattering characteristics is convenient for studies in the aforementioned fields. In fact, a model with a phase changing screen (PCS) has been proposed in optical-field for continuous random media.

In this paper, we try to analyze wave scattering from a cylinder surrounded by a PCS as a boundary value problem. The geometry is shown in Fig. 1. Here the PCS is assumed as an infinitesimal thin layer which changes randomly the phases of waves after passing through it. Kirchhoff-Huygens's principle leads to the calculation of the incident wave on the cylinder and the scattered wave observed by a receiver. The ensemble average of bistatic radar cross-section (RCS) of a circular cylinder ( $\sigma_{\text{pcs}}$ ) normalized by that without the PCS ( $\sigma_{\text{free}}$ ) is shown in Fig. 2 as a function of the angle  $\theta_r$  between the transmitter and the receiver. There are a backscattering enhancement peak at  $\theta_r = 0$  and a depression of the RCS outside the peak. The normalized RCS tends to one for larger  $\theta_r$ , and the integral value of the RCS with respect to  $\theta_r$  becomes almost one. This fact means that the results agree with the law of energy conservation. These normalized RCS characteristics agree well with those obtained for a cylinder embedded in a continuous random medium [1].

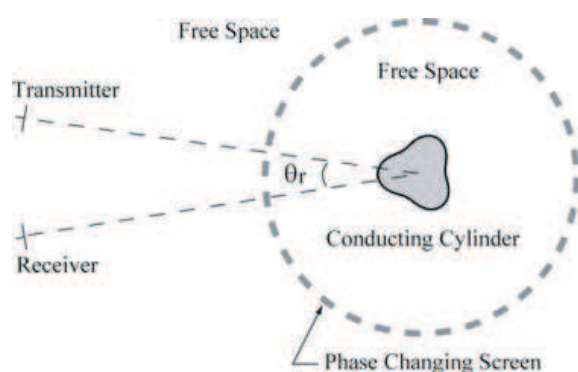


Figure 1: Geometry of the scattering problem.

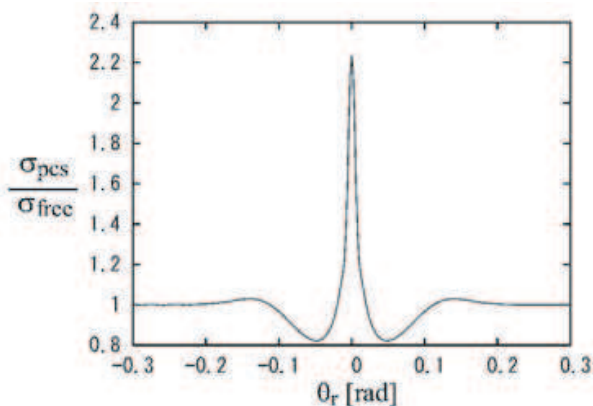


Figure 2: Normalized RCS.

### REFERENCES

1. Meng, Z.-Q., N. Yamasaki, and M. Tateiba, "Numerical analysis of bistatic cross-sections of conducting circular cylinders embedded in continuous random media," *IEICE Transactions on Electronics*, Vol. E83-C, No. 12, 1814–1819, 2000.

# FDTD Parallel Computing of Microwave Scattering and Attenuation Characteristics Due to Randomly Distributed Rainfalls

Yasumitsu Miyazaki<sup>1</sup>, Koichi Takahashi<sup>1</sup>, and Nobuo Goto<sup>2</sup>

<sup>1</sup>Department of Media Informatics, Aichi University of Technology  
50-2 Manori, Nishihassama-cho, Gamagori 443-0047, Japan

<sup>2</sup>Institute of Technology and Science, The University of Tokushima  
2-1 Minamijosanjima-cho, Tokushima 770-8506, Japan

**Abstract**— Rain measurement system using propagation characteristics of microwave and millimeter wave is very important for disaster prevention system to foresee and prevent the occurrence of disasters caused by strong rainfalls and for the sensor of ITS (Intelligent Transport Systems) to support safe and automatic driving and cruising. Measurement technique of electromagnetic scattering and attenuation characteristics by rain is one of accurate evaluation methods of rainfall rate. Rain measurement system using microwave and millimeter wave has the advantage of rapid measurement of rainfall rate in wide area compared with the direct measurement by rain gauges. In this study, propagation region is modeled as random media with randomly distributed rainfalls. Propagation of electromagnetic wave in random media is analyzed by three-dimensional FDTD method. FDTD analysis demonstrates the dynamic characteristics of wave scattering and absorption phenomena in rain region where raindrops are distributed randomly.

In this analysis, the shapes of raindrops are assumed to be cubic with several side lengths. Random scatterers are generated by giving the number of raindrops  $N$ , with lengths of side lengths of cubic  $a_i$ , positions of one apex  $(x_i, y_i, z_i)$  and complex dielectric constants  $\varepsilon_i^* = \varepsilon_i' - j\varepsilon_i''$ . For the incident wave, the Gaussian beam of x polarization that propagates along the  $z$  axis is assumed. For the analysis of microwave scattering by rain, the analysis space including many raindrops less than and comparable with the wavelength is required and analysis region is much larger than the wavelength and a few meters. Parallel computation of FDTD using grid computer is indispensably important. To perform parallel processing using grid computer, the total analysis space is divided into subdomains of  $Mz \times My$  as shown in Fig. 1 and one divided subdomain  $D_{u,v}$  is assigned to one of PC computers. The electromagnetic fields in  $D_{u,v}$  ( $1 \leq v \leq My$ ) are calculated by parallel processing. For the calculation of values on the boundary of subdomains, values in the adjacent subdomain are exchanged and matched for field boundary condition. To proceed the parallel processing, data transfer between adjacent subdomains is carried out using MPI. Along  $z$  direction, electromagnetic fields are calculated successively by storing the electromagnetic fields at the end point of subdomain in the  $z$  direction to computer memory. These stored electromagnetic fields are used as incident field in the domain boundary, to calculate the fields in the next subdomains  $D_{u+1,v}$  ( $1 \leq v \leq My$ ).

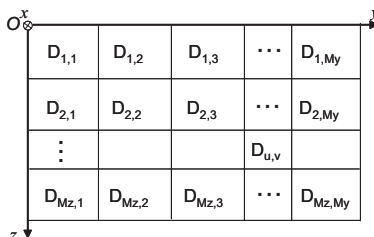


Figure 1: Parallel processing of microwave scattering and attenuation in rain region, subdomain  $D_{u,v}$  ( $1 \leq u \leq Mz, 1 \leq v \leq My$ ).

In this paper, propagation characteristics of microwave in rain region are discussed using FDTD method. The effects of multiple scattering and absorption due to randomly distributed raindrops are studied and the relationships between rainfall rate and specific attenuation are evaluated numerically. The numerical results of specific attenuation are compared with the experimental results to evaluate the accuracy of FDTD computer simulation.

**REFERENCES**

1. Oguchi, T., "Electromagnetic wave propagation and scattering in rain and other hydrometers," *IEEE Proc.*, Vol. 71, 1029–1078, 1983.
2. Takahashi, K. and Y. Miyazaki, "Scattering and attenuation characteristics of microwave and millimeter wave due to rainfall for its and weather measurement system," *Proc. of ISAP'04*, POS-B-4, 1081–1084, Sendai, Japan, 2004.
3. Miyazaki, Y. and K. Takahashi, "Computer simulation of X-Ray scattering characteristics for medical image diagnosis," *Trans. IEE Japan*, Vol. 126-C, No. 12, 1431–1440, 2006.
4. Rodriguez, G., Y. Miyazaki, and N. Goto, "Matrix-based FDTD parallel algorithm for big areas and its applications to high-speed wireless communications," *IEEE Trans. Antennas & Propagat.*, Vol. 54, No. 3, 785–796, 2006.



## Local Modes in Random Lasers

A. P. Mosk

MESA+ Institute for Nanotechnology and Department of Science and Technology  
University of Twente, P. O. Box 217, 7500 AE Enschede, The Netherlands

**Abstract**— Random lasers are complex, randomly scattering materials in which strong optical gain is present. In widely varying experiments by several different groups, intense, spectrally pure light has been observed from various types of random lasers (e.g., [1–5]). For a quantitative discussion of these experiments, see [6]. The origin of such spectrally narrow emission is explained by several different models. Experimental studies of very strongly scattering random lasers suggest that in the strongly scattering regime emission is dominated by a few local modes, which are effectively high-Q cavities for the laser light [7]. In this regime, the gain process finds the longest lived modes in the pumped laser material, and we may study such modes by looking at the emission light. We demonstrated an extremely strongly scattering random laser, based on Gallium Phosphide sponges infiltrated with laser dye [8]. In this system, we were able to measure the spatial extent of the local modes, as well as their statistical distribution in frequency space. This distribution shows mode repulsion, which is not explained by present theory. I will show new calculations, based on computer-generated random matrices, that indicate mode repulsion is generated by the way the random laser modes are selected.

### ACKNOWLEDGMENT

Work performed in collaboration with A. Lagendijk (AMOLF, Amsterdam), R. W. Tjerkstra and K. L. van der Molen.

### REFERENCES

1. Cao, H., et al., *Appl. Phys. Lett.*, Vol. 73, 3656, 1998.
2. Frolov, S. V., et al., *Opt. Commun.*, Vol. 162, 241, 1999.
3. Polson, R. C. and Z. V. Vardeny, *Phys. Rev. B*, Vol. 71, 045205, 2005.
4. Milner, V. and A. Z. Genack, *Phys. Rev. Lett.*, Vol. 94, 073901, 2005.
5. Noginov, M. A., J. Novak, and S. Williams, *Phys. Rev. A*, Vol. 70, 063810, 2004.
6. Van der Molen, K. L., A. P. Mosk, and A. Lagendijk, “Quantitative analysis of several random lasers,” *Opt. Commun.*, Vol. 278, 110, 2007.
7. Cao, H., et al., *Phys. Rev. E*, Vol. 66, 025601(R), 2002.
8. Van der Molen, K. L., R. W. Tjerkstra, A. P. Mosk, and A. Lagendijk, “Spatial extent of random laser modes,” *Phys. Rev. Lett.*, Vol. 98, 143901, 2007.

# An Iterative Progressive Numerical Method to the Computation of Scattering from Many Cylinders and Its Parallelization

N. Nakashima and M. Tateiba

Faculty of Computer Science and Communication Engineering, Kyushu University  
744 Moto-oka, Nishi-ku, Fukuoka 819-0395, Japan

**Abstract**— The authors work on a Monte Carlo simulation for multiple scattering by random media composed of several kinds of particles in shape, size and material. To efficiently compute scattering waves by realizations of random media, we combine an iterative progressive numerical method (IPNM) with a fast multipole algorithm (FMA). Considering the data structure of the FMA, we parallelize the computation. Numerical results provide the efficiency and accuracy for the computation.

We compute scattered wave from many objects by using the IPNM. If a primary wave is incident on many objects, the scattered wave from an object is incident on the other objects with the primary wave. In the IPNM, we repeatedly compute the scattered wave from each object. Here, the incident wave on an object is expressed in the sum of the primary wave and previously obtained scattered waves by the other objects. In actual computation, we extend “an object” to “a group of objects”.

The FMA can expedite the computations of scattered wave and incident wave in the IPNM. We use a hierarchical group expressed by a tree structure. Dividing the tree into subtrees, we can make groups of objects. We distribute them to processing nodes and compute independently the scattered wave from each group. The incident wave is computed in parallel by using the communication among the processing nodes. Using the above techniques, we can parallelize the IPNM with FMA.

As numerical examples, we consider scattering from regularly placed 100 and 400 cylinders in a square region. The radii, relative permittivities and relative permeabilities of cylinders are all the same and assumed as  $ka = 5.0$ ,  $\varepsilon_r = 2.0$  and  $\mu_r = 1.0$ , respectively. Here,  $k$  is the wavenumber of background medium. The number of groups, namely processing nodes, are 2 and 4. Numerical solutions are obtained in the cases of fractional volume  $f = 0.01$  and  $0.001$  and are in good agreement with those for the standard computation. Speed-up factor is close to the number of processing nodes for  $f = 0.01$ ; however, the factor is quite small for  $f = 0.001$ . We explain the reason for such behavior of the factor.

# Field Approximation for Reconstruction of 2D Perfectly Conducting Rough Surfaces

M. Spivack<sup>1</sup>, S. Bottone<sup>2</sup>, and O. Rath<sup>1</sup>

<sup>1</sup>Centre for Mathematical Sciences, University of Cambridge, CB3 0WA, UK

<sup>2</sup>DataPath Inc, 13025 Danielson St, Suite 200, San Diego CA 92064, USA

**Abstract**— The problem is considered of reconstruction of a rough two-dimensional surface from scattered field measurements along a plane parallel to the mean surface. Considerable progress has been made recently on this and related problems [1–4]. The method assumes the availability of full complex amplitudes, and is analogous to an approach previously applied to 1D surfaces [5], although here the restrictions on surface height and scattering regime are relaxed. In the particular case of predominantly forward scattering this provides a direct approximation for the surface  $S(x)$  (in the illuminated region). For more general regimes this may be refined by use of an iterative series, in which few terms are typically needed.

The problem is addressed as follows: The scattered field at each point  $\psi_s$  is expressed as an integral of the unknown surface current  $\mathbf{J}$  over the bounding surface  $S$ , say.  $\mathbf{J}$  depends in turn on the incident field  $\psi_{inc|S}$  along the surface via a similar boundary integral, and through  $\psi_{inc}$  on  $S$  itself. In each integral the Green function kernel varies as one or both arguments vary along  $S(x)$ , and the dependence on  $S$  is thus highly nonlinear. A simplifying approximation is now introduced for the dependence upon  $S$  in the first of these boundary integrals; this is applicable provided  $d \gg \lambda$  where  $d$  is the distance of the measurement plane to the mean surface and  $\lambda$  is a wavelength. The resulting expression, together with the second boundary integral can be recast as a set of coupled integral equations, relating the unknown current and incident field at the surface. These can be solved by a “marching” technique applied progressively in the predominant direction of propagation.

The accuracy of the method will be evaluated theoretically and by use of numerical simulation. Note that although this approach is deterministic, the above field approximation may also find application when the surface is stochastically rough and we wish to examine scattered field statistics.

## REFERENCES

1. Akduman, I., R. Kress, and A. Yapar, “Iterative reconstruction of dielectric rough surface profiles at fixed frequency,” *Inverse Problems*, Vol. 22, 939–954, 2006.
2. Ren, Y. C., L. X. Guo, and Z. S. Wu, “Direct solution of the inverse problem for rough surface scattering,” *Chinese Physics Letters*, Vol. 23, 2426–2429, 2006.
3. Cai, Z. J., D. Q. Chen, and S. Lu, “Reconstruction of a fractal rough surface,” *Physica D-Nonlinear Phenomena*, Vol. 213, 25–30, 2006.
4. Yapar, A., O. Ozdemir, H. Sahinturk, and I. Akduman, “A newton method for the reconstruction of perfectly conducting slightly rough surface profiles,” *IEEE Trans. Ant. & Prop.*, Vol. 54, 275–279, 2006.
5. Spivack, M., “Solution of the inverse scattering problem for grazing incidence on a rough surface,” *J. Opt. Soc. Am. A*, Vol. 9, 1352–1355, 1992.

## Radar Cross-section of Targets Using Beam Wave Incidence with Linear Polarization

Hosam El-Ocla

Department of Computer Science, Lakehead University, Ontario, Canada

**Abstract**— It has been proved that radar cross section (RCS) changes obviously with the illumination region curvature and polarization. Research on laser radar for target ranging, detection, and recognition has become the one key technology to evaluate and model the characteristics of scattering from a complex target in the military and civil applications. In this regard, the scattering characteristics are analyzed through studying the behaviour of laser RCS (LRCS) of the target. In fact, we can consider the beam wave as a plane wave when the mean size of the target becomes smaller than the beam width; however, this is not usually the general case practically. To detect targets of larger sizes, we should, therefore, handle the case where the beam width is smaller than the target size. Here, we evaluate the effects of the target configuration including size and curvature on the RCS of target for the two cases of plane and beam wave incidences. To achieve this aim, we draw on the method that solves the scattering problem as a boundary value problem and calculates the scattering waves using the current generated on the surface of the target. Numerical results are conducted for the RCS and LRCS of concave-convex targets in free space. Targets are taking large sizes up to about five wavelengths to be bigger enough than the beam width. Polarization of incident waves is one of the primary keys that affect the scattering waves. Here, we assume linear polarization including E-wave incidence and H-wave incidence.

Numerical results showed that target configuration together with beam width  $kW$  have major effects on LRCS. Creeping waves, produced in case of  $H$ -polarization, influence the LRCS obviously for limited  $ka$  and their impact diminishes gradually with  $ka$ . LRCS behaves differently from RCS for plane wave incidence in the range  $ka \geq kW$  where target complexity  $\delta$  has a clear effect especially with small  $kW$ . This behaviour contradicts with  $E$ -polarization case in which LRCS is almost invariant with  $\delta$  as a result of the absence of creeping waves. However, LRCS approaches certain values with  $ka > kW$  irrespective of linear wave polarization.

# Polarization of Waves in Reciprocal and Nonreciprocal Uniaxially Bianisotropic Media

Xiangxiang Cheng<sup>1,2</sup>, Jin Au Kong<sup>1,3</sup>, and Lixin Ran<sup>1,2</sup>

<sup>1</sup>The Electromagnetics Academy at Zhejiang University, Zhejiang University, Hangzhou 310058, China

<sup>2</sup>Department of Information and Electronic Engineering, Zhejiang University, Hangzhou 310027, China

<sup>3</sup>Research Laboratory of Electronics, Massachusetts Institute of Technology, Cambridge, MA 02139, USA

**Abstract**— We investigate the polarizations of waves in reciprocal and nonreciprocal uniaxially bianisotropic media, whose corresponding chirality parameter and Tellegen parameter appear only in one direction. By analyzing constitutive parameters for generating circularly polarized waves, we find that the optical-activity effects happen in such kind of uniaxially anisotropic chiral media under certain conditions. On the other hand, similar conditions give birth to linearly polarized waves in nonreciprocal uniaxially bianisotropic media.

## Selective Cancellation of Optical Scattering in Random Media

C. Amra, C. Deumié, G. Georges, L. Arnaud, and M. Zerrad

Institut Fresnel, UMR CNRST2I 6133, Université Paul Cézanne  
Ecole Centrale Marseille, Université de Provence, France

**Abstract**— We present an optical technique devoted to selective cancellation of light scattering in random media. It is based on tunable interferences of polarized light at each direction of space. Experimental data are recorded with an angle-resolved scatterometer, and compared with success to theoretical results based on electromagnetic theories. It is shown how bulk scattering can be eliminated while surface scattering remains quasi-constant, and inversely. A single interface or bulk within a multilayer can also be isolated with this procedure, as well as elastic and inelastic scattering. The technique is extended to diffraction process from several objects. In a more general way, the procedure allows a direct identification of the scattering centers (surface or bulk).

For slightly inhomogeneous samples, perturbative theories show that the angular cancellation conditions do not depend on the samples microstructure — but only on the scattering origins, which provides a practical probe. The case of arbitrary samples is more complex, since these conditions are microstructure dependent. Applications concern different fields such as biomedical and submarine optics, optical coatings and remote sensing . . . In a last step we show how defect-induced depolarization is responsible for the limitation of the technique.

### REFERENCES

1. Gilbert, O., C. Deumie, and C. Amra, “Angle-resolved ellipsometry of scattering patterns from arbitrary surfaces and bulks,” *Optics Express*, Vol. 13, Issue 7, 2403–2418, April 2005.
2. Amra, C., C. Deumié, and O. Gilbert, “Elimination of polarized light scattered by surface roughness or bulk heterogeneity,” *Optics Express*, Vol. 13, Issue 26, 10854–10864, December 2005.
3. Georges, G., C. Deumié, and C. Amra, “Selective probing and imaging in random media based on the elimination of polarized scattering,” *Optics Express*, Vol. 15, Issue 15, 9804–9816, July 2007.

# Session 4A7

## Extended/Unconventional Electromagnetic Theory, EHD/EMHD, Electrobiolgy 1

<b>Identification of Defects in Materials with Surface Conductivity Distribution</b>	
<i>Jarmila Dėdkov (Brno University of Technology, Czech Republic);</i> .....	792
<b>Image Reconstruction Using Combination Deterministic and Stochastic Method</b>	
<i>Jarmila Dėdkov (Brno University of Technology, Czech Republic);</i> .....	793
<b>Laplace Transform and FDTD Approach Applied to MTL Simulation</b>	
<i>Jarmila Dedkova (Brno University of Technology, Czech Republic); Lubomir Brancik (Brno University of Technology, Czech Republic);</i> .....	794
<b>Basic Experiments with Model of Inductive Flowmeter</b>	
<i>Pavel Fiala (Brno University of Technology, Czech Republic); Vaclav Sadek (Brno University of Technology, Czech Republic); Premysl Dohmal (Brno University of Technology, Czech Republic); T. Bachorec (Brno University of Technology, Czech Republic);</i> .....	795
<b>Experiments with Accuracy of Air Ion Field Measurement</b>	
<i>Miloslav Steinbauer (Brno University of Technology, Czech Republic); Pavel Fiala (Brno University of Technology, Czech Republic); Karel Bartuřek (Institute of Scientific Instruments, Academy of Sciences of the Czech Republic, Czech Republic); Zoltan Szabo (Brno University of Technology, Czech Republic);</i> .....	796
<b>Optical Methods Identifying of the Special Purpose Generator Pulses</b>	
<i>Pavel Fiala (Brno University of Technology, Czech Republic); Petr Drexler (Brno University of Technology, Czech Republic); Miloslav Steinbauer (Brno University of Technology, Czech Republic);</i> .....	797
<b>A Passive Optical Location with Limited Range</b>	
<i>Pavel Fiala (Brno University of Technology, Czech Republic); Tomas Jirku (Brno University of Technology, Czech Republic); Radek Kubasek (Brno University of Technology, Czech Republic); Zoltan Szabo (Brno University of Technology, Czech Republic); P. Konas (Brno University of Technology, Czech Republic);</i> .....	798
<b>Numerical Method of Simulation of Material Influences in MR Tomography</b>	
<i>Miroslav Steinbauer (Brno University of Technology, Czech Republic); Radek Kubasek (Brno University of Technology, Czech Republic); Karel Bartusek (Institute of Scientific Instruments, Academy of Sciences of the Czech Republic, Czech Republic);</i> .....	799
<b>Experiments with the Effect of Non-homogenous Parts into Materials</b>	
<i>Pavel Fiala (Brno University of Technology, Czech Republic); Eva Kroutilova (Brno University of Technology, Czech Republic); Miloslav Steinbauer (Brno University of Technology, Czech Republic); Premysl Dohmal (Brno University of Technology, Czech Republic); Michal Hadinec (Brno University of Technology, Czech Republic); Karel Bartusek (Institute of Scientific Instruments, Academy of Sciences of the Czech Republic, Czech Republic);</i> .....	802
<b>Optimization Method of EMI Power Filters and Its Measurement</b>	
<i>Zoltan Szab (Brno University of Technology, Czech Republic); J. Sedlcek (Brno University of Technology, Czech Republic); Michal Hadinec (Brno University of Technology, Czech Republic);</i> .....	803

## Identification of Defects in Materials with Surface Conductivity Distribution

J. Dědková

Department of Theoretical and Experimental Electrical Engineering  
Brno University of Technology  
Kolejní 2906/4, Brno 612 00, Czech Republic

**Abstract**— The images of the electrical surface conductivity distribution can be reconstructed from voltage measurement captured on boundaries of the object. This very well known technique is named Electrical Impedance Tomography. The image reconstruction problem is an ill-posed inverse problem of finding such conductivity  $\sigma_s$  that minimizes some optimisation criterion, which can be given for example by following primal objective function

$$\Psi(\sigma_s) = \frac{1}{2} \sum \|U_{\text{FEM}}(\sigma_s) - U_{\text{MEAS}}\|^2,$$

where  $U_{\text{FEM}}$  is the vector iteratively calculated using FEM,  $U_{\text{MEAS}}$  is the vector of measured nodal voltages. This paper describes new algorithms based on stochastic methods to be used for the acquirement of more accurate reconstruction results and stable solution. The proposed methods are expected to be used for the non-destructive testing materials. It will be shown example of the identification of voids or cracks in special structures called honeycombs. The advantages of new approach are compared with properties of deterministic approach to the same image reconstructions.



## Image Reconstruction Using Combination Deterministic and Stochastic Method

J. Dědková

Department of Theoretical and Experimental Electrical Engineering  
Brno University of Technology  
Kolejni 2906/4, Brno 612 00, Czech Republic

**Abstract**— This paper describes new algorithms based on the combination of deterministic and stochastic methods to be used to the best results of reconstruction process of surface conductivity distribution. The images of the electrical surface conductivity distribution can be reconstructed from voltage measurement captured on boundaries of the object. The image reconstruction problem is an ill-posed inverse problem of finding such surface conductivity  $\sigma_s$  that minimizes some optimisation criterion, which can be given for example by following primal objective function

$$\Psi(\sigma_s) = \frac{1}{2} \Sigma \|U_{\text{FEM}}(\sigma_s) - U_{\text{MEAS}}\|^2,$$

where  $U_{\text{FEM}}$  is the vector iteratively calculated using FEM,  $U_{\text{MEAS}}$  is the vector of measured nodal voltages. The advantages of new approach are compared with properties of deterministic and stochastic approach to the same image reconstructions. It will be shown that it is very effective way to obtain satisfying identifications of voids or cracks in special structures called honeycombs.

## Laplace Transform and FDTD Approach Applied to MTL Simulation

J. Dědková<sup>1</sup> and L. Brančík<sup>2</sup>

<sup>1</sup>Department of Theoretical and Experimental Electrical Engineering

Brno University of Technology

Kolejní 2906/4, Brno 612 00, Czech Republic

<sup>2</sup>Department of Radio Electronics, Brno University of Technology

Purkyňova 118, Brno 612 00, Czech Republic

**Abstract**— The paper proposes two different approaches to simulation of the multiconductor transmission line. Numerical results of MTL simulations based on both the Laplace transform and Finite Difference Time Domain method are presented and compared. Fundamental algorithms were programmed in Matlab language. Some typical situations are solved as an illustration of the results.

## Basic Experiments with Model of Inductive Flowmeter

P. Fiala<sup>1</sup>, V. Sadek<sup>1</sup>, P. Dohnal<sup>2</sup>, and T. Bachorec<sup>1</sup>

<sup>1</sup>Department of Theoretical and Experimental Electrical Engineering  
Brno University of Technology, Kolejní 2906/4, 612 00 Brno, Czech Republic

<sup>2</sup>Department of Languages, Brno University of Technology  
Udolní 53, 602 00 Brno, Czech Republic

**Abstract**— This article deals with physical and chemical processes during measurement with inductive flowmeter. There are presented theoretical model and example numerical solution. We prepared numerical models based on combined finite element method (FEM) and finite volume method (FVM) of one of three variants and computed output voltage of flowmeter electrodes. The model joins magnetic, electric and current field, flow field and chemical nonlinear ion model. Results were obtained by means of FEM/FVM as a main application in ANSYS software.

**Introduction** The full electro-hydro-dynamical (EHD) model of inductive flowmeter is coupled problem. There are coupled electric, magnetic, fluid flow field and electric circuit and chemical (ions) models, Fig. 1. This model was solved with combined finite element methods (FEM) and finite volume methods (FVM). Results from numerical model and experiments were compared and the numerical equality was very good.

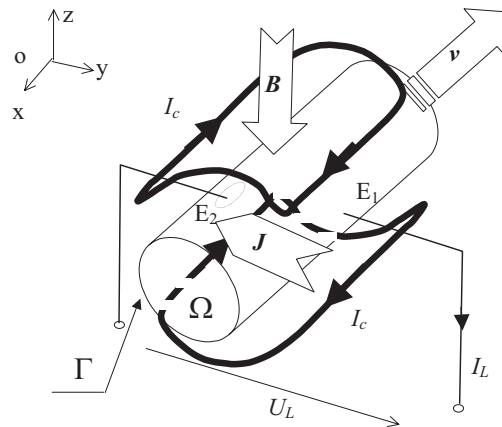


Figure 1: Principle of the induction flowmeter.

### REFERENCES

1. Fala, P., "Model of inductive flowmeter DN-100," Research report No. 2/01, Laboratory of Modelling and Optimisation of Electromechanical Systems BUT FECT, 1–23, Brno, Czech Republic, June 21, 2001.
2. Fleischner, P., *Hydromechanika*, Paperback VUT FS, VUT Brno, ISBN 80-214-0266-1, 1990.
3. Černoch, S., *Strojně technická příručka*, SNTL Praha, 1968.
4. Moore, J. W., *Fyzikální chemie*, SNTL Praha, 1981.
5. Brdička, R. and J. Dvořák, *Základy fyzikální chemie*, Academia Praha, 1977.

## Experiments with Accuracy of Air Ion Field Measurement

M. Steinbauer<sup>1</sup>, P. Fiala<sup>1</sup>, K. Bartušek<sup>2</sup>, and Z. Szabo<sup>1</sup>

<sup>1</sup>Department of Theoretical and Experimental Electrical Engineering  
University of Technology Brno, Kolejní 4, 612 00 Brno, Czech Republic

<sup>2</sup>Institute of Scientific Instruments, Academy of Sciences of the Czech Republic  
Královopolská 147, 612 64 Brno, Czech Republic

**Abstract**— An analysis of the electric state of air shows the presence of various ion sorts. The therapeutic effect of negative high-mobility ions of proper concentration is known. This positive effect was observed in caves that are used for speleotherapy. This article presents the capability of methods for measuring ion concentration and for ion spectral analysis.

**Introduction:** Air ion concentration and composition belong to the frequently monitored parameters of the atmosphere [5]. Their influence on living organisms has been the subject of intensive studies. Earlier research has demonstrated the positive influence of light negative ions and air cleanness on human health. The Department of the Theoretical and Experimental Electrical Engineering of Brno University of Technology and the Institute of Scientific Instruments of the Academy of Sciences of the Czech Republic are involved in the research of ion field in office and living spaces. The objective is to increase the concentration of light air ions in these spaces. Another task is to set up a simulated therapy room, with conditions similar to speleotherapy caves. It sets the requirements for accurate measurement of ion field with good repeatability. The article deals with the design of gerdien condenser and peripheral measuring devices. An optimal design is important for eliminating the inaccuracy of ion concentration measurement.

### REFERENCES

1. Bartušek, K., Měření speleoterapeutických parametrů jeskyní pro lékařské účely, Interní text UPT AV ČR, 1997.
2. Buřival, Z., Vliv prostorového náboje v atmosféře na znečištění vzduchu v technologických provozech, Knihnice odborných a vědeckých spisů VUT Brno.
3. Spurný, Z., Atmosferická ionizace, Praha, Academia 1985.
4. Puškeilerová, L., Nové poznatky o měření volných záporných iontů v laboratorním prostředí, Příspěvek k VŠTČ FEI, Brno, 2000.
5. Israël, H., Atmosphärische Elektrizität, Akademische Verlagsgesellschaft Leipzig, 1957.
6. Smutný, T., Vliv obvodových prvků na přesnost měření iontových polí, Diplomová práce 2004 VUT Brno.
7. Kafka, V., Saturační a spektrální charakteristika iontového pole, Diplomová práce 2004 VUT Brno.

## Optical Methods Identifying of the Special Purpose Generator Pulses

P. Fiala, P. Drexler, and M. Steinbauer

Department of Theoretical and Experimental Electrical Engineering  
Brno University of Technology  
Kolejní 2906/4, 612 00 Brno, Czech Republic

**Abstract**— There are some suitable methods for the measurement of ultra-short solitary electromagnetic pulses (EMP) that are generated by high power microwave generators. The characteristics of EMPs are high power level ( $P_{\max} = 250$  MW) and very short time duration ( $t_p \in < 1, 60 >$  ns). Special requirements for measurement methods have to be considered because of the specific EMPs properties. In the paper, two suitable methods for this application are presented. The first one, the calorimetric method, utilizes the thermal impacts of microwave absorption. The second method presented — the magneto-optic method — uses the Faraday's magneto-optic effect as a sensor principle. A combined calorimetric sensor was realized and there were made some experimental EMP measurements with good results. The sensor utilizing the magneto-optic method is still in development.

**Introduction:** In connection with the events of the last few years and with the increased number of terrorist activities, the problem of identifying and measuring the impact of electromagnetic weapons or other systems occurred. Among these weapons or systems there are also microwave sources which can reach extensive peak power of up to  $P_{\max} = 250$  MW. Solitary, in some cases several times repeated, pulses lasting from  $t_p \in < 1, 60 >$  ns cause the destruction of semiconductor junctions. The analysis of possible measuring methods convenient for the identification and measurement of the ultra-short solitary electromagnetic (EM) pulses is presented in this paper; some of the methods were selected and used for practical measurement.

### REFERENCES

1. Ott, H., *Noise Reduction Techniques in Electronic Systems*, John Wiley & Sons, 1988.
2. Booske, J. H., "Studies of non-thermal effects during intense microwave heating of crystalline solids," *Proceedings of the 3-rd Symposium Microwave Processing of Materials*, 269, Pittsburgh, 1992.
3. Barker, R. J. and E. Schamiloglu, *High-power Microwave Sources and Technologies*, IEEE Press, 2001.
4. Fiala, P., *Non-conventional Sources of Electrical Energy*, BUT FEKT, Brno, 2003.
5. Kasal, M., *Multinuclear Measuring Channel of NMR Spectrometer*, FE BUT, Brno, 1984.
6. Pfeffer, M. and M. Kasal, "Automatic impulse reflectometer," *Sdělovací technika*, Vol. 10/11, Czech Republic, 1986.
7. Šuka, P., Verbal information, UFP AVČR, Praha 6, 2003.

## A Passive Optical Location with Limited Range

P. Fiala<sup>1</sup>, T. Jirku<sup>2</sup>, R. Kubasek<sup>3</sup>, Z. Szabo<sup>4</sup>, and P. Konas<sup>5</sup>

<sup>1,2,3,4</sup>Department of Theoretical and Experimental Electrical Engineering, Brno University of Technology  
Kolejni 2906/4, 612 00 Brno, Czech Republic

<sup>5</sup>Department Wood Science, Mendel University of Agriculture and Forestry  
Brno Zemedelska 3, 613 00 Brno, Czech Republic

**Abstract**— We know active and passive methods of a location. This article deals only with a passive location of dynamic targets (see [1–7]). The passive optics location is suitable just for tracking of targets with mean velocity which is limited by the hardware basis. The aim of this work is to recognize plasma, particles etc. It is possible to propose such kind of evaluation methods which improve the capture probability markedly. Suggested method is dealing with the short-distance evaluation of targets. We suppose the application of three independent principles how to recognize an object in a scanned picture. These principles use similar stochastic functions in order to evaluate an object location by means of simple mathematical operations. Methods are based on direct evaluation of picture sequence by the help of the histogram and frequency spectrum. We find out the probability of unidentified moving object in pictures. If the probability reaches a setting value we will get a signal. The processing of dynamic pictures and their filtration are a significant part of work [8–13]. Static objects, background (trees, buildings) must be filtered off before. This filtration is being also done by means of the probability function. Probability distribution of an object position is gained from a sequence of more pictures.

### REFERENCES

1. Herman, S. and P. Moulin, “A particle filtering approach to FM-band passive radar tracking and automatic target recognition,” *Proceedings of IEEE Aerospace Conference*, Boston, 2002.
2. Internet source: <http://www.ifp.uiuc.edu/smherman/darpa/>.
3. Ehrman, L. M. and A. D. Lanterman, “Automated target recognition using passive radar and coordinated flight models,” *Proceedings of SPIE International Conference*, Orlando, Florida, 2003.
4. Lanterman, A. D. and D. C. Munson, “Deconvolution techniques for passive radar imaging,” *Proceedings of SPIE International Conference*, Orlando, Florida, 2002.
5. Wu, Y. and D. C. Munson, Jr., “Multistatic passive radar imaging using the smoothed pseudo Wigner-Ville distribution,” *Proceedings of IEEE Image Processing Conference*, 604–607, 2001.
6. Lind, F. D. and J. D. Sahr, “Passive radar and the low frequency array,” *Proceedings of General Assembly of the International Union of Radio Science*, Maastricht, Netherlands, 2002.
7. Neyt, X., J. Raout, M. Kubica, V. Kubica, S. Roques, M. Acheroy, and J. G. Verly, “Feasibility of STAP for passive GSM-based radar,” *Proceedings of the IEEE Radar Conference*, 546–551, Verona, NY, April, 2006.
8. Töeyin, B. U., A. E. Cetin, A. Aksaya, and M. B. Akhan, “Moving object detection in wavelet compressed video,” *Signal Processing: Image Communication*, Vol. 20, 225–264, 2005.
9. Morimoto, C., D. DeMenthon, L. Davis, and R. Chellappa, “Detection of independently moving objects in passive video,” *Proceedings of Intelligent Vehicles Symposium*, 270–275, Detroit, MI, 1995.
10. Nguyen, H. T., M. Worrington, and A. Dev, “Detection of moving objects in video using a robust motion similarity measure,” *IEEE Transactions on Image Processing*, Vol. 9, 137–141, 2000.
11. Vese, L. A., “Multiphase detection and image segmentation,” UCLA C.A.M. Report 02-36, June 2002.
12. Chang, K., *Handbook of Optical Components and Engineering*, Wiley-Interscience, New Jersey, 2003.
13. Gonzales, C. G., R. E. Woods, and S. L. Eddins, *Digital Image Processing Using Matlab*, Pearson Prentice Hall, New Jersey, 2004.

# Numerical Method of Simulation of Material Influences in MR Tomography

M. Steinbauer<sup>1</sup>, R. Kubasek<sup>1</sup>, and K. Bartusek<sup>2</sup>

<sup>1</sup>Faculty of Electrical Engineering and Communications, Brno University of Technology, Czech Republic

<sup>2</sup>Institute of Scientific Instruments, Academy of Sciences of the Czech Republic, Czech Republic

**Abstract**— Generally all Magnetic Resonance Imaging (MRI) techniques are affected by magnetic and electric properties of measured materials, resulting in errors in MR image. Using numerical simulation we can solve the effect of changes in homogeneity of static and RF magnetic fields caused by specimen made from conductive and/or magnetic material in MR tomography. This paper deals with numerical simulation of material susceptibility influence to magnetic field.

## 1. INTRODUCTION

In MR tomography, strong magnetic field is used (above 1 T). Because MR is very sensitive to inhomogeneity of this field, even such weak induced magnetic field as from para- or diamagnetic material is significant. Second mechanism, which affects field homogeneity, is magnetic field of eddy current induced by RF impulse in conductive material. Aim of this paper is in simulation of weakly magnetic material influence to static magnetic field.

For numerical simulation, two approaches can be used: normal Finite Element Method (FEM) and calculation of reaction field considering the induced polarity in the region. These approaches have been discussed in [6] and [7], where the accuracy consideration and possible reduction of numerical method errors can be found. Using FEM for calculation of magnetic field in MR tomography requires double precision arithmetic and sufficiently fine mesh, because change of the magnetic field in vicinity of slightly magnetic materials is weak in comparison to basic static magnetic field. Second approach may use single precision arithmetic, because only reaction field (induced own field of magnetic material) is computed.

## 2. 2D ANALYTIC SOLUTION

Let's have specimen with susceptibility  $\chi_{m1}$  surrounded by reference medium with known susceptibility  $\chi_{m2}$  and placed into static primal magnetic field with magnetic intensity vector  $\mathbf{H}_0$  oriented in  $\mathbf{u}_z$  direction — see Fig. 1 left. We have to determine magnetic intensity  $\mathbf{H}$  of incurred field, which is superposition of primal and reaction field  $\mathbf{H}_r$  (effect of specimen magnetization).

Because there are not variable currents in whole area, magnetic field is irrotational ( $\text{rot } \mathbf{H} = 0$ ) and we can use scalar magnetic potential

$$\mathbf{H} = -\text{grad}\varphi_m. \quad (1)$$

Magnetic potential of primal field of intensity  $\mathbf{H}_0$  is

$$\varphi_{m0} = - \int \mathbf{H}_0 \cdot \mathbf{u}_z dz = -\mathbf{H}_0 z. \quad (2)$$

Incidence of magnetized specimen from Fig. 1 left we can replace with effect of field of surface magnetic charge with density  $\sigma_m$  on boundary of areas  $\Omega_1$  a  $\Omega_2$  — see Fig. 1 right, whereas susceptibility of areas is now zero. First we have to compute magnetic charge density distribution on bound  $\Gamma$  and consequently the intensity of reaction field  $\Delta\mathbf{H} = \mathbf{H} - \mathbf{H}_0$

$$\Delta\mathbf{H}(\mathbf{r}) = \frac{1}{2\pi} \oint_{\Gamma} \sigma_m(\mathbf{r}') \frac{\mathbf{u}_r}{R(\mathbf{r}, \mathbf{r}')} d\Gamma. \quad (3)$$

Surface magnetic charge invokes scalar magnetic potential [5]

$$\varphi_{mr}(\mathbf{r}) = -\frac{1}{2\pi} \oint_{\Gamma} \sigma_m(\mathbf{r}') \ln R(\mathbf{r}, \mathbf{r}') d\Gamma. \quad (4)$$

Total scalar magnetic potential at point  $\mathbf{r}$  is superposition of static primal field intensity (2) and contribution from charged bound (4)

$$\varphi_m(\mathbf{r}) = -Hz - \frac{1}{2\pi} \oint_{\Gamma} \sigma_m(\mathbf{r}') \ln R(\mathbf{r}, \mathbf{r}') d\Gamma. \quad (5)$$

Using condition of magnetic flux  $\mathbf{B}_n = B_n \mathbf{u}_n$  we obtain an integral formula for surface magnetic charge density normal component conjunction on bound  $\Gamma$  (see Fig. 1 middle)

$$B_n = \mu_0(1 + \chi_{m1})H_{1n} = \mu_0(1 + \chi_{m2})H_{2n} \quad (6)$$

Analogically to the Gauss theorem causes magnetic charge of density  $\sigma_m$  at point A magnetic field of intensity

$$\Delta H_n = \pm \frac{\sigma_m(A)}{2}. \quad (7)$$

Using (5) and (1) we have the normal components of magnetic field intensity at point A (Fig. 1 middle)

$$H_{1n} = H_0 \mathbf{u}_z \cdot \mathbf{u}_n + \frac{1}{2\pi} \text{grad} \oint_{\Gamma, r \in \Omega_1} \sigma_m(\mathbf{r}') \ln R(\mathbf{r}, \mathbf{r}') d\Gamma \mathbf{u}_n, \quad (8)$$

$$H_{2n} = H_0 \mathbf{u}_z \cdot \mathbf{u}_n + \frac{1}{2\pi} \text{grad} \oint_{\Gamma, r \in \Omega_1} \sigma_m(\mathbf{r}') \ln R(\mathbf{r}, \mathbf{r}') d\Gamma \mathbf{u}_n. \quad (9)$$

Whenever  $A \in \Gamma$  and thus  $\mathbf{r} \in \Gamma$ , has integral in formulas (8) a (9) singularity at point A (where  $\mathbf{r} = \mathbf{r}'$ ). We can remove this singularity omitting point  $\mathbf{r} = \mathbf{r}'$  from integration and taking field contribution of this point using (7) instead. So we can write

$$H_{1n} = H_0 \mathbf{u}_z \cdot \mathbf{u}_n + \frac{1}{2\pi} \oint_{\substack{\Gamma \\ r \neq r'}} \sigma_m(\mathbf{r}') \frac{1}{R(\mathbf{r}, \mathbf{r}')} d\Gamma \mathbf{u}_R \cdot \mathbf{u}_n - \frac{\sigma_m(A)}{2}, \quad (10)$$

$$H_{2n} = H_0 \mathbf{u}_z \cdot \mathbf{u}_n + \frac{1}{2\pi} \oint_{\substack{\Gamma \\ r \neq r'}} \sigma_m(\mathbf{r}') \frac{1}{R(\mathbf{r}, \mathbf{r}')} d\Gamma \mathbf{u}_R \cdot \mathbf{u}_n + \frac{\sigma_m(A)}{2}, \quad (11)$$

where was used

$$\text{grad} \ln R(\mathbf{r}, \mathbf{r}') = \frac{1}{R(\mathbf{r}, \mathbf{r}')} \mathbf{u}_R. \quad (12)$$

Substituting from (10) and (11) into (6) we have after some rearrangement

$$\frac{\chi_{\Delta}}{2\pi} \oint_{\substack{\Gamma \\ r \in \Gamma, r \neq r'}} \frac{\sigma_m(\mathbf{r}')}{R(\mathbf{r}, \mathbf{r}')} d\Gamma \mathbf{u}_R \cdot \mathbf{u}_n + \frac{\sigma_m(\mathbf{r})}{2} = -\chi_{\Delta} H_0 \mathbf{u}_z \cdot \mathbf{u}_n, \quad (13)$$

where differential susceptibility was introduced

$$\chi_{\Delta} = \frac{\chi_{m1} - \chi_{m2}}{\chi_{m1} + \chi_{m2} + 2}. \quad (14)$$

Formula (13) is not analytically solvable, thus we solve it numerically by mean of boundary element method. After solution of (13) using collocation method described in [5] we have obtained results, shown in next figure. Shape of magnetic flux density is in the Fig. 2. In this simulation the aluminium specimen ( $\Omega_1$ ) was considered with  $\chi_{m1} = 22 \cdot 10^{-6}$ , length of specimen  $z = 20$  mm, thickness  $a = (3, 5 \text{ and } 7)$  mm. Specimen was immersed into the water with  $\chi_{m2} = -9 \cdot 10^{-6} - (\Omega_2)$ .



### 3. 3D NUMERICAL SOLUTION

Three dimensional numerical modeling was provided using FEM and Ansys software. The scalar magnetic potential was computed by solving of Laplace's equation

$$\Delta\varphi_m = \operatorname{div} \mu (-\operatorname{grad} \varphi_m) = 0. \quad (15)$$

One of used model is in Fig. 3. Here weakly paramagnetic specimen is surrounded by diamagnetic reference substance. The model was meshed with Solid96 element type. Boundary conditions were set up to achieve induction  $B_0 = 4,700$  T in  $z$ -axes direction:  $\varphi_m = \text{const.}$  on the surfaces  $\Gamma_1, \Gamma_2$ ,  $\frac{\partial\varphi_m}{\partial n} = 0$  on the shell surface  $\Gamma_3$ .

FEM modeling and solution is described in [8]. One of obtained results — the module of magnetic induction  $B$  along the “path” marked in Fig. 3 — is shown in the figure in the right.

### 4. CONCLUSIONS

Both method of numerical modeling of magnetic field deformation in MRI, caused by weakly magnetic specimen, which were described here, was compared with experimental results [3, 8]. Proximity of measured and numerically modeled data was good — see [5]. To enable comparison, simulation was adjusted to the same conditions as experiment: size of sample, susceptibilities and magnetic field of  $B = 4.7$  T.

Based on this simulation, MR measuring technique was founded [8], which is suitable for substances with no signal in MR tomography. The method uses Gradient Echo (GE) method and benefits from magnetic induction field shape in specimen vicinity, which is immersed in reference medium with measurable MR signal. After an optimization this method can be used for investigation of the materials used in MR tomography as well as of biological tissues affecting quality of MR images.

### ACKNOWLEDGMENT

This work is supported by the grants GAAV B208130603 and GAAV B208130604.

### REFERENCES

1. Ernst, R. R., G. Bodenhausen, and A. Wokaun, *Principles of NMR in One and Two Dimensions*, Oxford Science Publishing, 1987.
2. Sepúlveda, N. G., I. M. Thomas, and J. P. Wikswo Jr., “Magnetic susceptibility tomography for three-dimensional imaging of diamagnetic and paramagnetic objects,” *IEEE Transaction on Magnetics*, Vol. 30, No. 6, 5062–5069, 1994.
3. Kubasek, R., M. Steinbauer, and K. Bartusek, “Material influences in MR tomography, measurement and simulation,” *Journal of Electrical Engineering*, Vol. 8, 58–61, Zilina, 2006.
4. Wang, Z. J., S. LI, and J. C. Hasselgrove, “Magnetic resonance imaging measurement of volume magnetic susceptibility using a boundary condition,” *Journal of Magnetic Resonance*, Vol. 142, 477–481, 1999.
5. Hwang, S. N. and F. W. Wehrli, “Experimental evaluation of surface charge method for computing the induced magnetic field in trabecular bone,” *Journal of Magnetic Resonance*, Vol. 139, 35–45, 1999.
6. Eastham, J. F., R. J. Hill-Cottingham, I. R. Young, and J. V. Hajnal, “A method of inverse calculation for regions of small susceptibility variations,” *IEEE Transaction on Magnetics*, Vol. 33, No. 2, 1212–1215, 1997.
7. Eastham, J. F., R. J. Hill-Cottingham, I. R. Young, J. V. Hajnal, P. J. Leonard, and W. Lin, “Use of finite element analysis to calculate field changes in low susceptibility materials,” *Proceedings of Compumag 95 International Conference*, 546–547, Berlin, Germany, 1995.
8. Steinbauer, M., “Magnetic susceptibility measurement using MRI methods,” PhD thesis, Brno University of Technology, 2005.

## Experiments with the Effect of Non-homogenous Parts into Materials

Pavel Fiala<sup>1</sup>, Eva Kroutilova<sup>1</sup>, Miloslav Steinbauer<sup>1</sup>  
Premysl Dohnal<sup>1</sup>, Michal Hadinec<sup>1</sup>, and Karel Bartušek<sup>2</sup>

<sup>1</sup>Brno University of Technology, Czech Republic

<sup>2</sup>Academy of Science of the Czech Republic, Czech Republic

**Abstract**— This article deals with the verification of experimental results obtained by numerical simulation. We solved the effect of changes in the homogeneity of magnetic fields evoked by different samples from conductive and/or magnetic materials and the different types of inhomogeneity in the MR tomograph. Moreover, the paper will describe the suitable magnetic resonance techniques.

### REFERENCES

1. Ansys User's Manual. Huston (USA): SVANSON ANALYSYS SYSTEM, Inc., 1994–2006.
2. Fiala, P., E. Kroutilová, and T. Bachorec, Modelování elektromagnetických polí, počítačová cvičení, vyd. Brno: VUT v Brně FEKT, Údolní 53, 602 00, s. 1–69, Brno, 2005.
3. Steinbauer, M., Měření magnetické susceptibility technikami tomografie magnetické rezonance. vyd. Brno: VUT v Brně FEKT, Údolní 53, 602 00, Brno, 2006.

# Optimization Method of EMI Power Filters and Its Measurement

Z. Szabó, J. Sedláček, and M. Hadinec  
BUT FEKT Brno, Czech Republic

**Abstract**— Electromagnetic interference (EMI) can be reduced to acceptable level using EMI filter circuits. Unfortunately, many known methods of filter design and optimization cannot be applied directly to power electronics, which has its own peculiarities. In comparison to EMI data communication filters EMI power filters operate typically under mismatched impedance conditions. One of the important manner of a filter design and optimization process there is a filter modeling. The paper deals with methods of filter design and optimization useful in area of EMI power filter synthesis. Synthesis and optimization of different types of EMI power filters with required insertion loss and using of their equivalent models here are discussed in some practical examples.

**Introduction** In present time the world is becoming more densely populated with devices that are increasingly sensitive to electromagnetic disturbances. In industrial spheres, electronic control systems, data processing equipment and other sensitive devices play an increasingly important role. Therefore solution of problems coupled with problematic of EMC (electromagnetic compatibility) is very important. In electrical engineering practice now are used many new circuit elements for electromagnetic interference (EMI) suppression. We can observe, that in area of EMC are growing different requirements to solve problems of electromagnetic emissions and electromagnetic susceptibility.

In area of EMC there are very often used EMI filters. Their using can be differed to solution of two different problems. At first it is the essential decreasing of undesirable electromagnetic pollution, on the other hand are used to increase electromagnetic immunity of any electrical equipments.

In telecommunications adequate methods for computing and solving EMC problems have been developed over the last years. Unfortunately, many of these methods cannot be applied directly to power electronics, which has its own peculiarities [1].

## REFERENCES

1. Thayne, L., *Electromagnetic Compatibility in Power Electronics*, IEEE PRESS, J. K. Eckert, Sarasota, USA, 1995, 2004.
2. Williams, T. and K. Armstrong, *EMC for Systems and Installations*, Newnes, Butterworth-Heinemann, Oxford, Great Britain, 2000.
3. Rybak, T. and M. Steffka, *Automotive Electromagnetic Compatibility (EMC)*, Kluwer Academic Publishers, Norwell, Massachusetts, USA, 2004.
4. Dřínovský, J. and J. Svačina, "Estimation of EMI filter performance for the "worst-case" system," *Radioengineering*, Vol. 15, No. 4, ISSN 04-510-79, Brno, 2006.



# Session 4A8

## Electromagnetic Techniques for Subsurface Detection and Imaging: Theory, Algorithms, and HW Implementations

<p><a href="#">Qualitative Microwave Subsurface Imaging by Means of a Multi-resolution Multi-region Level Set Method</a></p> <p><i>Manuel Benedetti (University of Trento, Italy); Dominique Lesselier (CNRS-SUPELEC-UPS 11, France); Lorenzo Poli (University of Trento, Italy); Andrea Massa (University of Trento, Italy); ...</i></p> <p><a href="#">A Comparison between Deterministic and Stochastic Inversions of Phaseless Data for Microwave Imaging</a></p> <p><i>Gabriele Franceschini (University of Trento, Italy); Davide Franceschini (University of Trento, Italy); Manuel Benedetti (University of Trento, Italy); Paolo Rocca (University of Trento, Italy); Andrea Massa (University of Trento, Italy); ...</i></p> <p><a href="#">A Method for the Shape Reconstruction of a Perfectly Conducting Object Buried in a Half-space</a></p> <p><i>İbrahim Akduman (Istanbul Technical University, Turkey); Mehmet Çayören (Istanbul Technical University, Turkey); Ali Yapar (Istanbul Technical University, Turkey); ...</i></p> <p><a href="#">Improving a Shape Reconstruction Method by Means of Frequency and Angle Diversity</a></p> <p><i>Mehmet Çayören (Istanbul Technical University, Turkey); Hulya Şahintürk (Yıldız Technical University, Turkey); Lorenzo Crocco (National Research Council - Institute for Electromagnetic Sensing of Environment, Italy); ...</i></p> <p><a href="#">Estimation Method of Quasi-wavefronts for UWB Radar Imaging with LMS Filter and Fractional Boundary Scattering Transform</a></p> <p><i>Takuya Sakamoto (Kyoto University, Japan); K. Teshima (Kyoto University, Japan); T. Sato (Kyoto University, Japan); ...</i></p> <p><a href="#">EM Inverse Scattering from Phaseless Data of the Total Field Based on Born Approximation</a></p> <p><i>Zheng Hu (Institute of Electronics, Chinese Academy of Sciences, China); Lianlin Li (Institute of Electronics, Chinese Academy of Sciences, China); Fang Li (Institute of Electronics, Chinese Academy of Sciences, China); ...</i></p> <p><a href="#">Detection of a Dielectric Target in a Half-space Using Extinction-pulse (E-pulse) Technique</a></p> <p><i>Shantanu K. Padhi (The University of Queensland, Australia); Hoi-Shun Lui (The University of Queensland, Australia); Nick Shuley (The University of Queensland, Australia); Feng Liu (The University of Queensland, Australia); ...</i></p> <p><a href="#">Structural and Multiferroic Properties of BiFe<sub>0.5</sub>Co<sub>0.5</sub>O<sub>3</sub> Ceramics</a></p> <p><i>Hai-Xia Lu (Yangzhou University, China); Xiang-Yu Mao (Yangzhou University, China); Wei Wang (Yangzhou University, China); Xiao-Bing Chen (Yangzhou University, China); ...</i></p> <p><a href="#">A Novel Method for Passive Shim Design: I</a></p> <p><i>Hector Sanchez Lopez (The University of Queensland, Australia); Feng Liu (The University of Queensland, Australia); Ewald Weber (The University of Queensland, Australia); Stuart Crozier (The University of Queensland, Australia); ...</i></p> <p><a href="#">Subsurface Sounding in Northern Hemisphere of Mars by Marsis: Mars Express Mission</a></p> <p><i>Giovanni Picardi (University of Rome "La Sapienza", Italy); D. Biccari (University of Rome "La Sapienza", Italy); M. Cartacci (University of Rome "La Sapienza", Italy); A. Cicchetti (University of Rome "La Sapienza", Italy); A. Marini (University of Rome "La Sapienza", Italy); A. Masdea (University of Rome "La Sapienza", Italy); F. Piccari (University of Rome "La Sapienza", Italy); R. Seu (University of Rome "La Sapienza", Italy); J. J. Plaut (Jet Propulsion Laboratory, USA); P. T. Melacci (University of Perugia, Italy); O. Bombaci (Alenia Spazio ALS, Italy); D. Calabrese (Alcatel Alenia Space, Italy); E. Zampolini (Alenia Spazio ALS, Italy); P. Edenhofer (Universität Bochum, Germany); D. Plettmeier (Fakultaet für Elektrotechnik und Informationstechnik Lehrstuhl und Laboratorium für Theoretische, Germany); E. Flamini (ASI, Agenzia Spaziale Italiana, Italy); ...</i></p>	<p>806</p> <p>807</p> <p>808</p> <p>809</p> <p>810</p> <p>811</p> <p>812</p> <p>813</p> <p>814</p> <p>816</p>
--	---

# Qualitative Microwave Subsurface Imaging by Means of a Multi-resolution Multi-region Level Set Method

M. Benedetti<sup>1,2</sup>, D. Lesselier<sup>2</sup>, L. Poli<sup>1</sup>, and A. Massa<sup>1</sup>

<sup>1</sup>ELEDIA Research Group at DIT, University of Trento, Via Sommarive 14, I-38050 Trento, Italy

<sup>2</sup>Laboratoire des Signaux et Systèmes, Département de Recherche en Électromagnétisme  
CNRS-SUPELEC-UPS 11, 3 rue Joliot-Curie, 91192 Gif-sur-Yvette CEDEX, France

**Abstract**— Subsurface sensing is a wide branch of non-invasive diagnostic concerned with the detection of unexploded ordnance as well as oilfield discovery. In this framework, many approaches have been proposed by considering different probing techniques as for instance x-rays, ultrasonics, eddy currents, and microwaves. As far as microwaves are concerned, such techniques have been recently recognized as suitable and effective tools [1]. Within microwave methodologies, inverse scattering approaches are aimed at retrieving a complete image of the region under test. Unfortunately, the underlying mathematical model is intrinsically ill-posed as well as non-linear. In order to cope with the ill-posedness, multi-view and multi-illumination systems are generally used to collect a sufficient amount of independent data. However, the amount of independent data is an upper-bounded quantity [2]. Therefore, the number of unknowns cannot be very large. Consequently, in order to achieve satisfactory reconstructions with a sufficient spatial accuracy without the presence of local minima, multi-resolution approaches have been proposed [3]. Besides multi-resolution techniques, another method for counteracting the lack of information lies in the exploitation of the available *a-priori* knowledge. In subsurface sensing, the scenario under test might often be represented by a binary contrast where the electromagnetic properties of both the target and the host-medium are known quantities. Under these assumptions, the imaging problem reduces to the search of position and shape of the scatterer lying in the host medium and optimization methods such as Level Set can be profitably employed [4].

In order to exploit both the available *a-priori* information and independent data from scattering measurements, this paper proposes an innovative approach based on a multi-resolution multi-region Level Set aimed at dealing with complex scenarios characterized by the presence of more-than-one target. Such a technique is based on a multi-step procedure aimed at increasing the spatial resolution inside limited regions of interest where the scatterers are more carefully localized. Moreover, only the shapes of the objects are iteratively estimated by means of a multi-regions Level Set procedure.

The proposed approach is assessed by means of a selected set of results and compared with the single-resolution as well as the multi-resolution single-region approaches in order to point out potentialities and current limitations.

## REFERENCES

1. Zoughi, R., *Microwave Nondestructive Testing and Evaluation*, Kluwer Academics Publishers, Dordrecht, The Netherlands, 2000.
2. Bucci, O. M. and T. Isernia, "Electromagnetic inverse scattering: retrievable informations and measurement strategies," *Radio Science*, Vol. 32, 2123–2138, 1997.
3. Caorsi, S., M. Donelli, and A. Massa, "Detection, location, and imaging of multiple scatterers by means of the iterative multiscaling method," *IEEE Trans. Microwave Theory Tech.*, Vol. 52, No. 4, 1217–1228, 2004.
4. Dorn, O. and D. Lesselier, "Level set methods for inverse scattering," *Inverse Problems*, Vol. 22, R67–R131, 2006.

## A Comparison between Deterministic and Stochastic Inversions of Phaseless Data for Microwave Imaging

G. Franceschini, D. Franceschini, M. Benedetti, P. Rocca, and A. Massa

ELEDIA Research Group at DIT, University of Trento, Via Sommarive 14, I-38050 Trento, Italy

**Abstract**—The development of microwave imaging techniques and their application are strongly related to the possibility to realize fast and cheap measurement systems. On the contrary, the phase acquisition usually requires complex and expensive apparatus and it turns out to be critical especially at high frequencies. Moreover, holographic and interferometric methods, often used in optical applications [1], are usually characterized by a high computational burden because of the time-consuming data post-processing.

Consequently, the study of efficient algorithms for the reconstruction from amplitude-only data is necessary in several applications. Toward this end, different strategies have been proposed. A two step method has been proposed in [2], where firstly a phase-retrieval problem is solved and then (i.e., at the second step) a standard inversion is performed. Alternatively, single step approaches have been investigated. In such cases, customized algorithms have been developed to directly process amplitude-only data [3].

In this paper, the two step strategy presented in [4] is considered. Such an approach is aimed at solving an inverse source problem at the first step to retrieve the distribution of the incident field in the investigation domain [4]. Then, such an information is exploited at the second step in order to recast the phaseless inversion problem to the minimization of a suitable multi-resolution cost function with phaseless data. Because of the non-differentiability of the functional, the optimization is carried out by means of a gradient-free stochastic optimizer [5]. Alternatively, a new formulation is proposed where a differentiable cost function is defined thus allowing the exploitation of a conjugate gradient minimization [6]. The results of a comparative analysis between deterministic and stochastic two-step approaches are presented and discussed in order to point out the potentialities and the limitations of the two strategies in terms of reconstruction accuracy, robustness, and computational efficiency. Moreover, some comparisons with full-data approaches are performed, as well.

### REFERENCES

1. Faris, G. W. and H. M. Hertz, "Tunable differential interferometer for optical tomography," *Appl. Opt.*, Vol. 28, 4662–4667, 1989.
2. Crocco, L., M. D'Urso, and T. Isernia, "Inverse scattering from phaseless measurements of the total field on a closed curve," *J. Opt. Soc. Am. A*, Vol. 21, Apr. 2004.
3. Maleki, M. H., A. J. Devaney, and A. Schatzberg, "Tomographic reconstruction from optical scattered intensities," *J. Opt. Soc. Am. A*, Vol. 9, 1356–1363, 1992.
4. Franceschini, G., M. Donelli, R. Azaro, and A. Massa, "Inversion of phaseless total field data using a two-step strategy based on the iterative multiscaling approach," *IEEE Trans. Geosci. Remote Sens.*, Vol. 44, 3527–3539, Dec. 2006.
5. Donelli, M. and A. Massa, "Computational approach based on a particle swarm optimizer for microwave imaging of two-dimensional dielectric scatterers," *IEEE Trans. Microwave Theory Tech.*, Vol. 53, 1761–1776, May 2005.
6. Harada, H., D. J. N. Wall, T. T. Takenaka, and T. Tanaka, "Conjugate gradient method applied to inverse scattering problem," *IEEE Trans. Antennas Propagat.*, Vol. 43, 784–792, Aug. 1995.

# A Method for the Shape Reconstruction of a Perfectly Conducting Object Buried in a Half-space

İ. Akduman, M. Çayören, and A. Yapar

Electrical and Electronics Engineering Faculty, Istanbul Technical University, Istanbul, Turkey

**Abstract**— Determination of the location and/or shape of a perfectly conducting object buried in a layered medium constitutes one of the basic and important class of problems in inverse scattering theory due to the wide range of applications such as microwave remote sensing, underwater acoustics, non-destructive testing, mine detection, and geophysical exploration etc. In these problem one tries to recover the geometrical properties, i.e., location and shape of a perfectly conducting object buried in a half space through the scattered field measurements performed on a certain limited domain in the upper half space [1, 2].

The main aim of this work is to give a simple and fast method to determine the location and shape of a perfectly conducting object buried in a half space. By this configuration one can model any real world applications related to the conducting objects buried underground. For the sake of simplicity, we consider only two-dimensional (2D) objects which enable us to reduce the problem to a scalar one. The buried body is illuminated by a plane wave, incident from the upper half-space at a fixed frequency and the scattered field measurements are also performed in a limited domain inside the upper half space.

The method is based on the representation of the scattered field in the upper half space as a single layer potential integral whose domain is a circle covering the object under test. Then using the scattered field data, an ill-posed integral equation is solved by a regularized technique to obtain the unknown density function. The field inside the circle is expressed as a Taylor series expansion (made of a few terms) whose coefficients are computed using the field arising from the single-layer potential representation. The unknown shape is then reconstructed using the condition that the total electric field must vanish on the boundary of the scatterer. The resulting non-linear equation is solved iteratively via Newton method. Since the solution is sensitive to errors on data, regularization in the least square sense is also applied. As shown through several numerical examples, the method yields satisfactory reconstructions especially for the multi-view case.

## REFERENCES

1. Cakoni, F., M. Fares, and H. Haddar, “Analysis of two linear sampling methods applied to electromagnetic imaging of buried objects,” *Inverse Problems*, Vol. 22, No. 3, 845–867, 2006.
2. Baussard, A., E. Miller, and D. Lesselier, “Adaptive multiscale reconstruction of buried objects,” *Inverse Problems*, Vol. 20, S1–S15, 2004.



# Improving a Shape Reconstruction Method by Means of Frequency and Angle Diversity

M. Çayören<sup>1</sup>, H. Şahintürk<sup>2</sup>, and L. Crocco<sup>3</sup>

<sup>1</sup>Istanbul Technical University, Istanbul, Turkey

<sup>2</sup>Yıldız Technical University, Istanbul, Turkey

<sup>3</sup>National Research Council — Institute for Electromagnetic Sensing of Environment, Naples, Italy

**Abstract**— Reconstruction of the shape and location of a perfectly electric conducting (PEC) object by means of probing electromagnetic waves is a relevant problem in a large number of applications, such as microwave remote sensing, subsurface imaging or non-destructive testing. Accordingly, this problem has been extensively investigated in the open literature and several methods based on different approaches have been developed [1–3].

Recently, a method has been proposed to reconstruct the shape of a 2D PEC target using a single plane wave at a fixed frequency and collecting the data on a curve surrounding the object [3]. This method belongs to the class of the “decomposition” methods, in which the non-linear ill-posed inverse scattering problem is split into two parts. In [3], a linear ill-posed inverse problem is first solved in order to reconstruct the scattered field in any point of the region exterior to the unknown target. Then, a polynomial equation arising from the known boundary condition is iteratively solved to retrieve the target’s shape. However, while being simple and computationally inexpensive, the method becomes less effective when electrically large targets are dealt with.

A general strategy to improve the quality of shape reconstruction methods is that of using frequency and angle diversity. As a matter of fact, by using multiple frequencies and multiple illumination directions, one can enlarge the available data and therefore hopefully improve the quality of the reconstruction [2]. Accordingly, in this communication we pursue the extension of the method in [3] to this different measurement configuration. Remarkably, such an extension is done in an almost natural fashion and without any approximation. As a matter of fact, as the unknown function is actually independent of the incident wave’s direction and frequency, the method can be simply formulated in the multiview/multifrequency case as the solution of a system of polynomial equations (each one arising from a single view monochromatic experiment). Therefore, after working out the first step for each single experiment, the unknown contour is achieved by solving the non-linear system in an iterative fashion using Gauss-Newton method and regularized least squares.

The obtained results show that, while the computational burden of the imaging procedure is still negligible, the use of diversity in angle and in frequency allows us to tackle scatterers of larger dimensions with respect to the original formulation.

## REFERENCES

1. Liu, C. Y. and Y. W. Kiang, “Inverse scattering for conductors by the equivalent source method,” *IEEE Trans. Antennas Propagat.*, Vol. 44, 310–316, 1996.
2. Soldovieri, F., A. Brancaccio, G. Leone, and R. Pierri, “Shape reconstruction of perfectly conducting objects by multiview experimental data,” *IEEE Trans. Geosci. Remote Sens.*, Vol. 43, 65–71, 2005.
3. Çayören, M., I. Akduman, A. Yapar, and L. Crocco, “A new algorithm for the shape reconstruction of perfectly conducting objects,” *Inverse Problems*, Vol. 23, 1087–1100, 2007.

# Estimation Method of Quasi-wavefronts for UWB Radar Imaging with LMS Filter and Fractional Boundary Scattering Transform

T. Sakamoto, K. Teshima, and T. Sato

Graduate School of Informatics, Kyoto University  
Yoshida-Honmachi, Sakyo-ku, Kyoto 606-8501, Japan

**Abstract**— UWB (Ultra Wide-Band) radars have a variety of applications including security surveillance systems. SEABED algorithm is a fast imaging method for UWB radars, which utilizes the reversible transform between the real and data spaces [1]. We have introduced the intermediate space between the real and data spaces [2]. The curves can be smooth in the intermediate space, which can be utilized to extract quasi-wavefronts (equi-phase surface of data). In this paper, we utilize LMS (Least-Mean-Square) filters in the intermediate space for the imaging of arbitrary target shape.

A mono-static radar system with an omni-directional antenna is assumed.  $s(X, Y)$  is defined as the received signal at the receive antenna  $(x, y) = (X, 0)$ , where these parameters are normalized by the center wavelength  $\lambda$ .  $Y$  is defined as  $Y = ct/(2\lambda)$  with the delay  $t$  and the wave velocity  $c$ . SEABED algorithm estimates a quasiwavefront  $(X, Y)$ , which is the equi-phase surface of  $s(X, Y)$ . By applying IBST (Inverse Boundary Scattering Transform) [1] to the quasi-wavefront and obtain the estimation of target shapes.

The intermediate space between the real space  $(x, y)$  and the data space  $(X, Y)$  is called fractional transform space  $(x_\alpha, y_\alpha)$ , which is expressed with the FBST (Fractional Boundary Scattering Transform) as

$$x_\alpha = X - \alpha Y dY/dX \quad (1)$$

$$y_\alpha = Y \sqrt{1 - \alpha(dY/dX)^2}. \quad (2)$$

For suitably selected  $0 < \alpha < 1$ , the curves in the fractional transform space are smooth regardless of the target shape [2]. Here, we empirically adopt  $\alpha = 0.5$ .

A new extraction method of quasi-wavefronts is proposed here. 100 undesired interference points are assumed with the true quasi-wavefront points for each antenna position  $X$ . The first 10 true points are assumed to be known as the initial value. We apply the FBST to the estimated quasi-wavefront to obtain the curve in the intermediate space, and apply 5th-order LMS filter to estimate the entire curve. Then we apply the inverse FBST and obtain the predicted points. We adopt the nearest point to the prediction as the estimation in the next step. This procedure is repeated. Fig. 1 shows the comparison between the proposed method and the conventional method which applies the LMS filter in the data space, not in the intermediate space. The results show that the proposed method effectively works while the conventional method gives poor estimation.

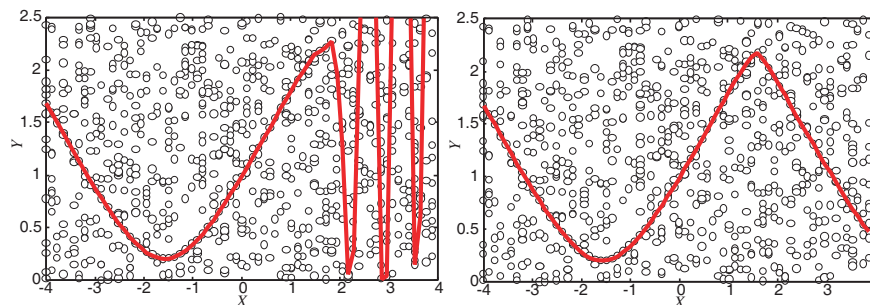


Figure 1: The estimated quasi-wavefronts with the conventional method (left) and the proposed method (right).

## REFERENCES

1. Sakamoto, T. and T. Sato, *IEICE Trans. on Commun.*, Vol. E87-B, No. 5, 1357–1365, 2004.
2. Sakamoto, T., *IEICE Trans. on Commun.*, Vol. E90-B, No. 1, 131–139, 2007.

# EM Inverse Scattering from Phaseless Data of the Total Field Based on Born Approximation

Zheng Hu<sup>1,2</sup>, Lianlin Li<sup>1</sup>, and Fang Li<sup>1</sup>

<sup>1</sup>Institute of Electronics, Chinese Academy of Sciences, Beijing, China

<sup>2</sup>Graduate University of Chinese Academy of Sciences, Beijing, China

**Abstract**— A new reconstruction algorithm for the object of complex permittivity based on Born approximation from phaseless data is presented. The key of the algorithm is to find the relationship between the real and imaginary part of the scattered electrical field. To solve this problem, we separate the electrical integral equation into two equations about the real part and the imaginary part of the scattered field. By discrete the test domain into a uniform grid of form of  $N \times N$  subsquare, assumed the contrast and fields to be piecewise constant, two electrical integral equations can be expressed as the form of product of a matrix and the contrast respectively. The relationship of real part and imaginary part of the scattered field can be connected through the same contrast of the two equations. Using the weak scattering approximation, the total electrical field can be substituted by the incident field which can be known. Then the relationship of real and imaginary part of scattered field is determined based on the weak scattering approximation. The second step is to reconstruct the real part and imaginary part of scattered field based on the optimization procedure and their relationship. Firstly a functional as the norm of the difference between the measured intensity of the total field and the calculated one is defined. Then an estimate of the imaginary part of scattered field by applying the Polak-Ribiere conjugate gradient method is obtained. Using the relationship, both the real part and the imaginary part of the scattered field can be reconstructed. The final step is to tomography the object of the complex permittivity using the reconstructed scattered field. The standard Born inversion is used as the method to reconstruct the object's complex permittivity profile. It is noted that the Tikhonov regularization was used in the Born inversion method. At the last, the proposed algorithm is verified by the numerical testing. The measured data are the results from simulation by solving the direct scattering problem with the help of method of moment (MoM). The numerical testing shows that the algorithm works effectively.

## Detection of a Dielectric Target in a Half-space Using Extinction-pulse (E-pulse) Technique

Shantanu K. Padhi, Hoi-Shun Lui, N. V. Shuley, and Feng Liu

School of Information Technology and Electrical Engineering

The University of Queensland, 4072, Australia

**Abstract**— This paper describes an approach to model the impulse response of a dielectric target buried inside a half-space using a time domain deconvolution technique. The Singularity Expansion Method (SEM) has been used for a long time in the detection and recognition of targets in free space. In this approach, the scattered signals are represented as a sum of exponentials and can be extracted by using a deconvolution process if the incident signal is known. A finite difference time domain (FDTD) code is used to calculate the transient responses of a dielectric scatterer in a half-space. A singular value decomposition algorithm is used to estimate the impulse response of the target by removing the response from interface and a robust algorithm such as the matrix pencil method (MPOF) is used to calculate the complex natural resonances (CNRs) of the scatterer. The extracted poles are compared with the poles scattered by the target in free space. An automated E-pulse scheme has been used to discriminate the change in physical properties of target. The discrimination performance is calculated quantitatively by using an energy discrimination number (EDN) and the discrimination ratio (DR). The calculated results successfully discriminate the targets with small changes in conductivity. This approach has wide scale application in finding the signatures of dielectric target buried in half space. This result may be useful in determining the existence of a subcutaneous tumor in a biomedical application.

## Structural and Multiferroic Properties of $\text{BiFe}_{0.5}\text{Co}_{0.5}\text{O}_3$ Ceramics

Hai-Xia Lu, Xiang-Yu Mao, Wei Wang, and Xiao-Bing Chen

College of Physics Science and Technology, Yangzhou University, Yangzhou 225002, China

**Abstract**— The crystal and magnetic structure of polycrystalline  $\text{BiFe}_{0.5}\text{Co}_{0.5}\text{O}_3$  prepared by a solid-state reaction method with multiple calcination. The starting materials were  $\text{Bi}_2\text{O}_3$ ,  $\text{Co}_2\text{O}_3$ ,  $\text{Fe}_2\text{O}_3$ , mixed together at the stoichiometric ratios designed for  $\text{BiFe}_{0.5}\text{Co}_{0.5}\text{O}_3$  compositions with 5.0% excess  $\text{Bi}_2\text{O}_3$  to compensate for the likely loss of  $\text{Bi}_2\text{O}_3$  at elevated temperatures. The oxide mixture was calcined repeatedly and sintered for 1 h at  $830^\circ\text{C}$ . The X-ray diffraction (XRD) study shows that relatively pure phase were achieved in  $\text{BiFe}_{0.5}\text{Co}_{0.5}\text{O}_3$  samples. Comparing with the XRD of  $\text{BiFeO}_3$ , the pattern indicates that Co-doped  $\text{BiFeO}_3$  have a structural transformation. The ferroelectricity of the samples has been confirmed by the hysteresis loops measurement but the leakage current is quite large, implying that Co substitution has no effect of the improvement on ferroelectricity in  $\text{BiFe}_{0.5}\text{Co}_{0.5}\text{O}_3$  samples. The high leakage current is due to the existence of  $\text{Co}^{2+}$ ,  $\text{Fe}^{2+}$  and oxygen deficiency. The magnetization measurement performed at room temperature showed a perfect hysteresis loop with large remnant magnetization ( $M_r \approx 0.55 \text{ emu/g}$ ) and low coercive field ( $H_c \approx 197 \text{ Oe}$ ). It is different from the hysteresis of  $\text{BiFeO}_3$  that behaved a small non-linearity at room temperature. The excellent ferromagnetism in  $\text{BiFe}_{0.5}\text{Co}_{0.5}\text{O}_3$  may attribute to the ferromagnetic interaction of  $\text{Co}^{3+} - \text{O} - \text{Fe}^{3+}$ . The temperature dependence of magnetization of the sample shows that below  $230^\circ\text{C}$  the ferromagnetic phase exists and above  $390^\circ\text{C}$  the phase is paramagnetic. There is an intermediate magnetic phase in between  $230 \sim 390^\circ\text{C}$ . The frequency dependence of admittance ( $Y'$ ) at room temperature turn out a resonance curve centered at  $f \sim 12.6 \text{ MHz}$  and a negative overshoot as a typical of resonancelike behavior. The dielectric property of the  $\text{BiFe}_{0.5}\text{Co}_{0.5}\text{O}_3$  ceramics were investigated at intermediate frequencies ( $10^2 \sim 10^6 \text{ Hz}$ ) in the temperature range of  $100 \sim 560^\circ\text{C}$ . The results show that dielectric constant ( $\epsilon'$ ) have two peaks with their heights decreasing as frequency increases. At low frequencies, the temperature of the first peak,  $T_1 \sim 322^\circ\text{C}$ , almost does not vary with frequency, while the second peak,  $T_2 \sim 400^\circ\text{C}$ , shifts to lower temperature side with frequency increasing. Above  $T_2$  the dielectric constant ( $\epsilon'$ ) reduces rapidly and behaves a negative value; At high frequencies when  $f > 5.8 \text{ kHz}$ , the second peak was completely suppressed, meanwhile the first peak,  $T_1$  also shifts to lower temperature as frequency increasing. The  $T_1$  is in the intermediate magnetic phase and may be related to the ferroelectric phase transition. The interpretation of occurrence of negative dielectric permittivity might be taken into account the peculiar phase-separation formed by space-charge or interfacial polarization.

## A Novel Method for Passive Shim Design: I

Hector Sanchez Lopez, Feng Liu, Ewald Weber, and Stuart Crozier

School of Information Technology and Electrical Engineering, The University of Queensland  
St. Lucia, Brisbane Qld 4072, Australia

**Abstract**— This paper presents a new passive shim design method and a novel shimming procedure to correct the magnetic field inhomogeneities generated by horizontal Magnetic Resonance Imaging magnets. The method produces passive shim solutions capable of generating harmonics with high purity and using a minimal number of ferroschims.

**Introduction:** Magnetic resonance imaging (MRI) requires a main magnet to produce a strong and very homogeneous magnetic field (a few parts per million) within the imaging region. Reproducing the magnet theoretical dimensions as accurately as possible in the manufacturing process is very difficult. Due to machining tolerances and cooling the magnet to liquid helium temperatures, unavoidable errors are introduced in coil positions and therefore in the expected magnetic field homogeneity and as a consequence a passive and/or active correction process is required [1]. The passive shimming process generally arranges pieces of ferromagnetic materials in a convenient way to produce the same amplitude and opposite sign of the contaminant harmonics present in the magnetic field once the magnet is energised. In this paper we present a novel passive shimming approach where the shim thickness is expressed as a sum of orthogonal functions multiplied by unknown amplitudes. For first time, the thickness is expressed as a function of the azimuthal angle and cylinder length and hence, an optimal shimming procedure can be achieved for a set of particular harmonics impurities, DSV size, and cylinder radius.

**Materials and Methods:** Let us assume an isotropic and homogenous ferromagnetic cylindrical shell of radius  $R$  and axial length  $L$ , uniformly magnetized ( $M_z e_z$ ) along the axial axis. Assuming that the ferromagnetic shell is in the saturated state we can write the element volume as  $dV' = R \cdot t(z', \phi') dz' d\phi'$ , where the scalar magnitude  $t(z', \phi')$  represents the element thickness at the point  $(z', \phi')$  and can be expressed as a sum of orthogonal functions as follows:

$$t(z', \phi') = \sum_{n'=1}^N \sum_{m'=0}^M (a_{m'} \cos m' \phi' + b_{m'} \sin m' \phi') (c_{n'} \cos K_{n'} z' + d_{n'} \sin K_{n'} z'); \quad -\frac{L}{2} \leq z' \leq \frac{L}{2}, \quad (1)$$

and  $t(z', \phi') = 0$  outside of the domain in  $z$  defined in (1). The parameters  $(a_{m'}, b_{m'})$  and  $(c_{n'}, d_{n'})$  represents the unknown amplitudes of the  $t(z', \phi')$  oscillating modes along the azimuthal and axial direction, respectively.  $K_n = (\pi n)/L$ . The parameter  $N$  and  $M$  defines the number of modes along the axial and azimuthal direction, respectively. The amplitudes corresponding to the magnetic field oscillating harmonics are written as:

$$A_{nm} = \int_{-\frac{L}{2}}^{\frac{L}{2}} \int_0^{2\pi} C_{nm}(z', \phi') \cos m \phi' dz' d\phi', \quad B_{nm} = \int_{-\frac{L}{2}}^{\frac{L}{2}} \int_0^{2\pi} C_{nm}(z', \phi') \sin m \phi' dz' d\phi',$$

where  $C_{nm}$  contains the function  $t(z', \phi')$ . A least squares optimization algorithm is used to obtain the optimal amplitudes  $(a_{m'}, b_{m'})$  and  $(c_{n'}, d_{n'})$ , that minimizes the cylinder shell weight  $W(z', \phi')$  and at the same time, cancel the target harmonics and control the high orders field components excluded in the target set. From the continuous thickness map, a valid domain (regions with positive thickness) is set and discrete pieces of shim are chosen. A linear programming optimization algorithm is then employed to obtain the discrete thickness distribution.

**Results and Conclusions:** This approach was applied for a case where a combination of harmonics forms the harmonic target set. The target harmonic produces a peak-to-peak magnetic field inhomogeneity equivalent to 588.34 ppm. Figs. 1(a, b) shows the continues thickness map and the valid domain (the starting point for placing discrete shim pieces). The addition of the un-shimmed magnetic field and the magnetic field generated by the discrete shim array shown in Fig. 1(c) reduces the peak-to-peak magnetic field inhomogeneity to 20.5 ppm. The figure of merit value corresponding to the discrete array was  $\eta = 7.06 \cdot 10^{-5} \text{ T}/(\text{kg}\cdot\text{ppm})$  and the weight of the iron shim set was 0.7 kg. Fig. 1(e) shows a ferroschim profile to correct the target harmonic, considering the field contribution of all the shims uniformly distributed on the cylinder surface. The figure of merit  $\eta = 2.97 \cdot 10^{-5} \text{ T}/(\text{kg}\cdot\text{ppm})$ , was 2.4 times smaller than the same parameter produced with our approach. The corrected peak-to-peak field inhomogeneity was 25.6 ppm using

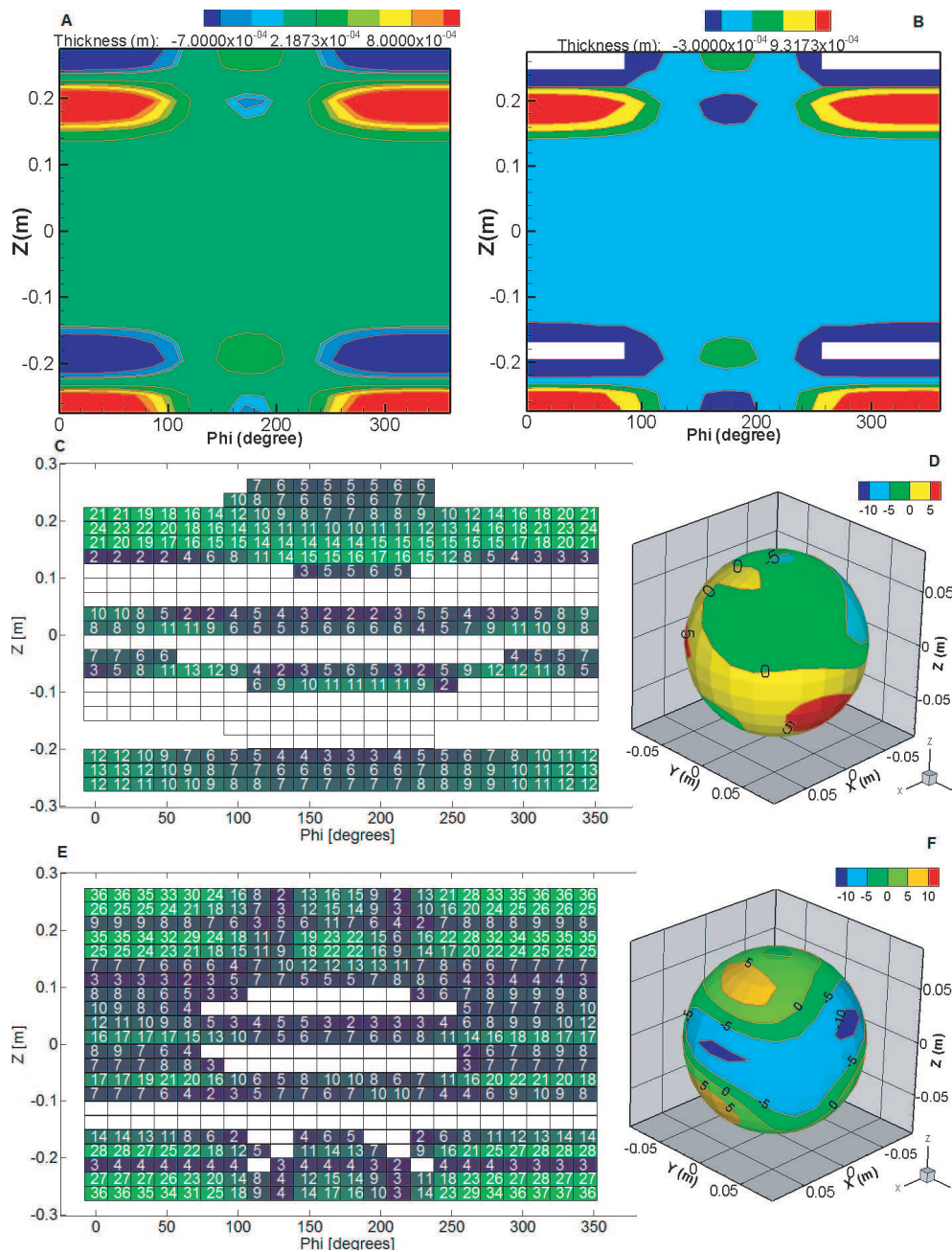


Figure 1.

1.48 kg of iron. The total shim set weight was roughly half of that needed when using a classical approach (i.e., to search directly for the shimming solution without using a continuous map as a starting point) and the homogeneity was improved 1.25 times using the profile shown in Fig. 1(c). The ferroschims thickness expressed as a sum of orthogonal series in functions of the azimuthal angle and cylinder length, provides a useful map where the shim shape and thickness is well defined. The placement of the ferroschim pieces in the effective domain significantly reduces the shim weight and improves the field homogeneity. The new shim profiles presented in this research generates highly pure harmonics and high orders in an efficient manner.

**ACKNOWLEDGMENT**

Financial support for this project from the Australian Research Council is gratefully acknowledged.

**REFERENCES**

1. Brideson, M. A., L. K. Forbes, and S. Crozier, *Concepts Magn. Reson.*, Vol. 14, 9–18, 2002.

## Subsurface Sounding in Northern Hemisphere of Mars by Marsis: Mars Express Mission

G. Picardi<sup>1</sup>, D. Biccari<sup>1</sup>, M. Cartacci<sup>1</sup>, A. Cicchetti<sup>1</sup>, A. Marini<sup>1</sup>  
A. Masdea<sup>1</sup>, F. Piccari<sup>1</sup>, R. Seu<sup>1</sup>, J. J. Plaut<sup>2</sup>, P. T. Melacci<sup>3</sup>, O. Bombaci<sup>4</sup>  
D. Calabrese<sup>4</sup>, E. Zampolini<sup>4</sup>, P. Edenhofer<sup>5</sup>, D. Plettemeier<sup>6</sup>, and E. Flamini<sup>7</sup>

<sup>1</sup>Infocom Dept., University of Rome "La Sapienza", Via Eudossiana, 18-00184 Rome, Italy

<sup>2</sup>Jet Propulsion Laboratory, 4800 Oak Grove Drive, Pasadena, CA-91109, USA

<sup>3</sup>Computer Science Dept., University of Perugia, Via Vanvitelli 1, 06123 Perugia, Italy

<sup>4</sup>Alcatel Alenia Space, Via Saccomuro, 24-00131 Rome, Italy

<sup>5</sup>Institut für HochfrequenztechnikArbeitsgruppe Antennen und Wellenausbreitung Fakultät für Elektrotechnik und Informationstechnik Ruhr, Universität Bochum 44780 Bochum, Germany

<sup>6</sup>Fakultaet für Elektrotechnik und Informationstechnik Lehrstuhl und Laboratorium für Theoretische Germany

<sup>7</sup>ASI, Viale Liegi, 26-00198 Rome, Italy

**Abstract**— The primary scientific objective of MARSIS (Mars Advanced Radar for Subsurface and Ionosphere Sounding), in the MEX (Mars Express) mission, is to map the distribution of water, both liquid and solid, in the upper portions of the crust of Mars. Detection of such reservoirs of water will address key issues in the hydrologic, geologic, climatic and possible biologic evolution of Mars. Three secondary objectives are defined for the MARSIS subsurface experiment: subsurface geologic probing, surface characterization, and ionosphere sounding. The MARSIS observations are optimized during the periods in which the pericenter of the orbit is near or below zero degrees sun elevation ("night side"). This condition existed during July 2005, in the last year of the MEX nominal mission, in the northern latitude of Mars regions. This paper provides a description of the modelling approach and of the expected performance of MARSIS in the northern hemisphere of Mars. Several models, utilized for the radar design and suitable for a preliminary analysis of the MARSIS performance, are reported. In particular the data analysis is addressed to the SCR (Signal to Clutter Ratio) performance and to the penetration depth capability of the radar. The knowledge of this performance characteristics, evaluated according to the model used for the surface and subsurface of the Martian crust, has been utilized in order to select, during the planning activity of the mission, the operative mode of the radar. The models utilized are an effective tool for the simulator that has to perform the process of the radar data inversion in order to numerically evaluate, by means of the measured radar returns, the surface and subsurface dielectric characteristics. First results of scientific analysis for the surface and subsurface characteristics, based on radar measurements taken during the night side operation of MARSIS, and a typical simulation result of the surface and subsurface echo behaviour are reported in the paper as preliminary data inversion example. Few frames from the real data are shown and their analysis reveals some feature of a boundary layer interfacing within the first km downward into the Mars subsurface. It has to be emphasized that the described inversion process represents a starting point for a better interpretation of the surface and the subsurface characteristics, taking into account the constraints related to the results of other payloads or missions.



# Session 4P1a

## Photonic Crystals

<b>A New Broadband L-shaped Bend Based on Photonic Crystal Ring Resonators</b>	818
<i>Mehrdad Djavid (K.N.Toosi University of Technology, Iran); F. Monifi (K.N.Toosi University of Technology, Iran); A. Ghaffari (K.N.Toosi University of Technology, Iran); Mohammad Sadegh Abrishamian (K.N.Toosi University of Technology, Iran); .....</i>	
<b>Magneto-optics of a 1D Magnetophotonic Crystal</b>	819
<i>Alexey P. Vinogradov (Russian Academy of Sciences, Russia); Alexander M. Merzlikin (Russian Academy of Sciences, Russia); Alexander V. Dorofeenko (Russian Academy of Sciences, Russia); Alexander B. Granovsky (Moscow State University, Russia); Alexander A. Lisyansky (The City University of New York, USA); Mitsuteru Inoue (Toyohashi University of Technology, Japan); .....</i>	
<b>Photonic Lattice of Coupled Microcavities in Nonpermanent Gravitational Field Produced by Rotation</b>	820
<i>Dmitri L. Boiko (Ecole Polytechnique Federale de Lausanne, Switzerland); .....</i>	
<b>Magnetic Anisotropy and the Stop Band of Magnetic Photonic Crystals at Microwave Frequency</b>	821
<i>Rui-Xin Wu (Nanjing University, China); Ping Chen (Nanjing University, China); Aimin Jiang (Nanjing University, China); Ji Xu (Nanjing University, China); .....</i>	
<b>Optical Properties of Photonic Crystals Made of Deep Nanopores in Silicon</b>	822
<i>A. P. Mosk (University of Twente, The Netherlands); A. Hartsuiker (FOM Institute for Atomic and Molecular Physics, The Netherlands); L. A. Woldering (University of Twente, The Netherlands); R. W. Tjerkstra (University of Twente, The Netherlands); W. L. Vos (University of Twente, The Netherlands); W. L. Vos (University of Twente, The Netherlands); .....</i>	
<b>Perfectly Periodic Photonic Quasi-Crystals</b>	823
<i>Robert C. Gauthier (Carleton University, Canada); .....</i>	
<b>Mode Localization and Bandstructure Formation in Photonic Quasicrystal Systems via Crystal Angular Momentum States</b>	824
<i>Khaled Mnaymneh (Carleton University, Canada); Robert C. Gauthier (Carleton University, Canada); .....</i>	

## A New Broadband L-shaped Bend Based on Photonic Crystal Ring Resonators

M. Djavid, F. Monifi, A. Ghaffari, and M. S. Abrishamian

Department of Electrical Engineering, K.N.Toosi University of Technology, Tehran, Iran

**Abstract**— In this paper, we propose a new type of 2D photonic crystal L-shaped bent waveguide based on ring resonator with broadband acceptable bandwidth; FDTD method concludes output efficiency over 90%.

# Magneto-optics of a 1D Magnetophotonic Crystal

A. P. Vinogradov<sup>1</sup>, A. M. Merzlikin<sup>1</sup>, A. V. Dorofeenko<sup>1</sup>  
A. B. Granovsky<sup>2</sup>, A. A. Lisyansky<sup>3</sup>, and M. Inoue<sup>4</sup>

<sup>1</sup>Institute for Theoretical and Applied Electromagnetism, Russian Academy of Sciences, RF

<sup>2</sup>Faculty of Physics, Moscow State University, RF

<sup>3</sup>Department of Physics, Queens College, the University of New York, USA

<sup>4</sup>Department of Electrical and Electronic Engineering  
Toyohashi University of Technology, Japan

**Abstract**— Photonic crystals consisting of magneto-optical (MO) materials (magnetophotonic crystals or MPCs) often exhibit unusual magneto-optical properties. It is well known that when MPC is diluted so that the volume fraction of an MO material is significantly smaller than unity, MO Kerr, Faraday, and magnetorefractive effects may be enhanced considerably [1–6].

In this communication, we focus our attention on 1D photonic crystals because of their comparative robustness in manufacturing and of their comparative insensitivity to losses. We produce a unified explanation of the enhancement of MO effects in different resonant structures, such as the MO defect in 1D photonic crystals, the Tamm state at the 1D photonic crystal — 1D MPC interface, and a slab of 1D MPC. For this purpose, we generalize the Airy's method to treat multilayer structures, taking into account that the eigensolutions of the Maxwell equations in a photonic crystal are Bloch waves with complicated intracellular structure.

We also show that some intracellular feature of the Bloch waves in MPC may lead to many effects unobserved in the usual magnetoordered crystals: e.g., enhancement of MO effects, formation of new band gaps inside the Brillouin zones, and the Borrmann effect in MPCs.

It turns out that, in spite of the natural weakness of MO phenomena, the effects caused by the magnetization of MPCs may be substantial, such as the magnetic super-prism effect [7], the controllable Tamm state [8], etc.

## REFERENCES

1. Inoue, M., T. Yamamoto, K. Isamoto, and T. Fujii, *J. Appl. Phys.*, Vol. 79, 5988, 1996.
2. Inoue, M., K. Arai, T. Fujii, and M. Abe, *J. Appl. Phys.*, Vol. 85, 5768, 1999.
3. Vinogradov, A. P., S. G. Erokhin, A. B. Granovski, and M. Inoue, *J. Communication Technology and Electronics*, Vol. 49, 88, 2004.
4. Vinogradov, A. P., S. G. Erokhin, A. B. Granovski, and M. Inoue, *J. Communication Technology and Electronics*, Vol. 49, 682, 2004.
5. Lyubchanskii, I. L., N. N. Dadoenkova, M. I. Lyubchanskii, et al., *J. Phys. D: Appl. Phys.*, Vol. 36, R277, 2003.
6. Boriskina, J. V., S. G. Erokhin, A. P. Vinogradov, M. Inoue, and A. B. Granovsky, *JMMM*, Vol. 300, e251, 2006.
7. Merzlikin, A. M. and A. P. Vinogradov, *Optics Comm.*, Vol. 259, 700–703, 2006.
8. Merzlikin, A. M., A. P. Vinogradov, A. V. Dorofeenko, M. Inoue, M. Levy, and A. B. Granovsky, *Physica B*, Vol. 394, No. 2, 277, 2007.

# Photonic Lattice of Coupled Microcavities in Nonpermanent Gravitational Field Produced by Rotation

D. L. Boiko

Ecole Polytechnique Fédérale de Lausanne, Quantum Architecture group, 1015  
Lausanne, Switzerland

**Abstract**— The impact of nonpermanent gravitational field on band structure of a rotating photonic crystal is analyzed theoretically. Rotation-induced Coriolis-Zeeman (CZ) splitting of the otherwise degenerate photonic bands is reported here for the two-dimensional square symmetry photonic lattices of evanescently coupled optical microcavities. The symmetry-broken energy splitting is similar to the Zeeman splitting of atomic levels in a magnetic field. Another example of similar behavior in magnetic fields can be found in semiconductor crystals, showing splitting of the conduction and valence bands into magnetic subbands. Coriolis-Zeeman splitting in a solitary Fabry-Pérot (FP) cavity rotating about its optical axis is known to be small (of the order of rotation rate). Here, the CZ splitting is shown to be enhanced by a factor of 1000 if the FP microcavities are arranged side-by-side in a two-dimensional (2D) periodic lattice, forming thus a photonic crystal structure of evanescently coupled optical microresonators. Their photonic band structure is analyzed here by introducing a paraxial gauge transformation which converts the Maxwell's equations into the Schrödinger equation with respect to two nonzero components of photonic spinor wave function. Apart from the kinetic in-plane energy and effective periodic crystal potential, its Hamiltonian contains relativistic term  $\propto \hbar\Omega(\hat{\mathbf{L}} + \hat{\mathbf{S}})$  with  $\Omega$  being the angular rotation rate. The impact of this term on photonic band structure is similar to the effect of an external magnetic field interacting with electron magnetic moment, which in the case of semiconductors, is usually modeled using the Luttinger k.p-approximation Hamiltonian. In photonic crystals, such term is responsible for the Coriolis-Zeeman splitting of photonic bands, and it is treated here using the 8x8 k.p-approximation of our Hamiltonian for photons. Its solutions show that the CZ splitting in photonic crystals can be measured with available experimental techniques. Estimates of the intraband matrix elements  $\langle r^2 \rangle$  indicate that the enhancement of the CZ splitting can be attributed to the fact that photons are delocalized over the large lattice domains incorporating thousands of FP microcavities composing the lattice. Following the mentioned analogy with the Hamiltonian for electrons, our Hamiltonian for photons suggests that nonstationary rotation or high frequency gravitational waves will induce quantum transitions between photonic states. Furthermore, formally it allows the inverse process to take place as well. Thus on the basis of such formalism, one can expect that a superposition of nonstationary photonic states representing the system undergoing quantum transition might produce high frequency gravitational waves.

## REFERENCES

1. Boiko, D. L., "Coriolis-Zeeman effect in rotating photonic crystal," ArXiv, 0705.1509, 2007.

# Magnetic Anisotropy and the Stop Band of Magnetic Photonic Crystals at Microwave Frequency

Rui-Xin Wu, Ping Chen, Aimin Jiang, and Ji Xu

Department of Electronic Sciences and Engineering, Nanjing University, Nanjing 210093, China

**Abstract**— Photonic crystals (PCs) have been the subject of intensive theoretical and experimental research. Up to now, most studies are done on the PCs made of dielectrics or metals. However, the PCs made of magnetic materials (MPCs) are attracted some attention recently. Magnetic response of meta-materials makes the MPCs possible at optical frequencies.

At microwave or radio frequencies MPCs can be realized by ferromagnetic materials such as ferrites. Previously, we experimentally studied the transmission characters of MPCs made of ferrite and found the stop band with some differences from the band calculation by plan-wave expansion method. In this work, using the multiple-scattering method, we further investigated the effect of magnetic anisotropy on their transmission properties. We find that magnetic anisotropy can changes the stop band width clearly. Under applied magnetic field, frequency shift rate is different for the top and the bottom frequencies of the stop band. At lower applied fields, the shift rate for top and bottom frequencies are almost the same, which has been verified in our experiments. However, at higher fields, the shift rate for bottom frequency is higher than that of top frequency, consequently the MPCs shows a stop band shift to higher frequency while a decrease of bandwidth.

## ACKNOWLEDGMENT

This work is supported by the National Natural Science Foundation of China (under project 60471020).

# Optical Properties of Photonic Crystals Made of Deep Nanopores in Silicon

A. P. Mosk<sup>1</sup>, A. Hartsuiker<sup>2</sup>, L. A. Woldering<sup>1</sup>, R. W. Tjerkstra<sup>1</sup>, and W. L. Vos<sup>1,2</sup>

<sup>1</sup>MESA+ Institute for Nanotechnology and Department of Science and Technology  
University of Twente, P. O. Box 217, 7500 AE Enschede, The Netherlands

<sup>2</sup>FOM Institute for Atomic and Molecular Physics  
Kruislaan 407, 1098 SJ Amsterdam, The Netherlands

**Abstract**— Photonic crystals offer unprecedented opportunities to control the generation and propagation of light. To maximize this control in realistic applications, scalable and precise fabrication methods are needed. We demonstrate fabrication, optical measurements and band structure calculations of two-dimensional photonic crystals made of deep nanopores in silicon. These extremely regular structures can possess a two-dimensional bandgap, and can be used to fabricate intricate three-dimensional photonic crystals.

Several different lattices of extremely deep nanopores in Si, were etched to a high aspect ratio using reactive ion etching. The structures were patterned by means of deep-UV scan- and step lithography [1], resulting in well-defined arrays of deep pores with negligible tapering.

Light from a supercontinuum light source was focused on the side of the crystals, to obtain broadband reflectivity spectra, in the range of 4000 to 15000  $\text{cm}^{-1}$ . The spectra show several reflectivity peaks with heights up to 75%, confirming the high quality of the photonic crystals. The spectra were analyzed with the help of *ab initio* band structure calculations [2], confirming that the observed reflectivity peaks correspond to the band gaps and stop gaps of the crystal.

Our fabrication methods are flexible, extremely scalable, and compatible to industrial CMOS processes. Therefore these structures may be of considerable interest, not only for research on spontaneous emission control [3] and ultrafast switching [4], but also for high-volume applications such as chemical sensors, telecom signal multiplexers, and miniature lasers and LEDs.

## REFERENCES

1. Woldering, L. A., R. W. Tjerkstra, H. V. Jansen, I. D. Setija, and W. L. Vos, (submitted), 2007.
2. Johnson, S. G. and J. D. Joannopoulos, *Opt. Express*, Vol. 8, 173, 2001.
3. Lodahl, P., A. F. van Driel, I. S. Nikolaev, A. Irman, K. Overgaag, D. Vanmaekelbergh, and W. L. Vos, *Nature*, Vol. 430, 654–657, 2004.
4. Euser, T. G., H. Wei, J. Kalkman, Y. Jun, A. Polman, D. J. Norris, and W. L. Vos, *J. Appl. Phys.*, 102, (in press), Sept. 2007.

## Perfectly Periodic Photonic Quasi-Crystals

**Robert C. Gauthier**  
Carleton University, Canada

**Abstract**— The new term “Perfectly Periodic Photonic Quasi-Crystals” ( $P^3QC$ ) applies to 2-D and 3-D dielectric arrangements that possess a high rotational order about a central pivot point (standard photonic quasi-crystal) and in the same pattern possess a radial periodicity as viewed from the same central pivot point. These structures do not possess translational symmetry as associated with standard photonic crystals. In a 2-D structure,  $P^3QC$  periodicity is observed for the polar coordinates  $(r, \theta)$  and a unit cell of surface  $dS = r dr d\theta$  serves as the building block of the pattern at each of the radial “Lattice Points”. A generating algorithm based on orthogonal functions is used to produce many different types of  $P^3C$  patterns for analysis through FDTD simulations. The presence of bandgaps in the transmission spectrum for these structures is observed when the dielectric fill factor, rotational order and dielectric contrast are carefully selected. The presence of bandgaps enables the researcher to design in defect states and construct waveguide structures.

# Mode Localization and Bandstructure Formation in Photonic Quasicrystal Systems via Crystal Angular Momentum States

Khaled Mnaymneh and Robert C. Gauthier

Department of Electronics, Carleton University, Ottawa K1S5B6, Canada

**Abstract**— Photonic quasicrystals are the rotational analogy of photonic crystals. These structures give rise to rotational extended states similar to the translational extended states, known as Bloch states, in photonic crystals. These rotational extended states appear as defect states because they are localized to certain sites within the photonic quasicrystal pattern. The pattern is not physically defected to yield these states as in the case with photonic crystals. This paper puts forward the case that these rotational extended states arise from crystal rotational symmetry. The rotational foldness of this photonic quasicrystal can be identified with an orbital angular momentum quantum number,  $l$ , which leads to  $2m + 1$  rotational extended states. We call these states crystal angular momentum states and they are similar to central potential states in atomic systems. The analogy is strengthened further by the discovery of Lamb shift states similar to those in atomic systems. Group theory predicts less than  $2m + 1$  localized states but it is the unconventional scatterer shapes of the photonic quasicrystal that manifests the  $2m + 1$ . This paper presents theoretical, simulated and experimental evidence for the case of crystal angular momentum states in photonic quasicrystals.



# Session 4P1b

## Plasmonics and Photonic Crystals for Electromagnetic Field Enhancement

<b>Surface-Polariton-Enhanced Reflected THz-Field</b>	
<i>Danhong Huang (Air Force Research Laboratory, USA); G. Gumbs (The City University of New York, USA); Paul M. Alsing (Air Force Research Laboratory, USA); David A. Cardimona (Air Force Research Laboratory, USA);</i> .....	826
<b>An Efficient Approach to Identifying a Complete Photonic Band Gap in Two-dimensional Photonic Crystals with Omnidirectional Light Propagation</b>	
<i>Ruei-Fu Jao (Fu Jen Catholic University, Taiwan, R.O.C.); Ming-Chieh Lin (National Cheng Kung University, Taiwan, Republic of China);</i> .....	827
<b>Finite Element Modeling of Transmission Characteristics of the Plasmonic Crystal Structures</b>	
<i>Dong Xiao (University of Illinois at Urbana-Champaign, USA); H. T. Johnson (University of Illinois at Urbana-Champaign, USA);</i> .....	828
<b>Photonic Crystal Enhanced Longwave Infrared Light-emitter Based on Intersubband Transitions in InAs/GaAs Quantum Dots</b>	
<i>Xuejun Lu (University of Massachusetts Lowell, USA);</i> .....	829
<b>Limitation of Spontaneous Emission Enhancement Using Surface Plasmon Polaritons</b>	
<i>Greg Sun (University of Massachusetts Boston, USA); Jacob B. Khurgin (Johns Hopkins University, USA);</i> .....	830
<b>Defect Modes in Photonic Crystals: An Asymptotic Theory for Isolated and Compound Defects</b>	
<i>Lindsay C. Botten (University of Technology, Australia); K. B. Dossou (University of Technology, Australia); C. G. Poulton (University of Technology, Australia); A. A. Astryan (University of Technology, Australia); S. Mahmoodian (University of Sydney, Australia); Ross C. McPhedran (University of Sydney, Australia); C. Martijn de Sterke (University of Sydney, Australia);</i> .....	831

## Surface-Polariton-Enhanced Reflected THz-Field

D. H. Huang<sup>1</sup>, G. Gumbs<sup>2</sup>, P. M. Alsing<sup>1</sup>, and D. A. Cardimona<sup>1</sup>

<sup>1</sup>Air Force Research Laboratory, Space Vehicles Directorate  
Kirtland Air Force Base, NM 87117, USA

<sup>2</sup>Department of Physics and Astronomy, Hunter College of the City University of New York  
695 Park Avenue, New York, NY 10021, USA

**Abstract**— Our previous study on the effect of plasma-wave induced longitudinal field [4] is generalized by further incorporating a conductive grating on top of a conducting sheet for the generation and mixing of diffraction modes of a reflected/transmitted electromagnetic field. Moreover, it expands our recent work on the coupling of an electronically-modulated two-dimensional plasmon and the surface plasmon [3] by including radiation modes as well as longitudinal-field effects in the calculation for the diffracted near and far electromagnetic fields. The highlight of this work is the prediction of a huge enhancement in the reflected far THz field, which is explained as a consequence of the strong mixing of specular and diffraction modes of the reflected THz field by the induced optical polarization in a surface conductive grating.

### ACKNOWLEDGMENT

We acknowledge partial support from the National Science Foundation under grant Nos. DMR-0303574 and CREST 0206162, PSC-CUNY grant # 68387-00-37 as well as grant # P120A050057-06 from the US Department of Education, and partial support from the Air Force Office of Scientific Research (AFOSR).

### REFERENCES

1. Raether, H., *Surface Plasmons on Smooth and Rough Surfaces and on Gratings*, Springer-Verlag, Berlin, 1988.
2. Forstmann, F. and R. R. Gerhardts, *Metal Optics Near the Plasma Frequency*, Springer-Verlag, Berlin, 1986.
3. Gumbs, G. and D. H. Huang, “Electronically modulated two-dimensional plasmons coupled to surface plasmon modes,” *Phys. Rev. B*, Vol. 75, No. 11, 115314(9), 2007.
4. Huang, D. H., C. Rhodes, P. M. Alsing, and D. A. Cardimona, “Effects of longitudinal field on transmitted near field in doped semi-infinite semiconductors with a surface conducting sheet,” *J. Appl. Phys.*, Vol. 100, No. 11, 113711(10), 2006.
5. Zayats, A. V., I. I. Smolyaninov, and A. A. Maradudin, “Nano-optics of surface plasmon polaritons,” *Phys. Rep.*, Vol. 408, No. 3–4, 131–314, 2005.
6. Stern, F., “Polarizability of a two-dimensional electron gas,” *Phys. Rev. Lett.*, Vol. 18, No. 14, 546–548, 1967.

# An Efficient Approach to Identifying a Complete Photonic Band Gap in Two-dimensional Photonic Crystals with Omnidirectional Light Propagation

Ruei-Fu Jao<sup>1,2</sup> and Ming-Chieh Lin<sup>1</sup>

<sup>1</sup>NanoScience Simulation Laboratory, Department of Physics, Fu Jen Catholic University  
Taipei County 24205, Taiwan, Republic of China

<sup>2</sup>Department of Physics, National Cheng Kung University  
Tainan 701, Taiwan, Republic of China

**Abstract**— Omnidirectional light propagation in two-dimensional (2D) photonic crystals (PCs) is investigated. An efficient approach to identifying a complete photonic band gap (PBG) in 2D PCs has been developed. The in-plane band structure of 2D photonic crystals is calculated by an adaptive finite element method. With adopting the suitable boundary conditions, the eigenvalues can be easily and rapidly calculated no matter how complex the geometric structures are. By symmetry, the omnidirectional photon density of states (PDOS) can be calculated based on the in-plane dispersion relation within the irreducible Brillouin zone. The PDOS corresponding to both the radiation and evanescent waves can be obtained accurately and efficiently. We demonstrate that the “complete band gaps” showed by some previous work due to considering only the radiation modes will be closed by including the contributions of the evanescent modes. Therefore, the complete PBGs do not exist in 2D PCs where evanescent waves can propagate. These results are of general importance and relevant to the spontaneous emission by an atom, or to dipole radiation in two-dimensional periodic structures.

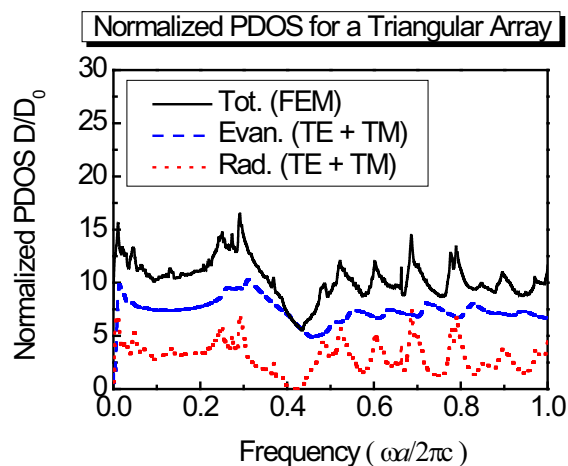


Figure 1: PDOS normalized to that of the vacuum for radiation and evanescent waves.

# Finite Element Modeling of Transmission Characteristics of the Plasmonic Crystal Structures

D. Xiao and H. T. Johnson

Department of Mechanical Science and Engineering, University of Illinois at Urbana-Champaign  
Urbana, Illinois 61801, USA

**Abstract**— Optical transmission suppression and enhancement through metal films with periodically arranged holes has been studied since 1998 [1, 2]. While it is well known that surface plasmon polaritons (SPPs) play an important role in the optical transmission, many models such as SPP Bloch waves, localized SPPs, coupling of SPPs excited on different interfaces, field localization inside the nanoholes, and Wood's anomalies *etc.* [3–8] have been proposed in efforts to provide a more detailed and clear picture of the mechanism. Until now, the finite difference time domain (FDTD) method has been the most successful numerical method for calculating the transmission spectrum of these plasmonic crystal structures since it is capable of simulating the frequency dependent materials. To apply this method, the dielectric function of the metal is normally assumed to follow the Drude form

$$\varepsilon_m(\omega) = 1 - \frac{\omega_p^2}{\omega(\omega + i\gamma)}, \quad (1)$$

where  $\omega_p$  is the plasma frequency and  $\gamma$  is the damping factor. However, using the Drude form as the dielectric function of a metal in the visible and near-infrared range is not accurate in describing the optical properties of the metal. Here, we use the finite element method (FEM) to carry out the calculations. Instead of the Drude form, we use well-recognized experimental data [9] to describe the optical properties of the metal directly.

First we focus on transmission suppression in the transmission spectra. We observe that the first region of the transmission suppression located at around 800 nm, is insensitive to the film thickness. We also find the wavelength of the first transmission suppression  $\lambda_S$  is insensitive to the hole radius, when the hole radius is not increased too much. The wavelength  $\lambda_S$  has a linear dependence on the period  $a$ , unless the holes are very close to each other. We further observe a linear relationship between the wavelength  $\lambda_S$  and the dielectric constant of the background  $\varepsilon_b$ . Finally, with a new set of the experimental data from Ref. [9], we calculate the transmission spectrum for normal light propagating through the Ag film and discover the wavelength  $\lambda_S$  is not relevant to the metal.

Second, we establish an approximate one-dimensional (1-D) model according to the SPP Bloch wave theory to study the transmission enhancement. We show that a single fitting parameter can be used to estimate the effective dielectric constant of the plasmonic crystal with light propagating normally through the film. The first transmission peaks, calculated from the transmission spectra and the 1-D analytical model, match reasonably well with varying dielectric constant of the background from 1 to 2.

## REFERENCES

1. Ebbesen, T. W., H. J. Lezec, H. F. Ghaemi, T. Thoi, and P. A. Wolff, *Nature*, Vol. 391, 667, 1998.
2. Ghaemi, H. F., T. Thoi, D. E. Grupp, T. W. Ebbesen, and H. J. Lezec, *Phys. Rev. B*, Vol. 58, 6779, 1998.
3. Wannemacher, R., *Opt. Commun.*, Vol. 195, 107, 2001.
4. Prikulis, J., P. Hanarp, L. Olofsson, D. Sutherland, and M. Kall, *Nano Lett.*, Vol. 4, 1003, 2004.
5. Chang, S. H., S. K. Gray, and G. C. Schatz, *Opt. Express*, Vol. 13, 3150, 2005.
6. Sarrazin, M., J. P. Vigneron, and J. M. Vigoureux, *Phys. Rev. B*, Vol. 67, 085415, 2003.
7. Salomon, L., F. Grillot, A. V. Zayats, and F. de Fornel, *Phys. Rev. Lett.*, Vol. 86, 1110, 2001.
8. Darmanyan, S. A. and A. V. Zayats, *Phys. Rev. B*, Vol. 67, 035424, 2003.
9. Lynch, D. W. and W. R. Hunter, *Handbook of Optical Constants of Solids*, edited by E. D. Palik, Academic, Boston, 1991.

## Photonic Crystal Enhanced Longwave Infrared Light-emitter Based on Intersubband Transitions in InAs/GaAs Quantum Dots

Xuejun Lu

University of Massachusetts Lowell, Lowell, MA 01854, USA

**Abstract**— Two-dimensional (2-D) infrared (IR) emitter arrays are of great importance in numerous military and commercial applications, including IR object and background simulation, infrared detection system testing, radiometric duplication and counter measurement, as well as medicine and spectroscopic trace-gas sensing. Current existing mid-infrared (MIR, 3–5  $\mu\text{m}$ ) and longwave infrared (LWIR, 8–14  $\mu\text{m}$ ) light emission technologies include resistive IR emitter array, MIR/LWIR light emitting diodes (LED) based on narrow bandgap and type II strained-layer superlattice materials such as  $\text{Hg}_{1-x}\text{Cd}_x\text{Te}$  and InAsSb-InSb, and quantum well cascaded lasers. Resistive IR emitter arrays are limited by a maximum apparent temperature of 700 K, and a low frame rate of 200 Hz. In addition, they are not able to produce negative luminescence to simulate cold scene temperature below ambient. In this paper, a longwave infrared (LWIR) light-emitter is reported based on intersubband transitions in InAs/GaAs quantum dots. Due to the suppressed nonradiative electron-phonon rate in the 3-D confined QD heterostructures, the QD MIR/LWIR emitter is expected to high emission efficiency. 2-D photonic crystal cavity is used to enhance the surface normal emission of the LWIR QD light emitter. Such IR emitter arrays are promising for wide-range scene simulations from below ambient to over 3000 K.

# Limitation of Spontaneous Emission Enhancement Using Surface Plasmon Polaritons

Greg Sun<sup>1</sup> and Jacob B. Khurgin<sup>2</sup>

<sup>1</sup>Department of Physics, University of Massachusetts Boston  
100 Morrissey Boulevard, Boston, Massachusetts 02125, USA

<sup>2</sup>Department of Electrical and Computer Engineering, Johns Hopkins University  
3400 N. Charles Street, Baltimore, Maryland 21218, USA

**Abstract**— Recently, there has been a great deal of interest in enhancing the efficiency of spontaneous emission (fluorescence) using the surface plasmon polariton (SPP) in the vicinity of a metal-dielectric boundary. The first definite sign of improvement was attained in GaN photoluminescence by placing a thin Ag film atop the GaN. Ninety-fold enhancement of the spontaneous recombination rate in a similar structure was subsequently demonstrated. Since then, SPP enhancement of spontaneous emission has been shown in a large number of different light emitting media. The coupling of normally non-radiative SPPs into the radiation mode has been accomplished with 1-D dielectric gratings, or 2-D corrugated silver films, or more complicated cavity-like structures.

With all the results reported, it is far from clear whether the schemes involved in the aforementioned experiments are actually optimal for the given emitters and collection optics. There were a number of analytical and numerical calculations that describe the SPP coupling into the radiation mode. Some of the calculations completely disregard the issues of Ohmic losses in SPPs and thus give an overly optimistic prognosis for the SPP enhancement. Others require extensive numerical modeling for each particular case. To the best of our knowledge, there has been no comprehensive study aimed at answering two simple questions: What should be the optimum configuration of the SPP structure for an emitter with a given radiative efficiency in a given light-collection geometry and what, if any improvement, will such an apparatus offer?

This work is aimed precisely at developing such a theory: a framework that provides unambiguous answers about the maximum improvement in radiative efficiency that one can expect using SPP and about the optimal configuration in which such improvement can be achieved. The theory relies only upon a very limited number of parameters, namely the intrinsic luminescence efficiency of the emitter and the imaginary part of the dielectric constant of a metal. Using the GaN/Ag system as an example we obtain easy-to-interpret analytical results that unequivocally indicate that using SPP pays off only for emitters that have medium-to-low luminescence efficiency; thus the SPP applications should be limited to those in sensing and analysis rather than in the development of efficient light sources.

# Defect Modes in Photonic Crystals: An Asymptotic Theory for Isolated and Compound Defects

L. C. Botten<sup>1</sup>, K. B. Dossou<sup>1</sup>, C. G. Poulton<sup>1</sup>, A. A. Astryan<sup>1</sup>  
S. Mahmoodian<sup>2</sup>, R. C. McPhedran<sup>2</sup>, and C. M. de Sterke<sup>2</sup>

<sup>1</sup>CUDOS and University of Technology, Sydney, Australia

<sup>2</sup>CUDOS and University of Sydney, Australia

**Abstract**— We consider 2D photonic crystal defect modes and deduce and demonstrate a simple exponential law linking the frequency difference of the mode and band gap edge to the relative change in modal electric energy.

The study of photonic band-gap systems has evolved from an early focus on devising structures with total band gaps, through the creation of defects that are the foundation of useful devices, e.g., cavities, waveguides etc, and, most recently, to the application of unusual and interesting properties, including high dispersion and slow light (including band-edge properties of photonic crystals). In this paper, we consider the properties of defect modes in two-dimensional (2D) photonic crystals (PC), created by making a small perturbation in an otherwise infinite, periodic photonic crystal. Such defect modes are well understood for electrons [1], and since the wave equation and the boundary conditions are similar for the 2D TM polarized electromagnetic case (i.e., with the electric field parallel to the cylinder axes), one might be confident that the behaviour exhibited by electrons should carry over to photons. However, for the case of an electric field polarized perpendicular to the axes (i.e, TE polarization), the boundary conditions for electrons and photons differ, and thus it is an open issue whether the asymptotics for TE polarization will be similar to, or quite different from, that exhibited by electrons.

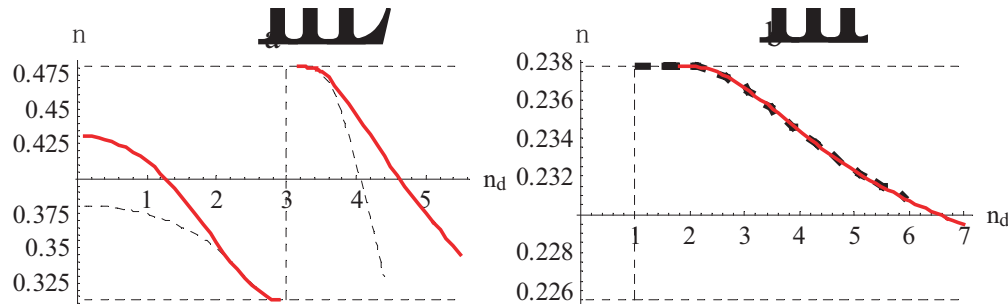


Figure 1: Evolution of a defect mode in a hexagonal PC with varying refractive index  $n_d$  of a single defect cylinder. Red line: results from FSS method; Dashed black line: reconstruction from (1) using computed sensitivity parameter. (a) TM polarization for rod-type PC ( $n_b = 1$ ,  $n_c = 3$ ); (b) TE polarization for hole-type PC  $n_b = 3$ ,  $n_c = 1$ . Cyl. radius is  $a/d = 0.2$ ,  $\nu = \omega d/(2\pi)$ .

Our treatment combines analytic and numerical studies. In the near vicinity of the band edge, we assume the band surface is parabolic, and deduce that the Green function of this 2D system is dominated by the contribution associated with the mode at the band edge — due a logarithmic dependence on the frequency difference between the defect mode  $\omega$  and the band edge  $\omega_L$ . This allows us to undertake a first-order perturbation treatment, leading to the following key result, valid for both TM and TE polarization

$$\frac{1}{\ln|\omega - \omega_L|} = -\frac{1}{S} \frac{\delta E_{\text{WSC}}}{E_{\text{WSC}}} = -\frac{1}{S} \frac{\int_{\text{WSC}} \delta\varepsilon(\mathbf{r}') ||E(k_L, \mathbf{r}')||^2 d^2\mathbf{r}'}{\int_{\text{WSC}} \varepsilon(\mathbf{r}') ||E(k_L, \mathbf{r}')||^2 d^2\mathbf{r}'},$$

$$\text{or } |\omega - \omega_L| = A \exp\left(-\frac{S}{\delta E_{\text{WSC}}/E_{\text{WSC}}}\right), \quad (1)$$

in which  $\delta\omega = \omega - \omega_L$  is related exponentially to the relative change in the electric energy ( $\delta E_{\text{WSC}}/E_{\text{WSC}}$ ) (due to the defect permittivity change  $\delta\varepsilon$ ) evaluated over the Wigner-Seitz cell, and where  $S = 2/(\omega_L N_L)$  is the sensitivity parameter, involving the density of states  $N_L$ .

We have validated [2] this formalism using our accurate *fictitious source superposition* (FSS) method [3], designed specifically to compute defect modes that are highly extended, e.g., near band edges of modal cut-off. Fig. 1 shows the evolution of the defect mode, with the red curves displaying FSS dispersion  $\omega$  and the dashed black curves displaying the reconstruction from the fitted model (1). Table 1 shows values of the sensitivity parameter ( $S_{\text{FSS}}$ ) generated by the fitting process and values ( $S_{\text{asym}}$ ) according to our asymptotic theory, with the agreement being very good in all cases.

The presentation will outline the theory, demonstrate its application for simple and compound defects.

Table 1: Tabulation of model fit parameters and the calculated sensitivity value based on the asymptotic model for the hexagonal rod-type lattice in TM polarization, and for the hole-type structure in TE polarization. (LE)/(UE) denotes the lower/upper edge of the band gap.

	$\tilde{\nu}_L$	$A_{\text{FSS}}$	$\varepsilon_{C_0} S_{\text{FSS}}$	$\varepsilon_{C_0} S_{\text{asym}}$
TM: (LE)	0.313183	0.14635	6.9536	6.9319
TM: (UE)	0.480299	0.76399	16.846	16.862
TE: (LE)	0.225548	-	-	899.68
TE: (UE)	0.237806	0.011883	18.553	18.506

## REFERENCES

1. Economou, E. N., *Green's Functions in Quantum Physics*, 2nd ed., Springer-Verlag, Berlin, 1983.
2. Dossou, K. B., R. C. McPhedran, L. C. Botten, A. A. Asatryan, and C. M. de Sterke, "Gap edge asymptotics of defect modes in 2D photonic crystals," *Optics Express*, Vol. 15, 4753–62, 2007.
3. Wilcox, S., L. C. Botten, R. C. McPhedran, C. G. Poulton, and C. M. de Sterke, *Phys. Rev. E*, Vol. 71, 056606, 2005.



# Session 4P2

## Vector Properties of Bound Light Beams and Their Physical Effects

<a href="#">Generation of Vortex Beams by Multimode Fibers</a>	
<i>Xuanhui Lu (Zhejiang University, China); He Chen (Zhejiang University, China); Chengliang Zhao (Zhejiang University, China);</i> .....	834
<a href="#">Integral Transformation Solution of Maxwell's Equations and Modified Bessel-Gaussian Cylindrical Vector Beams</a>	
<i>Chun-Fang Li (Shanghai University, China);</i> .....	835
<a href="#">Ultrafast Optical Nonlinearity Enhancement in Metalodielectric Multilayer Stacks</a>	
<i>Guohong Ma (Shanghai University, China); Sing Hai Tang (National University of Singapore, Singapore);</i> .....	836
<a href="#">Generated One Special Polarization Distribution Light Beam</a>	
<i>Pengcheng Jin (Xi'an Institute of Optics and Precision Mechanics of CAS, China); T. Duan (Xi'an Institute of Optics and Precision Mechanics of CAS, China); C. F. Li (Xi'an Institute of Optics and Precision Mechanics of CAS, China);</i> .....	837
<a href="#">Origin of Anomalous Displacements in Layered Structure: Interference between Multiple Finite-sized Light Beams</a>	
<i>Xi Chen (Shanghai University, China); Chun-Fang Li (Shanghai University, China); Qi-Biao Zhu (Shanghai University, China);</i> .....	838
<a href="#">Microwave Measurement of Dielectric Thin-film Goos-Hänchen Displacement</a>	
<i>Tao Duan (Xi'an Institute of Optics and Precision Mechanics, China); Chun-Fang Li (Shanghai University, China);</i> .....	839
<a href="#">Influence of Spatial Coherence on the Goos-Hänchen Shift at Total Internal Reflection</a>	
<i>Li-Qin Wang (Zhejiang University, China); Li-Gang Wang (Zhejiang University, China);</i> .....	840
<a href="#">Large Negative and Positive Lateral Displacement of Light Beams in a Left-handed/Right-handed Periodical Layered Structures</a>	
<i>Qi-Biao Zhu (Shanghai University, China); Chun-Fang Li (Shanghai University, China); Xi Chen (Shanghai University, China);</i> .....	841
<a href="#">Transverse Displacement of a Polarization Gaussian Beam at a Sharp Boundary</a>	
<i>Bao-Ying Liu (Xi'an Institute of Optics and Precision Mechanics, Chinese Academy of Sciences, China); Chun-Fang Li (Xi'an Institute of Optics and Precision Mechanics, Chinese Academy of Sciences, China);</i>	842
<a href="#">Polarization and Dynamical Properties of Propagation Invariant Optical Fields</a>	
<i>Karen Volke-Sepulveda (Universidad Nacional Autonoma de Mexico, Mexico); Eugenio Ley-Koo (Universidad Nacional Autonoma de Mexico, Mexico);</i> .....	843

## Generation of Vortex Beams by Multimode Fibers

Xuanhui Lu, He Chen, and Chengliang Zhao

Institute of Optics, Department of Physics, Zhejiang University  
Hangzhou 310027, China

**Abstract**— In recent years, optical vortices have been studied in details and attracted great attention for its wide applications in trapping and manipulating atoms or micro particles. They have a helical wave front with a phase term  $e^{(i\theta)}$  along the beam propagation direction and possess an orbital angular momentum (OAM) of  $l\hbar$  per photon where  $l$  is the topological charge. Many different methods for generating optical vortices have been reported, such as directly from the laser cavity, using spiral phase plates (SPPs), computer-generated holograms (CGHs), cylindrical lens converters, or a wedgelike glass platelets. In this paper, we show experimentally a novel method to generate optical vortices by multimode fibers. A laser of fundamental Gaussian mode is coupled to a multimode fiber with a certain misalignment. At the output end of the fiber, a vortex beam with helical wave front is generated. By changing the misalignment angle or position, vortex beams with different topological charges can be obtained. This approach offers an alternative to existing methods based on tilting and angular offsets for the multimode fibers.

# Integral Transformation Solution of Maxwell's Equations and Modified Bessel-Gaussian Cylindrical Vector Beams

Chun-Fang Li<sup>1,2</sup>

<sup>1</sup>Department of Physics, Shanghai University, Shanghai 200444, China

<sup>2</sup>State Key Laboratory of Transient Optics and Photonics

Xi'an Institute of Optics and Precision Mechanics of CAS

Xi'an 10119, China

**Abstract**— A cylindrical vector beam is of spatially inhomogeneous polarization that is rotationally symmetric with respect to the propagation axis. Due to its unique polarization properties, the cylindrical vector beam has attracted much attention in both optical physics and applied optics. The mathematical expression for a paraxial cylindrical vector beam is usually obtained by solving the paraxial wave equation. In this paper, we present a unified description for the cylindrical vector beam. It is shown that this beam description represents an integral transformation solution of the Maxwell's equations.

The electric-field vector of a beam that propagates in the positive  $x$  direction in source-free space can be represented by the following integral over the plane-wave angular spectrum,

$$\mathbf{E}(\mathbf{x}) = \int \int_{k_\rho < k} \frac{d\Omega}{2\pi} \mathbf{A}(k_\rho, \varphi) \exp(i\mathbf{k} \cdot \mathbf{x}), \quad (1)$$

in the cylindrical coordinate system, where

$$\mathbf{A}(k_\rho, \varphi) = \mathbf{P} \tilde{A}(k_\rho, \varphi) \quad (2)$$

is the vectorial amplitude of the angular spectrum,

$$\tilde{A}(k_\rho, \varphi) = \begin{pmatrix} A_s \\ A_p \end{pmatrix} \quad (3)$$

is the two-form amplitude [1] of the angular spectrum,

$$\mathbf{P} = \begin{pmatrix} s_x & p_x \\ s_y & p_y \\ s_z & p_z \end{pmatrix} \quad (4)$$

is a  $3 \times 2$  matrix that plays the role of extending the two-form amplitude  $\tilde{A}$  to the three-component vectorial amplitude  $\mathbf{A}$ . For the cylindrical vector beam, we choose [1]

$$\mathbf{s} = \mathbf{e}_\varphi, \quad (5)$$

$$\mathbf{p} = -\mathbf{e}_x \frac{k_\rho}{k} + \mathbf{e}_\rho \frac{k_x}{k}. \quad (6)$$

Equation (1), together with Eqs. (2)–(6), constitutes the integral-transformation solution to the vector Helmholtz's equation subject to the transversality condition. The advantage of this solution is that the two-form amplitude of the angular spectrum can be arbitrary.

Extension matrix (4), the elements of which are given by Eqs. (5) and (6), is symmetric with respect to the  $x$  axis. If the two-form amplitude is chosen to be rotationally symmetric, the electric-field vector produced by Eq. (1) is rotationally symmetric. Apart from the known Bessel-Gaussian [2] and Laguerre-Gaussian [3] cylindrical vector beams, this solution also predicts new beams, including the modified-Bessel-Gaussian cylindrical vector beams.

## ACKNOWLEDGMENT

This work was supported in part by the National Natural Science Foundation of China (Grant 60377025), Science and Technology Commission of Shanghai Municipal (Grant 04JC14036), and the Shanghai Leading Academic Discipline Program (T0104).

## REFERENCES

1. Li, C.-F., *Phys. Rev. A*, Vol. 76, 013811, 2007.
2. Jordan, R. H. and D. G. Hall, *Opt. Lett.*, Vol. 19, 427, 1994.
3. Tovar, A. A., *J. Opt. Soc. Am. A*, Vol. 15, 2705, 1998.

# Ultrafast Optical Nonlinearity Enhancement in Metallodielectric Multilayer Stacks

Guohong Ma<sup>1</sup> and Sing Hai Tang<sup>2</sup>

<sup>1</sup>Department of Physics, Shanghai University, Shanghai 200444, China

<sup>2</sup>Department of Physics, National University of Singapore, 117542, Singapore

**Abstract**— Nonlinear materials with large third-order nonlinear susceptibility,  $\chi^{(3)}$  and ultrafast response are essential requirement for future photonic device applications. In the past decades, metallic nanoparticles (especially for novel metal nanoparticles, such as Au, Ag and Cu etc.) embedded into a transparent dielectric matrix has attracted much attention because of its large nonlinear susceptibility and ultrafast response. In general, the large  $\chi^{(3)}$  is attained when laser wavelength involved falls in the range of the surface plasmon resonance of the nanoparticles. A common drawback of this kind of material is the close association of large  $\chi^{(3)}$  with resonance absorption, which may lead to thermal damage of device and loss of light. From point of view of applications, nonlinear materials with a large off-resonance value of  $\chi^{(3)}$  are very important. In recent year, it is realized that metal-dielectric multiplayer structures behave a high transmission within a certain controllable spectral range due to multiple Bragg reflections, even when the total thickness of metal significantly exceeds the conventional skin depth. The transmission window can be tuned by adjusting the thickness of metal and dielectric layers, or by changing the number of metal layers. This artificial structure provides another candidate material for fabricating all-optical devices. In this article, we investigated the nonlinear optical response of a metal-dielectric multiplayer structure. By designing the thickness of metal and dielectric layers, the transmission window can be tuned to be on-resonance with the laser wavelength, 800 nm. By employing femtosecond pump-probe and optical Kerr effect measurement, enhanced nonlinear optical response was investigated. Our results demonstrate that metal-dielectric composite structure is a suitable candidate for fabricating photonic devices.

## Generated One Special Polarization Distribution Light Beam

P. C. Jin<sup>1</sup>, T. Duan<sup>1</sup>, and C. F. Li<sup>1,2</sup>

<sup>1</sup>State Key Laboratory of Transient Optics and Photonics  
Xi'an Institute of Optics and Precision Mechanics of CAS  
Xi'an 710119, China

<sup>2</sup>Department of Physics, Shanghai University, Shanghai 200444, China

**Abstract**— A light beam have two symmetry axis in free space, one symmetry axis describe the beam's direction, and the other describe the extension matrix. The odditional symmetry axis of the extension matrix is identified due to the transversality property of the electromagnetic wave in free space. When the symmetry axis of the extension matrix is neither perpendicular nor parallel to the propagation axis of the beam, we arrive at such beams that show the observable evidence of the Beauregard effect. We try to generating the special light beam, make sure the two axis have a random angle. This beam must have a special polarization distribution, in the experiment, the beam was composed of radially and azimuthally polarized beams. The radially and azimuthally polarized beams was generated by radial polarization converter, which consisted of the polarization converter, a phase shifter that permits to compensate the  $\lambda/2$  phase step between the upper and the lower half of the theta cell and a twisted nematic cell capable to rotate the entrance polarization by  $90^\circ$  and permits to switch between the azimuthal and radial polarization distribution.

# Origin of Anomalous Displacements in Layered Structure: Interference between Multiple Finite-sized Light Beams

Xi Chen<sup>1</sup>, Chun-Fang Li<sup>1,2</sup>, and Qi-Biao Zhu<sup>1</sup>

<sup>1</sup>Department of Physics, Shanghai University, Shanghai 200444, China

<sup>2</sup>State Key Laboratory of Transient Optics and Photonics, Xi'an Institute of Optics and Precision Mechanics of CAS, Xi'an 710119, China

**Abstract**— It is well known that a light beam totally reflected from an interface between two dielectric media undergoes lateral displacement from the position predicted by geometrical optics [1, 2]. This phenomenon is referred to as the Goos-Hänchen (GH) shift. The investigations of the GH shifts have been extended to frustrated total internal reflection, partial reflection and to other areas of physics, such as acoustics and quantum mechanics. In early 1970s, Reesor et al. once discussed the lateral displacements of light beams incident on an dielectric slab. It was shown that when the slab's thickness is comparable with the wave-length of light, the lateral displacement is different from the prediction of geometrical optics, that is, the Snell's law of refraction. Recently, Li et al. have further predicted theoretically [3] and demonstrated experimentally [4] that the displacement can be zero and negative as well as positive.

What is the mechanism for the anomalous displacements? Historically, the phenomena of the GH shift is usually believed to be associated with the evanescent wave in optically thin medium. It was explained [5] by the reshaping of the reflected beam, due to the interference between each plane wave components undergoing different phase shift after the total internal reflection. However, the displacement discussed here have nothing to do with the evanescent wave as in the case of total internal reflection. Because of the feature of partial reflection and thus partial transmission, Hsue and Tamir [6, 7] have shown that the lateral displacements are produced by distortion of the beam profiles. As a matter of fact, when the concept of lateral displacement is applicable, it is implied that the actually transmitted beam has approximately the same shape as that of incident beam. On the other hand, the displacement keeps the feature of GH shift, that is, it is attributed to the finite width of the light beam. So the beam shift can't be simply considered as the result of the multiple interference of plane waves in much the same way as that in Fabry-Perot interferometer.

In this paper, we give a clear picture of the reshape mechanism of the transmitted beam to explain the anomalous displacements in the slab configuration. The reshaping of the whole transmitted beam results from the coherent interference its different constituents, which are not plane wave components but all finite-sized beam, arising from the multiple reflections inside the slab. It is shown that the lateral displacements of the whole transmitted beam can be negative, while each successively transmitted constituents is displaced a positive displacement predicted from geometrical optics. A physical condition was advanced that is required for the transmitted beam to maintain the shape of incident beam. We believe that the reshaping mechanism of finite-sized beam discussed here is also applicable to other phenomena, such as the Goos-Hänchen displacement in frustrated total internal reflection and the anomalous lateral displacement of light beam transmitted through other layered configurations.

## ACKNOWLEDGMENT

This work was supported in part by the National Natural Science Foundation of China (Grants 60377025), Science and Technology Commission of Shanghai Municipal (Grants 04JC14036), and the Shanghai Leading Academic Discipline Program (T0104).

## REFERENCES

1. Goos, F. and H. Hänchen, *Ann. Phys. (Leipzig)*, Vol. 1, 333, 1947.
2. Goos, F. and H. Hänchen, *Ann. Phys. (Leipzig)*, Vol. 5, 251, 1949.
3. Li, C.-F., *Phys. Rev. Lett.*, Vol. 91, 133903, 2003.
4. Li, C.-F., Q.-B. Zhu, G. Nimtz, X. Chen, and Y. Zhang, *Opt. Comm.*, Vol. 259, 470, 2006.
5. Artmann, K. V., *Ann. Phys. (Leipzig)*, Vol. 2, 87, 1948.
6. Hsue, C. W. and T. Tamir, *Opt. Commun.*, Vol. 49, 383, 1984.
7. Hsue, C. W. and T. Tamir, *J. Opt. Soc. Am. A*, Vol. 2, 978, 1985.

# Microwave Measurement of Dielectric Thin-film Goos-Hänchen Displacement

Tao Duan<sup>1,3</sup> and Chun-Fang Li<sup>1,2</sup>

<sup>1</sup>State Key Laboratory of Transient Optics Technology, Xi'an Institute of Optics and Precision Mechanics  
Academia Sinica, Xi'an 710119, China

<sup>2</sup>Department of Physics, Shanghai University, 99 Shangda Road, Shanghai 200444, China

<sup>3</sup>Graduate School of the Chinese Academy of Sciences, Beijing 100049, China

**Abstract**— The Goos-Hänchen displacement occurring at single interface is only of the order of wavelength. The smallness of the GH displacement impedes its experimental observation in a single reflection, especially in the optical domain and its applications in optical devices. Recently, it was predicted that the GH displacement of totally reflected beam can be greatly enhanced at resonance when a low refractive index slab is coated onto the high refractive index prism, especially when the incidence angle is smaller than but close to the critical angle for total reflection at the prism-slab interface. Due to the effect of resonance enhancement, the GH displacement can be modulated by both the angle of incidence and the thickness of the slab. Since the thickness of the slab should be of the order of wavelength in order that the concept of GH displacement is valid, it is hard in optical experiments to observe the dependence of GH displacement on the thickness of the slab. On the other hand, the wavelength of X-band microwave is about 30 mm. So it is easy for us to change the thickness of the slab in microwave experiments by use of dielectric slabs of different thickness. The purpose of this paper is to report our experimental results on the relation of the GH displacement with the thickness of the slab. In this case, the displacements for TE and TM polarizations can be measured independently by comparing the position of the reflected beam with the slab with that without the slab. As a result, the measured data are in a good agreement with the result of the numerical simulations by use of a Gaussian shaped incident beam.

## Influence of Spatial Coherence on the Goos-Hänchen Shift at Total Internal Reflection

Li-Qin Wang and Li-Gang Wang

Department of Physics, Zhejiang University, Hangzhou 310027, China

**Abstract**— In this paper, the influence of spatial coherence on the Goos-Hänchen (GH) shift at total internal reflection is investigated. A general integral expression of the cross-spectral density for a partially coherent beam reflected from an interface is derived. By means of the numerical simulation, it is found that the GH shift of the reflected beam will greatly depend on the spatial coherence, and the GH shift is greatly reduced with the decreasing of spatial coherence.

### ACKNOWLEDGMENT

This work is supported by NSFC (No. 10604047) and Zhejiang Province Education Foundation (G20630).



# Large Negative and Positive Lateral Displacement of Light Beams in a Left-handed/Right-handed Periodical Layered Structures

Qi-Biao Zhu<sup>1</sup>, Chun-Fang Li<sup>1,2</sup>, and Xi Chen<sup>1</sup>

<sup>1</sup>Department of Physics, Shanghai University, Shanghai 200444, China

<sup>2</sup>State Key Laboratory of Transient Optics and Photonics

Xi'an Institute of Optics and Precision Mechanics of CAS, Xi'an 710119, China

**Abstract**— It is well known that a light beam totally reflected from an interface between two dielectric media undergoes lateral displacement from the position predicted by geometrical optics [1, 2]. This phenomenon is referred to as the Goos-Hänchen (GH) displacement. Because of their potential applications in the microdevices, the investigations of the lateral displacements have been extended to frustrated total internal reflection, partial reflection and to other areas of physics, such as acoustics and quantum mechanics.

In the past a few years, photonic crystals (PCs) have inspired considerable interest in both the physics and the engineering communities because of their interesting electromagnetic behaviors, such as the super-prism phenomenon and the ultra-refractive effect, which have potential applications in integrated optics. Recently, GH displacements in PCs have attracted much attention. Felbacq et al. [3, 4] have shown that obvious GH displacement exists for PCs at frequencies both in- side and outside a bandgap. By choosing an appropriate thickness for the homogeneous cladding layer, giant negative GH displacement can also occur for PCs with a negative refractive index [5, 6]. More recently, we have investigated the giant bistable shifts for one-dimensional (1-D) nonlinear PCs [7].

In this paper, we study the large negative and positive lateral displacement of light beams transmitting through a periodical layered structures (1-D PCs) consisting of alternating slabs of two materials with positive-index medium (PIM) and negative-index medium (NIM). It is shown that the lateral displacement can be negative as well as positive, which is dependent on the evenness or oddness of the number of interfaces between different types of media (such as PIM-NIM and NIM-PIM). Furthermore, the negative and positive lateral displacements are also closely related to the incidence angle, refractive index, and the thickness of the slab. These phenomena will lead to novel applications, such as spatial modulator, optical waveguide switches, and optical sensors.

## ACKNOWLEDGMENT

This work was supported in part by the National Natural Science Foundation of China (Grants 60377025), Science and Technology Commission of Shanghai Municipal (Grants 04JC14036), and the Shanghai Leading Academic Discipline Program (T0104).

## REFERENCES

1. Goos, F. and H. Hänchen, *Ann. Phys. (Leipzig)*, Vol. 1, 333, 1947.
2. Goos, F. and H. Hänchen, *Ann. Phys. (Leipzig)*, Vol. 5, 251, 1949.
3. Felbacq, D. and R. Smaali, *Phys. Rev. Lett.*, Vol. 92, 193902, 2004.
4. Felbacq, D., A. Moreau, and R. Smaali, *Opt. Lett.*, Vol. 28, 1633, 2003.
5. He, J., J. Yi, and S. He, *Opt. Express*, Vol. 14, 3024, 2006.
6. Wang, L.-G. and S.-Y. Zhu, *Opt. Lett.*, Vol. 31, 101, 2006.
7. Hou, P., Y.-Y. Chen, X. Chen, J.-L. Shi, and Q. Wang, *Phys. Rev. A*, Vol. 75, 045802, 2007.

# Transverse Displacement of a Polarization Gaussian Beam at a Sharp Boundary

Bao-Ying Liu and Chun-Fang Li

State Key Laboratory of Transient Optics and Photonics  
Xi'an Institute of Optics and Precision Mechanics, Chinese Academy of Sciences  
Xi'an 710119, China

**Abstract**— It has been already known that the reflected and transmitted light beam undergo shift of position in the plane of incidence (longitudinal) or normal to the plane of incidence (transverse). The transverse displacement includes the polarization dependent transverse Imbert-Fedorov shift (usually called as IF effect) in the reflection or refraction of the beam on a sharp boundary, and the splitting of rays of different polarizations in a smoothly inhomogeneous medium. The theoretical predictions and issues of the previous papers about the IF displacement in partial reflection and refraction, remain still controversial. And, the displacement of the transmitted light beam has not been experimentally measured so far. We present solutions to the problem of transverse displacement of the reflected and transmitted beam at an interface between two homogeneous media, through representing the vectorial angular spectrum and the vectorial amplitude of a 3D light beam in terms of a two-form angular spectrum and an expansion matrix. We have derived the general formula for the transverse displacement of the reflected and transmitted beam in the paraxial approximation, and have discussed the influences of the polarization feature of the vectorial angular spectrum on the transverse displacement. It is found that only the non-uniformly polarized beams bear the transverse displacement, it also shows that the displacement is concerned with the polarization state of the angular spectrum, and is quantized with the ellipticity, so it is quantized with eigenstates the two orthogonal circular polarizations and it is in fact the translational inertial spin effect happening to the interface of two homogeneous dielectric media. The results are found to be in agreement with the Schilling's theoretical result and Pillon's recent experimental result.

# Polarization and Dynamical Properties of Propagation Invariant Optical Fields

Karen Volke-Sepulveda and Eugenio Ley-Koo

Instituto de Fisica, Universidad Nacional Autonoma de Mexico  
Apdo Postal 20-364, Mexico City 01000, DF, Mexico

**Abstract**— In 1987, Durnin and co-workers introduced the lowest order Bessel beams [1] as the first example of non-diffracting or propagation invariant optical fields (PIOFs), and they were studied under the scope of the scalar theory. Afterwards, the complete family of Bessel beams was extensively analyzed and, in recent years, other families of PIOFs with different geometries, namely the elliptic Mathieu beams [2] and the parabolic non-diffracting beams [3], have been studied also within the scalar approach. In this work we present a general vector description for all the families of PIOFs, allowing the identification of different polarization states. Furthermore, we obtain general expressions for the energy density and Poynting vector, which lead to an extended characterization of the different kinds of vector PIOF, incorporating information on their polarization properties. Finally, we discuss the geometrical and dynamical meaning of the separation constants in the solution of Helmholtz equations associated PIOFs. The characteristics of the operators and dynamical quantities behind such constants, including their connections and differences, are important in extending the familiarity with Bessel POIFs to the two other families, in both the scalar and vector versions.

## REFERENCES

1. Durnin, J., et al., *Phys. Rev. Lett.*, Vol. 58, 1499–1501, 1987.
2. Gutierrez-Vega, J. C., et al., *Opt. Lett.*, Vol. 25, 1493–1495, 2000.
3. Bandres, M. A., et al., *Opt. Lett.*, Vol. 29, 44–46, 2004.



# Session 4P3

## Wave Propagation and Superresolution in Active and Passive Metamaterials 3

<a href="#">Potential of Micro/Nanotechnology for Metamaterials</a>	
<i>Herbert O. Moser (National University of Singapore, Singapore);</i>	846
<a href="#">Finite Difference Time Domain Analysis of Imaging Properties in a Metallic Photonic Crystal System</a>	
<i>Dong Xiao (University of Illinois at Urbana-Champaign, USA); K. W. Kim (North Carolina State University, USA); H. T. Johnson (University of Illinois at Urbana-Champaign, USA);</i>	847
<a href="#">Terahertz Transmission Properties of Multi-layer Planar Electric Metamaterials</a>	
<i>Abul K. Azad (MPA-CINT, Los Alamos National Laboratory, USA); Elshan Akhadov (MPA-CINT, Los Alamos National Laboratory, USA); Nina R. Weisse-Bernstein (Space and Remote Sensing, Los Alamos National Laboratory, USA); Hou-Tong Chen (MPA-CINT, Los Alamos National Laboratory, USA); Antoinette J. Taylor (MPA-CINT, Los Alamos National Laboratory, USA); John F. O'Hara (MPA-CINT, Los Alamos National Laboratory, USA);</i>	848
<a href="#">Metamaterial Techniques for Automotive Applications</a>	
<i>K. Sato (Toyota Central R and D Labs., Japan); T. Nomura (Toyota Central R and D Labs., Japan); S. Matsuzawa (Toyota Central R and D Labs., Japan); H. Iizuka (Toyota Central R and D Labs., Japan);</i>	849
<a href="#">Terahertz and Microwave Energy Focusing onto Extremely Rectangular Slits</a>	
<i>Dai-Sik Kim (Seoul National University, Korea);</i>	850
<a href="#">Anisotropic Metamaterial from Layered Metal-dielectric System: Application to Optical Invisibility Cloaking and Polarization Beam Splitting</a>	
<i>Yijun Feng (Nanjing University, China);</i>	851
<a href="#">Left-handed and Right-handed Metamaterials Sensitive to the Polarization</a>	
<i>Miguel Beruete (Universidad Publica de Navarra, Spain); Miguel Navarro-Cía (Universidad Publica de Navarra, Spain); Mario Sorolla (Universidad Publica de Navarra, Spain); Igor Campillo (CIC nanoGUNE Consolider, Spain);</i>	852
<a href="#">Plasmonic Metamaterials with Negative Magnetism and Refractive Index for the Visible Range</a>	
<i>Vladimir P. Drachev (Purdue University, USA); Uday K. Chettiar (Purdue University, USA); Hsiao-Kuan Yuan (Purdue University, USA); Wenshan Cai (Purdue University, USA); Alexander V. Kildishev (Purdue University, USA); Vladimir M. Shalaev (Purdue University, USA);</i>	853
<a href="#">Photonic Meta Materials, Nano-scale Plasmonics and Super Lens</a>	
<i>Xiang Zhang (University of California, USA);</i>	854
<a href="#">Discussion of Some Problems of Wave Propagation in Passive Metamaterials</a>	
<i>Chao Li (Institute of Electronics, Chinese Academy of Sciences, China); F. Li (Institute of Electronics, Chinese Academy of Science, China);</i>	855
<a href="#">Novel Smart Sensory Composites with Magnetoimpedance Wires for Stress Monitoring at Microwave Frequencies</a>	
<i>Larissa V. Panina (University of Plymouth, UK); D. P. Makhnovskiy (University of Plymouth, UK); Arcady P. Zhukov (Universidad del Pais Vasco, Spain); J. Gonzalez (Universidad del Pais Vasco, Spain);</i>	856
<a href="#">Nano-photonic Devices and Wave Propagation in Organic Nano-structures</a>	
<i>Vellaisamy Arul Lenus Roy (The University of Hong Kong, China); Stephen C. F. Kui (The University of Hong Kong, China); Chi-Ming Che (The University of Hong Kong, China);</i>	857

## Potential of Micro/Nanotechnology for Metamaterials

H. O. Moser

Singapore Synchrotron Light Source, National University of Singapore  
5 Research Link, 117603, Singapore

**Abstract**— The development of metamaterials and of their applications strongly depends on the availability of reasonable amounts of high-quality samples. For electromagnetic metamaterials with resonance frequencies ranging from the far infrared to the visible ( $1 - > 400$  THz), micro/nanomanufacturing was successfully applied during the past years to produce a variety of different designs, materials, and resonance frequencies. Besides the production by primary pattern generation via electron beam, proton beam and photon beam (laser) writing, lithography is taking center stage when it comes to the fast parallel cost-effective production of comparably large areas of metamaterials. Deep X-ray lithography with synchrotron radiation is particularly well suited for producing tall high-aspect-ratio microstructures. Such architectures may be particularly well suited for side-on incidence of the electromagnetic wave, thus maximising coupling with the magnetic field component. Tall microstructures also facilitate the production of substantial volumes of metamaterials. The status and future directions of development will be discussed including current challenges to the materials, the process technology and the designs.

# Finite Difference Time Domain Analysis of Imaging Properties in a Metallic Photonic Crystal System

D. Xiao<sup>1</sup>, K. W. Kim<sup>2</sup>, and H. T. Johnson<sup>1</sup>

<sup>1</sup>Department of Mechanical Science and Engineering, University of Illinois at Urbana-Champaign  
Urbana, Illinois 61801, USA

<sup>2</sup>Department of Electrical and Computer Engineering, North Carolina State University  
Raleigh, North Carolina 27695, USA

**Abstract**— In left-handed media (LHM), so named by Veselago [1] in the late 60's, the electromagnetic wave, in the form of wave vector  $\vec{k}$ , electric field  $\vec{E}$  and magnetic field  $\vec{H}$ , forms a left-handed vector set. These hypothetical materials have many interesting properties, including a negative refractive index. Pendry suggested that these materials could be used to fabricate a perfect lens [2], since both propagating and evanescent waves contribute to the resolution of the image to overcome the conventional resolution limit of the wavelength  $\lambda$ . The scarcity of LHMs in nature has triggered a search for an artificially structured LHM. Pendry et al. proposed a periodic array of thin wires and ring cavities with negative electric permittivity and magnetic permeability respectively for electromagnetic waves with frequencies of 1–10 GHz [3]. Progress in engineering these periodic arrays of metallic elements stimulated significant interest in the photonic crystals (PCs), especially metallic PCs, due to their obvious similarities [4–8]. Very recently, some studies suggested the possibility of far-field imaging in metallic PCs obeying the rule of geometric optics. In the present paper, through a comparison of the imaging properties of a metallic PC and the ideal LHM system, we suggest although the light propagation in such a metallic PC system does exhibit negative refraction, the scattering effect as mentioned in Ref. 9 has a huge impact on the imaging properties of the system. This effect influences the imaging so significantly that it may prevent the use of a 2D PC based medium as a superlens.

We consider a PC structure that consists of a triangular array of metallic rods with the radius  $r = 0.25 \mu\text{m}$  in a dielectric host medium of  $\varepsilon = 6$ . The lattice constant  $a$  is chosen to be  $1 \mu\text{m}$ . The dielectric constant of the metal follows the Drude form

$$\varepsilon = 1 - \frac{\nu_p^2}{\nu(\nu + i\gamma)} \quad (1)$$

and the permeability  $\mu = 1$ . Here  $\nu_p$  is the plasma frequency of the metal and  $\gamma$  is the Drude relaxation rate. By the comparison, the dielectric properties of an ideal LHM are expressed as

$$\begin{cases} \varepsilon = 1 - \frac{K_\varepsilon^2}{\nu(\nu + i\gamma\varepsilon)} \\ \mu = 1 - \frac{K_\mu^2}{\nu(\nu + i\gamma\mu)} \end{cases}, \quad (2)$$

where all constants are set so that  $\varepsilon = \mu \approx -1$ . The analysis by the finite difference time domain (FDTD) method shows that in a metallic PC based system, far-field images do follow the rule of geometric optics with respect to changes in the source position. However, the similarity with the ideal LHM may end here as the PC based system cannot be described as a homogeneous composite medium. The imaging mechanism in the metallic PC is also based on the multiple scattering process.

## REFERENCES

1. Veselago, V. G., *Sov. Phys. Usp.*, Vol. 10, 509, 1968.
2. Pendry, J. B., A. J. Holden, and W. J. Stewart, *Phys. Rev. Lett.*, Vol. 76, 4773, 1996.
3. Pendry, J. B., A. J. Holden, D. J. Robbins, and W. J. Stewart, *IEEE Trans. Microwave Theory Tech.*, Vol. 47, 2075, 1999.
4. Zhang, X., *Phys. Rev. B*, Vol. 70, 195110, 2004.
5. Hu, X. and C. T. Chan, *Appl. Phys. Lett.*, Vol. 85, 1520, 2004.
6. Wang, Y., X. Wang, J. Rybczynski, D. Z. Wang, K. Kempa, and Z. F. Ren, *Appl. Phys. Lett.*, Vol. 86, 153120, 2005.
7. Wang, X. and K. Kempa, *Phys. Rev. B*, Vol. 71, 233101, 2005.
8. Ao, X. and S. He, *Appl. Phys. Lett.*, Vol. 87, 101112, 2005.
9. Li, Z. and L. Lin, *Phys. Rev. B*, Vol. 68, 245110, 2003.

# Terahertz Transmission Properties of Multi-layer Planar Electric Metamaterials

Abul K. Azad<sup>1</sup>, Elshan Akhadov<sup>1</sup>, Nina R. Weisse-Bernstein<sup>2</sup>, Hou-Tong Chen<sup>1</sup>  
Antoinette J. Taylor<sup>1</sup>, and John F. O'Hara<sup>1</sup>

<sup>1</sup>MPA-CINT, Los Alamos National Laboratory

P. O. Box 1663, MS K771, Los Alamos, NM 87544, USA

<sup>2</sup>Space and Remote Sensing, Los Alamos National Laboratory

P. O. Box 1663, MS B244, Los Alamos, NM 87545, USA

**Abstract**— Presently, there are a number of approaches to defining the effective thickness of a single-layer planar metamaterial, or metafilm. The optical properties of a metafilm can be extracted from experimental measurements, but they are critically dependent on this choice of thickness. Measuring the transmission properties of multiple stacked metafilm layers is an intriguing process because it illustrates the transition from a single-layer effective thickness to a quasi-bulk thickness, both of which should result in the same optical properties under the effective medium approximation. In this work, we study the transmission properties of metamaterials comprised of multiple metafilm layers using terahertz time domain spectroscopy.

Periodic subwavelength electric split-ring-resonators (eSRRs) of gold film were fabricated in square arrays on multiple insulating substrates using conventional photolithography. These metafilms were aligned and stacked together to form quasi three dimensional effective medium. The layers were separated by a distance of 1.5 times the transverse lattice parameter to minimize the inter-layer interaction. The transmission measurements were performed under normal incidence. Measured transmission spectra reveal clear resonances at 1.2 THz due to the effective inductive-capacitive response of the eSRRs. The transmission was also measured through the multiple layers and was then compared with a single layer sample. The transmission spectra show band-stop filtering behavior that increases in strength with an increasing number of layers. After adding four layers of metamaterial the effective medium becomes completely band-stop at the resonance frequency whereas the single layer can only reduce the transmission by 40%. The resonance linewidth also increases with number of layers which indicates possible interactions between layers. However, there is no shift in the resonance frequency of single layer and multi layer samples. This demonstrates that the resonance frequency is mostly determined by the SRR structural parameters. Extraction of the optical properties of the multiple layer materials initially indicates that as greater numbers of layers are added the composite material's properties converge to steady value, indicating a "true" effective medium response. We show that the complex refractive index of the composite media and that of the individual metafilm layers are not in agreement for our samples.



## Metamaterial Techniques for Automotive Applications

**K. Sato, T. Nomura, S. Matsuzawa, and H. Iizuka**  
Toyota Central Research & Development Labs., Inc., Japan

**Abstract**— Metamaterials are artificially constructed materials that have unusual electromagnetic properties such as backward wave, reduced wavelength with decreasing frequency, nonlinear frequency characteristic of resonances, and so on. In the view point of engineering, metamaterials having such unusual electromagnetic properties are expected to extend significantly the design degrees of freedom for materials, devices, components and systems, resulting in new applications, drastic improvement of performance, simple architectures, low cost, and so on. This paper presents automotive applications that metamaterials could work effectively. They include beam scanning antenna systems for radars and mobile communication antennas, novel magnetic materials for electric motors, the high-performance absorbing and shielding materials for electromagnetic compatibility. Metamaterials could be applied to optical devices such as LED headlights and night vision systems using infrared cameras. Then, research activities undertaken at Toyota Central R and D Labs (TCRL) are reviewed. Two types of metamaterial-based antennas are presented. One is a leaky-wave antenna for future millimeter-wave radar systems that need wide scanning angle with simple architecture. The other is a dipole for UHF band applications. The dipole provides small size, or opposite polarization to conventional one. Also, design techniques are desired to maximize the performance of metamaterials. A topology design optimization technique for periodic structures of metamaterials is presented with an example model.

## Terahertz and Microwave Energy Focusing onto Extremely Rectangular Slits

Dai-Sik Kim

Department of Physics, Seoul National University, Seoul 151-742, Republic of Korea

**Abstract**— Plasmonics has attracted growing attention in the photonics community in the last decade. The concept of surface plasmon polariton has been extended to perforated structures with local resonances in the microwave and terahertz frequency range where metals are highly conducting. In perfect metals, the lightning rod effect becomes singular and a large field enhancement is expected. Recently, it has been predicted that a rectangle aperture with a large aspect ratio acts as a strong local antenna at its fundamental resonance, focusing the incoming wave onto its small area. Here, we performed terahertz near-field experiments on single rectangular holes grown on an electro-optic crystal substrate. We found that the near-field enhancement becomes larger as the rectangle becomes narrower, strongly suggesting that a constant energy passes through the rectangle no matter how narrow it is. We expect that the enormous field enhancement will have wide ranging implications in many areas where strong terahertz fields are much desired.

# Anisotropic Metamaterial from Layered Metal-dielectric System: Application to Optical Invisibility Cloaking and Polarization Beam Splitting

Yijun Feng

Department of Electronic Science and Engineering, Nanjing University, Nanjing 210093, China

**Abstract**— In addition to isotropic left-handed metamaterials (LHMs), anisotropic metamaterials (AMMs) having permittivity and permeability tensors with parts of the elements being negative have drawn a lot of attentions due to their extraordinary electromagnetic wave propagation properties and easier realizations comparing with the isotropic LHMs. The AMMs have been identified into four types based on their wave propagation properties, which are called the cutoff, always-cutoff, never-cutoff and anti-cutoff media. Negative refraction [1], anomalous electromagnetic wave refraction and reflection [1–3] have been demonstrated at the interface between normal medium and the AMM medium. Anisotropic materials with desired permittivity properties can be produced by a layered structure of thin, alternating dielectric layers (or metal and dielectric layers). Such planar systems have been proposed to demonstrate the subwavelength imaging [4], and to build photonic funnels for sub-diffraction light compression and propagation [5].

In this presentation, we will report our recent progress on utilizing the anomalous wave propagation properties of AMM. We will show two examples of optical device applications based on AMM designed from the layered metal-dielectric system. The first example is the approach of realizing the optical cloaking by concentric layered structures. We will show that by properly designing the realization of the anisotropic distribution of the permittivity required for the cloak through layered structure of homogeneous isotropic materials, the low-reflection and power-flow bending properties of the electromagnetic cloaking could be obtained. The second example is a novel polarization beam splitter (PBS) utilizing the anomalous reflection and transmission of an anisotropic metamaterial slab. We will show that by proper design of the constitutive tensors of the slab, PBS is achieved with little dependence on the incident angle and slab thickness. We will also discuss the realization of the proposed PBS in the optical range by layered metal-dielectric nano-structured system, which could be modeled as an effective anisotropic metamaterial with the desired constitutive tensors.

## ACKNOWLEDGMENT

Supported by the National Basic Research Program of China (2004CB719800), the National Nature Science Foundation (No. 60671002), and the Specialized Research Fund for the Doctoral Program of Higher Education (No. 20030284024).

## REFERENCES

1. Smith, D. R. and D. Schurig, *Phys. Rev. Lett.*, Vol. 90, 077405, 2003.
2. Grzegorzcyk, T. M., et al., *IEEE Tran. Microwave Theory and Techniques*, Vol. 53, 1443–1450, 2005.
3. Feng, Y., et al., *J. Appl. Phys.*, Vol. 100, 114901, 2006.
4. Wood, B., J. B. Pendry, and D. P. Tsai, *Phys. Rev. B*, Vol. 74, 115116, 2006.
5. Govyadinov, A. A. and V. A. Podolskiy, *Phys. Rev. B*, Vol. 73, 155108, 2006.

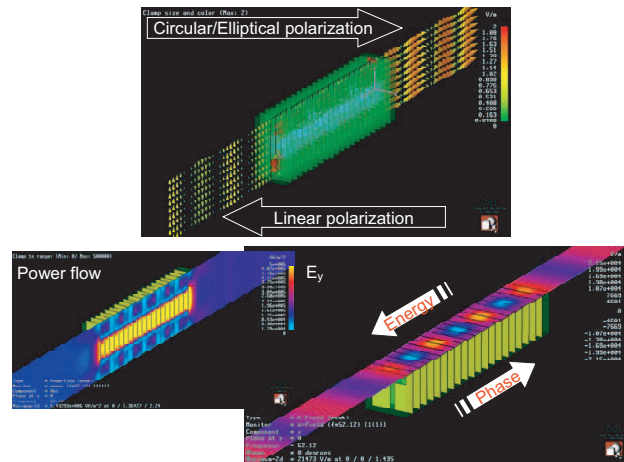
# Left-handed and Right-handed Metamaterials Sensitive to the Polarization

Miguel Beruete<sup>1</sup>, Miguel Navarro-Cía<sup>1</sup>, Mario Sorolla<sup>1</sup>, and Igor Campillo<sup>2</sup>

<sup>1</sup>Millimeter Wave Laboratory, Universidad Pública de Navarra  
Campus Arrosadía s/n, 31006-Pamplona, Spain

<sup>2</sup>CIC nanoGUNE Consolider, Paseo Mikeletegi 56, 301, Donostia 20009, Spain

**Abstract**— Recently, metamaterial structures which are sensitive to the polarization have been demonstrated in the sub-terahertz range [1]. By using an stacked subwavelength hole array that exhibits simultaneously Extraordinary Optical Transmission (EOT) and Left-Handed (LHM) propagation [2]. The dispersion diagram shows that LHM propagation can be achieved for the principal polarization whereas the cross-polarization can be inhibited or allowed to propagate as in standard media. Measurements results of the fabricated prototypes are in close agreement with our proposals. In this way, novel polarization control metamaterials are envisaged [3].



## REFERENCES

1. Beruete, M., M. Navarro-Cía, M. Sorolla, and I. Campillo, *Opt. Exp.*, Vol. 15, 8125, 2007.
2. Beruete, M., M. Sorolla, and I. Campillo, *Opt. Exp.*, Vol. 14, 5445, 2006.
3. Werner, D. H., D. H. Kwon, I. C. Khoo, A. V. Kildishev, and V. M. Shalaev, *Opt. Exp.*, Vol. 15, 3342, 2007.

## Plasmonic Metamaterials with Negative Magnetism and Refractive Index for the Visible Range

Vladimir P. Drachev, Uday K. Chettiar, Hsiao-Kuan Yuan  
Wenshan Cai, Alexander V. Kildishev, and Vladimir M. Shalaev  
Birck Nanotechnology Center and School of Electrical and Computer Engineering  
Purdue University, West Lafayette, IN 47907, USA

**Abstract**— Metal nanostructures support localized surface plasmons and propagating waves, known as surface plasmon-polaritons. The variety of applications of plasmonic nanostructures includes molecular sensing and imaging, all-optical devices, sub-wavelength waveguides and integrated circuits, and metamaterials with optical magnetism and negative refractive index. Advanced fabrication and computation methods allow the engineering of optimal nanostructure geometries of metal dielectric composites aimed at particular application. The fundamental properties of the metal and the artificially designed geometries of the structural units enable the needed functionality for the nanostructures.

Metamaterials with optical magnetism and negative refractive index employ the effect of circular currents in double layered metal nanostructures separated by a dielectric spacer. We present the results of experimental realization of such metamaterials for the visible spectral range. The samples of a subwavelength bi-periodic cross-grating, consisting of two perforated thin metal layers separated by a thin dielectric show both a negative effective permeability and a negative effective permittivity for linearly polarized light with a wavelength between 799 and 818 nm, and the real part of its refractive index is about  $-1.0$  at 813 nm. The ratio  $-\text{Re}(n)/\text{Im}(n)$  is close to 1.3 at 813 nm. For an orthogonal polarization, the same sample exhibits a negative refractive index at 772 nm. The magnetism across the whole visible spectrum by creating a family of paired-strip samples with varying geometries has been demonstrated.

In this talk we focus also on the basic properties of metal nanostructures, including effect of the size-dependent permittivity and surface roughness on metamaterial effective parameters. The permittivity of a metal nanostructure differs from the ideal bulk metal, especially in its imaginary part,  $\epsilon''_m$ . With a fine adjustment of the fabrication protocol we are able to control not only dimensions but also the roughness of a metal-dielectric interface. We will present, in particular, our experiments on negative metamagnetics with differing silver surface roughness or with different dimensions, and discuss the effect of these factors on the electron relaxation rate. Surprisingly, the geometrical effect of roughness is mostly responsible for increased losses at the plasmon resonances of the nanostructure, while the surface roughness does not affect the Ag permittivity. Anisotropy in  $\epsilon''_m$  observed in the experiments indicates a significant contribution from the quantum size effect and the chemical interface effect. The size-dependent terms of  $\epsilon''_m$  for two polarizations have relatively large A-parameters. The spectra of  $\epsilon''_m$  for the electric field parallel to the strips suggest good quality of the Ag crystal structure since the absolute values of  $\epsilon''_m$  for samples with large widths are between the literature values for bulk Ag.

# Photonic Meta Materials, Nano-scale Plasmonics and Super Lens

**Xiang Zhang**

NSF Nano-scale Science and Engineering Center (NSEC)  
University of California, 5130 Etcheverry Hall, Berkeley, CA 94720, USA

**Abstract**— Recent theory predicted a new class of meta structures made of engineered sub wavelength entities — meta “atoms” and “molecules” which enable the unprecedented electromagnetic properties that do not exist in the nature. For example, artificial plasma and artificial magnetism, and super lens that focuses far below the diffraction limit. The metamaterials may have profound impact in wide range of applications such as nano-scale imaging, nanolithography, and integrated nano photonics.

I'll discuss a few experiments that demonstrated these intriguing phenomena. We showed, for the first time, the high frequency magnetic activity at THz generated by artificially structured “meta molecule resonance”, as well as the artificial plasma. Our experiment also confirmed the key proposition of super lens theory by using surface plasmon. We indeed observed optical superlensing which breaks down so called diffraction limit. I'll also discuss nano plasmonics for imaging and bio-sensing. The surface plasmon indeed promises an exciting engineering paradigm of “x-ray wavelength at optical frequency”.

## Discussion of Some Problems of Wave Propagation in Passive Metamaterials

C. Li and F. Li

Institute of Electronics, Chinese Academy of Science, China

**Abstract**— In the past few years, there has been growing interest in artificial fabricated structures with peculiar electromagnetic responses, which are classified as metamaterials (MTMs). MTMs includes electromagnetic band gap (EBG) structures, complex surfaces such as high-impedance planes (HIPs), and left-handed materials (LHMs). In this paper some issues related to the wave propagation in passive metamaterials are discussed.

**Implementation of Resonant Metamaterial Particles (RMPs) for Controlling Wave Propagation in Planar Microwave Structures:** Recently, RMPs have been successfully applied to design novel microwave circuits and devices, or to improve their performance. The most commonly used RMPs are Split Ring Resonators (SRRs) and their dual counterparts — Complementary Split Ring Resonators (CSRRs). Originally, SRRs were inspired by the first experimental demonstration of left handedness. The presence of SRRs leads to the negative permeability in a narrow band above resonance. CSRRs can be made by etching the negative image of SRRs in a conducting plane. Hence they are the dual counterpart of the SRRs and exhibit negative permittivity upon their resonance.

Here, we present our researches on the interaction between RMPs and the planar microwave structures, and the coupling between the adjacent RMPs. Some experiments are given to show the methods to control the wave propagation in planar microwave structures with these resonant elements.

**Resolution Ability and Surface Plasmon of a Left-Handed Material Slab:** Subwavelength focusing with LHM slab was first proposed by Prof. Pendry and attracted great attention. Here we study the imaging properties of a LHM slab using a spectrum decomposition method. The solution of the interaction between a line source and a LHM slab is obtained. It's found that, for a slab with appropriate amount of absorption, the surface plasmon (SP) can be excited and the evanescent wave amplification can be realized to some extent. It's also found that the distribution of SP is heavily relevant to the resolution ability of the slab.

# Novel Smart Sensory Composites with Magnetoimpedance Wires for Stress Monitoring at Microwave Frequencies

L. V. Panina<sup>1,2</sup>, D. P. Makhnovskiy<sup>1</sup>, A. P. Zhukov<sup>2</sup>, and J. Gonzalez<sup>2</sup>

<sup>1</sup>School of Computing, Communications and Electronics, University of Plymouth, PL4 8AA, UK

<sup>2</sup>Departamento de Física de Materiales, Facultad de Química  
UPV/EHU, 1072, 20080 San Sebastian, Spain

**Abstract**— Composite materials with sensing capabilities that can provide the information on their current condition constitute an important class of smart materials and are in high demand for structural evaluation and rehabilitation. In particular, the development of sensory materials enabling continuous monitoring of stress and strain is an important aspect of health monitoring of structural components. Recently, optic fibres and piezoelectric ceramic fibres have become preferable stress-sensing elements combining small size, high sensitivity and high frequency response. However, their main drawback is the need of intimate bounding either at external surface or composite laminates limiting the number of sensors that can be deployed. Large-scale applications in civil structures require the development of innovative distributed sensors concepts. This can be achieved by incorporating an additional active phase into the composite matrix during initial build or retrofit. This paper reviews our recent results on *novel sensory composites with embedded magnetoimpedance wires showing large change in electrical impedance or polarisation with respect to mechanical stress at MHz and GHz frequency bands*. The material will benefit from low cost, very high sensitivities at low concentrations, consistency with structural integrity, and remote wireless monitoring of stress with the use of microwave scanning techniques at low energies.

Magnetic wires in composite matrix behave as electric dipoles which experience a resonance at half wave-length condition. They constitute the effective electric polarisation and permittivity which also can have a resonant dispersion within the frequency band easily adjusted by the wire length and the matrix permittivity. The permittivity is lossy and the loss factor may be controlled by the wire magnetoimpedance which can be changed by external stimuli, such as a stress or a dc magnetic field. For high impedance state (magnetisation is along the wire), the dipole resonances are strongly damped and the composite is transparent for electromagnetic field. In opposite case of low impedance (magnetisation is along circumference) the resonance behaviour of the effective permittivity will result in suppressing the wave propagation in this frequency band. The possibility to control the electromagnetic interaction with composite media by changing magnetic properties of the constituent fibres was originally proposed by authors [1, 2] and simultaneously by Acher and co-workers [3]. We have recently proven experimentally [4] a very strong impact of the external magnetic field and stress on the reflection/transmission in tissue composites containing  $\text{Co}_{68}\text{Fe}_4\text{Cr}_3\text{B}_{14}\text{Si}_{11}$  glass coated amorphous wires. For wires with induced helical anisotropy, a change of nearly 10 dB is observed by applying a tensile stress of 0.1 MPa which causes the magnetisation to align along the circumference and, thus, the reduction in the wire impedance.

## REFERENCES

1. Makhnovskiy, D. P. and L. V. Panina, *J. Appl. Phys.*, Vol. 93, 4120, 2003.
2. Panina, L. V., S. I. Sandacci, and D. P. Makhnovskiy, *J. Appl. Phys.*, Vol. 97, 13701, 2004.
3. Reynet, O., A. L. Adent, S. Deprot, O. Acher, and M. Latrach, *Phys. Rev. B*, Vol. 66, 94412, 2002.
4. Makhnovskiy, D. P., L. V. Panina, C. Garcia, A. Zhukov, and J. Gonzalez, *Phys. Rev. B*, Vol. 74, 64205, 2006.



# Nano-phonic Devices and Wave Propagation in Organic Nano-structures

V. A. L. Roy, Stephen C. F. Kui, and Chi-Ming Che

The University of Hong Kong, China

**Abstract**— We have demonstrated that organoplatinum(II) complexes self assemble into nanowires through intermolecular Pt(II)...Pt(II) and ligand  $\pi$ - $\pi$  interactions. These intermolecular interactions direct the cationic Pt(II) molecules to assemble into a linear chain with high crystallinity, with intriguing charge transport and electroluminescent properties. The first ambipolar light emitting transistors with promising mobility and balanced charge transport using organometallic complexes has been fabricated. Moreover, wave propagation on these nano-structures has been discovered and explained in detail using confocal microscopy imaging.

## REFERENCES

1. Hissler, M., J. E. McGarrah, W. B. Connick, D. K. Geiger, S. D. Cummings, and R. Eisenberg, *Coord. Chem. Rev.*, Vol. 208, 115, 2000.
2. McMillin, D. R. and J. J. Moore, *Coord. Chem. Rev.*, Vol. 229, 113, 2002.
3. Lu, W., B. X. Mi, M. C. W. Chan, Z. Hui, C. M. Che, N. Zhu, and S. T. Lee, *J. Chem. Soc.*, Vol. 126, 7639, 2004.
4. Lin, Y. Y., S. C. Chan, M. C. W. Chan, Y. J. Hou, H. Zhu, C. M. Che, Y. Liu, and Y. Wang, *Chem. Eur. J.*, Vol. 9, 1263, 2003.
5. Osborn, R. J. and D. Rogers, *J. Chem. Soc., Dalton Trans.*, 1002, 1974.
6. Connick, W. B., R. E. Marsh, W. P. Schaefer, and H. B. Gray, *Inorg. Chem.*, Vol. 36, 913, 1997.
7. Yam, V. W. W., K. M. C. Wong, and N. Zhu, *J. Am. Chem. Soc.*, Vol. 124, 6506, 2002.



## Session 4P4a

# Semiconductor Homostructures and Heterostructures 2

### Force Constants and Dispersion Relations in GaN

*D. G. Santiago-Perez (Centro Universitario Jose Marti Perez, Cuba); F. De Leon-Perez (Universidad de Zaragoza, Spain); Miguel Eduardo Mora-Ramos (Universidad Autonoma del Estado de Morelos, Mexico); R. Perez-Alvarez (Universidad Autonoma del Estado de Morelos, Mexico);* ..... 860

### Longwave Phonon Tunnelling Using an Impedance Concept

*D. Villegas (Central University Marta Abreu of Las Villas, Cuba); F. De Leon-Perez (Universidad de Zaragoza, Spain); R. Perez-Alvarez (Universidad Autónoma del Estado de Morelos, México);* ..... 861

### Cantor Dielectric Heterostructures Made of Nanostructured Multilayers of Porous Silicon

*V. Agarwal (Universidad Autónoma del Estado de Morelos, México); B. Alvarado-Tenorio (Universidad Autónoma del Estado de Morelos, México); J. Escorcía-García (Universidad Autónoma del Estado de Morelos, México); Luis M. Gaggero-Sager (Universidad Autónoma del Estado de Morelos, México);* .. 862

### Hydrostatic Pressure and Magnetic Field Effects on the Exciton States in Vertically Coupled GaAs-(Ga, Al) As Quantum Dots

*Miguel Eduardo Mora-Ramos (Universidad Autónoma del Estado de Morelos, México); Arezky H. Rodríguez (Universidad Autónoma de la Ciudad de México, México); S. Y. López (Universidad de Antioquia, Colombia); C. A. Duque (Universidad de Antioquia, Colombia);* ..... 863

### Internal Mobility Edge in Doped Graphene: Frustration in a Renormalized Lattice

*Gerardo G. Naumis (Universidad Nacional Autonoma de Mexico (UNAM), Mexico);* ..... 864

## Force Constants and Dispersion Relations in GaN

D. G. Santiago-Pérez<sup>1</sup>, F. de León-Pérez<sup>2</sup>, M. E. Mora-Ramos<sup>3</sup>, and R. Pérez-Álvarez<sup>3</sup>

<sup>1</sup>Centro Universitario José Martí Pérez, Avenida de los Mártires 360, Sancti Spiritus, Cuba

<sup>2</sup>Departamento de Física de la Materia Condensada, Universidad de Zaragoza, E-50009 Zaragoza, Spain

<sup>3</sup>Universidad Autónoma del Estado de Morelos, Ave. Universidad 1001, 62209 Cuernavaca, México

**Abstract**— We have investigated the lattice dynamics of wurtzite phase of bulk group-III nitride using the linear chain models. Along high symmetry directions such as either the [0001] directions, for semiconductors with wurtzite structures, the three-dimensional (3D) equations of motion are decoupled into one longitudinal and two transverse oscillations which can be described by linear chain models. This exact result for the bulk is useful for the study of heterostructures. In fact, for heterostructures grown along high symmetry directions, it is usually assumed that the force constants in each constituent layer are equal to the bulk force constant. In this way the phonon equations of motions are obtained. As group-III nitride are ionic materials we separate the contribution of the macroscopic field, consider a given number of atoms and assume harmonic interaction between a limited number of neighbors for interaction of microscopic character. Then, the dynamical matrix is constructed, taking into account the symmetry of the underlying lattice. Interesting properties of the equations are found in this way. In particular, we check explicitly how the 3D problem reduces to decoupled linear chain equations for high symmetry directions, with the aim of obtaining the relation between the 3D and one-dimensional (1D) force constants. To the best of our knowledge, this relations has not been explored so far. Our study helps to understand better the richness of the linear chain models. We also show how to fit the 3D bulk force constants (and consequently the whole dynamical matrix) from a few points, either experimental or theoretical.

### REFERENCES

1. Narayamurti, V., H. L. Störmer, M. A. Chin, A. C. Gossard, and W. Wiegmann, “Selective transmission of high-frequency phonons by a superlattice: The ‘dielectric’ phonon filter,” *Phys. Rev. Lett.*, Vol. 43, No. 27, 2012–2016, 1979.
2. Tamura, S., “Focusing of high-frequency dispersive phonons,” *Phys. Rev. B*, Vol. 25, No. 2, 1415–1418, 1982.
3. Yao, T., “Thermal properties of AlAs/GaAs superlattices,” *Appl. Phys. Lett.*, Vol. 51, No. 22, 1798–1800, 1987.
4. Hicks, L. D. and M. S. Dresselhaus, “Effect of quantum-well structures on the thermoelectric figure of merit,” *Phys. Rev. B*, Vol. 47, No. 19, 12727–12731, 1993.
5. Hyldgaard, P. and G. D. Mahan, “Phonon superlattice transport,” *Phys. Rev. B*, Vol. 56, No. 17, 10754–10757, 1997.
6. Fasolino, A., E. Molinari, and K. Kunc, “Planar force-constant method for lattice dynamics of structures,” *Phys. Rev. B*, Vol. 41, No. 12, 8302–8312, 1990.
7. Santiago-Pérez, D. G., F. de León-Pérez, and R. Pérez-Álvarez, “Force constants and dispersion relations for the zincblende and diamond structures revisited,” *Rev. Mex Fis.*, Vol. 52, No. 2, 163–171, 2006.
8. Born, M. and K. Huang, *Dynamical Theory of Crystal Lattices*, Oxford, Clarendon Press, 1954.
9. Ashcroft, N. W. and N. D. Mermin, *Solid State Physics*, Saunders College, Philadelphia, 1976.
10. Tütüncü, H. M. and G. B. Srivastava, “Phonons in zinc-blende and wurtzite phases of GaN, AlN, and BN with the adiabatic bond-charge model,” *Phys. Rev. B*, Vol. 62, No. 8, 5028–5035, 2000.

## Longwave Phonon Tunnelling Using an Impedance Concept

D. Villegas<sup>1</sup>, F. de León-Pérez<sup>2</sup>, and R. Pérez-Álvarez<sup>3</sup>

<sup>1</sup>Physics Department, Central University Marta Abreu of Las Villas, Santa Clara, Cuba

<sup>2</sup>Departamento de Física de la Materia Condensada, Universidad de Zaragoza

E-50009 Zaragoza, Spain

<sup>3</sup>Universidad Autónoma del Estado de Morelos

Ave. Universidad 1001, 62209 Cuernavaca, México

**Abstract**— In this paper we study numerically the transmission, reflexion and dwell times of phonon packets propagating through semiconductor multilayer structures. The tunneling of optical and acoustic phonon at normal incidence on multiple layers systems is analyzed. We adopt the continuum model valid for long-wavelength oscillations, i.e., an elasticity approach for acoustical modes and the so called Full Phenomenological Model for the optical ones in which a quasistatic electric field is coupled with mechanical oscillations. The isomorphism between acoustical and optical propagation in heterostructures, and electromagnetic waves in transmission lines, is analyzed. We use an impedance concept similar to the quantum-mechanical one introduced by Khondker and collaborators.

### REFERENCES

1. De León-Pérez, F. and R. Pérez-Álvarez, "Phonon propagation in nonpolar semiconductor heterostructures," *Phys. Rev B*, Vol. 63, 245304, 2001.
2. Villegas, D., F. de León-Pérez, and R. Pérez-Álvarez, "Tunneling time of long-wavelength phonons through semiconductors heterostructures," *Phys. Rev. B*, Vol. 71, 035322, 2005.
3. Khondker, A. N., M. R. Khan, and A. F. M. Anwar, "Transmission line analogy of resonance tunneling phenomena: The generalized impedance concept," *J. Appl. Phys.*, Vol. 63, No. 10, 5191–5193, 1988.
4. Tung, H. T. and C. P. Lee, "An energy band-pass filter using superlattice structures," *IEEE Journal of Quantum Electronics*, Vol. 32, No. 3, 507–512, 1996.
5. Trallero-Giner, C., R. Pérez-Álvarez, and F. García-Moliner, *Long Wave Polar Modes in Semiconductor Heterostructures*, Pergamon/Elsevier Science, London, 1998.
6. Born, M. and K. Huang, *Dynamical Theory of Crystal Lattices*, Clarendon Press, Oxford, 1954.

## Cantor Dielectric Heterostructures Made of Nanostructured Multilayers of Porous Silicon

V. Agarwal<sup>1</sup>, B. Alvarado-Tenorio<sup>1</sup>, J. Escorcia-Garcia<sup>1</sup>, and L. M. Gaggero Sager<sup>2</sup>

<sup>1</sup>Centro de Investigación en Ingeniería y Ciencias Aplicadas, Universidad Autónoma del Estado de Morelos  
Av. Universidad 1001, Col. Chamilpa, CP 62209, Cuernavaca, Morelos, México

<sup>2</sup>Facultad de Ciencias, Universidad Autónoma del Estado de Morelos  
Av. Universidad 1001, Col. Chamilpa, CP 62209, Cuernavaca, Morelos, Mexico

**Abstract**— The fabrication and the optical properties of the one dimensional Cantor porous silicon-based photonic heterostructures are investigated [1]. Cantor multilayer heterostructures were fabricated by the porous silicon layers having the refractive indices of 1.9 (A) and 1.45 (B) for the low and high porosity respectively [2, 3]. Different generations of Cantor structure were generated taking the total physical thickness of the structure as 9000 nm. Hence in the second generation had three layers (ABA) with the thicknesses of 3000 nm each. For making the Cantor heterostructures up to 7th generation, the thicknesses of the layers was varied from 3000 nm to 12 nm. In the reflectance spectra of the Cantor structure of 5th (31) and 6th order (63 layers), major photonic band gaps are observed in the visible region. On the contrary, the reflectance spectra of the 7th generation shows the presence of equidistant fringes between 500–700 nm with no photonic bandgap in the visible region.

### REFERENCES

1. Gaggero-Sager, L. M., E. R. Pujals, and O. Sotolongo, “Self-similarity in a Cantor like semiconductor quantum well,” *Physica Status Solidi (b)*, Vol. 220, 167, 2000.
2. Agarwal, V. and M. E. Mora-Ramos, “Optical characterization of poly-type Fibonacci and Thue-Morse quasiregular dielectric structures made of porous silicon,” *Journal of Physics D: Applied Physics*, Vol. 40, 3203–3211, 2007.
3. Becerra, D. and V. Agarwal, “Fabrication of UV filters from porous silicon at low temperatures,” *Physica Status Solidi (c)*, Vol. 4, No. 6, 1956–1960, 2007.

## Hydrostatic Pressure and Magnetic Field Effects on the Exciton States in Vertically Coupled GaAs-(Ga, Al) As Quantum Dots

M. E. Mora-Ramos<sup>1</sup>, A. H. Rodríguez<sup>2</sup>, S. Y. López<sup>3</sup>, and C. A. Duque<sup>4,5</sup>

<sup>1</sup>Universidad Autónoma del Estado de Morelos, Ave. Universidad 1001, 62209 Cuernavaca, México

<sup>2</sup>Universidad Autónoma de la Ciudad de México, Plantel Iztapalapa, México DF, México

<sup>3</sup>Facultad de Educación, Universidad de Antioquia, AA 1226, Medellín, Colombia

<sup>4</sup>Instituto de Física, Universidad de Antioquia, AA 1226, Medellín, Colombia

<sup>5</sup>Instituto de Física, Unicamp, CP 6165, Campinas-SP, 13083-970, Brazil

**Abstract**— The variational procedure, in the effective-mass and parabolic-band approximations, is used in order to investigate the combined effects of hydrostatic pressure and in-plane-direction-applied magnetic field on the exciton states in vertically coupled GaAs-(Ga,Al)As quantum dots. Calculations are performed for two cylindrical-shape quantum dots. The exciton envelope wave function is obtained through a variational procedure using a hydrogenic 1 *s*-like wave function and an expansion in a complete set of trigonometric functions for the electron and hole wave functions. The anticrossing effects on the dispersion with applied magnetic field and hydrostatic pressure of the photoluminescence peaks associated with direct and indirect excitons are studied as well. Calculated results are compared with available experimental and theoretical findings.

## Internal Mobility Edge in Doped Graphene: Frustration in a Renormalized Lattice

Gerardo G. Naumis

Departamento de Física-Química, Instituto de Física  
Universidad Nacional Autónoma de México (UNAM)  
Apartado Postal 20-364, México DF 01000, Mexico

**Abstract**— We show that an internal localization mobility edge can appear around the Fermi energy in graphene by introducing impurities in the split-band regimen, or by producing vacancies in the lattice. The edge appears at the center of the spectrum and not at the band edges, in contrast with the usual picture of localization. Such result is explained by showing that the bipartite nature of lattice allows to renormalize the Hamiltonian, and the internal edge appears because of frustration effects in the renormalized lattice. The size in energy of the spectral region with localized states is similar in value to that observed in narrow gap semiconductors.



# Session 4P4b

## Nano-Semiconductors and Devices

<b>Electronic States of Strained Semiconductor Nano-wires</b>	
<i>Zhixun Ma (Lawrence Berkeley National Laboratory, US); Todd Holden (CUNY, USA); Zhiming M. Wang (University of Arkansas, USA); Gregory J. Salamo (University of Arkansas, USA); Samuel S. Mao (Lawrence Berkeley National Laboratory, USA);</i>	866
<b>Small Nano-dot Incorporated High-efficiency Phosphorescent Blue Organic Light-emitting Diode</b>	
<i>Jwo-Huei Jou (National Tsing Hua University, Taiwan, China); Wei-Ben Wang (National Tsing Hua University, Taiwan, China); Mao-Feng Hsu (National Tsing Hua University, Taiwan, China); Chi-Ping Liu (National Tsing Hua University, Taiwan, China); Cheng-Chung Chen (National Tsing Hua University, Taiwan, China); Chun-Jan Wang (National Tsing Hua University, Taiwan, China); Yung-Cheng Tsai (National Tsing Hua University, Taiwan, China); Yung-Cheng Tsai (National Tsing Hua University, Taiwan, China); Jing-Jong Shyue (Research Center for Applied Sciences Academia Sinica, Taiwan); Sung-Cheng Hu (Chung-shan Institute of Science and Technology, China); Chung-Che Chiang (National Chi Nan University, Taiwan); He Wang (Tsinghua University, China);</i>	867
<b>Structure and Optical Properties of Pb<sub>8</sub>S<sub>8</sub></b>	
<i>Shenglan Xu (Donghua University, China); Huaizhong Xing (Donghua University, China); Zongling Ding (Donghua University, China); Xiaoshuang Chen (Shanghai Institute for Technical Physics, Chinese Academy of Sciences, China);</i>	868
<b>Coherent Transient Terahertz Radiation from Photoexcited Semiconductor Supperlattices</b>	
<i>T. Y. Zhang (Xi'an Institute of Optics and Precise Mechanics, Chinese Academy of Science, China); W. Zhao (Xi'an Institute of Optics and Precise Mechanics, Chinese Academy of Science, China);</i>	869
<b>A Contradictory Spectral Phenomenon with Quantum Confinement Effect in ZnO Nano-particles</b>	
<i>Shu-Lin Zhang (Peking University, China); J. Z. Jiang (Zhejiang University, China);</i>	870

## Electronic States of Strained Semiconductor Nano-wires

Zhixun Ma<sup>1</sup>, Todd Holden<sup>2</sup>, Zhiming M. Wang<sup>3</sup>  
Gregory J. Salamo<sup>3</sup>, and Samuel S. Mao<sup>1</sup>

<sup>1</sup>Lawrence Berkeley National Laboratory, Berkeley, CA 94720, USA

<sup>2</sup>Department of Physics, Queensborough Community College of the City University of New York  
Bayside, NY 11364, USA

<sup>3</sup>Department of Physics, University of Arkansas, Fayetteville, Arkansas 72701, USA

**Abstract**— Similar to quantum dot structure, vertically stacked quantum wire structures can be formed by the penetrated strain, while the strain distribution reveals an anisotropic nature, that is, the strain is released to some extent in the direction perpendicular to the wires but remains along the wires, leading to the formation of triaxial strain in wires. The strain-induced effects, such as change of band gap, state splitting of heavy hole and light hole, have been extensively studied experimentally and theoretically in the well material, but have not been well understood in the strained barrier layers. In this paper, we report our experimental observations and theoretical calculations of band-gap shrinkage and the hh-lh splitting of the GaAs barrier in layered InGaAs/GaAs (001) quantum wires and quantum dot chains oriented along  $[-110]$ . It has been found that the anisotropic strain relaxation across the wires has a strong effect on the hh-lh splitting but little on band gap in quantum wires. The PZ electric field has been estimated to be on an order of  $10^5$  V/cm in barriers while one order of magnitude less within wires. These studies are beneficial to strain engineering for quantum-wire-based optoelectronic devices such as quantum-wire-based infrared detectors.

## Small Nano-dot Incorporated High-efficiency Phosphorescent Blue Organic Light-emitting Diode

Jwo-Huei Jou<sup>1</sup>, Wei-Ben Wang<sup>1</sup>, Mao-Feng Hsu<sup>1</sup>, Chi-Ping Liu<sup>1</sup>, Cheng-Chung Chen<sup>1</sup>,  
Chun-Jan Wang<sup>1</sup>, Yung-Cheng Tsai<sup>1</sup>, Jing-Jong Shyue<sup>2</sup>, Sung-Cheng Hu<sup>3</sup>,  
Chung-Che Chiang<sup>4</sup>, and He Wang<sup>5</sup>

<sup>1</sup>Department of Materials Science and Engineering, National Tsing Hua University  
Hsin-Chu, Taiwan 30013, China

<sup>2</sup>Research Center for Applied Sciences Academia Sinica  
128 Academia Rd., Sec. 2 Nankang, Taipei 115, Taiwan, China

<sup>3</sup>Chung-shan Institute of Science and Technology, Armament Bureau, M. N. D.  
No. 481, Sec. Chia An, Zhongzheng Rd., Longtan Shiang, Taoyuan County 325, China

<sup>4</sup>Department of Applied Chemistry, National Chi Nan University  
Nantou Hsien, Taiwan 545, China

<sup>5</sup>Department of Materials Science and Engineering, Tsinghua University  
Beijing 100084, China

**Abstract**— High efficiency phosphorescent blue organic light-emitting diode (OLED) was obtained by incorporating small amino or hydroxyl functional group-modified polymeric nano-dot (APND or HPND) in the hole transporting layer (HTL), poly (ethylenedioxythiophene): poly (styrene sulfonic acid) (PEDOT:PSS). The device comprised a 1250 Å anode layer of indium tin oxide, a 350 Å HTL of PEDOT:PSS doped with APND or HPND, a 400 Å blue emissive layer composed of a molecular host of 4,4'-bis (carbazol-9-yl) biphenyl doped with 14 wt% blue dye of bis (3,5-difluoro-2-(2-pyridyl)-phenyl-(2-carboxypyridyl) iridium (III), a 320 Å electron-transporting layer of 2, 2', 2''-(1,3,5-benzenetriyl)-tris (1-phenyl-1-H-benzimidazole), a 7 Å electron-injection layer of lithium fluoride and a 1500 Å cathode layer of aluminum. The resultant power efficiency at 100 cd/m<sup>2</sup>, for example, was increased from 10.3 to 21.0 lm/W, an increase of 203%, as 7 wt% APND of 8 nm in size was added. By employing 7 wt% HPND, the power-efficiency was 17.5 lm/W. The resultant luminance markedly increased with the incorporation the nano-dots until the doping concentration was above 7 wt%. Whilst, the resultant current density continuously decreased as these two nano-dot concentrations increased. These results indicate that the marked efficiency improvement may be attributed to a better balance of carrier-injection resulted from the hole-blocking-function possessed APND and the hole-trapping-function possessed HPND, which respectively exhibited positive and negative charge on the surface. Moreover, the chromaticity coordinate at 100 cd/m<sup>2</sup>, for example, was (0.19, 0.34), barely changed in the presence of the nano-dots. Importantly, since the nano-dot was not employed in the emissive layer, the same concept may be applied to fluorescent type OLEDs.

## Structure and Optical Properties of $\text{Pb}_8\text{S}_8$

Shenglan Xu<sup>1</sup>, Huaizhong Xing<sup>1</sup>, Zongling Ding<sup>1</sup>, and Xiaoshuang Chen<sup>2</sup>

<sup>1</sup>Department of Applied Physics, Donghua University

Ren Min Road 2999, Songjiang District, Shanghai 201620, China

<sup>2</sup>National Lab. Of Infrared Physics, Shanghai Institute for Technical Physics

Chinese Academy of Sciences, Yu Tian Road 500, Shanghai 200083, China

**Abstract**— Based on gradient-corrected density functional theory and genetic global optimization approach that directly searches for the configuration of  $\text{Pb}_8\text{S}_8$  cluster, three possibly structural isomers are found. After several initial geometric configurations are relaxed, the global minimum of  $\text{Pb}_8\text{S}_8$  cluster with a four-faced polyhedron is found. Its each face is built of a  $\text{Pb}_2\text{S}_2$  and  $\text{Pb}_3\text{S}_3$  ring which are rotated in order to build the next face and six rombi and four hexagons are found in this structure. The configuration of the metastable may be viewed as being built of two parallel  $\text{Pb}_4\text{S}_4$  rings linked together by  $\text{Pb}_2\text{S}_2$  rings. The third isomer is a distorted non-planar ring. The density of states calculations display the behavior of  $\text{Pb}_8\text{S}_8$  cluster close to the bluck behavior of PbS. The calculated vibrational spectrum implies that the optimized geometry is located at the minimum point of the potential surface. The strong peaks of IR absorption are primary distributing the range from  $200\text{ cm}^{-1}$  to  $270\text{ cm}^{-1}$ .

## Coherent Transient Terahertz Radiation from Photoexcited Semiconductor Supperlattices

T. Y. Zhang and W. Zhao

State Key Laboratory of Transient Optics and Photonics  
Xi'an Institute of Optics and Precise Mechanics, Chinese Academy of Science  
17 Xixi Road, 710119 Xi'an, China

**Abstract**— Coherent transient terahertz electromagnetic radiation induced by homogeneous electric field from semiconductor superlattices is analyzed. The analysis is based on the extended semiconductor Bloch equations, which include the applied electric field, in addition to the many-body effects of Coulomb interaction in the time-dependent Hartree-Fock approximation. The influence of the Coulomb interaction on the Bloch oscillations and the Wannier-Stark-ladder is investigated.

# A Contradictory Spectral Phenomenon with Quantum Confinement Effect in ZnO Nano-particles

Shu-Lin Zhang<sup>1</sup> and J. Z. Jiang<sup>2</sup>

<sup>1</sup>School of Physics, Peking University, China

<sup>2</sup>Department of Materials Science and Engineering, Zhejiang University, China

**Abstract**— The quantum confinement effect (QCE) is the one of universal and basic effects of nano-materials and the technological applied base of nano-semiconductors, which has been conformed by theoretical and experimental researches including spectroscopic methods solidly.

Recently, our spectroscopic studies on the ZnO nano-particles (NPs) found that the QCE is shown in the photoluminescence (PL) spectra and not in the Raman spectra.

From the TEM measurements, the sizes of ZnO NPs,  $\bar{R} \pm \Delta R$ , are estimated to be  $5.7 \pm 0.6$ ,  $7.5 \pm 0.9$ ,  $18.2 \pm 1.7$ ,  $27.4 \pm 1.84$  for samples Z1, Z2, Z3 and Z4, respectively, in which  $\bar{R}$  is the average sizes and the  $\Delta R$  is deviation from  $\bar{R}$ . The above results indicates that the  $\Delta R$  is around 10% or less for all samples and the used samples are of nearly uniform sizes.

It was observed that the peak energies of photoluminescence (PL) spectra were changed with sample sizes. It indicated that the QCE exists in the electronic structures. But we found for the same group of ZnO samples used in the PL measurement that the peak energies of Raman spectra were not changed with sample sizes in single- and multiple-phonon Raman spectra. This means that the Raman peak energy is independent of the sample size.

The above results exhibit an interesting phenomenon that in the same group of ZnO NP samples with nearly uniform sizes, QCE exists in PL but not in Raman scattering. The origin of this novel phenomenon and its significance for device applications were discussed.

# Session 4P5a

## Applied Inverse Problems

<p>Determination of Electron Spectra in Solar Flares through Regularized Inversion of Observed X-ray Spectra</p> <p><i>Gordon Emslie (Oklahoma State University, USA);</i> .....</p> <p>Linear Sampling Method: Physical Interpretation and Guidelines for a Successful Application</p> <p><i>Ilaria Catapano (Institute for Electromagnetic Sensing of Environment, National Research Council, Italy); Lorenzo Crocco (National Research Council, Italy); Tommaso Isernia (Mediterranea University of Reggio Calabria, Italy);</i> .....</p> <p>Properties of Regularization Operators in Learning Theory</p> <p><i>Andrea Caponnetto (City University of Hong Kong, China);</i> .....</p> <p>Parametrical Imaging in Solar Astronomy Using Visibilities</p> <p><i>Michele Piana (Universita di Verona, Italy); Anna Maria Massone (CNR-INFN, Italy); A. G. Emslie (Universita di Verona, Italy); G. J. Hurford (Universita di Verona, Italy); E. P. Kontar (Universita di Verona, Italy); M. Prato (Universita di Verona, Italy); R. A. Schwartz (Universita di Verona, Italy);</i></p> <p>A SVM-based Three-dimensional Multi-resolution Approach for Biomedical Inverse Scattering Problems</p> <p><i>Federico Viani (University of Trento, Italy); Massimo Donelli (University of Trento, Italy); Paolo Rocca (University of Trento, Italy); Andrea Massa (University of Trento, Italy);</i> .....</p>	<p>872</p> <p>873</p> <p>874</p> <p>875</p> <p>876</p>
---	--

## Determination of Electron Spectra in Solar Flares through Regularized Inversion of Observed X-ray Spectra

Gordon Emslie

Oklahoma State University, USA

**Abstract**— X-ray radiation from a solar flare provides prompt and direct information on the accelerated electron population in the flare. Because the solar atmosphere is largely transparent to X-rays, the relation between the accelerated electron flux  $F(E)$  and the emergent X-ray spectrum  $I(\epsilon)$  is a simple integral equation:

$$I(\epsilon) \propto \int_E F(E) Q(\epsilon, E) dE$$

where  $Q(\epsilon, E)$  is the *cross-section* for production of a photon of energy  $\epsilon$  by an electron of energy  $E$ , in general a complicated function of  $\epsilon, E$  and possibly other variables, such as the polarization state of the emitted photon and the angle between the emitting electron velocity vector and the direction to the observer.

Using Tikhonov regularization techniques, we have used X-ray observations from the NASA Ramaty High Energy Solar Spectroscopic Imager (RHESSI) mission to reconstruct electron energy spectra for the flare. Further, through the application of spatial Fourier transform (“visibility”) techniques, we have also determined the variation of the electron spectrum throughout the flare region. By construction, these spectra, both spatially-integrated and imaged, behave smoothly with  $E$  and are so suitable for further analysis of the mechanisms responsible for electron acceleration and propagation.



# Linear Sampling Method: Physical Interpretation and Guidelines for a Successful Application

Ilaria Catapano<sup>1</sup>, Lorenzo Crocco<sup>1</sup>, and Tommaso Isernia<sup>2</sup>

<sup>1</sup>National Research Council - Institute for Electromagnetic Sensing of Environment, CNR-IREA  
Naples, Italy

<sup>2</sup>Mediterranea University of Reggio Calabria, Reggio Calabria, Italy

**Abstract**— The use of electromagnetic waves to characterize inaccessible targets is a basic problem in the inverse scattering theory, which receives a huge interest in all those applications wherein a non invasive diagnostics is required. In this framework, efficient strategies aiming at reconstructing the shape of unknown objects from the measured scattered field are worth to be considered. As a matter of fact, they not only provide a satisfactory information in several contexts such as diagnostic of cracks and detection of voids or utilities, but they also offer a useful a priori information when the permittivity and conductivity profiles of the investigated region have to be retrieved.

The shape reconstruction problem can be efficiently addressed by means of the Linear Sampling Method (LSM), which allows one to get the geometrical features of metallic as well as dielectric objects by simply observing the behavior of a function, which is bounded inside the scatterers and unbounded elsewhere. Such a function, which is obtained by solving in a regularized fashion an auxiliary (ill-posed) linear problem, it is thus referred to as support indicator. Notably, LSM has a straightforward implementation and requires an almost negligible computational burden even in the case of large scale 3D problems. As a matter of fact, it only entails simple matrix operations and involves a matrix whose size is determined by the amount of available data.

Notwithstanding the remarkable above mentioned features, LSM seems to be largely neglected outside of the mathematical community, where it was originally proposed. As this is possibly due to the (apparent) lack of “physical” meaning behind the mathematical theory, our effort has been that of providing a physical interpretation of LSM for the case of dielectric objects. In particular, by showing the relationship between LSM and the electromagnetic problem of focusing into a point the current induced by a collection of sources, we can review and explain from a different perspective merits and limitations of the LSM. In particular, concerning the key role played by the number of illuminations and measurements which is exploited, we provide some guidelines for a successful application of LSM. Examples with experimental data from the “Marseille” data-set confirm the proposed physical interpretation, allow us to validate the introduced guidelines and stress the reconstruction capabilities of LSM against non-convex scatterers.

# Properties of Regularization Operators in Learning Theory

Andrea Caponnetto

City University of Hong Kong, China

**Abstract**— We discuss the properties of a large class of learning algorithms defined in terms of classical regularization operators for ill-posed problems. Popular algorithms from this class, such as Regularized Least-Squares (RLS) and Landweber Algorithm were studied in [1] and [2]. In particular, in [1], a minimax analysis was performed, and it was showed that RLS attains optimal rates of convergence over a suitable family of priors. We describe similar optimality results for general regularization operators in the supervised setting of learning theory. We show that suitable data-dependent criteria for the choice of the regularization parameter enforce adaptation over the considered family of priors.

## REFERENCES

1. Caponnetto, A. and E. de Vito, “Optimal rates for regularized least-squares algorithm,” *Foundations of Computational Mathematics*, 2006.
2. Yao, Y., L. Rosasco, and A. Caponnetto, “On early stopping in gradient descent learning,” *Constructive Approximation*, 2007.

## Parametrical Imaging in Solar Astronomy Using Visibilities

M. Piana<sup>1</sup>, A. M. Massone<sup>2</sup>, A. G. Emslie<sup>1</sup>  
G. J. Hurford<sup>1</sup>, E. P. Kontar<sup>1</sup>, M. Prato<sup>1</sup>, and R. A. Schwartz<sup>1</sup>

<sup>1</sup>Universita di Verona, Italy

<sup>2</sup>CNR-INFN, Italy

**Abstract**— Visibilities are calibrated measurements of sampled Fourier components of a source distribution. In astronomical imaging they are provided, for instance, by rotation modulation collimators in X-ray imaging or by pairs of antennas in a radio interferometer. Here we present a novel technique which allows the imaging of important physical parameters in the source from the analysis of measured visibilities. This method is based on the application of a regularization approach in the spatial frequency domain. We show its effectiveness in an application to X-ray solar imaging spectroscopy with real visibilities measured by the Reuven Ramaty High Energy Solar Spectroscopy Imager (RHESSI).

# A SVM-based Three-dimensional Multi-resolution Approach for Biomedical Inverse Scattering Problems

F. Viani, M. Donelli, P. Rocca, and A. Massa

ELEDIA Research Group at DIT, University of Trento, Via Sommarive 14, I-38050 Trento, Italy

**Abstract**— In the last few years, microwave imaging techniques have been successfully used to provide the spatial distribution of tissues. In particular, because of the significant contrast of the dielectric properties between the normal tissue and the malignant tissue at microwave frequencies, microwave methods seem to be very promising diagnosis methods for the early cancer detection [1]. The cancer detection problem can be reformulated in terms of an inverse scattering one where the problem unknowns (i.e., the presence, the position, its dimensions, and the characteristics of the malignant region) are obtained starting from the measurement of the electromagnetic interactions between the biological specimen under investigation and a probing electromagnetic source. However, although inverse scattering methods are very promising, unfortunately their practical application is strongly limited by the need of 3D reconstructions, high spatial resolutions, and fast processing. An alternative to use inverse scattering techniques lies in considering learning by example techniques. In such a case, the detection problem is reformulated into a classification one, where the data (i.e., the measures of the scattered field collected in an external spatial region called observation domain) and the unknowns (i.e., the geometrical and dielectric characteristics of the malignant tissue) are related by means of a transfer function estimated through an off-line procedure called training phase. The approaches based on neural networks (NN) [2] and support vector machine (SVM) have been satisfactorily applied in various and complex electromagnetic problems. In this paper, an integrated strategy based on a SVM classifier and on an iterative multi-zooming procedure is proposed. After the training procedure, which can be performed once and off-line, the geometrical and dielectric characteristics of the malignant region are estimated in real time and with a limited amount of computational resources. In particular, a succession of approximations of a probability map of the presence of malignant tissue is determined starting from the same training set. At each step, the spatial resolution is increased in a limited set of spatial regions (called “regions of interest”, ROIs) defined at the previous zooming step and characterized by a greater value (with respect to the remaining part of the investigation domain) of the occurrence probability of a malignant tissue. The multi-step procedure is stopped when a detailed spatial reconstruction is reached in the ROIs. Because of the favorable trade-off among computational complexity and spatial resolution, the proposed method seems to be suitable for real time detection of cancer regions. Therefore, to preliminary assess the effectiveness and the potentialities of method, a large number of numerical experiments has been performed and a representative set of results concerning different kind of pathologies both in noiseless and noisy conditions is reported and discussed.

## REFERENCES

1. Xie, Y., B. Guo, L. Xu, J. Li, and P. Stoica, “Multistatic adaptive microwave imaging for early breast cancer detection,” *IEEE Transactions on Biomedical Engineering*, Vol. 53, No. 8, 1647–1657, Aug. 2006.
2. Rekanos, I. T., “Neural-network-based inverse-scattering technique for online microwave medical imaging,” *IEEE Trans. on Magnetics*, Vol. 38, No. 2, 1061–1064, Mar. 2001.

# Session 4P5b

## Remote Sensing of the Earth, Ocean, Atmosphere and Land/Monitoring the earth

<a href="#">Soil Moisture Estimation and Validation Using WindSat Observations</a>	
<i>Jingyang Du (USDA ARS Hydrology and Remote Sensing Lab, USA); Thomas J. Jackson (USDA ARS Hydrology and Remote Sensing Lab, USA); M. H. Cosh (USDA Agricultural Research Service Hydrology and Remote Sensing Lab, USA); Li Li (Naval Research Lab, USA); .....</i>	
	878
<a href="#">Soil Dielectric Model Accounting for Contribution of Bound Water Spectra through Clay Content</a>	
<i>V. L. Mironov (Kirensky Institute of Physics, Siberian Branch, Russian Academy of Sciences, Russia); L. G. Kosolapova (Kirensky Institute of Physics, Siberian Branch, Russian Academy of Sciences, Russia); S. V. Fomin (Kirensky Institute of Physics, Siberian Branch, Russian Academy of Sciences, Russia); .</i>	
	879
<a href="#">Operational Soil Moisture and Ocean Salinity Mission</a>	
<i>Manuel Martin-Neira (European Space Agency, ESTEC, The Netherlands); .....</i>	
	880
<a href="#">Monitoring of Satellite Thermal Patch Formed by A Wave Facet Ocean Surface Water Waves</a>	
<i>S. Nakamura (Kyoto University, Japan); .....</i>	
	881
<a href="#">Monitoring of Satellite Thermal Patch on the Ocean Surface Generated by Strong Wind Duration in Mid-night</a>	
<i>S. Nakamura (Kyoto University, Japan); .....</i>	
	882

## Soil Moisture Estimation and Validation Using WindSat Observations

Jinyang Du<sup>1,2</sup>, Thomas J. Jackson<sup>1</sup>, Rajat Bindlish<sup>1</sup>, M. H. Cosh<sup>1</sup>, and Li Li<sup>3</sup>

<sup>1</sup>USDA ARS Hydrology and Remote Sensing Lab, Beltsville, MD 20705, USA

<sup>2</sup>Institute of Remote Sensing Applications, CAS, Beijing 100101, China

<sup>3</sup>Naval Research Lab, Washington, DC, USA

**Abstract**— An accurate estimate of soil moisture is highly desirable in the study of global water and energy cycles as well as the carbon cycle. Microwave remote sensing is the most feasible technique for large-scale soil moisture monitoring and mapping. Only a few satellite sensor systems have been available that have the potential to implement this approach. WindSat is a spaceborne multi-frequency polarimetric microwave radiometer operating at 6.8, 10.7, 18.7, 23.8 and 37.0 GHz. WindSat is in a sun synchronous polar orbit with an ascending node at 6:00 PM. It is designed to demonstrate the use of passive microwave polarimetry in measuring ocean surface wind speed and direction. However, there is a growing interest in using WindSat observations for retrieving land variables. Low frequencies are preferable for soil moisture retrieval since perturbing factors such as vegetation are less significant. However, the presence of Radio Frequency Interference (RFI) has made C-band observations unsuitable for land applications. In this study, the single channel algorithm is applied to X-band WindSat data to estimate global soil moisture. Comprehensive validation was performed by comparing the retrievals with in situ soil moisture observations from networks at four carefully designed satellite soil moisture validation sites. The four sites have very different climate and vegetation conditions. The overall standard error of estimates of soil moisture for the four sites was  $0.038 \text{ m}^3/\text{m}^3$ . Analysis showed that WindSat soil moisture retrievals for all four validation sites for both ascending and descending orbits were reasonable and within acceptable error bounds. Global soil moisture maps were also generated and showed a spatial distribution of soil moisture that was consistent with the known global climatology. This is the first attempt at estimating global soil moisture from WindSat observations. With their different overpass time and spatial coverage, WindSat, AMSR-E and future Chinese FY-3 will be complementary in achieving global soil moisture monitoring and mapping.

## Soil Dielectric Model Accounting for Contribution of Bound Water Spectra through Clay Content

V. L. Mironov, L. G. Kosolapova, and S. V. Fomin  
Kirensky Institute of Physics SB RAS, Russia

**Abstract**— In this paper, there was studied correlation of dielectric predictions for moist soils with the dielectric constant and loss factor measured, regarding the well known and prevalent in common usage semiempirical mixing dielectric model (SMDM) proposed by M. C. Dobson et al. [1], on the one hand, and recently developed generalized refractive mixing dielectric model (GRMDM) proposed by V. L. Mironov et al. [2], on the other hand. The latter explicitly takes into account a bound water impact on the permittivity of moist soils, thus providing for predictions to be on the same order as the errors of dielectric measurements themselves. The analysis is based on the measured dielectric data borrowed from the Technical Report EL-95-34, December 1995 by J. O. Curtis et al. [3], in which an ansamblage of soils measured included all of grain-size distributions that are observed in nature, with measurements being performed over the frequency range from 45 MHz to 26.5 GHz at the moistures spanning from the neary dry samples to ones saturated close to total moisture capacity. The equations for both the SMDM and GRMDM are presented to make clear a conceptual difference between the two models. Using the granulometric mineralogy data available in the Technical Report EL-95-34, dielectric spectra predictions both for the dielectric constant and loss factor were calculated with the use of the SMDM, and correlation anlysis, regarding their values mesured and predicted. was carried out. Simultaneously, based on the dielectric data of the Technical Report EL-95-34, the spectroscopic parameters of the GRMDM developed by Mironov et al. were derived, and dielectric predictions, obtained with the use of those, correlated to the measured dielectric constants and loss facors. The SMDM was found to provide for good dielectric predictions in the case of the typological soils it was based on, failing to make predictions with good accuracy for the soils studied in the Technical Report EL-95-34, which fall beyond the scope of soils measured by Dobson et al. While the GRMDM appeared to ensure good dielectric prediction for the soils both studied in the Technical Report EL-95-34 and measured by M. C. Dobson et al. To bring the GRMDM into the same state of convenience for the users, in which only soil granulometric mineralogy parameters are needed to make dielectric predictions, the spectroscopic parameters of the GRMDM were linked to the clay content in the soil types considered. As a result, a new type of dielectric model was developed, named the mineralogy based soil dielectric model (MBSDM). The accuracy of dielectric predictions using the MBSDM was found to be the same as that for the GRMDM. This result was achieved due to employing a clear physical hypothesis about dependence of soil water spectroscopic parameters on the soil mineralogy, which were previously introdused and well substantiated by V. L. Mironov et al.

### REFERENCES

1. Dobson, M. C., F. T. Ulaby, M. T. Hallikainen, and M. A. El-Rayes, "Microwave dielectric behavior of wet soil-Part II: Dielectric Mixing Models," *IEEE Trans. Geosci. Remote Sensing*, Vol. 23, No. 1, 35–46, 1985.
2. Mironov, V. L., M. C. Dobson, V. H. Kaupp, S. A. Komarov, and V. N. Kleshchenko, "Generalized refractive mixing dielectric model for moist soils," *IEEE Trans. Geosci. Remote Sensing*, Vol. 42, No. 4, 773–785, 2004.
3. Curtis, J. O., C. A. Weiss, Jr., and J. B. Everett, "Effect of soil composition on dielectric properties," Technical Report EL-95-34, December 1995.

## Operational Soil Moisture and Ocean Salinity Mission

M. Martin-Neira

European Space Agency, ESTEC, Keplerlaan 1, 2200-AG Noordwijk, The Netherlands

**Abstract**— SMOS is ESA's second Earth Explorer mission with the objective of producing global maps of Soil Moisture and Ocean Salinity over the Earth. Launch date is expected at the end of 2008. The only instrument on board SMOS is an L-band Microwave Imaging Radiometer with Aperture Synthesis (MIRAS). The life time of SMOS is 3 years although its consumables have been sized for 5 years.

Once launched, SMOS data will be used, amongst others, by the European Centre for Medium range Weather Forecasting (ECMWF) to assess their impact in weather predictions. Other scientific groups involved in a variety of applications, covering land desertification, agriculture production, floods, ocean circulation, long term climate prediction and global warming, will also extract as much information as possible from SMOS data.

In preparation for a possible operational follow-on mission that would ensure users with a continuity of SMOS products, the European Space Agency has started a system study of SMOSops (SMOS-Operational Mission). The main objective of this mission, driven by scientists request, is the improvement of the accuracy of the SMOS products. For this goal, the new MIRAS-2 instrument will have more sensitive receivers and possibly an additional X-band interferometer from CSSAR (China) is intended to be embarked, as well as a GNSS reflectometry experiment for sea surface roughness corrections.



## Monitoring of Satellite Thermal Patch Formed by A Wave Facet Ocean Surface Water Waves

**S. Nakamura**  
Kyoto University, Japan

**Abstract**— In a case of monitoring a satellite thermal patch, frequently found a wave facets on the sea surface. Assuming a concave facet of a part of the sea surface waves, a simple model is introduced in order to realize that the facet acts an infrared beam out of the ocean surface as a black body. Supporting satellite thermal patterns has been obtained by a direct receiving of the satellite signals. A note is given in relation to special spectrum of the sea surface waves.

## Monitoring of Satellite Thermal Patch on the Ocean Surface Generated by Strong Wind Duration in Mid-night

S. Nakamura  
Kyoto University, Japan

**Abstract**— This work concerns monitoring thermal plateau on the ocean surface generated by a strong wind duration in mid-night time of a cold season. This problem was raised first at a satellite thermal monitoring of a data set directly received signals at the satellite passing time just above the station of a system for receiving the satellite signal directly. There has been introduced a physical model for our understanding of a thermal high in a part of the reduced thermal pattern. The author has considered to introduce an application of Stefan-Boltzmann's criteria for a reasonable model with a radiation of an infrared beam out of the earth's surface.

# Session 4P6a

## Design and Applications of UWB Antennas

<p><b>CPW-fed Bow-tie Slot Antenna for the Application of UWB Antenna Array</b>  <i>Dua-Chyrh Chang (Oriental Institute of Technology, Taiwan); Bing-Hao Zeng (Yuan Ze University, Taiwan); Ji-Chyun Liu (Ching Yun University, Taiwan);</i> .....</p> <p><b>Study of a Circular Disc Monopole Ultrawide-band Miniature Antenna</b>  <i>Lingling Zhong (Harbin Institute of Technology, China); Bo Sun (Harbin Institute of Technology, China); Jinghui Qiu (Harbin Institute of Technology, China); Ning Zhang (Harbin Institute of Technology, China);</i> .....</p> <p><b>Feasibility Studies of Transversely Electromagnetic Coupled Microstrip Based Array Using Various Feeding Structures</b>  <i>Ka-Sing Lim (Multimedia University, Malaysia); Lei-Teen Teo (Multimedia University, Malaysia);</i> .</p> <p><b>A Study on a Printed Planar Crescent-like Antipodal Antenna</b>  <i>Yao-Chiang Kan (Yuan Ze University, Taiwan, R.O.C.); Li-Hsiang Chin (Ming Chuan University, Taiwan, R.O.C.); Chien-Hsun Chen (Ming Chuan University, Taiwan, R.O.C.); Huey-Ru Chuang (National Cheng Kung University, Taiwan, R.O.C.);</i> .....</p> <p><b>Wideband Cavity Backed Spiral Antenna for Dual Mode Operation</b>  <i>Hongli Wang (Tongji University, China); Min Zhang (Tongji University, China);</i> .....</p>	<p>884</p> <p>886</p> <p>887</p> <p>889</p> <p>890</p>
--	--

## CPW-fed Bow-tie Slot Antenna for the Application of UWB Antenna Array

Dua-Chyrh Chang<sup>1,2</sup>, Bing-Hao Zeng<sup>2</sup>, and Ji-Chyun Liu<sup>3</sup>

<sup>1</sup>Oriental Institute of Technology, Taiwan

<sup>2</sup>Yuan Ze University, Taiwan

<sup>3</sup>Ching Yun University, Taiwan

**Abstract**— In order to develop an UWB antenna array, UWB CPW-fed Bow-tie slot antenna element is proposed as shown in Fig. 1. The antenna structure is composed of a linear tapered transition slot line between the feeding CPW and the bow-tie slot antenna. By using this linear tapered transition, a 120% impedance bandwidth with 10 dB return loss is obtained as shown in Fig. 2. The Fig. 3 shows the phase response of the antenna is measured by impulse time domain



Figure 1: Structure of antenna element.

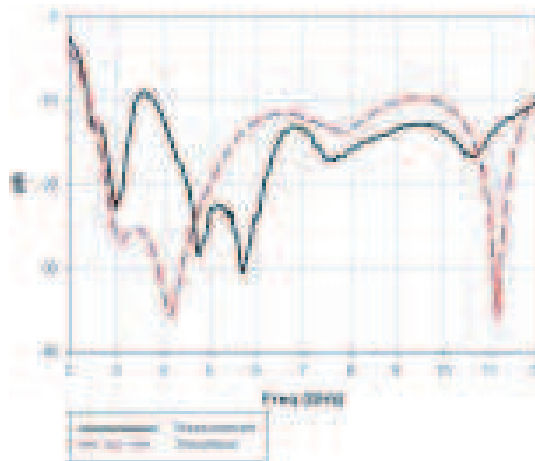


Figure 2: Return loss of the antenna.

network analyzer. Good phase linearity is obtained over the desired frequency band. Fig. 4 shows the  $XZ$ -plane radiation pattern (solid line) at 8 GHz which measured by the spherical near field range with impulse time domain vector network analyzer. The maximum gain and average gain is 4.8 dBi and 2.2 dBi respectively.

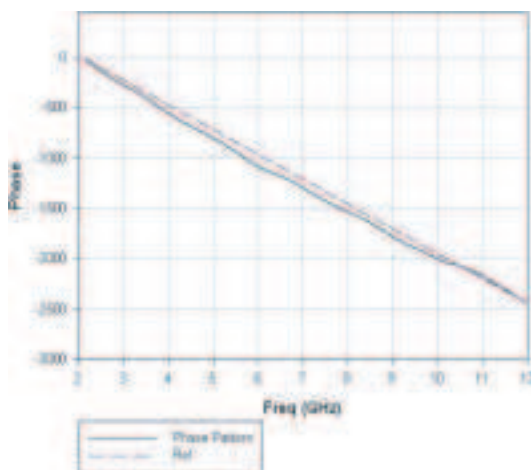


Figure 3: Phase response of antenna element.

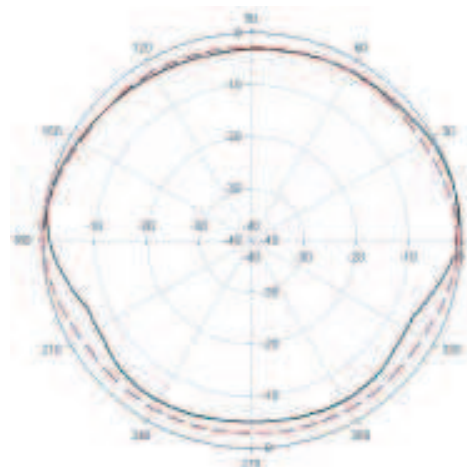


Figure 4: Radiation pattern at 9 GHz.

By using the developed bow-tie slot antenna as an antenna element, the UWB antenna array is implemented as shown in Fig. 5. By using the impulse time domain with frequency range is from 3.1 GHz to 10.6 GHz, the test result of the UWB array pattern is shown in Fig. 6. The test results are agreed with that of simulation.

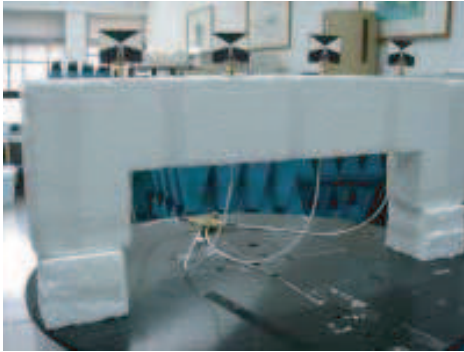


Figure 5: UWB antenna array.

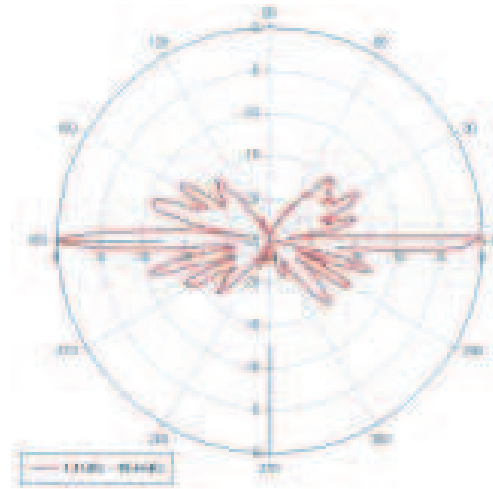


Figure 6: Radiation pattern of UWB antenna array.

## Study of a Circular Disc Monopole Ultrawide-band Miniature Antenna

Lingling Zhong, Bo Sun, Jinghui Qiu, and Ning Zhang

Department of Electronics and Communication Engineering

Harbin Institute of Technology, Harbin 150001, China

**Abstract**— Study of a novel planar circular disc monopole ultrawide-band antenna fed by coaxial line is presented in this paper. The radiator, ground plane and the feeder equipment of the antenna are placed on the same plate. The special structure reduces the spatial volume, and it is used to realize the miniaturization of the antenna. The basic theory and design method are analyzed, and detailed exploration is conducted to determine the antenna's properties. The current distributions, return loss, radiation patterns and gain of the antenna are discussed. In addition, the time domain performance of the proposed antenna is also evaluated in simulations. The research results show that this kind of planar antenna can radiate and receive short pulse signals without distortion. The 10 dB return loss bandwidth is from 2.5 GHz to 55 GHz. And it can realize near omnidirectional pattern in the H-plane. It is a real planar structure and can really reduce the spatial volume. On this basis, the structure of the planar circular disc monopole antenna is improved. The radiator moves around the upper edge of the ground plane. The new structure reduces the antenna height to a certain degree and it is used to achieve further miniaturization. Analyses are conducted to determine the novel antennas' properties. The result of study indicates that the improved antenna can realize good bandwidth performance as the planar circular disc monopole antenna, and it has low-cost, simple structural characteristics. The novel miniature antenna and the improved type are suitable for the wireless communications, satellite communications and mobile communications systems with good prospects.

# Feasibility Studies of Transversely Electromagnetic Coupled Microstrip Based Array Using Various Feeding Structures

Ka-Sing Lim and Lei-Teen Teo

Faculty of Engineering, Multimedia University, Persiaran Multimedia  
Cyberjaya 63100, Selangor, Malaysia

**Abstract**— This paper presents the design and development of various Electromagnetically Coupled Arrays (EMCA) using two feeding structures, namely Series Feed (SF-EMCA) and Parallel Feed (PF-EMCA). The advantages of EMC dipoles are they provide higher bandwidth and frequency compared to traditional fed printed antennas [1, 2]. EMCA designs require proximity coupling technique that excites radio wave from its feeding network to radiation elements. Therefore, both SF-EMCA and PF-EMCA feed networks are designed using three layers of conductor cascaded between two dielectric layer substrates. Preliminary design of SF-EMCA and PF-EMCA are simulated using a threedimensional electromagnetic simulation tool for design evaluation. Prototypes of both designs are constructed based on simulation models. Series of antenna parameters measurements are conducted in multipurpose and wideband anechoic chamber to verify the actual performance of the designs.

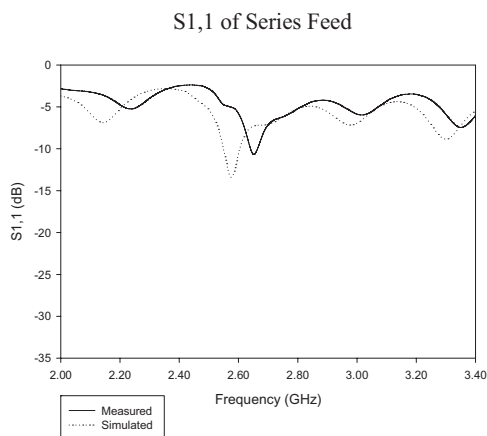


Figure 1: Simulated and measured  $S_{11}$  of SF-EMCA.

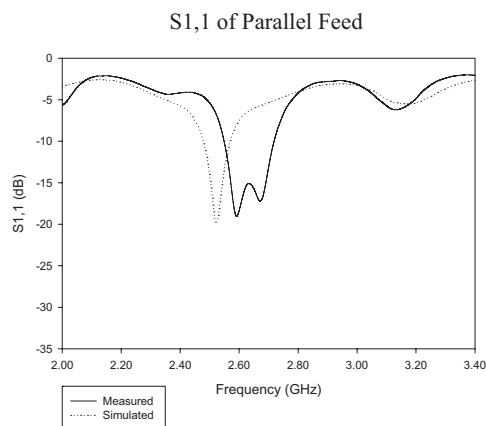


Figure 2: Simulated and measured  $S_{11}$  of PF-EMCA

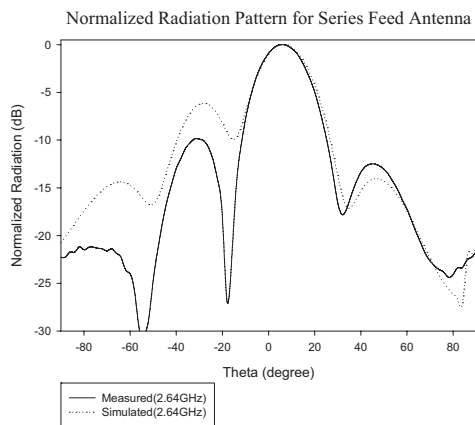


Figure 3: Simulated and measured  $S_{11}$  of SF-EMCA.

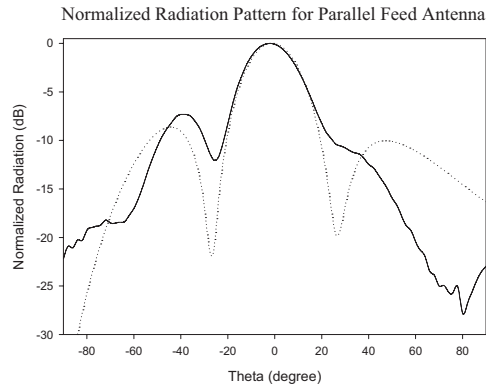


Figure 4: Simulated and measured  $S_{11}$  of PF-EMCA.

Comparison between simulated and measured results for both SF-EMCA and PFEMCA is carried out. Figure 1 shows the simulated and measured results for SF-EMCA. The simulated

resonant frequency occurs at 2.58GHz with a value of  $-13.28$  dB. The measured resonant frequency recorded  $-10.7$  dB at 2.65 GHz. The simulated and measured bandwidths are 50 MHz and 20 MHz, respectively. The simulated and measured results for FP-EMCA are depicted in Figure 2. The simulated resonant frequency of FP-EMCA displayed at 2.52 GHz with  $S_{11}$  of  $-19.86$  dB while the measured resonant frequency is 2.59 GHz with  $-19$  dB. The bandwidth FP-EMCA clearly shows improvement by approximately 160 MHz or 6.15% from its center frequency. The simulated and measured radiation pattern of SF-EMCA and PF-EMCA are shown in Figure 3 and Figure 4, respectively.

#### REFERENCES

1. Yang, H.-Y., N. G. Alexpoulos, P. M. Lepeltier, and G. J. Stern, "Design of transversely EMC microstrip dipole arrays including mutual coupling," *IEEE Transactions on Antennas and Propagation*, Vol. 38, No. 2, Feb. 1990.
2. Potharazu, P. K. and D. R. Jackson, "Analysis and design of a leaky-wave EMC dipole array," *IEEE Transactions on Antennas and Propagation*, Vol. 40 No. 8, Aug. 1992.



## A Study on a Printed Planar Crescent-like Antipodal Antenna

Yao-Chiang Kan<sup>1</sup>, Li-Hsiang Chin<sup>2</sup>, Chien-Hsun Chen<sup>2</sup>, and Huey-Ru Chuang<sup>3</sup>

<sup>1</sup>Department of Communications Engineering, Yuan Ze University  
No. 135 Yuan-Tung Road, Chung-Li 32003, Taiwan, R.O.C.

<sup>2</sup>Department of Information and Telecommunications Engineering, Ming Chuan University  
5 De Ming Rd., Gui Shan District, Taoyuan County 333, Taiwan, R.O.C.

<sup>3</sup>Department of Electrical Engineering, National Cheng Kung University, Tainan, Taiwan, R.O.C.

**Abstract**— A printed planar crescent-like antipodal antenna (PCLA) is proposed and studied. This antenna utilizes a pattern with a crescent-like shape on one side and an antipodal one on the other side, i.e., so-called Tai-Chi pattern. This crescent-like shape can be constructed with carefully arrangement of three circles with different radii. The centers of the middle and the smallest circles are located at the half and quarter of the radius of the largest circle, respectively. In addition, the radius of the largest circle is always twice of that of the middle circle. The source is fed by penetrating through the center of the antenna on the ground side and then connected to the radiating side. The impedance bandwidths, defined by VSWR equal or smaller than 2, are measured while the radii of the largest and the smallest are changed independently. A continuous bandwidth band above 12 GHz, but below 17 GHz, is observed and the bandwidths oscillate when the radius of the smallest circle increases. Similarly, increasing the radius of the largest circle not only makes the bandwidth oscillation but also features some lower frequency components. The measured radiation patterns at several frequencies of this antenna are satisfactory omnidirectional. The simulation by using the FDTD is also performed to verify those observations. This antenna possesses a high frequency bandwidth above 12 GHz and the bandwidth could be controlled by changing the radii of the largest and the smallest circles. Hence, a modified PCLA could be applied to the WiMax application for the light-of-sight (LOS) frequency range.

# Wideband Cavity Backed Spiral Antenna for Dual Mode Operation

Hongli Wang and Min Zhang

Modern Integrated Electromagnetic Simulation R&D Center (MIEMS)  
Tongji University, Shanghai 201203, China

**Abstract**— Spiral antennas can be used to obtain multiple-mode patterns over very broad frequency ranges. This paper simulates a low profile four-arm dual-mode spiral antenna. The spiral antenna is backed with a cone-shaped reflecting cavity in order to suppress back radiation and to conserve the radiated energy. The cavity backed four-arm spiral antenna is designed to work from 3 GHz to 12 GHz for both Mode 1(sum-beam) and Mode 2(differential-beam). The antenna is fed by a coplanar transmission line. The two radiation modes of the antenna are generated by exciting the even and odd modes on the coplanar transmission line. Both radiation patterns can be excited simultaneously. Good performance over an octave bandwidth is achieved. The directivity pattern of mode 1 is kept in the normal direction and the directivity is kept as split beam for mode 2 pattern. The total cumulative phase is 360 degrees for mode 1 pattern and 720 degrees for mode 2 pattern at the design elevation. Phase linearity over the entire bandwidth is well maintained. The standard deviation of phase is controlled within design requirement for both Mode 1 and Mode 2. The average axial ratio is below 3.5 dB throughout the operating range of the antenna.

CST MICROWAVE STUDIO® (CST MWS) is extensively used to study effects of various antenna parameters including a thinner substrate, feeding balun, and cone-shaped cavity. CST MWS® is based on the Finite Integration Technique(FIT) and provides different simulation methods for 3D EM analysis. FIT can be formulated as a time domain technique, which is well suitable to obtaining the wideband results for EM simulations. A prototype antenna based on the simulation design is fabricated. The measured data show a good agreement with the simulation results.

# Session 4P6b

## EM Theory and Applications

<b>Electric Field Distribution Near the End of a Thin Wire</b>	
<i>A. V. Goncharenko (Research Center for Applied Sciences, Taiwan); M. M. Dvoynenko (Natl. Acad. of Sci. of Ukraine, Ukraine); Yia-Chung Chang (Research Center for Applied Sciences, Taiwan); . . . . .</i>	892
<b>Artificial Material and Maxwell's Equations</b>	
<i>Arun K. Saha (Georgia Southern University, USA); Osamu Mizue (Ryukoku University, Japan); Ikuo Awai (Ryukoku University, Japan); . . . . .</i>	893
<b>Virtual Sources for a Sinh-Gaussian Beam</b>	
<i>Y. C. Zhang (Xichang College, China); Z. R. Chen (Xichang College, China); Z. X. Shi (Xichang College, China); J. Q. Dong (Xichang College, China); Z. L. Wu (Xichang College, China); N. Zhang (Xichang College, China); . . . . .</i>	895
<b>Localized Waves as Relativistically Boosted EM Fields</b>	
<i>Peter Saari (University of Tartu, Estonia); . . . . .</i>	896
<b>Effect of Incident Electromagnetic Waves on the Earthing Ground Grids and the Surrounding Soils at GSM Frequency</b>	
<i>Adel Mohamed Abdin (Shorouk Academy, Egypt); Mohamed Salah Kheir (German University in Cairo, Egypt); Mohamed Gamal Ashmawy (Shorouk Academy, Egypt); . . . . .</i>	897
<b>High-frequency Ferromagnetic Properties of Uniaxial Anisotropy as-deposited FeCoTa Films</b>	
<i>Shandong Li (Fujian Normal University, China); Meimei Liu (Fujian Normal University, China); Liya Lu (Nanjing University, China); Jenq-Gong Duh (National Tsing Hua University, Taiwan); . . .</i>	898
<b>Metamagnetic Transition in <math>RFe_2(H,D)_{4.2}</math> Compounds under Strong Magnetic Field</b>	
<i>Maurice Guillot (LCMI, CNRS-MPI, France); Valerie Paul-Boncour (LCMTR, CNRS, France); . . .</i>	899

## Electric Field Distribution Near the End of a Thin Wire

A. V. Goncharenko<sup>1,2</sup>, M. M. Dvoynenko<sup>2</sup>, and Yia-Chung Chang<sup>1</sup>

<sup>1</sup>Research Center for Applied Sciences, Academia Sinica, Nankang, Taipei 115, Taiwan

<sup>2</sup>Institute of Semiconductor Physics, Natl. Acad. of Sci. of Ukraine, Kyiv 03028, Ukraine

**Abstract**— At present, near-field optical properties of thin wires have aroused considerable interest from the point of view of such applications as scanning near-field optical microscopy where the wires were proposed to mount on a standard probe, integrated plasmon optics where the wires can be used for surface plasmon waveguiding and optical addressing, nanotweezers, sensorics, SERS-active substrates, etc. To evaluate the electric near field in various structures, one usually deals with numerical techniques. However, numerical techniques do not provide as much insight into the physics as analytical approaches. So, the computations are limited by certain sizes and specific materials that hinders the search for general regularities in behavior of the field. We develop analytical methods which are readily applicable to the general problems that arise when dealing with a thin wire illuminated by a plane wave.

Generally speaking, the problem of electromagnetic scattering by a thin wire can be considered in terms of the Pocklington's integro-differential equation or Hallen's integral equation [1]. As a result, closed-form solutions for the induced currents can be obtained iteratively. Once the currents have been obtained, the magnetic and electric fields can be determined. At the same time, in spite of its importance, the problem of the calculation of the electric field distribution near the end of the illuminated wire has not been addressed so far.

While an accurate solution of the Pocklington's equation involves some difficulties, its approximate closed-form solution can be obtained by Galerkin's method. In essence, the method consists in choosing a trial function for the current, inserting it in the equation, and integrating over the length of the wire [2]. In specific cases, the simplest approach making use of the Born approximation is shown to be applicable [3].

Using the above approaches, we show that in some cases the analytical solutions for the electric near field of a thin finite-length wire can be obtained. In other cases, the problem can be reduced to relatively simple semi-analytical calculations. To check the applicability of our calculations, we use the finite-difference time-domain method.

### REFERENCES

1. Balanis, C. A., *Antenna Theory. Analysis and Design*, Wiley, New York, 1997.
2. Waterman, P. C. and J. C. Pedersen, *J. Appl. Phys.*, Vol. 78, 656, 1995.
3. Hao, J. and G. W. Hanson, *Phys. Rev. B*, Vol. 75, 165416, 2007.

## Artificial Material and Maxwell's Equations

Arun K. Saha<sup>1</sup>, Osamu Mizue<sup>2</sup>, and Ikuo Awai<sup>2</sup>

<sup>1</sup>Georgia Southern University, Statesboro, USA

<sup>2</sup>Ryukoku University, Otsu, Japan

**Abstract**— Disk resonators are fabricated with isotropic artificial dielectrics made of Teflon-coated spherical copper balls for the first time. These artificial resonators are placed inside a cylindrical metal shield and excited with a horizontal loop probe. The shifting of resonant frequencies of the first few modes, as the height of the sample varies, occurs in a similar fashion as seen in the natural dielectric resonator. Investigation will be extended to resonators made of artificial anisotropic dielectric too.

**Introduction:** Natural material parameters represent the vibration of *bounded* electron clouds inside atoms as described in Maxwell's equations. Macroscopically, artificial material parameters represent the vibration of *free* electron clouds inside unit metallic particles (artificial molecules) as described in various works starting from Lewin [1].

In the present work, we will show experimentally that electromagnetic behavior of resonators made of artificial dielectrics, where  $\epsilon$ ,  $\mu$ , are *macroscopic* quantity, can also be governed by the Maxwell's equations just as natural dielectric resonators, where  $\epsilon$ ,  $\mu$ , are *microscopically* determined parameters.

**Experiment:** Artificial dielectric resonators are fabricated by pouring various numbers of insulated copper balls (dia = 1 mm) into a cylindrical-shaped container of fixed diameter as shown in Fig. 1. The resonators are excited being placed inside a cylindrical metal shield as shown in Fig. 2. Shifting of resonant frequencies are observed for various resonator heights as shown by dots in Fig. 3.

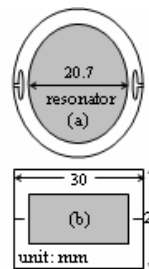
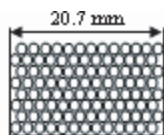


Figure 1: Artificial dielectric resonator made of insulated copper balls.

Figure 2: Experimental system (a) top view, (b) side view.

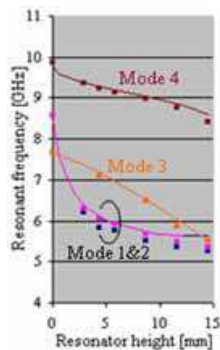


Figure 3: Experimental and simulated resonant frequencies.

**Calculation and Simulation:** Material parameters  $\epsilon$ ,  $\mu$ , are extracted assuming unit cells of standard lattice structures of crystals and verified with theoretical values from Lewin [1]. HFSS

eigen value simulations are done for various heights of resonators using those extracted parameters and shifting of resonant frequencies are shown by solid lines in Fig. 3.

**Conclusions:** Experimental shifting of resonant frequency with resonator height occurs in a similar fashion as obtained by simulation. This proves that macroscopically determined  $\varepsilon$ ,  $\mu$ , can also be used in Maxwell's equation to solve modes of artificial dielectric resonators. Investigation is extended to anisotropic case too.

#### REFERENCES

1. Lewin, L., *J. IEE*, Vol. 94, Part III, 65-68, London, Jan. 1947.

## Virtual Sources for a Sinh-Gaussian Beam

Y. C. Zhang, Z. R. Chen, Z. X. Shi, J. Q. Dong, Z. L. Wu, and N. Zhang

Department of information science and technology, Xichang College, Xichang 615500, China

**Abstract**— On the basis of the superposition of beams, a group of virtual sources that generate a sinh-Gaussian wave is identified. A closed-form expression is derived for the sinh-Gaussian wave, which, in the appropriate limit, yields the paraxial approximation for the sinh-Gaussian beam. From this expression, the paraxial approximation and the nonparaxial corrections of all orders for the corresponding paraxial sinh-Gaussian beam are determined.

# Localized Waves as Relativistically Boosted EM Fields

Peeter Saari

Institute of Physics, University of Tartu, Riia 142, Tartu 51014, Estonia

**Abstract**— There are many potential applications for highly localized EM pulses in free space or linear media. These include imaging, fabrication for optoelectronic, nano- and microparticle acceleration and manipulation, medical applications, lidar and laser weapons. Defeating spatial and temporal spreading of a wavepacket is an intriguing task in context of wave optics and diffraction particularly. In recent years a lot of effort have been put into theoretical and experimental study of such few — and subcycle nonspreading pulses — so-called localized waves (see reviews [1, 2]) — which are represented by somewhat exotic non-separable solutions of source-free linear wave equations. A simplest type of them — the so-called X-waves — have been launched and studied experimentally, incl. their superluminal propagation over large distances without spread [3, 4].

It is instructive that the localized waves are treatable as manifestations of relativistic Doppler shift and aberration if one boosts certain (almost text-book-simple) waves into relativistically moving reference frames. Despite generating different types of localized waves — subluminal, luminal and superluminal ones — from simple solutions of the scalar wave equation seems a purely theoretical method [1, 2], it is applicable also in real devices involving circular or cylindrical diffraction gratings [5]. If applied to quantized EM field, certain types of localized waves force to revise the notion of localizability of photon [6].

In the paper illustrated with animated 3D plots we present our new results of study of localized waves. In particular, we consider startling examples of “backward light” in vacuum, where negative group velocity (and velocity of the whole pulse intensity profile) originates from angular dispersion in 3D space instead of well-known mechanism — being caused by anomalies in the dispersion of the 1D propagation medium.

## REFERENCES

1. Besieris, I., M. Abdel-Rahman, A. Shaarawi, and A. Chatzipetros, *Progr. in Electromagn. Research*, Vol. 19, 1, 1998.
2. Saari, P. and K. Reivelt, *Phys. Rev. E*, Vol. 69, 036612, 2004.
3. Saari, P. and K. Reivelt, *Phys. Rev. Lett.*, Vol. 79, 4135, 1997.
4. Alexeev, I., K. Y. Kim, and H. M. Milchberg, *Phys. Rev. Lett.*, Vol. 88, 073901, 2002.
5. Valtna, H., K. Reivelt, and P. Saari, *Opt. Commun.*, Vol. 278, 1–7, 2007.
6. Saari, P., M. Menert, and H. Valtna, *Opt. Commun.*, Vol. 246, 445–450, 2005.



## Effect of Incident Electromagnetic Waves on the Earthing Ground Grids and the Surrounding Soils at GSM Frequency

Adel M. Abdin<sup>1</sup>, Mohamed S. Kheir<sup>2</sup>, and Mohamed G. Ashmawy<sup>3</sup>

<sup>1</sup>Department of Communications and Electronics, Shorouk Academy, Cairo, Egypt

<sup>2</sup>Department of Information Engineering, German University in Cairo, Cairo, Egypt

<sup>3</sup>Department of Electrical Power Engineering, Shorouk Academy, Cairo, Egypt

**Abstract**— A simple and new study investigates the effect of electromagnetic waves on the earthing ground grids is hereby introduced. The aim of this study is to inspect the electric and magnetic fields distribution on and around these earthing grids due to GSM(Global System for Mobile Communications) mobile communications radiation from Base Transceiver Stations (BTSs). The paper considers both the 900 and 1800 MHz standards with different radiated power levels. Normal and oblique incident plane waves are also considered in order to make this model as close as possible to reality.

The first section of the paper gives a brief introduction about the grounding grids, their construction and importance in our daily life.

The second section illustrates the basic model used in our simulation which, in principle, consists of the following basic elements:

1. The grid drawn into scale to a real construction.
2. The soil below and above this grid with scaled heights. (Four different homogenous soil types have been investigated within this study).
3. Incident uniform plane waves
4. A free-space boundary surrounding this setup.

The third section discusses the output results from this model, namely:

- The magnitude of electric field distribution on the grid.
- The magnitude of magnetic field distribution on the grid.
- The volume current density of the soil below and above the grid.

All simulations have been carried out using the Ansoft High Frequency Structure Simulator (HFSS) as a finite elements based solver which provides a complete description of the problem.

In the last section, some concluding remarks and comments are discussed so as to evaluate this research and its feasibility. However, some proposed solutions for protecting this grounding system, which may result in a better electromagnetic compatibility to our environment, are also offered.

## High-frequency Ferromagnetic Properties of Uniaxial Anisotropy as-deposited FeCoTa Films

Shandong Li<sup>1,2,3</sup>, Meimei Liu<sup>1</sup>, Liya Lü<sup>3</sup>, and Jenq-Gong Duh<sup>2</sup>

<sup>1</sup>Department of Physics, Fujian Normal University, Fuzhou 350007, China

<sup>2</sup>Department of Materials Science and Engineering, National Tsing Hua University  
Hsinchu 30013, Taiwan

<sup>3</sup>National Laboratory of Solid State Microstructure, Nanjing University  
Nanjing 210093, China

**Abstract**— Introducing high-frequency ferromagnetic (HFFM) film into monolithic integrated circuits (MICs) is an effective way to miniaturize the electromagnetic components and to enhance the reliability of electronic devices. Nanocrystalline FeCoTa films with Ta composition gradient were prepared by gradient sputtering (GS) method at room temperature. It is interesting to note that as-deposited GS films without pre- and/or post-magnetic-annealing exhibited promising high-frequency ferromagnetic properties with resonance frequency over 3 GHz and strong uniaxial magnetic anisotropy (UMA) with anisotropy field,  $H_k$ , up to 280 Oe. The magnitudes of  $H_k$  can be adjusted by controlling the composition gradient of doping element Ta. The origin of UMA can be attributed to the uniaxial stress gradient, which is resulted from the composition gradient. In general, the UMA in ferromagnetic films is obtained by magnetic annealing at 300–600°C, however, the MICs require to be fabricated at room temperature. This contradiction can be resolved by this gradient sputtering method.

# Metamagnetic Transition in $\text{RFe}_2(\text{H,D})_{4.2}$ Compounds under Strong Magnetic Field

Maurice Guillot<sup>1</sup> and Valerie Paul-Boncour<sup>2</sup>

<sup>1</sup>LCMI, CNRS-MPI, BP166, 38042 Grenoble Cedex 9, France

<sup>2</sup>LCMTR, CNRS, 2 rue H. Dunant, 94320 Thiais Cedex, France

**Abstract**—  $\text{RFe}_2$  Laves phases compounds absorb hydrogen or deuterium up to 5 H(D)/mol. Below a critical temperature the  $\text{RFe}_2\text{D}_x$  (R: Rare earth atom) phases display various structural distortions of the cubic C15 structure due to the ordering of the H(D) atoms in preferential interstitial sites (see [1] and ref. therein). Hydrogen absorption strongly influences the magnetic properties. The  $\text{YFe}_2\text{D}_x$  deuterides are ferromagnetic with an increase of the mean Fe moment and a decrease of  $T_C$  for  $x \leq 3.5$  D/mol. For  $x = 4.2$ , the monoclinic compound is ferromagnetic at low temperature then undergoes a sharp first-order magnetovolumic transition towards an antiferromagnetic structure at 84 K.

Surprisingly this transition is very sensitive to the H for D substitution, which increases the mean Fe moment at 4.2 K and shift the transition temperature to 130 K, i.e., of 50%; Since the cell volume of the hydride is 0.78% larger than the deuteride such large isotope effect can be related to the strong sensitivity of the IEM behaviour to the volume.

In this paper the magnetic properties are studied in the 4.2–300 K temperature range under high continuous magnetic field up to 25 tesla. *The techniques of the high field production are described* in a first part of the paper; in the second one the home made magnetometer is presented. The influence of different parameters on the first order metamagnetic transition, in particular its sensitivity to the large (H,D) isotope effect is finally analyzed.

## REFERENCES

1. Paul-Boncour, V., et al., *Phys. Rev. B*, Vol. 72, 174430, 2005.



# Session 4P7

## Extended/Unconventional Electromagnetic Theory, EHD/EMHD, Electrobiolgy 2

<b>Method for Magnetic Field Approximation in MR Tomography</b>	
<i>Michal Hadinec (Brno University of Technology, Czech Republic); Pavel Fiala (Brno University of Technology, Czech Republic); Eva Kroutilová (Brno University of Technology, Czech Republic); Miloslav Steinbauer (Brno University of Technology, Czech Republic); Karel Bartušek (Institute of Scientific Instruments, Academy of Sciences of the Czech Republic, Czech Republic);</i>	902
<b>Design Simulation and Optimization the Source of Light</b>	
<i>Eva Kroutilova (Brno University of Technology, Czech Republic); Tomas Kriz (Brno University of Technology, Czech Republic); Pavel Fiala (Brno University of Technology, Czech Republic); Michal Hadinec (Brno University of Technology, Czech Republic);</i>	903
<b>Inversion Reconstruction of Signals Measured by the NMR Techniques</b>	
<i>Eva Kroutilova (Brno University of Technology, Czech Republic); Miroslav Steinbauer (Brno University of Technology, Czech Republic); Premysl Dohal (Brno University of Technology, Czech Republic); Michal Hadinec (Brno University of Technology, Czech Republic); Eva Gescheidtova (Brno University of Technology, Czech Republic); Karel Bartusek (Institute of Scientific Instruments, Academy of Sciences of the Czech Republic, Czech Republic);</i>	904
<b>Numerical Modeling of Electromagnetic Field a Tornado</b>	
<i>Pavel Fiala (Brno University of Technology, Czech Republic); Vaclav Sadek (Brno University of Technology, Czech Republic); T. Kriz (Brno University of Technology, Czech Republic);</i>	905
<b>The Numerical Modeling and Conformal Mapping Method Applied to the Strip-centered Coaxial Line Analysis</b>	
<i>Vaclav Sadek (Brno University of Technology, Czech Republic); Pavel Fiala (Brno University of Technology, Czech Republic); Michal Hadinec (Brno University of Technology, Czech Republic);</i>	906
<b>A Novel Hypothesis for Quantum Physics, Model with Telegraphs Equation</b>	
<i>Pavel Fiala (Brno University of Technology, Czech Republic); Karel Bartusek (Institute of Scientific Instruments, Academy of Sciences of the Czech Republic, Czech Republic); Miloslav Steinbauer (Brno University of Technology, Czech Republic);</i>	907
<b>Extending the Concept of Debye Length for Chasmas</b>	
<i>Dirk K. Callebaut (University of Antwerp, Belgium); Hiroshi Kikuchi (Institute for Environmental Electromagnetics, Japan);</i>	908
<b>Further Results on Post-MHD</b>	
<i>Dirk K. Callebaut (University of Antwerp, Belgium); Geoffrey K. Karugila (Sokoine University, Tanzania);</i>	909
<b>Non-quasi-neutral Plasmas or Chasmas</b>	
<i>Dirk K. Callebaut (University of Antwerp, Belgium);</i>	910
<b>Usefulness of a Universal Electric-cusp Type Plasma Reactor in Basic Studies and a Variety of Applications in Dust Dynamics, Ionization and Discharge Physics Based on Electrohydrodynamics</b>	
<i>Hiroshi Kikuchi (Institute for Environmental Electromagnetics, Japan);</i>	911
<b>Magnetoplasmons in Graphene Structures</b>	
<i>Oleg L. Berman (City University of New York, USA); Godfrey Gumbs (City University of New York, USA); Yurii E. Lozovik (Institute of Spectroscopy, Russian Academy of Sciences, Russia);</i>	912

## Method for Magnetic Field Approximation in MR Tomography

Michal Hadinec<sup>1</sup>, Pavel Fiala<sup>1</sup>, Eva Kroutilová<sup>1</sup>  
Miroslav Steinbauer<sup>1</sup>, and Karel Bartušek<sup>2</sup>

<sup>1</sup>Institute of Scientific Instruments of the ASCR, v.v.i  
Královopolská 147, 612 64, Brno, Czech Republic

<sup>2</sup>Department of Theoretical and Experimental Electrical Engineering  
Faculty of Electrical Engineering and Communication, Brno University of Technology  
Kolejní 2906/4, 612 00, Brno, Czech Republic

**Abstract**— This paper describes a method, which can be used for creating map of magnetic field. Method has a great usage in magnetic resonance tomography, when we need to get information about homogeneity and characteristics of magnetic field inside the working space of the MR tomograph. The main purpose of this article is to describe basic principles of magnetic resonance phenomenon and mathematical method of Legendre polynoms which can be used for signal processing of FID (Free Induction Decay) signal obtained from tomograph detection coils. In the end of my article is experimental solution of magnetic field and models of magnetic field created by Matlab.

**Introduce** Magnetic resonance tomography is an imaging technique used primary in medical setting to produce high quality images of the human body. Magnetic resonance imaging is based on the principles of nuclear magnetic resonance (NMR) and at the present time it is the most developed imaging technique at biomedical imaging [2]. Lately, medical science lays stress on the measuring of exactly defined parts of human body, especially human brain. If we want to obtain the best quality images we have to pay attention to homogeneity of magnetic fields, which are used to scan desired samples inside the tomograph. We should know how to reduce inhomogeneity, which can cause misleading information at the final images of samples. Generally, inhomogeneity of magnetic fields at magnetic resonance imaging cause contour distortion of images. To eliminate these inhomogeneity correctly, we need to know the map of the magnetic field and we also need to have an exact information about parameters of the magnetic field. This paper presents the experimental method, which can easily create the map of electromagnetic induction at any defined area inside the tomograph. This method uses mathematical theory of Legendre polynoms, which are used for approximation of magnetic field, if we know specific coefficients. The coefficients of Legendre polynoms, which are computed using measured values of magnetic induction at exactly defined discrete points are used for creating map of magnetic field. If we know these coefficients, we are able to compute magnetic induction at any point of defined area. At the ideal case, there should be no difference between measured data and approximated data.

### REFERENCES

1. Fiala, P., E. Kroutilová, and T. Bachorec, Modelování elektromagnetických polí, počítačová cvičení vyd. Brno: VUT v Brně, FEKT, Údolní 53, 602 00, Brno, 2005.
2. Haacke, E. M., R. W. Brown, M. R. Thomson, and R. Venkatesan, Magnetic resonance imaging-physical principles and sequence design, John Wiley & Sons, ISBN 0-471-48921-2, 2001.
3. Stratton, J. A., Teorie elektromagnetického pole, SNTL Praha, 1961.
4. Angot, A., Užitá matematika, Státní nakladatelství technické literatury, Praha 1972.
5. Morris, P. G., *Nuclear Magnetic Resonance Imaging in Medicine and Biology*, Clearendon Press, Oxford, 1986.

## Design Simulation and Optimization the Source of Light

Eva Kroutilová, Tomáš Kříž, Pavel Fiala, and Michal Hadinec

Department of Theoretical and Experimental Electrical Engineering, Brno University of Technology  
Kolejní 4, 612 00 Brno, Czech Republic

**Abstract**— This paper presents information about design of light sources, which is intended for commercial use. Required properties were continuous spectral characteristic with respect to active wavelength area, 3D light characteristics. Design of light source consisting of classical used light source, as well as experimental results, are presented. The light source was designed, optimized and tested for the research activity.

### REFERENCES

1. GM Electronic, Katalog elektronických součástek, 2005.
2. Světlo, ISSN 1212-0812, FCC Public s.r.o., Pod Vodárenskou věží 4, 182 08, Praha 8, ČR.
3. Plch, J., J. Mohelníková, and P. Suchánek, Osvětlení neosvětlitelných prostor, ERA, 2004.
4. *LEOS Newsletter Magazine*, Lasers and Electro-Optics Society of the Institute of Electrical and Electronics Engineers, Inc., Corporate Office: 3 Park Ave., 17th Floor, New York, NY 10016-5997, USA.
5. Plch, J., *Světelná technika v praxi*, IN-EL 1999, Praha, 210 stran, ISBN 80-86230-09-0.
6. Habel, J. a. K., *Světelná technika a osvětlování*, FCC Public, Praha, 448 stran, ISBN 800-901985-0-3, 1995.
7. Govindjee, *Bioenergetics of Photosynthesis*, Academic Press, New York, 1975.
8. Campbell, N. and J. Reece, Benjamin Cummings., *Biology* 7th ed., San Francisco, 2005.
9. <http://www.esim.ca/2002/documents/Proceedings/other2.pdf>.

# Inversion Reconstruction of Signals Measured by the NMR Techniques

Eva Kroutilova<sup>1</sup>, Miloslav Steinbauer<sup>1</sup>, Premysl Dohal<sup>1</sup>  
 Michal Hadinec<sup>1</sup>, Eva Gescheidtova<sup>1</sup>, and Karel Bartušek<sup>2</sup>

<sup>1</sup>Brno University of Technology, Czech Republic

<sup>2</sup>Academy of Science of the Czech Republic, Czech Republic

**Abstract**— The paper describes the magnetic resonance imaging method applicable mainly in MRI and MRS in vivo studies. We solved the effect of changes of magnetic fields in MR tomography. This article deals with the reverse reconstruction results obtained from the numerical simulation of MR signals by various techniques, which will be usable for the experimental results verification.

**Geometrical Model:** Figure 1 describes the sample geometry for the numerical modeling. On both sides, the sample is surrounded by the referential medium. During the real experiment, the reference is represented by water, which is ideal for obtaining the MR signal.

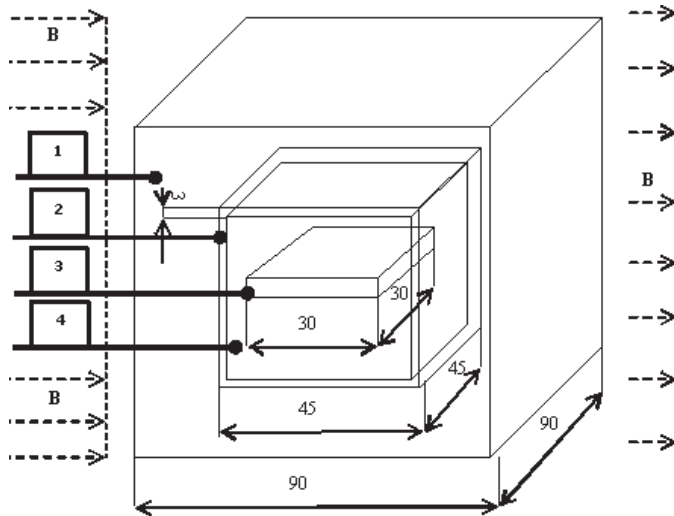


Figure 1: The sample geometry for numerical modeling.

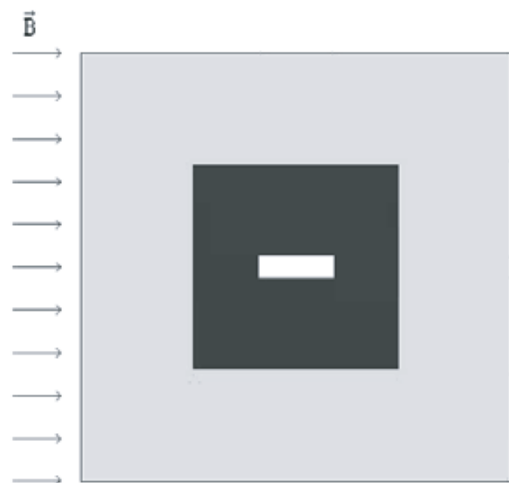


Figure 2: The geometrical model in the system Ansys.

## REFERENCES

1. Fiala, P., E. Kroutilová, and T. Bachorec, Modelování elektromagnetických polí, počítačová cvičení, vyd. VUT v Brně, Brno, FEKT, Údolní 53, s. 1–69, 602 00, Brno, 2005.
2. Steinbauer, M., Měření magnetické susceptibility technikami tomografie magnetické rezonance, vyd. VUT v Brně, Brno, FEKT, Údolní 53, 602 00, Brno, 2006.



# Numerical Modeling of Electromagnetic Field a Tornado

P. Fiala, V. Sadek, and T. Kriz

Department of Theoretical and Experimental Electrical Engineering  
Brno University of Technology, Kolejní 2906/4, 612 00 Brno, Czech Republic

**Abstract**— This article deals the numerical model with physical and chemical processes in the tornado. There are presented basic theoretical model and numerical solution. We prepared numerical models based on combined finite element method (FEM) and finite volume method (FVM). The model joins magnetic, electric and current field, flow field and chemical nonlinear ion model. Results were obtained by means of FEM/FVM as a main application in ANSYS software.

**Introduction:** The full electro-hydro-dynamical (EHD) model of inductive tornado is coupled problem. There are coupled electric, magnetic, fluid flow field and electric circuit and chemical (ions) models. This model was solved with combined finite element methods (FEM) and finite volume methods (FVM). Results from numerical model were tested.

## REFERENCES

1. Fala, P., "Model of inductive flowmeter DN-100," Research report No. 2/01, 1–23, Laboratory of modelling and optimisation of electromechanical systems BUT FECT, Brno, Czech Republic, June 21, 2001,
2. Fleischner, P., Hydromechanika, Paperback VUT FS, VUT Brno, ISBN 80-214-0266-1, 1990.
3. Černoch, S., Strojně technická příručka, SNTL Praha, 1968.
4. Moore, J. W., Fyzikální chemie, SNTL Praha, 1981.
5. Brdička, R. and J. Dvořák, Základy fyzikální chemie, Academia Praha, 1977.

# The Numerical Modeling and Conformal Mapping Method Applied to the Strip-centered Coaxial Line Analysis

V. Šádek, P. Fiala, and M. Hadinec

Faculty of Electrical Engineering and Communication, Brno University of Technology  
Kolejní 2906/4, Brno 612 00, Czech Republic

**Abstract**— The boundary element method (BEM) is used for the strip centered coaxial line (SCCL). The common microstrip line has one disadvantage — a lot of electromagnetic field is spread outside the dielectric substrate. This field moves  $\sqrt{\epsilon_r}$  times faster than field under the microstrip inside the dielectric substrate. This deformation of the field (HEM wave) complicates the application of the microstrip line on frequencies over c. 20 GHz. Described complication can be eliminated in the structure, which cumulates major part of power density of the EM field in dielectric substrate to the detriment of free space above the strip.

**Introduction:** A lot of different electronic equipments have to work together. Unfortunately the power levels among them are over 200 dB very often. Coaxial structures are widely used because of their good shielding effect, which suppress the fields around strong distortion sources (e.g., transmitting antenna feeder) and protect sensitive parts of receivers, measurements etc. [1, 2].

Whereas coaxial line (two concentric cylindrical electrodes) is widely known, strip-centered coaxial line (SCCL, Fig. 1.) is mentioned rarely (found only in very special literature like [3]). The SCCL structure also offers a very attractive occasion of matching to microstrip line, coplanar waveguide, etc.

## REFERENCES

1. Svačina, J., *Electromagnetic Compatibility — Lectures*, Textbook of Brno University of Technology, FEKT VUT Brno, 2002.
2. Armstrong, K., Design Techniques for EMC, [http://www.compliance-club.com/keith\\_armstrong.asp](http://www.compliance-club.com/keith_armstrong.asp).
3. Wadell, B. C., *Transmission Line Design Handbook*, Artech House, Boston/London, 1991.
4. Driscoll, T. A., SC-Toolbox, for MATLAB, <http://www.math.edu/driscoll/SC/>.
5. Paris, F. and J. Canas, *Boundary Element Method*, Oxford University Press, Oxford, 1997.
6. Bongiani, W. L., “Fabrication and performance of strip-centered microminiature coaxial cable,” *Proceeding of the IEEE*, Vol. 72, No. 12, 1810–1811, December 1984.
7. Hilberg, W., *Electric Characteristics of Transmission Lines*, 122, Artech House Nooks, Dedham, MA, 1979.

# A Novel Hypothesis for Quantum Physics, Model with Telegraphs Equation

P. Fiala<sup>1</sup>, K. Bartusek<sup>2</sup>, and M. Steinbauer<sup>1</sup>

<sup>1</sup>Department of Theoretical and Experimental Electrical Engineering  
University of Technology Brno, Kolejní 4, 612 00 Brno, Czech Republic

<sup>2</sup>Institute of Scientific Instruments, Academy of Sciences of the Czech Republic  
Královopolská 147, 612 64 Brno, Czech Republic

**Abstract**— The article describes a test of numerical model of the electron beam according to present knowledge of references [1–5]. The basic configuration of the electron beam was verified in Institute of Scientific Instruments Academy of Sciences of the Czech Republic experimentally. We prepared the numerical model which is based on the particle theory. Actually, it respects classical Electrodynamics Material Wave Theory (MWT). Numerical results were evaluated. The second model was prepared in respect to theory of wave packet (Louis de Broglie) and solved again. Results of both models were the same in their quality, we evaluated electric field intensity  $E$  on the electron impact area, and they corresponded with results from experiments.

## REFERENCES

1. Van Vlaenderen, K. J. and A. Waser, “Electrodynamics with the scalar field,” *Physics*, Vol. 2, 1–13, 2001.
2. Kikuchir, H., “Electrohydrodynamics in dusty and dirty plasmas, gravito-electrodynamics and EHD,” *Kluwer academic publishers*, Dordrecht/Boston/London, 2001.
3. Van Vlaenderen, K. J., “A charge space as the origin of sources, fields and potentials,” *Physics*, arXiv: physics/9910022 v1, 1–13, 16 Oct., 1999.
4. Hofer, W. A., “A charge space as the origin of sources, fields and potentials,” *Physics*, arXiv: quant-ph/ 9611009 v3, 1–13, 17 Apr., 1997.
5. Prosser, V a K., “Experimentální metody biofyziky,” *Academia*, Praha, 1989.
6. Delong, A., “Verbal information,” Czech Academy of Science, ISI Brno, Brno, 7. 2. 2006.
7. Bartusek, K. and P. Fiala, “A simple numerical simulation of internal structure of particles test,” *PIERS 2007*, Beijing, China, March 2007.

## Extending the Concept of Debye Length for Chasmas

D. K. Callebaut<sup>1</sup> and H. Kikuchi<sup>2</sup>

<sup>1</sup>Physics Dept., CDE, University of Antwerp, Antwerp, B-2610, Belgium

<sup>2</sup>Institute for Environmental Electromagnetics, Tokyo 170, Japan

**Abstract**— Chasmas are a generalization of plasmas, i.e., the condition of quasi-neutrality is dropped. That means that in chasmas the quasi-neutrality may be (strongly) violated over distances many times the Debye length which requires special circumstances (double layers, electric fields, ...). The question arises what the meaning is of a shielding length in chasmas. It was demonstrated that the so-called chasma (angular) frequency has an expression similar to the plasma frequency:

$$\omega_c^2 = \frac{|n_- - n_+|e^2}{\epsilon m_-},$$

with an obvious notation. However, this chasma frequency plays a role as well in the equilibrium (or steady state) as in the stability. For the ‘Debye length in chasmas’ we obtained

$$\lambda_c^2 = \frac{\epsilon k_B T}{(n_+ + n_-)e^2},$$

supposing the temperature of electrons and ions is the same, that the ions are only once ionized and that  $kT \gg e\varphi$  (kinetic energy much larger than potential energy). This means that the chasma shielding length is much the same as the Debye length and that  $\lambda_c \omega_p \sim \lambda_D \omega_p \sim k_B T$  while  $\lambda_c \omega_c$  make a rather different combination involving the temperature and the degree of non-quasi-neutrality

$$\frac{n_- - n_+}{n_- + n_+}.$$

However, some comments are in place. First the equilibrium has the same structure, so that the general shape of the chasma and the shape near the extra charge introduced in it have a different amplitude, but the same shape. (Cf. the same situation for  $\omega_c$  which plays a role in the equilibrium and in the perturbation.) Second, the question of the universality of the expression for  $\lambda_c$  arises, although we obtained it for two cases (one equilibrium and one steady state). Indeed, chasmas require extra forces or conditions to exist and each case needs a somewhat adapted treatment. However, on general grounds we expect the expression rather general.

### REFERENCES

1. Callebaut, D. K., G. K. Karugila, and A. H. Khater, “Chasma perturbations,” *Proc. PIERS 2005*, 720–723, Hangzhou, China, August 22–26, 2005.
2. Callebaut, D. K. and A. H. Khater, “Chasma including magnetic effects,” *Proc. PIERS 2006*, 404–411, Cambridge, USA, March 26–29, 2006.
3. Callebaut, D. K. and H. Kikuchi, “Debye shielding in chasmas,” *Proc. PIERS 2007*, Prague, 27–30 August, 2007.

## Further Results on Post-MHD

D. K. Callebaut<sup>1</sup> and G. K. Karugila<sup>2</sup>

<sup>1</sup>Physics Department, CDE, University of Antwerp, Antwerp, B-2610, Belgium

<sup>2</sup>Sokoine University, Morogoro 3038, Tanzania

**Abstract**— This paper continues the previous work on post-magnetohydrodynamics [3]. In magnetohydrodynamics (MHD) Maxwell's displacement current is neglected. From the evolution equation for MHD (either ideal or not) one obtains the magnetic field and through Maxwell's equations one may calculate the electric field, the current and the electric charge. This allows to verify the neglect of the displacement term. The exact solution obtained by Callebaut for ideal MHD allows a rigorous calculation (for a given velocity profile and a given initial field) of the neglected term. The displacement current yields a correction term which may require an iteration. This corresponds to pass from MHD to Post-MHD. In Ref. 3 it was shown that the displacement current exceeds the MHD current when the time derivative divided by  $c^2$  exceeds the second order space derivatives multiplied by the time lapse in the case treated. Further examples are given. It results that precisely at the start of a magnetic phenomenon the displacement current may play a role: this is related to Lenz law. For longer times the displacement current fades out. As a side result the question of quasi-neutrality is considered (cf. the concept of non-quasi-neutral plasmas or "chasmas").

### REFERENCES

1. Callebaut, D. K. and V. I. Makarov, "Generation of sunspots and polar faculae from a kinematic dynamo," *Proc. IX Pulkovo International Conference on Solar Physics: Solar Activity as a factor of Cosmic Weather*, (Pulkovo) Main Astronomical Observatory, 4–9 July 2005 (A. V. Stepanov, A. A. Solov'ev & V. A. Dergachev, directors), (Mostly in Russian), 196140 St. Petersburg, Russia, 379–388, 2005.
2. Callebaut, D. K. and A. H. Khater, "Generation of sunspot and polar faculae butterflies using bipolar and quadripolar seed field," *Proc. IAU Symposium 233, Solar Activity and Its Magnetic Origin*, 9–16, Eds. V. Bothmer and A. A. Hady, Cairo, Egypt, March 31–April 4, 2006.
3. Callebaut, D. K. and A. H. Khater, "Post-Magnetohydrodynamics," *PIERS07*, 989–993, (+ CD-Rom), Beijing, China, March 26–30, 2006.

## Non-quasi-neutral Plasmas or Chasmas

D. K. Callebaut

Physics Department, CGB, University of Antwerp, Antwerp, B-2020, Belgium

**Abstract**— By definition a plasma is quasi-neutral over distances of the order of the Debye length. However, there are many cases in which there is no quasi-neutrality over distances of many Debye lengths. Such a “charged plasma” has been called plasma. Several types of this may occur in the cavities of particle accelerators or in (re-entrant) cavities according to the sign of the ionizing beam (+, 0 or  $-$ ), its orientation, the residual gas pressure, the geometry and the presence of a magnetic field (parallel or perpendicular). This may be studied using a (partial) integro-differential equation or more geneneral, using the Maxwell equations from the start in 1D, 2D or 3D. We define the chasma frequency, similar to the plasma frequency, but playing a role in the equilibrium or steady state as well as in the stability analysis. The extension of the Debye length and potential is considered. Other cases of chasmas are briefly considered (chasma surrounded by isolating walls, double layers, double current layers, pure electron gas in crossed magnetic field and rotation, It may be noted that plasma instabilities often show non-quasi-neutrality which may lead to wrong results if the corresponding frequencies are used instead of the ones for chasmas. Clearly a cavity filled with a chasma has a different resonance frequency then when empty.

# Usefulness of a Universal Electric-cusp Type Plasma Reactor in Basic Studies and a Variety of Applications in Dust Dynamics, Ionization and Discharge Physics Based on Electrohydrodynamics

H. Kikuchi

Institute for Environmental Electromagnetics, 3-8-18, Komagome, Toshima-ku, Tokyo 170, Japan

**Abstract**— A universal electric-cusp type plasma reactor designed more than a decades ago by the present author has successfully been in operation for the last couple of years and has been proved useful for basic studies and a variety of applications in dust dynamics, ionization and discharge physics, including laboratory simulation of universe, atmospheric and space electricity and plasmas, based on 'Electrohydrodynamics (EHD)/Electromagnetohydrodynamics (EMHD)'. This paper aims to present the structure and operation of this plasma reactor and to show how this device is useful for basic studies and applications, citing a number of examples. The new device is a square box with two lead electrodes (15 mm in diameter and 5 cm in interval) inside, suspended 2.75 ~ 5 cm above a metallic plate. When a tiny object or dust grain, conducting or dielectric, is placed in the cusp center, electric field line merging toward it occurs from the four or two poles, inducing or polarizing electric charges on its surface or in its volume, negative or positive facing positive or negative poles, respectively. Then a catastrophe occurs, namely zero-electric field without the object or dust suddenly tends to sufficiently high electric fields, almost infinity, around it. We are now ready to be advanced to one of entirely different two directions, depending upon the background gas pressure. One is the case of energy transfer from fields to kinetic energy leading to dust dynamics in a pair of electric mirror for the background gas pressure below the breakdown threshold, and the other is the case of energy transfer from fields to ionization resulting in an electric discharge for the background gas pressure beyond the breakdown threshold. First we deal with the former case. When an uncharged dust grain, conducting or dielectric, is placed onto the center of a quadrupole, dust starts moving between conjugating mirror points and is going back and forth undulating the mid-plane. If a dust grain is negatively or positively charged its motion in periodic cusps and mirrors in the midplane of a quadrupole forming an electric mirror. Next we proceed to three dimensional motion of an uncharged or charged dust grain not in the ecliptic plane of a quadrupole, Then the dust grain is going to helical motion due to helicity generation of an electric quadrupole. The second case when the background gas pressure is beyond the breakdown threshold leads to a variety of electric discharge phenomena, laboratory evidence of 'electric cusp-mirror and reconnection model' as well as the first case and provides basic studies of ionization and discharge processes, laboratory simulations of universe, atmospheric and space electric electricity and plasma phenomena, applications to industrial plasmas, including plasma processing, new material production such as diamond, electric precipitator and so on.

# Magnetoplasmons in Graphene Structures

Oleg L. Berman<sup>1</sup>, Godfrey Gumbs<sup>2</sup>, and Yurii E. Lozovik<sup>3</sup>

<sup>1</sup>Physics Department, New York City College of Technology, City University of New York, USA

<sup>2</sup>Department of Physics, Hunter College, City University of New York, USA

<sup>3</sup>Institute of Spectroscopy, Russian Academy of Sciences, Russia

**Abstract**— Recent progress in technology has allowed the production of graphene, which is a two-dimensional honeycomb lattice of carbon atoms that form the basic planar structure in graphite. [1, 2] Graphene has attracted strong theoretical attention as a gapless semiconductor with an unusual massless Dirac-fermion band structure. The unusual many-body interactions in graphene have been investigated. [5] The integer quantum Hall effect (IQHE) has been discovered in graphene in recent experiments. [6–8] The quantum Hall ferromagnetism in graphene has been studied theoretically. [9] The spectrum of plasmon excitations in a single graphene layer immersed in a material with effective dielectric constant  $\epsilon_s$  without magnetic field ( $B = 0$ ) was calculated in Ref. [10]. We calculated the spectrum of magnetoplasmon excitations in graphene layer immersed in a dielectric in strong magnetic fields  $B = 5T$  and  $B = 10T$  applying the random phase approximation (RPA). Besides, we have calculated the spectrum of magnetoplasmon excitations in graphene bilayer and an infinite superlattice of graphene layers immersed in a dielectric. We analyze the dispersion relation in detail. Our numerical calculations reveal symmetric and antisymmetric plasmon modes for bilayer graphene as well as a negative group velocity for a range of wave vectors. There is Landau damping of the plasmon excitations by the particle-hole modes in some regimes of the wavelength of the collective plasmon branches. Our formalism is valid for arbitrary filling factor and temperature. Plasma instabilities associated with these layered structures will be explored as a source of electro-magnetic radiation.

## REFERENCES

1. Novoselov, K. S., et al., *Science*, Vol. 306, 666, 2004.
2. Zhang, Y., et al., *Phys. Rev. Lett.*, Vol. 94, 176803, 2005.
3. DiVincenzo, D. P. and E. J. Mele, *Phys. Rev. B*, Vol. 29, 1685, 1984.
4. Kane, C. L. and E. J. Mele, *Phys. Rev. Lett.*, Vol. 78, 1932, 1997.
5. Sarma, S. D., E. H. Hwang, and W.-K. Tse, *Phys. Rev. B*, Vol. 75, 121406(R), 2007.
6. Novoselov, K. S., et al., *Nature*, Vol. 438, 197, London, 2005.
7. Zhang, Y. B., et al., *Nature*, Vol. 438, 201, London, 2005.
8. Zhang, Y., et al., *Phys. Rev. Lett.*, Vol. 96, 136806, 2006.
9. Nomura, K. and A. H. MacDonald, *Phys. Rev. Lett.*, Vol. 96, 256602, 2006.
10. Sarma, S. D. and E. H. Hwang, *Phys. Rev. Lett.*, Vol. 81, 4216, 1998.



# Session 4P8a

## Advanced CEM Techniques

<a href="#">On the Analysis of Discrete-Time Electromagnetic Problems</a> <i>Hsi-Tseng Chou (Yuan Zi University, Taiwan); Shih-Chung Tuan (Oriental Institute of Technologies, Taiwan);</i> .....	914
<a href="#">Diagonalization of Translation Operators for Elastic Wave Equations</a> <i>Bo He (University of Illinois at Urbana-Champaign, USA); Weng Cho Chew (University of Illinois at Urbana-Champaign, USA);</i> .....	915
<a href="#">A Hybrid Finite/Boundary Element Method for Periodic Structures on Non-periodic Meshes Using an Interior Penalty Formulation</a> <i>Seung-Cheol Lee (The Ohio State University, USA); Vineet Rawat (The Ohio State University, USA); Jin-Fa Lee (The Ohio State University, USA);</i> .....	916
<a href="#">A Hybrid Technique for Combining Macro Basis Functions and AIM Approach</a> <i>Irene Ang (National University of Singapore, Singapore); Ban leong Ooi (National University of Singapore, Singapore);</i> .....	917

## On the Analysis of Discrete-Time Electromagnetic Problems

Hsi-Tseng Chou<sup>1</sup> and Shih-Chung Tuan<sup>2</sup>

<sup>1</sup>Department of Communications Eng., Yuan Ze University, Taiwan

<sup>2</sup>Department of Communications Eng., Oriental Institute of Technologies, Taiwan

**Abstract**— Numerical analysis of electromagnetic (EM) problems directly in time-domain (TD) for a general TD input pulse has attracted significant efforts for years such as finite difference time domain (FDTD) and TD integral equation. Those existing numerical techniques are generally referred as low frequency (LF) techniques because it suffers from cumbersome numerical inefficiency as the structure under consideration becomes extreme large. Since the general TD pulses are generally consisted of LF and HF (high frequencies) components, and thus it is of increasing interest to develop hybrid techniques that combines LF and HF techniques while in the mean time retaining the HF physical interpretation phenomena.

This paper presents studies based on the time discretization of TD Maxwell's equations (referred to Discrete-Time (DT) Maxwell's equations) and results in a scenario that allows the TD EM problems to be solved directly in TD via utilizing the existing FD (frequency domain) solutions in a hybrid fashion. The DT equations are matrix equations and created via the coefficients of a basis expansion on the TD pulses at any space locations. The coefficients become dependent on the space parameters of  $(x, y, z)$ , and make the DT equations analogous to FD equations. Examples will be presented to demonstrate the concepts of this work.

# Diagonalization of Translation Operators for Elastic Wave Equations

B. He<sup>1</sup> and W. C. Chew<sup>1,2</sup>

<sup>1</sup>Center for Computational Electromagnetics and Electromagnetics Laboratory  
Department of ECE, University of Illinois at Urbana-Champaign, Urbana, IL 61801, USA

<sup>2</sup>University of Hong Kong, Hong Kong, SAR, China

**Abstract**— Elastic wave equations are difficult to solve because they are composed of a longitudinal wave and transverse wave propagating at different speeds. Furthermore, for some boundary conditions, longitudinal waves produce transverse waves on reflection, and vice versa. This difficulty has been overcome by solving the integral formulation of the elastic waves. This integral formulation also facilitates the use of the fast multipole method (FMM) to solve the problems of elastic wave scattering.

The crucial step in the FMM for solving the wave equations is the diagonalization of the translation operators. Recently, the diagonalizations of the translation operators have been extended to vector and general tensor cases. It shows that the longitudinal waves and transverse waves are translated separately. Thus, the diagonalization of the translation operators of the longitudinal waves and transverse waves can be treated separately. However, since Hansen (vector) spherical harmonics and multipole fields are complete set, the translation operators of the longitudinal waves and transverse waves can be diagonalized simultaneously.

We introduce compact notations for Hansen spherical harmonics and multipole fields, which one can express the vector addition for elastic waves in terms of. We show that the dyadic Green's function of elastic wave equations can be factorized in terms of vector translators. Then, the derivation of diagonalization of translation operators for elastic wave equations is presented.

The diagonalization of the translation operators facilitate in applying FMM to study elastic wave propagation in complex media, in particular for some cases where large number of unknowns are needed.

## A Hybrid Finite/Boundary Element Method for Periodic Structures on Non-periodic Meshes Using an Interior Penalty Formulation

Seung-Cheol Lee, Vineet Rawat, and Jin-Fa Lee

Electro Science Lab., ECE Department, The Ohio State University, Columbus, OH 43210, USA

**Abstract**— Recent interests in analyzing/designing large finite arrays, frequency selective surfaces (FSS), and metamaterials speak volume of the need for a robust and efficient numerical method for arbitrary and inhomogeneous periodic structures in 3D. The development in general numerical methods for analyzing arbitrary 3-dimensional periodic structures is nothing new. Many existing literature has thoroughly addressing this issue, including the hybridization of finite and boundary element method utilizes the Ewald transform to quickly compute the needed periodic Green's function. However, most of the work on modeling periodic structures relies on the availability of periodic meshes. Although such a constraint may not seem much a burden in many problem geometries, however, the relief of such a constraint still contributes greatly to the flexibility of applying the computer codes to periodic structures. This attribute has been the focus of a few recent publications on using non-periodic meshes for analyzing periodic structures.

The technical difficulties remain in modeling periodic structures using non-period meshes can be broadly summarized into two: One is that none of the existing approaches is able to combine finite/boundary element methods on the non-periodic meshes, and, the other is an efficient matrix solution technique for the resulting matrix equations. We are reporting in this paper our attempt in hybridizing finite/boundary element methods for periodic structures using non-periodic meshes. The breakthrough came from the adoption of the classical interior penalty method, or the Nitsch mortar method. The details of the final formulation and its performances will be presented in full.

# A Hybrid Technique for Combining Macro Basis Functions and AIM Approach

Irene Ang and B. L. Ooi

National University of Singapore, Singapore

**Abstract**— The method of moments (MoM) has been widely used for the analysis of microstrip structures. However the conventional MoM using subsection basis functions becomes highly inefficient for the analysis of large or complex antennas and arrays. As the number of unknowns,  $N$  becomes very large, there will be a tremendous increase in time usage and memory, giving rise to dense matrices that are expensive to store and solve,  $O(N^2)$  memory and  $O(N^3)$  time. As the size of the system matrix increases, direct numerical technique bears progressive degradation of accuracy of the near-field solution.

To circumvent the computational difficulties, a number of works have been devoted to solve large scale problems. These include the fast multipole method (FMM), the adaptive integral method (AIM) and the conjugate-gradient fast Fourier transform method (CG-FFT). The recent development in fast algorithms use  $O(N \log N)$  memory and close to  $O(N \log N)$  time. These methods employ iteration solver which can lead to convergence difficulties when dealing with either very large scale or multi-scale features objects.

Recently, some methods such as subdomain multilevel approach with macro-basis functions (MBF) and sub-entire-domain (SED) basis function based on the concept of segmentation have been developed to solve large scale problems. Using MBF or SED basis functions, the number of unknowns can be reduced significantly. However the bottleneck of the method is the computation of the MoM matrices for interactions between all basis and testing functions located on different cells. Two methods have been reported to improve the MoM matrix filling. The first strategy is based on reducing MBFs to equivalent moments and the second strategy is based on Multipole expansions which is strongly dependence on the integral equation kernel.

In this paper, we present an efficient hybrid MBF-AIM approach to improve the computational speed. The interaction between basis and testing functions when sufficiently far apart can be carried out by using compressed representation through the AIM method. The compressed representation is obtained by constructing, for each individual original basis function, an auxiliary basis function representing collections of auxiliary pointlike sources located at nodes of a regular Cartesian grid, with strength chosen so as to approximate the far field. The procedures can be summarized as follows:

- All the cells are enclosed in identical rectangular grids.
- The MBFs and the testing functions on the cell are projected to the surrounding grids.
- The mutual coupling is then computed with the aid of fast Fourier transform.
- The computed mutual coupling is interpolated back to the elements on the cell.

Numerical result for a microstrip antenna array, a linear series-fed array and a bandpass filter will be presented to demonstrate the efficiency and accuracy of the proposed method.



# Session 4P8b

## Computational Electromagnetic Methods

<b>Finite Element Method Simulation of Photoinductive Imaging for Cracks</b>	
<i>Cheng-Chi Tai (National Cheng Kung University, Taiwan); Yen-Lin Pan (National Cheng Kung University, Taiwan);</i> .....	920
<b>A New Scheme of Spectral Integral in Low-frequency Fast Multipole Method</b>	
<i>Zu-Hui Ma (University of Electronic Science and Technology of China, China); Jun Hu (University of Electronic Science and Technology of China, China);</i> .....	921
<b>Equivalent Charge Formulation of the Multilevel Green's Function Interpolation Method for Capacitance Extraction in RFIC</b>	
<i>Y. F. Leung (City University of Hong Kong, China); Haogang Wang (Zhejiang University, China); Chi Hou Chan (City University of Hongkong, China);</i> .....	922
<b>Solving Scattering from Multiple Conducting Objects by Hybrid MLFMA with Generalized Forward-backward Method</b>	
<i>Rui Xi (University of Electronic Science and Technology of China, China); Jun Hu (University of Electronic Science and Technology of China, China);</i> .....	923
<b>Staggered-grid Pseudospectral Time Domain (PSTD) Method Using Real Fourier Transform for 2.5D Electromagnetic Wave Propagation</b>	
<i>Lanbo Liu (University of Connecticut, USA); Benjamin Barrowes (Cold Regions Research and Engineering Laboratory, USA); Zhao Zhao (University of Connecticut, USA);</i> .....	924
<b>Microscopic Biological Cell Level Model Using Modified Finite-difference Time-domain at Mobile Radio Frequencies</b>	
<i>Chan H. See (University of Bradford, UK); Raed A. Abd-Alhameed (University of Bradford, UK); Peter S. Excell (University of Bradford, UK); Dawei Zhou (University of Bradford, UK);</i> .....	925
<b>Generalized One-port Network Model for Arbitrarily-shaped Homogeneous Scatterers</b>	
<i>Gaobiao Xiao (Shanghai Jiao Tong University, China); Junfa Mao (Shanghai Jiao Tong University, China); Bin Yuan (Shanghai Jiaotong University, China);</i> .....	926
<b>A Hybrid of Genetic Algorithm and Particle Swarm Optimization for Antenna Design</b>	
<i>Wen Tao Li (Xidian University, China); L. Xu (Xidian University, China); Xiao Wei Shi (Xidian University, China);</i> .....	927
<b>Hydrodynamics Investigation of Ferrofluid Flows through Randomly Packed Beds in the Presence of an External Magnetic Field</b>	
<i>Arezou Jafari (Lappeenranta University of Technology, Finland); T. Tynjala (Lappeenranta University of Technology, Finland); S. M. Mousavi (Sharif University of Technology, Iran); P. Sarkomaa (Lappeenranta University of Technology, Finland);</i> .....	928

# Finite Element Method Simulation of Photoinductive Imaging for Cracks

Cheng-Chi Tai and Yen-Lin Pan

Department of Electrical Engineering, National Cheng Kung University, Tainan, Taiwan

**Abstract**— Crack sizing is a critical issue in quantitative nondestructive evaluation (NDE). The ultrasonic method is used predominantly to detect subsurface discontinuities, while the eddy current (EC) method is effective for surface cracks. One main disadvantage of conventional eddy current methods is the low spatial resolution, which is limited by the size of eddy current probes. The photoinductive imaging (PI) method is a hybrid NDE technique that combines eddy current and laser-based thermal wave methods. The use of a focused laser beam provides the method with a microscopic resolution while using eddy current pickup sensors.

Photoinductive mapping of eddy current fields interacting with cracks is a newly devised technique that is similar to photothermal (PT) imaging. The photothermal effect is the generation of thermal waves in a given medium under illumination by an intensity-modulated light flux. Measuring the magnitude of the PT effect yields information on the material's structure due to the interaction of thermal waves with the material. A focused laser beam generates a localized hot spot on the specimen surface, causing a local change of electrical conductivity and/or permeability, which can be detected by a nearby eddy current coil through its impedance changes.

In this paper, the numerical simulations of PI imaging method have been performed with the 2D transient using the finite element method (FEM) to characterize corner cracks at the edge of a bolt hole. The PI imaging results have higher spatial resolution in the area of the defect in 2D models as compared with the conventional EC images. The FEM simulation results of 0.25-mm, 0.50-mm, and 0.75-mm rectangular defects are showed and analyzed. The dependencies of PI signals on EC frequencies and temperature of the thermal spot are also examined. The results demonstrate that the PI method is applicable to examine the geometric shape of corner cracks.



# A New Scheme of Spectral Integral in Low-frequency Fast Multipole Method

Zu-Hui Ma and Jun Hu

College of Electronic Engineering

University of Electronic Science and Technology of China

Chengdu 610054, China

**Abstract**— The method of moments is the most widely used tool for electromagnetic scattering problems, it has the advantages of high accuracy, versatility, and the ability to compute near-zone as well as far-zone parameters. However, it lead to large dense linear system and needs huge computational costs.

The fast multipole method (FMM) is very efficient for solving electrically large scattering and radiation problems. There are two different version about FMM. One is developed by Prof. Rokhlin, based on the multipole expansion of the Green function, the other is based on the plane-wave expansion of the Green function, proposed by Prof. W. C. Chew. However, because the asymptotic behaviors of the spherical Hankel and spherical Bessel functions with small arguments would result in large errors, the dynamic FMM and MLFMA proposed by Chew cannot be applied directly at low frequencies.

There are at least two different ways to implement the FMM in low-frequency regime: one is based multipole-series, the other one is based the spectral representation, or the low-frequency stable inhomogeneous plane-wave expansion, of the Green function .

The FMM based spectral representation of the Green function is stable at all frequency, but unfortunately, the representation is direction dependent. So, we need to split the translation procedures into six directions(+z, -z, +y, -y, +x, -x), and consider each direction separately. In order to expedite matrix-vector product, data of all six directions are needed to storage. We propose a new scheme of integral rule. Using the scheme, we can reduce a half of memory consumption in the aggregation and disaggregation. Numerical results show the validity and efficiency of the present method.

# Equivalent Charge Formulation of the Multilevel Green's Function Interpolation Method for Capacitance Extraction in RFIC

Y. F. Leung<sup>1</sup>, Haogang Wang<sup>2</sup>, and Chi Hou Chan<sup>1</sup>

<sup>1</sup>Wireless Communication Research Center, City University of Hong Kong, Hong Kong SAR, China

<sup>2</sup>Electromagnetics Academy, Zhejiang University, Hangzhou, China

**Abstract**— This paper presents a computational and memory efficient method for capacitance extraction of three-dimensional structures in radio-frequency integrated circuits (RFICs). The method is based on the equivalent charge formulation (ECF) in which the resulting method-of-moments (MoM) matrix is solved using the recently developed multilevel Green's function interpolation method (MLGFM) that has an  $O(N)$  computational complexity.

In ECF, a free-space Green's function approach is adopted in which arbitrarily shaped dielectric interfaces with moderate permittivity ratios and conducting traces can be modeled with relative ease. For complicated RFIC capacitance extraction, the difficulty in solving a large MoM matrix is alleviated by using the fast matrix-vector-multiplication scheme MLGFM in which a hierarchical partitioning is applied in such a way that only the computation of influences of the interpolation points of a cube to those of another cube is required. The interpolation is effectively carried out using the orthonormal inverse multi-quadric radial basis functions even when the number of interpolation points is small. These interpolation functions are particularly useful as we have employed a staggered interpolation grid that comprises two interpolation grids with different grid sizes. The number of levels of partitioning depends on the complexity and number of unknowns of the problems at hand. The larger the number of unknowns, the higher the level of partitioning; and this would result in more savings in computer memory requirement and CPU time for each matrix-vector multiplication.

In this paper, several examples are analyzed and compared with published results whenever available. These include coupled transmission lines with and without an air bridge, crossing buses and fractal capacitors. The number of unknowns varies from tens of thousands to four hundred thousands. Our simulation results indicate that the combination scheme of ECF and MLGFM provides a flexible, accurate and efficient analysis approach which has a complexity of  $O(N)$  for capacitance extraction of three-dimensional RFIC structures.

## ACKNOWLEDGMENT

The work presented in this paper is supported by the Hong Kong Research Grant Council, Grant CityU 110606.

## Solving Scattering from Multiple Conducting Objects by Hybrid MLFMA with Generalized Forward-backward Method

Rui Xi and Jun Hu

University of Electronic Science and Technology of China, Chengdu 610054, China

**Abstract**— To speed up the solution of scattering from multiple conducting objects with complex structures, a hybrid MLFMA with generalized forward-backward method is developed. The region involving multiple conducting objects is divided into finite uniform sub-regions. The induced current in each sub-region is solved by GFB method. Different from traditional multi-region iterative (MRI), only the coupling in the forward or backward direction is taken into account. The interaction between sub-regions and the induced current in each sub-region are computed by the MLFMA. The present method has the memory requirement of  $O(N_{\max} \log N_{\max})$ , where  $N_{\max}$  is the maximum value among the number of unknowns in these regions. The GFB method is shown to provide accurate results while maintaining the efficiency and fast convergence of the conventional FB method. Some numerical results demonstrate the efficiency and accuracy of the present method for complex scattering problems. An airplane array model is calculated by MRI combined with GFB method. It has 425,520 unknowns. The memory requirement is about 870 MB with MRI method, 3,018 MB with traditional MLFMA. The MRI method hybrid MLFMA with GFB method can further accelerate the convergence. Using this iterative method, a large multiple conducting objects can be solved with less memory requirement.

# Staggered-grid Pseudospectral Time Domain (PSTD) Method Using Real Fourier Transform for 2.5D Electromagnetic Wave Propagation

Lanbo Liu<sup>1,2</sup>, Benjamin Barrowes<sup>2</sup>, and Zhao Zhao<sup>1</sup>

<sup>1</sup>Department of Civil & Environmental Engineering, University of Connecticut, USA

<sup>2</sup>Cold Regions Research and Engineering Laboratory, USA

**Abstract**— In the published literature in pseudospectral time domain (PSTD) simulation for the propagation of electromagnetic waves, the discretized grids for the electric field and the magnetic field are not staggered for simplicity. In contrast, the staggered grid approached gained wide popularity in the original finite difference time domain (FDTD) method such as the done in the famous Yee's approach.

Nevertheless, using staggered grid to the pseudospectral scheme will make the time marching more stable and the numerical dispersion much suppressed for models with large contrast in material properties. Thus it is highly desirable for models with high material contrasts. To the best of the author's knowledge, amount those published papers, no detailed discussion on the application of the staggered grid PSTD to model the electromagnetic wave propagations. The staggered grid scheme is realized by shifting and makes the Nyquist wave number a non-zero pure real value of  $-\pi/\Delta x$ . By doing this the Nyquist information of the original spatial function is preserved and makes the differentiation operator more stable. In the Fourier domain, adding trigonometric factors in the classic Fourier coefficients is equivalent to the staggered grid approach in the original space domain [Zhao et al. 2001]. We will discuss this approach and apply it to model a situation of a mobile subsurface discrimination system.

# Microscopic Biological Cell Level Model Using Modified Finite-difference Time-domain at Mobile Radio Frequencies

C. H. See, R. A. Abd-Alhameed, P. S. Excell, and D. Zhou

Mobile and Satellite Communications Research Centre, University of Bradford  
Richmond Road, Bradford, West Yorkshire, BD7 1DP, UK

**Abstract**— The presented paper demonstrates the modelling of the interaction mechanism between the biological tissues and electromagnetic field at mobile communication frequency by implementing modified FDTD numerical method. By adopting frequency scaled FDTD with floquet periodic boundary conditions and modified PMLs [1,2], microdosimetric modelling of bioelectromagnetic interactions at cellular level, is established. In order to include the membrane effect on the biological tissues model in the analysis, the LE-FDTD is exploited to embed the lumped element cell-membrane model on the surface of the proposed tissue model in the FDTD computational domain.

Two different types of the biological tissue are modelled, which are made by a cluster of cubical and cylindrical cells respectively. Floquet periodic boundary conditions are imposed on the proposed model to imitate the effect of periodic replication of the assemblages. Thus, the analysis of a large structure of cells is made more computationally efficient than the modeling of the entire structure. The total fields of the simulated structures are shown to give reasonable and stable results at 900 MHz, 1800 MHz and 2450 MHz. This leads to the conclusion that the application of the lumped element model allows cells of arbitrary geometries to be handled and demonstrates the viability of embedding other types of lumped-element model for membrane function. Moreover, use of the Floquet boundary condition enables a non-trivial region of connected biological tissue to be simulated. Such a tool will facilitate deeper investigation of the phenomena in the interaction between EM fields and biological systems at various levels of spatial definition.

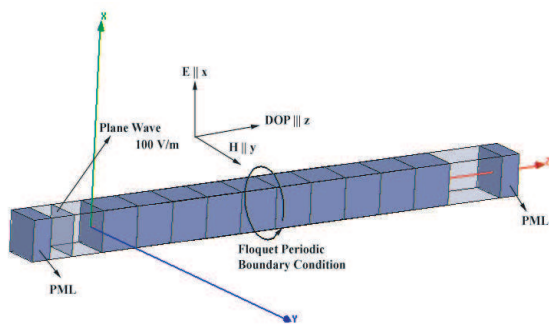


Figure 1: The 3D view of the simulated cubical biological structures in FDTD computational domain.

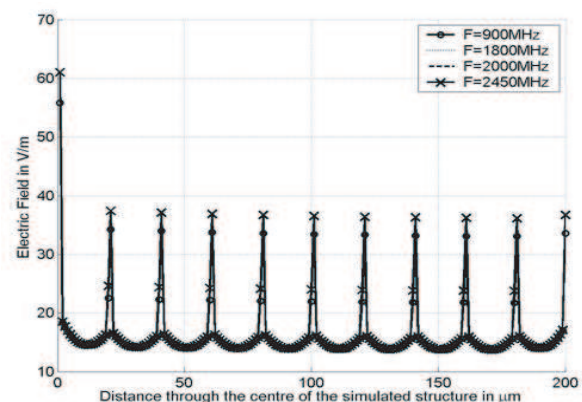


Figure 2: Penetration of Electric Field along  $z$  axis, through the centre of the simulated structure

## REFERENCES

1. Emili, G., A. Schiavoni, F. L. Roselli, and R. Sorrentino, "Computation of electromagnetic field inside a tissue at mobile communications frequencies," *IEEE Trans. on MTT*, Vol. 51, 178–186, 2003.
2. See, C. H., R. A. Abd-Alhameed, and P. S. Excell, "Electromagnetic modelling biological tissues equivalent cluster of spheres using LE-FDTD," accepted to be published in *International Union of Radio Science (URSI) Conference*, New Delhi, India, October 23–29, 2005.

# Generalized One-port Network Model for Arbitrarily-shaped Homogeneous Scatterers

Gaobiao Xiao, Junfa Mao, and Bin Yuan  
Shanghai JiaoTong University, China

**Abstract**— A large scale scattering system usually consists of a lot of individual scatterers with various shapes, structures and materials. To solve the corresponding scattering problem as a whole is a difficult work that always challenges our computation ability. An alternative method is to divide the system into building blocks at first, then solve the scattering problem of each building block independently, and finally combine the scattering characteristics of all buildings blocks to get the whole scattering characteristics. This paper presents a generalized one-port model for each building blocks. Each building block is associated with a generalized port parameter, with can characterize the scattering characteristics of the scatterer with required accuracy. The reference surface of the port is originally selected to be the surface of the scatterer with normal unit vector pointing outwardly. By analogous to network theory, if the scatterer is surrounded by homogeneous media, the reference surface can also be moved from the surface of the scatterer to a regular-shaped surface in the homogeneous media. The network port parameters defined in different reference surfaces can be easily transformed from each other. Therefore, arbitrarily-shaped scatterers can be handled efficiently by using their associated network parameters defined on regular shaped reference surfaces. When two building blocks are placed in a homogeneous environment, interaction exists and the system can be handled using an equivalent circuit model: two one-port devices connected by a segment of generalized transmission. In this manner, a large scale scattering system can be equivalent to a network circuit with many generalized one-port devices connected with generalized transmission lines. The total scattering fields can be obtained by network circuit analysis technique.

A formulation of boundary integral equation system based from Huygens' principle is revisited and port variables are defined proportional to the rotated tangential field components. Numerical examples for building blocks of 2-D homogeneous dielectric and perfect conducting scatters are provided, which show that the presented method is effective.

# A Hybrid of Genetic Algorithm and Particle Swarm Optimization for Antenna Design

W. T. Li, L. Xu, and X. W. Shi

National Key Laboratory of Antenna and Microwave Technology, Xidian University  
Xi'an 710071, China

**Abstract**— In this paper, a new effective optimization algorithm called PGHA is presented, which combines in the most effective way the properties of two of the most popular evolutionary optimization approaches now in use for the optimization of electromagnetic structures, the Particle Swarm Optimization (PSO) and Genetic Algorithms (GA). In order to overcome the drawbacks of standard particle swarm optimization and genetic algorithm, such as prematurity and easily trapping in local optimum, some improved genetic mechanisms based on non-linear ranking selection, competition and selection among several crossover offspring and adaptive change of mutation scaling are adopted in the paper. In the algorithm the new population is produced through three approaches, which are elitist strategy, improved PSO strategy and the improved genetic algorithm strategy. This algorithm is essentially, as PSO and GA, a population-based heuristic search technique, which can be used to solve combinatorial optimization problems. The key feature of this algorithm is that it maintains the integration of GA and PSO for the entire run. In each iteration the population is divided into two parts which are evolved with the two techniques respectively. The two different parts are then recombined in the updated population for the next iteration, and after that the new population is again divided randomly in the next runs, to take advantage of both genetic and particle swarm operators, so while speeding up the convergence process, this algorithm can avoid premature effectively. Furthermore, the proposed algorithm is successfully applied to design the line array with ten elements and the circle array with thirty one elements and obtain the desired beam forms. We try to use a modified Bernstein polynomial to reduce the number of variables when calculating the circle array, and simulation results show the abroad foreground of PGHA in the antenna array design.

# Hydrodynamics Investigation of Ferrofluid Flows through Randomly Packed Beds in the Presence of an External Magnetic Field

A. Jafari<sup>1</sup>, T. Tynjälä<sup>1</sup>, S. M. Mousavi<sup>2,3</sup>, and P. Sarkomaa<sup>1</sup>

<sup>1</sup>Laboratory of Engineering Thermodynamics, Lappeenranta University of Technology  
53850, Lappeenranta, Finland

<sup>2</sup>Department of Chemical and Petroleum Engineering, Sharif University of Technology, Tehran, Iran

<sup>3</sup>Department of Chemical Engineering, Lappeenranta University of Technology  
53850, Lappeenranta, Finland

**Abstract**— Ferrofluids are suspension of single domain particles of magnetic materials in a carrier liquid [1]. Flow of ferrofluids through porous media is poorly considered in the literature and it was restricted to Darcy flow regime [2]. Therefore hydrodynamics investigation of a Kerosene-based ferrofluid flows through random packing of non-overlapping spheres in a cylindrical geometry (Fig. 1) and at different regimes (Darcy and post Darcy) is simulated in this attempt. Commercial computational fluid dynamics package (FLUENT) was used to solve governing equations, and a user defined function was implemented on the software to apply an external magnetic field. It is assumed that the ferrofluid treats as an isothermal and incompressible single-phase Newtonian fluid. Different magnetic fields strengths in different directions (parallel and perpendicular to the flow) were used in the system. Numerical results illustrate that compare to the field free case, in the presence of magnetic field the transport processes will enhance. This makes ferrofluids find a variety of applications in various fields. In addition it is found that the magnetic field mitigates wall channeling.

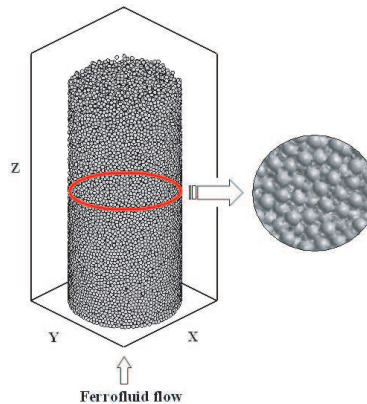


Figure 1: Particles configuration for the simulations.

## REFERENCES

1. Tynjälä, T., "Theoretical and numerical study of thermomagnetic convection in magnetic fluids," PhD Thesis, Lappeenranta University of Technology press, Finland, 2005.
2. Larachi, F., "Ferrofluid induced-field effects in inhomogeneous porous media under linear-gradient dc magnetic fields," *Chemical Engineering and Processing*, Vol. 46, No. 8, 729–735, 2007.



# Session 5A1

## Nano Scale Electromagnetics, MEMS

<b>Fabrication and Analysis of Valve-less Micro Pumps</b>	
<i>Nan-Chyuan Tsai (National Cheng Kung University, Taiwan); Wei-Ming Huang (National Cheng Kung University, Taiwan); Chao-Wen Chiang (National Cheng Kung University, Taiwan); Rong-Mao Lee (National Cheng Kung University, Taiwan);</i>	930
<b>Ray-optical Negative Refraction and Local Ray Rotation with Microprism Structures</b>	
<i>Johannes Courtial (University of Glasgow, UK); J. Nelson (University of Glasgow, UK);</i>	931
<b>Performance and Dynamic Characteristics of Diamagnetic Bearings in Micro Systems</b>	
<i>Jie-Yu Chen (Shanghai Jiao Tong University, China); Jian-Bin Zhou (Shanghai Jiao Tong University, China); Guang Meng (Shanghai Jiao Tong University, China);</i>	932
<b>RF MEMS Extended Tuning Range Varactor and Varactor Based True Time Delay Line Design</b>	
<i>Yaping Liang (University of California, USA); Calvin W. Domier (University of California, USA); Neville C. Luhmann, Jr. (University of California, USA);</i>	933
<b>Free Energy Surface of Protein Folding Determined Using Single-molecule Force Spectroscopy</b>	
<i>Ching-Hwa Kiang (Rice University, USA);</i>	934
<b>Designing Environmentally Responsive Drug Carriers</b>	
<i>Jiunn-Ren Roan (National Chung Hsing University, Taiwan);</i>	935
<b>Au Nanowire Arrays for Negative Index Metamaterial Applications</b>	
<i>Latika Menon (Northeastern University, USA); W. Lu (Northeastern University, USA); S. Bennett (Northeastern University, USA); D. Heiman (Northeastern University, USA); S. Sridhar (Northeastern University, USA);</i>	936
<b>Coupled Magnetic Plasmon Modes in Chains of Metallic Trilayer Structures</b>	
<i>Shu-Ming Wang (Nanjing University, China); T. Li (Nanjing University, China); H. Liu (Nanjing University, China); F. M. Wang (Nanjing University, China); S. N. Zhu (Nanjing University, China);</i>	937
<b>Optical Transmission through Nanostructured Metal/Dielectric Multilayers</b>	
<i>Zi-Jian Zhang (Nanjing University, China); Z. H. Tang (Nanjing University, China); Ru-Wen Peng (Nanjing University, China); Z. Wang (Nanjing University, China); Xin Wu (Nanjing University, China); Wei-Hua Sun (Nanjing University, China); Mu Wang (Nanjing University, China);</i>	938
<b>Playing with Optical Tweezers Forces Induced on Structured Micro-nano Objects</b>	
<i>Jean-Pierre Galaup (Universite Paris XI, France); Mariela Rodriguez-Otazo (Universite Paris XI, France);</i>	939

## Fabrication and Analysis of Valve-less Micro Pumps

Nan-Chyuan Tsai, Wei-Ming Huang, Chao-Wen Chiang, and Rong-Mao Lee

Department of Mechanical Engineering, National Cheng Kung University

No. 1, University Road, Tainan 70101, Taiwan

**Abstract**— Due to dramatic progress in microfluidic devices and their applications, the development of microfluidic systems become more and more pertinent in recent years, such as fluidic activation devices, micro-sensors and micro-pumps. In this research, micro-electro-mechanical fabrication technologies are employed to fabricate an innovative valve-less micro-pump under magnetic control. The micro-coil is fabricated by electroforming and utilized to generate control force. *Prior to* fabrication of micro-pump, commercial software *CFD-RC* and *ANSOFT* are used first to simulate the performance of the designed micro-pump. *CFD-RC* is to observe the flow field and pressure in the micro-channel, and *ANSOFT* to evaluate if the magnetic force is sufficient enough to activate the membrane of the micro-pump. Finally, the micro-pump is equipped with a personal computer, in which *dSPACE* simulation module *DS1104* is embedded, to realize the closed-loop micro-system.

# Ray-optical Negative Refraction and Local Ray Rotation with Microprism Structures

J. Courtial and J. Nelson

Department of Physics and Astronomy, University of Glasgow, UK

**Abstract**— Metamaterials are arrays of simple optical components that have been miniaturized to a scale where they act as a homogeneous medium. In standard metamaterials, the simple optical component is a resonant electro-magnetic circuit; the scale below which they start to behave as a homogeneous medium is the wavelength scale. We investigate here arrays of Dove prisms that have been miniaturized below the scale where only the change in ray direction is relevant. In the sense of the above definition, this would make such arrays ray-optical metamaterials.

Dove prisms have the property of reflecting the direction of incoming light rays with respect to a plane through the prism. They also offset the ray position on the scale of the prism's aperture. In principle, the entire prism, and with it its aperture, can always be miniaturized until an offset of the ray position becomes irrelevant for the intended application. The change in ray direction is not affected by this miniaturization. A two-dimensional array of sufficiently miniaturized and suitably oriented Dove prisms then reflects the local ray direction with respect to the normal to the array.

We investigate here the imaging properties of Dove-prism arrays, on their own and in combination with other Dove-prism arrays. We find that their optical properties are highly unusual. Specifically, combinations of Dove-prism arrays can act like the interface between optical media with equal but opposite refractive indices. (The same effect has previously been achieved with GRIN-lenslet arrays [F. Okano and J. Arai, *Appl. Opt.* 41, 4140 (2002)]. In reflection, a similar effect can be achieved with an array of miniaturized corner-cube reflectors.) and exhibit pseudoscopic imaging (that is, they make nearer objects appear further away than objects that actually are further away). Different combinations of Dove-prism arrays can rotate the local ray direction through arbitrary angles around the normal to the array plane.

We will demonstrate these very unusual properties here with movies that simulate the view through Dove-prism arrays.

# Performance and Dynamic Characteristics of Diamagnetic Bearings in Micro Systems

Jie-Yu Chen, Jian-Bin Zhou, and Guang Meng

State Key Laboratory of Mechanical System and Vibration, Shanghai Jiao Tong University  
800 Dongchuan Road, Shanghai 200240, China

**Abstract**— The limitation of friction loss in bearings for micro-engineered systems which contain moving components is a great engineering challenge. At the micro scale, the tribology and the subsequent wear and rub impact severely on the system operation, especially for high speed rotational machines. Therefore non-contact bearings are essential to achieve desirable performance of the device. The cube-square law dictates that fluidic bearings have comparatively high specific load capacity. But the major drawbacks of these bearings are that hydrostatic bearings require connections to external sources of pressurized gas, while hydrodynamic bearings cannot respond to varying loading conditions without adjusting the speed of the rotor. For electromagnetic approach, the electrostatic or permanent magnetic bearings need to be in combination with displacement sensors so as to achieve close loop control of the system. The high-frequency response of the device and the dearth of the sensor dynamics database make active bearings less attractive at the micro scale.

As an alternative candidate to address this issue, this paper presents investigation into the diamagnetic bearing, which figures patterned micro-permanent magnets array as the stator and diamagnetic disk as the rotor. There is little research being done on the use of diamagnetic material such as bismuth or graphite in the magnetic bearings compared to the use of superconductors. This is mainly because the stability provided by the diamagnetic material at the macro scale is not strong enough. However, scale reduction laws for magnetism indicate that diamagnetism is highly efficient for magnetic MEMS. Also, this simple configuration does not need energy supply and is stable at some geometric parameters space at room temperature, thereby leading to a compact passive solution that might be suitable for some applications.

We study the performance of the diamagnetic bearing in terms of the load-carrying capacity, the associated axial, lateral and tilting stiffness and also the necessary PM array configuration so as to ensure three dimensional stability of the bearing. And then we investigate the linear and nonlinear vibrational characteristics of the bearing. The intrinsic small damping of the mechanism implicates that complicated phenomena of dynamics due to nonlinearity in its magnetic force may occur. We specifically focus on the parametric resonances induced by the nonlinear cross-coupling between the vibrational modes in the vertical, lateral and inclinational directions. Results obtained show that even if the system is stable in the linear sense, it can undergo severe instability owing to the small stiffness and the nonlinearity of the system at some parametric spaces. Therefore, this research may serve as useful guidelines for design optimization of diamagnetic bearing-enabled MEMS.

## RF MEMS Extended Tuning Range Varactor and Varactor Based True Time Delay Line Design

Yaping Liang<sup>1</sup>, C. W. Domier<sup>2</sup>, and N. C. Luhmann, Jr.<sup>2</sup>

<sup>1</sup>Department of Electronics and Information Engineering, Hangzhou Dianzi University, China

<sup>2</sup>Department of Applied Science, University of California, Davis, USA

**Abstract**— MEMS varactors are one of the important passive MEMS devices. Their applications include use in VCOs, tunable impedance matching networks, tunable filters, phase shifters, and true time delay lines. The shunt capacitive structure has been employed in most of the conventional MEMS varactors designs because of its simplicity. However, the capacitance ratio of this conventional shunt capacitive MEMS varactor is limited to 1.5 because of the MEMS Pull-In effect, which happens when the deflection between the MEMS top and bottom metal plates increase beyond 1/3 of the whole airgap of the two metal plates. At that time, the top metal plate will quickly snap down. This effect is the major limitation in MEMS varactor designs and can cause nonlinearity and mechanically instability. In order to eliminate this Pull-In effect, the author employed the so-called MEMS extended tuning range structure. This structure, utilizes a variable height top metal beam with separate actuation parts. The airgap between the center part of the top beam and the bottom plate has been designed to be smaller than 1/3 of the airgap between the top beam and the bottom actuation pads. When DC bias is applied to the actuation parts, the entire top beam will move down together. Consequently, before the Pull-In effect happens at the actuation parts, the center part has already traveled through its entire tuning range, which means that the capacitance ratio of this kind of MEMS varactor can go to infinity.

A fabrication process on GaAs substrate has been designed based on the surface micromachining technology. The maximum capacitance ratio of the designed MEMS extended tuning range varactor is 5.39 with a  $C_{\max}$  value of 167 fF. Based on this MEMS varactor design, a Ka-band MEMS varactor based distributed true time delay line has been designed. This distributed true time delay line includes a high impedance CPW transmission line with  $70\ \Omega$  unloaded impedance at 28 GHz and eight MEMS extended tuning range varactors based on the varactor design periodically loaded on the CPW line. The testing results show that a  $56^\circ$  phase delay variation has been achieved at 28 GHz. The measured insertion loss at 28 GHz is  $-1.07$  dB at the up-state and  $-2.36$  dB at the down-state. The measured return losses,  $S_{11}$  and  $S_{22}$ , are both below  $-15$  dB at 28 GHz and below  $-10$  dB over the entire tested frequency range of 5 GHz to 40 GHz.

## Free Energy Surface of Protein Folding Determined Using Single-molecule Force Spectroscopy

Ching-Hwa Kiang

Department of Physics & Astronomy, Rice University, USA

**Abstract**— The development of precision tools to measure the dynamic response of single molecules to mechanical forces allows one to probe molecular interactions at the nanometer scale. We used the atomic force microscope to manipulate and unfold individual molecules of titin I27 domain and to reconstruct its free energy surface using Jarzynski's equality. The free energy surface for both the stretching and unfolding was reconstructed, and the unfolding free energy barrier was determined.

## Designing Environmentally Responsive Drug Carriers

**Jiunn-Ren Roan**

Department of Physics, National Chung Hsing University, Taiwan

**Abstract**— Drug carriers that can respond to local physiological changes are of great interest to biomedical and pharmaceutical research. Although much progress has been made in recent years, it remains rather difficult, if not impossible, to manufacture such carriers with pre-designated responsive polymorphism. This contribution will discuss and demonstrate by computer simulations how this may be accomplished.

It has been recognized for some time that drug carriers coated with certain polymers such as PEG can escape immune clearance and thus circulate in the bloodstream for a prolonged period of time. A major class of polymer-coated carriers is liposomes formed by amphiphilic block copolymers. In all cases the block copolymers employed are of the same type, leaving the world of mixed-copolymer liposomes unexplored. Here I consider two types of block copolymers, A-C and B-C, in which A and B are hydrophilic but mutually immiscible and C is hydrophobic. In a mixed aqueous solution of A-C and B-C, a typical liposome will contain both, with the C blocks inside being shielded from water by a surface coat composed of A and B. The immiscibility causes the two surface blocks to undergo phase separation, dividing the surface coat into A-rich and B-rich domains.

Computer simulations demonstrate that there are several structure transition sequences that can be induced by varying composition or block length. This shows that liposomes formed by mixed block copolymers will adapt their surface structures to local physiological environment. It also shows that one may pre-designate on these liposomes a specific sequence of structure transitions.

## Au Nanowire Arrays for Negative Index Metamaterial Applications

L. Menon, W. Lu, S. Bennett, D. Heiman, and S. Sridhar

Northeastern University, USA

**Abstract**— Nanowire arrays of metals such as gold and silver electrodeposited in dielectrics such as aluminum oxide are highly interesting, particularly with respect to their plasmonic properties. We have prepared nanowire arrays of gold and silver inside nanoporous alumina templates by means of electrodeposition. The aspect ratio (diameter and length) of the wires are controlled by adjusting the electrodeposition conditions. From transmission and reflection spectra, we have calculated the absorption spectra of such metal-dielectric structures as a function of varying wire dimensions and for varying angles of incidence. Transverse and longitudinal surface plasmon resonance peaks are observed in the absorption and the peak intensity and position is seen to depend strongly on wire dimensions and angle of incidence — consistent with modeling results obtained in our laboratory.



## Coupled Magnetic Plasmon Modes in Chains of Metallic Trilayer Structures

S. M. Wang, T. Li, H. Liu, F. M. Wang, and S. N. Zhu

National Laboratory of Solid State Microstructures  
Nanjing University, Nanjing 210093, China

**Abstract**— Sub-wavelength waveguides made of chains of noble metal nanoparticles have attracted considerable attention recently. Because of the strong coupling of surface plasmon resonances of the nanoparticles, electromagnetic field is highly confined around the chains. In this work, the coupled magnetic plasmon modes have been investigated theoretically in periodic chains of metallic trilayer nanostructure (nanoburger). We have employed the Fourier Transformation method and directly observe the magnetic Plasmon modes excited in these chains from the Fourier Transformation map. It is observed that different magnetic plasmon modes are excited in the chain with different exciting sources, which gives out a lot of physics about the system. The propagating lengths of the magnetic field in the chains have also been investigated. For their long propagating lengths, these chains can well work as waveguides to transport magnetic field. And by changing the parameters of these chains, one can easily tune the frequency region and band width of the magnetic plasmon modes.

Besides of making a sub-wavelength waveguide, the chain of nanoburgers with the interparticle spacing between nanoburgers linearly increasing can even work as a selective switch. This kind of graded nanoburger chain sustains different types of localizations of magnetic field at different frequency regions. Therefore, one can precisely control the region that magnetic field can reach in the chain. By applying this property, one can easily guide the magnetic field to different ports of the switch with different frequencies, which may have potential application in the integrate Optics and Plasmonics. The working frequency can also be tuned by changing the parameters of the chain.

## Optical Transmission through Nanostructured Metal/Dielectric Multilayers

Zi-Jian Zhang, Z. H. Tang, R. W. Peng, Z. Wang, X. Wu, W. H. Sun, and Mu Wang

National Laboratory of Solid State Microstructures and Department of Physics

Nanjing University, Nanjing 210093, China

**Abstract**— In 1998, Ebbesen et al. reported the extraordinary optical transmission (EOT) through a two-dimensional (2D) array of sub-wavelength holes perforated on silver film. It is found that the EOT in the sub-wavelength holes originates from the surface plasmon in resonance with the lattice structure. In this work, we demonstrate here that transmission optical enhancement originates not only from surface plasmons (SPs) but also from the coupling of SPs on the silver film perforated with a periodic array of subwavelength holes. We fabricate samples by coating films with magnetron sputtering then drilling holes with focused-ion-beam facility. The optical measurements are in good agreement with numerical calculations. It is shown that the coupling of SPs strongly depends on the detailed structure, and in our system the coupled SPs can be characterized by using an effective-permittivity model. In the sandwiched structure with nanostructured silver, the coupling of SPs leads to the shift of transmission peaks. While in a nanostructured silver and silicon oxide multilayer, the coupling of SPs yields a new resonant mode with increased quality factor of the transmission peak, which originates from multiple scatterings and the coupling of electromagnetic waves on the interfaces of the multilayers. These properties may be utilized to tune electromagnetic wave in subwavelength optics.

### ACKNOWLEDGMENT

This work is supported by the grant from National Natural Science Foundation of China.

# Playing with Optical Tweezers Forces Induced on Structured Micro-nano Objects

Jean-Pierre Galaup<sup>1</sup> and Mariela Rodriguez-Otazo<sup>1,2</sup>

<sup>1</sup>Laboratoire Aimé Cotton, CNRS UPR 3321 & Université Paris XI, Bat. 505, 91405 Orsay cedex, France

<sup>2</sup>Centro de Aplicaciones Tecnológicas (CEADEN) & Instituto Superior de Tecnologías, Avanzadas (InSTEC), La Habana, Cuba

**Abstract**— Two main problems concerned with the use of optical forces for manipulating micro sized objects are addressed.

One problem arises if one wants to work with the smallest objects as possible as the trapping force decreases with the size of the dielectric particle. Situation is opposite with metallic beads as they are known to experience enhanced optical strengths for a given size, therefore the use of hybrid particles with a metallic core and a dielectric envelope which could also be functionalized shall present many attractive possibilities.

Trapping forces have been evaluated for different type of objects: 1  $\mu\text{m}$  latex sphere, 400 nm silica grains and 100 nm hybrid particles where a 50 nm metallic core (gold) is embedded in silica. The beads were immersed in water.

The second problem concerns the manipulation of non-spherical object which is not fully understood. Single crystals of the organic molecule NBD-C8 were prepared by the reprecipitation method with typical size of  $10 \times 3 \times 0.2 \mu\text{m}^3$ . These crystals are fluorescent. An interesting aim would be to control the crystal growth of a unique single crystal trapped in an optical tweezers with polarized light.

Main conclusions of this work are:

- 1) For structured colloidal particles: (i) efficient trapping even on the smallest particles with a gold core has been revealed and complete 3D control has been demonstrated; (ii) trapping forces are in the range of 1.2 to 1.4 pN for the three studied particles and a incoming laser power of about 10 mW; (iii) the efficiency of the trapping increases with the laser power output for all studied particles although the rate of increase of this efficiency differs. The trapping efficiency reaches a saturation level. More work is still needed to make more effective the comparison by using particles with the same diameter and outer composition, just differing by their internal structure.
- 2) For organics micro-crystals: (i) the crystals are oriented in the direction of the linearly polarized light. (ii) with circularly or elliptically polarized light, the crystals are put on rotation with frequencies approaching several hundred Hz. (iii) The rotation frequency reaches a maximum value and then decreases irreversibly. This last point is not precisely understood and deserves more future work.

## ACKNOWLEDGMENT

This work is part of the PhD thesis in progress of M. R.-O.



# Session 5A2

## Optics and Photonics, Quantum Well Devices and Technology

<b>Conductance and Wave Impedance of Electrons</b>	
<i>Raphael Tsu (University of North Carolina at Charlotte, USA); Timir Datta (University of South Carolina, USA);</i> .....	942
<b>A New Definition of Capacitance of Few Electron Systems</b>	
<i>Tim LaFave Jr. (University of Iowa, USA); Raphael Tsu (University of North Carolina at Charlotte, USA);</i> .....	943
<b>Macroscopic Quantum Electrodynamics in Linear Media — the Green Tensor of Maxwell’s Equations in Quantum Optics</b>	
<i>Stefan Scheel (Imperial College London, United Kingdom);</i> .....	944
<b>Quantum Wires and Field Theory</b>	
<i>B. Bellazzini (INFN and Scuola Normale Superiore, Italy); M. Mintchev (Università di Pisa, Italy); Paul Sorba (University de Savoie, France);</i> .....	945
<b>Modulation Spectroscopy Study of Arsenic-doped Narrow-gap HgCdTe Epilayers</b>	
<i>Junhao Chu (Shanghai Institute of Technical Physics, Chinese Academy of Sciences, China); Jun Shao (Shanghai Institute of Technical Physics, Chinese Academy of Sciences, China); Xiang Lu (Shanghai Institute of Technical Physics, Chinese Academy of Sciences, China); Fangyu Yue (Shanghai Institute of Technical Physics, Chinese Academy of Sciences, China); Wei Huang (Shanghai Institute of Technical Physics, Chinese Academy of Sciences, China); Lili Ma (Shanghai Institute of Technical Physics, Chinese Academy of Sciences, China); Wei Lu (Shanghai Institute of Technical Physics, Chinese Academy of Sciences, China); Jun Wu (Shanghai Institute of Technical Physics, Chinese Academy of Sciences, China); Li He (Shanghai Institute of Technical Physics, Chinese Academy of Sciences, China);</i> .....	946
<b>Noise Associated with Microwave Intensity Modulation of Semiconductor Lasers</b>	
<i>Moustafa Ahmed (Minia University, Egypt); Minoru Yamada (Kanazawa University, Japan);</i> .....	947
<b>Temperature Effects Induced a Radically Different Behavior on the Transport Properties of Si Delta-doped GaAs Quantum Wells</b>	
<i>Luis M. Gaggero-Sager (Universidad Autonoma del Estado de Morelos, Mexico); Isaac Rodriguez-Vargas (Universidad Autonoma de Zacatecas, Mexico);</i> .....	948
<b>Evaluation of Leakage Losses in Optical Bragg Waveguides</b>	
<i>Jie Li (City University of Hong Kong, China); Kin Seng Chiang (City University of Hong Kong, China);</i> .....	949
<b>Numerical Investigation of an Ultra-compact and Ultra-wideband Polarization Beam Splitter Design Using Coupled Plasmonic Waveguide Arrays</b>	
<i>Chao-Yi Tai (National Central University, Taiwan); Sheng Hsiung Chang (National Central University, Taiwan); Tsen Chieh Chiu (National Central University, Taiwan);</i> .....	950
<b>Progress in Theoretical Design and Numerical Simulation of High Power Terahertz Backward Wave Oscillator</b>	
<i>Hai Zhang (Xi’an Jiaotong University, China); Jianguo Wang (Xi’an Jiaotong University, China); Changjiang Tong (Northwest Institute of Nuclear Technology, China);</i> .....	951
<b>Modeling of Passively Mode-locked Broadband Dual-gain-media Nd:glass Laser</b>	
<i>Song Han (University of Maryland, USA); Li Yan (University of Maryland Baltimore County, USA);</i>	952

# Conductance and Wave Impedance of Electrons

Raphael Tsu<sup>1</sup> and Timir Datta<sup>2</sup>

<sup>1</sup>University of North Carolina at Charlotte, Charlotte, NC 28223, USA

<sup>2</sup>University of South Carolina, Columbia, SC 29208, USA

**Abstract**— Quantum conductance from various systems and concepts are examined for a better understanding of the concept of conductance involving the wave nature of electrons. The tunneling between two contacts for electrons at temperature  $T \rightarrow 0$  is given by the conductance  $G = 2G_0 \sum_t |T|^2(E_F, E_t)$ , with  $G_0 = e^2/h = 38.6 \mu\text{S}$ , and its inverse  $Z_0 = 25.9 \text{k}\Omega$ .  $G_0$  is known as the universal conductance. The conductance of an electron quantum waveguide, EQW, consists of a region with sides bounded by impenetrable barriers in the transverse plane is given by  $G = \sum_{n,m} 2G_0 \theta(E_F + eV - \hbar^2 k_{t,nm}^2/2m)$ , where  $k_{t,nm}$  is the transverse momentum of the (n,m) mode, and  $\theta$  is the unit step function, and  $V$  is the applied potential difference between the input plane and the rest of the space containing the electron wave guide. Using the same definition for electromagnetic definition of the wave impedance, the electron wave impedance in a solid with a plane wave in one dimension is given by  $Z = \frac{\hbar}{2e^2} \frac{k_0 L}{\sqrt{1 - k_c^2/k_0^2}}$  [1], where  $k_c$  is same as  $k_t$  for the EQW. Without the transverse degree of freedom,  $Z = Z_0$ . However, with the transverse degree of freedom, the electron wave impedance is given by [2]  $Z_{\ell,m,n} = Z_0 \Xi_{\ell,m,n}$ , where  $\Xi_{\ell,m,n} = \left[ \frac{\ell^2 + \frac{m^2}{a^2} + \frac{n^2}{b^2}}{\ell^2 + \frac{m^2}{a^2} + \frac{n^2}{b^2}} \right]$ . Note that only in a one dimensional system  $Z_{\ell,m,n}$  is given by an integral multiple of  $Z_0$ . Furthermore, experimentally the measured conductance for tunneling through a quantum dot, QD, involves peaks and steps. Since conductance peaks represent tunneling via QD, and conductance steps represent tunneling via quantum well, QW, for conductance peak leading conductance step, it is argued that an electron captured by a QD is responsible for the coupling of the QDs into a 2D-like system. [3] Thus many body effects are involved. *Identifying  $Z_0$  with electron wave impedance is as important as the case for electromagnetic waves where matching in transmission lines and antennas are off primary importance.*

## REFERENCES

1. Tsu, R., *Superlattice to Nanoelectronics*, Chapter 11, Elsevier, 2005.
2. Datta, T. and R. Tsu, QWILLANE2.19. Nov. 2003. <http://arXiv.org/condmat/0311479>
3. Tsu, R., *Microelectronic J.*, MEJ.2184, 2007.

## A New Definition of Capacitance of Few Electron Systems

Tim LaFave Jr.<sup>1</sup> and Raphael Tsu<sup>2</sup>

<sup>1</sup>Department of Physics and Astronomy, University of Iowa, Iowa, IA 52242, USA

<sup>2</sup>Department of Computer and Electrical Engineering  
University of North Carolina at Charlotte, Charlotte, NC 28223, USA

**Abstract**— When considering nanoscale systems the spatial symmetry properties of electrons play an important role in the characterization of its electronic properties. These symmetry properties are most important for systems consisting of few electrons since the resulting potential landscape shapes its electrostatic boundary conditions. While the quantum mechanical Schrödinger equation provides an accurate evaluation of kinetic energy, here a classical electrostatic interactions model is demonstrated to provide the total electrostatic potential energy using only the Poisson equation to properly account for spatial symmetry properties resulting from the discrete nature of electrons. Within this model, developed using an ideal dielectric sphere, an expression characterizing the capacitance is derived using the fundamental relation  $C \equiv Q/V$ . However, this traditional definition assumes an equal potential boundary, where electrons were assumed to be infinitesimally spread over a well defined surface or pushed together into a supercharge situated at the center, point of maximum symmetry. Taking  $V$  as an average potential of  $N$  electrons, and requiring consistency with traditional configuration for  $N = 1$  and  $N \rightarrow \infty$ , the  $N$ -dependent expression of capacitance is defined by  $C(N) \equiv \frac{Q}{V_{TOT}(r_i)} = N \frac{Q}{V(N)} = \frac{(Ne)^2}{E(N)}$ , with the  $N$ -dependent energy given by this interactions model,  $E(N) = e[\phi_C(N) + \phi_P(N) + \phi_S(N)] = E_C(N) + E_P(N) + E_S(N) + W(N)$  where subscripts  $C, P$  and  $S$  correspond to electrostatic Coulomb, polarization and self-polarization interactions, respectively, and  $W(N)$  is the work done on the system by a collection of  $N$  electrons as given by the total self-polarization energy,  $E_s(r_i) = e\phi(r_i) - W$ . This *monophasic* capacitance is a direct consequence of the symmetry properties resulting from the discreteness of electron charge, rather than the wave-nature of electrons. Each  $N$ -electron system is afforded a unique range of symmetry properties and may arguably be treated as a unique phase of the system. The monophasic capacitance characterizes the purely time-independent electrostatic ground state of the system and is shown to mathematically agree with the traditional expressions for the special case of a single electron in a dielectric sphere and in the ‘conducting limit’ as  $N \rightarrow \infty$ . *This new definition in terms of an average potential should be applicable even including quantum effects, as well as in biological systems.*

# Macroscopic Quantum Electrodynamics in Linear Media — the Green Tensor of Maxwell's Equations in Quantum Optics

Stefan Scheel

Imperial College London, United Kingdom

**Abstract**— In this contribution, I will present the basic concepts of macroscopic quantum electrodynamics in arbitrary linearly responding media. The theory is based on a source-quantity representation of the electromagnetic fields in terms of the classical dyadic Green function. I will show that this theory is consistent with the fundamental requirements of quantum theory as well as statistical physics. The calculation of physical quantities (expectation values, transition rates etc.) then reduces to the evaluation of the dyadic Green function of the underlying classical scattering problem which contains all information about the dielectric/paramagnetic properties and the geometrical arrangement of the dielectric bodies. The theory generalizes, but contains as a limiting case, the familiar mode expansion of vacuum quantum electrodynamics. With regard to practical applications, I will address the surface impedance method for the calculation of the Green tensor of the macroscopic Maxwell equations.

This theory has numerous applications in both quantum optics and atomic physics as well as in the quantum optics/condensed matter interface. In quantum optics, one is primarily interested in propagation of nonclassical light (squeezed, entangled etc.) and its interaction with atomic systems. I will provide examples of the application of the quantum theory of light in dielectric media to decoherence problems in propagation of nonclassical states of light through passive optical elements.

One particularly interesting consequence of the theory is that it provides information about absorption-induced electromagnetic-field fluctuations that influence the dynamics and the coherence of microscopic systems such as clouds of cold atoms, ions, or molecules. In that way, atomic systems can be used as sensitive probes of surface properties of dielectric, metallic and superconducting materials. I will describe recent progress in atomic relaxation studies near superconducting surfaces and carbon nanotubes.



## Quantum Wires and Field Theory

B. Bellazzini<sup>1</sup>, M. Mintchev<sup>2</sup>, and P. Sorba<sup>3</sup>

<sup>1</sup>INFN and Scuola Normale Superiore, Piazza dei Cavalieri 7, Pisa 56127, Italy

<sup>2</sup>INFN and Dipartimento di Fisica, Università di Pisa, Largo Pontecorvo 3, Pisa 56127, Italy

<sup>3</sup>LAPTH, CNRS, University de Savoie, BP 110, F-74941 Annecy-le-Vieux cedex, France

**Abstract**— Quantum graphs are networks of one-dimensional wires connected at nodes. The interest for such structures increased these recent times with the development of nano-scale technology. We focus our attention on star graphs made of  $n$  edges with one junction. The related bosonic fields propagate in the bulk, either freely or submitted to a four-fermion interaction, and interact at the vertex, which can be considered as a defect. Hereafter, a quantum field theoretical framework is developed and applied to the computation of physical quantities, such that the electric and spin conductance. More precisely, our approach combines results from the spectral theory of the Schrödinger operator on quantum graphs with an algebraic technique for dealing with quantum fields with defects (impurities). At the vertex, all possible interactions preserving unitarity are taken into account, but special attention is given to scale-invariant ones, which lead to the critical properties of the system. Then bosonization and vertex operators on quantum graphs are investigated to solve exactly, for scale invariant boundary conditions, the four-fermion bulk interaction (Tomonaga-Luttinger model). At this point, we are in position to derive the charge and spin transport, and establish a simple relationship among them.

# Modulation Spectroscopy Study of Arsenic-doped Narrow-gap HgCdTe Epilayers

Junhao Chu<sup>1,2</sup>, Jun Shao<sup>1</sup>, Xiang Lu<sup>1</sup>, Fangyu Yue<sup>1</sup>, Wei Huang<sup>1</sup>, Lili Ma<sup>1</sup>, Wei Lu<sup>1</sup>  
Jun Wu<sup>3</sup>, and Li He<sup>3</sup>

<sup>1</sup>National Lab for Infrared Physics, Shanghai Institute of Technical Physics, Chinese Academy of Sciences  
Shanghai 200083, China

<sup>2</sup>ECNU-SITP Joint Laboratory for Image Information, East China Normal University  
Shanghai 200062, China

<sup>3</sup>Research Center for Advanced Materials and Devices  
Shanghai Institute of Technical Physics, Chinese Academy of Sciences  
Shanghai 200083, China

**Abstract**— Hg<sub>1-x</sub>Cd<sub>x</sub>Te as a narrow-gap semiconductor has found wide applications in infrared detection. To realize large-scale high-performance infrared detector focal plane arrays, p-type in-situ doping is crucial, of which arsenic (As) is the most favorite dopant. For identifying the activation and the energetic positions of the dopant, electrical techniques were frequently employed. In contrast, optical studies by, e.g., photoluminescence (PL) and photoreflectance (PR) were very limited, due to the difficulties in implementing the experiments in the mid- and far-infrared spectral regions.

In this presentation, we report new experimental results established in temperature-dependent PL and PR studies of *in situ* As-doped narrow-gap Hg<sub>1-x</sub>Cd<sub>x</sub>Te films grown by molecular beam epitaxy.

In the PL study, a modulated Fourier transform infrared (FTIR) spectrometer-based PL technique, which was testified to be powerful in eliminating room-temperature environmental thermal emission, is employed and different excitation and different temperature in the range of 11 ~ 300 K is used. Experimental data reveal besides the band-to-band transition the information about shallow levels. Analyses indicate that the shallow levels are related to Hg vacancy and As as either donor or acceptor.

A FTIR PR technique recently developed in our group is employed for the PR study, which ensures a rapid and sensitive detection of PR signal with high signal-to-noise ratio and spectral resolution and hence provides a possibility for quantitative characterization of near bandgap electronic levels and transitions. By fitting the temperature-dependent PR spectra taken for a series Hg<sub>1-x</sub>Cd<sub>x</sub>Te samples with third-order derivative Lorentzian lineshapes, critical point energies are determined and their evolution with temperature is identified. These lead to a reliable determination of the band gap and the dopant/defect related energy levels. The activation of As as p dopant is then discussed.

The results of this study also illustrate that the modulation spectroscopy based on FTIR spectrometer is powerful and may play an important role in optical study of narrow-gap demiconductors.

## Noise Associated with Microwave Intensity Modulation of Semiconductor Lasers

Moustafa Ahmed<sup>1</sup> and Minoru Yamada<sup>2</sup>

<sup>1</sup>Department of Physics, Faculty of Science, Minia University, El-Minia 61519, Egypt

<sup>2</sup>Division of Electrical Engineering and Computer Science  
Graduate School on Natural Science and Technology, Kanazawa University  
Kakuma-machi, Kanazawa 920-1192, Japan

**Abstract**— Relative intensity noise (RIN) and frequency noise (FN) associated with gigahertz intensity modulation of semiconductor lasers are investigated. The study is based on numerical solution of the laser rate equations augmented by a sinusoidal current source and Langevin noise sources. The frequency spectra of RIN and FN are evaluated as the fast Fourier transforms of the corresponding intensity and frequency-shift fluctuations, respectively. The laser dynamics under modulation are classified into six types with distinct dynamic characteristics in both time and frequency domains. These types are continuous signal (CS), continuous signal with relaxation oscillation (CSRO), continuous signal with period doubling (CSPD), periodic pulse (PP), periodic pulse with relaxation oscillation (PPRO), and periodic pulse with period doubling (PPPD). The classification is achieved over wide ranges of the modulation index and frequency when the laser is biased above threshold. We characterize the frequency spectra of RIN and FN in each dynamic type. The results show that the GHz components of both RIN and FN are higher when the laser output has discontinuous pulses than when it varies continuously with the time variation. The noise spectra of the CS and PP types are characterized by the modulation frequency and its multiples. For CSPD and PPPD types, the noise spectra are characterized by both the modulation frequency and its half-harmonic. For both CSRO and PPRO types, the spectra are characterized by the modulation and relaxation frequencies. The low-frequency noise levels are flat, lowest and almost equal for CS, CSRO and CSPD types. These noise levels are highest when the laser output is either PP or PPRO.

# Temperature Effects Induced a Radically Different Behavior on the Transport Properties of Si Delta-doped GaAs Quantum Wells

L. M. Gaggero-Sager<sup>1</sup> and I. Rodriguez-Vargas<sup>2</sup>

<sup>1</sup>Universidad Autónoma del Estado de Morelos, Ave. Universidad 1001, 62209 Cuernavaca, México

<sup>2</sup>Unidad Académica de Física, Universidad Autónoma de Zacatecas  
Calzada Solidaridad Esquina con Paseo la Bufa S/N, 98060 Zacatecas, ZAC., México

**Abstract**— The electronic structure of a delta-doped quantum well of Si in GaAs matrix is studied for different temperatures. The calculation is carried out self-consistently in the framework of the Hartree approximation. The energy levels and the mobility trends are reported for various impurity densities. The apparent contradictory temperature dependence of the mobility reported between Zheng and Gurtovoi et al. [1, 2] can be explain by means of the temperature variation of the electronic structure. Values of 1.9 and 0.9 are obtained for the ratio of the mobility at 300 K and 77 K corresponding to impurity densities of  $5 \times 10^{12} \text{ cm}^{-2}$  and  $3 \times 10^{12} \text{ cm}^{-2}$ , respectively, in excellent agreement with the experimental ones, 2.1 and 0.85.

## REFERENCES

1. Zheng, X., T. K. Carns, K. L. Wang, and B. Wu, *Appl. Phys. Lett.*, Vol. 62, 504, 1993.
2. Gurtovoi, V. L., V. V. Valyaev, S. Y. Shapoval, and A. N. Pustovit, *Appl. Phys. Lett.*, Vol. 72, 1202, 1998.

## Evaluation of Leakage Losses in Optical Bragg Waveguides

Jie Li and Kin Seng Chiang

Department of Electronic Engineering, City University of Hong Kong  
83 Tat Chee Avenue, Hong Kong, China

**Abstract**— Optical Bragg waveguides exhibit many unusual properties, such as strong wavelength-dependence transmission, giant dispersion effects, and sharp polarization discrimination, which can find new applications in optical signal transmission and processing. An ideal Bragg waveguide consists of a Bragg reflector that is made up of infinite multilayer stacks of alternating refractive indices (an infinite periodic structure). A practical Bragg waveguide, however, has a truncated Bragg reflector (a finite periodic structure), which unavoidably introduces leakage losses. It is therefore of fundamental importance to calculate the leakage losses caused by a truncated Bragg reflector for the design and fabrication of such waveguides. In general, the leakage losses are calculated by numerical methods, such as the finite-difference time-domain method and the transfer-matrix method, which are time consuming and provide limited physical insight. In this paper, we present an analytical expression for the evaluation of the leakage losses in a Bragg waveguide that contains a guiding layer sandwiched between two identical truncated Bragg reflectors. Our analysis is based on the ray-optics model, which allows a simple intuitive interpretation of the wave propagation phenomenon in the waveguide. To be specific, we treat a finite periodic structure as a perturbation of an infinite periodic structure and derive a complex reflection coefficient, from which we can calculate efficiently the leakage losses for different modes of the waveguide. Using this method, we analyze a number of Bragg waveguides and determine how the leakage losses in these waveguides depend on the number of the periods in the Bragg reflector.

# Numerical Investigation of an Ultra-compact and Ultra-wideband Polarization Beam Splitter Design Using Coupled Plasmonic Waveguide Arrays

Chao-Yi Tai<sup>1</sup>, Sheng-Hsiung Chang<sup>2</sup>, and Tsen-Chieh Chiu<sup>2</sup>

<sup>1</sup>Department of Optics and Photonics, National Central University, Taiwan

<sup>2</sup>Department of Electric Engineering, National Central University, Taiwan

**Abstract**— We present the design of an ultra-compact polarization beam splitter where three symmetrical dielectric channel waveguides are hybrid integrated with Au plasmonic waveguide arrays. In contrast to a flat mirror which reflects both transverse electric (TE) and transverse magnetic (TM) waves when operating below plasma frequency, small slit openings here provide an opportunity for the TE wave to penetrate through the waveguide array in form of coupled surface plasmon polaritons, leading to the discrimination of the two polarizations. Simultaneously satisfying a high reflection of the TM wave and high transmission of the TE wave will inherently place no fundamental limit for the operational bandwidth. The only restriction arises from the absorption of the consisting metal and the junction loss between interfaces that may limit the propagation distance. To compromise between the total insertion loss and the extinction ratio, finite-difference time-domain (FDTD) method is used in the optimization process in which various structural parameters are scanned to establish a design atlas. To optimize the position of the input/output (I/O) waveguides, successive snapshots of the field distributions for both TE and TM polarizations before incidence and after reflection/refraction are recorded. The extrapolation of the direction of the reflected/refracted beams toward to the waveguide array enables one to take into account of the Goos-Hänchen phase shift due to reflection and the transverse shift due to negative refraction and thereby minimize the total insertion loss. Ultra-wideband operation over 50 THz with the insertion loss less than 2 dB for both TE and TM mode are predicted. The extinction ratio is better than 15 dB for both polarizations and it is realizable using practical materials on a chip size as small as  $0.93 \times 4.2 \mu\text{m}^2$ .

# Progress in Theoretical Design and Numerical Simulation of High Power Terahertz Backward Wave Oscillator

Hai Zhang<sup>1</sup>, Jianguo Wang<sup>1,2</sup>, and Changjiang Tong<sup>2</sup>

<sup>1</sup>School of Electronics and Information Engineering, Xi'an Jiaotong University, Xi'an 710049, China

<sup>2</sup>Northwest Institute of Nuclear Technology, Xi'an 710024, China

**Abstract**— Terahertz signals were until recently an almost unexplored area of research due to the difficulties in generation and detection of electromagnetic fields at these wavelengths. Neither optical nor microwave techniques are directly applicable in the terahertz range since optical wavelengths are too short and microwave wavelengths are too long compared to terahertz field wavelengths. The developments of ultra fast optical techniques, the manufacturing of semi-insulating semiconductors and the micromachining of vacuum electron devices have boosted the terahertz fields as a new research area. This paper presented the recent results of design and simulation of 0.14 THz high power relativistic backward wave oscillator in our laboratory.

It is known that with the frequencies of microwave tubes increasing into the THz regime, the geometrical dimensions of devices decrease rapidly. This phenomenon inevitably reduces the power capacity of the tube and enhances the difficulties of its manufacturing. In order to solve these problems, a rectangular corrugated overmoded slow wave structure (SWS) was proposed. We investigated the dispersion relation and field distribution of the SWS in two different ways: analytical method and simulation method. And the results from two methods agreed very well. We also studied the effect of certain structural parameters of SWS on the dispersion curves and finally a set of optimal parameter values were achieved.

For the purpose of obtaining the distinct fundamental physical image of the radiation generation, a three-dimensional moving process of the electron beam was studied and the mechanism of beam interaction with synchronous spacial harmonic wave was also illuminated with both linear theory and 2.5-dimensional particle-in-cell (PIC) simulation programme. In this “hot test” simulation, a 2-dimensional axial symmetrical BWO model was constructed, and the resulting output characteristics were gained under appropriate running conditions. Meanwhile, the optimization of the system parameters, such as total number of the single periodic structure, length of the back transition portion, value of the magnetic field, etc, were also accomplished according to the output power requirements. Mode competition problem was seriously considered in the paper as well, and the eventual result of pure  $TM_{01}$  mode was procured in our generator. It is also worth indicating that the prototype BWO in our research operated in the near  $\pi$  mode, which enabled the device behave as a surface wave oscillator (SWO) at higher frequencies.

In conclusion, for the success of high power terahertz wave generator, a novel THz relativistic BWO was proposed in this paper. Since the optimization of certain parameters is critical to obtaining useful amount of AC power, a 2.5-dimensional PIC code was employed to gain the optimal operation parameters. Under the condition of 500 ~ 650 KV beam voltage, simulation achieved the output power of approximate 40 MW at the frequency of 0.146 THz with perfect time plot and fine spectrum characteristics.

# Modeling of Passively Mode-locked Broadband Dual-gain-media Nd:glass Laser

Song Han and Li Yan

Department of Computer Science and Electrical Engineering  
University of Maryland, Baltimore County, Baltimore, MD 21250, USA

**Abstract**— An ultrafast dual-gain-media Nd:glass laser, which contains both the Nd:fluorophosphate glass and the Nd:silicate glass in a single laser resonator, can effectively reshape and broaden the overall gain. Previously, it generated record-short pulses of 34 fs through passive mode-locking. The gain of neodymium-doped glass is inhomogeneously broadened and consists of multiple Stark-split sub-transitions. Each sub-transition has different peak cross-section, which leads to an asymmetric gain profile. Multiple Stark-split lines are involved when the pulse shortening mechanism is strong. A full gain model that includes the Stark-split sub-transitions is necessary to accurately predict the performance of this type of oscillator.

We modeled the gain of Nd:glass laser by considering Stark-split sub-transitions in addition to homogeneous broadening and inhomogeneous broadening. The peak cross-sections of sub-transitions are adjusted so that the small signal gain profile fits well with the published fluorescence of the Nd:glass, with a linewidth of  $\sim 26$  nm. With this full gain model, the simulated free running and passive mode-locking characteristics are in good agreement with the experiments. The simulation shows that for the single-medium Nd:glass laser,  $\geq 5\%$  unsaturated absorber loss  $\delta_{a0}$  is needed to generate a pulse bandwidth comparable to the gain linewidth. For the dual-gain-media Nd:glass laser, the simulation shows that a gain ratio (Nd:fluorophosphate to Nd:silicate) of  $\sim 2$  broadens best the overall gain. As a result, broader pulse bandwidth and shorter pulses are obtained, as compared with the single-medium Nd:glass laser. A relatively larger gain broadening can be obtained when the mode-locking strength is less strong. The generated pulse bandwidth is 30% broader than that from a single-medium Nd:glass laser when  $\delta_{a0} = 6\%$ . The simulated pulse bandwidths are within 10% with respect to the experimental results.



# Session 5A3

## Wave Propagation and Superresolution in Active and Passive Metamaterials 4

<b>Active Cut-Rod Metamaterial with Microwave Varactors</b>	
<i>Dongqing Wang (Zhejiang University, China); Hongsheng Chen (Zhejiang University, China); Baolian Wu (Massachusetts Institute of Technology, USA); Jin Au Kong (Massachusetts Institute of Technology, USA);</i> .....	954
<b>Metamaterials on the Basis of Precise Micro- and Nanoshells</b>	
<i>Victor Yakovlevich Prinz (Institute of Semiconductor Physics, SB RAS, Russia); E. V. Naumova (Institute of Semiconductor Physics, SB RAS, Russia); S. V. Golod (Institute of Semiconductor Physics, SB RAS, Russia); V. A. Seleznev (Institute of Semiconductor Physics, SB RAS, Russia); R. A. Soots (Institute of Semiconductor Physics, SB RAS, Russia);</i> .....	955
<b>Chiral Swiss Rolls</b>	
<i>Michael Wiltshire (Imperial College London, UK);</i> .....	956
<b>Sub-wavelength Imaging with RF Metamaterials</b>	
<i>Michael C. K. Wiltshire (Imperial College London, UK);</i> .....	958
<b>Optical Magnetism and Plasmonic Nanolaser</b>	
<i>Alexei L. Bogdanov (Canadian Photonics Fabrication Centre, Canada); Andrey N. Lagarkov (Institute of Theoretical and Applied Electrodynamics, Russia); Andrey K. Sarychev (Institute of Theoretical and Applied Electrodynamics, Russia);</i> .....	959
<b>Metamaterial Structures for Compact Millimeter Wave Antenna Applications</b>	
<i>Cuong Tran Manh (UniversitéParis X, Nanterre, France); Habiba Hafdallah Ouslimani (UniversitéParis X, Nanterre, France); Geraldine Guida (UniversitéParis X, Nanterre, France); Alain C. Priou (UniversitéParis X, Nanterre, France); Herve Teillet (THALES Communications, France); J. Y. Daden (THALES Communications, France);</i> .....	960
<b>Design and Characterization of Metamaterial Media Using Space Filling Curve</b>	
<i>Redha Abdeddaim (UniversitéParis X, Nanterre, France); Habiba Hafdallah Ouslimani (UniversitéParis X, Nanterre, France); Alain C. Priou (UniversitéParis X, Nanterre, France);</i> .....	961
<b>Overcoming the Diffraction Limit with a Volumetric Negative-Refractive-Index Transmission-Line Slab</b>	
<i>Jiang Zhu (University of Toronto, Canada); George V. Eleftheriades (University of Toronto, Canada);</i>	963
<b>Application of Band Theory to the Imaging Problem in Stackable Lenses</b>	
<i>Alexey P. Vinogradov (Russian Academy of Sciences, Russia); Alexander M. Merzlikin (Russian Academy of Sciences, Russia); Alexander V. Dorofeenko (Russian Academy of Sciences, Russia); Alexander A. Lisiansky (The City University of New York, USA); Said Zouhdi (University Paris Sud, France); J. P. Clerc (Universite de Provence, France);</i> .....	964

## Active Cut-Rod Metamaterial with Microwave Varactors

Dongxing Wang<sup>1,2</sup>, Hongsheng Chen<sup>1,2</sup>, Bae-Ian Wu<sup>1,2</sup>, and Jin Au Kong<sup>1,2</sup>

<sup>1</sup>The Electromagnetics Academy at Zhejiang University, China

<sup>2</sup>Research Laboratory of Electronics at MIT, USA

**Abstract**— In the present paper, a Cut-Rod Shaped metamaterial structure collaborated with microwave varactors are proposed and its tunable electromagnetic properties are verified in numerical simulations. From Figure 1(a), it can be noticed that the passband of such controllable metamaterial is shifted to lower frequency bands, when the capacitance of varactors are increased. In the meanwhile, at a fixed frequency within the passbands, the phases of the transmission is tuned also as shown in Figure 1(b), which is a useful property for various cases, such as beam steering and so on. As shown in Figure 2, the simplicity of the metamaterial structure make itself easy to be controlled by external voltage biases which give feasibilities for the practical applications.

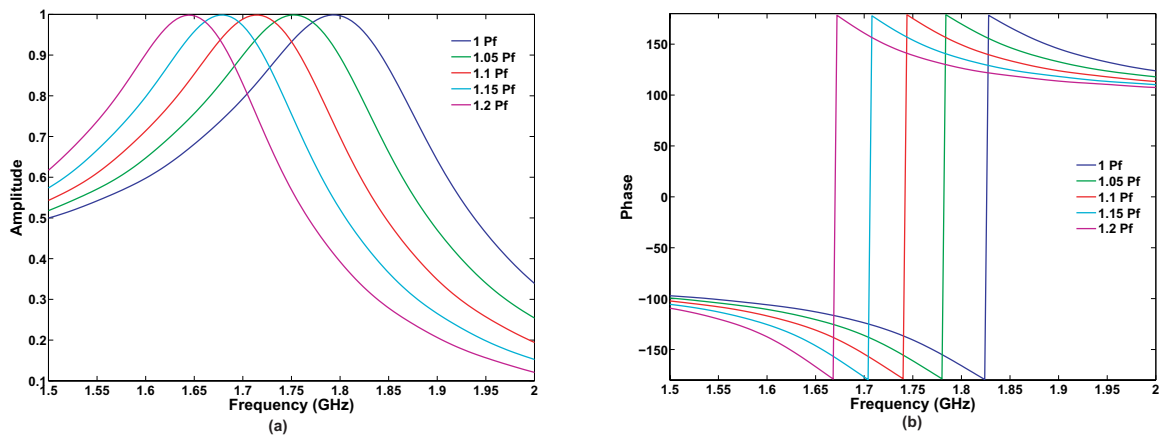


Figure 1: The transmission properties of the controllable Cut-Rod structure for the cases with different capacitances of the microwave varactors. (a) The amplitude of the transmission curves. (b) The phases of the transmission curves.

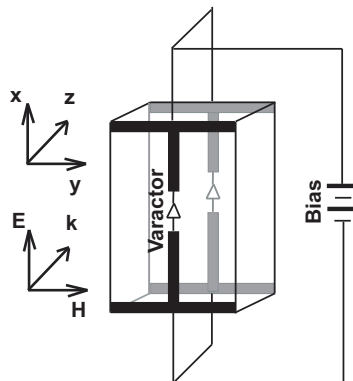


Figure 2: The structure of the controllable metamaterial with external bias voltage control.

### ACKNOWLEDGMENT

This work is supported by National Natural Science Foundation of China under Contract Nos. 60531020 and 60671003, the China Postdoctoral Science Foundation under Grant No. 20060390331, and in part by GF Basic Research Program (No. ZJDX2008179), the National Key Laboratory Foundation (No. 9140C5304020704) and ZJNSF under Grant R105253.

# Metamaterials on the Basis of Precise Micro- and Nanoshells

V. Ya. Prinz, E. V. Naumova, S. V. Golod, V. A. Seleznev, and R. A. Soots

Institute of Semiconductor Physics, SB RAS, Lavrent'eva, 13, Novosibirsk 630090, Russia

**Abstract**— Nowadays, for fabrication of micro- and nanoelements of metamaterials a traditional planar IC technology is mainly used. This technology meets such essential requirements as precision and reproducibility of elements, however, it is inappropriate for fabrication of 3D elements and uniform isotropic 3D arrangement of micro- and nanoelements, that significantly restrains the freedom of tailoring electromagnetic properties of metamaterials. Some variants of solutions which allows getting over these limitations are presented in this work. These solutions are based on the method of formation of 3D micro- and nanostructures from strained thin films [1, 2] and application of this method to formation of 3D arrays of elements.

In short, the fabrication process is as follows: multilayered thin film containing layers of different strains is grown on the substrate and lithographically patterned; being detached from the substrate (for instance, by etching of underlying sacrificial layer) the planar thin-film structures transform into 3D shells under action of internal strains. The method allows fabrication of precise 3D shells with thicknesses from hundreds of nanometers to a few angstroms and with curvature radii from 100 micrometers to a few nanometers from different materials: dielectrics, metals, semiconductors. Freedom and precision in control of strains, thicknesses and patterns of layers of the planar structures provides a great variety of possible 3D designs.

Highly-ordered 2D and 3D arrays of precise metal-semiconductor and semiconductor micro- and nanoshells are presented. Variants of formation of micro- and nanocomposites containing highly-ordered 3D arrays of micro- and nanoshells are considered. Rotation of the polarization plane of radiation by 2D array of metal-semiconductor microhelices fabricated by this method was studied in THz range, that was the first demonstration of artificial chirality in THz range [3]. Full compatibility of the used method with IC technology encourages proceeding to metamaterials with dynamically controlled properties and creation of active metamaterials, some possible solutions are suggested and discussed. Variants of the presented approach having prospects for mass fabrication of metamaterials from microwave to optical range are considered.

## REFERENCES

1. Prinz, V. Y., V. A. Seleznev, A. K. Gutakovskiy, A. V. Chehovskiy, V. V. Preobrazenskii, M. A. Putyato, and T. A. Gavrilova, "Free-standing and overgrown InGaAs/GaAs nanotubes, nanohelices and their arrays," *Physica E*, Vol. 6, No. 1-4, 828–831, 2000.
2. Prinz, V. Y., "Precise, molecularly thin semiconductor shells: From nanotubes to nanocorrugated quantum systems," *Phys. Stat. Sol. (b)*, Vol. 243, No. 13, 3333–3339, 2006/DOI 10.1002/pssb.200669132.
3. Naumova, E. V., V. Y. Prinz, V. A. Seleznev, S. V. Golod, V. V. Kubarev, B. A. Knyazev, G. N. Kulipanov, S. A. Kuznetsov, P. V. Kalinin, and N. A. Vinokurov, "Polarization rotation of THz radiation by an array of helices," *Proc. of Joint 31st International Conference on Infrared and Millimeter Waves and 14th International Conference on Terahertz Electronics*, Shanghai, China, Sept. 18–22, 2006.

# Chiral Swiss Rolls

M. C. K. Wiltshire<sup>1,2</sup>

<sup>1</sup>Imaging Sciences Department, Clinical Sciences Centre, Imperial College London  
Hammersmith Hospital Campus, Ducane Road, London W12 0NN, UK

<sup>2</sup>The Blackett Laboratory, Department of Physics, Imperial College London  
South Kensington, London SW7 2AZ, UK

**Abstract**— “Swiss Rolls” [1–3] have proved to be extremely effective metamaterials in the radiofrequency (RF) regime. Their low resonance frequency and intense magnetic activity have been exploited to demonstrate RF flux guiding [4] at the resonant frequency and sub-wavelength imaging [5] when the permeability  $\mu = -1$ . It has also been shown that strongly chiral metamaterials could offer an alternative route [6] to negative refraction and sub-wavelength imaging, and the chiral Swiss Roll was proposed as a possible metamaterial element to achieve this.

Chiral Swiss Rolls have been made by the helical winding of 5 mm wide NovaClad tape (Sheldahl G2202) onto glass fibre rod mandrels with a winding pitch between  $5^\circ$  and  $2^\circ$ . A custom-built machine [7] was used to carry out the winding, and an example of a finished roll is shown in Fig. 1.

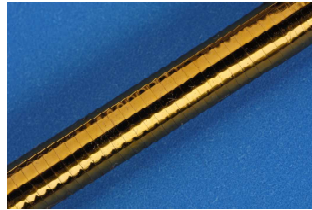


Figure 1: A chiral Swiss roll.

The definitive signature of a chiral material is the coupling of the electric and magnetic response through the constitutive relations

$$\mathbf{D} = \epsilon\epsilon_0\mathbf{E} + \sqrt{\epsilon_0\mu_0}\xi\mathbf{H}, \quad \mathbf{B} = \sqrt{\epsilon_0\mu_0}\zeta\mathbf{E} + \mu\mu_0\mathbf{H}$$

The rolls were characterised by exciting them with a magnetic field from a small (5 mm diameter) loop placed at one end, and probing the axial magnetic field with a second loop and the axial electric field with a small dipole aerial. This revealed a strong electric field response that is not seen in a conventional Swiss Roll (Fig. 2).

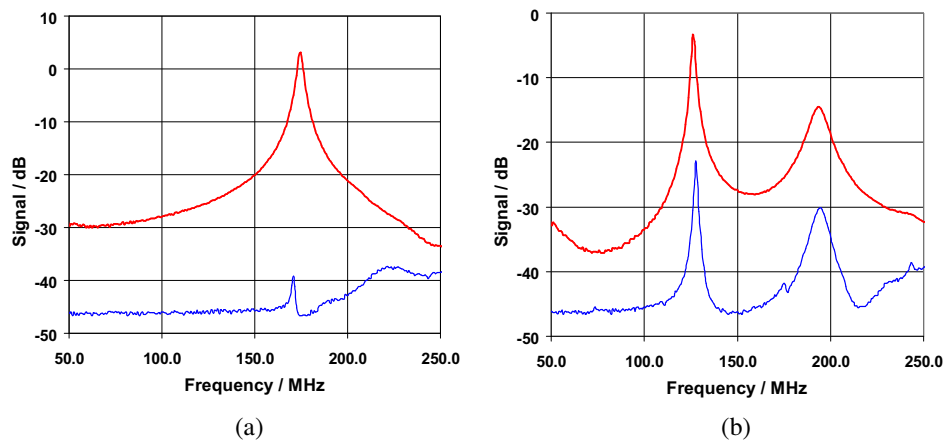


Figure 2: Spectra of the axial magnetic (red) and electric (blue) fields for (a) non-chiral and (b) chiral Swiss Rolls excited by an axial magnetic field, showing the strong electric response in the chiral rolls.

In this paper, the development and characterisation of chiral Swiss Rolls will be reviewed, and their properties and the excitations of these highly chiral objects, both the individual elements and in the bulk material, will be discussed.

**REFERENCES**

1. Pendry, J. B., et al., *IEEE Trans. Microw. Theory Tech.*, Vol. 47, 2075, 1999.
2. Smith, D. R., J. B. Pendry, and M. C. K. Wiltshire, *Science*, Vol. 305, 788, 2004.
3. Wiltshire, M. C. K., *Phys. Stat. Sol (b)*, Vol. 244, 1227, 2007.
4. Wiltshire, M. C. K., et al., *Opt. Express*, Vol. 11, 709, 2003.
5. Wiltshire, M. C. K., J. B. Pendry, and J. V. Hajnal, *J. Phys.: Condens. Matter*, Vol. 18, L315, 2006.
6. Pendry, J. B., *Science*, Vol. 306, 1353, 2004.
7. Constructed by 3Pinnovation Ltd., Budbrooke Industrial Estate, Warwick, CV34 5WP, UK.

# Sub-wavelength Imaging with RF Metamaterials

M. C. K. Wiltshire<sup>1,2</sup>

<sup>1</sup>Imaging Sciences Department, Clinical Sciences Centre, Imperial College London  
Hammersmith Hospital Campus, Du Cane Road, London W12 0NN, UK

<sup>2</sup>The Blackett Laboratory, Department of Physics, Imperial College London  
South Kensington, London SW7 2AZ, UK

**Abstract**— There are several advantages of working in the radiofrequency (RF) regime to study metamaterials. Because the wavelength is large, typically several metres, all structures are electrically small and the effective medium description of the metamaterial should be accurate. Secondly, experiments can be carried out in the very near field,  $r \ll \lambda$ , where the electric and magnetic fields are essentially decoupled, thus simplifying both the experiment and its interpretation. In particular, Pendry's prescription for the "perfect lens" [1], in which a slab of material with refractive index  $n = -1$  focuses both the propagating and the evanescent radiation, can be relaxed so that the material only needs to have  $\varepsilon = -1$  to focus the electric field or  $\mu = -1$  to focus the magnetic field. Swiss Rolls" [2-4] have proved to be extremely effective metamaterials in the radiofrequency (RF) regime. Their low resonance frequency and intense magnetic activity have been exploited to demonstrate RF flux guiding [5] at the resonant frequency. Above the resonant frequency, the permeability is negative, and a variety of surface resonances can be demonstrated [6]. When the permeability  $\mu = -1$ , sub-wavelength imaging of magnetic objects has been observed [7]. Because the "lens" is very thin compared to the wavelength and the material loss is quite low, a resolution of  $\lambda/64$  could be achieved, much higher than that obtained at optical frequencies. In this paper, I will describe the development of the RF metamaterials and how they have been used to show sub-wavelength imaging, and also discuss the potential for improved performance.

## REFERENCES

1. Pendry, J. B., *Phys. Rev. Lett.*, Vol. 85, 3966, 2000.
2. Pendry, J. B., et al., *IEEE Trans. Microw. Theory Tech.*, Vol. 47, 2075, 1999.
3. Smith, D. R., J. B. Pendry, and M. C. K. Wiltshire, *Science*, Vol. 305, 788, 2004.
4. Wiltshire, M. C. K., *Phys. Stat. Sol (B)*, Vol. 244, 1227, 2007.
5. Wiltshire, M. C. K., et al., *Opt. Express*, Vol. 11, 709, 2003.
6. Wiltshire, M. C. K., et al., *J. Phys.: Condens. Matter*, Vol. 19, 456216, 2007.
7. Wiltshire, M. C. K., J. B. Pendry, and J. V. Hajnal, *J. Phys.: Condens. Matter*, Vol. 18, L315, 2006.

## Optical Magnetism and Plasmonic Nanolaser

Alexei L. Bogdanov<sup>1</sup>, Andrey N. Lagarkov<sup>2</sup>, and Andrey K. Sarychev<sup>2</sup>

<sup>1</sup>Canadian Photonics Fabrication Centre, Ottawa, Canada

<sup>2</sup>Institute of Theoretical and Applied Electrodynamics RAS, Moscow, Russia

**Abstract**— We consider plasmonic nanoantennas immersed in active host medium. Specifically shaped metal nanoantennas can exhibit strong magnetic properties in the optical spectral range due to the excitation of magnetic plasmon resonance. A case when a metamaterial comprising such nanoantennas can demonstrate both left handedness and negative permeability in the optical range is considered. We show that high losses predicted for optical left-handed materials can be compensated in the gain medium. Gain allows achieving local generation in such magnetic active metamaterials. We propose plasmonic nanolaser, where the metal nanoantenna operates similar to a resonator. The size of the proposed plasmonic laser is much smaller than the wavelength. Therefore, it can serve as a very compact source of coherent electromagnetic radiation.

Extending the range of electromagnetic properties of naturally occurring materials motivates the development of artificial metamaterials. For example, it has been demonstrated recently that optical metamaterials may exhibit such exotic properties as, negative dielectric permittivity, negative magnetic permeability, and even both. Situations when a negative refractive index can be realized in practice are particularly interesting because of possibility of the perfect lens with subwavelength resolution, which is not restricted by the diffraction limit. Negative refraction and subwavelength imaging has been demonstrated in the microwave and optical range. However, the loss becomes progressively important with decreasing the wavelength towards the optical range. High loss inside the left-handed superlens dramatically reduces the resolution of such lens and made a dream of a full-scale superlens unattainable. To reduce the loss we suggest filling the metal plasmonic resonator with an active medium. We consider the interaction of such nanoantenna with a two-level amplifying system, which can be represented by quantum dot in the semiconductor host, quantum well, dye molecules, or another high gain medium.

# Metamaterial Structures for Compact Millimeter Wave Antenna Applications

Cuong Tran Manh<sup>1</sup>, Habiba Hafdallah Ouslimani<sup>1</sup>, Geraldine Guida<sup>1</sup>  
Alain Priou<sup>1</sup>, Herve Teillet<sup>2</sup>, and J. Y. Daden<sup>2</sup>

<sup>1</sup>Applied Electromagnetic Group (GEA), Université Paris X, Nanterre  
50 rue de Sevres, Ville d'Avray 92410, France

<sup>2</sup>THALES Communications, 160 Boulevard de Valmy, Colombes 92704, France

**Abstract**— This paper proposes the study of some high impedance surface (HIS) structures [1] for compact antenna applications in the millimeter-wave domain. The millimeter wave domain is now very important for high speed wireless and high bit rate optical (> 40 Gbits/s) communications systems. The HIS structures provide many advantages for antenna as they enhance their performances; they have capability to block the surface wave, to reduce the coupling effect, to present high real impedance at the resonance frequency ( $R_e(Z) \gg 377 \Omega$ ) and to reduce the global thickness of the low profile antenna. Several high impedance surfaces structures are analyzed and their properties compared. We perform this analysis on structures which composed of rectangular lattices patches periodic arrangements, Jerusalem lattices shape and 2LC shape (two LC split loops [2]). For each structure, we are interested in the frequency behavior of the reflection phase to determine the resonance frequency and the band-gap as well as in the losses (joule effect) in the structure. All the dimensions and shapes of the unit cell geometry are optimized in order to use the dielectric substrate available in our laboratory. The high impedance surface is modeled using HFSS (Ansoft) code based on finite element methods. We chose the structure presenting the best performances to design the metamaterial antenna [3, 4] with coaxial fed and finite surface witch is modeled with  $7 \times 7$  and  $9 \times 9$  double rang unit cells. In comparison with conventional antenna type placed above a metal ground plan, the antenna placed above the HIS has smoother radiation profile, less power wasted in the backward direction, better return loss (at least 10 to 15 dB better) and higher gain and directivity [4] (at least 1 dB). The layout of the HIS structures circuits (many varieties) are now edited and the manufacturing process in progress. The results of the HFSS simulations will be compared with the experimental free space and coaxial measurements in the millimeter-wave domain.

## REFERENCES

1. Daniel Sievenpiper Thesis, University California, Los Angeles, 1999.
2. Schurig, D., J. J. Mock, and D. R. Smith, *Appl. Physics Letter*, Vol. 88, 041109, 2006.
3. Abdelwaheb Ourir Thesis, University Paris X, 2006.
4. Engheta, N. and R. W. Ziolkowski, *Electromagnetic Metamaterials: Physics and Engineering Explorations*, Wiley-IEEE Press, August 2006.



## Design and Characterization of Metamaterial Media Using Space Filling Curve

Redha Abdeddaim, Habiba Hafdallah Ouslimani, and Alain Priou

Groupe d'Electromagnétisme Appliquée: GEA, Pôle scientifique et technique de Ville d'Avray

**Abstract**— Left handed media is a combination of a thin wire structure and magnetic resonant structures. Several models of magnetic structures are present in the literature, like single and broadside split ring resonators (SRR) or spiral inductors [1]. In this paper we propose to explore the properties of space filling curve [2] to realize an artificial resonant magnetic medium with a reduction of the electrical size. A space filling curve is fractal surface which is in general a continuous mapping of repetitive geometric forms. In comparison with the other SRR structures, the resonant frequency of the fractal structure depend on either the dimensions of the structure and also the order of the curve ( $n=3, 4, \dots$ ). Initially we study the response of third order “Peno”

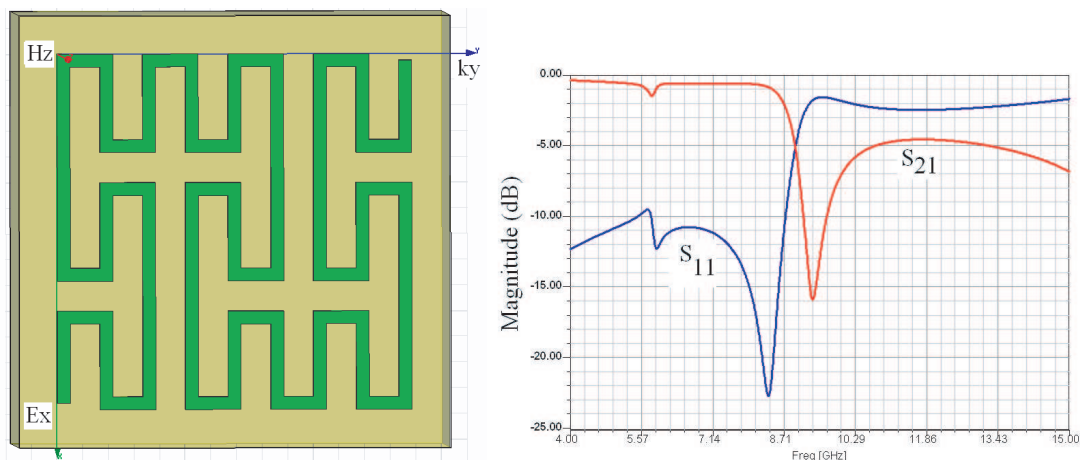


Figure 1: Magnetic resonance of the “Peno” structure.

curve under different orientation of the electric polarisation. Like the SRR [3] structure, it exhibits magnetic (Fig. 1) or magnetoelectric behaviour. Fig. 2 shows a metamaterial medium realized with the bianisotropic structure (Fig. 1) and parallel wires disposed along the electrical direction. In order to suppress the bi-anisotropic effect, we placed back to back two space filling curve layers on a thin dielectric substrate (broadside structure) and we try to find the best orientation of

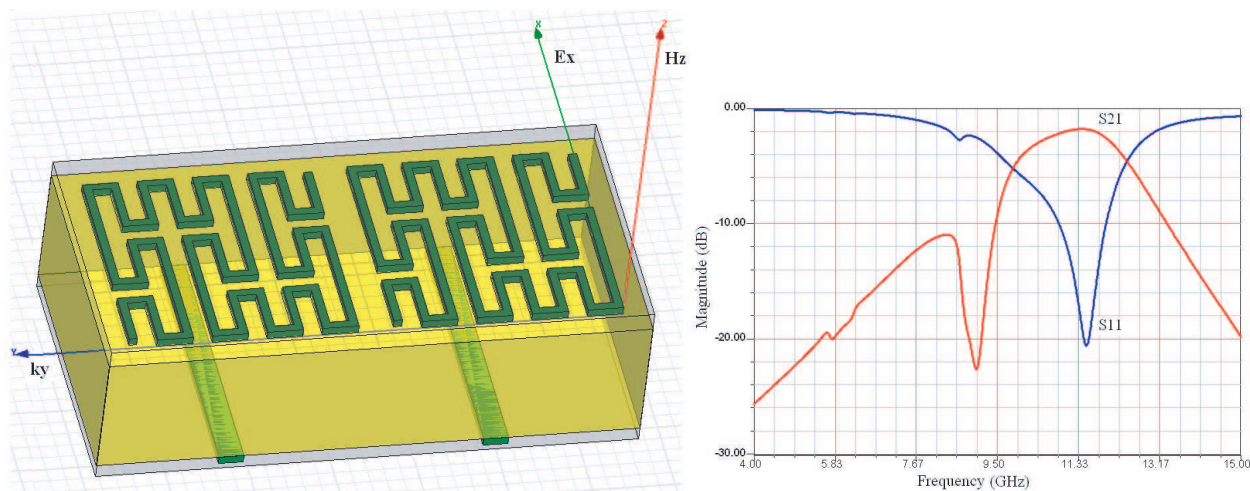


Figure 2: Metamaterial structure.

the second layer to compensate the electrical resonance and obtained a quasi purely magnetic media. Since this orientation is not easy to determine because there are no evident symmetry in the structure, in the experimental measurements we test only four orientations of the bottom layer: at  $0^\circ$ ,  $90^\circ$ ,  $180^\circ$  or  $270^\circ$  from the top layer. We present in this paper the results of the electromagnetic simulations compared to the free space measurements in the X band frequency.

#### REFERENCES

1. Baena, J. D. and all, "Artificial magnetic metamaterial design by using spiral resonators," *Physical Review B*, Vol. 69; 014402-1–014402-5, 2004.
2. Engata, N. and R. W. Ziolkowski, *Metamaterials Physics Explorations*, Wiley-Interscience, 2006.
3. Pendry, J. B., J. A. Holden., J. D. Robin, and J. W. Stewart, "Magnetism from conductor and enhanced nonlinear phenomena," *IEEE. Trans. MTT.*, Vol. 47, 2075–2077, 1999.

## Overcoming the Diffraction Limit with a Volumetric Negative-Refractive-Index Transmission-Line Slab

Jiang Zhu and George V. Eleftheriades

The Edward S. Rogers Sr. Department of Electrical and Computer Engineering, Electromagnetics Group  
University of Toronto, Toronto, Ontario, M5S 3G4, Canada

**Abstract**— Volumetric negative-refractive index (NRI) metamaterials can be created by stacking layers of planar NRI transmission lines (NRI-TLs). This approach is a natural extension of the two dimensional (2D) NRI-TL media of [1] to the third dimension [2]. In this paper, this approach is implemented using a shunt-node TL structure to synthesize fully printed NRI-TL metamaterials. The dispersion and transmission characteristics of such a quarter-wavelength thick slab are analyzed by multiconductor transmission line (MTL) theory and a full-wave finite-element method (FEM) using Ansoft's HFSS. These analysis results reveal the broadband and low-loss properties of the proposed structure. These attributes are essential for achieving sub-diffraction imaging. Using this approach, a volumetric NRI-TL flat Veselago-Pendry lens with a relative refractive index of  $-1$  is designed. Experimental results suggest that focusing beyond the diffraction limit is actually achieved at microwave frequencies.

### REFERENCES

1. Eleftheriades, G. V., A. K. Iyer, and P. C. Kremer, "Planar negative refractive index media using periodically L-C loaded transmission lines," *IEEE Trans. on Microwave Theory and Techniques*, Vol. 50, No. 12, 2702–2712, Dec. 2002.
2. Stickel, M., F. Elek, J. Zhu, and G. V. Eleftheriades, "Volumetric negative-refractive-index metamaterials based upon the shunt-node transmission-line configuration," *Journal of Applied Physics*, Vol. 102, 094903, Nov. 2007.

# Application of Band Theory to the Imaging Problem in Stackable Lenses

A. P. Vinogradov<sup>1</sup>, A. M. Merzlikin<sup>1</sup>, A. V. Dorofeenko<sup>1</sup>  
 A. A. Lisyansky<sup>2</sup>, S. Zouhdi<sup>3</sup>, and J. P. Clerc<sup>4</sup>

<sup>1</sup>Institute for Theoretical and Applied Electromagnetics, Russian Academy of Sciences, Russia

<sup>2</sup>Department of Physics, Queens College, the City University of New York, USA

<sup>3</sup>Laboratoire de Génie Electrique de Paris Supélec

Plateau de Moulon, 91192, Gif sur Yvette Cedex, France

<sup>4</sup>Universite de Provence, IUSTI, Technopole de Chateau-Gombert

5 rue E. Fermi, 13453 Marseille, France

**Abstract**— It is shown that the transfer functions of Pendry-Ramakrishna, and Alù-Engheta stackable lenses are well described by the application of the band theory of photonic crystals.

In 1968 Veselago [1] predicted that a slab of a metamaterial (a material with negative permittivity and permeability) can perfectly focus the far-fields of a point source. As a result, one can obtain an image by using a slab of a double-negative medium. In 2000, Pendry [2] showed that this slab “focused” evanescent waves. Thus, one can obtain an ideal image. The key point is that evanescent waves resonantly excite surface plasmons and magnons. Being resonant by origin, the subwavelength resolution is very sensitive to losses. In Ref. [3], in order to overcome this problem, the use of a stackable lens was suggested. This lens can be obtained by splitting a single-layer lens into a set of thinner layers. In 2003, a stackable lens with single-epsilon-negative (ENG) and single-mu-negative (MNG) layers was suggested [4].

The stackable lens may be considered as a 1D photonic crystal (PC). A distinct feature of a 1D PC containing layers with negative constitutive parameters is the existence of traveling Bloch waves, which are locally, in each layer, of evanescent nature [5]. It is these waves that transfer the subwavelength field structure over the stackable lens. Our analysis [6] of the Pendry-Ramakrishna lens shows that (i) stackable lens forms a resonator cavity for the traveling Bloch waves that cannot leave the PC resonator due to total internal reflection; (ii) imaging is possible outside the band gaps only and no imaging can be achieved in the vicinity of the eigenstates of the PC resonator as well as near the state associated with the excitation of the volume plasmon; (iii) an expected advantage is due to thinning the layers, which results in shifting of both the band edge and the eigenstates toward higher values of the wave number; and (iv) a single-layer lens has the broadest working range compared to a stackable lens with the same elementary layer thickness.

It was shown [7] that the Alù-Engheta lens may be considered as a 1D PC made of successive layers of ENG and MNG media. Such a PC can have a photonic band gap of zero width. Although this band gap consists of band edges only, the normal component of group velocity does not vanish. It is shown that the condition for the existence of a zero-width band gap coincides with the Alù-Engheta conditions [4]. At this very frequency, the restoration of the amplitude and phase of an electromagnetic wave by means of ENG-MNG bilayers exists. At the conjugate Alù-Engheta conditions [4], the restoration exists at any frequency that allows for using this PC for perfect imaging. The origin and robustness of these effects were studied.

## REFERENCES

1. Veselago, V. G., *Sov. Phys. Usp.*, Vol. 10, 509, 1968.
2. Pendry, J. B., *Phys. Rev. Lett.*, Vol. 85, 3966, 2000.
3. Ramakrishna, S. A., J. B. Pendry, M. C. Wiltshire, and W. J. Stewart, *J. Mod. Optics*, Vol. 50, 1419, 2003.
4. Alù, A. and N. Engheta, *IEEE Tr. AP*, Vol. 51, 2558, 2003.
5. Vinogradov, A. P. and A. V. Dorofeenko, *J. Comm. Technology and Electronics*, Vol. 50, 10, 2005.
6. Dorofeenko, A. V., A. A. Lisyansky, A. M. Merzlikin, and A. P. Vinogradov, *Phys. Rev. B*, Vol. 73, 235126, 2006.
7. Zouhdi, S., A. V. Dorofeenko, A. M. Merzlikin, and A. P. Vinogradov, *Phys. Rev. B*, Vol. 75, 035125, 2007.

# Session 5A4

## Interaction of EM Waves and Media

<b>Force Generation of Selemion Governed by the Charge Quantity</b>	966
<i>H. Tamagawa (Gifu University, Japan); .....</i>	
<b>Electro-optic Properties and Phase Behavior of Chiral-nematic Molecules</b>	
<i>Kyongok Kang (Forschungszentrum Juelich, IFF, Germany); Samuel Sprunt (Kent State University, USA); Jan K. G. Dhont (Forschungszentrum Juelich, IFF, Germany); .....</i>	
<b>Biological Effects of Pulsed Microwaves</b>	
<i>Jozef Mendecki (Montefiore Medical Center, USA); Daniel D. Mawhinney (MMTC, Inc., USA); Fred Sterzer (MMTC, Inc., USA); .....</i>	
<b>Universal Statistical Electromagnetic Properties of Ray-chaotic Enclosures</b>	
<i>Steven M. Anlage (University of Maryland, USA); Thomas Antonsen (University of Maryland, USA); James Hart (University of Maryland, USA); Elliott Bradshaw (University of Maryland, USA); Edward Ott (University of Maryland, USA); .....</i>	
<b>Design of Composite Electromagnetic Wave Absorber Made of Soft Magnetic Materials Dispersed and Isolated in Polystyrene Resin</b>	
<i>Kenji Sakai (Doshisha University, Japan); Yoichi Wada (Doshisha University, Japan); Shinzo Yoshikado (Doshisha University, Japan); .....</i>	
<b>Spectral Density Function Approach as Applied to Dielectric Properties of Biological Cell Suspensions</b>	
<i>A. V. Goncharenko (Research Center for Applied Sciences, Taiwan); Yia-Chung Chang (Research Center for Applied Sciences, Taiwan); .....</i>	
<b>Non-thermal Effect of Electrolyte Aqueous Solution under Microwave Radiation</b>	
<i>Ka-Ma Huang (Sichuan University, China); Xiao-Qing Yang (Sichuan University, China); .....</i>	

## Force Generation of Selemion Governed by the Charge Quantity

H. Tamagawa

Department of Human and Information Systems, Faculty of Engineering  
Gifu University, Japan

**Abstract**— It has been well known that ion exchange polymer membrane sandwiched between thin metal layers exhibits bending under an applied voltage. It has been widely accepted that it will become a polymer actuator near future. Previously, it was reported that the ion exchange polymer membrane called Selemion (Asahi glass, Co. Ltd., Japan) containing  $-\text{SO}_3\text{H}$  functional atomic group, sandwiched between thin silver layers, retained a simple relationship between the charge quantity given to Selemion and its bending curvature — linear relationship —. Consequently, it was found possible to control the bending curvature of such a Selemion simply by controlling the charge quantity. At the same time, it was observed that the force generated by the same Selemion sandwiched between thin silver layers appeared to be controllable by the control of charge quantity as well. In order to verify if the generated force was truly governed by the charge quantity, the further experiments were carried out in this work. In consequence, it was firmly observed that the force was correlated with the charge quantity merely by a linear relationship just like the relationship between the charge quantity and bending curvature, as long as the redox reaction of silver layers on Selemion surfaces was induced. Such an observation stimulated us to expect that the control of charge quantity given to Selemion could be simply reflected as the control of generated force. In fact, it was experimentally confirmed true, and the force behavior responded precisely even to the complicatedly controlled charge quantity.

# Electro-optic Properties and Phase Behavior of Chiral-nematic Molecules

Kyongok Kang<sup>1</sup>, Samuel Sprunt<sup>2</sup>, and Jan K. G. Dhont<sup>1</sup>

<sup>1</sup>Forschungszentrum Juelich, IFF-Weiche Materie, D-52425, Juelich, Germany

<sup>2</sup>Department of Physics, Kent State University, Kent, OH, USA

**Abstract**— We will discuss electro-optic properties and phase-behavior of lyotropic chiral-nematic materials under electric fields.

(I) Fingerprint rolls of a chiral nematic between two antiparallel-rubbed ITO substrates are formed at low electric field strengths. This pattern can be photo-stabilized through UV polymerization of added monomers by means of an UV focal-conic Gaussian laser beam. The chiral nematic liquid crystalline molecules are still free to diffuse within the polymer-stabilized confining structure. The resulting stabilized pattern can be used as a highly diffractive electrically switchable polymer-stabilized cholesteric diffraction grating (PSCDG). The regular spatial variation of chiral nematic material gives rise to strong light intensity in forward diffraction peaks, together with weaker intensity peaks of half the spacing from the polymer matrix. The electro-optic properties and dynamical modes of these gratings depend on the dynamics of the chiral nematic liquid within the polymer matrix, which is found to depend on whether isotropic or mesogenic monomers are used. We found a strong effect of confinement on the dynamics of chiral nematic order fluctuations in the mesogenic polymer network for scattering vectors along the helicoidal axis of the fingerprint-roll structures.

(II) Preliminary experiments on the phase-behavior of fd-virus suspensions under external electric fields will be shortly discussed. Phase diagrams in the field-amplitude versus frequency plane with the external electric AC field will be presented for various fd-virus concentrations. At low ionic strengths, electric field-induced polarization of the double layer induces an isotropic to chiral-nematic phase transition. At higher field strengths we observe melting of the chiral nematic state, which is probably due to either induced dipole-dipole interactions or the finite relaxation time of the double-layer charge density.

## Biological Effects of Pulsed Microwaves

Jozef Mendecki<sup>1</sup>, Daniel D. Mawhinney<sup>2</sup>, and Fred Sterzer<sup>2</sup>

<sup>1</sup>Montefiore Medical Center, Bronx, NY, USA

<sup>2</sup>MMTC, Inc., 12 Roszel Road, Princeton, NJ, USA

**Abstract**— The paper will describe *in vivo* animal experiments using pulsed microwaves and will discuss physical mechanisms that could account for the observed effects. In one experiment accelerated wound healing was demonstrated in Wistar rats. Linear skin incisions were made on each flank of the rats under sterile conditions. The incision on one flank was exposed to 30 minutes of pulsed microwaves twice daily for six days. The incision on the other flank was allowed to heal naturally without any intervention. The unexposed could be spread apart along the healed incisions with much less force than the incisions exposed to microwave pulses. In another series of experiments it was demonstrated that pulsed microwaves could enhance the uptake of pharmaceuticals and other substances. These experiments were carried out using 3-month-old male Copenhagen rats with a tumor model whose natural course simulates that of human prostatic cancer. The rats were implanted subcutaneously with 3 mm<sup>3</sup> of tumor tissues into the right and left sides of the lower chest abdomen plate. Eight days following the implantation when the tumors had grown to about 10 mm in diameter a series of experiments were performed. In one series of experiments the animals were injected with chemotherapeutic agents (Bleomycin 750 μ/kg or Taxol 5 mg/kg) and one of the tumors in each animal was exposed to microwave pulsing for 30 minutes at a time while the contralateral tumor was not pulsed. The pulsing was repeated twice at four-day intervals. After 26 days, the tumor volumes of the pulsed tumors were much smaller than those of the tumors that were not pulsed. Similar experiments using Trypan Blue and Fluorescin Dextran showed much larger uptakes of these substances in pulsed versus non-pulsed tumors. The physical mechanisms that might account for the results of these experiments include the unidirectional forces that are produced by microwave fields at the interfaces between low and high dielectric bodies, field enhancements caused by non-uniform shaped cells, and pulsed expansion/contractions caused by pulsed thermal effects.



# Universal Statistical Electromagnetic Properties of Ray-chaotic Enclosures

Steven M. Anlage, Thomas Antonsen, James Hart, Elliott Bradshaw, and Edward Ott  
Physics Department, University of Maryland  
College Park, MD 20742-4111, USA

**Abstract**— We are concerned with the universal electromagnetic properties of enclosures that show ray-chaos. Ray-chaos means that rays undergoing specular reflection from the interior of an enclosure show extreme sensitivity to initial conditions. This condition is quite common in real life. We investigate the electromagnetic wave properties of an ensemble of such enclosures, and this subject is known as ‘wave chaos’. One way to create such an ensemble of ray-chaotic enclosures is with a mode-stirred chamber. Our prior experimental work has examined the statistical properties of nearest-neighbor eigenvalue spacing [1], eigenfunctions [2], and the scattering and impedance matrices for 1- and 2-port single-channel systems [3, 4]. In wave chaotic scattering, statistical fluctuations of the scattering matrix  $S$  and the impedance matrix  $Z$  depend both on universal properties and on nonuniversal details of how the scatterer is coupled to external channels. We remove the non-universal effects of the coupling from the experimental  $S$  data using the radiation impedance obtained directly from the experiments [5], thus eliminating one of the most significant complications in electromagnetic scattering measurements. The results apply to scattering measurements on any wave chaotic system. The underlying universal statistical properties of the enclosures are well described by random matrix theory, and are independent of many details of the enclosure [6, 7]. We next identified an additional complication coming from short orbits created by the antenna and the walls of the enclosure. This leads to a correction of the radiation impedance to explicitly remove the non-universal short orbits, resulting in a clear determination of the underlying statistical properties.

## ACKNOWLEDGMENT

This work is supported by ONR MURI N000140710734 and ONR DURIP N000140710708.

## REFERENCES

1. So, P., et al., *Phys. Rev. Lett.*, Vol. 74, 2662, 1995.
2. Wu, D.-H., et al., *Phys. Rev. Lett.*, Vol. 81, 2890, 1998.
3. Hemmady, S., et al., *Phys. Rev. E*, Vol. 74, 036213, 2006.
4. Hemmady, S., X. Zheng, T. M. Antonsen, E. Ott, and S. M. Anlage, “Universal statistics of the scattering coefficient of chaotic microwave cavities,” *Phys. Rev. E*, Vol. 71, 056215, 2005.
5. Hemmady, S., et al., *Phys. Rev. Lett.*, Vol. 94, 014102, 2005.
6. Zheng, X., T. M. Antonsen Jr., and E. Ott, “Statistics of impedance and scattering matrices in chaotic microwave cavities: single channel case,” *Electromagnetics*, Vol. 26, 3, 2006.
7. Zheng, X., T. M. Antonsen Jr., and E. Ott, “Statistics of impedance and scattering matrices of chaotic microwave cavities with multiple ports,” *Electromagnetics*, Vol. 26, 37, 2006.

## Design of Composite Electromagnetic Wave Absorber Made of Soft Magnetic Materials Dispersed and Isolated in Polystyrene Resin

K. Sakai, Y. Wada, and S. Yoshikado

Department of Electronics, Doshisha University, Japan

**Abstract**— Development of an electromagnetic wave absorber suitable for the frequency band above 1 GHz is requested. The purpose of this study is to design composite electromagnetic wave absorber suitable for this frequency band. To design an absorber with desired absorption characteristics, the frequency dependences of the relative complex permeability  $\mu_r^*$ , relative complex permittivity  $\varepsilon_r^*$ , and conductivity  $\sigma$  of absorbing material are important. Thus, we have investigated to control the frequency dependences of  $\mu_r^*$ ,  $\varepsilon_r^*$  and  $\sigma$  by optimizing the structure of composite absorber. For optimization of structure, we attempt to disperse and isolate soft magnetic material particles in the polystyrene resin without the contact of each magnetic material particle. The composite absorber is composed of Permalloy or Sendust dispersed in the polystyrene resin. To isolate magnetic material particles, the surfaces of the magnetic material particles were coated by very fine polystyrene particles less than 1  $\mu\text{m}$  diameter. As a result, contact of each magnetic material particle could be prevented and the values of  $\varepsilon_r^*$  decreased. The frequency dependence of  $\mu_r^*$  did not obey the Lichtenecker's law, which explain the frequency dependences of  $\mu_r^*$  and  $\varepsilon_r^*$  of composite material, as magnetic material particles isolated in the polystyrene resin. Large magnetic loss related to eddy current loss occurred, because the values of  $\mu_r''$  had local maximum in the range of GHz. For the mixture ratio above 70 vol%, the values of  $\mu_r'$  was smaller than unity above 8 GHz due to the diamagnetism. This result shows that electromagnetic wave above 10 GHz can be absorbed, because the values of  $\mu_r'$  is to be less than one above several GHz from the theoretical calculation. It is concluded that both  $\mu_r^*$  and  $\varepsilon_r^*$  can be controlled in the wide range. Therefore, the sample could absorb electromagnetic wave energy above 99% in the frequency range above several GHz.

# Spectral Density Function Approach as Applied to Dielectric Properties of Biological Cell Suspensions

A. V. Goncharenko<sup>1,2</sup> and Yia-Chung Chang<sup>1</sup>

<sup>1</sup>Research Center for Applied Sciences, Academia Sinica, Nankang, Taipei 115, Taiwan

<sup>2</sup>Institute of Semiconductor Physics, Natl. Acad. of Sci. of Ukraine, Kyiv 03028, Ukraine

**Abstract**— Modern dielectric spectroscopy is known to be able, in principle, to estimate the average electrical properties of biological cells, that, in turn, allows one to extract a useful information from dielectric spectra of cell suspensions using an appropriate mixture rule [1]. However, while the cells can have a complicated shape and structure, in practice, for mathematical treatment, they usually restrict themselves to dealing with the simplest geometry such as two confocal ellipsoids. There were also rare attempts to consider more complicated shapes, such as axially symmetric particles (see, e.g., [2]). To describe the dielectric spectra of the cell suspensions, we suggest to adopt a more general approach based on an extension of the so-called Bergman-Milton (BM) spectral representation [3, 4].

The BM formalism enables one to separate the material parameters of the phases (in our cases — dielectric constants and conductivities) and geometrical parameters, which are specified by the so-called spectral density function. The effective dielectric response of a suspension can be represented via an integral equation with the integrand being the product of the kernel which is nothing but the polarizability of a spheroid and the spectral density function which can be considered as a shape distribution function of the spheroids. The function describes geometric arrangement of the real particles, their shapes, as well as mutual interaction. Some ideas how to construct this function are suggested in [5].

Although any shape can be considered within this framework, so far the approach was limited by two-phase systems only. As the cells consist of at least three phases (cell cytoplasm, membrane, and extracellular medium), the approach in its conventional form is inapplicable for describing cell suspensions. To extend the BM approach to the suspensions of the cells (which are modeled as shelled particles) we make use of an equivalent permittivity of a shelled spheroid. The equivalent permittivity of the inhomogeneous (shelled) spheroid 1 may be defined as such the permittivity of a *homogeneous* spheroid 2 (having the same dimension as the spheroid 1) that if the permittivity of the ambient medium is equal to it, the field and the potential at any point of the ambient medium is unperturbed by the introduction of the spheroid 1 [6]. Our main idea is to substitute the equivalent permittivity in the expression for the spheroid polarizability; in such a way we obtain a three-phase extension of the BM representation to suspensions of the shelled particles. We show that this approach can be especially efficient and useful when dealing with dielectric properties of biological cells having a thin membrane. In addition, the multilayer (and, in particular, bilayer) membranes can be considered within the framework of our approach.

## REFERENCES

1. Asami, K., *Prog. Polym. Sci.*, Vol. 27, 1617, 2002.
2. Gheorghiu, E., *Ann. New York Acad. Sci.*, Vol. 873, 262, 1999.
3. Bergman, D., *Phys. Rep.*, Vol. 43, 377, 1978.
4. Milton, G. W., *Appl. Phys. Lett.*, Vol. 37, 300, 1980.
5. Goncharenko, A. V., *Phys. Rev. E*, Vol. 68, 041108, 2003.
6. Bilboul, R. R., *Brit. J. Appl. Phys.*, Vol. 2, 921, 1969.

## Non-thermal Effect of Electrolyte Aqueous Solution under Microwave Radiation

Ka-Ma Huang and Xiao-Qing Yang

College of Electronics and Information Engineering, Sichuan University, Chengdu 610064, China

**Abstract**— The reflection coefficients from a coaxial line probe, which is merged in the electrolyte aqueous solutions with constant temperature are measured under the different microwave powers. The measured results show that there is a new phenomenon: the amplitude of reflection coefficient can be influenced by microwave power. As to sodium chlorid, by the multiphysics calculation and temperature measurement during the experiment, the thermal effect can be excluded. So, it should be a non-thermal effect of sodium chloride aqueous solution under microwave radiation. Furthermore, the new phenomenon is analyzed and explained, it is reason that the microwave power can influence directly the conductivity of electrolyte aqueous solution.

# Session 5A5

## Remote Sensing and Scattering Problem

<p>An Unsupervised Classification Method for Polarimetric SAR Images Based on Inhomogeneous Markov Random Field and Graph Cuts</p> <p><i>Xing Rong (Tsinghua University, China); Jian Yang (Tsinghua University, China); Weijie Zhang (Tsinghua University, China); Wen Hong (Institute of Electronics, Chinese Academy of Sciences, China); Fang Cao (Institute of Electronics, Chinese Academy of Sciences, China);</i> .....</p>	974
<p>Spatial Distribution Pattern of MODIS-NDVI and Correlation between NDVI and Meteorology Factors in Shandong Province in China</p> <p><i>Dongmei Song (China University of Petroleum, China); Peng Guo (China University of Petroleum, China); Hui Sheng (China University of Petroleum, China);</i> .....</p>	976
<p>Development of the Microwave Calibrated Infrared Split-window Technique (MIST) for Rainfall Estimation</p> <p><i>Roongroj Chokngamwong (George Mason University, USA); Long Sang Chiu (Chinese University of Hong Kong, China);</i> .....</p>	977
<p>High Temporal Resolution Atmospheric Soundings from GOES Sounder and Applications</p> <p><i>Zhenglong Li (University of Wisconsin-Madison, USA); Jun Li (University of Wisconsin-Madison, USA); W. Paul Menzel (University of Wisconsin-Madison, USA); Timothy J. Schmit (NOAA/NESDIS, USA);</i> .....</p>	978
<p>Domain Decomposition Method with Iterative Robin Boundary Condition for Bistatic Scattering from Large 3D Rough Surface</p> <p><i>Peng Liu (Fudan University, China); Ya-Qiu Jin (Fudan University, China);</i> .....</p>	979
<p>Research Progress in Polarimetric Scattering and SAR Imagery in WASRSI</p> <p><i>Ya-Qiu Jin (Fudan University, China);</i> .....</p>	980
<p>Investigation on the RCS Measurement Technique of Large Targets at Near Distance</p> <p><i>Nan-Jing Li (Northwestern Polytechnical University, China); Wei-Jun Chen (Northwestern Polytechnical University, China); Chu-Feng Hu (Northwestern Polytechnical University, China); Lin-Xi Zhang (Northwestern Polytechnical University, China);</i> .....</p>	981
<p>Application of DSP in the Step-Frequency RCS Measurement System</p> <p><i>Chu-Feng Hu (Northwestern Polytechnical University, China); Jia-Dong Xu (Northwestern Polytechnical University, China); Nan-Jing Li (Northwestern Polytechnical University, China); Jin Cao (Northwestern Polytechnical University, China);</i> .....</p>	982
<p>Effects of Complex Models in Deriving Lightning Return-stroke Currents from Fields</p> <p><i>Robert L. Gardner (6152 Manchester Park Circle, USA);</i> .....</p>	983

# An Unsupervised Classification Method for Polarimetric SAR Images Based on Inhomogeneous Markov Random Field and Graph Cuts

Xing Rong<sup>1</sup>, Jian Yang<sup>1</sup>, Weijie Zhang<sup>1</sup>, Wen Hong<sup>2</sup>, and Fang Cao<sup>2</sup>

<sup>1</sup>Dept. of Electronic Eng., Tsinghua University, Beijing 100084, China

<sup>2</sup>National Key Lab of Microwave Imaging Technology  
Institute of Electronics, CAS, Beijing 100080, China

**Abstract**— Cloude and Pottier proposed an unsupervised classification method based on their target decomposition theory [1]. Lee proposed a method based on the Wishart classifier [2]. Both methods are based on the assumption that the pixels are independent. Markov Random Field (MRF) has been applied to classification in remote sensing [5]. The standard Markov Random Field (homogeneous MRF) can incorporate the spatial interaction of pixels but cannot represent the label scale variability because it assumes that the coupling between pixel labels (the parameter  $\beta$ ) is constant throughout the whole image. When we classify an image by using the homogeneous MRF model, it is difficult to keep details of a region associated with a small  $\beta$  and prevent another region associated with a large  $\beta$  from being divided simultaneously.

In this paper, we employ the Inhomogeneous MRF [3] to solve the above problem and convert the unsupervised classification problem of POLSAR images into finding a labeling for minimizing an energy function by using maximum a-posteriori probability (MAP) estimator. We develop a new iteration method consisting of two steps: (1) to fix the labeling (a classification result) and estimate the cluster parameters and the smoothness parameter  $\beta$  in the energy function; (2) to fix the parameters and estimate a labeling that minimizes an energy function by using an expansion algorithm [4] based on Graph Cuts. In Step (1), if the covariance matrix of the  $m$ -th cluster center is denoted as  $\Sigma_m$ , then the estimation of  $\Sigma_m$  is the mean of covariance matrices of the pixels corresponding to the label  $m$  in the last iteration [2]. For Inhomogeneous MRF,  $\beta$  is variant in different sites of an image, and the estimation of  $\beta_{ij}$  is intractable because  $\beta_{ij}$  appears in both the exponent of the probability density model and the normalizing constant. So the Pseudo Likelihood Estimator (PLE) can be used here. We separate the whole image into  $16 \times 16$  equal partitions, and in each partition  $\beta$  is treated as a constant which is estimated in each partition. In this way,  $\beta$  can approximately represent the local label scale and its estimation is tractable. To make the labeling to be discontinuity preserving, we chose the Potts model in Step (2) because the potential function of the Smoothness term has to be non-convex, which made computing the global minimum of the energy function to be NP-hard. We use an expansion algorithm based on Graph Cuts other than the Iterated Conditional Modes(ICM) or Simulated Annealing(SA) to compute the approximation of the global minimum. In contrast to standard moves adopted in ICM and SA which can be trapped in a local minimum that may be arbitrarily far from the global minimum, the expansion moves are adopted in the expansion algorithm based on Graph Cuts which can rapidly reach the result that is within a factor of two of the global minimum. In this algorithm, we can find the approximation of the global minimum by setting a suitable graph and finding the minimum cut in the graph.

The procedure of the proposed method is given as follows: (1) Initialize the labeling and compute the corresponding covariance matrices of cluster centers. (2) Divide the image into  $16 \times 16$  equal partitions; for each partition compute  $\beta$  by using the labeling obtained from the last iteration. Let  $\beta = \beta/6$  if the time of the iteration is odd. (3) Find the new labeling by using the expansion algorithm based on Graph Cuts. (4) Update covariance matrices of cluster centers  $\Sigma_m$  by using the new labeling. (5) Go to Step (2) unless termination condition is satisfied.

The excellent performance of the proposed method has been illustrated by a NASA/JPL AIRSAR L-band image of San Francisco. In contrast to much noise and falsely assigned labels by using the method proposed in [2], the proposed method keeps both the spatial coherence and the details of the image.

## ACKNOWLEDGMENT

This work was supported by the research fund of National Key Lab of Microwave Imaging Technology, Institute of Electronics, Chinese academy of sciences.

**REFERENCES**

1. Cloude, S. R. and E. Pottier, "An entropy based classification scheme for land applications of polarimetric SAR," *IEEE Trans. Geosci. Remote Sensing*, Vol. 35, No. 1, 68–78, Jan. 1997.
2. Lee, J. S., M. R. Grunes, and et al., "Unsupervised classification using polarimetric decomposition and the complex Wishart classifier," *IEEE Trans. Geosci. Remote Sensing*, Vol. 37, No. 5, 2249–2257, Sept. 1999.
3. Cadez, I. and P. Smyth, "Modeling of inhomogeneous Markov random fields with applications to cloud screening," University of California, Technical Report UCI-ICS, 98–21, 1998.
4. Boykov, Y., O. Veksler, and R. Zabih, "Fast approximate energy minimization via Graph Cuts," *Proc. IEEE Trans. Pattern Analysis and Machine Intelligence*, Vol. 23, No. 11, 1222–1239, Nov. 2001.
5. Chen, Y., et al., "Supervised polarimetric SAR classification method using graph-cut," submitted to *IEEE Geoscience and Remote Sensing Letters*.

## Spatial Distribution Pattern of MODIS-NDVI and Correlation between NDVI and Meteorology Factors in Shandong Province in China

Dongmei Song, Peng Guo, and Hui Sheng

Earth Resource and Information Institute, China University of Petroleum, Qing Dao 266555, China

**Abstract**— The vegetation index research was necessary for monitoring plant growth. Based on the data of 250 m spatial resolution NDVI (Normalized Difference Vegetation Index) of MODIS (Moderate Resolution Imaging Spectroradiometer), this paper analyzed the spatial distribution pattern of NDVI in Summer in Shandong province in the east of China. With the data of six meteorologic sites and the average NDVI in January, April, July and October in 2006 and the average values of atmosphere temperature, relative humidity, rainfall, sunlight hours and the SPSS statistics software, the correlation between NDVI and meteorology factors was researched. The results were showed as follows: there was obvious character of spatial distribution pattern of NDVI in Shandong Province. The value of NDVI in plain region was higher than that of mountain and hill region, and there was little change range of NDVI in plain, in which the most of NDVI was greater than 0.7–0.8. In the mountain region, NDVI was falling off with the decreasing of the altitude, where NDVI was about 0.6–0.7. Deeply research showed that NDVI was affected by human activity distinctly, and the NDVI in the city was lower than 0.4, as such lower than that of the suburb. The atmosphere temperature and quantity of the rainfall were the two main factors affecting the change of NDVI, at the same time the seasonal sunlight hours was second-class factor that caused the change of the NDVI. The research results also showed that with the decreasing of the latitude, the correlation between NDVI and temperature was decreasing too, on contrast, the correlation between NDVI and the quantity of rainfall was increasing. In Spring and Summer, the atmosphere temperature was the most main factor that caused the change of NDVI in Shandong province, however, in Autumn the main factor was the quantity of the rainfall.



## Development of the Microwave Calibrated Infrared Split-window Technique (MIST) for Rainfall Estimation

Roongroj Chokngamwong<sup>1</sup> and Long S. Chiu<sup>2</sup>

<sup>1</sup>Center for Earth Observing and Space Research  
George Mason University, Fairfax, VA 22030, USA

<sup>2</sup>Institute of Space and Earth Information Science  
Chinese University of Hong Kong, Shatin Hong Kong, China

**Abstract**— An Infrared rainfall estimation technique that includes information from a split window is developed. The split-window refers to the difference in the brightness between the far infrared channels situated at around 10 and 12 microns and has been used to estimate atmospheric water vapor and for rain area detection. The technique, called the Microwave calibrated Infrared Split-window Technique, or MIST, can be considered an extension of the Adjusted GOES Precipitation Index (AGPI). IR rain rates are first estimated from an IR-rain rate relation derived from matching the monthly histograms of combined microwave rain estimates (3B40RT) produced by the Tropical Rainfall Measuring Mission (TRMM) Multi-satellite Precipitation Analysis (TMPA) and the infrared data observed from a geostationary satellite. The novelty is the inclusion of the split-window information to eliminate non-rainy pixels as a second step. The technique has been applied to GMS and GOES data and tested for a dry and a wet period. The results show that the MIST has comparable biases and better rain event detection skill than the TMPA, although the TMPA is constrained by the gauge analysis by design while the MIST has no direct gauge input.

# High Temporal Resolution Atmospheric Soundings from GOES Sounder and Applications

Zhenglong Li<sup>1</sup>, Jun Li<sup>1</sup>, W. Paul Menzel<sup>1</sup>, and Timothy J. Schmit<sup>2</sup>

<sup>1</sup>Cooperative Institute for Meteorological Satellite Studies (CIMSS)  
University of Wisconsin-Madison

1225 West Dayton Street, Madison, WI 53706, USA

<sup>2</sup>Center for Satellite Applications and Research, NOAA/NESDIS

1225 West Dayton Street, Madison, WI 53706, USA

**Abstract**— Both infrared (IR) and microwave sounders are currently being used for remote sensing of atmospheric and surface conditions, such as temperature and moisture, the surface emissivities and skin temperature. The microwave sounder has the advantage of all weather conditions, but the spatial and temporal resolutions are usually low compared with IR due to weak signal strength. Current technology can only put microwave sensors on polar-orbit satellites, which usually takes about 12 hours to visit the same area. For short-term severe weather forecast, IR sounders on geostationary satellites perform much better than microwave sounders on polar-orbit satellites for better temporal and spatial resolutions. The disadvantage is the remote sensing can only be done for cloud-free area only with current geostationary infrared sounders.

By using a realistic error covariance matrix of background information, an improved fast radiative transfer model (RTM), a radiance bias adjustment scheme, a first guess from regression, a reliable surface emissivity scheme, and inverted cone averaging, an improved physical retrieval algorithm is applied to the Geostationary Operational Environmental Satellite-12 (GOES-12) Sounder radiances. A comparison with the microwave radiometer (MWR) measured total precipitable water (TPW) at the Southern Great Plains (SGP) Cloud and Radiation Testbed (CART) site from June 2003 to May 2005 shows that the TPW retrievals are improved by 0.4 mm over the previous legacy GOES Sounder TPW product. A case study on a deadly tornadic supercell at Eagle Pass, Texas on 24 April 2007 reveals that the improved physical retrieval is able to identify the pre-convective environment while the numerical model forecast failed to do so. Another supercell case on 13 April 2006 demonstrated that the improved physical algorithm is able to detect the low level moisture much better than the GFS forecast. These hourly products greatly help the forecasters determine the further development of the current weather system. With future GOES hyperspectral IR sounding system, temperature and moisture profiles with full disk coverage can be achieved with much higher vertical resolution and accuracy than the current GOES Sounders.

# Domain Decomposition Method with Iterative Robin Boundary Condition for Bistatic Scattering from Large 3D Rough Surface

Peng Liu and Ya-Qiu Jin

Key Laboratory of Wave Scattering and Remote Sensing Information  
(Ministry of Education), Fudan University, Shanghai 200433, China

**Abstract**— A non-iterative domain decomposition method with Iterative Robin Boundary Condition (IRBC) is developed for bistatic scattering from large 3D rough surface. The coupling boundary conditions on the interface between two adjacent subdomains are derived when the IRBC is used as the truncation boundary of the Finite Element Method (FEM), and the final coupling matrices are obtained by using the inward-looking approach. This matrix has a sparse block structure, through which the interactions between DDM subdomains are described. By using an efficient solver, the unknown expansion coefficients on the DDM interfaces can be obtained by solving the DDM coupling matrix equation. Then the field distributions in each subdomain can be obtained from a field summation procedure.

The IRBC is used as an open-region boundary condition to solve the electromagnetic (EM) scattering problem. The IRBC is expressed as the localized operator embodying the Sommerfeld radiation condition on the fictitious boundary, where its right-hand side residual is iteratively updated by field integral equation in the computational region. In the case of planar structure such as large-scale rough surface, most time consuming of the algorithm is spent on evaluating the IRBC on the planar fictitious boundary. In this paper, the field integral equation is written as the 2D (2-dimensional) convolution form and is solved efficiently by using the fast Fourier transform (FFT). Computation complexity of the IRBC is reduced from  $O(N_s^4)$  to  $O(N_s^2 \log N_s^2)$ , where  $N_s$  is the number of sampling points in one direction of the planar fictitious boundary.

The formulation of this technique is presented, and a numerical simulation of the EM scattering from large scale 3D random rough surface is carried out to show the accuracy and efficiency.

## Research Progress in Polarimetric Scattering and SAR Imagery in WASRSI

Ya-Qiu Jin

Key Laboratory of Wave Scattering and Remote Sensing Information (WSRS, MOE)  
Fudan University, Shanghai 200433, China

**Abstract**— Synthetic aperture radar (SAR) imagery technology is one of most important advances in space-borne microwave remote sensing during recent decades. Completely polarimetric scattering from complex terrain surfaces can be measured. Fully understanding and quantitatively retrieving information from polarimetric scattering signatures of natural media have become a key issue for SAR remote sensing and its broad applications.

During recent years, there has been extensive research on polarimetric scattering for SAR imagery, including Pol-InSAR, BiSAR etc.

In this presentation, a brief report on the research progress of polarimetric scattering and information retrieval from SAR imagery in our Laboratory (WSRS) is presented. It includes: polarimetric scattering modeling of the terrain surface via parameterized Mueller matrix solution, polarimetric pulse propagation through inhomogeneous vegetation canopy, deorientation theory and unsupervised terrain surface classification, multi-aspect SAR image and 3-D object reconstruction, image simulation of comprehensive terrain scene for polarimetric SAR and bistatic SAR techniques, and polarimetric radar exploration of Lunar surface etc.

## Investigation on the RCS Measurement Technique of Large Targets at Near Distance

Nan-Jing Li, Wei-Jun Chen, Chu-Feng Hu, and Lin-Xi Zhang

UAV Speciality Technique Key Labrotary of National Defense Technology

Northwestern Polytechnical University, Xi'an, Shaanxi 710072, China

**Abstract**— In general, RCS measurement must meet the far-field condition, which needs a vast measuring area or a costly compact range. To solve the problem, a new extrapolating correction technique by dealing with near-distance RCS measurement of aircraft targets is set up. The RCS of aircraft targets under spherical wave illuminating can be adopted to extrapolate far-field RCS of them. The extrapolating convolution arithmetic utilizing conductive board as a reference target deduces the phase-correction coefficient  $g(x)$  between spherical and plane wave, and in fact the extrapolating convolution calculation of  $g(x)$  can be replaced by Fast Fourier Transform, which is related to the scattering field of the reference target measured in near-distance, thus the calculating procedure could be completed simply and quickly. By theoretical simulation for simple target, such as conductive board and cylinder, the RCS extrapolated can be obtained correctly. Experimental results of complex aircraft target show that this new technique is makes experiment agree to theory precisely, moreover, it permits the measurement distance reduced by 15 percent of the minimum distance of far-field. Also, there is no serious limitation to target in dimension of aperture and depth during the measurement.

## Application of DSP in the Step-Frequency RCS Measurement System

Chufeng Hu, Jiadong Xu, Nanjing Li, and Jin Cao

National Defense Technology Institute, Northwestern Polytechnical University  
Xi'an, Shaanxi 710072, China

**Abstract**— Step-Frequency RCS measurement system is a new and remarkable RCS measurement system, which can obtain the response of target at each frequency point in an anecho chamber. Comparing it with traditional way of CW RCS measurement, more information gains in the new system. IFFT, zero insertion and the use of additional windows are some of familiar DSP techniques, which can improve the results if they are applied to the measurement. Using IFFT, the frequency domain data of whole chamber obtained by the measurement can be interpreted into time domain value, and the unwanted signals can be removed by adding a gate of range. Inserting zero in the frequency domain for increasing the points of IFFT will be good for finding response of target in the time domain exactly. The measurement of finite frequency spectrum makes the cut of data, the use of windows can reduce the effect of side lobe. Two metal spheres are measured in the anecho chamber. Two sorts of diameter are 50 mm and 400 mm respectively. The former is used for a target, the latter for scaling. The span of frequency is 8 GHz ~ 12 GHz, and the test frequency points are 801. Hamming windows are added to frequency domain data of the target and the scaler, then a number of zero as many as three times of frequency domain data are inserted for IFFT. A range gate is added to the target region where energy of target returns is much higher than the background. Returning to the frequency domain again, according to the results scaled, it shows that the accuracy of measurement is obviously improved. The value of RCS measurement is waved less than 1 dB around the center of frequency over 80%, in comparison with 4 dB waving over all test frequencies before, so it's significant that integrating DSP techniques mentioned above is specially useful for RCS measurement of low scattering targets.

## Effects of Complex Models in Deriving Lightning Return-stroke Currents from Fields

**Robert L. Gardner**

6152 Manchester Park Circle, Alexandria, VA 22310-4957, USA

**Abstract**— Lightning return-stroke currents are large broadband sources of electromagnetic fields. These currents may be 100s of kA and last for 10s of microseconds and so produce a very hostile environment around the channel. Further, unless the experimenter is very careful, the measurement process will substantially change the currents of interest. These currents produce electromagnetic fields that can be used to remote sense the currents in the channel, but the models predicting the direct phenomena are very approximate. For example, the most used model is one that assumes that the channel current propagates without change in waveform up the channel at the speed of light and the electromagnetic wave propagates over perfectly conducting ground consequently with the same waveform. In fact, the channel is lossy with loss terms that are dependent on height and current and are dispersive. Further, the ground has losses, particularly in the frequency range of lightning return-strokes. The effect of the channel losses is that the source of the high-frequency radiation from the channel is limited to the region near the ground and is not spread over the channel as required by the simpler model above. Calculation of the degree of dispersion requires a complex non uniform, nonlinear transmission line model that, at least approximates the hydrodynamic development of the channel. An analytic hydrodynamic model is inserted into a transmission line model to show the variation in attenuation with frequency and height. Propagation over lossy ground limits the amount of information that can be derived from the fields on the early time part of the pulse and, for some cases, the information cannot be recovered. Use of these more complex models suggests that standard current waveforms may have high frequency components that cannot be derived using the simple field inversion technique.





# Session 5A6

## Microwave and Millimeter Wave Circuits and Devices

### 2

<p>Electromagnetic Absorption by Conducting Fiber Filled Composite in the Centimeter- and Millimeter-wave Regions  <i>Ling Yun Liu (Hubei University of Technology, China); Lin Zhang Wu (Hubei University of Technology, China); Shi Bing Pan (Nonmetal Institute of Jinan, China); Xian Wang (Huazhong University of Science and Technology, China); Rong Zhou Gong (Huazhong University of Science and Technology, China); Hua Hui He (Huazhong University of Science and Technology, China);</i> .....</p>	986
<p>A Novel Compact Balun for DVB-H Application  <i>Kengyi Huang (National Central University, Taiwan, R.O.C.); Tsenchieh Chiu (National Central University, Taiwan, R.O.C.); Chao Ping Hsieh (National Central University, Taiwan, R.O.C.);</i> .....</p>	987
<p>Analysis of the Optimal Gap Width and Gap-to-gap Distance in <math>\pi</math>-mode Double-gap Cavities for Broad-band Klystrons  <i>Fu-Min Lin (Shantou University, China);</i> .....</p>	988
<p>Analysis and Design of Power Generator on Passive RFID Transponders  <i>Fan Jiang (Xiamen University, China); Donghui Guo (Xiamen University, China); L. L. Cheng (City University of Hong Kong, China);</i> .....</p>	989
<p>An Injection-locked Millimeter Wave Oscillator Based on Field-emission Cathodes  <i>Ming-Chieh Lin (Fu Jen Catholic University, Taiwan, R.O.C.); Pu-Shih Lu (Fu Jen Catholic University, Taiwan, R.O.C.);</i> .....</p>	990
<p>Miniaturized Planar Microstrip Line Broadband Branch-line Coupler  <i>Shry-Sann Liao (Feng-Chia University, Taiwan); Kun-Ying Lin (Nan Kai Institute of Technology, Taiwan); Pou-Tou Sun (Feng-Chia University, Taiwan); Hung-Liang Lin (Feng-Chia University, Taiwan); Yu-Fang Chang (Feng-Chia University, Taiwan);</i> .....</p>	991
<p>A New Tunable Wideband Ring Filter with Merged Stubs and Miniaturized Geometry for Bluetooth Technology  <i>Mohamed Salah Kheir (German University in Cairo, Egypt); Adel Mohamed Abdin (Shorouk Academy, Egypt);</i> .....</p>	992

## Electromagnetic Absorption by Conducting Fiber Filled Composite in the Centimeter- and Millimeter-wave Regions

L. Y. Liu<sup>1</sup>, L. Z. Wu<sup>1</sup>, S. B. Pan<sup>2</sup>, X. Wang<sup>3</sup>, R. Z. Gong<sup>3</sup>, and H. H. He<sup>3</sup>

<sup>1</sup> School of Electrical and Electronic Engineering, Hubei University of Technology  
Wuhan 430068, China

<sup>2</sup> Nonmetal Institute of Jinan, Jinan 250031, China

<sup>3</sup> Department of Electronic Science and Technology, Huazhong University of Science and Technology  
Wuhan 430074, China

**Abstract**— We observed strong electromagnetic absorption by the conducting fiber filled foam composite with a low fiber concentration in a wide frequency range. The strong absorption in millimeter-wave region can be attributed to the magnetic property which originates from the interaction of fibers in high frequency region. The experimental data are in good agreement with the theoretical computations. With the aspect ratio of the fiber increasing and the conductivity decreasing, strong absorption would emerge throughout the centimeter- and millimeter-wave regions. The conducting fiber filled composite can be employed to develop light microwave absorbing materials with strong absorbing ability in wide waveband.

## A Novel Compact Balun for DVB-H Application

Kengyi Huang, Tsenchieh Chiu, and Chao Ping Hsieh

Department of Electrical Engineering, National Central University, Taiwan, R.O.C.

**Abstract**— The novel miniaturized baluns designed for digital TV (UHF 470–710 MHz) applications will be presented in this paper. Conventional Marchand baluns employ  $\lambda/4$  coupled lines and yield broadband characteristics. These  $\lambda/4$  coupled lines occupy large circuit areas, especially for low frequency applications (ex, DVB, GSM). Broadband design is not always required for commercial applications. Thus, some trade-offs can be made between bandwidth and the size of the circuits. In the paper, the proposed design replaces the open-terminal of traditional Marchand balun with a grounded capacitor which regulates the bandwidth of the Marchand balun. Furthermore, by replacing the open-terminal with short-terminal, a narrow bandwidth characteristic is obtained, while the electrical length of the coupled lines is reduced to  $\lambda/10$ . Baluns are devices for converting signals between an unbalanced circuit structure ( $Z_{in}$ ) and a balanced circuit structure ( $Z_{out}$ ). This novel balun is suitable for low impedance-transforming ratio ( $Z_{out}/Z_{in} \leq 1$ ) application. However, it is sensitive to output impedance.

For the complex impedance component designs (ex, amplifiers), circuit structures insensitive to output impedance are proposed. The miniature, narrow band and insensitive balun is realized by using one series capacitor at unbalanced port and two shunt capacitors at balanced port. This design provides a wide impedance-transforming ratio  $Z_{out}/Z_{in}$  from  $0.5 \sim 1.6$ . The balun bandwidth is controllable, and the required coupled-line lengths of this balun structure can be as short as  $\lambda/25$ . All circuits are fabricated on FR4 substrate, and the measurement results are in good agreement with simulations by HFSS. The proposed baluns achieve 0.5 dB amplitude balance and  $5^\circ$  phase balance.

## Analysis of the Optimal Gap Width and Gap-to-gap Distance in $\pi$ -mode Double-gap Cavities for Broadband Klystrons

Fu-Min Lin

Department of Physics, Shantou University, Guangdong 515063, China

**Abstract**— Double-gap cavities are usually used as output cavities of klystrons to widen the frequency band and upgrade the peak power of the output. An accurate design of the gap width and the gap-to-gap distance is very important to the efficiency of klystron. Unsuitable gap width or distance between two gaps will cause parasitic oscillation or instability.

Equal two gaps is generally used in  $\pi$ -mode double-gap cavity, but it is not the optimal gap width to get maximal efficiency, because of the different speed or transit angle of electrons in two gaps. It is also not the best choice that the transit angle of the distance between two gaps in  $\pi$ -mode double-gap cavity is  $\pi$ , just as which in many conventional design. The paper is to analysis the interaction process of ideal clustering electron beam with the resonant E-field in the gaps of asymmetric  $\pi$ -mode double-gap cavities by single electron approximate approach, and the optimal gap width and the distance between two gaps for maximal conversion efficiency are calculated. The results are

$$\theta_1 = \omega t_1 = \frac{\pi}{2}, \quad \theta_2 = \omega t_2 = \pi, \quad \theta_L = \omega t_L = 2\pi$$

$$d_1 = \frac{\pi V_0}{2\omega} \left( 1 - \frac{2}{\pi} \frac{eE_0}{m_e \omega V_0} \right), \quad d_2 = \frac{\pi V_0}{\omega} \left( 1 - \frac{2eE_0}{m_e \omega V_0} \right), \quad L = \frac{2\pi V_0}{\omega} \left( 1 - \frac{eE_0}{m_e \omega V_0} \right)$$

The transit angle of the distance between the middles of two gaps is  $2.75\pi$ . The maximal efficiency is

$$\eta_{\text{opt}} = 1 - \left( 1 - \frac{3eE_0}{m_e \omega V_0} \right)^2$$

# Analysis and Design of Power Generator on Passive RFID Transponders

Fan Jiang<sup>1,3</sup>, Donghui Guo<sup>1,2,3</sup>, and L. L. Cheng<sup>4</sup>

<sup>1</sup>EDA Lab, Department of Physics, Xiamen University, Xiamen 361005, China

<sup>2</sup>Department of Electronic Engineering, Xiamen University, Xiamen 361005, China

<sup>3</sup>Xiamen RichIT Microelectronic Technologies LTD, Xiamen 361005, China

<sup>4</sup>Electronic Engineering Department of City University of Hong Kong, Hong Kong, China

**Abstract**— Rectifier is the essential part of passive RFID transponders. This paper based on two types of conventional rectifier, such that several factors which influence the output voltage and Power Conversion Efficiency (PCE) of the rectifier are being studied. From the analysis results of these two types of rectifier, we proposed a modified version of the rectifier which has high output voltage and high PCE. Simulation results are also studied and presented in this paper.

# An Injection-locked Millimeter Wave Oscillator Based on Field-emission Cathodes

Ming-Chieh Lin<sup>1</sup> and Pu-Shih Lu<sup>1,2</sup>

<sup>1</sup>NanoScience Simulation Laboratory (NSSL), Department of Physics  
Fu Jen Catholic University, Taiwan, R.O.C.

<sup>2</sup>Institute of Optoelectronic Sciences, National Taiwan Ocean University, Taiwan, R.O.C.

**Abstract**— We investigate an injection-locked millimeter wave source based on field emission mechanism by following the previous successful designs of the THz and millimeter wave devices. The design of the device has been carried out and verified by the finite-difference time-domain particle-in-cell simulations. The well phase/frequency controllability is demonstrated and the simulation results are consistent with the prediction of Adlers equation. A band width about 60 MHz is obtained and the corresponding efficiency 7.38% is achieved without employing any external magnetic circuit. The quality factor is also calculated. The preliminary results show that our design seems to promise useful and compact millimeter wave sources.

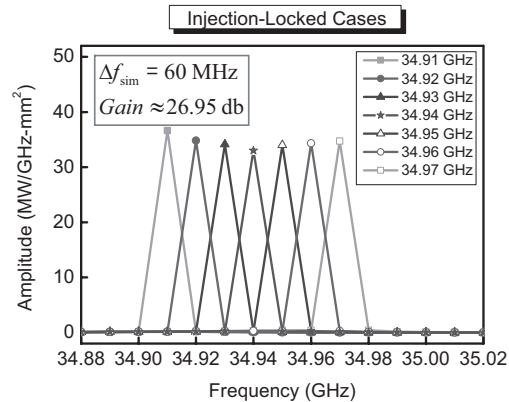


Figure 1: Power spectrum of successfully locked cases with injected frequency from 34.91 to 34.97 GHz.

# Miniaturized Planar Microstrip Line Broadband Branch-line Coupler

Shry-Sann Liao<sup>1</sup>, Kun-Ying Lin<sup>2</sup>, Pou-Tou Sun<sup>1</sup>, Hung-Liang Lin<sup>1</sup>, and Yu-Fang Chang<sup>1</sup>

<sup>1</sup>RF&MW Circuits Design Laboratory, Department of Communication Engineering  
Feng-Chia University, 100, Wen-Hua Rd., Taichung, Taiwan 407, R.O.C.

<sup>2</sup>Department of Electronic Engineering, Nan Kai Institute of Technology  
568, Chung Cheng Rd.,Tsaotun Nantou Taiwan 542, R.O.C.

**Abstract**— Branch-line coupler is one of the most popular circuits with the convenient design and implementation for the realization of balanced circuits and matched attenuators. However, the narrow-band characteristics and the large circuit dimension are the major disadvantages. The traditional multi-branch design can enlarge the bandwidth [1, 2], but they increase the circuit dimension. Many methods have been proposed to overcome this problem [3, 4]. In this study, several methods are considered to increase bandwidth up to 50%, it shows the size reduction more than 89% compared with the conventional wideband branch-line coupler design.

This novel broadband branch-line coupler is designed and realized at the band group one of the Ultra-Wideband (UWB) system, i.e., 3.1 GHz  $\sim$  4.7 GHz. All the simulated S-parameters of this coupler are obtained from the full-wave Sonnet em simulator and measurement results are shown in Fig. 1. The prototype circuits are fabricated on the RO4003C substrate ( $\epsilon_r = 3.38$ ,  $\tan \delta = 0.0027$ , thickness = 0.813 mm, and the metal thickness = 0.022 mm) and is measured by Agilent 8510C. The element size of the component can easily be patterned by using standard printed-circuit etching processes. It is very useful in the modern communication systems.

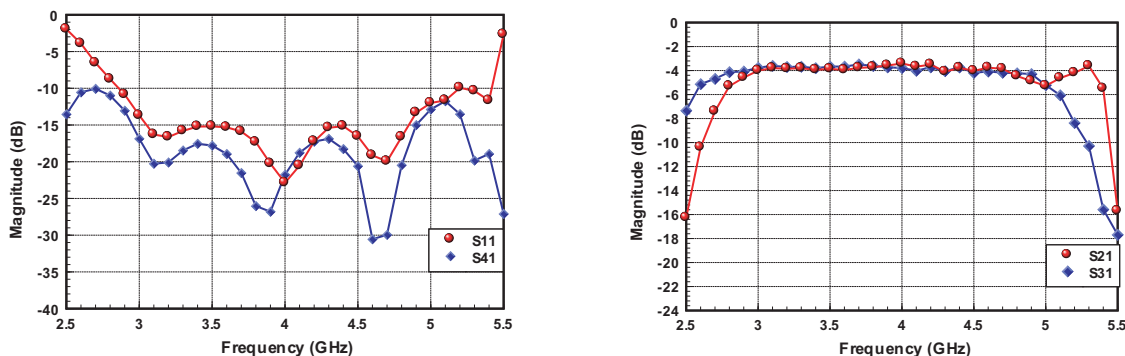


Figure 1: Measurement of S-parameters.

## ACKNOWLEDGMENT

The authors are grateful to support from the National Science Council of Taiwan in this project. (Project No. NSC 96-2221-E-035-003).

## REFERENCES

1. Lin, C. T., C. L. Liao, and C. H. Chen, "Finite-ground coplanar-waveguide branch-line couplers," *IEEE Trans. Microwave Theory Tech.*, Vol. 43, No. 3, Mar. 2001.
2. Knöchel, R., "Broadband flat coupler for two-branch and multibranch directional couplers," *IEEE MTT-S*, 1999.
3. Tung, W. S. and Y. C. Chiang, "Wide-band lumped-element directional coupler with arbitrary coupling coefficient," *IEE Proc.-Microwave Antennas Propag.*, Vol. 151, No. 4, Aug. 2004.
4. Chun, Y.-H. and J.-S. Hong, "Design of a compact broadband branch-line hybrid," *Microwave Symposium Digest IEEE MTT-S International*, 997–1000, June 2005.

# A New Tunable Wideband Ring Filter with Merged Stubs and Miniaturized Geometry for Bluetooth Technology

M. S. Kheir<sup>1</sup> and A. M. Abdin<sup>2</sup>

<sup>1</sup>Department of Information Engineering, German University in Cairo, Cairo, Egypt

<sup>2</sup>Department of Communications Engineering, Shorouk Academy, Cairo, Egypt

**Abstract**— A new miniaturized bandpass filter geometry is hereby presented. The structure of this filter is based on microstrip annular ring resonators with a wide bandwidth and precise tuning capability. The center frequency of the filter is 2.45 GHz and the 3-dB Fractional Bandwidth (FBW) is 104 % with a sharp out-of-band rejection. The size of the designed filter, excluding the I/O wave ports, is only  $7 \times 7 \text{ mm}^2$  by using an RT/Duroid substrate material with a dielectric constant ( $\epsilon_r = 10.2$ ) and a substrate thickness ( $h = 0.635 \text{ mm}$ ). According to the best knowledge of the authors, no such size has been implemented before in such application.

The filter geometry is based on a new technique that is to merge the open-stubs which allows a noticeable size reduction, 30% of the primary design, maintaining the same filter characteristics. The validity of the design has been verified using two dissimilar electromagnetic full-wave numerical solvers, ADS-Momentum and Ansoft- HFSS, where a very good agreement between each other has been achieved which proved the validity of the design.

Several investigations on the tuning parameters of the filter have been gone through. According to the achieved results, it was concluded that the most significant parameters that affect the tuning of the filter are the stub-length and the via-hole radius. The FBW increases as the length of the stub decreases and the center frequency can be controlled by the radius of both via-holes.

The overall size and the wideband characteristics made it convenient for wireless communication systems which require high bit-rate connectivity such as Bluetooth.



# Session 5A8

## Novel Antennas and Array Design

<a href="#">High-performance Universal GNSS Antenna as a New and Practical Approach</a>	
<i>Johnson Jenn-Hwa Wang (Wang Electro-Opto Corporation, USA); David J. Triplett (Wang Electro-Opto Corporation, USA);</i> .....	994
<a href="#">A Circular Polarization Microstrip Stacked Structure Broadband Antenna</a>	
<i>Huan-Cheng Lien (Wu Feng Institute of Technology, Taiwan, R.O.C.); Huei-Chiou Tsai (Wu Feng Institute of Technology, Taiwan, R.O.C.); Yung-Cheng Lee (Wu Feng Institute of Technology, Taiwan, China); Wen-Fei Lee (Wufeng Institute of Technology, Taiwan, R.O.C.); Wen-Fei Lee (Wu Feng Institute of Technology, Taiwan, R.O.C.);</i> .....	995
<a href="#">A Wide-band Circular Polarization Stacked Patch Antenna for the Wireless Communication Applications</a>	
<i>Huan-Cheng Lien (Wu Feng Institute of Technology, Taiwan, R.O.C.); Huei-Chiou Tsai (Wu Feng Institute of Technology, Taiwan, R.O.C.);</i> .....	996
<a href="#">A Low-profile Switchable Quadri-polarization Diversity Aperture-coupled Patch Antenna</a>	
<i>Don-Yen Lai (National Chiao Tung University, Taiwan); Shi-Yung Wang (National Chiao Tung University, Taiwan); Fu-Chiang Chen (National Chiao Tung University, Taiwan);</i> .....	997
<a href="#">Reflector Antenna with Artificial Magnetic Conductor Structure</a>	
<i>Jwo-Shiun Sun (National Taipei University of Technology, Taiwan); Guan-Yu Chen (National Taipei University of Technology, Taiwan); Cheng-Hung Lin (National Taiwan Ocean University, Taiwan); Kwong-Kau Tiong (National Taiwan Ocean University, Taiwan); Y. D. Chen (High Tech Computer Corp. (HTC), Taiwan);</i> .....	998
<a href="#">A High-gain Metallic Patterns Loaded Dielectric EBG Resonator Antenna at 5.0 GHz</a>	
<i>Yuehe Ge (Macquarie University, Australia); Karu P. Esselle (Macquarie University, Australia);</i> ...	999
<a href="#">Slot-coupled Planar Antenna's Mutual Coupling Reduction Characteristics Due to Reed-shaped Element</a>	
<i>Huiling Jiang (NTT DoCoMo, Inc., Japan); Ryo Yamaguchi (NTT DoCoMo, Inc., Japan); Keizo Cho (NTT DoCoMo, Inc., Japan);</i> .....	1000
<a href="#">Design of Controlled RF Switch for Beam Steering Antenna Array</a>	
<i>Musa. M. Abusitta (University of Bradford, UK); Dawei Zhou (University of Bradford, UK); Raed A. Abd-Alhameed (University of Bradford, UK); Peter S. Excell (University of Bradford, UK);</i> .	1001
<a href="#">Passive and Active Beam Steering of a Metamaterial-based Directive Subwavelength Cavity</a>	
<i>Abdelwaheb Ourir (Universite Pairs-Sud, France); S. N. Burokur (Universite Paris-Sud, France); A. de Lustrac (Universite Pairs-Sud, France);</i> .....	1003
<a href="#">Ultra Low Side Lobe Level Synthesis with Particle Swarm Optimization for Symmetrical Non-uniform Linear Array Antennas</a>	
<i>Xiaomiao Zhang (Xidian University, China); Kwai Man Luk (City University of Hong Kong, China); Xue Bai (Xidian University, China); Yinhang Wang (Xidian University, China); Jinyang Li (Xidian University, China);</i> .....	1004
<a href="#">An Efficient Density Weighting Approach for Side-lobe Level Suppression of Linear Array Antennas</a>	
<i>Xiaomiao Zhang (Xidian University, China); Kwai Man Luk (City University of Hong Kong, China); Weiwei Song (Xidian University, China); Wei Zhao (Xidian University, China); Yang Liu (Xidian University, China);</i> .....	1005

# High-performance Universal GNSS Antenna as a New and Practical Approach

Johnson J. H. Wang and David J. Triplett

Wang Electro-Opto Corporation (WEO), Marietta, Georgia 30067, USA

**Abstract**— In anticipation of the addition of the new Galileo satellite navigation system to the present GPS and GLONASS constellations, GNSS (Global Satellite Navigation System) receivers and antennas capable of operating on all three services are envisioned. The availability of more signals in the constellations can be used to greatly enhance the precision for geolocation, which is highly desirable for certain applications such as geodetic survey.

However, coverage of all three systems requires a broadband antenna having a wide frequency bandwidth of 1.164–1.610 GHz with a phase center stable with spatial and frequency variations. Fortunately, successful development of such an antenna has been reported [1, 2]. A key component in both approaches is a planar four-arm spiral as the radiating aperture, which is uniquely suitable, with performance not achievable by conventional GNSS antenna approaches such as the patch antenna or other broadband antennas, as noted in [1].

Although the details of the design in [1] have not been fully disclosed, those of [2] can be traced back to as early as 1995 [3] with a number of papers and patents. This paper will address new and practical considerations of this type of GNSS antenna.

It has been noted for more than three decades that the performance of a multiarm planar spiral antenna is critically sensitive to errors in its feed network [4]. Therefore, a significant effort is being made to improve the excitation accuracy, in both phase and amplitude, from the feed network to the feed region of the spiral.

Other major sources of errors in GPS are multipath scattering and noises, generally at low elevation angles. Conventional method for reduction of these interferences at the antenna level was made by antenna pattern shaping with sharply reduced gain at low angles; but this measure also results in a reduction of the available constellation, thus limiting the geolocation accuracy.

A new approach for GNSS antenna design now takes advantage of the denser constellation. A narrower antenna beamwidth optimized for the particular low-elevation-angle noise/interference environment, yet wide enough for the greatly expanded constellation, can immensely improve the performance in the new age of combined GPS/GLONASS/Galileo constellation.

Other advantages and features of this new antenna approach will also be discussed.

## REFERENCES

1. Granger, R., P. Readman, and S. Simpson, "Ready to receive: developing a professional antenna for galileo," *GPS World*, Feb. 1, 2007.
2. Wang, J. J. H. and D. J. Triplett, "High-performance universal GNSS antenna based on SMM antenna technology," *IEEE MAPE (Microwave, Antennas, Propagation and EMC) 2007*, Hangzhou, China, August 2007.
3. Wang, J. J. H. and J. K. Tillery, "Mobile SMM antennas with pattern-diversity and dual-mode operations," *1995 Radio Science Meeting*, Newport Beach, CA, June 1995.
4. Wang, J. J. H., "Physical limitations of the multimode current ring DF antennas," *Proc. ECOM-ARO Workshop on Electrically Small Antennas*, Ft. Monmouth, NJ, May 1976.

## A Circular Polarization Microstrip Stacked Structure Broadband Antenna

Huan-Cheng Lien, Huei-Chiou Tsai, Yung-Cheng Lee, and Wen-Fei Lee

Department of Electrical Engineering, Wufeng Institute of Technology  
No. 117, Chian-Ku Rd., Sec. 2, Ming-Hsiung (621), Chiayi, Taiwan, R.O.C.

**Abstract**— This paper described a single-feed S-Ring type stacked microstrip structure antenna for broadband applications. The antenna is designed for RHCP/LHCP at a center frequency of 2.1 GHz. The design of the antenna is aimed at obtaining both wider bandwidth on the impedance and better circular polarization AR (Axial-Ratio) for GPS applications. The feeding technique and structures of the present antenna has been analyzed. The Simulations and measurements results show that the antenna has an impedance bandwidth (VSWR.  $\leq 2$ ) of 28% and a 3-dB AR bandwidth more than 23%.



Figure 1: Antenna configuration of proposed. (a) Top view, (b) Side view.

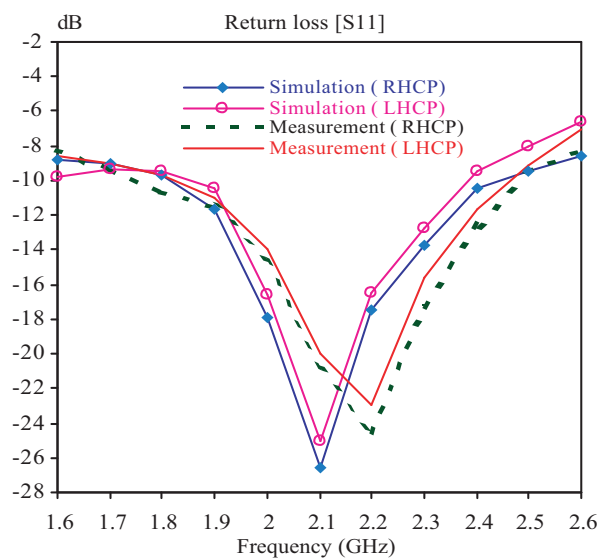


Figure 2: Return loss vs. frequency.

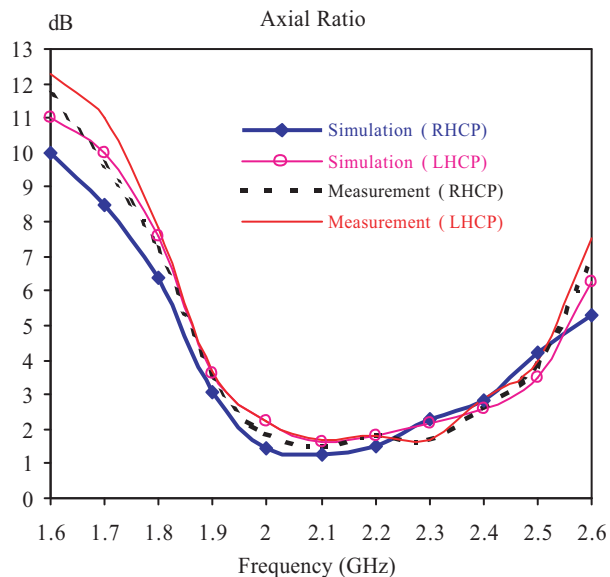


Figure 3: Axial vs. frequency.

# A Wide-band Circular Polarization Stacked Patch Antenna for the Wireless Communication Applications

Huan-Cheng Lien and Huei-Chiou Tsai

Department of Electrical Engineering, Wufeng Institute of Technology  
No. 117, Chian-Ku Rd., Sec. 2, Ming-Hsiung 621, Chiayi, Taiwan, R.O.C.

**Abstract**— A wide-band “corners-truncated rectangular” stacked patch antenna for using in the circular polarized applications was proposed. The antenna in this paper, which is proposed an axial ratio of less than 3 dB and a VSWR of less than 2:1 were shown to be achievable over a 25% bandwidth for using in the wireless communication applications, moreover, this antenna can achieves higher gain, lower side lobes and wider bandwidth compared to the traditional microstrip patch antenna. The designed picture, return loss, and axial ratio versus frequency are shown in following:

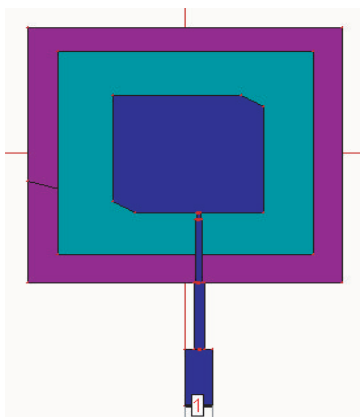


Figure 1: Diagram of microstrip antenna.

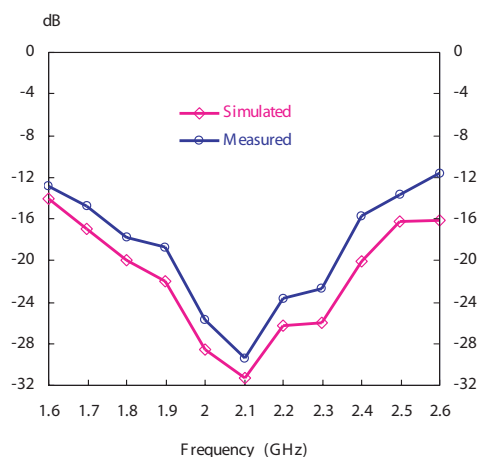


Figure 2: Return loss.

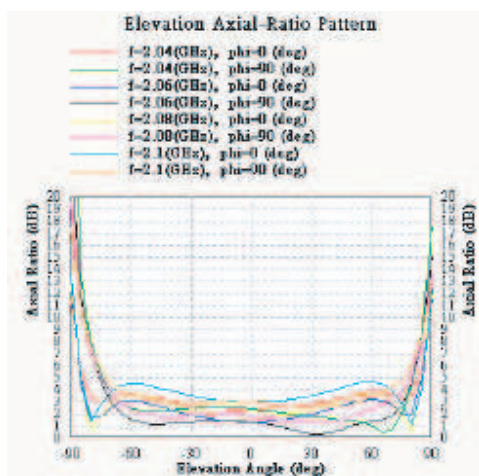


Figure 3: Elevation axial ratio pattern.

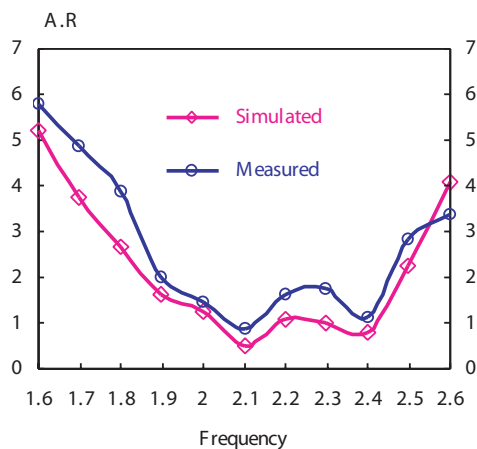


Figure 4: Axial ratio vs. frequency.

## A Low-profile Switchable Quadri-polarization Diversity Aperture-coupled Patch Antenna

Don-Yen Lai, Shi-Yung Wang, and Fu-Chiarng Chen

Department of Communication Engineering, National Chiao Tung University  
1001 Tahsueh Rd., Hsinchu 300, Taiwan

**Abstract**— Polarization diversity has gained significant attention in modern wireless communication systems. It is effective to avoid the fading loss caused by multipath effects, reach the goal of frequency reuse and extremely improve the communications capacity. Pin-diodes play an important role in providing versatility for polarization diversity applications. In [1], the antenna can operate in different excitation modes by controlling the on/off states of the pin diodes in the antenna structures. In [2], a novel reconfigurable quadri-polarization diversity aperture-coupled patch antenna can provide four polarization states. By controlling the eight pin diodes at ON/OFF states on the feeding network, the proposed antenna can provide a pair of orthogonal linear polarizations (LP) and a pair of orthogonal circular polarizations (CP).

In this paper, we present a novel low-profile switchable aperture-coupled patch antenna, which uses only four pin-diodes to provide four polarization states (dual linear polarization states and dual circular polarization states) for polarization diversity. The antenna designed to operate at 2.45 GHz consists of an aperture-coupled patch antenna and a new feeding network fabricated on the 0.8-mm FR4 substrates. The proposed antenna can provide four polarization states by switching the four pin-diodes embedded in the feeding network. The feeding network consists of a quadrature hybrid, four DC block capacitors, three RF chokes, and four pin-diodes. The hybrid can generate output signals for different polarization states resulting from changing ON/OFF states of the pin-diodes. Therefore, by controlling the DC bias voltage of the four pin-diodes properly, the antenna can provide either a pair of orthogonal linear-polarizations or a pair of orthogonal circular-polarizations. The measured return loss and insertion loss show that both LP and CP can operate at 2.45 GHz. Besides, the maximum measured gain of LP pattern in E-plane is about 5 dBi while the maximum measured gain of CP pattern is about 3 dBi with 65° 1-dB axial-ratio beamwidth. The experimental results validate this low-profile antenna provides the features of polarization diversity for wireless applications.

### REFERENCES

1. Sung, Y. J., T. U. Jang, and Y. S. Kim, "A reconfigurable microstrip antenna for switchable polarization," *IEEE Microwave and Wireless Components Letters*, Vol. 14, No. 11, 534–536, November 2004.
2. Wu, Y. F., C. H. Wu, D. Y. Lai, and F. C. Chen, "A reconfigurable quadri-polarization diversity aperture-coupled patch antenna," *IEEE Transactions on Antennas and Propagation*, Vol. 55, No. 3, 1009–1012, March 2007.

## Reflector Antenna with Artificial Magnetic Conductor Structure

Jwo-Shiun Sun<sup>1</sup>, Guan-Yu Chen<sup>1</sup>, Cheng-Hung Lin<sup>2</sup>, Kwong-Kau Tiong<sup>2</sup>, and Y. D. Chen<sup>3</sup>

<sup>1</sup>Department of Electronic Engineering, National Taipei University of Technology, Taiwan

<sup>2</sup>Department of Electrical Engineering, National Taiwan Ocean University, Taiwan

<sup>3</sup>Antenna and EMC Laboratory, High Tech Computer Corp. (HTC), Taiwan

**Abstract**— The design of a meta-material realization of artificial magnetic conductor (AMC) surfaces for a high-gain reflector antenna application is presented. Planar or corner periodic metallic array behave as AMC placed on a grounded dielectric substrate.

The AMC structure with periodic metallic array is shown in Fig. 1 which may reduce the surface wave and enhance the radiation performance. The traditional reflector antenna with PEC ground plane is shown in Fig. 2 which introduces comparable worse cross-polarization. The proposed reflector antenna with AMC structure in Fig. 3 can reduce the surface wave interference, reduce cross-polarization and also improve the antenna gain (Fig. 4).

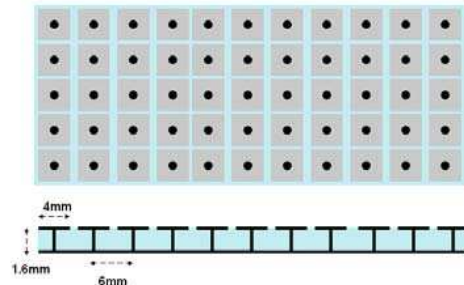


Figure 1: The artificial magnetic conductor (AMC) structure.

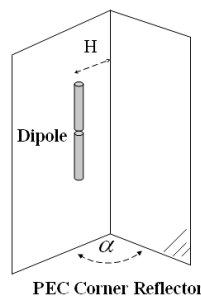


Figure 2: The traditional reflector antenna.

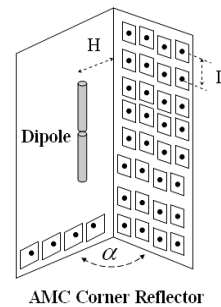


Figure 3: Proposed reflector antenna with AMC structure.

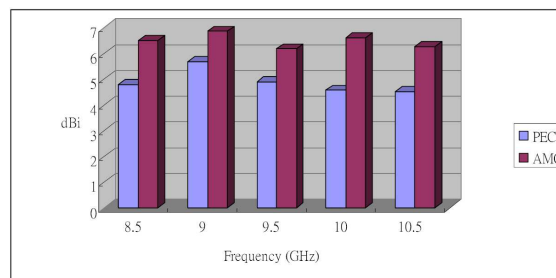


Figure 4: Compared data with PEC and AMC reflector.

The AMC structure of a high-impedance ground plane applied for a reflector antenna with dipole radiator has been developed. The designed antenna exhibits fairly high gain with the frequencies from 8.5 GHz to 10.5 GHz. It is believed to be useful for microwave antenna applications.

## A High-gain Metallic Patterns Loaded Dielectric EBG Resonator Antenna at 5.0 GHz

Yuehe Ge and Karu P. Esselle

Electronics Department, Macquarie University, Australia

**Abstract**— In recent years, electromagnetic band-gap (EBG) structures, also known as photonic bandgap (PBG) structures, have been widely investigated for enhancing antenna performance. Among them, dielectric EBG structures and frequency selective surfaces (FSS) have the advantages of low-cost and ease to be fabricated and mounted. Based on them, recently, the authors have designed high-gain, low-profile EBG resonator antennas by increasing the Q-factor of the corresponding EBG resonant structures. It is well known that EBG structures with a high permittivity will lead to a high Q-factor. While in our design, a higher Q-factor can be obtained by loading periodic metallic patterns on one or both surfaces of a single dielectric layer. The design and optimisation are carried out by combining a genetic algorithm (GA) with the FDTD method.

Theoretically, the thickness of the dielectric layer of the EBG structure forming an EBG resonator antenna should be a quarter of guide-wavelength ( $\lambda_g$ ). For example, in our previous design operating at 12 GHz, the thickness of the dielectric superstrate is about 3.1 mm, which is the standard dimension of the commercial material FR4/Epoxy and can be directly obtained from the market. However, if the operating frequency is lower, the thickness of the superstrate or FSS will increase. For example, at the operating frequency of the design in this paper, 5.0 GHz, if the EBG structure uses the same FR4/Epoxy material, the thickness of it should be about 7.2 mm, which is not the standard dimension and unavailable. The fabrication will increase the cost. Another disadvantage is the increase of the weight of the antenna.

In this paper, the thinner dielectric layer is applied to the design of high-gain low-cost lowprofile dielectric EBG resonator antennas. The operating frequency is 5.0 GHz ( $f_0$ ). The EBG or FSS structures considered here are FR4/Epoxy superstrate, which has a thickness of 1.6 mm ( $< 1/16\lambda_g$ ) and a low dielectric constant of 4.4. The EBG resonant structure is composed of the FSS and the ground. By optimising the periodic metallic patterns on the top and bottom surfaces of the FSS, a high Q-factor of the EBG cavity and hence a high gain can be obtained when forming the EBG resonator antenna. In our optimisation, the final Q-factor is about 18.0 while it is less than 1.0 when without loading the periodic metallic patterns. In our simulation of the EBG resonator antenna, the size of the FSS (superstrate) is  $240 \times 240 \text{ mm}^2$  ( $4.0\lambda_0 \times 4.0\lambda_0$ ). The distance between the superstrate and the ground is 31.1 mm (about  $1/2\lambda_0$ ). The simulated directivity at operating frequency 5.0 GHz is 19.2 dB. Details of the simulations and the measurements will be presented in the conference.

## Slot-coupled Planar Antenna's Mutual Coupling Reduction Characteristics Due to Reed-shaped Element

Huiling Jiang, Ryo Yamaguchi, and Keizo Cho

NTT DoCoMo, Inc., 3-5 Hikarino-oka, Yokosuka-shi, Kanagawa, 239-8536, Japan

**Abstract**— The base station antenna for the IMT-advanced systems is required to have broadband and polarization diversity property. An RF integrated antenna is considered a useful configuration to decrease the feeding loss due to the use of high frequency band and ensure the sufficient power for broadband transmission. Miniaturization of antenna and RF circuit are required because RF components and antenna elements are integrated in same radome.

This study investigates a filter integrated antenna configuration for Rx and Tx antennas integrated on same substrate. In this paper, we propose a bow-tie slot coupled patch antenna comprising multiple reed-shaped elements. The elements are installed on Rx antenna's substrate between coupling slot and radiation element. After an investigation of mutual coupling characteristics due to reed-shaped elements, the proposed configuration integrate a part of the duplexer function without increase antenna's outer size and Rx antenna's bandwidth is also maintained. By installing multiple reed-shaped elements between the feed layer and radiation layer, up to 5.7 dB reduction on mutual coupling in transmitting frequency band can be achieved. This paper describes the mechanism of antenna's filtering function and design guide of reed-shaped elements is also illustrated.

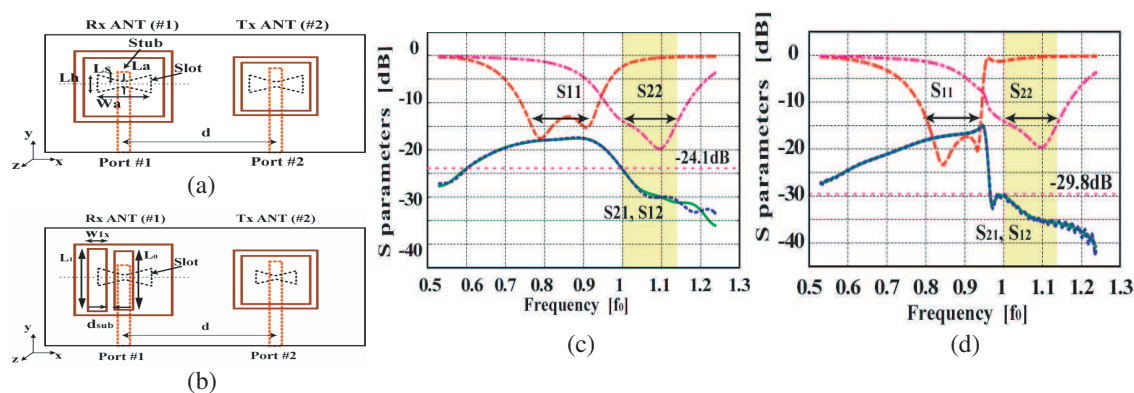


Figure 1: (a) Conventional model, (b) proposed model, (c) S-parameters of conventional model, (d) S-parameters of proposed model.



## Design of Controlled RF Switch for Beam Steering Antenna Array

M. M. Abusitta, D. Zhou, R. A. Abd-Alhameed, and P. S. Excell  
 Mobile and Satellite Communications Research Centre, University of Bradford  
 Richmond Road, Bradford, West Yorkshire, BD7 1DP, UK

**Abstract**— The use of adaptive array antennas for cellular base station application has recently become an active area of research and development [1–3]. Base station antennas normally radiate omni-directionally or in broad sectors, and most power is radiated in other directions than toward the user. This causes waste of power and interference for other users. Therefore new versions of base station antennas are now being made to overcome the problem by using antennas that have narrow steerable beams. These can give large increment in capacity, and the possibility of tracking mobile phones or vehicles. In authors' previous work, a set of simple design procedures for beam steering single circular and concentric circular ring antenna arrays was proposed and analyzed theoretically (see Fig. 1) [4]. In the paper, the design theory was formulated and the results of the proposed analytical model, validated by a numerical model, were presented. Beam steering was achieved by implementing an ON/OFF system concept to excite only specific elements of the array dipole antenna.

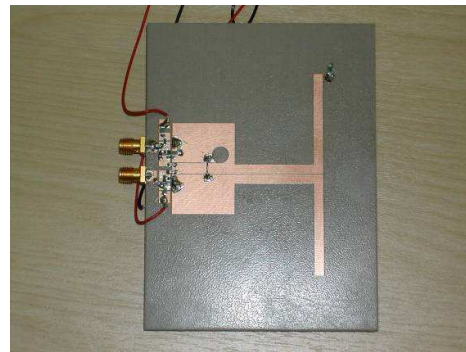
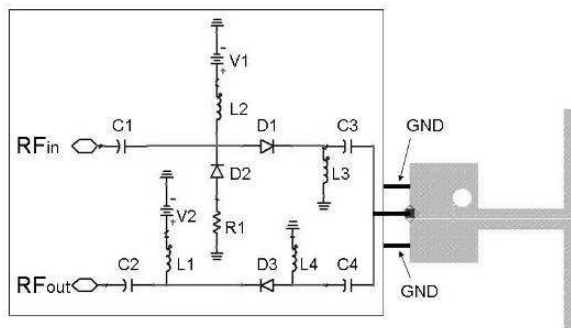


Figure 1: Overall circuit diagram of the RF switching circuit, balun and the dipole.

Figure 2: Prototype circuit configuration for CWP-fed CPS dipole with sensor element included.

Moreover, an investigation on hardware implementation of a CPW-to-CPS dipole antenna controlled by a RF switching circuit for duplex operation was carried out. The performance of the overall circuit (i.e., the switch and the dipole) was analyzed and evaluated using a commercial RF and EM simulator (see Fig. 1). The design of CPW-to-CPS balun and dipole antenna was designed and discussed (see Fig. 2). A novel technique for measuring the antenna resonance frequency and accepted power by the CPW input was investigated. The theory of the RF switching circuit was demonstrated, including the evaluation measurements of overall circuit performance in full duplex operation as shown in Figs. 3 and 4.

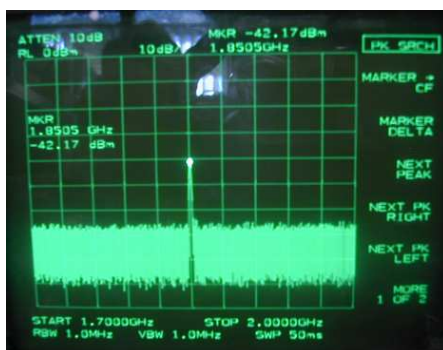


Figure 3: The output of the back to back baluns when the switch mode is off.

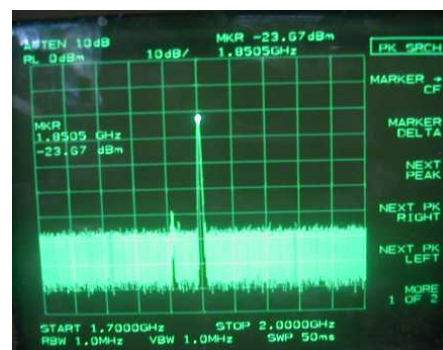


Figure 4: The output of the back to back baluns when the switch mode is on.

**REFERENCES**

1. Irie, Y., S. Hara, Y. Nakaya, T. Toda, and Y. Oishi, "A beamforming method for a reactively steered adaptive array antenna with RF-MEMS device," *IEEE Topical Conference on Wireless Communication Technology*, 396–397, Oct. 2003.
2. Imamura, K. and H. Morishita, "Analysis of the mobile terminal adaptive array antenna in consideration of a case and elements," *IEEE Antennas and Propagation Society Symposium*, Vol. 3, 3195–3198, June 2004.
3. Nakaya, Y., T. Toda, S. Hara, and Y. Oishi, "MIMO receiver using an RF-adaptive array antenna with a novel control method," *IEEE International Conference on Communication*, Vol. 5, 2568–2572, June 2004.
4. Abd-Alhameed, R. A., N. T. Ali, P. S. Excell, M. K. Atiya, and C. H. See, "Beam steering antenna array for mobile base stations," *3rd IEEE International Conference on Systems, Signals & Devices SSD'05*, Sousse, Tunisia, Paper Ref. SSD05-CSP-118, March 2005.

## Passive and Active Beam Steering of a Metamaterial-based Directive Subwavelength Cavity

A. Ourir, S. N. Burokur, and A. de Lustrac

IEF, Université Paris-Sud, UMR 8622, CNRS, Orsay F-91405, France

**Abstract**— Metamaterials that produce in-phase reflections (High Impedance Surface (HIS), Artificial Magnetic Conductors (AMC), ...) were used to miniaturize and minimize the cost of communication components [1–4]. Current research involves the development of metamaterial based ground planes, substrates and superstrates to the directive compact antennas [3, 5, 6]. By incorporating tunable structures into such metamaterials, D. Sievenpiper expanded their capabilities to perform active control of electromagnetic waves [7]. We have recently proposed an active Partially Reflective Surface (PRS) based on a phase varying metamaterial to make the shift of the cavity resonance frequency [8].

In this paper, a passive and active PRS metamaterial based on microstrip technology is proposed for the design of a steerable ultra-compact directive cavity. This material, based on a composite metamaterial, is made of a constant inductive grid and a locally phase varying capacitive grid. It presents a high reflectivity and a negative reflection phase for normal incident waves over a wide frequency band. This negative phase combined with the phase at the surface of the substrate (very close to  $180^\circ$ ) above a conventional ground plane leads to the design of a subwavelength cavity. Using the idea of phased-arrayed antennas, we impose reflection phase differences to our metamaterial in order to make our antenna steerable. By changing the metallic gap or the varicap bias voltage between the metallic strips of the capacitive grid of the PRS in one direction, the capacitance of the metamaterial will also vary along this same direction. As a consequence, the phases of the reflection and transmission coefficients vary. Hence, the steering of the radiated beam can be controlled. Thereby, the proposed cavity can provide a low-cost alternative to traditional electrically scanned antennas.

### REFERENCES

1. Sievenpiper, D., "High-impedance electromagnetic surfaces with a forbidden frequency band," *IEEE Trans. Microwave Theory Tech.*, Vol. 47, 2059, 1999.
2. McVay, J., N. Engheta, and A. Hoorfar, "High-impedance metamaterial surfaces using Hilbert-curve inclusions," *IEEE Microwave and Wireless Components Lett.*, Vol. 14, 130, 2004.
3. Ourir, A., A. de Lustrac, and J.-M. Lourtioz, "All-metamaterial-based sub-wavelength cavities ( $\lambda/60$ ) for ultrathin directive antennas," *Appl. Phys. Lett.*, Vol. 88, 084103-1–084103-3, 2006.
4. Bilotti, F., M. Manzini, A. Alu, and L. Vegni, "Polygonal patch antennas with reactive impedance surfaces," *J. Elect. Waves and Applications*, Vol. 20, 169, 2006.
5. Feresidis, A. P., G. Goussetis, S. Wang, and J. C. Vardaxoglou, "Artificial magnetic conductor surfaces and their application to low-profile high-gain planar antennas," *IEEE Trans. Antennas Propag.*, Vol. 53, No. 1, 209–215, Jan. 2005.
6. Zhou, L., H. Li, Y. Qin, Z. Wei, and C. T. Chan, "Directive emissions from subwavelength metamaterial-based cavities," *Appl. Phys. Lett.*, Vol. 86, 101101-1–101101-3, 2005.
7. Sievenpiper, D. F., "Forward and backward leaky wave radiation with large effective aperture from an electronically tunable textured surface," *IEEE Trans. Antennas Propag.*, Vol. 53, No. 1, 236–247, Jan. 2005.
8. Ourir, A., S. N. Burokur, and A. de Lustrac, "Electronically reconfigurable metamaterial for compact directive cavity antennas," *Electron. Lett.*, Vol. 43, No. 13, 2007.

# Ultra Low Side Lobe Level Synthesis with Particle Swarm Optimization for Symmetrical Non-uniform Linear Array Antennas

Xiaomiao Zhang<sup>1</sup>, Kwai Man Luk<sup>2</sup>, Xue Bai<sup>1</sup>, Yinhang Wang<sup>1</sup>, and Jinyang Li<sup>1</sup>

<sup>1</sup>National Key Laboratory of Antennas and Microwave Techniques, Xidian University  
Xi'an 710071, Shaanxi Province, China

<sup>2</sup>Department of Electronic Engineering, City University of Hong Kong  
83 Tat Chee Avenue, Kowloon, Hong Kong, China

**Abstract**— Ultra low side lobe level (ULSLL) array antennas have important applications in radar and communication systems, ULSLLs are usually realized with uniform linear array (ULA) or planar array antennas by excitation amplitude weighting, such as the current distributions resulted from Dolph-Chebyshev or Taylor synthesis. Lower SLL, however, implies lower aperture efficiency and larger excitation amplitude ratio (EAR), which makes the feed network more complicated and more difficult to fabricate; lower SLL is also very sensitive to the excitation amplitude/phase errors. In order to mitigate this difficulty, both the excitation amplitudes and the element positions are used for ULSLL synthesis, where the element positions act as extra freedoms for further SLL suppression. A symmetrical non-uniform linear array (SNULA) is proposed, the full information particle swarm optimization (FIPSO) based on the Von Neumann local neighborhood topology is adopted for ULSLL pattern synthesis, because it is effective for multi-dimensional, multi-local-minimum, non-linear complex problems and robust convergence. In the algorithm, the inertia weight is improved via the sigmoid limiting function; the boundary conditions are dealt with a randomized damp reflection. Two numerical examples are given, the first one is an 8-element  $-40$  dB SLL array antenna, for comparison, a ULA with the same aperture size, element number and peak SLL is synthesized by Dolph-Chebyshev method, the results obtained show that they have nearly identical main beam and equal side lobes, but the SNULA has lower EAR and higher aperture efficiency than those of the ULA. The second example is a 12-element  $-45$  dB SLL array, similar rules are obtained.

## An Efficient Density Weighting Approach for Side-lobe Level Suppression of Linear Array Antennas

Xiaomiao Zhang<sup>1</sup>, Kwai Man Luk<sup>2</sup>, Weiwei Song<sup>1</sup>, Wei Zhao<sup>1</sup>, and Yang Liu<sup>1</sup>

<sup>1</sup>National Key Laboratory of Antennas and Microwave Techniques, Xidian University  
Xi'an 710071, Shaanxi Province, China

<sup>2</sup>Department of Electronic Engineering, City University of Hong Kong  
83 Tat Chee Avenue, Kowloon, Hong Kong, China

**Abstract**— Most likely, there are two techniques existed to reduce the side lobe level (SLL) of array antennas: The conventional excitation amplitude tapering (AT) and the unusual element space density tapering (DT). The AT technique, such as triangular, cosine, cosine-square and raised-cosine amplitude distributions, as well as the Dolph-Chebyshev or Taylor current coefficients, provides efficient means for low SLL (LSLL) and ultra-low SLL (ULSLL) pattern synthesis, and also affords significant dynamic ranges control of the aperture distributions. The feed network, however, becomes complicated and narrow bandwidth, the aperture efficiency decreased rapidly as the amplitude getting much tapered. The DT technique offers another way for limited SLL reduction while the aperture efficiency is maintained, the antenna is a uniformly excited non-uniformly spaced array with element positions thinned from the center element (odd number array) or center two elements (even number array), the main advantage is that it simplifies the bulk and lossy feed network. In this paper, A uniformly excited symmetrical array antenna, which is compose of a uniform central sub-array (central part) and two density tapered side sub-arrays (side parts), is presented for SLL suppression, a power function characterized by two-parameter is employed to express the increments between adjacent elements of the two side parts, the optimum values of the two parameters are searched by the Min-max method according to the peak SLL. Numerical examples are given for the cosine-element, one half wavelength least spacing, and 4-element central part arrays, 8-, 10-, and 12-element arrays are simulated; Dolph-Chebyshev like patterns are observed,  $-19.5$  dB,  $-20.8$  dB and  $-21.4$  dB SLLs are achieved, respectively.

# Author Index

- Çayören Mehmet, 808, 809  
Şahintürk Hulya, 809  
Čizrnár T., 366, 367, 447, 572  
Šiler M., 367, 447  
no J. A. Reyes-Avenda 250
- Abajo F. Javier Garcia de, 219  
Abd-Alhameed Raed A., 516,  
518, 925, 1001  
Abdalla Mahmoud A., 472  
Abdallah Esmat Abdel-Fattah,  
75  
Abdeddaim Redha, 961  
Abdel-Rhim Abdel-Hamid, 75  
Abdelaziz Abdelaziz Abdel-  
monem, 121  
AbdelMalek F., 747  
Abdin Adel Mohamed, 92, 623,  
897, 992  
Abernathy C. R., 596  
Abrishamian Mohammad  
Sadegh, 818  
Abubakar Aria, 630  
Abugalia A., 401  
Aburakawa Yuji, 264  
Abusitta Musa. M., 1001  
Adamashvili G. T., 419  
Adams Laura, 672  
Ade Peter, 77  
Afsahi Majid, 468  
Agarwal V., 862  
Ahmed Ghufra, 690, 694  
Ahmed Moustafa, 373, 947  
Akduman İbrahim, 808  
Akhadov Elshan, 848  
Al-Nuaimi Miqdad, 614  
Albagory Yasser, 302  
Albert Mohan Dass, 493  
Alfredo-Badillo U., 536  
Alsing Paul M., 826  
Alvarado-Tenorio B., 862  
Amagai Jun, 265  
Ammann M. J., 86, 380  
Amooshahi Majid, 402  
Amra Claude, 790  
Ams Martin, 735  
Andersson Ulf, 718  
Andrade-Herrera J., 323  
Ang Irene, 917  
Anlage Steven M., 404, 550,  
672, 969  
Antonsen Thomas, 550, 969  
Ao Faliang, 415  
Aramini R., 540  
Arima Takuji, 526  
Ariza-Flores A. David, 754, 755
- Arnaud L., 790  
Asavei T., 654  
Asboth Janos, 570  
Ashmawy Mohamed Gamal,  
897  
Askari Gholamreza, 87  
Astryan A. A., 831  
Atalla Ashraf, 430  
Attari Amir Reza, 56, 60, 369  
Averitt Richard D., 160  
Awai Ikuo, 22, 893  
Aydin Koray, 467, 746  
Azad A. K., 163  
Azad Abul K., 158, 160, 848  
Azadi-Tinat Nima, 506
- Ba Jing, 304, 306, 314  
Ba Rongsheng, 157  
Babu G. Santosh, 180, 185  
Bachorec T., 795  
Bahadorzadeh M., 331  
Bai Jianping, 429  
Bai Xue, 1004  
Bai Yang, 398  
Bain C. D., 577  
Bain Colin D., 576, 660  
Baluyot Stein C., 446  
Balyakin Artem A., 336  
Balzano Quirino, 523  
Ban Dayan, 258  
Banadkok Mitra Torabipour,  
685  
Banciu G. M., 693  
Bao Di, 246  
Bao Xiu Long, 86, 380  
Barabanenkov M. Yu., 247  
Barabanenkov Yurii Nicolae-  
vich, 247  
Barile Lucio, 442  
Barrowes Benjamin, 924  
Bartušek Karel, 796  
Bartušek Karel, 902  
Bartusek Karel, 379, 799, 802,  
904, 907  
Bayat Alireza, 685  
Baykal Yahya, 377, 607  
Baykal Yahya Kemal, 610  
Begbie Mark, 724  
Bellarbi L., 635  
Bellazzini B., 945  
Belotelov Vladimir I., 225  
Bendali A., 332  
Benedetti Manuel, 628, 806,  
807  
Beneduci A., 383  
Bennett S., 936
- Beran Mark J., 780  
Berg Peter M. van den, 630  
Bergman David J., 432, 664,  
744  
Berman Oleg L., 912  
Bernet S., 657  
Bertani Francesca, 442  
Beruete Miguel, 852  
Bhooshan S., 70  
Biccari D., 816  
Bilge Serafettin, 467  
Bingham Kenrick, 546  
Blanco J. M., 462  
Blokhina Elena V., 336  
Boerner Wolfgang-Martin, 124,  
126, 127  
Bogdanov Alexei L., 959  
Boiko Dmitri L., 820  
Boix Rafael R., 298, 646  
Bombaci O., 816  
Borderies Pierre, 332, 495, 651  
Botten Lindsay C., 831  
Bottone S., 787  
Boules Raouf N., 615  
Bozza Giovanni, 540  
Bradley Michael P., 722  
Bradshaw Elliott, 969  
Brancik Lubomir, 794  
Bredow Jonathan W., 489  
Bri Seddik, 635  
Brignone Massimo, 540  
Brzobohatý O., 366, 572  
Bu J., 682  
Buchanan M., 600  
Buchanan Margaret, 258  
Burokur S. N., 1003  
Buyanova I. A., 596  
Byun Joon-Ho, 117
- Cai Hongjun, 170  
Cai Wenshan, 853  
Cai Xiaobing, 592  
Cai Xinlun, 283  
Cai Yangjian, 377, 607, 610,  
611  
Cai Zhiyin, 428  
Calabrese D., 816  
Callebaut Dirk K., 908–910  
Caloz Christophe, 242  
Camacho Luis M., 491  
Campbell Mark A., 634  
Campi C., 633  
Campillo Igor, 852  
Camposeo A, 448  
Canning John, 236–240  
Cao Fang, 974

- Cao Fuquan, 16  
 Cao Jin, 982  
 Cao L. S., 425, 426  
 Cao Wei, 556  
 Cao Yao-Yu, 222  
 Cao Yunjian, 463  
 Cao Zhuangqi, 360  
 Capineri Lorenzo, 274  
 Caponnetto Andrea, 874  
 Cappelli M., 383  
 Cardimona David A., 826  
 Cargill Matthew R., 576  
 Carlo Flavia De, 442  
 Carruthers Antonia, 574  
 Cartacci M., 816  
 Catapano Ilaria, 632, 873  
 Censor Dan, 293  
 Cesar C. L., 448  
 Chai Lu, 156, 159, 161, 162  
 Chakrabarty Ajay, 49, 54  
 Chakravarty T., 70  
 Chan C. T., 137, 590  
 Chan Che Ting, 433, 450, 575  
 Chan Chi Hou, 922  
 Chan V., 774  
 Chan Wai Kin, 604  
 Chang Chew Wai, 175  
 Chang Dua-Chyrh, 884  
 Chang Hung-Chun, 644  
 Chang Hung-Wen, 282, 286, 290  
 Chang Kihun, 619  
 Chang L. W., 183  
 Chang Sheng Hsiung, 950  
 Chang The-Nan, 81, 82  
 Chang Tzu-Yin, 353  
 Chang Won-Seok, 740  
 Chang Yi-Hao, 505  
 Chang Yia-Chung, 892, 971  
 Chang Yu-Fang, 991  
 Chau Yuan-Fong, 481  
 Che Chi-Ming, 675, 857  
 Cheah Kok Wai, 223, 674  
 Chen B. C., 232  
 Chen Bing-Hung, 278  
 Chen C. D., 474  
 Chen Cheng-Chung, 867  
 Chen Chien-Chang, 382  
 Chen Chien-Hsun, 889  
 Chen Chih-Hao, 29  
 Chen Chow-Son, 211  
 Chen Dapeng, 310  
 Chen Fu-Chiang, 997  
 Chen Guan-Yu, 19, 63, 66, 79, 83, 93, 514, 998  
 Chen H. M., 184  
 Chen He, 834  
 Chen Hong, 190  
 Chen Hongsheng, 135, 138, 588, 589, 591, 954  
 Chen Hou-Tong, 160, 848  
 Chen Hua-jun, 520  
 Chen Huanyang, 137, 590  
 Chen Jer-Long, 17, 62  
 Chen Jia Bin, 488  
 Chen Jianhua, 341  
 Chen Jie-Yu, 932  
 Chen Juan, 46  
 Chen K. J., 679  
 Chen Kuan-Ren, 435  
 Chen Kun-Shan, 127, 490  
 Chen Lin, 360  
 Chen Minfeng, 644  
 Chen Mingsong, 415  
 Chen Ping, 821  
 Chen Q., 774  
 Chen Ru, 688  
 Chen Sheng Chung, 436  
 Chen Shude, 428  
 Chen Songyan, 416  
 Chen W. M., 596  
 Chen Wei, 163, 164  
 Chen Wei-Jun, 981  
 Chen Wei-Qiang, 147, 222  
 Chen Xi, 838, 841  
 Chen Xiao-Bing, 813  
 Chen Xiaoqun, 624  
 Chen Xiaoshuang, 595, 868  
 Chen Y. D., 19, 63, 66, 79, 83, 93, 514, 998  
 Chen Y. W., 334  
 Chen Yan, 340  
 Chen Yifang, 219  
 Chen Yimin, 361  
 Chen Yongyao, 418  
 Chen Yu-Hsiang, 40  
 Chen Z. R., 895  
 Chen Ziyang, 609  
 Cheng A. T., 424  
 Cheng Hsiu-Fung, 185, 334, 335  
 Cheng L. L., 520, 989  
 Cheng Ming-Kum, 381  
 Cheng Qiang, 246, 460  
 Cheng Wei-Chi, 286  
 Cheng Xiangxiang, 789  
 Cheng Y., 224  
 Cheng Ya, 370, 371, 563  
 Cheng Yinqin, 328  
 Cheng Zuhai, 417  
 Chettiar Uday K., 853  
 Chevallier Jacques, 236  
 Chew Weng Cho, 915  
 Chi Cheng-Chung, 181  
 Chia Chih-Ta, 180, 185  
 Chiang Chao-Wen, 930  
 Chiang Chung-Che, 867  
 Chiang Jung-Sheng, 285  
 Chiang Kin Seng, 949  
 Chiang Pei-Yuan, 39, 44  
 Chiang Po-Jui, 284, 289  
 Chichkov Boris N., 144  
 Chimenti Isotta, 442  
 Chin Jessie Yao, 246, 460  
 Chin Li-Hsiang, 889  
 Chin See Leang, 734  
 Chiou Yih-Peng, 358  
 Chiu Kuo Pin, 436  
 Chiu Long Sang, 977  
 Chiu Tsen Chieh, 950  
 Chiu Tsenchieh, 987  
 Chiu Wei-Hsuan, 211  
 Cho Keizo, 1000  
 Cho Sung-Hak, 740  
 Choi Hyengcheul, 625  
 Choi Jaehoon, 622  
 Choi Jaewon, 618  
 Chokngamwong Roongroj, 977  
 Chon Kwon Su, 410  
 Chou Chung-Kwang, 534  
 Chou Hsi-Tseng, 914  
 Chu Junhao, 719, 946  
 Chu Keping, 428  
 Chua S. J., 675  
 Chuah Hean-Teik, 171, 492, 493  
 Chuang Huey-Ru, 889  
 Chuang Wei-Ching, 480  
 Chue Y., 224  
 Chung Chia-Hsin, 82  
 Cicchetti A., 816  
 Cingolani R., 448  
 Cizmar Tomas, 574  
 Clerc J. P., 964  
 Cojoc Dan, 456  
 Connor Kenneth, 513  
 Contreras-Solorio D. A., 762  
 Cosh M. H., 878  
 Courtial Johannes, 569, 931  
 Coyle J., 540  
 Crocco Lorenzo, 632, 809, 873  
 Crossley Maxwell J., 240  
 Crozier Stuart, 385, 636, 642, 814  
 Csaki Andrea, 221  
 Cui Naxin, 636  
 Cui Tie Jun, 246, 460  
 Cui Wan-Zhao, 43, 195, 584  
 Cui Wanzhao, 190  
 Curto S., 380  
 D'Emilia Enrico, 442  
 D'Urso Michele, 632  
 Díaz-Guerrero D. S., 760

- Dědková Jarmila, 792, 793  
 Da H. X., 412  
 Da Hai-Xia, 112  
 Daden J. Y., 960  
 Dai Xiaoyu, 748  
 Daigle Andrew, 78  
 Damoah-Afari Peter, 774  
 Daniels David J., 274  
 Das Yogadhish, 272, 273  
 Datta Timir, 942  
 Decat Gilbert, 103  
 Dedkova Jarmila, 794  
 Dekker Peter, 735  
 Delaune David, 510, 512  
 Delbary F., 540  
 Deng Ke, 340  
 Deng S.-G., 305  
 Deng Xiaoxu, 360  
 Depollier C., 214  
 Derouard J., 568  
 Dessouky Moawad, 302  
 Deumié C., 790  
 Dholakia Kishan, 574  
 Dhont Jan K. G., 967  
 Di Qingyun, 308  
 Dimitrov Dimitar, 333  
 Ding C. R., 232  
 Ding Xiao-Li, 774  
 Ding Yanfang, 16  
 Ding Zongling, 868  
 Diodati Paolo, 686  
 Diry Fabienne, 420  
 Djavid Mehrdad, 818  
 Djurišić Aleksandra B., 604  
 Dohal Premysl, 904  
 Dohnal Premysl, 795, 802  
 Dolinsky Yu., 406  
 Domier Calvin W., 933  
 Domokos Peter, 570  
 Donchev V. T., 756  
 Donderici Burkay, 136  
 Donelli Massimo, 538, 628, 876  
 Donetsky Dmitry, 361  
 Dong Bo, 391  
 Dong Hongtao, 157  
 Dong J. Q., 895  
 Dong Jian-Wen, 232, 433  
 Dong Shi-Wei, 190  
 Dong Shiwei, 192  
 Dong Xian-Zi, 147, 222  
 Dong Zhihong, 35  
 Dorkenoo Kokou D., 375  
 Dorofeenko Alexander V., 819, 964  
 Dossou K. B., 831  
 Drachev Vladimir P., 853  
 Drexler Petr, 797  
 Du Bo, 399  
 Du Hua Kun, 202  
 Du Jingyang, 878  
 Du Qiang, 562  
 Du Yang, 95–100, 496, 497  
 Duan T., 837  
 Duan Tao, 330, 839  
 Duan Xuan-Ming, 147, 222  
 Dubois-Fernandez Pascale, 495  
 Duh Jenq-Gong, 215, 898  
 Duque C. A., 863  
 Dvoynenko M. M., 892  
 Dybov V. A., 616  
 Economou E. N., 671  
 Ede Ch., 552  
 Edenhofer P., 816  
 Egorov V. S., 417  
 El-Ocla Hosam, 788  
 Elder Joe A., 534  
 Eleftheriades George V., 963  
 Elkamchouchi Hassan M., 104–106  
 Elperin T., 406  
 Emslie A. G., 875  
 Emslie Gordon, 872  
 Escorcia-Garcia J., 862  
 Eshaghi Armaghan, 369  
 Esselle Karu P., 999  
 Ewe Hong Tat, 492  
 Ewe Hong-Tat, 171, 493  
 Excell Peter S., 516, 518, 925, 1001  
 Eyyuboğlu Halil Tanyer, 607, 610  
 Eyyuboglu Halil Tanyer, 377  
 Fürhapter S., 657  
 Fabrizio Enzo Di, 453, 456  
 Falorni Pierluigi, 274  
 Fan Dianyuan, 748  
 Fan Juan, 307  
 Fan Jun, 212  
 Fan Xiaoyan, 199, 345  
 Fang Dai-Ning, 279  
 Fang Shuai, 95–97  
 Fang Weihai, 393  
 Fatholoulumi Saeed, 258  
 Fato F. Di, 456  
 Fear Elise C., 634  
 Fedeli J.-M., 568  
 Fedotov Ilya, 713  
 Fedotov Vasily, 219  
 Fellah M., 214  
 Fellah Z. E. A., 214  
 Feng Gang, 212  
 Feng X. J., 674  
 Feng Xuebing, 333  
 Feng Yijun, 132, 851  
 Ferrari E., 456  
 Ferret P., 568  
 Ferrières X., 651  
 Fiala Pavel, 795–798, 802, 902, 903, 905–907  
 Firouzeh Zaker Hossein, 87  
 Flamini E., 816  
 Flores-Tapia Daniel, 629  
 Flourey N., 495  
 Foletti Alberto, 442  
 Fomin S. V., 879  
 Fontes A., 448  
 Forooraghi Keyvan, 74  
 Forró László, 658  
 Fournier Jean-Marc R., 655, 656  
 Franceschini Davide, 807  
 Franceschini Gabriele, 807  
 Frandsen Lars H., 236  
 Frankenthal Shimshon, 780  
 Franosh Thomas, 658  
 Freni Angelo, 111  
 Freymann G. Von, 150  
 Fritzsche Wolfgang, 221  
 Fructos A. L., 646  
 Fu H., 543  
 Fu Junmei, 196  
 Fu Lan, 677  
 Fu Liwei, 244  
 Fu Yi, 43  
 Fujisaki C., 782  
 Fukuda Seisuke, 775  
 Fung K. S., 774  
 Fung Kin Hung, 433  
 Furuya Hirotaka, 512  
 Gétin Stephane, 568  
 Gaetani Roberto, 442  
 Gaggero-Sager Luis M., 759, 760, 763, 764, 862, 948  
 Galaup Jean-Pierre, 939  
 Gamaly E. G., 146  
 Gao F., 426  
 Gao Xiumin, 362, 400  
 García C., 462  
 Garcia Daniel Jaque, 148  
 Gardner Robert L., 983  
 Gaugiran S., 568  
 Gauthier Robert C., 153, 823, 824  
 Ge W. K., 679  
 Ge Yuehe, 999  
 Geffrin Jean Michel, 541  
 Genov D. A., 243  
 George Thomas F., 423  
 Georges G., 790  
 Gescheidtova Eva, 346, 379, 904



- Ghaffari A., 818  
 Ghassemi N., 65  
 Ghosh Saswati, 49, 54  
 Ghosh Soham, 53  
 Giessen Harald W., 244  
 Girasole M., 383  
 Giuliani Livio, 442  
 Glückstad Jesper, 452  
 Gnanavel M., 122  
 Golod S. V., 955  
 Golovanov Oleg A., 714, 715  
 Golovanov Oleg. A., 650  
 Golshan M. M., 364  
 Goncharenko A. V., 892, 971  
 Gong Mufei, 158  
 Gong Qihuang, 738  
 Gong Rong Zhou, 986  
 Gonzalez J., 462, 856  
 Gossard Arthur C., 160  
 Goto Nobuo, 783  
 Gou Y. S., 182  
 Granovsky Alexander B., 745, 819  
 Grant Peter, 258  
 Greenleaf Allan, 131, 139  
 Grimaldi Settimio, 442  
 Grime Paul, 77  
 Gu C. Z., 41  
 Gu Jianqiang, 156, 159, 161, 162  
 Gu Min, 149, 152, 220, 557, 567  
 Gu Zu-Han, 608, 613, 683  
 Guan Ning, 510, 512  
 Guida Geraldine, 960  
 Guillot Maurice, 899  
 Gumbs G., 826  
 Gumbs Godfrey, 912  
 Gunnala Suman K., 489  
 Guo Donghui, 520, 989  
 Guo Fangmin, 719  
 Guo H. C., 363  
 Guo Hongcang, 244  
 Guo Peng, 976  
 Guo Qiaohong, 338, 339  
 Guo Yuchun, 624, 648  
 Gupta J. A., 600  
 Gupta Shulabh, 242  
 Guy Meynen, 103  
  
 Habashy Tarek M., 630  
 Habibi M., 635  
 Hadinec Michal, 802, 803, 902–904, 906  
 Hai Ming, 688  
 Hajivandi J., 364  
 Halevi Peter, 250, 294, 536  
 Han Hainian, 562  
 Han Jianguang, 158, 163, 164  
 Han Lu, 582  
 Han Man-na, 397  
 Han Pin, 354  
 Han Song, 952  
 Hanada Yasutaka, 739  
 Hang Zhihong, 575  
 Hansen Volkert, 528  
 Hao Chao-Kun, 24  
 Hao Jiaming, 134, 249  
 Harris Louis-Ray, 645  
 Hart James, 550, 969  
 Hartikainen Juha, 531  
 Hartsuiker A., 822  
 Haruta K., 782  
 Hashimoto Shinsuke, 659  
 Haxha S., 747  
 Hayasaki Y., 732  
 Hayashi Shinichiro, 260  
 He Bo, 915  
 He Fei, 371  
 He Hongyang, 176  
 He Hua Hui, 986  
 He Jinliang, 324  
 He Li, 946  
 He Mingxia, 162, 163, 165  
 He Ning, 415  
 He Wu-Jie, 405  
 He Xinyang, 191  
 Heckenberg N. R., 449, 654  
 Hedman Antti, 531  
 Heiman D., 936  
 Helmerson Kristian, 661  
 Her Man-Long, 40  
 Hietanen Maila, 531  
 Higashino Takeshi, 264  
 Highstrete Clark, 160  
 Hikage Takashi, 645  
 Hikita Mitsutaka, 177  
 Hinata Takashi, 649, 710  
 Hiraizumi Yasushi, 177  
 Hirao K., 229, 733  
 Hirao Kazuyuki, 230  
 Hirono Masahiko, 645  
 Ho Hsin-Chia, 181  
 Holden Todd, 866  
 Holdsworth John, 238  
 Hong Chin-Yih, 483  
 Hong Wen, 974  
 Horii Yasushi, 72, 73  
 Horng H. E., 483  
 Horng Heng-Er, 482  
 Hou Ling Li, 460  
 Hou Shang-Lin, 387  
 Hou Zheng-Zheng, 24, 25  
 Hsieh Chao Ping, 987  
 Hsieh P. F., 344  
 Hsu Heng-Shou, 486  
 Hsu Heng-Tung, 76, 485  
 Hsu Kuo-Chien, 181  
 Hsu Mao-Feng, 867  
 Hsu Yuk Fan, 604  
 Hu Chu-Feng, 981, 982  
 Hu Dong Liang, 169  
 Hu Gengkai, 592, 749  
 Hu Hao, 392  
 Hu Jin, 749  
 Hu Jun, 921, 923  
 Hu S. F., 184  
 Hu Shan, 341  
 Hu Shu-Fen, 187  
 Hu Sung-Cheng, 867  
 Hu Tiancun, 198  
 Hu Wei, 340  
 Hu Wenyi, 630  
 Hu Y., 654  
 Hu Yongxiang, 343  
 Hu Zheng, 811  
 Hu Zhirun, 438, 472  
 Huang Chao-Yuan, 187  
 Huang Danhong, 826  
 Huang Dexiu, 283  
 Huang F. M., 219  
 Huang Guiling, 21, 347, 378, 389–391  
 Huang Hao, 16  
 Huang J., 719  
 Huang Jintang, 689  
 Huang Ka-Ma, 972  
 Huang Kengyi, 987  
 Huang Lina, 566  
 Huang Meng, 581  
 Huang Wei, 946  
 Huang Wei-Ming, 930  
 Huang Wen-Lung, 17  
 Huang Wenhao, 231  
 Huang Xueguang, 399  
 Huang Yi Jen, 188  
 Huang Ying, 132  
 Huang Zhaohui, 52  
 Huang Zhaoniu, 389, 390  
 Huang Zhaoran (Rena), 513  
 Huangfu Jiangtao, 33, 41, 588, 589, 591  
 Hui Pak Ming, 440  
 Hung C. C., 334  
 Hurford G. J., 875  
 Hwang Seong In, 772  
 Hwang Soon-Ho, 117  
 Hwang Taekjin, 120  
  
 Ide Takanori, 547  
 II Nathaniel P. Hermosa, 446  
 Iizuka H., 849  
 Inoue Mitsuteru, 819  
 Ioachim A., 693  
 Ipatov M., 462

- Isernia Tommaso, 632, 873  
 Isozaki Hiroshi, 548  
 Ito H., 374  
 Ito Koichi, 510, 512  
 Iu Hei, 441  
 Ivans Veronica, 529  
 Ivashov Sergey I., 276  
 Ivrisimtzis Leonidas P., 614  
 Iwakiri Munetoshi, 771  
 Izutsu Masayuki, 265
- Jákl P., 447  
 Jackson Thomas J., 878  
 Jacquot Pierre, 655  
 Jafari Arezou, 928  
 Jagadish Chennupati, 677  
 Jahr Norbert, 221  
 Jang Byoung-Jun, 90  
 Jao Ruei-Fu, 827  
 Jaque Francisco, 148  
 Jazi Mahmud Niroo, 87  
 Jen Cheng-Min, 81  
 Jeney Sylvia, 658  
 Jeon Sinhyung, 625  
 Jeon Sung-Keun, 90  
 Jeremic Aleksandar, 430  
 Jesacher A., 657  
 Ji Wei, 676  
 Ji Weili, 372  
 Ji Xiaoling, 612  
 Ji Yang, 599  
 Jia Baohua, 149, 567  
 Jiang Ai-Min, 470  
 Jiang Aimin, 821  
 Jiang Dagang, 340  
 Jiang Fan, 989  
 Jiang Huiling, 1000  
 Jiang J. Z., 870  
 Jiang Lingling, 32  
 Jiang Tao, 42, 584, 585  
 Jiang Tian, 132  
 Jiang Xunya, 590  
 Jiang Yansheng, 392  
 Jiao Binbin, 310  
 Jiao Yong-Chang, 69, 119  
 Jin Kui-Juan, 601  
 Jin Pengcheng, 837  
 Jin Shun-jing, 407  
 Jin Ya-Qiu, 773, 979, 980  
 Jin Zhaoyang, 636  
 Jin Zhen, 333  
 Jirku Tomas, 798  
 John Sajeev, 142, 143  
 Johnson H. T., 828, 847  
 Johnson William T. K., 766  
 Johnston Sheila A., 532  
 Jones Stephen H., 504  
 Jordan G., 552
- Joseph P. T., 334, 335  
 Jou Christina F., 27–29, 39, 44  
 Jou Jwo-Huei, 867  
 Jr. Neville C. Luhmann., 933  
 Jr. Tim LaFave, 943  
 Juang Jenh-Yih, 182  
 Juodkasis Saulius, 146, 151
- Käs Josef A., 454  
 Kabir Humayun, 205  
 Kado Yuichi, 255  
 Kafesaki Maria, 671  
 Kagawa Naoki, 659  
 Kaiser Stefan, 244  
 Kalish A. N., 225  
 Kam Pooi Yuen, 543  
 Kamal Hanan A., 121  
 Kamei Toshihisa, 500  
 Kan Yao-Chiang, 889  
 Kanai T., 560  
 Kanevsky Mikhail, 351  
 Kang Kyongok, 967  
 Kang Kyung Sik, 553  
 Kang Lei, 398, 399  
 Kang Tong, 308, 477, 484  
 Kang Woo Suk, 619  
 Kani Junichi, 263  
 Kanilowski Hypolito, 239  
 Kanno Atsushi, 261  
 Kao Y. H., 36  
 Karásek V., 572  
 Karaev Vladimir Yurjevich, 351  
 Karimabadi Sara Sadat, 60  
 Karle T., 421  
 Karugila Geoffrey K., 909  
 Kasai S., 374  
 Katsube T. J., 273  
 Kawamura Hiroshi, 768, 770  
 Kawanishi Tetsuya, 265  
 Kawase Kodo, 260  
 Kawata Satoshi, 222  
 Kawata Yoshimasa, 228  
 Kazansky Peter G., 230  
 Kazaura Kamugisya, 264  
 Khalefa S., 401  
 Khalid Zubair, 696  
 Khan Noor M., 690, 694, 696  
 Kheir Mohamed Salah, 897, 992  
 Kheirandish Fardin, 402  
 Khurgin Jacob B., 830  
 Kiang Ching-Hwa, 934  
 Kikuchi Hiroshi, 908, 911  
 Kildishev Alexander V., 853  
 Kim Dai-Sik, 850  
 Kim Hojeong, 625  
 Kim Hyeong Dong, 625
- Kim Hyoungjun, 618  
 Kim Jae-Goo, 740  
 Kim Jeongpyo, 622  
 Kim K. W., 847  
 Kim Kwang Ik, 477  
 Kim Kyung Taec, 553  
 Kim Min-Seong, 620  
 Kim Nam, 88–90  
 Kisel Vladimir N., 668, 669  
 Kitaeva G. Kh., 363  
 Kitamura Kenji, 146  
 Kitamura Toshiaki, 72, 73  
 Kiuchi Hitoshi, 265  
 Knorr A., 419  
 Ko Dong Hyuk, 553  
 Ko Kyung Hyun, 37  
 Koay Jun-Yi, 492  
 Kobayashi Kazuya, 708, 709, 711  
 Kojima Toshitaka, 72, 73  
 Komaki Shozo, 264  
 Komiyama Akira, 781  
 Konas P., 798  
 Kong Jin Au, 31, 135, 138, 496, 497, 583, 588, 589, 591, 789, 954  
 Konig Friedrich, 299  
 Kontar E. P., 875  
 Korotkova Olga, 606  
 Koschny Th., 671  
 Kosolapova L. G., 879  
 Kraus Jonas, 658  
 Krausz Ferenc, 730  
 Kristensen Martin, 236, 240  
 Kriz T., 905  
 Kriz Tomas, 903  
 Krolikowski Wieslaw, 146  
 Kroutilová Eva, 902  
 Kroutilova Eva, 802, 903, 904  
 Kubasek Radek, 346, 798, 799  
 Kui Stephen C. F., 857  
 Kukutsu Naoya, 262  
 Kumar Pradeep, 70  
 Kundu Anindya, 53  
 Kuo Watson, 474  
 Kurylev Yaroslav, 131, 139, 546, 548  
 Kuusela Tom, 531
- López S. Y., 863  
 López-Rodríguez F. J., 764  
 Labib Mohamed A., 104–106  
 Lacroux F., 525  
 Laframboise Sylvain R., 258  
 Lagarkov Andrey N., 668, 669, 959  
 Lai Don-Yen, 997  
 Lai Hongkai, 416

- Lai Jiali, 395  
 Laishram J., 456  
 Lam H. L., 674  
 Lamela Jorge, 148  
 Lan Pengfei, 556  
 Lan Yung-Chiang, 434  
 Langenberg Karl Joerg, 292  
 Larar Allen, 349  
 Lassas Matti, 131, 139, 546, 548  
 Lassouaoui Nadia, 326, 356  
 Lauprette C., 495  
 Lauriks W., 214  
 Ledda Mario, 442  
 Lee Chongmin, 618  
 Lee El-Hang, 218  
 Lee Ho-Min, 88  
 Lee Jin-Fa, 136, 916  
 Lee Kun-Yi, 480  
 Lee Mark, 160  
 Lee Rong-Mao, 930  
 Lee Seung-Cheol, 916  
 Lee Seung-Woo, 88, 90  
 Lee Seung-Yeup, 89  
 Lee Seungwoo, 89  
 Lee Wei-Yu, 480  
 Lee Wen-Fei, 995  
 Lee Young Chul, 37, 38  
 Lee Yung-Cheng, 995  
 Lei Danyuan, 439  
 Lei Jing-Li, 387  
 Lei Wei, 719  
 Lencrerot Raphael, 541  
 Leon-Perez F. De, 860, 861  
 Leonhardt Ulf, 130, 299  
 Lesegno Bruno Viaris de, 420  
 Leskova Tamara A., 613  
 Lesselier Dominique, 628, 806  
 Leung Y. F., 922  
 Levenson A., 421, 422  
 Lewis Amanda, 660  
 Ley-Koo Eugenio, 843  
 Li B. K., 679  
 Li Bo, 398, 399  
 Li C. F., 837  
 Li Chao, 15, 397, 403, 855  
 Li Chaobo, 310  
 Li Cheng, 416  
 Li Chun-Fang, 330, 835, 838, 839, 841, 842  
 Li De, 123, 425, 426  
 Li Derong, 376  
 Li Desheng, 338, 339  
 Li F., 855  
 Li Fang, 15, 355, 403, 537, 638, 701, 702, 811  
 Li G. X., 223  
 Li H. L., 109  
 Li Henghua, 311  
 Li Honggen, 360  
 Li J., 123  
 Li Jia, 440, 441  
 Li Jia-Han, 224  
 Li Jia-Qi, 251  
 Li Jianhua, 203, 206, 210, 306–309, 311–313, 476, 484  
 Li Jie, 199, 345, 949  
 Li Jing, 206, 309, 311  
 Li Jinyang, 1004  
 Li Jun, 978  
 Li Kai, 300  
 Li Le-Wei, 465  
 Li Li, 878  
 Li Lianlin, 355, 537, 638, 701, 702, 811  
 Li Lijie, 724–726  
 Li Longtu, 399  
 Li Meng, 165  
 Li Minqi, 352  
 Li N., 595  
 Li Nan-Jing, 981, 982  
 Li Pei. Ci., 278  
 Li Qing, 677  
 Li Quanlu, 52  
 Li Ruxin, 563  
 Li S. W., 232  
 Li Shandong, 215, 898  
 Li Shang-Bin, 252  
 Li Sheng, 423  
 Li Shengxian, 196  
 Li Shuhong, 21, 347  
 Li Suo-Ping, 387  
 Li T., 937  
 Li T. X., 595  
 Li Tao, 243, 251  
 Li Wen Tao, 927  
 Li Xi, 16  
 Li Xing-Xing, 24  
 Li Xinhua, 678  
 Li Xuan, 345  
 Li Y., 543  
 Li Ya-Nan, 465  
 Li Yan, 738  
 Li Yan Ping, 194  
 Li Yanfeng, 156, 159, 161, 162  
 Li Yanrui, 414  
 Li Yuan, 52, 414  
 Li Yuanchun, 395, 396  
 Li Yuhua, 556  
 Li Z. W., 774  
 Li Zengchang, 688, 689  
 Li Zhaofeng, 467  
 Li Zhen-Ya, 112, 412  
 Li Zhenglong, 978  
 Li Zhibin, 341  
 Liang Chang-Hong, 25  
 Liang Dong, 159  
 Liang Yaping, 933  
 Liao Jiping, 21, 347  
 Liao Jun, 513  
 Liao Leng, 601  
 Liao Shry-Sann, 505, 991  
 Liao Shu-Hsien, 482  
 Liao Ting-Wei, 187  
 Liao Yang, 371  
 Liao Yu-Shun, 27  
 Liao Yu-Jie, 284, 285  
 Lien Huan-Cheng, 995, 996  
 Liew Soo Chin, 174, 175  
 Lim Ka Sing, 502  
 Lim Ka-Sing, 887  
 Lin Cheng-Hung, 19, 63, 66, 79, 83, 93, 514, 998  
 Lin Chi-Feng, 40  
 Lin Chien-Chang, 307, 309, 312, 313  
 Lin Chih-Peng, 39  
 Lin Ching-Ren, 211  
 Lin Fu-Min, 988  
 Lin Guijiang, 416  
 Lin Han-Nien, 17, 62  
 Lin Hung-Liang, 505, 991  
 Lin I-Nan, 180, 185, 334, 335  
 Lin J., 682  
 Lin J. H., 344  
 Lin J.-Y., 182  
 Lin Jon-Hong, 36  
 Lin Kun-Ying, 991  
 Lin Maoliu, 170  
 Lin Ming-Chieh, 827, 990  
 Lin Rufeng, 99, 100  
 Lin Shih-Chiang, 284, 285  
 Lin Tsung-Ting, 39  
 Lin Xian Qi, 246  
 Lin Yen-Juei, 480  
 Lin Zen-Chi, 181  
 Lin Zheng Yu, 436  
 Lindholm Harri, 531  
 Ling Yan, 115  
 Liou Saxon, 474  
 Liou Yuei-An, 353  
 Lisi Antonella, 442  
 Lisyansky Alexander A., 819, 964  
 Litman Amelie, 541  
 Liu Bao-Ying, 842  
 Liu Bo, 391  
 Liu Chang Sheng, 202  
 Liu Chi-Ping, 867  
 Liu Dawei, 496, 497  
 Liu Dayong, 738  
 Liu Feng, 162, 385, 636, 642, 812, 814  
 Liu H., 937

- Liu H. C., 258, 597, 598, 600  
 Liu Hong, 372  
 Liu Hsiang-Lin, 185  
 Liu Hui, 243, 251  
 Liu Ji-Chyun, 884  
 Liu Jie, 555  
 Liu Jing, 16  
 Liu Ken, 233  
 Liu Lanbo, 924  
 Liu Li, 417  
 Liu Liang, 300  
 Liu Lie, 750  
 Liu Ling Yun, 986  
 Liu Meimei, 215, 898  
 Liu Na, 244  
 Liu Peng, 979  
 Liu Qizhong, 191  
 Liu Ru-Shi, 184  
 Liu Ruopeng, 460  
 Liu S. F., 69  
 Liu Sen-Eon, 290  
 Liu Shao-Dong, 69, 475  
 Liu Shu-Fang, 475  
 Liu Songfen, 389  
 Liu W. M., 363  
 Liu Xiao, 15  
 Liu Xiuli, 742  
 Liu Xu, 349  
 Liu Yang, 1005  
 Liu Yanli, 638  
 Liu Yongxin, 609  
 Liu Yue Feng, 488  
 Liu Zhiyang, 504  
 Lizzi Leonardo, 538  
 Lo Kuang-Yao, 188  
 Loke Vincent L. Y., 449, 654  
 Long J., 33  
 Long J. P., 774  
 Longo G., 383  
 Lopera Olga Lucia, 274  
 Lopez Hector Sanchez, 385, 814  
 Love G. D., 577  
 Lozovik Yurii E., 912  
 Lu Chieh-Han, 180  
 Lu Fang, 115  
 Lu Guangyue, 168  
 Lu Hai-Xia, 813  
 Lu Hui-Bin, 601  
 Lu Liya, 898  
 Lu Mingyu, 489, 491, 494  
 Lu Peixiang, 556  
 Lu Pu-Shih, 990  
 Lu Shih-Ming, 282  
 Lu W., 936  
 Lu Wei, 595, 946  
 Lu Xiang, 946  
 Lu Xinchao, 158, 164  
 Lu Xuanhui, 834  
 Lu Xuejun, 829  
 Lu Ye, 425  
 Lu Z., 774  
 Lu Z. Y., 338  
 Lu Zheng, 409  
 Lu Zhiyuan, 339  
 Lucyszyn Stepan, 204  
 Lue Juh Tzeng, 183, 186  
 Lui Hoi-Shun, 812  
 Luk Kwai Man, 1004, 1005  
 Luk Wai Chun, 440  
 Lukić Branimir, 658  
 Luo Bin-feng, 169  
 Luo C. W., 182  
 Luo Hai Hui, 599  
 Luo Hui, 258  
 Luo Qingming, 376, 742  
 Luo Yanhua, 688, 689  
 Luo Ying, 169  
 Luo Yu, 138, 588  
 Lustrac A. de, 1003  
 Luukkonen O., 464  
 Lv Junfeng, 21, 378  
 Lv Xiaohua, 376, 564  
 Ma Changzheng, 168  
 Ma Da, 301  
 Ma Guohong, 836  
 Ma Haihong, 197  
 Ma Hongru, 137, 590  
 Ma Lili, 946  
 Ma Mingbo, 18  
 Ma Qian, 18  
 Ma Wei, 43, 101, 190, 192, 195, 198, 345, 584  
 Ma Xiang, 409  
 Ma Yi Ming, 194  
 Ma Zhixun, 866  
 Ma Zu-Hui, 921  
 Machac Jan, 248  
 Madrigal-Melchor J., 757  
 Mahmoodian S., 831  
 Mahmoudian A., 47  
 Mahmoodian Alireza, 74  
 Makeeva Galina S., 650, 714, 715  
 Makhnovskiy D. P., 856  
 Malekabadi S. A., 369  
 Mamouni Ahmed, 635  
 Manh Cuong Tran, 960  
 Mao Junfa, 926  
 Mao Samuel S., 866  
 Mao Wenhui, 396  
 Mao Xiang-Yu, 813  
 Maradudin Alexei Alexei, 613  
 Maria Alberto Di, 111  
 Marini A., 816  
 Marklein René, 292  
 Marshall Graham D., 735  
 Martel Jesús, 503  
 Martelli Cicero, 236, 239, 240  
 Martin Olivier J. F., 566  
 Martin-Neira Manuel, 880  
 Masdea A., 816  
 Massa Andrea, 538, 628, 806, 807, 876  
 Massone Anna Maria, 875  
 Matitsine Serguei, 750  
 Matsumoto Mitsuji, 264  
 Matsuoka Takeshi, 767  
 Matsuzawa S., 849  
 Maurer C., 657  
 Mauskopf Philip, 77  
 Mawhinney Daniel D., 968  
 Mayer Klaus, 292  
 Mazilu Michael, 569  
 Mbonjo H. Ndoumbè Mbonjo, 528  
 McCall Martin W., 293, 670  
 McPhedran Ross C., 831  
 Medina Francisco, 298, 459, 503, 646  
 Mehnert Andrew, 636  
 Melacci P. T., 816  
 Mellor Christopher D., 660  
 Mendecki Jozef, 968  
 Mendez Cruz, 148  
 Meng Guang, 932  
 Meng Kuo, 257  
 Meng Max Q.-H., 703  
 Meng Z.-Q., 782  
 Menon Latika, 936  
 Menzel W. Paul, 978  
 Merenda Fabrice, 655, 656  
 Merzlikin Alexander M., 819, 964  
 Mesa Francisco L., 298, 459, 646  
 Meshkov Eugeny, 351  
 Mestre Michael, 420  
 Metzger Klaus, 574  
 Meziani Yahya Moubarak, 256  
 Miao H. Y., 183  
 Miao Yinping, 347, 391  
 Midorikawa Katsumi, 560, 739  
 Milszczewski Maura, 239  
 Min Kyeong-Sik, 620  
 Minami Keiya, 177  
 Mintchev M., 945  
 Mirmohammad-Sadeghi Hamid, 87  
 Mironov V. L., 268, 879  
 Mirsalehi M. M., 56, 369  
 Misawa H., 146, 151  
 Mitake Yuta, 539  
 Miteva A. M., 756

- Miura K., 229, 733  
 Miura Kiyotaka, 230  
 Miyamoto M., 228  
 Miyanaga Noriaki, 741  
 Miyazaki Yasumitsu, 778, 783  
 Mizeikis V., 146  
 Mizue Osamu, 893  
 Mnaymneh Khaled, 824  
 Moeller Robert, 221  
 Moghadasi S. Mahdi, 56, 58, 60  
 Moghaddasi M. Naser, 331  
 Mohan D. Bharathi, 122  
 Mohsenzadeh Yalda, 60  
 Monifi F., 818  
 Monnier P., 422  
 Montoya J. J. F., 760  
 Mora-Ramos Miguel Eduardo, 759, 761, 860, 863  
 Moser Herbert O., 846  
 Mosig Juan R., 465  
 Mosk A. P., 751, 822  
 Mosk Allard P., 785  
 Mousavi S. M., 928  
 Mouysset V., 651  
 Muhi-Eldeen Zaid, 614  
 Murayama A. A., 596  
 Murray W. A., 359  
 Murthy V. R. K., 180, 185
- Néel D., 568  
 Nabekawa Y., 560  
 Nadai Akitsugu, 767  
 Nagalingam Manimaran, 502  
 Nagatomi Kenzo, 539  
 Nagatsuma Tadao, 255, 262  
 Naishadham Krishna, 78  
 Nakabayashi M., 228  
 Nakamura Ryosuke, 72  
 Nakamura S., 881, 882  
 Nakamura Takuya, 264  
 Nakashima Norimasa, 786  
 Nakata Yoshiki, 741  
 Nakheli A., 635  
 Nam Chang Hee, 553  
 Naumis Gerardo G., 764, 864  
 Naumova E. V., 955  
 Navarro-Cía Miguel, 852  
 Nelson J., 569, 931  
 Nemati Hoggat-Allah, 287  
 Neshati Mohammad Hassan, 65  
 Neves Antonio A. R., 448  
 Ng Jack, 450, 575  
 Ng Man Ching Alan, 604  
 Nieminen Timo A., 449, 654  
 Nikitov S. A., 247  
 Ning J. Q., 597, 598  
 Nino Juanita, 531
- Nishimura Taichi, 22  
 Niu Jia-Jun, 110, 113, 114  
 Nojima Toshio, 645  
 Nomura T., 849  
 Noor Adnan, 438  
 Novotna Katerina, 700  
 Nugent K. A., 542
- O'Hara John F., 160, 848  
 Ogam E., 214  
 Ogawa Yuichi, 260  
 Oka Soichi, 262  
 Oka Y., 596  
 Okoniewski Michal M., 634  
 Okubo Kensuke, 466  
 Omae Kazunori, 264  
 Ong H. C., 439  
 Ong Hock Chun, 440, 441  
 Ooi Ban leong, 917  
 Oppl Ladislav, 700  
 Oraizi Homayoon, 287, 468, 506  
 Oristaglio Michael, 210, 304, 312, 313  
 Orloff Nathan, 672  
 Oskouei Hamidreza Dalili, 74  
 Osman Husam El-Din Ahmed, 75  
 Ostendorf Andreas, 731  
 Otani Chiko, 260  
 Otsuji Taiichi, 256  
 Ott Edward, 550, 969  
 Ou Yi, 310  
 Oubram Outmane, 763  
 Ouchi K., 769  
 Ouchi Kazuo, 771–773  
 Ouchi T., 374  
 Ourir Abdelwaheb, 1003  
 Ouslimani Habiba Hafdallah, 326, 356, 960, 961  
 Ozaki Ryosuke, 649, 710  
 Ozbay Ekmel, 467, 746
- Pérez-Álvarez R., 760  
 Pérez-Álvarez R. P., 759  
 Pérez-Alvarez R., 761  
 Pérez-Rodríguez F., 250  
 Padhi Shantanu K., 812  
 Padilla Willie J., 160  
 Pai Hung-Yao, 530  
 Pai Shyh-Shii, 181  
 Pan E., 128  
 Pan Shi Bing, 986  
 Pan Yen-Lin, 920  
 Pan Yongmei, 394  
 Pang Xiao-Feng, 208, 478  
 Panina Larissa V., 462, 856  
 Pao-An Lin, 181
- Pardavi-Horvath Martha, 650, 714, 715  
 Park Chul-Keun, 620  
 Park Ju Yun, 553  
 Park Kyu-Bok, 117  
 Park Sang-Myeong, 88–90  
 Park Sung-Wu, 88, 89  
 Parkin S. J., 654  
 Parsons J., 359  
 Pascarella A., 633  
 Paul-Boncour Valerie, 899  
 Pearton S. J., 596  
 Pei Y., 279  
 Peng Gangding, 688, 689  
 Peng R. W., 123, 425  
 Peng Ru-Wen, 426, 938  
 Peng Yufeng, 417  
 Perez-Alvarez R., 860, 861  
 Persson M., 654  
 Peschel Ulf, 611  
 Peschke Peter, 639  
 Philbin Thomas G., 130, 299  
 Piana Michele, 540, 633, 875  
 Picardi Giovanni, 816  
 Piccari F., 816  
 Picon O., 525  
 Pisignano D., 448  
 Pistorius Stephen, 629  
 Plaut J. J., 816  
 Plettemeier D., 816  
 Poirier J.-R., 332, 495  
 Poli Lorenzo, 806  
 Poplau Gisela, 296  
 Poulton C. G., 831  
 Pourush P. K. S., 91  
 Pozzi Deleana, 442  
 Prato M., 875  
 Prinz Victor Yakovlevich, 955  
 Priou Alain C., 326, 356, 960, 961  
 Pruvost Laurence, 420  
 Pu Jixiong, 609
- Qi J., 471  
 Qiao Lingling, 370  
 Qiao Peng, 98  
 Qiao Shan, 33, 41, 42  
 Qin Xiaogang, 329, 337  
 Qin Yiqiang, 156  
 Qiu Cheng-Wei, 465  
 Qiu Jianrong, 229, 230, 733  
 Qiu Jiawen, 329, 337  
 Qiu Jinghui, 684, 886  
 Qiu Kai, 678  
 Qiu Ledo, 101, 195  
 Qiu Min, 718
- Räisänen A. V., 464

- Raineri F., 421, 422  
Raj R., 421, 422  
Raja J., 626  
Ramer Rodica, 690, 693, 694, 696  
Ramundo-Orlando Alfonsina, 383  
Ran Lixin, 31–33, 41, 42, 138, 583–585, 789  
Rao P. Nageswara, 85  
Rashed-Mohassel Jalil A., 47, 65  
Rath O., 787  
Rawat Vineet, 916  
Ray S., 163  
Razevig Vladimir V., 276  
Reece Peter, 574  
Ren Hongliang, 703  
Ren Zheng Yong, 202  
Ren ZhiXing, 409  
Repacholi Michael H., 522  
Reyes-Ayona E., 250  
Reznik A. N., 275  
Rho Sung Jung, 619  
Ricci Michael, 672  
Rienen Ursula van, 296  
Righi M., 456  
Ritsch Helmut, 570  
Ritsch-Marte Monika, 657  
Ritter Kathrin, 221  
Ro Ru-Yen, 284, 285  
Roan Jiunn-Ren, 935  
Rocca Paolo, 538, 807, 876  
Rode A. V., 146  
Rodenas Airan, 148  
Rodríguez Arezky H., 863  
Rodriguez-Otazo Mariela, 939  
Rodriguez-Vargas Isaac, 754, 755, 757, 758, 762, 948  
Rogatkin Dmitrii A., 616  
Rohini G., 721  
Rohner Johann, 655, 656  
Rong Lu, 95–100  
Rong Xing, 974  
Rong Yu, 110, 113, 114  
Roso Luis, 148  
Rosolen Grahame, 259  
Roy Atanu, 49, 54  
Roy Vellaisamy Arul Lenus, 857  
Ruan Lizhen, 359, 443  
Ruan X. Z., 597, 598  
Ruan Xue Zhong, 599  
Rubinsztein-Dunlop Halina, 449, 654  
Saadi A., 635  
Saari Peter, 896  
Sadek Vaclav, 795, 905, 906  
Saeedi Shahrokh, 506  
Saha Arun K., 893  
Saillard Joseph, 176  
Sakai Kenji, 970  
Sakakura Masaaki, 230  
Sakamoto Takahide, 265  
Sakamoto Takuya, 810  
Salamo Gregory J., 866  
Salathe Rene Paul, 655, 656  
Saliminia A., 734  
Salinas Santo V., 174, 175  
Salivahanan S., 721  
Saltykov Evgeny Grigoryevich, 216  
Sambles J. Roy, 359, 443  
Samokhin Alexander B., 713  
Sanchez Hector, 636  
Sanchez-Barbosa O. Y., 762  
Sang Mei, 164  
Sano Eiichi, 256  
Santiago A. del RÍo De, 758  
Santiago A. del Rio de, 757  
Santiago-Perez D. G., 860  
Sardari Dariush, 705  
Sarkomaa P., 928  
Sarman N. V. S. N., 85  
Sarychev Andrey K., 959  
Sasagawa Kiyotaka, 261  
Sasilatha Thankappan, 626  
Satake Makoto, 767  
Sato K., 849  
Sato T., 810  
Saxena Naveen Kumar, 91  
Sbeta M., 401  
Scheel Stefan, 944  
Schluessel Peter, 349  
Schmit Timothy J., 978  
Schueler Thomas, 221  
Schwaighofer A., 657  
Schwartz R. A., 875  
Schweizer H., 244  
Scrinzi Armin, 552  
Sebaa N., 214  
Sedláček J., 803  
See Chan H., 925  
Sekikawa Taro, 554  
Seleznev V. A., 955  
Semenenko V. N., 668, 669  
Seo Chulhun, 618  
Sery M., 447  
Seu R., 816  
Shadrivov Ilya V., 752  
Shah Alam Mohammad, 264  
Shahapure R., 456  
Shalaev Vladimir M., 853  
Shang Erhao, 709  
Shang She, 190, 345  
Shang Yuanbo, 119  
Shao Che-Min, 62  
Shao Jun, 946  
Shao Zhenghai, 463  
Sharma Vikrant Kumar, 55  
Shashar Hamdy, 302  
Shen Dong, 341  
Shen L.-F., 305  
Shen Linfang, 481  
Shen Qishun, 360  
Sheng Hui, 976  
Sheppard Asher R., 523  
Shestopalov Yury V., 711, 712  
Shevchenko E. A., 225  
Sheyko Anton P., 276  
Shi Jiancheng, 490  
Shi S. L., 675  
Shi Shali, 310  
Shi Wei, 372  
Shi Xiao Wei, 927  
Shi Xiaowei, 624, 648  
Shi Yanling, 16  
Shi Z. X., 895  
Shi Zhiguo, 42, 585  
Shih N.-Y., 358  
Shimada Teruhisa, 768  
Shimotsuma Yasuhiko, 230  
Shuley Nick, 812  
Shyue Jing-Jong, 867  
Sihvola Ari Henrik, 458, 471  
Siltanen Samuli, 546, 549  
Simba Ally Y., 526  
Simoes Jose, 239  
Simovski C. R., 464  
Singh Bhoopendra, 91  
Singh G., 70  
Skivesen Nina, 236, 240  
Smirnov Yury G., 711, 712  
Smith William L., 349  
Somersalo E., 131  
Song C. Y., 600  
Song Dongmei, 976  
Song J., 733  
Song Jinglu, 414  
Song S. H., 218  
Song Shupeng, 157  
Song Weiwei, 1005  
Soots R. A., 955  
Sorba Paul, 945  
Sorolla Mario, 459, 852  
Sorrentino A., 633  
Soukoulis C. M., 671  
Spivack Mark, 787  
Sprunt Samuel, 967  
Sridhar S., 936  
Steinbauer Miloslav, 796, 797, 802, 902, 907  
Steinbauer Miroslav, 799, 904

- Steinbrueck Andrea, 221  
 Sterke C. Martijn de, 831  
 Sterzer Fred, 968  
 Stevenson Michael, 239  
 Streckert Joachim, 528  
 Strelniker Yakov, 744  
 Stricker Josef, 411  
 Stukach O. V., 48  
 Su Hua, 108  
 Su T. H., 344  
 Su Wei, 689  
 Su Yan-Kuin, 424  
 Subramanian V., 185  
 Subramanian Venkatachalam, 180  
 Suemitsu Tetsuya, 256  
 Suen Y. W., 474  
 Sugioka Koji, 739  
 Sui Qiang, 397  
 Sun Bao Quan, 599  
 Sun Bo, 684, 886  
 Sun Greg, 830  
 Sun Guoqing, 496  
 Sun Haiyi, 371  
 Sun Hua, 112  
 Sun J. L., 344  
 Sun Jian, 770  
 Sun Jiawei, 207  
 Sun Jwo-Shiun, 19, 63, 66, 79, 83, 93, 514, 998  
 Sun Nai-Hsiang, 284, 285, 289  
 Sun Nian-Xiang, 78  
 Sun Pou-Tou, 505, 991  
 Sun Q., 734  
 Sun Qiong, 408  
 Sun Wei-Hua, 425, 938  
 Sun Xin, 423  
 Sun Yi, 408  
 Sunandana C. S., 122  
 Sung Guo-Ming, 50  
 Suzuki Hirotsuke, 500  
 Suzuki Toshiji, 264  
 Swicord Mays L., 523  
 Szabó Zoltan, 803  
 Szabo Zoltan, 796, 798
- Taddese Biniyam, 550  
 Tagashira Katsuhisa, 73  
 Tahvanainen Kari, 531  
 Tai Chao-Yi, 950  
 Tai Cheng-Chi, 381, 382, 920  
 Tai Nyan-Hwa, 334, 335  
 Takahashi E. J., 560  
 Takahashi Koichi, 264, 783  
 Takahashi Yoshilide, 526  
 Takahashi Satoru, 659  
 Takekawa Shunji, 146  
 Takenaka Takashi, 539, 631
- Takeyasu Nobuyuki, 222  
 Takimoto Koki, 177  
 Talaia Paolo, 239  
 Talanov V. V., 275  
 Tam H. L., 223  
 Tamagawa H., 966  
 Tamosiunaite Milda, 102  
 Tamosiunas Stasys, 102  
 Tamosiuniene Milda, 102  
 Tan Chue-Poh, 171  
 Tan H. Hoe, 677  
 Tan Hwee Siang, 168  
 Tan Peng Khiang, 750  
 Tan Qinggui, 193  
 Tanabashi A., 374  
 Tanaka Takuo, 222  
 Tanaka Toshiyuki, 539, 631  
 Tang Jing Tian, 202  
 Tang Sing Hai, 363, 836  
 Tang Xiaohong, 197  
 Tang Xiaoli, 108  
 Tang Yi-Ping, 405, 407  
 Tang Z. H., 938  
 Tarricone L., 383  
 Tateiba Mitsuo, 782, 786  
 Taylor Antoinette J., 160, 848  
 Taylor Jonathan M., 577  
 Tchernyi Vladimir V., 107, 616  
 Teillet Herve, 960  
 Teixeira Fernando Lisboa, 136  
 Teng Hao, 562  
 Teo Lei-Teen, 887  
 Teshima K., 810  
 Tetu Amelie, 236  
 Thanh Nguyen, 500  
 Thiel M., 150  
 Thomas Gabriel, 629  
 Thomson L. C., 569  
 Tian Zhen, 156, 159, 161, 162  
 Tiong Kwong-Kau, 19, 63, 66, 79, 83, 93, 514, 998  
 Tjerkstra R. W., 822  
 Tjuatja Saibun, 489, 491, 494  
 Togni Paolo, 639  
 Togo Hiroyoshi, 262  
 Tong Changjiang, 951  
 Torchia Gustavo, 148  
 Torre V., 456  
 Tortel Herve, 541  
 Tournier S., 495  
 Toutain Y., 525  
 Trakic Adnan, 642  
 Tran Chanh Q., 542  
 Trasi Kartik, 494  
 Tretyakov Sergei, 464  
 Triplett David J., 994  
 Truschi Nicola, 111  
 Tsai Din Ping, 436
- Tsai Huei-Chiou, 995, 996  
 Tsai Nan-Chyuan, 930  
 Tsai Yung-Cheng, 867  
 Tsu Raphael, 942, 943  
 Tsuchida Kunio, 741  
 Tsuchiya Masahiro, 261, 265  
 Tsukamoto Katsutoshi, 264  
 Tsutsumi Makoto, 466  
 Tu Dingyuan, 99  
 Tuan Shih-Chung, 914  
 Tynjala T., 928
- Uen T. M., 182  
 Uhlmann Gunther, 131, 139  
 Umansky V., 599  
 Umehara Toshihiko, 767  
 Uno Toru, 526  
 Uratsuka Seiho, 767  
 Usman Muhammad, 518  
 Ustinov Alexey V., 404  
 Utsumi Yozo, 500  
 Uttamchandani Deepak, 724–726
- Vallée R., 734  
 Vannucci Luca, 639  
 Vasilyev Igor A., 276  
 Vecchi G., 421  
 Velázquez-Ahumada Maria del Castillo, 503  
 Velasco Victor R., 761  
 Venkov George, 293  
 Verga N., 705  
 Veselago V. G., 665  
 Vesely A. A., 26  
 Vesely Sara Liyuba, 26  
 Viani Federico, 876  
 Villagrán-Muniz Mayo, 323  
 Villard Ludovic, 495  
 Villegas D., 861  
 Villoresi Paolo, 561  
 Vinogradov Alexey P., 819, 964  
 Visek Lukas, 639  
 Vlaev Stoyan Jelevev, 756–758, 762  
 Vogel Horst, 455  
 Vogel R., 654  
 Volke-Sepulveda Karen, 843  
 Vos W. L., 822  
 Vrba David, 700  
 Vrba Jan, 639, 700, 704  
 Vu Manh Dat, 620
- Wada Yoichi, 970  
 Wakamori Kazuhiko, 264  
 Wan Jones Tsz-Kai, 441  
 Wang Anting, 608, 683  
 Wang Changlei, 156, 159, 161, 162

- Wang Chao, 45  
 Wang Chen, 370  
 Wang Ching-Yue, 418  
 Wang Chun-Jan, 867  
 Wang Dao-bin, 387  
 Wang Dongxing, 584, 589, 591, 954  
 Wang F. M., 937  
 Wang F. Y., 223  
 Wang Fei, 21, 347  
 Wang Fu-Ming, 243, 251  
 Wang Haipeng, 771, 773  
 Wang Haogang, 922  
 Wang He, 867  
 Wang He-Zhou, 232, 433  
 Wang Hong, 408  
 Wang Hongli, 890  
 Wang Hua, 642  
 Wang Ji, 329, 337  
 Wang Jian, 362  
 Wang Jian-Nong, 679  
 Wang Jianguo, 46, 951  
 Wang Jiannong, 678  
 Wang Johnson Jenn-Hwa, 994  
 Wang Jun, 101, 199, 352  
 Wang Keyi, 689  
 Wang Lei, 192  
 Wang Li-Gang, 840  
 Wang Li-Qin, 840  
 Wang Mengyu, 31  
 Wang Mu, 425, 426, 938  
 Wang Qing, 648  
 Wang Qingyue, 156, 159, 161, 162  
 Wang Shi-Yung, 997  
 Wang Shu-Ming, 243, 251, 937  
 Wang Tao, 609  
 Wang W. P., 595  
 Wang Wei, 339, 813  
 Wang Wei-Ben, 867  
 Wang Wei-Kang, 222  
 Wang Weihua, 249  
 Wang Xian, 986  
 Wang Xiao-Qing, 350  
 Wang Xiaobin, 333  
 Wang Xiaochuan, 324  
 Wang Xinlin, 556  
 Wang Xue-Hua, 145  
 Wang Yanhua, 257  
 Wang Ye, 202  
 Wang Yide, 176  
 Wang Ying, 43  
 Wang Yinhang, 1004  
 Wang Yuqi, 678  
 Wang Z., 426, 938  
 Wang Zhigong, 30  
 Wang Zhiguo, 413  
 Wang Zhiming M., 866  
 Wang Zhiyu, 584  
 Ward Andrew D., 660  
 Wasilewski Z. R., 600  
 Wasilewski Zbig R., 258  
 Watanabe Soichi, 526  
 Weber Ewald, 385, 814  
 Weder Ricardo, 133  
 Wegener M., 150  
 Wei K., 123, 426  
 Wei Lien-Sheng, 28  
 Wei Qing, 636  
 Wei S. C., 424  
 Wei Wenbo, 68  
 Wei Zhiyi, 562  
 Weikle Robert M., 504  
 Weiland Thomas, 297  
 Weisse-Bernstein Nina R., 848  
 Wen Guangjun, 463  
 Wen Haiyan, 162  
 Wen Shuangchun, 748  
 Wen Xiuzhi, 16  
 Wiart Joe, 525  
 Wilczek Daniel, 103  
 Wiltshire Michael, 956  
 Wiltshire Michael C. K., 958  
 Windsor Colin G., 274  
 Withford Michael, 735  
 Withington Stafford, 77  
 Woldering L. A., 822  
 Wong Kam Sing, 602  
 Wong Luen Yan, 576  
 Wong M. S., 674  
 Wong Man-Fai, 525  
 Woods David, 660  
 Wright Ewan, 574  
 Wu Bae-Ian, 135, 588, 589, 591, 954  
 Wu Bian, 25  
 Wu Chien-Jang, 479  
 Wu Guoguang, 504  
 Wu H., 497  
 Wu Hui I, 39  
 Wu J. C., 412  
 Wu J. Y., 483  
 Wu Jian-Chun, 112  
 Wu Jun, 946  
 Wu K. H., 182  
 Wu Kuo-Liang, 66, 93  
 Wu Lin Zhang, 986  
 Wu P. L., 674  
 Wu Rui-Xin, 470, 821  
 Wu T. D., 490  
 Wu Tongning, 525  
 Wu Tsungyin, 494  
 Wu X., 425  
 Wu Xin, 123, 938  
 Wu Xinglong, 594  
 Wu Xuda, 196  
 Wu Z. L., 895  
 Xi Rui, 923  
 Xi Sheng, 589, 591  
 Xi Yan Yan, 604  
 Xia Lei, 116  
 Xia Ling, 636  
 Xia Ruohong, 428  
 Xiang R., 774  
 Xiang Yin, 355  
 Xiang Yuanjiang, 748  
 Xiao Dong, 828, 847  
 Xiao Gaobiao, 720, 926  
 Xiao Jiang, 350  
 Xiao Jianhua, 277, 322  
 Xiao Q. W., 497  
 Xiao Xiao, 202  
 Xie Feng, 203, 476  
 Xie Ganquan, 203, 206, 210, 304, 308, 309, 311–314, 476, 484  
 Xie Kang, 463  
 Xie L., 210  
 Xie Lee, 203, 206, 476  
 Xie Qin, 399  
 Xie Xinhua, 552  
 Xing Huaizhong, 868  
 Xing Qirong, 156, 159, 161, 162  
 Xing Xiaohang, 684  
 Xiong Shi-Jie, 603  
 Xu Feng, 45  
 Xu Fu Yong, 460  
 Xu Haisheng, 341  
 Xu Hao, 249  
 Xu Hua, 672  
 Xu Ji, 821  
 Xu Jia-Dong, 982  
 Xu Jian, 371  
 Xu K. Y., 128  
 Xu L., 927  
 Xu Lisheng, 703  
 Xu Qiang, 95–97, 100  
 Xu Ruimin, 116  
 Xu S. J., 597, 598, 603, 675, 677  
 Xu Shanjia, 393–396, 580–582  
 Xu Shenglan, 868  
 Xu Wenlong, 636  
 Xu Xiaofei, 132  
 Xu Yi Hui, 300  
 Xu Zheng, 414  
 Xu Zhizhan, 370, 371, 563, 733  
 Xu Zhong Ying, 599  
 Xu Zhuo, 392  
 Xue Linyan, 16  
 Yachin Vladimir, 295  
 Yacomotti A. M., 421, 422  
 Yamada Masumi, 265



Yamada Minoru, 373, 947  
 Yamaguchi Ryo, 1000  
 Yamasaki Tsuneki, 649, 710  
 Yamashita M., 374  
 Yan Bo, 116  
 Yan Lei, 488  
 Yan Li, 952  
 Yan Qing, 689  
 Yan Wenzhe, 496, 497  
 Yang C. S., 769  
 Yang Fuzi, 443  
 Yang Guangdi, 99  
 Yang Guangli, 118  
 Yang Guo-Zhen, 601  
 Yang Guomin, 78  
 Yang H. C., 483  
 Yang Hong, 738  
 Yang Hong-Chang, 482  
 Yang Hua, 409  
 Yang Huizhu, 304, 306, 314  
 Yang Ji, 597, 598  
 Yang Jian, 974  
 Yang Jianzhong, 727  
 Yang Liu, 720  
 Yang S. Y., 482  
 Yang Shieh-Yueh, 483  
 Yang Tianxin, 157  
 Yang Tzong-Jer, 481  
 Yang Xiao-Qing, 972  
 Yang Xin Mi, 246  
 Yang Yaru, 414  
 Yao Kan, 403  
 Yao Zoushi, 340  
 Yapar Ali, 808  
 Yasumoto Kiyotoshi, 295  
 Ye Dexin, 583  
 Ye Hongbo, 16  
 Ye Lezhi, 338, 339  
 Ye Wei-Min, 233  
 Yeh W.-L., 358  
 Yeh Yi-Chen, 186  
 Yeo Tat Soon, 168  
 Yin Xiang, 701  
 Yin Yingzeng, 68  
 Ying Heping, 440  
 Yoneyama H., 374  
 Yoon Hyung Kuk, 619  
 Yoon Kwon-Ha, 410  
 Yoon Young Joong, 619  
 Yoshikado Shinzo, 970  
 You Zheng, 727  
 Yu Chih-Ping, 50  
 Yu Jia Cheng, 488  
 Yu Jinzhong, 416  
 Yu Ming, 205  
 Yu Siyuan, 283  
 Yu Tsan-Yuan, 180  
 Yu Ying, 350  
 Yuan Bin, 110, 113, 114, 926  
 Yuan Hsiao-Kuan, 853  
 Yuan Shih-Yi, 505  
 Yuan Xiao-Cong, 682  
 Yuan Xiao-Dong, 233  
 Yue Fangyu, 946  
 Yvinec Yann, 271  
 Zajicek Radim, 700  
 Zakharin Boris, 411  
 Zampolini E., 816  
 Zehentner Jan, 248  
 Zemánek Pavel, 366, 367, 447, 572  
 Zeng Bing-Hao, 884  
 Zeng Qunli, 428  
 Zeng Rong, 324  
 Zeng Shaoqun, 376, 564, 742  
 Zeng Y. S., 169  
 Zenkour L., 635  
 Zerrad M., 790  
 Zhan G. Z., 719  
 Zhang Anxue, 392  
 Zhang Baile, 135, 589  
 Zhang Bo, 324  
 Zhang Chenghui, 636  
 Zhang Danying, 428  
 Zhang F. S., 69, 119  
 Zhang Fujun, 414  
 Zhang Hai, 951  
 Zhang Hong-Tai, 190  
 Zhang Hongtao, 68  
 Zhang Huaiwu, 108  
 Zhang J., 163  
 Zhang J. S., 123  
 Zhang Ji Feng, 202  
 Zhang Jin, 77  
 Zhang Jing, 340  
 Zhang Jingjing, 138, 588, 591  
 Zhang Jun, 395, 580  
 Zhang Junping, 173  
 Zhang Lamei, 170, 173  
 Zhang Lin-Xi, 981  
 Zhang Min, 207, 890  
 Zhang Minggao, 417  
 Zhang N., 895  
 Zhang Ning, 886  
 Zhang Peng, 340  
 Zhang Qijin, 688, 689  
 Zhang Qijun, 205  
 Zhang Qun, 169  
 Zhang R. L., 123  
 Zhang Shu-Lin, 870  
 Zhang T., 119  
 Zhang T. Y., 869  
 Zhang W. J., 537  
 Zhang Weijie, 974  
 Zhang Weili, 158, 163–165  
 Zhang Wen Xun, 301  
 Zhang Wenji, 702  
 Zhang X., 243  
 Zhang Xia, 310  
 Zhang Xiang, 854  
 Zhang Xiaomiao, 1004, 1005  
 Zhang Xin-Hai, 675  
 Zhang Xing, 398  
 Zhang Y. C., 895  
 Zhang Yan, 257  
 Zhang Yaoju, 429  
 Zhang Ye, 173  
 Zhang Yi, 199  
 Zhang Yukun, 428  
 Zhang Yun, 324  
 Zhang Z. J., 123  
 Zhang Zi-Jian, 938  
 Zhang Ziyang, 718  
 Zhao Bing, 98  
 Zhao Chengliang, 834  
 Zhao Hongjie, 398, 399  
 Zhao Jiuzhou, 109  
 Zhao Kezhong, 136  
 Zhao Kun, 601  
 Zhao Luming, 21, 347, 378  
 Zhao Qian, 398, 399  
 Zhao Qida, 21, 347, 378, 391  
 Zhao Suling, 414  
 Zhao W., 869  
 Zhao Wei, 1005  
 Zhao Y., 163  
 Zhao Zeng, 426  
 Zhao Zhao, 924  
 Zhao Zhen-Shang, 147  
 Zheludev Nikolay, 219  
 Zheng Boren, 463  
 Zheng H. Z., 597, 598  
 Zheng Jianping, 708  
 Zheng Rongsheng, 688  
 Zhong Fei, 678  
 Zhong Lingling, 684, 886  
 Zhong Zhiyong, 108  
 Zhou Bin, 191  
 Zhou Daniel K., 348, 349  
 Zhou Dawei, 516, 925, 1001  
 Zhou Guangyong, 152  
 Zhou Hui, 631  
 Zhou Ji, 398, 399  
 Zhou Jian-Bin, 932  
 Zhou Jianzheng, 30  
 Zhou Jingli, 689  
 Zhou Lei, 134, 249  
 Zhou Quan, 101, 352  
 Zhou Wei, 742  
 Zhou Xiaoming, 749  
 Zhou Yi, 528  
 Zhu Bin, 340  
 Zhu Bing, 688

Zhu Jianfeng, [636](#)

Zhu Jiang, [963](#)

Zhu Jiangfeng, [562](#)

Zhu Ka-Di, [427](#)

Zhu Min-Hui, [350](#)

Zhu Minhua, [636](#)

Zhu Qi, [395](#), [396](#), [580](#), [582](#)

Zhu Qi-Biao, [838](#), [841](#)

Zhu S. N., [937](#)

Zhu Shi-Ning, [243](#), [251](#)

Zhu X.-R., [305](#)

Zhu Yi-Hua, [405](#)

Zhu Yongyuan, [156](#)

Zhu Z. Q., [719](#)

Zhukov Arcady P., [462](#), [856](#)

Zhukova V., [462](#)

Zhuravel Alexander, [404](#)

Zhuravlev A. V., [276](#)

Zide Joshua M. O., [160](#)

Zilinskas Mindaugas, [102](#)

Zou Bin, [170](#), [173](#)

Zouhdi Said, [964](#)

Zuo Daxin, [206](#), [311](#)

Zvezdin A. K., [225](#)

